

# INDIAN JOURNAL OF PHYSICS

VOL. 27

AND

PROCEEDINGS

OF THE

*Indian Association for the Cultivation of Science, Vol. 36*

*(Published in Collaboration with the Indian Physical Society)*

---

( With Thirty Plates )

---

Printed by Sibendranath Kanjilal, Superintendent Calcutta University Press,  
48, Hazra Road, Ballygunge, Calcutta and published by the Registrar,

Indian Association for the Cultivation of Science.

Jadavpur, Calcutta 32

1953

## BOARD OF EDITORS

K. BANERJEE	S. K. MITRA
D. M. BOSE	P. RAY
S. N. BOSE	K. R. RAO
K. R. DIXIT	M. N. SAHA

S. C. SIRKAR (*Secretary*)

## EDITORIAL COLLABORATORS

DR. R. K. ASUNDI, M.A., PH.D.  
PROF. H. J. BHABHA, PH.D., F.R.S.  
DR. P. K. KICHLU, D.Sc.  
PROF. K. S. KRISHNAN, D.Sc., F.R.S.  
PROF. G. P. DUBE, M.Sc.  
DR. B. D. NAG CHOWDHURY, PH.D.  
DR. N. N. DASGUPTA, M.Sc., PH.D.  
PROF. N. R. SEN, D.Sc., F.N.I.  
PROF. P. C. MAHANTI, D.Sc., F.N.I.  
PROF. S. R. PALIT, D.Sc., F.N.I.  
DR. H. RAKSHIT, D.Sc.  
DR. VIKRAM A. SARABHAI, M.A., PH.D.  
DR. P. S. GILL, PH.D.  
DR. S. R. KHASTGIR, D.Sc., F.N.I.,  
F.R.S.E.  
DR. D. BASU, PH.D.  
DR. D. S. KOTHARI, D.Sc., F.N.I.

 ASSISTANT EDITOR 

MR. A. N. BANERJEE, M.Sc.

## NOTICE TO INTENDING AUTHORS

Manuscripts for publication should be sent to Mr. A. N. Banerjee, Assistant Editor, 2 & 3, Lady Willingdon Road, Jadavpur, Calcutta 32.

The manuscript of each paper should contain in the beginning a short abstract of the paper.

All references to published papers should be given in the text by quoting the surname of the authors followed by the year of publication within braces, *e.g.*, Sen (1942). The actual references should be given in a list at the end of the paper according to the following specimen :

Sen, B. K., 1942, *Ind. J. Phys.*, **16**, 329.

The references should be arranged alphabetically in the list.

All diagrams should be drawn on thick white paper in Indian ink, and letters and numbers in the diagrams should be written neatly in capital type in Indian ink. The size of the diagrams should be at least three times that of the intended size of the actual figure.

Annual Subscription—

Indian Rs. 30

Foreign £. 2



# CONTENTS

PAGE

## No. 1

Scattering Domains around the Reciprocal Lattice Points of Benzil Crystal by Photographic Photometry—By R. K. Sen ... ..	1
2. Phosphorus in Steel—By K. C. Mazumder and M. K. Ghosh ... ..	11
3. Absolute Neutron Flux from a $Ra\alpha + Be$ Source—By N. K. Saha and L. Kasturi Rangan ... ..	18
4. Structure of Tetraphenyl Ethylene—By M. N. Datta ... ..	25
5. On the Spectral Characteristics of Ozoniser Discharge in Pure Nitrogen at 20 mm Pressure—By N. Appalanarasimham ... ..	31
6. On the Faithful Reproduction of the Flat top of a Pulse in a High Fidelity Pulse Amplifier—By Bimal Krishna Bhattacharyya ... ..	39
7. Ultraviolet Absorption Bands of Crystals of Ortho and Para-Dichlorobenzene at Low Temperatures—By H. N. Swamy ... ..	55

## No. 2

8. Change of Frequency of Resonance Lines of Sodium during Transmission through Sodium Vapour—By G. S. Kastha ... ..	67
Sound Velocity Measurements in Organic Liquids—By S. Parthasarathy and N. N. Bakhshi ... ..	73
10. The Effect of Fluid Motion on Heat Transmission. Part I. Vertical Cylinders—By D. G. Kapadnis ... ..	77
11. The Raman Spectra of 1, 3 Dibromopropane and 1, 2, 3-Trichloropropane in the Solid State—By B. M. Bishui ... ..	90
12. The Comparative Influence of Short and Long Range Electric Fields in the Salts of the Iron Group of Elements. Part III.—By A. Bose and S. C. Mitra ... ..	95
13. Streamer Mechanism in A. C. Silent Discharges—By S. R. Khastgir and C. M. Srivastava ... ..	109

## No. 3

14. Absorption Spectra of Organic Substances in the Liquid and Solid States. VI. Some Disubstituted Benzenes—By H. N. Swamy ... ..	119
15. An X-ray Investigation of the Tetraphenylethylene Crystal—By M. N. Datta ... ..	126
16. Temperature Dependence of Anisotropy of some Ortho and Para Disubstituted Benzenes—By Monomohan Mazumder ... ..	129
17. On the Large Load Characteristics of Vapour Pumps—By S. K. Mukherjee and P. K. Dutt ... ..	137
18. Molecular Diameter of a Liquid—By M. G. Bhatawdekar ... ..	145

19. A Discussion on the Spectroscopic State of Tetravalent Carbon in the Halogen Substituted Derivatives of Methane as revealed by Absorption Spectra—By Prabhat K. Sen Gupta ... .. 149
20. An Accurate Determination of the Torsion Constant of Quartz Fibres used in the Measurement of the Magnetic Anisotropy of Crystals—By Sunil Kumar Datta ... .. 155

No. 4

21. Raman Spectra of Methyl Methacrylate in the Solid State at  $-180^{\circ}\text{C}$ —By N. K. Roy ... .. 167
22. Proton-Proton Scattering and the Pseudoscalar Meson Theory—By C. C. Banerjee ... .. 173
23. On the Electronic Spectra of Dibenzyl, Diphenylmethane and Ethylbenzoate in the Solid State at  $-180^{\circ}\text{C}$ —By A. R. Deb ... .. 183
24. Production of Penetrating Showers in Paraffin and Lead—By R. L. Sen Gupta, K. K. Roy and T. Roy ... .. 191
25. Covariant Theory of Radiation Damping and the Scattering of Charged Scalar Mesons by Nucleons—By S. N. Biswas ... .. 197
26. On the Concentration of Stress round the Edge of a Hole bounded by two Intersecting Circles in a Large Plate—By B. Karunes ... .. 208
27. Cross Sections of (p, 2n), (p, pn) and (p, 2p) Reactions for Copper Bombarded with High Energy Protons—By S. N. Ghoshal and T. N. Dave ... .. 213

No. 5

28. Moisture Sensitivity of Dielectric Constant of Raw Jute and Cotton—By B. L. Banerjee ... .. 223
29. Correlation between Variations of Surface Pressure and Ionospheric Parameters—By M. R. Kundu ... .. 235
30. Relative Cross Sections of (n, p) Reactions in Sulphur 32 and Phosphorus 31—By N. K. Saha and M. Choudhury ... .. 244
31. Electronic Spectra of Molecules containing six and five membered Rings. Part I. Calculation of Energy Levels—By G. Viswanath ... .. 251
32. Oblique Propagation of Radio Waves over a Curved Earth—By B. Chatterjee 257
33. Effect of Steepness of Pulse Fronts on the Response of Differentiating and Integrating Circuits—By Bimal Krishna Bhattacharyya ... .. 269

No. 6

34. Absorption of U. H. F. Radio Waves in the Range 250-920 Mc/sec by Substituted Benzenes. III.—By Dimp Kumar Ghosh ... .. 285

35.	Electrical Properties of Indian Mica. V. D. C. Resistivity—By S. S. Mandal and P. C. Mahanti	294
36.	Ultraviolet Absorption Spectra of Diphenyl in the Liquid and Solid States—By A. R. Deb	305
37.	Classical Theory of Charged Meson—By N. C. Sil	311
38.	On the Raman Spectra of Solutions of 1, 2, 3-Trichloropropane—By T. A. Hariharan	323
39.	Measurement of Ferromagnetic Permeability at Microwave Frequencies—By G. S. Sanyal and J. S. Chatterjee	328
Corrigendum :		
	On the Solutions of Maxwell's Equations in an Infinite Medium, etc.—By K. V. Krishna Prasad.	340

No. 7

40.	On the Raman Spectrum and Structure of 1, 3, 5-Triphenyl Benzene—By S. K. Mukerji, L. Singh and R. S. Singh	341
41.	Production of $\pi$ Mesons in Neutron-Proton Collisions—By D. Basu	347
42.	The Band Spectrum of Nickel Fluoride—By V. G. Krishnamurty	354
43.	Oscillographic Measurements of Valve Noise in Audio Frequency Channels—By Miss G. V. Subhadramma	359
44.	Intensities in $^4\Sigma - ^4\Sigma$ Transitions—By K. Suryanarayana Rao	368
45.	On the Distribution of Stress Round the Edge of a Hole in a Deep Beam under a uniform Bending Moment—By B. Karunes	373
46.	The Raman Spectra of 1, 1, 1 and 1, 1, 2 -Trichloroethane in the Solid State at $-180^\circ\text{C}$ .—By D. C. Biswas	379

No. 8

47.	Spectroscopic Study of Amethyst Quartz in the Ultraviolet and Infrared Regions—By M. K. Vainu Bappu	385
48.	On the Temperature Effect in Geiger Müller Counters—By C. P. Joshi	393
49.	The Complex Band Spectrum of the Diatomic Molecule CbO in the Photographic Infrared—By V. Ramakrishna Rao and D. Premaswarup	399
50.	On the Raman Spectra of 1, 2-Dichloroethane and 1, 1, 2-Trichloroethane in the Vapour state—By Monomohan Mazumder	406
51.	Intensity Formulæ for Bands involving High Multiplicity Terms. Part I. $^5\Sigma - ^5\Sigma$ and $^6\Sigma - ^6\Sigma$ Transitions—By D. Premaswarup	415
52.	Global Characteristics of the Separation between the $F_1$ and $F_2$ Layers of the Ionosphere—By (Miss) Mrinmayee Ghosh	441

## No. 9

53. On the Law of Variation of the E-Region Maximum with the Zenith Distance of the Sun—By A. K. Saha ... .. 431
54. Stress Distribution in an Infinite Plate with an Elliptic Hole acted upon by a Force and a Couple at an Internal Point—By B. Karunes ... .. 439
55. On the Raman Spectra and Fluorescence of Ortho and Parachlorotoluene in the solid state—By S. B. Sanyal . . . . . 447
56. Oscillation of Viscous Liquids in Tubes and the Criterion of Stream Line Motion—By S. Venkataraman ... .. 452
57. The Ultraviolet Absorption Spectra of Phenetole and *n*-Butylbenzoate in Different States—By A. R. Deb ... .. 457
58. Radiation Properties of the Open End of a Rectangular Waveguide when the End Plane is Inclined to the Guide Axis—By G. S. Sanyal ... .. 465

## No. 10

59. On the Relaxation Time of Polar Molecules in the Liquid State—By S. C. Sirkar ... .. 475
60. On the Use of the Scintillation Counter as a Gamma Ray Spectrometer, using Stilbene Crystal—By Sobhana Dhar and Sunil Kumar Sen ... .. 483
61. Limit of Interference in Optical Instruments—By Amar Nath Nigam, Yatendra Pal Varshni and Mahendra Singh Sodha ... .. 491
62. On the Generation of High Intensity Ultrasonic Energy and Measurement of the Output Power Density of a Quartz Crystal—By T. C. Bhadra ... .. 496
63. Calculation of the Excited Levels of Indene—By S. Ramamurty ... .. 504
64. On the Absorption Maxima exhibited by some Organic Liquids in the Microwave Region. I.—By Dilip Kumar Ghosh ... .. 511
65. Latent Heat of Sublimation of Fifteen Salts from Spectroscopic and Thermochemical Data—By Mahendra Singh Sodha and Yatendra Pal Varshni ... .. 520
66. The Focusing and Magnetic Analysis of a Beam from a Radio Frequency Ion Source—By A. N. Banerjee ... .. 523

## No. 11

67. The Effect of Fluid Motion on Heat Transmission—By D. G. Kapadnis ... .. 533
68. Dynamics of Plastic Deformation in a Bar Exhibiting Strain-Rate Effect and subjected to Alternating Stress—By S. K. Ghosh ... .. 541
69. On the Study of Bi-Partition and Tri-Partition of Uranium Nucleus—By S. P. Dutta ... .. 547
70. Proton-Proton Scattering at High Energies—By Prabuddha Banerjee ... .. 557

	PAGE
71. Motion of a Single Cloud in the Ionosphere—By S. N. Mitra ... ..	562
72. On the Faithful Reproduction of the Flat Top of a Pulse in a High Fidelity Pulse Amplifier—By Bimal Krishna Bhattacharyya ... ..	565
73. Intensity Formulae for Bands involving High Multiplicity Terms. Part II. $^3\Pi-^5\Sigma$ , $^3\Pi-^3\Pi$ and $^4\Pi-^4\Pi$ Transitions—By D. Premaswarup ... ..	578

No. 12

74. Term Values in the Spectrum of Chromium II—By V. Suryanarayana and V. Ramakrishna Rao ... ..	585
75. On the Photoconductivity of Amethyst Quartz—By M. K. Vainu Bappu ...	591
76. On the Ultraviolet Absorption Spectra of Toluidines in the Liquid and Solid States—By (Miss) Usha Rani Guha Biswas ... ..	603
77. Calculation of Partial Molar Volume at Infinite Dilution from Refractive Index Measurements—By Anil K. Sircar and Santi R. Palit ... ..	610
78. A Study of D. C. Resistivity of Calcutta Soil—By S. P. Bhattacharyya and P. C. Mahanti ... ..	615
79. On a Consistency Test of the Theories of Strong Electrolytes in Solution—By M. Sengupta ... ..	628

Author	Subject	Page
Sanyal, G. S. and Chatterjee, J. S.	Measurement of Ferromagnetic Permeability at Microwave Frequencies	328
Sanyal, G. S.	Radiation Properties of the Open End of a Rectangular Waveguide when the End Plane is Inclined to the Guide Axis	465
Sanyal, S. B.	On the Raman Spectra and Fluorescence of Ortho and Parachlorotoluene in the Solid State	447
Sen, R. K.	Scattering Domains Around the Reciprocal Lattice Points of Benzil Crystal by Photo- graphic Photometry	1
Sen, Sunil Kumar	(See Dhar, Sobhana and ...)	483
Sengupta, M.	On a Consistency Test of the Theories of Strong Electrolytes in Solution	628
Sen Gupta, Prabhat K	A Discussion on the Spectroscopic State of Tetravalent Carbon in the Halogen Subs- tituted Derivatives of Methane as revealed by Absorption Spectra	149
Sen Gupta, R. L., Roy, K. K. and Roy, T.	Production of Penetrating Showers in Paraffin and Lead	191
Sil, N. C.	Classical Theory of Charged Meson	311
Singh, L.	(See Mukerji, S. K. and ...)	341
Singh, R. S.	(See Mukerji, S. K. and ...)	341
Sircar, Anil K. and Palit, Santi R.	Calculation of Partial Molar Volume at Infinite Dilution from Refractive Index Measure- ments	610
Sinkar, S. C.	On the Relaxation Time of Polar Molecules in the Liquid State	475
Sodha, Mahendra Singh	(See Nigam, Amar Nath and ...)	491
Sodha, Mahendra Singh and Varshni, Yatendra Pal	Latent Heat of Sublimation of Fifteen Salts from Spectroscopic and Thermochemical Data	520
Subhadramma, (Miss) G. V.	Oscillographic Measurements of Valve Noise in Audio Frequency Channels	359
Suryanarayana, V. and Rao, V. Ramakrishna	Term Values in the Spectrum of Chromium II	585
Srivastava, C. M.	(See Khastgir, S. R. and ...)	109

# Author Index

xiii

Author	Subject	Page
Swamy, H. N.	Ultraviolet Absorption Bands of Crystals of Ortho- and Para-Dichlorobenzene at Low Temperatures	55
„ „	Absorption Spectra of Organic Substances in the Liquid and Solid States. VI.	119
Varshni, Yatendra Pal	(See Nigam, Amar Nath and ...)	491
„ „	(See Sodha, Mahendra Singh ...)	520
Venkataraman, S.	Oscillation of Viscous Liquids in Tubes and the Criterion of Stream Line Motion	452
Viswanath, G.	Electronic Spectra of Molecules containing six and five Membered Rings. Part I. Calculation of Energy Levels	251

# SUBJECT INDEX

Subject	Author	Page
Absorption Maxima Exhibited by some Organic Liquids in the Microwave Region. I. On the	Dilip Kumar Ghosh	511
Absorption Spectra of Organic Substances in the Liquid and Solid States. VI. Some Substituted Benzenes	H. N. Swamy	119
Amethyst Quartz in the Ultraviolet and Infrared Regions. Spectroscopic Study of	M. K. Vainu Bappu	385
Anisotropy of some Ortho and Para Disubstituted Benzenes. Temperature Dependence of	Monomohan Mazumder	129
Band Spectrum of the Diatomic Molecule CbO in the Photographic Infrared. The Complex	V. Ramakrishna Rao and D. Premaswarup	399
Band Spectrum of Nickel Fluoride. The	V. G. Krishnamurty	354
Beam from a Radio Frequency Ion Source. The Focusing and Magnetic Analysis of	A. N. Banerjee	523
Charged Meson. Classical Theory of	N. C. Sil	311
Cross Sections of (n, p) Reactions in Sulphur 32 and Phosphorus 31	N. K. Saha and M. Choudhury	244
Cross Sections of (p, 2n), (p, pn) and (p, 2p) Reactions for Copper Bombarded with High Energy Protons	S. N. Ghoshal and T. N. Dave	213
D. C. Resistivity of Calcutta Soil. A Study of	S. P. Bhattacharyya and P. C. Mahanti	615
Dielectric Constant of Raw Jute and Cotton. Moisture Sensitivity of	B. L. Banerjee	223
Electronic Spectra of Dibenzyl, Diphenylmethane and Ethylbenzoate in the Solid State at $-180^{\circ}\text{C}$ . On the	A. R. Deb	183
Electronic Spectra of Molecules Containing six and five Membered Rings. Part I. Calculations of Energy Levels	G. Viswanath	251
Excited Levels of Indene. Calculation of	S. Ramamurty	504
Flat Top of a Pulse in a High Fidelity Pulse Amplifier. On the Faithful Reproduction of the	Bimal Krishna Bhattacharyya	39



# Subject Index

xv

Subject	Author	Page
Flat Top of a Pulse in a High Fidelity Pulse Amplifier. On the Faithful Reproduction of the	Bimal Krishna Bhattacharyya	565
F <sub>1</sub> and F <sub>2</sub> -Layer of the Ionosphere. Global Characteristics of the Separation Between	(Miss) Mrinmayee Ghosh	421
Ferromagnetic Permeability at Microwave Frequencies. Measurement of	G. S. Sanyal and J. S. Chatterjee	328
Geiger Müller Counters. On the Temperature Effect in	C. P. Joshi	393
Heat Transmission. Effect of Fluid Motion On. Part I. Vertical Cylinders	D. G. Kapadnis	77
Heat Transmission. The Effect of Fluid Motion On	Do.	533
Indian Mica. Electrical Properties of. V. D. C. Resistivity	S. S. Mandal and P. C. Mahanti	294
Intensity Formulae for Bands Involving High Multiplicity Terms. Part I. $^5\Sigma - ^5\Sigma$ and $^6\Sigma - ^6\Sigma$ Transitions	D. Premaswarup	415
Intensity Formulae for Bands involving High Multiplicity Terms. Part II. $^5\Pi - ^5\Sigma$ , $^5\Pi - ^5\Pi$ and $^4\Pi - ^4\Pi$ Transitions	Do.	578
Interference in Optical Instruments. Limit of	Amar Nath Nigam, Yatendra Pal Varshni and Mahendra Singh Sodha	491
Latent Heat of Sublimation of Fifteen Salts from Spectroscopic and Thermochemical Data	Mahendra Singh Sodha and Yaten- dra Pal Varshni	520
Law of Variation of the E-Region Maximum with Zenith Distance of the Sun. On the	A. K. Saha	431
$\pi$ -Mesons in Neutron-Proton Collisions. Production of	D. Basu	347
Molecular Diameter of a Liquid	M. G. Bhatawdekar	145
Motion of a single Cloud in the Ionosphere	S. N. Mitra	562
Neutron Flux from a Ra $\alpha$ + Be Source. Absolute	N. K. Saha and L. Kasturi Rangan	18
Oscillation of Viscous Liquids in Tubes and the Criterion of Stream Line Motion	S. Vankataraman	452
Ozonizer Discharge in Pure Nitrogen at 20 mm. Pressure. On the Spectral Characteristics of	N. Appalanara- simham	31

Subject	Author	Page
Partial Molar Volume at Infinite Dilution from Refractive Index Measurements. Calculation of	Anil K. Sircar and Santi R. Palit	610
Penetrating Showers in Paraffin and Lead. Production of	R. L. Sengupta, K. K. Roy and T. Roy	191
Phosphorus in Steel	K. C. Mazumder and M. K. Ghosh	11
Photoconductivity of Amethyst Quartz. On the	M. K. Vainu Bappu	591
Plastic Deformation in a Bar Exhibiting Strain-Rate Effect and subjected to Alternating Stress. Dynamics of	S. K. Ghosh	541
Propagation of Radio Waves Over a curved Earth. Oblique	B. Chatterjee	257
Proton-Proton Scattering at High Energies	Prabuddha Banerjee	557
Proton-Proton Scattering and the Pseudoscalar Meson Theory	C. C. Banerjee	173
Radiation Damping and the Scattering of Charged Scalar Mesons by Nucleon. Covariant Theory of	S. N. Biswas	197
Radiation Properties of the Open End of a Rectangular Waveguide when the End Plane is Inclined to the Guide Axis	G. S. Sanyal	465
Raman Spectra of 1, 1, 1 and 1, 1, 2-Trichloroethane in the Solid State at $-180^{\circ}\text{C}$ . The	D. C. Biswas	379
Raman Spectra of 1, 2-Dichloroethane and 1, 1, 2-Trichloroethane in the Vapour State. On the	Monomohan Mazumder	406
Raman Spectra of 1, 3-Dibromopropane and 1, 2, 3-Trichloropropane in the Solid State	B. M. Bishui	90
Raman Spectra and Fluorescence of Ortho and Parachlorotoluene in the Solid State. On the	S. B. Sanyal	447
Raman Spectra of Methyl Methacrylate in the Solid State at $-180^{\circ}\text{C}$	N. K. Roy	167
Raman Spectra of Solutions of 1, 2, 3-Trichloropropane. On the	T. A. Hariharan	323
Raman Spectrum and Structure of 1, 3, 5-Triphenyl Benzene. On the	S. K. Mukerji, L. Singh and R. S. Singh	341
Relaxation Time of Polar Molecules in the Liquid State. On the	S. C. Sirkar	475

# Subject Index

xvii

Subject	Author	Page
Resonance Lines of Sodium during Transmission through Sodium Vapour. Change of Frequency of	G. S. Kastha	67
Salts of the Iron Group of Elements. The Comparative Influence of Short and Long Range Electric Fields in the	A. Bose and S. C. Mitra	95
Scattering Domains around the Reciprocal Lattice Points of Benzil Crystal by Photographic Photometry	R. K. Sen	1
Scintillation Counter as a Gama Ray Spectrometer, Using Stilbene Crystal. On the Use of the	Sobhana Dhar and Sunil Kumar Sen	483
Sound Velocity Measurements in Organic Liquids	S. Parthasarathy and N. N. Bakhshi	73
Spectroscopic State of Tetravalent Carbon in the Halogen Substituted Derivatives of Methane as revealed by Absorption Spectra. A Discussion on the	Prabhat K. Sen Gupta	149
Steepness of Pulse Fronts on the Response of Differentiating and Integrating Circuits. Effect of	Binal Krishna Bhattacharyya	269
Streamer Mechanism in A. C. Silent Discharges	S. R. Khastgir and C. M. Srivastava	109
Stress Distribution in an Infinite Plate with an Elliptic Hole acted upon by a Force and a Couple at an Internal Point	B. Karunes	439
Stress Round the Edge of a Hole bounded by two Intersecting Circles in a Large Plate. On the Concentration of	Do.	208
Stress Round the Edge of a Hole in a Deep Beam under a uniform Bending Moment. On the Distribution of	Do.	373
Surface Pressure and Ionospheric Parameters. Correlation Between the Variations of	M. R. Kundu	235
Term Values in the Spectrum of Chromium II	V. Suryanarayana and V. Ramakrishna Rao	585
Tetraphenyl Ethylene. Structure of	M. N. Datta	25
Tetraphenyl Ethylene Crystal. An X-ray Investigation of the	Do.	126

Subject	Author	Page
Theories of Strong Electrolytes in Solution. On a Consistency Test of the	M. Sengupta	628
Torsion Constant of Quartz Fibre used in the Measurement of Magnetic Anisotropy of Crystals. An Accurate Determination of the	Sunil Kumar Datta	155
' $\Sigma$ '-' $\Sigma$ ' Transitions. Intensities in	K. Suryanarayana Rao	368
U. H. F. Radio Waves in the Range 250-920 Mc/sec by Substituted Benzenes. III. Absorption of	Dilip Kumar Ghosh	285
Ultrasonic Energy and Measurement of the Output Power Density of a Quartz Crystal. On the Generation of High Intensity	T. C. Bhadra	496
Ultraviolet Absorption Bands of Crystals of Ortho and Para Dichlorobenzene at Low Temperatures	H. N. Swamy	55
Ultraviolet Absorption Spectra of Diphenyl in the Liquid and Solid States	A. R. Deb	305
Ultraviolet Absorption Spectra of Phenctole and <i>n</i> -Butylbenzoate in Different States. The	Do.	457
Ultraviolet Absorption Spectra of Toluidines in the Liquid and Solid States. On the	(Miss) Usha Rani Guha Biswas	603
Uranium Nucleus. On the Study of Bi-partition and Tri-Partition of	S. P. Dutta	547
Valve Noise in Audio Frequency Channels. Oscillographic Measurements of	Miss G. V. Subhadramma	359
Vapour Pumps. On the Large Load Characteristics of	S. K. Mukherjee and P. K. Dutt	137

# ERRATA

(No. 2—February, 1953)

Page	Line	For	Read
80	6th line from below	$\log\left(-\frac{1}{A\Delta\theta}\frac{dQ}{dT}\frac{D}{\xi}\right)$	$\log\left(\frac{1}{A\Delta\theta}\frac{dQ}{dT}\frac{D}{K}\right)$
85	Ordinate of Fig. 3	of heat transfer	Rate of heat transfer
87	Ordinate of Fig. 5		10, 2, 3 ... 8, 10 <sup>3</sup> , 2...
	Abcissa of Fig. 5		10 <sup>3</sup> , 2, 3, ..., 8, 10 <sup>4</sup> 2, 3, .., 8, 10 <sup>5</sup> ...

(No. 5—May, 1953)

Page	Line	For	Read
272	2	$Lt_r^{-1}f_r(p)$	$L^{-1}f_n(p)$
„	8 (from bottom)	$\phi(p)(p)$	$\phi(p)$
278	Eq. 35	$D/(-\beta_r)$	$D'(-\beta_r)$
280	1	figures 11—14	figures 11—13
„	4 (from bottom)	$t_r/T=1.5$	$t_r/T=1.0$
282	Eq. 44	$D/(-\beta_r)$	$D'(-\beta_r)$
283	19	figures ... and	figures 12 and 13

(No. 7—July, 1953)

342	Table I, last column, top	1. 2. 3 tri ...	1, 3, 5-tri...
-----	---------------------------	-----------------	----------------

# Errata (contd.)

(No. 10—October, 1953)

Page	Line	For	Read
523	3 (Abstract)	0.22 kv	2.2 kv
529	Under Table III	Magnet current for peak mass $i$ ion current in $\mu$ amperes	$i$ in amps (for peak mass $I$ , ion current)
529	Under Table IV (a)	Shap of cathode, sharp and tip uncovered	shape of cathode-sharp, tip uncovered
530	Under Table IV (b)	Shape of cathode, flat tip covered with pyrex tubing	shape of cathode-flat, tip covered with pyrex tubing
531	16	$I = KV^{2.15}X^2$	$I = KV^{2.15}X^{-2}$
532	24	ions from the cone of the discharge	ions from the core of the discharge
532	2-3 (from bottom)	Thonemonn ,..., <i>Proc. Phys. Soc. (Lond.)</i> 61, 433	Thonemann ,..., <i>Proc. Phys. Soc. (Lond.)</i> 61, 483

# SCATTERING DOMAINS AROUND THE RECIPROCAL LATTICE POINTS OF BENZIL CRYSTAL BY PHOTOGRAPHIC PHOTOMETRY \*

By R. K. SEN

DEPARTMENT OF X-RAYS AND MAGNETISM INDIAN ASSOCIATION  
FOR THE CULTIVATION OF SCIENCE, CALCUTTA 32.

(Received for publication, August 29, 1952)

Plates I A-C

**ABSTRACT.** Equi-intensity lines around the  $(40.0)$ ,  $(22.0)$  and  $(40.2)$  reciprocal lattice points of benzil in the different reciprocal lattice planes have been drawn from the measurements of the intensity distribution in the different extra spots observed in the Laue photographs of benzil. The shapes of the equi-intensity surfaces have been discussed in the light of the thermal theories. The observed surfaces agree with the results of the thermal theories.

## INTRODUCTION

In previous communications, Lonsdale and Smith (1951), Banerjee, Sen and Khan (1945) and Sen (1947) reported a number of interesting results of the measurements of the positions of the extra spots and streaks in the Laue photographs of benzil. For a proper understanding of how far these extra spots of benzil conform to thermal diffuse-scattering it is necessary that the scattering domains around the reciprocal lattice points are mapped from a study of these extra reflections. Such mappings were first carried out by Laval (1939) who drew iso-diffusion lines or lines drawn through points having equal diffuse scattering power around the reciprocal lattice points of sylvine. Since then the scattering domains round the reciprocal lattice points of a number of crystals, mostly cubic, have been studied. Since benzil is a noncubic molecular crystal, its investigation is expected to be very interesting. For determining the intensity distributions in the extra spots, ionisation methods have been universally used by the earlier investigators. Since a photographic method has its obvious advantages such a method has been developed in the present investigation. The mapping of equi-intensity lines around the reciprocal lattice points of benzil and discussing their shapes and forms in the light of the thermal theories of the origin of the extra reflections have been aimed at in this paper.

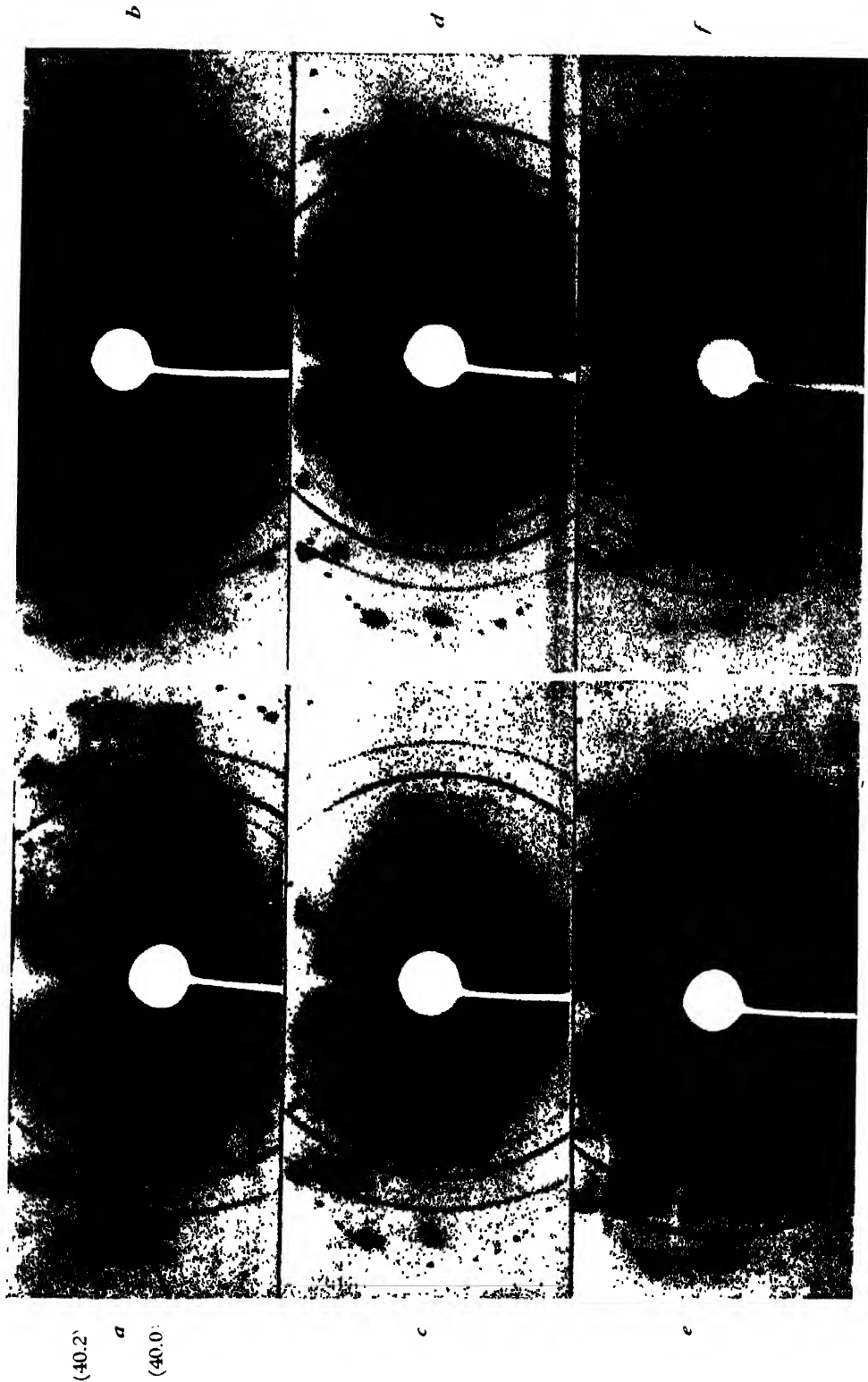
\* Communicated by Prof. K. Banerjee

## EXPERIMENTS

(a). A small crystal of benzil was mounted on the axis of a cylindrical camera with the  $[00.1]$  axis coinciding with the axis of the camera. Unfiltered X-rays, from a North American Philips X-ray diffraction unit with copper anticathode at a voltage of 45 K. V. and 15 ma, after being collimated through a 7 cm. long slit with a cylindrical hole of about .5 mm. diameter at the narrow part, was incident on the crystal normal to the axis of the camera. Stationary crystal photographs were then taken with the X-ray beam making various angles with the  $[10.0]$  axis. In each of these photographs a number of aluminium powder diffraction lines, arising out of diffraction of X-rays by a small amount of aluminium powder dusted on the crystal, were also recorded. These photographs are shown in Plates I, A-C. The whole series could not be completed with one crystal but two crystals were actually used. Same type of film and same conditions of development were used for all the photographs. The Laue photographs consisted of the usual Laue spots, corresponding to the diffraction of general X-radiations by the crystal lattice, the diffuse spots and the weak streak between these diffuse spots and comparison lines from aluminium powder. The indices of the planes giving rise to the diffuse spots were determined in the manner indicated in the previous communication by the present author (Sen, 1947).

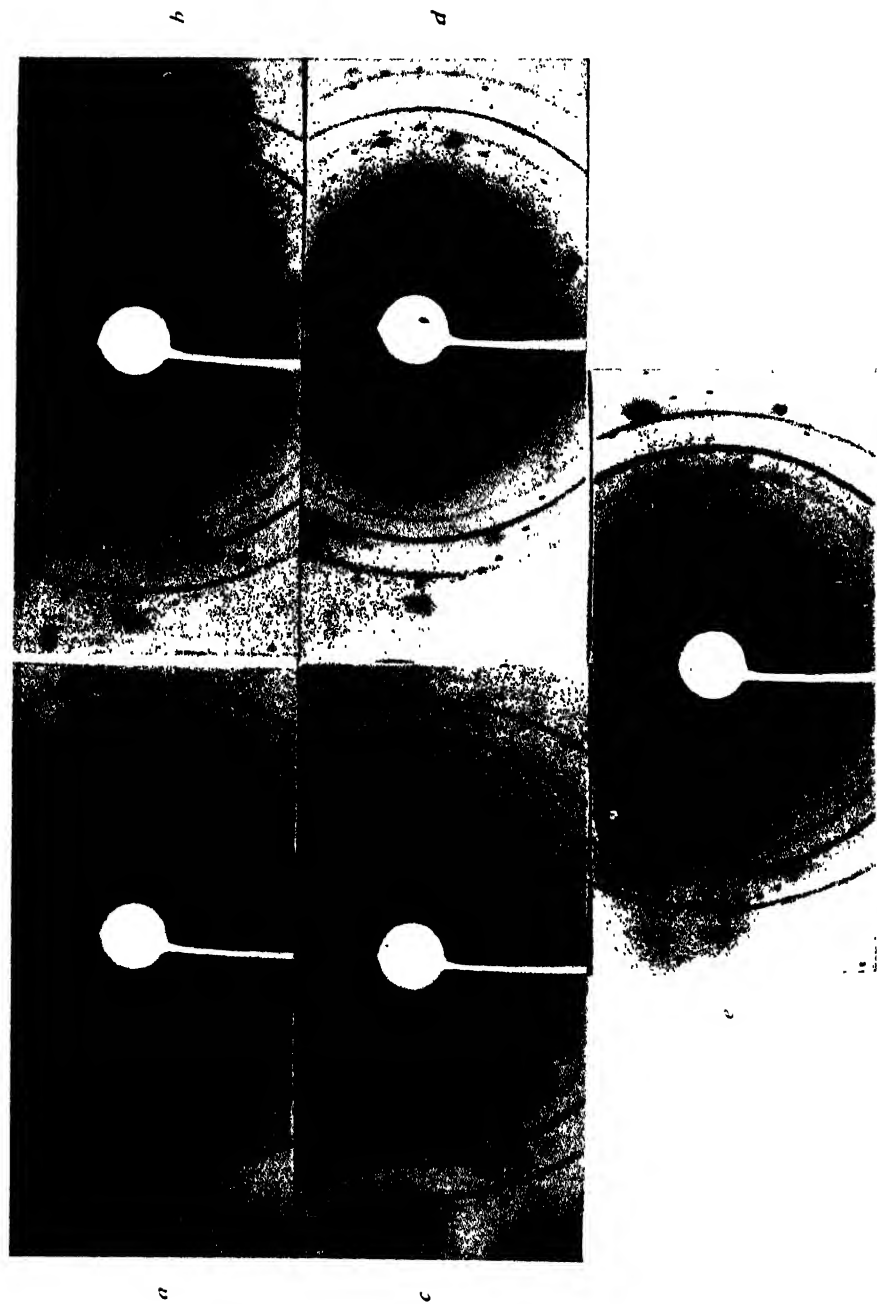
(b) *Intensity measurements.* The intensity distribution in the diffuse spots and streaks were measured with the help of a Moll recording microphotometer. For spots lying on the equatorial line, the photographs were mounted on the carriage of the photometer in such a manner as to allow the scanning spot of light (width .02 mm. and height .5 mm) to traverse through the spots along the equatorial line when the carriage is driven by the motor of the instrument. In the same traversal two aluminium powder lines were also traversed along with the spots. For spots lying above or below the equatorial line, a traversal was given through the spots and aluminium lines parallel to the equatorial line at a height corresponding to the different layer lines to which the spots belong. Similarly for the weak streak connecting the (40.0) diffuse spot with the (40.2) diffuse spot traversals parallel to the equatorial lines at heights of 1 mm., 2 mm., 3 mm., etc. were given. The photometric curve obtained from each of these traversals gives the galvanometer deflections against distances traversed. From these curves we have to obtain intensity versus crystal orientation curves. The ordinates of the recorded photometric curves were therefore converted into intensity on an arbitrary scale by comparing them with the deflections of photometric curve of a calibration wedge obtained by the method of Robinson (1933). The abscissa of the photometric curves were converted into the corresponding angles of diffraction with the help of the observed distance between the peaks corresponding to the aluminium lines whose angles of diffractions are already known. Thus from the photometric records, the intensity (in an arbitrary





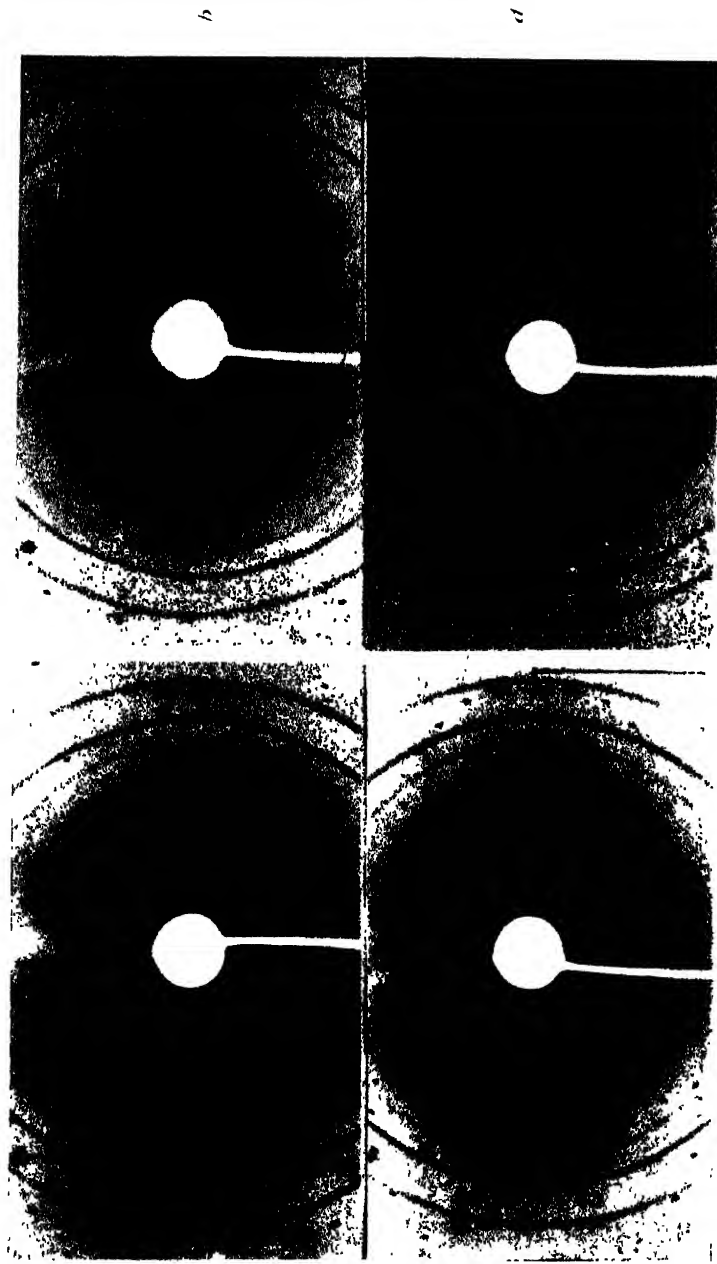
Laue photographs with incident beam making angles :

(a).  $0^{\circ}50'$  ; (b).  $1^{\circ}24'$  ; (c).  $2^{\circ}18'$  ; (d).  $3^{\circ}6'$  ; (e).  $3^{\circ}24'$  and (f).  $4^{\circ}6'$  with the  $[10.0]$  axis.  
 $[00.1]$  axis vertical.



Laue photographs with incident beam making angles :

(a),  $5^{\circ}10'$ ; (b),  $6^{\circ}$ ; (c),  $6^{\circ}20'$ ; (d),  $6^{\circ}48'$  and (e),  $8^{\circ}6'$  with  $[10.0]$  axis,  $[00.1]$  axis vertical.



220

Laue photographs with incident beam making angles : (a)  $20^{\circ}30'$ , (b)  $21^{\circ}6'$ , (c)  $22^{\circ}18'$  and (d)  $22^{\circ}48'$  with  $[10.0]$  axis.  $[001]$  axis vertical.



scale)-angle of diffraction curves for the different spots and streaks observed in different photographs were computed.

In the different photographs the total intensity of the incident beam was not the same. The intensities of the diffuse scattering measured from the different photographs were brought to the same scale with the help of the ratios of the peak intensities of a particular aluminium line observed in the different photographs. The photograph taken with the incident beam making  $4^{\circ}6'$  with the  $[10.0]$  direction was taken as the standard and the maximum intensity in the  $(40.0)$  diffuse spot of this photograph was taken as 10. The relative intensities of the diffuse spots observed in all the photographs were then computed in the manner indicated above. For bringing to the same scale the photographs taken with different crystals, photograph in one identical position of each of the crystals was taken. The orientation in which the incident beam makes an angle of  $4^{\circ}6'$  with  $[10.0]$  direction was taken as the standard orientation. By comparing the intensity distribution of the same diffuse spot  $(40.2)$  in these two photographs the ratio for the conversion of the intensity of the one set to that corresponding to the other was determined. These intensity curves in arbitrary scale are shown in figures 1, 2, 3 and 4.

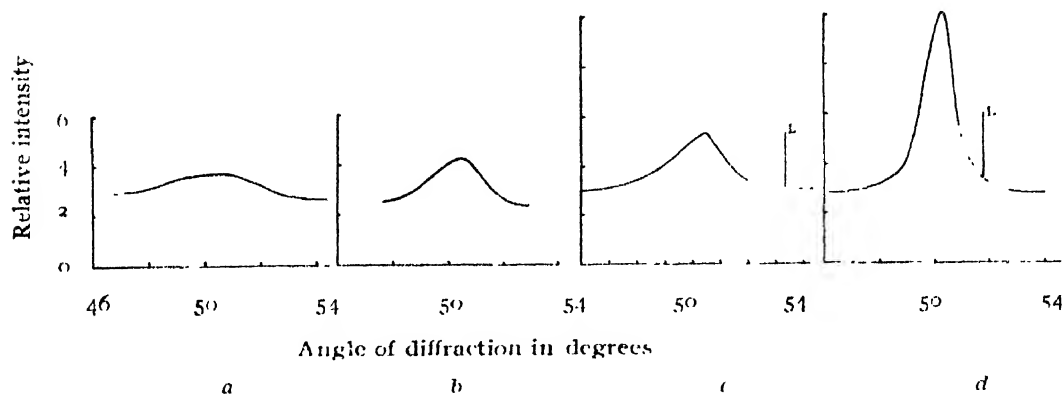


FIG. 1

Intensity distribution curve for the  $(40.0)$  extra reflection observed in the photographs taken with the incident beam making (a)  $2^{\circ}18'$  ( $\theta = \theta_B + 2^{\circ}36'$ ), (b)  $3^{\circ}6'$  ( $\theta = \theta_B + 1^{\circ}48'$ ), (c)  $3^{\circ}24'$  ( $\theta = \theta_B + 1^{\circ}80'$ ), and (d)  $4^{\circ}6'$  ( $\theta = \theta_B + 0^{\circ}48'$ ) with  $[10.0]$  axis. L corresponds to the Laue reflections from the plane  $(40.0)$

*Representation on the reciprocal lattice.* The reciprocal lattice of benzil (figure 5) was constructed as usual. By taking a vector  $OC$  of length  $1/\lambda$ , where  $\lambda$  is the wave-length of the radiation used ( $\text{CuK}\alpha = 1.54 \text{ \AA}$ ), in the reciprocal lattice parallel to the incident ray such that its extremity coincides with the origin  $O$  of the reciprocal lattice and another vector  $CP$  equally of length  $1/\lambda$  parallel to the diffuse ray, one finds that the vector  $OP$

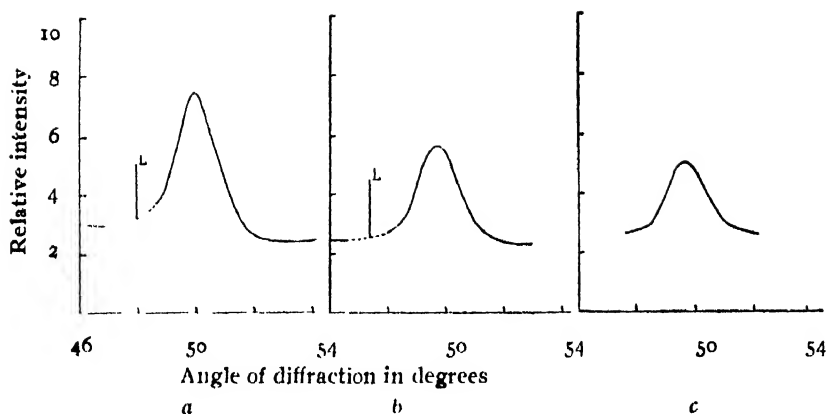


FIG. 2

Intensity distribution curve for the (40.0) extra reflection observed in the photographs taken with the incident beam making (a)  $6^\circ$  ( $\theta = \theta_B - 1^\circ 0'$ ), (b)  $6^\circ 20'$  ( $\theta = \theta_B - 1^\circ 26'$ ) and (c)  $6^\circ 48'$  ( $\theta = \theta_B - 1^\circ 54'$ ) with  $[10.0]$  axis. L represents the Laue reflection from the (40.0) plane.

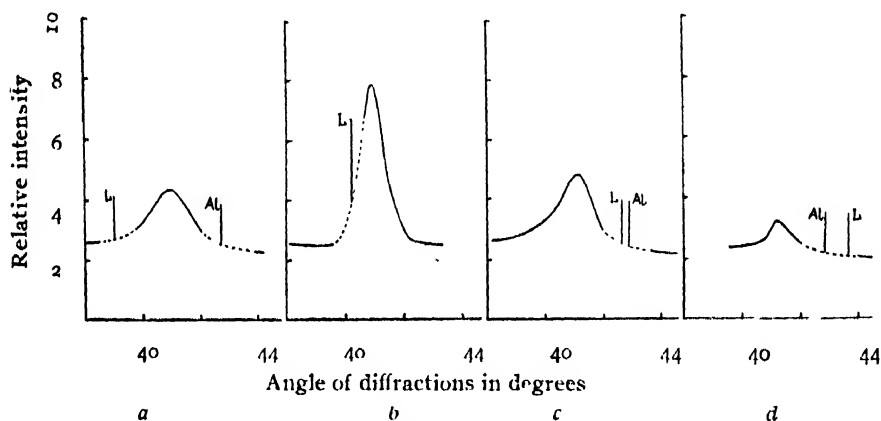


FIG. 3

Intensity distribution curve for the (22.0) extra reflection observed in the photographs taken with the incident beam making (a)  $20^\circ 30'$  ( $\theta = \theta_B - 0^\circ 56'$ ), (b)  $21^\circ 6'$  ( $\theta = \theta_B - 0^\circ 20'$ ), (c)  $22^\circ 18'$  ( $\theta = \theta_B + 0^\circ 52'$ ) and (d)  $22^\circ 48'$  ( $\theta = \theta_B + 1^\circ 23'$ ) with  $[10.0]$  axis. L represents the Laue reflection from (22.0) plane. Al represents the aluminium (200) diffraction line.

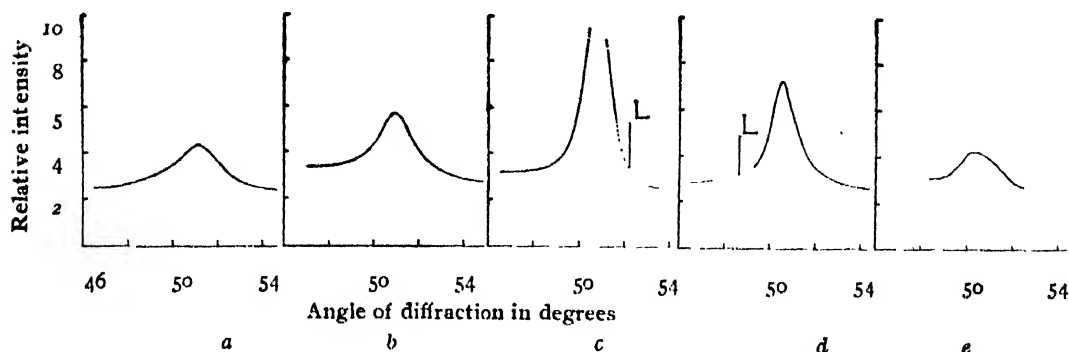


FIG. 4

Intensity distribution curve for the (40.2) extra reflection observed in the photographs with the incident beam making (a)  $0^\circ 50'$ , (b)  $1^\circ 24'$ , (c)  $2^\circ 18'$ , (d)  $4^\circ 6'$  and (e)  $5^\circ 10'$  with  $[10.0]$  axis. L represents the Laue reflection from (40.2) plane.

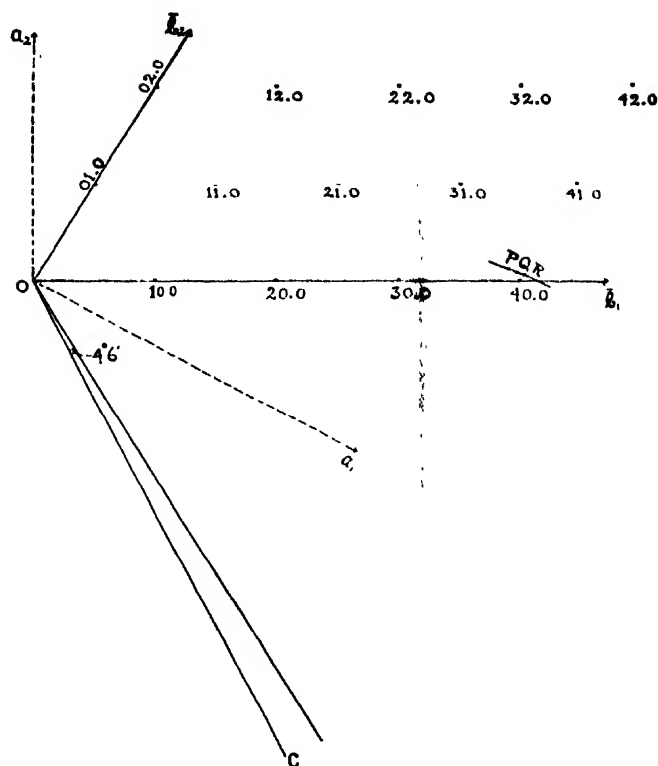


FIG. 5

A section of the reciprocal lattice of benzil normal to  $[001]$  axis, which is also the  $b_2$  reciprocal lattice axis. — reciprocal lattice axes — crystal lattice axes. P, Q, R. are the poles corresponding to angles of diffraction  $49^\circ$ ,  $50^\circ$  and  $51^\circ$  respectively

(figure 5) is the reciprocal lattice vector responsible for the diffusion in the direction under consideration. The vector  $OP$  is called the 'vector of diffusion' and  $P$  is the 'pole of diffusion'. The selective Bragg reflection takes place when the pole of diffusion  $P$  coincides with any node  $M$ . A section of the reciprocal lattice of benzil normal to the  $[00.1]$  axis and the corresponding crystal lattice is shown in figure 5. In order to draw equiscattering surfaces (*i.e.* surfaces having equal intensity of scattering), the 'poles of diffusion', corresponding to the different points of observations in the diffuse spots, were plotted in the reciprocal lattice. From the considerations laid down above it is clear that the plotting of the 'poles of diffusion' is carried on by drawing a circle of radius  $1/\lambda$  with centre  $C$  through the origin  $O$  ( $CO$  being the direction of the incident X-ray beam) and then drawing another line  $CP$  making with  $CO$ , the observed angle of diffusion corresponding to a point in the diffuse spot, when the point  $P$ , where  $CP$  meets the circle, gives the 'pole' corresponding to the point of observation considered. Some of the 'poles of diffusion', corresponding to different points in the  $(40.0)$  diffuse spot observed in the photograph with the incident beam making  $4^\circ 6'$  with  $[10.0]$  axis, are shown in figure 5. At the various

poles of diffusion thus plotted, the values of the relative intensities observed at the corresponding points of the relative intensity curves, were then noted. It must be noted here that relative intensity values are the values obtained by subtracting the intensity of the background from the total intensity observed at those points. Again, since the same scanning spot of light was used for the photometry of all the spots, the solid angle over which the observation is made is different for the different spots. For if  $ds$  be the area of the scanning spot of light used in photometry and  $ds/R$  be the radius of the camera used, then  $ds/R^2$  is the solid angle over which the intensity has been measured in the case of spots lying on the equatorial line, whereas for the spots lying above or below the equatorial line this solid angle is

$$\frac{ds \cos \mu}{(R/\cos \mu)^2} = \frac{ds \cos^3 \mu}{R^2}, \text{ where } \mu \text{ is the vertical angular coordinate corresponding to the layer lines to which the spot belongs. The intensities of the spots lying on different layer lines above or below the equatorial}$$

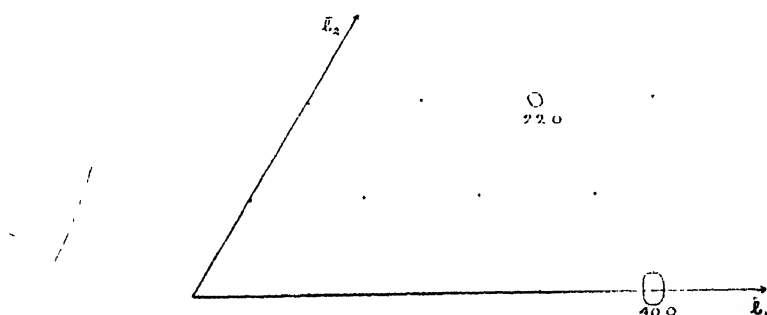


FIG. 6

Equi-intensity lines around the  $(40.0)$  and  $(22.0)$  reciprocal lattice points in the plane normal to the  $\bar{b}_3$  axis.

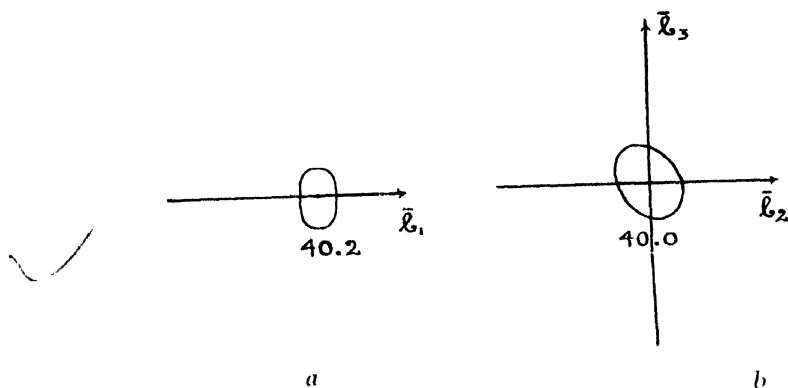


FIG. 7

(a) Equi-intensity lines around the  $(40.2)$  reciprocal lattice point in the plane perpendicular to the  $[00.1]$  axis.

(b) Equi-intensity lines around  $(40.0)$  reciprocal lattice point in the  $\bar{b}_2 - \bar{b}_3$  plane



line were, therefore, divided by the factor  $\cos^3\mu$  in order to convert it to the intensities corresponding to the solid angle of observation used in the intensity measurement for the spots on the equatorial line. For the (40.2) spot the relative intensity values corrected in the above manner were plotted in the reciprocal lattice. Lines were then drawn through points having equal values of the relative intensities plotted. Thus equi-scattering surfaces around the different reciprocal lattice points were obtained. In figure 6 are shown the sections of the equi-scattering surfaces around the (40.0) and (22.0) reciprocal lattice points by a plane normal to the [00.1] axis. A section of the scattering domain around the (40.0) reciprocal lattice point by the  $\bar{b}_2b_3$  reciprocal lattice plane is shown in figure 7.

# DISCUSSION OF RESULTS

The shapes of the equi-scattering lines in the plane parallel to  $b_1b_2$  around the reciprocal lattice points (40.0), and (22.0) are more or less elliptical with the major axis along the normal to the reciprocal lattice vector. This indicates that the amplitudes of vibration due to the transverse waves are much larger than those due to the longitudinal waves. In the case of NaCl, KCl, Al also it has been observed that the thermal diffuse scattering due to transverse waves are more intense than that due to longitudinal waves. Again, the strong regions of equi-scattering lines around the reciprocal lattice points in the plane normal to [00.1] axis are more or less symmetrical about the reciprocal lattice vector and its normal. The section of the equi-scattering surface around the (40.0) reciprocal lattice point by the  $b_2\bar{b}_3$  plane shows that the strong scattering regions are more or less elliptical in shape but they are not symmetrical about the  $b_3$  axis and  $b_1b_2$  plane. These features of the scattering domains around the reciprocal lattice points can be qualitatively explained on the thermal theories of diffuse scattering (Born, 1942-43, Zachariasen, 1940). According to these theories, the intensity of scattering  $I_s$  corresponding to a point near the reciprocal lattice points is given by the relation,

$$I_s = I_e NKT \cdot F^2 \cdot d(q)/m,$$

where 
$$I_e = I_0 \left( \frac{e^2}{m_0 c^2} \right)^2 \left( \frac{1 + \cos^2 \phi}{2} \right) = \text{Thomson factor.}$$

$N$  = no. of cells in the crystal

$K$  = Boltzmann constant

$T$  = Temperature

$m = \sum m_k$  where  $m_k$  is the mass of the  $k$ th atom of the cell

$F$  = Crystal structure factor of the plane in question.

$$d(\bar{q}) = \Sigma D_{\alpha\beta}^{-1}(\bar{q}) q_{\beta}^{(h)}$$

$$D_{\alpha\beta}^{-1}(\bar{q}) = \text{adj}_{\alpha\beta} D(\bar{q}) / \det D(\bar{q})$$

$$\rho D(\bar{q}) = \begin{bmatrix} C_{11} & C_{66} & C_{55} & C_{65} & C_{51} & C_{16} \\ C_{66} & C_{22} & C_{44} & C_{24} & C_{46} & C_{62} \\ C_{55} & C_{44} & C_{33} & C_{43} & C_{35} & C_{54} \\ C_{65} & C_{24} & C_{43} & \frac{1}{2}(C_{23} + C_{41}) & \frac{1}{2}(C_{45} + C_{36}) & \frac{1}{2}(C_{64} + C_{15}) \\ C_{51} & C_{46} & C_{35} & \frac{1}{2}(C_{15} + C_{36}) & \frac{1}{2}(C_{31} + C_{55}) & \frac{1}{2}(C_{56} + C_{14}) \\ C_{16} & C_{62} & C_{54} & \frac{1}{2}(C_{61} + C_{25}) & \frac{1}{2}(C_{56} + C_{14}) & \frac{1}{2}(C_{12} + C_{66}) \end{bmatrix} \begin{bmatrix} \bar{q}_1^2 \\ \bar{q}_2^2 \\ \bar{q}_3^2 \\ 2\bar{q}_2\bar{q}_3 \\ 2\bar{q}_3\bar{q}_1 \\ 2\bar{q}_1\bar{q}_2 \end{bmatrix}$$

$\bar{q}$  is the vector joining the reciprocal lattice point to the point of observation.  $q_{\alpha}^{(h)}$ ,  $q_{\beta}^{(h)}$  are the components of the reciprocal lattice vector along and normal to the  $\bar{b}_1$  axis.

$C_{\alpha\beta}$  are the elastic constants.  $\rho$  is the density.

For hexagonal crystals of  $D_3$  class to which the present crystal belongs, the determinant  $\rho D(\bar{q})$  reduces to

$$\rho D(\bar{q}) = \begin{bmatrix} C_{11} & C_{66} & C_{44} & C_{14} & 0 & 0 \\ C_{66} & C_{11} & C_{44} & -C_{14} & 0 & 0 \\ C_{44} & C_{44} & C_{33} & 0 & 0 & 0 \\ C_{14} & -C_{14} & 0 & \frac{1}{2}(C_{13} + C_{44}) & 0 & 0 \\ 0 & 0 & 0 & 0 & \frac{1}{2}(C_{44} + C_{13}) & C_{14} \\ 0 & 0 & 0 & 0 & C_{14} & \frac{1}{2}(C_{12} + C_{66}) \end{bmatrix} \begin{bmatrix} \bar{q}_1^2 \\ \bar{q}_2^2 \\ \bar{q}_3^2 \\ 2\bar{q}_2\bar{q}_3 \\ 2\bar{q}_3\bar{q}_1 \\ 2\bar{q}_1\bar{q}_2 \end{bmatrix}$$

where,

$$\left. \begin{aligned} \rho D_{11}(\bar{q}) &= C_{11} \bar{q}_1^2 + C_{66} \bar{q}_2^2 + C_{44} \bar{q}_3^2 + 2C_{14} \bar{q}_2 \bar{q}_3 \\ \rho D_{22}(\bar{q}) &= C_{66} \bar{q}_1^2 + C_{11} \bar{q}_2^2 + C_{44} \bar{q}_3^2 - 2C_{14} \bar{q}_2 \bar{q}_3 \\ \rho D_{33}(\bar{q}) &= C_{44} (\bar{q}_1^2 + \bar{q}_2^2) + C_{33} \bar{q}_3^2 \\ \rho D_{23}(\bar{q}) &= C_{14} (\bar{q}_1^2 - \bar{q}_2^2) + (C_{13} + C_{44}) \bar{q}_2 \bar{q}_3 \\ \rho D_{31}(\bar{q}) &= (C_{44} + C_{13}) \bar{q}_2 \bar{q}_1 + 2C_{14} \bar{q}_1 \bar{q}_2 \\ \rho D_{12}(\bar{q}) &= 2C_{14} \bar{q}_3 \bar{q}_1 + (C_{13} + C_{66}) \bar{q}_1 \bar{q}_2 \end{aligned} \right\} \dots \quad (1)$$

For (ho.o) planes, for points lying in the plane normal to [00.1] axis and along the normal to the reciprocal lattice vector,  $q_3=0$ ,  $q_1=0$  and  $q=\bar{q}_2$ , then equation (1) reduces to,

$$\rho D_{11}(\bar{q}) = C_{66} \bar{q}^2, \rho D_{22}(\bar{q}) = C_{11} \bar{q}^2, \rho D_{33}(\bar{q}) = C_{44} \bar{q}^2$$

$$\rho D_{23}(q) = -C_{14} \bar{q}^2, \rho D_{31}(\bar{q}) = 0, \rho D_{12}(\bar{q}) = 0$$

$$\det D(q) = \frac{\bar{q}^6}{\rho^3} (C_{66}(C_{11}C_{44} - C_{14}^2))$$

$$\text{and } adj D_{11}(q) = \frac{q^4}{\rho^2} (C_{11}C_{44} - C_{14}^2)$$

$$\therefore D_{11}^{-1}(\bar{q}) = \frac{\rho}{\bar{q}^2} \cdot \frac{1}{C_{66}}$$

For the (40.o) reciprocal point, therefore,

$$d(q) = D_{11}^{-1}(\bar{q}) q^{(h)2}$$

$$\frac{\rho}{q^2} \cdot \frac{1}{C_{66}} \cdot q^{(h)2}$$

where,  $q^{(h)}$  is equal to the reciprocal lattice vector and  $q$  is the distance of the point of observation, lying on the normal to  $q^{(h)}$ , from the reciprocal lattice point. It is observed, therefore, that since  $q^2$  is involved in the expression for the intensity, the intensity will be practically the same so long as  $\bar{q}$  remains the same in magnitude no matter whether the point of observation lies on one side or the other. It must be mentioned here, however, that the intensity will vary very slightly for the very small difference in the corresponding angles of diffraction. Similarly it can be shown that for all points lying on the plane normal to [00.1 axis] the intensity depends on  $\bar{q}^2$ , that is to say the intensity depends on the magnitude of  $\bar{q}$  and not on its sign except for the small difference in angle of diffraction. Thus it is found that according to the thermal theories, the section of the scattering surface around (40.o) by the  $\bar{b}_1\bar{b}_2$  plane will be practically symmetrical about  $\bar{b}_1$  axis and the normal to it. This is in agreement with the observations.

Again, for points lying in the  $\bar{b}_2\bar{b}_3$  plane but not falling on  $\bar{b}_2$  or  $\bar{b}_3$ , none of the values of  $\bar{q}_1$ ,  $q_2$  and  $q_3$  are zero, so in this case, the expressions for  $D_{11}(\bar{q})$ ,  $D_{22}(\bar{q})$ ,  $D_{33}(\bar{q})$  etc., will be those given by equation (1). For the  $\bar{b}_2\bar{b}_3$  plane through (40.o) reciprocal lattice point, the expression for  $d(q)$  is given by,  $d(q) = D_{11}^{-1}(q) \bar{q}^{(h)2}$ , since  $q_2^{(h)}$  and  $q_3^{(h)}$  are zero.

$$D_{11}^{-1}(\bar{q}) = \frac{D_{22}(q)D_{33}(q) - D_{23}^2(q)}{\det D(q)}$$

$$\therefore d(q) = \frac{D_{22}(q)D_{33}(\bar{q}) - D_{23}^2(q)}{\det D(\bar{q})} \cdot q^{(h)}$$

Now, in the expression for  $D_{22}(\bar{q})$  there is a term  $-2C_{14}\bar{q}_2 q_3$ . Hence  $D_{22}(\bar{q})$  will have different values for the positive and negative values of  $\bar{q}_3$  having the same magnitude. So  $d(q)$  and consequently the intensity of scattering corresponding to points in  $b_2 b_3$  plane at equal distances from the (40.0) reciprocal lattice point on the two sides of the  $b_1 b_2$  plane will have different values. The scattering surface will not therefore be symmetrical about the  $b_1 b_2$  plane. The present observations are therefore quite in agreement with the theory. Quantitative comparison cannot be carried on as the elastic constants are not known. However, from the above considerations it is clear that so far as the strong diffuse scatterings are concerned the intensity distribution is in general agreement with the thermal theories.

#### ACKNOWLEDGMENT

Thanks are due to Prof. K. Banerjee, D. Sc., F. N. I. for constant help and guidance during the progress of the work.

#### REFERENCES

- Banerjee, K., Sen, R. K., and Khan, Md Ferdouse, 1945, *Proc. Nat. Inst. Sci. Ind.*, **11**, 4.  
 Born, M., 1942-43, *Rep. Phys. Soc. Progr. Phys.*, **9**, 294.  
 Laval, J., 1939, *Bull. Soc. franc. Minér.*, **62**, 137.  
 Lonsdale, K and Smith, H., 1941, *Proc. Roy. Soc. A*, **179**, 8.  
 Robinson, B. W., 1933, *J. Sci. Instr.*, **10**, 233.  
 Sen, R. K., 1947, *Ind. J. Phys.*, **21**, 285.  
 Zachariasen, W. H., 1944, *Theory of X-ray diffraction in Crystals* John Wiley and Sons, Inc. New York.

## PHOSPHORUS IN STEEL

BY K. C. MAZUMDER AND M. K. GHOSH

THE NEW CONTROL & RESEARCH LABORATORY,  
T. I. & S. CO. LTD., JAMSHEDPUR*(Received for publication, May 25, 1952, received after revision, December 5, 1952)*

## Plate II

**ABSTRACT.** By means of the medium quartz spectrograph and a 20 KVA transformer the spectral lines of phosphorus contained in steel were photographed and its contents evaluated. The accuracy was fairly good. It is suggested that the inaccurate ones were due to segregation

## INTRODUCTION

The spectro-chemical determination of phosphorus in both ferrous and non-ferrous alloys have been found to be extremely difficult. The spectrum of the element does not consist of many bright lines. The few tolerably bright lines it has, lie in the range  $4500-5000 \text{ \AA}$  which is not suitable for spectro-chemical analysis. Moreover, the amounts of phosphorus found in these alloys generally being very small, the ordinary method of excitation is rather inadequate to bring out the P-lines in the presence of the more excitable elements contained in the alloys also in much larger percentages. The arc method of excitation has, therefore, been tried for the spectro-chemical determination of phosphorus, (e.g. Norman and Johnson, 1945). Since 1947, we have also been trying the above method of excitation for this work. But with the large quartz spectrograph the P-lines for samples containing 0.03 % or less of phosphorus appear hardly on the plate even with fairly long exposures, the current being about 8 amp. As has been shown by Mazumder and Ghosh (1948), the medium quartz spectrograph can be used for spectro chemical analysis of the ferrous alloys as suitable lines for intensity determinations of all the elements excepting carbon contained in these alloys, can be found in the low wave length range where the dispersion is not very poor. In Plate II, it will be seen that the phosphorus line  $2136.20 \text{ \AA}$  is clearly separated from the interfering copper line  $2135.98 \text{ \AA}$ . With this apparatus the P-line  $2136.20 \text{ \AA}$  can be photographed for samples containing as low a percentage as 0.020, the arc current being only 2 or 3 amp. Though the general proportionality of intensities with percentages can always be found the consistencies are rather poor. The standardisation of the arc conditions and keeping them constant are extremely tedious. But by giving 4 or 5 exposures with each sample using freshly ground surface for each exposure and by averaging the readings

fairly good curves can be obtained (figure 1). This is too much time absorbing and cannot be adopted for routine work. These difficulties arise

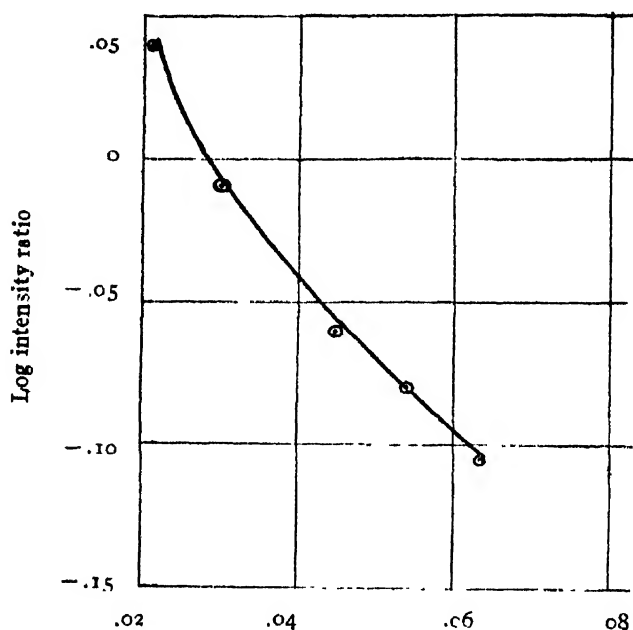


FIG. 1  
Percentage of phosphorus

out of the fact that the intensity of the P-line is very poor. To obviate these troubles the direct method of intensity measurement by placing a G-M counter (or a photocoell) on the focal plane of the spectrograph, has been adopted in some laboratories for the spectro-chemical determination of phosphorus. This method has been specially developed in the laboratory of the Ford Motor Company and adopted for the routine analysis of P in steel, (Bryan and Nahstall 1949). It has been corroborated by Hans (1950). We have been trying for some time past to have the attachment necessary for holding the counters in the plane of the photographic plate and for accurately adjusting its position by some reliable firm but have not yet been successful. On the contrary, we have been informed that M/s. Ford Company have given up this method of phosphorus determination and have adopted the colorimetric technique which has been found to be simple and rapid.

Their equipment, is, however still being used for 'phosphorus determination in relation to experimental foundry work'. M/s. Applied Research Laboratory also now claim that phosphorus in steel can be determined by their quantometer, another direct intensity measuring spectrograph but using photo-tubes instead of G-M counter. They have made a very special study of the phosphorus determinations by the quantometer in collaboration with the British Cast Iron Research Association and claim to have achieved highly satisfactory results. We have made fairly wide

F<sub>1</sub> 135.96 Å  
P 36.2 Å



Sample  
(spark)  
P - 0.55%

Cu (spark)

—  
Cu 2135.98 Å





enquiries but have failed to find any place where the quantometer has been put to regular routine work for the phosphorus estimation. It seems still to be in the research stage. It is apparent that considerable attention has been paid to improving the means of observation and very little attempt has been made to excite the P-lines more strongly so as to make the observation easier. The direct intensity measurement by G-M counter or photo tube cannot yield correct results if the intensities of the phosphorus lines are not appreciable. More powerful method of exciting the spectrum should, therefore, be adopted if phosphorus in steel is to be successfully determined by spectrograph. With this end in view we have a 20 KVA transformer made which gives one ampere current in the secondary. It has not, however, been possible to arrange to have the secondary voltage and current in steps but by introducing inductance in the secondary circuit some variation in the sparking power can be effected. With this excitation source together with the adoption of the medium quartz spectrograph considerable success has been achieved in determining phosphorus spectro-chemically.

#### EXPERIMENTAL

As soon as we became aware that P-lines could not be easily photographed unless a heavy current arc was used for excitation we designed and placed an order with M/S Adam Hilger Ltd for a 20 KVA transformer mentioned above. Our plan for having intermediate steps in secondary output could not, however, be carried out. Two condensers, one of capacity 0.01 and the other of 0.015  $\mu$ F, were placed in parallel with the secondary; two inductances with the total value 1.5 MH but having steps, the minimum being 0.015 MH, were connected in series with the secondary of the

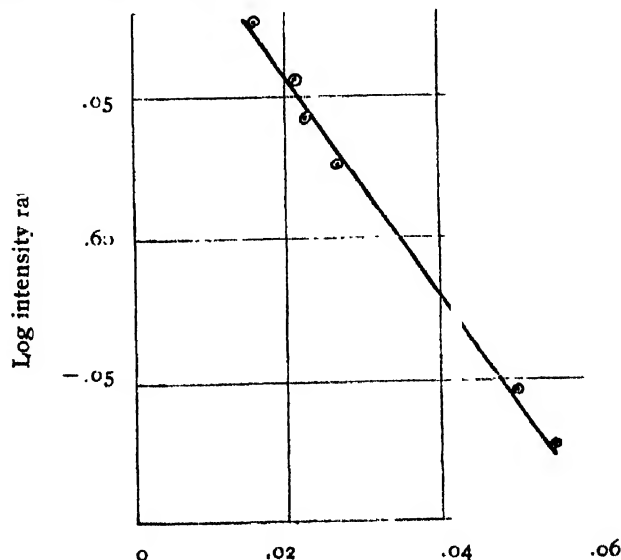


FIG. 2

Percentage of phosphorus

transformer. With an inductance of 0.03 MH the phosphorus contents

were determined fairly accurately even up to 0.016 %-(Figures 2 & 3.) Still lower percentages could not be tried as suitable standards were not available. It should be mentioned here that nitrogen from a cylinder was blown against the spark gap at 2"-4" pressure as in the case of carbon determination by spectrograph (Mazumder and Ghosh, 1949). By this

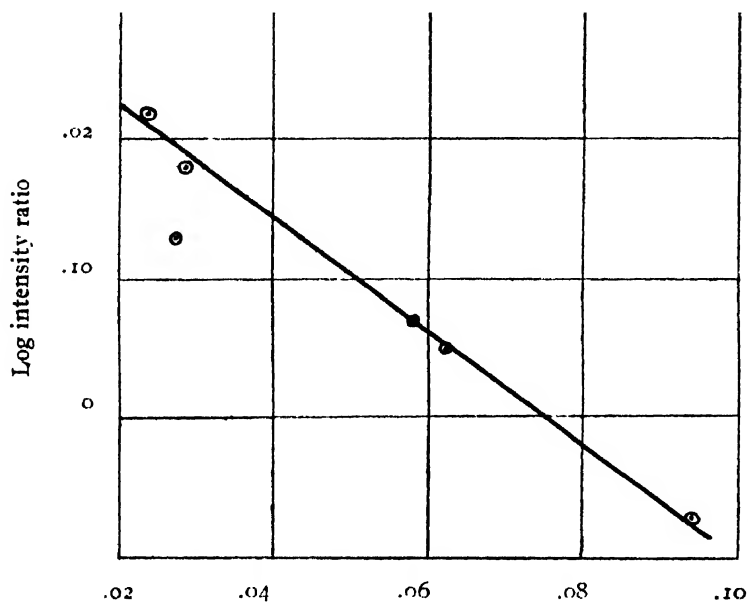


FIG. 3  
Percentage of phosphorus

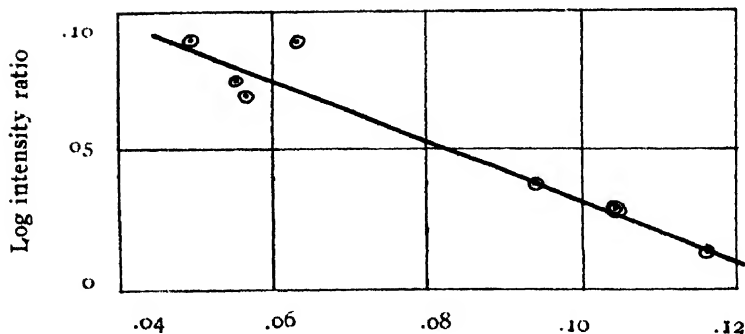


FIG. 4  
Percentage of phosphorus

means cleaner plates and more consistent results were obtained. Lines used were P 2136.2Å and Fe 2138.6Å. Attempts have also been made

to determine Mn and Si contents of the sample from the same spectrograph used for phosphorus determination. There have been some initial difficulties as the region, where the suitable lines of Mn and Si appear, become so dark that the intensity measurement becomes impossible. By introducing inductance up to 1.0 MH success has been achieved in this connection

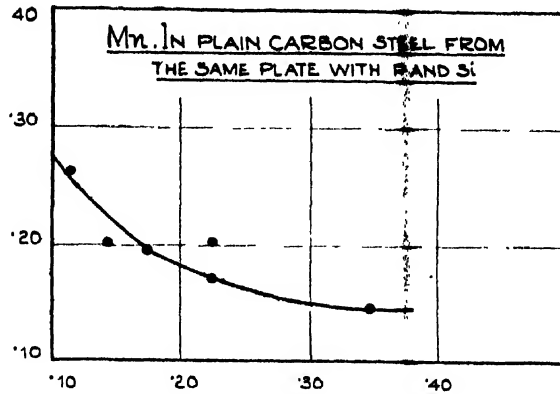


FIG. 5  
Percentage of manganese

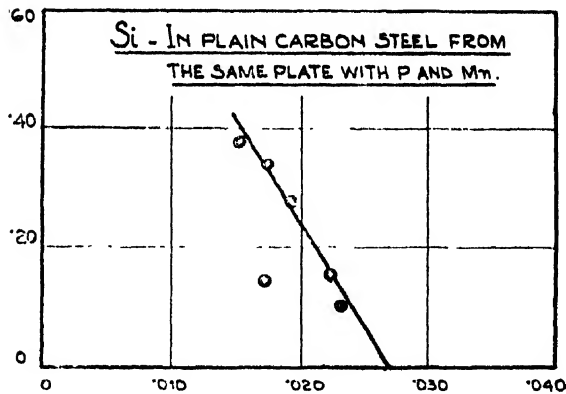


FIG. 6  
Percentage of silicon

also (see figures 5 and 6). The phosphorus determination is fairly accurate even with high inductance in the circuit (figure 4).

## RESULTS AND DISCUSSION

In the Table I, some data are given from which the degree of accuracy of the phosphorus determination can be obtained. The reasons for inaccuracy of a part of the data are discussed.

It is seen that most of the determinations are accurate considering the smallness of the phosphorus contents. If we now scrutinise the inaccurate ones some interesting features will become apparent :

(1) Consider the samples 10842 (2) and 10842 (5) ; the first two

TABLE J

Sample No.*	No. of estimations.	Spectro-chemical % of P.			Chemical % of P.
		Min.	Max.	Avg.	
7621 Forged	10	.060	.066	.063	.064
7643 "	12	.052	.059	.055	.054
7557 "	4	.024	.038	.030	.045
34573 "	4	.062	.072	.063	.038
34574 "	4	.038	.047	.043	.030
34570 "	4	.015	.015	.014	.015
17	6	.003	.008	.004	.004
6558	6	.021	.036	.027	.031
6699	9	.026	.031	.029	.029
10720 (1)	14	.051	.060	.055	.055
10720 (2)	13	.034	.062	.050	.051
10720 (3)	1	.058	.058	.058	.063
10771 (1)	13	.010	.021	.018	.016
10771 (3) unhardened	9	.018	.029	.021	.023
10771 (3) hardened	13	.025	.040	.032	.027
10842 (1)	5	.044	.052	.047	.044
10842 (2)	3	.035	.054	.053	.053
10842 (3) unhardened	2	.064	.070	.067	.064
10842 (3) hardened	2	.104	.104	.104	.104
10842 (4)	4	.022	.026	.025	.028
10842 (5)	2	.026	.027	.027	.030

\* All these samples were bath samples

determinations are quite different from the chemical ones. The drillings for the chemical analysis were taken from one end of the rods and the other ends were sparked. On noticing the differences in the estimations by the two methods the sparking ends were changed and the results of the spectro-chemical analysis became practically equal to the chemical ones.

(2) Two rods cast with metals taken from the same spoon, one hardened by dipping into water and the other air cooled yielded different values of the phosphorus contents found either chemically or spectro-chemically.

(3) The sample, 34570, yielded the same value for the first four determinations but all the subsequent 6 determinations differed considerably from the chemical ones, and they have been omitted from the table.

(4) The samples forged and those cast sometimes yield spectro-chemically different results though their chemical determinations are equivalent. This has been noticed in the case of some other elements also.

These observations lead one to the conclusion that segregations are rather common in the phosphorus distribution in steel. The chemical analysis, it should be remembered, gives more or less average results. In the

spectro-chemical work, however, only particular spots are arced or sparked ; the results obtained thereby are far from being the average.

ACKNOWLEDGMENTS

The authors take this opportunity of thanking Dr. J. C. Ghosh, the Chief Chemist and the Tata Management for giving the necessary research facilities for carrying out the work.

REFERENCES

- Bryan, F. R. and Nahstall, G. A., 1949, *H. S. T. M. Bulletin* No. 157.  
Hans, A , 1950, *J. Iron & Inst. Oct.*  
Mazumder, K. C and Ghosh M. K., 1948, *Ind. J. Phys.*, **22**, 460.  
Mazumder, K. C. and Ghosh M. K., 1949, *Ind. J. Phys.*, **23**, 477.  
Normal, D P. and Johnson, W. W. A., 1945. *Indust. Engr. Chem. (Anal. Ed.)* 17, 233.

# ABSOLUTE NEUTRON FLUX FROM A $\text{Ra}\alpha + \text{Be}$ SOURCE \*

BY N. K. SAHA AND L. KASTURI RANGAN

PHYSICS DEPARTMENT, UNIVERSITY OF DELHI

(Received for publication, August 27, 1952)

**ABSTRACT.** The absolute flux of neutrons from a ( $\text{Ra}\alpha + \text{Be}$ ) source has been determined by the method of 'thermalisation' (Barschall, 1952). A large volume of  $\text{MnSO}_4$  solution is activated by thermalised neutrons from the  $\text{Ra}\alpha + \text{Be}$  source held at the centre and the solution activity measured by a specially constructed immersion  $\beta$ -ray counter. The activity of  $\text{Mn}^{56}$  with reference to the neutron beam is calibrated with the help of an end window  $\beta$ -ray counter designed for the purpose. Detailed corrections for back-scattering, and self absorption of the  $\beta$ -rays, geometry and efficiency of the end-window counter, finite size of the source etc. have been applied. The absolute flux has been determined to be  $F_0 = 13.2 \times 10^6$  neutrons per gram per second with a probable error of  $\pm 25\%$ . Values of  $F_0$  determined by other workers for a similar source have been compiled for comparison. The approximate value supplied by the manufacturer of the neutron-source is  $1.3 \times 10^6$  neutrons per sec. for a 100 mgm  $\text{Ra} + \text{Be}$  source of this type and it agrees well with the present determination.

## INTRODUCTION

The neutron flux from a ( $\text{Ra} + \text{Be}$ ) source has been defined as the number of neutrons of all velocities emitted in all directions from the source per second per gramme of its radium-content. The knowledge of the absolute neutron flux from a permanent neutron source is essential in determining the cross section of nuclear reactions produced by the neutrons from the source. Measurement of neutron flux is also necessary in determining the cross section of reactions in which charged particles interact with nuclei to produce neutrons. Various methods exist for the measurement of neutron flux from a source. An excellent review of these methods has recently been given by Barkchall, Rosen, Tasches and Williams (1952). If the neutron source is a mono-energetic one, the methods of 'recoil particle' and 'the associated particle method' are considered to be quite accurate. In the recoil particle method a thin foil of radiator made of a light material is chosen in which the elastic scattering of the fast neutrons is practically the only important interaction of the neutrons with the nuclei of the material. If the cross section of the elastic scattering process is known from separate transmission experiments, the flux of the neutrons can be determined by counting the number of recoil nuclei from the radiator in a fixed geometry. Any single absorption process, such as,  $(n, \alpha)$ -reaction in boron<sup>10</sup>, can also be used likewise. The associated particle method is quite simple in principle. Certain nuclear reactions which act as sources of deutrones emit a charged particle with each neutron produced in the reaction. If the charged particle is sufficiently energetic and also

\* Communicated by Prof R. C. Mazumder, University of Delhi.

otherwise suitable to produce ionisation pulses, detection of these would give the number of neutrons emitted from the source. For example, the neutrons produced from the reaction  $D^2 (d, n) He^3 + Q$  can be counted by counting the  $He^3$  nuclei produced in the reaction. The method, however, is limited in its applicability, as in many neutron sources the angular distribution of the associated particle is not known; moreover in many cases suitable associated particles are not available, and the technique of measuring ionisation pulses due to associated particles which are not very light is as yet undeveloped. Both these methods are also not very suitable when the neutrons from the source have got a wide energy spectrum, since the charged particles in the above methods may not be detectable if they are of very low energy. The method of 'thermalisation' would be particularly suitable to determine neutron flux from a polynenergetic neutron source such as the  $(Ra\alpha + Be)$  neutron source. The neutron source in this method is placed in a moderating medium distributed symmetrically about the source. A radioactive indicator such as a metal foil ( $In$  116; 57 minutes) or a substance like  $Mn^{56}$  (2.5 hours) as sulphate in solution can be used to detect the thermalised neutrons. The volume of the moderator must be so large that (1) neutrons of all velocities from the source are thermalised by elastic collision with its nuclei and brought within the energy range in which the detector is sensitive and (2) no neutron escapes out of the system. The activity of the detector has to be calibrated in terms of a standard neutron source strength. The principle of the method was first given by Amaldi and Fermi (1936) and has been used by many workers (Walker, 1945, Neal *et al.* 1946, Alder and Huber, 1949) with minor variations in the method of calibration or the technique of measurement employed. In the present work the method of thermalisation has been employed with an aqueous solution of manganese sulphate using the 2.5 hour  $Mn^{56}$  as detector. The radioactivity produced in  $Mn$  powder by neutron capture is also absolutely determined by using a small carefully calibrated end-window counter, which instrument, we believe, would be a simple but powerful tool for such calibrations if its technique can be perfected.

For equilibrium activation of a radioactive indicator by a neutron source, the rate of neutron capture would be equal to the initial rate of decay of the active indicator nuclei and the rate of activation would thus be given by

$$A_1 = \int_{E_t}^{E_0} n_0 \sigma(E) F(E) dE,$$

where  $n_0$  = the number of the target nuclei present,  $F(E)$  = the flux of neutrons in the energy range  $E$  and  $E + dE$ ,  $\sigma(E)$  is the corresponding neutron capture cross section, and the detector is sensitive to the thermal neutrons between the threshold energy  $E_t$  and the upper limit  $E_0$ . If the activity produced in the solution is mechanically integrated by thoroughly mixing up the solution, the integrated activity  $A_0 \approx \text{const}$ ,  $F_0$  would be a direct measure of the total neutron flux. If now the solution is surrounded by a uniform

layer of an absorber, and exposed as before to the indicator, some of the neutrons will be captured in the absorber and the rest will go to activate the indicator. Let this number transmitted through the absorber be  $F$  and the reduced initial integrated activity of the indicator  $A \approx \text{const. } F$ . Hence it follows :

$$\frac{F}{F_0} = \frac{A}{A_0} = R ; 1 - R = \frac{F_0 - F}{F_0} = \frac{a}{F_0}, \text{ i.e. } F_0 = \frac{a}{1 - R}$$

where  $a$  denotes the absolute activity of the absorber in the second experiment. Thus the required neutron flux  $F_0$  would be obtained by measuring the absolute  $\beta$ -activity of the absorber,  $a$ , and the ratio  $R$  of the initial activities of the solution exposed to the source with and without the absorber.

#### EXPERIMENT AND OBSERVATIONS

(i) The indicator substance  $\text{Mn}^{56}$  in the form of  $\text{MnSO}_4$  was dissolved in water (moderator) to make a 10% solution. The solution was kept in a cylindrical drum, 30" high, 20" diameter, nearly full. These dimensions ensure, as some preliminary experiments showed, the slowing down of all the fast neutrons from a  $\text{Ra} \alpha + \text{Be}$  source to thermal velocities within the volume of the solution. The neutron source, kept at the centre of the solution, irradiated the solution for 15 hours. After removal of the of the source, the solution was thoroughly stirred for mechanical integration

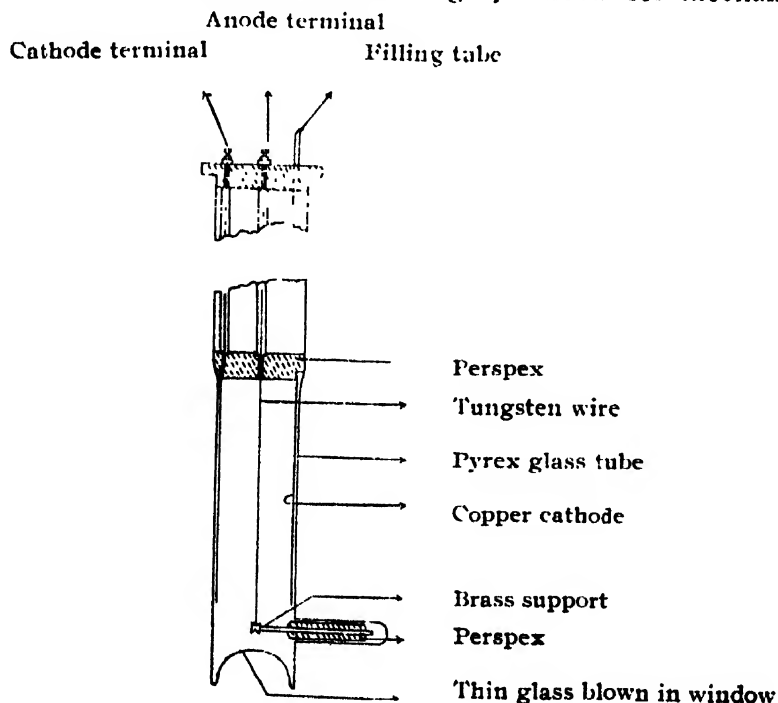


FIG. 1

Immersion counter: cathode length  $\sim 8.5$  cm, total length  $\sim 57$  cm, cathode inner diameter  $\sim 2.2$  cm.



of its activity. The solution activity was measured by a specially designed immersion counter (figure 1). Sixteen reliable sets of observations were taken and in each case the activity was followed for a period of 4 hours. Average of all sets of readings (after subtracting the back-ground) is shown in figure 2(a) on a semi-logarithmic plot. An extrapolation of the straight

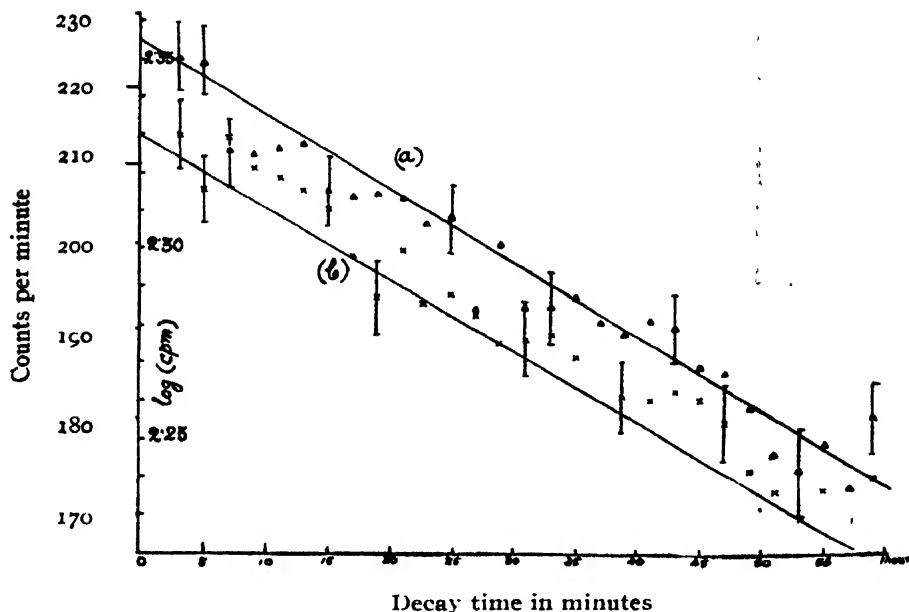


FIG. 2

Activity of manganese sulphate solution

(a) Without absorber

(b) With Mn-absorber

Initial activity of (a) = 227 count per min., (b) = 214 count per min.

line to zero time gives the initial activity of  $\sim 227$  counts per minute.

(ii) The neutron source is covered on all sides by a uniform layer of

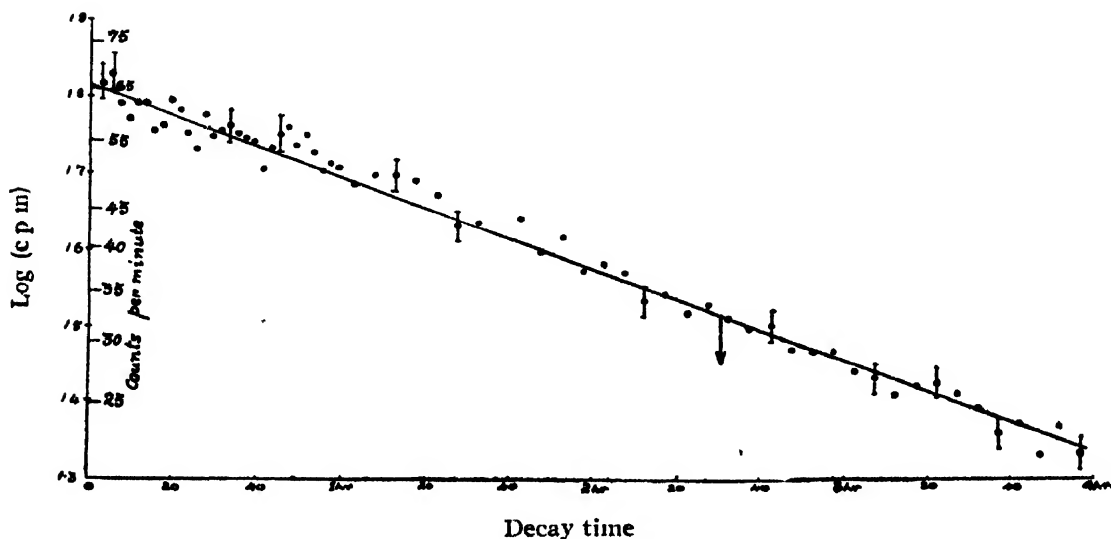


FIG. 3

Manganese powder activity

pure metallic manganese powder (absorber, total weight = 500 gm) and the solution exposed to this source for 15 hours. The initial activity of the solution, after removal of the source, is determined in an identical fashion as above. The initial activity obtained was  $\sim 214$  cpm, as follows from figure 2(b). It will be seen from the plots that the statistical error of the observed initial activity is less than 2 %. But the reduction in activity in the second case (b) being small, though finite, the probable error of the ratio  $R$  becomes quite considerable. It was felt, however, that in order to obtain better statistics, an inconveniently large number of observations would be necessary, in course of which it would be difficult to maintain constancy of counting conditions. Within the limits of the present accuracy therefore we obtain  $R = 214/227$ , giving  $(1 - R) = 5.8$  % with a probable error of about 20 %.

(iii) For determining  $a$  the absolute activity of the absorber, the Mn powder in experiment (ii) was thoroughly mixed up after removing the source and the initial activity of a small sample (average weight  $\sim 0.0607$  gm.) was found by means of a well calibrated end-window counter under well defined geometry. Knowing the mass of the sample and the total mass exposed,  $a$  is calculated (after correcting for geometry, back scattering, self-absorption of the  $\beta$ -rays etc.)

The effective aperture of the window of the counter was found out by measuring the rate of counting when a collimated  $\beta$ -ray source was scanned across the counter window, both along the two mutually perpendicular diameters of the window with the source held normal to the window, and the source held against the window-centre at various angles with the counter axis. Out of an aperture of 10.4 mm. of the window, about 7.0 mm. was found to be effective. Correction experiments for the determination of the amount of back scattering of  $\beta$ -rays from the source holder was performed similar to that given by Brutt (1949) and a correction factor of 0.9 was obtained. The method given by Aten (1950) was slightly modified for the measurement of self-absorption of the  $\beta$ -rays in the sample layer. A correction factor of 1/0.62 was estimated. The usual solid angle and planar source corrections were also applied. Absorptions due to the window and air gap between the Mn sample and the window were found negligible. With an initial activity of 65.3 cpm observed for the sample (figure 3), we obtain

$$a = \frac{65.3 \text{ counts}}{60 \text{ sec.}} \cdot \frac{500 \text{ gm.}}{0.0607 \text{ gm.}} \cdot \frac{0.9}{0.62} \cdot \frac{4\pi}{0.425 \times 2\pi} \cdot \frac{1}{0.85}$$

$$= 7.25 \times 10^4 \text{ disintegrations per second.}$$

This gives a total neutron flux

$$F_0^* = \frac{a}{1 - R} = 1.25 \times 10^6 \text{ neutrons per sec.}$$

from the 95 mgm Ra + Be neutron source used, which is equivalent to  $F_0 = 13.2 \times 10^6$  neutrons per gm per sec with a probable error of about  $\pm 25$  %.

## CONCLUSION

The absolute neutron flux of a 100 mgm ( $Ra\alpha + Be$ ) source of this type has been roughly indicated by the manufacturer of the source to be  $\sim 1.3$  million neutrons/sec. This compares very well with the value determined by us. Similar measurements made on the ( $Ra\alpha + Be$ ) neutron sources by other workers are also available. The values obtained by some of the authors are collected below for comparison.

Author	Absorber used	$F_0$ (neutrons per gm/sec)
Paneth, Gluckauf and Lohleit (1936)	Boron	$6.7 \times 10^6$
Ladenburg, Kanner (1937)	?	6.0 "
Walker (1945)	Boron	11.8 "
Seidel, Harris (1947)	Boron	11.0 "
O'Neal and Scharff-Goldhaber (1946)	Manganese	6.8 "
Alder and Huber (1949)	"	6.3 "
Bracci, Facchini and Germagnoli (1950)	Indium	6.0 "

As is well known the ( $Ra\alpha + Be$ ) source cannot be regarded as a very permanent neutron source, since its neutron flux is likely to vary slightly from source to source depending on factors like coarseness and packing of the grains constituting the source and alterations in these with time. This may account for differences in the values observed by various authors. Modern improvements in the technique of preparation of natural neutron sources may be responsible for the higher values of the flux we have obtained. It must be stressed, however, that the estimated accuracy of the present value is quite low (certainly not better than  $\pm 20\%$ ), the main uncertainties being the fluctuations observed in the solution activity and the low reduction in the activity with absorber screening the neutron source. The method of thermalisation can therefore be applied only for calibrating good secondary neutron sources in a laboratory.

## ACKNOWLEDGMENTS

A preliminary measurement of the neutron flux from the  $Ra\alpha + Be$  source, which forms the basis of the present work, was done in collaboration with M. Choudhury of this laboratory in the last winter and was reported in the Indian Science Congress Session in January 1952. The work has been carried out with the financial support of the Atomic Energy Commission, Government of India. We are grateful to Prof. D. S. Kothari and Prof. R. C. Majumder Physics Department, University of Delhi for their constant encouragement in this work. Our thanks are also due to Prof. P. S. Gill of the University of Aligarh for many helpful discussions in connection with this work.

## REFERENCES

- Alder E. and Huber, P. 1949, *Helv. Phys. Acta.*, **22**, 368  
 Amaldi, E. and Fermi, E. 1936, *Phys. Rev.*, **50**, 898.

Aten, A. H. W. *Nucleonics* VI, 68, (Jan. 1950).

Barchall, H. H. Rosen, L. Taschek R. F. and Williams, J. H. 1952, *Rev. Mod. Phys.* 24/1, 1.

Bracci, A. Facchini U. and Germaguoli, E. *Nuovo Cimento* 1950, 715, 1.

Brutt, B. P. *Nucleonics*, V, 28 (Aug. 1949).

Ladenburg P. and Kanner, H. H. 1937, *Phy. Rev.*, 51, 1022

Paneth, F. A. Gluckauf E. and Loleit, H. 1936, *Proc. Roy. Soc.* 87 412

Neal R. D. O' and Scharff-Goldhaber, G. 1946, *Phy. Rev.* 69, 368

Seidel F. G. P. and Harris, S. P. 1947, *Rev. Sc. Instr.* 18. 897.

Walker, R. L. 1945, *MDDC*, 414.

## STRUCTURE OF TETRAPHENYL ETHYLENE\*

By M. N. DATTA

KHAIRA LABORATORY OF PHYSICS, UNIVERSITY COLLEGE OF SCIENCE, CALCUTTA

*(Received for publication, June 12, 1952)*

## Plate III

**ABSTRACT.** The structure of tetraphenyl ethylene has been studied in the present investigation. The crystal was found to belong to holoaxial monoclinic system with the axial ratio  $a : b : c = 1.413 : 1 : 1.078$ ,  $\beta = 68^\circ 20'$ . The crystal has a high refractive index which is due to (C=C) atoms which has a high absorption band near ultraviolet spectrum. Number of molecules per unit cell has been found to be one which shows that the crystal has neither glide plane nor screw axis.

## INTRODUCTION

Uptil now tetraphenyl ethylene crystal is not known to have any crystallographic data. The present paper reports morphological data, different optical properties and a preliminary X-ray investigation with the help of fixed film camera.

It is interesting to determine the structure of tetraphenyl ethylene on account of its importance in organic chemistry. This compound consists of four phenyl groups and one C=C double bond. It is interesting to determine the positions of four phenyl groups around the C=C double bond. The valency angles between C=C double bond and four phenyl groups are also to be determined. The crystal has also interesting optical properties ; these are studied, as they give some information about the atomic arrangement in the crystal.

*Preparation of crystal.*

The substance was dissolved in alcohol which was heated till it dissolved completely ; then benzene was added. The whole mixture was allowed to evaporate slowly, when the crystal of tetraphenyl ethylene was obtained.

## GONIOMETRIC STUDY

(i) The crystal shows elongation of the cross section, being of uniform or non-uniform width.

(ii) The elongation may be along *c*-or *b*-axis, less likely along *a*-axis.

(iii) Apparently the plane perpendicular to the elongation of the crystal is a symmetry plane, supported by parallel extinction under microscope.

(iv) The distribution and the angular relation of the face called

\*Communicated by Prof. S. N. Bose.

originally in goniometry as  $c$  suggest a lack of symmetry plane parallel to the direction of elongation of the crystal, which is possibly an axis of symmetry.

Thus a monoclinic holohedral symmetry is obtained.

(v) The faces  $b$  and  $d$  are in the same zone, they cannot constitute the form  $(hko)$ , probably  $(110)$ .

(vi) The so-called  $a$  and  $c$  faces constitute (i) 2 domes of the type  $(\bar{h}ol)$  and  $(hol)$  or (ii)  $(001)$  and  $(\bar{h}ol)$ .

(vii) Plotting on assumption and using angular relations  $(110) \wedge (001) = 78^\circ$ .

$$110 \wedge 110 = 85^\circ : 001 \wedge \bar{1}01 = 50^\circ, 001 \wedge 011 = 45^\circ$$

$\bar{1}01 \wedge 011 = 63^\circ$ ,  $110 \wedge 011 = 47^\circ$ , the stereogram has been drawn. This has the advantage of having simple indices and confirms the symmetry already assumed.

#### OPTICAL CHARACTERS

(1) Non-pleochroic characters.

(2) The crystal, being of monoclinic system, the monoclinic axis is one of the principal axes, (Sen, 1946) while the other two, which are at right angles to each other, lie in a plane normal to this axis. For the determination of the directions of these basal axes, the crystal was mounted on Fedorov stage, placed between crossed nicols of a polarising microscope, and the crystal was rotated about the direction until the extinction was observed. The angle between the direction of the electric vector of the polarised light and a crystal edge was measured accurately and hence the directions of the principal axes were fixed. For the determination of the principal refractive indices, the Becke method has been utilised. For this purpose the crystal was immersed in a drop of a liquid whose refractive index is intermediate between two principal indices of the crystal, and was mounted on the Fedorov stage with the plane containing the two principal directions normal to the axis of optical system. The crystal was illuminated by polarised light and liquid of higher refractive index was mixed until the Becke line just disappeared. Then the refractive index of the mixture was measured by refractometer. This is the refractive index of the crystal. The refractive indices in three principal directions were measured on the Fedorov stage (Datta, 1947). They are :

$$\alpha = 1.690$$

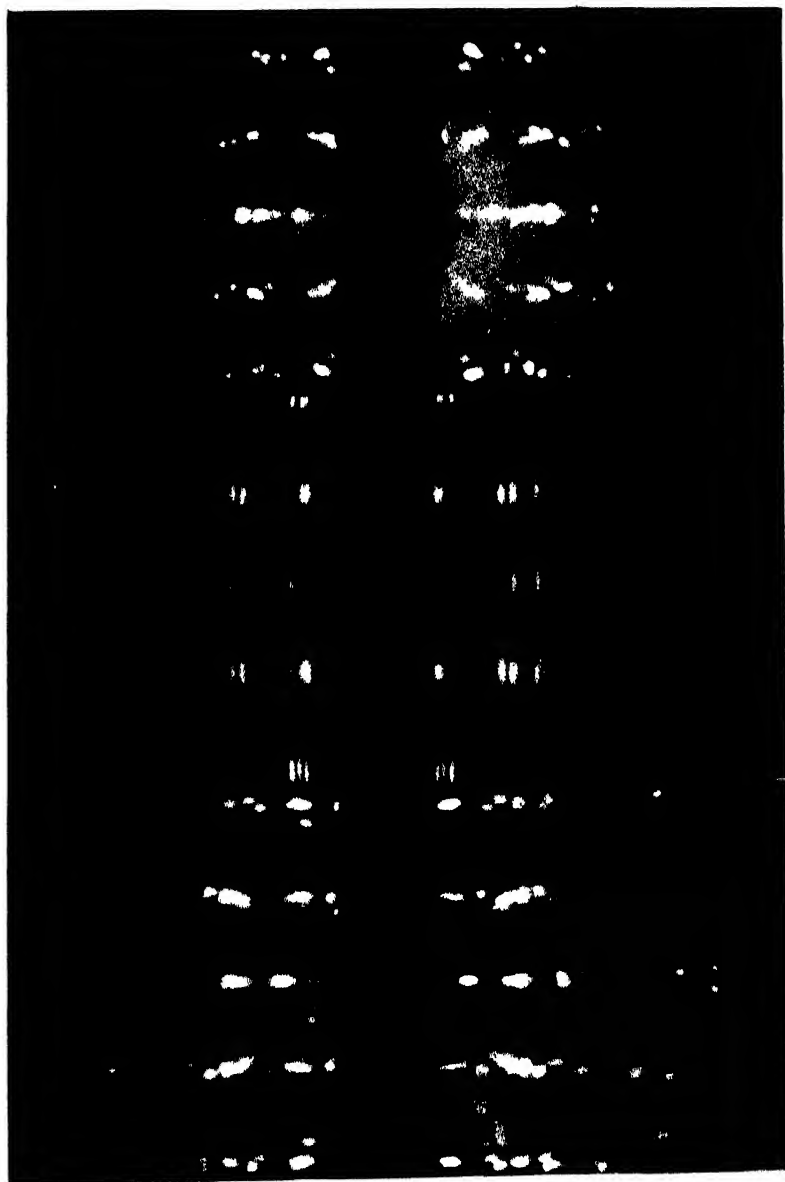
$$\beta = 1.757$$

$$\gamma = 1.762$$

(3) Birefringence is high.

(4) The crystal is biaxial, optically negative, the optic-axial angle was measured in Fedorov stage, as well as by observing interference in convergent polarised light ;  $2V = 46^\circ$ .

(5) The crystal possesses a high dispersion, which is chiefly axial. The optic-axial plane for red light makes an angle of  $7^\circ$  with  $(001)$  face,



Rotation photographs of tetraphenylethylene

(a) about  $a$ -axis,      (b) about  $b$ -axis,      (c) about  $c$ -axis.





Axes feebly dispersed  $v > \rho$

(6) Extinction straight on (001) (101) inclined on  $b$  (010).

(7) The crystallographic axis  $a$  makes an angle  $13^\circ$  with principal axis  $a$ .

*Actual face-angle measurement.* A single crystal of tetraphenyl ethylene was mounted on a goniometer head, and the angles between the faces were measured. The following are the measurements

$$\begin{array}{lll}
 \left. \begin{array}{l} 134^\circ 53' \\ 57^\circ 11' \end{array} \right\} ab \ 77^\circ 42'; & \left. \begin{array}{l} 209^\circ 35' \\ 277^\circ 55' \end{array} \right\} bc \ 68^\circ 20'; & \left. \begin{array}{l} 269^\circ 39' \\ 323^\circ 58' \end{array} \right\} cc \ 54^\circ 23'; \\
 \left. \begin{array}{l} 234^\circ 0' \\ 312^\circ 22' \end{array} \right\} bc \ 78^\circ 13'; & \left. \begin{array}{l} 175^\circ 0' \\ 237^\circ 12' \end{array} \right\} ac \ 62^\circ 12'; & \left. \begin{array}{l} 58^\circ 34' \\ 144^\circ 4' \end{array} \right\} bd \ 85^\circ 20'; \\
 \left. \begin{array}{l} 237^\circ 12' \\ 286^\circ 13' \end{array} \right\} cd \ 49^\circ 1' & & 
 \end{array}$$

From the measurements above as well as from the appearances of faces it is found that (ac) forms one zone and (acda) forms another zone.

The stereogram has been drawn. This has the advantage of having simple indices and confirms the symmetry already assumed.

*Density measurement.* The density of the crystal was measured by floatation method, using zinc sulphate solution, and was found to be 1.057.

*The measurement of  $2V$  by Fedorov stage* The thin section was placed in a horizontal position and rotated to extinction about the axis of microscope. This angle was plotted in stereographic projection. The inner stage was turned by successive  $5^\circ$  rotations, and at the same time this was determined by rotation about the horizontal axis of Fedorov stage. The values are plotted in stereographic projection. The curves thus obtained must pass through the point of emergence of the optic axis of the crystal, and also through the centre of projection.

*Dispersion in monoclinic crystals.* Tetraphenyl ethylene crystals show dispersion of monoclinic type when examined in convergent polarised light under polarising microscope. The acute bisectrix parallel to  $b$ -axis, and the obtuse bisectrix and the optic normal lie in the crystallographic plane of symmetry. In this case interference figures show crossed dispersion

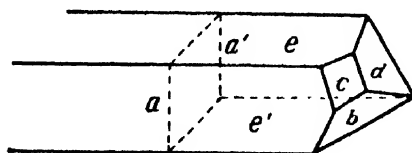


FIG. 1

Tetraphenyl ethylene crystal

in the acute bisectrix figure. The red colour fringes are spaced farther apart than the blue fringes. This is shown in the figures. Crossed dispersion produces in the parallel position similar coloured fringes on diagonally opposite sides of the isogyres. In the 45-degree position, the fringes border the convex sides of the isogyres and lie on a diagonal line passing through the centre of the field.

*X-ray study.* The rotation pictures about three crystallographic axes were taken. At first the crystal was placed on a goniometer head, with  $(a, c)$  zone axis or  $b$ -axis vertical. The rotation picture was taken by using Ni-radiation. The axis  $b$  is calculated from the relation

$$b \sin \mu = \lambda$$

where,  $\tan \mu = \frac{y}{R}$  :  $\frac{\text{distance from the first layer to zero layer}}{\text{radius of the camera}}$

Here,  $y = 1.05$  cm and  $R = 5.73$  cm,  
from which  $\mu = 10^\circ 19$ , and  $b = 9.371$  A.U.

For  $a$ -axis,  $\tan \mu = \frac{.85}{5.73} = .1480$

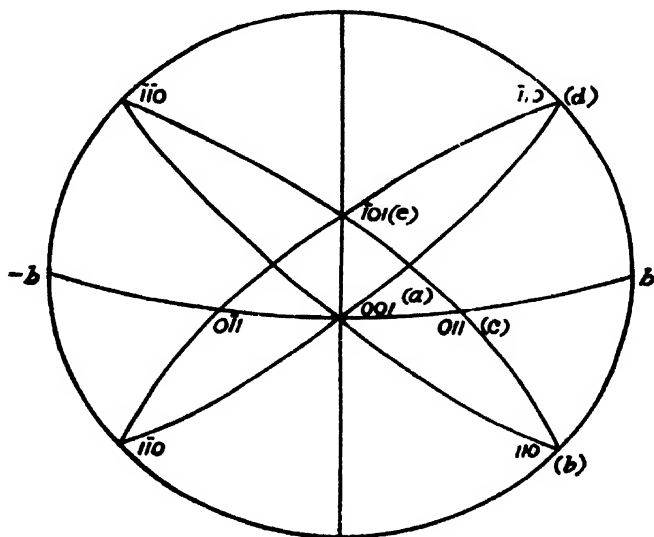


FIG. 2  
Stereographic projection

Hence,  $\mu = 8^\circ 25$ ; and  $a = 11.36$  A.U.

For  $c$ -axis,  $\tan \mu = \frac{.95}{5.73} = .1655$

Hence,  $c = 10.10$  A.U.

The monoclinic angle  $\beta$  which is between  $a$  and  $c$  is calculated from rotation picture about  $b$ -axis

$$\xi^2 = h^2 a^{*2} + l^2 c^{*2} - 2 h l a^* c^* \cos \beta$$

where  $\xi = \frac{\chi}{R}$ , where  $\chi$  = distance of Bragg spot ( $hol$ ) from centre of undeviated

beam, and  $a^* = \frac{\lambda}{d}$  and  $c^* = \frac{\lambda}{d}$

The spot chosen is (101) ;  $\xi = \frac{1}{5.73} = .1742$  ;  $(a^*) = .1452$ ,  $(c^*) = .1633$ .

Hence,  $\cos \beta = .3677$  and  $\beta = 68^\circ 20'$ .

The axial ratio is  $a : b : c = 1.213 : 1 : 1.078$

Calculation of number of molecule per unit cell.

The number of molecules per unit cell is calculated from the relation

$N = \frac{\rho V}{AM_H}$  , where  $\rho$  = density ;  $V$  = volume =  $abc \sin \beta$  ;  $A$  = atomic weight and  $M_H$  = mass of hydrogen atom.

On substitution of the values,  $N$ , the number of molecules per unit cell is found to be one.

#### CONCLUSION

The possible conclusions regarding the structure of tetraphenyl ethylene are.

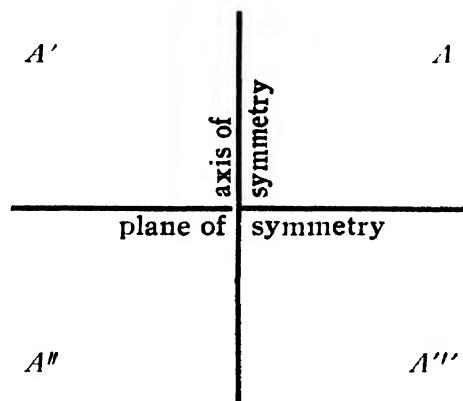
(1) C=C double bond possibly is either along the axis of symmetry or in the plane of symmetry.

(2) The angle between the phenyl groups is  $108^\circ$  which is monoclinic  $\beta$  angle and the valency of C=C double bond is also  $108^\circ$ .

(3) High refractive index is due to (C=C) group which has a strong absorption band in near ultra violet region the frequency of the radiation used is nearly equal to natural frequency of the atoms, given by the formula

$$\mu^2 = 1 + \sum \frac{A}{v_i^2 - \gamma_0^2}$$

(4) The four  $A$  positions represent the positions of phenyl groups, the reflections are due to axis of symmetry and due to plane of symmetry.



#### ACKNOWLEDGMENTS

The author wishes to express his grateful thanks to Prof. S. N. Bose for suggesting the problem and advice and to Dr. S. K. Roy of Presidency

College, Calcutta, for guidance in carrying out the experiments on optical crystallography.

## REFERENCES

Datta, M. N., 1947, *Ind. Jour. Phys.*, **21**, 362

Sen, S. N., 1940, *Sci. and Cull.*, **5**, 719.

# ON SPECTRAL CHARACTERISTICS OF OZONISER DISCHARGE IN PURE NITROGEN AT 20 mm. PRESSURE

By N. APPALANARASIMHAM

SPECTROSCOPIC LABORATORY, BANARAS HINDU UNIVERSITY

(Received for publication, June 14, 1952)

Plates IV A, B

**ABSTRACT.** In the ozoniser discharge through nitrogen at 20 mm pressure are excited a large number of known band systems involving the following initial electronic levels,  $D^3\Sigma_u^+$ ,  $C^3\Pi_u$ ,  $B^3\Pi_g$ ,  $c_2^1\Sigma_u^+$ ,  $m^1\Pi_u$ ,  $l$ ,  $s^1\Sigma_u^+$ ,  $h^1\Sigma_u^+$ ,  $r^1\Sigma_u^+$ ,  $z$ ,  $y(^1\Pi_g)$  and  $x(^1\Sigma_g^-)$ , with relative intensities visually estimated, ranging from 100 in the case of second positive to 0.5 for the first positive system of bands with 30 for the fourth positive and 20 for the singlet systems. Also, the first negative bands of  $N_2^+$  are excited with intensity 60 in the above scale. Besides, there is evidence of three progressions of new bands which probably involve transitions from hitherto unknown electronic singlet levels to the  $a^1\Pi_g$  state.

It is generally accepted that excitation of a molecule by electron collisions favours such excited states for which the inter-nuclear distance is not much different from that of the lower state while excitation by collisions with ions or atomic particles favours excited states which have greatly altered inter-nuclear distances. From this principle, the excitation of the  $D^3\Sigma_u^+$  state ( $r = 1.103$ ) and of  $B^3\Sigma_u^+$  of the first negative bands of  $N_2^+$  ( $r = 1.075$ ) can be understood to be due to collisions of normal  $N_2$  molecules with high speed electrons while that of the singlet electronic levels which involve a big change in the inter-nuclear distance (from 1.22 and 1.33 to 1.094, the  $r_0$  in the ground state) is due to collisions with particles of atomic masses. The excitation of all these states simultaneously in the ozoniser discharge, indicates the significance of this type of discharge.

The abnormally low intensity of the first positive bands in this type of ozoniser discharge is attributed to deactivation of the initial electronic level  $B^3\Pi_g$ , due to collisions with atomic particles and a possible radiationless transfer to repulsive states.

## INTRODUCTION

The spectrum of an uncondensed discharge through nitrogen consists of the systems of the first and second positive bands which lie in the regions from the near infra-red to about 5000 Å and 4900 Å to 2820 Å respectively while the spectrum of a condensed discharge (Fowler and Strutt, 1911) contains in addition a single progression of the fourth positive system extending from 2900 Å to 2250 Å. But for this, the spectrum of nitrogen does not usually comprise of any strong systems in the quartz ultra-violet region. Recently, a number of weak band systems (Gaydon, 1944 ; Rosen and Herman, 1951 ; Herman, 1950 ; Janin, 1949, 1950 ; Janin and Crozet, 1948 ; Gaydon and Herman, 1946) have been discovered in this region of the spectrum under different conditions of excitation. In the course of the experiments of the spectroscopic studies of an ozoniser discharge through nitrogen (Appalanarasimham, 1950-51) in relation to the Joshi effect, it was

observed that the spectrum consists of the second positive system quite strong in intensity and the fourth positive system weaker than the second positive and in addition, a number of weak bands in the ultra-violet region many of which are identified with the new singlet systems, the fifth positive and the Kaplan's second systems. Besides these, three more groups of bands are obtained which could be arranged in progressions probably involving new electronic levels. In view of the development of almost all the systems of bands in the ozoniser discharge at comparatively high pressure of nitrogen, a detailed study of the spectrum has been made.

#### EXPERIMENTAL PROCEDURE

The ozoniser used in the present experiments was originally prepared for the spectroscopic study of the Joshi effect in nitrogen. The ozoniser tube was filled with chemically pure and dry nitrogen at 20 mm pressure where the negative Joshi effect was found to be maximum at the 'threshold potential' (780 volts). The preparation of the tube has been described in detail in an earlier paper (Appalanarasimham, 1950-51). This ozoniser is excited in all the present studies by a transformer working off 110 volts A.C., 50 cycles primary and delivering about 6000 volts in the secondary. The spectrum is photographed on small and medium Hilger Quartz spectrographs. Kodak P 1200 Super Panchro Press and B 20 process regular plates have been used to photograph the respective spectra. Exposures of less than 4 hours were enough to record the more intense second positive bands on the medium instrument, whereas, the less intense bands in the ultra-violet needed exposures of 20 hours or more. The order of the intensities of the band systems of nitrogen obtained in the present experiments is roughly estimated visually and given in the following table with certain other relevant data. For this purpose a value of 100 is chosen for the intensity of the second positive system which is the most intense system and relative to it, the intensities of the other systems are estimated. Generally, the intense bands in any system are taken for the relative intensity estimation.

It was easy to identify directly from the spectrograms the bands obtained when these belonged to the well known second positive, first positive or fourth positive systems of nitrogen or to the negative bands of  $N_2^+$ . The wavelengths of the band heads of all other nitrogen bands were determined in the usual way by measuring the spectrograms and calculating the values from the Hartmann formula. The average discrepancy between the mean calculated values and the values given in literature was  $\pm 0.5 \text{ \AA}$ . The bands could thus be definitely identified with the known ones. The values given in literature are therefore employed in the discussion. In the course of the new classified and unclassified bands, the band head data obtained in the present experiments have been presented and used,

#### OBSERVATIONS

(a) *Triplet systems of nitrogen.* The most intense of the triplet

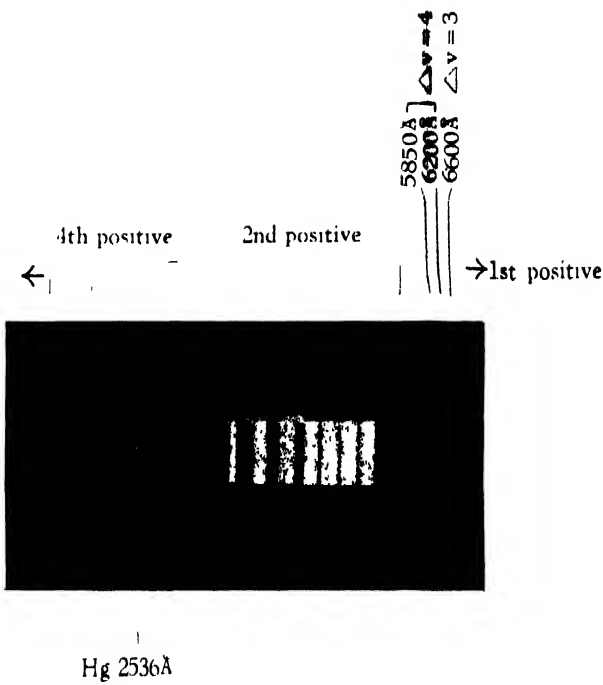


Fig 1

2nd positive bands

2976.8 (2,0)

3159.3 (1 0)

3371.3 (0,0)

3576.9 (0,1)

3642 (4,6)

3804.9 (0,2)

4059.4 (0,3)

4343.6 (0,4)

4667.3 (0,5)

a



8  
2932

Q(0,2)

Q(0,3)

P<sub>1</sub>(0,5)  
3661

2492 Cu

1st h + ve  
0.3

2618 Cu

4th h + ve  
0.4

2776  
Cu<sup>+</sup>  
h + ve  
0.5  
8

2819.8 2nd pos  
2827.1 P sys  
2839 Cu

2932 8

b



T(0,1)

S(0,0)

T(0,2)

S(0,1)

P<sub>2</sub>(2,0)

T(0,3)

S(0,2)

Fig 2

R(0,0)

T(0,4)

Q(0,0)

P(1,2)

P(0,0)

Q(0,0)



systems of the nitrogen molecule is the second positive group. Long exposures of the ozoniser discharge bring out the fourth positive group and also very weak groups of bands belonging to the sequences  $\Delta v=3$  and 4 only of the first positive system (figure 1, Plate IV A).

The excitation of the fourth positive group (excitation potential  $\sim 12.6$  e.v.) indicates that the mechanism of excitation approximates to the vigorous type as is generally met with in condensed discharges and is probably due to electrons of high velocity. Electronic collisions favour transitions to states in which the inter-nuclear distance does not suffer large changes. From this principle, the first negative,  $N_2^+(r_e=1.075)$  and the fourth positive ( $r_e=1.108$ ) are to be regarded as being excited by electronic collisions in these experiments. The weak intensity of the first positive bands is probably a case of deactivation (Tawde and Patankar, 1947; Gaydon, 1944) of the initial level of the first positive system due to collisions and a possible radiationless transfer into a repulsive state.

(b) *Singlet systems of nitrogen.* In emission, eight systems of short progressions of bands are now known which have been obtained under different conditions of excitation by different authors, each of them obtaining some of these systems selectively depending upon the method of excitation employed. The discharge conditions under which the different band systems are excited are briefly as follows: Gaydon (1944) excited five of the band systems (*P*, *Q*, *R*, *S*, *T* systems) in a hollow cathode discharge through a capillary tube of 2 mm bore and 20 cm long and the discharge was maintained by an ordinary induction coil with a small condenser and  $\frac{1}{2}$  inch spark gap. A flow of chemically dry and oxygen-free nitrogen was maintained in the discharge tube at a few mm pressure of mercury. Mme. Renee Herman (1950) obtained the *P*,  $\delta$  ( $v'=0$ ,  $v'=1^*$ ), *S*, *T*,  $\theta$ ,  $\eta$  systems in an ordinary discharge at low pressures through a very long tube (25 m). Janin (1949, 1950) obtained the *P*,  $\delta$  ( $v=0$  and  $v'=1^*$ ) systems in an electrodeless discharge of the ozoniser type at low pressure of nitrogen while Janin and Crozet (1948) got the  $\delta$  ( $v'=0$  and  $v'=1^*$ ) systems in low pressure discharges in the presence of rare gases. Thus we see that there is a pronounced effect of the discharge conditions in bringing out the different systems. We shall now compare the systems excited in the present experiments with those described above. In every system only the recorded bands in the present experiments are given with the quantum numbers (figure 2, Plate IV B). These form the strongest bands in each system. The other bands of the systems are either absent or very weak.

1. *P* system : 2827 (0,0), 2967 (0,1), 3283 (0,3), 3661 (0,5)  
2785 (1,1), 2516 (2,0) and 2918 (1,2).

Of all the bands of the singlet systems excited in the present experiments the 2827 (0,0) band of this system is the strongest. This band is in fact

\* This is the same as Gaydon's *Q* progression.

stronger than the 2819 (3,0) band of the second positive system (see figure 2). Some of the bands of this system are superposed by the rotational lines of the second positive bands. Gaydon obtained only the (0,0), (0,1) and (0,2) bands of the progression  $v'=0$  while Janin and Crozet (1948) obtained two more progressions viz.,  $v'=1$  and  $v'=2$ . In the present experiments only the stronger of these two progressions is obtained. However, the bands at 2662 (1,0) and 2871 (2,3) are not present on our plates though they are assigned intensity values of (10) and (6) by Janin and Crozet.

2. *Q system* : 2746 (0,0), 2878 (0,1), 3020 (0,2) and 3175 (0,3).

The (0,3) band at 3175 Å is not included by Gaydon (1944). All the four have been observed by Janin (1949, 1950) in the luminescence spectrum of a silent electric discharge at low pressure of nitrogen.

3. *δ system* : 2796 (0,0), 2932 (0,1), 3080 (0,2) and 3241 (0,3),

This progression and the *Q* progression were grouped into the same system by Gaydon and Herman (1946) who called it *δ* system. Janin (1949, 1950) also obtained both these progressions and tentatively put them into the same system. But Gaydon got only the *Q* system in his experiments of a mildly condensed discharge through a flowing stream of nitrogen through a capillary tube at low pressure. In a joint publication, Gaydon and Herman (1946) discussed this point and finally Gaydon put them as belonging to two systems in view of the incompatibility of the  $\omega_{1/2}$  (640  $\text{cm}^{-1}$ ) with the *B* value of about 1.36 obtained from a rotational analysis of the 2746 (0,0) band. In the present experiments, both these systems are recorded with almost equal intensity. In view of the rather widely differing discharge conditions, the excitation of the *δ* system of bands is probably characteristic of the ozoniser discharges of the type used by Janin and us, while it is not favoured in the hollow cathode discharges. The other sources favourable for the production of these bands are luminescence discharges and discharges in the presence of rare gases (Rosen and Herman, 1951).

In a compilation of the data of the nitrogen band systems made by Rosen and Herman (1951) which came to our hand rather late, Herman designates the 3080 Å band of the *δ* system as the (1,2) band of a system whose origin is at 2841 Å = 35188  $\text{cm}^{-1}$ . This means that the above progression of the *δ* system is not the  $v'=0$  progression but  $v'=1$  progression. If this is true, there will be strong evidence for regarding the *δ* and *Q* as two different systems. A further point in favour of this view consists in the fact that Herman considers the two progressions  $v'=0$  and  $v'=1$  of the *δ* system are themselves the  $v'=4$  and  $v'=5$  progressions respectively of a system whose origin locates the 101456.0  $\text{cm}^{-1}$  electronic level found in absorption by Worley (1943).

4. *R system* : 2672 (0,0) and 2796 (0,1).

The (0,0) band at 2672 Å is present while the band at 2796 Å is rather crowded by two more bands viz., (0,5) of the *T* system and (0,0) of the system and as such its presence is not certain. It may be mentioned here

that this system has been obtained only in a hollow cathode discharge by Gaydon. Further, Gaydon observed the band at  $2672\text{\AA}$  to be the most outstanding of the new bands. But on our plates the (0,0) band at  $2827\text{\AA}$  of the *P* system is probably the strongest of all the bands of the singlet systems.

5. *S and T systems* : *S* system : 2397 (0,0), 2497 (0,1), 2603 (0,2) and 2718 (0,3). *T* system : 2282 (0,0), 2372 (0,1), 2467 (0,2), 2570 (0,3) and 2796 (0,5).

Both these systems are equally strong on our plates. The (0,2) band of the *T* system was not observed earlier either by Gaydon or by Herman. This band is quite weak on our plates but it is clearly visible.

6.  *$\theta$  System* : In addition to these bands, we find a weak structure of bands at  $2358\text{\AA}$  which is also the strongest band of the system of Herman. The other bands of the system are, however, not present.

*Other band systems of nitrogen* : Kaplan's second system . 2354 (0,0), 2537 (0,2), 2636 (0,4) and 2619 (1,4).

This system is rather weak and only the above bands are present on the plates. These bands are also the strongest bands of this system.

*Fifth positive (Van der Ziel's) system* : 2412 (1,4), 2586 (1,6) and 2681 (1,7).

This system is the weakest of all the systems of bands described in these studies. The progression  $v'=0$  is not observed at all. In fact, only the bands of the progression,  $v'=1$ , were observed originally by Van der Ziel, and later Gaydon and Herman (1946) observed a further weak progression which fitted into the  $v'=0$  of this system.

*New band systems, probably singlet* : In addition to these systems, we got a number of other bands some of which are noticeable on Gaydon's published spectrograms (Gaydon, 1944) also. Eight of these could be arranged into three progressions as shown below.

$v'$	$v''$	0	1	2	3
(i) 0	$\lambda$ 2462.3 $\nu$ 40600	$\Delta\nu$ (1653)	2567.5 38937	$\Delta\nu$ (1631)	2679.7 37306
(ii) 0	$\lambda$ 2723 V $\nu$ 36713	$\Delta\nu$ (1665)	2852.4 V 35048		$\Delta\nu$ (1610)
(iii) 0	$\lambda$ 2839 $\nu$ 35213	$\Delta\nu$ (1665)	2980 33547		2810.6 35696

The vibrational wave number differences in the (i) system agree closely with those of the  $a' {}^1\Pi_u$  state viz., 1666, 1638, and  $1610\text{ cm}^{-1}$ . These bands, therefore, locate a new level at  $109557\text{ cm}^{-1}$  of the  $\text{N}_2$  molecule,

The progressions (ii) and (iii) are represented by only two bands each and are therefore less definite. It is, however, to be noted that Janin (1949) also recorded the bands of the (iii) progression. The band at  $2839\text{\AA}$  is definitely present in Gaydon's spectrogram. The bands at  $2980\text{\AA}$  is likely

to be missed in the structure of strong  $2977\text{\AA}$  band (2,0) of the second positive group. In our experiments the bands stand out clearly in a plate which records the  $2977\text{\AA}$  second positive band comparatively weakly, whereas, usually the band at  $2980\text{\AA}$  is masked by the structure of the strong second positive band at  $2977\text{\AA}$ .

The two bands at  $2723$  and  $2852\text{\AA}$  which are tentatively shown to form a new progression are not recorded by previous workers.

#### *Unclassified bands :*

The following bands are also present on our plates.  $2417.9$ ,  $2424.0$ ,  $2459.6$ ,  $2612.0$ ,  $2673.0$  and  $2907.5$  Some of these viz.,  $2424.0$  and  $2459.6$  are present on Gaydon's plate.

### SUMMARY AND CONCLUSIONS

The prominent features of the spectrum excited in the ozoniser discharge through nitrogen at a pressure of 20 mm are the following .

- (1). The first positive system is extremely weak while in the ordinary discharges the first positive system is comparable in intensity to the second positive system.
- (2). The fourth positive system is excited. This system is usually excited only in condensed and other vigorous types of discharges through nitrogen.
- (3). Seven systems out of the eight known singlet band systems are obtained in emission with the single mode of excitation employed, namely, ozoniser discharge through nitrogen at 20 mm. pressure. Previously these systems of bands have been excited under different excitation conditions like (a) the electrodeless discharge in the presence of rare gases (b) discharges through nitrogen at moderate but controlled pressures (c) hollow cathode discharge through nitrogen at low pressures.
- (4). Other systems like the Kaplan's second system, the fifth positive system and several new bands for some of which a classification is proposed, are excited only weakly.

These features can be understood in the following way. It is generally known that the addition of a small amount of oxygen decreases the intensity of the first positive bands by deactivation (Tawde and Patankar, 1947 ; Gaydon, 1944) due to collisions with oxygen atoms. It is also likely that at high pressures collisions with particles of atomic masses may drift the molecules into a radiationless transition. In either case, collisions with atomic particles are essential. That this happens in the present ozoniser discharge through nitrogen is shown also by independent observations given below and elsewhere (Appalanarasimham 1952-53). The second observation is indicative of the excitation of the nitrogen molecule to high energy states, the excitation energy of the fourth positive bands being 12.6 e.v. thus indicating the availability of high energy electrons in the ozoniser discharge. The third feature is significant. The molecule in these singlet states has an internuclear distance much larger (1.20 to 1.33) than in the ground state

TABLE I

No. Band system	Transition	Sources favourable	$r$ , in the initial state	Visually estimated intensity
<i>Triplet systems :</i>				
1. 2nd positive	$C^3\Pi_u \rightarrow B^3\Pi_u$	Positive column discharges	1.2123	100
2. 4th positive	$D^1\Sigma^+_u \rightarrow B^3\Pi_u$	Condensed discharges	1.108 (70)	30
3. 1st positive	$B^3\Pi_u \rightarrow A^3\Sigma^+_u$	Positive column discharges	1.293	0.5
<i>Singlet systems :</i>				
4. P system	$c_3^1\Sigma^+_u \rightarrow a^1\Pi_u$	Ozoniser discharges at low pressures	1.12 (70)	40
5. Q "	$m^1\Pi_u \rightarrow a^1\Pi_u$	Discharges at strong press., ozoniser discharges	1.328 (70)	20
6. δ "	$1 \rightarrow a^1\Pi_u$	Luminescence and ozoniser discharges : also in the presence of rare gases	(1.27)	"
7. R "	$r^1\Sigma^+_u \rightarrow a^1\Pi_u$	Electrodeless discharges, medium pressures, mildly condensed discharges	1.20 (70)	"
8. S "	$s^1\Sigma^+_u \rightarrow a^1\Pi_u$	Electrodeless discharges, medium pressures, mildly condensed discharges	1.232 (70)	"
9. T "	$h^1\Sigma^+_u \rightarrow a^1\Pi_u$	Moderate pressures, mildly condensed discharges	1.22 (70)	"
10. Kalpan's and systems	$y(^1\Pi_u) \rightarrow \bar{u}$	Moderate pressures	1.16 (70)	15
11. 5th positive of Van der Ziel's	$x(^1\Sigma^+_u) \rightarrow a'(^1\Sigma^+_u)$	"	1.18	5
12. θ system	$z \rightarrow a^2\Pi_u$	Strong current	—	—

$r$ , of the grand state  $\times 10^4$

The spectrum also records two bands of  $N^+_2$ , first negative system, (0,0) and (0,1), with a visual intensity of 60 in scale employed.

In addition to the above, the following lines and band heads due to trace of impurities have been recorded on the long exposure plates, with intensities ranging from 10 to 20 on the above scale. 2883 Å and 2896 Å due probably to  $CO^+$ ; 3064 Å due to OH and 3536 Å due to Hg

The designations of the electronic levels given in column 3 and the data of the  $r$ , and  $r$ , values and the sources favourable are taken from Rosen and Herman (1951).

( $r_e = 1.094$ ). Electronic transitions involving relatively large changes in internuclear distance are known to be favoured either by atomic collisions or by discharges in the presence of rare gases. That in the ozoniser discharge employed almost all the singlet levels are excited is thus indicative of the appreciable availability for excitation, also of atomic collisions.

#### ACKNOWLEDGEMENT

The author extends his sincere thanks to Prof. R. K. Asundi for guidance and help.

#### REFERENCES

- Appalanarasimham, 1950, 51, *Jour. Sc. Res., B- H. U.*, 1, 78.  
 Appalanarasimham, 1952-53, *Jour. Sc. Res., B. H. U.*, 2 (under publication).  
 Fowler and Strutt, 1911, *Proc. Roy. Soc.*, **85**, 377.  
 Gaydon and Herman, 1946, *Proc. Phys. Soc.*, **58**, 292.  
 Gaydon, 1944, *Proc. Roy. Soc.*, **182A**, 286.  
 Gaydon, 1944, *Proc. Phys. Soc.*, **56**, 85.  
 Janin, 1949, " " **52**, 737  
 " 1950, " " **53**, 178.  
 Janin and Crozet, 1948, *Science Abstracts*, **51**, 154.  
 Mme. Renee Herman 1950, *Science Abstracts*, **53**, 126.  
 Tawde and Patankar, 1947, *Phil. Mag*, Ser. 7, **38**, 65.  
 Rosen B. and Herman, R. 1951, "Constantes Selectionees Donnees Spectroscopiques concernant les Molecules Diatomiques," Hermann and Cie, Depositaires, Paris-Ve.  
 p 199 f  
 Worley, 1943, *Phys. Rev.*, **64**, 207.

# ON THE FAITHFUL REPRODUCTION OF THE FLAT TOP OF A PULSE IN A HIGH FIDELITY PULSE AMPLIFIER\*

BY BIMAL KRISHNA BHATTACHARYYA

INSTITUTE OF NUCLEAR PHYSICS, 97, UPPER CIRCULAR ROAD, CALCUTTA

(Received for publication, September 10, 1952)

**ABSTRACT.** The response of a pulse amplifier to the flat top of a pulse has been studied in two different ways. The complicated interactions of the three circuits, e.g., the  $R_g C_g$  grid circuit,  $R_k C_k$  cathode circuit and  $R_{s\eta} C_{s\eta}$  screen circuit, have been considered. The effect of the plate-supply decoupling network  $R_d C_d$  is also taken into consideration and it is shown that it permits compensation for the flat top distortion due to  $R_g C_g$  combination in the grid. The conditions which are to be satisfied by the circuit elements in order to make the sag less pronounced, have been given. The expression for the overall transfer function of the amplifier is derived. The output voltage is found to be a combination of several exponential terms which arise due to the various resistance-capacitance networks in the amplifier.

## INTRODUCTION

Pulse amplifiers are generally studied by considering their steady-state phase and frequency responses or by determining the pulse or transient response, that is, the shape of the output waveform as a function of time for a certain input pulse. When the shape of the input pulse is known, the transient response method is generally used. The input pulse may be of various shapes, (i) rectangular (ii) delta-function (iii) triangular, etc. In a linear amplifier the response to any of the above pulses completely determines the response to any other.

The subject of analysis in this paper is the reproduction of the flat top of a rectangular pulse in a typical pulse amplifier. This is nothing but the faithful amplification of the direct current by the amplifier. The nature of the response of an amplifier to the flat top of a rectangular pulse is shown in figure 1.

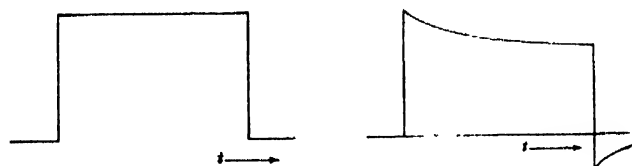


FIG. 1

Reproduction of the flat top of a rectangular pulse

The amount of non-faithful transmission of the flat top is determined by the sag and so the problem is to minimise the sag to have an almost exact replica of the input rectangular pulse in the output.

\* Communicated by Prof. M. N. Saha, F. R. S.

The basic pulse amplifier stage uses a pentode with resistance-capacitance coupling between successive stages as shown in figure 2. A pentode or a tetrode with a high gain is generally used due to their low interelectrode capacities and low input capacity because of Miller effect.

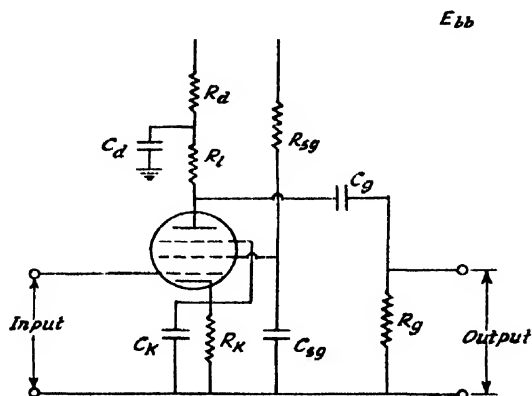


FIG. 2

Resistance capacitance coupled amplifier

The transmission of direct current is prevented by the series  $R_d C_d$  grid circuit, the parallel  $R_{sg} C_g$  screen circuit and the  $R_k C_k$  cathode circuit. An exact analysis of the circuit (figure 2) is attempted in this paper in two ways considering the interaction of the three circuits.

In the first process the reduction factors in the overall amplification of the pulse amplifier stage due to the effect of voltages developed across the parallel  $R_{sg} C_g$  screen circuit and  $R_k C_k$  cathode circuit, have been derived in a conventional way. These reduction factors are utilised to find out the current flowing in the plate and thus the output voltage.

The second method of analysis takes advantage of the superposition principle by means of which the total plate current may be taken to be the combination of currents resulting from three voltage sources, (i) the input voltage  $e_g$  at the grid, (ii) the voltage developed across the screen impedance and (iii) the cathode voltage  $e_k$  developed across  $R_k C_k$  circuit. Since the plate current is now known, the total response of the amplifier may be found out.

#### FIRST METHOD OF ANALYSIS

When a signal voltage is applied to the control grid of a pentode tube, a variation in current results in the screen, plate and cathode. Such currents cause a voltage drop in the impedance  $Z_{sg}$  of the screen circuit as well as in the impedance  $Z_k$  of the cathode. The voltages thus developed across the two impedances in the screen and cathode reduce the amplified plate current of the pentode. Thus the amplification will be diminished by certain reduction factors which will now be determined considering the effect of voltages across the screen and cathode circuits.



The variation in screen current when an alternating voltage is impressed between the cathode and grid, will develop an amplified voltage across the screen circuit impedance  $Z_{sg}$  which is assumed to be a parallel combination of a resistance  $R_{sg}$  and a condenser  $C_{sg}$ . This amplified voltage is developed between screen and cathode and reduces the amplification by affecting the plate current. We shall assume that the plate voltage is sufficient to make the plate current independent of the plate voltage and so although the screen circuit voltage variation affects the plate current, the reverse is not true. Then the equivalent screen grid circuit (figure 3) is drawn where  $\mu_s$  is the  $\mu$ -factor of the screen grid relative to the control grid.

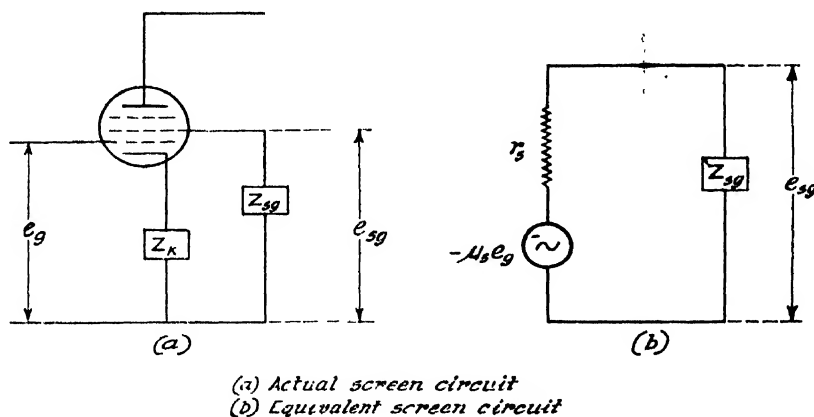


FIG. 3

From figure 3 the voltage developed across  $Z_{sg}$  is given by

$$e_{sg} = -\mu_s e_g \frac{Z_{sg}}{Z_{sg} + r_s} \quad (1)$$

The voltage developed across  $Z_{sg}$  has an effect equivalent to reducing the signal voltage from  $e_g$  to  $e_g + e_{sg}/\mu_s$ . So the actual amplification in plate voltage is reduced by a factor :

$$A = \frac{e_g + e_{sg}/\mu_s}{e_g} = 1 + \frac{1}{\mu_s} \cdot \frac{e_{sg}}{e_g} \quad \dots (2)$$

Substituting from equation (1),

$$A = 1 - \frac{Z_{sg}}{r_s + Z_{sg}} \quad \dots (3)$$

Since

$$Z_{sg} = \frac{R_{sg}}{1 + pC_{sg}R_{sg}} \quad \dots (4)$$

where  
we have

$$p = j\omega,$$

$$A = \frac{p + a}{p + b'}, \quad \dots (5)$$

where

$$a = 1/C_{sg}R_{sg} \quad \dots (6)$$

and

$$b' = \frac{r_s + R_{sg}}{C_{sg}R_{sg}r_s}$$

If we consider the effect of screen circuit only in reducing the amplification, the plate current  $i_p$  will be given by the transform equation.

$$L(i_p) = Ag_m L(e_a) \quad \dots (7)$$

where  $L$  denotes the Laplacian operator.

If the input voltage is the unit step voltage, the step function response  $f(t)$  is the Laplace transform of  $F(p)$ , where  $F(p)$  is given by

$$F(p) = \frac{1}{p}, \quad A(p) = \frac{1}{p} \cdot \frac{p + a}{p + b'}, \quad (8)$$

leaving out the constant term  $g_m$ .

So

$$f(t) = L^{-1}F(p) = L^{-1} \frac{1}{p} \cdot \frac{p + a}{p + b'} = \frac{(b' - a)e^{-b't} + a}{b'} \quad (9)$$

where  $L^{-1}$  denotes the inverse Laplacian operator.

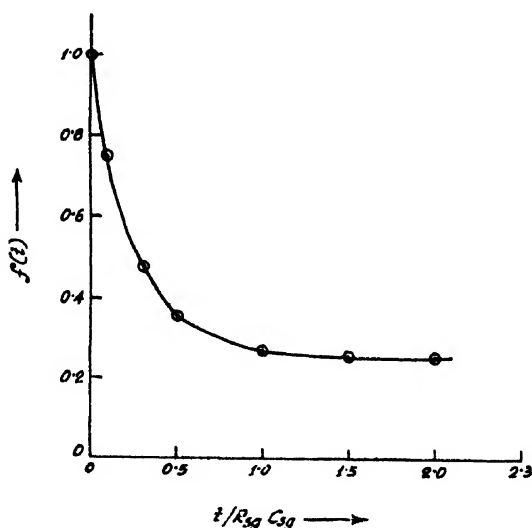


FIG. 4

Step function response of a pulse amplifier when the effect of the screen circuit is only considered.

$f(t)$  is now plotted as shown in figure 4 assuming the following values of the circuit elements :

For tube type 6AC7,  $r_s = 20000 \Omega$ ,  $C_{sg} = 2.5 \mu f$ ,  $R_{sg} = 60000 \Omega$

The slope of  $f(t)$  at  $t=0$  is given by

$$\left. \frac{df(t)}{dt} \right|_{t=0} = a - b' = -\frac{I}{r_s C_{sg}} \quad \dots (10)$$

Hence, if the sag in time  $t_1$  is very small so that the graph of equation (9) may be assumed to be practically linear in this interval of time and if 1 per cent sag is allowed, we have

$$\frac{I}{100 t_1} = \frac{I}{r_s C_{sg}}$$

so,

$$C_{sg} = \frac{100 t_1}{r_s} \quad \dots (11)$$

But when the sag is considerable, the fractional sag in time  $t_1$  is given by the equation,

$$\text{Fractional sag} = \frac{f(0) - f(t_1)}{f(0)} \quad \dots (12)$$

If we substitute from equation (9), the sag is found out to be

$$\frac{f(0) - f(t_1)}{f(0)} = \frac{(b' - a')(1 - e^{-b't})}{b'} \quad \dots (13)$$

**Cathode Circuit.** The cathode circuit is a parallel  $R_k C_k$  combination (figure 2). The amplified signal current flowing through this impedance causes a voltage drop across the combination which appears as a voltage across the control grid and cathode in addition to the applied signal  $e_g$ .

The voltage present between cathode and grid is  $e_g - e_k$ , where  $e_k$ , the voltage developed across  $Z_k$ .

$$\text{Now,} \quad Z_k = R_k / 1 + p R_k C_k \quad \dots (14)$$

The voltage  $e_k$  is given by

$$e_k = A g_m (e_g - e_k) \cdot Z_k$$

and so

$$e_k = \frac{A g_m Z_k}{1 + A g_m Z_k} \cdot e_g \quad \dots (15)$$

The output current of the tube is given by

$$i_p = \frac{e_k}{Z_k} = \frac{A}{1 + A g_m Z_k} \cdot g_m e_g \quad \dots (16)$$

So the cathode circuit has an effect equivalent to reducing the plate current and hence amplification by the factor

$$B = \frac{A}{1 + A g_m Z_k} \quad \dots (17)$$

Substituting the values of  $A$  and  $Z_k$  from equations (5) and (14) respectively, we have

$$B = \frac{\frac{p+a}{p+b'}}{1 + \frac{p+a}{p+b'} \cdot \frac{g_m R_k}{1 + p R_k C_k}} = \frac{p^2 + a_0 p + a\alpha}{(p+c)(p+d)} \quad \dots (18)$$

where,

$$\left. \begin{aligned} \alpha &= \frac{1}{R_k C_k} \\ a_0 &= a + \alpha \\ c + d &= b' + \alpha + g_m / C_k \\ cd &= b' \alpha + a g_m / C_k \end{aligned} \right\} \quad \dots (19)$$

and

Thus  $c$  and  $d$  can be determined from equation (19).

So the step-function response  $f(t)$  is the Laplace transform of

$$\frac{1}{p} \cdot \frac{p^2 + a_0 p + a\alpha}{(p+c)(p+d)}$$

Hence

$$\begin{aligned} f(t) &= L^{-1} \frac{1}{p} \cdot \frac{p^2 + a_0 p + a\alpha}{(p+c)(p+d)} \\ &= \frac{a\alpha}{cd} + \frac{1}{d-c} \left[ \left( a_0 - c - \frac{a\alpha}{c} \right) e^{-ct} - \left( a_0 - d - \frac{a\alpha}{d} \right) e^{-dt} \right] \quad \dots (20) \end{aligned}$$

Equation (20) is now plotted as shown in figure 5.

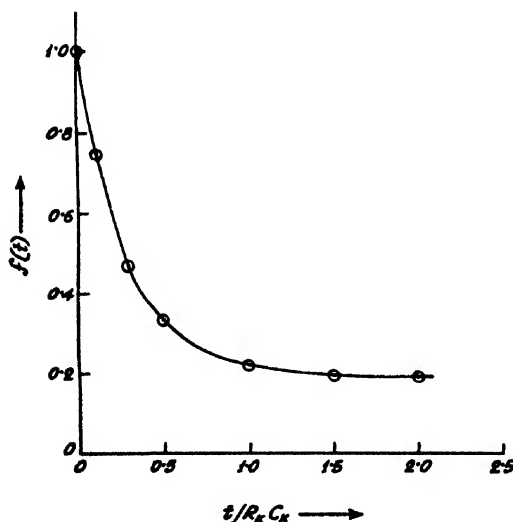


FIG. 5

Step-function response of a pulse amplifier when the combined effect of the screen and cathode circuits is taken into account.

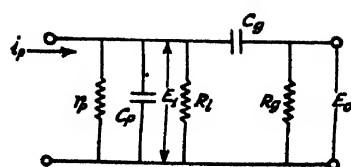


FIG. 6

Equivalent plate circuit of the pulse amplifier using a pentode.

The slope of equation (20) at  $t=0$  is given by

$$\left. \frac{df(t)}{dt} \right|_{t=0} = \frac{I}{d-c} \left[ d \left( a_0 - d - \frac{a\alpha}{d} \right) - c \left( a_0 - c - \frac{a\alpha}{c} \right) \right] \quad (21)$$

If 1 per cent sag is allowed in time  $t_1$ , the relation to be satisfied by the circuit components is

$$\frac{I}{100t_1} = \frac{I}{d-c} \left[ d \left( a_0 - d - \frac{a\alpha}{d} \right) - c \left( a_0 - c - \frac{a\alpha}{c} \right) \right] \quad (22)$$

When the sag is marked, it will be calculated with the help of the equation (12).

*Plate circuit.* The equivalent plate circuit of the basic pentode amplifier (figure 2) is drawn in figure 6.

$r_p$  = plate resistance of the pentode.

$C_p$  = plate-cathode tube capacitance plus stray wiring capacitances.

$R_c$  = coupling resistance.

$C_g$  = coupling condenser.

$R_g$  = grid-leak resistance.

We shall assume that the plate load resistor is small compared to the grid leak resistance. The plate-resistance  $r_p$  of the pentode is very large compared to the load-resistance  $R_L$  and in the transmission of the flat top of a pulse the reactance of  $C_p$  is so high that it can be taken to be the practical equivalent of an open circuit. If the effect of the voltages developed across the screen circuit and the cathode is taken into account, the voltage across the load resistance may be written as

$$E_1 = G \cdot A \cdot B \cdot e_g \quad \dots \quad (23)$$

where  $G$  is a gain factor determined by the tube and circuit constants.

Since  $R_L$  is small compared to  $R_g$ , the ratio of the output voltage  $E_0$  and  $E_1$  is given by

$$\begin{aligned} \frac{E_0}{E_1} &= \frac{p R_g C_g}{1 + p R_g C} \\ &= \frac{p}{p + \beta} \end{aligned} \quad (24)$$

where

$$\beta = \frac{1}{R_g C_g}$$

So

$$E_0 = G \cdot A \cdot B \cdot \frac{p}{p + \beta} \cdot e_g$$

Substituting the values of  $A$  and  $B$ , the step-function response  $f(t)$  is given by

$$f(t) = L^{-1} \frac{1}{p} \cdot \frac{p}{p+\beta} \cdot \frac{p+a}{p+b'} \cdot \frac{p^2+a_0p+a\alpha}{(p+c)(p+d)}$$

Breaking the righthand part into partial fractions, we can write  $f(t)$  in the following form with the help of a table of inverse Laplace transforms.

$$f(t) = \frac{(a-\beta)(a\alpha-a_0\beta+\beta^2)}{(b'-\beta)(c-\beta)(d-\beta)} e^{-\beta t} + \frac{(a-b')(a\alpha-a_0b'+b'^2)}{(\beta-b')(c-b')(d-b')} e^{-b't} \\ + \frac{(a-c)(a\alpha-a_0c+c^2)}{(\beta-c)(b'-c)(d-c)} e^{-ct} + \frac{(a-d)(a\alpha-a_0d+d^2)}{(\beta-d)(b'-d)(c-d)} e^{-dt} \quad (25)$$

The slope of equation (25) at time  $t=0$  is given by

$$\frac{df(t)}{dt} \Big|_{t=0} = -\beta \cdot \frac{(a-\beta)(a\alpha-a_0\beta+\beta^2)}{(b'-\beta)(c-\beta)(d-\beta)} - \frac{b'(a-b')(a\alpha-a_0b'+b'^2)}{(\beta-b')(c-b')(d-b')} \\ - \frac{c(a-c)(a\alpha-a_0c+c^2)}{(\beta-c)(b'-c)(d-c)} - \frac{d(a-d)(a\alpha-a_0d+d^2)}{(\beta-d)(c-d)(b'-d)} \quad (26)$$

The expression on the left side of equation (26) is equal to  $1/100 t_1$  if 1 percent sag is allowed in time  $t_1$ . Whenever the sag is prominent, equation (12) must be utilised to find out the fractional sag.

*Compensation for the flat-top distortion.* The distortion in the transmission of the flat top of a pulse due to  $R_g C_g$  network is compensated by the plate-supply decoupling network  $R_d C_d$ .

The pentode tube may be conveniently assumed to be a constant current generator. Since the plate resistance  $r_p$  of a pentode is very large, it may be omitted from the following equivalent plate circuit.

First of all, assuming that the screen  $R_{s,g} C_{s,g}$  circuit and the cathode  $R_k C_k$  combination have no effect on the plate current,  $i_p$  may be written as:

$$i_p = -g_m e_g$$

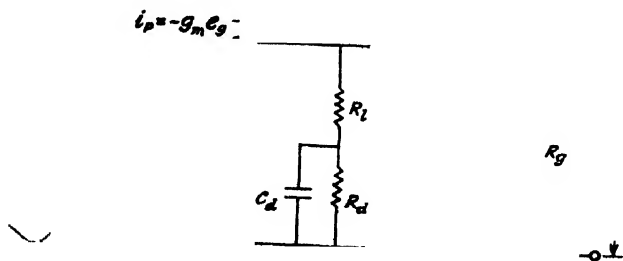


FIG. 7

Equivalent plate circuit of a pulse amplifier with decoupling filter network in the plate

Taking

$$R_g C_g = \frac{1}{R_L C_d}, \quad \beta' = \frac{1}{R_d C_d} \quad \text{and} \quad p = ja$$

the output voltage  $e_o$  is given by

$$e_o = g_m e_u \left\{ R_l + \frac{1}{C_d} \cdot \frac{1}{p + \beta'} \right\} \left\{ \frac{R_u}{p} (p + \alpha') \right\} \cdot \frac{p}{p + \alpha'} \dots \quad (27)$$

Since  $R_u$  is generally large compared to  $R_l$ , equation (27) can be simplified to

$$e_o = \frac{g_m e_u R_l}{R_u} \left\{ 1 + \frac{\alpha'}{p + \beta'} \right\} \cdot R_u = g_m e_u R_l \cdot \frac{p(p + \alpha' + \beta')}{(p + \alpha')(p + \beta')} \quad (28)$$

The step-function response  $f(t)$  of this network is given by

$$f(t) = \frac{\alpha' e^{-\beta' t} - \beta' e^{-\alpha' t}}{\alpha' - \beta'}, \quad \alpha' \neq \beta' \quad (29)$$

or 
$$f(t) = e^{-\beta' t} (1 + \beta' t), \quad \alpha' = \beta' \quad (30)$$

The slope of  $f(t)$  at  $t=0$  (figure 8) is zero and so the condition  $R_u C_u = R_l C_d$  which was assumed earlier, is necessary for proper compensation.

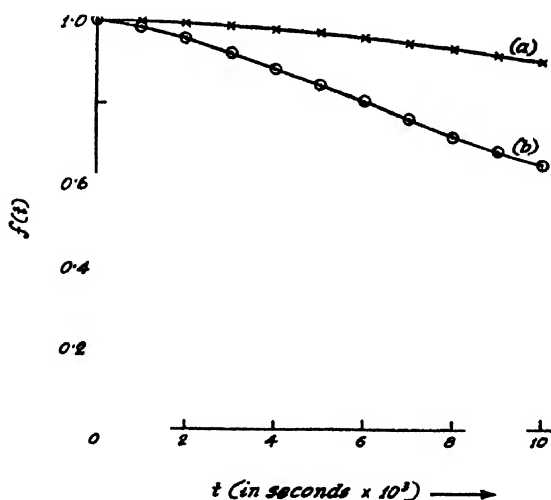


FIG. 8

Curve of response for flat top compensation

(a)  $\alpha' = \beta'$

(b)  $\alpha' \neq \beta'$

If the effect of screen and cathode circuits is to be considered, the plate current should be written as

$$i_p = g_m \cdot A \cdot B \cdot e_u$$

So in this case the response  $f(t)$  of the amplifier to a unit step-function voltage is the inverse Laplace transform of  $F(p)$  where  $F(p)$  is given by

$$F(p) = \frac{1}{p} \cdot \frac{p(p + \alpha' + \beta')}{(p + \alpha')(p + \beta')(p + b')} \cdot \frac{p^2 + a_0p + a_2}{(p + c)(p + d)} \quad (31)$$

The inverse transform can be found using the Heaviside expansion theorem, namely,

$$x^{-1} \left\{ \frac{\phi(p)}{f(p)} \right\} = \sum_{r=1}^n \frac{\phi(p_r)}{f'(p_r)} e^{p_r t} \quad (32)$$

where

$$f(p) = \prod_{r=1}^n (p - p_r) \quad (33)$$

and  $p_r$ 's are all distinct. Heaviside's theorem demands that the degree of the denominator  $f(p)$  will be at least as high as that of the numerator  $\phi(p)$ . This condition is satisfied by the function where

$$\begin{aligned} \phi(p) = & p^4 + p^3(a_0 + \alpha + \alpha' + \beta') + p^2\{a(\alpha' + \beta') + \alpha\alpha + a_0(\alpha + \alpha' + \beta')\} \\ & + p\{a\alpha(\alpha + \alpha' + \beta') + aa_0(\alpha' + \beta')\} + a^2\alpha(\alpha' + \beta') \end{aligned} \quad \dots (34)$$

and

$$f(p) = (p + \alpha')(p + \beta')(p + b')(p + c)(p + d) \quad \dots (35)$$

Thus the response  $f(t)$  of the amplifier to a unit step-function voltage can be determined as given below :

$$f(t) = A_1 e^{-\alpha' t} + A_2 e^{-\beta' t} + A_3 e^{-b' t} + A_4 e^{-c t} + A_5 e^{-d t} \quad \dots (36)$$

where the coefficients are found out from equations (32) and (33).

The response  $f(t)$  in equation (36) when multiplied by certain circuit constants, will give the output voltage of the amplifier as a function of time. From this expression of  $f(t)$  it is found that the output voltage consists of a number of terms with negative exponentials. The various RC combinations in the amplifier stage are responsible for these terms.

## SECOND METHOD OF ANALYSIS

In the previous treatment we have not considered the effect of the cathode current on the voltage developed across  $Z_{kg}$  which determined the reduction factor  $A$ . To take this effect into account we shall draw a modified

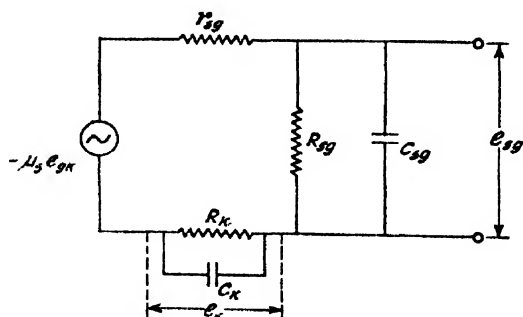


FIG. 9

Equivalent screen grid circuit when the effect of the cathode current is considered.



equivalent screen grid circuit. It will be assumed that plate voltage is sufficient to make the plate current independent of plate voltage. So, though any change in screen circuit voltage affects the plate current, the reverse is not true.

Now the equivalent screen grid circuit is drawn (figure 9) where

$$e_{gk} = \text{grid-cathode voltage} = e_g - e_k$$

and  $e_k$  is the voltage developed across  $Z_k$  due to the flow of plate current and screen current through the cathode impedance. The plate current source has not been shown in figure 9 to avoid complexity.

A simple analysis of the circuit shows that the screen current is given by

$$i_{sg} = \mu_s e_g / r_{sg} + Z_{sg} + Z_k \{1 + \mu_s (K + 1)\} \quad \dots (37)$$

where  $K$  is a factor greater than unity, and is determined by the ratio of plate and screen currents.

To find out the voltage  $e_k$ , the plate current which will vary similarly, may now be conveniently written as

$$i_p = K \cdot \frac{\mu_s e_g}{r_{sg} + Z_{sg} + Z_k \{1 + \mu_s (K + 1)\}} \quad (38)$$

So the actual voltage developed across the cathode impedance due to the flow of  $i_p$  and  $i_{sg}$  through the cathode is given by

$$\frac{\mu_s e_g (K + 1)}{r_{sg} + Z_{sg} + Z_k \{1 + \mu_s (K + 1)\}} \quad (39)$$

which can be expressed as

$$e_k = \frac{\mu_s (K + 1)}{C_k r_{sg}} \cdot e_g \cdot \frac{p + c}{p^2 + 2bp + \omega_0^2} \quad (40)$$

where  $c = 1/R_{sg}C_{sg}$

$$2b = \frac{r_{sg}(R_{sg}C_{sg} + R_k C_k) + R_{sg}R_k C_k + R_k \{1 + \mu_s (K + 1)\} R_{sg}C_{sg}}{R_{sg}C_{sg}R_k C_k r_{sg}}$$

$$\text{and } \omega_0^2 = \frac{r_{sg} + R_{sg} + R_k \{1 + \mu_s (K + 1)\}}{R_{sg}C_{sg}R_k C_k r_{sg}}$$

So leaving out the constant factors, we can express the step-function response of equation (40) as

$$f(t) = \frac{C}{nm} + \frac{(C-m)}{m(m-n)} e^{-mt} + \frac{(C-n)}{n(n-m)} e^{-nt} \quad \dots (41)$$

where  $(-m)$  and  $(-n)$  are the roots of  $p^2 + 2bp + \omega_0^2 = 0$ .

If 1 per cent sag is allowed in time  $t_1$  the relation to be satisfied is

$$\frac{1}{100f t_1} \cdot \frac{df(t)}{dt} \bigg|_{t=0} = 1 \quad (42)$$

If the sag is pronounced, equation (12) will be used to find out the fractional sag.

With the aid of equation (37) the voltage developed across  $Z_{sg}$  can be written as

$$e_{sg} = i_{sg} Z_{sg} \\ = \frac{-\mu_s e_g Z_{sg}}{r_{sg} + Z_{sg} + Z_K \{1 + \mu_s (K + 1)\}} \quad \dots (43)$$

$$= -\frac{\mu_s e_g}{C_{sg} r_{sg}} \cdot \frac{p + c'}{p^2 + 2bp + \omega_0^2} \quad \dots (44)$$

where

$$C' = 1/R_K C_K$$

Equation (44) is similar in form to equation (40). So the step function response  $f(t)$  is given by

$$f(t) = \frac{C'}{mn} + \frac{(C' - m)}{m(m - n)} e^{-mt} + \frac{(C' - n)}{n(n - m)} e^{-nt} \quad \dots (45)$$

The slope of equation (45) at  $t=0$  is given by 1. Hence for 1 per cent sag allowed in time  $t_1$ , we have

$$1/100 t_1 = 1. \quad \dots (46)$$

Three voltage sources may now be taken to be responsible for having marked contribution to the plate current  $i_p$  of the pentode. They are (i) the input voltage  $e_g$  at the grid (ii) the voltage developed across  $Z_{sg}$  and (iii) the cathode voltage  $e_k$  across  $Z_K$ . The total plate current will be the sum of currents resulting from these sources and can, therefore, be written as

$$i_p = G_m e_g + G_{m2} e_{sg} + G_K e_K \quad \dots (47)$$

where

$G_m$  = transconductance of the tube with respect to grid =  $\partial i_p / \partial e_g$

$G_{m2}$  = transconductance of the tube with respect to screen =  $\partial i_p / \partial e_{sg}$   
and

$G_K$  = transconductance of the tube with respect to cathode =  $-\partial i_p / \partial e_K$

From the equivalent plate circuit (figure 6) we have

$$E_0 = i_p \cdot R_L \cdot \frac{p}{p + \beta} \quad \dots (48)$$

where  $\beta = 1/R_g C_g$  and the effect of  $r_p$  and  $C_p$  has been neglected.

Substituting the value of  $i_p$  from equation (47) we find that the step-function response  $f(t)$  is the inverse Laplace transform of

$$F(p) = R_L \left[ G_m \cdot \frac{1}{p + \beta} - G_{m2} \cdot \frac{\mu_s}{C_{sg} r_{sg}} \cdot \frac{1}{p + \beta} \cdot \frac{p + c'}{(p + m)(p + n)} \right. \\ \left. + G_K \frac{\mu_s (K + 1)}{C_K r_{sg}} \cdot \frac{1}{p + \beta} \cdot \frac{p + c}{(p + m)(p + n)} \right] \quad \dots (49)$$

Taking the inverse Laplace transform of equation (49), we have

$$f(t) = A e^{-\beta t} + B e^{-mt} + C e^{-nt} \quad \dots (50)$$

where,

$$A = R_L G_m + R_L \left[ G_{m2} \cdot \frac{\mu_s (\beta - C)}{C_{sq} r_{sq}} - G_K \cdot \frac{\mu_s (K + 1)}{C_{K} r_{sq}} \cdot (\beta - C) \right] \cdot \frac{1}{(m - \beta)(n - \beta)}$$

$$B = R_L \left[ \frac{G_{m2} \mu_s}{C_{sq} r_{sq}} (m - C) - G_K \cdot \frac{\mu_s (K + 1)}{C_K r_{sq}} (m - C) \right] \times \frac{1}{(m - \beta)(m - n)}$$

and

$$C = R_L \left[ \frac{G_{m2} \mu_s}{C_{sq} r_{sq}} (n - C) - G_K \cdot \frac{\mu_s (K + 1)}{C_K r_{sq}} (n - C) \right] \cdot \frac{1}{(\beta - n)(m - n)}$$

The slope of equation (50) at time  $t=0$  is given by

$$\frac{df(t)}{dt} \bigg|_{t=0} = -[\beta A + mB + nC] \quad (51)$$

The slope will be equal to  $\frac{1}{\text{root}_1}$  if 1 per cent sag is allowed in time  $t_1$ .

*Flat-top compensation*: It has been previously stated that the plate-supply decoupling network  $R_d C_d$  is used to compensate for the flat-top distortion. The equivalent circuit is shown in figure 7 where  $i_p$  is given by equation (47). The output voltage  $e_o$  is given by

$$e_o = i_p \cdot R_L \cdot \frac{p(p + \gamma + \beta)}{(p + \alpha)(p + \beta)} \quad (52)$$

where

$$\alpha = \frac{1}{R_d C_d}, \beta = \frac{1}{R_d C_d} \text{ and } \gamma = \frac{1}{R_L C_d}.$$

Inserting the value of  $i_p$ , we find that the step-function response  $f(t)$  is the Laplace transform of

$$F(p) = R_L \left[ G_m \frac{(p + \gamma + \beta)}{(p + \alpha)(p + \beta)} - G_{m2} \frac{p + C'}{C_{sq} r_{sq}} \cdot \frac{(p + \gamma + \beta)}{(p + \alpha)(p + \beta)} \right. \\ \left. + G_K \frac{\mu_s (K + 1)}{C_K r_{sq}} \cdot \frac{(p + C)}{(p^2 + 2bp + \omega_0^2)} \cdot \frac{(p + \gamma + \beta)}{(p + \alpha)(p + \beta)} \right] \quad (53)$$

By means of Heaviside Expansion Theorem, as given in equation (32), the inverse transform of equation (53) can be obtained as given below:

$$f(t) = P e^{-\alpha t} + Q e^{-\beta t} + R e^{-m t} + S e^{-n t} \quad \dots \quad (54)$$

where the constants can be easily found out.

*A comparison of the two methods*: In the first method of analysis we did not consider the mutual interaction of cathode circuit and screen circuit fully, which determines to a great extent the influence of the two circuits on the flow of current in the plate. In the second method we have tried to study this interaction more closely and the procedure followed is more rigorous in this case

For the sake of comparison we shall write down the expressions of the plate current obtained in two ways. In the first method, the plate current is given by

$$\begin{aligned} \frac{i_p}{g_m} = & \frac{a^2\alpha}{b'cd} + \frac{(a-b')(a\alpha - a_0b' + b'^2)}{(-b')(c-b')(d-b')} e^{-b't} \\ & + \frac{(a-c)(a\alpha - a_0c + c^2)}{(-c)(b'-c)(d-c)} e^{-c't} + \frac{(a-d)(a\alpha - a_0d + d^2)}{(-d)(b'-d)(c-d)} e^{-d't} \end{aligned} \quad (55)$$

If the second method is followed, the plate current is given by

$$i_p = G_m e_0 + G_{m2} e_{s\eta} + G_K e_K$$

which can be written as

$$\begin{aligned} \frac{i_p}{G_m} = & \left[ 1 + \frac{G_K \mu_s (K+1)}{G_m C_K r_{s\eta}} \cdot \frac{C}{\omega_0^2} - \frac{G_{m2} \mu_s}{G_m C_{s\eta} r_{s\eta}} \cdot \frac{C'}{\omega_0^2} \right] \\ & \frac{e^{-mt}}{n-m} \left[ \frac{G_K}{G_m} \cdot \frac{\mu_s (K+1)}{C_K r_{s\eta}} \left( 1 - \frac{C}{m} \right) - \frac{G_{m2}}{G_m} \cdot \frac{\mu_s}{C_{s\eta} r_{s\eta}} \left( 1 - \frac{C'}{m} \right) \right] \\ & + \frac{e^{-nt}}{n-m} \left[ \frac{G_{m2}}{G_m} \cdot \frac{\mu_s}{C_{s\eta} r_{s\eta}} \left( 1 - \frac{C}{n} \right) - \frac{G_K}{G_m} \cdot \frac{\mu_s (K+1)}{C_K r_{s\eta}} \left( 1 - \frac{C'}{n} \right) \right] \end{aligned} \quad (56)$$

Equations (55) and (56) have been plotted in figure 10 assuming the following values of the circuit elements :

Type 6AC7 tube

$$\mu_s = 40, r_s = 20 K, C_{s\eta} = 2.5 \mu f,$$

$$R_{s\eta} = 60 K, R_K = 150 \Omega, C_K = 500 \mu f$$

$$G_m = -G_K = 9000 \mu \text{ mhos}, G_{m2} = 225 \mu \text{ mhos and } K=4,$$

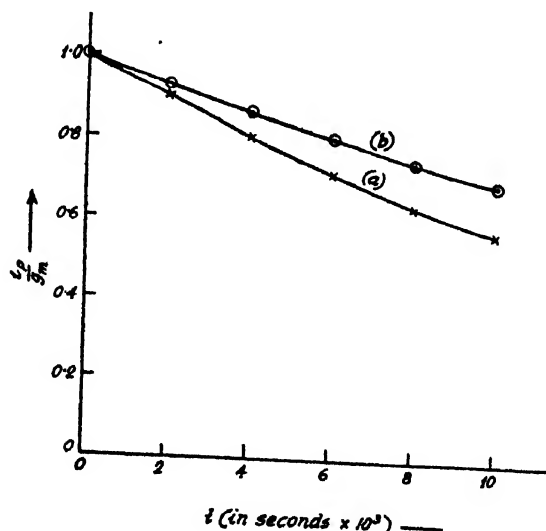


FIG. 10

Plot of plate current with time

(a) for the first method

(b) for the second method

It is clear from figure 10 that both the plate currents predicted by the two methods of analysis of the pulse amplifier are not very much different from each other. The plate current *vs.* time curve shows almost identical exponentially decaying characteristic though the plate current calculated by the more rigorous way of analysis is a bit larger than that found with the help of the first method.

With the help of equations (25) and (50), the output voltage waveform is plotted with time (figure 11) assuming  $R_L = 10K$ ,  $C_\theta = .01 \mu f$ ,  $R_g = 200K$ . The waveforms for the two cases are similar.

That the flat top distortion is very much minimised when the decoupling

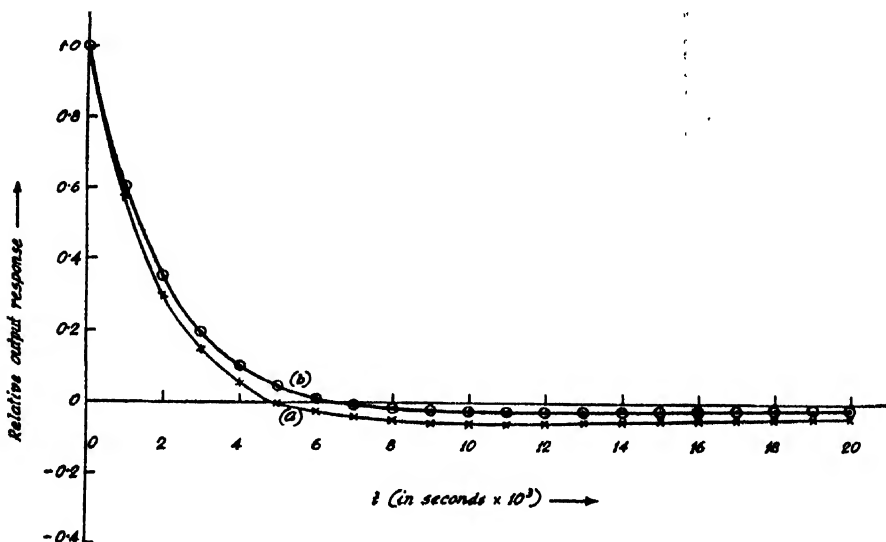


FIG. 11  
Relative output response curve (without decoupling network)  
(a) for the first method, (b) for the second method

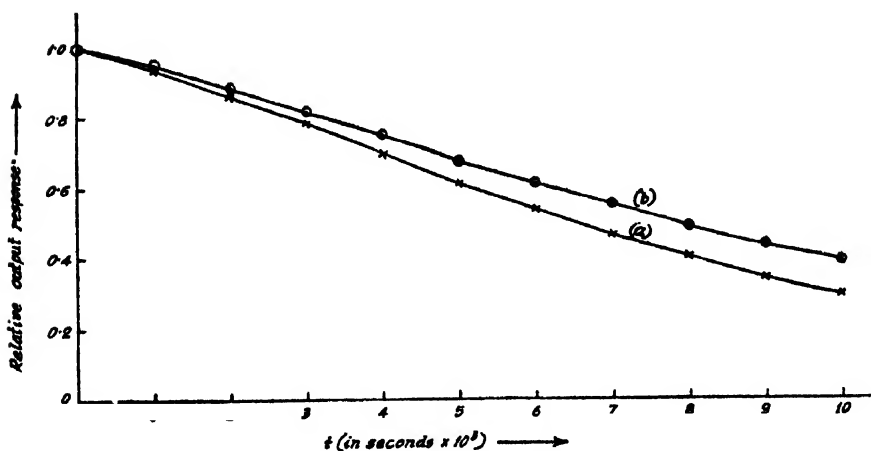


FIG. 12  
Relative output response curve (with decoupling network)  
(a) for the first method (b) for the second method

filter network is used, is shown in figure 12 with the help of equations (36) and (54). The values of the circuits constants chosen are

$$R_L = 2K, R_d = 18K, C_d = 1 \mu f,$$

$$R_g = 200 K \text{ and } C_g = .01 \mu f.$$

There is very little difference between the two sets of results obtained in all these curves for the two methods of analysis. These curves show definitely that any of the two methods may be adopted to analyse a pulse amplifier critically.

#### ACKNOWLEDGMENTS

The author is deeply indebted to Prof. M. N. Saha, D. Sc., F. R. S., for his kind interest in the work. He also wishes to express his grateful thanks to Mr. B. M. Banerjee for suggesting the second method of analysis and for his constant active help. He is also grateful to Dr. B. D. Nag and Dr. A. K. Saha for helpful discussions.

#### REFERENCES

- Gardner, M. F. and Barnes, J. L., 1947, *Transients in linear systems* Vol I.; Wiley, New York.
- Moskowitz and Racker 1951, *Pulse Techniques*.
- Pipes, L. A. 1946, *Applied Mathematics for Engineers and Physicists*, Mc Graw-Hill Book Co, New York.
- Terman, F. E., 1947, *Radio Engineering*.
- Valley, G. E. and Wallman, H., 1948, *Vacuum Tube Amplifiers*, Mc Graw-Hill Book Co, New York.

# ULTRAVIOLET ABSORPTION BANDS OF CRYSTALS OF ORTHO- AND PARADICHLORO BENZENE AND PARADIBROMOBENZENE AT LOW TEMPERATURES\*

By H. N. SWAMY

OPTICS DEPARTMENT, INDIAN ASSOCIATION FOR THE CULTIVATION OF SCIENCE, CALCUTTA

(Received for publication, September 2, 1952)

## Plates V A-C

**ABSTRACT.** The ultraviolet absorption spectra of thin films of *o*-dichlorobenzene in the liquid state at 30°C and in the solid state at -50°C and -180°C and of *p*-dichlorobenzene and *p*-dibromobenzene in the liquid state and in the solid state at 30°C and -180°C have been investigated. In the latter two cases the solid films were also once cooled to -180°C and after bringing them to 30°C their absorption spectra were photographed. In the case of *o*-dichlorobenzene in the liquid state only three bands are observed with intervals of about 1030 cm<sup>-1</sup>. Each of these is split up into two when the liquid is solidified at -50°C, and at -180°C each of the three bands for the liquid is split up into three bands. The intervals between the principal band and the satellites do not agree with any of the vibrational frequencies observed in the case of the vapour. It is suggested that formation of virtual bonds between neighbouring molecules may be responsible for such splitting of the electronic energy level.

In the case of *p*-dichlorobenzene, the liquid as well as the crystal at 30°C yield three broad bands at intervals of about 1030 cm<sup>-1</sup>. When the crystal is cooled to -180°C and again brought to room temperature three more new bands corresponding to the vibration frequency 764 cm<sup>-1</sup> are observed. At -180°C, the number of bands increases owing to the appearance of other new bands corresponding to vibrational frequency 569 cm<sup>-1</sup>. In the case of *p*-dibromobenzene, the solid at 30°C either before or after once being cooled to -180°C exhibits bands similar to those observed in the case of the liquid. When the solid is cooled to -180°C the bands become sharp and extra bands corresponding to vibrational frequencies 329, 537, 693, 1004, 1202 and 1431 cm<sup>-1</sup> appear. The appearance of these extra bands in both the cases is assumed to be due to sharpening of the broad bands caused by the cessation of angular oscillations at -180°C. It is suggested that formation of virtual bonds may be responsible for the damping of angular oscillations at low temperatures.

## INTRODUCTION

The ultraviolet absorption spectra of several substituted benzene compounds in the liquid state above their melting points and in the solid state at low temperatures were studied previously (Swamy, 1951, 1952 *a*, 1952 *b*) and it was observed that in some cases changes take place in the number and position of the bands with solidification of the liquid and subsequent lowering of the temperature, while in other cases only the bands observed in the case of the liquid shift slightly with solidification of the liquid. Besides these changes, the solidification and cooling down to -180°C

\* Communicated by Prof. S. C. Sirkar.

of *o*-dichlorobenzene and *m*-chlorotoluene were observed to bring about a splitting of the electronic energy levels of these molecules (Sirkar and Swamy 1952, Swamy 1952 c). In *o*-chlorotoluene the two new components were on the two sides of the principal band while in *m*-chlorotoluene both the new components were on the longer wavelength side. Also, the absence of such splitting of the energy level in the case of *p*-chlorotoluene led to the conclusion that splitting of the electronic energy level depends on the relative positions of the substituent groups and does not take place when the permanent electric moment is small. Kronenberger (1930), however, had previously observed that in the case of benzene, the *o-o* transition, which is forbidden in the vapour state, appears at  $-180^{\circ}\text{C}$ . It was pointed out (Sirkar and Swamy, 1932) that this might be due to the distortion of the molecule and absence of the centre of symmetry in the solid state at  $-180^{\circ}\text{C}$ .

Ortho- and para-dichlorobenzene are other examples of disubstituted benzene molecules, one having a strong permanent electric moment and the other having no such moment. The para compound is interesting for the reason that in the solid state just below its melting point the substance yields new Raman lines in the low frequency region, the positions of these lines depending on whether the substance has once been cooled in ice or not (Vuks 1936, Sirkar and Gupta, 1936, Sirkar and Ray, 1951). It was thought worthwhile to investigate whether the electronic energy level of the molecule undergoes any change with such cooling in ice and whether the changes observed in these absorption bands with lowering of temperature upto  $-180^{\circ}\text{C}$  throw any light on the changes in the positions of the Raman lines in the low-frequency region which take place with the lowering of temperature upto  $-180^{\circ}\text{C}$ . The absorption spectra of *p*-dichlorobenzene in different states and at different temperatures have therefore been investigated and the results have been discussed in the present paper. The absorption spectra of *p*-dibromobenzene in different states and at different temperatures have also been studied to find out whether these are similar to the spectra observed in the case of *p*-dichlorobenzene. The results for *o*-dichlorobenzene briefly reported earlier (Sirkar and Swamy, 1952) have also been discussed in detail in this paper.

#### EXPERIMENTAL

The experimental arrangement is that employed in earlier investigations by the author (Swamy, 1951, 1952). A hydrogen discharge tube running at 3 K. V. served as the source of continuous spectrum. Spectrograms were taken on Ilford HP 3 films with a Hilger E. I spectrograph having a dispersion of 3 Å. U. per mm in the region, 2600 Å. Chemically pure substances distilled under vacuum were used in this investigation.

Paradibromobenzene was obtained from Merck's original packing and the other two substances were obtained from U. S. A. In each case a film



of thickness about 0.2 mm was found to produce absorption bands in the near ultraviolet region. For recording absorption spectra of *p*-dichlorobenzene, and *p*-dibromobenzene in the liquid state the two quartz plates between which the film was produced were held in a brass frame which was suspended at the centre of a heater, the current through the heating coil being adjusted so that the temperature at the centre of the heater was just above the melting point of the substance under study. Absorption spectra in the solid state at  $-180^{\circ}\text{C}$  were photographed with the technique described previously (Swamy 1951, 1952). An exposure of about 12 minutes was required to record the spectrum for the liquid state and for the solid state at room temperature, while the exposure required to record the spectra for the solid at  $-180^{\circ}\text{C}$  was about 40 minutes. For comparison, mercury arc spectrum was recorded with the help of Hartmann diaphragm on each spectrogram.

TABLE I

Absorption bands of *o*-dichlorobenzene;  $\nu$  in  $\text{cm}^{-1}$ .

Vapour (Prominent bands) Spomer, 1949.		Present author						
		Liquid at 30°C	Assign- ment	Solid at -50°C		Solid at -180°C	Assign- ment	
36230 vs	$\nu_0$	35848 (vs) broad	$\nu_0$	35933 (s)	$A_0$	35587 (m) 35939 (vs)	$C_0$ $A_0$	
36545 ms	$\nu_0 + 315$			36368 (w)	$B_0$	36399 (m) 36636 (m)	$B_0$ $C_1$	
36615 ms	$\nu_0 + 385$	36876 (v-) broad	$\nu_0 + 1028$			36971 (s)	$A_1$	36983 (vs)
36670 vs	$\nu_0 + 440$							
36840 ms	$\nu_0 + 610$			37403 (w)	$B_1$	37450 (m)	$B_1$	
36954 m	$\nu_0 + 724$							
37062 ms	$\nu_0 + 832$					37690 (vw)	$C_2$	
37110 ms	$\nu_0 + 880$							
37187 ms	$\nu_0 + 957$			38000 (m)	$A_2$	38036 (s)	$A_2$	
37250 s	$\nu_0 + 1010$							
37319 vs	$\nu_0 + 1089$					38447 (vw)	$B_2$	
37420 w	$\nu_0 + 880 + 315$							
37504 w	$\nu_0 + 832 + 440$	37910 (m)	$\nu_0 + 2 \times 1031$	38447 (vw)	$B_2$	$B_2$		
37563 w	$\nu_0 + 1020 + 315$							
37631 m	$\nu_0 + 957 + 440$			39030 (w)	$A_3$		39081 (s)	$A_c$
37719 m	$\nu_0 + 880 + 610$							
37759 w	$\nu_0 + 1089 + 440$							
38159 m	$\nu_0 + 2 \times 957$							
38215 s	$\nu_0 + 1020 + 957$							
38275 vs	$\nu_0 + 2 \times 1020$							
38395 ms	$\nu_0 + 2 \times 1089$							



TABLE III

 Absorption bands of *p*-dibromobenzene;  $\nu$  in  $\text{cm}^{-1}$ .

Vapour, (Sreenan & Murthy 1951), Prominent bands	Present author			
	Liquid, $9^\circ\text{C}$	Assignment	Solid, $30^\circ\text{C}$	Assignment
35643 s	35560 (sb)	$\nu_0$	35362 (vsb)	$\nu_0$
36113 ms	36268 (sb)	$\nu_0 + 1002$	36380 (S)	$\nu_0 + 1018$
36320 ms				
36657 m				
36787 w				
37071 m				
37092 m	37290 (m)	$\nu_0 + 2 \times 1010$	37400 (s)	$\nu_0 + 2 \times 1019$
37660 w				
37751 vw				
38106 w				
38299 vw				

$\nu_0$   
 $\nu_0 + 329$   
 $\nu_0 + 537$   
 $\nu_0 + 693$   
 $\nu_0 + 1004$   
 $\nu_0 + 1202$   
 $\nu_0 + 1004 + 329$   
 $\nu_0 + 1431$   
 $\nu_0 + 1004 + 537$   
 $\nu_0 + 1004 + 693$   
 $\nu_0 + 2 \times 1005$   
 $\nu_0 + 1202 + 1004$   
 $\nu_0 + 1431 + 1004$   
 $\nu_0 + 2 \times 1004 + 693$   
 $\nu_0 + 3 \times 1004$   
 $\nu_0 + 2 \times 1004 + 1202$   
 $\nu_0 + 2 \times 1004 + 1432$   
 $\nu_0 + 3 \times 1004 + 693$   
 $\nu_0 + 2 \times 1202 + 1004 + 693$

## RESULTS

Spectrograms for *o*-dichlorobenzene in the liquid state at 30°C and solid state at -50°C and -180°C are reproduced in figures 1-3, Plate VA. Spectrograms for *p*-dichlorobenzene in the liquid state at 60°C and in the solid state at 30°C and -180°C as well as for the sample at 30°C after it had been once cooled to -180°C are also included in Plate VA (figures, 4-7). Microphotometer records of the absorption spectra of *p*-dibromobenzene in the liquid state at 90°C as well as in the solid state at 30°C and -180°C are reproduced in figure 8 (Plate VB), and those for *o*- and *p*-dichlorobenzene in figures 9 and 10 (Plate VC). Measurements were made for the centre of the absorption peak, as the bands are broad. The wave numbers of the principal bands observed by previous workers for the vapour state are included in Tables I, II and III in which the wave numbers of the bands observed in the present investigation are given. Assignments for the absorption bands of *o*-dichlorobenzene in the solid state at -180°C have been made on the assumption that the electronic energy level is split up into three components.

## DISCUSSION

(a) *Orthodichlorobenzene.*

The spectrograms published by Sponer (1942) for the absorption spectra of *o*-dichlorobenzene in the vapour state show that the  $\nu_0$  band is at 36230  $\text{cm}^{-1}$ . The band is very strong in agreement with the fact that the  $o \rightarrow o$  transition is allowed in this case. There are also prominent bands at 36670, 37250 and 37319  $\text{cm}^{-1}$  which can be assigned as  $\nu_0 + 440$ ,  $\nu_0 + 1020$  and  $\nu_0 + 1089$   $\text{cm}^{-1}$ . There are, however, companions on the red side of all the main bands at least two of which are probably due to  $v \rightarrow v$  transitions, their separations from the principal ones being only 25 and 60  $\text{cm}^{-1}$  respectively.

In the present investigation the substance produces only three broad bands in the liquid state, the  $\nu_0$  band being at 35848  $\text{cm}^{-1}$ . The fine structure found in the vapour state is absent. The centres of the bands are separated by intervals of 1030  $\text{cm}^{-1}$ . In the solid state at -180°C the substance produces four intense bands marked  $A_0$ ,  $A_1$ ,  $A_2$  and  $A_3$ . Each of the first three of the above bands is accompanied by two fainter bands, one on each side marked  $C_0$ ,  $B_0$ ;  $C_1$ ,  $B_1$  and  $C_2$ ,  $B_2$  respectively. The fainter band on the longer wavelength side of the first principal band at 35587  $\text{cm}^{-1}$  cannot be due to a  $v \rightarrow o$  transition, as the distance between the two bands is about 352  $\text{cm}^{-1}$ , and at -180°C the number of molecules present in the excited state in this mode of vibration is negligible. It is to be concluded that the electronic energy level is split up into three components in the case of the substance in the solid state at -180°C. The assignments made on the basis of this assumption are given in Table I. The companions of

Fig. 1

.. 3

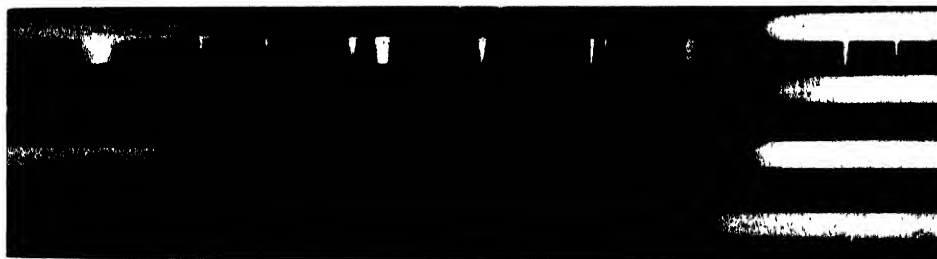


Fig 4

.. 5

.. 6

.. 7



Hg 2537Å

Hg 2652Å

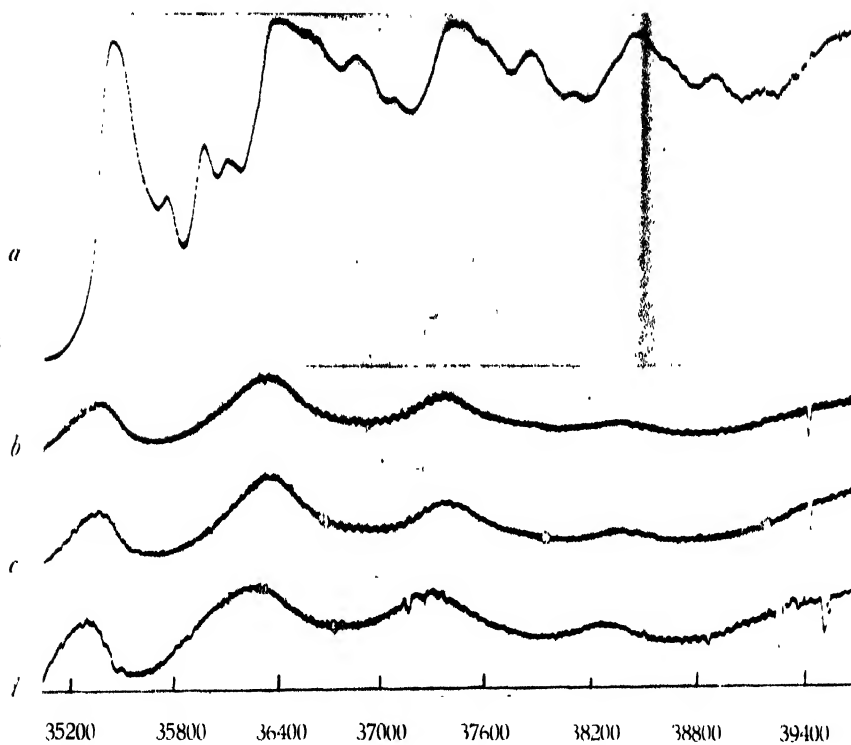
Hg 2752.9Å

## Ultraviolet absorption spectra

1. Ortho dichlorobenzene - liquid at 30°C
2. " " solid .. - 50°C
3. " " solid .. - 180°C
4. Para dichlorobenzene - liquid .. 60°C
5. " " solid .. 30°C
6. " " " " 30°C after cooling  
to - 180°C
7. " " " " - 180°C



Fig 8

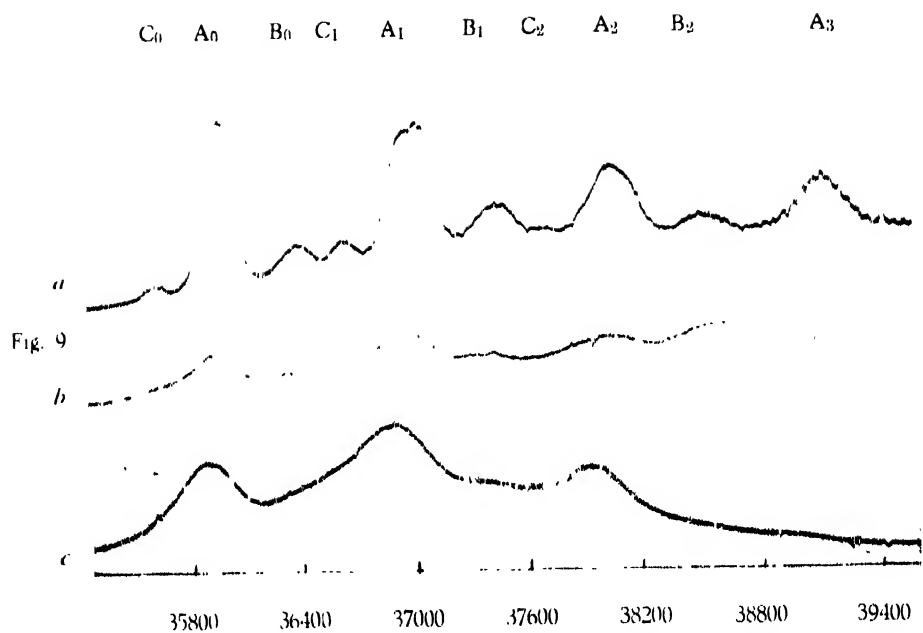


(a) *p*-Dibromobenzene, solid at -180°C

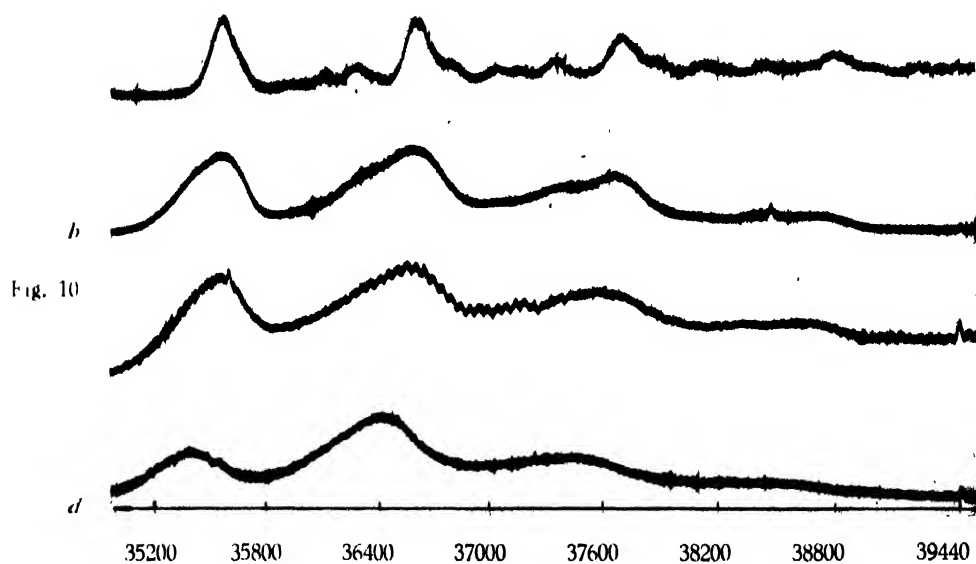
(b) " " " " 30°C after cooling  
to -180°C

(c) " " " " 30°C

(d) " " liquid at 90°C



- (a) *o*-Dichlorobenzene, solid at -180°C  
 (b) " " " " about -50°C  
 (c) " " liquid at -30°C



- (a) *p*-Dichlorobenzene, solid at -180°C  
 (b) " " " " 30°C after cooling to -180°C  
 (c) " " " " 30°C  
 (d) " " liquid at 60°C



the principal absorption bands are much feebler than the main bands. Similar phenomenon has been observed in the case of benzene in the solid state at  $-259^{\circ}\text{C}$  by Kronenberger (1930). The  $0,0$  band of benzene which is forbidden in the vapour state appears strongly at  $-180^{\circ}\text{C}$ , and at  $-259^{\circ}\text{C}$  owing to the interaction of neighbouring molecules, the energy level is split up. The splitting of the energy level and the destruction of the symmetry of the electronic configuration in the benzene ring cannot be due to Van der Waals' forces in the lattice. This phenomenon may be due to the formation of virtual bonds between neighbouring molecules in the lattice as concluded from the results of study of the Raman spectra of benzene by Sirkar and Ray (1950). Such virtual bonds are more likely to be formed in the case of *o*-dichlorobenzene, as the molecule is strongly polar and the splitting of the energy level in this case also may be due to formation of such virtual linkages. The large shift of the  $\nu_0$  band towards longer wavelengths, which takes place with solidification of the substance, probably indicates that such an association of the molecules takes place in the lattice.

The absorption spectrum of the solid at  $-50^{\circ}\text{C}$  indicates that besides the bands corresponding to those for the liquid state, there are four extra feeble bands, as shown in Table I and these can be accounted for by assuming that the energy level is split up into two components giving bands of unequal intensities. As the temperature of the solid is lowered, probably besides the close neighbours, the distant neighbours also exert influence on the energy level of each molecule, producing thereby a third component of the level.

The intermolecular field in the liquid state also is expected to have some influence on the electronic energy level. The molecules, however, have greater freedom for rotational oscillation in the liquid state and this oscillation is likely to broaden the level. The large width of the absorption bands observed in the case of the liquid actually corroborates this view. The splitting of the level in the solid state at  $-180^{\circ}\text{C}$ , however, shows that some fundamental change takes place in the intermolecular field with solidification and this may be due to formation of virtual bonds among neighbouring molecules as stated above. The frequency-difference between successive bands for the liquid state is about  $1030\text{ cm}^{-1}$  and for the solid state it is about  $1044\text{ cm}^{-1}$ . This discrepancy may be due to the large width of the bands in the former case. The value  $1044\text{ cm}^{-1}$  for the solid state, however, is about the mean of the two frequencies  $1020\text{ cm}^{-1}$  and  $1089\text{ cm}^{-1}$  observed in the case of the vapour. The results of this investigation confirm the view mentioned in an earlier paper (Swamy, 1952c) that the splitting of the electronic energy level depends on the position of the substitution group and takes place in this isomer since the dipole moment has a large value *viz.*,  $2.4 - 2.5\text{D}$  (Spouer, 1942).

(b) *Paradichlorobenzene.*

The data given in Table II show that in the case of *p*-dichlorobenzene the new absorption bands which appear when the solid is cooled down to  $-180^{\circ}\text{C}$  can be explained satisfactorily on the assumption that these are due to transitions to upper vibrational levels in the excited state. In this case there is no band on the longer wavelength side of the  $\nu_0$  band, and therefore, it is concluded that no splitting of the energy level with lowering of temperature occurs in this particular case. This may be due to the absence of permanent electric moment in the molecule. In the case of benzene also the splitting of electronic energy level occurs only at  $-259^{\circ}\text{C}$  and no such splitting is observed at  $-180^{\circ}\text{C}$  (Kronenberger, 1930). The vibrational frequencies derived from the absorption spectrum in the solid state at  $-180^{\circ}\text{C}$  are slightly different from those derived from the absorption spectrum of the vapour (Sponer, 1942).

It is observed from a comparison of the data in Table II and the microphotometric records reproduced in figure 10, that the absorption spectra of *p*-dichlorobenzene in the liquid state and in the solid state at  $30^{\circ}\text{C}$  are similar, but in the case of the solid the bands shift by about  $210\text{ cm}^{-1}$  towards shorter wavelengths from their respective positions in the case of the liquid. The bands are broad and diffuse in both the cases. When, however, the solid is once cooled in liquid air and brought to  $30^{\circ}\text{C}$ , extra bands corresponding to the transitions  $\nu_0 + 764$  and  $\nu_0 + 1031 + 764$  are observed. On further cooling down the solid to  $-180^{\circ}\text{C}$ , the bands become narrower and additional feeble bands corresponding to the vibrational frequency  $569\text{ cm}^{-1}$  appear. On comparing the position of the  $\nu_0$  band observed in the case of the liquid with that observed for the vapour (Sponer, 1942), it is found that the band shifts by about  $400\text{ cm}^{-1}$  towards longer wavelengths with the liquefaction of the vapour. This shows that the intermolecular field has much influence on the electronic energy level. The molecules are expected to execute angular oscillation in the liquid and the intermolecular field acting on each molecule may fluctuate resulting in the broadening of the electronic energy level of the molecule in the liquid state. As all the bands become broad due to such a cause, the feeble bands are not resolved and only the intense bands appear as broad bands. In the case of the solid at  $30^{\circ}\text{C}$  also the bands are observed to be broad and therefore it is to be concluded that such angular oscillations of about the same amplitude are present also in the case of the solid at  $30^{\circ}\text{C}$ . When, however, the solid is once cooled in liquid oxygen and brought to  $30^{\circ}\text{C}$  again, the bands become a little sharper owing probably to cessation of such angular oscillation about one of the axes. Consequently, the bands become slightly narrower, so that the bands corresponding to the vibration frequency  $764\text{ cm}^{-1}$  are resolved from those due to the vibration frequency  $1031\text{ cm}^{-1}$ . When the solid is cooled down to  $-180^{\circ}\text{C}$  the amplitude of the angular oscillations diminishes to a very small value, and therefore, the fluctuation of the intermolecular field is negligible. Conse-

quently, the bands become very narrow and the feeble bands are observed in this case owing to their sharpness. This sharpness of the bands of *p*-dichlorobenzene in the solid state at  $-180^{\circ}\text{C}$  thus indicates almost complete cessation of angular oscillations of the molecules in the lattice at this low temperature.

It would be interesting to compare these changes observed in the absorption bands with lowering of temperature of the solid with those observed in the positions and intensities of the Raman lines in the low frequency region (Sirkar and Gupta, 1936 ; Ray, 1952). It is observed that the number of these lines increases and the frequency-shifts and intensities of some of them increase with the cooling down of the solid to  $-180^{\circ}\text{C}$ . These changes as well as the large diminution of the amplitude of angular oscillation indicated by the changes observed in the absorption spectra definitely contradict the hypothesis that the Raman lines are due to angular oscillation of the molecules in the lattice. The diminution of the amplitude of angular oscillation may be due to linking up of neighbouring molecules through virtual bonds and the results obtained in the present investigation corroborate the hypothesis put forward by Sirkar (1937) that the new Raman lines in the low frequency region may be due to vibrations in associated groups of molecules.

(c) *p*-dibromobenzene.

The data reported by Sree Ramamurthy (1951) for the absorption spectra of *p*-dibromobenzene in the vapour state show that the  $\nu_0$  band which is allowed in the present case is at  $35643\text{ cm}^{-1}$ . There are other strong bands at  $36113$ ,  $36657$ ,  $37092\text{ cm}^{-1}$  which have been assigned as  $\nu_0 + 470$ ,  $\nu_0 + 1014$  and  $\nu_0 + 1449\text{ cm}^{-1}$ . There are of course close lying bands on the longer wavelength side of all the strong bands.

In the present investigation, the substance is observed to produce four broad bands in the liquid state. The  $\nu_0$  band is at  $35260\text{ cm}^{-1}$ , being shifted by about  $400\text{ cm}^{-1}$  towards longer wavelength side from the position in the vapour state. The centres of the bands are separated by  $1008\text{ cm}^{-1}$ . In the solid state at  $30^{\circ}\text{C}$  again, the same four bands are observed, but their positions are shifted by about  $100\text{ cm}^{-1}$  towards shorter wavelengths. The absorption spectrum of the sample brought to room temperature after once being cooled to  $-180^{\circ}\text{C}$ , is exactly identical with that for the solid at room temperature which has not been cooled down below  $0^{\circ}\text{C}$ . This behaviour of the substance is different from that observed in the case of *p*-dichlorobenzene, because in the latter case new bands appear if the crystal is once cooled to  $-180^{\circ}\text{C}$  and again brought to room temperature. In the solid state at  $-180^{\circ}\text{C}$ , *p*-dibromobenzene produces a large number of bands. The position of the  $\nu_0$  band shifts by about  $80\text{ cm}^{-1}$  from its position in the solid state at  $30^{\circ}\text{C}$ . The first four bands just on the higher frequency side of the  $\nu_0$  band can be assigned as  $\nu_0 + 320$ ,  $\nu_0 + 537$ ,  $\nu_0 + 693$  and  $\nu_0 + 1004\text{ cm}^{-1}$ . After this we get new frequencies giving bands at  $\nu_0 + 1202$  and  $\nu_0 + 1431\text{ cm}^{-1}$ .

The band at  $\nu_0 + 1004 + 329 \text{ cm}^{-1}$  is very feeble and the band  $\nu_0 + 1004 + 537 \text{ cm}^{-1}$  is just separated from the band at  $\nu_0 + 1431 \text{ cm}^{-1}$ . The bands  $\nu_0 + 2 \times 1004 + 537 \text{ cm}^{-1}$  and  $\nu_0 + 3 \times 1004 + 537 \text{ cm}^{-1}$  are not separated from the adjacent bands corresponding to the vibrational frequency  $1431 \text{ cm}^{-1}$  probably because the frequency  $537 \text{ cm}^{-1}$  becomes a little lower in these cases. The large width of the bands in the case of the solid at  $30^\circ \text{ C}$  may be due to angular oscillations, as in the case of *p*-dichlorobenzene. The appearance of new sharp bands at  $-180^\circ \text{ C}$  may also be due to cessation of such angular oscillation at the low temperature.

The difference between the behaviour of the crystals of *p*-dichlorobenzene and *p*-dibromobenzene once cooled to  $-180^\circ \text{ C}$  and brought to  $30^\circ \text{ C}$  may be due to the difference in the chemical affinity of the two halogen atoms, the bromine atom being less reactive than chlorine atom. It may also be due to difference in their crystal structure. The absorption bands are equally broad both in the liquid and the solid states, but in the latter case the  $\nu_0$  band has its position shifted by  $100 \text{ cm}^{-1}$  towards shorter wavelengths from its position in the former case. So this indicates a change in the intermolecular field with solidification. It is also known that new Raman lines appear with solidification. Their absence in the liquid state and appearance in the solid state are thus connected with this change in the intermolecular field with solidification. It is not unlikely that formation of virtual bonds is responsible for the apparent change in the intermolecular field and the appearance of new Raman lines in the low frequency region. The fluctuation of the intermolecular field due to angular oscillation of the molecules is probably responsible for broadening of the absorption bands as well as of the new Raman lines and cessation of such fluctuation at low temperatures probably causes sharpening of the bands and the Raman lines. This view is corroborated by the fact that in the absence of intermolecular field the absorption bands are sharp, as in the case of vapour,

The investigations are being continued with other substances and the results will be reported shortly.

#### ACKNOWLEDGMENTS

The author is indebted to Prof. S. C. Sirkar, D. Sc., F. N. I., for his kind interest and helpful guidance throughout the progress of the work and to the Govt. of India, for the award of a scholarship,

#### REFERENCES

- Kronenberger, A., 1930, *Z. f. Phys*, **63**, 494.
- Ray, A. K., 1952, *Ind. J. Phys.*, **28**, 226.
- Sirkar, S. C., 1936, *Ind. J. Phys*, **10**, 110.
- Sirkar, S. C., 1937, *Ind. J. Phys.*, **11**, 343.
- Sirkar, S. C., and Gupta, J., 1936, *Ind. J. Phys.*, **10**, 473.
- Sirkar, S. C., and Ray, A. K., 1950, *Ind. J. Phys.*, **24**, 189.

- Sirker, S. C., and Ray, A. K. 1951, *Ind J Phys*, **25**, 489  
Sirker, S. C., and Swamy, H. N., 1952, *J Chem. Phys*, **20**, 1177  
Sponer, H., 1942, *Rev. Mod Phys*, **14**, 229.  
Sreeramamurthy, C. 1951, *Current Science*, **20**, 176.  
Swamy, H. N., 1951, *Ind J Phys.*, **25**, 262.  
Swamy, H. N., 1952a, *Ind J. Phys.* **26**, 119.  
Swamy, H. N., 1952b, *Ind. J Phys*, **26**, 223.  
Swamy, H N, 1952c, *Ind J. Phys.*, **28**, (in press)  
Vuks, M, 1936, *Comptes Rendus. (De Klady)* **1**, 73.



# CHANGE OF FREQUENCY OF RESONANCE LINES OF SODIUM DURING TRANSMISSION THROUGH SODIUM VAPOUR

By G. S. KASTHA

OPTICS DEPARTMENT, INDIAN ASSOCIATION FOR THE CULTIVATION  
OF SCIENCE, CALCUTTA 32

(Received for publication, November 15 1952)

## Plate VI

**ABSTRACT.** The structure of the D-lines of sodium filtered through an absorption cell containing sodium vapour at temperatures ranging from  $465^{\circ}\text{K}$  to  $563^{\circ}\text{K}$  and pressures ranging from  $8.4 \times 10^{-5}$  to  $9.1 \times 10^{-3}$  mm. of Hg has been studied using a 12 ft. concave grating spectrograph in its third order. It has been observed that at lower temperatures and pressures the transmitted D-lines appear as doublets owing to the absorption of the central part and that as the pressure is increased the distance between the components of each doublet increases rapidly, so that at a pressure of  $9.1 \times 10^{-3}$  mm the distance from resonance is  $1.13 \text{ cm}^{-1}$  for  $\text{D}_1$  and  $1.58 \text{ cm}^{-1}$  for  $\text{D}_2$ . It is pointed out that in the incident radiation filtered through Hg vapour at a pressure of about  $10^{-4}$  mm of Hg, there is no intensity at these distances from resonance and therefore this alteration in frequency takes place in a process of absorption of the quantum just before collision and its re-emission at the instant of collision.

## INTRODUCTION

It was observed previously (Kastha, 1949) that when the mercury resonance line  $2537 \text{ \AA}$  is passed through an absorbing layer of mercury vapour and the line is examined with a high dispersion spectrograph the line appears as a doublet, the separation between the components of which depends upon the temperature of the absorption cell containing the drop of mercury used to produce the absorbing layer of mercury vapour. At a temperature of about  $100^{\circ}\text{C}$  the separation between the two components is about  $18.6 \text{ cm}^{-1}$ . It was further observed that the intensity of the two components in the doublet diminishes very rapidly with the increase of temperature of the absorption cell and at about  $100^{\circ}\text{C}$  the  $2534 \text{ \AA}$  line is found to be many times more intense than the total intensity of the components of the doublet at  $2537 \text{ \AA}$ . It was pointed out that such a broadening of the  $2537 \text{ \AA}$  line could not be explained on the hypothesis that it was a Doppler broadening. Previous investigations on the resonance line of mercury are so numerous that it would appear to be almost impossible that the facts mentioned above had been overlooked by previous workers.

\* Communicated by Prof. S. C. Sirkar

Although the absorption coefficient of the resonance line given out by a resonance cell has been measured using a photo-electric cell by several previous workers (e.g., Kunze, 1928, Fairbrother and Tuck, 1936 etc.), the width of the resonance lines of sodium in absorption was studied using a high dispersion instrument only by Korff (1932), who used a 30 ft. concave grating for the purpose. He, however, used a continuous radiation as the incident light and the phenomenon mentioned above in the case of the mercury resonance line could not be observed with such an arrangement. Zehden (1933) separated the two D-lines by using two double image prisms and a quartz plate, but the thickness of the absorbing layer was such that only a small fraction of the whole intensity was absorbed in order that the absorption coefficient could be measured. So, the phenomenon mentioned above could not be observed with such an arrangement. It was, therefore, thought worth while to investigate whether the D-lines of sodium filtered through sodium vapour at different temperatures show a structure similar to that observed (Kastha, 1949) in the case of the Hg line 2537 Å. The results obtained in such an investigation are discussed in the present paper.

#### EXPERIMENTAL

The absorption cell was made of Pyrex glass tubing with windows at the two ends made approximately plane and parallel by carefully blowing the molten ends. Two side tubes were provided through one of which the cell was connected to the sodium distillation apparatus and the other was connected to the pump system. The distillation apparatus consisted of three small bulbs of Pyrex glass joined in a line with Pyrex glass tubing one after another. Metallic sodium carefully purified was introduced through a side tube into the first of the three bulbs by evaporation under vacuum and a small quantity of the metal was introduced in the absorption tube by successive distillation in the other two bulbs. The absorption cell was then sealed off at the constrictions in the two side tubes. Two such absorption cells, one of length 12 cms and the other 5 cms were used.

The absorption cell was placed axially in a cylindrical heating oven the temperature of which could be controlled by varying the current through its heating coil. The temperatures for different currents were measured with a gas-filled mercury thermometer. Light from an Osram sodium vapour lamp made parallel with a lens passed through the absorption cell. It was then focussed on the slit of a grating spectrograph with a second lens.

In the former investigation (Kastha, 1949) on the absorption of resonance line of mercury filtered through mercury vapour, the dispersing medium used was an E<sub>1</sub>-Hilger quartz spectrograph. The dispersion was quite high, being about 3 Å/mm. at 2536 Å. In the present case no such spectrograph could be used due to very low dispersion in the region of 5890 Å. So, a 12 ft.



concave grating (Littrow type) having a ruled surface about 5 inches long was used in the third order. The dispersion in this order is about 1.5 A.U. per mm. The grating gives strong ghost lines in the neighbourhood of the principal maxima, but fortunately, these ghost lines due to anyone of the  $D_1$  and  $D_2$  lines of Na do not overlap on either the principal maximum or the ghost lines of the other wavelength. The width of the slit used was .05 mm and its length was about 1 cm. The theoretical resolving power of the grating is about 120,000 in the third order. Gevaert panchromatic plates were used to photograph the lines, the exposures ranging from 1 hour to 10 hours.

First, the width of the line emitted by the Osram sodium lamp was examined by photographing the D-lines produced in the third order of the grating. The width was found to be less than 0.10 A.U. The longer absorption tube was first used and the D-lines transmitted by the cell at different temperatures from 185°C to 265°C were photographed with exposures ranging from 1 to 3 hours. Next, the investigation was repeated with the shorter absorption cell, the temperature being raised in this case upto 290°C. Three photographs of the D-lines were also taken on the same plate with an exposure of 1 hour in each case, the temperatures of the absorption cell being 185°C, 198°C and 217°C, respectively. The strongest of the ghost lines accompanying each of the  $D_1$  and  $D_2$  lines was recorded with moderate density in each of these photographs so that the width of the transmitted line and its structure could be determined. Microphotometer traces were also taken with a self-recording Moll microphotometer of Kipp and Zonen type and the separation of the components of the transmitted doublets was determined in each case from these records. The separation was also measured with an Adam-Hilger comparator.

#### RESULTS AND DISCUSSION

Some of the spectrograms obtained with different temperatures of the absorption cell and enlarged four times are reproduced in Plate VI. In figures 7 and 8 the spectrograms obtained with an exposure of one hour and with the absorption cell at 198°C and 217°C respectively are also reproduced. The separations of the components in the doublets produced by the absorption of  $D_1$  and  $D_2$  lines for different temperatures of the cell are given in Table I. The vapour pressures of Na at these temperatures have been calculated from the formula (Ladenburg and Thiele, 1930)

$$\log p = \frac{-26077}{4.573 T} - 1.178 \log T + 11.329$$

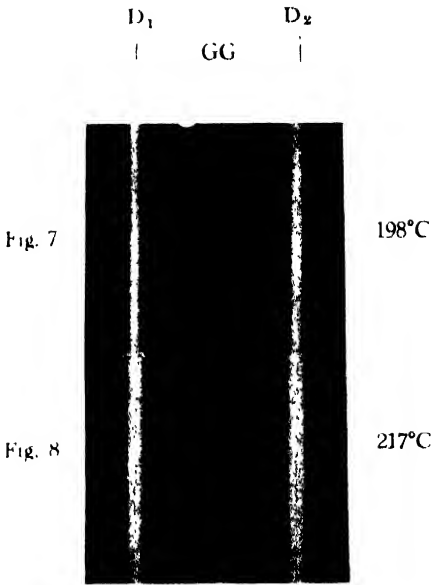
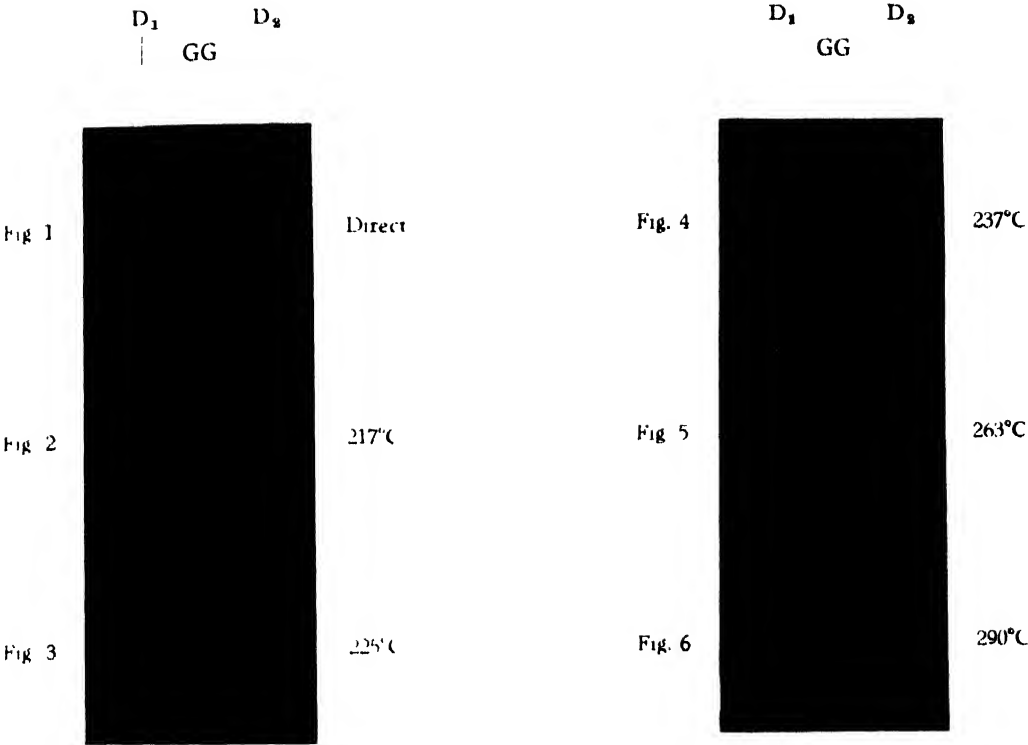
These vapour pressures are given in Table I. In order to find out whether there is any simple relation between the vapour pressure and the separation, the logarithms of separations have been plotted against the logarithms of vapour pressures in figure 9.

TABLE I

$T = \text{Temperature}$ in $^{\circ}\text{K}$	Vapour pressure $p$ in mm. of Hg.	Separation in $\text{cm}^{-1}$	
		$D_1$	$D_2$
465	$8.4 \times 10^{-5}$	.252	347
471	$1.18 \times 10^{-4}$	.315	.428
478	$1.75 \times 10^{-4}$	.347	.518
490	$3.38 \times 10^{-4}$	.482	.653
498	$5.18 \times 10^{-4}$	.630	.792
510	$9.1 \times 10^{-4}$	.752	.977
536	$2.98 \times 10^{-3}$	1.175	1.643
563	$9.1 \times 10^{-3}$	2.250	3.150

It can be seen from figures 1-6 that the separations between the components of the doublet formed by the  $D_1$  and  $D_2$  lines filtered through sodium vapour increases with temperature of the cell. Since the increase in temperature is small the increase in separation is evidently due to increase in the pressure of the vapour inside the absorption cell.

The curves in Fig. 9 show that the separation increases linearly with the pressure. It is, of course, evident from the figures that the intensity of the components in the doublet also diminishes with increase in pressure of the absorbing vapour, but a comparison of figures, 7 and 8 clearly shows that at a distance equal to that of the centre of the component observed with the absorption cell at  $217^{\circ}\text{C}$  from the centre of the doublet there is no appreciable intensity in the doublet obtained with the cell at  $198^{\circ}\text{C}$  (Fig 7). This can be clearly seen from a comparison of the ghosts between the principal lines in figures 7 and 8. Since the exposure is the same in both the cases, and the components of the doublet in figure 8 appear at the position at which there is no intensity in the incident line, the change of frequency of the transmitted line observed in figure 8 is caused by the absorbing vapour. This phenomenon is different from the anomalous widening of absorption band with increase in pressure of absorbing vapour observed by Korff (1932). In the present investigation the transmitted radiation of modified wavelength is actually produced during the process of absorption and re-emission while Korff (1932) observed that the opacity varies inversely with square of wavelength distance from resonance up to a certain pressure above which the width of the absorption line was found to be much higher than the theoretical value. This anomaly was assumed to be due to the influence of interaction between Na-atoms on the frequency of resonance at higher



Resonance lines of Na filtered through Na vapour  
G, G—ghost lines.



pressure. He, however, could not detect with the arrangement used by him any change of frequency of radiation emitted by the absorption cell, because he used a continuous radiation as the incident beam.

It can be seen from Table I that the distance of any of the components of the transmitted doublet from resonance varies from .058 Å at 185°C to .5 Å at 290°C for the  $D_2$  line, while the corresponding values for  $D_1$  are .04 Å and .38 Å respectively. Also the components of the transmitted doublet become broader and diffuse at higher temperatures, the width of each component being about .5 Å at 290°C. The maximum shift observed in the case of  $D_2$  is about  $1.5 \text{ cm}^{-1}$  at 290°C while in the case of resonance line of Hg the maximum shift observed was  $9 \text{ cm}^{-1}$  (Kastha, 1949). Thus the percentage change in the frequency of the transmitted line is larger in

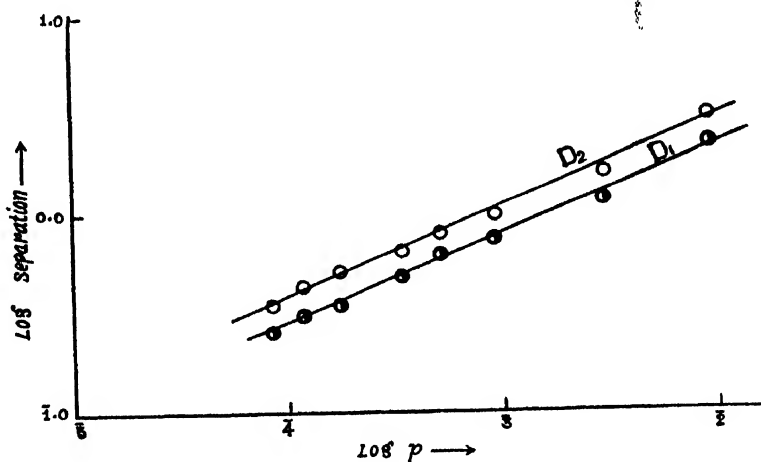


FIG. 9

the latter case than in the case of the D lines. The absorption tube is expected to act as a resonance lamp, the intensity of radiation emitted in any direction being only a very small fraction of that of the radiation absorbed. Evidently, due to interaction of the atoms not only the frequency of absorption but also that of the emitted radiation is slightly altered. If we also postulate the alteration of frequency at each process of emission after that of absorption, the change of frequency of the emitted radiation is expected to be larger than that of the absorbed radiation. Such a phenomenon can take place when the radiation is absorbed by an atom just before its collision with another atom and the energy is re-emitted at the instant of collision. There may be absorption of the emitted radiation again by some other Na-atom impinging with each other and the frequency of the radiation re-emitted may be changed to a greater extent. The probability of such a re-absorption and re-emission of the radiation is much less than that of single absorption and re-emission. So the intensity of the transmitted radiation at larger distance from resonance is expected to be smaller. This may be the explanation for the feebleness of the doublet observed at 290°C, the intense portion of the

transmitted component nearer to the resonance in this case being completely absorbed owing to larger width of the absorption band at this temperature, as observed by Korff (1932). Thus the results of both the previous investigation (Kastha, 1949) and the present investigation definitely prove the fact that besides the Doppler and other known types of collisional broadening of resonance line, there is a new type of broadening of the resonance line which is produced during absorption and re-emission of the resonance line by the vapour of the emitting element at suitable pressures.

It may finally be pointed out that in any method in which the vapour of the element is used to absorb its resonance line, the absorption is never complete and there is always a feeble radiation of modified frequency transmitted by the absorbing vapour, the intensity of this transmitted radiation falling off rapidly with increase of pressure of the absorbing vapour.

#### ACKNOWLEDGMENT

The author is indebted to Prof. S. C. Sirkar for his kind interest and guidance during the progress of this work.

#### REFERENCES

- Fairbother, F. and Tuck, J. L., 1936, *Trans. Farad. Soc.*, **32**, 624.  
Kastha, G. S., 1949, *Ind. J. Phys.*, **23**, 247.  
Korff, S. A., 1932, *Astrophys. Jour.*, **76**, 124.  
Kunze, P., 1928, *Ann d Phys.*, **85**, 1013.  
Ladenburg, R. and Thiele, E., 1930, *Z. f. Phys. Chem.*, B, **7**, 161.  
Zehden, W., 1933, *Z. f. Phys* **86**, 855.

# SOUND VELOCITY MEASUREMENTS IN ORGANIC LIQUIDS

BY S. PARTHASARATHY AND N. N. BAKHSHI

NATIONAL PHYSICAL LABORATORY OF INDIA, NEW DELHI

(Received for publication November 13, 1952)

**ABSTRACT.** Sound velocity measurements have been redetermined in 48 organic compounds of various molecular structures with a view to checking previous results. Rules obtained previously by one of us (S. P.) regarding the relation between sound velocity and chemical constitution have been applied to them and are found to hold good.

## INTRODUCTION

Sound velocity measurements have been made in 48 organic liquids by the light diffraction method. The authors in the course of their investigations on the dispersion of the sound velocity in organic liquids observed that some of their velocity values differed considerably compared to the values determined by previous workers. Therefore, with a view to checking the velocity measurements the present work was undertaken. A few of the determinations are new. The empirical rules (Parthasarathy, 1935, 1936, 1937, 1938) derived by one of us previously between sound velocity and chemical constitution are applied here and reviewed further.

## EXPERIMENTAL AND RESULTS

The well known diffraction method of Debye-Sears and Lucas-Biquard was employed in the determination of sound velocity. Care was taken to have each liquid, which was pure, freshly distilled again before the measurements. The accuracy claimed for these values is of the order of 1 metre in a thousand.

As examples we give in Table I a few liquids where velocities given by earlier workers do not agree among themselves :—

TABLE I

Liquid	Authors		From Bergmann's "Der Ultraschall"	
	Temp °C	Vel. m/s	Temp. °C	Vel. m/s
1. Ethylene glycol	25	1656	20	1616
2. Diethyl oxalate	22.4	1292	22	1392
3. Ethyl acetoacetate	24	1341	25.5	1417
4. o-Nitrotoluene	23.2	1460	20	1432
5. α-Picoline	25	1392	28	1453

We have redetermined with great care the sound velocity measurements in about 50 liquids. The values and the temperatures at which they were taken are given in the Table II. The sound velocities in these liquids are

given in Bergmann's "Der Ultraschall" 1949 edition and are also being given here for the purpose of comparison.

TABLE II

Liquid	Authors		From Bergmann's "Der Ultraschall".	
	Temp. °C	Vel. m/s	Temp. °C	Vel. m/s
<i>(i) Alcohols</i>				
1. Methyl alcohol	23.8	1126	20	1123
2. Ethyl alcohol	24	1176	20	1180
3. Iso-propyl alcohol	21.8	1170	20	1170
4. N-ethyl alcohol	21.8	1261	20	1268
5. Iso-butyl alcohol	23.2	1203	20	1222
6. Amyl alcohol	21.4	1263	20	1294
7. N-ethyl alcohol	22.6	1358	20	1358
8. Capryl alcohol	22.8	1319		
9. Benzyl alcohol	25.5	1529	20	1540
10. Iso-amyl alcohol	23	1241		
11. Cyclohexanol	25	1465	20	1493
12. Ethylene glycol	25	1656	20	1616
13. Allyl alcohol	26	1251		
<i>(ii) Esters</i>				
14. Methyl acetate	26	1154	25	1154
15. Ethyl acetate	23.6	1152	20	1176
16. N-butyl acetate	23	1203	26	1271
17. N-amyl acetate	23.5	1200	26	1168
18. Methyl salicylate	23.2	1419	28	1408
19. Diethyl oxalate	22.1	1292	22	1392
20. Diethyl benzoate	21.8	1300		
21. Ethyl-acetoacetate	24	1341	25.5	1417
22. Ethyl butyrate	24.5	1179	23.5	1171
23. Diethyl malonate	25.8	1306	22	1386
24. Diethyl phthalate	26	1423	23	1471
25. Amyl formate	26.6	1195	26	1201
<i>(iii) Ketones</i>				
26. Acetone	23.5	1177	20	1192
27. Methyl ethyl ketone	23.5	1204	20	1207
28. Acetophenone	24.6	1479	20	1496
29. Cyclohexanone	23.2	1419	20	1449
<i>(iv) Other Compounds</i>				
30. Benzene	21.8	1317	20	1326
31. Toluene	22.2	1318	20	1328
32. Xylene	22.8	1334		
33. p-Cymene	21.4	1331		
34. Bromobenzene (mono)	22.2	1162	20	1170
35. Chloroform	25.6	985.7	20	1005
36. Cyclohexane	24.6	1259	20	1284
37. o-Nitrotoluene	23.2	1460	20	1432
38. m-nitrotoluene	23.8	1467	20	1489
39. Pyridine	25.5	1416	20	1445
40. Dipentene	24.2	1327	23.8	1328
41. Nitrobenzene	25.2	1457	20	1473
42. o-Chlorotoluene	24.4	1305	20	1344



TABLE II (contd.)

Liquid	Authors		From Bergmann's "Der Ultraschall "	
	Temp. °C	Vel. m/s	Temp. °C	Vel. m/s
43. Aniline	24.8	1643	20	1656
44. Carbon tetrachloride	21.8	933	20	938
45. $\alpha$ -Picoline	25	1392	28	1453
46. Quinoline	25.4	1561	20	1600
47. Benzaldehyde	26.6	1456	20	1479
48. Dioxane	24.5	1351	20	1389

## DISCUSSION

In this connection we may restate the rules (Parthasarathy, 1935, 1936, 1937, 1938) obtained between sound velocity and chemical constitution.

It will be useful to split these rules, for considerations of simplicity, into two groups, (i) General rules applicable in all cases and (ii) particular rules which apply only in special cases, like substitution of radicals, atoms etc.

*General Rules*

There are only three of them out of those enunciated in our earlier paper. They are:

(1) *Aliphatics and aromatics.* Aromatic compounds have usually higher velocities than the aliphatics. This is amply confirmed by part (iv) of Table II. It is observed that aromatic compounds like, benzene, toluene, xylene etc., have usually higher velocities as compared to the aliphatic compounds like acetone and methyl ethyl ketone.

(2) Compounds having higher viscosities have in general higher velocities

On an examination of Table II we find that as stated earlier, acetophenone and aniline have higher velocities than the parent compound. Therefore this rule also holds good.

(3) *Isomers.* Among isomers, if isomerism is not of the optical kind there is a difference in the acoustic velocity.

This is borne out clearly by the examples of *n*- and isobutyl alcohols, *n*- and iso-amyl alcohols, and *o*- and *m*-nitro-toluenes. Therefore these findings confirm the rule.

*Particular Rules*

(1) *Lengthening of the chain.* As the length of the molecule increases, the velocity of sound also increases. This is amply borne out by the

members of the homologous series in the aliphatic alcohols and benzene hydrocarbons from Table II parts (i) and (iv), which go to show that the rule holds. Increase in molecular weight does not always go with increase in the length of the chain and it is not therefore correct to say that with increase in molecular weight the velocity increases, e.g. molecules which have heavy atoms substituted possess lower velocities.

(2) *Introduction of a heavier atom.* Introduction of a heavier atom into the molecules brings down the velocity. Examples are toluene and *o*-chloro-toluene; chloroform and carbon tetrachloride. This rule is also confirmed.

(3) *Introduction of a double bond.* It has been observed that usually the introduction of a double bond lowers the velocity.

(4) *Electric moment.* It has been shown that molecules possessing an electric moment tend to show enhanced sound velocities. Examples confirming the above statement are.

(i) Benzene and nitrobenzene.

(ii) Cyclohexane and cyclohexanone.

(iii) Toluene and *o*-nitro toluene.

As regards esters, the earlier rule says that they form a class by themselves as they show a diminution in velocity with increasing length of the alcohol radical. But from the Table II we observe that the values of sound velocities for esters *i.e.* for the esters of acetic acid do not differ much from each other. Therefore, it is difficult to say anything on this just yet. Further work is necessary to confirm this rule.

On a re-examination of the empirical rules derived earlier in 1936-37 we find that all of them hold good as evidenced by this further work.

#### REFERENCES

- Parthasarathy, S., 1935, *Proc. Ind. Acad. Sci. (A)*, **2**, 497.  
" " 1936, *ibid*, **3**, 285, 482, 519.  
" " 1936, *ibid*, **4**, 59, 213.  
" " 1937, *Curr. Sci*, **6**, 215.  
" " 1938, *ibid*, **7**, 322.

# THE EFFECT OF FLUID MOTION ON HEAT TRANSMISSION. PART I—VERTICAL CYLINDERS

BY D. G. KAPADNIS

NATIONAL PHYSICAL LABORATORY OF INDIA, NEW DELHI.

(Received for publication, September 15, 1952)

**ABSTRACT.** In this investigation the effect of air stream on convective heat transfer rate has been studied under different ambient conditions and the experimental data are compared with those of previous workers in this field. The experimental results show that

(1) The heat transmission does not increase quite so fast as the air velocity—the rate of heat transfer being proportional to 0.517th power of air velocity ;

(2) As the characteristic dimension of the vessel is reduced its convective heat transfer per unit area per unit temperature excess increases ;

(3) For an air stream striking the cylinder at an angle of 45 degrees the heat transfer rate is about three-quarters, and for flow parallel to the axis about one-half that for flow at right angles to the axis ; there is a small variation in heat dissipation for inclinations above 60 degrees ;

(4) Clothing affects the heat transfer rate but the efficiency of insulation deteriorates with the increase in air velocity ; the double layer of clothing increases the effectiveness of insulation, but at higher velocities the protection effect of the garments is negligible in comparison with the effect of wind penetration.

A hot body in steady motion through any real fluid or at rest in a moving current loses heat by three modes of heat transfer. Losses by conduction and radiation can be minimized by suitable arrangements and under these conditions most of the heat dissipation will be due to convection—natural as well as forced. In natural or free convection the fluid motion is caused solely by gravity forces due to difference of density between the hotter and cooler parts, while in forced convection the fluid motion is caused by forces independent of the temperature of the fluid, such as externally imposed differences of pressure. The magnitude of forced convection depends upon the relative velocity, the physical properties of the fluid, the excess of temperature of the body over that of the fluid and the size and form of the body.

Because of the immense variety of forms of heat exchangers there exists a vast variety of experimental results. These experimental results are mostly applicable only to cases which are similar to the special arrangements employed. Numerous formulae have been, and still are, conceived, and their field of application is more or less restricted. Only very few amongst them satisfy the theoretical requirements as to their mathematical form.

In the cases of flow of hot gases through the tubes of a boiler (Nicholson, 1909), flow of liquids and gases through pipes (Stanton, 1897 ; Jordan,

1909 ; Nusselt, 1909), heat losses from honeycomb radiators, etc. , the rate of heat transfer is proportional to the  $n$ -th power of air velocity where  $n$  varies from 0.75 to unity ; while the experiments on heat dissipation from hot wires of small diameter in an air current show that the value of  $n$  is about 0.5 (Davis, 1926). Büttner (1934), interested in heat losses from human body, arrives at  $n=0.52$  in experiments on convective heat losses from spheres of various sizes in a current of air. The experimental data of Winslow and others (1939) who treat the human body as a 7 cm cylinder or 15 cm sphere fits in either of the two formulae in which the value of  $n$  is 0.5 or unity. Hilpert (1933) carried out a systematic series of experiments for thin wires as well as cylindrical tubes of different diameters in air and found that his results could be expressed as

$$(\text{Nusselt's number}) = B (\text{Renold's number})^n$$

The values of  $B$  decrease while those of  $n$  increase with the Renold's number. They can, however, within the limits of experimental error, be treated as constant quantities in limited ranges of Renold's number.

Cylindrical bodies chosen by various workers were either thin solid wires or hollow tubes and pipes heated electrically or by some mechanical means. Horizontal cylinders have been studied in detail in both gases and liquids, but very scattered information is available for vertical cylinders. As more experimental evidence is necessary for the satisfactory understanding of the thermodynamics of heat-interchange between the body and the surroundings under different ambient conditions it was thought worthwhile to try an experiment of heat dissipation from vertical cylindrical vessels of different sizes filled with hot water and placed in a current of air under different ambient conditions in order to study the effect of fluid motion on heat transmission, and to compare the results obtained with those of previous workers in this field.

#### EXPERIMENTAL ARRANGEMENT

A partial theoretical solution of this problem of determining the rate of heat transfer per unit area per unit difference of temperature for a heated vessel in a gas can easily be arrived at by using the well-known method of dimensional analysis dealing with the dimensions of mass, length, time and temperature as fundamental. Based on various assumptions as to the factors involved dimensional analysis gives for forced convection the Nusselt's equation.

$$\left( \frac{1}{A \Delta \theta} \frac{dQ}{dT} \frac{D}{K} \right) = B' \left( \frac{VDC}{K} \right)^n \left( \frac{C\xi}{K} \right)^m \quad \dots (1)$$

where  $\frac{dQ}{dT}$  = the rate of heat transmission,

$D$  = the characteristic dimension of the vessel,

$A$  = area of the vessel exposed,

$\Delta\theta$  = excess of temperature of the surface of the vessel over that of the surrounding fluid,

$K$  = thermal conductivity of the fluid,

$V$  = fluid velocity,

$C$  = product of the specific heat and the density of the fluid,

$\xi$  = ratio of the viscosity of the fluid to its density,

$B'$  = a constant,

and  $m, n$  are unassigned numbers the values of which are to be determined from experimental data.

Expression (1) can be simplified because from both kinetic theory and experiment the numeric  $\frac{C\xi}{K}$  is constant for gases.

Thus 
$$\left( \frac{1}{A\Delta\theta} \quad \frac{dQ}{dT} \quad \frac{D}{K} \right) = B \left( \frac{VD}{\xi} \right)^n \quad \dots (2)$$

where  $B$  is the convection constant. The rate of heat transfer per unit area can be measured for different values of fluid velocity, characteristic dimension of the vessel, temperature excess and also for different fluids. If we plot the logarithms of the quantities in the parentheses against each other, a straight line having a slope equal to  $n$  will result.

Let us compute the effect of changing the velocity of the fluid stream alone on the heat transfer rate per unit area, all other factors remaining unchanged. Representing the logarithm of the quantity in the parenthesis on the right of equation (2) by  $X$  and that on the left by  $Y$  and expanding we have

$$X = \log D + \log V - \log \xi,$$

and 
$$Y = \log \left( \frac{1}{A\Delta\theta} \quad \frac{DQ}{dT} \right) - \log K + \log^a D$$

Taking differentials for the two cases involving a change of  $V$  only we get

$$\Delta X = \Delta \log V,$$

and 
$$\Delta Y = \Delta \log \left( \frac{1}{A\Delta\theta} \quad \frac{dQ}{dT} \right)$$

combining these, we get 
$$\Delta \log \left( \frac{1}{A\Delta\theta} \quad \frac{dQ}{dT} \right) = \frac{\Delta Y}{\Delta X} \cdot \Delta \log V \quad \dots (3)$$

The effect of changing the characteristic dimension of the vessel alone

on the rate of heat transfer per unit area can be computed in a similar fashion. In this case we get

$$\Delta \log \left( \frac{1}{A \Delta \theta} \frac{dQ}{dT} \right) = \left( \frac{\Delta Y}{\Delta X} - 1 \right) \cdot \Delta \log D \quad \dots (4)$$

The experimental arrangement used by the present author and Gogate (1952) in studying the shape constant of the vessels was tried by the author in these investigations. Repetition is, therefore, avoided. Some necessary modifications were, however, made. The short focus telescope was not used, the surface temperatures of the vessels were measured by means of thermocouples and preliminary experiments were carried out in still air in order to obtain the radiation losses which also included the heat dissipation due to natural convection currents, and all the observations were corrected for these losses.

The effect of fluid motion was studied by varying the air velocity from 80 cm/sec to 1100 cm/sec. This air stream was forced on cylindrical vessels of different sizes ranging from 2.4 cm to 21.8 cm. The observations were repeated for three different values (30°, 50° and 68°C) of the excess of surface temperature of the vessel over that of the surrounding air stream. The air velocity and the rate of heat transfer were measured in the same manner (Kapadnis and Gogate, 1952) followed in their previous investigations.

The electric fan was then slowly turned round its horizontal axis by steps in order to get the beam of air current striking the vessel at different angles, thus enabling the author to study the effect of inclination of the air current on heat transmission for different air velocities.

The insulation effect due to single and double layers of clothing made up as cylindrical covers to fit the vessel properly and covering it completely was finally studied for different air velocities by measuring the heat losses in the cases of bare vessels, vessels covered with single garments and those with two.

## RESULTS AND DISCUSSION

Figure 1 gives a plot of the logarithms of the quantities in the parentheses of equation (2) namely,  $\log \left( \frac{1}{A \Delta \theta} \frac{dQ}{dT} \frac{D}{\xi} \right)$  against  $\log \left( \frac{VD}{\xi} \right)$ ,

which slightly concaves upwards, but is practically a straight line in all the cases of vessels tried for different air velocities and for different values of temperature excess, a typical set of the actual observations being recorded in Table I. The slope of this line, i.e. the value of the index  $n$ , in these experiments, is equal to 0.517, showing clearly that the rate of heat

transfer is proportional to 0.517th power of air velocity. The experimental data lie reasonably close to the curve which is represented by

$$\left( \frac{1}{A\Delta\theta} \frac{dQ}{dT} \frac{D}{K} \right) = 0.56 \left( \frac{VD}{\xi} \right)^{0.517} \quad (5)$$

A few points shown by the letter *b* in figure 1, however, deviate considerably from the straight line representing the logarithmic plot of equation (5). As these points correspond to velocities of the air stream higher than about ten metres per second, it means that at about this velocity of ten metres per second the linear relationship represented by the straight line (figure 1) breaks down.

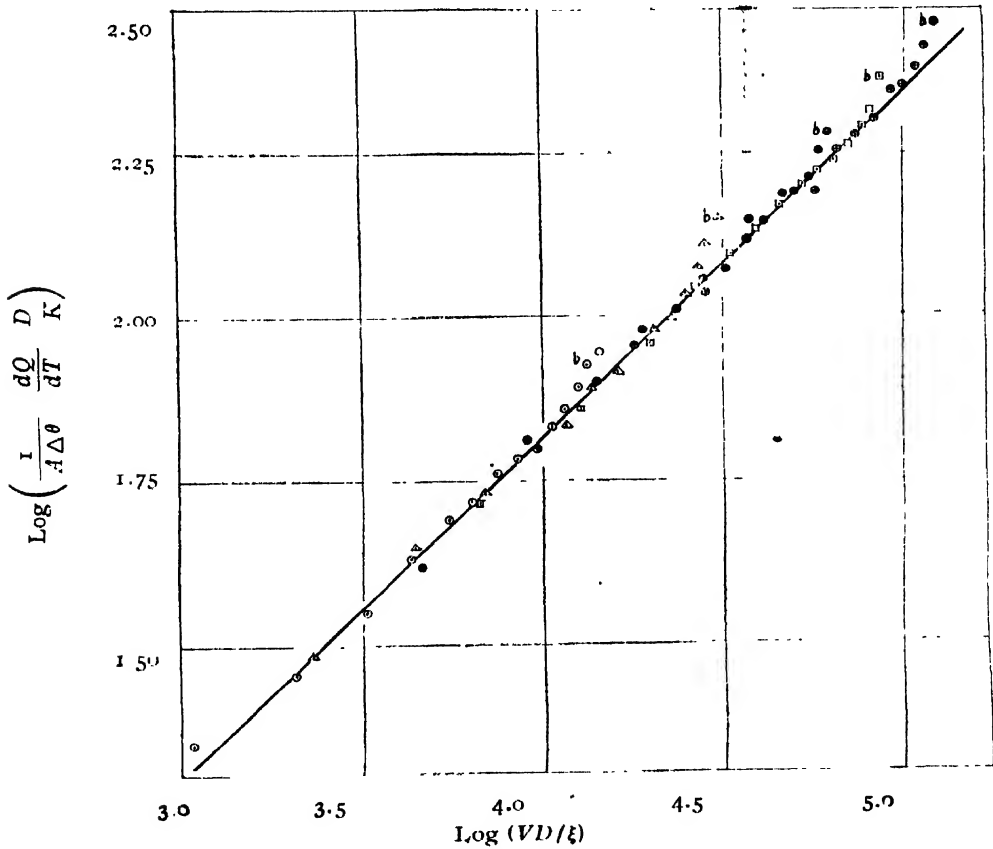


FIG. 1

Buttner (1934), in his experiments of heat losses from spheres of various sizes in a current of air, arrived at a similar result.

The experimental value of the term  $\frac{\Delta Y}{\Delta X}$ , i.e., the slope of the straight line, found in these investigations is less than unity. Substitution in equation (3) gives

$$\Delta \log \left( \frac{1}{A\Delta\theta} \frac{dQ}{dT} \right) = 0.517 \cdot \Delta \log \quad \dots (6)$$

TABLE I

Effect of wind velocity on heat transmission in case of vessels of different sizes

Mean value of heat loss in still air ... 0.00052 cal/sec/cm<sup>2</sup>/°C

Temperature excess ... 30.0°C

Diameter of the vessel, cm,	ir velocity, cm/sec	Heat transfer rate cals/cm <sup>2</sup> /sec/°C,	$\frac{VD}{\xi}$	$\frac{1}{A \Delta \theta} \frac{dQ}{dT} \frac{D}{K}$
2.4	80	$5.04 \times 10^{-14}$	1060	22.4
	155	6.42	2060	28.5
	242	7.95	3220	35.3
	326	9.60	4340	42.7
	405	11.08	5390	49.2
	487	11.76	6480	52.2
	563	12.80	7470	57.3
	644	13.62	8570	60.5
	721	14.20	9590	63.1
	805	15.30	10700	68.4
	882	16.34	11700	72.6
	967	17.75	12900	78.9
	1020	18.98	13600	84.3
	1095	21.00	14600	93.3
5.2	80	3.19	2310	30.7
	155	4.65	4470	44.8
	242	5.63	6970	54.2
	326	6.43	9400	61.9
	405	7.22	11700	69.5
	487	8.06	14000	77.6
	563	8.38	16200	80.7
	644	9.21	18600	90.8
	721	9.94	20800	95.7
	805	10.34	23200	99.5
	882	11.13	25400	107.2
	967	12.37	27900	110.1
	1020	13.47	29400	120.7
	1095	14.67	31600	141.3
10.3	80	2.11	4740	41.8
	155	3.35	9190	66.4
	242	4.01	14400	79.4
	326	4.82	19300	95.5
	405	5.12	24000	101.4
	487	5.66	28000	112.2
	563	5.96	33400	118.0
	644	6.67	38200	132.1
	721	6.97	42800	138.0
	805	7.64	47700	151.4
	882	7.76	52300	153.8
	967	8.17	57400	161.8
	1020	8.97	60500	177.8
	1095	9.68	64900	191.9
	80	1.89	6650	52.5
	155	2.67	12900	74.1
	242	3.23	20100	89.7
	326	4.02	27100	111.7
	405	4.43	33700	123.0
	487	4.85	40500	134.6



TABLE I (contd)

Diameter of the vessel, cm	Air velocity, cm/sec	Heat transfer rate, cal/cm <sup>2</sup> sec/°C	$\frac{VD}{\xi}$	$\frac{I}{A \Delta \theta} \frac{dQ}{dT} \frac{D}{K}$
15.0	563	5.33	46800	147.9
	614	5.68	53600	157.8
	721	5.97	59900	196.0
	805	6.23	66600	173.0
	882	6.51	73300	180.7
	967	7.02	80100	105.0
	1020	7.54	84800	209.4
	1095	8.31	91000	230.7
	80	1.56	9670	63.1
	155	2.21	18700	89.1
	242	2.66	29200	107.2
	326	3.44	39400	139.0
	405	3.60	49000	145.2
	487	3.70	58800	153.1
21.8	563	4.31	68000	175.4
	614	4.01	77800	186.2
	721	4.95	87100	200.0
	805	5.44	99500	219.8
	882	5.55	107000	223.9
	967	6.02	117000	243.2
	1020	6.34	121000	255.9
	1095	6.95	132000	280.5

For a specific case, consider an air stream blowing with a speed of 326 cm/sec on the hot vessel of 15 cm diameter. For a change of  $V$  to 644 cm/sec, nearly two-fold increase, the change in the rate of heat transfer per unit area per unit temperature excess will be an increase of 1.53 fold. The calculated and the experimentally observed values for the rate of heat transfer for this specific case cited are  $6.14 \times 10^{-4}$  and  $5.68 \times 10^{-4}$  units respectively, showing a fairly good agreement within the limits of experimental error. Expressed qualitatively equation (6) means that the rate of heat transmission does not increase quite so fast as the air velocity.

Similar reasoning, applied to equation (4) which gives

$$\Delta \log \frac{1}{A \Delta \theta} \frac{dQ}{dT} = -0.483 \Delta \log D \quad (7)$$

after substitution, reveals that for a change of  $D$  from 2.4 cm to 10.7 cm, a 4.46 fold increase, there will be a 3.14 fold decrease in the rate of heat

dissipation, because the term  $\left(\frac{\Delta Y}{\Delta X} - 1\right)$  is negative. The experimental value

of the rate of heat transmission at a velocity of 563 cm/sec for  $D=10.7$  cm is  $5.66 \times 10^{-4}$  units while that calculated is  $4.16 \times 10^{-4}$  units in this case. Equation (7) interpreted in words means that as the characteristic dimension of the vessel is reduced its convective heat transfer rate per unit area per unit excess of temperature increases.

The experimental data for these two cases is represented graphically

in figure 2 in which the convective heat transfer rate is plotted as a function of air velocity for five cylinders of different sizes. With the increase in air velocity all these curves in figure 2 rise

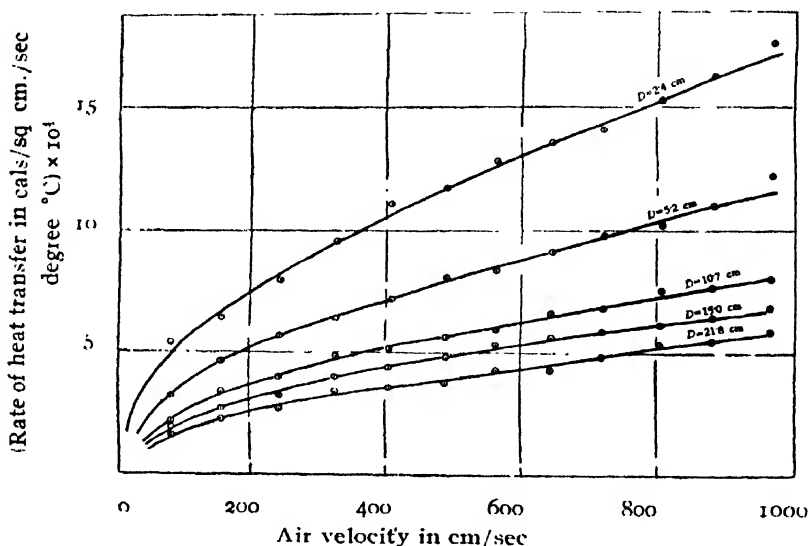


FIG. 2

steadily with a continuous decrease in slope. This is in close agreement with the interpretation of equation (6). For all the five vessels tried the heat transfer rate increases, of course, with increasing velocity, but the curves for vessels bigger in size lie below those for the smaller ones, a very good agreement, indeed, with equation (7). The importance of this fact that as the diameter of a cylinder is reduced its convective heat transfer rate per unit area per unit temperature excess increases, in the design of gas-filled incandescent lamps, is, therefore, obvious. This also suggests that, in order to measure the temperature of the fluid with a thermocouple one should prefer very fine wires. This will help increasing the ease of heat exchange between the couple and the fluid.

In figure 3, the convective heat transfer rate is plotted against the inclination of the air stream to the axis of the cylinder for different air velocities, the actual observations being given in Table II. The variation of convective heat losses for the inclinations above 60 degrees is very small. For the air stream striking the cylinder at an angle of 45 degrees the heat transfer rate is about three-quarters, and for flow parallel to the axis about one-half that for flow at right angles to the axis.

Figure 4 represents graphically the variation of the rate of heat transfer with air velocity for a bare vessel and that covered with different layers of a piece of cloth. A typical set of observations is recorded in Table III. It is found in these investigations that the wind destroys insulation as it penetrates into clothing. The efficiency of insulation deteriorates at air velocities above 500 cm/sec. It means that more clothing may have to be worn in

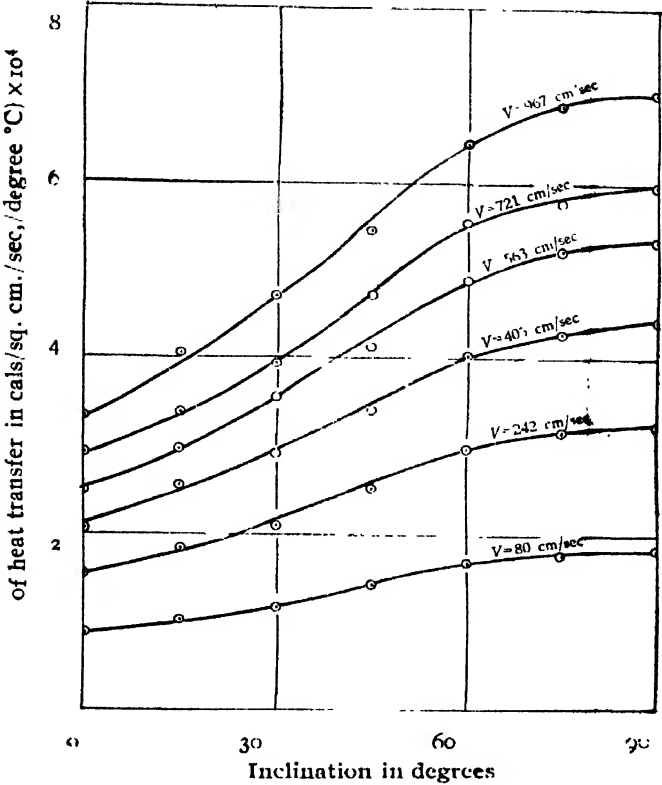


FIG. 3

TABLE II

Effect of inclination of air stream to the cylinder on heat transmission  
Characteristic dimension of the vessel = 15.0 cm

Air velocity cm/sec	Rate of heat transfer per unit area per unit temperature excess in cals/sq. cm/sec/deg C for inclinations of						
	0°	15°	30°	45°	60°	75°	90°
	$\times 10^{-4}$	$\times 10^{-4}$	$\times 10^{-4}$	$\times 10^{-4}$	$\times 10^{-4}$	$\times 10^{-4}$	$\times 10^{-4}$
80	0.93	1.08	1.25	1.49	1.74	1.85	1.89
242	1.55	1.84	2.10	2.52	2.97	3.17	3.23
405	2.08	2.57	2.92	3.42	4.03	4.30	4.43
563	2.50	2.98	3.57	4.15	4.90	5.22	5.33
721	2.93	3.41	3.94	4.72	5.56	5.80	5.97
967	3.37	4.07	4.70	5.48	6.46	6.88	7.02

the wind to furnish a specified amount of insulation. Clothing principally

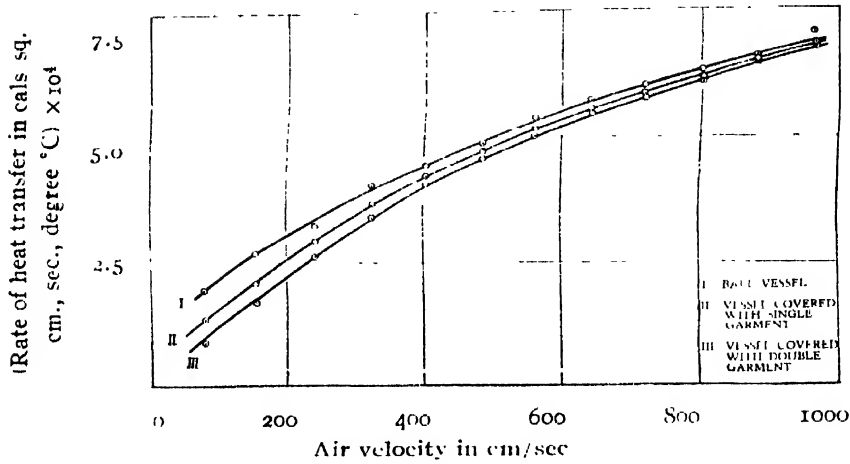


FIG. 4

affects the heat transfer. There is another physical phenomenon which is of considerable consequence in this case, and that is the tendency of the gases to form relatively thick and stable layers at surfaces, the thickness of which decreases rapidly with the increase in air velocity (Newburgh and Harris, 1945). At a velocity of about 25 metres/sec the layer is reduced to a fraction of a millimetre and is negligible as insulation.

TABLE III

Effect of insulation on heat transmission  
Characteristic dimension of the vessel = 21.8 cm

Air velocity cm/sec	Rate of heat transfer per unit area per unit temperature excess in cal/sq. cm./sec/deg C for		
	bare vessel	vessel with single cover	vessel with double cover
80	$1.80 \times 10^{-4}$	$1.35 \times 10^{-4}$	$0.85 \times 10^{-4}$
155	2.67	2.08	1.70
242	3.23	2.92	2.61
326	4.02	3.66	3.40
405	4.43	4.23	4.03
487	4.85	4.70	4.56
563	5.33	5.10	4.97
644	5.68	5.50	5.40
721	5.97	5.80	5.71
805	6.23	6.12	6.04
882	6.51	6.46	6.39
967	7.02	6.78	6.73

This layer of air, therefore, acts as insulation to the vessel—bare as well as clothed. The layers of clothing trap additional layers of air, thus, increasing the effectiveness of insulation. But at higher velocities the thick-

ness of these insulating layers of air rapidly decreases and also the protection effect of garments becomes negligible in comparison with the effect of wind penetration. This is obvious from figure 4. The insulation effect will also depend upon the nature, size and material of the fabrics of which the piece of cloth is made.

The range of data for air flowing normal to single cylinders tried by various workers are recorded in Table IV in order to give the comparative idea of the experimental work done in this field. Figure 5 shows a logarithmic plot of the experimental data of these workers with that of the present author in the range of  $\frac{VD}{\xi}$  from  $10^3$  to  $10^5$ . The results of the author for Renold's numbers upto about  $10^4$  show somewhat higher rates of heat transmission than those of

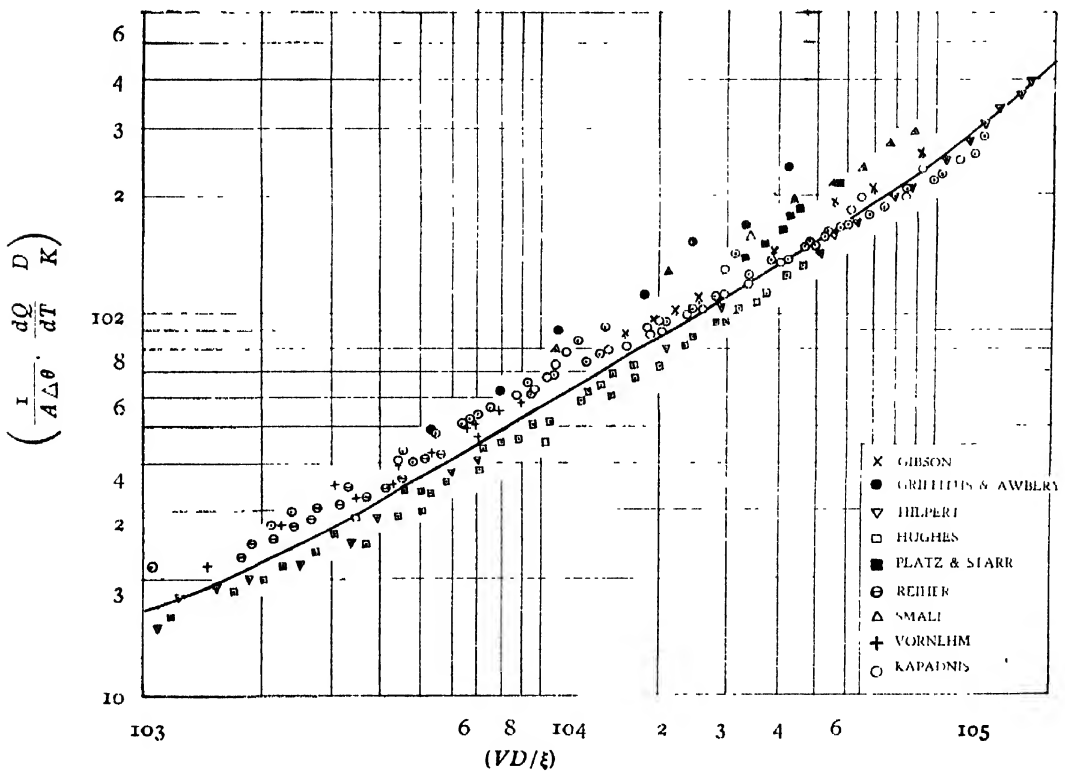


FIG. 5

other workers. The values obtained are, however in line with those of Reiher (1925) and Vornehm (1932), but hot air stream was forced on cold pipes in their experiments while the reverse was the case in the present author's experiments.

Still, however, for single cylinders in the range of  $\frac{VD}{\xi}$  from  $10^3$  to  $10^5$  the dimensionless equation (5) obtained from the experimental data of the present author represents the data of various workers in this field within  $\pm 20\%$ . The curve recommended by McAdams (1951) which represents the experimental data more closely is also drawn in the same figure.

TABLE IV

Range of data for air flowing normal to single cylinders  
Atmospheric pressure = one atm.

Observer	Cylinder or pipe diameter in cm	Air temp. deg C	Surface temp. of pipe or cylinder deg C	Air velocity cm/sec
Gibson (1924)	9.5	10	88	271-1554
Griffiths and Awberv (1933, 1937)	3.18-8.26	18.3	28-49	76-610
Hilpert (1933)	0.0019-15.0	21	93-110	183-2957
Hughes (1916)	0.43-5.50	15.6	100	0-1524
Paltz and Starr (1931)	8.26	21	100	700-1220
Reiher (1925)	1.5-2.8	260	21-35	274-579
Small (1935)	11.4	21	77-92	152-1219
Vornehm (1932)	2.41-3.05	199	27-41	122-762
Present Author	2.4-21.8	30	60-98	8-1095

This work is expected to throw some light on the understanding of the thermodynamics of the heat-interchange between the body and the surroundings under different ambient conditions.

#### ACKNOWLEDGMENTS

The author wishes to place on record his deep gratitude to Dr. K. S. Krishnan, Director of the National Physical Laboratory, New Delhi, for his kind permission to publish this paper.

This research work was carried out in the Physics Laboratory of the Faculty of Science of M. S. University of Baroda. The author desires to thank very heartily the authorities for all the facilities they gave during the progress of this work.

The author tenders his grateful thanks to Dr. D. V. Gogate for his keen interest and inspiring guidance ; to Messrs K. R. Chaudhari and H. N. Patil, for their unfailing help and suggestions during the investigation ; and to Mr. R. N. Pawar of Architectural Division of the Council of Scientific and Industrial Research, for his precious help in drawing graphs.

#### REFERENCES

- Buttner, K., 1934, *Publication of Prus. Met. Inst.*, **10**, 404.  
 Davis, A. H., 1926, *Collected Researches*, Nat. Phys. Lab., (Teddington), **19**, 205.  
 Gibson, A. H., 1924, *Phil. Mag.*, (6) **47**, 324.  
 Griffiths, R., and Awberv, J. H., 1933 *Proc. Inst. Mec. Engrs.*, (London), **126**, 319 ;  
*Loc. Cit.* 1937, **137**, 195.  
 Hilpert, R., 1933, *Forschg. Geb. Ing. wes.*, **4**, 215.  
 Hughes, J. A., 1916, *Phil. Mag.*, (6) **31**, 118.  
 Jordan, H. P., 1909, *Proc. Inst. Mec. Engrs.*, P. 1317.  
 Kapadnis, D. G., and Gogate, D. V., 1952, *Ind. J. Phys.*, **26**, 171.

- McAdams, W. H., 1951, *Heat Transmission*, (McGraw-Hill Publishing Co., London), 2nd ed, P. 221.
- Newburgh, L. H., and Harris, M., 1945, *Nat. Res. Council, Washington, C. A. M. Report*, 390, 37.
- Nicholson, J. T., 1909, *Trans. Inst. Engrs and Shipbuilders*, p. 54.
- Nusselt, W. Z, 1909, *Zeitschrift des Vereines deuts. Ing.*,
- Paltz, W. J., and Starr, C. E, 1931, Thesis in Chem. Eng., M. I. T.
- Reiher, H., 1925, *Mitt Forsch.*, 269, 1
- Small, J., 1935, *Phil Mag.*, (7) 19, 251.
- Stanton, T. E., 1897, *Trans. Roy Soc., London, A* 190, 97.
- Stanton, T. E., Booth, R., and Marshall, D., 1917, *Brit. Aeronaut. Res. Comm., Rept. and Memo.*, p. 271.
- Vornehm, L., 1932, *Forsch. Gebiete Ings.*, 3, 94.
- Winslow, C. E. A., Herrington, L. P., and Gagge, A. P, 1939, *Am. J. Physiol.*, 127, 595.

# THE RAMAN SPECTRA OF 1, 3-DIBROMOPROPANE AND 1, 2, 3-TRICHLOROPROPANE IN THE SOLID STATE\*

By B. M. BISHUI

OPTICS DEPARTMENT, INDIAN ASSOCIATION FOR THE CULTIVATION OF SCIENCE, CALCUTTA 32

(Received for publication, October 29, 1952)

## Plate VII

**ABSTRACT.** The Raman spectra of 1, 3-dibromopropane and 1, 2, 3 trichloropropane have been investigated in the solid state at  $-180^{\circ}\text{C}$ . It has been observed that in the first case some of the Raman lines disappear with solidification, while in the case of the second liquid all the prominent Raman lines persist even when the liquid is solidified and cooled to  $-180^{\circ}\text{C}$ . It is pointed out that although the results reported by previous workers indicate the presence of two rotational isomers even in the case of normal paraffins in the liquid state and disappearance of one of the rotational isomers with the solidification of the liquids, the results observed in the case of 1, 2, 3-trichloropropane do not indicate such disappearance of one of the isomers with the solidification of the liquid. It is pointed out that the presence of extra lines cannot be due to presence of two isomeric molecules in the liquid state of this compound

## INTRODUCTION

The Raman spectra of many substituted paraffins have been studied previously by several workers at different temperatures and in different states, and results have been interpreted on the assumption that the liquid state contains two isomers, one of which disappears in the solid state. Even in the case of some monosubstituted propanes, e.g., propyl halides also, such a disappearance of some of the Raman lines has been observed previously (Mizushima *et al*, 1940 ; Bishui, 1948a).

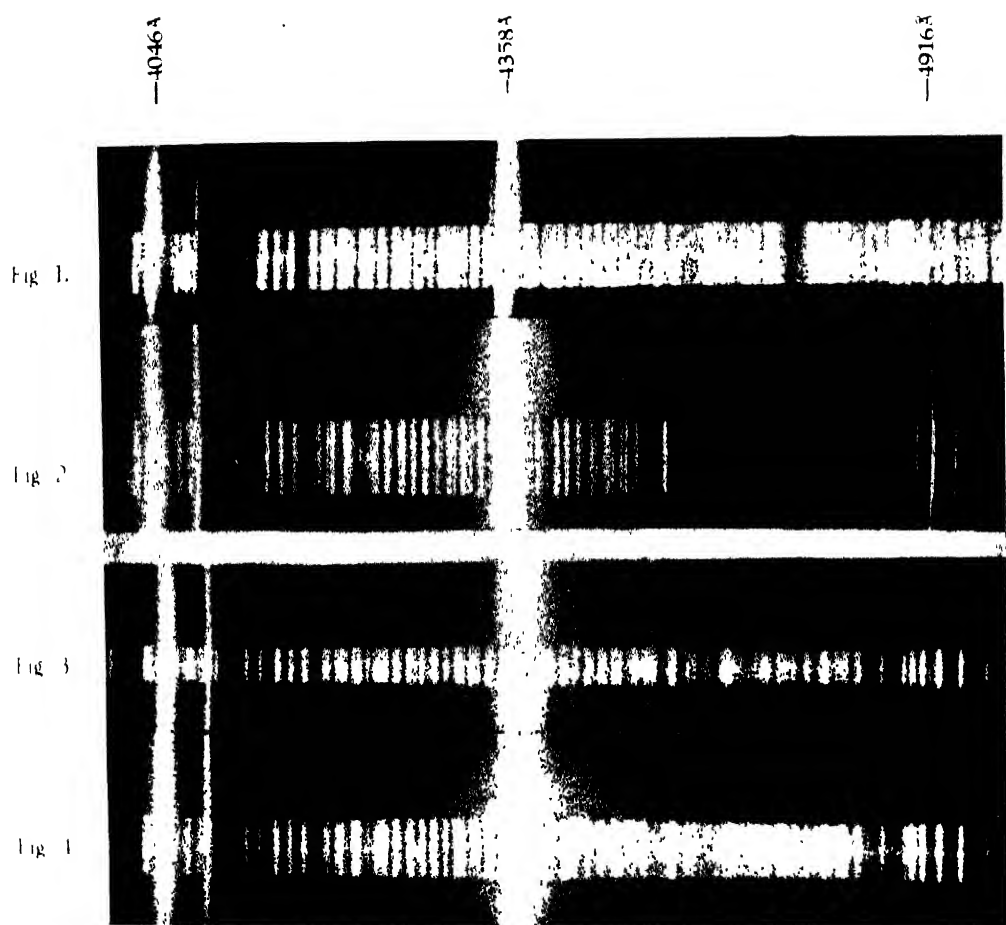
In order to verify whether disubstituted and trisubstituted propanes also behave in the same way as monosubstituted propane, the Raman spectra of 1, 3-dibromopropane and 1, 2, 3-trichloropropane have been studied in the liquid and solid states in the present investigation.

## EXPERIMENTAL

The liquids 1, 3-dibromopropane and 1, 2, 3-trichloropropane were procured from B. D. H. (London) and Fisher Scientific Company (New York) respectively and redistilled in vacuum. The apparatus used in the present investigation for the study of the Raman spectra of the substances in the solid state at low temperatures was the same as described earlier (Bishui, 1948b). The liquid was put in a Pyrex glass tube held in a vertical position in the transparent liquid oxygen container of Pyrex glass. The liquid oxygen was transferred to the transparent Dewar vessel by an arrangement with Cenco

\* Communicated by Prof. S. C. Sirkar





Raman spectra

Fig. 1. 1, 3-Dibromopropane at 30°C.

Fig. 2. " " " -180°C.

Fig. 3. 1, 2, 3-Trichloropropane at 30°C.

Fig. 4. " " " -180°C.



Hyvac pump so that the level of the liquid oxygen was initially much below the bottom of the container containing the liquid, which was thus cooled very slowly. Consequently, the process of solidification was very slow. The frozen mass thus produced was transparent.

A Fuess glass spectrograph having a dispersion of about  $14 \text{ \AA}$  per mm in the region of  $4046 \text{ \AA}$  was used. The transparent solid mass was illuminated by light from two vertical mercury arcs condensed by two glass condensers placed on opposite sides of the container. Cobalt glass filters were placed in the path of the incident rays to cut off continuous background in the blue-green region of the spectrum. The Raman spectra of the liquids at room temperature were photographed in the usual way.

# RESULTS AND DISCUSSION

The spectrograms for the liquid and the solid states of the two substances are reproduced in Plate VII. The frequency-shifts are given in Tables I and II in which the data for liquid state reported by previous workers are also included for comparison. The visually estimated intensities of the lines are given in the parentheses.

TABLE I

1, 3-Dibromopropane  $\text{BrCH}_2\text{CH}_2\text{CH}_2\text{Br}$

Liquid at $30^\circ\text{C}$		Solid at $-180^\circ\text{C}$
Kohlrausch and Ypsilanti (1936)	Present author	Present author
187(6)	188(3) e, k	-----
211(2b)	210(2b) e, k	230(0) e, k
313(2)	315(1b) e, k	-----
378(3)	374(3) e, k	-----
421(7)	428(4) e, k	426(1) e, k
550(10)	552(5) e, k	552(2) e, k
562(10)	564(5) e, k	-----
580(15)	580(6) e, k	594(3) e, k
648(9)	654(5) e, k	-----
696(4)	696(2) e, k	-----
757(3)	768(1b) e, k	-----
855(4)	861(1b) e, k	861(0) e, k
943(3)	951(1) e, k	-----
998(8)	998(2) e, k	-----
1046(2)	-----	-----
1117(3)	1240(3) e, k	-----
1170(2)	1295(3) e, k	-----
1236(8b)	1353(1) e, k	-----
1291(4)	1417(2) e	-----
1340(1)	1438(4) e, k	-----
1417(5)	2830(1) k	-----
1437(6)	2858(2) k	-----
2840(2)	2909(5) e, k	2909(4) e, k
2908(7)	2930(4b) e, k	2930(3) e, k
2966(10)	2972(6) e, k	2972(4) e, k
3016(3)	3008(4) e, k	2998(2)
		3012(4) e, k

TABLE II

1, 2, 3-Trichloropropane Cl.  $\text{H}_2\text{C} \cdot \text{CH}(\text{Cl}) \cdot \text{CH}_2\text{Cl}$ 

Liquid at 30°C		Solid at -180°C
Kohlrausch and Ypsilanti (1936)	Present author	Present author
	88(2) e, k	94(2) e, k
	128(0) e	
	190(0) e	
	237(0) e	
188(0)	294(6) e, k	292(2) e, k
227(0)	357(3) e, k	357(0) e, k
288(5)	387(2) e, k	---
356(2)	418(2) e, k	---
381(1)	524(4) e, k	524(1) e, k
412(1)	637(0) e, k	632(1) e, k
510(3)	667(6) e, k	664(3) e, k
628(1)	710(5) e, k	718(3) e, k
660(6)	752(6b) e, k	752(4) e, k
716(4)	872(3) e, k	872(c) e, k
746(8)	905(0) e, k	---
863(3)	934(0) e, k	---
906(0)	995(2) e, k	1005(1) e, k
931(0)	1094(4b) e, k	1094(1) e, k
990(2)	1190(0) e, k	---
1090(2)	1285(2b) e, k	1280(0) e, k
1198(2)	1347(1b) e, k	1347(0) e, k
1283(3)	1438(5b) e, k	1440(1) e, k
1338(1)	2962(8b) e, k	2966(2) e, k
1432(3b)	3015(4b) e, k	3024(2) e, k
2860(2) ?		
2960(10b)		
3008(6)		

## DISCUSSION

The results given in Table I show that in the case of 1, 3-dibromopropane in the liquid state all the lines observed by Kohlrausch and Ypsilanti (1936) are observed in the present investigation excepting the lines 1046, 1117 and 1170  $\text{cm}^{-1}$ . The first of the three lines was found to be definitely absent and the other two supposed to be excited by 4046 Å are actually the antistokes frequencies 650 and 597  $\text{cm}^{-1}$  excited by the 4358 Å line. The corresponding lines excited by the 4358 Å lines could not be detected. So the liquid studied was the same as that studied by Kohlrausch and Ypsilanti (1936). It is observed from Table I that the strong lines 374, 564, 654 and 1438  $\text{cm}^{-1}$  disappear with the solidification of the liquid. In the case of *n*-propyl bromide only one of the lines due to C-Br valence oscillation disappeared with solidification (Bishui, 1948a) while in the present case the two lines 564 and 654  $\text{cm}^{-1}$  probably due to such oscillations disappear when the liquid is frozen. Similar results observed in the case of *n*-propyl chloride were explained by Mizushima, Morino and Nakamura (1940) on the assumption that the liquid contains two types of isomeric molecules one

of which disappears with solidification. If similar hypothesis is applied in the present case it is found that the disappearance of the strong line  $1438\text{ cm}^{-1}$  due to C-H deformation oscillation cannot be explained.

It is observed that the lines due to C-H valence oscillation become sharper with solidification of the liquid and the line  $3008\text{ cm}^{-1}$  splits up into two lines at  $2998$  and  $3012\text{ cm}^{-1}$  respectively. If it is assumed that the two lines  $564$  and  $654\text{ cm}^{-1}$  are due to C-Br vibration in one of the isomeric forms of the molecule the other two lines  $582$  and  $594\text{ cm}^{-1}$  are the corresponding lines due to the other form. If these frequencies for the two forms be so different from each other the frequencies of C-H oscillations of the two forms also ought to have been slightly different from each other, but actually all the prominent lines due to C-H valence oscillation persist in the case of the solid state.

The results given in Table II show that all the prominent lines observed in the case of 1, 2, 3-trichloropropane persist when the liquid is solidified at  $-180^{\circ}\text{C}$ . As the three chlorine atoms are attached to three different carbon atoms, different isomeric molecules can be formed by rotation about the C-C bond. Even in the case of *n*-paraffins Sheppard and Szasz (1949) have observed that some of the Raman lines disappear with the freezing of the liquid and they have explained the results on the assumption that one of the two isomeric forms disappears in the solid state. The persistence of all the lines in the case of solid 1, 2, 3-trichloropropane thus shows that the presence of two types of isomers in the liquid state of this compound cannot be assumed to explain the presence of any extra lines in the Raman spectrum of this substance. There are 17 lines of frequency-shifts below  $1100\text{ cm}^{-1}$  excluding the line  $88\text{ cm}^{-1}$  in the Raman spectrum of this liquid, while in the case of 1, 3-dibromopropane there are 14 such lines. The number of heavy atoms in the former molecule is six while in the latter case it is five. So the extra three lines in the former case is due to the additional chlorine atom attached to the central carbon atom. The 14 lines in the case of 1, 3-dibromopropane, however, are not due to a single molecule, as some of them disappear when the liquid is frozen. Hence in the case of 1, 2, 3-trichloropropane also these seventeen lines cannot be due to a single molecule. Since all of them persist in the case of the solid they cannot be due to two isomeric forms of the molecule. The only other alternative explanation which can be offered is that in this particular case the presence of three chlorine atoms in molecule makes the molecule strongly polar and the molecules are strongly associated both in the liquid and solid states. This hypothesis can be tested only by investigating the Raman spectrum of the substance in the vapour state, but as it is very difficult to record the feeble Raman lines in the case of vapour no attempt has been made to verify the hypothesis.

## ACKNOWLEDGMENT

The author is indebted to Prof. S. C. Sirkar for his kind interest and helpful discussions throughout the progress of the work.

## REFERENCES

- Bishui, B. M., 1948a, *Ind. J. Phys.*, **22**, 333.  
Bishui, B. M., 1948b, *Ind. J. Phys.*, **22**, 167.  
Kohlrausch, K. W. F., and Ypsilanti, Gr. Prinz, 1936, *Zett. Phys. Chem. B.*, **32**, 407.  
Mizushima, S., Morino, Y. and Nakamura, S., (1940), *Sci. Papers Inst. Phys. Chem. Research (Tokyo)*, **37**, 205.  
Sheppard, N., and Szasz G. J., 1949, *J. Chem. Phys.*, **17**, 86.

# THE COMPARATIVE INFLUENCE OF SHORT AND LONG RANGE ELECTRIC FIELDS IN THE SALTS OF THE IRON GROUP OF ELEMENTS. PART III.

By A. BOSE AND S. C. MITRA

DEPARTMENT OF X-RAYS AND MAGNETISM, INDIAN ASSOCIATION FOR THE CULTIVATION OF SCIENCE, CALCUTTA - 32

(Received for publication, September 20, 1952)

**ABSTRACT.** In Part II of the present paper it was found that several instances of the existence of the effect of the long range fields, in paramagnetic salts of the first half of the iron group of elements, arose, in spite of the conditions there being unfavourable for such observations. In the second half of the iron group the removal of orbital degeneracy by the cubic field in the first approximation, is less perfect. In consequence, Jahn-Teller distortions of the whole crystal lattice occur, giving rise to deviations from cubic field and hence further removal of the orbital degeneracy and to some extent the spin degeneracy. The spin-orbit coupling restores some of the orbital moment and at the same time causes a restraint on the orientations of the spins. These also lead to Jahn-Teller repercussions throughout the crystal lattice and to the final stabilization of the Stark-energy levels. It is thus seen that the final stabilization of the energy in the paramagnetic salts is dependent on the long range fields, especially when removal of orbital degeneracy by the cubic field is imperfect. Clear evidence of this is found from the salts of the ions  $\text{Fe}^{++}$ ,  $\text{Co}^{++}$ , and to a smaller extent of  $\text{Ni}^{++}$ . Evidence from  $\text{Cu}^{++}$  salts is inconclusive for various reasons.

## 1 INTRODUCTION

In the previous part of this paper (Bose and Mitra, 1952) we found a small but appreciable effect of the changes in the crystalline electric fields, on the magnetic behaviour of the ions of the first half of the iron group, arising from the changes of the ions and dipoles lying outside the immediate neighbours of the paramagnetic ion. It was discussed there that the Jahn-Teller conditions of stability for a paramagnetic ionic cluster, when extended to the entire crystal lattice may be enough to explain the removal of the degeneracy of both the spin and the orbital states of the paramagnetic ion.

In the second half of the iron group the orbital contributions to the magnetic moments are in general large, even when the lowest cubic state in the Stark-pattern of an ion is non-degenerate, and we expect here a correspondingly larger deviation of the moments from salt to salt and from solid to solution, containing the same paramagnetic ion.

## DISCUSSIONS

The experimental data are much more extensive and reliable in the latter half of the iron group than the first. But here again the variations of

the results from author to author make it extremely difficult to compare the absolute magnitudes of the actions of the long and short range fields. We take up, as before, the results represented in the form of graphs of the square of mean effective moments against the absolute temperatures (figures 1-7)\*.

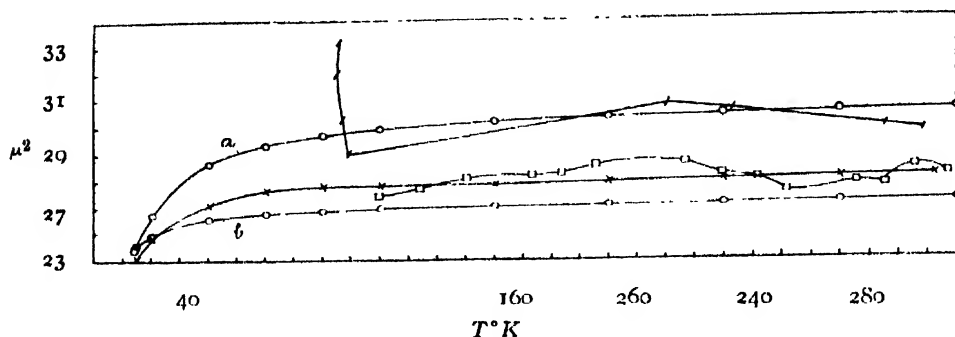


FIG. 1

$\mu^2$  versus  $T$  curves for  $\text{Fe}^{++}$  salts.

1.  $\circ$  --- Jackson.—(a)  $\text{Fe}(\text{NH}_4\text{SO}_4)_2 \cdot 6\text{H}_2\text{O}$ ; (b)  $\text{FeSO}_4 \cdot 7\text{H}_2\text{O}$
2.  $\times$  --- Onnes and Oosterhuis— $\text{FeSO}_4 \cdot 7\text{H}_2\text{O}$
2.  $\square$  --- Ishiwara— $\text{FeSO}_4 \cdot 7\text{H}_2\text{O}$
4.  $|$  --- Foex— $\text{Fe}(\text{NH}_4\text{SO}_4)_2 \cdot 6\text{H}_2\text{O}$ .

(1)  $\text{Fe}^{++}$  salts. From the fact that an orbital triplet  $1^1_3$ , lies lowest in the Stark-pattern of the octahedrally coordinated salts of  $\text{Fe}^{++}$  ion we should expect large orbital Jahn-Teller distortions of both the long and the short range structures in such salts (Bose and Mitra, 1952). Thus, in the two salts studied, namely,  $\text{FeSO}_4 \cdot 7\text{H}_2\text{O}$  and  $\text{Fe}(\text{NH}_4\text{SO}_4)_2 \cdot 6\text{H}_2\text{O}$  in both of which  $\text{Fe}^{++}$  ions are surrounded by an octahedron of 6 water molecules, the differences observed in the temperature variation curves of the moments (figure 1) must be due to differences in the long range fields alone. On an examination of the curves, we can immediately discard Ishiwara's (1915) and Foex's (1921) measurements as being wholly unreliable. Then, even admitting rather large differences in Jackson's (1924) and Onne's (1924) curves for  $\text{FeSO}_4 \cdot 7\text{H}_2\text{O}$  as being due to systematic errors in calibration or tendency for oxidation of the salt, it will be seen that a fairly large difference exists between the curves of the above two salts. It is known from the X-ray structures of the two salts (Hofmann (1931); Beccers and Schwartz (1935)) that the crystals of the two salts, though both monoclinic, are not in the same space group, the single salt belonging to  $C_{2h}^6$  with 16 molecules in the unit cell and the Tutton salts to  $C_{2h}^6$  with two molecules. Of the two salts, the former evidently has a lesser internal symmetry and it is therefore very satisfactory that it actually shows a larger quenching of the effective moment. It is further interesting to note that at low temperatures the curve for  $\text{FeSO}_4 \cdot 7\text{H}_2\text{O}$  is less steep than that for the Tutton salt, showing lesser influence of the spin quenchings as also of the higher order field terms in this region. Represen-

\* For full references please see Part I of the present paper (Bose and Mitra)



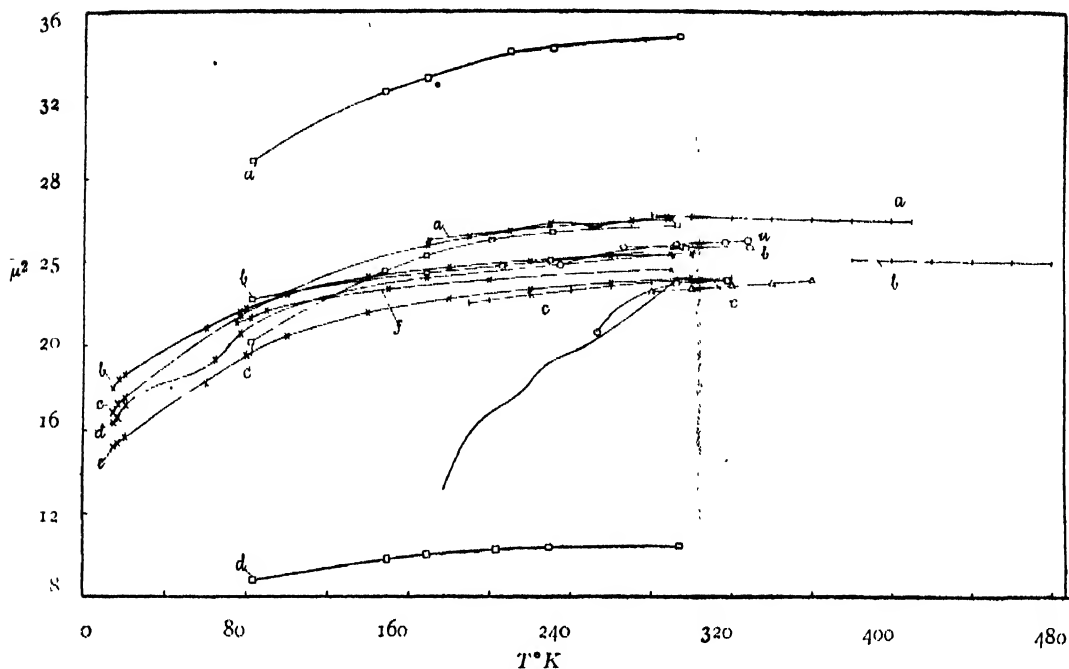


FIG. 2

 $\mu^2$  versus  $T$  curves for  $\text{Co}^{++}$  salts

Bartlett --- ○

a.  $\text{Co}(\text{KSO}_4)_2 \cdot 6\text{H}_2\text{O}$ b.  $\text{Co}(\text{NH}_4\text{SCN})_2 \cdot 6\text{H}_2\text{O}$ c.  $\text{CoSO}_4 \cdot 7\text{H}_2\text{O}$ 

2. Janes --- □

a.  $\text{CoSO}_4 \cdot 6\text{NH}_3$ b.  $\text{K}_2\text{Co}(\text{SCN})_4 \cdot 4\text{H}_2\text{O}$ c.  $\text{CoCl}_2 \cdot 6\text{NH}_3$ d.  $\text{Co}(\text{CN})_2 \cdot 2\text{H}_2\text{O}$ 

3. Jackson --- ×

a.  $\text{Co}(\text{KSO}_4)_2 \cdot 6\text{H}_2\text{O}$ b.  $\text{CoSO}_4 \cdot 7\text{H}_2\text{O}$ c.  $\text{Co}(\text{RbSO}_4)_2 \cdot 6\text{H}_2\text{O}$ d.  $\text{Co}(\text{KSO}_4)_2 \cdot 6\text{H}_2\text{O}$ e.  $\text{Co}(\text{NH}_4\text{SO}_4)_2 \cdot 6\text{H}_2\text{O}$ f.  $\text{CoSO}_4 \cdot 7\text{H}_2\text{O}$ 

Chatillon --- |

a.  $\text{CoCl}_2 \cdot \text{H}_2\text{O}$ b.  $\text{CoCl}_2 \cdot 6\text{H}_2\text{O}$  molten bluec.  $\text{CoCl}_2 \cdot 6\text{H}_2\text{O}$  solid.

5. Serres --- Δ

 $\text{CoSO}_4 \cdot 7\text{H}_2\text{O}$ 

6. Mercier --- —

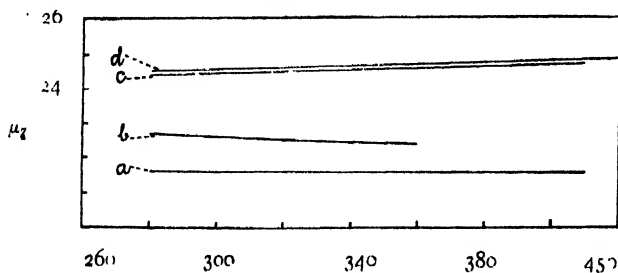
 $\text{CoCl}_2$  soln in methanol.

FIG. 3a

 $\mu^2$  versus  $T$  curves for solutions of  $\text{Co}^{++}$  salts.Author - Chatillon— a.  $\text{CoCl}_2$  soln in amyl alcohol.b.  $\text{CoCl}_2$  soln. in ethyl alcohol.c.  $(\text{CoNO}_3)_2$  aq. soln.d.  $\text{CoCl}_2$  and  $\text{CoSO}_4$  aq. soln.

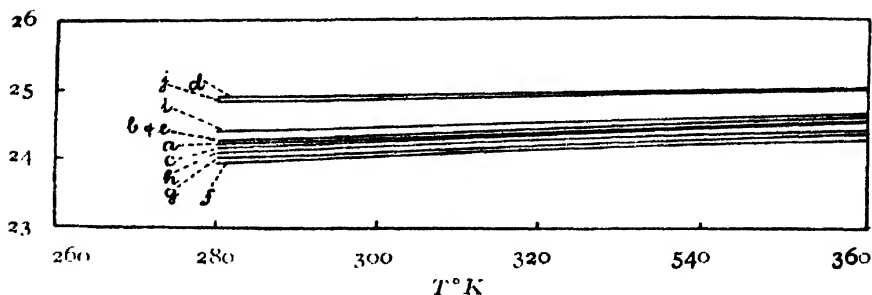


FIG. 3b

Author—Lallemand— $\text{CoCl}_2$  aq. soln, conc. in gms. per gm. soln.

Indep. of Conc.

1.  $a = .041$ ;  $b = .0207$ ;  $c = .091$ ;

Dependent on conc. & mode of preparation

2.  $d = .017$ ;  $e = .325$ ;  $f = .072$ ;  $g = .046$ ;

$h = .031$ ;  $i = .022$ ;  $j = .0125$ .

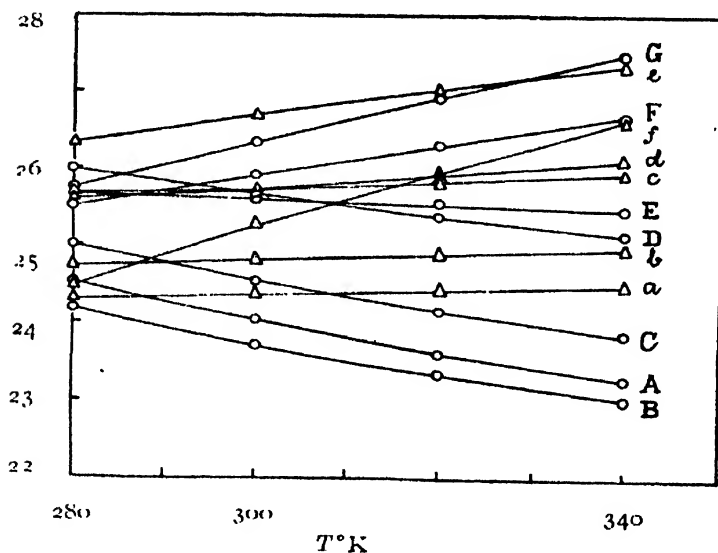


FIG. 4

$\bar{\mu}^2$  versus  $T$  curves for solutions of  $\text{Co}^{++}$  salts.

Author—Zahlenbrach.

$\text{CoCl}_2 \cdot 6\text{H}_2\text{O}$  aq. soln.

A = 7.382 conc. gms./100 c.c. soln.

B = 4.434

C = 2.957

D = 1.477

E = .743

F = .236

G = .118

$\text{CoCl}_2$  anhyd. aq. soln

$a = 2.636$  conc. gms./100 cc. soln

$b = 1.757$  „

$c = 1.054$  „

$d = .527$  „

$e = .264$  „

$f = .132$  „

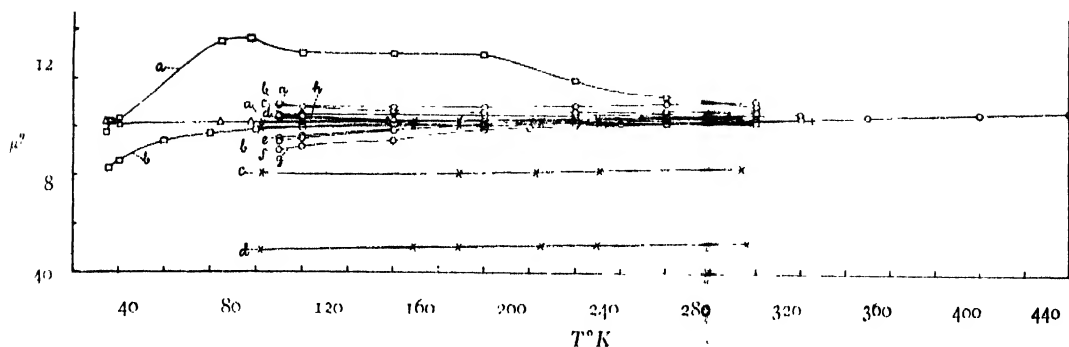


FIG. 5

 $\mu^2$  versus  $T$  curves for  $\text{Ni}^{2+}$  salts.

Serres - - - O

a.  $\text{NiSO}_4 \cdot 8.5\text{H}_2\text{O}$ ; b.  $\text{Ni}(\text{NH}_4\text{SO}_4)_2 \cdot 6\text{H}_2\text{O}$ ; c.  $\text{NiSO}_4 \cdot 4\text{H}_2\text{O}$ ; d.  $\text{NiSO}_4 \cdot 6\text{H}_2\text{O}$ ;  
 e.  $\text{NiCl}_2 \cdot 6\text{H}_2\text{O}$ ; f.  $\text{NiSO}_4 \cdot 1.13\text{H}_2\text{O}$ ; g.  $\text{NiSO}_4 \cdot \text{H}_2\text{O}$ ; h.  $\text{NiSO}_4 \cdot 7\text{H}_2\text{O}$ .

Jackson - - □ - a.  $\text{NiSO}_4 \cdot 7\text{H}_2\text{O}$ ; b.  $\text{Ni}(\text{NH}_4\text{SO}_4)_2 \cdot 6\text{H}_2\text{O}$ .de Haas and Gorter - - Δ -  $\text{NiSO}_4 \cdot 7\text{H}_2\text{O}$ Janes - - x - a.  $\text{Ni}(\text{NO}_3)_2 \cdot 6\text{H}_2\text{O}$ ; b.  $\text{NiSO}_4 \cdot 6\text{H}_2\text{O}$ ; c.  $\text{Ni}(\text{NO})_2 \cdot 4\text{NH}_3$ ; d.  $\text{Ni}(\text{CN})_2\text{C}_6\text{H}_6\text{NH}_3$ 

15

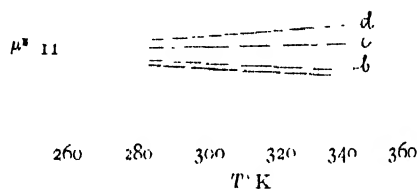


FIG. 6

 $\mu^2$  versus  $T$  curves for solutions of  $\text{Ni}^{2+}$  salts.Author—Fahlenbrach.  $\text{NiCl}_2$  Solution

- After aging, independent of conc.  
 $a = 7.310, 3.412, 1.707, .5845$  gms. per 120 cc. soln.
- Freshly prepared; dependent on conc.  
 $b = 4.271$      $c = 1.073$      $d = 0.429$

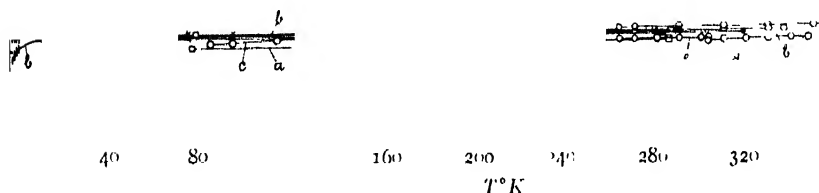


FIG. 7

 $\mu^2$  versus  $T$  curves for  $\text{Cu}^{2+}$  salts and their solutions.

- ⊙ - - - Birch—*a.*  $\text{CuSO}_4 \cdot 5\text{H}_2\text{O}$ ; *b.*  $\text{CuCl}_2 \cdot 2\text{H}_2\text{O}$ ; *c.*  $\text{Cu}^{2+}\text{O} \cdot \text{H}_2\text{O}$ ; *d.*  $\text{CuCl}_2$  soln.; *e.*  $\text{CuCl}_2$  soln.
- - - - Bartlett— $\text{Cu}(\text{KSO}_4)_2 \cdot 6\text{H}_2\text{O}$  and  $\text{Cu}(\text{NH}_4\text{SO}_4)_2 \cdot 6\text{H}_2\text{O}$ .
- Δ - - - de Haas and Gorter— $\text{CuSO}_4 \cdot 5\text{H}_2\text{O}$ .
- x - - - Hupse— $\text{Cu}(\text{KSO}_4)_2 \cdot 6\text{H}_2\text{O}$ .
- - - - Janes—*a.*  $\text{CuSO}_4 \cdot 4\text{NH}_3 \cdot \text{H}_2\text{O}$ ; *b.*  $\text{Cu}(\text{KSO}_4)_2 \cdot 6\text{H}_2\text{O}$  &  $\text{Cu}(\text{NH}_4\text{SO}_4)_2 \cdot 6\text{H}_2\text{O}$ .
- ! - - - Reckie—*a.*  $\text{Cu}(\text{KSO}_4)_2 \cdot 6\text{H}_2\text{O}$ ; *b.*  $\text{CuSO}_4 \cdot 5\text{H}_2\text{O}$ .

ting the curves by a three constant formula of the type,  $\overline{\mu^2_{eff}} - 24 = A + BT + \frac{C}{T}$ , as we did in the previous part of the paper (*l.c.*) we find for the constants the following values (Table I). The differences in the A terms are

TABLE I

Author	Salt	A	B	C
Omnes and Oosterhuis	$\text{FeSO}_4 \cdot 7\text{H}_2\text{O}$	+4.57	-.001	-51.4
Jackson	$\text{FeSO}_4 \cdot 7\text{H}_2\text{O}$	+3.21	0	-25.6
Do	$\text{Fe}(\text{NH}_4\text{SO}_4)_2 \cdot 6\text{H}_2\text{O}$	+6.23	+0.017	-66.

mostly due to differences in the short range fields, induced by differences in long range fields. The differences in the C terms which are well pronounced should be especially noted, as these come mostly from the differences in long range asymmetric fields, acting on both orbital and spin degeneracies, becoming more prominent at low temperatures. Unfortunately, no temperature variation data on solutions of  $\text{Fe}^{++}$  salts are available from which we could estimate the full action of the long range fields in these salts.

(7)  $\text{Co}^{++}$ . In the Stark-pattern of the octahedrally coordinated red  $\text{Co}^{++}$  salts an orbitally degenerate triplet  $\Gamma_1$ , lies lowest and hence their behaviours should not be very much different from the similarly constituted  $\text{Fe}^{++}$  salts. It has been, however, found that the case is complicated by the tendency of many  $\text{Co}^{++}$  salts to form a blue complex with a tetrahedral coordination, in the Stark-pattern of which a singlet  $\Gamma_2$  lies lowest so that the behaviour approaches that of octahedrally coordinated  $\text{Cr}^{+++}$  or  $\text{Ni}^{++}$  salts. Especially, in the state of solutions the two types of complexes may be concurrently present, their relative amounts depending on temperature, concentration, mode of preparation, previous treatment, etc., so that the interpretation of the results is not easy. Corresponding to the large orbital contributions to the moment in the red salts of  $\text{Co}^{++}$  ion and also to a high degree of restraint on the spins through spin-orbit coupling and the rhombic fields, we should expect a large Jahn-Teller effect upon both short range and long range clusters. (Bose and Mitra Part II)

Let us take the graphical representations of the moments of the solid salts first (figure 2) and for obvious reasons only such as do not depend on the mode of preparations or previous history. Of the salts studied, the best for comparison would be the isomorphous monoclinic Tutton salts in which X-ray data give an octahedron of water molecules immediately surrounding each  $\text{Co}^{++}$  ion, the difference in the distant atoms being only due to the different alkali ions, *e.g.*  $\text{K}^+$ ,  $\text{NH}_4^+$  or  $\text{Rb}^+$ . The interatomic distances increase from salt to salt in the sequence of increasing ionic radius of the alkali ions. The

water octahedron has a pseudo-tetragonal symmetry and the distant atoms have monoclinic symmetry about the  $\text{Co}^{++}$  ion. Unfortunately, the magnetic data on the moments vary considerably even for the same salt done twice by the same observer,—vide the graphs for the potassium salt, also those for monoclinic  $\text{CoSO}_4 \cdot 7\text{H}_2\text{O}$  by Jackson (1923, 1924, 1927 1933). It is also rather disquieting that the graph of the ammonium salt by the same author should show the highest quenching of the effective moment. Much significance, however cannot be attached to these as also to the inflexions in the curve of the potassium salt nearabout  $80^\circ\text{K}$ , which are not confirmed by the other observations. Bartlett's (1932) curves for the same two Tutton salts are not very different from each other and actually cross. The importance of these data is, however, dubious owing to the very small range of temperature used.

In  $\text{CoSO}_4 \cdot 7\text{H}_2\text{O}$ , which is isomorphous with  $\text{FeSO}_4 \cdot 7\text{H}_2\text{O}$ , the  $\text{Co}^{++}$  ion is surrounded by a water octahedron but the actual internal symmetries of the atoms both near and distant are less than the Tutton salts. The data by Jackson (*l.c.*), Serres (1932) and Bartlett (*l.c.*) differ much from one another. On the whole, however, comparing all these salts one has to admit that without laying too much stress on the sequence of the changes from salt to salt, there exist fairly large differences in the moment curves of the salts, least quenching being for the rubidium salt and the highest perhaps for the heptahydrated sulphate, as it should be, in view of the increasing asymmetry of internal structure along the series.

The clustering immediately round  $\text{Co}^{++}$  ion in the hexahydrated chloride is exactly as in the previous salts but the presence of  $\text{Cl}^-$  ions marks the difference in distant atoms, of which the exact arrangements are not known, causing a larger quenching of the moment than most of the Tutton salts, as shown by Mlle. Serres' data (*l.c.*).

$\text{CoCl}_2 \cdot 6\text{NH}_3$  done by Janes (1935), in which  $\text{Co}^{++}$  is surrounded by an octahedral cluster of  $\text{NH}_3$  instead of  $\text{H}_2\text{O}$  as in the previous salts, shows a much smaller quenching effect of the  $\text{NH}_3$  molecules compared to  $\text{H}_2\text{O}$ , the case being similar to the rubidium Tutton salt. We might have expected the salt  $\text{CoSO}_4 \cdot 6\text{NH}_3$  by the same author to behave not very differently. But the tremendous difference actually observed leads us to suspect that the magnetic behaviour of these ammines may be highly sensitive to changes in the long range fields. Much higher moment in the amminosulphate is evidently due to an incomplete splitting of the ground  $1^1_4$  triplet in the Stark-pattern, the electric field on the  $\text{Co}^{++}$  ion being uniaxial; and an inversion in  $1^1_4$  triplet occurring owing to a comparable magnitude of the 2nd and the 4th order rhombic fields, causing the doubly degenerate component of  $1^1_4$  to lie lowest here, instead of the singlet as is probably the case in the aminochloride or the other  $\text{Co}^{++}$  salts (*vide*  $\text{V}^{+4}$  and  $\text{V}^{+3}$  salts, Bose and Mitra Part II; Van Vleck 1939).

On the other hand,  $\text{Co}(\text{CN})_2 \cdot 6\text{H}_2\text{O}$  (Jones, *l.c.*) shows an abnormally low moment much below even the spin only value of 15, no doubt owing to strong covalency common in all cyanides and this abnormality therefore is more the action of the near than the distant atoms.

$\text{CoCl}_2 \cdot \text{H}_2\text{O}$  done by Chatillon (1927) at high temperatures shows much higher moment than the hexahydrated chloride, which can only be explained as an effect of ferromagnetic spin couplings of similar ions, very likely to occur in view of its low magnetic dilution.

$\text{CoCl}_2 \cdot 6\text{H}_2\text{O}$  studied in the molten state (Chatillon, *l.c.*, figure 2) is somewhat complicated by the formation of a tetrahedral phase, but clearly shows the sudden rise in the moment as the lattice breaks down at the melting point and the long range fields vanish. The cobalt salts in aqueous solutions done by Lallemant (1935) and Chatillon (*l.c.*) (figures 3a and 3b) also show similar behaviour, though the same tendency for tetrahedral cluster formation mars the possibility of observing to the best advantage, the result of vanishing long range fields in these solutions. By the way, the enormous variations of the moments with concentration and temperature, of some cobalt salts observed by Fahlenbrach (1932; figure 2) can possibly be ascribed to such uncertain changes in the coordination of the  $\text{Co}^{++}$  ions. In the alcoholic solutions (figure 3) of the cobalt salts (1932) the effect of the above tetrahedral clustering is even more clearly marked. The case of methanol solution of  $\text{CoCl}_2$  (Mercier, 1935; figure 2) is, however, unlike anything else and the field here must be such as to cause an even heavier quenching of the spins at low temperatures than in the cyanide.

The causes of the deviations from the Curie law can be compared in the different salts by trying to fit the curves with a three constant formula :

$$\mu_{eff}^2 = 15 - A + BT + \frac{C}{T}.$$

The values of the constants for the different salts are tabulated below, some of the results for the solid salts and the solutions having been omitted as having been measured over a too restricted range of temperatures to serve much useful purpose.

Two of Jackson's results below, marked by query, might be explained as being due to the observer having picked up for measurement, as luck would have it, some different crystal modification of the corresponding salt, having quite different crystal field. But it would be better to repeat these results before coming to any conclusion. The other values on the same salts by Jackson were done at Leiden over a wider range of temperatures and are more reliable.

On a perusal of the rest of the table we can immediately divide it into two sets of similar results, leaving aside the solitary case of the dihydrated cyanide. The first set consists of the heptahydrated sulphate and the Tutton salts, all having comparatively small A values, indicating small

TABLE II

Salt	Author	A	B	C
1. $\text{CoSO}_4 \cdot 7\text{H}_2\text{O}$	Jackson	+9.00	+0.0016	-224. (?)
2. -do-	-do-	+6.81	+0.0091	-59.1
3. $\text{Co}(\text{KSO}_4)_2 \cdot 6\text{H}_2\text{O}$	-d -	+5.20	+0.0117	-60.6
4. -do-	-do-	+17.9	-0.0113	-1007 (?)
5. $\text{Co}(\text{NH}_4\text{SO}_4)_2 \cdot 6\text{H}_2\text{O}$	-do-	+5.06	+0.0115	-74.7
6. $\text{Co}(\text{RbSO}_4)_2 \cdot 6\text{H}_2\text{O}$	-do-	+6.02	+0.0185	-65.8
7. $\text{CoSO}_4 \cdot 7\text{H}_2\text{O}$	Seires	+5.77	+0.0069	—
8. $\text{CoCl}_2 \cdot 6\text{H}_2\text{O}$	Chatillon	+9.71	+0.001	-540
9. $\text{CoCl}_2 \cdot \text{H}_2\text{O}$	-do-	+11.8	-0.0018	—
10. $\text{CoSO}_4 \cdot 6\text{NH}_3$	Janes	+20.8	+0.0039	-597.
11. $\text{CoCl}_2 \cdot 6\text{NH}_3$	-do-	+13.7	-0.0015	-690
12. $\text{K}_2\text{Co}(\text{SCN})_4 \cdot 4\text{H}_2\text{O}$	-do-	+7.46	+0.0085	-77.8
13. $\text{Co}(\text{CN})_2 \cdot 2\text{H}_2\text{O}$	-do-	-1.19	+0.0005	-178.

spin-orbit contribution from the upper cubic levels. The C values are also comparatively smaller, pointing to a small exchange of population amongst the rhombic levels and only moderate restraint on the spins, through the spin orbit coupling in these salts. The values of the constants A, B, C change from salt to salt and though the variation is not systematic the general tendency is for the values to increase in magnitude towards the rubidium salt. This is in the right direction, comparing the internal symmetries of the sulphate and the double sulphates.

The salt  $\text{K}_2\text{Co}(\text{SCN})_4 \cdot 4\text{H}_2\text{O}$  (Janes, l. c.) appears to have the contributions from A, B and C terms not much different from the previous salts, the small difference seeming to indicate a crystalline field splitting of lesser magnitude in this salt.

The other set of salts comprising the chlorides, hexammines have a much higher numerical values of the constants A, B, and C, which is possible only if as already mentioned crystalline fields are smaller and more symmetric causing a large contributions from upper cubic levels, from the rhombic levels of the lowest  $1^1_4$  triplet as also large spin quenchings through spin-orbit coupling and the rhombic field. The order of decreasing strength of the of fields is evidently along the series  $\text{CoCl}_2 \cdot 6\text{H}_2\text{O}$ ,  $\text{CoCl}_2 \cdot \text{H}_2\text{O}$ ,  $\text{CoCl}_2 \cdot 6\text{NH}_3$  and  $\text{CoSO}_4 \cdot 6\text{NH}_3$ . However, as was mentioned previously in connection with the ammino-sulphate, it now appears probable that in all these cobalt salts the lowest triplet is only partially separated into a doublet and singlet by a (nearly) uniaxial field existing in these crystals and the 2nd and the 4th order rhombic fields are in such a ratio as to cause an inversion of the rhombic triplet  $\Gamma_4$  in passing from 1st set of salts to the 2nd set, so that the singlet is lowest in the first and the doublet in the 2nd. This strengthens our former belief that the cobalt salts are very sensitive to even small changes in the long and the short range electric fields and provides us with a nice example of the Jahn-Teller distortional effects of the long range fields.

That the spin quenchings are of the 1st order in  $\text{Co}(\text{CN})_2 \cdot 2\text{H}_2\text{O}$  is shown clearly by the -ve value of the temperature independent term A, and the variations of the orbital contributions are also large as shown by the C term.

(3)  $\text{Ni}^{++}$ . In the octahedrally coordinated salts of  $\text{Ni}^{++}$  ion, just like  $\text{Cr}^{+++}$  ion, the  $\Gamma_2$  nondegenerate state lies lowest in the Stark pattern. But the spin-orbit coupling in  $\text{Ni}^{++}$  ion is  $-335 \text{ cm}^{-1}$ , as against  $+87 \text{ cm}^{-1}$  in  $\text{Cr}^{+++}$ . Also in  $\text{Ni}^{++}$  ion with 8 electrons as against 3 in  $\text{Cr}^{+++}$ , there is no Kramer's spin degeneracy. Hence the spin-orbit contributions from the upper cubic levels as also spin quenchings will be much larger. Evidently the effect of the long range fields should be more pronounced in the  $\text{Ni}^{++}$  salts. The results of the measurements on the  $\text{Ni}^{++}$  salts are plotted in graphs of  $\overline{\mu_{eff}^2}$  against  $T$  (Fig). Excepting a few, e.g., the salt  $\text{NiSO}_4 \cdot 7\text{H}_2\text{O}$  by Jackson (l.c.) which are known to be in error, and the salts  $\text{Ni}(\text{NO}_2)_2 \cdot 4\text{NH}_3$  and  $\text{Ni}(\text{CN})_2 \cdot \text{C}_6\text{H}_6 \cdot \text{NH}_3$  by Janes (l.c.), which must have strong covalent fields acting in them, the rest only of the salts approximately obey the Curie Law, with squares of the moments differing appreciably from the spin only value of 8, as are to be expected. The percentage deviations of the moments from salt to salt are somewhat larger than in  $\text{Cr}^{+++}$  salts (vide Part II). Further, the slopes of the curves are markedly different at low temperatures.

A three constant formula  $\overline{\mu_{eff}^2} - 8 = A + BT + \frac{C}{T}$ , applied to these curves yields the values of the coefficients A, B and C as tabulated below.

TABLE III

Salt	Author	A	B	C
1. $\text{NiSO}_4 \cdot 11\text{H}_2\text{O}$	Serres	+2.28	+0.0017	-130.
2. $\text{NiSO}_4 \cdot 11\frac{1}{2}\text{H}_2\text{O}$	do	+1.68	+0.0038	-61.2
3. $\text{NiSO}_4 \cdot 4\text{H}_2\text{O}$ $300^\circ - 140^\circ \text{K}$	do	+1.21	+0.0034	+108.
do $140^\circ - 90^\circ \text{K}$	do	+1.79	+0.0038	+25.2
4. $\text{NiSO}_4 \cdot 6\text{H}_2\text{O}$	do	+1.25	+0.0035	+62.2
5. $\text{NiSO}_4 \cdot 7\text{H}_2\text{O}$	do	+1.17	+0.0033	+77.7
6. $\text{NiSO}_4 \cdot 8\frac{1}{2}\text{H}_2\text{O}$	do	+1.36	+0.0034	+107.
7. $\text{Ni}(\text{NH}_4\text{SO}_4)_2 \cdot 6\text{H}_2\text{O}$	do	+1.62	+0.0041	+72.9
8. $\text{NiCl}_2 \cdot 6\text{H}_2\text{O}$	do	+1.79	+0.0025	-48.5
9. $\text{NiSO}_4 \cdot 6\text{H}_2\text{O}$	Janes	+1.79	+0.014	—
10. $\text{Ni}(\text{NO}_3)_2 \cdot 6\text{H}_2\text{O}$	do	+1.93	+0.0017	—
11. $\text{Ni}(\text{NO}_2)_2 \cdot 4\text{NH}_3$	do	-5.45	+0.0023	-23.3
12. $\text{Ni}(\text{CN})_2 \cdot \text{C}_6\text{H}_6 \cdot \text{NH}_3$	do	-3.14	+0.0012	+6.04
13. $\text{NiSO}_4 \cdot 7\frac{1}{2}\text{H}_2\text{O}$	de Haas & Gorter	+1.82	+0.0022	+4.45
14. do	Jackson	+8.99(?)	-0.0193	-102. (?)
15. $\text{Ni}(\text{NH}_4\text{SO}_4)_2 \cdot 6\text{H}_2\text{O}$	do	+2.20	+0.0002	-31.4 (?)

The largest number of salts studied, are by Mlle Serres (1933) but unfortunately the structures in most cases are not known. Even, in the hexhydrated and heptahydrated sulphates and the ammonium Tutton salt, where structures are known, the salts are not isomorphous so that it is difficult to compare the



action of the distant atoms. In these three salts and the hexahydrated chloride the  $\text{Ni}^{++}$  ions are all surrounded by 6 water molecules. The heptahydrated sulphate, being the most asymmetric structure of these should have the smallest value of the coefficient A and next in order should come, the Tutton salt, the hexahydrated chloride and then the hexahydrated sulphate. Excepting the value for the last, which appears to be rather too small, the other salts fall in a right sequence. It may be noticed that Janes' measurements for the hexahydrated sulphate and nitrate place them approximately in their correct position in the sequence. The large discrepancies in the values of the constants in the salts  $\text{NiSO}_4 \cdot \text{H}_2\text{O}$  and  $\text{NiSO}_4 \cdot 1.13\text{H}_2\text{O}$  cannot be easily explained though it is note worthy that the compositions of the salts are rather uncertain and the coordinations unstable. Further, exchange interactions are of importance in such magnetically concentrated salts.

The negative value of the C terms in the above two salts as also in  $\text{NiCl}_2 \cdot 6\text{H}_2\text{O}$  should be noted indicating a total quenching of the moments below liquid hydrogen temperatures. The high +ve values of C for most of the other salts done by Serres may not have much significance in view of the fact that for the salt  $\text{NiSO}_4 \cdot 7\text{H}_2\text{O}$  Serres' value for C is +77.7, as against the value of +4.45 by Gorter and de Haas, (Leid. Comm) done with great care over a wider range of temperatures, though the absolute value of the moment may not be as accurate as that of Serres.  $\text{NiSO}_4 \cdot 4\text{H}_2\text{O}$  is interesting in that its crystalline fields above  $140^\circ\text{K}$ , resembling  $\text{NiSO}_4 \cdot 6\text{H}_2\text{O}$  and  $\text{NiSO}_4 \cdot 8.5\text{H}_2\text{O}$  are very much modified below  $140^\circ\text{K}$ , approaching the behaviour of  $\text{NiSO}_4 \cdot 7\text{H}_2\text{O}$  of Gorter and de Haas and of  $\text{NiCl}_2 \cdot 6\text{H}_2\text{O}$  of Serres, indicating very different internal symmetries above and below  $140^\circ\text{K}$ .

It is of course possible that differences in the signs and magnitudes of the C terms in different salts might be partly due to exchange effects and partly of the changes in the action of the distant atoms to which the rhomic field constants are highly sensitive. It is noteworthy that in the field theory of Penny and Schlapp (1932) they have taken into account only the A and B terms in the mean moment of  $\text{Ni}^{++}$ , C term being accurately zero. But they have not considered the action of the distance atoms in this theory which may have quite important contributions to the C term.

The two complex salts done by Janes (*l.c.*) are definitely strongly covalent as is shown by the strong quenching of the moments. The values of A, B, C for  $\text{Ni}(\text{NH}_4\text{SO}_4)_2 \cdot 6\text{H}_2\text{O}$  by Jackson (*l.c.*) are quite different from Serres' and incompatible with the previous accounts.

As regards the measurements on solutions at different temperatures the only data are by Fahlenbrach (*l.c.*; figure 6) giving wide variations of the moment, with concentration and temperature which are contrary to room temperature measurements by most of the other authors as indicated in Part I (*l.c.*), and are inexplicable except on grounds of large uncertain changes in the compositions. So we leave these out of our consideration.

(4)  $\text{Cu}^{++}$  ion. The doublet  $\Gamma_3$  being the lowest level in the Stark-pattern for octahedrally coordinated  $\text{Cu}^{++}$  salts, we should expect them to behave similarly to the  $\text{Cr}^{++}$  and  $\text{Mn}^{+++}$  salts. But the spin moments in the two cases are one Bohr magneton against four and also the spin orbit coupling is very much larger in  $\text{Cu}^{++}$  than in  $\text{Cr}^{++}$  or  $\text{Mn}^{+++}$ . Actually, the behaviour of  $\text{Cu}^{++}$  is more resembled by the tetrahedrally coordinated  $\text{Tl}^{+++}$  or  $\text{V}^{+4}$  ion if we do not consider the differences in the spin-orbit couplings. All of the copper salts discussed here appear to obey the Curie law very well over a wide range of temperatures, except the three salts by Birch (1928) of which  $\text{CuCl}_2 \cdot 2\text{H}_2\text{O}$  and  $\text{CuSO}_4 \cdot \text{H}_2\text{O}$  are certainly rather concentrated magnetically; and  $\text{CuSO}_4 \cdot 5\text{H}_2\text{O}$  by Reekie (1939) below about  $10^\circ\text{K}$ , in which specific heat anomalies are also marked in this region (Ashmead, 1939). Recent measurements on the paramagnetic resonance show exchange interactions to be the cause of these anomalies (Bagguley and Griffiths 1948). The high temperature results of Birch on  $\text{CuSO}_4 \cdot 5\text{H}_2\text{O}$ , showing a break in the  $\mu_{eff}^2 - T$  curve indicates probably a change in the electric fields marked by a greater freedom for the  $\text{Cu}^{++}$  ion. There is however, a large discrepancy in the slope of the curve with those of de Haas and Gorter (Leid Comm.) and of Reekie which are certainly more reliable.

The moment curves (figure 7) for the different salts show so little difference from salt to salt that it is difficult to estimate the effects of the long range fields. This is not very strange considering the low absolute value of the effective moment in  $\text{Cu}^{++}$ , in spite of the fact that the contributions to the orbital moments are relatively fairly large.

It would be better for the above purpose to compare the three constant series representation of the results as before, e.g.

$$\overline{\mu_{eff}^2} - 3 = A + BT + \frac{C}{T}.$$

TABLE IV

Salt	Author	A	B	C
$\text{CuSO}_4 \cdot \text{H}_2\text{O}$	Birch	+ 868	+ .00046	- 54.
$\text{CuSO}_4 \cdot 5\text{H}_2\text{O}$	Birch (195.1-273.1°K 273-430°K do	+ 942 + 1015 + 986	+ .00021 + .00005 + .00005	- 69 - 35. - 80.
$\text{CuCl}_2 \cdot 2\text{H}_2\text{O}$	de Haas and Gorter	+ .550	+ .00053	- 78
$\text{CuSO}_4 \cdot 5\text{H}_2\text{O}$	Reekie	+ .651	+ .00003	- 1.6
$\text{CuSO}_4 \cdot 0.5\text{H}_2\text{O}$	do	+ 6.6	+ .00027	- .044
$\text{Cu}(\text{KSO}_4)_2 \cdot 6\text{H}_2\text{O}$	do	+ .657	+ .00022	- .014
$\text{Cu}(\text{NH}_4\text{SO}_4)_2 \cdot 6\text{H}_2\text{O}$	James	+ .558	+ .0058	+ 4.4
$\text{Cu}(\text{KSO}_4)_2 \cdot 6\text{H}_2\text{O}$	do	+ .592	+ .0040	+ 2.5
$\text{CuSO}_4 \cdot 4\text{NH}_3 \cdot \text{H}_2\text{O}$	do	+ .1528	+ .0009	- 8.9
$\text{Cu}(\text{KSO}_4)_2 \cdot 6\text{H}_2\text{O}$	Hupse	+ .676	+ .0035	- .051

It will be seen that the high frequency term in all the copper salts is quite negligible. It is well known that the spin-degeneracy in the 9 electron  $\text{Cu}^{++}$  ion is entirely of the Kramer's type as in  $\text{Ti}^{+++}$  or  $\text{V}^{++}$  with one electron and hence the crystalline electric field has no effect on the two-fold spin degeneracy. Thus the origin of the small C term in the various salts are either due to exchange interaction or higher order orbital contributions. Measurements of Reekie (l.c.) and Hupse (Leid.Comm.) on the Tutton salts giving very small +ve values of C extend to helium temperatures and are hence more reliable than those of Janes (l.c.). Somewhat larger +ve values of C in Janes's measurement therefore cannot be given much significance. The most important temperature independent term A, is given by the upper level contributions through the large spin-orbit coupling in  $\text{Cu}^{++}$  ion. Both Janes' and Reekie's values for the two Tutton salts agree in giving a difference in the A term in the right direction, decreasing from potassium salt to ammonium salt. The absolute values by the two authors are however somewhat different. The absolute value of A for the potassium salt by Miss Hupse is the highest of all. Again, the absolute value of the term A in  $\text{CuSO}_4 \cdot 5\text{H}_2\text{O}$  by Reekie is about the same as his ammonium salt, which is surprising since the pentahydrate is a triclinic crystal with no internal symmetry except inversion. Hence the orbital quenching here should have been the largest. It is to be noted that absolute value of de Haas and Gorter for A term for  $\text{CuSO}_4 \cdot 5\text{H}_2\text{O}$  seems to give a better fit with Reekie's values for the Tutton salts, though it must be admitted that the results of the former authors being only down to  $14^\circ\text{K}$  give no indication of the steep downward fall in the curve below  $14^\circ\text{K}$  observed by Reekie. In fact, the higher value of A for  $\text{CuSO}_4 \cdot 5\text{H}_2\text{O}$  by Reekie might be ascribed to the inclusion of this steep part of the curve in calculating the constants of the series formula. The comparatively smaller value of A and larger -ve value of C in the salt  $\text{CuSO}_4 \cdot 4\text{NH}_3 \cdot \text{H}_2\text{O}$  done by Janes are no doubt owing to a much stronger field perhaps arising from a square coordination of the  $\text{Cu}^{++}$  ion with four  $\text{NH}_3$  molecules.

The data on solutions of  $\text{Cu}^{++}$  salts are not extensive enough to enable us to compare these with the solid salts.

#### CONCLUSION

From the previous discussions, we have been able to show definitely that the effects of the long range electric fields on the mean effective moments in the latter half of the ion group are by no means negligible, and are particularly prominent in the  $\text{Fe}^{++}$  and  $\text{Co}^{++}$  salts. Quantitative treatment of such fields are, however, out of the question primarily owing to lack of extensive and reliable data on a large number of similarly constituted salts as also their solutions. Further, it will have to be admitted that the mean values of the moments can only give us an idea of the long range cubic field

and the averaged effect of the rhombic fields, to the variations of which the moments are not very sensitive.

The long range rhombic fields are very structure sensitive and have large influence on the magnetic anisotropies and the principal moments in the crystals. The study of these, therefore, would give us a full picture of the Jahn-Teller mechanism for asymmetrically removing the magnetic degeneracy of the paramagnetic ions. The discussion on the magnetic measurements on single crystals of these salts which alone can give us the above informations, are left for some future papers.

One of us is grateful to the Government of India for the grant of a senior research scholarship in its 'Development Scheme'. Grateful thanks are also due to the authorities of the India Association for the Cultivation of Science for laboratory and other facilities.

#### REFERENCES

- Ashmead, J. 1939, *Nature*, **143**, 855.  
 Bartlett, R. W., 1932, *Phys. Rev.*, **41**, 818.  
 Baggeley, D. M. S., and Griffiths, J. H. R., 1948, *Nature*, **162**, 538.  
 Beevers, C. A. and Schwartz, 1935, *Zeit. f. Kryst.*, **91**, 157.  
 Birch, F., 1928, *Jour. de Phys.*, **9**, 137.  
 Bose, A and Mitra, S. C., Pt. I. 1952, *Ind. J. Phys.*, **26**, 393.  
 „ „ Pt. II, 1952, *ibid*  
 Chatillon, A., 1927, *Ann. de Phys.*, **9**, 187.  
 Fahlenbrach, H. 1932, *Ann. der. Phys.*, **13**, 265  
 Foex, G., 1921, *Ann de Phys.* **16**, 174.  
 de Haas, W. J., and Gorter, C. J., *Comm. Leid.* 210d.  
 „ „ *ibid.* 218d.  
 Hofmann, W. 1931, *Zeits. f. Kryst.* **78**, 279  
 Hupse, J. C. *Comm. Leid.* 265d.  
 Ishiware T., 1915, *Sci. Rep. Tohoku. Univ.*  
 Jackson, L. C. 1923, *Proc. Roy. Soc. A*, **104**, 671.  
 „ 1924, *Phil. Trans. Roy. Soc. A*, **224**, 1.  
 „ 1927, *ibid.* **226**, 107.  
 „ 1933, *Proc. Roy. Soc. A*, **140**, 695.  
 Janes, R. B., 1935, *Phys. Rev*, **48**, 78.  
 Lallemand, A., 1935, *Ann. de Phys.*, **3**, 97.  
 Mercier, R. 1935, *Ann. de Phys.*, **3**, 201.  
 Onnes, K. and Oosterhuis, 1911, *Proc. Roy. Soc. Amst.*, **13**, 1.  
 Pennev, W. G. and Schlapp, R., 1932, *Phys. Rev.*, **42**, 666.  
 Reckie, J. 1939, *Proc. Roy. Soc. A*, **173**, 367.  
 Serres, A. 1932, *Ann. de Phys*, **17**, 5.  
 „ 1933, *ibid.* **20**, 441.  
 Van Vleck, J. H. 1932, *Phys. Rev.* **41**, 208.  
 „ 1939, *Jour. Chem. Phys.*, **7**, 61.

# STREAMER MECHANISM IN A.C. SILENT DISCHARGES

By S. R. KHASTGIR AND C. M. SRIVASTAVA

PHYSICS DEPARTMENT, BENARES HINDU UNIVERSITY, BENARES

(Received for publication, October 23, 1955)

**ABSTRACT.** The streamer mechanism of Loeb and Meek, as applied to A. C. 'silent' discharges is developed in the paper. According to the streamer theory, when the applied field is adequate for Townsend's cumulative ionization, there is a conical column of positive ions drifting towards the cathode. In an A.C. 'silent' discharge, the negative charge formed on the intervening glass surface attracts the positive ions of the conical column near the anode and forms a stationary array of positive ions close to the glass surface, producing thereby an electrical double layer. A gap is also set up initially between the array of positive ions and the streamer by the time the latter touches the glass wall on the cathode side. A discharge is not, therefore, possible at the time due to this gap. It has been explained how this gap is subsequently bridged up, when the density of the charge on the glass surface attains a requisite value producing what has been called *Townsend pulses* at the peak values of the applied A.C. field. The discharge (or discharges) across the electrical double layer on and near the glass surface in the manner suggested by Mitra gives rise to a different type of pulses. Such pulses have been called *discharge pulses*. That the two types of pulses exist, at least in certain gases, is substantiated by the experimental results of Khastgir and Setty. In iodine vapour, there is experimental evidence to show that the critical voltage for the occurrence of the Townsend pulses is distinctly less than that for the occurrence of the 'discharge' pulses.

The effect of light on the two types of pulses has been considered in detail and the following conclusions have been drawn :

(i) Initiation of the Townsend pulses by irradiation may be possible under favourable conditions. This explains the *positive* Joshi effect observed near the threshold potential in certain gases.

(ii) At or near the 'threshold' potential, complete suppression or reduction of *either* type of pulses may be caused by irradiation.

(iii) In iodine vapour, the negative light effect is largely due to the disappearance or reduction of the 'discharge' pulses.

## INTRODUCTION

The photo-increase and photo-reduction of discharge current in A.C. discharge which are known as the *positive* and *negative* Joshi effect are now well established. It is also well known that the Joshi effect is associated with some current pulses which can be observed, when the potential difference across a suitable high resistance placed in series with the A.C. discharge circuit, is delineated on the fluorescent screen of an oscillograph. Several attempts have been made from time to time to explain experimental results on the subject. The views put forward by Joshi himself (1945, 1946, 1947) have been used by his associates (Ramana Rao and Sarma, 1949 Arnika,

1952) to explain in a general way the negative and positive light effect. A modification of the Klemenc-Hintenberger-Hofer mechanism (1937) of the A.C. silent discharge as suggested by Mitra was reported by Deb and Ghosh (1946, 1948) and formed the basis of an explanation of the negative Joshi effect. Recently, a photo-dissociation theory has been formulated by Harries and von Fögel (1951) to explain the negative Joshi effect in chlorine and such other gases where photo-dissociation is possible. This theory has not taken in its purview the consideration of the positive effect.

The object of the present paper is to consider the streamer mechanism of Loeb and Meek (1941) as applied to A.C. silent discharges. The insulating material (glass wall) that intervenes the gas or vapour and the electrodes introduces certain features which provide a fundamental basis for the occurrences of two distinct types of current pulses in such discharges. The origins of these pulses and the effect of light on them form the main subject matter of the paper. It is also shown that there is sufficient experimental evidence in favour of the conclusions arising out of the streamer mechanism in A.C. silent discharges.

#### STREAMER THEORY OF SPARK DISCHARGE

The streamer theory of spark discharge as given by Loeb and Meek (1941) is summarised as follows:

It is well known that electron avalanches are formed under an electric field adequate for the Townsend collisions to take place. As each avalanche advances from the cathode to the anode, it spreads laterally by the random diffusive movement of the electrons and a conical distribution of positive ions is formed with more positive ions towards the anode and only a few at the apex of the cone drifting slowly towards the cathode. The electrons soon disappear into the metallic anode and a positive space-charge 'boss' appears on it.

During the process of cumulative ionization, a number of excited atoms and molecules are formed and some of them are excited to an energy exceeding the ionization potential of these atoms and molecules. These excited atoms and molecules give rise to photons of very short wavelengths. These photons are absorbed by the gas and electron-positive ion pairs are produced. The electrons of these pairs are attracted to the positive ions in the conical column which soon becomes a highly conducting *plasma* containing both electrons and positive ions. This conducting column moves slowly towards the cathode and is called the streamer. When the advancing tip of the streamer comes near the cathode, the photo-electrons produced by photons at the cathode bring about intense ionization at the cathode, producing a cathode spot which may become a source of visible light. Ultimately, when the tip of the streamer reaches the cathode, there is a conducting filament across the two metal electrodes and there occurs a current pulse which passes up the pre-ionized conducting channel to the

anode with very high velocity and multiplies the electrons present by a large factor. Such a mechanism was also developed by Schonland (1936) in connection with the return stroke of a lightning discharge.

The streamers have actually been photographed in cloud tracks by Raether (1940, 1941) and the cathode spot appearing when the streamer is almost reaching the cathode has been recorded in Dunnington's (1931) Kerr cell photographs.

The streamer formation requires adequate photo-ionization and adequate field at the streamer tip. A satisfactory quantitative criterion for the streamer formation has been given by Meek (1940). Townsend's theory which was attended with serious difficulties has now been replaced by the streamer theory of Loeb and Meek.

It is to be noted that the current pulse flashing from the cathode to the anode according to the streamer mechanism can still be called a *Townsend pulse*, as it is significant that for a pulse to pass, the applied field must be sufficiently high to produce cumulative ionization by Townsend's collision process. As soon as the Townsend pulse occurs, the potential across the electrodes drops and the electrons proceeding from the cathode are not in a sufficient field to produce electron avalanches. The pulse then ceases momentarily till the potential is again built up to the former value by the external source. In this way there is an intermittent D.C. discharge with metal electrodes. The same picture is also true with A.C. discharges, at least for low frequencies.

#### MODIFIED PICTURE OF STREAMER FORMATION IN A.C. SILENT DISCHARGES

In A. C. silent discharges the picture of the streamer formation is somewhat different. The intervening glass wall in an ozonizer or in a discharge tube fitted with external metal electrodes, causes the formation of negative surface charge on its inner surface due to the deposit of negative charge by the electrons during the positive half cycle of the applied A. C. voltage. When the voltage is sufficient for Townsend collisions to take place, we soon get, for the positive half cycle, a conical distribution of positive ions which moves towards the cathode. An array of positive ions, at the base of the conical column and near the anode gets attached to the negative surface charge on the inner glass surface and remains stationary. The positive ions which are ahead of the stationary array in the conical column drift slowly towards the cathode producing a gap between the stationary array of positive ions and the moving conical column. As the conical column moves towards the cathode, it attracts to itself the neighbouring electron avalanches and the photo-ionized electrons in the same manner as in the streamer mechanism between metal electrodes. In the silent discharge, it is to be noted that even when the advancing tip of this highly conducting plasma containing positive ions and electrons touches the

cathode, a discharge is not possible due to the gap that is formed between the stationary array of positive ions  $GG$  (figure 1), attached to the negative charge on the inner glass surface ( $AA$ ) and the base ( $CC$ ) of the highly conducting streamer. This gap ( $GGCC$ ) illustrated in figure 1.

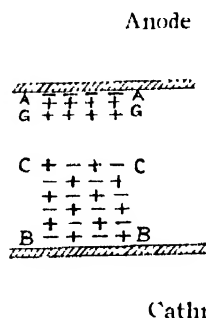


FIG. 1

The electrons from the cathode pass up the highly conducting plasma and move across the gap towards the anode. Within the gap the electrons are, of course, in an accelerating field and produce cumulative ionization by Townsend collisions. As a consequence, many electrons with very high velocity cross the stationary array of positive ions and move on in spite of the retarding field due to the negative surface charge on the glass wall. Only electrons with high velocity are, however, able to reach the glass surface. The negative charge on the inner glass surface is thus gradually built up. When the density of the surface charge attains a certain definite value, the electrons coming from the lower boundary of the gap are no longer able to penetrate through the stationary array of positive ions and get repelled. This repulsion brings back a large number of electrons within the gap, when there is already a number of positive ions due to Townsend collisions. Accordingly, the gap becomes highly conducting and gets bridged up causing a current pulse to flash across. The effect of the intervening glass is thus to produce initially a gap and to delay the discharge till such time as is required for the formation of a requisite density of charge on the inner glass surface, repelling the electrons moving up across the gap and ultimately bridging up the gap. It is to be noted that the magnitude of the applied voltage at which the requisite value for the density of surface charge is attained for bridging up the gap and for the occurrence of the Townsend pulse is to be identified with what is called 'threshold' potential in A.C. silent discharges.

It is evident, therefore, that when the applied A.C. voltage is such that the charge on the inner glass surface attains the requisite density at the peak value of the voltage, a Townsend pulse would occur at the peak in each half cycle. When the applied voltage is higher, the gap gets bridged up and a pulse is produced earlier at the required value. As the pulse flashes across, the voltage across the channel drops. The discharge, therefore, ceases, but voltage is again built up to the former value by the external



A.C. supply and another pulse is produced. Thus for a higher A.C. voltage a number of Townsend pulses is expected on either side of the peak. This is illustrated in figure 2.

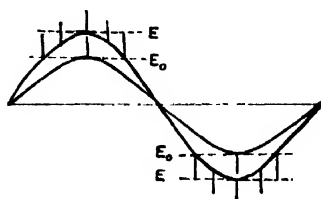


FIG. 2

#### 4. INITIATION OF TOWNSEND PULSE BY IRRADIATION

When the applied A.C. voltage across the two electrodes in an ozonizer or in a discharge tube fitted with external electrodes is critically adjusted to give just the sinuous current trace on the oscillograph, it is found that in certain gases irradiation produces pulses on the peaks of the A.C. cycle. This may be called positive Joshi effect which is observed near the threshold potential in certain gases. These pulses also appear in the dark when the applied voltage is slightly increased. If we accept the modified picture of the streamer formation in an A.C. silent discharge, the positive Joshi effect (near the 'threshold' potential) which indicates initiation of the Townsend pulses by irradiation in certain gases can be explained as follows :

Let us suppose that the applied voltage is so adjusted that Townsend's cumulative ionization is initiated but the discharge has not just started. This means that the gap is still there between the stationary array of positive ions and the base of the moving column and the negative charge on the glass surface has not attained, just yet, the requisite value for bridging up the gap. With the incidence of light on the negative charge on the inner glass surface, the photo-electrons emitted from this surface come nearer to the array of the positive ions and may at once cause the electrons coming from the lower boundary of the gap to be repelled and returned within the gap. The gap may thus be bridged up by the incidence of light on the negatively charged surface causing the Townsend pulses to flash across. Thus it can be said that the effect of light is to decrease slightly the value of the 'threshold' potential. In dark, however, when there is no photo-electric emission, the gap cannot be bridged up, as the applied voltage is not quite sufficient to build up the requisite negative charge on the inner glass surface so as to repel and return the electrons from the lower boundary of the gap. At higher voltages, of course, the gap is bridged up and the pulses persist even in the dark.

It is to be noted that the initiation of the Townsend pulses by irradiation is possible only in certain gases and under favourable conditions.

## 5. TWO TYPES OF PULSES IN A.C. SILENT DISCHARGES

From the picture of streamer formation in A.C. silent discharges, it is clear that with an applied voltage sufficient for Townsend collisions to take place, there is a layer of negative surface charge formed on the inner glass surface and a stationary array of positive ions very near the negative surface charge and further there is formed a gap between the stationary array of positive ions and the base of the conical column moving towards the cathode. It has already been explained how this gap is bridged up at the threshold potential when the requisite density of negative charge is formed on the glass surface, and a pulse flashes across the gap. This has been called a Townsend pulse. It may be mentioned that these pulses were identified by Deb and Ghosh (1948) as "low frequency" pulses. Their origin was also attributed to the alternate starting and stoppage of discharge under the combined action of the externally applied field and the opposing internal field (arising out of the separation of the electrons and positive ions caused by the application of the external field). The negative charge on the glass surface sufficient for the occurrence of a Townsend pulse may not be adequate to produce a discharge or discharges between the negative surface and the stationary array of positive ions in the manner already suggested by Deb and Ghosh. Such discharges may, however, take place at a certain higher voltage when the density of the negative charge attains a certain higher value. It is evident that when such discharges take place, there is neutralisation of the positive and negative charges and the opposing voltage due to the negative surface charge and the adjoining array of positive ions

removed. It is also evident that these discharges can only occur when the effective voltage is zero and the surface charge is free so that with the removal of the opposing voltage, due to the neutralisation of the negative surface charge and the positive charge on the array of positive ions, the effective voltage increases suddenly from zero to the value  $e$  and there is discharge current proportional to  $\frac{de}{dt}$ , which may be quite large. We have called this type of current pulse a 'discharge' pulse, as this is due to the discharge or discharges between the opposite charges in the electrical double layer on and near the glass surface. As these discharges occur when the effective voltage is zero the 'discharge' pulses should appear near the peaks of the A.C. current, there being a phase difference of nearly  $\frac{\pi}{2}$  between the discharge current and the applied voltage.

It is interesting to note that the electrical double layer consisting of a negative charge on the inner glass surface and an adjoining layer of positive charge which forms the basis of an explanation of the negative Joshi effect

by Mitra is only a logical consequence of the streamer mechanism in A.C. silent discharges.

That the two types of pulses exist, atleast in certain gases is abundantly clear from the oscillograms observed by Deb and Ghosh (1948) and by Khastgir and Setty (1952) in their experiments with ozonizers or with discharge tubes fitted with external electrodes. In iodine vapour, the two types observed by Khastgir and Setty are quite distinct in intensity, position and distribution. It has also been experimentally found with iodine vapour, that the critical 'threshold' voltage for the occurrence of the Townsend pulses is definitely less than the critical voltage for the occurrence of the 'discharge' pulses. A scrutiny of the two types of pluses with high sweep-frequency of the linear time-base of the oscillograph has also lent strong support to the view that the two types of pulses have altogether different origins.

#### EFFECT OF LIGHT ON THE TWO TYPES OF PULSES IN A.C. SILENT DISCHARGES

The effect of light is associated with photo-electric emission from the negative surface charge formed on the inner surface of the intervening glass wall. Starting from a low applied voltage, it has been observed that at least in certain gases, the Townsend pulses appear earlier than the discharge pulses, so that it can be said that the requisite density ( $\sigma_T$ ) of the negative surface charge for the Townsend pulses to occur is less than the requisite density ( $\sigma_D$ ) for the occurrence of the 'discharge' pulses. Let us now consider the effect of light, at some voltage, when both types of pulses co-exist. On irradiation, the negative charge is, of course, reduced due to photo-electric emission. If the density of surface charge is reduced, but not below  $\sigma_D$ , the discharge pulses are only reduced in size. If, however, on irradiation, the density of surface charge is reduced below  $\sigma_D$  but not below  $\sigma_T$ , the discharge pulses are completely quenched but the Townsend pulses persist. The photo-reduction of the discharge pulses and its dependence on the magnitude of the applied voltage has been discussed elsewhere by Khastgir and Setty (1952). The effect of light on the Townsend pulses will only be mentioned here.

We have already explained the initiation of the Townsend pulses by irradiation in certain gases and under favourable conditions. In some gases the initiation of the Townsend pulses by the incidence of light has not been observed. In such cases it may be said that the threshold potential remains practically unaffected by light. In considering the effect of light on the Townsend pulses, the fact that the emission of photo-electrons from the negatively charged layer is not an instantaneous process, has a very important bearing. Under light, when the photo-electric process is operative, it takes a little longer time for the attainment of the requisite surface charge for bridging up the gap and for the Townsend pulses to pass

than in the dark. Thus, on irradiation, the gap is widened to some extent due to the movement of the conducting column towards the cathode. Under the circumstances, when the gap length is slightly increased, the applied voltage or the requisite density of surface charge may not be just sufficient for the initiation of the Townsend pulses. Stoppage of Townsend pulses by irradiation may, therefore, be envisaged at or near the threshold potential, at least in those cases where the threshold value remains unaffected by irradiation. In cases where there is a slight decrease in the threshold potential due to irradiation, the Townsend pulses persist but their size may be reduced due to the increased resistance of the slightly wider gap through which the Townsend pulses pass. At higher voltages the photo-reduction of the Townsend pulses is induced very slight.

### CONCLUSIONS

The streamer mechanism as applied to A. C. silent discharges has been outlined. It has been shown that it is possible to have two types of current pulses, called the Townsend and the discharge pulses. There is experimental evidence of the two types of pulses in certain gases.

The effect of light on the two types of pulses has been discussed. It can be said in a general way that at or near the threshold potential, the negative effect may be caused by the suppression or reduction of either type of pulses. In the case of Townsend pulses, the reduction in size on irradiation is expected to decrease with the increase of the applied voltage. With regard to the discharge pulses the reduction in size should at first increase and attain a maximum and should subsequently fall off with the increasing voltage. In the case of iodine vapour there is definite experimental evidence to show that the negative effect is largely due to the disappearance or reduction of the discharge pulses. Regarding the positive Joshi effect that is unmistakably observed in iodine vapour just before the 'threshold' potential, it is considered as due to the initiation of the Townsend pulses by irradiation which may be possible under favourable conditions.

With regard to Joshi's theory and the photo-dissociation theory of Harries and von Engel (1951), it appears to us that the physical processes underlying these theories may be operative under suitable conditions, quite apart from what we have formulated regarding the occurrence of the Joshi effect.

In conclusion, it can be stated that the negative surface charge on the inner surface of the intervening glass wall is the main seat of the Joshi effect in A.C. silent discharges. The magnitude of the surface charge is dependent on the surface conditions, electron affinity etc. of the enclosed gas or vapour and as the work function of the surface depends on these factors, the photo-electric emission from the negative surface charge is also greatly affected

by them. It is now generally accepted that the Joshi effect is predominantly a surface phenomenon, although the possibility of volume effect is not ruled out altogether.

# REFERENCES

- Arnikar, H. J., 1952, *J. Chem. Phys.* **20**.
- Deb, S. C. and Ghosh, N., 1946, *Sci. and Cult.*, **12**, 17.
- "    "    "    1948, *Sci. and Cult.*, **14**, 39.
- "    "    "    1948, *J. Ind. Chem. Soc.*, **26**, 449.
- Dunnington, F. G., 1931, *Phys. Rev.*, **38**, 1535.
- Harries, W. L. and von Engel A , 1951, *J. Chem. Phys.* **19**, 514.
- Harries, W. L. and von Engel, A , 1951, *Proc. Phys. Soc. (Lond.)* **B64**, 915.
- Joshi, S. S , 1945, *Proc. Ind. Acad. Sci.* , **14**, 317.
- Joshi, S. S., 1946, *Curr. Sci.*, **16**, 281.
- Joshi, S. S., 1947, *Curr. Sci.*, **16**, 19.
- Klemenc, Hintenberger and Hofer, 1937, *Zeits. f. Elektrochemie*, **43**, 708.
- Khastgir, S. R. and Setty, P. S. V , 1952, *Proc. Phys. Soc. (Lond.)*, **B68**, 823.
- Khastgir, S. R. and Setty, P. S. V , 1952, *Sci. and Cult.*, **18**, 189, 394.
- Meek, J. M., 1940, *Phys. Rev.*, **67**, 722.
- Loeb, L. B. and Meek, J. M , 1949, *J. Appl. Phys.* **11**, 438, 459.
- Raether, H., 1941, *Zeits. f. Physik*, **117**, 375, 524.
- Raether, H., 1949, *Archiv. f. Electrotech.* **34**, 49.
- Ramana Rao and Sarma, 1949, *J. Phys. and Colloid Chem*, **53**, 753.
- Schonland, B. F. J., 1936, *Proc. Roy. Soc. A*, **164**, 132.
- Loeb, L. B. and Meek, J. M., 1941, "Mechanism of the Electric Spark" (Stanford University Press).



# ABSORPTION SPECTRA OF ORGANIC SUBSTANCES IN THE LIQUID AND SOLID STATES. VI. SOME DISUBSTITUTED BENZENES \*

BY H. N. SWAMY

OPTICS DEPARTMENT, INDIAN ASSOCIATION FOR THE CULTIVATION OF SCIENCE, CALCUTTA—32

(Received for publication November 6, 1952)

## Plates VIII A-C

**ABSTRACT.** Ultraviolet absorption spectra of *ortho* and *para* chlorophenol and bromotoluene have been investigated with the substances in the liquid and solid states at different temperatures, including that of liquid oxygen. In the case of *o*-chlorophenol three bands are observed in both liquid and solid states, the  $\nu_0$  band shifting by about  $270\text{ cm}^{-1}$  towards shorter wavelengths with solidification and cooling down to  $-180^\circ\text{C}$ . The shift is very small in the case of liquefaction of the vapour. In the case of the *para* compound the liquid state yields two broad bands while the solid state yields three bands with  $\nu_0$  band shifted by about  $180\text{ cm}^{-1}$  towards shorter wavelengths. With liquefaction of the vapour the  $\nu_0$  band shifts towards longer wavelengths by about  $150\text{ cm}^{-1}$ . In the case of *o*-bromotoluene in the liquid state three bands are observed with  $\nu_0$  band at  $36450\text{ cm}^{-1}$  and a progression of the frequency  $982\text{ cm}^{-1}$ . The solid at  $-180^\circ\text{C}$  yields nine bands which are explained on the assumption that the energy level splits into three components. In this case also the  $\nu_0$  band shifts by about  $400\text{ cm}^{-1}$  towards longer wavelengths with liquefaction of the vapour and the principal component of this band shifts by about  $726\text{ cm}^{-1}$  towards shorter wavelengths with solidification and cooling down to  $-180^\circ\text{C}$ . In the case of *p*-bromotoluene no such splitting is observed, but the  $\nu_0$  band shifts in the same directions as in the *ortho* compound with liquefaction and solidification. The results have been discussed and it is pointed out that these shifts may indicate formation of virtual bonds between neighbouring molecules.

## INTRODUCTION

The ultraviolet absorption spectra of several substituted benzene compounds in the liquid and solid states at low temperatures were studied previously (Swamy, 1951, 1952a, 1952b, 1952c) and it was observed that some changes in the spectra occur with solidification and lowering of temperature, the changes depending upon the nature and relative positions of the substituent groups. The solidification and cooling down to  $-180^\circ\text{C}$  of substances like *o*-dichlorobenzene (Sirkar and Swamy, 1952) and *o*- and *m*-chlorotoluene (Swamy, 1952c) produce a splitting of the electronic energy levels. In substances like *o*- and *p*-xylene, a number of new bands was observed at  $-180^\circ\text{C}$ , and these were assigned to vibrational frequencies allowed by the peculiar packing of molecules at  $-180^\circ\text{C}$ , and no splitting of the level was observed. In the case of some other disubstituted benzenes, also, *viz.*, *p*-dichlorobenzene, *p*-dibromobenzene (Sirkar and Swamy, 1953,

\* Communicated by Prof. S. C. Sirkar.

Swamy 1953), *o*-cresol and *m*-cresol (Swamy, 1952a) no splitting of the electronic energy level with solidification and lowering of temperature of the substances to  $-180^{\circ}\text{C}$  was observed, but transitions corresponding to some vibrational frequencies which were absent in the liquid state were observed in the case of the solid state at  $-180^{\circ}\text{C}$ . The present investigation was undertaken to study the influence of change of state and temperature on the absorption spectra of a few other disubstituted benzenes, viz., ortho- and para-chlorophenol, and ortho- and para bromotoluene, and the results have been discussed in the present paper.

#### EXPERIMENTAL

The experimental technique used was the same as that employed in earlier investigations by the author (Swamy, 1951, 1952). A hydrogen discharge tube running at 3 KV served as the source of continuous spectrum. Spectrograms were taken on Ilford HP 3 films with a Hilger E 1 quartz spectrograph having a dispersion of 3 Å. U. per mm. in the region, 2600 Å. (Ortho- and *p*-bromotoluene and *o*-chloro phenol were supplied by Eastman Kodak and *p*-chlorophenol was from Merck's original bottle. All the substances were distilled four times under vacuum before being used in the investigations.

The film of *o*- and *p*-bromotoluene that produced absorption bands had a thickness of about 0.2 mm. In the case of *o*- and *p*-chlorophenol only very thin films having thickness of a few microns, as in the case of cresols, produced the bands. The absorption spectra of *o*-bromotoluene in the vapour state were photographed using absorption a tube of length 25 cm. and diameter 12mm., quartz windows being fitted to the tube using sodium silicate cement. The liquid was contained in a small bulb attached to the tube and through another side tube, the absorption tube was connected to a Cenco Hyvac pump. After the tube had been evacuated, the stop cock leading to the pump was closed and the vapour was allowed to fill up the tube at the saturation pressure at room temperature. Absorption spectra at  $-180^{\circ}\text{C}$  were photographed with the technique described previously (Swamy, 1951). For comparison, mercury arc spectrum was recorded with the help of a Hartmann diaphragm on each spectrogram. An exposure of 10 minutes was required to record the absorption spectrum for the liquid state and about 30 minutes for the vapour state and the solid at  $-180^{\circ}\text{C}$ .

#### RESULTS

Spectrograms for *o*- and *p*-chlorophenol and *o*- and *p*-bromotoluene in the liquid state and solid state at  $-180^{\circ}\text{C}$  and those of *o*-bromotoluene in vapour state and *p*-chlorophenol in the solid state at about  $20^{\circ}\text{C}$  are reproduced in figures 1-4 in Plate VIIIA. The bands in the liquid and solid states being broad, microphotometric records were obtained to measure the frequencies accurately. These are reproduced in figures 5-8. Hg 2537 Å line in the spectrograms



served as the reference line in the microphotometric records and measurements were made of the centres of absorption peaks. (Only the prominent bands in the vapour state have been measured and assigned to particular transitions. The wave numbers of the bands observed for the vapour, liquid and solid states are given in Tables I-IV. Assignments of the bands of *o*-bromotoluene in solid state at  $-180^{\circ}\text{C}$  are made on the assumption that the electronic energy level is split up into three components. Bands of *o*- and *p*-chlorophenol and *p*-bromotoluene have been assigned to certain transitions on the assumption that no such splitting of the energy levels occurs in these cases.

TABLE I

Absorption bands of *o*-chlorophenol ;  $\nu$  in  $\text{cm}^{-1}$ 

Vapour (Ramasastry, 1951), Prominent bands	Assignment	Liquid at $30^{\circ}\text{C}$	Assignment	Solid at $-180^{\circ}\text{C}$	Assignment
35892 (vs)	$\nu_0$	35862 (vs,b)	$\nu_0$	36134 (sb)	$\nu_0$
36387 (w)	$\nu_0 + 496$	35475		35640	
36527 (m)	$\nu_0 + 635$				
36693 (m)	$\nu_0 + 801$				
36845 (s)	$\nu_0 + 953$	36810 (vs,b)	$\nu_0 + 948$	37040 (sb)	$\nu_0 + 916$
36982 (s)	$\nu_0 + 1090$				
37092 (w)	$\nu_0 + 1200$				
37337 (vw)	$\nu_0 + 1445$				
37639 (w)	$\nu_0 + 801 + 953$				
37789 (m)	$\nu_0 + 2 \times 953$	37760 (vw)	$\nu_0 + 2 \times 949$	37950 (w)	$\nu_0 + 2 \times 908$
38036 (w)	$\nu_0 + 1210 + 953$				
38733 (vw)	$\nu_0 + 3 \times 953$				

TABLE II

Absorption bands of *p*-chlorophenol ;  $\nu$  in  $\text{cm}^{-1}$ .

Vapour (Ramasastry, 1951), Prominent bands	Assignment	Liquid at $30^{\circ}\text{C}$	Assignment	Solid at $-180^{\circ}\text{C}$	Assignment
34820	$\nu_0$	34667 (s,b)	$\nu_0$	34848 (s,b)	$\nu_0$
35616	$\nu_0 + 795$				
35780	$\nu_0 + 960$				
35873	$\nu_0 + 1053$				
36032	$\nu_0 + 1212$	35501 (s,b)	$\nu_0 + 931$	35815 (s,b)	$\nu_0 + 957$
36270	$\nu_0 + 1450$				
36575	$\nu_0 + 960 + 795$			36760 (w)	$\nu_0 + 2 \times 956$
36740	$\nu_0 + 2 \times 960$				

TABLE III

Absorption bands of *o*-bromotoluene ;  $\nu$  in  $\text{cm}^{-1}$ .

Vapour, (Prominent bands).	Assignment	Liquid at $30^\circ\text{C}$	Assignment	Solid at $-180^\circ\text{C}$	Assignment
36780	$\nu_0 - 74$	36450 (v, sb)	$\nu_0$	36730 (m)	$\text{C}_0$
36854	$\nu_0$			36950 (w)	$\text{B}_0$
37280	$\nu_0 + 426$			37176 (s)	$\text{A}_0$
37330	$\nu_0 + 476$			37690 (m)	$\text{C}_1$
37825	$\nu_0 + 971$	37432 (s, l)	$\nu_0 + 982$	37912 (w)	$\text{B}_1$
37876	$\nu_0 + 1022$		$\nu_0 + 2 \times 982$	38140 (s)	$\text{A}_1$
38790	$\nu_0 + 2 \times 971$	38420 (m)		38655 (m)	$\text{C}_2$
38848	$\nu_0 + 941 + 1022$			38880 (w)	$\text{B}_2$
38900	$\nu_0 + 2 \times 1022$			39104 (w)	$\text{A}_2$

TABLE IV

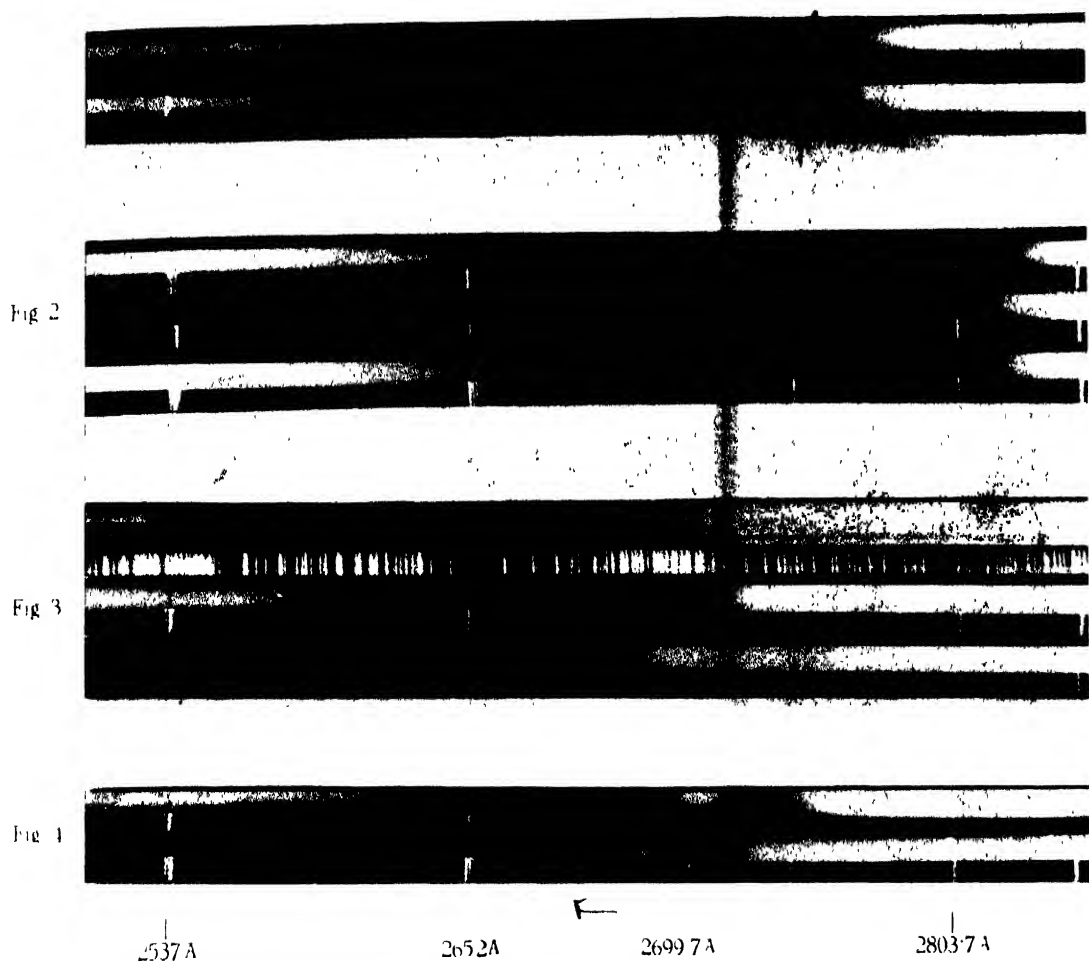
Absorption bands of *p*-bromotoluene ;  $\nu$  in  $\text{cm}^{-1}$ .

Vapour, (Prominent bands).	Assignment	Liquid at $30^\circ\text{C}$	Assignment	Solid at $-180^\circ\text{C}$	Assignment
36173	$\nu_0$	35803 (vs, l)	$\nu_0$	36102 (vs)	$\nu_0$
36928	$\nu_0 + 755$	36827 (s)	$\nu_0 + 1025$	36890 (m)	$\nu_0 + 788$
37189	$\nu_0 + 1016$				
37954	$\nu_0 + 1016 + 755$	37849 (w)	$\nu_0 + 2 \times 1023$	37123 (s)	$\nu_0 + 1021$
38205	$\nu_0 + 2 \times 1016$			37910 (w)	$\nu_0 + 1021 + 788$
				38154 (m)	$\nu_0 + 2 \times 1027$
				39166 (w)	$\nu_0 + 3 \times 1021$

## DISCUSSION

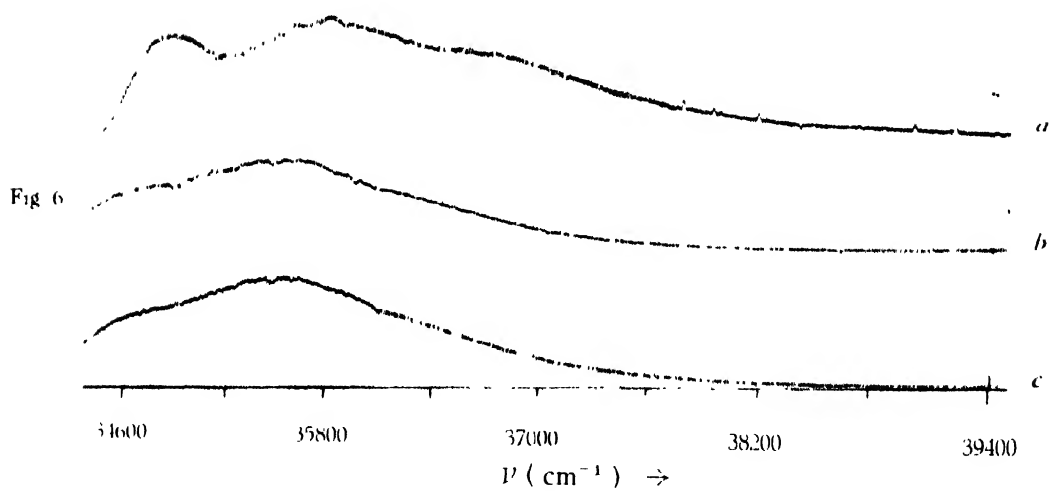
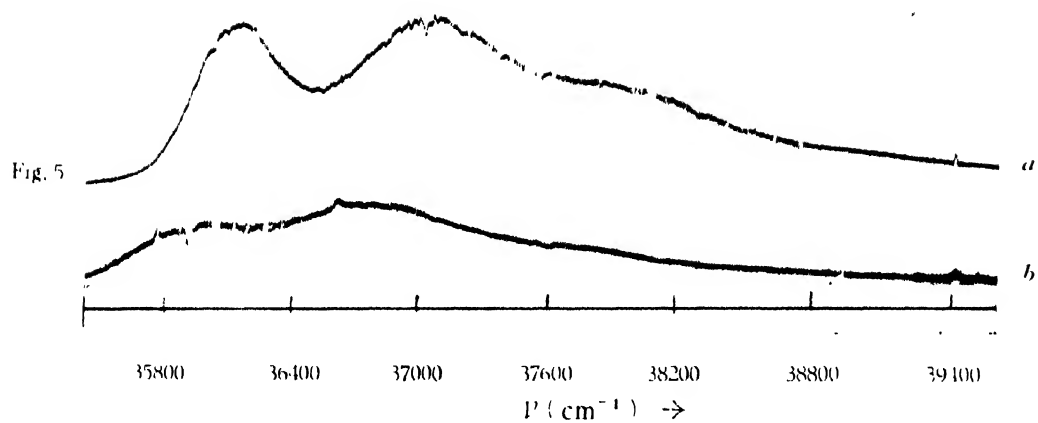
*Ortho and para chlorophenol :*

The data for *o*-chlorophenol reported by Ramasastriy (1951) show that the  $\nu_0$  band is at  $35892 \text{ cm}^{-1}$ . There are bands representing transitions  $\nu_0 + 495$ ,  $\nu_0 + 635$ ,  $\nu_0 + 801$ ,  $\nu_0 + 953$ ,  $\nu_0 + 1091$ ,  $\nu_0 + 1200$  and  $\nu_0 + 1445$  and their combinations and harmonics. The C-Cl vibration is weak. In the liquid state the substance produces three very broad bands, the first one being at  $35862 \text{ cm}^{-1}$ . There appears to be not much change in the position of the  $\nu_0$  band with the change from vapour to liquid state. In the solid state at  $-180^\circ\text{C}$ , the bands are a little sharper and the  $\nu_0$  band is found to have shifted towards shorter wavelengths by about  $270 \text{ cm}^{-1}$  from its position in the liquid state. It is concluded from these facts that the molecules get associated through virtual bonds only with solidification and lowering of temperature to  $-180^\circ\text{C}$ , and this causes the shift of the  $\nu_0$  band mentioned above.



## Absorption spectra

- Fig. 1. (a). *o*-Chlorophenol, liquid at 30°C  
 (b).     "     "     solid at 180°C
- Fig. 2. (a). *p*-Chlorophenol, liquid at 35°C  
 (b).     "     "     solid at 20°C  
 (c).     "     "     solid at 180°C
- Fig. 3. (a). *o*-Bromotoluene, vapour at 30°C  
 (b).     "     "     liquid at 30°C  
 (c).     "     "     solid at 180°C
- Fig. 4. (a). *p*-Bromotoluene, liquid at 30°C  
 (b).     "     "     solid at 180°C



### Mycrophotometric records

Fig. 5 (a). *o*-Chlorophenol, solid at  $-180^{\circ}\text{C}$

(b). " " liquid at  $30^{\circ}\text{C}$

Fig. 6 (a). *p*-Chlorophenol, solid at  $-180^{\circ}\text{C}$

(b). " " solid at  $20^{\circ}\text{C}$

(c). " " liquid at  $35^{\circ}\text{C}$

Fig. 7

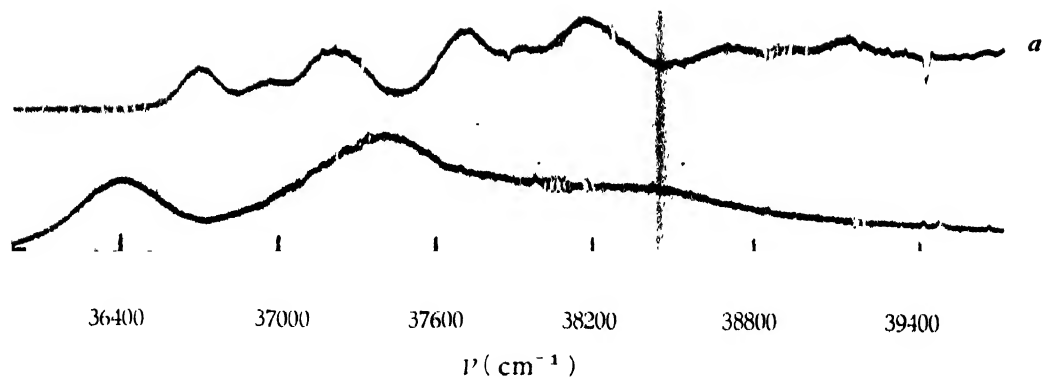
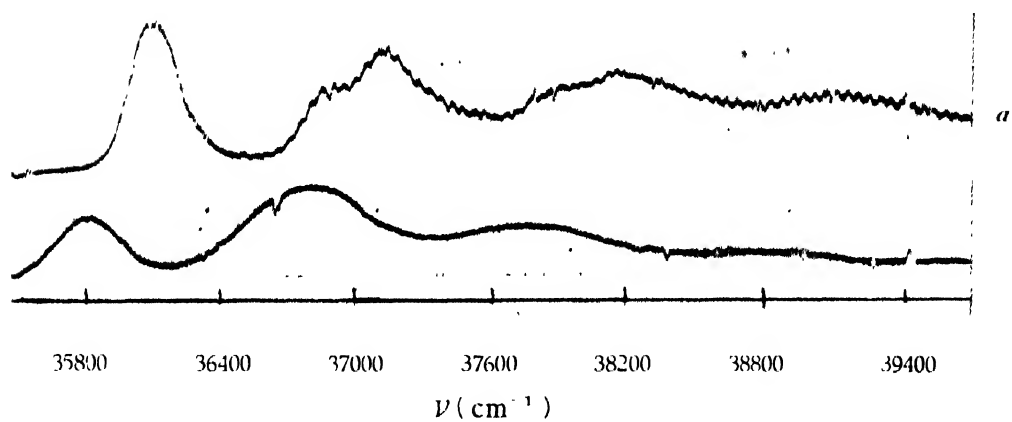


Fig. 8



## Microphotometric records

Fig. 7. (a) *o*-Bromotoluene, solid at -180°C

(b) " " liquid at 30°C

Fig. 8. (a) *p*-Bromotoluene, solid at -180°C

(b) " " liquid at 30°C



It can be further seen from figure 5 that the bands are broad and diffuse in the case of the liquid state while they become narrower with solidification. This shows that the intermolecular field has much influence on the position of the electronic energy level, because the thermal motion of the molecules in the liquid state widens the energy level considerably. Although translational motion ceases with solidification there may be angular oscillation of the molecules. If the molecules are linked to each other through virtual bonds such a motion is likely to produce a fluctuation of the intermolecular field, and consequently, to widen the electronic energy level even in the solid state. If the bond becomes stronger at very low temperatures the amplitude of angular oscillation is expected to diminish considerably and the bands may become sharper. Such a phenomenon appears to take place in the present case.

In the vapour state, *p*-chlorophenol has its  $\nu_0$  band at  $34820\text{ cm}^{-1}$  (Ramasastry, 1951). The C-Cl vibration is strong and there are bands representing transitions  $\nu_0 + 795$ ,  $\nu_0 + 960$ ,  $\nu_0 + 1063$ ,  $\nu_0 + 1212$ ,  $\nu_0 + 1450$  and their combinations and harmonics. In the liquid state at  $30^\circ\text{C}$ , the substance produces two broad bands, the first one being at  $34667\text{ cm}^{-1}$ . The  $\nu_0$  band is shifted by about  $160\text{ cm}^{-1}$  towards longer wave lengths from its position in the vapour state, and in the solid state at  $-180^\circ\text{C}$ , the  $\nu_0$  band shifts towards shorter wavelengths, to  $34848\text{ cm}^{-1}$ . There is also the formation of a weak band at  $36760\text{ cm}^{-1}$  representing a transition  $\nu_0 + 2 \times 956$ . The substance in the solid state at  $20^\circ\text{C}$  produces a spectrum almost identical with that of the liquid. The bands sharpen up only at  $-180^\circ\text{C}$ . This again shows that the intermolecular field has much influence on the electronic energy level and the molecules execute angular oscillation not only in the liquid state, but also in the solid state at  $20^\circ\text{C}$ . The intermolecular field acting on each molecule fluctuates during this oscillation resulting in the broadening of the electronic energy level of the molecule in the liquid state as well as in the solid state at  $20^\circ\text{C}$ . The slight sharpening of the band at  $-180^\circ\text{C}$  is less pronounced in this case than in the case of *o*-chlorophenol. This shows that in the present case the amplitude of angular oscillation diminishes only slightly with lowering of temperature to  $-180^\circ\text{C}$ . The shifts of the bands with liquefaction and solidification, however, show that the molecules get strongly associated through virtual bond in this case also, but probably the relative positions of the two substitution groups and the small value of the permanent electric moment in this case are responsible for the persistence of the angular oscillations of the molecules even at low temperatures.

*o*-Bromotoluene. The absorption spectrum of *o*-bromotoluene in the vapour state was studied previously by Tintea (1939). The data were not available to the author and hence the absorption spectrum of *o*-bromotoluene in the vapour state was photographed in the present investigation. A large number of bands was observed, but only the prominent bands produced by

# AN X-RAY INVESTIGATION ON TETRAPHENYLETHYLENE CRYSTAL\*

BY M. N. DATTA

KHAIKA LABORATORY OF PHYSICS, UNIVERSITY COLLEGE OF SCIENCE,  
CALCUTTA.

(Received for publication, November 15, 1952)

**ABSTRACT** A systematic study of X-ray reflections from a large number of planes, indicates that the space group of this crystal is  $P2_1/m$ . The estimated intensities of these planes show that the molecule does not lie in any simple crystallographic plane.

In the previous communication (Datta, 1953), we have seen that the crystal of tetraphenylethylene belongs to monoclinic holo-axial system. Morphological study and three rotation photographs about the three crystallographic axes using Ni-radiation gave the following values for the axial lengths and angles

$$a = 11.30 \text{ \AA.}$$

$$b = 9.37 \text{ \AA.}$$

$$c = 10.10 \text{ \AA.}$$

$$\beta = 72^\circ$$

$b$ -axis is the axis of symmetry and  $\beta$  is the angle between  $a$  and  $c$  axes. The density of the crystal (by floatation method) was found to be 1.057. (On substitution of these values in the formula

$$N = \frac{\rho V}{AM_H}$$

where  $N$  = No. of molecule per unit cell,  $\rho$  = density,  $V$  = volume,  $A$  = at weight,  $M_H$  = mass of hydrogen atom, the number of molecules per unit cell was found to be one. Hence the crystal has neither glide plane nor screw axis.

This is further confirmed by identifying a large number of reflecting planes on oscillation photographs. The  $b$ -axis of the crystal was made vertical. Oscillation photographs were taken over  $10^\circ$  oscillation. 18 photographs were taken from  $0^\circ$  to  $180^\circ$ . The spots were identified (usual method, Banerjee and Singh, 1937) on reciprocal lattice network of  $a^*$  and  $c^*$ . The relative intensities as determined by eye-estimation, were noted down against all the spots.

From the Table (Astbury and Yardley) it is shown that

all ( $h0l$ ) planes are present

all ( $oko$ ) planes are present,

\* Communicated by Prof. S. N. Bose.



so that *b*-axis is the axis of symmetry, and (*a*, *c*) plane is the plane of symmetry. There are a few absent spectra which are due to symmetrical arrangement of phenyl groups themselves. The space group of the this crystal will be, therefore,  $P2/m$ .

In the previous communication (Datta, 1953), we have seen that the crystal is bi-axial and optically negative with

$$\alpha = 1.690,$$

$$\beta = 1.757,$$

$$\gamma = 1.762.$$

The lowest refractive index being normal to the plane of molecule (Datta, 1947), since the above values are nearly equal, the molecule does not lie in any simple crystallographic plane. Our estimated intensities also support this view. Therefore, the complicated molecule as it is will not be planar.

TABLE I

The following planes have been identified.

Planes	Intensity	Planes	Intensity
002	S	313	V.S.
003	V.S.	314	W
004	S	315	W
005	W	400	S
010	S	401	W
012	V.S.	402	S
013	V.S.	403	S
014	S	404	W
020	V.S.	500	V.S.
022	V.S.	501	V.W.
023	S	502	S
024	S	303	W
025	S	504	W
030	V.S.	505	V.W.
032	S	600	W
033	W	601	W
033	W	603	S
100	S	604	S
101	S	606	S
102	S	701	W
103	W	702	W
104	V.V.W.	703	W
105	S	704	W
200	V.S.	803	V.W.
201	S	805	W
202	S	807	W
203	S	903	V.W.
204	W	005	V.V.W.
205	S	10 02	S
301	V.S.	110	V.W.
302	W	111	V.S.
303	W	112	V.S.
304	S	115	S
311	W	113	W
312	W	114	V.W.

TABLE I (contd.)

Planes	Intensity	Planes	Intensity
121	S	515	
122	V S	610	V.W.
123	S	711	W
124	V S	613	W
125	W	614	V.V.W.
130	V.S	711	W
131	S	711	W
132	W	713	S
133	S	714	W
134	V S	815	W
211	S	915	S
212	S	420	S
213	S	421	W
214	V S	422	W
215	W	423	V.W.
220	S	424	W
221	S	520	S
222	V S.	521	S
223	S	522	S
224	S	523	S
225	S	524	W
231	S	525	V.W.
232	S	620	W
233	S	621	S
234	S	623	W
235	W	624	W
321	W	724	W
322	S	821	W
323	S	825	W
324	W	430	S
331	S	431	V.W.
332	W	432	S
333	S	433	V.W.
410	S	434	S
411	S	530	V.W.
412	V.S	531	S
413	W	532	S
414	W	533	W
510	S	534	W
511	S	630	W
512	S	633	W
513	W	634	W
514	W	734	W
		835	W

## ACKNOWLEDGMENT

The author expresses his grateful thanks to Prof. S. N. Bose, Khaira Professor of Physics, Calcutta University, for his valuable guidance, and giving research facilities in the laboratory.

## REFERENCES

- Astbury, W. T. and Yardley, K., 1924, *Phil. Trans. Roy. Soc.*, **A 225**, 221.  
 Banerjee, K. and Singh, K. L., 1937, *Ind. J. Phys.*, **20**, 20  
 Datta, M. N., 1947, *Ind. J. Phys.*, **21**, 302  
 Datta, M. N., 1953, *Ind. J. Phys.*, **27**, 25.

# TEMPERATURE DEPENDENCE OF ANISOTROPY OF SOME ORTHO- AND PARA DISUBSTITUTED BENZENES\*

BY MONOMOCHAN MAZUMDER

OPTICS DEPARTMENT, INDIAN ASSOCIATION FOR THE CULTIVATION OF SCIENCE, CALCUTTA-32.

(Received for publication, November 28, 1952)

## Plate IX

**ABSTRACT.** The factor of depolarisation of the Rayleigh scattering in  $\text{CCl}_4$ , *o*-chlorotoluene, *p*-chlorotoluene, *o*-cresol and *p*-cresol at different temperatures due to the mercury lines 4047 Å and 5461 Å as the incident light has been determined by the method of spectrophotometry in order to find out whether the anisotropy changes with temperature in the same way in the case of both ortho and para compounds. By using Solier slits the corrected value of  $\rho$  in the case of carbon tetrachloride was found to be .054 at 34°C which changed to .039 at 65°C. The value of  $\delta$  was found to remain almost constant within this range of temperature. In the case *p*-chlorotoluene and *p*-cresol the values of  $\delta$  calculated from the observed values of  $\rho$  and  $\beta$  for different temperatures showed that  $\delta$  remains constant up to a temperature just below the boiling points of the liquids, while in the case of the ortho compounds it was found from similar data that  $\delta$  increases by about 50% with the rise of temperature mentioned above. It is concluded that in the case of the ortho compounds, breaking up of associated groups of molecules is responsible for the increase in  $\delta$  with temperature.

## INTRODUCTION

It was recently pointed out by Rank (1951) that from the values of the degree of depolarisation of the Rayleigh scattering in liquids having elongated molecules, it can be judged whether the molecules are associated in the liquid or not, because if the molecules, which are themselves highly anisotropic, become associated with each other, the anisotropy of the associated group is generally much less than that of the single molecule, and consequently the Rayleigh scattering becomes highly polarised. Many substituted benzenes have such molecules and from the results of investigation of the Raman spectra of a few such compounds in the liquid and solid states previous authors (e.g. Sirkar and Bishui, 1946) concluded that even in the liquid state the molecules of some substituted benzenes, such as benzyl alcohol and benzyl chloride may be associated. In the case of disubstituted benzenes the ortho and meta compounds may similarly have associated molecules in the liquid state while the para compounds may have only single molecules. A comparative study of the degree of depolarisation of Rayleigh scattering in the para compound and that in either ortho or meta

\* Communicated by Prof. S. C. Sirkar

compound is, therefore, expected to throw some light on the degree of association of the latter molecules in the liquid state.

The value of  $\rho$ , the factor of depolarisation of Rayleigh scattering in the liquid state, however, depends also on the temperature and compressibility of the liquid. By studying the temperature-dependence of  $\rho$  in the case of many liquids it was observed by Rao (1927, 1928) that the factor of depolarisation of Rayleigh scattering remains almost constant up to the boiling point and diminishes at higher temperatures in the case of many organic liquids. He also showed that the anisotropy of the molecule calculated from these results applying the formula deduced on the assumption of isotropic polarising field increases with the increase of temperature in almost all the cases including carbon tetrachloride. He got the liquid sealed in a spherical bulb which was placed in a bath kept at different temperatures. White light was used as incident radiation and  $\rho$  was determined by Cornu's visual method. The liquids studied by him, however, do not include disubstituted benzenes, and especially, the ortho, meta and para isomers of the same disubstituted compound, and therefore, the results published by him do not furnish any information regarding the state of association of the molecules in the the liquids. It was, therefore, thought worthwhile to study the factor of depolarisation of Rayleigh scattering quantitatively in a few such compounds. It was also thought desirable to employ the method of photographic spectrophotometry so that the results could be demonstrated by reproducing the spectrograms which would also furnish results for different wavelengths. Such results obtained in the case of ortho and para cresol, ortho and para chlorotoluene and carbon tetrachloride have been discussed in the present paper.

#### EXPERIMENTAL

The liquids were supplied by May and Baker and they were distilled in vacuum at least three times before being introduced in the experimental container. The ideal arrangement for studying the Rayleigh scattering should provide a parallel incident beam and a scattered light free from any extraneous light. The windows of the container should also be plane and free from strain so that the state of polarisation of the incident and emergent light does not undergo any change while passing through these windows. In a sealed container heated much above the boiling point of the liquid the pressure is likely to be a few atmospheres and this may produce some strain in the walls of the container. For this reason it was decided to study only liquids having high boiling points at temperatures below their boiling points. A Wood's tube of diameter about 26 mm. having a plane window for observation of the scattered light and tapering bent tail was used in the present investigation. The tube was painted with dull black paint leaving a horizontal slit in the window and another long horizontal slit on its side. The length of the latter slit was about 8 cm. and width about 5 mm. A

horizontal mercury arc was used to illuminate the tube and a Soller slit consisting of narrow thin copper strips fixed in a wooden frame parallel to each other so as to form channels each about 4 cm long, of width 5 mm and height 1 cm was used to make the light parallel. The copper strips were painted with dull black paint. The effective height of the channels was reduced to 5 mm, because the height of the long window on the Wood's tube was only 5 mm. The value of half the angle of convergence was therefore of the order of .12 radians. The same tube was used to study the depolarisation of the light scattered by all the liquids. The tube was placed in a cylindrical electric heater provided with a suitable window and the temperature of the liquid was varied by altering the current in the heater.

The scattered light coming out through the window at one of the ends of the tube was focussed with a lens on to the slit of a Fuess spectrograph in such a way that an image of the rectangular aperture of the window was formed on the slit. A quartz double image prism was then placed between the lens and the slit of the spectrograph to separate the vertical and horizontal components of the scattered light. Ilford Selochrome plates were used to record the spectra of the light scattered by the different liquids. The experimental arrangement is shown diagrammatically in figure 1. The

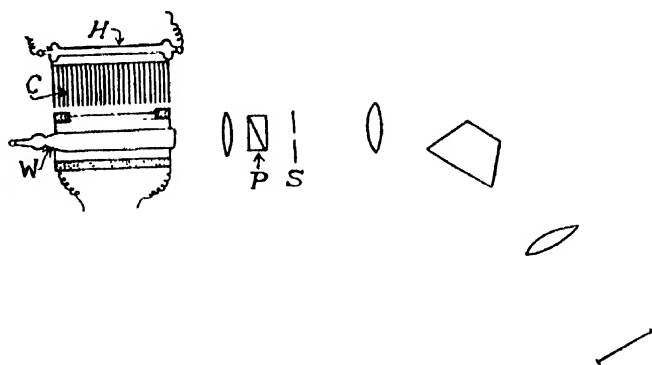


FIG. 1

H—Hg arc  
C—channels  
W—Woods tube

P—Wollaston prism  
S—slit of spectrograph

spectra of the light scattered by the liquid first with the liquid placed in the heater at 30° C and next at the higher temperature were photographed on the same plate. Different spectrograms were obtained for the same liquid in order to get the mean values of  $\rho$  from them.

The densities of the two components of the scattered light were determined by taking microphotometric records with a self-recording Moll microphotometer of Kipp and Zonen type. Intensity marks were also obtained on a plate taken from the same packet by photographing the spectrum of light of tungsten filament lamp scattered by white paper using different known widths of the slit of the spectrograph. All the plates were developed under

identical conditions. Intensities of the horizontal and vertical components were obtained from the densities of the lines with the help of blackening log-intensity curves drawn with the help of the densities of the known intensity marks. The value of  $\rho$  was first determined in the case of light scattered by pure dust-free carbon tetrachloride, using the arrangement mentioned above in order to test the accuracy of the method.

The values of  $\beta_*$ , the isothermal compressibility of the liquids at different temperatures, were not available from existing literature and therefore an experimental arrangement was set up to determine the values of  $\beta_*$  for the cresols and chlorotoluenes at temperatures ranging from 30°C up to 180°C. The apparatus used was essentially that described by Tyrer (1913) with a little modification. The tube containing the liquid was put inside a long cylindrical electric heater and the temperature inside the heater was maintained constant for a long time by adjusting the current flowing through it. The temperature was measured with a sensitive mercury thermometer. The arrangement is shown in figure 2. The volume of the tube

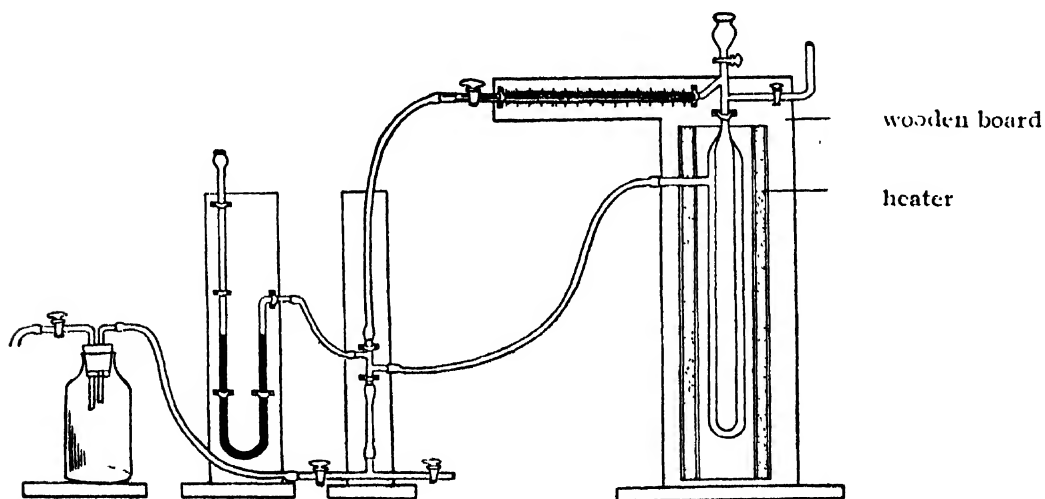


FIG. 2

used was 83 c. c. The values of isothermal compressibility was calculated from those of  $\beta_\gamma$ , the adiabatic compressibility using the relation,

$$\beta_* = \beta_\gamma + \frac{\Gamma \left( \frac{\partial v}{\partial T} \right)^2}{J C_p v} \times 1.013 \times 10^6$$

where  $v$  is the specific volume which was also measured. The values of  $\beta_*$  for  $\text{CCl}_4$  were known but to test the accuracy of measurements in the present investigation these values were redetermined.

## RESULTS

The values of  $\beta_\gamma$  and  $\beta_*$  are given in Tables I-III. The microphotometer traces of the two components of the scattered light of different wave-

lengths are reproduced in Plate IX. Preliminary calculations showed that in the case of  $\text{CCl}_4$  the value of  $\rho$  with the unpolarised incident light was '075. A correction was made for convergence error by simply subtracting half the square of the semi angle of divergence (Bhagavantam, 1940). The value of this quantity calculated from the geometry of the arrangement was .007. Even after applying this correction to the value of  $\rho$  for the chlorotoluenes and cresols, it was found that the corrected values of  $\rho$  for para compounds were almost unity. It was evident from this that there was some loss of intensity of the vertical component owing the reflection at the surface of the prism in the spectrograph. A correction factor was to be determined to take into account this loss. As the value of  $\rho$  in the case of  $\text{CCl}_4$  was found to be less than that observed by some previous authors (Krishnan, 1925 ; Rao, 1927) it was assumed that the coefficient of reflection was 0.2 and the loss was due to one such reflection. So the values corrected for convergence were multiplied by 0.8. The observed and corrected values of  $\rho$  for the liquids at different temperatures are given in Tables IV-VI. The values of  $\delta$ , the anisotropy of the molecule calculated from the formula  $\delta = \frac{5RT\beta_s\rho}{M(6-7\rho)}$  are given in the last columns of these tables,  $s$  being the density of the liquid.

TABLE I  
Carbon tetrachloride

Temp.	Adiabatic compressibility $\beta_\gamma \times 10^6$ per atmos	Isothermal compressibility $\beta_\epsilon \times 10^6$ per atmos.
20°C	73.28	105
34°C	80.5	116
64°C	101	150

TABLE II  
Chlorotoluenes

Liquid	Temp.	Adiabatic compressibility $\beta_\gamma \times 10^6$ per atmos.	Isothermal compressibility $\beta_\epsilon \times 10^6$ per atmos.
Para chloro- toluene	35°C	55.17	72.16
„	135°C	110.9	151.03
Ortho chloro- toluene	35°C	52	70.48
„	135°C	118	146.8

TABLE III

## Cresols

Liquid	Temp	Adiabatic compressibility $\beta_\gamma \times 10^6$ per atmos.	Isothermal compressibility $\beta_p \times 10^6$ per atmos.
Para cresol	34°C	48.3	52.16
"	180°C	99.5	136.31
Ortho cresol	34°C	42.5	49.65
"	150°C	88.57	115.45

TABLE IV

## Cresols

Liquid	Hg. lines	Temp.	Observed value of $\rho$	Corrected value of $\rho$	Isothermal compressibility $\beta_p \times 10^{12}$ per dyne	Optical anisotropy $\delta \times 10^3$
Para cresol	4047 Å	34°C	1	.795	51.84	100
	"	180°C	.81	.642	135.2	95
	5461 Å	34°C	.98	.778	51.84	82
	"	180°C	.81	.642	135.2	95
Ortho cresol	4047 Å	34°C	.81	.642	49.33	26
	"	150°C	.66	.522	114.3	42
	5461 Å	34°C	.81	.642	49.33	26
	"	150°C	.70	.554	114.3	47

TABLE V

## Chlorotoluenes

Liquid	Hg. lines	Temp.	Observed value of $\rho$	Corrected value of $\rho$	Isothermal compressibility $\beta_p \times 10^{12}$ per dyne	Optical anisotropy $\delta \times 10^3$
Para chlorotoluene	4047 Å	35°C	.85	.57	71.65	42
	"	135°C	.66	.52	150.1	43
	5461 Å	35°C	.89	.70	71.65	50
	"	135°C	.70	.544	150.1	50
Ortho chlorotoluene	4047 Å	35°C	.52	.41	69.5	10
	"	135°C	.40	.31	146	15.5
	5461 Å	35°C	.61	.48	69.5	13.1
	"	135°C	.46	.36	146	19.9



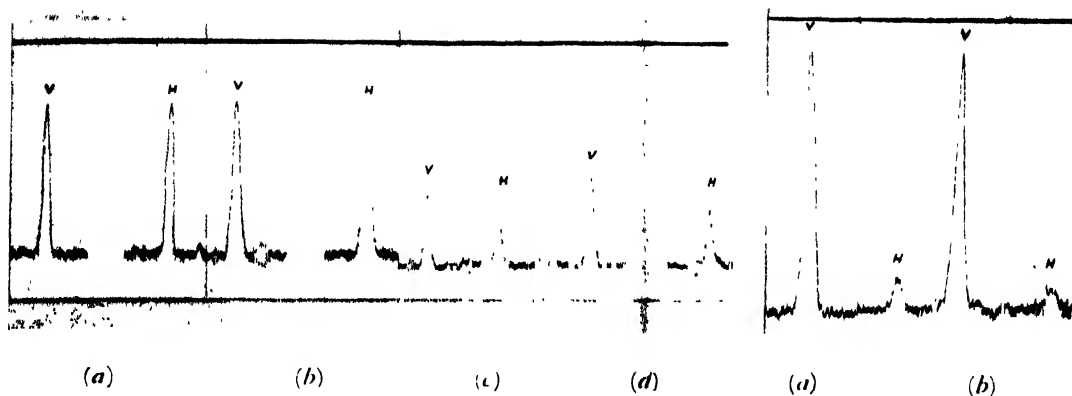


Fig. 1

Fig. 2

(a). *p*-Cresol at 34°C.

(b). " " at 180°C.

(c). *o*-Cresol at 34°C.

(d). " " at 150°C.

(a) CCl<sub>4</sub> at 34°C.

(b). " " at 65°C.

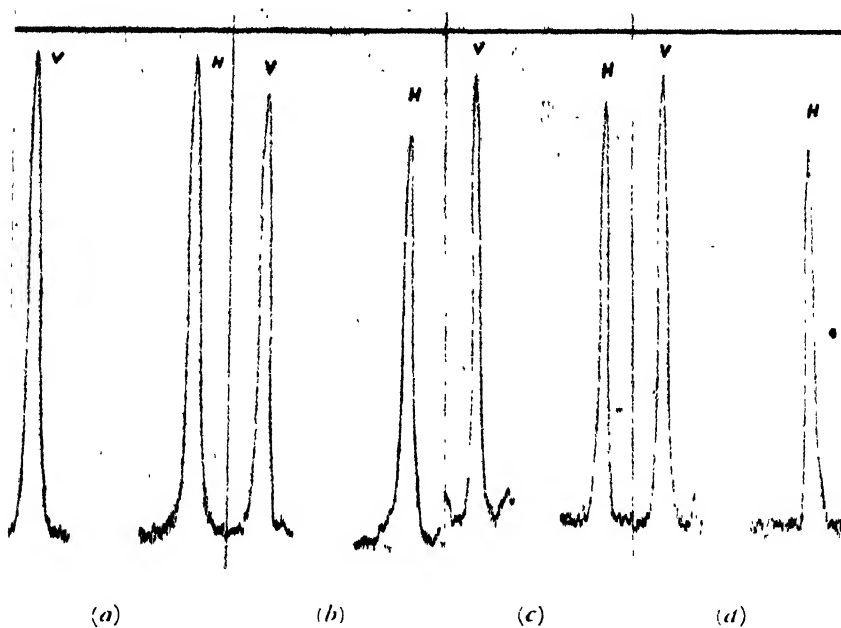


Fig. 3

(a). *p*-Chlorotoluene at 35°C.

(b). " " at 135°C.

(c). *o*-Chlorotoluene at 35°C.

(d). " " at 135°C.



TABLE VI  
Carbon tetrachloride

Liquid	Hg. lines	Temp.	Observed value of $\rho$	Corrected value of $\rho$	Isothermal compressibility $\beta_p \times 10^{12}$ per dyne	Optical anisotropy $\delta \times 10^3$
CCl <sub>4</sub>	4047 Å	34°C	.075	.054	115.3	1.46
"	"	65°C	.056	.039	149.1	1.49
"	5461 Å	34°C	.077	.056	115.3	1.50
"	"	65°C	.056	.039	149.1	1.49

## DISCUSSION

It will be seen from Table IV and V that the values of  $\rho$  for the para compounds are higher than those for the corresponding ortho compounds, while the percentage change of  $\rho$  with temperature is almost the same for both the para and the ortho compounds. The values of  $\rho$  for CCl<sub>4</sub> at 34°C and 65°C, as given in Table VI, are .054 and .039 respectively for the wavelength 4047 Å. It is therefore evident that the method of photographic photometry has yielded accurate values in this case and the values for the other two compounds given in Tables IV and V can be taken as fairly accurate. The value of  $\rho$  diminishes slightly with rise of temperature in the case of CCl<sub>4</sub>. Such a diminution was not observed by Rao(1927) who observed by visual method that  $\rho$  was constant up to 120°C in the case of CCl<sub>4</sub>. This diminution at higher temperature clearly indicates the absence of any influence of unresolved rotational wing on the value of  $\rho$ . The value of  $\rho$  decreases with increase of temperature in case of the cresols and the chlorotoluenes. The large value of  $\rho$  in the case of the para compounds is evidently due to the large anisotropy of the molecule and the smaller value for the ortho compounds is therefore due to the decrease of anisotropy caused by formation of associated groups of molecules as pointed out by Rank (1951), because the anisotropy of the single ortho molecule can not be very much less than that of the para molecule. Such a conclusion is supported by the changes in the values of  $\delta$  calculated from the values of  $\rho$  at different temperatures.

It is seen from Tables IV and V that the value of  $\delta$  for the two para compounds remains almost constant with rise of temperature, while it increases in the case of the ortho compounds. The increase in  $\delta$  is about 50% for a change of temperature of about 100°C in the case of *o*-chlorotoluene and 115°C in the case of *o*-cresol. These increased values at high temperatures are still much lower than the values for the corresponding para compounds. These results may be explained on the assumption that at the

room temperatures most of the molecules are associated, the value of  $\delta$  for the associated group being less than that of the single molecule at the higher temperatures. In the case of the para compounds no such association takes place and therefore the anisotropy of the molecule is higher and it remains constant with the rise of temperature. The persence of OH group with *p*-cresol molecule evidently makes the anisotropy of the molecule larger than that of the *p*-chlorotoluene molecule.

The values of  $\delta$  for carbon tetrachloride at 34°C and 65°C, given in Table V, show that the value is about .0014 at both the temperatures. This constancy of the value of  $\delta$  is also expected in this particular case, because the molecule being isotropic any change in the very small value of  $\delta$  with temperature can not be easily accounted for. Of course, Rao (1927) observed that the value of  $\delta$  for carbon tetrachloride increased from .0016 at 30°C to .005 at 260°C. The value of  $\delta$  for the vapour calculated from a value of  $\rho$  equal to 0.5% was found by him to be .004. The value of  $\rho$  for carbon tetrachloride vapour has since been corrected by Parthasarathy (1951) the revised value being 0.12%. The value of  $\delta$  calculated from this value of  $\rho$  is .0023. It has, however, been remarked by Parthasarathy (1951) that the corrected value of  $\rho$  for carbon tetrachloride vapour is almost negligible. As it is more difficult to measure small values of  $\rho$  by the visual method, the value observed in the present investigation for the  $\text{CCl}_4$  in the liquid state is probably the upper limit of the value of  $\delta$  for the carbon tetrachloride molecule. Probably the strain in the glass container which might develop at high temperatures was responsible for the high values of  $\rho$  for liquid carbon tetrachloride which were observed by Rao (1927) at these temperatures.

It is thus evident from the given discussions that a comparison of the values of  $\rho$  for polar and nonpolar molecules of similar structure can really furnish much information about the nature of association of the molecules in the liquid state.

#### ACKNOWLEDGMENTS

The author is indebted to Prof. S. C. Sirkar, D. Sc., F. N. I., for his kind interest and helpful guidance throughout the progress of the work and to the Government of India for the award of a scholarship.

#### REFERENCES

- Bhagavantam, S., 1930, Scattering of light and Raman Effect.
- Krishnan, K. S., 1925, *Phil. Mag.*, **80**, 697.
- Parthasarathy, S., 1951, *Ind. J. Phys.*, **34**, 21.
- Philip, N. M., 1938, *Proc. Ind. Acad. Sci.*, **9A**, 109.
- Rao, S. Ramchandra, 1927, *Ind. J. Phys.*, **2**, 179.
- Rao, I. Ramakrishna, 1927, *Ind. J. Phys.*, **2**, 61.
- Rank, D. H., 1951, *J. Chem. Phys.*, **19**, 311.
- Sirkar, S. C. and Bishui, B. M., 1946, *Ind. J. Phys.*, **20**, 111.
- Tyrer, D., 1913, *J. Ind. Chem. Soc.*, **2**, 1675.

# ON THE LARGE LOAD CHARACTERISTICS OF VAPOUR PUMPS

By S. K. MUKHERJEE AND P. K. DUTT

INSTITUTE OF NUCLEAR PHYSICS, CALCUTTA UNIVERSITY, CALCUTTA

(Received for publication, November 11, 1952)

**ABSTRACT.** The different characteristics of vapour pumps under various leak-load and forepressure conditions are studied. The leak load position dependence of forepressure is investigated from which different conditions of critical forepressure are distinguished.

## INTRODUCTION

Since the pioneer theory of Gaede (1915, 1923) and a much later attempt by Matricon (1932), on the performance of a "vapour stream pump", much work on its performance has been done to collect data in the attempts to verify the theories (Blears and Hill, 1948; Dayton, 1948, Ho; 1932). Specially the influence of heater input, forepressure and load, on the performance of a pump has been much discussed. The present paper is an investigation of the vacuum characteristics of a pump in their relation to leak-load and its position.

Normally, a vapour pump is characterised by three specific factors :

1. *The ultimate vacuum* : i. e. highest vacuum reached.
2. *The speed* : i. e. average litre-micron that is handled throughout the operating range.
3. *Maximum load handling capacity* : i. e. peak load that can be tolerated by the pump before jet-breakdown.

It is well-known that backing pressure in case of a good multiple jet pump has no effect on the speed until a certain critical value, called the critical forepressure, is exceeded when the speed drops rapidly. The relation of speed to fine pressure shows (figure 1) that fine pressure falls from

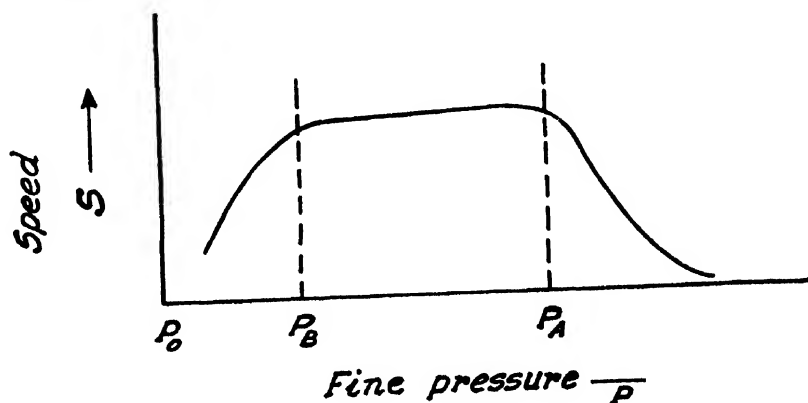


FIG. 1

the forepressure value to a value  $P_A$  when the vapour pump takes over from the backing pump. In this region the speed rises to a maximum value  $P_A$  and then remains constant upto  $P_B$  beyond which it gradually decreases until it reaches the ultimate vacuum  $P_0$ . Here the effective pump speed is zero because the real pump speed at this stage is just counter balanced by the evolution of gases and vapours from the system and operating pump fluid. It may be noted that real pumping speed is the same throughout the operating range. It is the effective pump speed which falls to zero from a maximum value. We consider a system directly connected to the vapour pump. We assume the validity of the equation of continuity in the case of the flow of air past different jets. For the sake of simplicity, we omit here the dependence of speed on the effect of back diffusion of air whose contribution to the lowering of speed is generally small for a well designed pump, specially at higher heater input. The pumping action is provided by the vapour stream of the operating fluid directed downwards by directed jets from high vacuum side to the fore vacuum side. The gas is compressed by the jets and fed to the backing pump at sufficient pressure to enable the backing pump to handle it before the jet breaks down. The pump remains in working condition so long as this pressure gradient is maintained from high side to fore side. This power of the jets to compress the gas (i. e. the critical forepressure) is dependent on jet design, number of stages in the pump, the operating fluid and the heater input. But the maximum gas load tolerated is determined by forepressure at which it is operating at a constant heater input. So breakdown forepressure is always associated with gas load or leak in the system. As against this condition, when a leak load is placed in the forevacuum part of the system, only a very slight increase of fine pressure will result until, of course, the leak will increase the forepressure to such an extent that the jets breakdown. These two jet breakdown forepressures may be completely different.

The following cases may conveniently be classified :

- 1 Leak-load, introduced on the fine side, is increased till jets breakdown corresponding forepressure, fine pressure relations observed and the critical forepressure noted.
2. Leak-load introduced in the fore side, the fine side of course, is considered to be leak-free.
3. Leak-load introduced in the fine side is kept at a certain level at a constant heat input. Additional leak-load introduced in the foreside is progressively increased till jets breakdown.

In each of the above cases, heat input is varied.

It is evident from the foregoing classification, the forepump used should be sufficiently large and the heat input in the vapour pumps should be set at an optimum value depending on the gas handling capacity. Also a series of values have been taken at different leak rates, so that the curves can be plotted over the entire range.

## EXPERIMENTAL ARRANGEMENTS

In our experimental set up, the vapour pump used is a three stage 4" diameter pump of our own make. It is backed by a mechanical pump of Leybold's type XI of pumping speed 0.5 litres/sec at  $10^{-3}$  mm. The forepump connection is short and of sufficiently large diameter so as to have little influence on the forepump speed and its measurements. There is a valve in between the mechanical and vapour pump, and leak valve is also connected there with a ballast. This leak valve is capable of controlling leak of the order of 2 lit-micron. There is the usual arrangements for measuring pressure by means of Pirani gauge (checked at interval against a Mcleod gauge), ion gauge etc. A test dome is used for gauge housing and leak entries. The diameter of this test dome is larger than the m.p.f. of the molecules of the vapour and the leak is introduced in such a way as to eliminate any directional characteristic due to beaming. The speed measuring apparatus is a constant pressure type and is a modification of Howard's (1935) apparatus. The essential alteration is an arrangement for keeping the pressure inside the measuring apparatus constant and entire elimination of the capillary system which is substituted by a precision leak valve. The actual experimental arrangement is shown in figure 2. The leak in the fine side is also controlled by a precision leak valve of the same type as that used in the fore vacuum part of the system. The pressure is measured by means of an ion gauge connected to the dome through a liquid air trap. A Mcleod type gauge is used for frequent checking.

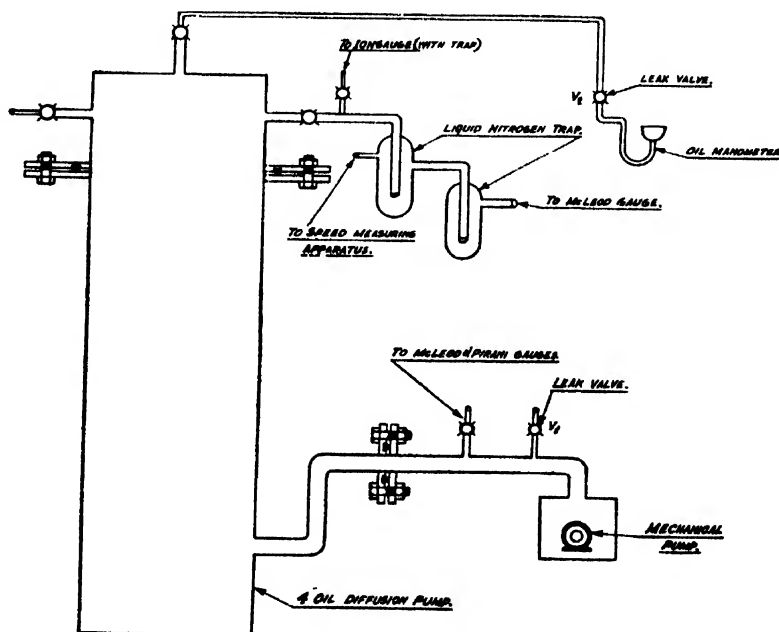


FIG. 2

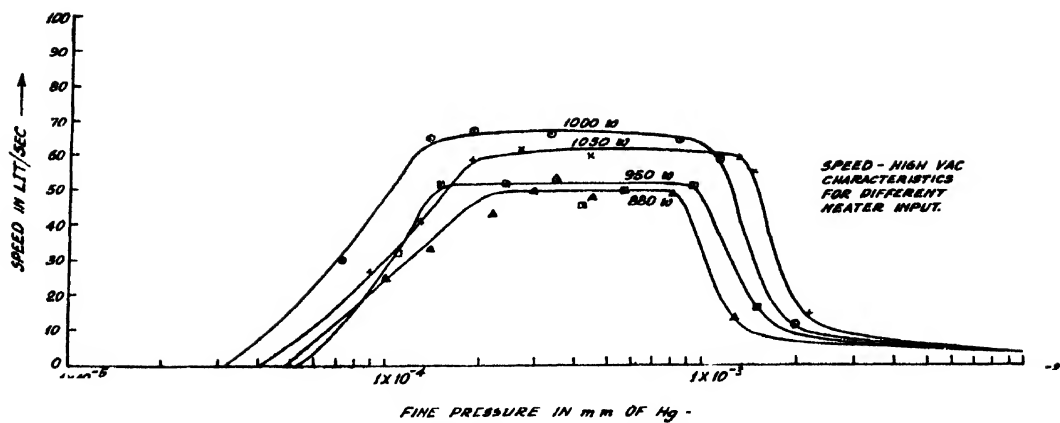


FIG. 3

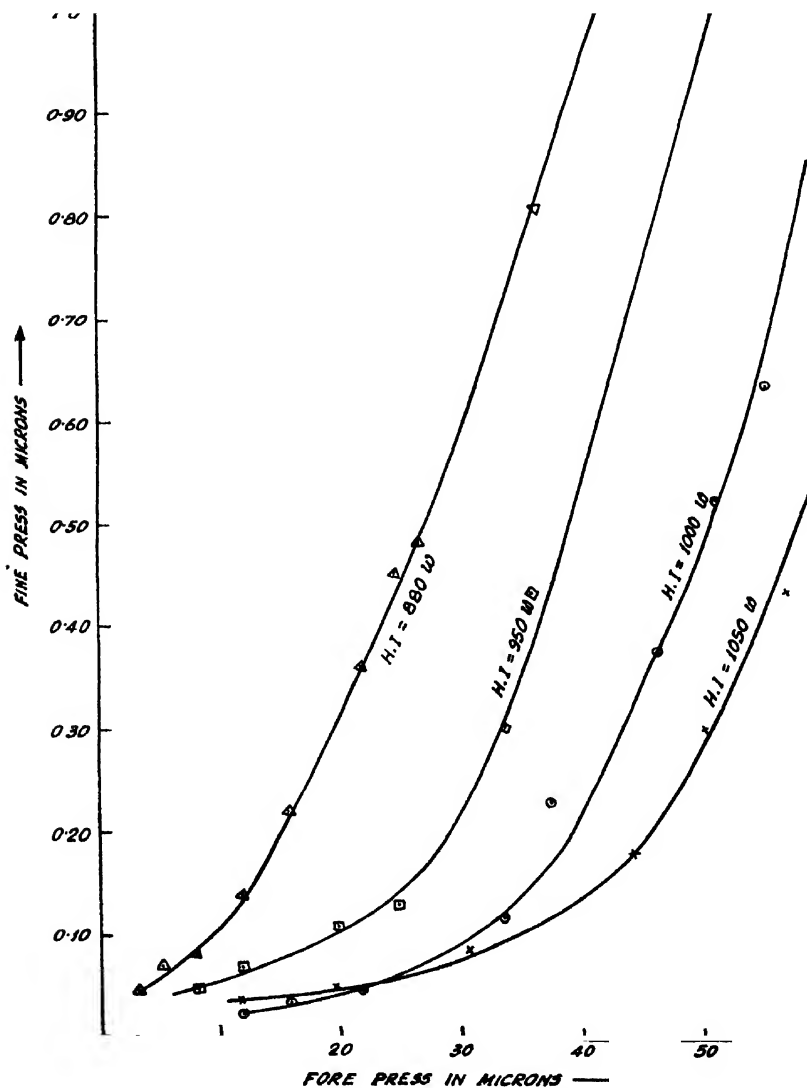


FIG. 4



## EXPERIMENTAL RESULTS

Using the method outlined above, speed and pressure measurements were made under conditions given below :

The usual fine pressure-speed characteristics of the pump at different heat inputs are shown in figure 3.

1. *Fine side leak : forepressure :*

The leak was introduced on the fine side by means of leak valve  $V_2$ . The forepressure at which the jets just break down was noted in each case of a particular heater input (figure 4). This jet breakdown is indicated by the sudden start of continuously increasing pressure in the ion gauge reading and the ultimate swing towards foreside pressure. The heat input variation ranges between 880 W-1050 W.

2. *Foreside leak : fine pressure :*

Quite distinct from the previous case, are the cases where the leak was introduced in the foreside (figure 5). The curves represent cases of different

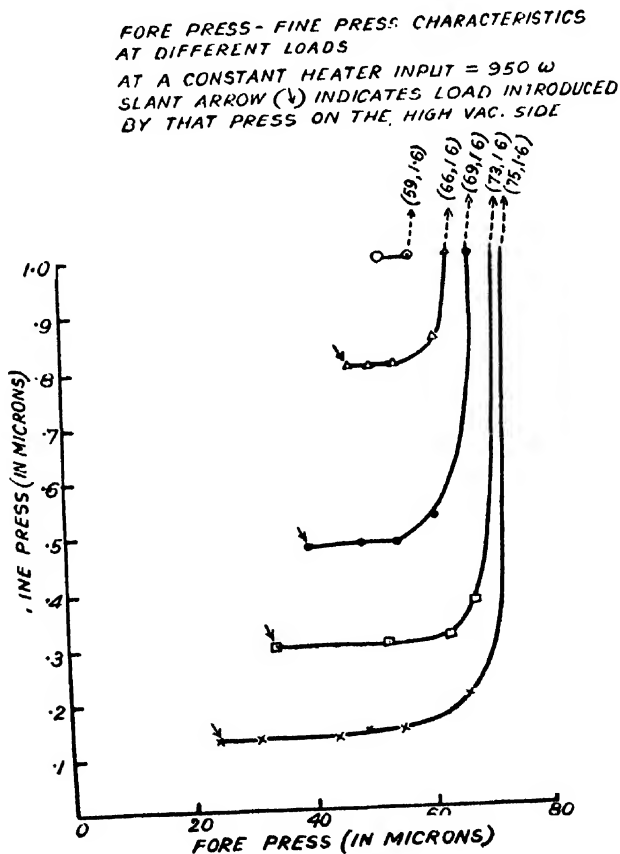


FIG. 5

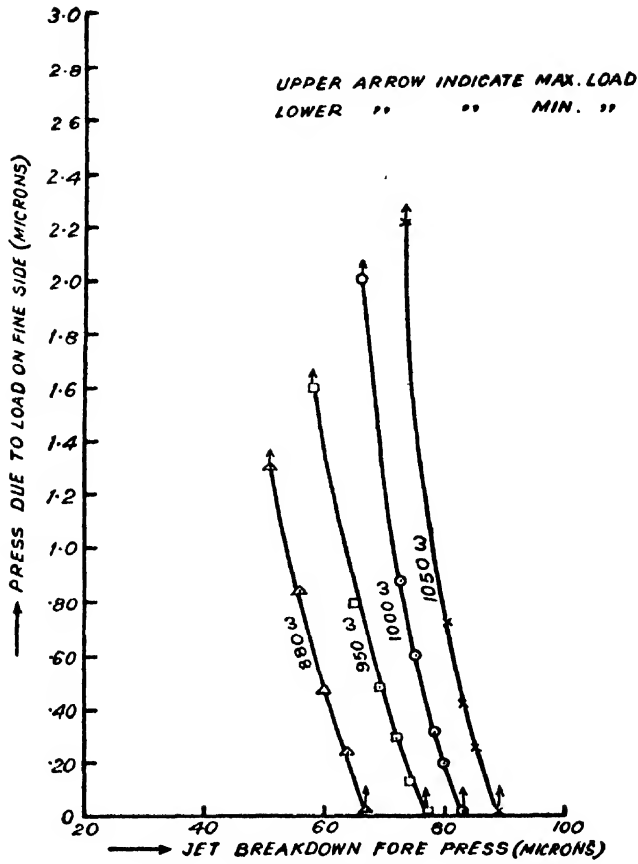


FIG. 6

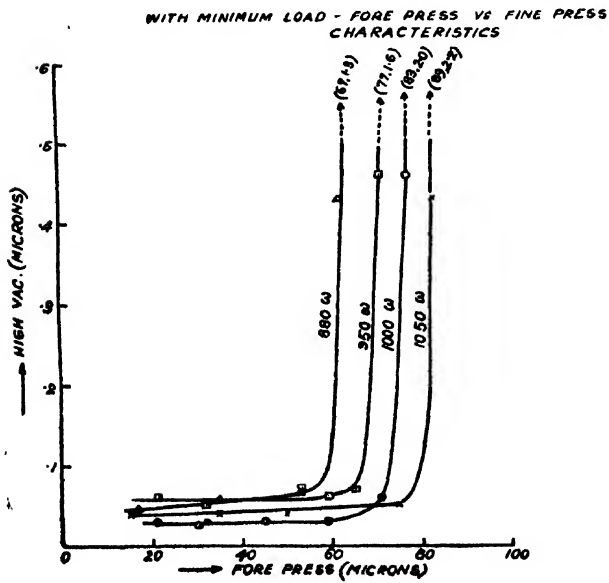


FIG. 7

heater inputs, the fine side is, of course, kept load free. The figures within bracket give the forepressure and fine pressure respectively recorded just when the jet breaks down.

3. Fore pressure: fine pressure of different load :

Figure 5 indicates the effects of additional leaks on the foreside till jets break down ; the fine side pressure in this case is kept at definite levels by means of leaks on fine side; the heat input is, of course, kept constant. The jet breakdown points are indicated by fine side pressure which means that up to that fine pressure can be measured after which jet breaks down.

Curves of figure 6 give the relation between jet breakdown forepressures with the fine side pressure due to leakload on that side at different heat-input. Figures 8 and 9 represent cases where relation of forepressure with speed is calculated for different fixed loads on the fine-side.

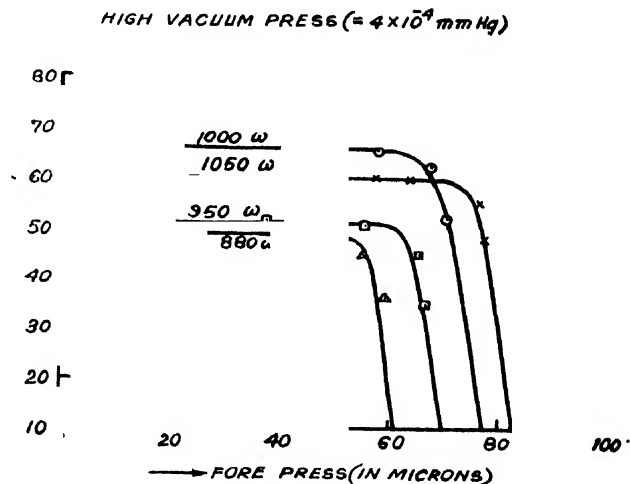


FIG. 8

(HIGH VACUUM SIDE PRESS  $= 2 \times 10^{-4}$  mm Hg)

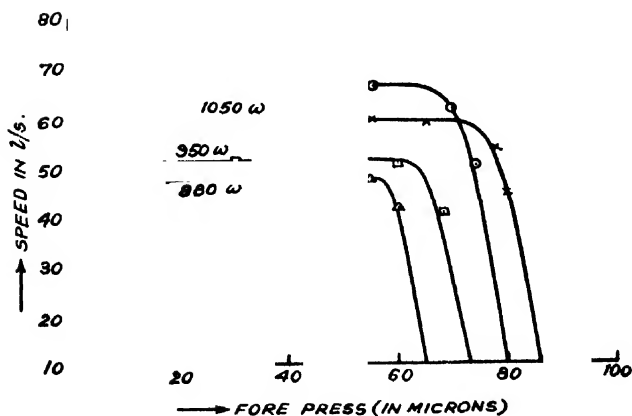


FIG. 9

## DISCUSSION

It is noteworthy that the effect of a small leak load on the ultimate vacuum produced will be small or pronounced according as it is situated on the fore or the fine side. This is amply borne out by the curves in figures 7 and 8. The very sharp critical forepressure is to be noticed, particularly in the case when the leak is introduced in the fore side. Quite different is the case when the leak is introduced in the fine side. Any rise in the forepressure is not reflected in the fine pressure until the critical forepressure is reached. The explanation is obvious from the working of the vapour pump. So long as the jets are able to maintain an effective seal between the two sides, any leak in the forepressure side will have little effect on the ultimate vacuum produced. Less heating than the rated minimum value may mean that the jets are not dense enough to stand a comparatively large pressure differential. On the other hand, when the rate of heating is too large, vapour molecules are imperfectly condensed on the pump walls, resulting in increased back-diffusion which will lead to reduction in speed and ultimate vacuum, (figure 4, curve-II. I. 1050). Another explanation offered by some authors is that at higher heat-inputs, a temporary cracking of fluid may take place giving off higher vapour pressure components, with consequent worsening of ultimate vacuum, which may take place concurrently with the first effect at higher heat inputs.

In our experiment we did not study individual jet breakdowns, but by jet breakdown the breakdown of all the jets is meant, as a result of which the vapourpump ceased functioning.

It is evident from the foregoing discussions that a knowledge of these characteristic curves under leak load should be very helpful particularly when used with kinetic systems with heavy loads. For example, in the case of vacuum smelting of magnesium, or similar other large kinetic systems used in industries, these pump characteristics are essential to choose proper types of pumping systems to be used.

## ACKNOWLEDGMENTS

The authors wish to thank Prof. M. N. Saha, D. Sc., F. R. S. Director of the Institute of Nuclear Physics, for his kind interest and encouragement in the work and express their appreciation to Dr. B. D. Nag for his helpful discussions.

## REFERENCES

- Blears J. and Hill, R. W., 1948, *Rev. Sci. Inst.*, **10**, 847.  
 Dayton B. B., 1948, *Rev. Sci. Instr.*, **10**,  
 Gaede, W. 1915, *Ann. d. Physik.*, **46**, 337.  
 Gaede, W. 1923, *Zeits. f. Tech. Physik*, **10**, 337.  
 Ho, T. L. 1932, *Physics.*, **2**, 386.  
 How H. C. ard, 1935, *Rev. Sci. Instr.*, **6**, 327.  
 Matricon, S. M. 1932, *J. de. Phys. et Rad.*, **3**, 127.

# MOLECULAR DIAMETER OF A LIQUID

By M. G. BHATAWDEKAR

DEPARTMENT OF PHYSICS, MAHARAJA'S COLLEGE, JAIPUR, (RAJPUTANA).

(Received for publication, August 25, 1952)

**ABSTRACT.** Knowing the potential energy of a liquid, an idea is gained about the molecular diameter. The pressure within liquid carbon dioxide and ethyl alcohol at different temperatures is calculated ; for the former, change in free energy and internal energy is also calculated.

This paper is in continuation of the previous ones by the author (Bhatawdekar, 1951 and 1952). As explained (Bhatawdekar 1951), the free energy  $H$ , internal energy  $E$ , and  $\frac{dH}{dT}$  are determined for carbon dioxide with the help of  $\beta$  (Tables I and II) Applying Virial theorem (Bhatawdekar, 1952), the pressure within carbon dioxide and ethyl alcohol is also calculated at different temperatures (Table III).

TABLE I

Temperature °C	Log $km$	No of maxima	$I$	$F$	$r - d/10$
-30	9.0405	70	715	$2.1 \times 10^3$	$3.4 \times 10^{-2}$
-20	9.0230	75	800	$8.6 \times 10^3$	$5.1 \times 10^{-2}$
-10	9.0061	75	875	$4.7 \times 10^4$	$7.4 \times 10^{-2}$
0	10.9899	80	890	$1.5 \times 10^5$	$1.1 \times 10^{-1}$
10	10.9743	85	1135	$9.9 \times 10^5$	$1.5 \times 10^{-1}$
20	10.9592	90	1335	$8.5 \times 10^6$	$2.5 \times 10^{-1}$
31.1°C	10.9431	95	2800	$3.9 \times 10^9$	$1.0 \times 10^0$

A general study of the variation of potential energy of a liquid with temperature shows that the author's earlier observation that water tends to show an anomalous behaviour is wrong. It is of general application. It is general occurrence with a liquid that its potential energy diminishes with diminishing temperature, becomes zero, and then reverses its sign. This change of sign is noted in the case of water and ethyl alcohol at temperatures between 70°C and 100°C, and 80°C and 120°C respectively. Similar observations are also possible in other liquids only if calculations can be carried at still

TABLE II

Temperature °C	$\beta \times 10^{10}$ ergs per gm.	$H \times 10^{-10}$ ergs	$P(V_2 - V_1)$ $\times 10^8$ ergs	$(H - E)$ $\times 10^{10}$ ergs	$\frac{(H - E)}{T}$ $\times 10^{-7}$ ergs per deg.	$dH/dT$ from graph	$\phi$ $k$ $\times 10^{13}$ ergs	$2\phi R$ $\times 10^{15}$ ergs per deg
-30	1.01	1.10	3.75	0.81	3.46	$3.0 \times 10^7$ ergs per degree	7.35	3.03
-20	1.18	1.13	3.50	0.89	3.51		8.36	3.42
-10	1.27	1.15	3.39	0.94	3.57		9.32	3.55
0	1.45	1.19	3.20	0.99	3.62		10.63	3.90
10	1.66	1.22	2.88	1.06	3.73		12.15	4.30
20	1.21	1.25	2.27	1.12	3.84		13.93	4.76
31.1	2.52	1.26	0.00	1.26	4.14		18.43	6.06

TABLE III

Sub- stance	Temper- ature °C	$r \times N^{1/3}$	$\xi \times 10^{13}$ ergs.	$\frac{d\xi}{dr} \times N^{-1/3}$ $\times 10^{12}$	$\Sigma r f(r)$ $\times 10^{-10}$	$RT \times 10^{-8}$	$V$ cc. per gm.	$P$ Atm $\times 10^{-4}$
<chem>C2H5OH</chem>	80	1.109	-0.08	?	?	6.37	1.361	?
	120	1.131	2.08	15.0	22.14	7.10	1.444	-4.998
	160	1.164	4.58	10.0	15.20	7.82	1.579	-3.082
	200	1.215	0.87	5.5	8.73	8.54	1.796	-1.539
	213	1.537	10.20	2.5	5.02	9.32	3.629	-0.430
<chem>CO2</chem>	-30	0.9761	3.68	5.8	7.70	4.59	0.9302	-2.675
	-20	0.9900	4.33	4.2	5.64	4.78	0.9699	-1.863
	-10	1.0070	4.66	3.3	4.48	4.97	1.0194	-1.396
	0	1.270	5.32	2.6	3.69	5.16	1.0811	-1.077
	10	1.0520	6.08	1.8	2.57	5.35	1.1628	-0.679

lower temperatures. The potential energy is assumed to be due to the existence of intermolecular forces. The change in the sign of the potential energy is interpreted as due to the change in the nature of the intermolecular forces which are known to depend on the intermolecular distances. Due to the dipole character of the molecule, they exert an attractive force  $F_a$  on each other which varies as  $1/r^4$ . When at lower temperatures, the two molecules approach very close to each other and due to the similar electronic shell charges they repel each other with a force  $F_r$  varying as  $1/r^t$ . Therefore, the resultant molecular force  $F = F_a - F_r = A/r^4 = B/r^t$ .

The value of  $r = r_0$  for which the resultant force becomes zero gives the equilibrium distance between the centres of two molecules and is equivalent to the molecular diameter  $\sigma$  (Saha and Shrivastava, 1935).

For a distance greater than  $r_0$ , (i.e. at higher temperatures) the resultant force will be the force of attraction and hence, the potential energy has plus sign, at smaller distances (i.e. at lower temperatures), the repulsive force will preponderate giving us the negative potential energy. When the resultant molecular force is zero the potential energy will also be zero. So, a graph is plotted between  $r$  [ $r = (1/d_v)^{1/3}$ , where  $d$  is the density of a liquid and  $N$  denotes the number of molecules in one gram of the liquid] and the potential energy. By extrapolation,  $r_0$  corresponding to zero potential energy and hence molecular diameter are known. The values of  $\sigma$  so determined are shown in Table IV, second column, while in the third and fourth columns are shown values calculated with the help of viscosity and Vander waals' constant data.

TABLE IV

Substance	From potential energy $\sigma r \times 10^8 \text{cm}$	From viscosity data $\sigma r \times 10^8 \text{cm}$	From Vander Waals constant $\sigma_v \times 10^8 \text{cm}$
$\text{CCl}_4$	5.50	5.09	4.64
$\text{NH}_3$	3.41	2.64	3.05
$\text{C}_2\text{H}_5\text{OH}$	4.67	3.90	4.05
$\text{CO}_2$	3.84	3.44	3.40
$\text{H}_2\text{O}$	3.14	2.53	2.75

The accuracy of  $\sigma$  will depend on the accuracy of the calculation of  $\beta$  and extrapolation in graph. The error is of the order of  $\pm 0.06 \times 10^{-8} \text{cm}$ .

In the case of  $\text{NH}_3$  and  $\text{CCl}_4$ , by plotting a graph between  $d\xi/dr$  and  $r$ , it is observed that  $d\xi/dr \propto 1/r^m$ , where  $m$  lies between 9 and 9.5. It is a matter of chance that the value of  $m$  comes out to be approximately the same for  $\text{NH}_3$  and  $\text{CCl}_4$ . It was, therefore, possible to get an equation of state where virial function is the same function of the specific volume of a liquid.  $S$  and  $t$  never have same values for all substances (Saha and Shrivastava, 1950) and hence the value of  $m$  will be different. Therefore, virial function will be a different function of volume of a liquid giving us different equations of state for different liquids. Further studies are under progress in this direction.

*Explanation, of the symbols used.*

$K = 1/2RT$  where  $R$  is the gas constant and  $T$  is the absolute temperature  
 $m$  = the mass of the particle

$$I = \int_0^\infty \frac{e^{-K m u^2} x^3 dx}{p x^2 \sqrt{x^2 + b} \cos^2 g x - \sqrt{x^2 + b} + \frac{x^2}{\sqrt{x^2 + b}}}$$

where

$$u^2 - b = x^2$$

$$p = \frac{16\pi^2 m^2}{1.2}$$

$$b = \frac{2U_1}{4mL} = \frac{4mL}{4mL} = 1$$

$$g = \frac{a}{2} \sqrt{p}$$

$a$  = thickness of potential barrier

$L$  = latent heat

$h$  = Planck's constant

$F$  = the total probability of a molecule crossing the boundary

$d$  = density of saturated vapour

$D$  = density of liquid

$\beta$  = the correction term

$$\phi/k = m\beta = \phi/2k = \xi$$

$\xi$  = potential energy of a liquid

$V_1, V_2$  = Volumes in liquid and gas phase respectively

#### A C K N O W L E D G M E N T

The author wishes to express his thanks to Prof. M. F. Soonawala, Maharaja's college, Jaipur, for his help and guidance.

#### R E F E R E N C E S

- Bhatawdekar, M. G. 1951, *Univ of Rajputana Studies*, **1**, 42,  
 Bhatawdekar, M. G., 1952, *Ind. J. Phys.*, **36**, 54.  
 Saha, M. N. and Shrivastava, B. N., 1935, *A Treatise on Heat*, 2nd Edition, p. 224.  
 Saha, M. N. and Srivastava, B. N., 1950, *A Treatise on Heat*, 3rd Edition p. 424.



# A DISCUSSION ON THE SPECTROSCOPIC STATE OF TETRAVALENT CARBON IN THE HALOGEN SUBSTITUTED DERIVATIVES OF METHANE, AS REVEALED BY ABSORPTION SPECTRA

By PRABHAT K. SEN GUPTA

METEOROLOGICAL OFFICE, SAHDARJANG AIR PORT, NEW DELHI

(Received for publication, December 10, 1952)

**ABSTRACT.** The view that tetravalent carbon in the halogen substituted derivatives of methane has the electronic configuration  $1s^2 2s^2 2p^2$  ( $^3P\ ^1D\ ^1S$ ) is supported by a comparison of energy values corresponding to the first long wavelength limit of continuous absorption in these compounds with the values of energy of carbon-halogen bond calculated with the aid of thermochemical data. In the calculations the latent heat of sublimation of graphite recently proposed by the author has been utilized.

## INTRODUCTION

For over two decades a number of papers and discussions have appeared on the absorption spectra of the halogen substituted derivatives of methane. Bands as well as continuous absorption regions have been found, but a common feature of all these compounds is that towards the longer wavelength region, the first absorption is a continuous one, beginning from a long wavelength limit. It is also seen that in the series... $\text{CH}_3\text{X}$ ,  $\text{CH}_2\text{X}_2$ ,  $\text{CHX}_3$ , and  $\text{CX}_4$ , where X is Cl, Br or I, the long wavelength limit of absorption shifts towards the longer wavelength side, as each H atom is substituted by the same halogen atom successively (Herzberg and Scheibe, 1930; Henrici, 1932; Saha, 1933; Hukumoto, 1935; Parti and Samuel, 1937). For instance, for the compounds  $\text{CH}_3\text{Cl}$ ,  $\text{CH}_2\text{Cl}_2$ ,  $\text{CHCl}_3$  and  $\text{CCl}_4$ , the long wavelength limits of continuous absorption are found to lie at  $\lambda\lambda$  2200, 2500, 2660, and 2800 Å respectively. The same effect has been observed in the in the series  $\text{CH}_3\text{Cl}$ ,  $\text{CH}_3\text{Br}$ , and  $\text{CH}_3\text{I}$  and other similar compounds as the halogen is successively substituted in the order Cl, Br, and I.

The author's experiments (Sen Gupta, 1933), however, showed that if the halogen is left undisturbed in a series like  $\text{CH}_3\text{Cl}$ ,  $\text{C}_2\text{H}_5\text{Cl}$ ,  $\text{C}_3\text{H}_7\text{Cl}$ ..., there is little shift in the long wavelength limit of continuous absorption. These results have led to the belief that it is the carbon-halogen bond in the compounds which is responsible for the first continuous absorption and the shift of its long wavelength limit towards the longer wavelength side. A region of continuous absorption is usually ascribed to a photo-dissociation of a molecule into some of its constituents. In this case

absorption of light quanta corresponding to the first long wavelength limit of continuous absorption is supposed to cause a rupture of the first carbon-halogen bond with the release of one halogen atom in the normal state (Sen Gupta, 1936). In terms of Franck-Condon diagram, this process is represented by a vertical transition from the stable ground state of the molecule to the first excited electronic state which happens in this case to be a repulsive  $U(r)$  curve (indicating dissociation). Hence the energy corresponding to the first long wavelength limit of absorption is expected to give an idea of the strength of the first carbon-halogen bond. The experimental value is, however, generally higher than the real value, as the repulsive  $U(r)$  curve has a slope at the point of transition, with the result that a small fraction of the absorbed quanta passes into the products of dissociation as kinetic energy. Therefore, while comparing experimental values with calculated values, it has to be borne in mind that the latter cannot be higher.

The experimental values are given in the second and third columns of Table V. Although the long wavelength limit should have a single value for each compound, there seems to be some disagreement in the results of different workers. The discrepancy is apparently due to the fact that with the experimental method adopted in some of the investigations it was not possible to reach the limiting value. In Table V, therefore, the values obtained by the author (Sen Gupta, 1933) and Saha (1933) have been given for the compounds investigated by them. For the other compounds, the highest wavelength limit available from different investigations for each compound has been selected as being most representative for our purpose.

#### CALCULATION OF BOND ENERGY

The energy of the carbon-halogen bond has been calculated with the aid of thermochemical equations and spectroscopic data. Our object is to find the energy required to rupture the first carbon-halogen bond, but the above method gives only the average value. The case of  $\text{CH}_4$  has been discussed by the author (Sen Gupta, 1951) recently. The four C-H bonds are situated symmetrically with respect to the same carbon atom, but from direct determinations it has been found that the energy required to break the first C-H bond is much higher than that for the last one (Anderson, Kistiakowsky and Van Artsdalen, 1942; Kistiakowsky and Van Artsdalen, 1944; Stevenson, 1942; Shidei, 1936; Voge, 1948). Voge has estimated that  $101 \pm 1$ , 90, 80, and 80 k.cal. are required for the removal of the H atoms in  $\text{CH}_4$  in succession. Accepting Voge's figures, the average bond energy comes out as  $(101 + 90 + 80 + 80) / 4$  that is equivalent to 88 k.cal., which is much lower than the energy required to rupture the first C-H bond ( $101 \pm 1$  k.cal.) If we postulate that the same proportion in bond energies is maintained amongst the different bonds of the halogen substituted

TABLE I.  $\text{CH}_3\text{X}$ 

Spectroscopic state of carbon-(x)	$s^2 p^2 3P$			$s^2 p^2 1D$			$s^2 p^2 1S$			$sp^3 3S$		
	Cl	Br	I	Cl	Br	I	Cl	Br	I	Cl	Br	I
Reactions $4\text{CH}_3\text{X} + 7\text{O}_2 \rightarrow 4\text{CO}_2 + 2\text{X}_2 + 6\text{H}_2\text{O}$ $2\text{X}_2 \rightarrow 4\text{X}$ $6\text{H}_2\text{O} \rightarrow 6\text{H}_2 + 3\text{O}_2$ $4\text{CO}_2 \rightarrow 4[\text{C}] + 4\text{O}_2$ $6\text{H}_2 \rightarrow 12\text{H}$ $4[\text{C}] \rightarrow 4\text{C}(\text{x})$	kcal	kcal	kcal	kcal	kcal	kcal	kcal	kcal	kcal	kcal	kcal	kcal
	692	736	802	692	736	802	692	736	802	692	736	802
	-116	-100	-90	-116	-100	-90	-116	-100	-90	-116	-100	-90
	-354	-354	-354	-354	-354	-354	-354	-354	-354	-354	-354	-354
	-36	-376	-376	-376	-376	-376	-376	-376	-376	-376	-376	-376
	-630	-630	-630	-630	-630	-630	-630	-630	-630	-630	-630	-630
	-475	-475	-475	-591	-591	-591	-721	-721	-721	-859	-859	-859
$\text{CH}_3\text{X} \rightarrow \text{C}(\text{x}) + 3\text{H} + \text{X}$	-515	-300	-281	-344	-329	-310	-376	-361	-342	-411	-396	-377
Total energy of last three C-H bonds, 90+80+80	250	250	250	250	260	250	250	250	250	250	250	250
Energy of C-X bond	65	50	31	94	79	60	126	111	92	161	146	127

 TABLE II.  $\text{CH}_2\text{X}_2$ 

Spectroscopic state of carbon ... (x)	$s^2 p^2 3P$			$s^2 p^2 1D$			$s^2 p^2 1S$			$sp^3 3S$		
	Cl	Br	I	Cl	Br	I	Cl	Br	I	Cl	Br	I
Reactions $2\text{CH}_2\text{X}_2 + 2\text{O}_2 \rightarrow 2\text{CO}_2 + 2\text{H}_2\text{O} + 2\text{X}_2$ $2\text{X}_2 \rightarrow 4\text{X}$ $2\text{CO}_2 \rightarrow 2[\text{C}] + 2\text{O}_2$ $2\text{H}_2\text{O} \rightarrow 2\text{H}_2 + \text{O}_2$ $2\text{H}_2 \rightarrow 4\text{H}$ $2[\text{C}] \rightarrow 2\text{C}(\text{x})$	kcal	kcal	kcal	kcal	kcal	kcal	kcal	kcal	kcal	kcal	kcal	kcal
	214	—	356	214	—	356	214	—	356	214	—	356
	-116	—	-90	-116	—	-90	-116	—	-90	-116	—	-90
	-188	—	-188	-188	—	-188	-188	—	-188	-188	—	-188
	-118	—	-118	-118	—	-118	-118	—	-118	-118	—	-118
	-210	—	-210	-210	—	-210	-210	—	-210	-210	—	-210
	-238	—	-238	-295	—	-295	-361	—	-361	-429	—	-429
$\text{CH}_2\text{X}_2 \rightarrow \text{C}(\text{x}) + 2\text{H} + 2\text{X}$	-328	—	-244	-357	—	-273	-390	—	-306	-424	—	-340
Total energy of last two C-H bonds, 80+80	160	—	160	160	—	160	160	—	160	160	—	160
energy of 2(C-X) bonds	168	—	84	197	—	113	230	—	146	264	—	180
Average energy of C-X bond	84	—	42	99	—	57	115	—	73	132	—	90
Energy required to rupture first C-X bond,	88	—	44	104	—	60	121	—	77	139	—	95
Average $\times \frac{101}{96}$												

TABLE III.  $\text{CHX}_3$ 

Spectroscopic state of carbon ... (x)	$s^2 p^2 3P$			$s^2 p^2 1D$			$s^2 p^2 1S$			$sp^3 {}^4S$		
X ... (Cl, Br or I)	Cl	Br	I	Cl	Br	I	Cl	Br	I	Cl	Br	I
Reactions	kcal	kcal	kcal	kcal	kcal	kcal	kcal	kcal	kcal	kcal	kcal	kcal
$4\text{CHX}_3 + 5\text{O}_2 \rightarrow 4\text{CO}_2 + 2\text{H}_2\text{O} + 6\text{X}_2$	281	—	548	281	—	648	281	—	648	281	—	648
$6\text{X}_2 \rightarrow 12\text{X}$	-348	—	-270	-348	—	-270	-348	—	-270	-348	—	-270
$2\text{H}_2\text{O} \rightarrow 2\text{H}_2 + \text{O}_2$	-118	—	-118	-118	—	-118	-118	—	-118	-118	—	-118
$2\text{H}_2 \rightarrow 4\text{H}$	-210	—	-210	-210	—	-210	-210	—	-210	-210	—	-210
$4\text{CO}_2 \rightarrow 4[\text{C}] + 4\text{O}_2$	-376	—	-376	-376	—	-376	-376	—	-376	-376	—	-376
$4[\text{C}] \rightarrow 4\text{C(x)}$	-475	—	-475	-591	—	-591	-721	—	-721	-859	—	-859
$\text{CHX}_3 \rightarrow \text{C(X)} + \text{H} + 3\text{X}$	-312	—	-200	-341	—	-229	373	—	-262	-408	—	-296
Energy of last C-H bond (80)	80	—	80	80	—	80	80	—	80	80	—	80
Total energy of 3(C-X) bonds	232	—	120	261	—	149	293	—	182	328	—	216
Average energy of (C-X) bond	77	—	40	87	—	50	98	—	61	109	—	72
Energy required to rupture the first C-X bond. Average $\times \frac{101}{90}$	86	—	45	98	—	56	110	—	68	122	—	81

TABLE IV.  $\text{CCl}_4$ 

Spectroscopic state of carbon ... (x)	$s^2 p^2 3P$	$s^2 p^2 1D$	$s^2 p^2 1S$	$sp^3 {}^4S$
Reactions	kcal	kcal	kcal	kcal
$\text{CCl}_4 + \text{O}_2 \rightarrow \text{CO}_2 + 2\text{Cl}_2$	45	45	45	45
$\text{CO}_2 \rightarrow [\text{C}] + \text{O}_2$	-94	-94	-94	-94
$2\text{Cl}_2 \rightarrow 4\text{Cl}$	-116	-116	-116	-116
$[\text{C}] \rightarrow \text{C(x)}$	-119	-148	-180	-215
$\text{CCl}_4 \rightarrow \text{C(x)} + 4\text{Cl}$	-284	-313	-345	-380
Average energy of C-Cl bond	71	78	86	95
Energy required to rupture the first C-Cl bond. Average $\times \frac{101}{88}$	82	89	100	109

TABLE V

Compound	First long wavelength limit of continuous absorption,		Energy of carbon-halogen bond taken from Tables I to IV	
	Wavelength in Å units	k-cal	Upper limit corresponding to configuration $1s^2 2s^2 2p^2 \dots 3p \ 1D \ 1S$	Configuration $1s^2 2s^2 2p^3 \ 3S$
			kcal	kcal
CH <sub>3</sub> Cl	2200 (Sen Gupta, 1933)	129	126	161
CH <sub>2</sub> Cl <sub>2</sub>	2500 (Saha, 1933)	114	121 (lower limit 88)	139
CHCl <sub>3</sub>	2660 (Saha, 1933)	107	110 (lower limit 86)	122
CCl <sub>4</sub>	2800 (Saha, 1933)	102	100	109
CH <sub>3</sub> Br	2415 (Hukumoto, 1935)	118	111	146
CH <sub>2</sub> Br <sub>2</sub>	2507 (Henrici, 1932)	113	..	..
CHBr <sub>3</sub>	2750 (Hukumoto, 1935)	103	..	..
CBr <sub>4</sub>	2932 (Parti and Samuel, 1937)	97	..	..
CH <sub>3</sub> I	2952 (Hukumoto, 1935)	96	92	127
CH <sub>2</sub> I <sub>2</sub>	3499 (Hukumoto, 1935)	81	77	95
CHI <sub>3</sub>	3730 (Parti and Samuel, 1937)	75	68	81
CI <sub>4</sub>	3930 (Parti and Samuel, 1937)	72	..	..

TABLE VI

Data used in calculations.

Heat of combustion		k cal.
	CH <sub>3</sub> Cl	173
	CH <sub>2</sub> Cl <sub>2</sub>	106.8
	CHCl <sub>3</sub>	70.3
	CCl <sub>4</sub>	44.5
	CH <sub>3</sub> Br	184
	CH <sub>3</sub> I	200.5
	CH <sub>2</sub> I <sub>2</sub>	178
	CHI <sub>3</sub>	162
Heat of formation ;	CO <sub>2</sub>	94
	2H <sub>2</sub> O	118
Heat of dissociation	Cl <sub>2</sub>	58
	Br <sub>2</sub>	50.2
	I <sub>2</sub>	45
	H <sub>2</sub>	105
Latent heat of sublimation of graphite into C(P <sup>3</sup> ) atoms. (Sen Gupta, 1951)		118.7
Spectroscopic term differences for C atom.		
	$s^2 \ 3P \sim s^2 \ 1D$	10194.5 cm <sup>-1</sup>
	$s^2 \ 3P \sim s^2 \ 1S$	21648.7 ..
	$s^2 \ 3P \sim sp^3 \ 5S$ (Shenstone, 1947) ..	33735.2 ..

compounds of CH<sub>4</sub> also, it is possible to estimate the energy required to break the first carbon-halogen bond in the following manner.

(a) CH<sub>3</sub>X: There is only one C-X bond. The total energy of the last three C-H bonds equivalent to 90+80+80=250 k.cal. has been allowed for in the calculations. (Table I).

(b)  $\text{CH}_2\text{X}_2$ : There are two C-X bonds, and therefore the energy of the first C-X bond is taken to be an equivalent to  $\frac{101}{(101+90)/2} = 101/96$  of the average value determined by the thermochemical calculations. In the calculations the value of the last two C-H bonds equivalent to  $80+80=160$  k.cal. has been taken into account. (Table II).

(c)  $\text{CHX}_3$ : There are three C-H bonds of which the first is being taken as equivalent to  $\frac{101}{(101+90+80)/3} = \frac{101}{90}$  of the average value. The last C-H bond has the energy value  $=80$  k.cal. (Table III).

(d)  $\text{CX}_4$ : There are four C-X bonds, of which the first has the energy value equivalent to  $\frac{101}{(101+90+80+80)/4} = \frac{101}{88}$  of the average. (Table IV).

#### SPECTROSCOPIC STATE OF TETRAVALENT CARBON

In a recent communication the author (Sen Gupta, 1951) supported the view that in  $\text{CH}_4$ , the carbon atom lies on the  $1s^2 2s^2 2p^2 - {}^3P \ ^1D \ ^1S$  state. As the alternative view that the carbon atom may lie in the  ${}^1S$  state of the configuration  $1s^2 2s^2 2p^2$  is also held by some investigators, it is proposed to examine both the views as applied to the halogen substituted compounds of  $\text{CH}_4$ . The calculations are given in each case in Tables I to III. Thermochemical and spectroscopic data used in these tables are given in Table VI. In Table V, the calculated values of the energy required to remove the first halogen atom, according as the carbon atom has the configuration  $s^2 p^2$  or  $sp^3$  are given in the last two columns, against the experimentally determined values of the first long wavelength limit of continuous absorption. It is seen that the figures corresponding to the  $sp^3 \ ^5S$  or carbon are much higher than the experimental limits and obviously absurd. There is much better agreement with column 5 of the same table, that is, if we assume that the carbon atom lies in the  $1s^2 2s^2 2p^2 - {}^3P \ ^1D \ ^1S$  state.

#### REFERENCES

- Anderson, H. G., Kistiakowsky, G. B., and Van Artsdalen, E. R., 1942, *J. Chem. Phys.*, **10**, 305.  
 Henrici, A., 1932, *Z. f. Phys.*, **77**, 35.  
 Herzberg, G. and Scheibe, G., 1930, *Z. f. Phys. Chem.*, **B 7**, 390.  
 Hukumoto, Y., 1935, *J. Chem. Phys.*, **3**, 164.  
 Iredale, T and Mills, 1931, *Proc. Roy. Soc. Lond.*, **A 133**, 430.  
 Kistiakowsky, G. B., and Van Artsdalen, E. R., 1944, *J. Chem. Phys.*, **12**, 469.  
 Partl, Y. P., and Samuel, R., 1937, *Proc. Phys. Soc. Lond.*, **49**, 568.  
 Saha, N. K., 1933, *Bull. Acad. Sci. U. P.*, **2**, 239.  
 Sen Gupta, P. K., 1933, *Bull. Acad. Sci. U. P.*, **2**, 115.  
 1936, *Bombay. Univ. Jour.*, **5**, 22.  
 1951, *Ind. J. Phys.*, **25**, 267.  
 Shenstone, A. G., 1947, *Phys. Rev.*, **72**, 411.  
 Shidei T., 1935, *Jap. J. Phys.*, **11**, 23.  
 Stevenson, D. B., 1942, *J. Chem. Phys.*, **10**, 231.  
 Voge, H. H., 1948, *J. Chem., Phys.*, **18**, 484.

# AN ACCURATE DETERMINATION OF THE TORSION CONSTANT OF QUARTZ FIBRES USED IN THE MEASUREMENT OF THE MAGNETIC ANISOTROPY OF CRYSTALS

BY SUNIL KUMAR DATTA

DEPARTMENT OF X-RAYS AND MAGNETISM, INDIAN ASSOCIATION FOR THE  
CULTIVATION OF SCIENCE, CALCUTTA 32

(Received for publication, September 11, 1952)

**ABSTRACT.** The torsional oscillations of circular discs with suspensions of quartz fibre have been studied for the determination of the torsion constant of the fibre. The correction of the time period for the damping of oscillations is found to be generally very small. The damping force is proportional to the first power of the angular velocity for small values of velocity, but to a higher power of velocity when it is large. The damping factor is found to be practically constant for the former case, dependent only on the dimensions of the vibrator and the factors affecting the viscosity of air. The effects of pressure, boundary conditions etc. have also been studied.

## 1. INTRODUCTION

In connection with the measurements of magnetic anisotropy of crystals, Krishnan and Banerjee (1935) have developed a method, depending upon the measurement of the critical torsional couple acting upon a crystal, suspended vertically in a homogeneous horizontal magnetic field, with a fine quartz fibre. The critical couple on the crystal is obtained when the direction of maximum magnetic susceptibility of the crystal in the horizontal plane makes an angle of  $\pi/4$  with the direction of the magnetic field, and is given by the equation :

$$\Delta X = \frac{2Mc}{mH^2} \left( \alpha_c - \frac{\pi}{4} \right) \quad \dots (1)^*$$

$m$  being the mass of the crystal and  $M$  its molecular weight,  $H$  the field strength and  $c$ , the torsion constant of the fibre.  $c$  is determined by suspending from the fibre a body of known moment of inertia,  $I$ , and observing the period of oscillation,  $T$ , where

$$T = 2\pi \sqrt{\frac{I}{c}} \quad \dots (2)$$

Since  $c$  is proportional to  $1/T^2$  it should be measured as accurately as possible. With due precautions it is not difficult to measure  $T$  with an

\* For small values of  $\alpha_c$  a correction term should be introduced (Krishnan, Mookerjee and Bose, 1939).

accuracy of 1 in 2000 which is all that we desire for our present purpose. Owing to the resistance of air, however, an oscillating body does not execute S. H. M., but has a damped oscillatory motion usually given by :

$$I \frac{d^2\theta}{dt^2} + R \frac{d\theta}{dt} + N \theta = 0 \quad \dots (3)$$

where  $I$  is the moment of inertia of the vibrating body,  $d\theta/dt$ , the angular velocity,  $R$ , the resisting force due to air (damping factor) and  $N$ , the restoring force. This equation may be written as

$$\frac{d^2\theta}{dt^2} + K \frac{d\theta}{dt} + \omega^2 \theta = 0 \quad \dots (3)$$

where,  $k$  is related to the logarithmic decrement of amplitude,  $\lambda$ , and the time period,  $T$ , of the damped motion is given by the relation

$$K = \frac{4\lambda}{T} \quad \dots (5)$$

The time period,  $T_0$ , of the system in the absence of damping is given by

$$T_0 = T \sqrt{\frac{\pi}{\pi^2 + \lambda^2}} \approx T \left( 1 - \frac{\lambda^2}{2\pi^2} \right) \quad \dots (6)$$

The above equation shows that the undamped period is less than the observed period by an amount  $T\lambda^2/2\pi^2$ . In determining  $c$  in connection with magnetic measurements, this damping correction of the time period has been neglected by previous workers.

In pursuance of a programme of improving the accuracy of measurement of the quantities involved in equation (1) to 0.1 % in order to determine the action of long range electric fields on paramagnetic ions (Bose and Mitra, 1952), this piece of work was undertaken to investigate : (i) whether the above correction factor is of sufficient order of magnitude to be introduced in the calculation of  $c$  ; and (ii) the conditions of experiment on which the damping factor,  $R$ , and hence,  $c$ , depend.

## 2. PREVIOUS OBSERVATIONS ON TORSIONAL OSCILLATIONS AND DAMPING FACTORS WITH QUARTZ FIBRE SUSPENSIONS

Torsional oscillations of a disc or cylinder have been employed for the determination of the modulus of rigidity of quartz fibres by Boys (1889), Thetfall (1899), Barnett (1898) and more elaborately by Horton (1905) who observed many precautions and corrected the period of oscillation for damping. It was observed that the rigidity of the fibres remained practically constant with time whilst it gradually increased linearly with temperature upto about 800°C and then decreased sharply. The period of oscillation and the logarithmic decrement also remained constant for small as well as for moderately large amplitudes. The logarithmic decrement, from which



the viscosity of the medium could be calculated, remained constant at lower pressures down to about 1/60th of an atmosphere and then decreased markedly (Maxwell, 1866; Kundt and Warburg, 1875). The logarithmic decrement,  $\lambda$ , at a pressure  $P$  is related to the logarithmic decrement,  $\lambda_0$ , at the normal pressure  $P_0$  by the equation (Dushman, 1910).

$$\frac{\lambda_0 - \mu}{\lambda - \mu} - 1 = P \frac{C'}{d} \quad \dots (7)$$

where  $\mu$  is the decrement due to the internal viscosity of the fibre and  $C'$  and  $d$  are constants involving  $P_0$  and the apparatus set-up.

Although the resisting force causing damping was at first assumed to be proportional to the first power of velocity, later work showed that damping might be proportional to the square of velocity. Thus :

$$\frac{d^2\theta}{dt^2} + k' \left( \frac{d\theta}{dt} \right)^2 + m^2\theta = 0 \quad \dots (8)$$

Peirce (1908) observed from photographic records of oscillations of galvanometer mirrors and other vibrating systems that there was an appreciable departure from the Gaussian law equation (1). The logarithmic decrement decreased rapidly for the first few oscillations after which the value of the decrement slowly decreased and for ordinary purposes could be regarded as constant. By increasing the restoring moment the coefficient of damping generally increased rapidly. Approximate solutions of the equations (8) for successive amplitudes and periods were obtained by van Zandt (1917) who gave the solution for the time period as

$$T_0 = \frac{2\pi}{\omega} \sqrt{\frac{c^2 k' \theta}{1 + 2k' \theta}} \quad \dots (9)$$

the value of  $k'$  being obtained by the method successive of approximation. Similar results were derived by Poschl (1928).

### 3. EXPERIMENTAL

Several pieces of cylindrical discs of various dimensions and materials (ebonite, glass, aluminium and steel) were procured, their diameters and thicknesses measured accurately with a screw gauge reading to 0.001 mm and their weights noted accurately to 0.0001 gm. They were suspended by means of short and thin pieces of glass rods from quartz fibres either vertically along any diameter or horizontally with their axes continuous with the fibres with the help of the hair line in a telescope set vertical with a fine plumb line. The fibres were of different lengths and thicknesses with their upper ends attached to a torsion head. Minute quantities of shellac were used in attaching the discs to the rods, the correction factor for shellac and the rod being assumed to be small. The torsion head was placed on the top of a wide glass tube with its bottom opening into a box, 20 × 15 × 15 cm<sup>3</sup> with a sliding glass front. The discs could be made to oscillate at the centre of

the box. Two other suspension chambers were used, one an air-tight glass tube capable of being evacuated through a side tube and with a plane glass window through which the vibrator could be viewed, and the other a narrow tube having a diameter 1 or 5 mm greater than two of the glass discs (Nos. 4 and 5) and with a similar glass window. Each of the ebonite, aluminium and steel discs corresponded in dimensions as nearly as possible with one of the two glass discs (Nos. 5 and 7). For vertical suspensions the reflection of an illuminated circular scale by the glass disc, either as it is, or with its surface thinly silver-coated, was observed in a telescope. In the case of discs of other materials, small portions of mirrored cover slips were attached to the discs, due account being taken of the inertia of the mirror. For horizontal suspensions, very small triangular (isosceles) portions of such mirrors (base about 3 mm, height 6 mm) were attached vertically to the glass rods bearing the discs. This procedure reduced the size of the mirror to a minimum giving at the same time a just sufficient view of the scale graduations. In order to estimate the small damping due to the mirror, a second mirror of about the same size and shape was fixed above the first one and the decrement was measured. It was found that the maximum increase in damping amounted to about 3 or 1%, according to the size of the vibrator, being less in case of large discs (cf. glass discs Nos. 5 and 9, Tables I and VII). The correction factor being uncertain, the data have been recorded without correction. The period was obtained by noting the passage of the rest point of the scale, determined previously, across the telescope crosswire for a sufficiently large period of time (300–500 sec.) using a stop-watch reading to the tenth of a second. The error was usually less than 0.1%. When the damping was small the logarithmic decrement was calculated by observing a set of even number of turning points of the image of the scale and after a number of complete oscillations ( $n$  semivibrations, say) when the amplitude had fallen to about a third of its initial value, the same number of turning points were noted. The elongations in one direction are then  $A_1, A_3, \dots A_{2r-1}$  for the first set and  $A_n, A_{n+2}, A_{n+4}, \dots A_{n+2r-1}$  for the second. The log decrement is then given by

$$(n-1)\lambda = \log e\{A_1 + A_3 + \dots A_{2r-1}\} - \log e\{A_n + A_{n+2} + \dots A_{n+2r-1}\} \dots (10)$$

For large dampings all the elongations were noted and the average of the ratios of successive elongations was used in calculating  $\lambda$ . The range of amplitude studied was always fairly small, although it was found that the decrement was constant within experimental errors for large ( $15^\circ - 20^\circ$ ) as well as for small ( $5^\circ - 7^\circ$ ) amplitudes. Measurements were made on: (i) different fibres with the same load, to see how the damping factor changes with time period as far as it depends on torsion constant; (ii) the same fibre with different loads for determining whether the torsion constant remains the same for the range of load investigated; (iii) the same fibre but with the vibrator in different orientation, *e.g.*, vertical or horizontal; (iv) comparison of results with silvered and unsilvered glass discs, or (v) discs of the same

dimensions but of different materials to see to what extent eddy currents and stray magnetic fields are responsible for damping in the latter and also to observe any changes of damping factor due to changes in moment of inertia ; (vi) the same fibre and vibrator but with different boundary conditions, e.g., the vibrating body placed in a narrow tube or in a wide box ; (vii) the same fibre and vibrator, but in air at ordinary pressure and in vacuum ; and (viii) the effects of temperature and moisture.

#### 4. RESULTS

The results of the present experiments are tabulated below.

TABLE I

(i) Variation of the damping factor ( $R$ ) of the vibrator with the time period of oscillation.

$R = kP = 4\lambda I/T$ , where  $\lambda$  is the logarithmic decrement, and  $T$  is the time period ( $T_0$  is the time period corrected for damping)

(i) Vertical suspension of the glass discs.

Disc No.	Fibre No.							19
G15	$T$	6.446	7.516	11.69	31.41	42.60		101.4
	$\lambda$	.0159	.0165	.0218	.0572	.0710		.1717
	$R \times 10^3$	3.87	3.14	2.93	2.61	2.61		2.66
	$T_0$	6.416	7.516	11.60	34.41	42.59		101.2
	Fibre No.	5	7	18	13	8		
G19	$T$	5.688	8.531	11.91	17.55	33.38		
	$\lambda$	.00811	.0096	.01128	.01647	.04763		
	$R \times 10^3$	17.51	13.82	11.63	11.52	10.99		
	$T_0$	5.688	8.531	11.63	17.55	33.38		

(ii) Horizontal suspension of the glass discs.

Disc No.	Fibre No.	16	1	11	14	9
G15	$T$	8.921	13.92	23.57	27.75	47.23
	$\lambda$	.00936	.01395	.0233	.0268	.0458
	$R \times 10^3$	3.25	3.10	3.06	2.99	3.00
	$T_0$	8.921	13.92	23.57	27.75	47.23
	Fibre No.	4	15	18	12	17
G19	$T$	4.171	7.870	17.51	23.92	42.48
	$\lambda$	.00293	.00503	.00891	.0116	.0200
	$R \times 10^3$	17.04	15.50	12.34	11.75	11.41
	$T_0$	4.171	7.870	17.51	23.92	42.48

The weights and dimensions of the discs are given in Table VII.

TABLE II

Variation of the torsion constant of the fibres with load.

$$c = 4\pi^2 I / T^2 \quad (\text{disc suspended vertically}).$$

Fibre No.	Disc No.	1	4	5	8	9
	Weight	.1968	.8402	1.5551	1.7290	5.2201
13	$T$	1.024	4.583	6.270	7.810	17.55
	$\lambda$	—	.00203	.0164	.0176	.01647
	$C$	.3945	.3945	.3936	.3947	.3950
11	$T$	5.632	25.31	34.40	42.91	
	$\lambda$	.0334	.0715	.0572	.0713	
	$C$	.1304	.1304	.1307	.1307	

TABLE III

Variation of the logarithmic decrement with factors affecting the viscosity of air :

(i) Effect of pressure (disc suspended vertically).

Disc No.		At atmos pressure	At 0.1 mm pressure	Disc No.	At atmos. pressure	At 0.1 mm pressure
G14	$T$ $\lambda$	5.900 .0232	5.885 .0146	G15	6.446 .00329	6.356 .0179

(ii) Effect of temperature (disc suspended horizontally ; aluminium)

Disc No.		At 28.2°C	At 30.8°C
A15	$T$ $\lambda$	21.57 .0211	21.54 .0215

(iii) Effect of moisture (disc suspended horizontally).

Disc No.		In air saturated with water vapour	In air dried by means of fused $\text{CaCl}_2$
A15	$T$ $\lambda$	21.56 .0215	21.57 .0223

TABLE IV

Variation of the logarithmic decrement with boundary conditions (discs suspended vertically).

Disc No.		In a box	In a tube	Disc No.	In a box	In a tube
G14	$T$ $\lambda$ $T_0$	4.622 .0166 4.622	4.626 .0205 4.626	G15	6.343 .0128 6.343	6.340 .0185 6.340

Dimensions of the box:  $20 \times 15 \times 15$  cm<sup>3</sup>; internal diam. of the tube: 25 mm.

TABLE V

The effect of earth's magnetic field and stray fields on the vibratory motion of bodies :

(i) Glass discs mirrored and unmirrored (suspension vertical). Thinnest discs (microscopic cover slips) were taken so as to reduce the inertia without reducing surface area much. Weight of the silver film was about one or two mgm whilst its resistance across any diameter was less than an ohm.

Disc No.		Unsilvered	Silvered
G16	$T$ $\lambda$ $R \times 10^3$	17.83 .2457 3.05	17.89 .2462 3.05

(ii) Glass and aluminium discs of nearly the same dimensions and not much different in weight (vertical suspension of the discs).

Disc No	Glass 5	Aluminium 5
$T$ $\lambda$ $R \times 10^3$	42.9 .0719 2.615	43.5 .0727 2.747

The weights and dimensions of the discs are given in Table VI.

TABLE VI

Variation of the damping factor of discs of the same dimensions but of different materials (*i.e.*, different moments of inertia). Horizontal suspension of the discs. (Diameter and thickness in cm ; weight in gm).

Disc No	Material	Ebonite	Glass	Aluminium	Steel
5	Diameter	1.982	1.996	1.991	1.989
	Thickness	.2023	.2013	.1819	.1982
5	Weight	.7880	1.5551	1.6351	4.7183
	$T$	40.14	47.23	43.38	38.18
5	$\lambda$	.0779	.0458	.0425	.0223
	$R \times 10^3$	3.08	3.00	3.16	3.45
	Diameter	2.370	2.369	2.397	2.396
	Thickness	.1778	.1575	.1620	.1385
	Weight	99.19	1.5981	1.7680	4.7177
	$T$	33.60	39.21	37.77	31.27
7	$\lambda$	.0950	.0413	.0388	.0127
	$R \times 10^3$	4.380	4.723	5.220	5.646

The values of  $R$  in the above table are taken for moderately large periods of vibration where  $R$  may be regarded as approximately constant.

### 5. DISCUSSIONS

The results set forth in Table I show that for the purpose of determining the torsion constant of quartz fibres the correction of time period for damping is inappreciable except for large periods. In order that  $\lambda^2/2\pi^2$  should exceed 1/1000,  $\lambda$  should be about 0.14 which is seldom the case. The damping factor,  $R$ , is approximately constant when the period is fairly large, whilst for smaller periods it increases rapidly with decreasing period. This is in agreement with the previous findings that the damping is proportional to a higher power of  $d\theta/dt$  than unity for small periods (Peirce, *loc. cit.*). An approximate value of  $\lambda$  can, however, be computed from the  $T$ - $R$  curve for any particular vibrator (*cf.* figure 1).

The logarithmic decrement is found to be decreased about 50% at a pressure of 0.1 mm of mercury (Table III i). The decrement due to the internal viscosity of the fibre, which is assumed to be low at ordinary pressures (Horton, *loc. cit.*) and is neglected in comparison with the decrement due to resistance of air, becomes appreciable at low pressures when the latter is small. This accounts for a still appreciable total damping at low pressures. Small changes in atmospheric pressure is known to be

without effect on the viscosity of air, and hence, on logarithmic decrement (Maxwell, loc. cit.), and has not been investigated in the present experiments. The effects of small variations of temperatures only, e. g., those arising from fluctuations of room temperature, have been studied. It has been found that the logarithmic decrement changes only slightly (by about 2%) per degree rise in temperature (Table III ii). This is in agreement with the observations of Horton that the logarithmic decrement increases by about 1% or less per degree rise in temperature. The effect of moisture content of air is also small.

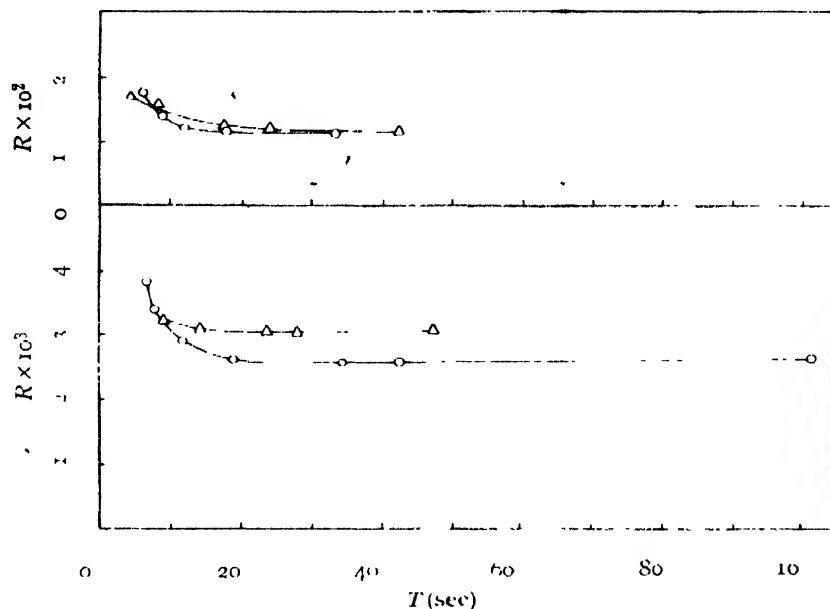


FIG. 1

Above, Disc no. G15      Δ—Horizontal suspension  
Below; Disc no. G19      O—Vertical suspension

Curves showing the variation of the damping factor ( $R$ ), of the discs with the period of oscillation ( $T$ ).

Damping is dependent to some extent on the boundary conditions (Table IV). For vertical suspension of the vibrator in a narrow tube with its walls at a few mm. from the disc the decrement due to viscous drag may be quite large, amounting sometimes to about 50% in excess of that within a large box. However, the change in the time period is usually inappreciable. Silvering a glass disc, even a thin one, does not produce any measurable change in the decrement, showing that the damping effects of any extraneous magnetic field (including that of the earth) by producing eddy currents, is quite negligible. The substitution of a metal disc for a glass one of the same dimensions and having comparable densities, however, results in an increase in the decrement (as is evident from an increase in the damping factor which takes into account the moments of inertia; Table V). This is also seen from Table VI which gives the damping factors of discs of the same dimensions but of different materials; the factors for discs of a

particular size are of the same order of magnitude in spite of widely different inertias, thus showing that they are dependent primarily on the size and shape of the vibrators. The values for glass and ebonite are nearly the same whilst for aluminium, and especially steel, they are markedly larger. This is perhaps due mainly to eddy currents causing magnetic damping (in the case of steel).

For vibrators of different sizes the damping factors are different and are also dependent on the diameters of the discs, as is seen from the following table in which the results for several glass discs are shown.

TABLE VII

Variation of the damping factor with the dimensions of the vibrator.

$A$  = area of the disc.

Disc No.	Weight (gm)	Diameter (cm)	Thickness (cm)	Vertical suspension $R \times 10^3 (R/A) \times 10^4$		Horizontal suspension $R \times 10^3 (R/A) \times 10^4$	
1	.1968	.9012	.1229	0.217	1.337	...	...
2	.0915	.9477	.0516	0.246	1.745	...	...
4	.8402	1.996	.1097	2.114	3.17	2.84	4.09
5	1.5551	1.905	.2013	2.61	3.47	3.00	3.99
6	.1809	.423	.0028	3.00	3.86	..	...
7	1.5981	2.369	.1472	4.30	4.24	4.71	4.76
8	1.7201	2.370	.1575	1.15	1.15	4.72	4.72
9	5.2201	3.048	.2931	10.99	6.32	11.4	6.55

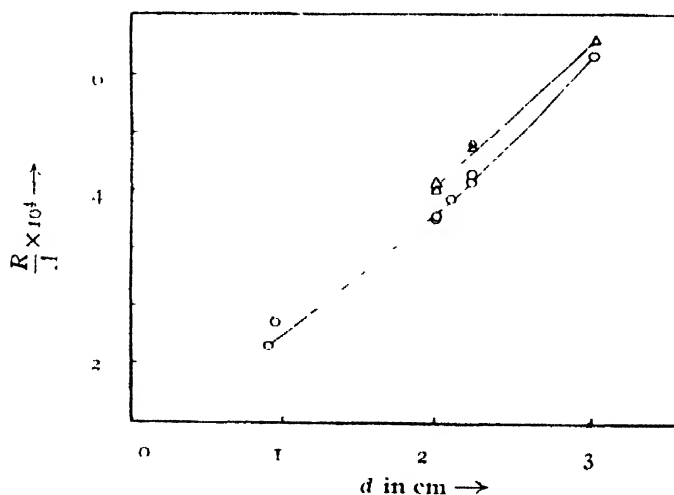


FIG. 2

$\Delta$  - Horizontal suspension

O - Vertical suspension

Curves showing the variation of the damping coefficient per unit surface of the disc ( $R/A$ ) with its diameter ( $d$ ).



It will be observed that the values obtained on dividing the damping factors by the surface area of the respective vibrators are nearly constant for discs of the same diameter (cf. No. 4 & 5 and 7 & 8), but increase with increasing diameter (figure 2). The value of  $R$  for horizontal suspension for any disc is greater than that for vertical suspension in almost all cases, the differences decreasing with increasing diameter. This may be due to the fact that the damping due to the mirror and other parts of suspension for horizontally suspended disc is not quite negligible in the case of the smaller discs. However, in view of the many effects associated with damping of a disc, e. g., edge effects and turbulence set up in the surrounding medium, it is hardly possible to assign any theoretical basis to the observations described above. Anyway, the extent of damping for a particular vibrator under the conditions mentioned above can still be estimated from its dimensions, since an approximate value of the decrement is all that is required for our present purpose.

The torsion constant of the fibre is found to be independent of load within the limits of experimental error (Table II). The range of load studied was from about 0.2 gm to 5 gm depending upon the thickness of the fibre used. From a knowledge of the length and approximate thickness of the fibre and using the accepted values of the Young's modulus,  $Y$ , ( $3.05 \times 10^{11}$  dynes/cm<sup>2</sup>) and Poisson's ratio (0.14), for fused quartz (cf. International Critical Tables, 1928), the ratio of the torsion constants before and after addition of load,  $c$  and  $c'$ , is given by :

$$c/c' = 1 - 1.56 f \quad \dots \quad (11)$$

where  $f$  is the elongation. For the thinnest fibre studied, 15 cm long and about 0.001 cm thick, the maximum load used was 0.2 gm. Using the above values in the formula:  $(S/\alpha)/Y = f$ , where  $\alpha$  is the area of cross section of the fibre and  $S$  the weight due to the load,  $f$  may be seen to be  $8.1 \times 10^{-4}$ . The correction for elongation is therefore about 0.1% which is just of the order of experimental errors.

Lastly, it may be said that for the purpose of calculating the torsion constant of quartz fibres in magne-crystalline experiments, horizontal suspension of the vibrator has no substantial point of advantage in comparison with vertical suspension. In actual practice, a vertically suspended cylindrical disc or mirror is more convenient for measuring the period accurately rather than one suspended horizontally, provided the conditions outlined above are fulfilled.

#### 6. ACKNOWLEDGMENT

The author expresses his gratitude to Dr A. Bose, D. Sc., for suggesting the problem and taking keen interest in connection with this work.

## REFERENCES

- Barnett, S. J. 1898, *Phys. Rev.*, **6**, 114.  
 Bose, A., and Mitra, S. C., 1952, *Ind. J. Phys.*, **26**, 398, 543.  
 Boys, C. V. 1899, *J. Soc. Arts* **37**, 827.  
 Dushman, S. 1949, "Scientific Foundations of Vacuum Technique", Wiley, N. Y., p. 282.  
 Horton, F., 1905, *Phil. Trans. Roy. Soc.*, **A204**, 412.  
 International Critical Tables 1928, **4**, 21.  
 Krishnan, K. S. and Banerjee, S., 1935, *Phil. Trans. Roy. Soc.*, **A234**, 265.  
 Krishnan, K. S., Mookerjee, A., and Bose, A., 1939, *ibid*, **A238**, 125.  
 Kundt, A., and Warburg, E., 1875, *Monats. der Berl. Akad.*, p. 162. *logg. Ann.*, 1875, **150**, 337, 525.  
 Maxwell, J. C., 1860, *Phil. Mag.* 4, **19**, 31. *Phil. Trans. Roy. Soc.* 1866, **A166**, 249.  
 Nilkantan, P. 1936, *Doctoral Dissertations* (Special publication, Indian Inst. Sci., Bangalore).  
 Peirce, B. O. 1908, *Proc. Amer. Acad. Arts and Sci.*, **44**, 11, 63.  
 Poschl, von T. 1928, *Phys. Zeits.*, **29**, 938.  
 Threlfall, 1890, *Phil. Mag.*, **30**, 99.  
 Van Zandt, J. P., 1917, *Phys. Rev.*, **10**, 415.

# RAMAN SPECTRA OF METHYL METHACRYLATE IN THE SOLID STATE AT $-180^{\circ}\text{C}^*$

By N. K. ROY

OPTICS DEPARTMENT, INDIAN ASSOCIATION FOR THE CULTIVATION OF SCIENCE, CALCUTTA 32

(Received for publication, March 7, 1953)

## Plate X

**ABSTRACT.** The Raman spectra of both monomeric methyl methacrylate in the solid state at  $-180^{\circ}\text{C}$  and polymethyl methacrylate at  $-180^{\circ}\text{C}$  have been photographed and compared with those of the substances at room temperature. It is observed that in agreement with results of earlier workers the line  $1640\text{ cm}^{-1}$  disappears and the line  $1722\text{ cm}^{-1}$  becomes feebler when the monomer is polymerized to form plexi glass, and when the monomer is solidified and cooled to  $-180^{\circ}\text{C}$  the intensity of line  $1640\text{ cm}^{-1}$  diminishes to half its value observed in the case of the liquid, while the line  $1722\text{ cm}^{-1}$  shifts to  $1700\text{ cm}^{-1}$ , but its intensity remains unaltered. It is concluded that in the latter case the  $\text{C}=\text{C}$  bond of some of the molecules disappears to form regular bonds between neighbouring molecules, but as the  $\text{C}=\text{O}$  group remains intact the bonds do not form permanent chains and they break up with rise of temperature of the monomer.

In the case of the polymer the frequencies of some of the lines due to  $\text{C}-\text{H}$  and  $\text{C}-\text{C}$  valence oscillations diminish with lowering of temperature to  $-180^{\circ}\text{C}$ .

## INTRODUCTION

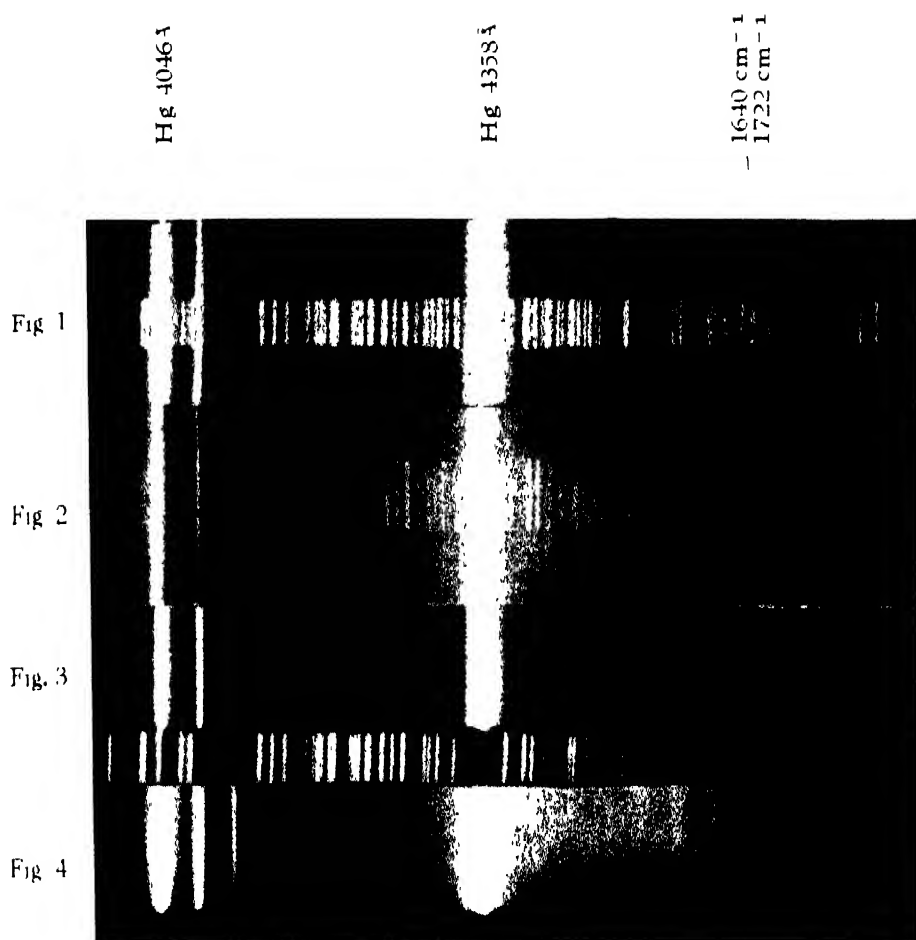
It was shown by Hibben (1937) that when methyl methacrylate is polymerised, the lines  $1404\text{ cm}^{-1}$  and  $1638\text{ cm}^{-1}$  of the monomer due to the  $\text{CH}_2$  deformation and  $\text{C}=\text{C}$  stretching vibration disappear completely and in place of the lines  $940$  and  $1008\text{ cm}^{-1}$  of the monomer two lines at  $974$  and  $1116\text{ cm}^{-1}$  are observed in the case of the polymer. It was concluded by him that the chain in the polymer is formed at the expense of the  $\text{C}=\text{C}$  bond. Yasumi (1942) showed that the intensity of the line due to  $\text{C}=\text{C}$  stretching oscillation in the monomer diminishes gradually as the degree of polymerization increases and finally the line disappears. Kojima (1949) also studied the Raman spectra of methyl methacrylate in different stages of polymerization and observed that the intensity of the line  $1638\text{ cm}^{-1}$  diminishes as the degree of polymerization of methyl methacrylate in solution in benzene increases. But he observed further that the intensity of the line  $1722\text{ cm}^{-1}$  due to  $\text{C}=\text{O}$  stretching vibration also diminishes with increase in the degree of polymerization. Patel (1949), on the otherhand, observed a line  $1598\text{ cm}^{-1}$  in the Raman spectrum of polymethyl methacrylate and concluded that

Hibben's conclusion that polymerization takes place at the expense of the  $C=C$  double bond has to be revised. The conclusions drawn by him are thus contradictory to those arrived at by the previous workers mentioned above. He, however overlooked the fact that the intensity of the line  $1638\text{ cm}^{-1}$  of the monomer is larger than that of the line  $1451\text{ cm}^{-1}$  while the line  $1598\text{ cm}^{-1}$  observed by him is too feeble to correspond to the line  $1630\text{ cm}^{-1}$ . The object of the present investigation was to study the Raman spectrum of the monomer in the solid state at  $-180^{\circ}\text{C}$  in order to find out whether in the solid state the monomer undergoes any change similar to that observed in the case of polymerization, and also to verify whether the line  $1598\text{ cm}^{-1}$  is actually present in the Raman spectrum of the polymer.

The Raman spectrum of the polymer at  $-180^{\circ}\text{C}$  has also been studied in order to find out whether the lowering of temperature has any influence on the position and intensity of the lines. The results of these investigations have been discussed in this paper.

#### EXPERIMENTAL

Blocks of polymethyl methacrylate were obtained from I. C. I. Ltd., and the monomer was prepared by purifying 'Kallodent' supplied by the same firm. The inhibitor mixed with the monomer in Kallodent was removed by washing the liquid repeatedly with 5% NaOH solution in a separating funnel. The caustic soda solution turned brown after the reaction with the inhibitor and after repeated washing with the caustic soda solution such a coloration did not take place. The liquid treated in this way was washed with distilled water several times and dried over anhydrous calcium chloride for 48 hours. The liquid thus made free from water was subjected to fractional distillation, and the fraction having the boiling point between  $99.4^{\circ}\text{C}$  and  $100^{\circ}\text{C}$  was collected. This purified liquid was then distilled in vacuum in a double bulb of Pyrex glass leaving a considerable residue, and the Raman spectrum of the pure liquid obtained in this way was studied at the room temperature immediately after the distillation. After the exposure the liquid was again distilled in another double bulb and the Raman spectrum of the distilled product solidified and cooled to  $-180^{\circ}\text{C}$  was photographed. A Fuess glass spectrograph having a dispersion of about 11.5 A. U. per mm. at  $4046\text{ \AA}$  was used in these two investigations and in the latter case the substance was solidified gradually by immersing slowly the Pyrex container containing the liquid in a transparent Dewar vessel containing liquid oxygen. The mouth of the latter vessel was covered with filter paper soaked in liquid oxygen to avoid formation of ice on the walls of the container. The solidified mass was illuminated by two vertical mercury arcs from two sides. A dilute solution of sodium nitrite was used to cut off all wavelengths below 3800 A. U. to avoid fluorescence. After the exposure, as the solid mass was allowed to attain gradually the room



## Raman spectra

Fig. 1. Methyl methacrylate monomer at 30°C

Fig. 2. " " " at -180°C

Fig. 3. " " polymer at 30°C

Fig. 4. " " " at -180°C



temperature it melted and became again a liquid having apparently the same properties as those of the liquid before solidification.

The Raman spectra of the polymer at room temperature and at  $-180^{\circ}\text{C}$  were photographed with a Hilger two-prism glass spectrograph of large light gathering power and giving a dispersion of about 20 Å. U. per mm. in the 4046 Å region. The specimen was in the form of a rectangular block about 2 cm. thick and 6 cm. long with all the six faces polished. In order to study its Raman spectrum at  $-180^{\circ}\text{C}$  the specimen was held in the transparent Dewar vessel mentioned above and liquid oxygen was poured into the Dewar vessel to cool the specimen. Iron arc spectrum was photographed on each of the spectrograms for comparison. The exposure for the liquid was 36 hours and for the monomer at  $-180^{\circ}\text{C}$  it was 14 hours.

Microphotometric records of the lines 1638 and  $1722\text{ cm}^{-1}$  due to the monomer at room temperature and of the corresponding lines of the monomer at  $-180^{\circ}\text{C}$  were next taken to find out the changes in relative intensities of these lines with solidification of the substance.

#### RESULTS AND DISCUSSION

The spectrograms are reproduced in figures 1-4, Plate X and the microphotometric records are reproduced in figure 5. The frequency-shifts are tabulated in Table I. The data reported by Hibben (1937) for the liquid and the polymer are also included in the table. Approximate intensities estimated visually are given in parentheses.

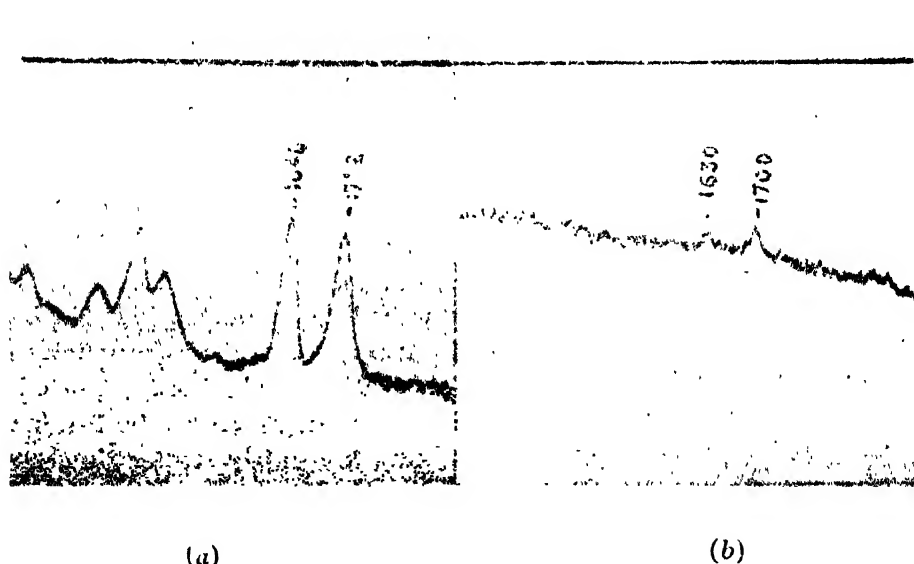


FIG. 5

Microphotometric records of methyl methacrylate monomer

(a) At  $30^{\circ}\text{C}$

(b) At  $-180^{\circ}\text{C}$

TABLE I  
Methyl methacrylate

Monomer, liquid		Monomer, solid at $-180^{\circ}\text{C}$ . $\Delta\nu$ in $\text{cm}^{-1}$ .	Polymer at room temperature		Polymer at $-180^{\circ}\text{C}$
Hibben (1937) $\Delta\nu$ in $\text{cm}^{-1}$ .	Present author $\Delta\nu$ in $\text{cm}^{-1}$		Hibben (1937) $\Delta\nu$ in $\text{cm}^{-1}$ .	Present author $\Delta\nu$ in $\text{cm}^{-1}$ .	Present author $\Delta\nu$ in $\text{cm}^{-1}$ .
		58 (2); e, k		88 (1b); e, 238 (ob); e, k	84 (1b); e, k
	228 (2); e, k 282 (1b); e, k 380 (5); e	380 (ob); e	209 (1) 367 (2, b) 487 (2, b, d)	300 (1); e, k 380 (2); e	375 (ob); e
377 (3)		506 (o); e, k		507 (2); e, k 602 (4); e, k	620 (1b); e, k
507 (2)	507 (2); e, k		596 (3)		
599 (2)	603 (3); e, k			812 (5); e, k	804 (2); e, k
656 (o)	658 (o); e, k	838 (2); e, k	806 (6)		
835 (6)	833 (8); e, k	937 (o); e, k			
940 (2)	937 (2); e, k 998 (1b); e, k	968 (o); e, k			
1008 (2)	1012 (2); e, k	1014 (1); e, k	974 (5, b, d)	976 (5); e, k 1002 (4); e, k 1122 (o); k 1188 (o); k	970 (3b); e, k
			1116 (1)		
1332 (1)	1335 (1); e, k	1327 (2b); e, k 1383 (1); e, k	1335 (o, b)	1340 (ob); e, k	1320 (ob); e, k
1404 (5)	1408 (5); e, k				
1451 (3)	1448 (3b); e, k	1460 (2b); e, k	1448 (1b, d)	1458 (5b); e, k	1450 (4); e, k
1638 (8)	1640 (10); e	1630 (3); k			
1722 (7)	1722 (8); e	1700 (5); k	1725 (3)	1731 (2); e	1728 (1b); e
2855 (o)	2850 (1); k	2852 (ob); k	2835 (o)	2853 (2); e, k	2852 (ob); k
2933 (3)	2934 (3); e, k 2954 (o); e, k	2934 (1); k 2953 (o); k	2917 (2)	2962 (2b); e, k	2945 (5); e, k
3005 (1)	3002 (2); e, k	2969 (o); k 2991 (2); e, k 3024 (2); e, k 3103 (2); e, k	3005 (1)	3024 (3b); e, k	2988 (3b); e, k
3100 (3)	3108 (2); e, k			3109 (ob); e, k	3100 (ob); k

It can be seen from Table I that the line  $1640\text{ cm}^{-1}$  due to the monomer is totally absent in the Raman spectrum of plexi glass. The line  $1598\text{ cm}^{-1}$  reported by Patel (1949) was not found in the spectrogram reproduced in Plate X. These results thus agree with those reported by Hibben (1937) and Yasumi (1942). There are, however, certain discrepancies between the results obtained in the present investigation and those reported for the monomer and the polymer at room temperature reported by Hibben (1937). The faint lines  $228$ ,  $282$ ,  $658$ ,  $998\text{ cm}^{-1}$  and the fairly strong line  $2954\text{ cm}^{-1}$  observed in the case of the liquid in the present investigation were not reported by Hibben (1937). Of course, in the case of the polymer there are lines at  $238$ ,  $300$  and  $2962\text{ cm}^{-1}$  and it might be suspected that the extra lines observed in the case of the liquid might be due to partial polymerization of the liquid during the exposure. There are, however, certain difficulties in drawing such a conclusion, because the intense lines  $816\text{ cm}^{-1}$



and  $976\text{ cm}^{-1}$  of the polymer were not observed in the spectrum due to the liquid. Also the frequency-shift  $2962\text{ cm}^{-1}$  due to the polymer is larger than  $2954\text{ cm}^{-1}$  observed in the case of the liquid. It is, therefore, concluded that the extra lines mentioned above may be due to the monomer.

On comparing the results given in columns 2 and 3 of Table I, it can be seen that when the monomer is solidified and cooled to  $-180^{\circ}\text{C}$  the line  $1640\text{ cm}^{-1}$  due to  $\text{C}=\text{C}$  stretching oscillation shifts to  $1630\text{ cm}^{-1}$  and its intensity relative to that of the  $1722\text{ cm}^{-1}$  line diminishes remarkably. Also the line  $1722\text{ cm}^{-1}$  shifts to  $1700\text{ cm}^{-1}$ . This can be seen from the spectrograms on Plate X as well as from the microphotometric records reproduced in figures 5a and 5b. In the case of the liquid the line  $1640\text{ cm}^{-1}$  is much stronger than the line  $1722\text{ cm}^{-1}$ , but in the case of the solidified monomer at  $-180^{\circ}\text{C}$  the line  $1630\text{ cm}^{-1}$  is only half as intense as the line  $1700\text{ cm}^{-1}$ . It has already been well established by the results reported by previous workers as well as by the results obtained in the present investigation that with polymerization and formation of plexi glass the  $\text{C}=\text{C}$  bond of methyl-methacrylate disappears. It is also found that the line  $1722\text{ cm}^{-1}$  also diminishes in intensity with polymerization. The diminution of intensity of the line  $1640\text{ cm}^{-1}$  with solidification and lowering of temperature of the monomer thus indicates that the  $\text{C}=\text{C}$  bond is transformed into  $\text{C}-\text{C}$  bond in some of the molecules in the solid state probably owing to formation of new bonds between some of the adjacent molecules. Such a diminution in intensity can not be due to passage of the scattered light through the solid mass, because the line  $1640\text{ cm}^{-1}$  is not very highly polarised. The appearance of the new Raman line  $58\text{ cm}^{-1}$  in the case of the solidified monomer may further indicate the formation of dimers in the solid state.

It can be concluded from these results that all the  $\text{C}=\text{C}$  bonds are converted to  $\text{C}-\text{C}$  and the  $\text{C}=\text{O}$  bond of some of the molecules are also changed to  $\text{C}-\text{O}$  bonds in the process of polymerization, while with solidification of the monomer and lowering of temperature to  $-180^{\circ}\text{C}$  only in some of the molecules the  $\text{C}=\text{C}$  bond is converted to  $\text{C}-\text{C}$  bond while the  $\text{C}=\text{O}$  group remains intact. The stability of the new bonds so formed depends on temperature, and as the temperature rises the new bonds break up and the monomer again becomes a liquid.

In the case of the polymer also a broad line at  $88\text{ cm}^{-1}$ , not reported by previous workers, has been observed in the present investigation. This line shifts to  $84\text{ cm}^{-1}$  when the polymer is cooled to  $-180^{\circ}\text{C}$ . With this lowering of temperature the frequencies of some of the other lines also diminish slightly. Thus the lines 976, 1340, 2962 and  $3024\text{ cm}^{-1}$  shift to 970, 1320, 2945 and  $2988\text{ cm}^{-1}$  respectively. These changes again indicate an influence of neighbouring atoms on the strength of the  $\text{C}-\text{H}$  and  $\text{C}-\text{C}$  bonds at the low temperature.

## ACKNOWLEDGMENT

The author is indebted to Prof. S. C. Sirkar for kindly suggesting the problem and for his guidance throughout the progress of the work.

## REFERENCES

- Hibben, J. H., 1937, *J. Chem. Phys.*, **5**, 704.  
Kojima, K., 1949, *J. Chem. Soc. Japan*, **70**, 147.  
Patel, M. M., 1949, *Current Science*, **18**, 436.  
Yasumi, M., 1942, *J. Chem. Soc., Japan*, **63**, 988

# PROTON - PROTON SCATTERING AND THE PSEUDOSCALAR MESON THEORY

By C. C. BANERJEE

DEPARTMENT OF THEORETICAL PHYSICS; INDIAN ASSOCIATION FOR THE CULTIVATION OF  
SCIENCE, CALCUTTA 32

(Received for publication, November 26, 1952)

**ABSTRACT** The paper embodies a study of the p-p scattering in the light of pseudoscalar meson theory using Born approximation. The theoretical findings have been numerically tested for energies of 150, 240, 340 Mev. The analysis indicates that either the pseudoscalar theory or a combination of the central and tensor force term of the interaction is unable to explain the isotropy in scattering observed experimentally.

## INTRODUCTION

With the discovery and operation of different types of high energy particle accelerators, a considerable amount of data on the differential cross section for p-p scattering are now available. The energy region for p-p scattering ranges from 0 to 340 Mev. These experiments show that the p-p scattering is nearly isotropic except at small angles where deviations from isotropy occur for small energy particles due to relative importance of the Coulomb field. It is our object here to see how best we can fit the experimental results with the theoretical findings based on interactions derived from the field-theories. The investigation is based upon the assumption that the interaction between two nucleons may be represented by means of a static potential that may have a charge and spin dependence. The static potential signifies that the terms in the potential expression which depend on nucleon velocities are neglected in the expression for the interaction considered.

The 340 Mev scattering experiments indicate a nearly spherically symmetric distribution over a wide angular range ( $15^\circ$  to  $90^\circ$ ) in the centre of mass system with a value close to  $4.5 \times 10^{-27} \text{cm}^2/\text{steradian}$ . The experimental values suggest that the process bears a similarity to scattering of plane waves by a perfectly rigid sphere which represents a short range potential of range equal to its radius. To explain isotropy with such a model the wavelength of the proton should be large compared to the range. The numerical value of the range which would give an isotropic differential cross section of magnitude  $4.5 \times 10^{-27} \text{cm}^2/\text{steradian}$  is approximately  $1 \times 10^{-13} \text{cm}$ . This is greater than the wavelength of the proton at this energy and is approximately double of it. So it is not possible to explain isotropy with such a model. The experiments also indicate that the differential cross

section exhibits isotropy at all energies down to 100 Mev with a little increase in the absolute magnitude. An attempt to explain the phenomena with a central force model is unsuitable because it gives a strong forward scattering. The results obtained do not exhibit isotropy in the differential cross section even over a small angular range at high or low energies. The presence of electrical quadrupole moment of deuteron suggests that the nuclear forces are non-central in character. Hence the potential energy of a pair of nucleons depends not only on their distance of separation but also on their relative orientation with respect to the spin axis. This non-central or tensor force might compensate the magnitude of the differential cross sections obtained from central forces in such a way that the resultant effect exhibits isotropy both at high and low energies. Rarita and Schwinger (1941) first considered the effect of the tensor force with  $n$ - $p$  scattering assuming that the radial dependence of both the central and non-central forces is the same. The results of their investigation explain the quadrupole moment of deuteron but cannot explain the scattering results at 90 Mev.

### TENSOR FORCE

To get an idea about the effect of tensor force on the  $p$ - $p$  differential cross section, we discuss the same below using Born approximation and a potential of the form :

$$S_{12} \cdot \frac{f^2}{4\pi} e^{-\gamma r} \quad (1)$$

where  $S_{12} \equiv$  the tensor force operator

$$= 3(\underline{\sigma}_1 \mathbf{r})(\underline{\sigma}_2 \mathbf{r}) - (\underline{\sigma}_1 \underline{\sigma}_2) \quad (2)$$

Let the momentum of the incident porton in the centre of mass system be  $k\hbar \mathbf{n}_0$  and let  $k\hbar \mathbf{n}$  be its momentum after scattering. The vectors  $\mathbf{n}_0$  and  $\mathbf{n}$  (figure 1) represent the unit vectors in the directions of initial relative motion and scattering respectively. We would consider  $\mathbf{n}_0$  also as the axis of quantisation of the relevant spin-functions.

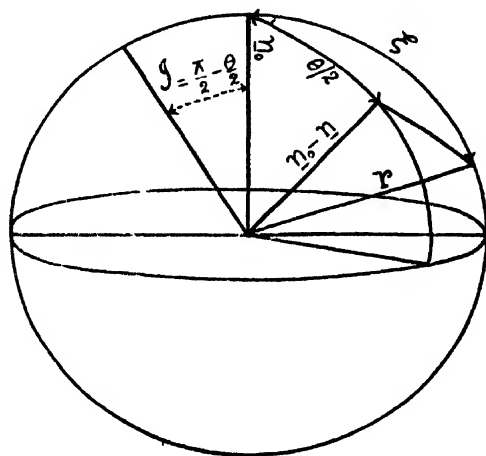


FIG. 1

With the above tensor force the amplitude of scattering according to Born's approximation takes the following form :

$$F(\theta) = -\frac{M}{4\pi\hbar^2} \int e^{i(\mathbf{r}-\mathbf{n})K} \chi_{ms'} \left\{ \frac{3(\boldsymbol{\sigma}_1 \cdot \mathbf{r})(\boldsymbol{\sigma}_2 \cdot \mathbf{r})}{r^2} - \boldsymbol{\sigma}_1 \cdot \boldsymbol{\sigma}_2 \right\} \chi_{ms''} \cdot \frac{e^{-\lambda r}}{4\pi} d\tau \quad \dots (3)$$

The tensor force operator for the proton-proton system when applied to any singlet state gives zero as its eigen value. So we consider here its effect on triplet scattering only. If the spins of the two protons are parallel the system is said to be in the triplet state and if the spins are antiparallel the system is said to be in the singlet. The spin dependent parts of the wave functions are :

$$\begin{aligned} {}^1\chi_0 &= \frac{1}{\sqrt{2}} \left\{ \alpha(1)\beta(2) - \alpha(2)\beta(1) \right\} \text{ (singlet)} \\ {}^3\chi_1 &= \alpha(1)\alpha(2) \quad \dots (4) \\ {}^3\chi_0 &= \frac{1}{\sqrt{2}} \left\{ \alpha(1)\beta(2) + \alpha(2)\beta(1) \right\} \text{ (triplet)} \\ {}^3\chi_{-1} &= \beta(1)\beta(2) \end{aligned}$$

The symbols (1) and (2) of the right hand side of equation (4) refer to the spin coordinates of proton number one and two respectively. The numbers 1, 0, -1 on the left hand side represent the magnetic quantum numbers.  $\alpha$  and  $\beta$  are the ordinary spin functions of a nucleon. The result of operating the tensor force operator  $S_{12}$  on the triplet spin functions for various values of magnetic quantum numbers (1, 0, -1) yields the following matrix :

$ms$	$ms'$	1	0	-1
1	1	$(3 \cos^2 \xi - 1)$	$3\sqrt{2} \cos \xi \sin \xi e^{-i\eta}$	$3e^{-2i\eta} \sin^2 \xi$
0	0	$3\sqrt{2} \sin \xi \cos \xi e^{i\eta}$	$-2(3 \cos^2 \xi - 1)$	$-3\sqrt{2} \cos \xi \sin \xi e^{-i\eta}$
-1	-1	$3 \sin^2 \xi e^{2i\eta}$	$-3\sqrt{2} \sin \xi \cos \xi e^{i\eta}$	$(3 \cos^2 \xi - 1)$

Substituting the elements of the above matrix in (3) and performing the integration in each case after transformation of coordinates from  $r, \xi, \eta$  to  $r, \theta, \phi$  as indicated in the diagram we would obtain the values of  $F(\theta)$  corresponding to each element of the matrix. For the case  $ms, ms' = 1, 1$  ; we get :

$$\begin{aligned} F(\theta) &= -\frac{Mf^2}{4\pi\hbar^2} \int e^{iK\tau \cos \theta'} \cdot 2 \frac{(3 \cos^2 \xi - 1)}{2} \cdot \frac{e^{-\lambda r}}{4\pi r} \cdot 2\pi r^2 d\tau d(\cos \theta') \\ &= -\frac{Mf^2}{4\pi\hbar^2} \cdot \frac{(3 \sin^2 \theta/2 + 1)}{2} \cdot 2 \int_0^\infty \left\{ \frac{3(\sin K\tau - K\tau \cos K\tau)}{K^3 \tau^3} - \frac{\sin K\tau}{K\tau} \right\} \times \\ &\quad \frac{e^{-\lambda r}}{r} \cdot r^2 d\tau \\ &= -\frac{Mf^2}{4\pi\hbar^2} \cdot \frac{(3 \sin^2 \theta/2 + 1)}{2} \cdot 2 \left[ \frac{3}{K^2} - \frac{3\lambda}{K^3} \tan^{-1} \frac{K}{\lambda} - \frac{1}{K^2 + \lambda^2} \right] \quad \dots (5) \end{aligned}$$

where  $K = 2k \sin \theta/2$

Obtaining thus the values of  $F(\theta)$  for other elements of the matrix an average of their squares over the various spin directions is determined. The sum of each averages would represent the intensity of scattering in the triplet state. Performing as stated above, we have,

$$I(\theta)_{\text{triplet}} = \left( \frac{Mf^2}{4\pi\hbar^2} \right)^2 \left( \frac{3 \sin^2 \theta/2 - 1}{2} \right)^2 \left( \frac{3}{K^2} - \frac{3\chi}{K^3} \tan^{-1} \frac{K}{\chi} - \frac{1}{K^2 + \chi^2} \right) \quad \dots (6)$$

It is clear from (6) that the intensity of the triplet scattering does not depend on  $\phi$  as during integration and averaging such terms vanish. This is evident because the scattering of an unpolarised beam of protons is axially symmetric.

For an unpolarised beam of protons, we have :

$$\begin{aligned} I(\theta) &= \frac{1}{4} I(\theta)_{\text{singlet}} + \frac{3}{4} I(\theta)_{\text{triplet}} \\ &= \frac{3}{4} I(\theta)_{\text{triplet}} \quad (\because I(\theta)_{\text{singlet}} = 0 \text{ in the case considered}) \\ &= \frac{3}{4} \cdot \left( \frac{Mf^2}{4\pi\hbar^2} \right)^2 (B_{msms'})^2 \cdot C^2(\theta) \\ &= 6 \left( \frac{Mf^2}{4\pi\hbar^2} \right)^2 (B_{msms'})^2 \cdot C^2(\theta) \end{aligned} \quad (7)$$

$$\text{where} \quad C^2(\theta) = \frac{3}{K^2} - \frac{3\chi}{K^3} \tan^{-1} \frac{K}{\chi} - \frac{1}{K^2 + \chi^2} \quad (8)$$

and  $B_{msms'}$  represents the diagonal elements of the matrix given below. The matrix here is derived from the matrix  $(A_{msms'})$  after transformation of coordinates as stated before.

$ms \backslash ms'$	$I$	$0$	$-I$
$I$	$(\sin^2 \theta/2 - 1)$	$3\sqrt{2} \sin \theta/2 \cos \theta/2 e^{-i\pi/3}$	$\cos^2 \theta/2 e^{-2i\pi}$
$0$	$3\sqrt{2} \sin \theta/2 \cos \theta/2 e^{i\pi}$	$-2(3 \sin^2 \theta/2 - 1) - 3\sqrt{2} \sin \theta/2 \cos \theta/2 e^{i\pi}$	
$-I$	$5 \cos^2 \theta/2 e^{i\pi}$	$-3\sqrt{2} \sin \theta/2 \cos \theta/2 e^{i\pi}$	$(3 \sin^2 \theta/2 - 1)$

The computed values of the differential cross sections at 240 Mev for various centre of mass angles are in Table II and represented in curve I(b) in figure 2. For comparison the corresponding values for simple Yukawa potential are given in Table I and represented in curve I(a).

The curves I(c), (d) and (e) represent the experimental values at 105, 240 and 340 Mev.

TABLE I

Centre of mass angles in degrees	30°	40°	50°	60°	70°	80°	90°
$\sigma(\theta)$ in mb/std	3.96	1.78	.88	.48	.29	.25	.18

TABLE II

Angles in degrees c. m. system	30°	40°	50°	60°	70°	80°	90°
$\sigma(\theta)$ mb/std.	.68	.44	.27	.211	.211	.197	.204

In these numerical computations we have taken the value of  $\frac{f^2}{\hbar c} = .7$  for the symmetrical case as has been obtained after normalising the value of the total n-p scattering cross section at 90 Mev determined experimentally by Fox, Leith, Wouters and Mackenzie (1950) and Dejuren (1950).

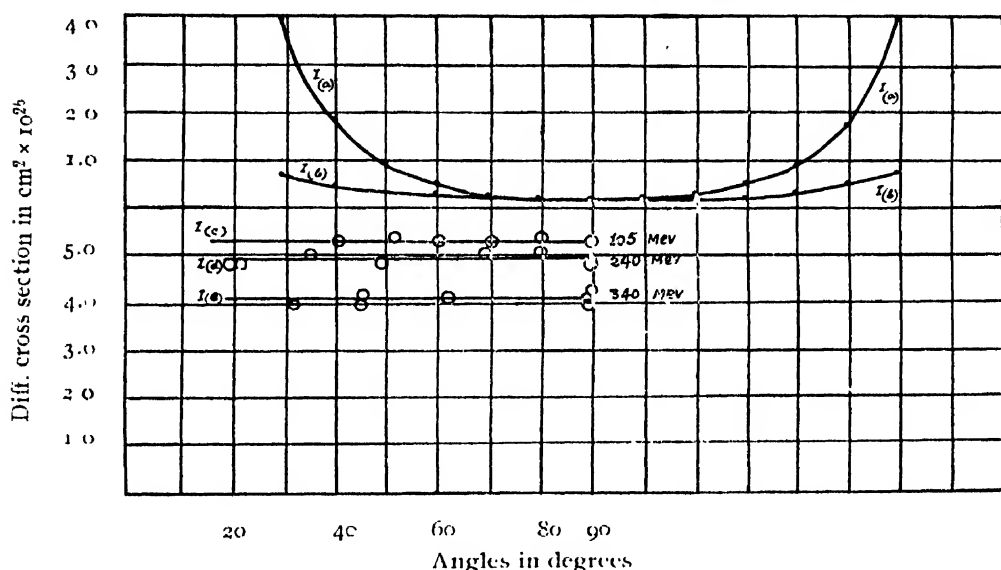


FIG. 2

Curves 1(a) and 1(b) represent the variation of  $\sigma(\theta)$  with angles at 240 Mev for Yukawa potential and for tensor force without singularity respectively. Curves 1(c), (d), and (e) represent experimental curves.

With central forces above the curve shows a tendency to drop down at 90°. The extent of dropping at 240 Mev is, however, not much perceptible. The tensor above gives a peak at 90° which also is not very marked at this energy. It is therefore expected that a combination of the two for triplet scattering would flatten the curve at 90°. Ashkin and Wu have, however, shown that the peak at 90° turns to a trough at 90° with increase of energy. If the symmetrical forces are considered the trough or the peak becomes so small that the curve at 90° is practically flat. The magnitude of the differential cross section drops to a very small value if the tensor force alone is taken into consideration. The curve, however, remains fairly flat over the angular range 50° to 90°. A combination of the central and tensor forces, however, increases the magnitude of the differential cross section at

small angles but at large angles the values remain still smaller. In case of symmetrical forces also the magnitude of the differential cross sections is too low particularly at large angles though the curve is sufficiently flat as in the case of tensor forces. If the symmetrical forces are not considered the curve is no longer flat and though there is an increase in the magnitude of differential cross section at small angles ( $30^\circ$ ) but at large angles it drops to a very small value as has been observed in the case of simple Yukawa potential. It is apparent, therefore, that such combinations of central and non-central forces will not lead to the results that would exhibit isotropy over the angular range in which the experiments show isotropic scattering and at the same time would increase the magnitude of the differential cross section even approximately to the experimental value.

### PSEUDOSCALAR INTERACTION

Meson field theories based on the assumption of weak coupling between nucleon and meson fields suggest that the main contribution to the interaction energy arises from the static part of the meson field. Each one of the possible types of meson fields gives rise to a form of static interaction between a pair of nucleons.

Recent experiments on meson-nucleon interaction favours the pseudoscalar nature of the meson. On decay a  $\pi^0$  meson gives two  $\gamma$ -rays. So its spin cannot be unity. The reactions which arise in the capture of  $\pi^-$  meson by deuteron indicate that it is not scalar. An analysis of the cross sections of production (p-p collision) and of absorption (in deuteron) of  $\pi^+$  meson indicates that its spin value should be zero. The fact that the cross section for production of  $\pi^+$  meson is very large compared to that of  $\pi^0$  meson, suggests that the  $\pi^0$  meson is pseudoscalar in nature. Since it is quite natural to assume the same nature for all the three kinds of mesons for symmetry, the  $\pi$  meson, supposed to be responsible for nuclear forces, should preferably be regarded pseudoscalar in nature.

We investigate here, using non-relativistic Born approximation, the extent to which the differential cross sections as calculated from the static potential of the interaction suggested by the symmetrical pseudoscalar meson theory agrees with the experiments.

The static potential obtained from the symmetrical pseudoscalar theory is given by

$$V_{ps} = \frac{1}{3}(\boldsymbol{\tau}_1 \boldsymbol{\tau}_2) \left[ (\boldsymbol{\sigma}_1 \boldsymbol{\sigma}_2) + \left\{ 3 \frac{(\boldsymbol{\sigma}_1 \mathbf{r})(\boldsymbol{\sigma}_2 \mathbf{r})}{r^2} - (\boldsymbol{\sigma}_1 \boldsymbol{\sigma}_2) \right\} \left\{ 1 + \frac{3}{\chi r} + \frac{3}{\chi^2 r^2} \right\} \right] \frac{f^2}{4\pi} \frac{e^{-\chi r}}{r} \quad \dots (9)$$

The amplitude scattered, using Born-appx. is,

$$F(\theta) = -\frac{Mf^2}{4\pi\hbar^2} \cdot \frac{1}{3}(\boldsymbol{\tau}_1 \boldsymbol{\tau}_2) \cdot \frac{1}{4\pi} \left[ \int_0^\infty \int_{-1}^{+1} e^{iK_1 \cos \theta'} \chi_{ms'} \left\{ (\boldsymbol{\sigma}_1 \boldsymbol{\sigma}_2) + S_{12} \left( 1 + \frac{3}{\chi r} + \frac{3}{\chi^2 r^2} \right) \right\} \right. \\ \left. \times \chi_{ms} \frac{e^{-\chi r}}{r} \cdot dt \right] \quad \dots (10)$$



For singlet states  $\chi_{ms}(\sigma_1\sigma_2)\chi_{ms} = -3$  and for triplet states it is equal to unity. The effect of the tensor force operator on singlet and triplet states has been discussed before. Similar calculations yield,

$$\begin{aligned}
 F(\theta) &= -\frac{M}{4\pi h^2} \cdot \frac{f^2}{4\pi} \cdot \frac{1}{3} (\tau_1 \tau_2) \left[ \left( \begin{array}{c} -3 \\ 1 \end{array} \right) \int_0^\infty \int_{-1}^1 e^{iK_1 \cos \theta'} \cdot \frac{e^{-\chi r}}{r} d\tau \right. \\
 &\quad \left. + \left( \begin{array}{c} 0 \\ A_{msms'} \end{array} \right) \int_0^\infty \int_{-1}^1 e^{iK_1 \cos \theta'} \cdot \frac{e^{-\chi r}}{r} dl \right] \\
 &= -\frac{M}{4\pi h^2} \cdot \frac{f^2}{4\pi} \cdot \frac{(\tau_1 \tau_2)}{3} \cdot 4\pi \left[ \left( \begin{array}{c} -3 \\ 1 \end{array} \right) \int_0^\infty \frac{\sin K_r}{K_r} \cdot \frac{e^{-\chi r}}{r} \cdot r^2 dr - \left( \begin{array}{c} 0 \\ B_{msms'} \end{array} \right) \right. \\
 &\quad \left. 2 \int_0^\infty \left\{ \frac{3(\sin K_r - K_r \cos K_r)}{K^3 r^3} - \frac{\sin K_r}{K_r} \times \left( 1 + \frac{3}{\chi r} + \frac{3}{\chi^2 r^2} \right) \right\} r^2 dr \right] \\
 &= -\frac{Mf^2}{4\pi h^2} \cdot \frac{(\tau_1 \tau_2)}{3} \left[ \left( \begin{array}{c} -3 \\ 1 \end{array} \right) \frac{1}{K^2 + \chi^2} - 2 \left( \begin{array}{c} 0 \\ B_{msms'} \end{array} \right) \frac{K^2}{\chi^2} \cdot \frac{1}{K^2 + \chi^2} \right] \quad \dots (11)
 \end{aligned}$$

$A_{msms'}$  and  $B_{msms'}$  represent the elements of the matrices  $(A_{msms'})$  and  $(B_{msms'})$ . In the case of p-p interaction,  $(\tau_1 \tau_2) = 1$ , since the system is always charge symmetric.

$$\begin{aligned}
 \therefore I_{\text{singlet}}(\theta) &= \left( \frac{Mf^2}{4\pi h^2} \right)^2 \cdot \left( \begin{array}{c} 1 \\ K^2 + \chi^2 \end{array} \right)^2 \\
 &= \left( \frac{Mf^2}{4\pi h^2} \right)^2 \cdot f^2(\theta) \quad \dots (12)
 \end{aligned}$$

$$\begin{aligned}
 \text{and } I_{\text{triplet}}(\theta) &= \left( \frac{M}{4\pi h^2} \right)^2 \cdot \frac{f^4}{9} \left\{ f^2(\theta) + 8 \frac{(3 \sin^2 \theta/2 - 1)^2}{4} \cdot \left( \begin{array}{c} K^2 \\ \chi^2 \cdot K^2 + \chi^2 \end{array} \right)^2 \right\} \\
 &= \left( \frac{M}{4\pi h^2} \right)^2 \cdot \frac{f^4}{9} \cdot \left[ f^2(\theta) + 8C^2(\theta) \right] \quad \dots (13)
 \end{aligned}$$

where  $f(\theta) = \frac{1}{K^2 + \chi^2}$  and  $C^2(\theta) = \frac{K^2}{\chi^2} \cdot \frac{1}{K^2 + \chi^2} P_2(\sin \theta/2)$

For the symmetrical case the expressions for the singlet and triplet differential cross sections are,

$$I_{\text{singlet}}(\theta) = \left( \frac{M}{4\pi h^2} \right)^2 \cdot f^4 (f(\theta) + f(\pi - \theta))^2 \quad \dots (14 a)$$

$$\begin{aligned}
 I_{\text{triplet}}(\theta) &= \left( \frac{M}{4\pi h^2} \right)^2 \cdot \frac{f^4}{9} \left[ \left\{ f(\theta) - f(\pi - \theta) \right\}^2 + 8 \left\{ C^2(\theta) + C^2(\pi - \theta) \right. \right. \\
 &\quad \left. \left. + C(\theta) C(\pi - \theta) \right\} \right] \quad \dots (14 b)
 \end{aligned}$$

Hence the differential cross section for an unpolarised beam of protons is,  
 $I(\theta) = \frac{1}{3} I(\theta)_{\text{sing}} + \frac{2}{3} I(\theta)_{\text{triplet}}$

sing triplet

$$\begin{aligned} & \left( \frac{Mf^2}{4\pi h^2} \right)^2 \left[ \frac{1}{3} \left( f(\theta) + f(\pi - \theta) \right)^2 + \frac{2}{3} \left( f(\theta) - f(\pi - \theta) \right)^2 \right. \\ & \quad \left. + \frac{1}{9} \cdot \frac{3}{4} \cdot 8 \left( C^2(\theta) + C^2(\pi - \theta) + C(\theta)C(\pi - \theta) \right) \right] \\ & \left( \frac{Mf^2}{4\pi h^2} \right)^2 \left[ \frac{1}{3} \left( f(\theta) + f(\pi - \theta) \right)^2 + \frac{2}{3} \left( f(\theta) - f(\pi - \theta) \right)^2 \right. \\ & \quad \left. + \frac{2}{3} \left( C^2(\theta) + C^2(\pi - \theta) + C(\theta)C(\pi - \theta) \right) \right] \quad \dots (15) \end{aligned}$$

The computed values of the differential cross sections from the equations (11) to (15) above for energies 150 Mev, 240 Mev and 340 Mev for various angles in the centre of mass system are given in Table III and the relevant curves are shown in II (a) (b) (c) in figure 3. A separate study of the effect

of the factor  $\left( \frac{1}{3} + \frac{1}{\chi^2} + \frac{1}{\chi^2 r} \right)$  occurring along with the tensor force operator

appearing in the pseudoscalar expression for potential, has also been made. Table IV gives the values of the differential cross sections for this part of the potential only. The relevant curves are represented in curves III (a), (b) and (c) in figure 4. The procedure is quite justified since the central and tensor forces contribute separately to the cross section.

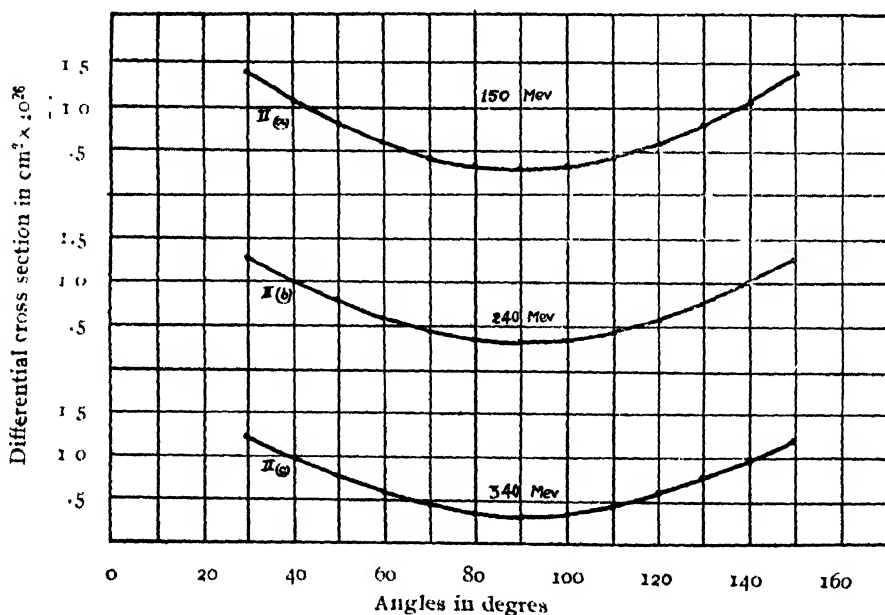


FIG. 3

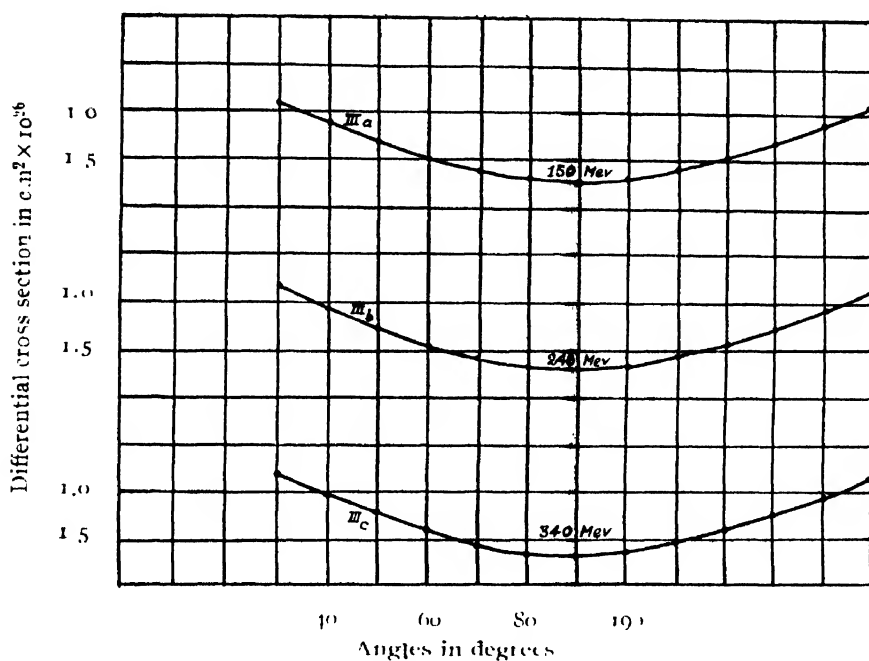


FIG. 4

TABLE III

Angles in degrees, c. m. system		30°	40°	50°	60°	70°	80°	90°
$\sigma(\theta)$ mb/std	150 Mev	13.71	10.52	8.02	5.99	4.46	3.53	3.16
	240 Mev	12.81	9.93	7.93	5.88	4.43	3.56	3.20
	340 Mev	12.37	9.78	7.83	5.91	4.54	3.60	3.21

TABLE IV

Angles in degrees, c. m. system		30°	40°	50°	60°	70°	80°	90°
$\sigma(\theta)$ mb/std	150 Mev	10.80	8.90	7.02	5.30	3.94	3.08	2.74
	240 Mev	11.16	9.03	7.64	5.57	4.21	3.37	3.02
	340 Mev	11.31	9.28	7.56	5.77	4.42	3.50	3.11

## CONCLUSION

The above analysis shows that the differential cross section at small angles is larger in magnitude than that at large angles. In the angular range  $30^\circ$  to  $60^\circ$ , the magnitude of the differential cross section decreases quite rapidly, whereas, in the interval  $60^\circ$  to  $90^\circ$ , the rate of decrease is comparatively small. Moreover, the decrease of the value of the differential cross section with angle becomes smaller as the energy of the particles becomes larger, this shows that the curves show a tendency to flatten as the energy increases. A comparison of Tables III and IV shows that the contribution to the value of the differential cross section comes mostly from the tensor force term which has  $1/r^3$  singularity; it is worth noting that the scattering cross section due to the tensor force with the  $1/r^3$  singularity increases with increasing energy, whereas, the scattering cross section due to the tensor force without the  $1/r^3$  singularity term decreases with energy (cf. Ashkin and Wu 1948). This means that for the pseudoscalar interaction the increase of the scattering cross section with increasing energy is entirely due to the  $1/r^3$  singularity term of the interaction.

The pseudoscalar interaction consists of a central force and a tensor force both of which give decreasing values of the scattering cross section with increasing angle, that being so it is not possible to explain the isotropy of scattering with different combinations of these two forces alone.

## ACKNOWLEDGMENT

The author desires to express his sincere thanks to Dr. D. Basu, Ph.D., for his kind suggestion of the problem and helpful guidance throughout the progress of the work.

## REFERENCES

- Ashkin, J., and Wu, T., 1948, *Phy. Rev.*, **73**, 973.  
 Burhop, E. H. S.; and Yadav, H. N., 1949, *Proc. Roy. Soc.*, **A**, **197**, 505.  
 Dejuren, J., 1950, *Phy. Rev.*, **80**, 27.  
 Fox, Leith, Wouters and Mackenzie, 1950, *Phy. Rev.*, **80**, 23.  
 Rarita and Schwinger, 1941, *Phy. Rev.*, **59**, 436, 556.

# ON THE ELECTRONIC SPECTRA OF DIBENZYL, DIPHENYLMETHANE AND ETHYLBENZOATE IN THE SOLID STATE AT $-180^{\circ}\text{C}.$ \*

By A. R. DEB

OPTICS DEPT., INDIAN ASSOCIATION FOR THE CULTIVATION OF SCIENCE,  
JADAVPUR, CALCUTTA 32

(Received for publication, December 22, 1952)

**ABSTRACT.** The ultraviolet absorption spectra of  $(\text{C}_6\text{H}_5\text{CH}_2)_2$ ,  $\text{C}_6\text{H}_5\text{CH}_2\text{C}_6\text{H}_5$ ,  $\text{C}_6\text{H}_5\text{COOC}_2\text{H}_5$  in the liquid and solid states at different temperatures have been photographed using very thin films of the substances, and the observed bands have been analysed. Dibenzyl in the liquid state yields eight bands with the  $\nu_0$  band at  $37122\text{ cm}^{-1}$  and the other bands corresponding to vibrational frequencies 561, 970, and  $1283\text{ cm}^{-1}$ . These vibrational frequencies diminish slightly in the case of the solid at  $30^{\circ}\text{C}$ . In the case of the solid at  $-180^{\circ}\text{C}$ , however, the bands are found to be sharper and more numerous. The vibrational frequencies at  $-180^{\circ}\text{C}$  are a little larger than the corresponding frequencies at  $30^{\circ}\text{C}$ , but smaller than those observed in the case of the liquid at  $80^{\circ}\text{C}$ .

In the case of diphenylmethane in the liquid state only six bands with the  $\nu_0$  band at  $36981\text{ cm}^{-1}$  and other bands corresponding to vibrational frequencies 1008 and  $1384\text{ cm}^{-1}$  are observed. In the solid state at  $-180^{\circ}\text{C}$  the substance yields 17 bands with the  $\nu_0$  band at  $36821\text{ cm}^{-1}$  and other bands corresponding to vibrational frequencies 593, 932, 1370 and  $1592\text{ cm}^{-1}$ .

In the case of ethylbenzoate in the liquid state only three bands with the  $\nu_0$  band at  $35596\text{ cm}^{-1}$  are observed. The solid at  $-180^{\circ}\text{C}$  also yields three bands with  $\nu_0$  band shifted to  $35500\text{ cm}^{-1}$ . The bands are broad in both these states. In the vapour state several bands with  $\nu_0$  band at  $36136\text{ cm}^{-1}$  and other bands corresponding to vibrational frequencies 312, 546 and  $917\text{ cm}^{-1}$  have been observed. All these results have been discussed in detail.

## INTRODUCTION

Previous investigations on the ultraviolet absorption spectra of organic substances in the liquid and solid states showed that some changes in the absorption spectra occur with solidification of the substances and lowering of the temperature up to  $-180^{\circ}\text{C}$ . These changes are, however, different for different substances. For instance, in the case of some disubstituted benzenes (Sirkar and Swamy, 1952; Swamy, 1952a, 1952b) containing halogen atoms each of the bands was found to be split up into three components with lowering of temperature of the solid up to  $-180^{\circ}\text{C}$ . In the case of other molecules containing no halogen atoms the bands observed in the liquid state were found to become sharper when the substances were cooled to about  $-180^{\circ}\text{C}$  (Deb, 1951, 1952). As a result of this sharpening some bands due to vibrational transitions which were not

\* Communicated by Prof. S. C. Sirkar.

visible in the liquid state were resolved from the more intense bands. It was the object of the present investigation to study the absorption spectra of a few more substituted benzenes to find out whether any fundamental change takes place in the electronic energy levels with lowering of the temperature of the substances in the solid state at about  $-180^{\circ}\text{C}$ .

#### EXPERIMENTAL

The experimental technique used in the present investigation was the same as that used in earlier investigations in this laboratory and described in detail previously (Deb, 1951). The compounds studied were  $(\text{C}_6\text{H}_5\text{CH}_2)_2$ ,  $\text{C}_6\text{H}_5\text{CH}_2\text{C}_6\text{H}_5$  and  $\text{C}_6\text{H}_5\text{COOC}_2\text{H}_5$ , supplied by B. D. H. The substances were of chemically pure quality and were distilled in evacuated double bulbs repeatedly to get rid of the traces of impurities. Ilford Q1 plates were used to photograph the spectra produced by a Hilger E1 quartz spectrograph giving a dispersion of about 3 Å. U. per mm. in the region of  $2600\text{Å}$ . Iron arc comparison was photographed on each spectrogram. A hydrogen discharge tube run by a 3 KV transformer was used as the source of continuum. Microphotometric records were obtained with a self-recording microphotometer supplied by Kipp & Zonen. The frequencies of the bands were measured from these microphotometric records in which the record of a known iron line was taken as reference line at one end of the spectrum. The ratio 1:1.6 was used in the microphotometer.

As the absorption spectrum of ethylbenzoate in the vapour state had not been reported by any previous worker it was studied in the present investigation using an absorption tube 77 cm long filled with the vapour at its saturation pressure at  $40^{\circ}\text{C}$ .

#### RESULTS AND DISCUSSION

The microphotometric records of the spectrograms are reproduced in figures 1, 2 and 3 and the bands are tabulated in Tables I, II and III. The data for dibenzyl and diphenylmethane in the vapour state were taken from the results reported by Seshan (1936) and these have been included in Tables I and II respectively. The band due to electronic transition not associated with any vibrational transition has been designated as the  $\nu_0$  band. approximate intensities have been indicated in parenthesis as usual.

It can be seen from Table I that in the case of dibenzyl the spectrum due to the liquid shows vibrational frequencies  $564$ ,  $990$  and  $1283\text{ cm}^{-1}$ . These frequencies diminish respectively to  $478$ ,  $947$  and  $1197\text{ cm}^{-1}$  with solidification. When the temperature of the solid is lowered to  $-180^{\circ}\text{C}$  the frequencies again increase respectively to  $494$ ,  $964$  and  $1202\text{ cm}^{-1}$ . Seshan (1936) only showed differences between frequencies of successive bands and did not assign the bands. The  $\nu_0$  band shifts slightly towards longer wavelengths with liquefaction of the vapour, if the band at  $37160\text{ cm}^{-1}$  reported by Seshan (1936) is taken as the  $\nu_0$  band for the vapour,

but with solidification it shifts to shorter wavelengths. When the solid is cooled to  $-180^{\circ}\text{C}$  the  $\nu_0$  band further shifts towards shorter wavelengths. This indicates that the intermolecular field changes the position of at least one of the energy levels responsible for this band. It is seen from a

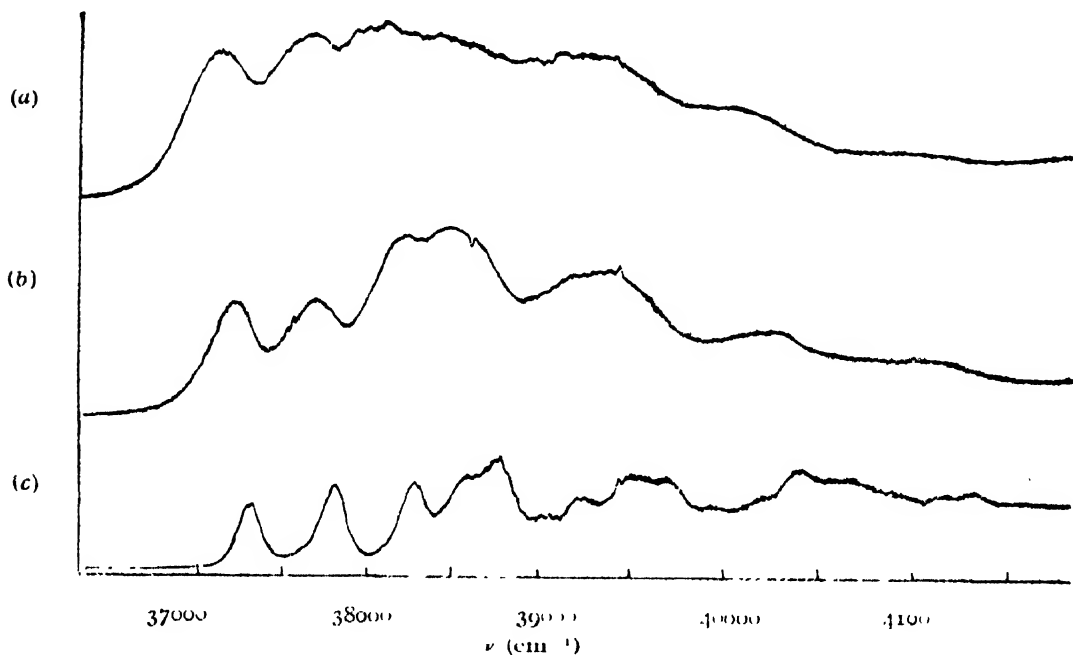


FIG. 1

Microphotometric records of the absorption spectra of dibenzyl

Curve (a)—Liquid at  $80^{\circ}\text{C}$ . Curve (b)—Solid at  $30^{\circ}\text{C}$ . Curve (c)—Solid at  $-180^{\circ}\text{C}$ .

comparison of curves *a*, *b*, and *c* in figures 1 that the bands are very broad in the liquid state and they become only slightly narrower with solidification and cooling to  $30^{\circ}\text{C}$ . This shows that the broadening is not mainly due to the random orientation of the molecules because in the case of the solid the arrangement of the molecules in the lattice is regular. When the crystal is cooled to  $-180^{\circ}\text{C}$ , however, the bands become much sharper so that the bands which merged into each other in the case of the solid at  $30^{\circ}\text{C}$  are resolved from each other at  $-180^{\circ}\text{C}$ . This sharpening is evidently due to cessation of some motion of the molecules in the lattice at  $-180^{\circ}\text{C}$ . The only motion of the molecules which can be assumed to be present in the lattice is the rotational oscillation about their axes. The sharpening of the bands at  $-180^{\circ}\text{C}$  shows that the amplitude of such oscillation decreases to negligible values.

In the case of diphenylmethane in the liquid state seven bands have been observed with the  $\nu_0$  band at  $36984\text{ cm}^{-1}$ . The data for the vapour reported by Seshan (1936) show that probably the  $\nu_0$  band for the vapour is at  $37440\text{ cm}^{-1}$ . There is thus a shift of about  $456\text{ cm}^{-1}$  towards longer wavelengths. The bands due to the liquid show vibrational frequencies of  $1008$  and  $1384\text{ cm}^{-1}$ . All the bands observed in the case of the liquid except the  $\nu_0$  band

are very broad. This shows that the electronic energy levels associated with vibrational transitions are themselves broad. This is evidently due to large influence of intermolecular field on the position of the electronic energy level and to the fluctuation of the intermolecular field due to movements of molecules. The  $\nu_0$  band becomes a little sharper with solidification and lowering of the temperature of the substance to  $-180^\circ\text{C}$ . The width of the other bands, however, diminishes to a greater extent with the lowering of temperature to  $-180^\circ\text{C}$ . Thus there is still another cause responsible for the large width of the bands due to the liquid. As mentioned earlier, this may be angular oscillations of the molecules in the liquid. The sharpening of the bands at  $-180^\circ\text{C}$  shows that in this case also the amplitude of such oscillation diminishes greatly at low temperatures. The vibrational frequencies  $932$  and  $1370\text{ cm}^{-1}$  are found to diminish in the case of combinational frequencies.

TABLE I. Dibenzyl

Vapour (Seshan, 1936).		Liquid at $80^\circ\text{C}$		Solid at $30^\circ\text{C}$		Solid at $-180^\circ\text{C}$	
$\nu$ ( $\text{cm}^{-1}$ )	Diff. Between successive bands	$\nu$ ( $\text{cm}^{-1}$ ) and intensity	Assign- ment	$\nu$ ( $\text{cm}^{-1}$ ) and intensity	Assignment	$\nu$ ( $\text{cm}^{-1}$ ) and intensity	Assignment
37160		37122 (vs)	$\nu_0$	37260 (vs)	$\nu_0$	37316 (vs)	$\nu_0$
37580	420	37080 (vs)	$\nu_0 + 564$	37738 (vs)	$\nu_0 + 478$	37180 (vs)	$\nu_0 + 494$
38010	430	38112 (vs)	$\nu_0 + 990$	38207 (vvs)	$\nu_0 + 947$	38280 (vs)	$\nu_0 + 964$
38450	440	38405 (s)	$\nu_0 + 1283$	38457 (vvs)	$\nu_0 + 1197$	38518 (ms)	$\nu_0 + 1202$
38900	450	39096 (s)	$\nu_0 + 2 \times 990$	39154 (s)	$\nu_0 + 2 \times 947$	38775 (vs)	$\nu_0 + 494 + 964$
39360	460	39397 (s)	$\nu_0 + 990 + 1283$	39401 (s)	$\nu_0 + 947 + 1197$	39245 (ms)	$\nu_0 + 2 \times 964$
39750	390	40002 (ms)	$\nu_0 + 3 \times 990$	40100 (w)	$\nu_0 + 3 \times 947$	39482 (s)	$\nu_0 + 964 + 1202$
40230	480			40351 (w)	$\nu_0 + 2 \times 947 + 1197$	39722 (ms)	$\nu_0 + 2 \times 964 + 494$
40640	410			41015 (w)	$\nu_0 + 4 \times 947$	40209 (w)	$\nu_0 + 3 \times 964$
		41080 (vw)	$\nu_0 + 4 \times 990$			40410 (s)	$\nu_0 + 2 \times 964 + 1202$
						40704 (w)	$\nu_0 + 3 \times 964 + 494$
						41173 (vvw)	$\nu_0 + 4 \times 964$

In the case of this particular molecule a remarkable change in absorption spectrum takes place with solidification and lowering of temperature of the



crystal to  $-180^{\circ}\text{C}$ . A very large number new bands not observed even in the case of vapour appear in the case of solid at  $-180^{\circ}\text{C}$ . The new vibrational frequencies 593 and  $1592\text{ cm}^{-1}$  are observed in the case of the solid. Evidently there is complete absence of fluctuation of the intermolecular field in this case and the packing of the molecules is favourable for the excitation of these vibrational modes.

TABLE II. Diphenylmethane

Vapour (Seshan, 1936)		Liquid at $30^{\circ}\text{C}$		Solid at $-180^{\circ}\text{C}$	
$\nu$ ( $\text{cm}^{-1}$ )	Diff. Between successive bands	$\nu$ ( $\text{cm}^{-1}$ ) and intensity	Assignment	$\nu$ ( $\text{cm}^{-1}$ ) and intensity	Assignment
37440		36984 (vs)	$\nu_0$	36821 (vvs)	$\nu_0$
37870	430			37414 (vs)	$\nu_0 + 593$
38300	430	37091 (vs)	$\nu_0 + 1008$	37753 (vvs)	$\nu_0 + 932$
38750	450			38101 (vvs)	$\nu_0 + 1370$
39220	470	38368 (w)	$\nu_0 + 1381$	38413 (vw)	$\nu_0 + 1812$
39670	450			38601 (s)	$\nu_0 + 2 \times 922$
40070	400			38793 (ms)	$\nu_0 + 593 + 1370$
		39002 (ms)	$\nu_0 + 2 \times 1008$	39000 (vs)	$\nu_0 + 922 + 1347$
		40011 (ms)	$\nu_0 + 3 \times 1008$	39335 (vw)	$\nu_0 + 922 + 1592$
				39592 (w)	$\nu_0 + 3 \times 922$
				39858 (w)	$\nu_0 + 2 \times 922 + 2 \times 593$
		41021	$\nu_0 + 1 \times 1008$	40021 (s)	$\nu_0 + 2 \times 922 + 1347$
				40255 (vw)	$\nu_0 + 2 \times 922 + 1592$
				40780 (w)	$\nu_0 + 3 \times 922 + 2 \times 593$
				40937 (vw)	$\nu_0 + 3 \times 922 + 1347$
				41182 (vww)	$\nu_0 + 3 \times 922 + 1592$
				41860 (vww)	$\nu_0 + 4 \times 922 + 1347$

The results for ethylbenzoate in the vapour state obtained in the present investigation show that the  $\nu_0$  band is at  $36136\text{ cm}^{-1}$  and three progressions corresponding to vibrational frequencies 312, 546 and  $917\text{ cm}^{-1}$ . The bands of some substituted benzenes, such as dihalobenzenes, are in this region. Evidently, the bands observed in the present case are due to the transitions in the benzene ring. The Raman spectrum of the substance (Magat, 1934) shows, besides other lines, three lines at 330, 616 and  $1001\text{ cm}^{-1}$  respectively.

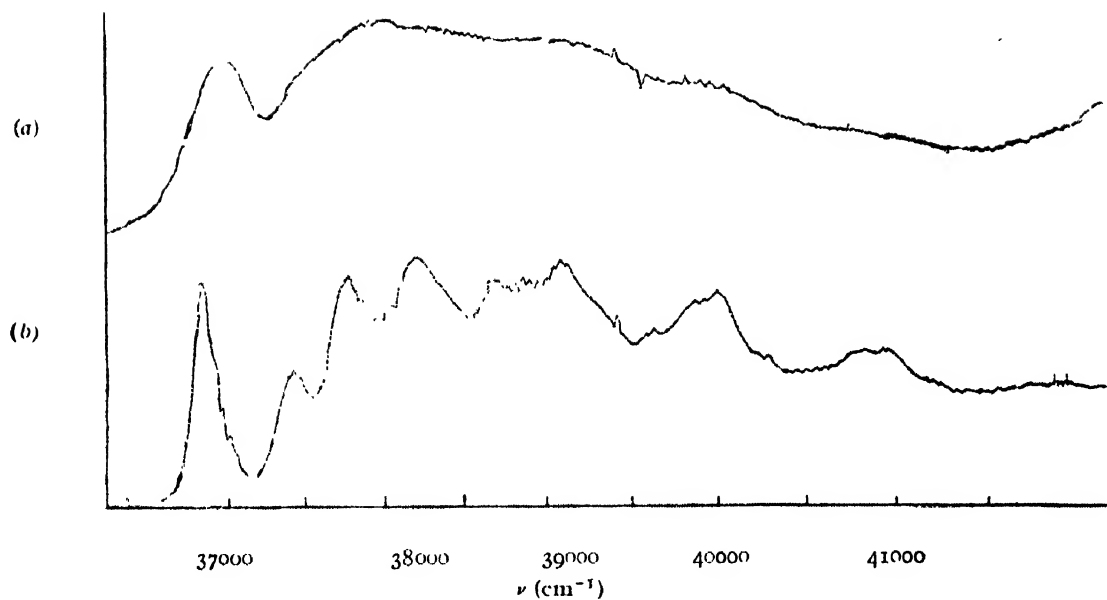


FIG. 2

Microphotometric records of the ultraviolet absorption spectra of diphenylmethane  
 Curve (a) Liquid at 30°C.                      Curve (b)—Solid at -180°C.

TABLE III  
 Ethylbenzoate

Vapour at 40°C		Liquid at 28°C		Solid at -180°C	
$\nu$ (cm <sup>-1</sup> ) and intensity	Assignment	$\nu$ (cm <sup>-1</sup> ) and intensity	Assignment	$\nu$ (cm <sup>-1</sup> ) and intensity	Assignment
36136 (vs)	$\nu_0$	35596 (vs)	$\nu_0$	35500 (vs)	$\nu_0$
36448 (w)	$\nu_0 + 312$				
36672 (vw)	$\nu_0 + 546$				
37053 (vvs)	$\nu_0 + 917$	36500 (vs)	$\nu_0 + 913$	36412 (vs)	$\nu_0 + 912$
37365 (ms)	$\nu_0 + 917 + 312$				
37599 (vw)	$\nu_0 + 917 + 546$				
37970 (s)	$\nu_0 + 2 \times 917$	37421 (w)	$\nu_0 + 2 \times 913$	37324 (w)	$\nu_0 + 2 \times 912$
38288 (vw)	$\nu_0 + 2 \times 917 + 312$				
38886 (s)	$\nu_0 + 3 \times 917$				
39200 (vw)	$\nu_0 + 3 \times 917 + 312$				

Probably the three frequencies observed in the absorption spectra are the corresponding frequencies in the excited state. In the liquid state ethylbenzoate yields only three broad bands with the  $\nu_0$  band at  $35596\text{ cm}^{-1}$ , and a progression of the vibrational frequency  $913\text{ cm}^{-1}$ . The bands are very broad, the width of each band being about  $240\text{ cm}^{-1}$ . In the case of the solid state also three similar bands are observed. The  $\nu_0$  band in this case is at  $35500\text{ cm}^{-1}$ . The bands have the same widths as in the case of the liquid. Thus in the case of this compound the  $\nu_0$  band shifts towards longer wavelengths both with liquefaction of the vapour and solidification of the liquid. The sharpening of the bands observed with solidification and cooling down to  $-180^\circ\text{C}$  in the case of dibenzyl and diphenylmethane is not observed in the case of ethylbenzoate. The cessation of rotational oscillation of the molecules in the lattice mentioned earlier is thus caused not by the lowering of temperature direct but probably by the linking of neighbouring molecules with each other through some virtual bonds at the low temperature. In the case of ethylbenzoate no such linking seems to take place on all sides of the molecule probably because the presence of the  $\text{C}_2\text{H}_5$  group makes the molecule highly asymmetric and makes the packing of the molecules less dense than that in the other two compounds.

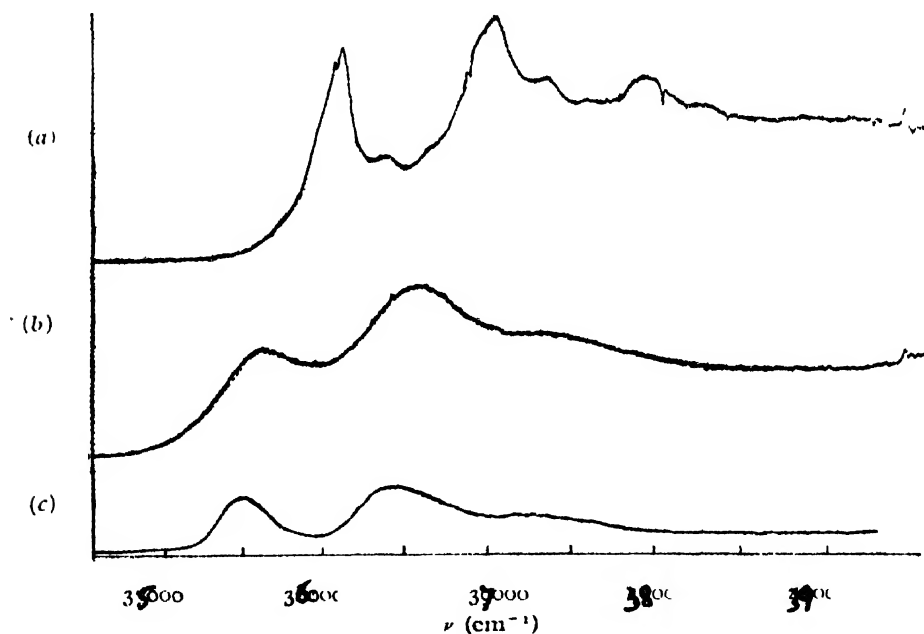


FIG. 3

Microphotometric records of the ultraviolet absorption spectra of ethylbenzoate

Curve (a) Vapour at  $40^\circ\text{C}$

„ (b) Liquid at  $38^\circ\text{C}$

„ (c) Solid at  $-180^\circ\text{C}$

The results obtained in this investigation thus show that in the case of some of the substituted benzene compounds in the solid state the amplitude

of rotational oscillations in the solid state diminishes greatly at low temperatures and, therefore, if there would be any Raman lines due to such oscillations, their intensities would diminish enormously at low temperatures. Such a conclusion has also been drawn by Sirkar and Swamy (1953) from results of investigation on the electronic absorption of *p*-dichloro and *p*-dibromobenzene at different temperatures. Actually, the new Raman lines which appear in the neighbourhood of the Rayleigh line when these substances are solidified do not become weaker with further lowering of temperature of the solid. It is thus evident that these lines cannot be due to rotational oscillations of the molecules in the lattice.

Similar investigations with some other compounds are being carried on and the results will be reported shortly.

#### ACKNOWLEDGMENT

The author is indebted to Prof. S. C. Sirkar for his kind guidance and interest during the progress of the work.

#### REFERENCES

- Deb A. R., 1951, *Ind. J. Phys.*, **25**, 233.  
 „ „ , 1952, *Ibid*, **26**, 201.  
 Magat, M., 1934, *Annual Tables*, Paris, **26**, 85.  
 Seshan, P. K , 1936, *Proc. Ind. Acad. Sci.*, **A3**, 148.  
 Sirkar, S. C. and Swamy, H. N., 1952, *J. Chem. Phys.*, **20**, 1177.  
 „ „ „ „ 1953, *Proc. 40th Ind. Sci. Cong.*, **20**, Physics Abstracts.  
 Swamy, H. N , 1952a, *Ind. J. Phys.*, **26**, 233  
 „ „ 1952b, *Ibid*, **26**, 445.  
 „ „ 1953, *Ibid*, **27**, 55.

# PRODUCTION OF PENETRATING SHOWERS IN PARAFFIN AND LEAD

BY R. L. SÉN GUPTA, K. K. ROY AND T. ROY  
PHYSICAL LABORATORY, PRESIDENCY COLLEGE, CALCUTTA

(Received for publication, December 23, 1952)

## Plates XIA-B

**ABSTRACT.** Size-frequency distribution of penetrating showers generated in lead and paraffin at the sea-level has been investigated by means of counter-controlled cloud chamber. It has been observed that the average multiplicity of penetrating showers and also their largest size are very closely the same in both the materials. From the results of observation it seems unlikely that the penetrating showers are generated in the nucleus in cascades (plural process) as suggested by Heitler and Janossy. The experimental results are more clearly understood on the basis of genuine multiplication of mesons, in which the particles are created in a single nucleon-nucleon collision.

## INTRODUCTION

The generation of penetrating particles in groups have been recorded by Fussel (1938), Wataghin, Santos and Pompeia (1940), Janossy and Ingleby (1940), Rochester, Butler and Runcorn (1947), Green (1950), Frier and Ney (1950), Brown and McKay (1950), Fretter (1949), Brown, Camerini, *et al.*, (1949), using counters, counter-controlled cloud chambers and photographic emulsion. Multiplate counter-controlled cloud chambers have been utilised by Frier and Ney (1950), Brown and McKay (1950), Fretter (1949) to investigate the generation of penetrating particles and also their interactions with the materials of the plates. Production of penetrating showers in light materials has been studied by Green (1950) and Fretter (1950). The present paper will report the measurements on locally produced penetrating showers at sea-level in lead and paraffin with a multiplate counter-controlled cloud chamber. The particular aspect of the problem to be investigated is to find out the size-frequency distribution of penetrating showers in lead and paraffin, and to compare them with the predictions of various existing theories assuming that the events have been initiated by incident nucleons.

## APPARATUS

The cloud chamber, used for the investigation is shown schematically in figure 1, which contains three lead plates, the top and the bottom plates being 1 cm. each and the central one 2.3 cm. in thickness. The consecutive plates are separated by a clear space of about 5 cms. The photo-

graphs (Plates XIA-B) have been taken stereoscopically by a pair of T. T. H. lenses with 5 cm. focal length. The chamber was counter-controlled and operated by a four-fold coincidence arrangement requiring at least one ionising

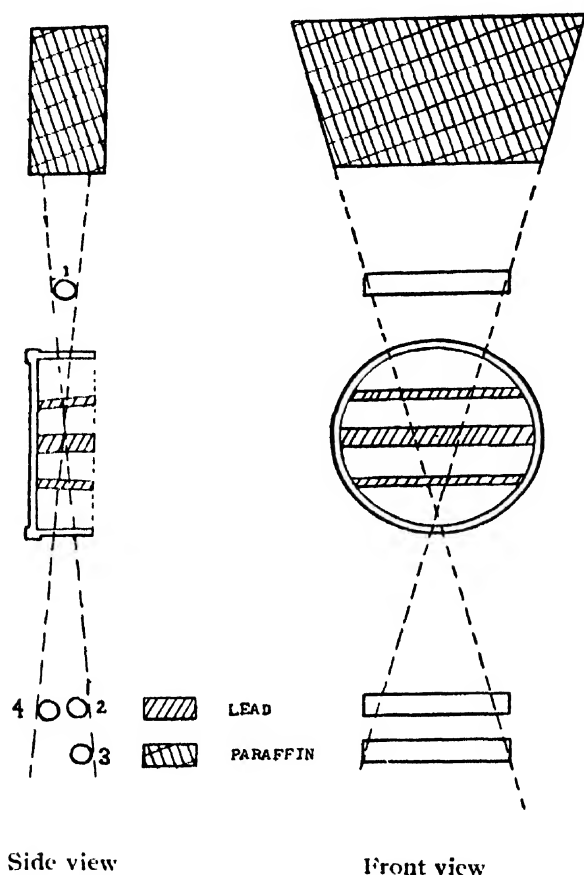


FIG. 1

The two perpendicular sections showing the arrangement of counters and the cloud chamber. The chamber was operated by four-fold coincidence

particle at the top and two below the cloud chamber and subsequent triggering of the cloud chamber. The cloud chamber was run automatically and took three minutes, after each expansion, for cleaning and resetting operations. The counters were arranged so as to avoid a rigid selection of any particular type of shower. The counter (3) was introduced to reduce the rate of random coincidences. All the counters were 2.5 cms. in diameter and 20 cm. long. The cloud chamber was 30 cm. in diameter and 8 cm. in depth and was filled with commercial argon. Moreover, rubber diaphragm was utilised for the expansion mechanism to increase the speed of expansion and thus reducing the diffusion of tracks. The condition imposed for the selection of the locally produced showers was to see whether the tracks produced backward would meet in the absorber.

# THEORETICAL ASPECTS

The theory of size-frequency distribution of penetrating showers has been discussed mainly by Heisenberg (1939), Janossy (1943) and Heitler and Janossy (1949). According to Heisenberg (1939), when a particle of sufficient energy collides with a nucleon, then in a meson field surrounding the nucleus a turbulence is set up and results in the generation of multiple mesons in a single collision. In the C-system Heisenberg (1939) assumed the meson spectrum to be of the form

$$dI = a \frac{dk_0}{k_0} \quad \dots (1)$$

where  $a$  is a constant and  $k_0$  is the energy. From the expression (1), one can calculate the average number of mesons which is

$$n = - \frac{\epsilon}{\chi \log \epsilon/\chi} \quad \dots (2)$$

where  $\epsilon$  is the total energy available,  $\chi$  is the meson mass. This expression clearly shows that the atomic weight of the medium in which the mesons are produced is quite immaterial, as it ought to be according to Heisenberg's picture of multiple meson production.

In the theory of Heitler and Janossy (1949), however, a single meson is produced in a single act of collision and thus  $n$  mesons are produced in  $n$  acts. These authors obtained the probability of  $n$  meson emissions as:

$$P_n = \omega_{\gamma+1}^n \left\{ \Gamma_n(a_1) - \frac{n(n+1)}{a_1^2} \Gamma_{n+2}(a_1) \right\} - \omega_{\gamma+1}^n \left\{ \Gamma_{n+1}(a_1) - \frac{(n+1)(n+2)}{a_1^2} \Gamma_{n+3}(a_1) \right\} \quad \dots (3)$$

where  $a_1 = \phi N d_A$

$$\text{and} \quad \Gamma_n(z) = \int_0^z \frac{z^{n-1}}{(n-1)!} e^{-z} dz \quad \dots (4)$$

$\phi$  being total emission cross section of meson,  $d_A$ , the diameter of the nucleus of the atom of atomic weight  $A$ ,  $N$ , the nuclear density.

$$\text{and} \quad \omega_{\gamma+1} = \int_0^E \omega \left( \frac{\epsilon}{E} \right) \left( 1 - \frac{\epsilon}{E} \right)^\gamma \frac{d\epsilon}{E}$$

where the function  $\omega \left( \frac{\epsilon}{E} \right)$  is connected with the cross-section of emission.

We thus see that in the theory of Heitler and Janossy the nature of the medium plays an important role. We shall consider this point in detail in the consideration of our experimental results

The calculations on the size-frequency distribution are based on (3). There is some difficulty in procuring the incomplete  $\Gamma$ -function (a remark which is also found in the paper by Heitler and Janossy already referred to).

To avoid this we note that when  $n$  is a positive integer the integral in (4) can be integrated in finite terms and is

$$\Gamma_n(z) = \int_z^\infty \frac{z^{n-1}}{(n-1)!} e^{-z} dz = 1 - e^{-z} \psi_{n-1}(z) \quad (5)$$

$$\text{where } \psi_{n-1}(z) = 1 + \frac{z}{1!} + \frac{z^2}{2!} + \frac{z^3}{3!} + \dots + \frac{z^{n-1}}{(n-1)!} \quad \dots \quad (6)$$

With the help of (5) and (6) it is now simple to obtain the value of  $\Gamma_n(z)$  which is required for the calculation of  $P_n$  given by (3). We shall calculate this  $P_n$  for different values of  $n$  and for paraffin and lead. The ratios of their relative frequencies for given multiplicities have been compared with our experimental results. In the case of paraffin and lead the values of  $a_A$  have been taken to be

$$a_A (\text{paraffin}) = 3.24$$

$$a_A (\text{lead}) = 7.95$$

We have also to remember that the values of the total number of mesons including neutral mesons is really equal to  $3/2$  times the value of the number of charged mesons which are observed on cloud chamber photographs.

#### EXPERIMENTAL RESULTS AND DISCUSSION

The distributions of the frequency of meson showers with their varying multiplicities have been plotted in figure 2 for paraffin and figure 3 for lead.

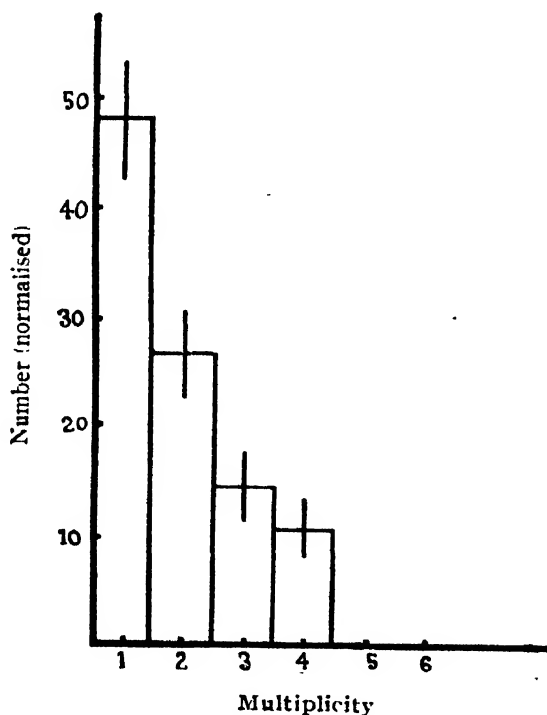
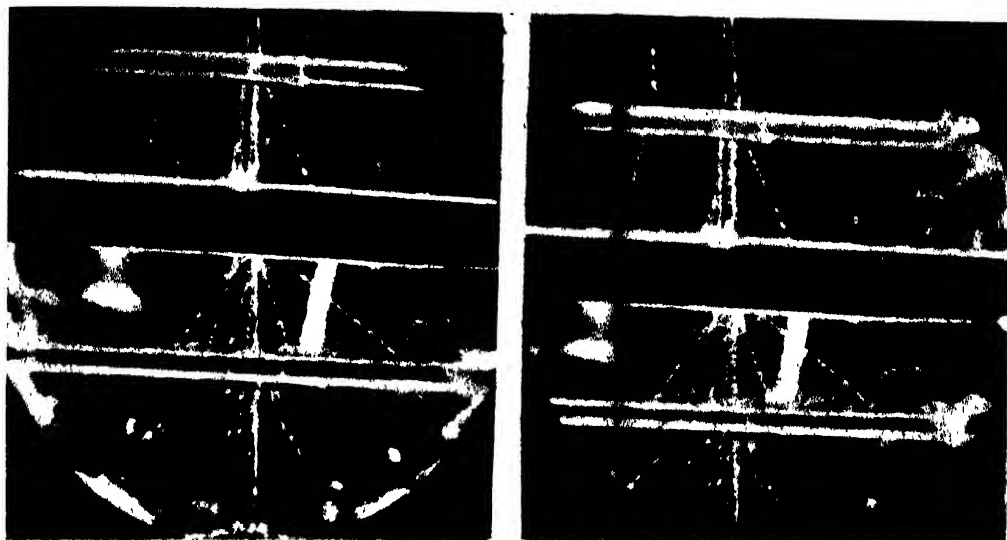


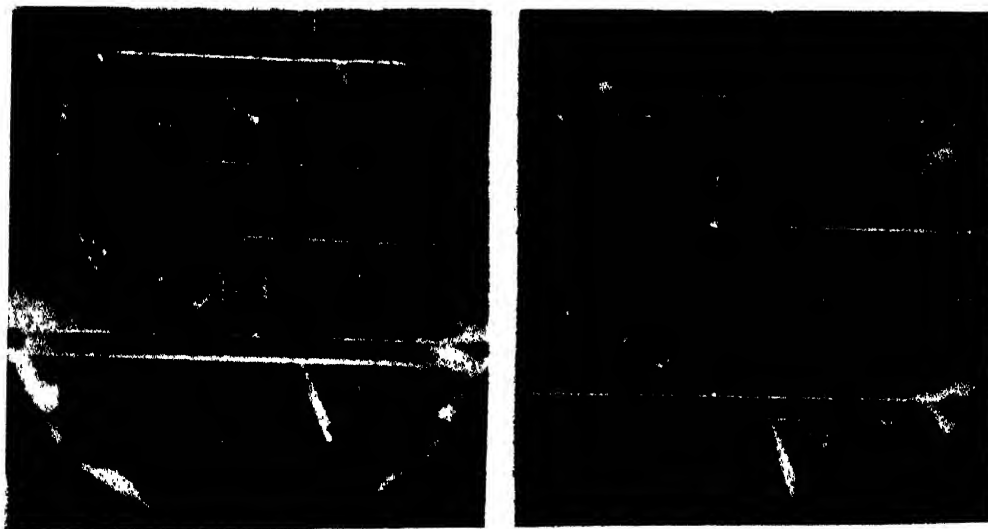
FIG. 2

Distribution of multiplicities of observed penetrating particles, normalised to an area of 100 particles under paraffin wax.

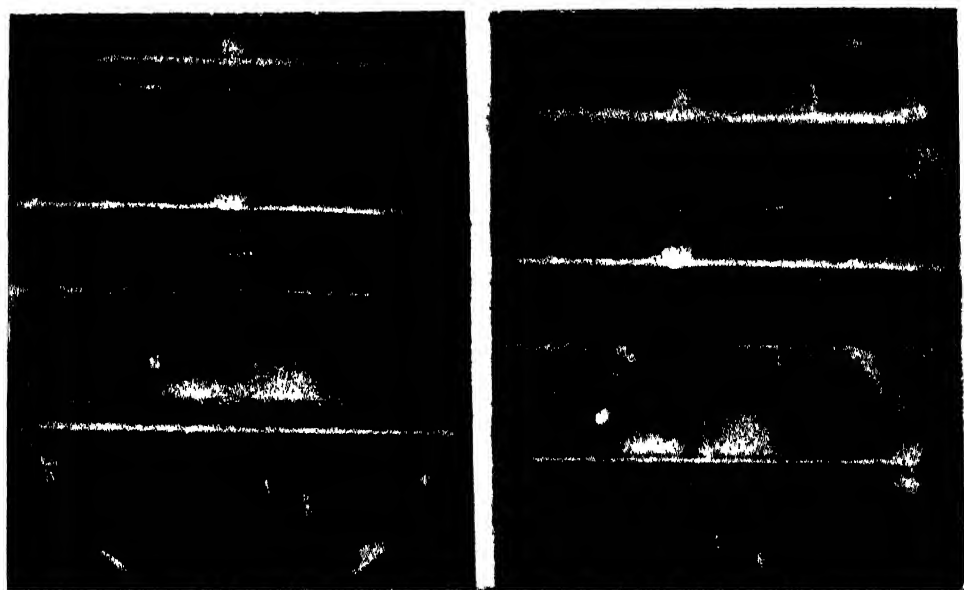




Stereo-pictures of a shower containing a penetrating particle on one side and probably a penetrating core.



Stereo-pictures of a local penetrating shower consisting of four penetrating particles produced under paraffin.



A pair of nearly parallel penetrating particles observed under paraffin.

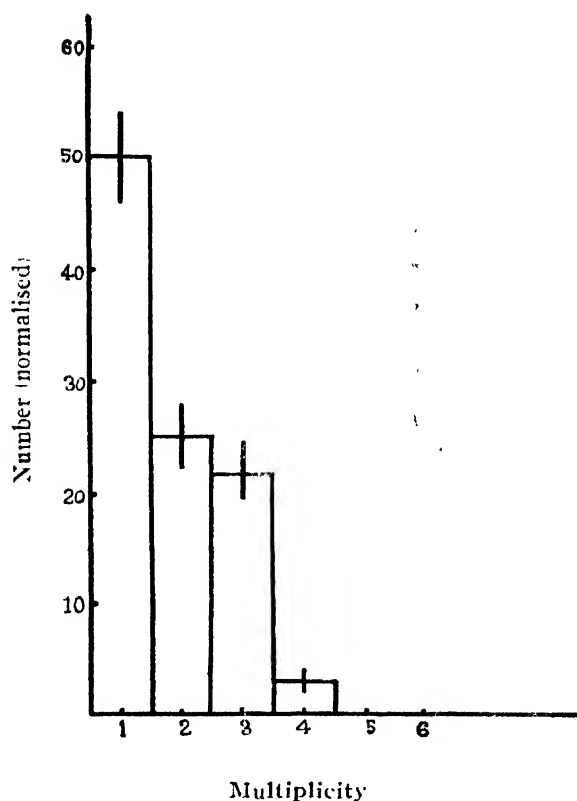


FIG. 3

Distribution of multiplicities of observed penetrating particles normalised to an area of 100 particles under lead.

It is clear from the diagrams that the increase in relative frequency of the meson showers for larger multiplicities, which is expected in the case of lead according to the theory of Heitler and Janossy, does not occur. The observed distribution curves for paraffin and lead do not appear to differ appreciably from each other. This may be explained by assuming that the saturation for meson production is already being attained in carbon nucleus. This, however, is not true since many cases are recorded both for carbon and lead where there are secondary nuclear interactions inside the cloud chamber after the incident nucleons have interacted in the top absorber. The theoretical values of the frequencies for various multiplicities, their ratios, and the ratios of the observed frequencies are given in Table I. It is quite clear that there is a very large discrepancy between the theoretical values of Heitler and Janossy and the experimental results for the showers of higher multiplicities in paraffin and lead.

The mechanism of production of meson showers can, however, be more readily explained in terms of the theory of multiple production of mesons suggested by Heisenberg, according to which, as mentioned in our theoretical discussions, the multiplicity should not depend on the atomic

numbers of the generating material. The low value of showers in lead for higher multiplicity is possibly due to the fact that for large multiplicity in the energy of the secondary mesons is low and so they are more likely to be absorbed in heavier absorbers like lead than in light materials like paraffin.

TABLE I

Relative frequency (%) of showers  $P_n$  with  $n$  mesons on H-J theory ( $\omega=0.6$ )

Absorber	$n$ $a_n$	1	2	3	4	5	6
Paraffin	3.24	—	—	9.1	—	0.83	0.20
Lead	7.95	—	—	14.2	—	3.98	1.95
Theoretical ratio for lead/paraffin	—	—	—	1.5	—	4.8	9.7
Experimental ratio	—	—	—	1.0	—	1.6	0.3

## ACKNOWLEDGMENT

Thanks are due to the authorities of the Presidency College, Calcutta for their continued co-operation during the progress of the work. The authors also take the opportunity of expressing their deep appreciation of the generous financial assistance of the Atomic Energy Commission, India, without which the investigation could not have been accomplished. One of the junior authors (K. K. Roy) expresses his gratefulness to the A. E. C. for awarding him a fellowship.

## REFERENCES:

- Brown and McKay, 1950, *Phys. Rev.*, **77**, 342  
 Brown, Camerini *et al.*, 1949 *Phil. Mag.*, **40**, 862  
 Fussell, 1938, reported in Euler and Heisenberg, *Ergebnisse der Exak. Natur Wiss.*, **17**,  
 Frier and Ney, 1950, *Phys. Rev.*, **77**, 337  
 Fretter, W. B., 1949, *Phys. Rev.*, **76**, 511  
 Fretter, W. B., 1950, *Phys. Rev.*, **80**, 921  
 Green, J. R., 1950, *Phys. Rev.*, **80**, 832  
 Heisenberg, 1939, *Zeit. Phys.*, **113**, 61  
 Heitler and Janossy, 1949, *Proc. Phys. Soc.*, **LXII**, 374  
 Janossy and Ingleby, 1940, *Nat. Lond.*, **145**, 511  
 Janossy, 1943, *Phys. Rev.*, **64**, 345  
 Rochester, Butler and Runcorn, 1947, *Nat. Lond.*, **159**, 227  
 Wataghin, Santos and Pompeia, 1940, *Phys. Rev.*, **57**, 61.

# COVARIANT THEORY OF RADIATION DAMPING AND THE SCATTERING OF CHARGED SCALAR MESONS BY NUCLEONS

By S. N. BISWAS

DEPARTMENT OF THEORETICAL PHYSICS, INDIAN ASSOCIATION FOR THE CULTIVATION  
OF SCIENCE, CALCUTTA 32

*(Received for publication, January 28, 1953)*

**ABSTRACT.** It is here shown that the strong increase of cross section with the increase of energy which is characteristic feature of all meson theories with derivative couplings and which remains unsolved from the covariant perturbation method of Feynman, can be removed by the inclusion of the influence of radiation damping. In this paper the Heitler's integral equation for the positive meson by proton and that of negative meson by neutron has been solved by the newly formulated variational technique of Goldberger, using the scalar meson field with vector coupling. A comparison of this result with the previous one obtained from the same scattering process using pseudoscalar meson field with pseudoscalar coupling, solved by the semi-variational procedure of Hsueh and Ma, shows that for a proper fit to the experimental result obtained by Steinberger, the value of the coupling constant has to be lowered to one third of the former value, 0.56 used in earlier paper by the author. The superiority of the variational technique of Goldberger to that of Ma and Hsueh has been established by considering the scattering of negative meson by proton. It is found that the exact solution corresponds to the approximate solution of Goldberger.

## 1. INTRODUCTION

The covariant formalism of Tomonaga and Schwinger (1948) on quantum electrodynamics has been applied successfully by many authors to remove the difficulties of meson theory. By the consistent use of the ideas of charge and mass renormalization, the divergencies arising from higher order radiative corrections have been removed from the covariant S-matrix of Schwinger by some authors. They have used the method of calculation devised by Feynman (1949) and Dyson (1949). Attempt has also been made to examine whether the cross section for meson scattering could remain finite even at high energy, on account of damping reaction.

This remains unsolved from the perturbation method of Dyson and Feynman unless we consider the Heitler's theory of radiation damping. From the relativistically covariant perturbation methods introduced by Feynman (1949), Ashkin, Simon and Marshak (1950) have calculated the lowest order scattering cross section for meson-nucleon interaction. The important feature to be noted is that the total cross sections decrease with incident meson energy for Ps (Ps) (*ie.* pseudoscalar meson theory with pseudoscalar

coupling) and  $S(S)$  (*ie.* scalar meson theory with scalar coupling) in contrast with their increase with energy for the  $PS(PV)$  (*ie.* pseudoscalar theory with pseudovector coupling) and  $S(V)$  theory (*ie.* scalar meson theory with vector coupling). It is clear that this strong increase of scattering cross section in case of  $PS(PV)$  and  $S(V)$  theories must be cut down by the damping reaction of the meson field. So we see that Heitler's theory is an effective and preferable alternative to the renormalisation procedure of Schwinger and Tomonaga. But the practical difficulty lies in the fact that the Heitler's integral equation of radiation damping cannot be exactly solved in most cases of the scattering processes. The nature of the difficulties has already been mentioned in an earlier paper. The general method is to solve this integral equation by a variational technique. Several authors have suggested different variational procedures of which the variational technique of Hsueh and Ma (1945) is worth mentioning. By this method Basu (1951) and Biswas (1952) have obtained fairly good results in the scattering of neutron by proton and the scattering of positive meson by proton respectively.

Recently, a more powerful variational procedure for the approximate solution of the scattering process has been devised by Goldberger (1952). As an example of the use of the variational method he has calculated the scattering process of positive meson by neutron assuming the pseudoscalar meson field using both pseudoscalar and pseudovector coupling. The superiority of this method may be observed from the fact that the result obtained by him is the same as that obtained by Ma and Hsueh (1944) from the exact solution of the integral equation.

In this paper this variational technique has been applied to solve the integral equation for the scattering process of positive meson by proton and that of negative meson by neutron taking into account of the damping reaction using a scalar meson field with vector coupling. The choice of this field is due to two points; (1) the matrix element for the process is simpler than that in the pseudoscalar theory, (2) the consideration of damping reaction is necessary in this theory with derivative coupling as the cross section increases with increasing energy.

Lastly, a comparison between the theoretical results obtained by the scalar theory and pseudoscalar theory (Biswas, 1952) has been made by means of a graph. The results in scalar theory seem to be too large. The cross section increases ten times in the scalar theory than in the pseudoscalar theory with the same value of the coupling constant which was chosen to be 0.56 for a proper fit to the experimental result of the scattering of  $\pi^+$  mesons by protons (Steinberger, 1951). Another feature to note is that the value of the coupling constant should be lessened by one third of the above mentioned value in order to be in agreement with the experimental value if we assume scalar meson theory.

In another section it has been shown that this variational technique gives exact solution in case of the scattering of the negative meson by proton

with  $S(V)$  theory as in  $PS(PS)$  theory. The consideration of the damping reaction seems to be unnecessary in  $PS(PS)$  theory since the cross section in this case decreases with increasing energy without damping influence. So this damping consideration will yield too low a result for the process. But this is not the case with  $S(V)$  theory.

The natural units  $\hbar = c = 1$  have been used throughout.

## 2. COVARIANT FORMALISM

The Schwinger equation in the interaction representation

$$i \frac{\delta}{\delta \sigma(x)} \Psi[\sigma] = H(x) \Psi[\sigma] \quad \dots (2.1)$$

is solved by the usual invariant perturbation  $S$ -matrix which is given by

$$S = 1 + \sum_{n=1}^{\infty} \frac{(-i)^n}{n!} S_n$$

with,

$$S_n = \int_{-\infty}^{\infty} d\lambda' \int_{-\infty}^{\infty} d\lambda'' \dots \int_{-\infty}^{\infty} d\lambda^{(n)} P \left( H(\lambda'), H(\lambda''), \dots, H(\lambda^{(n)}) \right) \quad \dots (2.2)$$

where symbol  $P$  stands for the Dyson's chronological product. In this form of  $S$ -matrix, the damping effect is not exhibited. To do this the usual method is to write the  $S$ -matrix in the Cayley form,

$$S = \frac{1 - \frac{i}{2} K}{1 + \frac{i}{2} K} \quad \dots (2.3)$$

where  $K$  is a hermitian matrix.

$$\text{Writing} \quad S = 1 - iR \quad \dots (2.4)$$

where  $R$  is the usual reaction matrix (it represents the amplitude of the scattered wave) we obtain from (2.3) and (2.4) the well known Heitler's (1941) and Pauli's (1946) equation of radiation damping, namely,

$$R = K - \frac{i}{2} K R \quad \dots (2.5)$$

This is the covariant form of Heitler's integral equation. This gives the scattering cross section with damping which is proportional to  $|R|^2$ .

It has been shown by Schwinger (1948) that the hermitian matrix,  $K$  is given by

$$K = \sum_{n=1}^{\infty} K_n$$

$$\text{with} \quad K_n = \left( \frac{-i}{2} \right)^{n-1} \int_{-\tau}^{\omega} d\lambda \dots \int_{-z}^x d\lambda^{(n)} H(\lambda') \dots H(\lambda^{(n)}) \epsilon[\sigma', \sigma''] \dots \epsilon[\sigma^{n-1}, \sigma^n] \quad \dots (2.8)$$

We can solve the integral equation (2.5) calculating  $K$  upto any order required.

Since the total energy-momentum is conserved, the matrix element  $S$ ,  $R$  and  $K$  must have the form (Pauli, 1946)

$$(p^1 \dots p^4 | A | p^1_0 \dots p^4_0) = \delta^4(p - p_0) (p^1 \dots p^4 | \bar{A} | p^1_0 \dots p^4_0) \quad \dots \quad (2.9)$$

where  $p_0 = \sum_{i=1}^n p^i_0$  and  $P = \sum_{i=1}^n p^i$

are the energy-momentum of four vectors of the initial and final states and  $\bar{A}$  is the submatrix of  $A$  belonging to the energy shell.

By means of this submatrix, the fundamental equation (2.5) reduces to the form

$$(p | R | p_0) = (p | K | p_0) - \frac{i}{2} \int (p | K | q) ((q | \bar{R} | p_0) \frac{d^4 q}{(2\pi)^3} \delta(q^2 + M^2) \delta^4(Q - p_0) \quad \dots \quad (1)$$

where  $Q = \sum_{i=1}^n q_i$

If we denote the initial and final energy-momentum of the nucleon and meson by  $p_0, k_0$  and  $p, k$ , respectively, the matrix element  $K$  for the meson scattering has the general form (see Fukuda and Miyazima, 1950)

$$(p, k | K | p_0 k_0) = (2\pi)^4 \phi_k^*(k) \phi_i(k_0) \{ \psi(p) \tau_k \tau_i A(p, k, p_0, k_0) \psi(p_0) + \bar{\psi}(p) \tau_i \tau_k B(p, k; p_0, k_0) \psi(p_0) \} \quad \dots \quad (2.10)$$

writing

$$(p, k | R | p_0, k_0) = (2\pi)^4 \phi_k^*(k) \phi_i(k_0) \{ \psi(p) \tau_k \tau_i X(p, k; p_0 k_0) \psi(p_0) + \bar{\psi}(p) \tau_i \tau_k Y(p, k; p_0, k_0) \psi(p_0) \} \quad \dots \quad (2.11)$$

and introducing this in (1) we get a pair of integral equations

$$X(p, k; p_0, k_0) = A(p, k; p_0 k_0) - \frac{ip}{(4\pi)^2 \omega} \int d\Omega' A(p, k; p_0', k_0') \Lambda(p') X(p', k'; p_0, k_0) \quad \dots \quad (2.12)$$

and

$$Y(p, k; p_0, k_0) = B(p, k; p_0 k_0) - \frac{ip}{(4\pi)^2 \omega} \int d\Omega' B(p, k; p', k') \Lambda(p') Y(p', k'; p_0, k_0) \quad \dots \quad (2.13)$$

The  $\Lambda(p')$  is the Feynman's projection operator,  $\Lambda(p') = \gamma \mathbf{p}' + M$ .

The first integral equation is for the process 'negative meson by proton' and the 2nd integral equation is for the process 'positive meson by proton'. Here we deal with the 2nd equation.

### 3. VARIATIONAL TECHNIQUE OF GOLDBERGER

We now proceed to derive a variational basis of the Heitler's integral equation (I, see. 2.) according to the newly formulated principle of Goldeberger (1952).



We write the equation (I) in an alternative but more convenient way namely,

$$R_{ba} = G_{ba} + i\pi \sum_c G_{bc} \delta^4(P_c - P_0) \delta(q^2 + M^2) R_{ca} \quad \dots (3.1)$$

where  $P_c$  and  $P_0$  are energy momentum four vectors of the initial and intermediate states, where

$$P_c = \sum q_i ; \quad P_0 = \sum p_0^i$$

and  $R_{ba}$  stands for  $(p \mid \bar{R} \mid p_0)$  and  $G_{ba}$  for  $(p \mid \bar{K} \mid p_0)$

Now defining the matrix multiplication by the following form

$$(RG)_{ba} = \sum_c R_{bc} \delta^4(P_c - P_0) \delta(q^2 + M^2) G_{ca}$$

we proceed to find out the stationary value of the expression  $L$ , given by

$$L = (RG)_{ba} (GR)_{ba} [(RR)_{ba} - i\pi (RG)_{ba}]^{-1}$$

Taking the arbitrary variation  $\delta L$  of  $L$  about  $R$  we easily see that the stationary value of  $L$  is given by

$$\left( \begin{array}{c} R - G \\ i\pi \end{array} \right) \quad (3.3)$$

Goldberger, however, started from the alternative form of the Heitler's integral equation made by Pauli (1949). His starting equation is

$$R_{ba} = G_{ba} + i\pi \sum_c G_{bc} \delta(E - E_c) R_{ca} ; \quad E - E_0 \quad \dots (3.4)$$

The transition probability per unit time from a state characterised by  $\phi_a$  to an initially unoccupied state  $\phi_b$  may be expressed as

$$w_{ba} = (2\pi/\hbar) |R_{ba}|^2 \delta(E_b - E_a) \quad \dots (3.5)$$

Remembering that for a collisional problems, the collision matrix

$$S_{ba} = \delta_{ba} + 2\pi i \delta(E_b - E_a) R_{ba} \quad \dots (3.6)$$

is both symmetric and unitary, so that  $R$  is symmetric and that  $G$  is real and symmetric.

Defining the matrix multiplication by

$$(RG)_{ba} = \sum_c R_{bc} \delta(E - E_c) G_{ca} \quad \dots (3.7)$$

we see that the stationary value of  $L$ , where

$$L = (RG)_{ba} (GR)_{ba} [(RR)_{ba} - i\pi (RG)_{ba}]^{-1} \quad \dots (3.8)$$

about the correct value of  $R$  is  $(R - G)/i\pi$

The difference between the variational method of Goldberger and that of Ma and Hsueh (1945) may be mentioned. Ma's procedure is based on the fact that the stationary value of  $M$ ,

$$M = \sum_a \delta(E - E_a) [R^+ (R - G - i\pi GR)]_{aa}$$

has been calculated about the correct value of  $R^+$  and not of  $R$ . The stationary value obtained is 0. It is also necessary to find out the variation of  $M$  about the correct value of  $R$ .

We will apply here the variational technique given in (3.2) for the solution of the problem in question.

## 4. CALCULATION OF MATRIX ELEMENT

We will solve equation (2.5) by calculating  $K$  upto 1st. order only, i.e., we will replace  $K$  by  $K_1$  in (2.5) and then apply the above variational technique for its solution. It has been shown by Gupta (1951) that upto 1st. order of  $K$ ,  $K_1$  is the same as  $S_1$  which is the lowest order scattering matrix element in the Feynman's perturbation method of calculation.

We consider here the scattering of scalar charged meson ( $\pi^+$  or  $\pi^-$ ) by neutrons or protons ( $N$  or  $P$ ), schematically shown by

$$\text{I : } \pi^- + P \longrightarrow \pi^- + P \text{ or } \pi^+ + N \longrightarrow \pi^+ + N$$

$$\text{II : } \pi^- + N \longrightarrow \pi^- + N \text{ or } \pi^+ + P \longrightarrow \pi^+ + P$$

The lowest order Feynman diagrams are shown for the above two types of processes (figure 1).

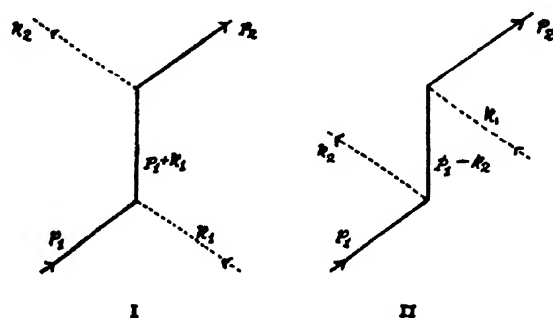


FIG. 1

In process I the incident meson is absorbed by the nucleon before the final meson is emitted since a proton can absorb but cannot emit negative meson and neutron can absorb but not emit positive meson. In process II the emission of the final meson precedes the absorption of the incident meson,

We may now write the covariant matrix element for each process from the corresponding diagram using the scalar meson theory with vector coupling. We should assume the nucleons to obey the Dirac equation. The Feynman's factors corresponding to the matrix element (meson energy-momentum four vector  $\mathbf{K}$ ) may be given as follows (see Ashkin, Simon and Marshak, 1950).

Type of Meson	Type of coupling	Absorption factor for meson $K$	Emission factor for meson
(1) Scalar	Vector	$(g/\mu)\mathbf{k}$	$-(g/\mu)\mathbf{k}$
(2) Propagation factors :		(i) $(\mathbf{p}_1 + \mathbf{k}_1 - M)^{-1}$	for process I
		(ii) $(\mathbf{p}_1 - \mathbf{k}_2 - M)^{-1}$	for process II
(3) At each vertex energy momentum conservation holds.			
(4) Each interaction with an external meson, contributes a factor- $i$ .			

$M$  denotes the nucleon mass,  $\mu$  the meson mass. The scalar product of two four vectors will be written in the form

$$\mathbf{A} \cdot \mathbf{B} = A_\mu B_\mu = A^4 B^4 - A_1 B_1 - A_2 B_2 - A_3 B_3$$

and each four vector  $\mathbf{p}$  is associated with a Dirac operator  $\mathbf{p} = p_\mu \gamma_\mu$  where  $\gamma_\mu$  are the four matrices  $\beta^z, \beta$ . The product of two operators  $A$  and  $B$  satisfies the relation  $\mathbf{A} \cdot \mathbf{B} + \mathbf{B} \cdot \mathbf{A} = 2\mathbf{A} \cdot \mathbf{B}$ . A nucleon of energy-momentum  $\mathbf{p}$  is characterised by a Dirac spinor,  $u$  obeying the Dirac equation

$$\mathbf{p}u = Mu \text{ or } u\mathbf{p} = Mu \text{ where } u = u^z \beta$$

( $u^*$  is the hermitian conjugate of  $u$ ). The  $\gamma_\mu$  differs from Pauli's by a factor  $i$ , for  $\mu = 1, 2, 3$ . And the  $\gamma_\mu$  satisfies

$$\gamma_\mu \gamma_\nu + \gamma_\nu \gamma_\mu = 2\delta_{\mu\nu} \text{ where } \delta_{14} = +1 \text{ and } \delta_{11} = \delta_{22} = \delta_{33} = -1$$

Let  $\mathbf{p}_1$  and  $\mathbf{p}_2$  denote the four vector energy-momentum of initial and final nucleons, and  $\mathbf{k}_1$  and  $\mathbf{k}_2$  the energy-momentum of initial and final mesons.

We have  $\mathbf{p}_1 + \mathbf{k}_1 = \mathbf{p}_2 + \mathbf{k}_2$  by energy-momentum conservation and  $\mathbf{p}_1^2 = \mathbf{p}_2^2 = M^2$ ;  $\mathbf{k}_1^2 = \mathbf{k}_2^2 = \mu^2$ . According to the Feynman's rules the matrix elements are given by S(V) theory

$$g^2 M_1 = -i(g^2/\mu_2) \mathbf{u}_2(-\mathbf{k}_2)(\mathbf{p}_1 + \mathbf{k}_1 - M)^{-1} \mathbf{k}_1 \mathbf{n}_1 \text{ for process I} \quad \dots \quad 4.1$$

$$g^2 M_1 = -i(g^2/\mu^2) \mathbf{u}_2(\mathbf{k}_1)(\mathbf{p}_1 - \mathbf{k}_2 - M)^{-1}(-\mathbf{k}_2)u_1 \text{ for process II} \quad \dots \quad 4.2$$

These reduce after a short calculation (Ashkin, Simon, Marshak 1950) to

$$\text{for process I, } i(g^2/\mu^2) \mathbf{u}_2(M - W\gamma_1)u_1 \quad \dots \quad 4.3$$

$$\text{for process II, } -i(g^2/\mu^2) \mathbf{u}_2(\gamma_4 \epsilon - \gamma p_2)u_1 \quad \dots \quad 4.4$$

where  $\epsilon$  is the meson incident energy,  $p_2$  the nucleon final momentum and  $W$  is the total energy of the system.

## 5. SOLUTION ( $\pi^+ + P \rightarrow \pi^{++} + P'$ )

The relevant matrix element for the process II,

$$(p_2, k_2 | G | p_1, k_1) = -(ig^2/\mu^2) u_2(\gamma_4 \epsilon - \gamma p_2) u_1$$

and in our reference system

$$p_1 + k_1 = p_2 + k_2 = 0, \epsilon = \sqrt{q^2 + \mu^2}; q = |p_1| = |p_2| = |k_1| = |k_2|$$

$$\left. \begin{aligned} \text{Writing} \quad (p_2, k_2 | R | p_1, k_1) &= \mathbf{u}_2 \mathbf{R} u_1 \\ (p_2, k_2 | G | p_1, k_1) &= \mathbf{u}_2 \mathbf{G} u_1 \end{aligned} \right\} \quad \dots \quad 5.1$$

We easily obtain the Heitler's integral equation as follows

$$\mathbf{R}(p_2, k_2; p_1, k_1) = (\mathbf{G} p_2, k_2; p_1, k_1) + \frac{iq}{32\pi^2 W} \int d\Omega' \mathbf{G}(p_2, k_2; p', k') (\gamma_\mu p_\mu + M) \mathbf{R}(p', k'; p_1, k_1) \quad \dots \quad 5.2$$

we now turn to the variational problem to solve the equation (4.5) Equation (3.1) has been used in the normal form as it stands.

Writing down the stationary value we get

$$\begin{aligned} r = \frac{\mathbf{R} - \mathbf{G}}{i\pi} &= \left( \frac{q}{32\pi^2 w} \right) \times \\ &\quad \left( \int d\Omega' \mathbf{G}(\gamma_\mu p_\mu' + M) \mathbf{R} \right) \left( \int d\Omega'' \mathbf{G}(\gamma_\mu p_\mu'' + M) \mathbf{R} \right) \\ &\quad \int d\Omega' \mathbf{R}(\gamma_\mu p_\mu + M) \mathbf{R} - \left( \frac{iq}{32\pi^2 W} \right) \int d\Omega' \int d\Omega'' \mathbf{R}(\gamma_\mu p_\mu' + M) \mathbf{G}(\gamma_\mu p_\mu'' + M) \mathbf{R} \quad \dots \quad 5.3 \end{aligned}$$

we now take  $\mathbf{R}=\mathbf{G}$ , as a trial function and we easily get

$$\mathbf{R}=\mathbf{G}+\frac{(iq/32\pi^2 W)(\int d\Omega' \mathbf{G}(\gamma_\mu p'_\mu + M)(\int d\Omega' \mathbf{G}(\gamma_\mu p'_\mu + M)\mathbf{G}))}{\int d\Omega' \mathbf{G}(\gamma_\mu p'_\mu + M)\mathbf{G}-(iq/32\pi^2 W')\int d\Omega' \int d\Omega'' \mathbf{G}(\gamma_\mu p'_\mu + M)\mathbf{G}(\gamma_\mu p''_\mu + M)\mathbf{G}} \dots 5.3$$

Putting  $\mathbf{G}=(-ig^2/\mu^2)(\gamma_4 e - \gamma p)$  (we will replace hereafter  $p_1$  and  $p_2$  by  $p_0$  and  $p$  denoting initial and final momenta) in the right hand side of the above integrals in (5.3), we perform the integrations which are simple but laborious.

After a straight forward calculation we get for  $\mathbf{R}$  the following

$$\mathbf{R}=\left\{\frac{S_1+S_2\gamma_1+S_3(\gamma p_0)+S_4\gamma_1(\gamma p_0)+D(\gamma p)}{T_1^2-T_2^2+T_3^2p^2-T_4^2p^2}\right\} \dots 5.4$$

where  $S_1, S_2, S_3, S_4, D, T_1, T_2, T_3$  and  $T_4$  are all functions of  $v$  (as given below) which is  $q/\mu$  where  $q$  denotes the absolute value of the momentum and  $\mu$  is the meson mass.

Hence the matrix element for the scattering process including radiation damping reduces to

$$R=(\mathbf{u}_2 \mathbf{R} \mathbf{u}_1) \text{ where } \mathbf{R} \text{ is given in (5.4).}$$

The differential cross section for the scattering process is in this case given by

$$d\sigma=\frac{d\Omega}{W^2} \frac{1}{(2\pi)^2} \frac{1}{8} \text{spur} (\Lambda(p)R\Lambda(p_0)\gamma_4 R^+ \gamma_1) \dots 5.5$$

where  $\Lambda(p)$  is the Feynman's projection operator,  $\Lambda(p)=(\gamma_\mu p_\mu + M)$  and we have also taken the average about the initial spin and the summation over the final spin of the nucleon. Performing the integration over all angles of scattering we get for the total scattering cross section,

$$\sigma=g^4 \frac{1}{2\pi W^2} \frac{F(x)}{\{D(v)\}^2} \dots 5.6$$

$$\begin{aligned} \text{where } F(x) &= (\lambda_2^2 + \rho^2) \{S_1(x) + S_2(x) - S_3(x) + S_4(x) - S_5(x)\} \\ &+ x^2 \{ \rho l_1(x) + 2v l_2(v) - 2x l_3(x) \} - 2\rho x l_4(v) - 2\lambda^2 l_5(x) \\ D(v) &= \{ \omega(x) \rho (1+x^2) + \rho x_1 l_1(x_1^2 x_2 - \lambda_1 x^2) \}^2 \\ &- \{ \omega(x) (x_1^2 v_2 - x_1 x^2) + x_1^2 \rho^2 l_1(1+x^2) \}^2 \\ &+ \{ x^2 \omega(x) (x_1 x_2 - \lambda^2) + \rho^2 x_1^2 l_1 v^2 \}^2 \\ &- \{ x^2 \omega(x) \cdot \rho \cdot x_1 + \rho x_1 l_1 (x_1 x_2 - x^2) \}^2 \end{aligned}$$

with,

$$\begin{aligned} S_1(x) &= l^2 \{ T_1(x) K(x) - T_2(x) L(x) + T_3(x) M(x) - T_4(x) N(x) \}^2 \\ S_2(x) &= l^2 \{ T_1(x) L(x) - T_2(x) K(x) - T_3(x) N(x) + T_4(x) M(x) \}^2 \\ S_3(x) &= l^2 \{ T_1(x) M(x) - T_2(x) N(x) - T_3(x) K(x) + T_4(x) L(x) \}^2 \\ S_4(x) &= l^2 \{ T_1(x) N(x) - T_2(x) M(x) - T_4(x) L(x) - T_4(x) K(x) \}^2 \\ S_5(x) &= D(x) \\ \Gamma_1(x) &= \{ S_1(x) S_2(x) \}^{1/2} \\ \Gamma_2(x) &= \{ S_1(x) S_4(x) \}^{1/2} \end{aligned}$$

$$\Gamma_3(x) = (S_3(x)S_2(x))^{1/2}$$

$$\Gamma_4(x) = (S_1(x)D(x))^{1/2}$$

$$\Gamma_5(x) = (S_3(x)D(x))^{1/2}$$

$$T_1(x) = \omega(x) \cdot \rho \cdot (1 + x^2) + \rho \lambda_1 l_1 (x_1^2 x_2 - x^2 x_1)$$

$$T_2(x) = \lambda_1 \rho^2 l_1 (1 + x^2) + \omega(x) (x_1^2 x_2 - x^2 x_1)$$

$$T_3(x) = x\omega(x) (\lambda_1 x_2 - x^2) + \rho^2 x_1^2 x^2 l_1$$

$$T_4(x) = x\omega(x) \rho x_1 + \rho x_1 l_1 (x_1 x_2 - x^2)$$

$$K(x) = \rho^2 x_1^2 (1 + 2x^2) + \lambda_1^2 x_2^2 + x^2 / x^2 - 2x_1 x_2$$

$$L(x) = (1 + x^2) \cdot \rho \cdot (\lambda_1^2 x_2 - x^2)$$

$$M(x) = (1 + x^2) \cdot \rho \cdot (x^2 - x_1 x_2)$$

$$N(x) = \rho x x_1^3$$

$$l = l_1 = g^2 / 8(x_1 + x_2)$$

$$M/\mu = \rho; \quad e/\mu = x_1; \quad E/\mu = x_2; \quad q/\mu = \lambda$$

$$\omega(x) = (x_1 x_2 l_1 - x^2 l_1 + 1)$$

$$x_1 = (1 + x_2)^{1/2}; \quad \lambda_1 = (\rho^2 + x^2)^{1/2}$$

## 6. THE SCATTERING OF $\pi$ MESON BY PROTON

In this section we conclude by remarking that the variational technique formulated by Goldberger is superior to that of Ma and Hsueh (1945). It is here shown that the exact solution of the integral equation regarding the scattering process of scalar negative  $\pi$ -meson by proton closely agrees to the solution obtained by the variational technique of Goldberger.

The matrix element for the process ( $\pi^- + p \rightarrow \pi^- + p'$ ) has been given in section 4.

From (4.3), the matrix element  $G = i(g^2/\mu^2)u_2(M - W\gamma_4)u_1$  can be written as  $u_2\mathbf{G}u_1$  with  $\mathbf{G} = a_1 - a_2\gamma_4$

where

$$a_1 = i(g^2/\mu^2)M$$

$$a_2 = i(g^2/\mu^2)W$$

The Heitler's integral equation is given by :

$$\mathbf{R}(p, k; p_0, k_0) = \mathbf{G}(p, k; p_0, k_0) + iq/32\pi^2 \omega \int d\Omega' \mathbf{G}(p, k; p', k') \Lambda(p') \mathbf{R}(p', k'; p_0, k_0) \quad \dots \quad 6.1$$

As in this case the  $\mathbf{G}$  is not involved with angles,  $\mathbf{R}$  may be expressed as  $\mathbf{R} = x\mathbf{G}$  where  $x$  is some constant not depending on angles. Substituting this value of  $\mathbf{R}$  in (6.1) we find the value of

$$x = \frac{1}{1 - i\lambda}$$

where

$$\lambda = (q/8\pi W)\mathbf{G}(E\gamma_4 + M)$$

Hence

$$\mathbf{R} = \frac{\mathbf{G}}{1 - i(q/8\pi W)\mathbf{G}(E\gamma_4 + M)} \quad \dots \quad 6.2$$

Now from the variational principle of Goldberger we write the stationary expression for  $\mathbf{R}$ , assuming the trial function  $\mathbf{R} = \mathbf{G}$

$$\frac{\mathbf{R} - \mathbf{G}}{i\pi} = \left( \frac{1}{32\pi^4 W} \int d\Omega' \mathbf{G}(\gamma_\mu p_\mu' + M) \mathbf{G} \right) \left( \int d\Omega'' \mathbf{G}(\gamma_\mu p_\mu'' + M) \mathbf{G} \right) \\ \int d\Omega' \mathbf{G}(\gamma_\mu p_\mu' + M) \mathbf{G} - \left( \frac{iq}{82\pi^2 W} \right) \int d\Omega' \int d\Omega'' \mathbf{G}(\gamma_\mu p_\mu' + M) \mathbf{G}(\gamma_\mu p_\mu'' + M) \mathbf{G}$$

On performing the integrations we may write

$$\mathbf{R} = \mathbf{G} + \frac{(iq/8\pi W) \mathbf{G}(E\gamma_4 + M)}{1 - (iq/8\pi W) \mathbf{G}(E\gamma_4 + M)} \\ = \frac{\mathbf{G}}{1 - i(q/8\pi W) \mathbf{G}(E\gamma_4 + M)},$$

which is the same result as (6.2) obtained by exactly solving (6.2).

Now from  $d\sigma = \frac{d\Omega}{W^2} \frac{1}{(2\pi)^2} \frac{1}{8} \text{spur} (\Lambda(p) \mathbf{R} \Lambda(p_0) \gamma_4 \mathbf{R}^* \gamma_4)$  we obtain for the total cross section,  $\sigma$  after performing the angular integrations

$$\sigma = \frac{8\pi}{p^2} \int \frac{k_1^2 + k_2^2 - (k_2^2 - k_1^2)^2}{1 + 2(k_1^2 + k_2^2) + (k_2^2 - k_1^2)^2}$$

$$\text{where } k_1(x) = \frac{ig}{8\pi} \left\{ \rho^2 - (\rho^2 + x^2)^{1/2} \left[ (1 + x^2)^{1/2} + (\rho^2 + x^2)^{1/2} \right] x / (x_1 + x_2) \right\}$$

$$k_2(x) = \frac{ig^2}{8\pi} \left\{ \rho(\rho^2 + x^2)^{1/2} - \rho \left[ (1 + x^2)^{1/2} + (\rho^2 + x^2)^{1/2} \right] x / (x_1 + x_2) \right\}$$

with  $\rho, x_1, x_2, x$  the same as in (5.6).

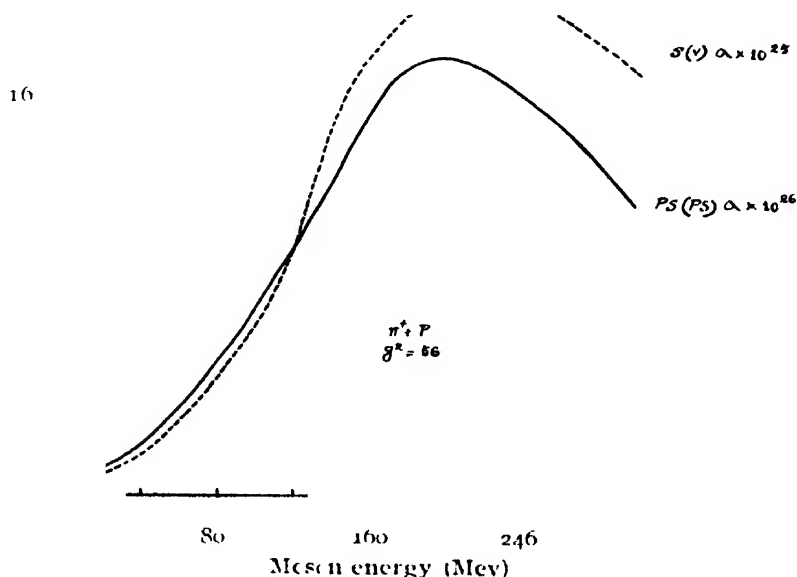


FIG. 2

## 7. COMPARISON WITH EXPERIMENT

The energy dependence of the total cross section including radiation damping has been shown by means of the accompanying graph (figure 2). The dotted curve drawn is from the theoretical result obtained here using the scalar meson field with vector coupling. The thicker line is from the previous result (Biswas, 1952) for the same process but using pseudoscalar meson field with pseudoscalar coupling. The value of the coupling constant assumed there was 0.56. The same value is also taken for the scalar theory, but with this value the scattering cross section is larger than that in the experimental result of Steinberger (1951). The value is 10 times larger than the former.

The ratio  $\rho$  for  $M/\mu$  is taken to be 6.67 since  $\mu = 276 \times m_e$  ( $m_e$  = mass of electron). In the scalar meson field the radiation reaction begins to assert itself from 180 Mev. In order to fit the theoretical values in agreement with the experimental one (Steinberger, Sachs and Anderson, 1951) it is necessary to lower down the value of the coupling constant to one third of the value assumed here. So we come to this conclusion that the coupling constant in scalar meson field with vector coupling should be lower than that in the pseudoscalar meson field with pseudoscalar coupling.

## ACKNOWLEDGMENT

The author wishes to express his sincere thanks to Dr. D. Basu for invaluable help and advice in the preparation of this paper and for his unfailing encouragement.

## REFERENCES

- Ashkin, J. and others, 1950, *Prog. Theor. Phys.*, **5**, 631.  
 Basu, D., 1951, *Ind. J. Phys.*, **25**, 246.  
 Biswas, S. N., 1952, *Ind. J. Phys.*, **26**, 613.  
 Dyson, F. J., 1949, *Phys. Rev.*, **75**, 1736.  
 Feynman, R. P. 1949, *Phys. Rev.*, **76**, 748, 760.  
 Goldberger, M. L., 1951, *Phys. Rev.*, **84**, 929.  
 Gupta, S. N., 1951, *Proc. Camb. Phil. Soc.*, **47**, 454.  
 Heiliter, W., 1941, *Proc. Camb. Soc.*, **37**, 291.  
 Hsueh and Ma, 1945, *Phys. Rev.*, **67**, 303.  
 Nobuyuki Fukuda and T. Miyazima, 1952, *Prog. Theor. Phys.*, **5**, 849.  
 Pauli, W., 1946, *Meson Theory of Nuclear forces* p. 39.  
 Schwinger, J., 1948, *Phys. Rev.*, **74**, 1439.  
 Steinberger, 1951, *Phys. Rev.*, **82**, 958.

# ON THE CONCENTRATION OF STRESS ROUND THE EDGE OF A HOLE BOUNDED BY TWO INTERSECTING CIRCLES IN A LARGE PLATE

By B. KARUNES

DEPARTMENT OF APPLIED PHYSICS, UNIVERSITY COLLEGE OF  
SCIENCE AND TECHNOLOGY, CALCUTTA.

(Received for publication, December 11, 1953)

**ABSTRACT.** A stress function in bipolar coordinates has been obtained to give the distribution of stress round the edge of a hole bounded by two intersecting circles in an infinite plate under uniform shear in the plane of the plate; and some particular cases have been discussed.

## INTRODUCTION

In a recent paper, Ling (1948) has studied the concentration of stress in an infinite plate containing a hole bounded by two equal intersecting circles when the plate is under (i) a uniform all round tension, (ii) a uniform longitudinal tension, and (iii) a uniform transverse tension, at infinity. We shall here consider the effect of the hole on the stress distribution in the plate when it is under a uniform shear  $S$  at infinity.

Using bipolar coordinates

$$\alpha + i\beta = \log \frac{x + i(y+a)}{x + i(y-a)} \quad \dots (1)$$

we take the boundary of the hole to be given by two equal intersecting circles  $\beta = \pm\beta_1$ , where  $\beta_1$  is a constant. The points of intersection of the two circles are given by  $\alpha = \pm\infty$ , and on each circle  $\alpha$  varies from  $-\infty$  to  $+\infty$ .

The stress function  $\chi$  satisfies the equation (Jeffery, 1921)

$$\left( \frac{\partial^4}{\partial \alpha^4} + 2 \frac{\partial^4}{\partial \alpha^2 \partial \beta^2} + \frac{\partial^4}{\partial \beta^4} - 2 \frac{\partial^2}{\partial \alpha^2} + 2 \frac{\partial^2}{\partial \beta^2} + 1 \right) (h\chi) = 0 \quad \dots (2)$$

The boundary conditions of no stress over this new type of holes are established in terms of Michell's constants of the boundary, as has been done by Jeffery for circular holes given by  $\alpha = \text{constant}$ .

## THE STRESS FUNCTION

Let us choose a solution of (2) of the type

$$h\chi = f(\beta) \cos n\alpha, \quad f(\beta) \sin n\alpha \quad \dots (3)$$



Then from (2) we get the differential equation for  $f(\beta)$  as

$$\left[ \frac{\partial^4}{\partial \beta^4} - 2(n^2 - 1) \frac{\partial^2}{\partial \beta^2} + (n^2 + 1)^2 \right] f(\beta) = 0 \quad (4)$$

the solution of which is (Ling, 1918)

$$\left[ f(\beta) = K_n \cos \beta \cosh n\beta + L_n \cos \beta \sinh n\beta \right. \\ \left. + M_n \sin \beta \cosh n\beta + N_n \sin \beta \sinh n\beta \right] \quad (5)$$

Hence we obtain an expression for  $h\chi$  in the form

$$h\chi = \int_0^\alpha \{ (A_n \cosh n\beta + B_n \sinh n\beta) \cos \beta \\ + (C_n \cosh n\beta + D_n \sinh n\beta) \sin \beta \} \cos n\alpha \\ + \{ (E_n \cosh n\beta + F_n \sinh n\beta) \cos \beta \\ + (G_n \cosh n\beta + H_n \sinh n\beta) \sin \beta \} \sin n\alpha \, d\beta \quad (6)$$

#### CONDITIONS FOR NO STRESS OVER A BOUNDARY

We have the stresses in bipolar coordinates given by (Jeffery, 1921,)

$$\widehat{\alpha\alpha} = \left\{ (\cosh \alpha - \cos \beta) \frac{\partial^2}{\partial \beta^2} - \sinh \alpha \frac{\partial}{\partial \alpha} - \sin \beta \frac{\partial}{\partial \beta} + \cosh \alpha \right\} (h\chi) \\ \widehat{\beta\beta} = \left\{ (\cosh \alpha - \cos \beta) \frac{\partial^2}{\partial \alpha^2} - \sinh \alpha \frac{\partial}{\partial \alpha} - \sin \beta \frac{\partial}{\partial \beta} + \cos \beta \right\} (h\chi) \quad \dots \quad (7) \\ \widehat{\alpha\beta} = -(\cosh \alpha - \cos \beta) \frac{\partial^2}{\partial \alpha \partial \beta} (h\chi)$$

If a boundary  $\beta = \pm \beta_1$  has to be free from stress,  $\widehat{\alpha\beta} = 0$  and  $\dot{\beta\beta} = 0$ , and we have on the boundary

$$\frac{\partial^2(h\chi)}{\partial \alpha \partial \beta} = 0$$

$$\text{therefore} \quad \frac{\partial(h\chi)}{\partial \beta} = \text{constant} = \rho (\text{say}) \quad \dots \quad (8)$$

Also on the boundary

$$(\cosh \alpha - \cos \beta) \frac{\partial^2(h\chi)}{\partial \alpha^2} - \sinh \alpha \frac{\partial(h\chi)}{\partial \alpha} + \cos \beta (h\chi) = \rho \sin \beta$$

the solution of which is

$$h\chi = \rho \tan \beta + \sigma (\cosh \alpha \cos \beta - 1) + \tau \sinh \alpha \quad \dots \quad (9)$$

$\rho$ ,  $\sigma$  and  $\tau$  are Michell's three constants of the boundary.

## THE SHEAR PROBLEM

Let the hole boundary be defined by  $\beta = \pm \beta_1$ ,  $\left(\beta_1 < \frac{\pi}{2}\right)$  so that if  $r$  be the radius of the intersecting circles which give the boundary of the hole and if  $2d$  be the distance between the centres of the circles, we have

$$r = \alpha \operatorname{cosec} \beta_1, \quad d = \alpha \cot \beta_1 \\ d/r = \cos \beta_1$$

If  $S$  be the applied shear in the plane of the plate, we may take the stress function at a great distance from the hole as

$$\chi_0 = -Sxy \quad \dots \quad (10)$$

so that

$$h\chi_0 = -aS \frac{\sinh \alpha \sin \beta}{\cosh \alpha - \cos \beta} \quad \dots \quad (11)$$

To obtain the condition of no stress over the boundary  $\beta = \pm \beta_1$  we need add another function  $\chi_1$  to  $\chi_0$  such that  $\chi_1$  produces no stress at infinity ( $\alpha = 0, \beta = 0$ ) and the sum of the two stress functions ( $\chi_0 + \chi_1$ ) produces no stress over  $\beta = \pm \beta_1$ .

Since  $h\chi_0$  is odd both in  $\alpha$  and in  $\beta$ , we may take only the terms in  $F_n$  and  $G_n$  in (6) and write for our complete solution

$$h\chi = -aS \frac{\sinh \alpha \sin \beta}{\cosh \alpha - \cos \beta} + aS \int_0^\infty [F_n \cos \beta \sinh n\beta + G_n \sin \beta \cosh n\beta] \sin n\alpha \, dn \quad \dots \quad (12)$$

From (12) it is clear that at infinity ( $\alpha = 0, \beta = 0$ ),  $h\chi = h\chi_0$ .

We have (Haan, 1867)

$$\int_0^\infty \frac{\sinh \alpha \sin n\alpha \, d\alpha}{\cosh \alpha - \cos \beta} = \pi \frac{\cosh n(\pi - \beta)}{\sinh n\pi}, \quad -\pi \leq \beta \leq \pi \quad \dots \quad (13)$$

whose Fourier Transform is

$$\frac{\sinh \alpha}{\cosh \alpha - \cos \beta} = 2 \int_0^\infty \frac{\cosh n(\pi - \beta) \sin n\alpha \, dn}{\sinh n\pi} \quad \dots \quad (14)$$

Substituting this value in (12) we get after a little reduction

$$h\chi = aS \int_0^\infty \{F_n \cos \beta \sinh n\beta + (G_n - 2 \coth n\pi) \sin \beta \cosh n\beta + 2 \sin \beta \sinh n\beta\} \sin n\alpha \, dn. \quad \dots \quad (15)$$

We now apply the boundary conditions (8) and (9) to (15) to calculate the values of  $F_n$  and  $G_n$  for no stress over the boundary  $\beta = \pm \beta_1$  and get

$$\left. \begin{aligned} F_n &= \frac{4n^2 \sin^2 \beta_1}{\sinh 2n\beta_1 - n \sin 2\beta_1} \\ G_n &= -\frac{4 \sinh^2 n\beta}{\sinh 2n\beta_1 - n \sin 2\beta_1} + 2 \coth n\pi \end{aligned} \right\} \quad \dots (16)$$

Substituting these values in (15) we have the stress function

$$h\chi = 4aS \int_0^\infty \{n \sin \beta_1 \sinh n\beta \sin (\beta_1 - \beta) - \sin \beta \sinh n\beta_1 \sinh n(\beta_1 - \beta)\} \frac{\sin n\alpha \, dn}{\sinh 2n\beta_1 - n \sin 2\beta_1} \quad \dots (17)$$

The circumferential stress  $\widehat{\alpha\alpha}$  over the edge of the hole is easily calculated with the help of (7) after obtaining the simple form

$$a(\widehat{\alpha\alpha} - \widehat{\beta\beta}) = \cosh \alpha - \cos \beta \left( \frac{\partial^2}{\partial \beta^2} - \frac{\partial^2}{\partial \alpha^2} + 1 \right) (h\chi) \quad \dots (18)$$

and putting  $\widehat{\beta\beta} = 0$  for the boundary  $\beta = \pm \beta_1$ , we get

$$\begin{aligned} \widehat{\alpha\alpha} &= 8S(\cosh \alpha - \cos \beta) \\ &\times \int_0^\infty \frac{n \cos \beta_1 \sinh n\beta_1 - n^2 \sin \beta_1 \cosh n\beta_1}{\sinh 2n\beta_1 - n \sin 2\beta_1} \sin n\alpha \, dn \end{aligned} \quad (19)$$

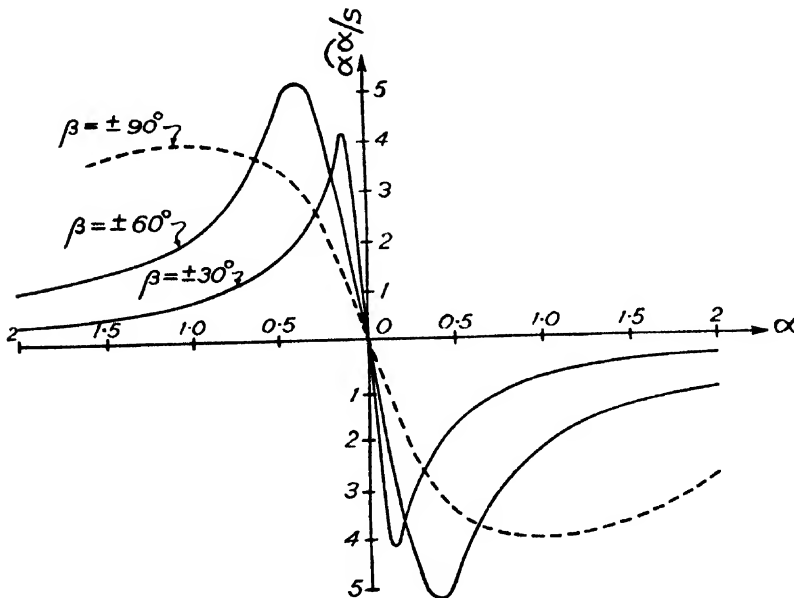


FIG. 1

In figure 1 we have plotted the graphs of edge stresses against different values of  $\alpha$  for the cases where (i)  $\beta = \pm 30^\circ$  when the distance between the centres of the intersecting circles is 1.732 times the radius of the circles, and (ii)  $\beta = \pm 60^\circ$  when the distance between the centres of the intersecting circles is equal to the radius of the circles. The maximum stresses in these two cases are  $\pm 4.2 S$  and  $\pm 5.3 S$  at  $\alpha = \pm 0.175$  and  $\alpha = \pm 0.436$  respectively. We see as  $\alpha$  tends to infinity the stresses tend to zero, which is obvious from the physical consideration that the points  $\alpha = \pm \infty$  are projected outwards from the main body of the plate. The dotted graph in the figure shows the edge stress when  $\beta = \pm 90^\circ$ , i.e. the hole is one complete circle. The maximum stress in this case is equal to  $4S$  which result is well known.

#### ACKNOWLEDGMENT

The author wishes to express his respectful thanks to Dr. S. Ghosh, under whose suggestion and guidance this paper has been prepared.

#### REFERENCES

- Haan, D. Bierns de, 1867, *Nouvells Tables D'integrales Definies*, p. 390.  
 Jeffery, G. B., 1921, *Phil. Trans. Roy. Soc.*, A, **221**, 265.  
 Ling, C. B., 1918, *J. App. Phys.*, **19**, 405.  
 ... 1947, *J. Math. & Phys.*, **26**, 284.

# CROSS SECTIONS OF (p, 2n), (p, pn) AND (p, 2p) REACTIONS FOR COPPER BOMBARDED WITH HIGH ENERGY PROTONS

BY S. N. GHOSHAL AND T. N. DAVE  
PHYSICS DEPARTMENT, LUCKNOW UNIVERSITY, LUCKNOW

(Received for publication, March 2, 1953)

**ABSTRACT.** A general expression for the cross section of a nuclear reaction involving the emission of  $n$  successive particles after the bombardment of the target nucleus with a suitable projectile has been developed. The possibility of emission of various types of particles, like protons, neutrons, etc. in each stage has been considered. The general equation has been applied to the cases of the emission of two and three particles respectively in a nuclear reaction. The explicit expressions for the cross sections in these two cases have been given. The energy region of the bombarding particle is assumed to be such that the compound nucleus hypothesis holds good.

Cross sections have been calculated, based on the equations derived, for (p, 2n), (p, pn) and (p, 2p) processes on  $\text{Cu}^{63}$  upto the incident proton energy of 22 Mev. Weisskopf's statistical theory of nuclear reactions has been applied to carry out the numerical calculations. The results have been compared with the experimentally determined cross sections for (p, 2n) and (p, pn) processes on  $\text{Cu}^{63}$ . The calculated values are in qualitative agreement with the experimental values. The possibility of the proton and the neutron being emitted as a single deuteron in the (p, p1) process has been considered. Its effect is, however, found to be very small upto the incident proton energy considered.

## INTRODUCTION

The cross section for the emission of two neutrons following the proton bombardment on a medium heavy nucleus has been derived by Weisskopf and Ewing (1910) from the statistical theory of nuclear reaction. Neglecting the probability of the emission of any other particle excepting the neutrons, they calculated the (p, 2n) cross section to be

$$\sigma(p, 2n) = \sigma_p [1 - (1 + \Delta E/kT)e^{-\Delta E/kT}]$$

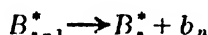
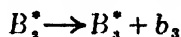
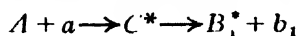
where  $\Delta E = E_p - T(p, 2n)$  is the excess energy of the incident proton over the threshold  $T(p, 2n)$  of the (p, 2n) reaction.  $T$  is the temperature of the nucleus corresponding to the excitation energy of the residual nucleus.

The above expression does not take into account the probability of the emission of particles other than neutrons. However, recent experiments have shown that this is by no means true. The probability of the emission of protons by not too heavy nuclei ( $A \sim 60$ ) is considerable, and seems to exceed that of the emission of neutrons in some cases. Thus the (p, pn) cross section on  $\text{Cu}^{63}$  has been found to be considerably higher than the

(p, 2n) cross section on the same nucleus (Ghoshal, 1950), even though the probability of the emission of protons from nuclei is expected to be considerably reduced by the Coulomb potential barrier. Rough calculations using a more correct formula showed that in the case of  $\text{Cu}^{63}$ , the (p, pn) cross section is of the same order of magnitude as the (p, 2n) cross section at a proton energy of about 20 Mev. The results of more exact calculations of these cross sections, taking into account the probability of deuteron emission, are reported in the present work.

#### CROSS SECTION OF THE EMISSION OF MORE THAN ONE PARTICLE

Let us consider a nuclear reaction of the type :



The energy of the bombarding particle  $a$  is sufficiently high to allow the emission of  $n$  successive particles  $b_1, b_2, b_3, \dots, b_n$ . The residual nuclei in the different stages are denoted by  $B_1^*, B_2^*, \dots, B_n^*$ . The emitted particles  $b$  may be protons, neutrons, deuterons, etc. If  $I_1(\epsilon_1) d\epsilon_1$  represents the energy distributions of the first particles emitted, then the total number of such particles will be

$$\sum_{b_1} \int_0^{\epsilon_1^m} I_1(\epsilon_1) d\epsilon_1$$

where  $\epsilon_1^m$  is the maximum permissible energy of the first particle emitted, consistent with the energy  $E_a$  of the incident particle.  $\epsilon_1^m = E_a + \beta_a - \beta_1$ , where  $\beta_a$  is the binding energy of the incident particle  $a$  to the compound nucleus  $C$  in its ground state and  $\beta_1$  is the binding energy of the first particle  $b_1$  to the same nucleus  $C$ . The summation in the denominator extends over the various types of the first particles  $b_1$  that can be emitted, e. g. neutrons, protons, etc.

A fraction of the total number of  $b_1$  emitted will be followed by the emission of the second particle  $b_2$ ; a smaller fraction will be followed by the emission of two particles  $b_2$  and  $b_3$ ; and so on. In each stage, the emitted particles may be protons, neutrons, etc. The maximum energy with which  $b_1$  can be emitted and can still be followed by the emission of  $(n-1)$  more particles is given by,

$$\epsilon_1^{(n)} = E_a + \beta_a - \sum_1^n \beta_v$$

where  $\sum_1 \beta_i$  denotes the sum over the binding energies  $\beta_1, \beta_2, \beta_3, \dots, \beta_n$  of the particles  $b_1, b_2, \dots, b_n$  to the respective nuclei  $C, B_1, B_2, \dots, B_{n-1}$ . The total number of  $b_1$  emitted with energies upto  $\epsilon_1^{(n)}$  is given by

$$\int_0^{\epsilon_1^{(n)}} I_1(\epsilon_1) d\epsilon_1$$

However, these first particles  $b_1$  may be followed by the emission of various types of the successive particles  $b_2$  to  $b_n$ . To get the number of  $b_1$  which will be followed by the emission of the particles  $b_2$  to  $b_n$  of the specified types, we have to multiply the integrand in the above expression by the respective probabilities of the emission of these specified types of  $b_2$  to  $b_n$ . Let  $P_2(\epsilon_2)d\epsilon_2, P_3(\epsilon_3)d\epsilon_3, \dots, P_n(\epsilon_n)d\epsilon_n$ , denote these probabilities within the proper energy ranges. Then the required number of  $b_1$  which will be followed by the emission of the proper types of  $b_2, b_3, \dots, b_n$  will be given by

$$\int_0^{\epsilon_1^{(n)}} \int_0^{\epsilon_2^{(n)}} \int_0^{\epsilon_3^{(n)}} \dots \int_0^{\epsilon_n^m} I_1(\epsilon_1) P_2(\epsilon_2) \dots P_n(\epsilon_n) d\epsilon_1 d\epsilon_2 \dots d\epsilon_n \quad \dots \quad (1)$$

where  $\epsilon_1^{(n)} = E_a + \beta_a - \sum_1^n \beta_i - \sum_1^{r-1} \epsilon_i$  is the maximum permissible energy of the  $r$ th particle which will allow the emission of  $n$  particles.  $\epsilon_n^m$  is the maximum energy of the  $n$ th particle emitted:

$$\epsilon_n^m = E_a + \beta_a - \sum_1^n \beta_i - \sum_1^{n-1} \epsilon_i$$

Then assuming the compound nucleus process to be valid in the energy regions concerned, the cross section will be given by (Weisskopf and Ewing, 1940)

$$\begin{aligned} \sigma(a, b_1 b_2 \dots b_n) \\ = \sigma_a \sum \int_0^{\epsilon_1^{(n)}} \int_0^{\epsilon_2^{(n)}} \dots \int_0^{\epsilon_n^m} I_1(\epsilon_1) P_2(\epsilon_2) \dots P_n(\epsilon_n) d\epsilon_1 d\epsilon_2 \dots d\epsilon_n \\ \sum_{b_1} \int_0^{\epsilon_1^m} I_1(\epsilon_1) d\epsilon_1 \end{aligned} \quad (2)$$

where  $\sigma_a$  is the cross section for the absorption of  $a$  to form the compound nucleus  $C$ .

In general, the calculation of the cross sections from the above formula involves the evaluation of the multiple integral by numerical integration. For nuclear reactions involving the emission of more than three particles, the calculations become very much involved.

## EMISSION OF TWO PARTICLES

This is a process of the type  $A(a, b_1 b_2)B_2$ . The cross section is given by

$$\sigma(a, b_1 b_2) = \sigma_a \frac{\int_{\epsilon_1^{(2)}}^{\epsilon_1^{(2)}} \int_{\epsilon_2^{(m)}}^{\epsilon_2^{(m)}} I_1(\epsilon_1) P_2(\epsilon_2) d\epsilon_2 d\epsilon_1}{\sum_{b_1 0}^{\epsilon_1^{(m)}} \int_{\epsilon_1^{(m)}}^{\epsilon_1^{(m)}} I_1(\epsilon_1) d\epsilon_1} \quad \dots \quad (3)$$

The second integral in the numerator can be written more explicitly as :

$$\int_{\epsilon_2^{(m)}}^{E_a + \beta_a - \beta_1 - \beta_2 - \epsilon_1} P_2(\epsilon_2) \alpha \epsilon_2 = \eta_2 (E_a + \beta_a - \beta_1 - \beta_2 - \epsilon_1) \quad (3a)$$

where  $\eta_2$  gives the total probability of the emission of  $b_2$  with the maximum energy  $\epsilon_2^{(m)} = E_a + \beta_a - \beta_1 - \beta_2 - \epsilon_1$ . Weisskopf and Ewing have shown this to be given by an expression of the form :

$$\eta_2 = \frac{f_2(\epsilon_2^{(m)})}{\sum_{b_2 0}^{\epsilon_2^{(m)}} f_2(\epsilon_2^{(m)})} = \frac{\int_0^{\epsilon_2^{(m)}} I_2(\epsilon_2) d\epsilon_2}{\sum_{b_2 0}^{\epsilon_2^{(m)}} \int_0^{\epsilon_2^{(m)}} I_2(\epsilon_2) d\epsilon_2} \quad (4)$$

where the summation in the denominator extends over the various possible types of  $b_2$  which can be emitted. Thus the expression for the cross section becomes :

$$\sigma(a, b_1 b_2) = \sigma_a \frac{\int_{\epsilon_1^{(2)}}^{E_a + \beta_a - \beta_1 - \beta_2} I_1(\epsilon_1) \eta_2 (E_a + \beta_a - \beta_1 - \beta_2 - \epsilon_1) d\epsilon_1}{\sum_{b_1 0}^{\overline{E_a + \beta_a - \beta_1}} \int_{\epsilon_1^{(m)}}^{\overline{E_a + \beta_a - \beta_1}} I_1(\epsilon_1) d\epsilon_1} \quad (5)$$

For nuclei which are not too light ( $A \sim 60$ ), protons and neutrons are the only two types of particles which can be emitted both as the primary ( $b_1$ ) and the secondary ( $b_2$ ) particles. However, in certain energy regions,  $\gamma$ -emission also becomes quite probable. This is particularly so when neutron emission is not energetically possible, whereas, proton emission can still take place. The probability of the emission of the latter is, however, small owing to the barrier effect (proton energy is small). The only alternative process for the excited nucleus is to decay by the emission of a  $\gamma$ -ray. There will be very small but finite probability for the emission of deuterons as primary particles, when sufficient energy is available. Thus the expressions (4) and (5) above can be rewritten as :

$$\sigma(a, b_1 b_2) = \sigma_a \frac{\int_{\epsilon_1^{(2)}}^{E_a + \beta_a - \beta_1 - \beta_2} I_1(\epsilon_1) \eta_2 (E_a + \beta_a - \beta_1 - \beta_2 - \epsilon_1) d\epsilon_1}{\int_{\epsilon_n^{(m)}}^{\overline{E_a + \beta_a - \beta_n}} I_n(\epsilon_n) d\epsilon_n + \int_{\epsilon_p^{(m)}}^{\overline{E_a + \beta_a - \beta_p}} I_p(\epsilon_p) d\epsilon_p + \int_{\epsilon_d^{(m)}}^{\overline{E_a + \beta_a - \beta_d}} I_d(\epsilon_d) d\epsilon_d} \quad (6)$$



$$= \frac{f_{b_1}(\epsilon_1^m)}{f_{n_1}(\epsilon_{n_1}^m) + f_{p_1}(\epsilon_{p_1}^m) + f_{\gamma_1}(\epsilon_{\gamma_1}^m)} \int_{\epsilon_1^m}^{\epsilon_1^m} I_2(\epsilon_2) d\epsilon_2 \dots (6a)$$

$$\int_{\epsilon_1^m}^{\epsilon_1^m} I_{n_1} d\epsilon_{n_1} + \int_{\epsilon_1^m}^{\epsilon_1^m} I_{p_1} d\epsilon_{p_1} + \int_{\epsilon_1^m}^{\epsilon_1^m} I_{\gamma_1} d\epsilon_{\gamma_1}$$

where we neglect the possibility of a second deuteron emission. The  $\gamma$ -emission is important in certain energy regions only (see above).

### EMISSION OF THREE PARTICLES

Here we have

$$\sigma(a, b_1 b_2 b_3) = \sigma_a \int_0^{\epsilon_1^{(3)}} \int_0^{\epsilon_2^{(3)}} \int_0^{\epsilon_3^m} I_1(\epsilon_1) P_2(\epsilon_2) P_3(\epsilon_3) d\epsilon_1 d\epsilon_2 d\epsilon_3 \quad (7)$$

$$\sum_{b_1} \int_0^{\epsilon_1^m} I_1(\epsilon_1) d\epsilon_1$$

As in the previous case,

$$\int_0^{\epsilon_3^m} P_3(\epsilon_3) d\epsilon_3 = \eta_3(\epsilon_3^m) = \eta_3(\epsilon_2^{(3)} - \epsilon_2) \quad (7a)$$

where  $\eta_3$  is the total probability of the emission of  $b_3$  with the maximum energy  $\epsilon_3^m$ . Considering the various types of  $b_3$  which can be emitted,  $\eta_3$  will be given by an expression of the form (4),  $\eta_3 = f_3 / \sum_{b_3} f_{b_3}$ . Putting this

expression for the third integral in (7), the second in it takes the form :

$$I_2^{(3)} = \int_0^{\epsilon_2^{(3)}} P_2(\epsilon_2) \cdot \eta_3(\epsilon_2^{(3)} - \epsilon_2) d\epsilon_2$$

$$= \frac{\int_0^{\epsilon_2^{(3)}} I_2(\epsilon_2) \cdot \eta_3(\epsilon_2^{(3)} - \epsilon_2) d\epsilon_2}{\sum_{b_2} \int_0^{\epsilon_2^m} I_2(\epsilon_2) d\epsilon_2} \quad (7b)$$

where  $\eta_3^{(3)}$  is the probability of the emission of the given types of  $b_2$  with the maximum energy  $\epsilon_2^{(3)}$  followed by the emission of the given types of  $b_3$ . The expression for the cross section then becomes

$$\sigma(a, b_1 b_2 b_3) = \sigma_a \int_0^{\epsilon_1^{(3)}} \int_0^{\epsilon_2^{(3)}} I_1(\epsilon_1) P_2(\epsilon_2) \eta_3(\epsilon_2^{(3)} - \epsilon_2) d\epsilon_1 d\epsilon_2 \dots (8)$$

$$\sum_{b_1} \int_0^{\epsilon_1^m} I_1(\epsilon_1) d\epsilon_1$$

where the explicit expression for the second integral is given as above (7b).

### APPLICATION

The above results have been applied to calculate the cross sections  $\sigma(p, 2n)$ ,  $\sigma(p, pn)$  and  $\sigma(p, 2p)$  for the nucleus  $\text{Cu}^{63}$ . Now the production

of the reaction  $(p, pn)$  is favoured by a number of factors over the  $(p, 2n)$  reaction : (1) Firstly,  $\sigma_t(p, pn)$  is made up of three parts.  $\sigma_t(p, pn) = \sigma(p, p_1n_2) + \sigma(p, n_1p_2) + \sigma(p, d)$ . In the first term, a proton is taken to be the first emitted particle, followed by a neutron as the second particle. In the second term, we have just the reverse of this, whereas, in the third term a deuteron is taken to be emitted as a single particle. The last is, therefore, a single particle emission case. (2) The reaction  $(p, 2n)$  on  $\text{Cu}^{63}$  leaves a residual nucleus  $\text{Zn}^{62}$  which is an even-even nucleus while the  $(p, pn)$  process leaves the residual nucleus  $\text{Cu}^{62}$  which is odd-odd. The number of levels available for decay in the latter is greater than those in the former (Weisskopf and Ewing, 1940), and hence the probability of decay by the former process will be smaller than that by the latter. This is due to the fact that level densities of the residual nuclei are involved in the explicit expression of the energy distribution term  $I(\epsilon)d\epsilon$ . (3) Finally, the binding energies of the protons and neutrons to the various nuclei involved are such that the threshold of the  $(p, pn)$  process is about 1.9 Mev lower than that for the  $(p, 2n)$  process. Hence more energy is available for the emission of the  $p$  and the  $n$  than for two neutrons only. This influences the cross section, since on the average, more energy and hence greater level density will be available for the residual nucleus in the former case.

The cross section  $\sigma(p, d)$  for the emission of the deuteron following the capture of the proton is given by the single particle emission formula (Weisskopf and Ewing, 1940) :

$$\sigma(p, d) = \sigma_p \cdot \frac{f_{d1}}{f_{n1} + f_{p1} + f_{d1}}$$

where the  $f$ -values are given by equation (10a).

The process  $\text{Cu}^{63}(p, 2p)$  leads to the stable end product  $\text{Ni}^{62}$ . Normally the preventive effect of the Coulomb barrier on the emission of two protons is expected to be more pronounced than that on the emission of a proton and a neutron. However, the product of the  $(p, pn)$  process,  $\text{Cu}^{62}$ , decays into  $\text{Ni}^{62}$  which is the product of the  $(p, 2p)$  process on  $\text{Cu}^{63}$ , by the emission of a positron of 2.9 Mev end point (Hayward, 1950). The energy release in this decay is thus 4.6 Mev, which makes the threshold of  $(p, 2p)$  reaction considerably lower than the  $(p, pn)$  threshold. The difference in the thresholds, calculated from the mass formula is about 5.2 Mev\*. Hence the energy available for the emission of the second proton is considerably higher than that for the emission of the neutron following the first proton emission. This increases the value of  $\sigma(p, 2p)$  very appreciably in those energy regions where  $(p, pn)$  process has either not yet started or is just starting.

\* Since the experimental values of the binding energies are not available in all cases, we have used the values of the binding energies calculated from the mass formula throughout the present work. These do not differ from the experimental values significantly as far as the present calculations are concerned.

The explicit expression for the energy distribution of the emitted particles,  $I(\epsilon)d\epsilon$  has been derived by Weisskopf (1947) and is given by (for a particle  $b$  emitted) :

$$I_b(\epsilon_b)d\epsilon_b = \frac{M_b}{\pi^2 \hbar^2} \sigma_b(\epsilon_b) \cdot \epsilon_b \cdot \omega_R(\epsilon_b^m - \epsilon_b) d\epsilon_b \quad (10)$$

where  $\sigma_b(\epsilon_b)$  is the cross section of the inverse process, viz., the capture of an incident particle  $b$  of energy  $\epsilon_b$  by the residual nucleus excited with energy  $(\epsilon_b^m - \epsilon_b)$ .  $\omega_R(\epsilon_b^m - \epsilon_b)$  gives the level density of the residual nucleus at the excitation energy  $(\epsilon_b^m - \epsilon_b)$  after the emission of  $b$ . The function  $f_b$  introduced above (Eqns 4 and 6) is given by the integral :

$$f_b(\epsilon_b^m) = \frac{M_b}{\pi^2 \hbar^2} \int_0^{\epsilon_b^m} \sigma_b(\epsilon_b) \cdot \epsilon_b \cdot \omega_R(\epsilon_b^m - \epsilon_b) d\epsilon_b \quad (10a)$$

$\epsilon_b^m$  being the maximum energy with which  $b$  can be emitted.

The values of  $f$  for different types of particles have been calculated by Weisskopf and Ewing (1940), by assuming the level density  $\omega_R$  to be given by an expression of the form :

$$\omega_R(E) = C e^{\sqrt{aE}}$$

where  $C$  is a constant depending on the mass number  $A$  of the nucleus. To take into account the fact that the residual nucleus may be even-even, odd-odd, or even-odd (see above), Weisskopf and Ewing (1940) have assumed the following ratios between the level-densities :

$$C_{\text{even-even}} = \frac{1}{2} C_{\text{even-odd}} = \frac{1}{4} C_{\text{odd-odd}}$$

However, in the present work, qualitative agreement between the calculated results and the observed values was obtained with the following ratios :

$$C_{\text{even-even}} = \frac{1}{6} C_{\text{even-odd}} = \frac{1}{6.4} C_{\text{odd-odd}}$$

These have, therefore, been used throughout our calculation.\*

The constant  $a$  also depends on  $A$ . In their calculations Weisskopf and Ewing have assumed  $a = A/5 \text{ (Mev)}^{-1}$

We have recalculated the  $f$  values using a slightly different expression for  $a$  (see Weisskopf, 1947)\*\*:

$$a = 3.35(A - 40)^{\frac{1}{2}} \text{ (Mev)}^{-1} \quad (11)$$

\* Recently Blatt and Weisskopf (1952) have predicted somewhat similar ratios for  $C$  between the different types of nuclei.

\*\* We are indebted to Professor Weisskopf for kindly supplying us with the tables of the cross sections  $\sigma_p$ ,  $\sigma_\alpha$  and  $\sigma_n$  for different nuclei. The cross sections which differ somewhat from the earlier calculations of Weisskopf (1947), have been used in the present work.

In their recent publication, Blatt and Weisskopf (1952) give the value of  $a$  somewhat different from the one given in eqn. (11). However, since the theory is very approximate, it can only show qualitative behaviours. Hence the above difference does not alter the nature of our results appreciably.

We have not assumed any explicit expression for  $C$ , since only ratios are always involved and  $C$  cancels out. We have neglected the slight variation of  $C$  and  $a$  between different nuclei involved ( $A$  varies between 62 and 64).

In the case of  $\gamma$ -emission, the following expression for  $f_\gamma$  has been used (Weisskopf, 1947) :

$$f_\gamma = \frac{C_\gamma}{2\pi^2 \hbar^2 c^2} \int_0^{E_c} \epsilon_\gamma^5 \omega_R (E_c - \epsilon_\gamma) d\epsilon_\gamma$$

where  $C_\gamma$  is a numerical constant whose value is given by  $C_\gamma = 0.65 \times 10^{-29} \text{ cm}^2/\text{Mev}^4$ .  $E_c$  is the excitation energy of the nucleus emitting the radiation and  $\epsilon_\gamma$  is the energy  $h\nu$  of the  $\gamma$ -ray emitted,  $c$  is the velocity of light.

Besides the cross sections  $\sigma(p, 2n)$ ,  $\sigma(p, pn)$  and  $\sigma(p, 2p)$  the cross sections  $\sigma(p, n)$  and  $\sigma(p, p)$  for single particle emission processes were also calculated at the same energy values as a check against possible mistakes in the calculations. For the sum of all these cross sections should give  $\sigma_p$ , the cross section for the absorption of the proton by  $\text{Cu}^{63}$  to form the compound nucleus  $\text{Zn}^{64}$ .

The results of the calculations are shown in figures 1 and 2. In figure 1, the cross sections  $\sigma(p, n_1 p_2)$ ,  $\sigma(p, p_1 n_2)$ ,  $\sigma(p, d)$  and  $\sigma_t(p, pn)$  which is the sum of the first three are plotted against the incident proton energy. In figure 2, the cross sections  $\sigma(p, 2n)$ ,  $\sigma_t(p, pn)$  and  $\sigma(p, 2p)$  are plotted.

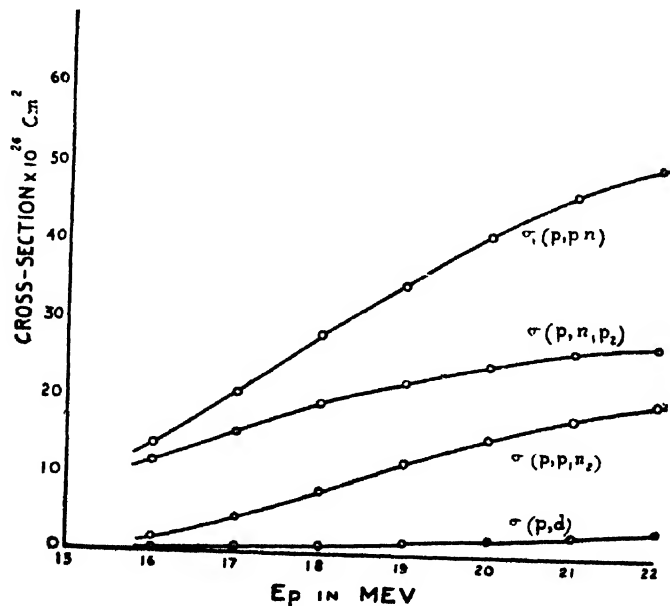


FIG. 1

Cross sections  $\sigma(p, p_1 n_2)$ ,  $\sigma(p, n_1 p_2)$ ,  $\sigma(p, d)$  and  $\sigma_t(p, pn)$  plotted as functions of the incident proton energy.  $\sigma_t(p, pn)$  is the sum of the first three cross-sections. ( $r = 1.3 \times 10^{-13}$ )

For the sake of comparison, the experimental values of  $\sigma(p, 2n)$  and  $\sigma_t(p, pn)$  are also plotted in the same diagram. The latter were measured

with the 32 Mev proton beam from the linear accelerator of the University of California, Berkeley, U.S.A. by one of us (Ghoshal 1950).

From figure 1, we see that the contribution to the  $\sigma(p, pn)$  cross section due to the emission of the deuteron is about 5% of  $\sigma(p, pn)$  at the incident proton energies considered.

The curves of figure 2 show qualitative agreement with the experimental values. The calculated ratio  $\sigma_t(p, pn) : \sigma(p, 2n)$  agrees with the experimental value at the peaks of the excitation curves. The agreement in other regions is very rough, owing to the fact that the cross sections depend significantly upon the thresholds of the various reactions and the ratio of the level densities in case of odd-odd, even-odd and even-even nuclei. There is also not very good agreement between the absolute values of the various cross sections as can be seen from figure 2.

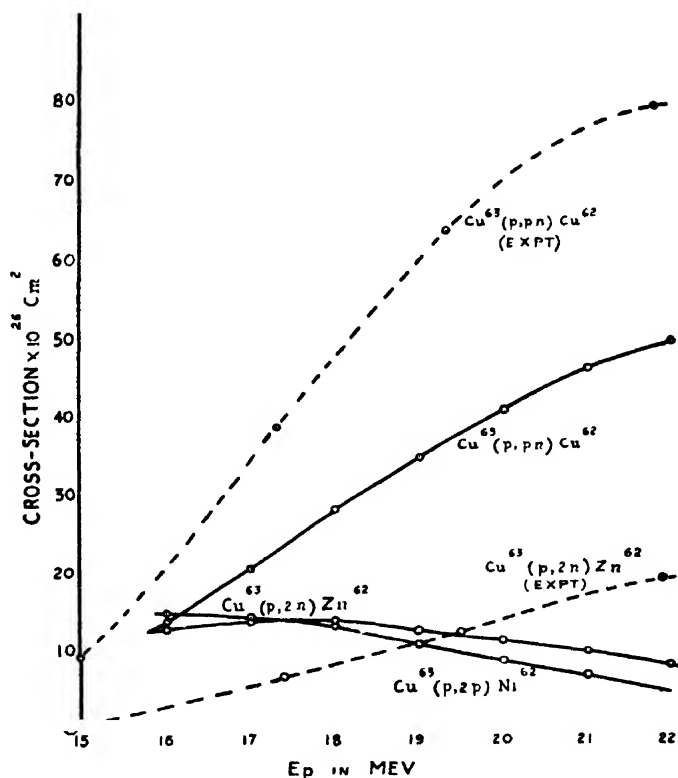


FIG. 2

Cross sections  $\sigma(p, 2n)$ ,  $\sigma_t(p, pn)$  and  $\sigma(p, 2p)$  as functions of the incident proton energy. Solid curves represent the calculated values ( $\tau_0 = 1.3 \times 10^{-13}$ ), while the broken curves represent the experimental values.

#### ACKNOWLEDGMENTS

The authors are indebted to the Atomic Energy Commission of the Government of India for sponsoring this research. One of us (T.N.D.) is

sincerely grateful to the A.E.C. for the award of a Research Assistantship which enabled him to carry out the work.

#### REFERENCES

Blatt and Weisskopf, 1952, *Theoretical Nuclear Physics*, 1st Ed., p. 372.373

Ghoshal, S.N., 1950, *Phys. Rev.*, **80**, 939.

Hayward, R., 1950, *Phys. Rev.*, **79**, 541.

Weisskopf, V. F., and Ewing, D.H., 1940, *Phys. Rev.*, **57**, 472.

Weisskopf, V F et al, 1947, *Lecture Series in Nuclear Physics*, U.S. Government Printing Office (MDDC-1175).

# MOISTURE-SENSITIVITY OF DIELECTRIC CONSTANT OF JUTE AND COTTON\*

By B. L. BANERJEE

[DIELECTRIC RESEARCH LABORATORY, DEPT. OF APPLIED PHYSICS, CALCUTTA UNIVERSITY

(Received for publication, August 4, 1952)

**ABSTRACT.** The effect of moisture on the dielectric constant of jute and cotton for both raw and chemically treated forms have been studied. The moisture-sensitivity of their dielectric constant is found to be different from one another but when dry, they have sensibly the same value of dielectric constant. Attempts have been made to explain this difference in their behaviour.

It is very much regretted that the size of the format in this particular issue has inadvertently been reduced to the royal size by the press at the time of printing.

and 1.5 cm. in diameter, are fixed centrally at right angles to the plane of the plates. On these rods threads are cut. The plates along with the rods are fitted face to face inside a horizontal pyrex glass tube of length 17.8 cm. Its inside diameter almost coincides with the diameter of the condenser plates. It is fitted with inlet and outlet tubes at its ends for the purpose of circulating air of desired humidities through it. Each end of the glass tube is closed by means of a flange and rubber gasket. At the back of each flange a nut, fixed on an ebonite hand-wheel, is fitted over the brass rod and its plate can be

\* Communicated by Prof. P. C. Mahanti.

sincerely grateful to the A.E.C. for the award of a Research Assistantship which enabled him to carry out the work.

#### REFERENCES

Blatt and Weisskopf, 1952, *Theoretical Nuclear Physics*, 1st Ed., p. 372.373

Ghoshal, S N., 1950, *Phys. Rev.*, **80**, 939.

Hayward, R., 1950, *Phys. Rev.*, **79**, 541.

Weisskopf, V. F., and Ewing, D.H., 1940, *Phys. Rev.*, **57**, 472.

Weisskopf, V F et al, 1947, *Lecture Series in Nuclear Physics*, U.S. Government Printing Office (MDDC-1175).



# MOISTURE-SENSITIVITY OF DIELECTRIC CONSTANT OF JUTE AND COTTON\*

By B. L. BANERJEE

DIELECTRIC RESEARCH LABORATORY, DEPT. OF APPLIED PHYSICS, CALCUTTA UNIVERSITY

(Received for publication, August 4, 1952)

**ABSTRACT.** The effect of moisture on the dielectric constant of jute and cotton for both raw and chemically treated forms have been studied. The moisture-sensitivity of their dielectric constant is found to be different from one another but when dry, they have sensibly the same value of dielectric constant. Attempts have been made to explain this difference in their behaviour.

## INTRODUCTION

The primary object with which the present work was started was to design a dielectric moisture meter for use in jute industry. From a preliminary survey of the effect of moisture on the different electrical properties of jute fibres, a study of moisture-sensitivity of their dielectric constant was found promising for the purpose. For a comparative study, it was also thought of interest to extend the observations to chemically treated samples of jute fibres, as well as to raw and chemically treated fibres of cotton. Measurements have been made therefore not only on samples of native raw jute and cotton, but also on five samples of chemically treated jute and one sample of chemically treated cotton. The chemically treated jute samples include three alkali-treated samples prepared by using 1%, 12.5% and 17.5% NaOH solutions at room temperature, one lignified and one holocellulose sample prepared by the use of usual chlorite method. The chemically treated cotton sample was a mercersized one using 5% NaOH solution also at the room temperature.

### *Experimental fibre-condenser.*

After many trials, a condenser as shown in figure 1, was suitably designed to contain a given weight of fibres at various conditions of relative humidities. It was essentially of parallel-plate type. The plates are circular brass discs of diameter 6.15 cm. and thickness 0.45 cm. and are nickel-plated to give a smooth shining surface. On one side of the plates, brass rods, about 15 cm. in length and 1.3 cm. in diameter, are fixed centrally at right angles to the plane of the plates. On these rods threads are cut. The plates along with the rods are placed face to face inside a horizontal pyrex glass tube of length 17.8 cm. Its inside diameter almost coincides with the diameter of the condenser plates. It is fitted with inlet and outlet tubes at its ends for the purpose of circulating air of desired humidities through it. Each end of the glass tube is closed by means of a flange and rubber gasket. At the back of each flange a nut, fixed with an ebonite hand-wheel, is fitted over the brass rod and its plate can be

\* Communicated by Prof. P. C. Mahanti.

moved inwards and outwards within the glass tube, as required by means of the hand-wheel. The plates are prevented from rotating during their movement

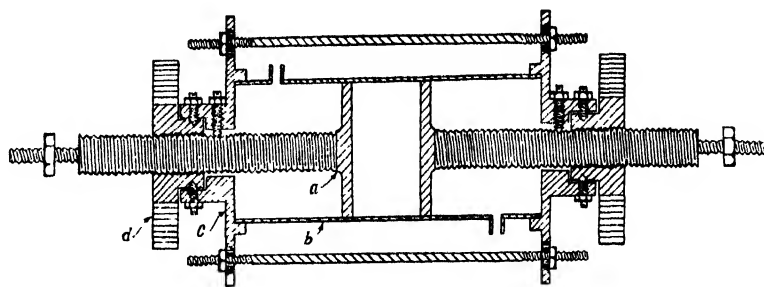


FIG. 1.

- |                     |                        |
|---------------------|------------------------|
| (a) Plate with rod. | (c) Flange and Gasket. |
| (b) Glass tube.     | (d) Ebonite hand wheel |

by means of a keyway fitting with the nut. Two binding screws at the ends of the two rods serve as the terminals of the condenser. The assembly is then suitably mounted in a horizontal position on a wooden frame.

In subsequent measurements, the plates were kept at 0.45 cm. apart and the capacity of the condenser under this condition with air as the medium, as measured on the Schering bridge, was about  $8.5 \mu\mu f.$  while that calculated from its dimensions was about  $6.1 \mu\mu f.$  For the purpose of this investigation, the parasitic capacity  $2.4 \mu\mu f.$ , as obtained from these data was assumed to remain constant throughout all measurements.

#### *Method of packing.*

Since dielectric constant depends on the alignment of the fibres with respect to the field, it was necessary to ensure a random packing of the fibres in the condenser. For this purpose the fibres were cut into small lengths mixed with a few drops of water and made into a plug which was inserted into the condenser for conditioning. The effect of air could not altogether be eliminated and hence the measured values would be lower than the actual dielectric constants of the fibres.

#### *Conditioning of fibres.*

The arrangement for conditioning the fibres in the condenser is as shown in figure 2. A given weight of fibres, 3.5 gm., was cut into small pieces and uniformly packed in the space between the condenser plates which were next screwed out to allow the inlet and outlet tubes to be introduced between them. The towers were filled with sulphuric acid-water mixtures of appropriate concentration for obtaining a particular relative humidity. Air was bubbled through the acid solutions and allowed to pass through the fibres and finally drawn out through the outlet tube of the condenser, a combined force/exhaust pump being used for the purpose. The object of having three towers was to ensure

that the concentration of the acid mixture in the tower nearest to the condenser remained practically constant during the period of circulation of air. About 4-5 hours of continuous flow at the rate of 2 litres per minute was found sufficient for the attainment of equilibrium humidity in the fibres. To avoid

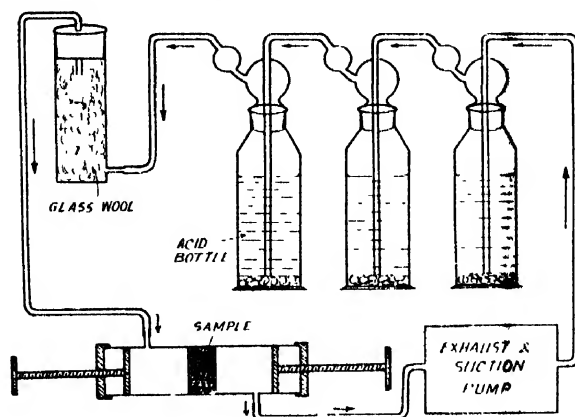


Fig. 2

uncertainty about the equilibrium point the fibres were conditioned for 20 hours by circulating humidified air continuously overnight at the end of which period the inlet and the outlet tubes of the condenser were closed, so that outside air could not disturb the condition of the fibres. The condenser plates were then brought closer to a distance of 1.35 cm. between their outer edges. To eliminate the effect, if there be any, of the previous history of the samples regarding the moisture absorption every sample was first conditioned at 0% relative humidity and its dielectric constant was measured, and the measurements continued after progressively increasing the relative humidity of conditioning and then similarly diminishing it so that a complete cycle of absorption and desorption could be taken.

#### *Measurement of dielectric constant.*

The circuit diagram of the bridge used is as shown in figure 3. All measurements were made at a frequency of oscillation of 2 Kc/sec. by the usual method of substitution. A standard air condenser  $C$  was placed in the fourth arm and the fibre condenser was inserted across the variable standard condenser  $C_{s1}$ . Balance was obtained by adjusting the power factor in the second arm and the capacity  $C_s$  in the third arm. Under this condition

$$C_{s1} + C_1 = \frac{R_1}{R_2} \quad (1)$$

( $C$  = capacity of the standard air condenser,  $C_{s1}$  = capacity of the variable condenser  $C_s$ ,  $C_1$  = capacity of the fibre condenser.  $R_1$  and  $R_2$  are impedances in the ratio arms 1 and 2 respectively.)

The fibre condenser was removed and again balance was obtained when

$$C = \frac{R_1}{R_2} \quad (2)$$

( $C_s$  = capacity of the variable condenser at the balance point.)

From (1) and (2)

$$C_t = C_s - C_{s1} \quad \dots (3)$$

From the observed value of  $C_t$ , the net capacitance ( $C'_t$ ) of the sample condenser at a given value of moisture content was obtained by making allowance

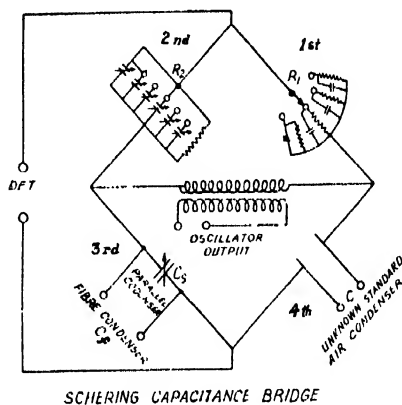


Fig. 3

for its parasitic capacitance and the value of dielectric constant was evaluated from the following relation,

$$K = \frac{11.31 C'_t t}{A},$$

where  $C'_t$  is given in  $\mu\mu F$ ,  $t$  is the thickness of the sample in cm. and  $A$  is the area of the condenser plates in  $\text{cm}^2$ .

Special care was taken to ensure the constancy of the frequency of oscillation during a measurement, for which purpose a stabilisation period of nearly half-an-hour was allowed to pass before a reading was taken. In order to check the accuracy of measurements, capacities of known laboratory standard capacitors were measured and it was found that the error did not exceed 1%. Replicate measurements with a given weight of fibres in the condenser confirmed the reproducibility of the results.

#### *Effect of pressure.*

It was considered important to investigate if the dielectric constant of a sample undergoes any appreciable variation when the separation between the electrodes for a given weight of the sample is slightly different from the value at which they were normally kept. It was found that the variations in the distance between the condenser plates over a range 0.35 - 0.60 cm. and hence the corresponding pressure variations, did not affect appreciably the dielectric constant of a sample, the maximum change being about 3% at the highest value of its moisture content.

## EXPERIMENTAL RESULTS

TABLE I

Jute samples

Sample	Adsorption results			Desorption results		
	% R.H.	% M.C.	K	% R.H.	% M.C.	K
Raw jute	0	0	1.80	73	16.5	3.80
	27	5.0	1.83	60	12.0	2.80
	37	6.2	1.93	51	9.7	2.10
	55	9.1	2.12	42	8.0	1.94
	60	10.0	2.18	39	7.5	1.89
	70	11.8	2.54	29	6.5	1.82
	79	13.7	3.60	2	0.1	1.80
	100	31.2	—	—	—	—
Holo-cellulose	0	0	1.83	66	10.5	8.84
	28	4.5	1.93	49	7.3	4.59
	51	6.6	3.12	33	6.0	2.26
	62	7.8	5.60	19	4.0	2.06
	69	8.9	8.30	0	0	1.71
	100	27.0	—	—	—	—
Delignified jute	0	0	1.85	61	13.1	4.27
	25	5.6	1.89	50	11.0	2.70
	42	8.2	2.05	38	9.2	2.60
	56	10.0	2.58	28	7.5	2.15
	71	12.0	4.37	14	4.5	2.06
	100	35.0	0	0	0	1.83
17.5% NaOH jute	0	0	1.80	87	21.5	2.66
	25	5.2	1.90	71	15.5	2.48
	38	6.9	1.98	51	11.0	2.29
	52	8.5	2.10	36	9.0	2.05
	65	10.5	2.19	19	6.0	1.90
	75	12.6	2.27	10	3.5	1.85
	100	28.2	3.60	0	0	1.81
12.5% NaOH jute	0	0	1.87	81	18.5	2.81
	26	5.2	2.00	70	14.1	2.41
	36	6.2	2.04	56	10.5	2.20
	51	8.0	2.15	42	8.2	2.07
	63	9.7	2.26	24	6.5	1.98
	85	15.6	2.66	10	3.5	1.88
	100	29.5	4.10	0	0	1.87
1% NaOH jute	0	0	1.88	82	19.0	3.15
	23	5.0	1.98	67	13.2	2.51
	36	6.2	2.05	48	9.0	2.16
	45	7.2	2.12	35	7.6	2.04
	61	9.5	2.32	20	6.5	1.97
	76	12.5	2.58	0	0	1.88
	88	17.5	3.30	—	—	—
	100	30.0	4.42	—	—	—

( $C_s$  = capacity of the variable condenser at the balance point.)

From (1) and (2)

$$C_t = C_s - C_{s1} \quad \dots (3)$$

From the observed value of  $C_t$ , the net capacitance ( $C'_t$ ) of the fibre condenser at a given value of moisture content was obtained by making allowance

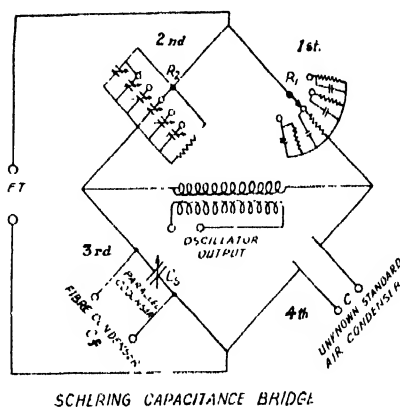


Fig. 3

for its parasitic capacitance and the value of dielectric constant was evaluated from the following relation,

$$K = \frac{11.31 C'_t t}{A},$$

where  $C'_t$  is given in  $\mu\mu F$ ,  $t$  is the thickness of the sample in cm. and  $A$  is the area of the condenser plates in  $\text{cm}^2$ .

Special care was taken to ensure the constancy of the frequency of oscillation during a measurement, for which purpose a stabilisation period of nearly half-an-hour was allowed to pass before a reading was taken. In order to check the accuracy of measurements, capacities of known laboratory standard capacitors were measured and it was found that the error did not exceed 1%. Replicate measurements with a given weight of fibres in the condenser confirmed the reproducibility of the results.

#### *Effect of pressure.*

It was considered important to investigate if the dielectric constant of a sample undergoes any appreciable variation when the separation between the electrodes for a given weight of the sample is slightly different from the value at which they were normally kept. It was found that the variations in the distance between the condenser plates over a range 0.35-0.60 cm. and hence the corresponding pressure variations, did not affect appreciably the dielectric constant of a sample, the maximum change being about 3% at the highest value of its moisture content.

## EXPERIMENTAL RESULTS

TABLE I  
Jute samples

Sample	Adsorption results			Desorption results		
	% R.H.	% M.C.		% R.H.	% M.C.	
Raw jute	0	0	1.80	73	16.5	3.80
	27	5.0	1.83	60	12.0	2.80
	37	6.2	1.93	51	9.7	2.10
	55	9.1	2.12	42	8.0	1.94
	60	10.0	2.18	39	7.5	1.89
	70	11.8	2.54	29	6.5	1.82
	79	13.7	3.60	2	0.1	1.80
	100	31.2		—	—	
Holo-cellulose	0	0	1.83	66	10.5	8.84
	28	4.5	1.93	49	7.3	4.59
	51	6.6	3.12	33	6.0	2.26
	62	7.8	5.60	19	4.0	2.06
	69	8.9	8.30	0	0	1.71
	100	27.0		—	—	
Delignified jute	0	0	1.85	61	13.1	4.27
	25	5.6	1.89	50	11.0	2.70
	42	8.2	2.05	38	9.2	2.60
	56	10.0	2.58	28	7.5	2.15
	71	12.0	4.37	14	4.5	2.06
	100	35.0		0	0	1.83
17.5% NaOH jute	0	0	1.80	87	21.5	2.66
	25	5.2	1.90	71	15.5	2.48
	38	6.9	1.98	51	11.0	2.29
	52	8.5	2.10	36	9.0	2.05
	65	10.5	2.19	19	6.0	1.90
	75	12.6	2.27	10	3.5	1.85
	100	28.2	3.60	0	0	1.81
2.5% NaOH jute	0	0	1.87	81	18.5	2.81
	26	5.2	2.00	70	14.1	2.41
	36	6.2	2.04	56	10.5	2.20
	51	8.0	2.15	42	8.2	2.07
	63	9.7	2.26	24	6.5	1.98
	85	15.6	2.66	10	3.5	1.88
	100	29.5	4.10	0	0	1.87
NaOH jute	0	0	1.88	82	19.0	3.15
	23	5.0	1.98	67	13.2	2.51
	36	6.2	2.05	48	9.0	2.16
	45	7.2	2.12	35	7.6	2.04
	61	9.5	2.32	20	6.5	1.97
	76	12.5	2.58	0	0	1.88
	88	17.5	3.30			
	100	30.0	4.42			

TABLE II

Cotton samples

Sample	Adsorption results			Desorption results		
	% R.H.	% M C	K	% R.H.	% M.C.	
Raw cotton ..	0	0	1.80	70	9.5	5.00
	7	2.0	1.80	57	7.5	3.70
	22	3.1	1.86	50	6.5	3.00
	37	4.0	2.15	43	5.6	2.61
	52	4.8	2.69	35	4.8	2.40
	62	6.0	4.11	28	4.2	2.05
	74	8.0	4.88	18	3.2	1.92
	100	—	—	0	0	1.83
Mercerised cotton	0	0	1.85	74	16.9	5.93
	26	6.0	1.88	63	13.6	3.66
	45	8.5	2.21	46	10.5	2.74
	59	10.3	2.58	29	7.7	2.10
	75	13.0	3.89	14	4.5	1.85
	100	35.0	—	0	0	1.83

TABLE III

Air dielectric

Adsorption results		Desorption results	
% R.H.		% R.H.	
0	1.00	100	1.35
30	1.05	90	1.17
80	1.10	80	1.10
90	1.17	30	1.05
100	1.35	0	1.00

## DISCUSSION

The variation of dielectric constant with relative humidity of conditioning for the various samples of jute and cotton is shown in figure 4 which includes also the results of measurements on the experimental condenser with air alone as medium between its plates. It will be noted that for a given change in the



relative humidity, the change in the dielectric constant of air is much smaller than that of the fibres. This is perhaps due to the more dispersed state of the

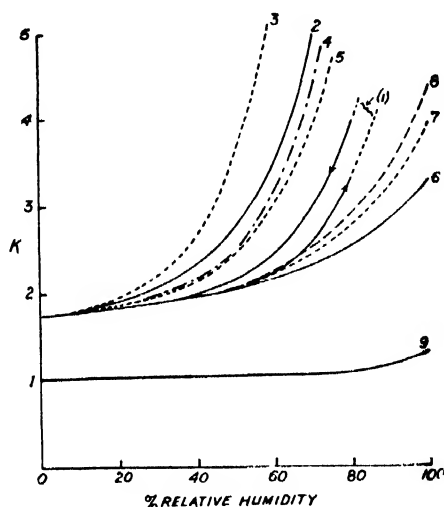


Fig. 4

Curve (1) — Jute (raw)	„ (6) — 17.5% NaOH treated jute
„ (2) — Cotton (raw)	„ (7) — 12.5% „ „ „
„ (3) — Holocellulose	„ (8) — 1% „ „ „
„ (4) — Delignified jute	„ (9) — Air condenser
„ (5) — Mercerised cotton	

molecules of water vapour in the former case. The main features of the results are :

(a) For a given sample, the dielectric constant at a particular relative humidity, depends upon whether it is conditioned by absorption or desorption, the dielectric constant in the latter case being higher, as can be seen from curve (1).

(b) The dielectric constant of jute is lower than that of cotton at any value of relative humidity although its moisture content corresponding to a given relative humidity is higher.

(c) Mercerisation or alkali treatment decreases the dielectric constant of jute and cotton.

(d) Delignification increases the dielectric constant of jute to a value nearing that for cotton at any value of relative humidity.

(e) The dielectric constant is sensibly the same for all dried samples of jute and cotton, irrespective of being raw or chemically treated.

The curves showing the variation of dielectric constant with moisture content of the different samples are given in figure 5. It may be noted that unlike the dielectric constant—relative humidity curve, the dielectric constant—moisture content curve is the same for both increasing and decreasing values of moisture content of conditioning of a sample.

It is now almost an established idea that the dielectric properties of fibres and polymeric substances in general can be explained in terms of an oscillation and relaxation spectrum. The former arises mainly out of electron and atom polarizations while the latter is the result of polarization on account of orientation of the molecules or their polar parts or displacement of ions, the translational or rotational diffusion as the case may be, requiring a supply of a statistical distribution of activation energy. The dielectric constant at frequencies of the applied field within the range  $10^3$ — $10^9$  c/sec. can be regarded as largely due to

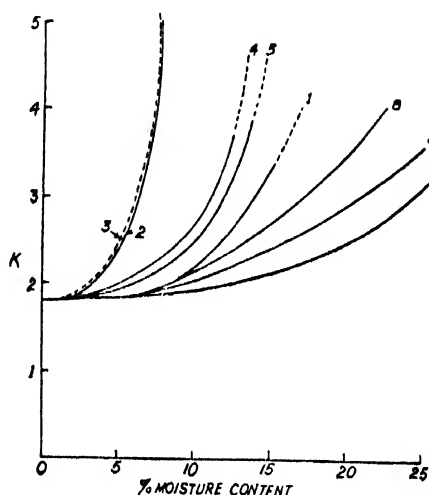


Fig. 5

polarization as a result of ionic displacement or dipolar orientation, whereas, that at higher frequencies due to electron and atom polarization. The dielectric properties, such as the dielectric constant and the loss angle, of inhomogeneous materials consisting of conducting or semi-conducting particles dispersed in an insulator can be explained with the help of Maxwell-Wagner equations and their subsequent modifications due to Sillars (1937) which relate these properties in terms of volume fractions, dielectric constants and conductivities of the components. Sillars has indicated that the shape of the conducting particles has a profound influence upon the dielectric constant. As for instance, a system having prolate (needle-like) particles will give a much higher dielectric constant than that with particles of oblate (lens-like) shape, the unique axis of both pointing toward the direction of the field.

The total quantities of moisture in fibres can be broadly regarded as composed of (1) bound and (2) free moisture. The small quantity of chemically bound moisture and that absorbed in the localised sites forming a unimolecular layer, both form the bound moisture; on the other hand, the free moisture inside fibres may be either (1) dispersed molecules in the multimolecular layers of adsorption and bound by the same force as between the molecules of liquid water or (2) liquid water in the capillaries of varying size and shape, or (3) both. Direct measurement of the relative proportions of bound and free moisture is rather difficult. For cotton, however, Peirce (1929) has

calculated these quantities from probability considerations. Since the ratio of dielectric constant of water and that of the fibre substance is very high (about 80:1.8) and the dielectric constant of water decreases with decrease in the freedom of movement of the molecules, one would expect that the dielectric constant will be very sensitive to the presence of water and, of the two states of water inside the fibres, the free moisture would affect it by a greater amount. The similarity in the nature of the curves as given in figure 4 and that showing the relation between free moisture and relative humidity for cotton, due to Peirce, also points to such calculation. The increase in the dielectric constant with moisture content can therefore be regarded as due to an increase in the amount of free moisture and is not likely to be the result of a decrease in the air content of the composite dielectric with swelling.

The fibre samples used in the the present investigation undoubtedly possess varying proportions of polar groups in the hydroxyls and the carboxyls of the constituents as well as in the associated water molecules, the moment and the freedom of motion of the dipole in each sample being different. It is therefore reasonable to expect their dielectric properties to be widely different on account of the difference in the dipole orientations resulting from the application of the alternating field. Figure 4 shows, however, that the fibres have almost the same dielectric constant at 0% relative humidity which suggests that in this case, the dipole mechanism is not effective. Since the frequency of the applied field, 2 Kc/sec., can be regarded as low, being about the lowest limit at which polarization due to ionic displacement or dipolar orientation is likely to occur, it will not be altogether without reason to exclude such a possibility. A small difference in the dielectric constant values for the various samples may arise out of a possible difference in the density of the fibre substances. It should be mentioned that the almost identical dielectric constant values for the various dry fibres may be due to the low order of accuracy of measurement in this region. If the effect of the intervening air could be eliminated by subjecting the fibres to a high pressure the dielectric constant values and therefore, the order of accuracy of measurement would certainly be higher as a result of which small differences, if there were any, between the dielectric constant values for the individual fibre sample would be revealed.

Accepting that the increase in the dielectric constant is due to an increase in the free moisture content as pointed out above and that the structure of the fibres is not likely to alter progressively with moisture absorption so as to effect increase either in the freedom of movement of the polar groups, or in the substance density, the observed relation between dielectric constant and moisture content can be explained by applying either Wagner model or its modification due to Sillars. Since the whole of moisture absorbed in the fibres is not in the free state, the volume fractions of free moisture need to be calculated. Using the Peirce's data for cotton the free moisture content at different relative humidities for jute can be deduced, if it is assumed that the proportions of bound moisture in jute and cotton are in the ratio of their non-crystalline constituents, 1.56, as indicated by Sen and Hermans (1949) disregarding the

content of the fibres. Assuming that lignin took part in the formation of the pores in jute and somehow blocked the cellulosic region having finer pores, its removal would lead to a fibrous material with finer pores which in respect of the dielectric properties would therefore approach cotton fibres.

The action of alkali on both jute and cotton can be regarded as to increase the bound moisture content on account of swelling due to which a greater number of reactive groups, hydroxyl or carboxyl, is likely to be available for moisture absorption. Simultaneously, fibres having larger pores may also result from alkali treatment.

#### A C K N O W L E D G M E N T S

The author acknowledges with pleasure his gratefulness to the Indian Jute Mills Association Research Institute and to its Research Director, Dr. W. G. Macmillan, for the award of a Scholarship to carry out the investigation. He is greatly indebted to Prof. P. C. Mahanti, Head of the Department of Applied Physics, and to Dr. M. K. Sen, Chief Physicist, IJMARI, for their guidance and helpful discussions during the course of the work.

#### R E F E R E N C E S

- Harmans, P. H., 1946, *Contribution to the Physics of Cellulose Fibres*, Elsevier.  
Macmillan, W. G., Mukherjee, R. R., and Sen, M. K., 1946, *J. Text Inst.*, **37**, T13.  
Muhlethaler, K., 1949, *Biochem. Biophys. Acta*, **3**, 15.  
Peirce, F. T., 1929, *J. Text. Inst.*, **20**, T133.  
Roy, M. M., 1951, Ph.D. Thesis, Calcutta University.  
Sen, M. K. and Harmans, P. H., 1949, *Revue Trav. Chim. Pays-Bas*, **68**, 1079.  
Sillars, R. W., 1937, *J. Inst. Elec. Eng.*, **8**, 378.  
Urquhart, A. R. and Williams, A. M., 1924, *J. Text Inst.*, **15**, T138.

# CORRELATION BETWEEN VARIATIONS OF SURFACE PRESSURE AND IONOSPHERIC PARAMETERS

By M. R. KUNDU

INSTITUTE OF RADIO PHYSICS AND ELECTRONICS; CALCUTTA UNIVERSITY.

(Received for publication, November 11, 1952)

**ABSTRACT.** Possible existence of correlation between variations of atmospheric pressure and variations of certain ionospheric parameters is examined by statistical analysis of the meteorological and ionospheric data of Calcutta for the years 1948-1951. It is found that in some months, at least, of a year the changes in the ionization value in course of the month (for a given hour of the day) have strong correlation with the pressure changes at the ground at the same hour in course of the same month. Further, for the same months, the variations of the average day- and night-time ionization densities of the E-region are found to have good correlation with pressure variations in course of the month at a particular hour. These results are in conformity with those obtained by Martyn and Pulley in Australia. The possible explanations of such correlations that have been suggested, namely, that variations of ozone content as occur in the ozonosphere (causing temperature variation) reach the ionospheric heights, or, that the effects of tropospheric disturbances reach the same heights by leaking through the stratosphere, are examined. It is maintained that before arriving at any definite conclusion regarding the correctness or otherwise of these explanations, it is essential that the types of the association that probably exist are established unambiguously, by long continued observations in the different parts of the world.

## INTRODUCTION

Attempts have been made from time to time by investigators in the different parts of the world to find out correlations, if any, between variations of barometric pressure at the ground and the variations of the ionospheric parameters (e.g., ionization density, height, etc.) of the different ionospheric layers. Thus, Jones and Jones (1950) have studied correlation between average variation of diurnal pressure at the ground and average diurnal variation of the semithickness of the  $F_2$ -layer. They found that the two oscillations are in opposite phase i.e., the semithickness is smallest when the surface barometric reading is the highest. Martyn and Pulley (1936), working at Sydney, Australia, investigated the correlation between variations of atmospheric pressure near the ground and variations of the ionization densities of the E and  $F_2$ -regions, as also of the height of the  $F_2$ -region. In certain cases, they found good correlation - direct for the former and indirect for the latter, but in most cases there was none. Definite associations were found, however, in the same country between the isobaric conditions near the ground and the  $F_2$ -ionizations in the ionosphere.

In the present paper, the possible existence of associations between the atmospheric pressure variations on the one hand and the variations of the semithickness and the critical frequency of the  $F_2$ -layer and the average day time and night time ionization densities of the E-region on the other, is examined afresh by statistical analysis of the records of the meteorological and ionospheric data of Calcutta. The ionospheric data were obtained from the records of the

Ionosphere Station at the University College of Science and Technology, Calcutta and the pressure data from the Meteorological Observatory, Alipore, situated at 7.5 km south of the ionospheric station.

### RESULTS OF ANALYSIS

(a) *Barometric pressure and  $F_2$ -layer semithickness* : For this analysis, the barometric and ionospheric data of Calcutta for the years 1948-1951 were utilised. The method of analysis was the same as employed by Jones and Jones.

To prevent masking of any possible association between the hourly values of the two parameters by large local changes due to disturbances or other causes, mean values were taken over intervals of 6 and 12 months. This is considered sufficient to eliminate random daily variations. Typical average three-hourly variation of pressure and semithickness of the  $F_2$ -layer are plotted in figures 1(a) and 1(b). It will be seen from the figures that the two oscillations are in

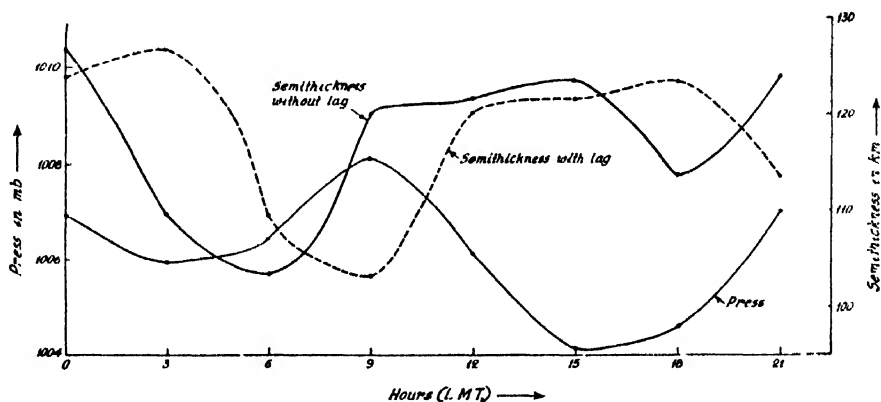


Fig. 1(a)

Diurnal variation of the mean values of the semithickness  $Y_m$  of the  $F_2$ -layer compared with the corresponding variations of surface pressure for the period July-Dec 1951

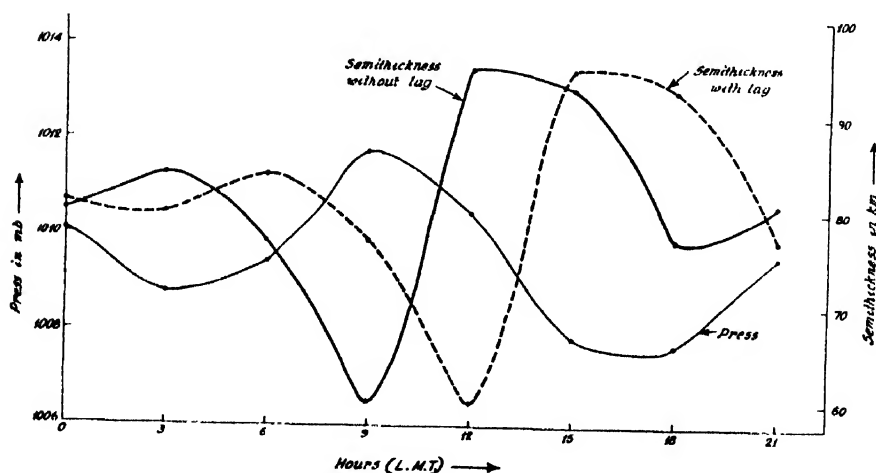


Fig. 1(b)

Diurnal variation of the mean values of the semithickness  $Y_m$  of the  $F_2$ -layer compared with the corresponding variations of surface pressure for the period Jan.-June, 1948.

composite phase only approximately. The best significant correlation is obtained by applying the so-called method of lag correlation in statistics, when a time lag of three hours is introduced between the two variations. The same result has been obtained from the data for all the years 1948-1951. The results of statistical analysis, allowing the time lag of three hours, are given in Table 1. It will be noticed that in most cases the probability of the association occurring by chance is small. It may therefore be concluded that in most cases the correlation is statistically significant. The significance test has also been carried out after Levy and Preidel (1944) (figure 2). Reference to Table 1 shows that

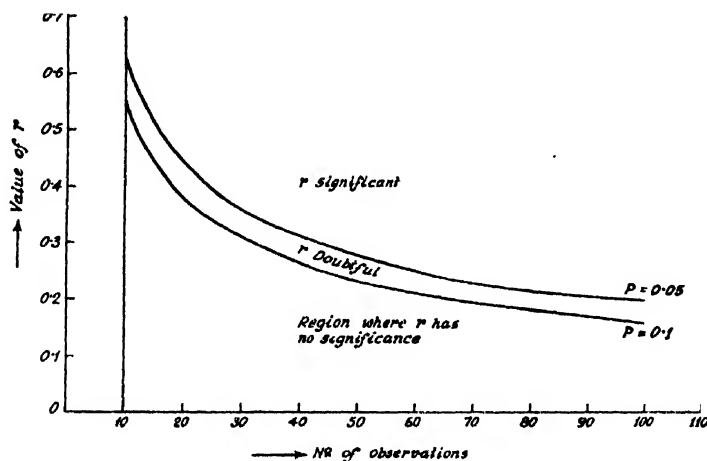


Fig. 2.

Test for the significance of the correlation coefficient.

in a number of cases the coefficient of correlation is small. This may perhaps be attributed to the limited accuracy of the ionospheric recorder used in the height measurements.

TABLE 1

Correlation between pressure and semithickness of the  $F_2$  layer

Year and months	Coefficient of correlation	Probability of occurrence by chance	Standard deviation of pressure	Standard deviation of semithickness
1948				
January-June	0.72	$0.66 \times 10^{-2}$	1.27 mb	10.10 km
January-December	0.65	$0.15 \times 10^{-1}$	1.36 mb	6.32 "
October-March '49	0.45	$0.90 \times 10^{-1}$	1.20 mb	6.10 "
1950				
January-June	0.62	$0.21 \times 10^{-1}$	1.16 mb	7.67 "
1951				
July-December	0.77	$0.43 \times 10^{-2}$	1.22 mb	7.61 "
1949				
January-December	0.62	$0.21 \times 10^{-1}$	1.08 mb	7.15 "

(b) *Pressure and ionization densities* : Only one year's data (Jan. 1949 to Dec. 1949) were analysed for the study of the correlation between the day to day variations of atmospheric pressure and of the ionization densities (data for three hours 0900, 1200, 1800 hours, L.M.T. were used). Figures 3 to 7 are

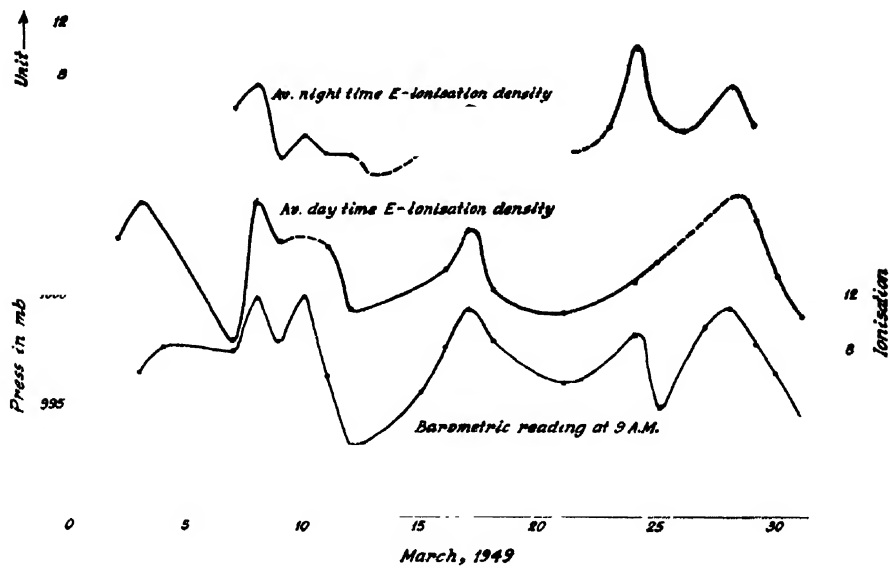


Fig. 3(a)

ustrating correlation between the day to day variations of surface pressure and the average E ionization density for March, 1949,

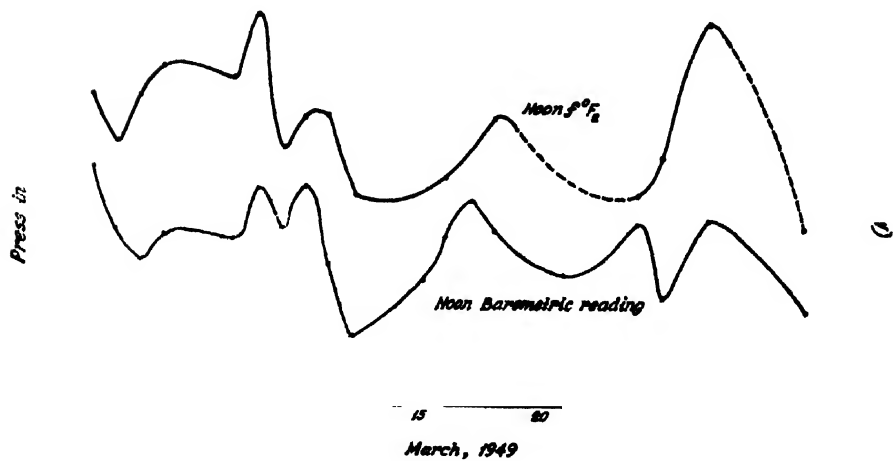


Fig. 3(b)

Illustrating correlation between the day to day variations of surface pressure and critical frequency of the F<sub>2</sub>-layer for March, 1949.



s of the variation curves. Visual comparison of the pressure curve with the spheric parameter curves at once reveals that there is correlation between two sets. This is in conformity with the observations of Martyn and Pulley Australia who found that the average day-time and night-time ionization

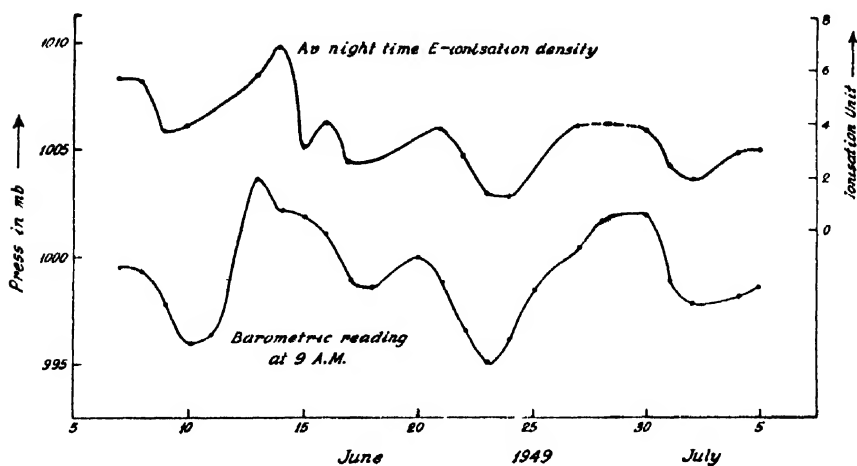


Fig. 4(a)

Illustrating correlation between the day to day variations of surface pressure and the average E ionization density for June, 1949.

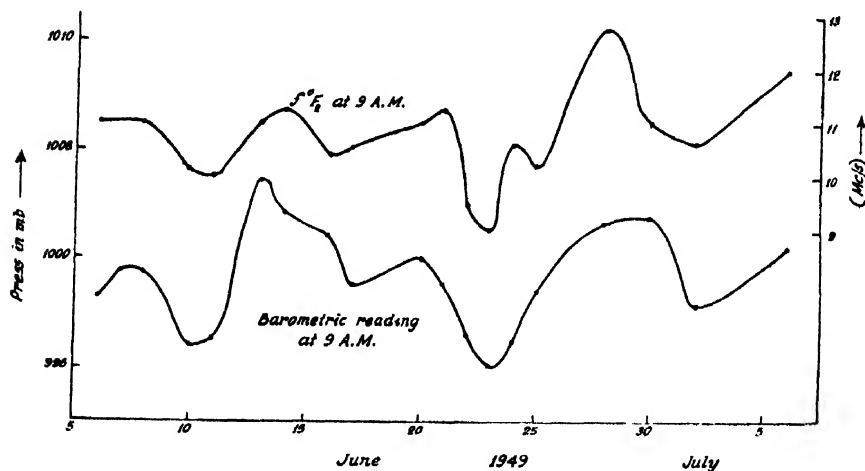


Fig. 4(b)

Illustrating correlation between the day to day variations of surface pressure and critical frequency of the  $F_2$ -layer for June, 1949.

densities of the E-region and the 9 A. M. and noon time critical frequencies of the  $F_2$ -region on the one hand correlate directly with the day to day pressure variations at the ground on the other. Closer scrutiny shows, however, that

the correlation is not of the same degree for all the months. Correlations for the months of March, June and September are better than those for July and December. Results of the statistical study of the correlation as shown in Table I.

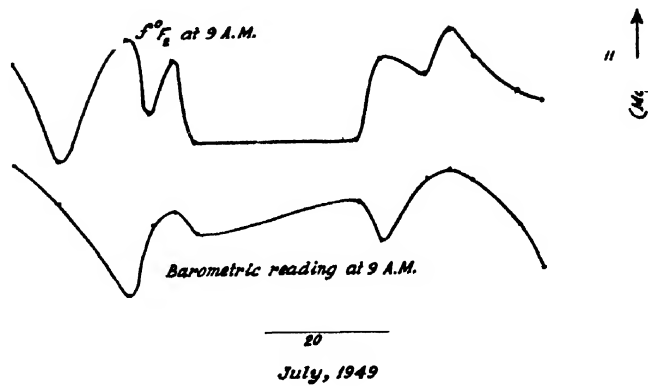


Fig. 5.  
Illustrating correlation between the day to day variations of surface pressure and critical frequency of the F<sub>2</sub>-layer for July, 1949.

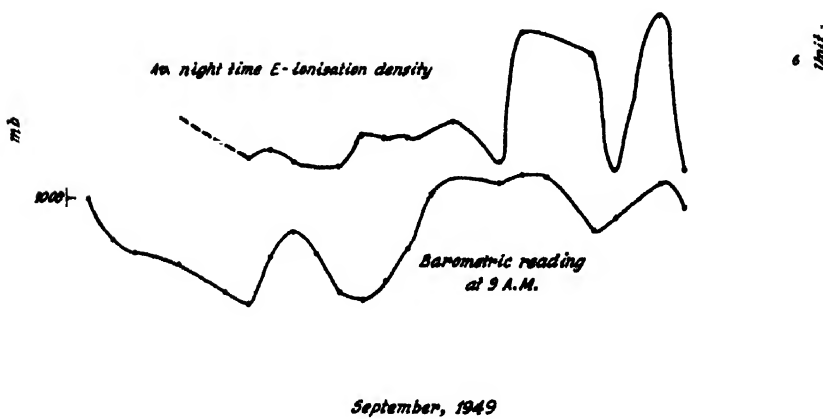


Fig. 6(a)  
Illustrating correlation between the day to day variations of surface pressure and the average E ionization density for September, 1949.

also confirm this. Examination of the probability of the correlation occurring by chance shows that whereas the correlation for the months of March, June and September is statistically significant that for the other months is less so.

TABLE II

Correlation between pressure and ionization densities

Year and month	Ionospheric parameter	Coefficient of correlation	Probability of occurrence by chance	Standard deviation of pressure	Standard deviation of the parameter
March, 1949	.. Noon time $f^oF_2$	0.70	$0.80 \times 10^{-4}$	2.34 mb	0.53 Mc/s
	Av. day time E-ionisation density	0.57	$0.13 \times 10^{-2}$	1.67 mb	2.94 unit
	Av. night time E-ionization density	0.50	$0.47 \times 10^{-2}$	1.68 mb	2.12 unit
June, 1949	.. $f^oF_2$ at 9 A.M.	0.73	$0.2 \times 10^{-4}$	2.4 mb	0.83 Mc/s
	Av. night time E-ionization density	0.65	$0.9 \times 10^{-1}$	2.27 mb	1.45 unit
July, 1949	.. $f^oF_2$ at 9 A.M.	0.07	$7.3 \times 10^{-1}$	1.85 mb	0.36 Mc/s
September, 1949	$f^oF_2$ at 9 A.M.	0.52	$0.14 \times 10^{-1}$	1.81 mb	0.58 Mc/s
	Av. night time E-ionisation density	0.53	$0.37 \times 10^{-2}$	1.98 mb	2.25 unit
December, 1949	$f^oF_2$ at 9 A.M.	0.02	$9.1 \times 10^{-1}$	2.45 mb	0.60 Mc/s

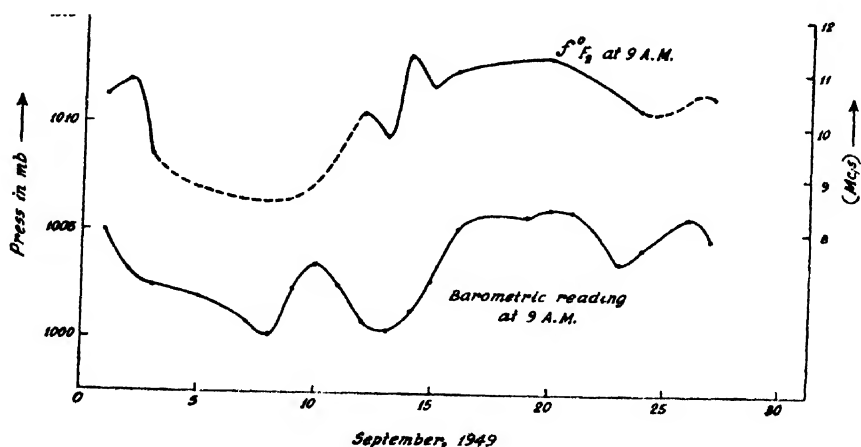


Fig. 6(b)

Illustrating correlation between the day to day variations of surface pressure and critical frequency of the  $F_2$ -layer for September, 1949.

## CONCLUDING REMARKS

The results of observation and statistical analysis described in the preceding section show that in some months, at least, of a year the changes in the ionization

value for a given hour of the day (in course of the month), have strong correlation with pressure changes at the ground at the same hour. Further, for the same months, the variations of the average day time and night time ionization density of the E-region, show good correlation with pressure variation in course of the month at a particular hour. These results are in conformity with those obtained by Martyn and Pulley (1936). We shall not attempt at any explanation of the correlation obtained by us, but shall only mention two suggestions that have been made regarding the modes by which effects of tropospheric pressure variations may be communicated to the ionospheric regions.

One of the suggestions is that the ionospheric variations are caused by variations in the ozone content in the ionospheric regions, it being well known that the ozone content of the ozonosphere is inversely correlated with the pressure variations at the ground. It is suggested that since atmospheric ozone, due to its strong absorption, acts as a solar heat reservoir, the variations of the

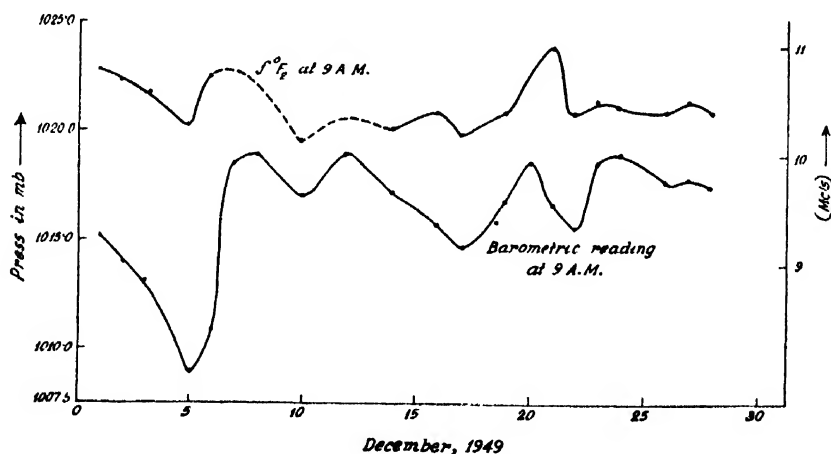


Fig. 7.

Illustrating correlation between the day to day variations of surface pressure and critical frequency of the  $F_2$ -layer for December, 1949.

ozone content will produce temperature variations in the ionospheric regions followed by corresponding variation of ionization density. This explanation may possibly be valid for the E-region, but is difficult to be accepted for the  $F_2$ -region. This is because, on account of the high temperature in this region, any ozone that might find its way there will be speedily dissociated. It has also been suggested (Bannon, *et al*, 1940) that the content of water vapour may be modified by the ozone content and that the effect of such changes of water vapour content may ultimately reach the ionospheric region. Simple considerations show, however, that the time required for water vapour to reach the upper F-region by diffusion is prohibitive.

The other suggestion, due to Kidson (1950), is as follows: It is ordinarily believed that the effects of circulations in the troposphere due to solar heating cannot reach the upper regions of the atmosphere due to the stratosphere acting as a barrier. Any circulatory motion in the high region of the atmosphere is, therefore, supposed to be caused by heat absorption in the upper region itself. It has to be remembered, however, that the wavelengths of these circulations being of the order of 100 km are also of the same order as the thickness of the stratosphere. As such, according to the wave theory, the stratosphere may not act as a perfect barrier to the effects of tropospheric circulations reaching the high ionospheric regions. A connection between disturbances in the troposphere with those in the ionosphere can thus be established.

The two explanations described above regarding the intriguing phenomenon of associations between tropospheric and ionospheric changes, no doubt merit careful consideration. But, they are still to be regarded as more or less tentative. In order that they may be fruitfully developed, it is first necessary to establish unambiguously, by systematic and long continued observations, in different parts of the world, the types of association that actually do exist between changes in surface pressure on the one hand and the ionospheric parameters on the other.

#### ACKNOWLEDGMENTS

Thanks are due to Prof. S. K. Mitra for his help, advice, and guidance throughout the progress of the work and to the Council of Scientific and Industrial Research, Government of India, for financial aid.

Thanks are also due to the Alipore Meteorological Office, Government of India for permitting the author to collect the meteorological data from their observatory.

#### REFERENCES

- Jones, M. W. and Jones, J. G., 1950, *Phys. Rev.*, **77**, 845.  
Martyn, D. F. and Pulley, O. O., 1936, *Proc. Roy. Soc. A*, **154**, 455.  
Levy, H. and Preidel, E. E., 1944, *Elementary Statistics* (Thomas Nelson & Sons Ltd, (London)).  
Bannon, J., Higgs, A. J., Martyn, D. F. and Munro, G. H., 1940 *Proc. Roy. Soc. A*, **174**, 298.  
Kidson, 1950, *Proceedings of the Conference on Ionospheric Physics, Pennsylvania*, p. 12 AA.  
Gerson, N. C., 1950, *Proc. I. R. E.*, **38**, 1456.

# RELATIVE CROSS-SECTIONS OF (n, p) REACTIONS IN SULPHUR 32 AND PHOSPHORUS 31

BY N. K. SAHA AND M. CHOUDHURY

PHYSICS DEPARTMENT, DELHI UNIVERSITY, DELHI.

(Received for publication, February 20, 1953)

**ABSTRACT.** Fast neutrons from a 100 milligram ( $\text{Ra}\alpha + \text{Be}$ ) source have been used to produce (n, p) reactions in  $\text{S}^{32}$  and  $\text{P}^{31}$ . The radioactive end products of the reactions  $\text{P}^{32}$  ( $T \sim 14.2$  days) in the case of  $\text{S}^{32}$ , and  $\text{Si}^{31}$  ( $T \sim 170$  min.) in the case of  $\text{P}^{31}$ , serve as indicators of the reactions. By the principle of 'threshold detector', the initial radioactivity of the end product in each case is a measure of the average cross section of the (n, p)-reaction over a narrow band of neutron-energy between the threshold of the reaction and the upper limit of the effective neutron-energy for capture. The saturation conditions of irradiation and measurement are found out by elaborate preliminary experiments. The initial activity, measured in this way by a G.M. counter under fixed geometry, comes out to be 367 counts per 2 mins for  $\text{S}^{32}$  and 240 counts/2 mins. for  $\text{P}^{31}$ . Various corrections for chemical or isotopic composition of the sample, self absorption of  $\beta$  rays, non-saturation of activity etc. are applied. The ratio of relative cross sections of (n, p) reaction for  $\text{S}^{32}$  to  $\text{P}^{31}$  is finally obtained as  $\sim 2$  with a probable error of about  $\pm 10\%$ . This agrees reasonably well with the ratio  $\sim 2.57$  obtained by Cohen with much higher energy of fast neutrons. Importance of works on these lines for the interpretation of high energy excitation states of nuclei is discussed.

## INTRODUCTION

### *Nuclear reactions with fast neutrons :*

In order to explore the structure of nuclear energy levels in the region of excitation energies higher than 8 Mev, recourse has to be taken primarily to reactions with fast neutrons. The position here is, however, somewhat more complicated than in the reactions with slow neutrons. In the fast neutron reactions, the resonance capture of the neutrons, so common with the capture of slow neutrons in heavy nuclei, is comparatively rare due to the over-lapping of the highly excited states of the compound nucleus. The cross section of fast neutron reactions, therefore, would be small. But here there are chances of sufficient excitation energy being available to the nucleus for the emission of a second particle after the first particle has been emitted ; more than one excited state of the compound nucleus and more than one state of the residual nucleus are likely to contribute to the reaction yield. Thereby the cross section of the neutron reactions may be sometimes considerably enhanced. The study of this reaction is also facilitated in favourable cases if the residual nucleus is radioactive.

On account of the strong short range forces existing between the constituent particles of a nucleus, it can be treated as a condensed phase of its constituents. As in a liquid drop, or in a solid body, an excited state of such a nucleus formed

the absorption of an incident particle cannot be far removed from its original ground state, yet it may possess an excitation energy large enough for the subsequent emission of a single particle. The compound nucleus thus formed has therefore a fairly long life and is a distinct intermediate stage in the nuclear reaction. Its state and decay are independent of the initial process of its formation. This picture will, however, be strictly true when a single quantum state of the compound nucleus has been formed. When a fast incident particle is absorbed in the nucleus, a superposition of several stationary states of a highly excited compound nucleus may result; the course of the nuclear process may then depend strongly on the relative phases of the states and may not be independent of the initial process of excitation. Bohr's method of calculation may not be strictly applicable in such a case. If, however, the density of states of the compound nucleus is very high, so that their widths overlap each other strongly, a great many states can be excited simultaneously by the incident particle. This phase relation of the states may be nearly at random and the resulting process again almost independent of the way of excitation. In such a case classical considerations may again be justified. Indeed, a statistical method assuming the existence of average values of certain magnitudes over states within not too wide interval of excitation-energy may then be applied. Weisskopf (1947) has shown that within the limits of validity of the statistical considerations discussed above, the cross section of a non-resonance process ( $a, b$ ) produced by the fast particles can be taken to be of the form:

$$\sigma(a, b) = \sigma_a \eta_b; \quad \eta_b = \Gamma_b / \Lambda \quad \dots\dots\dots (1)$$

where  $\sigma_a$  is the cross section for the formation of the compound nucleus by the capture of the particle  $a$  and  $\eta_b$  is the relative probability for the emission of the particle  $b$  from the compound nucleus. The quantity  $\eta_b$  is the ratio of the average (over all energy states) partial width  $\Gamma_b$  for the emission of  $b$ , to the average total width  $\Lambda$  for all kinds of particles. Based on the above model, Weisskopf has given the method of calculating the approximate cross sections of fast neutron reactions like (n, p), (n, n), (n, 2n), (n,  $\alpha$ ) etc. Confining our discussions to reactions with high energy neutrons alone as the incident particle, it is clear that

$$\sigma_a = \sigma_b \triangleq \pi r^2 \quad \dots\dots\dots (2)$$

where  $r$  is the nuclear radius. The process which may now result after the disintegration of the compound nucleus can be reactions of the type (n, p), (n, n), (n, 2n), (n,  $\gamma$ ) and (n,  $\alpha$ ), which are likely to compete with each other in accordance with the relative probabilities of these processes.

The (n, p) reactions are endothermic in character and can take place only with fast neutrons. They are generally less probable than the (n, n) reactions because of the potential barrier preventing the proton from escaping from the nucleus as easily as the neutron. They would predominantly proceed through closely lying energy states of high excitation energy and their cross section would be of measureable value only if neutron energies of several Mev above the threshold

energy of the reaction are employed, since the outgoing proton would need that much of energy to penetrate the potential barrier. If the incident neutron energy-surplus over the threshold is large compared to the nuclear temperature  $T$ , then the processes like  $(n, 2n)$  should be the dominant feature and the cross section for the  $(n, 2n)$  reaction would nearly be equal to  $\sigma_n$ . The  $(n, \alpha)$  reactions have an extremely small cross section in the heavy nuclei and in general their values will be smaller than those for the  $(n, p)$  reactions because of the higher potential barrier for the outgoing  $\alpha$ -particle. Further, the simple capture of the neutrons leading to radiative processes like  $(n, \gamma)$  should also possess very small cross section at neutron energies exceeding 1 Mev, when the cross section  $\sigma(n, n)$  for inelastic scattering of neutrons becomes considerable. The small chance of occurrence of the  $(n, \alpha)$  and  $(n, \gamma)$  reactions with fast neutrons in medium heavy nuclei can, therefore, be almost left out of account in the range of neutron energies in which the  $(n, p)$  reaction has generally a large cross section. The  $(n, 2n)$  reaction also does not compete seriously with the  $(n, p)$  reaction, when the energy of the neutrons employed is not more than a few Mev above the threshold energy of the  $(n, p)$  reaction.

Experiments have been performed by Jensen (1944), Dunlop and Little (1941), Cohen (1951) and others whose results can be used to verify the conclusions of Weisskopf's theory and to obtain approximate data on the structure of the energy levels in the high energy regions in some nuclei. The investigations are still in the initial stages. In most of these works, however, high energy neutrons produced by cyclotron-accelerated deuterons have been used. Although neutrons of more or less controlled energy can be produced by this method, the upper limit of the neutron energy spectrum generally obtained in this way is quite high (vide Cohen, 1951, figure 1). Consequently the  $(n, p)$  reactions produced by these neutrons are very often complicated by other types of reactions like  $(n, 2n)$ ,  $(n, \alpha)$ ,  $(n, n)$  etc., taking place simultaneously. We propose, therefore, to use the fast neutrons from a 100 mgm ( $Ra\alpha + Be$ ) neutron source available in this laboratory to study some  $(n, p)$  reactions with fast neutrons. The upper limit of the neutron energy spectrum from such a source is about 11 Mev (Teucher, 1949) and the spectrum has a flat maximum over the range about 2 to 4.5 Mev. With these average energies of the fast neutrons, reaction types  $(n, 2n)$ ,  $(n, \alpha)$  etc., are not likely to occur with any appreciable intensities, whereas, the  $(n, p)$  reactions are expected to be the predominant feature in the medium heavy nuclei, for which the  $(n, p)$  reaction threshold generally lies between 1 and 2.5 Mev. The average cross section of  $(n, p)$  reactions in these nuclei could therefore be studied with comparatively simple technique, as explained below, when a fairly strong ( $Ra\alpha + Be$ ) neutron source was employed.

#### METHOD OF THRESHOLD DETECTORS

In the cases where the  $(n, p)$  reactions in the nuclei lead to radioactive bodies, the relative cross section of the process can be determined by the method



of threshold detectors. For this a target material is chosen which becomes radioactive on absorbing neutrons of energies above a certain threshold value  $E_t$  and subsequently emits a  $\gamma$ -quantum, a proton or an  $\alpha$ -particle. It is important that the target nuclei are given an equilibrium exposure to the neutron source. If the neutrons from the source possess the proper threshold energy  $E_t$  and a wide spectrum extending up to the maximum energy  $E_m$  then assuming that there is no discontinuity in the capture cross section for activation in this region, the total initial activity produced can be written as

$$A = \int_{E_t}^{E_m} n_0 \cdot \sigma(E) \cdot F(E) \cdot dE$$

where  $n_0$  is the number of nuclei of the species to be activated by the neutrons in the target;  $\sigma(E) \equiv \sigma(n, p)$  denotes the cross section of the (n, p) reaction for the neutrons of energy  $E$ , to which the activity  $A$  is due,  $F(E)$  is the neutron flux in the energy range  $E$  and  $E+dE$ . The average cross section of the (n, p) reaction between  $E_t$  and  $E_m$  can thus be estimated by measuring the saturation activity  $A$  of the detector, if the flux  $F(E)$  and the fast neutron energy spectrum of the source are known;  $E_t$  can be determined from the energy balance of the (n, p) reaction under question. If, however, the neutron flux and the energy spectrum of the source are not absolutely known but remain constant, then careful measurements of the initial saturation activity of several detectors under strictly comparable geometrical conditions are expected to give relative cross sections of the (n, p) reactions in the detector nuclei. Such studies of the variation of  $\sigma(n, p)$  from element to element is expected to give useful information about the density of energy levels in the region of high excitation energy for these elements.

#### EXPERIMENTAL DETAILS

Samples of active material were placed as coaxial cylinders just outside a  $\beta$ -ray G. M. counter (0.1 mm. thick copper wall). Pure reprecipitated flower of sulphur was exposed to neutrons from the 100 mgm (Ra $\alpha$ +Be) source, filtered through about 1 mm of cadmium. For phosphorus, ammonium-dihydrogen-phosphate was used. Identical geometry of irradiation to the neutron source was employed throughout. Radio-active  $^{32}_{15}\text{P}$  of mean half-life 14.2 days was obtained by the (n, p) reaction in  $^{32}_{16}\text{S}$  and likewise  $^{31}_{14}\text{Si}$  of half-life 170 min. was obtained from  $^{31}_{15}\text{P}$ . In both the cases the threshold energy of the (n, p) reaction was about 1 Mev. In the case of  $^{31}_{15}\text{P}$ , an additional short period activity seems to have developed (vide figure 2), apparently due to  $^{30}_{15}\text{P}$  produced by the (n, 2n) reaction.

For quantitative comparison of cross sections, measurements should be made such that (1) saturation mass of the substance to be activated is exposed to the neutron-source, for saturation period; if possible, (2) saturation thickness of the well-mixed active substance should be examined for initial activity.

Condition (1) will ensure that even the fastest neutrons from the source may acquire the appropriate mean free path of collision in passing through the sample nuclei. Condition (2) will ensure that maximum possible number of  $\beta$ -rays from the active layer is reaching the counter. These saturation conditions have been discussed by Jensen (1944). Prolonged and painstaking investigations were made in order to determine these saturation conditions and from the results obtained it was finally decided to expose 407 gm of sulphur and 494 gm of the phosphate to the fast neutron source for final measurement.

The investigation of the saturation thickness of the active layers for measurement of the saturation activity was carried out with the activated saturation mass of the substance which was thoroughly mixed up to obtain the average effect. Thin cells of the active powder were then prepared in very thin paper cylinders supported by wide-meshed wire net inside and transparent alkathene cylinder outside. A saturation thickness of 0.6 gm/cm<sup>2</sup> for sulphur and 0.35 gm/cm<sup>2</sup> for the phosphate were obtained.

For the final measurement of the initial activity produced by the (n,p) reactions in sulphur a permanent cell was constructed with thin paper and wire gauge cylinder backing inside and a strong coaxial cylinder of brass outside. The inner cylinder was 4.25 cm in diameter and the well mixed activated sulphur was closely packed into a layer 8.9 cm high and 1.04 cm thick to give the required saturation layer of density 0.6 gm/cm<sup>2</sup>. The mass of this active layer was 90 gm. To measure the activity of this cell, the  $\beta$ -ray counter mentioned above was used under strictly reproducible geometry with 10 cm of lead shielding all around. The decay of the sample was followed regularly for 31 days. The semi-logarithmic plot of the nett activity is shown in figure 1, which clearly gives a half-life of 14.2 days.

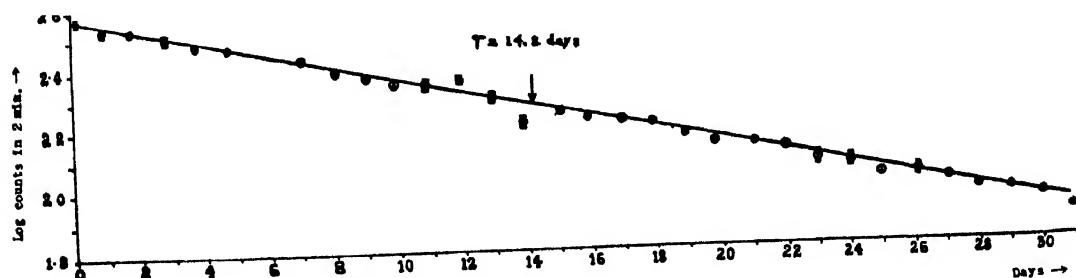


Fig. 1.

The decay curve of radio phosphorus  $P^{32}$  produced by the (n, p)-reaction in  $S^{32}$ .

Similar observations were made for a saturation mass of the activated phosphate (irradiated for 39 hrs to fast neutrons) and taken in the form of a shell similar to that of sulphur. The thickness of the shell was 0.26 cm and its weight was 42 gm, in order to give the saturation thickness of 0.35 gm/cm<sup>2</sup>. The activity of the shell was followed for 4½ hours. The average of three such sets of observations is shown as logarithmic plot in figure 2. The half-life of the activity is clearly 170 min.

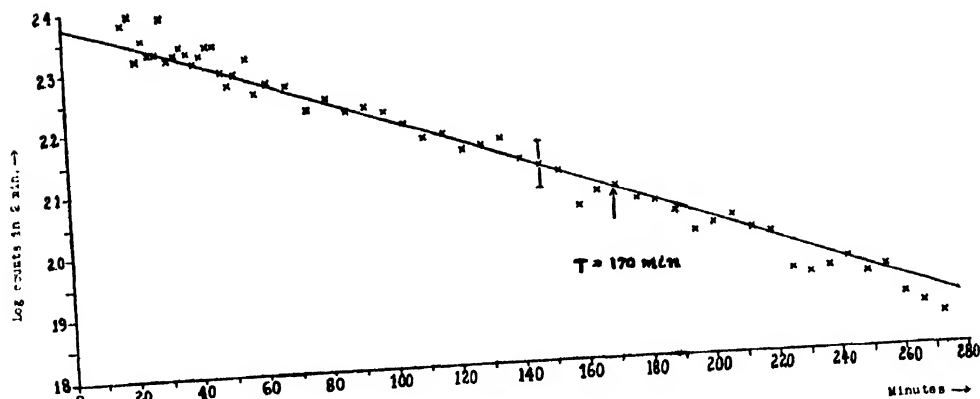


Fig. 2.

The decay curve of radio silicon  $\text{Si}^{31}$  produced by the (n, p)-reaction in  $\text{P}^{31}$ . The points near the beginning lie somewhat above the line and probably indicate the presence of a short period activity ( $\text{P}^{30} \sim 2.5$  min) produced by the (n, 2n) reaction in  $\text{P}^{31}$ .

### CORRECTIONS APPLIED

The initial activities obtained by extrapolating curves (1) and (2) to zero time are 367 counts per two min for sulphur and 240 counts per two min for the phosphate. The following corrections were applied to these values :

(a) A conversion factor of 1.05 to convert sulphur to the pure isotope  $\text{S}^{32}$ , there being 4.2% of  $\text{S}^{34}$  in the sample tested. Similarly a factor of 3.625 is necessary to convert the phosphate to the pure element.

(b) Since quite thick layers of the active substances were used for our measurements, the correction for self-absorption of  $\beta$ -rays in the layers is essential, but correction for back scattering of  $\beta$ -rays by the sample holder can be neglected (vide Metzger, Alder and Huber, 1948). The correction factors of 23% for sulphur and 18% for the phosphate were obtained by using the method given by the above authors. Almost identical results were obtained by another method suggested by Cohen (1951).

(c) In the case of sulphur, the half-life of activity being 14.2 days, the saturation activity was not attained by irradiating it for 94 hours, as we did. The correction factor on this account was calculated to be 5.7. The phosphate sample was always irradiated for saturation time and hence no correction was necessary for it on this account.

### RESULT

The corrected initial activity (which is proportional to the cross section of the (n, p)-reaction) for sulphur  $\text{S}^{32}$  therefore becomes :

$$\frac{367 \text{ counts}}{2 \times 60 \text{ sec.}} \times \frac{1.05 \times 5.7}{0.23} \doteq 79.$$

For phosphorus  $\text{P}^{31}$  :

$$\frac{240 \text{ counts}}{2 \times 60 \text{ sec.}} \times \frac{3.625}{0.18} \doteq 40.$$

The ratio of the two cross sections

$$\frac{\sigma(n, p)S^{32}}{\sigma(n, p)P^{31}} \simeq 2$$

The overall probable error of this determination is  $\pm 10$  to  $15\%$ .

#### REMARKS

The relative cross section for sulphur comes out to be about twice that for phosphorus. This result agrees within the limits of experimental error, with the (n, p) reaction cross section observed by Cohen (1951) who obtained  $28.5 \times 10^{-26} \text{ cm}^2$  for  $S^{32}$  and  $12.0 \times 10^{-26} \text{ cm}^2$  for  $P^{31}$ , which give a ratio 2.37. Fast neutrons of energy ranging upto  $\sim 18$  Mev were used for the reaction by Cohen. This energy limit being higher than the maximum neutron energy ( $\sim 11$  Mev, Teucher, 1949) from a (Raa+Be) source used by us, there may be difference in the state of excitation of the nuclei in the two cases leading to difference in the reaction cross sections. Metzger, Alder and Huber (1948) have observed a resonance effect in the excitation function of the reaction  $P^{31}(n, p)Si^{31}$ , the cross section slowly increasing linearly between the neutron energies 2.3 and 3 Mev, and reaching the maximum value of  $7.4 \times 10^{-26} \text{ cm}^2$  at 3 Mev. Thereafter the cross section begins to fall at high neutron-energies. For S some results of the total capture cross section as a function of neutron energy have been given by Adair (1950) and others. According to these authors a large number of resonance peaks exists for neutron capture in  $S^{32}$  between 0.1 and 4 Mev neutron energies, a region in which the (Raa+Be) neutron spectrum is particularly rich. The cross section for (n,p) reaction in  $S^{32}$  is therefore likely to be higher than in  $P^{31}$ . Further work on the absolute measurement of these cross sections would be necessary to clarify the position. Measurements of the absolute cross section of the (n, p) reaction in one of the nuclei and the relative cross section for a number of other cases are in progress. General considerations regarding the density and structure of the nuclear energy levels in the region of high excitation energy can probably be attempted in the light of the theory (vide Weisskopf, 1947) when these measurements are completed.

#### ACKNOWLEDGMENTS

We take this opportunity to express our sincere thanks to Professor D. S. Kothari and Prof. R. C. Majumdar for constant encouragement in course of this work and to Mr. S. K. Nandi and Mr. L. Kasturi Rangan for helping us with some of the measurements. The work has been done under the financial support of the Atomic Energy Commission, Ministry of Research and Natural Resources, Government of India.

#### REFERENCES

- Adair, R. K., 1950 *Rev. Mod. Phys.*, **22**/3, 249.
- Cohen, B. L., 1951, *Phys. Rev.*, **81**, 184.
- Dunlop, H. F. and Little, R. N., 1941, *Phys. Rev.*, **60**, 693.
- Jensen, P., 1944, *Z. f. Phys.*, **122**, 387.
- Metzger, F., Alder, F. and Huber, P., 1948, *Helv. Phys. Acta*, **21**, 278.
- Teucher, M., 1949, *Z. f. Phys.*, **126**, 410.
- Weisskopf, V., 1947, *Declassified Lecture Series in Nuclear Physics*, U.S.A.E.C.

# ELECTRONIC SPECTRA OF MOLECULES CONTAINING SIX AND FIVE MEMBERED RINGS.

## CALCULATION OF ENERGY LEVELS

BY G. VISWANATH

PHYSICS DEPARTMENT, ANDHRA UNIVERSITY, WALT AIR

*(Received for publication, October 23, 1952)*

**ABSTRACT.** Using atomic orbital method the region of absorption of the indene molecule has been predicted at  $\lambda$  3228 which agrees fairly with the experimental value at  $\lambda$  2952.

There are two independent methods of approach for the calculation of the ground and excited energy levels of polyatomic molecules—the valence bond or the atomic orbital method and the method of molecular orbitals (usually called the AO and MO methods). Both the methods give molecular ground states which are in satisfactory agreement with each other. The calculation of excited states is, however, more tentative. In recent investigations the two theoretical methods have been much improved by taking ionic structures into consideration in the atomic orbital method and antisymmetrization of molecular orbitals in the molecular orbital method. These improved methods have yielded better values which are in closer agreement with the experiment, within the limits of the approximations involved.

Sklar (1937) employed the AO method in the calculation of energy levels of benzene, fulvene and azulene. Without utilising the optical data of those molecules he could predict the longer wavelength region of absorption. There was slight disagreement in the values for absorption near 2000  $\text{\AA}$ . The calculated wavelengths are too short. In the case of benzene the predicted region of absorption was at 1400  $\text{\AA}$  but the experimentally observed absorption region is at 2000  $\text{\AA}$ . Calculations taking ionic structures into consideration, carried out by Craig (1949) have removed these discrepancies. Similar calculations were made in the case of naphthalene at first taking sixteen canonical structures which preserve the shape of the molecule and later taking all the 42 possible canonical structures to make the calculations more rigorous.

The molecular orbital method in its improved form was first applied in the calculations of energy levels of benzene by Sklar and Goppert Meyer (1938) for predicting the region of absorption and the determination of the relative intensities of benzene and its derivatives. Coulson and others (1948) have extended those calculations for naphthalene and higher hydrocarbons. Similar calculations were carried out in case of the diphenyl molecule, which belongs to a different series of molecules, by London (1945).

In the present paper the energy levels of fused five and six membered rings represented by molecules of the type of indene have been calculated by means of

the AO method as employed by Sklar. The actual state of any molecule can only be visualised as being represented by a set of structures which independently do not represent the actual state of molecule but only extreme states. It can be shown by quantum mechanics that the number of such independent (canonical) structures is given by

$$\frac{n}{2} ! \left( \frac{n}{2} + 1 \right) !$$

where  $n$  is the number of non-localized electrons.

Thus for benzene there are five canonical structures two of them being Kekule and three being Dewar ones. In the case of naphthalene which possesses ten non-localized electrons, the number of structures which contribute to the final state of the molecule is 42. In the case of anthracene which has 14 non-bonding electrons, the number of canonical structures is as large as 429. Sklar explained that the absorption bands are due to transitions between levels which arise from the resonance between the states corresponding to the various canonical structures. As the structure of the molecule becomes more and more complicated one has to resort to several approximations. Since the electronic transitions are dependent on the resonance between double bonds in complicated molecules the problems in aromatic systems can be simplified without much loss of accuracy by neglecting all electrons excepting those forming  $\pi$  bonds. Justification for doing such a simplification is that  $\pi$  wave functions have a node in the plane of the ring so that the overlapping between them and the function for an electron forming a bond in the plane is very small.

The number of canonical structures that should be taken into account for the calculation of the energy levels of indene molecule is 14. Of these, the number which preserve the shape of the molecule is seven; these are given below :

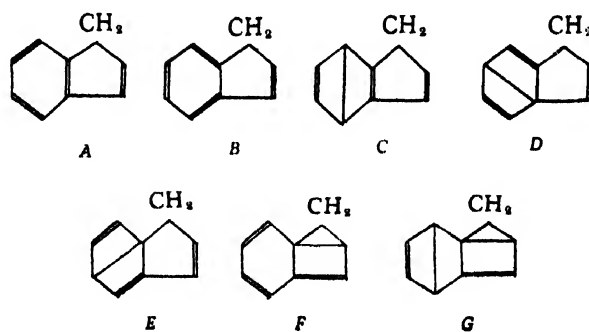


Fig. 1

The true state of the molecule may be considered as a resonance hybrid of the above seven structures (A to G). The carbon atom of  $\text{CH}_2$  group in the five membered ring is connected to two carbon atoms and two hydrogen atoms by 4  $\sigma$  bonds, because the bond formed from an  $s$  electron of one atom and  $p$  electron of

at other atom is a  $\sigma$  bond. As only  $\pi$  electrons are considered, the problem may be regarded as an eight-electron one, which is intermediate between benzene (6 electrons) and naphthalene (10 electrons).

The general method for the determination of energy levels is to set up and solve the secular equation as given below

$$|H_{LM} - \Delta_{LM} E| = 0$$

$$\text{where } H_{LM} = \int \psi_L H \psi_M d\tau \quad \text{and } \Delta_{LM} = \int \psi_L \psi_M d\tau$$

where  $\psi_L$  and  $\psi_M$  are the eigenfunctions of structures  $L$  and  $M$  and  $H$  being the Hamiltonian excluding electrons.

$H_{LM}$ 's can be calculated with the help of the following equation.

$$H_{LM} = -\frac{2x}{2y} \left[ Q + \frac{3}{2} \left\{ \Sigma J \left( \frac{\alpha}{\beta} \right) - \Sigma J (\alpha\beta) \right\} - \frac{1}{2} \Sigma J_{ij} \right]$$

where  $x$  = the number of islands formed by the superposition of structure  $L$  over  $M$ .

$y$  = the number of bonds.

$Q$  = coulombic integral

$\Sigma J (\alpha/\beta)$  = sum of single exchange integrals between electrons in the same island with opposite spins.

$\Sigma J (\alpha\beta)$  = sum of single exchange integrals between electrons in the same island with same spin.

By an island is meant a set of electrons so related that the spin of one fixes the spins of all others.  $\Delta_{LM}$ 's can be readily calculated by observing that it is equal to the coefficient of  $Q$  in  $H_{LM}$ 's.

In case of indene molecule the number of islands that are formed by superposing one canonical structure over another are given below :

	<i>A</i>	<i>B</i>	<i>C</i>	<i>D</i>	<i>E</i>	<i>F</i>	<i>G</i>
<i>A</i>	4	2	3	3	3	3	2
<i>B</i>	2	4	3	3	3	1	2
<i>C</i>	3	3	4	2	2	2	3
<i>D</i>	3	3	2	4	2	2	1
<i>E</i>	3	3	2	2	4	2	1
<i>F</i>	3	1	2	2	2	4	3
<i>G</i>	2	2	3	1	1	3	4

The islands themselves are shown below in the usual notation (i.e., the electrons with spin  $\alpha$  are given in the numerator and those with spin  $\beta$  in the denominator in one island and closed by a bracket). The  $\pi$  electrons in the ring are denoted by letters ' $a \dots i$ ' as shown below.

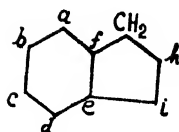


Fig. 2

Islands	
A.A.	$(a/b)(c/d)(c/f)(h/i)$
A.B.	$(ace/hdf)(h/i)$
A.C.	$(ac/bd)(c/f)(h/i)$
A.D.	$(ae/bf)(c/d)(h/i)$
A.E.	$(a/b)(ce/fd)(h/i)$
A.G.	$(ac/bd)(ch/fi)$
B.B.	$(a/f)(b/c)(d/c)(h/i)$
B.C.	$(ac/fd)(b/c)(h/i)$
B.D.	$(a/f)(bd/cc)(h/i)$
B.E.	$(ac/bf)(d/e)(h/i)$
B.F.	$(acch/bdif)$
B.G.	$(ach/dif)(b/c)$
C.C.	$(a/d)(b/c)(c/f)(h/i)$
C.D.	$(ace/dbf)(h/i)$
C.E.	$(ace/dbf)(h/i)$
C.F.	$(ac/bd)(ch/fi)$
C.G.	$(a/d)(b/c)(ch/fi)$
D.D.	$(a/f)(b/c)(c/d)(h/i)$
D.E.	$(ace/fdb)(h/i)$
D.F.	$(ahc/fib)(c/d)$
D.G.	$(abec/fibd)$
E.E.	$(a/b)(c/f)(d/c)(h/i)$
E.F.	$(a/b)(che/fid)$
E.G.	$(ache/bfid)$
F.F.	$(a/b)(c/d)(c/i)(f/h)$
F.G.	$(ac/bd)(c/i)(h/f)$
G.G.	$(a/d)(b/c)(c/i)(f/h)$

In this connection it must be remembered that the number of islands obtained by superposing structure  $L$  over  $M$  is equal to the number obtained by doing the converse.

Taking only the single exchange integrals between electrons on adjacent carbon atoms into consideration and treating all other single exchange integrals and multiple exchange integrals, as equal to zero the following values for  $H_{LM}$  are obtained.

$H_{AA} = Q + 5\alpha/2$	$H_{BG} = Q/4 + \alpha$
$H_{AB} = Q/4 + 7\alpha/4$	$H_{CC} = Q + \alpha$
$H_{AC} = Q/2 + 2\alpha$	$H_{CD} = Q/4 + 7\alpha/4$
$H_{AD} = Q/2 + 2\alpha$	$H_{DF} = Q/4 + \alpha$
$H_{AE} = Q/2 + 2\alpha$	$H_{DG} = Q/8 + 7\alpha/8$
$H_{AF} = Q/2 + 5\alpha/4$	$H_{EE} = Q + \alpha$
$H_{AG} = Q/4 + \alpha$	$H_{EF} = Q/4 + \alpha$
$H_{BB} = Q + 5\alpha/2$	$H_{EG} = Q/8 + 7\alpha/8$
$H_{BC} = Q/2 + 2\alpha$	$H_{FF} = Q - \alpha/2$
$H_{BD} = Q/2 + 2\alpha$	$H_{FG} = Q/2 + \alpha/2$
$H_{BE} = Q/2 + 2\alpha$	$H_{GG} = Q - 2\alpha$
$H_{BF} = Q/8 + 7\alpha/8$	

Putting  $Q - E = x$  the secular determinant\* is

$$\begin{vmatrix}
 x + 5\alpha/2 & x/4 + 7\alpha/4 & x/2 + 2\alpha & x/2 + 2\alpha & x/2 + 2\alpha & x/2 + 5\alpha/4 & x/4 + \alpha \\
 x/4 + 7\alpha/4 & x + 5\alpha/2 & x/2 + 2\alpha & x/2 + 2\alpha & x/2 + 2\alpha & x/8 + 7\alpha/8 & x/4 + \alpha \\
 x/2 + 2\alpha & x/2 + 2\alpha & x + \alpha & x/4 + 7\alpha/4 & x/4 + 7\alpha/4 & x/4 + \alpha & x/2 + \alpha/2 \\
 x/2 + 2\alpha & x/2 + 2\alpha & x/4 + 7\alpha/4 & x + \alpha & x/4 + 7\alpha/4 & x/4 + \alpha & x/8 + 7\alpha/8 \\
 x/2 + 2\alpha & x/2 + 2\alpha & x/4 + 7\alpha/4 & x/4 + 7\alpha/4 & x + \alpha & x/4 + \alpha & x/8 + 7\alpha/8 \\
 x/2 + 5\alpha/4 & x/2 + 7\alpha/8 & x/4 + \alpha & x/4 + \alpha & x/4 + \alpha & x - \alpha/2 & x/2 + \alpha/2 \\
 x/4 + \alpha & x/4 + \alpha & x/2 + \alpha/2 & x/8 + 7\alpha/8 & x/8 + 7\alpha/8 & x/2 + \alpha/2 & x - 2\alpha
 \end{vmatrix} = 0$$

\* The method of solving the determinant is given in the Appendix at the end of the paper.



To solve this determinant the value of  $\alpha$  is taken as -1.92 e.v. and substituted for  $\alpha$  in the above and the roots are determined. They are -103.75, -6.33, ~~1.53, -0.69i~~, 1.53 + 0.69i, 1.53 - 0.69i.

Rejecting the complex roots the energy values obtained are  $Q+103.75$ ,  $Q-1.92$ ,  $Q+6.33$ ,  $Q-1.92$ .

The only distinct element of symmetry of this molecule is molecular plane. So it belongs to the point group  $C_s$  and has the following character table.

$C_s$	$E$	$\sigma_h^2$	$n_i$
$A'$	+1	+1	34
$A''$	+1	-1	17
$U_r$	17	17	
$hpf_p$	51	17	

As there are two states only one band system can be observed. The energy value of this band system can be predicted by considering the differences in energies between levels represented by  $Q-1.92$  (ground level) and the rest. From the foregoing calculations, an electronic transition from the ground level to the excited level  $Q+1.92$  gives an energy difference of 3.84 electron volts, which corresponds to an absorption at  $\lambda$  3228 Å°. The experimentally observed absorption region is at  $\lambda$  2952. The discrepancy may not be considered as large comparing similar values for benzene obtained by the simple AO method. The calculated and observed absorption regions determined in case of benzene by Sklar are at  $\lambda$  2470 and  $\lambda$  2590 respectively.

#### A P P E N D I X

The secular equation to be solved is

$$\begin{vmatrix} 2a & 2b & c & c & c & a & d \\ 2b & 2a & c & c & c & b & d \\ c & c & 2c & 2b & 2b & d & c \\ c & c & 2b & 2c & 2b & d & b \\ c & c & 2b & 2b & 2c & d & b \\ a & b & d & d & d & f & c \\ d & d & c & b & b & c & g \end{vmatrix} = 0$$

$$\text{where } a = \frac{x}{2} + \frac{5a}{4}b - \frac{x}{8} + \frac{7a}{8}c - \frac{x}{2} + \frac{2a}{4}d - \frac{x}{4} + \frac{a}{2}e - \frac{x}{2} + \frac{a}{2},$$

$$f = x - \frac{a}{2}, g = x - 2a$$

$x$  is the unknown.  $\alpha = -1.92$ .

To simplify the left hand side determinant subtract the 2nd row from the 1st row, the 4th row from the 3rd, and the 5th row from the 4th, getting

$$\begin{vmatrix} 2(a-b) & 2(b-a) & 0 & 0 & 0 & a-b & 0 \\ 2b & 2a & c & c & c & b & d \\ 0 & 0 & 2(c-b) & 2(b-c) & 0 & 0 & c-b \\ 0 & 0 & 0 & 2(c-b) & 2(b-c) & 0 & 0 \\ c & c & 2b & 2b & 2c & d & b \\ a & b & d & d & d & f & c \\ d & d & c & b & b & c & g \end{vmatrix}$$

Now subtracting the 4th column from the 3rd column and the 5th column from the 4th column, this becomes

$$\begin{array}{ccccccc|c}
 2(a-b) & 2(b-a) & 0 & 0 & 0 & a-b & 0 & \\
 2b & 2a & 0 & 0 & c & b & d & \\
 0 & 0 & 4(c-b) & 2(b-c) & 0 & 0 & c-b & \\
 0 & 0 & 2(b-c) & 4(c-b) & 2(b-c) & 0 & 0 & \\
 c & c & 0 & 2(b-c) & 2c & d & b & \\
 a & b & 0 & 0 & d & f & e & \\
 d & d & c-b & 0 & b & c & g & \\
 \hline
 = (a-b) & (c-b) & 2(b-c) & 2 & -2 & 0 & 0 & 0 & 1 & 0 \\
 & 2b & 2a & 0 & 0 & c & b & d & & \\
 & 0 & 0 & 4 & -2 & 0 & 0 & 1 & & \\
 & 0 & 0 & 1 & -2 & 1 & 0 & 0 & & \\
 & c & c & 0 & 2(b-c) & 2c & d & b & & \\
 & a & b & 0 & 0 & d & f & e & & \\
 & d & d & c-b & 0 & b & c & g & & 
 \end{array}$$

Equating this to zero we get at once  $a-b=0$ ,  $c-b=0$ ,  $2(b-c)=0$  giving us the roots  $x = -a$ ,  $x = +a$ ,  $x = +a$  ( $a$  being 1.92). The remaining part of the equation is then

$$\begin{array}{ccccccc|c}
 2 & -2 & 0 & 0 & 0 & 1 & 0 & \\
 2b & 2a & 0 & 0 & c & b & d & \\
 0 & 0 & 4 & -2 & 0 & 0 & 1 & \\
 0 & 0 & 1 & -2 & 1 & 0 & 0 & \\
 c & c & 0 & 2(b-c) & 2c & d & b & \\
 a & b & 0 & 0 & d & f & e & \\
 d & d & c-b & 0 & b & c & g & 
 \end{array} = 0$$

Substituting for  $a, b, c, d, e, f, g$ , expanding and clearing fractions this becomes, on putting  $a = -1.92$ .

$$x^4 + 107.03 x^3 + 329.19 x^2 + 1102.89 x + 4955.14 = 0$$

A preliminary examination shows this has two negative and two complex roots

This equation has been solved by the root squaring method of Whittaker and Robinson. The roots are

$$-103.75, -6.33, 1.53 \pm 0.69i \text{ (to the second decimal place).}$$

#### ACKNOWLEDGMENT

The author is deeply indebted to Prof. K. R. Rao for his valuable guidance during the course of this investigation.

#### REFERENCES

- Sklar, A. L., 1937, *J.C.P.*, **5**, 669.  
 Goppert Meyer, M. and Sklar, A. L., 1938, *J.C.P.*, **6**, 645.  
 Craig, D. P., 1949, *P.R.S.*, **200**, 401.  
 Coulson, C. A., 1948, *Proc. Phy. Soc.*, **60**, 257.  
 London, A., 1945, *J.C.P.*, **13**, 396.

# OBLIQUE PROPAGATION OF RADIO WAVES OVER A CURVED EARTH \*

By B. CHATTERJEE

INSTITUTE OF RADIOPHYSICS, UNIVERSITY COLLEGE OF SCIENCE, CALCUTTA

(Received for publication, February 7, 1953)

**ABSTRACT.** Booker's analysis of oblique propagation of radio waves through the ionosphere over a flat earth, taking into considerations the effect of terrestrial magnetic field, has been extended to the case of the curved earth. This is done by introducing appropriate correction factors into the equations for the flat earth case to take account of the curvature effect. It

and that for the case of curved ionosphere, the value of  $x$ , ( $x = \frac{4\pi e^2}{mp} N$ , where  $N$  is the ionization density) is higher at the point of reflection in the deviating region. As a result of this, the values of group retardation, lateral deviation and attenuation in the deviating region as calculated for the curved earth case, are higher than those for the flat earth. These values for the curved earth are found to agree better with experimental results

## 1. INTRODUCTION

Study of the modes of propagation of radio waves incidents obliquely on the ionospheric layers is of great practical importance, because, all long distance radio communications are carried out by such obliquely propagated waves. Unfortunately, generalised mathematical treatment of oblique propagation, taking into account the effects of both the curvature of the ionospheric layers and of the terrestrial magnetic field, is too involved and laborious to be of much practical use. All workers in this field have, therefore, treated simplified cases by neglecting the one or the other effect. For example, Appleton and Beynon (1940) in their analysis of ionospheric propagation over the curved earth have neglected the effect of the terrestrial magnetic field. Booker (1938) in his analysis, on the other hand, while considering the effect of the terrestrial magnetic field, simplified the treatment by neglecting the earth's curvature. The same simplification has also been made by Gerson and Seaton (1948) in their extension of Booker's analysis, in which they took into considerations the polarization induced in the ionosphere considered as a dielectric.

Consideration of the general case of oblique propagation problem is, however, important, not only on account of its practical value, but also because it serves to check how far the effects of neglecting the terrestrial curvature or the terrestrial magnetic field lead to errors of significant importance. An attempt has been made in this paper to treat the oblique propagation problem by taking both the effects into account. In making this attempt it was soon found that the general analysis is not only long and laborious but also that the interpretation of the results of such analysis would be difficult. As such it was thought advisable to start with Booker's method of analysis for the plane earth and to introduce

\* Communicated by Prof. S. K. Mitra.

into it corrections in the appropriate stages to take into account the effect of the curvature of the ionospheric strata.

It is to be remembered that Booker's analysis is based on the ray treatment, that is, on the so called "slowly varying" approximation. Such treatment is applicable only to short and medium waves with which all practical radio communications are carried out. It is inapplicable to the cases of long and very long waves for which wave treatment is necessary. Such wave treatment for the general case of oblique propagation is also wanting, though, some special cases have been studied, e.g. Wilkes (1940, 1947) and Stanley (1950) on vertical incidence and Heading and Whipple (1952) on oblique incidence in presence of a vertical magnetic field.

## 2. WAVE PROPAGATION IN THE IONOSPHERE AT OBLIQUE INCIDENCE

For simplifying the analysis and also for obtaining a clearer picture of the modes of oblique propagation, we shall assume that the ionosphere consists of

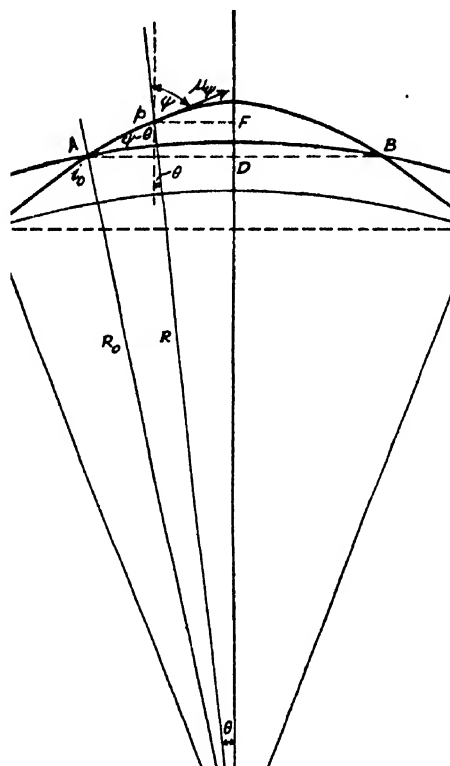


FIG. 1.

Approximate ray path  $T.ABZ$  for propagation through a curved ionosphere concentric with the curved earth. (not to the scale).

$R_0 = Op$  = distance from the earth-centre of the point in the ionosphere where the propagation is being considered.

spherically stratified layers of ionization concentric with the earth and the ionization density changes only along the radial direction. The results obtained with this simplified analysis may be modified, as necessary, to take into consideration the effects of tides, winds, etc.

In figure 1, let  $T$  be the transmitter and  $Z$  the receiver, and let the radio linkage be made by single hop ionospheric reflection. Let the ray meet the bottom layer of the ionosphere, making an angle  $i$  with the radial direction. The rectangular co-ordinates are so chosen that the vertical direction is along  $OM$ , being denoted by direction 3, and the horizontal plane contains the line  $AB$  which is parallel to the chord  $TZ$ . Let the 23 plane be the plane of incidence, the direction 2 lying along  $AB$  (figure 2). We can write the expressions for the polarization vector  $\mathbf{P}$  and the electric intensity  $\mathbf{E}$  of a magneto-ionic component of the electromagnetic wave as

$$\left. \begin{aligned} \mathbf{P} &= a \exp [ik (ct - \mu l)] \\ \mathbf{E} &= b \exp [ik (ct - \mu l)] \end{aligned} \right\} \quad (1)$$

where

$k = \frac{2\pi}{\lambda}$  ( $\lambda$  being the wave length);  $c$  = velocity of light in vacuo;  $\mu = a$  small path length  $l =$  time and  $i = \sqrt{1 - \mu^2}$ .

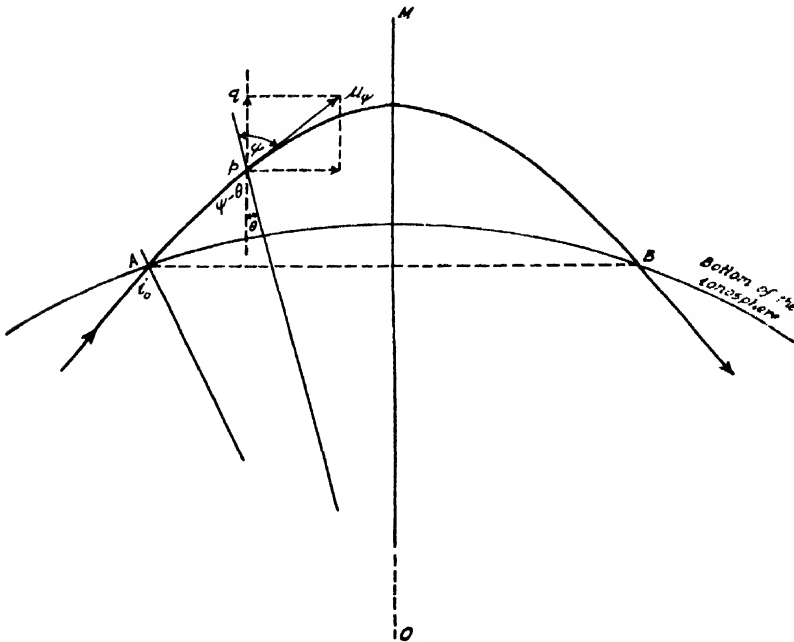


FIG. 2(a)

Illustrating components of the propagation vector ( $\mu\psi$ ) and the mode of propagation at any point  $p$  in the ionosphere. (not to the scale).

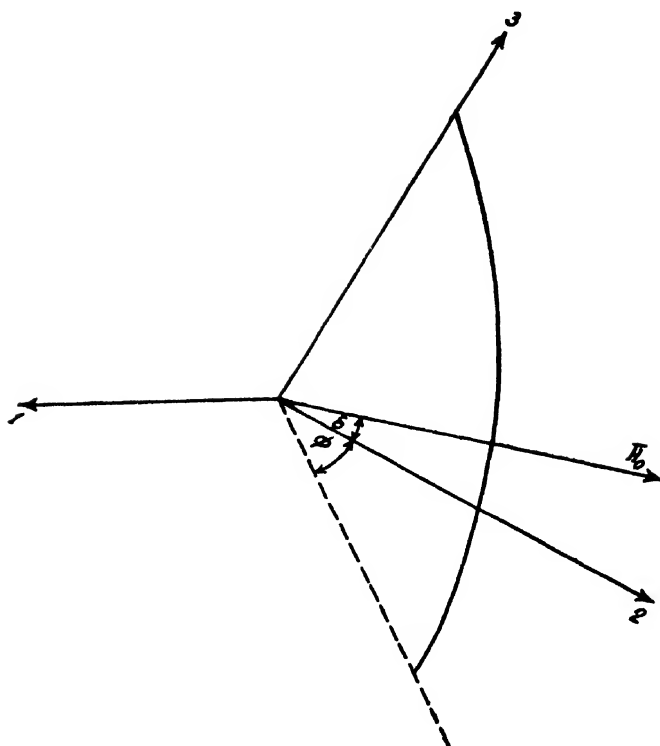


FIG. 2(b)

Co-ordinate axes as chosen in the analysis.  $\delta$  is the angle of magnetic dip and  $\phi$  is the angle between the magnetic meridian plane and the plane of incidence

Considering propagation at any point  $p$  in the ionized region, where the direction of propagation makes an angle  $\psi$  with the radius vector i.e. an angle  $(\psi - \theta)$  with the vertical direction (figure 1), an elementary length of path can be resolved into its components along the directions 2 and 3 (figure 2) as follows :

$$\begin{aligned} \mu_{\psi} l &= \mu_{\psi} [x_2 \sin (\psi - \theta) + x_3 \cos (\psi - \theta)] = x_3 \mu_{\psi} \cos (\psi - \theta) + x_2 [\mu_{\psi} \sin \psi \cos \theta \\ &- \mu_{\psi} \cos \psi \sin \theta] \end{aligned}$$

(where,  $x_2$  and  $x_3$  denote distances along the directions 2 and 3, and  $\theta = \angle pOM$  in figure 1).

Now  $\mu_{\psi} \cos (\psi - \theta)$  is the component of  $\mu_{\psi}$  in the vertical direction and can be denoted by  $q$  (5). Also, as  $\theta$  is small and  $\psi$  is large, the product

$$\cos \psi \sin \theta \ll \sin \psi \cos \theta$$

Therefore,

$$\mu_\psi l = qx_3 + (\mu_\psi \sin \psi \cos \theta) x_2 = qx_3 + x_2 \sin i_o (1 + \eta)^*$$

where  $\eta$  is the correction factor due to curvature of the earth

Thus equation (1) becomes :

$$\begin{aligned} \mathbf{P} &= a \exp [ik \{ct - qx_3 - x_2 \sin i_o (1 + \eta)\}] \\ \mathbf{E} &= b \exp [ik \{ct - qx_3 - x_2 \sin i_o (1 + \eta)\}] \end{aligned} \quad (2)$$

From Maxwell's equations

$$\left. \begin{aligned} \text{Curl } \mathbf{H} &= \frac{1}{c} (\mathbf{E} + 4\pi \dot{\mathbf{P}}) \\ \text{Curl } \mathbf{E} &= -\dot{\mathbf{H}} \end{aligned} \right\} \text{the dots representing derivatives with respect of time.}$$

$$\text{from which } \nabla^2 \mathbf{E} - \text{grad div } \mathbf{E} = \frac{1}{c^2} (\ddot{\mathbf{E}} + 4\pi \ddot{\mathbf{P}}) = 0$$

Substituting the values of  $\mathbf{P}$  and  $\mathbf{E}$ , as given by Eq. (2), to the above equation, the components along the three cartesian co-ordinates become

$$\left. \begin{aligned} E_1 [1 - s^2 (1 + \eta)^2 - q^2] + 4\pi P_1 &= 0 \\ (1 - q^2) E_2 + s(1 + \eta) q E_3 + 4\pi P_2 &= 0 \\ s(1 + \eta) q E_2 + [1 - s^2 (1 + \eta)^2] E_3 + 4\pi P_3 &= 0 \end{aligned} \right\} \quad \dots (3)$$

[where  $S = \sin i_o$  and  $c = \cos i_o$ ]

From these,

$$\left. \begin{aligned} E_1 &= \frac{4\pi P_1}{q^2 - c^2 + 2\eta s^2 + s^2 \eta^2} \\ E_2 &= 4\pi \frac{P_2 [2\eta^2 s^2 + \eta^2 s^2 - c^2] + p_3 s q (1 + \eta)}{c^2 - q^2 - 2\eta s^2 - \eta^2 s^2} \\ E_3 &= 4\pi \frac{P_2 s q (1 + \eta) - P_3 (1 - q^2)}{c^2 - q^2 - 2\eta s^2 - \eta^2 s^2} \end{aligned} \right\} \quad (4)$$

Neglecting the effect of the magnetic field on the incident wave, as it is very small compared to the steady terrestrial magnetic field, the relation between  $\mathbf{P}$  and  $\mathbf{E}$  is given by

$$\ddot{\mathbf{P}} + v \dot{\mathbf{P}} = \left( \frac{N\rho^2}{m} \right) \mathbf{E} + \left( \frac{e}{mc} \right) \dot{\mathbf{P}} \mathbf{H}_o \quad \dots (5)$$

(where  $\mathbf{H}_o$  is the terrestrial magnetic field vector). Substituting from (2) and solving for  $\mathbf{E}$

$$\mathbf{E} = 4\pi [\rho_0 + i \mathbf{P} \cdot \rho] \quad \dots (6)$$

\* From Snells law in spherically stratified layers (referring to figure 1).

$$R \mu_\psi \sin \psi = R_o \sin i_o \text{ and } \cos \theta = \frac{h_o}{R}$$

$$\therefore \mu_\psi \sin \psi \cos \theta = \frac{R_o h_o}{R^2} \sin i_o = \sin i_o (1 + \eta)$$

$$\text{or } 1 + \eta = \frac{R_o h_o}{R^2} = 1 - \frac{2r}{R_o}$$

$$\text{or } \eta = - \frac{2r}{R_o} \quad \dots 1(a)$$

where,

$$\rho_0 = -\frac{u}{\epsilon}, \quad \rho = -\frac{\mathbf{r}}{x} \text{ and } \mathbf{Y} = \frac{\mathbf{r}}{p}$$

$$\lambda = \frac{m\omega}{mp^2} N, \quad u = 1 + i z; \quad z = \nu/p,$$

taking,

$\nu$  = collisional frequency,  $N$  = electron density,  $\frac{p}{2\pi}$  = wave frequency and

$\frac{pH}{2\pi}$  = gyrofrequency.

On equating the components of (6) and (3)

$$\begin{aligned} \rho_0 &= \epsilon^2 - q^2 - 2\eta - S^2\eta^2 S^2 & P_1 + i\rho_3 P_2 - i\rho_2 P_3 &= 0 & \dots \\ i\rho_3 P_1 + \left( \rho_0 + \frac{\epsilon^2 - 2\eta S^2 - \eta^2 S^2}{\epsilon^2 - q^2 - 2\eta S^2 - \eta^2 S^2} \right) P_2 + \left( i\rho_1 - \frac{S q (1 + \eta)}{\epsilon^2 - q^2 - 2\eta S^2 - \eta^2 S^2} \right) P_3 &= 0 & (7b) \\ i\rho_2 P_1 + \left( i\rho_1 - \frac{S q (1 + \eta)}{q^2 - 2\eta S^2 - \eta^2 S^2} \right) P_2 + \left( \rho_0 + \frac{1 - q^2}{q^2 - 2\eta S^2 - \eta^2 S^2} \right) P_3 &= 0 & (7c) \end{aligned}$$

Finding out the values of  $P_1$  and  $P_2$  in terms of  $P_3$ , from Eqs 7(a) and 7(b), substituting the values of  $\rho_0$ ,  $P$ , etc. we get,

$$\alpha q^4 + \beta q^3 + \gamma q^2 + \delta q + \epsilon = 0 \quad \dots \quad (8)$$

where

$$\alpha = u(u^2 - y^2) - v(u^2 - y_3^2) \quad \dots \quad (9a)$$

$$\beta = 2y_2 y_3 S(1 + \eta) \quad \dots \quad (9b)$$

$$\begin{aligned} \gamma &= (\epsilon^2 - 2\eta S^2) (2u^2 v - 2u^3 + 2u y^2 - y_3^2 v) \\ &\quad - 2u \lambda^2 + 2u^2 \lambda + y_2^2 \lambda S^2 (1 + 2\eta) \quad \dots \quad (9c) \end{aligned}$$

$$\delta = -2y_2 y_3 v S(1 + \eta) (\epsilon^2 - 2\eta S^2) \quad \dots \quad (9d)$$

$$\begin{aligned} \epsilon &= (u - v) [u^2 (\epsilon^4 - 4\eta S^2 \epsilon^2) - 2u x (\epsilon^2 - 2\eta S^2) + x^2] \\ &\quad (\epsilon^2 - 2\eta S^2) [u y^2 (\epsilon^2 - 2\eta S^2) - y_2^2 x + y_2^2 S^2 \lambda (1 + 2\eta)] \quad \dots \quad (9e) \end{aligned}$$

[neglecting the terms containing  $\eta^2$ , as they are very small]

For a flat earth, the correction factor becomes zero; and, under that condition the values of the above co-efficients become identical with those of Booker. In the deviating E and F regions, which are important for ionospheric propagation, the collisional damping is negligible and we may take  $u = 1$ .

Even under the simplified condition of negligible collisional damping ( $z = 0$ ), the above quartic equation is very difficult to solve. But, as shown by Booker for the flat earth case, the problem is simplified if propagation curves are drawn for the equatorial region, which is of course much easier (Booker, 1949).

For propagation across the equatorial region or in a magnetic latitudinal plane, the above quartic equation in  $q$  is reduced to a quadratic equation, and under the condition it can be solved easily, as in the cases  $\beta = \delta = 0$ ,

The simplified propagation equation for transmission across equatorial region



neglecting the collisional damping (since  $\nu/\rho < 1$  in the deviating E or F region), is given by

$$q^2 = 2\eta S^2 - \frac{x(1-x)}{(1-x) + \frac{1}{2}\{y_2^2 S^2(1+\eta)^2 - y^2\} \pm \sqrt{\frac{1}{4}\{y_2^2 S^2(1+\eta)^2 - y^2\}^2 + y_2^2(1-x)(1+\eta)^2 S^2}}$$

As the correction factor  $\eta < 1$ , the terms containing square and higher powers of  $\eta$  can be neglected. The equation then becomes

$$q^2 = 2\eta S^2 - \frac{x(1-x)}{(1-x) + \frac{1}{2}\{y_2^2 S^2(1+2\eta) - y^2\} \pm \sqrt{\frac{1}{4}\{y_2^2 S^2(1+2\eta) - y^2\}^2 + y_2^2 S^2(1-x)(1+2\eta)}}$$

From the above equation and the expression for  $\eta$ , it is evident that in this case, the value of  $q$  not only depends on the value of  $x$  at a point, but also on its variation along the radius. Thus  $q^2-x$  curves can only be drawn for known distributions of the ionization density.

### 3. PLOTTING OF PROPAGATION CURVES ACROSS EQUATORIAL REGION

A few typical curves have been drawn over equatorial region (figures 3 and 4) illustrating the variation of  $q^2$  with  $x$  on the assumption of a parabolic gradient of ionization.

For parabolic ionization density, we have  $x = x_{\max} \left(1 - \frac{t'^2}{4H^2}\right)$

where

$$\frac{4\pi e^2}{mp^2} = Nm,$$

$Nm$  being the maximum ionization density in the layer. The thickness  $t'$  is measured from the point of maximum ionization density ( $x_{\max}$ ) and  $H$  is the scale height of the layer. Or, from figure 1,  $r = t_m \left[ \sqrt{1 - \frac{x}{x_{\max}}} \right]$  [ $t_m$  being the semithickness of the layer].

$$\therefore \text{The correction factor } \eta = -\frac{2r}{R_r} = -\frac{t_m}{R_0} \left[ 1 - \sqrt{1 - \frac{x}{x_{\max}}} \right]$$

substituting this value of  $\eta$  in Eq. (10) we get, for propagation across the equatorial region

$$\begin{aligned} & \frac{4S^2}{R_0} t_m \left[ 1 - \sqrt{1 - \frac{x}{x_{\max}}} \right] \\ & - \frac{x(1-x)}{(1-x) + \frac{1}{2}\left[y_2^2 S^2 \left\{ 1 - \frac{4t_m}{R_0} \left( 1 - \sqrt{1 - \frac{x}{x_{\max}}} \right) \right\} - y^2\right] \pm \sqrt{\frac{1}{4}\left[y_2^2 S^2 \left\{ 1 - \frac{4t_m}{R_0} \left( 1 - \sqrt{1 - \frac{x}{x_{\max}}} \right) \right\} - y^2\right]^2 + S^2 y_2^2 (1-x) \left\{ 1 - \frac{4t_m}{R_0} \left( 1 - \sqrt{1 - \frac{x}{x_{\max}}} \right) \right\}}} \dots \quad (11) \end{aligned}$$

As an illustration of the computation, let us consider the particular case when,  $\frac{t_m}{R_0} = 100$ , (i.e.  $t_m = 65$  km.) and the vertical incidence critical frequency of the

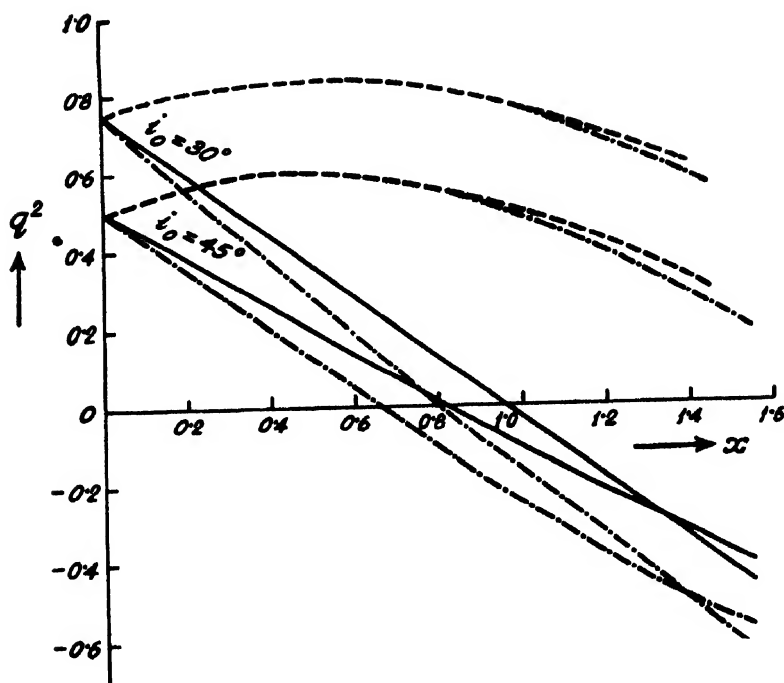


FIG. 3.

Propagation curves for propagation across the equatorial region and for  $f = \frac{1}{2}f_h$ . The plane of propagation makes an angle of  $\pm 45^\circ$  with the magnetic meridian plane. Two cases of different angles of incidence,  $30^\circ$  and  $45^\circ$ , are shown. The full lines represent the ordinary and the dotted lines the extra-ordinary components (both for the curved earth case). The propagation curves for the flat earth (chained lines) are also drawn for comparison.

layer at the point of reflection is  $f_c = 10 f_h$  which is approximately the value of daytime  $f^\circ F_2$  (These assumption simplify the computation). Hence,

$$x_{\max} = \frac{f_c^2}{f^2} = 100 f_h^2 / f^2 = 100 y^2$$

The illustrative curves are drawn for a direction of propagation making an angle of  $\pm 45^\circ$  with the magnetic meridian plane; so that

$$y_1^2 = y_2^2 = 0.5 y^2$$

Figure 3 shows the propagation curves for  $f = \frac{1}{2}f_h$  (i.e. for wave frequency less than gyro frequency) and for angles of incidence ( $i_0$ ) of  $30^\circ$  and  $45^\circ$ . The curves for the flat earth case (Chatterjee, 1952) according to Booker's formula, are also drawn to illustrate the effect of considering the curvature of the earth. It is seen that the difference between the two sets of curves is very small for the smaller values of  $x$ . But near the point of reflection (i.e. for values of  $x$  for which  $q^2$  tend to zero), there is noticeable deviation—the value of  $x$  for  $q^2 = 0$  being larger for the curved earth case by about 15% (the other conditions remaining identical). This is because, for the curved earth, the increase in ionization density

also the ray path is less than that for the flat earth case. The above deviations have important effects on the calculated values of attenuation and group retardation of an obliquely propagated radio wave, as discussed in the next section.

Figure 4 illustrates the propagation curves for  $f = 2f_h$  (i.e. for wave frequency greater than the gyro frequency) and for angles of incidence of  $30^\circ$ ,  $45^\circ$  and  $60^\circ$ . As in figure 3, the nature of the variations is same as that for the flat earth case, though the values of  $q^2$  for given values of  $x$  differ to a certain extent. Like the flat earth case, the value of  $q^2$  attains an infinite value corresponding to the fourth condition of reflection (Mitra, 1952).

#### 1. GROUP RETARDATION, ATTENUATION AND LATERAL DEVIATION.

In the previous sections, the plane of incidence was chosen to be coincident with the 23-plane of the co-ordinate axes. But it is inconvenient for some purposes to have the plane of incidence coinciding with a co-ordinate plane. In this section, we shall therefore, take the plane of incidence at any angle  $\phi_0$  to the  $31$  plane as shown in figure 5. Under this condition, the wave function of a magneto-ionic component becomes

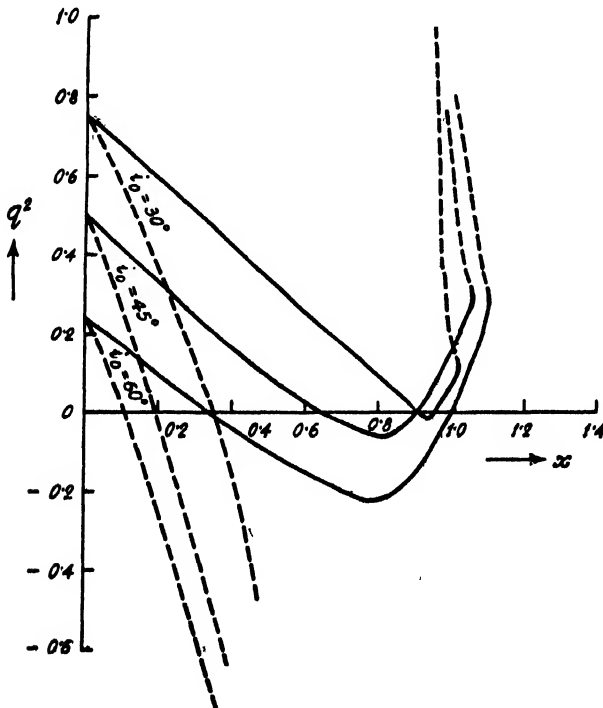


FIG. 4.

Propagation curves for propagation across the equatorial region and for  $f = \frac{1}{2}f_c$ . The plane of propagation makes an angle of  $\pm 45^\circ$  with the magnetic meridian plane. Three cases of different angles of incidence,  $30^\circ$ ,  $45^\circ$  and  $60^\circ$ , are shown. The ordinary and extraordinary components are as shown in figure 3.

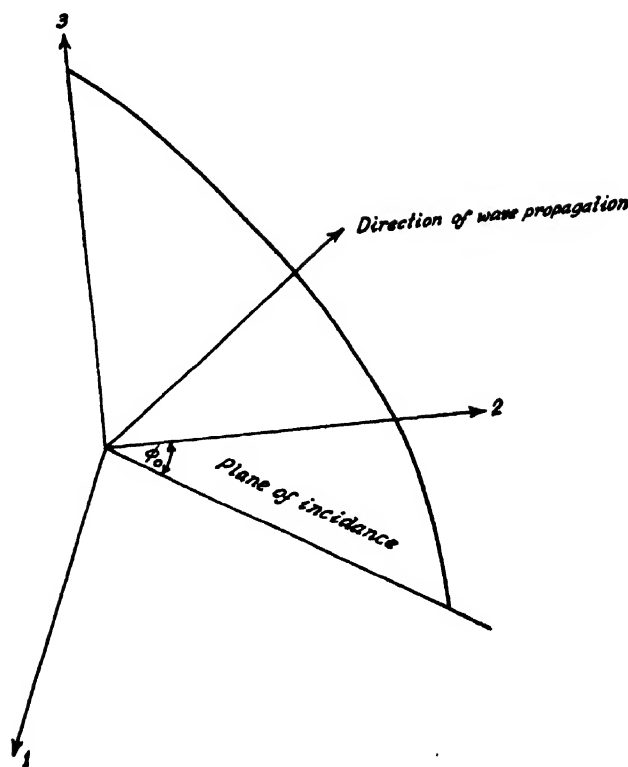


FIG. 5.

Co-ordinate axes for the general case of propagation, when the plane of incidence makes any angle  $\phi_0$  with the 23 plane.

$$\exp [i\kappa\{ct - (S_1x_1 + S_2x_2)(1 + \eta) - \int_0^x qdh\}] \quad \dots (12)$$

where  $S_1 = S \cos \phi_0$  and  $S_2 = S \sin \phi_0$

The co-efficients of the propagation equation (8) are also modified to

$$\alpha = u(u^2 - y^2) - x(u^2 - y_3^2) \quad \dots (13a)$$

$$\beta = 2y_3x(S_1y_1 + S_2y_2)(1 + \eta) \quad \dots (13b)$$

$$\gamma = (c^2 - 2\eta S^2)(2u^2x - 2u^3 + 2uy^2 - y_3^2x) - 2ux^2 + 2u^2x - y^2x + x(S_1y_1 + S_2y_2)^2(1 + 2\eta) \quad \dots (13c)$$

$$\delta = -2y_3x(S_1y_1 + S_2y_2)(1 + \eta)(c^2 - 2\eta S^2) \quad \dots (13d)$$

$$\epsilon = (u - x)[u^2(c^4 + 4\eta S^2c^2) - 2ux(c^2 - 2\eta S^2) + x^2] - (c^2 - 2\eta S^2)[uy^2(c^2 - 2\eta S^2) - y^2x + (S_1y_1 + S_2y_2)^2(1 + 2\eta)x] \quad \dots (13e)$$

Energy propagation in the ionosphere takes place with the group velocity--the velocity of the wave packet as a whole. To follow the wave packet in the ionosphere, we have to follow the point of constructive interference of these waves. This means that the partial derivatives of the wave function [eq. 12] are to be equated to zero. Thus

$$ct - (S_1 x_1 + S_2 x_2)(1 + \eta) - \int_0^h \frac{\delta(\kappa q)}{dh} dh = 0 \quad (14)$$

$$(1 + \eta) x_1 + \int_0^h \frac{dq}{dS_1} dh = 0 \text{ or } x_1 = - \frac{1}{1 + \eta} \int_0^h \frac{dq}{dS_1} dh \quad \dots \quad (15)$$

$$(1 + \eta) x_2 + \int_0^h \frac{dq}{dS_2} dh = 0 \text{ or } x_2 = - \frac{1}{1 + \eta} \int_0^h \frac{dq}{dS_2} dh \quad \dots \quad (16)$$

All the above expressions are for the wave packet in going from zero height to height  $h$ . If the total group retardation time be  $t_0$  then the equivalent path length  $p_{eq}$  is given by

$$\begin{aligned} p_{eq} - ct_0 &= \int_0^h \frac{d(ct)}{dh} dh = (S_1 x_1 + S_2 x_2)(1 + \eta) + \int_0^h \frac{d(kq)}{dk} dh \\ &= \int_0^h \left\{ \frac{d(kq)}{dk} - \frac{S_1}{1 + \eta} \frac{dq}{dS_1} - \frac{S_2}{1 + \eta} \frac{dq}{dS_2} \right\} dh \end{aligned} \quad (17)$$

$$\text{and the total lateral deviation } x_1 = - \int_0^h \frac{dx_1}{dh} dh = - \frac{1}{1 + \eta} \int_0^h \frac{dq}{dS_1} dh \quad (18)$$

The values of  $\frac{dq}{dS_1}$ ,  $\frac{dq}{dS_2}$  and  $\frac{d(kq)}{dk}$  can be calculated by simple differentiation as done by Booker for the flat earth case. The total amounts of group retardation and lateral deviation suffered in the deviating region can be calculated by the same procedure of graphical integration.

It is evident from figure 3 that for the curved earth case, the calculations will give a higher value of group retardation, as the wave penetrates deeper into the ionized layer (the value of  $x$  for  $q^2 = 0$  being higher for the curved earth case). This gives better agreement with experimental results. Calculations of Waterman (1952) neglecting the earth's field also gives a higher value of group retardation, when earth's curvature is taken into account.

To calculate the attenuation, it is to be noted that, in the deviating E or F region (reflections from these layers only being considered in this paper), the attenuation suffered by the waves is very small. Thus in the Taylor expansion of the function  $q(u) = q(1 - iz)$  we can neglect the higher terms and write.

$$q(\mu) = q(1) - iz \left( \frac{dq}{du} \right)_{u=1}$$

Substituting this value in Eq. (12), the wave function becomes

$$\exp \left[ ik \left\{ ct - (S_1 x_1 + S_2 x_2)(1 + \eta) - \int_0^h \left( q - iz \frac{dq}{du} \right) dh \right\} \right] \\ = \exp \left\{ -k \int_0^h z \left( \frac{dq}{du} \right) dh \right\} \exp \left[ ik \left\{ ct - (S_1 x_1 + S_2 x_2)(1 + \eta) - \int_0^h q dh \right\} \right]$$

the term  $\left[ -kz \left( \frac{dq}{du} \right) \right]$  giving attenuation per unit height. Thus we see that the expression giving attenuation per unit height in the deviating region for the curved earth case is identical with that for the flat earth; the total attenuation is, however, greater for the curved one, as the wave penetrates deeper into the ionosphere.

## 5. CONCLUDING REMARKS

The results of analysis for the case of the curved earth, as carried out in the previous sections, show that the corrections applicable to Booker's result for the case of a flat earth become appreciable only in the deviating 'reflecting' region. This is because the value of  $x$  at the reflecting points (i.e. for  $q^2=0$ ) is higher for the case of the curved earth than that for the flat earth. The values of attenuation and group retardation in the deviating region are thus also higher when the curvature effect is taken into account. Since, during day time the main absorption is caused in the non-deviating region below, the flat earth approximation does not significantly affect the calculated signal intensity and a good agreement with experimental results is possible. During night time, however, the main absorption is in the deviating (reflecting) region. Hence the absorption value is significantly higher when the curvature of the earth is taken into account. These results are in general agreement with observations. The measured values of absorption are always found to be greater than the values as calculated for the flat earth case. The analysis also shows that the lateral deviation of the ray is greater than that calculated from the flat earth consideration. The increase is, however, expected to be significant only for directions of propagation making angles of about  $\pm 45^\circ$  with the magnetic meridian plane.

## ACKNOWLEDGMENTS

The author's grateful thanks are due to Prof. S. K. Mitra for his constant guidance and help throughout the progress of the work. Thanks are also due to the Scientific Man Power Committee, Government of India, for financial help.

## REFERENCES

- Appleton, E. V. and Naismith, R. 1940, *Proc. Phys. Soc.*, **52**, 518.
- Booker, H. G., 1938, *Phil. Tran. Roy. Soc. A*, **237**, 411.
- Booker, H. G., 1949, *Jour. Geo. Res.*, **54**, 243.
- Chatterjee, B., 1949, *Ind. Jour. Phys.*, **26**, 297.
- Mitra, S. K., 1952, *The Upper Atmosphere* (Second Edition).
- Gerson, N. C. and Seaton, S. L., 1948, *Jour. Frank. Inst.* **246**, No. 6.
- Heading, J. and Whipple, R. T. P., 1952, *Phil. Trans. Roy. Soc. A*, **244**, 469.
- Stanley, J. P., 1950, *Jour. Atoms. Terr. Phys.*, **1**, 65.
- Wilkes, M. V., 1940, *Proc. Roy. Soc. A*, **175**, 143.
- Wilkes, M. V., 1947, *Proc. Roy. Soc. A*, **189**, 130.
- Waterman, A. T. (Jr.), 1952, *Tech. Rep. No. 142*, (Office of the Naval Research U.S.A.)

# EFFECT OF STEEPNESS OF PULSE FRONTS ON THE RESPONSE OF DIFFERENTIATING AND INTEGRATING CIRCUITS\*

BY BIMAL KRISHNA BHATTACHARYYA

INSTITUTE OF NUCLEAR PHYSICS, CALCUTTA UNIVERSITY

(Received for publication, February, 23, 1953)

**ABSTRACT.** The responses of integrating and differentiating circuits to a pulse front that rises linearly upto a certain time and then flattens out have been studied. Generally, the analysis of such circuits is made by assuming the input pulse to be a step-function. That the responses obtained by such an analysis are much different from those found in the case of a linearly rising pulse that flattens out after a certain time, has been shown clearly in both cases of cascaded differentiating and integrating circuits. When the rise time is very short, the output pulse shape becomes almost similar to that in the case of step-function input pulse. As the rise time and the number of cascaded sections increase, the magnitude as well as the rate of rise of the integrated output pulse sharply begins to diminish. In the case of differentiation, the maximum output voltage depends very much upon the rise time.

## I N T R O D U C T I O N

In calculating the responses of pulsed circuits it is the normal practice to assume the input voltage to be a unit step-function (figure 1) which is defined to be

$$e(t) = \begin{cases} 0 & t < 0 \\ 1 & t > 0 \end{cases} \dots \dots \dots (1)$$

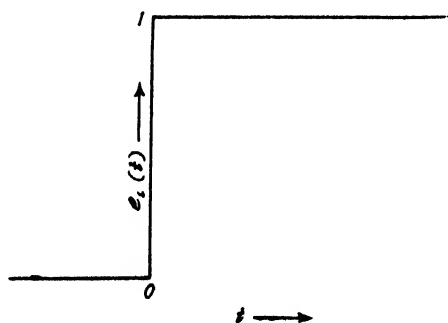


FIG. 1

A step function of unit height.

It is seen from the figure that the voltage changes instantaneously from one value to another. So the wavefront has an infinite slope as indicated by the function.

But it is not physically possible for a voltage or current to jump from one value to another instantaneously. So the responses of pulsed circuits calculated by taking the input voltage to be a step function do not indicate physically accurate pictures. Though the assumption of a perfectly square pulse front is a good approximation of a sharply rising pulse, yet it sometimes leads to erroneous results

\* Communicated by Prof. M. N. Saha, F.R.S.

as pointed out by Rubin (1952) and Schwartz (1946) in the case of analysis of pulse differentiation.

A sharply rising pulse can be represented by a linearly rising pulse front as a very good approximation (figure 2). This assumption is often accurate as the rise of the pulse is linear until before flattening out.

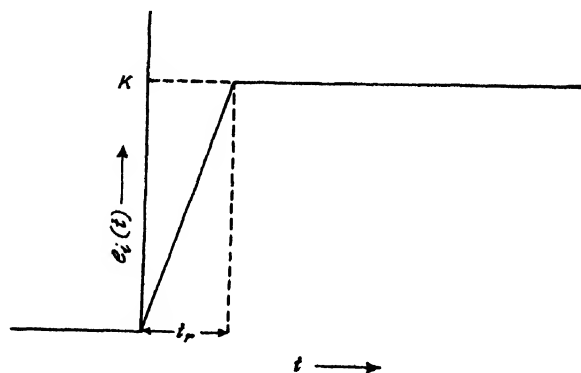


FIG. 2

A ramp function of height  $k$  with rise of time  $t_r$ .

The responses of cascaded differentiating and integrating circuits to a pulse (figure 2) which rises linearly upto a time  $t_r$  and then flattens out, will be obtained in the following analysis with the help of the theory of Laplace transforms. Such functions are called ramp functions.

It is shown that the shapes of differentiated and integrated pulses are much different in this case from those obtained when the input pulse is a step function. When the rise time is very short, the output pulse in both cases of differentiation and integration is practically similar to the output pulse when the input is as shown in figure 1.

#### *Analysis of Integrating Circuits :*

The pulse which is shown in figure 2 can be analytically represented by the following expression :

$$e_1(t) = \frac{Ku(t)t}{t_r} - \frac{Ku(t-t_r)(t-t_r)}{t_r} \quad (2)$$

where,  $t_r$  indicates the rise time of the pulse and  $u(t)$  and  $u(t-t_r)$  are unit step functions (figure 1) beginning at times  $t = 0$  and  $t = t_r$  respectively.  $K$  represents the height of the pulse.

So the excitation transform which is the Laplace transform of  $e_1(t)$  is given by

$$e_1(p) = \frac{K}{t_r} \left[ \frac{1}{p^2} - \frac{e^{-pt_r}}{p^2} \right] \quad (3)$$

The transfer function or system transform of  $n$  stages of cascaded integrating circuits (figure 3) is given by the equation (Bhattacharyya, 1952) :

Transfer function

$$\frac{e_n(p)}{e_1(p)} = \frac{1}{1 + a_1 T p + \dots + a_{n-1} T^{n-1} p^{n-1} + a_n T^n p^n} \quad (4)$$



where  $e_n(p)$  and  $e_i(p)$  are respectively the response transform and excitation transform

and

$$a_m = \frac{n+m}{n-m} C_{n-m} \\ = \frac{(n+m)!}{(n-m)! (2m)!} \quad (5)$$

and  $T = RC$

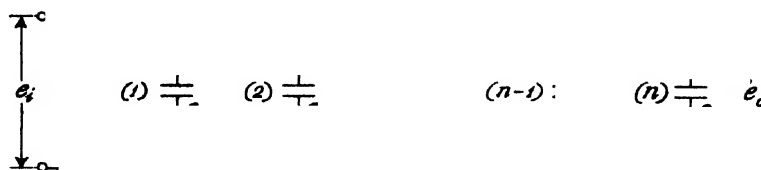


FIG. 3

The  $n$ -stage  $RC$ -integrating circuit.

To avoid complicated results in obtaining the response  $e_n(t)$  let us denote,

$$f_n(p) = \frac{K}{t_r} \cdot \frac{1}{p^2 (1 + a_1 T p + a_2 T^2 p^2 + \dots + T^n p^n)} \quad \dots (6)$$

so that the response  $e_n(t)$  is given by

$$e_n(t) = f_n(t) = f_n(t - t_r) u(t - t_r) \quad (7)$$

So the problem is now to find out the inverse Laplace transform of  $f(p)$ . The expression of the  $n$ th degree in the denominator of equation (6) is to be broken up into linear factors so that the inverse Laplace transform can be found by applying Heaviside's expansion theorem.  $f(p)$  can then be written as

$$f_n(p) = \frac{K}{t_r} \cdot \frac{1}{p^2 (T p + a_1) (T p + a_2) \dots (T p + a_n)} \quad \dots (8)$$

where  $-a_1$ 's are the roots of the polynomial

$$1 + a_1 T p + \dots + a_n T^n p^n \quad \dots (9)$$

It can be shown with the help of the theory of equations that the roots are distinct, irrational negative real numbers. Kenyon (1951) has given a table of the roots of the polynomial for values of  $n = 1, 2, 3, 4$ .

From the theory of Laplace transforms we know that if  $x(p)$  is the transform of  $x(t)$  and  $\theta$  is a real positive number, then  $\frac{1}{\theta} x(p/\theta)$  is the transform of  $x(\theta t)$ . Put  $\theta = 1/T$

Then  $T x(T p)$  is the transform of  $x(t/T)$ . Equation (8) can be written as

$$f_n(p) = \frac{KT}{t_r} \cdot \frac{T}{(T p)^2 (T p + a_1) (T p + a_2) \dots (T p + a_n)} \quad (10)$$

So we can normalize equation (10) by substituting  $t = t/Rc$  and  $f_n(t) = \frac{f_n(t)}{K}$

to obtain

$$f_n(p) = \frac{1}{t_r \cdot p^2(p+a_1)(p+a_2)\dots(p+a_n)} \quad (11)$$

So the response function  $f_n(t)$  that equals  $L^{-1}f_n(p)$  is given by

$$\begin{aligned} f_n(t) &= L^{-1}f_n(p) \\ &= \frac{1}{2\pi j} \cdot \frac{T}{t_r} \cdot \int_{C-j\infty}^{C+j\infty} \frac{e^{pt}}{p^2(p+a_1)(p+a_2)\dots(p+a_n)} \cdot p \dots \end{aligned} \quad (12)$$

where  $L^{-1}$  is the inverse Laplacian operator. We, therefore, have,

$$f_n(t) = \frac{T}{t_r} \cdot \sum \text{Residues of poles of} \quad \frac{e^{pt}}{p^2(p+a_1)(p+a_2)\dots(p+a_n)} \quad (13)$$

by the Cauchy Residue theorem.

$f_n(t)$  has a pole of second order at  $p=0$  with residue

$$\frac{d}{dp} \left( \frac{e^{pt}}{(p+a_1)(p+a_2)\dots(p+a_n)} \right)_{p=0} \quad (14)$$

and poles of order unity at points  $p = a_1, a_2, \dots, a_n$  with residues

$$\frac{e^{-a_r t}}{r-1} \cdot \phi'(-a_r) \quad (15)$$

where

$$\phi(p) = p^2(p+a_1)(p+a_2)\dots(p+a_n) \quad (16)$$

and  $\phi'(p)$  denotes differentiation of  $\phi(p)$  with respect to  $p$

So with the help of the expressions (14) and (15), we have

$$f_n(t) = \frac{T}{t_r} \cdot \sum_{r=1}^n \frac{e^{-a_r t}}{\phi'(-a_r)} + \frac{T}{t_r} \cdot \frac{d}{dp} \left( \frac{e^{pt}}{(p+a_1)\dots(p+a_n)} \right)_{p=0} \quad (17)$$

Equation (17) is expanded below for  $n = 1, 2, 3, 4$ .

$$f_1(t) = \frac{T}{t_r} (\epsilon^{-t} + t - 1) \quad (18)$$

$$f_2(t) = \frac{T}{t_r} \left[ 3.06522 \epsilon^{-0.88197 t} - 0.08271 \epsilon^{-2.61803 t} + t - 3 \right] \quad (19)$$

$$\begin{aligned} f_3(t) = \frac{T}{t_r} \left[ 6.16180 \epsilon^{-0.19806 t} - 0.18013 \epsilon^{-1.55496 t} + 0.01838 \epsilon^{-3.24698 t} \right. \\ \left. + t - 6 \right] \quad (20) \end{aligned}$$

$$i(t) = \frac{T}{t_r} \left[ 10.29129 e^{-0.12061 t} - 0.33333 e^{-t} + 0.05106 e^{-2.34730 t} - 0.00783 e^{-3.53209 t} + t - 10 \right] \quad \dots (21)$$

Now the responses of multimesh  $RC$  integrating circuits can be found out with the aid of equations (7) and (18-21). The responses for sections from one to four are shown in figures 4—7 for three values of  $t_r/T$  to show distinctly the three cases

- (i)  $t_r/T < 1$  ( $t_r/T = 0.5$ )
- (ii)  $t_r/T = 1$
- (iii)  $t_r/T > 1$  ( $t_r/T = 1.5$ )

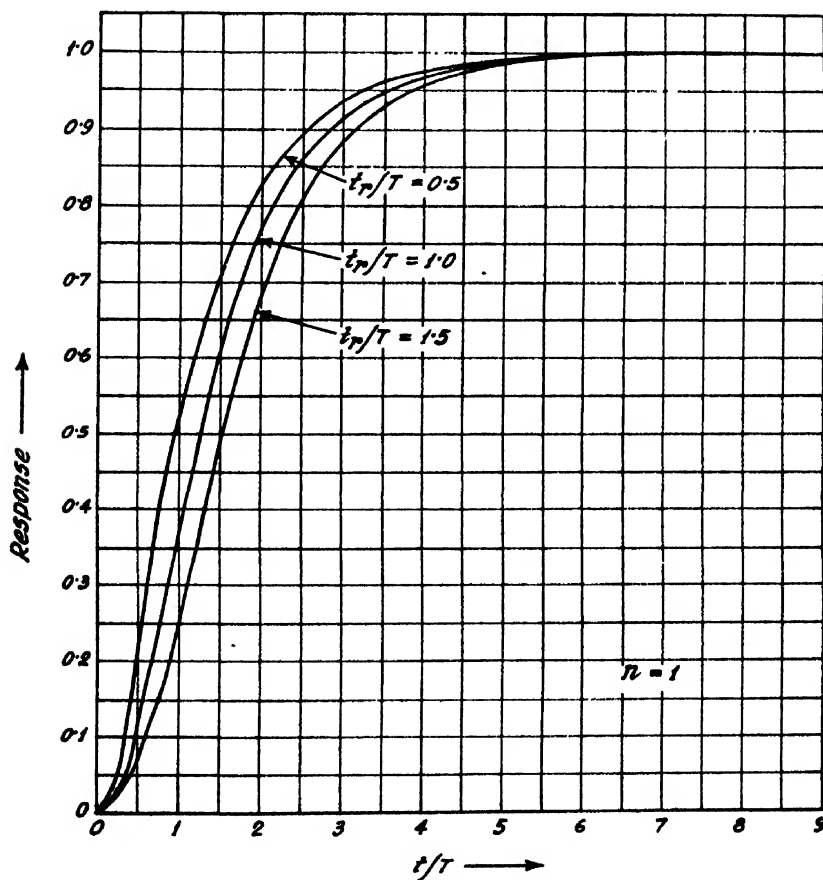


FIG. 4

Response to a ramp function of a single stage integrating circuit ( $n=1$ ).

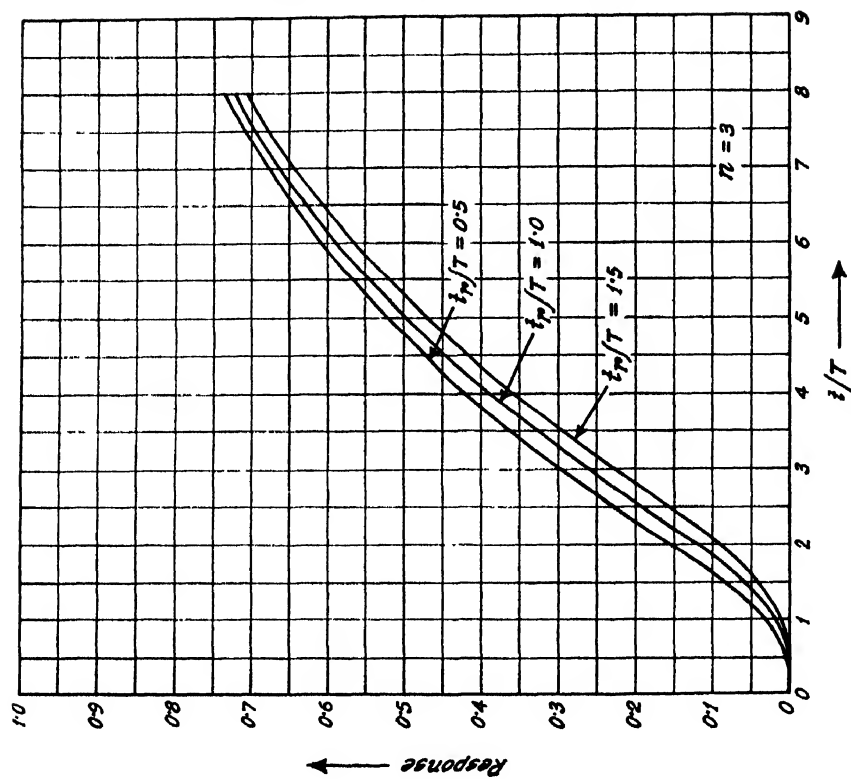


FIG. 6

Response to a ramp function of a three-stage integrating circuit ( $n=3$ ).

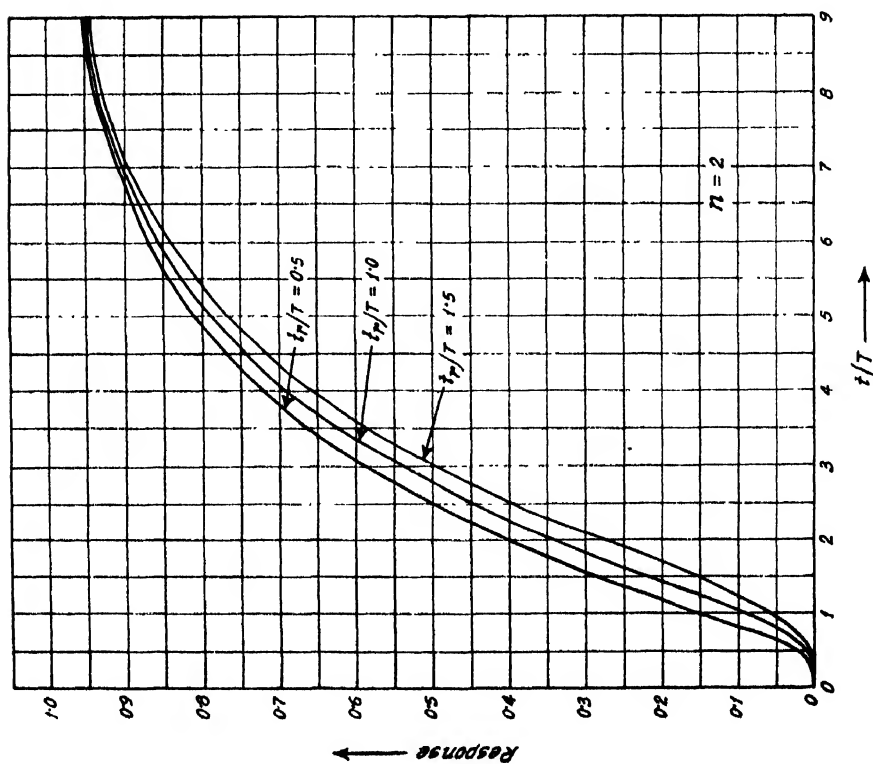


FIG. 5

Response to a ramp function of a two-stage integrating circuit ( $n=2$ ).

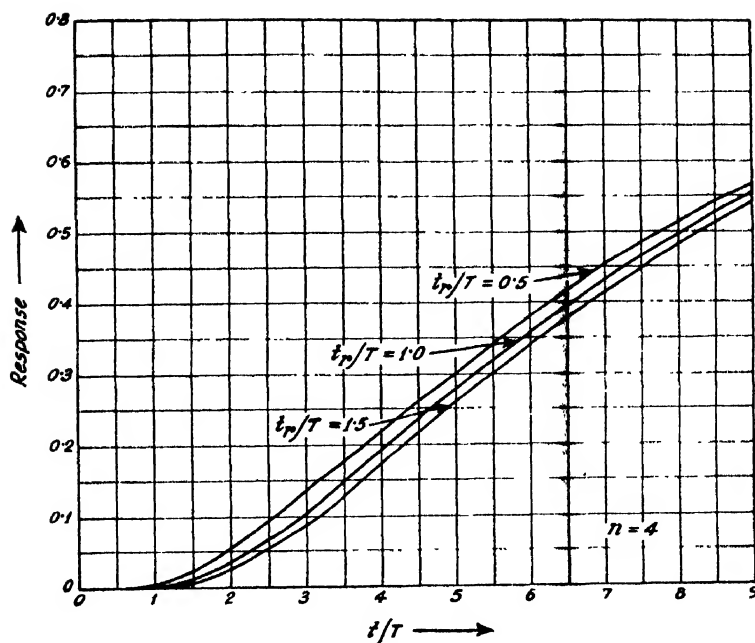


FIG. 7

Response to a ramp function of a four-stage integrating circuit ( $n=4$ ).

It is seen from the figures that the output is dependent on the rise time  $t_r$  of the pulse. As  $t_r$  increases, the rate of increase of output is also diminished. With the increase of the number of sections the magnitude as well as the rate of rise of the output pulse sharply begin to fall.

We shall now study the case when the rise time is very short. It is natural that as the rise time is diminished, the output pulse-shape will be almost similar to that found in the case of step-function input pulse.

The excitation transform of the unit step-function pulse is given by

$$e_1(p) = \frac{1}{p} \quad \dots (22)$$

So the transform of the output pulse is found to be

$$e_n(p) = \frac{1}{p} \cdot \frac{1}{1 + a_1 T p + a_2 T^2 p^2 + \dots + T^n p^n} \quad \dots (23)$$

which can be expressed as

$$e_n(p) = \frac{1}{p} \cdot \frac{1}{(T p + a_1)(T p + a_2) \dots (T p + a_n)} \quad \dots (24)$$

Normalizing equation (24) by putting  $t = t/RC$  we obtain,

$$e_n(p) = \frac{1}{p} \cdot \frac{1}{(p + a_1)(p + a_2) \dots (p + a_n)} \quad (25)$$

Applying Heaviside's Expansion Theorem to equation (25), we obtain (Kenyon, 1951)

$$e_n(t) = \sum_{r=1}^n \frac{\epsilon^{-a_r t}}{f'(-a_r)} + f'(0) \quad (26)$$

where

$$f(a_r) = p \cdot (p + a_1) \dots (p + a_r) \dots (p + a_n) \quad \dots (27)$$

The responses of cascaded integrating circuit to a step-function input voltage is now drawn in figure 8 with the help of equation (26).

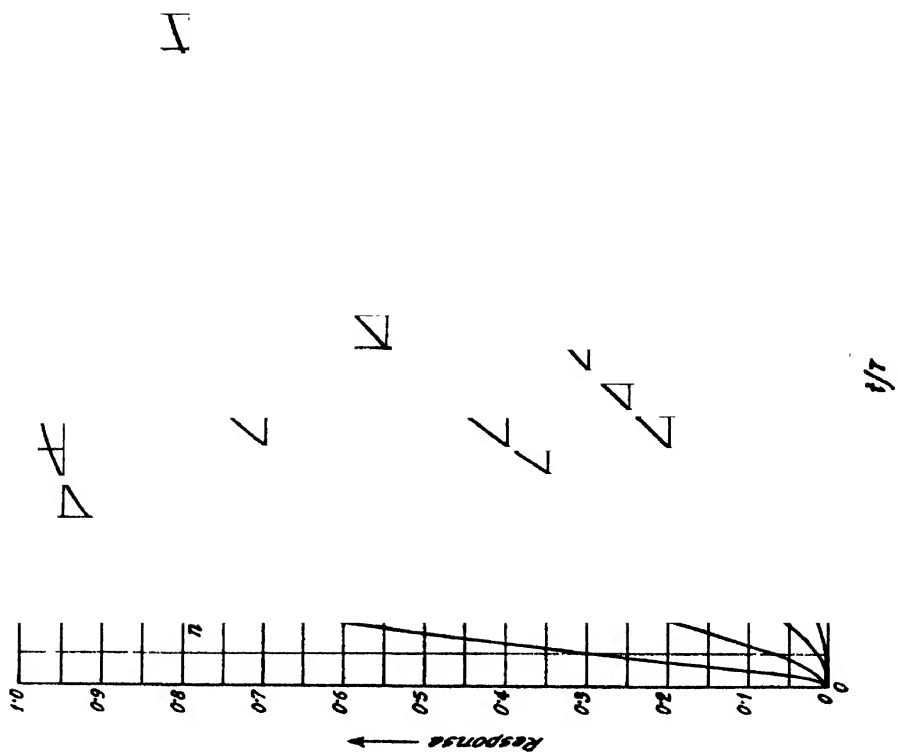


FIG. 8

Response to a step function input voltage of cascaded integrating circuits

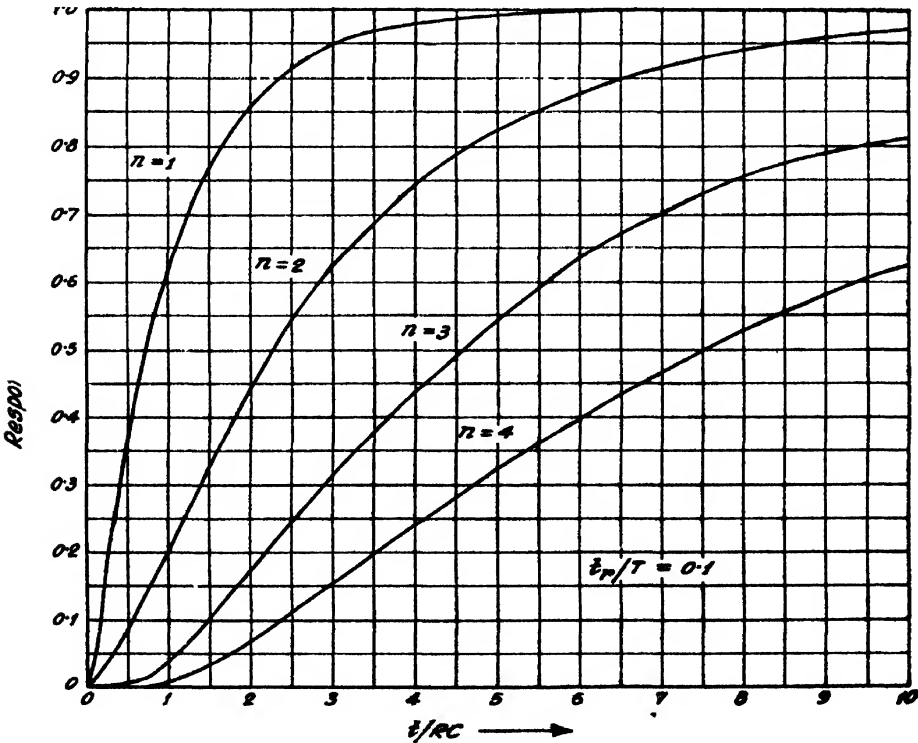


FIG. 9

Response to a ramp function of cascaded integrating circuits.

When the rise time is very short, e.g.  $t_r/T = 0.1$  the output pulses for various stages of integration are shown in figure 9.

It is evident from figures 8 and 9 that the response curves of integrating circuits to a pulse with a very short rise time is very much similar to the curves obtained in the case of step-function input voltage. In this case the assumption of a perfectly square pulse front is, no doubt, a good approximation of the sharply rising pulse.

#### Analysis of Differentiating Circuits :

The transfer function of  $n$  stages of cascaded differentiating circuits (figure 10) is given by the equation (Bhattacharyya, 1952) :

Transfer function:

$$\frac{e_n(p)}{e_1(p)} = \frac{(Tp)^n}{1 + t_1 Tp + \dots + t_r T^r p^r + \dots + T^n p^n} \quad (28)$$

where,

$$\begin{aligned} t_r &= 2n-rC_r \\ &= \frac{(2n-r)!}{r! (2n-2r)!} \\ \text{and } T &= RC \end{aligned} \quad (29)$$

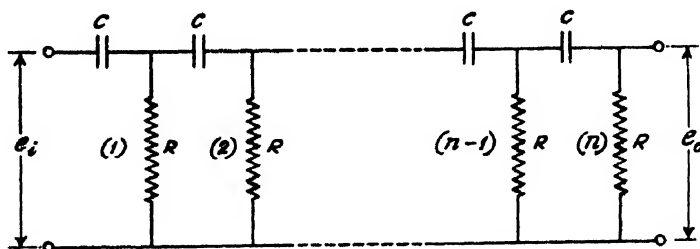


FIG. 10  
A cascaded differentiating circuit.

If we denote

$$g_n(p) = \frac{K}{t_r} \cdot \frac{(Tp)^n}{p^2 (1 + t_1 Tp + \dots + t_r T^r p^r + \dots + T^n p^n)} \quad (30)$$

then the response  $e_n(t)$  to a pulse given by equation (2) is given by

$$e_n(t) = g_n(t) - g_n(t-t_r) \cdot u(t-t_r) \quad \dots (31)$$

It can be proved by the theory of equations that the roots of the polynomial

$$1 + t_1 Tp + \dots + t_r T^r p^r + \dots + T^n p^n \quad \dots (32)$$

are the reciprocals of the roots of (9). So if  $\beta_1, \beta_2, \dots, \beta_n$  denote the reciprocals of  $\alpha_1, \alpha_2, \dots, \alpha_n$ , equation (30) can be written as

$$g_n(p) = \frac{K}{t_r} \cdot \frac{(Tp)^n}{p^2 (Tp + \beta_1) (Tp + \beta_2) \dots (Tp + \beta_n)} \quad \dots (33)$$

As in the case of the integrating circuits, we can normalize (33) by putting  $t = t/RC$  and  $g_n(t) = g_n(t)/K$  to obtain

$$g_n(p) = \frac{T}{t_r} \cdot \frac{p^{n-2}}{(p+\beta_1)(p+\beta_2)\dots(p+\beta_n)} \quad \dots \quad (34)$$

As the denominator of (34) is of higher degree in  $p$  than the numerator, Heaviside's expansion theorem can be applied to obtain the inverse transform

$$g_n(t) = \frac{T}{t_r} \sum_{r=1}^n \frac{e^{-\beta_r t}}{D'(\beta_r)} \quad (35)$$

where

$$D(p) = (p+\beta_1)(p+\beta_2)\dots(p+\beta_r)\dots(p+\beta_n) \quad (36)$$

Equation (35) is expanded below for  $n$  from one to four.

$$g_1(t) = \frac{T}{t_r} \left[ 1 - e^{-t} \right] \quad (37)$$

$$g_2(t) = \frac{T}{t_r} 0.44721 \left[ e^{-0.38197 t} - e^{-2.61803 t} \right] \quad (38)$$

$$g_3(t) = \frac{T}{t_r} \left[ 0.43554 e^{-0.64310 t} - 0.24171 e^{-5.04892 t} - 0.19384 e^{-0.30798 t} \right] \quad \dots \quad (39)$$

$$g_4(t) = \frac{T}{t_r} \left[ 0.09771 e^{-0.28312 t} - 0.28133 e^{-0.42602 t} + 0.33333 e^{-0.14969 t} \right] \quad (40)$$

With the help of equations (31) and (37)---(40) the responses of cascaded differentiating circuits to a pulse as shown in figure 2 can be easily obtained. The responses for sections from one to three are shown in figures 11—13 for three values of  $t_r/T$  as in the case of the analysis of integrating circuits.

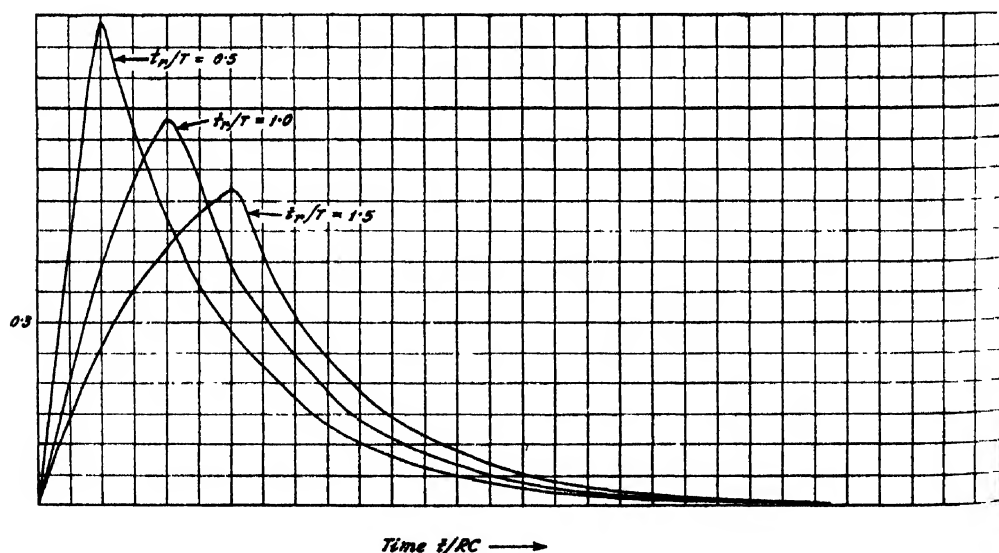


FIG. 11  
Response to a ramp function of a single-stage differentiating circuit ( $n=1$ ).



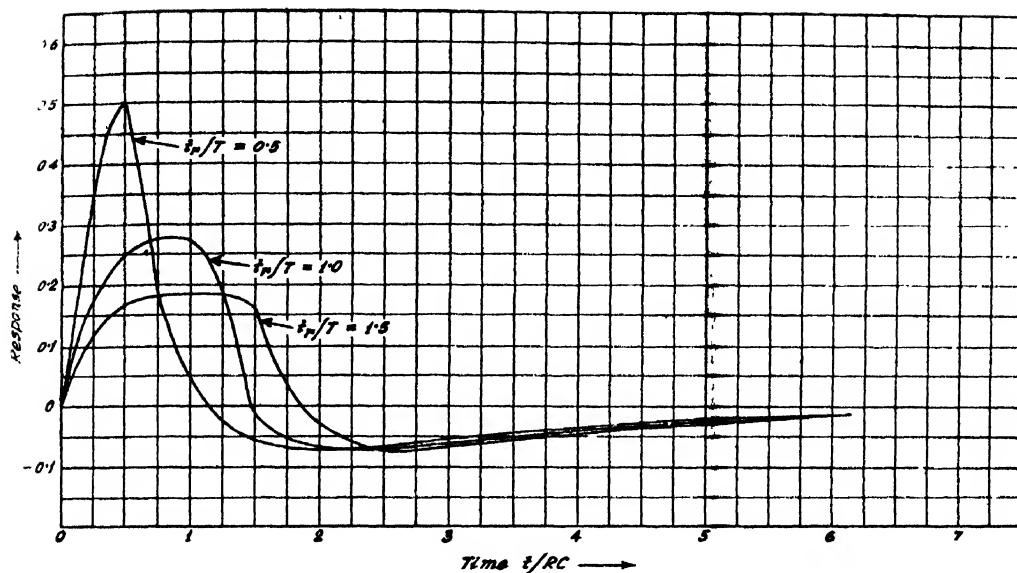


FIG. 12

Response to a ramp function of a two stage differentiating circuit ( $n=2$ ).

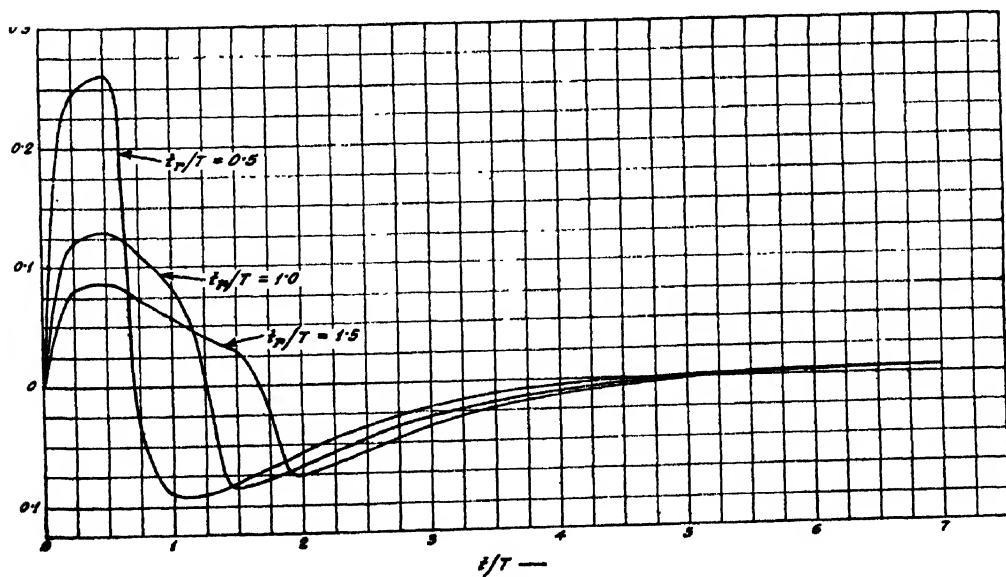


FIG. 13

Response to a ramp function of a three-stage differentiating circuit ( $n=3$ ).

It is evident from the figures 11—14 that the characteristics of the output pulse shape depends very much upon two parameters: (i) the rise time  $t_r$  of the input pulse and (ii) the number of cascaded sections.

The effect of the rise time  $t_r$  can easily be seen from the following table which shows the maximum output voltage that can be obtained for an input pulse of specified rise time and the half amplitude widths of the output pulses in terms of  $t/RC$ .

$$t_r/T = 0 \quad (\text{Step function input pulse}):$$

$n$	1	2	3	4
Maximum output voltage ..	1	1	1	1
Half amplitude widths ..	0.690	0.225	0.100	0.051

$$t_r/T = 0.1$$

$n$	1	2	3	4
Maximum output voltage ..	0.952	0.864	0.748	0.618
Half amplitude widths ..	0.75	0.26	0.16	0.13

$$t_r/T = 0.5$$

$n$	1	2	3	4
Maximum output voltage ..	0.787	0.497	0.260	0.158
Half amplitude widths ..	0.95	0.53	0.25	0.21

$$t_r/T = 1.5$$

$n$	1	2	3	4
Maximum output voltage ..	0.632	0.275	0.130	0.079
Half amplitude widths ..	1.32	1.05	0.51	0.31

$$t_r/T = 1.5$$

	1			
Maximum output voltage	0.518	0.182	0.087	0.053
Half amplitude widths	1.68	1.55	0.56	0.28

From this table we find that the maximum amplitude of the output voltage varies directly with the rise time  $t_r$ . In the case of single section differentiating circuit, the maximum output voltage is obtained at  $t = t_r$ . But as the number of sections increases, the maximum output voltage occurs at an earlier time because of the rounded shape at the peak of the differentiated output in the case of  $n = 1$ . This is the reason why with the increase of  $n$ , the time at which the voltage response reaches its maximum becomes shorter.

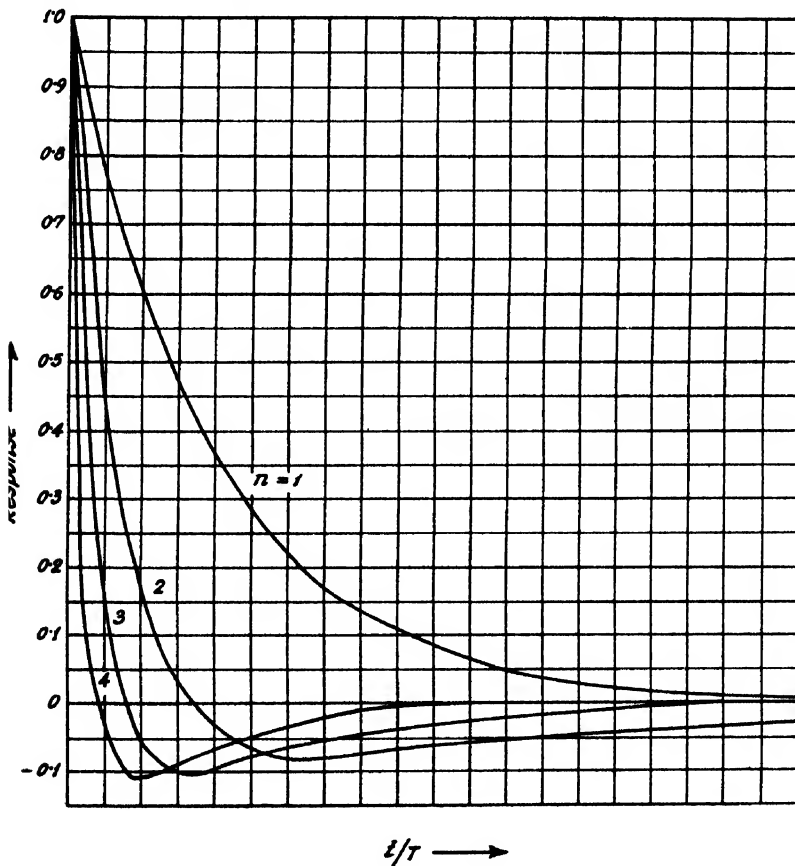


FIG. 14

Response to a step pulse of  $n$ -stage differentiating circuits.

A negative overshoot arises when  $n > 1$  and it begins to oscillate from negative to positive value as the number of sections increases.

In the previous table we have also inserted the case when a unit step function voltage is applied to the input. The response can be found easily since we know both the system transform and excitation transform (Kenyon, 1951). The transform of the output voltage is then given by

$$e_n(p) = \frac{1}{p} \frac{(Tp)^n}{[1 + t_1 Tp + \dots + t_r T^r p^r + \dots + t_n T^n p^n]} \quad (41)$$

which can be written as

$$e_n(p) = \frac{1}{p} \frac{(Tp)^n}{(Tp + \beta_1)(Tp + \beta_2) \dots (Tp + \beta_n)} \quad (42)$$

This can be normalized by substituting  $t = t/RC$  to obtain

$$e_n(p) = \frac{p^{n-1}}{(p + \beta_1)(p + \beta_2) \dots (p + \beta_n)} \quad (43)$$

By applying Heaviside's Expansion theorem we have,

$$e_n(t) = \sum_{r=1}^n \frac{(-\beta_r)^{n-1}}{D'(-\beta_r)} e^{-\beta_r t} \quad (44)$$

where

$D(p)$  is given by the expression (36).

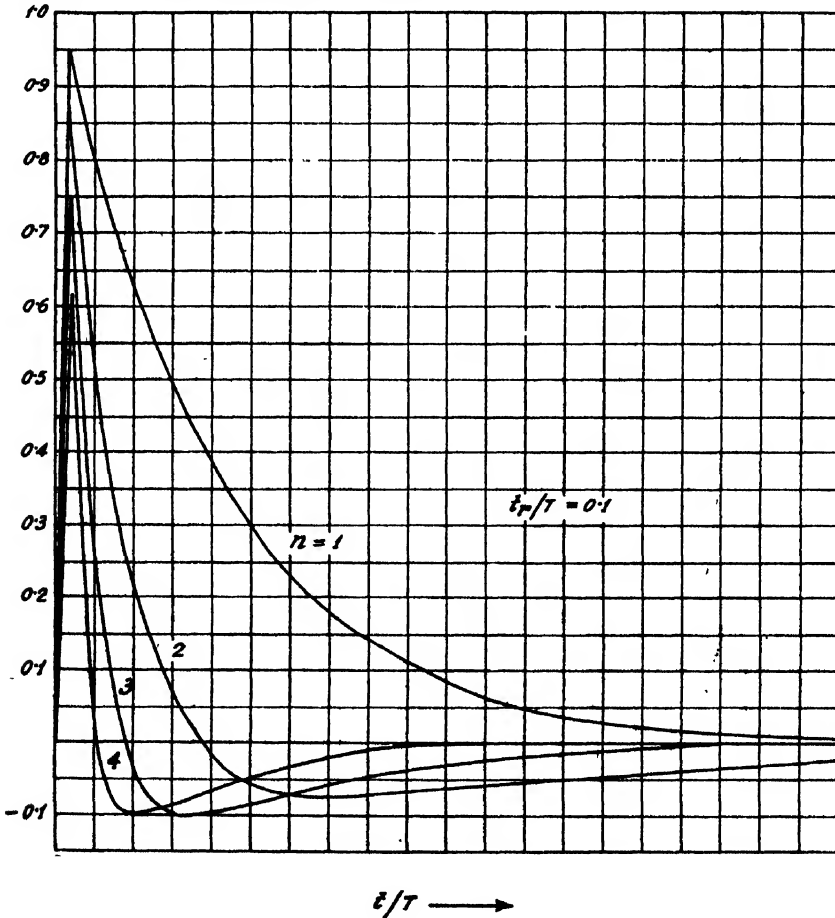


FIG. 15  
Response to a ramp function of  $n$ -stage differentiating circuits.

So with the help of equation (44), we can find out the responses of cascaded differentiated circuits to step function input voltages as shown in figure 15.

As the rise time  $t_r$  will be diminished, the responses will gradually be identical with that in figure 15. This can clearly be seen if we compare figures 14 and 15 where figure 15 is drawn for the case  $t_r/T = 0.1$ . Though in the latter case the maximum output voltage drops very much when  $n > 1$ , the exponential fall of the two curves shows marked similarity.

It is seen from figure 15 that even when  $n > 1$ , the maximum output voltage occurs at time  $t = t_r$  because of the short rise time and the absence of rounded peak.

### CONCLUSION

The present analysis of integrating and differentiating circuits has been done in order to show the importance of rise time of the input pulse in modifying their responses. In the case of integration the major effect of the rise time is to delay the integrated output to reach its maximum value. While in differentiation, the rise time practically determines the maximum output voltage that can be obtained. This limitation may become serious when the differentiated response is applied for the purpose of triggering a circuit.

Again, the flat top of the output that has been shown in some cases, e.g. in figures      and      , is sometimes very unsuitable for triggering.

### ACKNOWLEDGMENTS

The author is indebted to Prof. M. N. Saha, F.R.S. and Dr. B. D. Nag for their kind interest in the work. Sincere thanks are also due to Mr. B. M. Bauerjee and Dr. A. K. Saha for valuable discussions.

### REFERENCES

- Bhattacharyya, B. K., 1952, *Ind. J. Phys.*, **26**, 563.
- Kenyon, R. R., 1951, *Proc. I. R. E.*, **39**, 557.
- Rubin, M. D., 1952, *Electronics for Communication Engineers*, McGraw-Hill Book Co.
- Schwartz, L. S., 1946,—*Proc. I. R. E.*, **34**, 862.



# ABSORPTION OF U. H. F. RADIO WAVES IN THE RANGE 250-920 Mc/sec BY SUBSTITUTED BENZENES. III \*

BY DILIP KUMAR GHOSH

OPTICS DEPARTMENT, INDIAN ASSOCIATION FOR THE CULTIVATION OF SCIENCE, CALCUTTA 32

(Received for publication, March 13, 1953)

**ABSTRACT.** The absorption of U. H. F. radio waves in the range 250-920 Mc/sec in chlorobenzene, bromobenzene, *o*-xylene and *m*-xylene at room and lower temperatures has been investigated by optical method, using a G.R. 1209 A oscillator as the source of radio waves. In the case of chlorobenzene a peak has been observed at 820 Mc/sec at room temperature and this is observed to shift to 580 Mc/sec at 0°C. The peak is found to be due to a dimer. In the case of bromobenzene the peak at room temperature is beyond 920 Mc/sec, but it is at 880 Mc/sec at 0°C. The peak is due to a monomer. Indication of a peak below 250 Mc/sec at 0°C due to dimers has also been observed. In the case of *o*-xylene no absorption is observed at room temperature, but the liquid shows an absorption peak at 570 Mc/sec at 0°C, which shifts to 500 Mc/sec at -20°C. This peak is due to dimers. In the case of *m*-xylene at 0°C no absorption is observed, but at -30°C an absorption peak at 820 Mc/sec is observed. This peak is also due to dimers.

It is concluded from these results that with the lowering of temperatures of the liquids mentioned above associated groups of molecules, each group containing two molecules, are formed and the number of such groups increases with further lowering of temperature.

## INTRODUCTION

It was recently shown by Kastha (1952) that cresols absorb radio waves in the frequency range 700-900 Mc/sec and that the shift and diminution of height of the peak with dissolution of the liquid in non-polar solvents observed in the case of *m*-cresol is different from that observed in the case of *o*-cresol. The results obtained by him indicate that some of the molecules of all the three cresols exist as dimers in the liquid state and these dimers dissociate to form monomers when the liquids are either heated or dissolved in non-polar solvents. The data reported by him further show that the radius of the rotor calculated from Debye's theory, taking the macroscopic viscosity as the inner viscosity, is of the order of the radius of the single molecule in the case of meta- and paracresols. This fact not only proves the validity of Debye's theory in the frequency range mentioned above but also shows that in the case of the liquids mentioned above the macroscopic viscosity is identical with the inner viscosity mentioned in Debye's theory.

\* Communicated by Prof. S. C. Sirkar

The method also furnishes information regarding the nature of association of molecules in the liquid state. It is, however, not possible to draw a general conclusion from results obtained in the case of a few liquids. The question whether formation of stationary waves in the absorption cell affects the absorption coefficient obtained by the optical method, is also to be investigated thoroughly. A programme has, therefore, been undertaken to study the absorption of radio waves of frequencies in the range 250-920 Mc/sec in substituted benzenes in liquid state at different temperatures and in solution in different non-polar solvents. In the present paper the results obtained in the case of chlorobenzene, bromobenzene, orthoxylene and metaxylene have been discussed.

### EXPERIMENTAL

The liquids were all of chemically pure quality and were supplied by B. D. H. They were all distilled before being used in the investigation. A G.R.1209A oscillator with its shield removed was used as source of radio waves of frequencies ranging from 250 Mc/sec to 920 Mc/sec and a crystal detector was used as the receiver. Two absorption cells of inner thickness 1.7 and 3.5 cms respectively were used in the case of chlorobenzene to find out whether the values of absorption coefficient deduced in the two cases agree with each other. Reading of the tuned detector were taken first with an empty cell as absorber and then with a similar cell filled with the particular liquid, the detector being tuned again. In order to take readings for the liquid at low temperatures the cell containing the liquid was immersed in absolute alcohol, cooled to the proper temperature by being mixed with liquid oxygen. When the thermometer, inserted in the liquid through the stopper of the cell, indicated the proper temperature the cell was taken out and was placed in front of the tuning circuit of the detector, and after tuning the circuit again, the reading was noted. Care was taken to remove all obstacles from the vicinity of the oscillator and the detector to avoid reflection of the radio waves. The investigation was carried out in a large room so that the distance of the nearest wall from the oscillator was about 12 ft. No reflector was used in these investigations. The values of attenuation coefficient were calculated from the formula  $\mu = \frac{2.34}{x} \log_{10} \left( \frac{I_0}{I} \right)$  where  $x$  is the thickness of the liquid absorber.

### RESULTS AND DISCUSSION

The values of  $\mu$  calculated for different thicknesses of the cell in the case of chlorobenzene were found to be identical. The values of  $\mu$  for different frequencies for the liquids at different temperatures are given in Tables I-VII. In order to locate the absorption maxima accurately absorp-



tion curves have been drawn in figures 1-5. The values of  $\tau$  deduced from the frequencies at absorption maxima and the values of dielectric constant for frequencies zero and infinity according to Debye's theory are given in Table VIII. Finally, the values of cubes of the radii of rotors calculated on the assumption that the molecules are spherical are given in the last column of Table VIII.

TABLE I

Chlorobenzene at 25°C.

The thickness of the liquid, 3.5 cms

Frequency in Mc/sec.	$\frac{I_0}{I}$	Attenuation coefficient, $\mu$	$\mu \times 10^2$	Remarks
600	1	0	0	$\mu$ was calculated with thickness of the liquid 1.7 cms and it was found that $\mu = .0784$ at 820 Mc/sec
650	1	0	0	
700	1	0	0	
730	1	0	0	
780	1	0	0	
800	1.10	0.0505	5.05	
820	1.31	0.0784	7.84	
840	1.08	0.0223	2.23	
860	1	0	0	
880	1	0	0	
900	1	0	0	

TABLE II

Chlorobenzene at 0°C.

The thickness of the liquid, 3.5 cms

Frequency in Mc/sec.	$\frac{I_0}{I}$	Attenuation coefficient, $\mu$	$\mu \times 10^2$
550	1.33	.0827	8.27
565	1.5	.1175	11.75
580	1.62	.1397	13.97
600	1.51	.1175	11.75
620	1.16	.0431	4.31
640	1	0	0
700	1	0	0

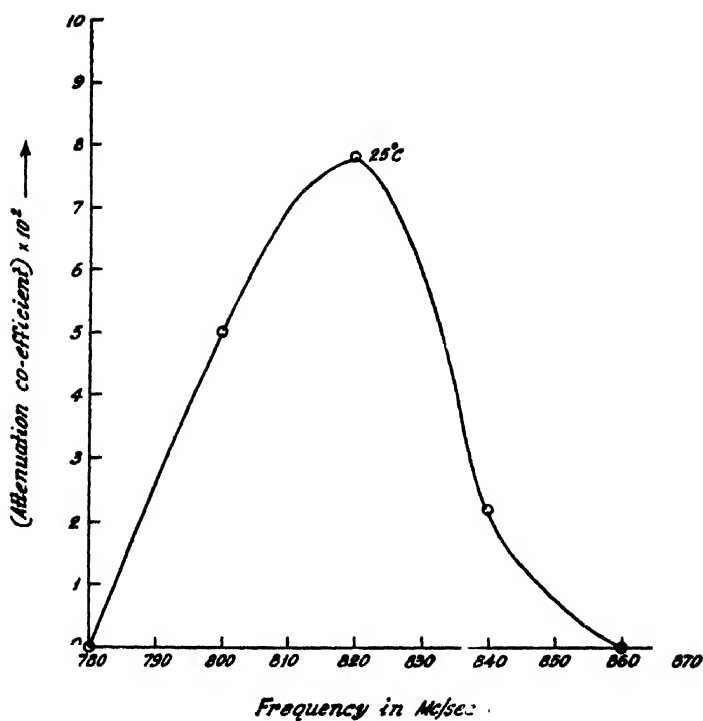


FIG. 1  
Chlorobenzene at 25°C

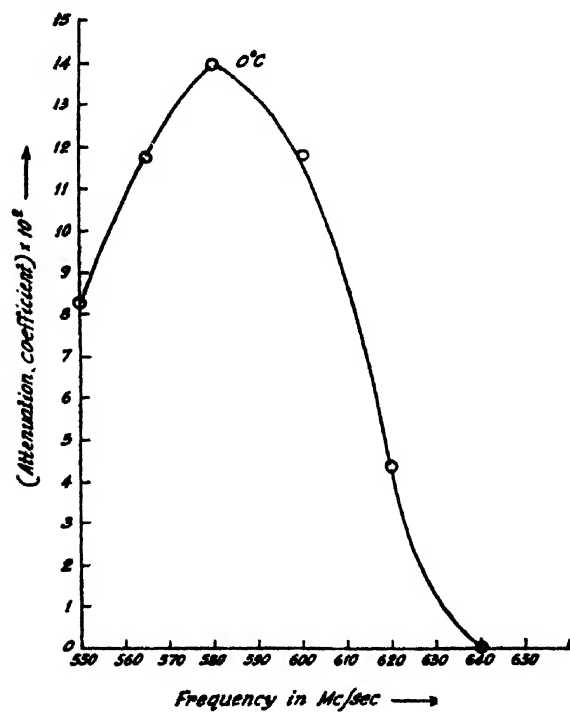


FIG. 2  
Chlorobenzene at 0°C

TABLE III

Bromobenzene at 30°C,  
The thickness of the liquid, 3.5 cms.

Frequency in Mc/sec.	$\frac{I_0}{I}$	Attenuation coefficient, $\mu$	$\mu \times 10^2$
860	1	0	0
880	1.04	.0114	1.14
900	1.25	.0648	6.48
920	1.71	.1540	15.40

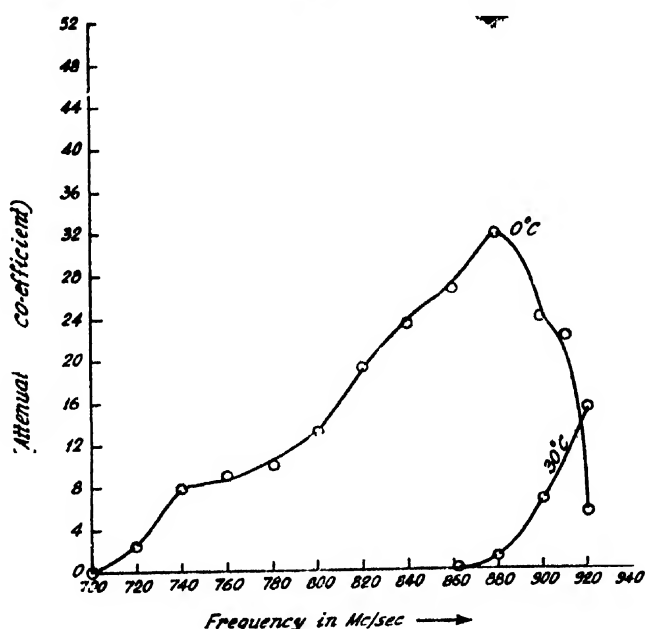


FIG. 3

Bromobenzene

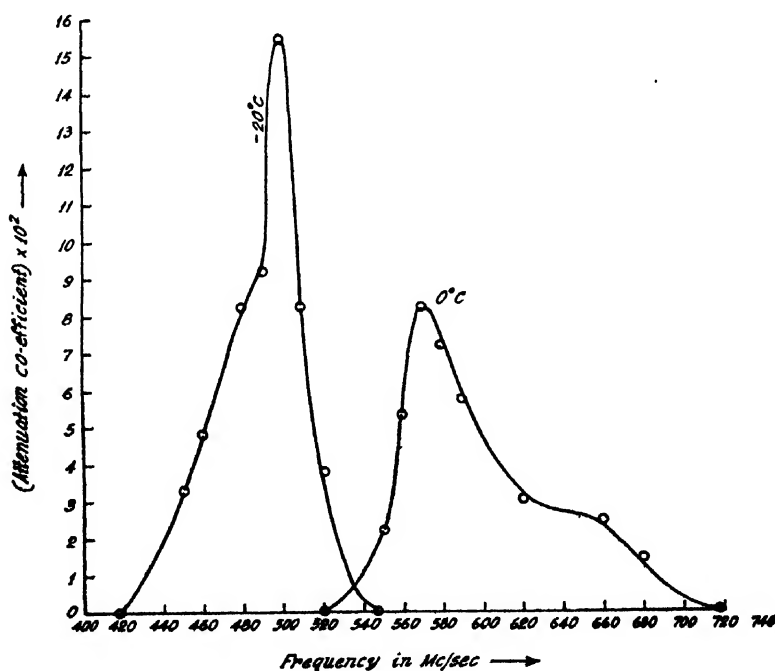
The results for chlorobenzene at 0°C agree with those reported by Sen (1950), because with his oscillator the maximum frequency was 520 Mc/sec and for this frequency the attenuation coefficient observed by him agrees with that observed in the present investigation. The absorption maximum at 0°C is at 580 Mc/sec and this shifts to 820 Mc/sec when the temperature of the liquid rises to 25°C. Although the shift is large, being about 240 Mc/sec, the values of  $a$ , the radius of the rotor calculated for the two temperatures are not widely different from each other. As the calculated radius is greater than  $4 \times 10^{-8}$  cm, the rotor cannot be a single molecule. It is evidently a dimer. As the height and the width of the absorption peak increase with the lowering of temperature from 25°C to 0°C, the number of such dimers increases with the lowering of temperature.

TABLE IV

Bromobenzene at 0°C.

The thickness of the liquid, 3.5 cms.

Frequency in Mc/sec.	$\frac{I_0}{I}$	Attenuation coefficient, $\mu$	$\mu \times 10^3$
720	1.09	.0450	2.50
740	1.31	.0784	7.84
760	1.36	.0893	8.93
780	1.42	.1018	10.18
800	1.57	.1309	13.09
820	1.94	.1944	19.24
840	2.25	.2354	23.54
860	2.5	.2661	26.61
880	3	.3189	31.89
900	2.27	.2380	23.80
910	2.14	.2209	22.09
920	1.2	.0530	5.30

FIG. 4  
Ortho xylene

In the case of bromobenzene at 30°C on the other hand, no absorption peak is observed in the frequency range 250-920 Mc/sec, but the attenuation coefficient increases rapidly as the frequency increases from 880 to 920 Mc/sec. This indicates that the absorption maximum occurs at still higher frequencies. When the liquid is cooled to 0°C an absorption peak at

TABLE V  
o-Xylene at 0°C.  
Thickness of the liquid, 3.5 cms.

Frequency in Mc/sec.	$\frac{I_0}{I}$	Attenuation coefficient, $\mu$	$\mu \times 10^2$
500	1	0	0
520	1	0	0
550	1.08	.0223	2.23
560	1.20	.0530	5.30
570	1.33	.0827	8.27
580	1.28	.0716	7.16
590	1.22	.0577	5.77
620	1.11	.0303	3.03
660	1.09	.0250	2.50
680	1.05	.0142	1.42
720	1	0	0
740	1	0	0

TABLE VI  
o-Xylene at -20°C.  
The thickness of the liquid, 3.5 cms.

Frequency in Mc/sec.	$\frac{I_0}{I}$	Attenuation coefficient, $\mu$	$\mu \times 10^2$
420	1	0	0
450	1.12	.0329	3.29
460	1.18	.0401	4.81
480	1.33	.0827	8.27
490	1.37	.0914	9.14
500	1.71	.1540	15.40
510	1.33	.0827	8.27
520	1.14	.0380	3.80
550	1	0	0
560	1	0	0
570	1	0	0

TABLE VII  
m-Xylene at -30°C.  
Thickness of the liquid, 3.5 cms.

Frequency in Mc/sec.	$\frac{I_0}{I}$	Attenuation coefficient, $\mu$	$\mu \times 10^2$
780	1	0	0
800	1.11	.0303	3.03
820	1.33	.0827	8.27
840	1.16	.0431	4.31
860	1.05	.0142	1.42
380	1	0	0

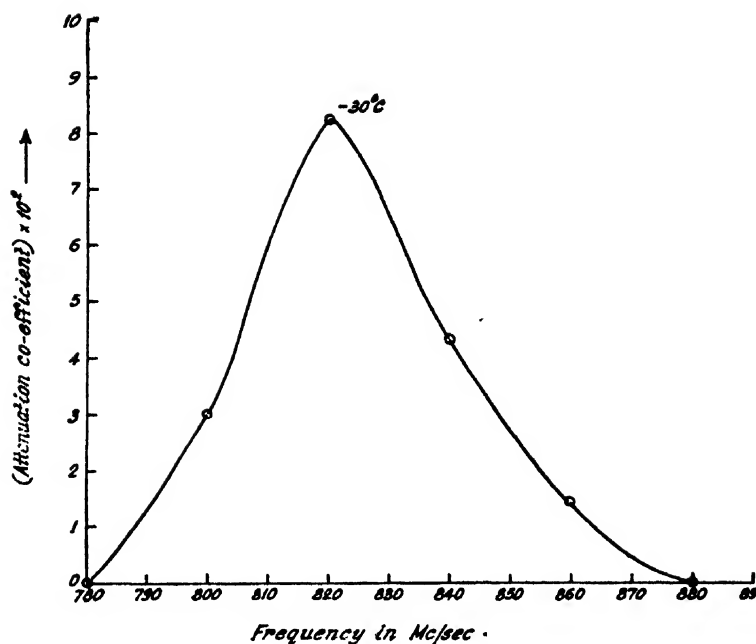


FIG. 5  
Meta xylene

TABLE VIII

Liquid	$\frac{\omega}{2\pi}$ in Mc/sec	Temperature in °C	$\eta \times 100$	$\tau \times 10^{10}$	$\epsilon_0$	$\epsilon_1$	$a^3 \times 10^{24}$ c.c
Chloro- benzene	820	25	.751	1.708	2.325	5.621	73.96
	580	0	1.053	2.370		6.0	66.97
Bromo- benzene	880	0	1.573	1.592	2.433	5.74	30.09
<i>o</i> -Xylene	570	0	1.105	2.763	2.268	2.648	74.39
<i>m</i> -Xylene	820	-30	1.08	1.527	2.243	2.462	47.26

880 Mc/sec is observed. The value of the radius of the rotor comes out as  $3.10 \times 10^{-8}$  cm. The calculated volume of the rotor being half of that found in the case of chlorobenzene, the peak observed at 880 Mc/sec in the case of bromobenzene is due to single molecules. A search was made for another peak due to the dimer at lower frequencies but no such peak was observed. This shows that at 0°C most of the molecules of this liquid are monomers. This may be due to the fact that the chemical affinity of

bromine atom is less than that of the chlorine atom. Dimers may, however, be found even in the case of bromobenzene at temperatures below  $0^{\circ}\text{C}$ . The liquid was, therefore, cooled to  $-8^{\circ}\text{C}$  and at this temperature the liquid was found to exhibit a little absorption at about 280 Mc/sec. The attenuation coefficient increased gradually as the frequency diminished to 250 Mc/sec. This shows that at  $-8^{\circ}\text{C}$  there is a peak in the region of about 240 Mc/sec. This peak is probably due to dimers which are formed only at temperatures below  $0^{\circ}\text{C}$  in this case.

Ortho and metaxylene at  $30^{\circ}\text{C}$  did not show any appreciable absorption in the frequency range 250-920 Mc/sec. Metaxylene did not show any absorption in the above range even when cooled to  $0^{\circ}\text{C}$ . At  $-30^{\circ}\text{C}$ , however, a low absorption peak was exhibited by the liquid at 820 Mc/sec. The value of radius of the rotor calculated from the viscosity and  $\tau$ , the relaxation time, assuming the rotor to be spherical, is  $3.61 \times 10^{-8}$  cm. The peak is probably due to dimers. The peak due to the monomer at  $-30^{\circ}\text{C}$  lies at frequencies much higher than 920 Mc/sec in this case. In the case of *o*-xylene at  $0^{\circ}\text{C}$  a low peak is observed at 570 Mc/sec. The peak increases in height and shifts to 500 Mc/sec when the liquid is cooled to  $-20^{\circ}\text{C}$ . The radius of the rotor in this case is about  $4.2 \times 10^{-8}$ . So in this case also the rotor is a dimer. The peak due to the monomer is evidently at a frequency larger than 920 Mc/sec.

The difference in the viscosity of the liquids accounts for the difference in position of the peaks due to the dimers. It has to be mentioned in this connection that Sirkar and Sen (1949) observed a gradual increase of the absorption coefficient with increase of frequency beyond 500 Mc/sec in case of xylene which was a mixture of the three isomers. This lowering of frequency of the absorption peak is probably due to formation of groups of molecules in the mixture larger than dimers.

Incidentally, it may be pointed out that the values of  $\tau$  observed for these four molecules are of the order of  $10^{-10}$  second. The corresponding frequencies are less than  $1 \text{ cm}^{-1}$ . Hence the Raman lines having frequency shifts in the range  $10-120 \text{ cm}^{-1}$  due to these substances in the solid state must be due to vibrations in which the intermolecular field is many times stronger than that in the liquid.

#### ACKNOWLEDGMENT

The author's thanks are due to Prof. S. C. Sirkar for his kind interest and guidance throughout the progress of the work.

#### REFERENCES

- Kastha, G. S., 1952, *Ind. J. Phys.*, **62**, 103.  
Sen, S. N., 1950, *Ind. J. Phys.*, **24**, 163.  
Sirkar, S. C. and Sen, S. N., 1949, *Nature*, **164**, 1948.

# ELECTRICAL PROPERTIES OF INDIAN MICA. V. D. C. RESISTIVITY

By S. S. MANDAL AND P. C. MAHANTI

DEPARTMENT OF APPLIED PHYSICS, UNIVERSITY COLLEGE OF SCIENCE, CALCUTTA.

*(Received for publication, November 11, 1952)*

**ABSTRACT.** The present paper reports the results of measurement of volume and surface resistivities of different qualities of the more abundant red and green Indian muscovite mica and the effect of humidity, temperature and preheating on them.

## INTRODUCTION

It is wellknown that one of the important electrical properties of an electrical insulating material is its d.c. resistivity which is the reciprocal of its conductivity. In the case of a solid insulating material, this resistivity is determined by measuring its insulation resistance, which is usually considered to be the resultant of two components, *viz.*, the volume resistance and the surface resistance, owing to the fact that when such a material is subjected to a difference of potential across it, there is a flow of current not only throughout its volume but also along all its surfaces. The volume resistivity of mica and its variation with temperature has been studied by many investigators before 1934. They found the volume resistivity of different kinds of mica to vary over wide limits, the muscovite having the highest value. The variation with temperature followed practically a linear law between 0°C and 100°C, after which it underwent a slow but gradual diminution. It is not clearly mentioned whether they took any Indian mica in their observations.

The present investigation was undertaken with the object of determining the volume as well as surface resistivities of different qualities of the more abundant red and green varieties of Indian muscovite mica of different qualities and origins and the effect of humidity and temperature on their resistivities. It was also thought of interest to ascertain how these resistivities were affected by pre-conditioning the samples at different temperatures.

Measurement has been made on the following muscovite micas. They were obtained in the form of booklets from the Geological Survey of India.

1. Bihar Red (Bengal Ruby), clear.
2. Bihar Red, stained.
3. Bihar Red, stained and slightly spotted.
4. Madras Green, clear.
5. Madras Green, stained.
6. Madras Green, stained and slightly spotted.



The most direct method of measuring the d.c. resistivity of an electrical insulating material is to apply a known potential difference between two points on opposite sides of the material and to measure by any suitable method the current which is usually very feeble. But when desired the two components, *viz.*, the volume and the surface resistivities can be determined separately. For this purpose Curtis (1914) devised a guard-ring method using mercury electrodes; but if the resistivities are very high, the measurement of this extremely small current becomes difficult even with a highly sensitive galvanometer or a quadrant electrometer. The ballistic discharge method which consists in charging a condenser made from the material and discharging it through a highly sensitive ballistic galvanometer, is also not satisfactory. Fortunately, the electron tube method has been successfully used in recent years for the measurement of such a feeble current. Special vacuum tubes, called electrometer tubes, are used for this purpose. A pilotron F. P-54 tube of International General Electric Company of America has been used by several investigators notably by Rose (1931), Hill (1931), Du Bridge (1931), Du Bridge and Brown (1933), Turner and Seigelin (1933) and Penick (1935) in developing circuits for the measurement of such feeble currents. The Penick circuit, as modified by Armistead (1948), gives a rapid measurement of such current. The R. C. A. miniature tube 12BE6 has also been used for this purpose as a high sensitivity stabilized d.c. amplifier by Anker (1947), Caldecourt (1949) and others. But the circuit developed by Cherry (1937), using Westinghouse RH-507 electrometer triode is very simple and, therefore, in the present investigation a similar circuit has been developed, using a Philips 4060 electrometer tube as an amplifier. A sensitive moving coil galvanometer served as the detector. The parameters of this valve were determined by Thae (1939).

#### THE MEASURING CIRCUIT.

The circuit is developed as shown in figure 1. As stated before a Philips 4060 electrometer valve is used here as a d.c. amplifier. For a smooth operation of the valve it is necessary to adjust the filament voltage to 0.64 volts with a plate voltage of 4 volts at zero grid-bias. A 5-megohm resistance is connected to the grid to obtain a stable working condition of the valve. To avoid electrostatic disturbances the valve is carefully screened by enclosing it inside a metallic case, (shown by a dotted line) properly earthed. The metal case has holes to allow connections to be made to the valve and contains fused calcium chloride in a porcelain pot to prevent any leakage of current due to deposition of moisture on the surface of the valve.

The main measuring circuit includes the mica test piece and a standard high resistance ( $R_1$ ) in series with a battery of dry cells giving a steady voltage of about 150 volts. A dummy high resistance ( $R_2$ ) of the same order of magnitude as the standard high resistance ( $R_1$ ) is connected across the

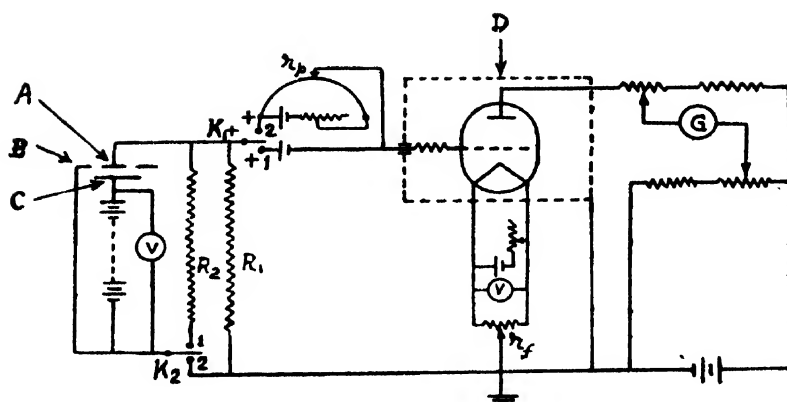


FIG. 1

- |                      |                    |
|----------------------|--------------------|
| A. Central electrode | B. Guard ring      |
| C. Lower electrode   | D. Metal enclosure |

test piece to by-pass the charging current to be fed through it. The high resistances are prepared and standardised, as advocated by Gemant, using solutions of picric acid, benzene, phenol and absolute alcohol in different proportions.

The plate circuit has two loading resistances, one having a floating contact. A wheatstone bridge network is formed by including the valve in one arm. The detector is connected across two floating points in the bridge in the usual way.

The special features of this measuring circuit are as follows :

1. The voltage across the standard high resistance ( $R_1$ ) is compensated by means of the potentiometer,  $r_p$ , so as to keep the grid at zero-potential during operation. The potentiometer is standardised with the help of a Weston standard cell, using the same amplifier and detector circuits. Such a compensation avoids the shifting of the working point of the valve when the grid-bias is likely to change because of a possible variation of current in the main measuring circuit.

2. A fine and accurate adjustment of the d.c. resistance of the bridge arm containing the valve can be carried out when necessary by changing the amplification of the valve with the help of the potential divider,  $r_f$ .

3. The charging current of the test piece can be by-passed by means of the dummy high resistance ( $R_2$ ). This prevents sudden application of higher voltage to the grid and helps the valve to operate under its normal working condition.

#### EXPERIMENTAL PROCEDURE

Mica samples were selected after examining visually their transparency, colour, spots and pits. From the selected samples were split out test-pieces of different thickness and cut in approximately 4 inches square size. They

were thoroughly cleansed with rectified spirit and stored in a desiccator at room temperature.

The measurement of thickness of a test-piece was ascertained before mounting between electrodes and conditioned at any desired value of humidity or temperature at which its resistance was to be measured.

The thickness was measured by means of dial micrometer to an accuracy of  $\pm 0.01$  mil. at several points. If the thickness at any point over its surface was found to vary by more than 2.5% from that at other points, it was excluded from test.

The conventional method of using mercury electrodes was found inconvenient for the present purpose. Highly polished brass electrodes were therefore, used and arranged as shown in figure 2. The lower electrode was

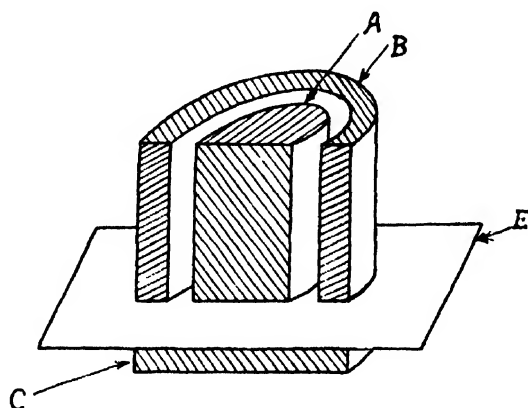


FIG. 2

- |                      |               |
|----------------------|---------------|
| A. Central electrode | B. Guard ring |
| C. Lower electrode   | E. Sample     |

comparatively light and had a diameter of 3 inches. The upper central electrode and the guard-ring were massive and thereby helped in securing an intimate contact with the surface of the test-piece. To ensure further intimate contact aqua-dag was used. The diameter of the central electrode was 1.5 inches while the inner diameter of the guard-ring was 1.75 inches. A groove to a depth of one inch was cut at the centre of the central electrode to hold a mercury-in-glass thermometer.

To condition a test-piece to a desired value of humidity, a desiccator containing the test piece fitted with electrodes was first evacuated and then filled with humidified air of that value of humidity at room temperature. The humidified air was obtained by bubbling dry air through calcium chloride tubes into humidity controlling jars containing glycerine solution of suitable concentration. An Edney paper hygrometer was fitted inside the desiccator to indicate directly the value of humidity to which a test-piece was conditioned. A conditioning of the test-piece for at least five hours at any value of humidity was found sufficient.

A heating plate on an asbestos board was also placed on the bottom platform of the desiccator. By varying the current through the heating element, any desired temperature could be easily maintained within the desiccator and read to an accuracy  $\pm 0.1^\circ\text{C}$ . from the thermometer fitted to the central electrode.

To study the effect of pre-heating, the resistance of a test-piece was first measured at the room temperature and then heated successively to  $100^\circ\text{C}$ ,  $200^\circ\text{C}$  and  $300^\circ\text{C}$ . At each such temperature the test-piece was kept for a sufficiently long time and then cooled down to the room temperature at which its resistance was again measured.

The following procedure was adopted to measure the resistance of a test-piece.

To begin with,  $K_1$  was first plugged at 1 and then the potentiometer standardised. For this purpose the voltage from the standard Weston cell was applied to the grid by closing  $K_1$  at 1. This produced a deflection in the galvanometer. By adjusting the two floating contacts of the galvanometer in the bridge circuit and also the floating contact of the potential divider ( $r_f$ ), a zero-deflection of the galvanometer was obtained.  $K_1$  was next plugged at 2, so that a voltage from the potentiometer was impressed on the grid. The dial of the potentiometer was then adjusted to the value indicating 1.0183 volts. This, however, produced a deflection in the galvanometer, indicating that the current through the potentiometer circuit had to be adjusted to bring back the condition of balance. This was done alone with the help of the rheostat in the circuit without disturbing the bridge-arms. It may be noted that the potentiometer thus standardised could indicate directly a voltage upto 1.7000 volts and correct to the fourth place of decimal. Thus with the help of this potentiometer one can apply to the grid any voltage from 0 to 1.7000 volts very conveniently.

After standardising the potentiometer as described above, a zero voltage from the potentiometer was applied to the grid and the bridge balanced by adjusting the bridge-arms. The key  $K_2$  was then plugged at 2. This allowed the current in the test-piece to flow through the standard high resistance  $R_1$ . The consequent voltage drop across the  $R_1$  was, therefore, impressed on the grid. This disturbed the condition of balance of the bridge again. But by means of the potentiometer, the effect of the application of voltage from the standard high resistance was compensated by applying a voltage in the opposite sense to the grid and the balance of the bridge restored. The reading of the potentiometer thus indicated the voltage drop ( $e$ ) across the standard high resistance. The resistance ( $R_x$ ) of the test-piece was then calculated from the following relation :

$$R_x = R_1 \left( \frac{E}{e} - 1 \right) \quad \dots (1)$$

where,  $E$  = total voltage impressed across the mica test-piece and the standard high resistance in series.

It may be noted that to determine the volume resistance ( $R_v$ ) of the test-piece, the stress was applied between the lower and the upper central electrode, the guard-ring being earthed. When measuring its surface resistance ( $R_s$ ), the stress was, however, applied between the guard-ring and the upper central electrode, the lower electrode being earthed.

The volume resistivity ( $\rho_v$ ) and the surface resistivity ( $\rho_s$ ) of a test-piece of thickness ( $t$ ) in inches were calculated as follows :

$$\rho_v = \frac{\pi D_c^2 \cdot R_v}{4t} \text{ ohm-inch} \quad (2)$$

$$\rho_s = \frac{2\pi \cdot R_s}{\log_e \frac{D_g}{D_c}} \text{ ohms} \quad (3)$$

where,  $D_g$  = internal diameter of the guardring in inches

and  $D_c$  = external diameter of the upper central electrode in inches.

Substituting the actual dimensions of the electrodes used, we have,

$$\rho_v = 1.768 \frac{R_v}{t} \text{ ohm-inch}$$

$$\rho_s = 4.0853 R_s \text{ ohms}$$

## RESULTS AND DISCUSSIONS

The data obtained to show the effect of humidity, temperature as well as preheating temperature on the resistivities of different qualities of Indian muscovite micas of different origins are presented graphically in figures 3-9. It will be seen from figures 3 and 4 that at the constant temperature of 30°C both the volume and surface resistivities decrease with the increasing values of humidity, the variation in no case following a linear law. The effect of temperature on the resistivities is very pronounced and the value of resistivity for any particular quality of mica changes very rapidly with the variation of temperature from its value at the room temperature (30°C) and normal humidity (60%).

Because of the wide variation of volume and surface resistivities over the temperature range 30°C-300°C, their logarithmic values have been given in figures 5-7.

From figures 8 and 9, the effect of preheating of the samples to different temperatures but at normal humidity (60%) will be evident. It may be noted that the effect of preheating temperatures on resistivities of the micas is similar to that as found previously (Mahanti and Mandal, 1948) in the case of their power factor.

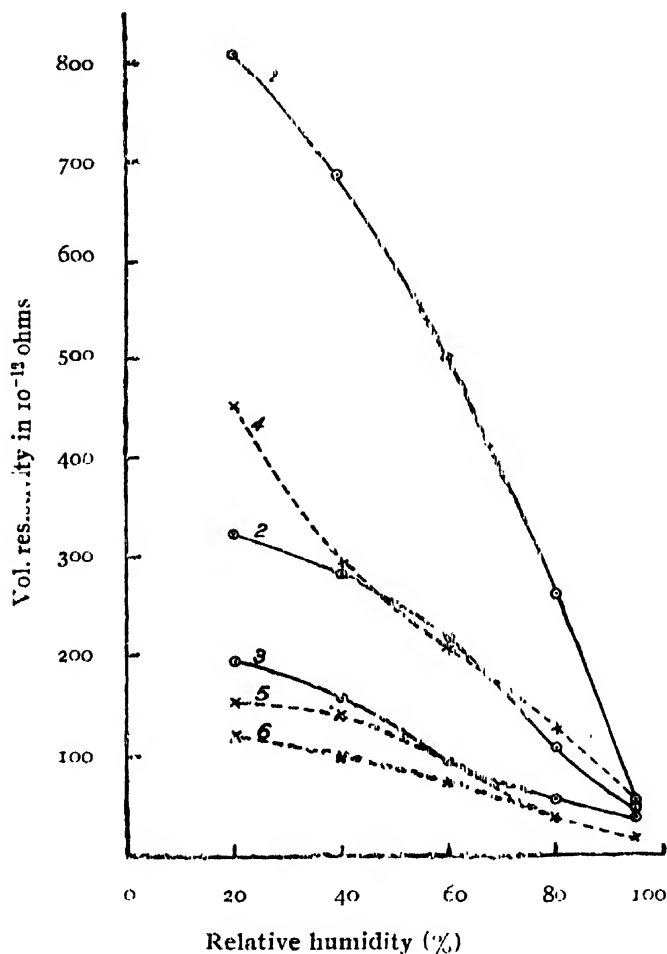


FIG. 3

Effect of humidity on vol. resistivity of Indian muscovite mica

1. Bihar Red (Bengal Ruby), clear
2. „ „ stained
3. „ „ stained & slightly spotted
4. Madras Green, clear
5. „ „ stained
6. „ „ stained & slightly spotted

From the above results, one is led to infer that the moisture in mica plays an important role in determining its electrical behaviour. we know that the moisture associated with mica may be traced to the following sources, viz (i) water deposition on its surface and (ii) moisture deposition inside its interlaminar spaces, besides its usual presence as water of crystallisation and water of constitution.

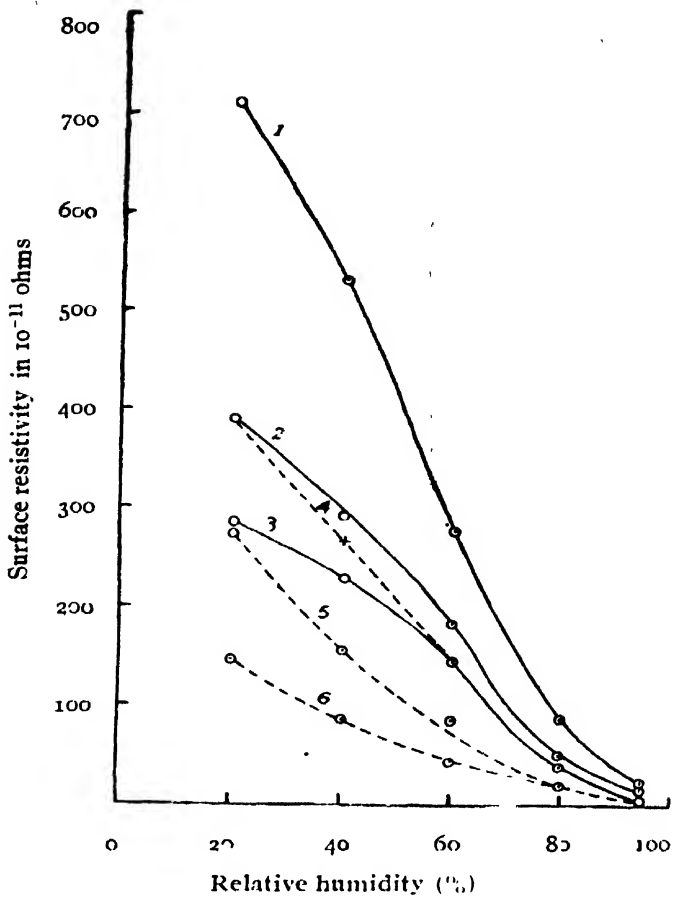


FIG. 4

Effect of humidity on surface resistivity of Indian muscovite mica

1. Bihar Red (Bengal Ruby) clear
2. „ „ stained
3. „ „ stained and slightly spotted
4. Madras Green, clear
5. „ „ stained
6. „ „ stained and slightly spotted

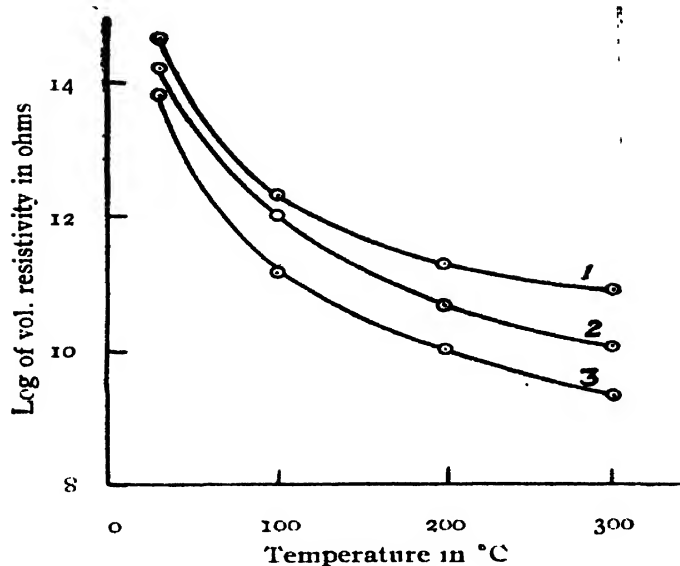


FIG. 5

Effect of temperature on vol. resistivity of Bihar Red mica

1. Clear, 2. Stained, 3. Stained and spotted

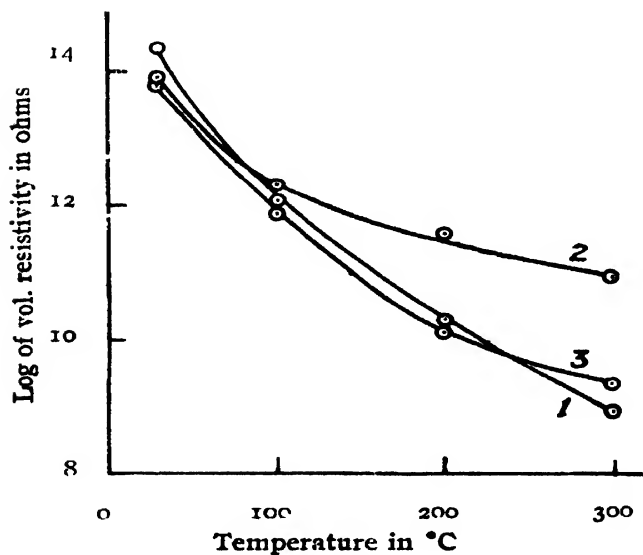


FIG. 6

Effect of temperature on volume resistivity of Madras Green mica

1. Madras Green, clear
2. " " stained
3. " " stained and spotted



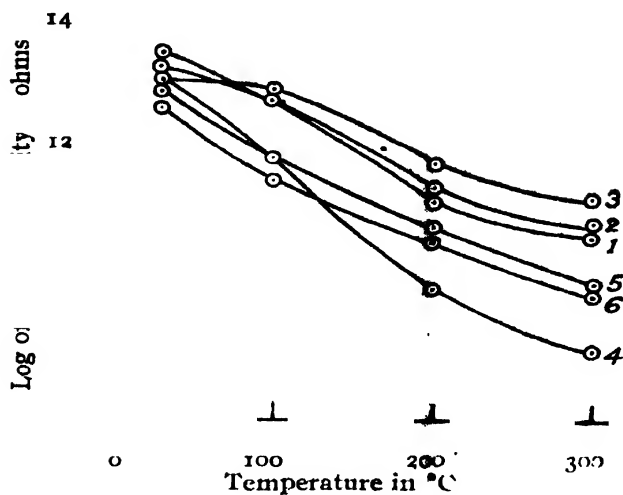


FIG. 7

Effective of temperature on surface resistivity of Indian muscovite mica

- |                            |                            |
|----------------------------|----------------------------|
| 1. Bihar Red, clear        | 4. Madras Green, clear     |
| 2. " " stained             | 5. " " stained             |
| 3. " " stained and spotted | 6. " " stained and spotted |

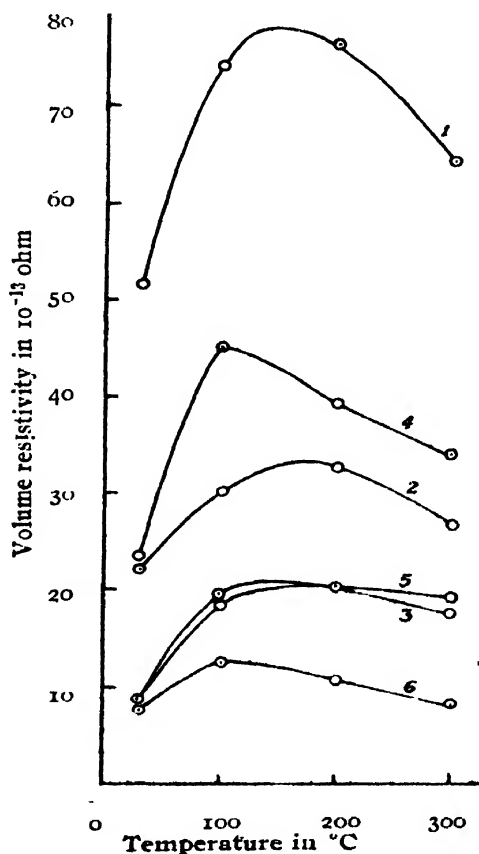


FIG. 8

Effect of pre-heating on volume resistivity of mica

- |                              |                                 |
|------------------------------|---------------------------------|
| Bihar Red :                  | Madras Green :                  |
| Clear                        | 4. Clear                        |
| Stained                      | 5. Stained                      |
| Stained and slightly spotted | 6. Stained and slightly spotted |

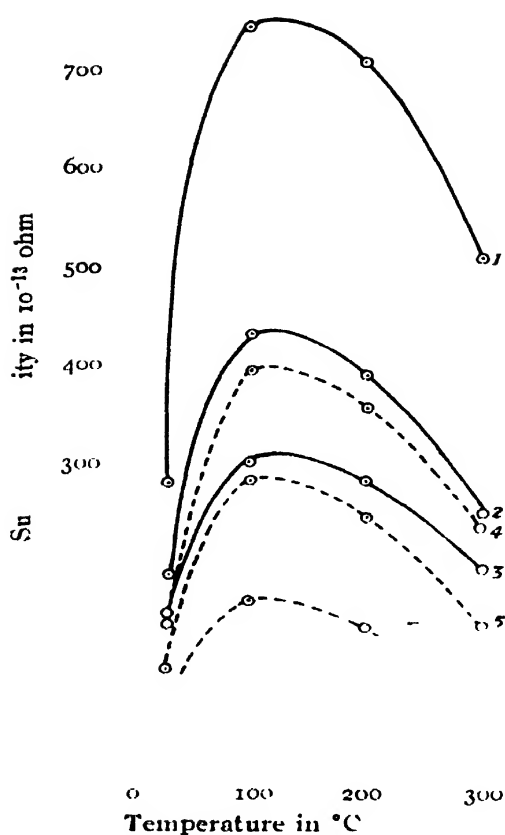


FIG. 9

Effect of preheating on surface resistivity of mica

Bihar Red :

Madras Green :

- |                                 |                                 |
|---------------------------------|---------------------------------|
| 1. Clear                        | 4. Clear                        |
| 2. Stained                      | 5. Stained                      |
| 3. Stained and slightly spotted | 6. Stained and slightly spotted |

## REFERENCES

- Anker, H. S., 1947, *Electronics*, 138.  
 Armistead, F. C., 1949, *Rev. Sci. Instr.*, **20**, 747.  
 Caldecourt, V. J., 1949, *Rev. Sci. Instr.*, **20**, 248.  
 Chety, R. H., 1937 *Trans. Electrochem. Soc.*, **72**, 33.  
 Curtis, H. L., 1914—1915, *Bull. Bur. Stands.*, **11**, 359.  
 Du Bridge, L. A., 1931, *Phys. Rev.*, **37**, 392.  
 Du Bridge L. A. and Brown, H. B., 1933, *Rev. Sci. Instr.*, **4**, 532.  
 Gemant, A., 1933, *Liquid Dielectrics* (J. Willey and Sons), 66.  
 Hill, 1931, *Science*, **78**, 529.  
 Mahanti, P. C. and Mandal, S. S., 1948, *Ind. J. Phys.*, **22**, 8.  
 Penick, D. B., 1935, *Rev. Sci. Instr.*, **6**, 115.  
 Rose, G. M., 1931, *Rev. Sci. Instr.*, **2**, 810.  
 Turner, L. A. and Seiglin C. O., 1933, *Rev. Sci. Instr.*, **4**, 429.  
 Thac, J. A. N., 1939, *Ind. J. Phys.*, **13**, 199.

# ULTRAVIOLET ABSORPTION SPECTRA OF DIPHENYL IN THE LIQUID AND SOLID STATES\*

By A. R. DEB

INDIAN ASSOCIATION FOR THE CULTIVATION OF SCIENCE, CALCUTTA 32

(Received for publication, March 25, 1953)

**ABSTRACT.** The ultraviolet absorption spectra of thin films of diphenyl of different thicknesses in the liquid state at 80°C and solid state at 30°C and -180°C have been investigated. It has been observed that the very broad band lying in the region 2900 Å 2300 Å in the spectrum due to the liquid is split up into two broad bands at 36306 and 37386 cm<sup>-1</sup> in the case of the solid at 30°C. There are also indications of broad feeble bands up to about 2850 Å. When the solid is cooled to -180°C these feeble bands become sharper and are clearly resolved into nine distinct narrow bands and each of the two broad intense bands observed in the case of the solid at 30°C, splits up into four components at the low temperature. The significance of these results has been discussed. It has been pointed out that these new feeble bands of the solid at -180°C may be due to transitions in one of the phenyl rings with the second one in the excited state.

## INTRODUCTION

Recent investigations on the absorption spectra of some organic compounds in the liquid and solid states at different temperatures including that of liquid oxygen (Deb, 1951a, 1951b, 1952; Swamy, 1951, 1952a, 1952b) yielded interesting results. It was found by comparing the results with those for the vapour that the bands shift to longer wavelengths when the vapour is liquefied and they shift some times towards shorter and some times towards longer wavelengths with freezing of the liquid and cooling down to -180°C. Splitting up and sharpening of bands, change of vibrational frequency, etc. were observed in some cases on cooling the substances to -180°C. The compounds studied in the recent investigations were mainly substituted benzene compounds. It was further observed that the changes taking place in the spectrum at low temperatures are different in the case of different substituents. The general similarity in the changes in the spectra, namely the disappearance in the liquid state of the fine structures of bands of vapour state and their partial reappearance at low temperatures is also not observed in some cases, for examples, in the methyl and ethyl benzoates, where the number of bands is the same in liquid and solid states at low temperatures and also the bands do not become appreciably sharp at -180°C.

\*Communicated by Prof. S. C. Sirkar.

In the present investigation the absorption spectrum of diphenyl at different temperatures have been studied in order to find out whether the presence of a phenyl group as a substituent produces any remarkable changes in the electronic energy levels of the molecule.

London (1945) has calculated the energy levels of diphenyl molecule from consideration of the perturbation of the original energy levels of benzene caused by the presence of the second benzene ring. According to him, four electronic transitions to the ground state are possible at about 2400 Å, 1900 Å, 1500 Å, and 1400 Å. The experimental results in the region about 2400 Å by Seshan (1936) and by Becke [unpublished work, reported by London, (1945)] have been compared and discussed in the present investigation.

#### EXPERIMENTAL

The experimental arrangement used was the same as that used by the author previously (Deb, 1951a). Chemically pure diphenyl obtained from Merck's original packing, was redistilled in evacuated double bulbs. A very thin film of the substance was necessary to produce bands and this was obtained by the method described earlier. It was found that the thickness of the absorbing film which produced bands distinctly in the region 2970 Å-2800 Å at low temperatures gave complete absorption for regions of shorter wavelengths. When the thicknesses was still further reduced it was possible to get bands in the region from 2800 Å to 2640 Å, beyond which again there was complete absorption. No bands could be observed at wavelengths below 2640 Å even when the thickness of the substance was reduced still further, though slight absorption was found upto about 2200 Å, the limit of the spectrograph. Films of different thickness were used in the case of the liquid as well as in the case of the solid at different temperatures.

Spectrograms were taken on Ilford Q 1 plates using an Adam Hilger E 1 quartz spectrograph which has a dispersion of about 4 Å.U. per mm in the region of 2800 Å. The exposure time was 8 minutes in the case of the liquid state and solid state at room temperature and 30 minutes for the solid at  $-180^{\circ}\text{C}$ . Iron arc comparison spectrum was taken in each photograph. A hydrogen discharge tube, run at about 3 K.V. was the source of the ultraviolet continuum. Microphotometric records of the spectra were taken using a self-recording microphotometer supplied by Kipp and Zonen. The frequencies of the bands were measured from these records in which the record of a known iron line at one end of the spectrum was taken as a reference line and the wavelengths were calculated from the known values of the enlargement (1.6 : 1) and the distances of the peaks from the iron line mentioned above.

## RESULTS AND DISCUSSION

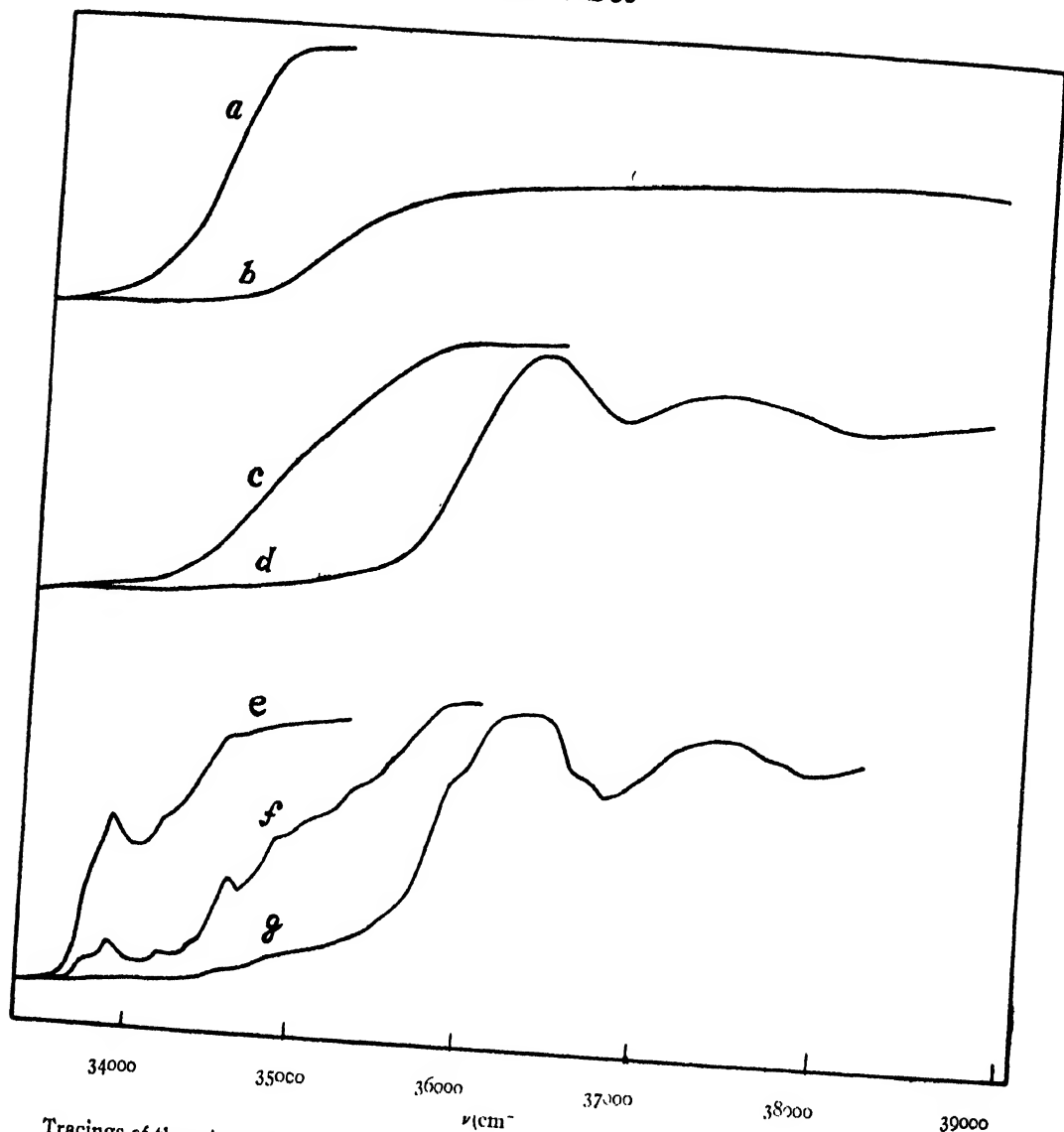
The tracings of the microphotometric records of the spectra are reproduced in figure 1, and the wave numbers of bands and their assignments are given in Table I.

TABLE I

## Ultraviolet absorption bands of diphenyl

Liquid at 80°C	Solid at 30°C		Solid at 180°C		
	$\nu$ (cm <sup>-1</sup> )	Assignment	Band no. and Int.	$\nu$ (cm <sup>-1</sup> )	Assignment
Continuous absorption commencing at about 2900 Å.	Very feeble broads absorption humps just preceptible.		1 (m)	33751	$\nu_0$
			2 (s)	33911	$\nu_0 + 160$
			3 (w)	34210	$\nu_0 + 468$
			4 (vw)	34460	$\nu_0 + 709$
			5 (s)	34627	$\nu_0 + 709 + 160$
			6 (s)	34803	$\nu_0 + 1142$
			7 (w)	35052	$\nu_0 + 1301$
			8 (w)	35350	$\nu_0 + 1142 + 160$
			9 (vw)	35608	$\nu_0 + 1142 + 468$
One structureless band between 2850Å-2300Å (with smaller thickness of the absorbing film).	36306	$\nu_0 + 1080$	1 (s)	35938	$\nu_0$ ( $A_0$ )
	37386		2 (vs)	36101	$\nu_0 + 266$ ( $B_0$ )
			3 (vs)	36405	$\nu_0 + 537$ ( $C_0$ )
			4 (ms)	36740	$\nu_0 + 812$ ( $D_0$ )
			5 (w)	37012	$\nu_0 + 1084$ ( $A_1$ )
			6 (ms)	37271	$\nu_0 + 1084 + 266$ ( $B_1$ )
			7 (w)	37554	$\nu_0 + 1084 + 537$ ( $C_1$ )
			8 (w)	37824	$\nu_0 + 1048 + 812$ ( $D_1$ )

As pointed out by previous workers (Seshan, 1936, London 1045) the absorption spectrum of diphenyl in the vapour state gives uniform absorption without any structure over the wide region between 2800 Å and 2200 Å, although the bands due to benzene and most of the substituted benzenes lying in this region have definite structures. The substance, however, shows absorption having banded structures (Carr and Stücklen, 1936) for other systems below 2000 Å, which is beyond the range of the quartz spectrograph. On liquefaction, no change in the absorption spectrum is observed but with the increase in thickness of the film, the region at which absorption begins shifts to about 2900 Å (figure 1, curves *a* and *b*). The solid at 30°C yields a spectrum quite different from that due to the liquid. The single broad absorption band splits up into two broad bands with centres at 36306 and 37386 cm<sup>-1</sup> (figure 1, curve *d*) respectively. The spectrum due to larger thickness of the absorber reveals the presence of very broad low absorption



Tracings of the microphotometric records of the absorption spectra of diphenyl

Curves (a, b) Liquid at 80°C

" (c, d) Solid at 30°C

" (e, f, g) Solid at -180°C

Curves (a), (c), (e) and (f) were obtained with absorbing films of nearly same thickness, and curves (b), (d) and (g) with a much thinner absorbing film.

humps between 2900 Å and 2750 Å (figure 1, curve c). These humps are resolved as sharp absorption peaks when the temperature of the solid film is reduced to -180°C (curve f) and the spectrum further undergoes remarkable changes. Each of the two broad bands observed at the room temperature is found to be split up into four components thus giving rise to several progressions (curve g). The wavenumber difference between the first components of the two bands is found to be 1084, which is equal to that

between the centres of the unresolved bands observed for the crystal at  $30^{\circ}\text{C}$ . The new absorption peaks lying between  $2900 \text{ \AA}$  and  $2750 \text{ \AA}$  increase in height with the increase of the thickness of the absorbing film at  $-180^{\circ}\text{C}$  (curve  $\epsilon$ ).

The analysis of the bands thus obtained offers considerable difficulty if all the bands from  $2963 \text{ \AA}$  are supposed to belong to the same system. The degrees of absorption at the new bands also suggest that these may belong to an entirely new system. Probably in the liquid state the feeble bands are also so broad that they merge into one another. Angular oscillations and translational motion of the molecules may be responsible for the for the width. In the case of the fairly thick film at  $30^{\circ}\text{C}$  the bands lying between  $2900 \text{ \AA}$  and  $2750 \text{ \AA}$  can be just identified but they are still very broad.

Angular oscillations persisting in the solid may be responsible for this large width of bands. The solid film at  $-180^{\circ}\text{C}$  yields sharp bands in the region mentioned above probably owing to cessation of the angular oscillation of the molecules. These feeble bands have been assumed to belong to the first system and the bands at  $36306$  and  $37386 \text{ cm}^{-1}$  form the second system in the case of the solid at  $30^{\circ}\text{C}$ . The weak system due to the crystal at  $30^{\circ}\text{C}$  cannot be analysed owing to the large width of the individual bands. In the case of the crystal at  $-180^{\circ}\text{C}$  the first band of this system at  $33751 \text{ cm}^{-1}$  has been taken as the 0, 0 band of the first system. On this assumption progressions of frequencies  $160$ ,  $468$ ,  $709$  and  $1142 \text{ cm}^{-1}$  have been observed in this system.

In the case of the second system the difference in frequencies of the two bands due to the crystal at  $30^{\circ}\text{C}$  is  $1084 \text{ cm}^{-1}$ . Each of these two bands is observed to be split into four bands when the crystal is cooled to  $-180^{\circ}\text{C}$ . Two alternative explanations can be suggested for this phenomenon. The difference between frequencies of successive components is about  $266 \text{ cm}^{-1}$ . Hence it can be assumed that this splitting of the bands is not due to the fact that the four components represent vibrational frequencies which are resolved only at  $-180^{\circ}\text{C}$  owing to the decrease in their width at the low temperature, but the splitting is due to the splitting of the energy levels by the intermolecular field in the crystal at  $-180^{\circ}\text{C}$ . Alternatively it can be assumed that the frequency differences  $266$ ,  $537$ ,  $812$  and  $1084 \text{ cm}^{-1}$  represent four vibrational frequencies of the excited state. In the case of this system only one of the phenyl rings is excited, the other being in the ground state. In the diphenyl molecule two carbon atoms of the two benzene rings are joined by C—C bond and the first feeble system may be due to energy levels of one of the rings when the second one is in the excited state. The difference in the excited state vibrational frequencies observed in the case of the two systems may also be due to the fact that the frequencies of vibration while both the rings of the molecule are in excited states are lower than those for the first ring with the second one in the ground state. The transi-

tion to the excited state of one of the rings when the other ring is at the excited state may lower the energy difference and this may be the reason why the feeble bands lie on the long wavelength side of the strong bands at 36306 and 37386  $\text{cm}^{-1}$  respectively. The probability of such transitions is very low and this explains the low intensity of the bands on the long wavelength side.

The centre of the group of components in each of the two bands in the second system seems to be slightly on the shorter wavelength side of the corresponding bands observed in the case of the solid at 30°C. The bands thus shift towards shorter wavelengths with lowering of temperature of the crystal. Such a phenomenon has been observed in the case of many substituted benzenes (Swamy, 1952, 1953). The splitting of the broad bands at low temperatures may be due to formation of virtual bonds between neighbouring molecules in the crystal.

Investigations with other substances are in progress.

#### ACKNOWLEDGMENT

The author wishes to express his indebtedness to Prof. S. C. Sirkar, D. Sc, F. N. I. for his kind permission to carry out the investigation in the laboratory of the Optics Department and for his guidance during the progress of the work.

#### REFERENCES

- Deb, A. R., 1951a, *Ind. J. Phys.*, **26**, 233.  
„ „ , 1951b, *ibid*, **26**, 433  
„ „ , 1952, *ibid*, **26**, 201.  
„ „ , 1953, *ibid*, **27**, 183  
Carr, R. and Stücklen, H., 1936, *J. Chem. Phys.*; **4**, 760  
London, A., 1945, *J. Chem. Phys.*, **13**, 396.  
Seshan, P. K., 1936, *Proc. Ind. Acad. Sci.*, **3**, 148  
Swamy, H. N., 1952a, *Ind. J. Phys.*, **26**, 119, 233.  
„ „ , 1952b, *ibid*, **26**, 445.  
„ „ , 1953, *ibid*, **27**, 55.



# CLASSICAL THEORY OF CHARGED MESON

BY N. C. SIL

DEPARTMENT OF THEORETICAL PHYSICS,  
INDIAN ASSOCIATION FOR THE CULTIVATION OF SCIENCE,  
JADAVPUR, CALCUTTA.

(Received for publication, February 15, 1953)

**ABSTRACT.** The equations of motion of the nucleon in interaction with the charged scalar meson field have been solved classically and the values of total scattering cross sections of charged mesons by nucleons have been calculated. The influence of radiation damping has also been investigated.

1. It is wellknown that the scattering cross sections of various processes become increasingly large with increasing energies if no account is taken of radiation reaction in the quantum mechanical calculations. However, it is not always possible to find exact solutions for scattering processes when the influence of radiation reaction is included in the mathematical formalism of quantum mechanics; it is often very difficult to estimate the degree of inaccuracy involved in the approximate solutions. Hence arises the necessity of approaching the problem from the classical theory in which the treatment of radiation reaction is much simpler. This scheme was originally introduced by Dirac (1938) in his 'classical theory of radiating electrons'. Bhabha (1939, 1941) and Harish Chandra (1946) extended the same method to the case of neutral meson field. It was not possible in Bhabha's theory to consider the charged mesons which are experimentally observed. The charge formalism was introduced by Fierz (1941) for the case of vector mesons, but he did not consider the dipole coupling. The complete treatment of electrically charged vector meson field was given by Le Couteur (1949). Recent experimental findings indicate, however, that the mesons involved in the nuclear interaction should be described by the pseudoscalar field. Now in a classical theory there should be no distinction between the scalar and pseudoscalar interactions. Hence it is worth while to investigate the case of electrically charged scalar meson field.

2. In the charge formalism each field quantity is considered as a vector in a three dimensional space which we may call 'charge space', denoted by three unit vectors  $\alpha, \beta, \gamma$ . The electrical charge density—an observable quantity—is represented as the  $\gamma$  component of a vector (Le Couteur, 1949).

We shall mostly keep to the notation of Le Couteur's paper. We take

the fundamental metric tensor  $g_{\mu\nu}$  (the suffixes  $\mu, \nu, \rho, \sigma$  as usual run from 0 to 3) defined by  $g_{00} = 1$ ,

$$g_{11} = g_{22} = g_{33} = -1,$$

with all the other components vanishing. Then we may describe the charged scalar meson field in interaction with the nucleons by a potential  $\mathbf{U}$  and field strengths  $\mathbf{G}_\mu$  which satisfy the following equations :

$$\mathbf{G}'_\mu = \partial_\mu \mathbf{U} - 4\pi \mathbf{S}_\mu = \mathbf{G}_\mu - 4\pi \mathbf{S}_\mu, \quad \dots (1)$$

$$\partial^\mu \mathbf{G}'_\mu + \chi^2 \mathbf{U} = 4\pi \mathbf{S}, \quad \dots (2)$$

where  $\chi = mc/\hbar$ ,  $m$  being the meson mass  $c$  and  $\hbar$  having their usual meanings.

and

$$\partial_\mu \equiv \frac{\partial}{\partial x^\mu}.$$

The source densities  $\mathbf{S}$  and  $\mathbf{S}_\mu$  are associated with the mesonic charge and dipole moment of the nucleons. The source densities arising from a single point particle may be assumed to be given by

$$\mathbf{S} = \int_{-\infty}^{\infty} \mathbf{s}(t) \delta(x - z(t)) dt, \quad (3)$$

$$\mathbf{S}_\mu = \int_{-\infty}^{\infty} \mathbf{s}_\mu(t) \delta(x - z(t)) dt, \quad (4)$$

where  $z_\mu(t)$  are the co-ordinates of the particle when its proper time is  $t$  (having the dimension of length) and  $\mathbf{s}(t)$  and  $\mathbf{s}_\mu(t)$  are continuous and differentiable functions of  $t$ .

From (1) and (2) we have

$$(\partial^\mu \partial_\mu + \chi^2) \mathbf{U} = 4\pi (\mathbf{S} + \partial^\mu \mathbf{S}_\mu). \quad \dots (5)$$

Previously, in Bhabha's theory (Bhabha, 1940) it was not possible to consider a charged meson field classically because of the commutability of all quantities in the classical theory. This difficulty is removed by defining the charge current vector  $J_\gamma^\mu$  as the 3rd. component of a vector product denoted by the symbol  $\wedge$  of two vectors in the charge space. Thus

$$4\pi \mathbf{J}^\mu = \left( \frac{e}{\hbar c} \right) \cdot \mathbf{G}'^\mu \wedge \mathbf{U}, \quad (6)$$

with the help of (1) and (2) we get

$$\partial^\mu \mathbf{J}_\mu = \left( \frac{e}{\hbar c} \right) \cdot \{ \mathbf{S} \wedge \mathbf{U} - \mathbf{S}_\mu \wedge \mathbf{G}_\mu \}. \quad (7)$$

The energy momentum tensor is given by

$$4\pi T_{\mu\nu} = \mathbf{G}_\mu \mathbf{G}_\nu - \frac{1}{2} g_{\mu\nu} \{ \mathbf{G}^\rho \mathbf{G}_\rho - \chi^2 \mathbf{U}^2 \}. \quad (8)$$

Hence we get after use of (1) and (2)

$$\partial^\nu T_{\mu\nu} = \mathbf{G}_\mu (\mathbf{S} + \partial^\rho \mathbf{S}_\rho) = \mathbf{G}_\mu \mathbf{S} - \partial^\rho \mathbf{G}_\mu \mathbf{S}_\rho + \partial^\rho (\mathbf{G}_\mu \mathbf{S}_\rho). \quad (9)$$

It is seen from (7) and (9) that in a source-free region

$$\partial_\mu J_\gamma^\mu = 0 \text{ and } \partial^\mu T_{\mu\nu} = 0$$

The angular momentum of the meson field is given by

$$M_{\mu\lambda} = x_\mu T_{\lambda} - x_\lambda T_{\mu} \quad \dots (10)$$

Hence

$$\partial^\lambda M_{\mu\nu\lambda} = \lambda_\mu \partial^\lambda T_{\lambda} - \lambda_\nu \partial^\lambda T_{\mu\lambda} \quad \dots (11)$$

With the help of (9) we get

$$\begin{aligned} \partial^\lambda M_{\mu\nu\lambda} &= \lambda_\mu \mathbf{S} \mathbf{G}_\nu - \lambda_\nu \mathbf{S}_\lambda \partial^\lambda \mathbf{G}_\nu - \mathbf{S}_\mu \mathbf{G}_\nu \\ &\quad - \lambda_\nu \mathbf{S} \mathbf{G}_\mu + \lambda_\nu \mathbf{S}_\lambda \partial^\lambda \mathbf{G}_\mu + \mathbf{S}_\nu \mathbf{G} \\ &\quad + \partial^\lambda \{x_\mu \mathbf{G}_\nu \mathbf{S}_\lambda - x_\nu \mathbf{G}_\mu \mathbf{S}_\lambda\}. \end{aligned} \quad \dots (12)$$

Let us now determine the electric charge current density  $J_\gamma^\mu$  and the average value of the energy momentum tensor for the special case of the plane wave as we shall require these afterwards for the evaluation of the scattering cross section. Following Le Couteur (1949) we have

$$U_\xi = A_\xi \sin (\omega_\mu x^\mu + \sigma_\xi), \quad \xi = \alpha, \beta \text{ or } \gamma. \quad \dots (13)$$

Then from equation (6)

$$J_\gamma^\mu = -\omega^\mu \left( \frac{c}{4\pi\hbar c} \right) A_\alpha A_\beta \sin (\sigma_\alpha - \sigma_\beta), \quad \dots (14)$$

and with the help of equation (8) the average value of the energy momentum tensor is given by

$$T_{\mu\nu} = \frac{1}{8\pi} \omega_\mu \omega_\nu \mathbf{A}^2. \quad \dots (15)$$

For a stream of positive or negative mesons we assume

$$A_\alpha = A_\beta, \quad A_\gamma = 0 \text{ and } \sigma_\alpha = \sigma_\beta \mp \frac{1}{2}\pi, \quad \dots (14a)$$

and in the case of neutral mesons

$$A_\alpha = A_\beta = 0.$$

3. The equations for the rates of change of the electric charge  $Q$ , the energy momentum  $A_\mu$  and the angular momentum  $b_{\mu\nu}$  carried by the nucleon are derived from the method of inflow calculation given by Harish Chandra (1946). In these calculations we have to use modified mean fields defined by

$$\mathbf{U}^{mean} = \mathbf{U}^m + \frac{1}{2} \mathbf{U}^{rad},$$

and

$$\mathbf{G}_\mu^{mean} = \mathbf{G}_\mu^m + \frac{1}{2} \mathbf{G}_\mu^{rad}. \quad \dots (16)$$

Hereafter we shall write  $\mathbf{U}$  for  $\mathbf{U}^{mean}$  and  $\mathbf{G}_\mu$  for  $\mathbf{G}_\mu^{mean}$ . Then from (7), (9) and (12)

$$\frac{dQ}{dt} = \frac{e}{\hbar c} \cdot \{ -\mathbf{s} \wedge \mathbf{U} + \mathbf{s}_\mu \wedge \mathbf{G}^\mu \} \quad \dots (17)$$

$$\frac{dA_\mu}{dt} = -\mathbf{s}\mathbf{G}_\mu + \mathbf{s}_\rho \partial^\rho \mathbf{G}_\mu. \quad \dots (18)$$

$$\begin{aligned} \frac{db_{\mu\nu}}{dt} = & -z_\mu \mathbf{s}\mathbf{G}_\nu + z_\mu \mathbf{s}_\lambda \delta^\lambda \mathbf{G}_\nu + \mathbf{s}_\mu \mathbf{G}_\nu \\ & + z_\nu \mathbf{s}\mathbf{G}_\mu - z_\nu \mathbf{s}_\lambda \delta^\lambda \mathbf{G}_\mu - \mathbf{s}_\nu \mathbf{G}_\mu. \end{aligned} \quad \dots (19)$$

The spin angular momentum  $B_{\mu\nu}$  is given by

$$\begin{aligned} \frac{dB_{\mu\nu}}{dt} = & \frac{db_{\mu\nu}}{dt} - \frac{d}{dt} (z_\mu A_\nu - z_\nu A_\mu) \\ = & (\mathbf{s}_\mu \mathbf{G}_\nu - \mathbf{s}_\nu \mathbf{G}_\mu) - (v_\mu A_\nu - v_\nu A_\mu), \end{aligned} \quad \dots (20)$$

where

$$v_\mu = \frac{dz_\mu}{dt}.$$

We may split any vector into two parts (i) one orthogonal to velocity  $v_\mu$  denoted by the sign  $\sim$  overhead, and (ii) the other parallel to  $v_\mu$ . Thus the dipole source function  $\mathbf{s}_\mu$  is split as follows

$$\mathbf{s}_\mu = \tilde{\mathbf{s}}_\mu + \mathbf{S}^* v_\mu,$$

where  $\tilde{\mathbf{s}}_\mu v^\mu = 0$  and  $\mathbf{S}^* = \mathbf{s}_\mu v^\mu$ .

It has been shown by Harish Chandra (1946) that with respect to the field producing properties the contribution of the part  $\mathbf{S}^*$  can be included within that of the charge function  $\mathbf{s}$ . Hence without loss of generality

we can take  $\tilde{\mathbf{s}}_\mu = \mathbf{s}_\mu$ .

Therefore

$$\mathbf{s}_\mu v^\mu = 0 \quad \dots (21)$$

We now express the source functions  $\mathbf{s}$  and  $\mathbf{s}_\mu$  in terms of  $\tau$  the classical analogue of the quantum mechanical isotopic spin vector. We assume

$$\mathbf{s} = g\tau, \quad \dots (22)$$

$$\mathbf{s}_\mu = fs_\mu\tau, \quad \dots (23)$$

where  $g$  and  $f$  are coupling constants.

$g$  has the dimension of electric charge and  $f$  has the dimension of electric dipole.

From (21) we see that

$$s_\mu v^\mu = 0. \quad \dots (21)$$

Thus in the rest system of co-ordinates  $v_\mu = (1, 0, 0, 0)$ ,  $s_0 = 0$  and the spatial parts are different from zero. In analogy with quantum mechanical results we assume that

$$\tau^2 = 1 \quad \text{so that} \quad \tau \frac{d\tau}{dt} = 0, \quad \dots (24)$$

and

$$s_\mu s^\mu = -1 \quad \text{whence} \quad s_\mu \frac{ds^\mu}{dt} = 0. \quad \dots (25)$$

Let  $\epsilon_{\mu\nu\rho\sigma}$  be a tensor which is antisymmetric in each pair of indices and  $\epsilon_{0123} = -1$ .

Then 
$$\frac{1}{2} \epsilon_{\mu\nu\rho\sigma} v^\mu s^\nu \epsilon^{\mu\nu\rho\sigma} v_\rho s_\sigma = 1. \quad (26)$$

Hence 
$$\epsilon_{\mu\nu\rho\sigma} v^\rho s^\sigma \frac{d}{dt} (\epsilon^{\mu\nu\rho\sigma} v_\rho s_\sigma) = 0. \quad (27)$$

Further

$$v^\rho s^\sigma \epsilon_{\mu\nu\rho\sigma} v^\mu = v^\rho s^\sigma \epsilon_{\mu\nu\rho\sigma} v^\nu = v^\rho s^\sigma \epsilon_{\mu\nu\rho\sigma} s^\mu = v^\rho s^\sigma \epsilon_{\mu\nu\rho\sigma} s^\nu = 0. \quad (28)$$

After use of (22) and (23), equation (17) is given by

$$\frac{d\mathbf{Q}}{dt} = -\frac{e}{\hbar c} \cdot \boldsymbol{\tau} \wedge \{g\mathbf{U} - fs_\mu \mathbf{G}^\mu\}. \quad (29)$$

From this we get following Le Couteur

$$\frac{d\boldsymbol{\tau}}{dt} = \frac{2}{\hbar c} \boldsymbol{\tau} \wedge \{g\mathbf{U} - fs_\mu \mathbf{G}^\mu + \mathbf{q}\}. \quad (30)$$

Let us write

$$A_\mu = A_\mu + M^* v_\mu, \quad (31)$$

where  $A_\mu v^\mu = 0$  and  $M^* = A_\mu v^\mu$ ,  
and

$$\mathbf{G}_\mu = \mathbf{G}_\mu + \mathbf{G}^* v_\mu,$$

where 
$$\tilde{\mathbf{G}}_\mu v^\mu = 0 \text{ and } \mathbf{G}^* = \mathbf{G}_\mu v^\mu = \frac{d\mathbf{U}}{dt} \quad (32)$$

Then contracting equation (20) with  $v^\nu$  and using (21), (31) and (32), we get

$$\tilde{A}_\mu = \frac{dB_{\mu\nu}}{dt} v^\nu - s_\mu \frac{d\mathbf{U}}{dt}, \quad \dots \quad (33)$$

$$\frac{dM^*}{dt} = v^\mu \frac{dA_\mu}{dt} + A_\mu \frac{dv^\mu}{dt}. \quad \dots \quad (34)$$

With the help of equations (33), (18) and (32), equation (34) may be written as

$$\frac{dM^*}{dt} = -g\boldsymbol{\tau} \frac{d\mathbf{U}}{dt} + fs_\rho \frac{d\mathbf{G}^\rho}{dt} + \frac{dB_{\mu\nu}}{dt} \frac{dv^\mu}{dt} v^\nu - fs_\mu \frac{d\mathbf{U}}{dt} \frac{dv^\mu}{dt}. \quad \dots \quad (35)$$

From (28) and (20) we see that

$$\epsilon^{\mu\nu\rho\sigma} v_\rho s_\sigma \frac{dB_{\mu\nu}}{dt} = 0.$$

On account of (27) and (28) we may take

$$\frac{dB_{\mu\nu}}{dt} = I \frac{d}{dt} ((\epsilon_{\mu\nu\rho\sigma} v^\rho s^\sigma) - (s_\mu V_\nu - s_\nu V_\mu)), \quad \dots \quad (36)$$

where  $I$  is a constant and  $V_\mu$  is an arbitrary vector.

From (20) and (36) we have

$$I\epsilon_{\mu\nu\rho\sigma}\left(\frac{dv^\rho}{dt}s^\sigma + v^\rho\frac{ds^\sigma}{dt}\right) = s_\mu(f\tau\mathbf{G}_\nu + V_\nu) - s_\nu(f\tau\mathbf{G}_\mu + V_\mu) - (v_\mu A_\nu - v_\nu A_\mu). \quad (37)$$

Multiplying both sides by  $\epsilon^{\mu\nu\alpha\beta}$  and using (Harish Chandra 1946)

$$\epsilon_{\mu\nu\rho\sigma}\epsilon^{\mu\nu\alpha\beta} = -2(\delta_\rho^\alpha\delta_\sigma^\beta - \delta_\sigma^\alpha\delta_\rho^\beta),$$

we get

$$I\left\{\left(\frac{ds^\alpha}{dt}v^\beta - \frac{ds^\beta}{dt}v^\alpha\right) + \left(s^\alpha\frac{dv^\beta}{dt} - s^\beta\frac{dv^\alpha}{dt}\right)\right\} = s_\mu(f\tau\mathbf{G}_\nu + V_\nu)\epsilon^{\mu\nu\alpha\beta} - v_\mu A_\nu\epsilon^{\mu\nu\alpha\beta}. \quad (38)$$

Omitting the parts proportional to  $v_\mu$  or  $v_\nu$  the equation (37) may be written as follows :

$$I\epsilon_{\mu\nu\rho\sigma}v^\rho\frac{ds^\sigma}{dt} = s_\mu\left(f\tau\tilde{\mathbf{G}}_\nu + \tilde{V}_\nu\right) - s_\nu\left(f\tau\tilde{\mathbf{G}}_\mu + \tilde{V}_\mu\right). \quad (39)$$

Contracting equation (38) with  $v_\beta\left(f\tau\mathbf{G}_\alpha + V_\alpha - f\tau v\frac{d\mathbf{U}}{dt}\right)$ ,

we obtain using (21), and  $v_\mu\frac{dv^\mu}{dt} = 0$ ,

$$f\tau\frac{ds^\alpha}{dt}\left(\mathbf{G}_\alpha - v_\alpha\frac{d\mathbf{U}}{dt}\right) + \frac{ds^\alpha}{dt}V_\alpha - \frac{ds^\beta}{dt}v^\alpha v_\beta V_\alpha = 0 \quad (40)$$

Also with the help of equation (28)

$$\frac{d}{dt}(\epsilon_{\mu\nu\rho\sigma}v^\rho s^\sigma)\frac{dv^\mu}{dt}v^\nu = -\epsilon_{\mu\nu\rho\sigma}v^\rho s^\sigma\frac{dv^\mu}{dt}\frac{dv^\nu}{dt} = 0 \quad (41)$$

Hence from (21) and (36) we get

$$\frac{d\mathbf{B}_{\mu\nu}}{dt}\frac{dv^\mu}{dt}v^\nu = s_\mu V_\nu\frac{dv^\mu}{dt}v^\nu = \frac{ds_\mu}{dt}V_\nu v^\mu v^\nu. \quad (42)$$

Therefore equation (35) may be written as

$$\begin{aligned} \frac{dM^*}{dt} = \frac{d}{dt}\left\{-g\tau\mathbf{U} + f\tau s_\mu\mathbf{G}^\mu\right\} + \frac{d\tau}{dt}\left\{g\mathbf{U} - f s_\mu\mathbf{G}^\mu\right\} \\ - f\tau\mathbf{G}_\mu\frac{ds^\mu}{dt} + f\tau\frac{ds_\mu}{dt}v^\mu\frac{d\mathbf{U}}{dt} + \frac{ds_\mu}{dt}V_\nu v^\mu v^\nu. \end{aligned}$$

Using (40) and (30) we finally get

$$\frac{dM^*}{dt} = \frac{d}{dt}\left\{-g\tau\mathbf{U} + f\tau\mathbf{G}^\mu s_\mu\right\} - \frac{d\tau}{dt}\mathbf{q} + \frac{ds_\mu}{dt}V^\mu. \quad (43)$$

Now  $\mathbf{q}$  and  $V_\mu$  may be so chosen that

$$\tau \wedge \mathbf{q}, (s_\mu V_\nu - s_\nu V_\mu) \text{ and } \frac{d\tau}{dt} \mathbf{q} - \frac{ds_\mu}{dt} V$$

are perfect differentials.

The simplest solution of course is  $\mathbf{q} = 0$ ,  $V_\mu = 0$ . Another simple solution is

$$\mathbf{q} = -\frac{1}{2}L \frac{d^2\tau}{dt^2}, V_\mu = -\frac{1}{2}K \frac{d^2s_\mu}{dt^2}. \quad \dots (4.4)$$

With the help of (4.4) the integration of (4.3) leads to

$$M^* = m^* - g\tau \mathbf{U} + f\tau \mathbf{G}^\mu s_\mu + \frac{1}{4}L \left( \frac{d\tau}{dt} \right)^2 - \frac{1}{4}K \frac{ds_\mu}{dt} \frac{ds_\mu}{dt}. \quad \dots (4.5)$$

Where  $m^*$  is the constant of integration.

Thus the equation of translational motion is solved completely.

4. We now evaluate the modified radiation fields  $\mathbf{U}'^{rad}$  and  $\mathbf{G}'^{rad}$  at points  $z_\mu(t)$  on the worldline of the nucleon. Following the calculations given in Harish Chandra's paper (1946) we obtain

$$\begin{aligned} \mathbf{U}'_{\mu(z_\mu(t))}^{rad} = & -2 \frac{d\mathbf{s}}{dt} - 2\chi \int_{-\infty}^t \mathbf{s} \frac{J_1(\chi u)}{u} dt' \\ & - \frac{2}{3} \mathbf{s}_\sigma \frac{d^2 v^\sigma}{dt^2} - 2 \frac{d\mathbf{s}_\sigma}{dt} \frac{dv^\sigma}{dt} - 2 \frac{d^2 \mathbf{s}_\sigma}{dt^2} v^\sigma \\ & + 2\chi^2 \int_{-\infty}^t u^\sigma \mathbf{s}_\sigma \frac{J_2(\chi u)}{u^2} dt', \end{aligned} \quad (4.6)$$

and  $\mathbf{G}'_{\mu(z_\mu(t))}^{rad} =$

$$\begin{aligned} & -\frac{2}{3} \mathbf{s} \frac{d^2 v^\mu}{dt^2} - 2 \frac{d\mathbf{s}}{dt} \frac{dv^\mu}{dt} - 2 \frac{d^2 \mathbf{s}}{dt^2} v^\mu - \chi^2 \mathbf{s} v^\mu \\ & + 2\chi^2 \int_{-\infty}^t u_\mu \mathbf{s} \frac{J_2(\chi u)}{u^2} dt' \\ & - \frac{2}{3} \mathbf{s}_\sigma v^\mu \frac{d^2 v^\sigma}{dt^2} - \frac{2}{3} \frac{d\mathbf{s}_\sigma}{dt} \left( v^\mu \frac{d^2 v^\sigma}{dt^2} + \frac{d^2 v^\mu}{dt^2} v^\sigma \right) \\ & - 4 \frac{d^2 \mathbf{s}_\sigma}{dt^2} \left( v^\mu \frac{dv^\sigma}{dt} + \frac{dv^\mu}{dt} v^\sigma \right) - \frac{8}{3} \frac{d^3 \mathbf{s}_\sigma}{dt^3} v^\mu v^\sigma + \frac{2}{3} \frac{d^3 \mathbf{s}_\mu}{dt^3} \\ & + \chi^2 \left( \frac{ds_\mu}{dt} - \mathbf{s}_\sigma v^\sigma \frac{dv^\mu}{dt} - \mathbf{s}_\sigma v \frac{dv^\mu}{dt} - 2 \frac{ds_\sigma}{dt} v^\mu v^\sigma \right) \end{aligned}$$

$$+ 2\chi^3 \int_{-\infty}^t \mathbf{s}_\mu \frac{J_2(\chi u)}{u^2} dt' - 2\chi^3 \int_{-\infty}^t u_\mu u^\sigma \mathbf{s}_\sigma \frac{J_2(\chi u)}{u^3} dt', \quad \dots \quad (47)$$

where  $u_\mu = x_\mu - z_\mu(t)$ ,  $x_\mu$  being the field point and  $u = |(u_\mu u^\mu)^{1/2}|$ .

in the above calculations we have neglected terms of the second degree

in  $\frac{dv}{dt}$ ,  $\frac{d^2v}{dt^2}$  and used the relation  $\mathbf{s}_\sigma v^\sigma = 0$ .

In the rest system of co-ordinates  $v_\mu = (1, 0, 0, 0)$ ,  $u_1 = u_2 = u_3 = 0$  and  $\mathbf{s}_0 = 0$  so that  $u^\sigma \mathbf{s}_\sigma = 0$ ,

$$\text{and } u = t - t' \text{ whence, } \int_{-\infty}^t dt' = \int_0^\infty du. \quad \dots \quad (48)$$

Hence in this system of co-ordinates, equations (46) and (47) can be simplified as follows :

$$\mathbf{U}'_{(z_\mu(t))} = -2g \frac{d\tau}{dt} - 2g\chi \int_{-\infty}^\infty \tau \frac{J_1(\chi u)}{u} du, \quad (49)$$

$$\begin{aligned} \text{and } \mathbf{G}'_{(z_\mu(t))} = & -2g \frac{d^2\tau}{dt^2} v_\mu - g\chi^2 \tau v_\mu + 2g\chi^2 \int_0^\infty \tau u_\mu \frac{J_2(\chi u)}{u^2} du \\ & + \frac{2}{3} \frac{d^3\mathbf{s}_\mu}{dt^3} + \chi^2 \frac{d\mathbf{s}_\mu}{dt} + 2\chi \int_{-\infty}^\infty \mathbf{s}_\mu \frac{J_2(\chi u)}{u^2} du \end{aligned} \quad (50)$$

Further equation (39) may be written in view of equation (44)

$$\text{as } \frac{dM}{dt} = M, f\tau \mathbf{H} - K \frac{d^2M}{dt^2} \Big], \quad (51)$$

where  $M$  is a three dimensional vector in ordinary space with components

$s_1, s_2, s_3$ ;  $M_k M_k = 1$ , and  $\tilde{\mathbf{H}}$  is a vector in ordinary space with components

$\tilde{\mathbf{G}}_1, \tilde{\mathbf{G}}_2$  and  $\tilde{\mathbf{G}}_3$ .  $[A, B]$  denotes vector product of vectors  $A$  and  $B$  in ordinary three dimensional space and  $(A B)$  denotes their scalar product. Similarly equation (30) becomes

$$\frac{d\tau}{dt} = \frac{2\tau}{\hbar c} \wedge \Big\{ g\mathbf{U} - f(M\tilde{\mathbf{H}}) - \frac{1}{2}L \frac{d^2\tau}{dt^2} \quad \dots \quad (52)$$

With the help of (48) and (50) we have

$$\begin{aligned} \tilde{\mathbf{H}} = & \tilde{\mathbf{H}}^{in} + \frac{1}{3}f \left( \tau \frac{d^3M}{dt^3} + 3 \frac{d\tau}{dt} \frac{d^2M}{dt^2} + 3 \frac{d^2\tau}{dt^2} \frac{dM}{dt} + \frac{d^2\tau}{dt^2} M \right) \\ & + \frac{1}{2}\chi^2 f \left( \tau \frac{dM}{dt} + \frac{d\tau}{dt} M \right) + \chi^2 f \int_0^\infty \tau M \frac{J_2(\chi u)}{u^2} du. \end{aligned}$$



Hence equations (51) and (52) become

$$I \frac{dM}{dt} \left| M, f\tau\tilde{H}^{in} - \frac{1}{2}K \frac{d^2M}{dt^2} \right. \\ \left. - f^2 \left[ M, \frac{1}{2} \frac{d^3M}{dt^3} + \tau \frac{d^2\tau}{dt^2} \frac{dM}{dt} + \frac{\chi^2}{2} \frac{dM}{dt} + \chi^2 \tau \int_0^\sigma \tau M \frac{J_2(\chi u)}{u^2} du \right] \right. \quad (51)$$

and

$$\frac{d\tau}{dt} = \frac{2\tau}{\hbar c} \wedge g\mathbf{U}^{in} - f(\mathbf{M}\mathbf{H}) \left\{ -\frac{L\tau}{\hbar c} \wedge \frac{d^2\tau}{dt^2} \right. \\ \left. - \frac{2\tau}{\hbar c} \wedge g^2 \left\{ \frac{d\tau}{dt} + \chi \int_0^\sigma \tau \frac{J_1(\chi u)}{u} du \right. \right. \\ \left. \left. - \frac{2\tau}{\hbar c} \wedge f^2 \left\{ M \frac{d^2M}{dt^2} \right\} \frac{d\tau}{dt} + \frac{M^2}{3} \frac{d^3\tau}{dt^3} + \frac{\chi^2 M^2}{2} \frac{d\tau}{dt} + \chi^2 M \int_0^\sigma \tau M \frac{J_2(\chi u)}{u^2} du \right\} \right. \quad (52)$$

5. We now try to solve the above equations assuming the incident field to be **weak** and simply periodic with frequency  $\omega$ . Equation (51) agrees with Le Couteur's equation (61) (Le Couteur, 1949), the solution of which is given by Bhabha in his neutral theory. We shall neglect the periodic oscillation of velocity.

To solve equation (52) we assume with Le Couteur that

$$\tau = a\gamma + \varepsilon_1 a \sin(\omega t + \sigma_1) + \varepsilon_2 \beta \sin(\omega t + \sigma_2), \quad (53)$$

where  $a \approx \pm 1$  depending upon whether the particle is initially a neutron or a proton, further  $\varepsilon_1$  and  $\varepsilon_2$  are quantities of smaller magnitude. To evaluate the radiation damping terms we notice that the terms proportional to  $f^2$  are the same as in Le Couteur's paper except for a factor  $\frac{1}{2}$ . Hence we need evaluate only the terms proportional to  $g^2$ . We shall carry our calculation for the case  $\omega > \chi$  as needed for the evaluation of the scattering cross section. Thus we get the radiation damping term

$$-Pa\gamma + R\varepsilon_1 a \cos(\omega t + \sigma_1) + R\varepsilon_2 \beta \cos(\omega t + \sigma_2), \quad (54)$$

where

$$P = 2g^2\chi + \frac{2}{3}f^2M^2\chi^3,$$

and

$$R = -2g^2(\omega^2 - \chi^2)^{1/2} + \frac{2}{3}f^2M^2(\omega^2 - \chi^2)^{3/2}. \quad (55)$$

Substituting (54) in (52) we obtain two equations by equating the coefficients of  $a$  and  $\beta$  on both sides. We write

$$\left\{ g\mathbf{U}^{in} - f(\mathbf{M}\tilde{H}^{in}) \right\} a = \delta_1 \sin \omega t + \delta_2 \cos \omega t, \\ \left\{ g\mathbf{U}^{in} - f(\mathbf{M}\tilde{H}^{in}) \right\} \beta = \delta_1 \sin\left(\omega t \pm \frac{\pi}{2}\right) + \delta_2 \cos\left(\omega t \pm \frac{\pi}{2}\right). \quad (56)$$

Comparing with (14 a) we associate the  $\pm$  signs with the positive or the negative meson. Further we take

$$\sigma_2 = \sigma_1 \pm \pi/2 \text{ and } \varepsilon_1 = \varepsilon_2 = \varepsilon, \quad \dots \quad (57)$$

where  $\sigma_1$  and  $\varepsilon$  are determined by the following relations :

$$\frac{\cos \sigma_1}{\delta_2 R + \delta_1 \left( \pm \frac{\omega \hbar c}{a} + L\omega^2 + P \right)} = \frac{\sin \sigma_1}{\delta_2 \left( \pm \frac{\omega \hbar c}{a} + L\omega^2 + P \right) - \delta_1 R} \quad \dots \quad (58)$$

and

$$\begin{aligned} \varepsilon^2 &= 4(\delta_1^2 + \delta_2^2) \left\{ \left( \frac{\omega \hbar c}{a} + L\omega^2 + P \right) + R^2 \right\}^{-1} \\ &= \frac{4}{\hbar^2 c^2} \cdot \frac{\delta_1^2 + \delta_2^2}{\omega^2} \left[ \left\{ 1 \pm \frac{a}{\hbar c} \left( L\omega + \frac{P}{\omega} \right) \right\}^2 + \frac{R^2}{\omega^2 \hbar^2 c^2} \right]^{-1} \quad \dots \quad (59) \end{aligned}$$

6. The contribution of  $\frac{dM}{dt}$  to the scattering cross section is of secondary importance and we need consider the contribution of  $\frac{d\tau}{dt}$  only. The variations of the charge function and the dipole function are respectively given by  $g \frac{d\tau}{dt}$  and  $fM \frac{d\tau}{dt}$ . The retraded potentials induced are respectively

$$\frac{eR}{r} \left[ \alpha \sin \left\{ \omega t - \sqrt{\omega^2 - \chi^2} \cdot r + \sigma_1 \right\} + \beta \sin \left\{ \omega t - \sqrt{\omega^2 - \chi^2} \cdot r + \sigma_2 \right\} \right], \quad \dots \quad (60)$$

and

$$\begin{aligned} \frac{ef\sqrt{\omega^2 - \chi^2}}{r^2} \frac{(rM)}{r^2} &\left[ \alpha \cos \left\{ \omega t - \sqrt{\omega^2 - \chi^2} \cdot r + \sigma_1 \right\} \right. \\ &\left. + \beta \cos \left\{ \omega t - \sqrt{\omega^2 - \chi^2} \cdot r + \sigma_2 \right\} \right]. \quad \dots \quad (61) \end{aligned}$$

The average of radial current density over all directions of orientation of  $M$  according to (14) and (14a) is given by

$$\left( \frac{e}{4\pi \hbar c} \right) \sqrt{\frac{\omega^2 - \chi^2}{r^2}} \left[ R^2 + f^2 M^2 (\omega^2 - \chi^2) \overline{\cos^2 \phi} \right] \varepsilon^2 \quad \dots \quad (62)$$

where  $\phi$  is the angle between  $r$  and  $M$  and the bar denotes an average over all possible directions of  $r$  with respect to  $M$

Let the incident meson wave be given by

$$\mathbf{U} = A \left[ \alpha \sin \left\{ \omega \lambda^0 - \sqrt{\omega^2 - \chi^2} \cdot \lambda^1 \right\} + \beta \sin \left\{ \omega \lambda^0 - \sqrt{\omega^2 - \chi^2} \cdot \lambda^1 \pm \frac{\pi}{2} \right\} \right], \quad \dots \quad (63)$$

the corresponding current density being given by

$$\pm \left( \frac{e}{4\pi\hbar c} \right) \cdot \sqrt{\omega^2 - \chi^2} \cdot A^2 \quad \dots \quad (64)$$

Comparing equation (63) with (56) we get the values of  $\delta_1$  and  $\delta_2$  and substitute these in (59) to calculate  $\epsilon^2$ . Thus from (62) and (64) the total cross section is given by

$$\frac{16\pi}{\omega^2 \hbar^2 c^2} \left\{ g^2 + f^2 M^2 (\omega^2 - \chi^2) \overline{\cos^2 \phi} \right\} \cdot \frac{\epsilon^2}{A^2} = \frac{\left\{ g^2 + f^2 M^2 (\omega^2 - \chi^2) \overline{\cos^2 \phi} \right\}}{\left\{ 1 \pm \frac{a}{\hbar c} \left( L\omega + \frac{P}{\omega} \right) \right\}^2 + \frac{R^2}{\omega^2 \hbar^2 c^2}}, \quad \dots \quad (65)$$

where  $\theta$  is the angle between  $M$  and  $\mathbf{H}^{in}$ .

In the quantum theory of nucleon spin  $\frac{1}{2}$  we have

$$\overline{\cos^2 \phi} = \overline{\cos^2 \theta} = 1 \text{ and } M^2 = 3. \quad \dots \quad (66)$$

7. To compare with experimental results we put  $L=0$  as has been done by Le Couteur (1949). As the values of the coupling constants in the pseudoscalar field are arbitrary to the extent of the cut-off distance, we assume, for our purpose here, their values to be the same as determined for the Möller-Rosenfeld mixed field from the deuteron binding energies;  $g^2/\hbar c = .024$  and  $f^2\chi^2/\hbar c = .096$ . The theoretical results are shown in curves I and II in figure 1. curve I ( $\pm a = -1$ ) gives the scattering of (negative/positive) mesons by (neutrons/protons) and curve II ( $\pm a = 1$ ) gives that of (negative/positive) mesons by (protons/neutrons). curve I shows that the maximum value of the scattering cross section is reached when the incident meson energy is 210 Mev; in case of curve II the corresponding meson energy is 270 Mev. The experimental results, though not very reliable, indicate that the maximum value of the cross section of the scattering of positive meson by proton is reached for 180 Mev energy of the incident meson. It may be mentioned here that the maximum values as obtained by Le Couteur (1949) for the above cross sections in the vector field with the same coupling constants occur round about 140 Mev meson energy. So it appears that in the

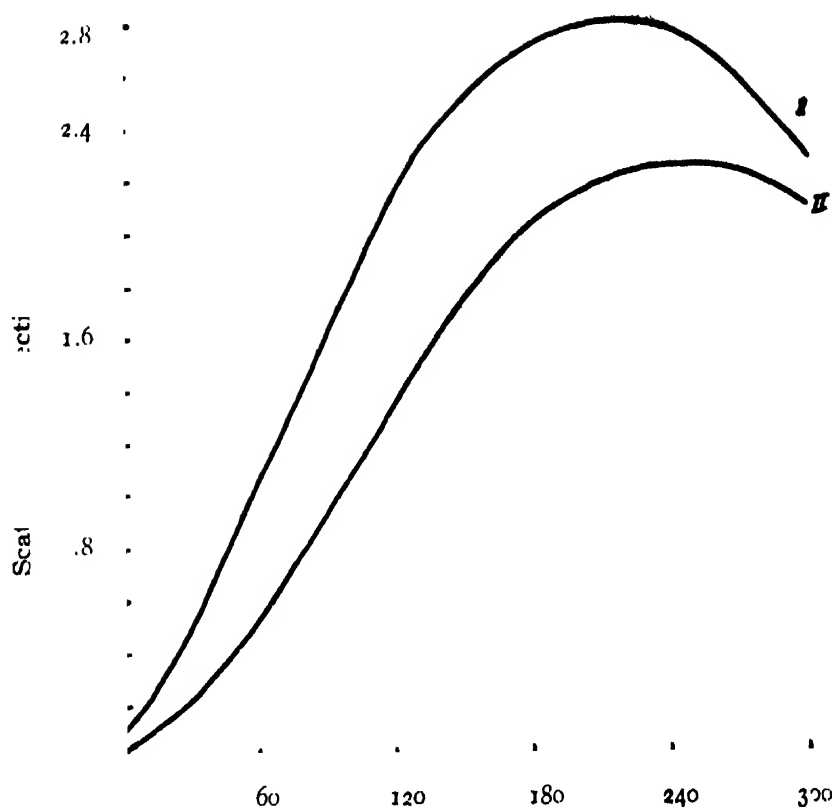


FIG. 1

Meson energy in Mev

pseudoscalar field the maximum value of the cross section is reached at meson energies higher than that in the vector field.

## ACKNOWLEDGMENT

The author wishes to thank Dr. D. Basu for suggesting the problem and for his kind help and guidance during the course of investigation.

## REFERENCES

- Bhabha, 1939, *Proc. Roy. Soc. A.*, **172**, 384.  
 „ 1940, *Proc. Ind. Acad. A.*, **11**, 347.  
 „ 1941, *Proc. Roy. Soc. A.*, **178**, 314.  
 Dirac, 1938, *Proc. Roy. Soc. A.*, **167**, 148.  
 Pierz, 1941, *Helv. Phys. Acta.*, **14**, 257.  
 Harish Chandra, 1946, *Proc. Roy. Soc. A.*, **188**, 269.  
 Le Conteur, 1949, *Proc. Cambridge. Phil. Soc.*, **45**, 429.

# ON THE RAMAN SPECTRA OF SOLUTIONS OF 1, 2, 3-TRICHLOROPROPANE\*

BY T. A. HARIHARAN

OPTICS DEPARTMENT

INDIAN ASSOCIATION FOR THE CULTIVATION OF SCIENCE, CALCUTTA 32

(Received for publication, March 3, 1953)

**ABSTRACT.** The Raman spectra of solutions of 1, 2, 3-trichloropropane in methyl alcohol, cyclohexane and dioxane have been investigated and microphotometric records of the spectrograms have been reproduced. It has been found that the line  $872\text{ cm}^{-1}$  of 1, 2, 3-trichloropropane diminishes in intensity greatly when the liquid is dissolved in dioxane. In the case of the solution in methyl alcohol also the intensity of the line seems to be slightly smaller than that in the case of the pure liquid. In the case of the solution in cyclohexane no such changes in intensity are observed. The line  $83\text{ cm}^{-1}$  also diminishes in intensity with dissolution of the substance in dioxane. In the case of *o*-chlorotoluene the intensity of the line  $164\text{ cm}^{-1}$  is found to diminish appreciably when the liquid is dissolved in benzene to make a dilute solution but no such diminution is observed in the case of solutions in either acetone or methyl alcohol.

## INTRODUCTION

It was reported previously (Hariharan, 1952) that the intensity of the line  $162\text{ cm}^{-1}$  of benzoylchloride diminishes to a large extent when the liquid is dissolved in benzene. The Raman spectra of solutions of a few other liquids in different solvents were next investigated and it was found that of these, solutions of 1, 2, 3-trichloropropane yielded some interesting changes. The results have been discussed in the present paper.

## EXPERIMENTAL

The liquids chosen in the present investigation are *o*-chlorotoluene and 1, 2, 3-trichloropropane which were supplied by Eastman Kodak Co., U. S. A. They were distilled in vacuum before use. The solvents were also of chemically pure quality and were distilled in vacuum. The Raman spectra of the pure liquids *o*-chlorotoluene and 1, 2, 3-trichloropropane and of the solutions of the former in benzene, methyl alcohol, and acetone and of the latter in cyclohexane, methyl alcohol and dioxane were photographed with a Fuess glass spectrograph having a dispersion of 12.5 A.U. in the 4000 A.U. region. The Wood's tube containing the solution was provided with an outer jacket containing a dilute solution of sodium nitrite which

\* Communicated by Prof. S. C. Sirkar

cut off all radiations of wavelengths shorter than 3800 Å. This removed the continuous fluorescence which was observed in the case of solutions if no such filter was used. Ilford Zenith plates were used for photographing the spectra and they were developed under identical conditions. Microphotometric records of some of the spectrograms were taken with a Moll type self-recording microphotometer.

The depolarisation of the Raman lines of pure 1, 2, 3-trichloropropane was also studied by photographing the horizontal and vertical components of the scattered light simultaneously using a Wollaston's prism of quartz. As light from a mercury arc focussed with a condensor was used as incident light, the spectrogram did not give the correct values of  $\rho$ , the factor of depolarisation, but to get an estimate of the errors due to convergence and

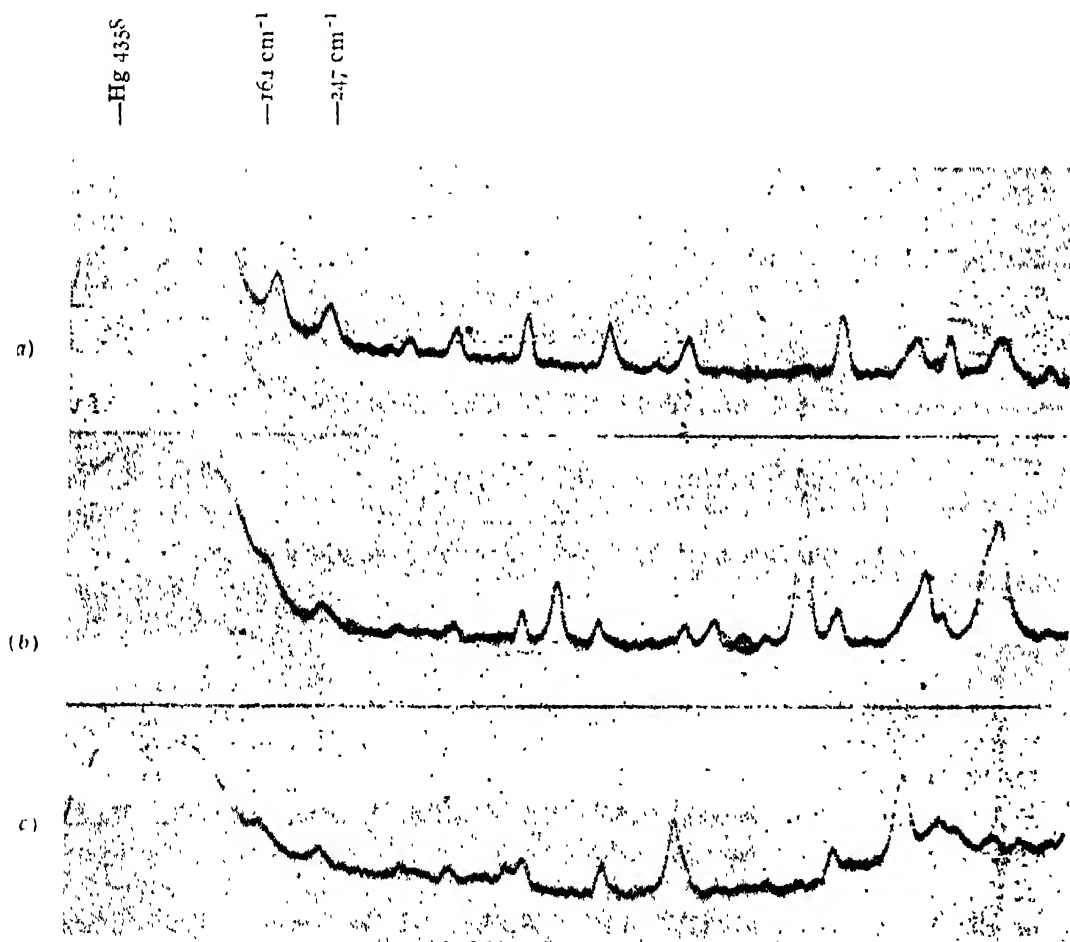


FIG. 1

Microphotometric records of Raman Spectra of *o*-chlorotoluene.

- (a) Pure liquid at room temperature
- (b) Solution in benzene (1:4 by volume).
- (c) Solution in acetone (1:4 by volume).

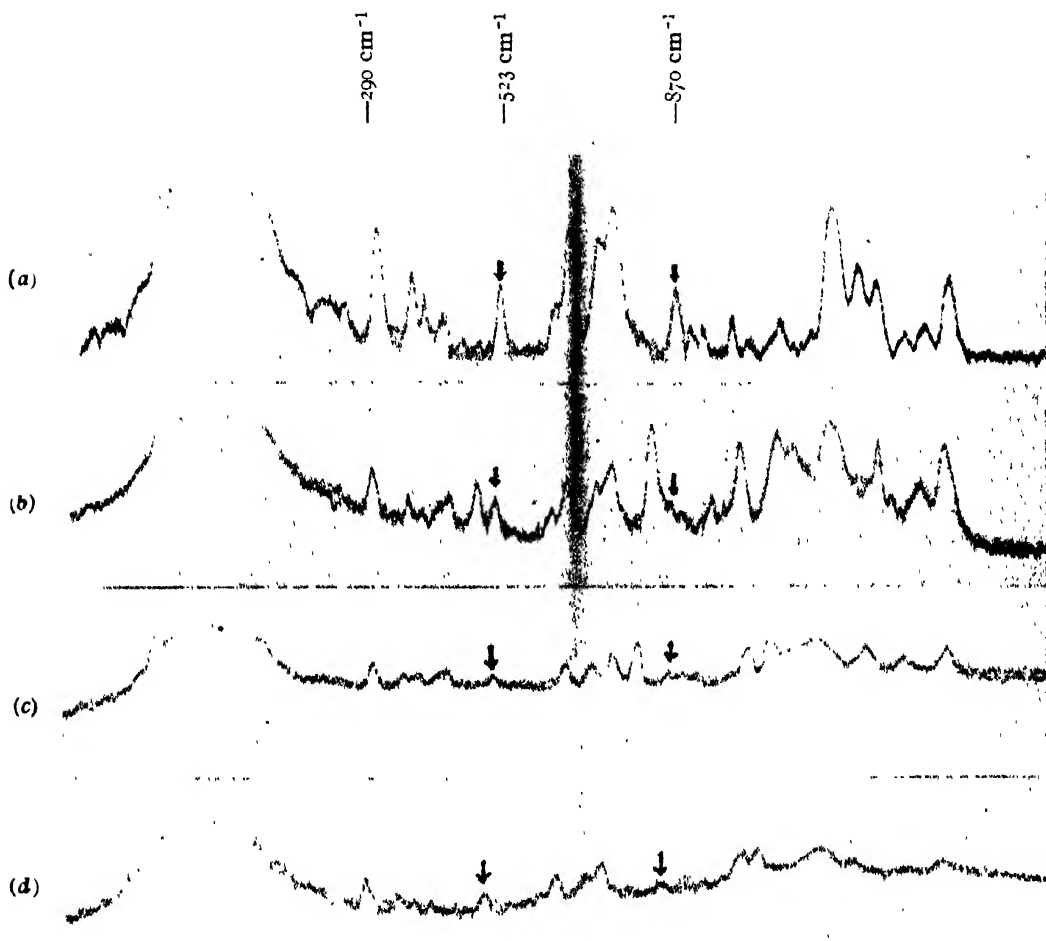


FIG. 2

Microphotometric records of the Raman spectra of 1, 2, 3-trichloropropane

- (a) Pure liquid at room temperature.
- (b) Solution in dioxane, 30% by volume.
- (c) Solution in cyclohexane, 30% by volume.
- (d) Solution in methyl alcohol, 30% by volume.

loss due to reflection at surfaces inside the spectrograph, the depolarisation of the Raman lines of carbon tetrachloride was studied under similar conditions and from a knowledge of the approximate values of  $\rho$ , thus found, and of its true value, the correct values of  $\rho$  in the case of the other liquids were estimated.

## RESULTS

The preliminary examination of the spectrograms revealed the fact that the intensities or positions of the Raman lines of *o*-chlorotoluene do not change markedly when the liquid is dissolved in either methyl alcohol or

acetone, but the line  $164\text{ cm}^{-1}$  seemed to be a little weaker in the case of the solution in benzene than in the case of the pure liquid, as can be seen from the microphotometric records reproduced in figure 1.

TABLE I  
Raman spectra of 1, 2, 3-trichloropropane.

Pure liquid at 28°C		Solution in dioxane	Solution in cyclohexane
Present author	Kohlrausch and Ypsilanti (1936)		
83 (2) e, k, $\pm$ D		83 (o) e	83 (o) e
104 (1) e, k, D?		140 (o) e	140 (o) e
176 (1) e, P		176 (o) e	176 (o) e
187 (1) e, P	188 (o)	187 (o) e	187 (o) e
230 (1) e, k, P	227 (o)	230 (o) e	230 (o) e
290 (10) $\pm$ e, k, i, P	288 (5)	290 (5) $\pm$ e, k	290 (8) $\pm$ e, k
356 (4) e, k, P	356 (2)	356 (2) e	356 (3) e
386 (2) e, P	381 (1)	386 (1) e	386 (3) e
418 (2) e, P	412 (1)	418 (1) e	
			422 (3b) e
523 (4) e, k, D	519 (3)	436 * (4) e	
632 (1) e	628 (1)	523 (3) e, k	523 (3) e
668 (10) $\pm$ e, k, P	660 (6)	632 (1) e	
718 (4) e, k, P	716 (4)	668 (5) $\pm$ e, k	668 (8) $\pm$ e, k
752 (10b) e, k, D	746 (5)	718 (3) e, k	718 (3) e
		752 (6) e, k	752 (8) e, k
872 (4) e, k, D	863 (2)	835 * (10) e, k	801 * (10) e, k, i
906 (1) e, P	906 (o)	872 (o) e	872 (2) e
933 (1) e, P	931 (o)	906 (o) e	
995 (2) e, P	990 (2)		
		995 (o) e	995 (1) e
1004 (1b) e, P	1090 (2)	1015 $\pm$ (12) e, k, i	1029 * (8) e, k
1190 (3b) e, k, P	1198 (2)	1106 * (6) e, k	
1280 (5) e, k, P	1283 (3)	1190 (2b) e, k	1190 (2) e
		1280 (1) e	1267 * (10) e, k
		1304 * (10) e, k	
1346 (1) e, P	1338 (2)	1346 (2) e, k	
1438 (6b) e, k, D	1432 (3b)	1438 (10) e, k	1438 (10b) e, k
		2660 * (1) e	2660 * (2) e, k
		2718 * (2) e	2689 * (1) e, k
2799 (1) e, k, D		2800 * (5) e	2799 * (3) e, k
2860 (1) e, k, P	2860 * (2)	2860 * (5) e, k, i	2860 * (10) e, k
		2888 * (3) e	
			2925 * (10) e, k, i
			2935 * (10) e, k, i
2960 (10b) e, k, i, P	2960 (10b)	2960 (10b) e, k, i	2960 (8) e, k
3014 (3) e, k, D	3008 (6)	3014 (1) e	3014 (2) e

N. B. Lines marked with asterisks are due to the solvents.

In the case of 1, 2, 3-trichloropropane, however, some changes were observed in the spectra with the dissolution of the substance in different solvents. The microphotometric records of the Raman spectra of the pure liquid and its solutions are reproduced in figure 2 to show these changes. The lines observed are given in Table I. The nature of polarisation of the



lines obtained are shown by letters P and D indicating values of  $\rho$  less than and equal to  $6/7$  respectively in Table I in which the data have been tabulated.

#### DISCUSSION OF RESULTS

It can be seen from a comparison of figures 2(a) and 2(b) that the relative intensities of the lines  $523$  and  $872\text{ cm}^{-1}$  are almost the same in the case of pure 1, 2, 3-trichloropropane while the latter line is much less intense than the former line in the case of the solution of the liquid in dioxane. A comparison of figures 2(c) and 2(d) also shows that the two lines mentioned above are of the same intensity in the case of the solution in cyclohexane while in the case of solution in methyl alcohol again the line  $872\text{ cm}^{-1}$  is less intense than line  $523\text{ cm}^{-1}$ . In comparison with the intensities of the other prominent lines, e. g., the line  $290\text{ cm}^{-1}$ , the intensity of the line  $523\text{ cm}^{-1}$  is found to remain the same in the solutions in the three different solvents. It is, therefore, evident that the intensity of the line  $872\text{ cm}^{-1}$  diminishes markedly when the liquid is dissolved in either dioxane or methyl alcohol.

As can be seen from Table I, the line  $872\text{ cm}^{-1}$  has a factor of depolarisation of the order of 0.87 while the line  $1438\text{ cm}^{-1}$  is also totally depolarised. Probably the line  $872\text{ cm}^{-1}$  is due to a mode of vibration of the group C-C-C, and the diminution of the intensity of this line probably indicates that the line is not due to a single molecule. As Bishui (1952) has shown that all the lines of 1, 2, 3-trichloropropane persist when the liquid is solidified and cooled down to  $-180^{\circ}\text{C}$  the question of co-existence of two isomeric forms in the liquid state does not arise. The line  $872\text{ cm}^{-1}$  therefore, may be due to some form of associated molecule, the number of which diminishes when the liquid is dissolved in either dioxane or methyl alcohol, but the solvent cyclohexane has no such effect. Visual examination of the spectrograms show that the line  $83\text{ cm}^{-1}$  also diminishes appreciably in intensity when the liquid is dissolved in dioxane.

The 1, 2, 3-trichloropropane molecule cannot have any element of symmetry. The fact that the line  $1438\text{ cm}^{-1}$  is totally depolarised, therefore, indicates that it is the symmetry of the two  $\text{CH}_2$  groups, the deformation C-H oscillation in which gives rise to this line, that determines the polarisation of the line and not the symmetry of the whole molecule

#### ACKNOWLEDGMENT

The author's thanks are due to Prof. S. C. Sirkar, D. Sc., F. N. I., for his kind interest and guidance throughout the progress of the work and to the Govt. of India, Ministry of Education, for the award of a research scholarship.

#### REFERENCES

- Hariharan, T. A., 1952 *Ind. J. Phys.*, **26**, 115.  
Kohlrausch and Ypsilanti, 1936, *Zeits. f. Phys. Chem.*, **32B**, 407.  
Bishui B. M., 1953, *Ind. J. Phys.* **27**, 90.

# MEASUREMENT OF FERROMAGNETIC PERMEABILITY AT MICROWAVE FREQUENCIES\*

By G. S. SANYAL AND J. S. CHATTERJEE

INSTITUTE OF RADIO PHYSICS AND ELECTRONICS UNIVERSITY OF CALCUTTA

(Received for publication, February 20, 1953)

**ABSTRACT.** The relative apparent permeabilities of soft iron and nickel (in the form of thick plates) are measured at a free-space wavelength of 3.2 cms. The method of measurement, which employs a resonant cylindrical cavity, is described. Expressions are derived relating the permeability,  $\mu_R$  with the cavity parameters and the resonant frequency. Approximate relations, from which  $\mu_R$  can be easily calculated, are given. The method gives value of  $\mu_R$  accurate within a few per cent. The effect of machining inaccuracy of one of the end walls of the cavity on the measurement of R. F. permeability is also discussed.

## 1 INTRODUCTION

The magnetic properties of ferromagnetic materials at v. h. f. and higher frequencies have been the subject of extensive studies in recent years. With the development of microwave technique during the war, it has been possible to extend these investigations to the frequency ranges of these waves. It has been found that the behaviour of ferromagnetic materials at such frequencies is not at all simple. Amongst other interesting effects, mention may be made of the dependence of the permeability on the frequency, on the magnitude and direction of the polarising d. c. magnetic field and on the surface conditions, temperature and tension of the sample.

The R. F. relative permeability can be expressed in terms of two real numbers,  $\mu_R$  and  $\mu_L$ , called apparent permeabilities, or by a complex number. It has been shown that  $\mu_R > \mu_L$  and that with the increase of frequency both  $\mu_R$  and  $\mu_L$  decrease. The different methods that have been developed for the determination of R. F. permeability are all based on the measurement of the impedance of a circuit element containing the ferromagnetic material under test. Some examples of such methods, as have been employed, are given below.

Johnson and Rado (1949) have determined both components of the complex permeability in the frequency range 200 to 975 Mc/s (as a function of a polarising magnetic field parallel to the H. F. field) by measuring the changes in the quality factor and in the resonant frequency of a half wave coaxial resonator, the inner conductor of which was of the ferromagnetic metal under test. Briks (1948) has determined the complex permeability by measuring the relative characteristic impedance and propagation

\* Communicated by Prof. S. K. Mitra

constant of a section of a rectangular guide filled with the substance in question in paraffin wax base. Griffiths (1946) has used a cylindrical cavity, with one of its end walls covered with a thin layer of the metal under test (electrolytically deposited), and has investigated the ferromagnetic resonance of the substances by measuring the  $Q$  of the cavity.

In the method adopted for the present investigation, a cylindrical cavity made of a non-magnetic material with one detachable end plate is used. The resonant frequency and the quality factor of the cavity are measured, once when the detachable end plate is made of the non-magnetic material and again when it is made of the ferromagnetic material under test. These measurements enable one to evaluate the  $\mu_r$  of the test material. The method is more accurate and, from certain expressions that have been derived, the calculations are made very simple. The method, is, however, not suitable for measurement of  $\mu_L$ , as this involves changes in the resonant frequencies of the cavity, too minute (0.0001%) to be detected with the equipment. Experiments are, however, in progress to develop a sufficiently precise method and the results will be communicated in due course.

## 2. EXPERIMENTAL ARRANGEMENT AND METHOD OF MEASUREMENT

A schematic diagram of the experimental arrangement is shown in figure 1 (a) and a photographic view of the same is given in figure 1 (b). Brief

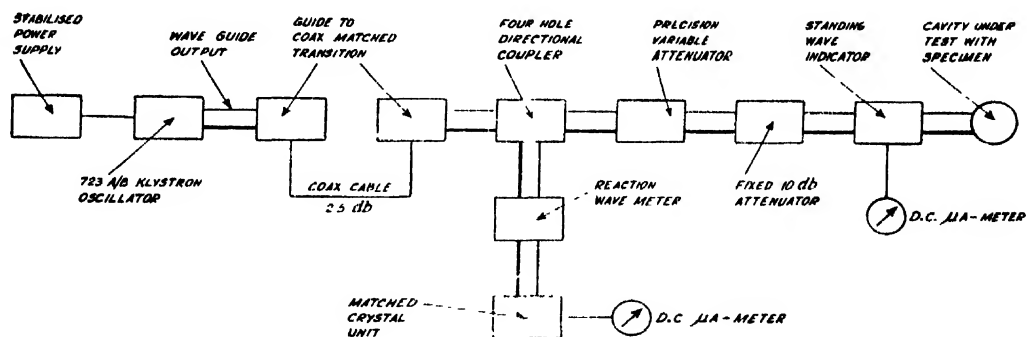


FIG. 1(a)

Block diagram of the experimental arrangement.

descriptions of the main units of the arrangement are given below. A 723 A/B klystron c.w. oscillator, having a stabilised power supply is used as the signal generator. A smooth variation of the frequency is obtainable by controlling the reflector voltage of the klystron round the optimum value. The signal generator feeds, *via* a coaxial-to-waveguide transition unit, into a four-hole directional coupler; the main branch of the directional coupler is utilised for the standing wave measurements and the subsidiary branch of the same for frequency measurements and monitoring. A fixed 10 db. attenuator and a variable precision

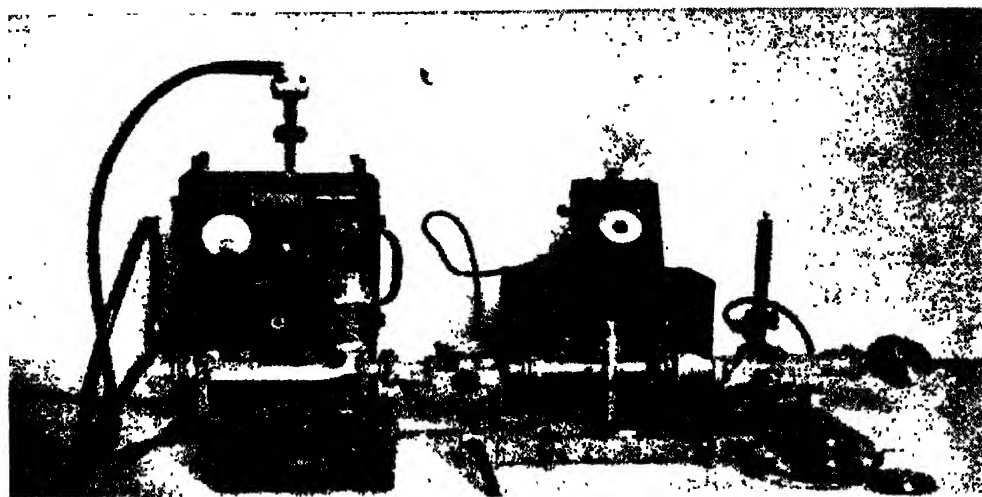


FIG. 1(b)

Photographic view of the experimental arrangement

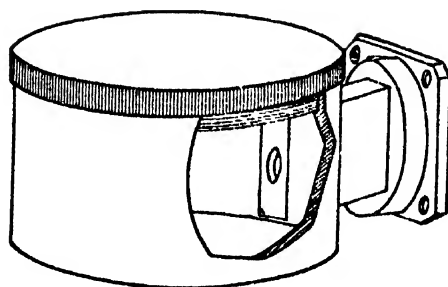


FIG. 2

Test cavity resonator with detachable end wall.

attenuator are interposed between the directional coupler and the standing wave measurement line (waveguide). The minimum attenuation between the signal generator and the load (i. e. the test cavity) is thus, including the 2.5 db. loss in the co-axial cable, 12.5 db. which is sufficient for eliminating any interaction between the two during the standing wave measurements. This means that the generator is always looking into a matched load.

The standing wave measurements are carried out by a precision wave-guide slotted section together with a broad band probe detector unit. The probe detector unit is tunable over a frequency range of 1,000 to 12,400 Mc/s and consists of three co-axial cylinders acting as two co-axial line pairs in series. The depth of the probe tip insertion inside the guide is adjustable and is always kept less than  $1/32$ " inch to minimise the distortion of the field inside the guide. The probe supplies power to a IN 23 crystal, which is held in pressure contact with the innermost conductor (the same conductor as the probe) of the co-axial line system and is used for R. F. detection. A 40  $\mu$ A full scale unipivot type d. c. microammeter measures the detected current.

The cavity under test is a right circular cylinder of brass with a detachable end wall, either of brass or of the ferromagnetic metal, as shown in figure 2. The cavity is coupled to the waveguide section (I. D.  $0.6'' \times 0.4''$ ), the broad side of which is parallel to the cavity axis, by a small circular hole ( $0.285''$  dia.) in the middle of the cylindrical wall of the cavity. By this method of coupling, only the  $TE_{011}$  mode is excited. Further, the end plates of the cavity are made accurately perpendicular to the cavity axis to prevent the simultaneous excitation of the degenerate  $TM_{111}$  mode which is undesirable. The resonant frequency of the cavity is dependent, amongst other factors, on  $\mu$  of the material of the end plate.

The voltage standing wave ratio (V. S. W. R.) at any frequency due to the test cavity was measured as follows. The detector carriage was placed at the minimum voltage position and the detected current and the position of minimum noted. The probe was then moved to the adjacent maximum position and the detected current was brought back to the previous minimum current value by the precision variable attenuator. The attenuation introduced by this attenuator was thus a measure of the V. S. W. R. The readings were checked for several minima and maxima.

The coupling hole between the test cavity and the waveguide section acts as a lossless transformer. At a certain reference plane in the cavity coupling system, the waveguide line (characteristic impedance  $Z_0$  in the equivalent transmission line circuit) looks, at resonance, into a pure resistance,  $R$  which accounts for the total loss inside the cavity. In general, the ratio  $Z_0/R$  may be greater, equal to or less than unity depending, amongst other parameters, on the diameter of the hole and the wall thickness. Referring to the Smith chart, it can be seen that if  $Z_0/R > 1$ , the position of the minimum in the slotted standing wave measuring guide shifts from that at resonance by a quarter guide wavelength at frequencies far off resonance; whereas, a shift of the minimum, much less than a quarter guide wavelength, indicates that  $Z_0/R$  is less than unity. By applying the above test the coupling parameter,  $Z_0/R$  of the test cavity was, in all cases, found to be less than unity.

For the accurate measurement of frequency difference off resonance, a wave meter is used in the secondary branch of the directional coupler. The wave meter (figure 3) is of a special reaction type and consists essentially of a brass cylindrical cavity. For the adjustment of its centre frequency, a brass rod  $9/32$  in. diameter is fitted and soldered (after adjustment) in the centre of one of the faces along the axis of the cavity. For the fine adjustment of frequency a much thinner rod,  $1/8$  in. in diameter, is fitted to a micrometer screw head to slide parallel to the axis at a distance of  $23/32$  in, from the centre. The wavemeter is calibrated separately and the wave-meter guide circuit is terminated in a matched  $1N21$  crystal unit. The crystal current also served the purpose of monitoring the R.F. power when the wavemeter was tuned off resonance. It is to be noted that since the

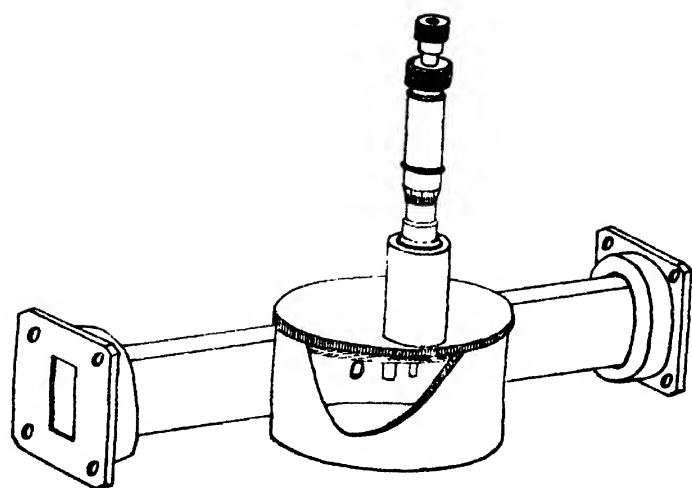


FIG. 3

Cutway view of the reaction type cavity wavemeter showing the fixed and the movable rod inside the cavity.

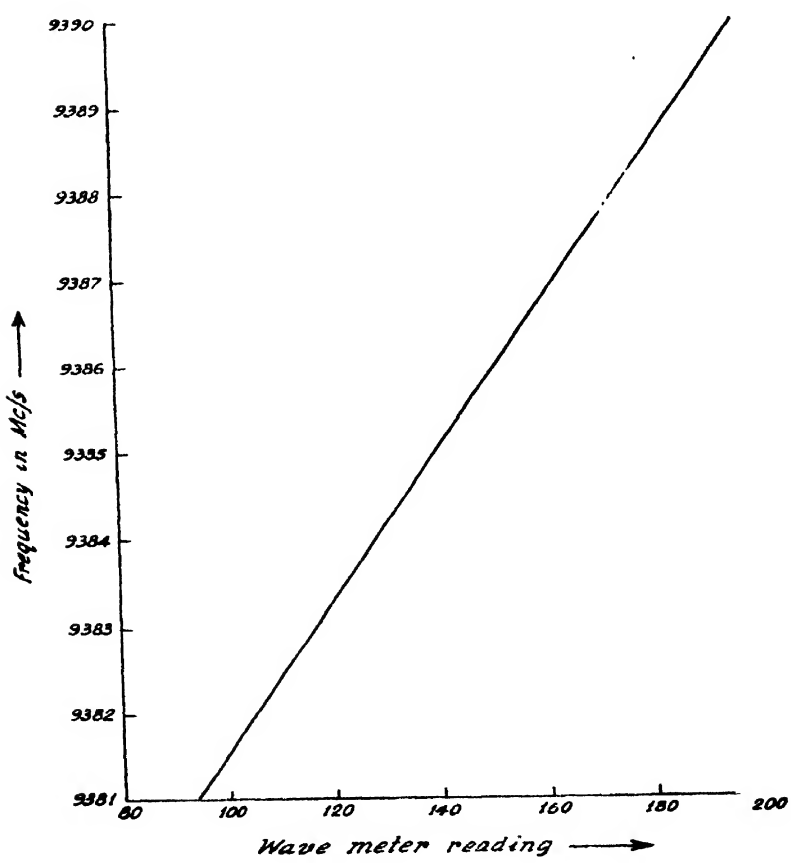


FIG. 4

Calibration curve of the reaction type cavity wavemeter.

attenuation introduced by the directional coupler between the primary and the secondary guide circuit is 20 db, it is ensured that there is no pulling effect between the signal generator and the wavemeter circuit. As the quality factor of the test cavity is very high, the difference in frequency that is to be determined round the resonant frequency of the test cavity, is necessarily very small. The reaction type of cavity wavemeter is, therefore, constructed having a direct reading accuracy of approximately 0.04 Mc/s and tunable over a frequency range of 9380 to 9398 Mc/s. In the small frequency range used in this experiment, the frequency varies linearly with the wavemeter setting as shown in figure 4. A sharp dip in the crystal current indicates the frequency. The constancy of this minimum reading is a check that the frequency of the signal generator remains steady during a particular measurement.

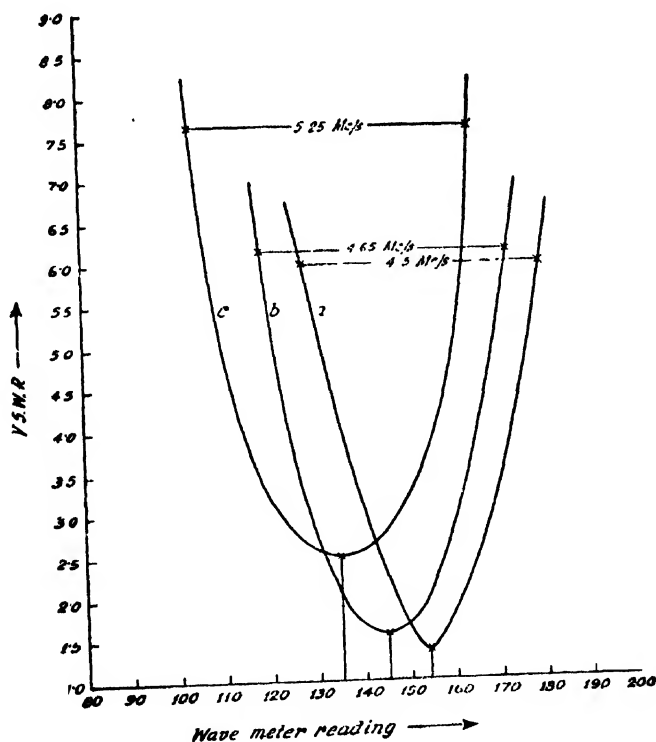


FIG. 5

V. S. W. R. in the waveguide versus frequency due to the test cavity resonator with various end plates. Curve *a* refers to the case of brass end plate; curves *b* and *c* are for nickel and soft iron end plates respectively.

V. S. W. R. versus frequency measurements were performed with the test cavity having detachable end plates made of brass, nickel, and soft iron. The results obtained are shown in figure 5.

In order to check the constancy of the geometry of the cavity, V.S. W.R. *versus* frequency measurements were carried out with several end plates of the same material. The measurements showed that though the quality factors were the same, the maximum deviation of resonant frequency for the different end plates of same material due to machining inaccuracy was  $\pm 0.4$  Mc/s. This amount of uncertainty of the resonant frequency, though small, is large enough to mask the minute change in the resonant frequency that would be produced due to change in the value of  $\mu_L$  of the ferromagnetic substance.

### 3. THEORETICAL ANALYSIS

The cylindrical cavity resonator used in this experiment has one end wall made either of brass or of some ferromagnetic metal. Ferromagnetic metals possess complex permeability and, as shown hereafter, the performances of a cavity (*e.g.* the resonant frequency and the quality factor) with an end plate made of such a material is different from that of a cavity made entirely of a non-magnetic material, *e.g.* brass. In what follows we shall derive expressions relating the R. F. permeability with the resonant frequency and quality factor of a cylindrical cavity, having one end plate made of some ferromagnetic material.

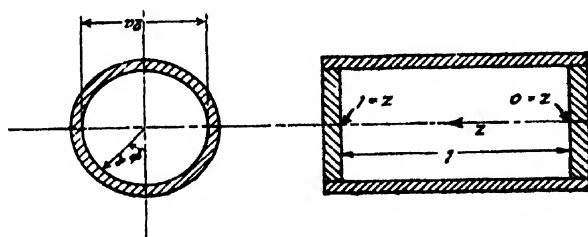


FIG. 6

Cylindrical cavity resonator illustrating the coordinate axes.

A lossless cylindrical air-dielectric cavity, such as shown in figure 6, when excited in the  $TE_{011}$  mode, has an oscillating electro-magnetic field given by (Sarbacher and Edson, 1943),

$$H_z = -jJ_0\left(\frac{p}{a}r\right)\sin\left(\frac{\pi z}{l}\right)e^{j\omega t}$$

$$H_r = j\beta\left(\frac{a}{p}\right)J_1\left(\frac{p}{a}r\right)\cos\left(\frac{\pi z}{l}\right)e^{j\omega t}$$

$$E_\phi = -\omega\mu_0\left(\frac{a}{p}\right)J_1\left(\frac{p}{a}r\right)\sin\left(\frac{\pi z}{l}\right)e^{j\omega t} \quad (1)$$



where,  $J_0$  and  $J_1$  are Bessel Functions of the first kind, of zero and first order respectively ;

$$\beta = \left| \left( \frac{\omega}{c} \right)^2 - \left( \frac{p}{a} \right)^2 \right|^{1/2} = \frac{\pi}{l} \quad \dots (2)$$

is the phase constant of the corresponding travelling wave mode ;  $p=3.832$ , the first root of the equation,  $J_0'(x)=0$ ,

$$c = \frac{1}{\sqrt{\mu_0 \epsilon_0}} = 3 \times 10^8 \text{ metres/sec.}$$

is the velocity of light in free space.

Equations (1) are also applicable, without serious error, to cylinders with high  $Q$ , i.e. low loss.

The maximum electric energy,  $W_E$  stored inside the cavity is

$$W_{EO} = \frac{1}{2} \epsilon_0 \int_0^{2\pi} \int_0^a \int_0^l |E_\phi|^2 r d\tau d\phi dz$$

Or, substituting for  $E_\phi$  from equation (1),

$$W_{EO} = \frac{1}{4} \left( \frac{a}{p} \right)^2 V \mu_0 \left( \frac{\omega_0}{c} \right)^2 J_0^2(p), \quad \dots (3)$$

where,  $V = \pi a^2 l$  is the volume of the cylindrical cavity.

The quality factor,  $Q$  of the cavity, without external loading, is given by

$$Q_0 = \frac{\omega_0 W_{EO}}{2P_{zo} + P_{ro}} \quad \dots (4)$$

where

$$\frac{\omega_0}{2\pi} = f_0 = \text{the resonant frequency}$$

$P_{ro}$  = power dissipated in the cylindrical wall perpendicular to the  $z$ -axis, and  $P_{zo}$  = power dissipated in each of the two faces perpendicular to the  $z$ -axis.

The power dissipated in the cylindrical wall is

$$P_{ro} = \frac{1}{2} R_c [Z_t] \int_0^l \int_0^{2\pi} |H_{tan}|^2 a d\phi dz, \quad \dots (5)$$

where,  $|H_{tan}|$  is the amplitude of the tangential component of the magnetic field at  $r=a$

and

$$t = \sqrt{\frac{j\omega_0 \mu_0}{\sigma_1}} \quad \dots (6)$$

is the intrinsic impedance (i.e. the ratio of transverse electric to magnetic field) of the wall material, and  $\sigma_1$  = electrical conductivity of the wall material.

Substitution of (6) in (5) yields

$$P_{r0} = \frac{1}{4} \sqrt{\frac{\pi f_0 \mu_0}{\sigma_1}} A_r J_0^2(p), \quad (7)$$

where,  $A_r = 2\pi al$  = the cylindrical surface area.

The power dissipated in each end wall is

$$P_{e0} = \frac{1}{2} R_c [z,] \int_0^{2\pi} \int_0^a |H_r|^2 r d\phi dr, \quad (8)$$

where,  $|H_r|$  is the amplitude of the tangential component of the magnetic field at the end walls, i.e. at  $z=0$  or  $z=l$ .

Then substituting for  $H_r$  from equation (1) and for  $Z_t$  from equation (6), we have for the power dissipated in one end wall,

$$P_{e0} = \frac{1}{2} \sqrt{\frac{\pi f_0 \mu_0}{\sigma_1}} \beta^2 \left( \frac{a}{p} \right)^2 A_e J_0^2(p), \quad (9)$$

where,  $A_e = \pi a^2$ , the area of one end wall.

In the above, the wall material is assumed to be made of a non-magnetic material (e.g., brass). If, however, the wall material be of a ferromagnetic metal (e.g., nickel), then  $\mu$  is complex and is given by

$$\mu = \mu_1 - j\mu_2 = |\mu| e^{-j\psi}. \quad \dots (10)$$

where  $|\mu| = \sqrt{\mu_1^2 + \mu_2^2}$  and  $\psi = -\tan^{-1} \frac{\mu_2}{\mu_1}$ .

The apparent permeabilities,  $\mu_R$  and  $\mu_L$ , are related to  $\mu$  as follows :

$$\mu_R = (|\mu| + \mu_2)/\mu_0 \text{ and } \mu_L = (|\mu| - \mu_2)/\mu_0.$$

For such case we have, therefore,

$$Z_t = \sqrt{\frac{j\omega\mu}{\sigma_2}} \sqrt{|\mu| + \mu_2 + j\sqrt{|\mu| - \mu_2}}, \quad (11)$$

where,  $\sigma_2$  is the conductivity of the ferromagnetic metal.

Hence, if a cylindrical cavity has one of its end walls made of a ferromagnetic material, the power dissipated in this wall will be given by

$$P_e = \frac{1}{2} \sqrt{\pi f (|\mu| + \mu_2)/\sigma_2} \beta^2 \left( \frac{a}{p} \right)^2 A_e J_0^2(p) \quad (12)$$

(Note: It is assumed in the above equations that the field configuration inside the cavity is not materially disturbed due to the presence of the ferromagnetic metal. This assumption is justified as the quality factor of the cavity remains high even with the ferromagnetic end-wall).

Now, when one of the end walls of the cavity is made of a ferromagnetic metal and the rest is of non-magnetic material, the quality factor is given by

$$Q_f = \frac{\omega_f W'_{EO}}{P'_{r0} + P'_e + P'_{s0}} \quad \dots (13)$$

where,  $\frac{\omega}{2\pi} = f$ , is the new resonant frequency of the cavity and the dashed symbols stand for the respective quantities at a frequency

It, therefore, follows from equations (4) and (13), that

$$\frac{I}{Q_f} - \frac{I}{Q_0} = \frac{P'_{r0} + P_Z + P'_{e0}}{\omega W_{E0'}} - \frac{P_{r0} + 2P_{e0}}{\omega_0 W_{E0}} \quad \dots (14)$$

Since the conductivity is very high, both for the non-magnetic and for the ferromagnetic metal, we can put  $\beta = \frac{\pi}{l}$  in the equations (9) and (12).

Substitution for  $P_r$  and  $P_e$  from appropriate equations, with due regard to the frequency, in equation (14) then yields;

$$\begin{aligned} \frac{I}{Q_f} - \frac{I}{Q_0} = & \frac{I}{4\pi^3} \sqrt{\frac{\pi}{\mu_0 \sigma_1}} \frac{h^2}{a^3} c^2 \left[ f^{-5/2} - f_0^{-5/2} \right] \\ & + \frac{I}{4\pi} \sqrt{\frac{\pi}{\mu_0 \sigma_1}} \frac{c^2}{l^3} \left[ f^{-5/2} - f_0^{-5/2} \right] \\ & + \left[ \frac{I}{4\pi} \sqrt{\frac{\pi \mu_R}{\mu_0 \sigma_2}} \frac{c^2}{l^3} f^{-5/2} - \frac{I}{4\pi} \sqrt{\frac{\pi}{\mu_0 \sigma_1}} \frac{c^2}{l^3} f_0^{-5/2} \right] \dots (15) \end{aligned}$$

Putting  $f_0 = f(1 + \delta)$ , where  $\delta \ll 1$  and remembering that  $\sigma_1/\sigma_2 \approx 1$ , simplification is usually possible by considering the relative values of the different terms. Each of the first two terms is of the order of  $10^{-3}$ . If then  $\mu_R = 1 + q$  say, the third term is about  $q/\delta$  times the other terms. Thus,

$$\frac{I}{Q_f} - \frac{I}{Q_0} = \frac{I}{4\pi} \sqrt{\frac{\pi}{\mu_0 \sigma_1}} \frac{c^2}{l^3} f_0^{-5/2} \left[ \left( \sqrt{\frac{\sigma_2}{\sigma_1}} \right) \mu_R^{1/2} - 1 \right] \quad \dots (16)$$

$Q_0$  and  $Q_f$  may be obtained from the standing wave measurement data as follows:

When a cavity coupling system has a single emergent transmission line, the V.S.W.R., produced in the line is given (Montgomery, 1947) by (see figure 7),

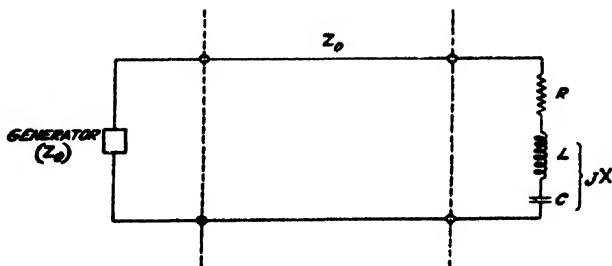


FIG. 7

Equivalent circuit of the cavity coupling system, at a particular reference plane, terminating a waveguide transmission line

$$\text{V.S.W.R.} = \frac{\sqrt{(Z_0 + R)^2 + X^2} + |\sqrt{(Z_0 - R)^2 + X^2}|}{\sqrt{(Z_0 + R)^2 + X^2} - |\sqrt{(Z_0 - R)^2 + X^2}|} \quad (17)$$

where,  $R + jX = R + j2RQ \frac{\Delta f}{f_0}$  is the equivalent line terminating impedance at some appropriate reference plane of the cavity coupling system,  $Z_0$  is the characteristic line impedance in the equivalent transmission line circuit,  $Q$  is the unloaded quality factor of the cavity, and  $f_0$  is the resonant frequency of the cavity.

At resonance, i.e.,  $\Delta f = 0$ , the V.R.W.R from equation (17) is

$$(i) \rho = R/Z_0, \text{ if } R > Z_0,$$

$$\text{or,} \quad (ii) \rho = Z_0/R, \text{ if } R < Z_0.$$

Since the cavity coupling in this case is such that  $R/Z_0 > 1$ ,

$$\rho = R/Z_0, \quad \dots (18)$$

For the frequencies,  $f_0 \pm \Delta F$  on either side of resonance,  $X = \pm (Z_0 + R)$  and the V.S.W.R. from equations (17) and (18) becomes

$$\rho_1 = \frac{1 + \rho + \sqrt{1 + \rho^2}}{1 + \rho - \sqrt{1 + \rho^2}} \quad \dots (19)$$

From the resonance curve (figure 5) the value of  $2\Delta F$  is obtained by knowing  $\rho_1$ .

The unloaded quality factor of the cavity thus is

$$Q = \frac{f_0}{2\Delta F} \left( 1 + \frac{1}{\rho} \right). \quad \dots (20)$$

#### 4. EXPERIMENTAL RESULTS AND DISCUSSION

Test cavity dimensions:

Diameter,  $2a = 4.95$  cms.

Length,  $l = 2.60$  cms,

Coupling hole diameter = 0.285"

The experimental results obtained are summarised in Table I.

TABLE I

Material	Resonant frequency $f_0$ in Mc/s.	V.S.W.R. at resonance, $\rho$	$\rho_1$	$2\Delta F$ in Mc/s.	Conductivity in mhos/metre $\times 10^{-7}$	$Q$	$\mu R$
Brass	9386.2	1.37	6.03	4.50	1.37	3620	1
Nickel	9385.45	1.55	6.17	4.65	1.3	3320	4.75
Soft iron	9384.55	2.5	7.65	5.25	1.0	2500	36

The experimentally obtained values of  $\mu_R$  are given in the last column of the table. These values, namely 36 for soft iron and 4.75 for nickel, agree closely with the values as obtained by other workers.

It is to be noted that the slight differences in the resonant frequencies, as given in the second column of the table for the cavity of same dimensions but of different materials for one of the end wells are to be ascribed more to machining inaccuracy than to differences in the value of  $\mu_L$  of the materials used. This was checked by an independent measurement in which the resonant frequencies of the cavity, with different end plates of the same material, were measured. The results obtained are given in Table II.

TABLE II.

End plate sample number	Resonant frequency in Mc/s.
1	9386.1
2	9385.8
3	9385.6
4	9386.4
5	9386.3
6	9386.2

Since the maximum error in the measurement of resonant frequency due to changes in geometry of the cavity is  $\pm 0.1$  Mc/s in 9385 Mc/s, i.e., 0.004%, it is seen from equation (21) that the error in  $Q$ -measurements for this reason is also of the same order. This will produce negligible error in the value of  $\mu_R$ .

#### 5. ACKNOWLEDGMENT

The authors take this opportunity to thank Professor S. K. Mitra for his encouragement and critical discussion and for his help in the preparation of the paper.

#### REFERENCES

- Birks, J. B., 1948, *Proc. Phys. Soc., Lond.*, **60**, 282.  
 Griffiths, J. H. B., 1946, *Nature*, **158**, 670.  
 Johnson, M. H., and Rado, G. T., 1949, *Phys. Rev.*, **75**, 841.  
 Montgomery, C. G., 1947. *Technique of Microwave Measurements* (Mc Graw-Hill), p. 334.  
 Sarbacher, R. I. and Edson, W. A., 1943, *Hyper, and Ultrahigh Frequency Engineering*, (Wiley), p. 378.

# **CORRIGENDUM**

## **ON THE SOLUTIONS OF MAXWELL'S EQUATIONS IN AN INFINITE MEDIUM, Etc.**

**BY K. V. KRISHNA PRASAD**

The material presented in my two papers entitled "On the approximate solutions of Maxwell's equations in an infinite medium with regions of finite conductivity" and "Rigorous solution for the case of electromagnetic wave propagation along a circular wave guide of finite conductivity", published in the Indian Journal of Physics, of August and September, 1951, respectively, are very much based on the material presented in the thesis by Dr. Glenn M. Roe, of March 1947, available from the University of Minnesota Library U. S. A. Several of the equations presented in the above papers are wrong and the correct equations are found in the thesis referred to above.

# ON THE RAMAN SPECTRUM AND STRUCTURE OF 1.3.5-TRIPHENYL BENZENE

By S. K. MUKERJI, L. SINGH AND R. S. SINGH

DEPARTMENT OF PHYSICS, AGRA COLLEGE, AGRA

(Received for publication, March 18, 1953)

## Plate XII

**ABSTRACT.** The Raman spectra of *s*-triphenyl benzene in various solutions have been studied for the first time. The spectrum of this substance resembles that of other substances of the diphenyl benzene family. The Raman frequencies obtained for this substance agree in most cases with those of diphenyl and of the ortho-, meta- and para-diphenyl benzene of this series investigated by previous authors.

The frequencies observed and found in all these various solutions are at 3046(1), 2987(4), 1603(8), 1406(7), 1458(5), 1350(6 bd), 1238(4), 1045(4), 1003(10), 603(1), 406(1), 384(5), 234(1), 170(5), 146(5) and 87(4)  $\text{cm}^{-1}$  respectively.

The results have been discussed with reference to the Raman spectra of diphenyl and of ortho-, meta- and para- diphenyl benzene. A comparative study of the spectra observed in all these substances lends support to the view that the substituent rings of this compound cannot be very appreciably tilted from the plane of the central ring.

## INTRODUCTION

In a previous communication to 'Nature' two of us (Mukerji and Singh, 1942) submitted a preliminary report giving the Raman frequencies obtained for *s*-triphenyl benzene in various solutions. During the last war this substance was practically unavailable, but now in the present investigation it has been possible to make a thorough study of the Raman spectra of this substance in various solutions. Discussions regarding the structures of the substances of this family of compounds with particular reference to 1, 3, 5-triphenyl benzene have also been incorporated in the present paper.

## EXPERIMENTAL

1, 3, 5-Triphenyl benzene obtained from the research laboratory of Eastman Kodak Company was further purified by crystallisation from absolute alcohol. The pure crystals thus formed were found opaque to light and hence were not studied for their Raman spectra in the solid state. The melting point of the substance is high (being  $170^{\circ}\text{C}$ ) and it tends to decompose at that high temperature. It was, therefore, studied in solutions in carbon-disulphide, carbon tetrachloride, acetic acid and chloroform respectively. The frequencies due to *s*-triphenyl benzene found common in all the above solutions are recorded here.

Wood's method was used to photograph the Raman spectra. With mercury arc as the exciting light, very intense scattering was obtained, but

there was also evidence of a very intense fluorescence spectrum on the plate. In order to reduce it considerably and to obtain a clean background a filter of concentrated solution of sodium nitrite was used which cut off the ultra violet portions of the mercury arc and suppressed  $\lambda$  4046 Å line considerably. The excitation was, therefore, only due to  $\lambda$  4358 Å mercury line which gave fairly good and intense spectra. The plates were exposed for a period of 40 hours.

The spectrograms were taken on Agfa Isochrome plates which were previously backed, speed H and D 4400, with a Fuess glass spectrograph having a dispersion of about 21 Å in the region of  $\lambda$  4358 Å. Measurements were made on a new accurate photo measuring micrometer. The wavelengths were calculated in the usual manner. The results for 1,3,5-triphenyl benzene have been tabulated in Table I in which the frequencies due to diphenyl, ortho-, meta- and para-diphenyl benzene have also been given for comparison.

TABLE I

Number	Diphenyl benzene (molten state) Mukerji and Aziz (1938)	<i>o</i> -diphenyl benzene (molten state) Mukerji and Aziz (1939).	<i>m</i> -diphenyl benzene (molten state) Mukerji and Aziz (1941).	<i>p</i> -diphenyl benzene Mukerji and Singh (1946).	1,2,3-triphenyl benzene in solutions (Authors).
1	—	Meltg. Pt. 57 <sup>0</sup>	—	42(5) solid	—
2	—	Boilg. Pt. 332 <sup>0</sup>	—	—	—
3	—	73(5) (bd)	80(4) (diff.)	85(5) solid	87(4)
4	—	—	—	93(3) molten	—
5	140(4) (bd)	112(5) (bd)	—	—	—
6	193(0)	114(6) (bd)	151(2) (diff.)	—	146(6)
7	—	—	—	—	170(5)
8	267(4) (bd)	238(6) (bd)	238(3) (diff.)	—	234(1)
9	313(4) (bd)	253(1)	275(3) (diff.)	—	—
10	358(0)	319(3)	—	—	—
11	408(5) (bd)	359(5)	—	—	384(5)*
12	—	406(6)	406(3)	—	406(1)
13	449(0)	—	—	409(1) molten	—
14	—	—	—	—	—
15	—	501(1)	—	—	—
16	548(1)	521(2)	—	—	—
17	614(4)	558(3)	—	—	—
18	—	615(5) (bd)	611(3)	508( $\frac{1}{2}$ ) solid	603(1)
19	—	—	—	593(0) molten	—
20	740(5)	708(6)	707(3)	—	—
21	779(4)	744(2)	—	—	—
22	—	774(5)	766(1)	773(5) solid	—
23	—	—	—	761(2) molten	—
24	838(4) (bd)	—	801( $\frac{1}{2}$ )	811(0) solid	—
25	—	839(4)	838(1)	—	—
26	898( $\frac{1}{2}$ )	874( $\frac{1}{2}$ )	—	—	—
27	—	—	901(1)	—	—
28	964(1)	—	964( $\frac{1}{2}$ )	940 molten	—
29	981(1)	—	—	—	—
30	1003(10)	993(8)	—	981(4) solid	—
31	—	1005(8)	1000(10)	1008(4) solid	1003(10)
32	1032(5)	—	—	1007(5) molten	—
33	—	1032(7)	1039(1)	1039(1)	1045( $\frac{1}{2}$ )
34	1090( $\frac{1}{2}$ )	1059(2)	—	—	—
35	1157(4)	—	1098( $\frac{1}{2}$ )	—	—
		1158(6)	1153(2)	1148(0) solid	—



TABLE I (contd.)

Number	Diphenyl benzene (molten state) Mukerji and Aziz (1938).	<i>o</i> -diphenyl benzene (molten state) Mukerji and Aziz (1939).	<i>m</i> -diphenyl benzene (molten state) Mukerji and Aziz (1941).	<i>p</i> -diphenyl benzene Mukerji and L. Singh (1946).	1,2,3-Triphenyl benzene in solutions (Authors).
36	1189(3)	1180(2)	—	—	—
37	—	—	—	1219(6) solid	—
38	1241(1)	1247(4)	—	1223(4) molten	1238(4)
39	1283(10)	1288(10)	1279(2)	1274(10) solid	—
40	—	—	—	1283(10) molten	—
41	1318(1)	—	1309(10)	—	—
42	—	—	1345(10)	—	1350(6) (bd)
43	1376(0)	—	—	1372(0) solid	—
44	—	—	—	1350(1) molten	—
45	—	—	1403(1)	—	—
46	1452(1)	1430(1)	1453(1)	—	1458(5) *
47	—	1471(1)	—	—	—
48	1506(4)	1503(5)	1494(4)	1503(1) solid	1496(1)
49	—	—	—	1523(2) diff. molten	—
50	—	—	—	1549(3)	—
51	—	1577(1)	1566(1)	—	—
52	1590(8)	1595(10)	1597(10)	1592(10) solid	—
53	—	—	—	1600(10) molten	—
54	1610(10)	1608(5)	1607(4)	1605(10)	—
55	—	—	—	1673(0) solid	1603(8)
56	—	—	—	1760(1) solid	—
57	—	—	—	2029(3) solid	2036(4)
58	—	—	—	2005(3) solid	—
59	—	—	—	2140(1) solid	—
60	—	—	—	2205(1) solid	—
61	—	—	—	2824(0) solid	—
62	2951(0)	—	—	—	—
63	—	—	—	—	—
64	3047(1)	3041(3)	—	3041(3) solid	2987(4) *
65	—	—	—	3043(2) molten	3046(1)
66	3063(5)	3059(6)	3062(2)	—	—
67	3192(0)	3196(0)	—	—	—

(bd) = broad

(diff.) = diffuse.

\* The three frequencies marked with asterisk were found only in acetic ether and chloroform solutions.

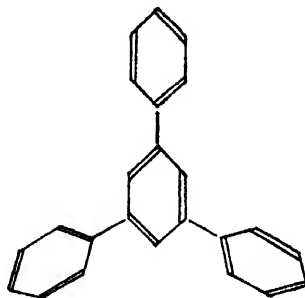


FIG. 1

1,3,5-Triphenylbenzene

## RESULTS AND DISCUSSION

Raman spectrum of diphenyl and of the ortho-, meta- and para- diphenyl benzene have been studied and reported by two of us (Mukerji and Aziz,

1938, 39, 41) and Mukerji and L. Singh (1946) previously. In this investigation we have studied the Raman spectra of *s*-triphenyl benzene. We can now compare the spectra of the substances of the diphenyl benzene family with those of symmetrical triphenyl benzene, as given in the foregoing table.

We know that in benzene there is a single ring with all the six carbon atoms free. In diphenyl one of the carbon atoms is loaded with a phenyl group. In the case of ortho- and meta- diphenyl benzene two of the carbon atoms are loaded with phenyl groups in the ortho- and meta- positions respectively. In *p*-diphenyl benzene two of the carbon atoms are also loaded with phenyl groups in the para position. The ortho, meta and para compounds have three benzene rings and in the para compound these benzene rings are joined end on in the para position.

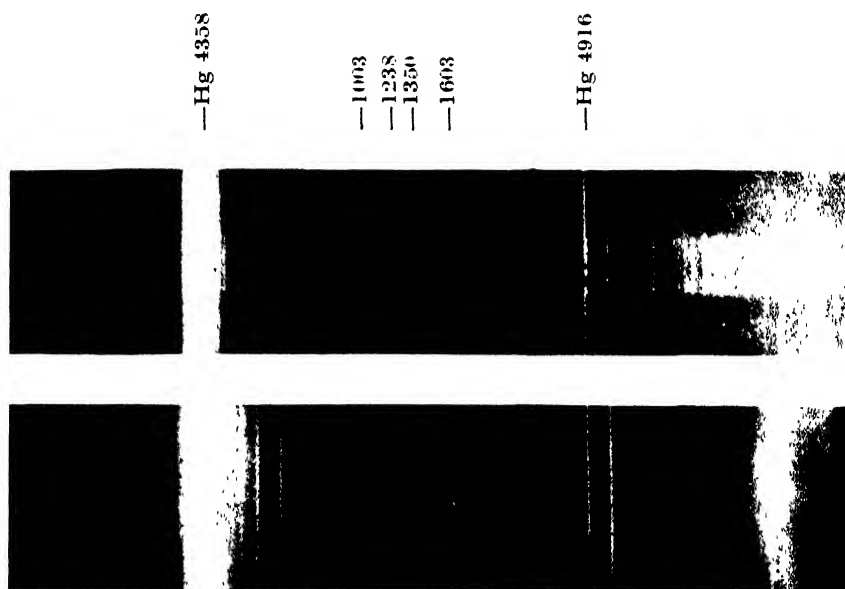
*s*-triphenyl benzene consists of four benzene rings, three of which are substituted in the fourth in positions 1, 3 and 5. Loss of any one of these benzene rings converts the substance into *m*-diphenyl benzene. It is, therefore, worthwhile to compare the frequencies of this substance with those of *m*-diphenyl benzene. It will be found, as given in Table I, that there is a close agreement between the majority of triphenyl benzene frequencies and those of *m*-diphenyl benzene. The strongest frequency of triphenyl benzene observed at  $1003\text{ cm}^{-1}$  is found equally strong by in *m*-diphenyl benzene and is also present in all the other compounds of this series. It may be observed here that in the case of the ortho- and para-diphenyl benzene, as will be seen in Table I, two strong lines are observed, in place of a single one, at  $1003\text{ cm}^{-1}$ , as observed in *s*-triphenyl benzene. This agrees remarkably well with the fact that the other line of this doublet has also completely disappeared in *m*-diphenyl benzene.

But the marked dissimilarity is that very strong line at  $1309\text{ cm}^{-1}$  observed in *m*-diphenyl benzene and also equally strongly in diphenyl and ortho and para compounds of this series with slightly lower frequencies is found to be completely missing in this compound.

It appears, therefore, that the addition of the extra benzene ring in position 5 of the central benzene ring of *m*-diphenyl benzene which makes *s*-triphenyl benzene a perfectly symmetrical compound is responsible for the disappearance of this line in the latter compound.

The other very marked difference is that the stronger frequency of the doublet at  $1597\text{ cm}^{-1}$ , also found in all the compounds of this series, is not observed in *s*-triphenyl benzene, although the other frequency of this doublet at  $1603\text{ cm}^{-1}$  appears in *s*-triphenyl benzene very strongly. It is possible that the two frequencies of this doublet have merged into one without being separated in *s*-triphenyl benzene, unless ethylene linkage  $\text{C}=\text{C}$  in the benzene rings of this compound has not been considerably weakened in the solution.

If we compare the frequencies of diphenyl with those of *s*-triphenyl benzene, which is obtained by the addition of two more benzene rings



Raman spectra of 1, 3, 5-triphenyl benzene

(a) In  $C_2S_2$  solution

(b) „  $CCl_4$  „



to diphenyl in the positions 3 and 5 of the central benzene ring, we find that many of the frequencies due to diphenyl are also present in *s*-triphenyl benzene. The two most prominent frequencies of diphenyl observed at  $1003\text{ cm}^{-1}$  and  $1610\text{ cm}^{-1}$  respectively appear almost equally strong in *s*-triphenyl benzene. Amongst the other frequencies common to these two compounds are 3046, 1496, 1458, 1238, 614 and  $146\text{ cm}^{-1}$  respectively, which are fairly strong in both these compounds.

It will be seen from Table I that many of the frequencies observed in ortho-diphenyl benzene have not appeared in *s*-triphenyl benzene. It is possible that since the Raman spectra of this substance were obtained in various solvents that many of the frequencies due to the ortho compound which are fairly weak have not appeared on the triphenyl benzene plate, being too feeble to be detected.

The frequency observed at  $3084\text{ cm}^{-1}$  as a weak line in *s*-triphenyl benzene evidently represents the C-H stretching vibration.

The line at  $1458\text{ cm}^{-1}$  which is also observed in other compounds of the series evidently corresponds to the transverse oscillation of hydrogen. The frequency at  $1350\text{ cm}^{-1}$  which appears as a broad band in *s*-triphenyl benzene is also observed as a very weak line at  $1345\text{ cm}^{-1}$  in *m*-diphenyl benzene. Similarly the line at  $1238\text{ cm}^{-1}$  is also observed with slightly varying frequencies in diphenyl and *o*-diphenyl benzene.

There are two other frequencies, one at  $603\text{ cm}^{-1}$  and the other at  $406\text{ cm}^{-1}$  observed in *s*-triphenyl benzene, are also found, as Table I will show, in all the other compounds of this series. The frequency at  $603\text{ cm}^{-1}$  then represents a carbon bending motion arising from the elongation and narrowing of the hexagonal configurations in this compound. The frequencies at  $384\text{ cm}^{-1}$  and  $234\text{ cm}^{-1}$  respectively due to *s*-triphenyl benzene are probably due to deformation oscillations of the molecule.

The frequency at  $146\text{ cm}^{-1}$  observed in *s*-triphenyl benzene as a fairly strong line is also found common to all other compounds of this series except *p*-diphenyl benzene. As it has not appeared in solid *p*-diphenyl benzene, although fairly strong, so it cannot possibly be due to lattice oscillations which is expected in the solid state. It may probably be due to the deformation oscillations of the molecule.

The frequency at  $73\text{ cm}^{-1}$  observed as a broad band in molten ortho-diphenyl benzene which has shifted to  $80\text{ cm}^{-1}$  as a diffuse band in molten *m*-diphenyl benzene and to  $93\text{ cm}^{-1}$  in molten *p*-diphenyl benzene, has appeared at  $87\text{ cm}^{-1}$  in *s*-triphenyl benzene, in solution. *p*-diphenyl benzene in the solid state gives this frequency as a strong line at  $85\text{ cm}^{-1}$ . This frequency appears, therefore, to be the lattice oscillation in the solid state of these compounds, which becomes weak and diffused when these compounds are in the molten state or in solution. The very low frequency at  $42\text{ cm}^{-1}$  also observed in solid *p*-diphenyl benzene, as Table I will show,

does not appear in *s*-triphenyl benzene in solution. This frequency evidently is due to lattice oscillations in the solid state.

It will be seen from Table I that there are hardly any frequencies observed in *s*-triphenyl benzene, in various solutions, which are not also present in one or the other compounds of this series, nor is there any strong frequency observed in this substance which can be said to be characteristic of this compound. There is not also much marked variation in the frequencies of this compound from those observed in other compounds of this series.

Diphenyl and *p*-diphenyl benzene have already been shown to be planer in structure. As regards ortho-diphenyl benzene, according to X-ray investigations of Clews and Lonsdale (1937), its most likely structure is one in which the two phenyl groups have their planes turned in the same direction out of the plane of the parent nucleus.

As regards *s*-triphenyl benzene its structure was studied by Orelkin and Lonsdale (1934) by X-ray investigation, who gave some preliminary data leading to its approximate structure. Their results are still inconclusive. In this investigation we have already pointed out that many of the frequencies of this substance agree remarkably well with those of diphenyl and also in many cases with those of the other compounds of the diphenyl benzene family. Diphenyl and *p*-diphenyl benzene have already been shown to be planer in structure, and as there is no marked dissimilarity between the frequencies of *s*-triphenyl benzene and those of the other compounds of the series, it is quite likely that the deviation from the planer configuration of this compound, if at all, cannot be very marked. Our results, therefore, lend support to the view that *s*-triphenyl benzene is planer in structure.

#### R E F E R E N C E S

- Aziz S. A., 1939, *Ind. J. Phys.*, **13**, 247.  
B. Clews, and K. Lonsdale, 1937, *Proc. Roy. Soc.*, **A**, **161**, 493,  
Orelkin, B. and K. Lonsdale, 1934, *Proc. Roy. Soc.*, **A**, **144**, 630.  
Mukerji S. K. and Aziz S. A., 1939, *Ind. J. Phys.*, **13**, 239.  
Mukerji S. K. and Aziz S. A., 1941, *Phil. Mag.* **31**, 231.  
Mukerji S. K. and L. Singh, 1942, *Nature*, **150**, 347.  
Mukerji S. K. and Aziz S. A., 1938, *Ind. J. Phys.*, **12**, 271.  
Mukerji S. K. and L. Singh., 1946 *Phil. Mag.*, **37**, 874.  
Mukerji S. K. and L. Singh., 1939 *Nature*, **144**, 382.  
Pickett L. W. 1933, *Proc. Roy. Soc. A*, **142**, 333.

# PRODUCTION OF $\pi$ -MESONS IN NEUTRON-PROTON COLLISIONS

By D. BASU

DEPARTMENT OF THEORETICAL PHYSICS, INDIAN ASSOCIATION FOR THE  
CULTIVATION OF SCIENCE, CALCUTTA 32

*(Received for publication, March 5, 1953)*

**ABSTRACT.** The cross section for the production of mesons in a neutron-proton collision, a third order process, is calculated on the basis of the 'charged pseudoscalar' theory with 'pseudoscalar coupling'. If the recoil of the nucleon initially at rest is neglected, the cross section vanishes. For  $g^2=0.3$ , the numerical value of the cross section is of the order of  $10^{-29}$  cm<sup>2</sup> and the total cross section increases as  $\log E_p$ ,  $E_p$  being the energy of the incident nucleon. The validity of our results for high energies is only restricted by the fact that radiation damping has been neglected.

## INTRODUCTION

The cross section for the production of mesons in a nucleon-nucleon collision depends essentially on the nature of the coupling of the meson with nucleons. At present the experimental trends indicate that the meson is to be described by a pseudoscalar field theory. In the present paper, the cross section for the production of meson has been evaluated as a third order process in which a meson is virtually emitted and re-absorbed and eventually emitted at the third step. We adopt the charged pseudoscalar theory with pseudoscalar coupling and treat the problem by the ordinary perturbation method (Born approximation) though it is a little precarious in the case of strongly coupled mesonic fields. The neglect of radiation damping is likely to matter only for extremely high energies. To include it is to make the handling of a third order process exceedingly difficult and imposes drastic simplifications which, in the energy region that is amenable to direct experimental verification, are likely to adulterate the result worse than the neglect of damping. Anyhow it is worthwhile trying to meet the experimental results in this way. The Born approximation in itself is justified since the threshold energy for meson production is well above 100 Mev.

## 2. METHOD OF CALCULATION

From the perturbation theory the differential cross section for meson production is given by

$$d\sigma = \frac{2\pi}{\hbar v} |H_{fi}|^2 \rho_f \quad \dots (1)$$

Here  $v$  is the relative velocity of the incident nucleon and  $V$  is the volume in which the state functions of the particles are normalised.  $\rho_f$  denotes the density functions of the final proton and meson. The third order matrix element  $H_{fi}$  stands for

$$H_{fi} = \sum_{m_1, m_2} \frac{\langle f^* | I | m_1 \rangle \langle m_1^* | I | m_2 \rangle \langle m_2^* | I | i \rangle}{(E_i - E_{m_1})(E_{m_1} - E_{m_2})} \quad \dots (2)$$

Here the letters  $f$ ,  $m_1$ ,  $m_2$  and  $i$  denote the wave functions of the two nucleons in the final, two successive intermediate and the initial states and  $E_i$ ,  $E_{m_1}$  and  $E_{m_2}$  stand for the total energies of the systems in the initial and the two successive intermediate states.  $I$  is the interaction Hamiltonian causing the emission and absorption of the meson, which for the pseudoscalar charged theory may be written thus

$$I = \sum \frac{1}{\sqrt{2\pi V}} \left\{ -ig_1 \mu \rho_2 (a_p^* - b_p) + g_2 (\boldsymbol{\sigma} \cdot \mathbf{p}) (a_p^* + b_p) + g_2 \epsilon \rho_1 (a_p^* + b_p) \right\} \tau_{NFC} e^{-\frac{2\pi i}{\hbar} (\mathbf{P} \cdot \mathbf{X})} \\ \left\{ +ig_1 \mu \rho_2 (a_p - b_p^*) + g_2 (\boldsymbol{\sigma} \cdot \mathbf{p}) (a_p - b_p^*) + g_2 \epsilon \rho_1 (a_p + b_p^*) \right\} \tau_{PNC} e^{+\frac{2\pi i}{\hbar} (\mathbf{P} \cdot \mathbf{X})} \dots (3)$$

$\epsilon$ ,  $\mu$  and  $p$  denote energy, mass and momentum of the meson respectively, all three in energy units.  $g_1$  and  $g_2$  are the two interaction constants corresponding to the pseudoscalar and pseudovector coupling respectively.  $a^*$  and  $a$  ( $b^*$  and  $b$ ) are the emission and absorption operators for the positive (negative) meson.  $\rho_1$ ,  $\rho_2$ ,  $\rho_3$  ( $=\beta$ ) and  $\boldsymbol{\alpha} = \rho_1 \boldsymbol{\sigma}$  are the usual Dirac matrices.

We consider the collision of a proton of initial momentum  $P_0$  with a neutron which, for simplicity, is taken to be at rest; in the final state we have two protons of momentum  $P_1$  and  $P_2$  and a negatively charged meson of momentum  $p$ . By  $P$  and  $N$  we shall denote a proton and a neutron while the superscripts 1 and 2 on  $P$  and  $N$  (or on  $E$ ) shall distinguish the two particles (or their energies).  $Y^+$  and  $Y^-$  stand for positively and negatively charged mesons respectively. The momentum of the particle follows in brackets the symbol for the particle. The transitions are considered according to the Hole theory; a square bracket enclosing the particle symbol denotes that the particle is in a state of negative energy, with the momentum indicated. The six transitions contributing to the third order matrix element for meson production are schematically represented as follows:



initial state :  $P^{(1)}(\mathbf{P}_0) + N^{(2)}(0) + [N'(\mathbf{P}_0 - \mathbf{p}')] \rightarrow$

$$(A) \quad N^{(1)'}(\mathbf{P}_0 - \mathbf{p}') + Y^{+'}(\mathbf{p}') + N^{(2)}(0) + [N'(\mathbf{P}_0 - \mathbf{p}')] \\ \rightarrow N^{(1)'}(\mathbf{P}_0 - \mathbf{p}') + P^{(2)}(\mathbf{p}') + [N'(\mathbf{P}_0 - \mathbf{p}')] ]$$

$$(B) \quad N^{(1)'}(\mathbf{P}_0 - \mathbf{p}') + Y^{+'}(\mathbf{p}') + N^{(2)}(0) + [N'(\mathbf{P}_0 - \mathbf{p}')] \\ \rightarrow P^{(1)}(\mathbf{P}_1) + Y^-(\mathbf{p}) + Y^+(\mathbf{p}') + N^{(2)}(0) + [N'(\mathbf{P}_0 - \mathbf{p}')] ]$$

$$(C) \quad P^{(1)}(\mathbf{P}_0) + P^{(2)}(\mathbf{p}') + Y^-(\mathbf{p}) + [N'(\mathbf{P}_0 - \mathbf{p}')] \\ \rightarrow N^{(1)'}(\mathbf{P}_0 - \mathbf{p}') + P^{(2)}(\mathbf{p}') + [N'(\mathbf{P}_0 - \mathbf{p}')] ]$$

intermediate states :

$$[A] \quad P^{(1)}(\mathbf{P}_0) + N^{(2)}(0) + P(\mathbf{P}_1) + Y^-(\mathbf{p}) \\ \rightarrow P^{(1)}(\mathbf{P}) + P(\mathbf{P}_1) + Y^-(\mathbf{p}) + P^{(2)}(\mathbf{p}') + Y^+(-\mathbf{p}')$$

$$[B] \quad P^{(1)}(\mathbf{P}_0) + P^{(2)}(\mathbf{p}') + Y^+(-\mathbf{p}) + [N'(\mathbf{P}_0 - \mathbf{p}')] \\ \rightarrow P^{(1)}(\mathbf{P}_0) + P^{(2)}(\mathbf{p}') + Y^+(-\mathbf{p}) + P(\mathbf{P}_1) + Y^-(\mathbf{p})$$

$$[C] \quad P^{(1)}(\mathbf{P}_0) + N^{(2)}(0) + P(\mathbf{P}_1) + Y^-(\mathbf{p}) \\ \rightarrow N^{(2)}(0) + P(\mathbf{P}_1) + Y^-(\mathbf{p}) + [N'(\mathbf{P}_0 - \mathbf{p}')] + Y^{+'}(\mathbf{p})$$

$$\text{final state} \rightarrow P^{(1)}(\mathbf{P}_1) + P^{(2)}(\mathbf{p}') + Y^-(\mathbf{p}) + [N'(\mathbf{P}_0 - \mathbf{p}')] , \quad \dots \quad (4)$$

$$\text{where} \quad \mathbf{P}_1 = \mathbf{P}_0 - \mathbf{p}' - \mathbf{p}, \quad \mathbf{P}_2 = \mathbf{p}' \quad \dots \quad (5)$$

On close inspection of the table it will be realised that the six cases of transition it describes in detail, differ with regard to the stage at which take place (a) the virtual emission (b) the virtual re-absorption (c) the emission of that meson that has come to stay. *E.g.* in (B) the virtual emission is at the first intermediate stage, its re-absorption is at the final stage, and the meson that will stay is emitted in the second intermediate state.

As can be seen from Eqn. 2, the contribution to the matrix elements is greatest when the resonance denominators are smallest, which means that cases of small momentum transfer between the nucleons, arising from very small values of momentum  $p'$  of the virtual meson, are of importance. The "exchange" terms corresponding to the transitions A, B and C arise when the two final protons interchange their momentum, the particle 1 having the momentum  $P_2$  and 2 having  $P_1$ ; such cases correspond to large values of  $p'$  which reduce the matrix elements in question by large denominators. Thus the contribution of the exchange terms will be small and we shall allow for them only in first approximation in the final integration of  $p'$  over all possible values. Remembering that only very small momentum transfers contribute considerably, we can put the final energy of the second particle  $E_{p'}^{(2)}$  very nearly equal to  $M$ . In this way we neglect the difference  $E_{p'}^{(2)} - M$  against  $E_{p'}^{(1)} - E_{N'}^{(1)}$  or  $\epsilon_{p'}$  (the energy of the virtual meson) in the denominators. For example, we put

$$(A) \quad E_1 - E_{m2} = E_{p'}^{(1)} - E_{N'}^{(1)} - E_{p'}^{(2)} + M^{(2)} \approx E_{p'}^{(1)} - E_{N'}^{(1)}, \quad \dots \quad (6)$$

$$\text{where} \quad | \mathbf{N}' | = | \mathbf{P}_0 - \mathbf{p}' |$$

In the same approximation the expression for the conservation of energy reads

$$E_{P_1} = E_{P_1'} + \epsilon_p \quad \dots \quad (7)$$

We prefer to drop the superscript on  $E$  from now on,  $E$  will indicate the energy of the nucleon with the momentum value denoted as a subscript.

We substitute (3) with  $g_2=0$  in (2) and, making use of (6) and (7), we notice that for the transition schemes (4), the matrix elements take a very simple form because the sum of the contribution due to  $A$  and  $B$  equals that of  $C$ . The matrix elements in the negative energy states would, by the way, be the same whether we regarded these states as empty or all filled (Hole theory). Writing  $\psi_{P_i}^{(1)}$  for the Dirac spin function of particle 1 having  $P_1$  as the value of the momentum, the expression for  $H_{fi}$  becomes

$$H_{fi} = \frac{2ig_1^3 \mu^3}{(2V)^{3/2} \epsilon'^2 \sqrt{\epsilon}} \sum_{\mathbf{L}} \frac{(\bar{\Psi}_{P_1}^{(1)*} \rho_2^{(1)} \Psi_{N'}^{(1)}) (\bar{\Psi}_{N'}^{(1)*} \rho_2^{(1)} \Psi_{P_2}^{(1)}) (\bar{\Psi}_{P_2}^{(2)*} \rho_2^{(2)} \Psi_0^{(2)})}{E_{P_2} - E_{N'}} \quad \dots (8)$$

where  $\epsilon'^2 = \mu^2 + p'^2$  and  $\epsilon^2 = \mu^2 + p^2$

Following the procedure of Heitler (1936), we multiply the numerator and denominator of (8) by  $E_{P_2} + E_{N'}$  and carry out the summation over the 4 possible states of the intermediate neutron. We then form the absolute square of (8) and, summing over the two spin states of the initial and final nucleons by the usual spur method, we obtain,

$$|H_{fi}|^2 = \frac{4g_1^6 \mu^6}{(2V)^3} \frac{1}{E_{P_2} E_{P_1}} \left( 1 - \frac{M}{E_{P_2}} \right) \frac{1}{\epsilon \epsilon'^4 (E_{P_2}^2 - E_{N'}^2)^2} \\ [E_{P_2} E_{P_1} \{2E_{P_2}^2 - (E_{P_2}^2 - E_{N'}^2)\} + \{(\mathbf{P}_1 \mathbf{P}_0) + M^2\} (E_{P_2}^2 - E_{N'}^2) \\ + 2\{(\mathbf{P}_0 \mathbf{N}') + M^2\} \{(\mathbf{P}_1 \mathbf{N}') + M^2\} - 2E_{P_2} \{E_{P_1} [(\mathbf{P}_1 \mathbf{N}') \\ + M^2] + E_{P_1} [(\mathbf{P}_0 \mathbf{N}') + M^2]\}] \quad \dots (9)$$

where  $(\mathbf{P}_0 \mathbf{P}_1)$  denotes the scalar product of  $P_0$  and  $P_1$

The factor  $\left(1 - \frac{M}{E_{P_2}}\right)$  in the above expression allows for the contribution of the square of the matrix element  $(\bar{\Psi}_{P_2} \rho_2 \Psi_0)$  of particle 2, which is initially at rest and then acquires the small momentum  $p'$  due to the virtual emission or the absorption of the meson. In the non-relativistic limit  $E_{P_2} \approx M$ , so the cross section vanishes. The negative sign within  $\left(1 - \frac{M}{E_{P_2}}\right)$  is a feature of the pseudoscalar interaction, where  $\rho_2$  anticommutes with  $\rho_3$  of the Hamiltonian; with scalar interaction the term involves  $\rho_3$  so that in the non-relativistic limit that factor becomes 2 (Urban and Schwarzl, 1949). The smallness of the cross section we shall find in the present pseudoscalar case is due to this factor.

The density function  $d\rho_f$  is

$$d\rho_f = \frac{p \epsilon d\epsilon}{(2\pi\hbar c)^3} \cdot \frac{P_1 E_{P_1}}{(2\pi\hbar c)^3} d\Omega_p d\Omega_{P_1} \quad \dots (9a)$$

Following Nordheim & Nordheim (1938) we write

$$\mathbf{Q} \equiv \mathbf{N}' = \mathbf{P}_0 - \mathbf{p}' = \mathbf{P}_1 + \mathbf{p} \quad \dots \quad (10)$$

With respect to  $P_0$  the polar angles of  $Q$  are denoted by  $\theta$  and  $\varphi$ ,  $\psi$  denotes the azimuthal angle of the plane  $(\mathbf{P}_1, \mathbf{p})$  around  $Q$ . In this notation

$$d\rho_f = \frac{6d\epsilon E_{P_1}}{(2\pi\hbar c)^6} d\varphi d\psi \sin\theta d\theta dQ \quad \dots \quad (11a)$$

$$\epsilon'^2 = \mu^2 + P_0^2 + Q^2 - 2P_0Q \cos\theta \quad \dots \quad (11b)$$

$$E_{P_0}^2 - E_{N'}^2 = P_0^2 - Q^2 \quad \dots \quad (11c)$$

$$(\mathbf{P}_1, \mathbf{N}') = \frac{Q^2 + P_1^2 - p^2}{2} \quad \dots \quad (11d)$$

Since only very small values of  $p'$  give a considerable contribution to the matrix element, we can write

$$\left(1 - \frac{M}{E_{p'}}\right) \approx \frac{1}{2} \frac{p'^2}{M^2} \quad \dots \quad (12)$$

Substituting (9), (11) and (12) in (1), we obtain for the differential cross section (after integration over  $d\psi$  and  $d\phi$ )

$$\begin{aligned} d\Phi = & \frac{4g_1^6 \mu^6}{(4\pi)^4 (\hbar c)^7 2M^2} \frac{d\epsilon}{P_0} \left( \frac{1}{\epsilon'^2} - \frac{\mu^2}{\epsilon'^4} \right) \frac{1}{(P_0^2 - Q^2)} \\ & \times [2E_{P_0} E_{P_1} - 2P_0^2 \{(\mathbf{P}_1, \mathbf{Q}) + M^2\} - 2E_{P_0} E_{P_1} M^2 \\ & + \{-E_{P_0} E_{P_1} + M^2\}(P_0^2 - Q^2) + (\mathbf{P}_1, \mathbf{P}_0)(P^2 - Q^2) \\ & + 2(\mathbf{P}_0, \mathbf{Q})\{(\mathbf{P}_1, \mathbf{Q}) + M^2\} - 2E_{P_0} E_{P_1} (\mathbf{P}_0, \mathbf{Q})] \sin\theta d\theta dQ. \quad \dots \quad (13) \end{aligned}$$

Integrating over  $d\theta$  and taking  $P_0^2 \gg \mu^2$  and  $P_0 \gg Q$  we obtain

$$\begin{aligned} d\Phi = & \frac{2}{\chi^2} \left( \frac{g_1^2 \chi^2}{4\pi\hbar c} \right)^3 \frac{\mu^2}{M^2} \frac{d\epsilon}{P_0} \left[ \frac{6E_{P_0} E_{P_1} - 3(E_{P_0}^2 + E_{P_1}^2 - p^2)}{(P_0^2 - Q^2)^2} \right. \\ & \left. + \frac{(5E_{P_0}^2 - E_{P_1}^2 - 4E_{P_0} E_{P_1} + p^2)}{2P_0^2 (P_0^2 - Q^2)} + \frac{1}{2P_0^2} \right] Q dQ, \quad \dots \quad (14) \end{aligned}$$

where

$$\chi = \mu/\hbar c.$$

On integrating over  $dQ$  between the limits  $\mathbf{P}_1 + \mathbf{p}$  and  $\mathbf{P}_1 - \mathbf{p}$ , the result becomes

$$\begin{aligned} d\Phi = & \frac{2g_1^6}{\chi^2} \frac{\mu^2}{M^2} \frac{d\epsilon}{P_0} \left[ \frac{(5E_{P_0}^2 - E_{P_1}^2 - 4E_{P_0} E_{P_1} + p^2)}{4P_0^2} \log \frac{P_0^2 - P_1^2 - p^2 + 2P_1 p}{P_0^2 - P_1^2 - p^2 - 2P_1 p} \right. \\ & \left. - \frac{3\mu^2}{2} - \frac{4P_1 P_0}{(P_0^2 - P_1^2 - p^2)^2 - 4P_1^2 p^2} + \frac{P_1 p}{P_0^2} \right] \dots \quad (15) \end{aligned}$$

$$\approx \frac{3g_1^6}{\chi^2} \frac{\mu^2}{M^2} \frac{E_{P_0} d\epsilon}{P_0^3} \log \frac{4E_{P_0} \epsilon}{\mu^2}, \quad \dots \quad (16)$$

when

$$p = \epsilon, P_1 = E_{P_1}.$$

and  $g^2 = \frac{g_1^2 \chi^2}{4\pi \hbar c}$  (a dimensionless constant)

Assuming that the maximum energy that the meson can have is  $\frac{1}{2}E_{P_0}$  the integration of (16) over  $d\epsilon$  then gives for the total cross section

$$\Phi = \frac{3}{4} \frac{g^6}{\chi^2} \frac{\mu^2}{M^2} \frac{E_{P_1}^3}{P_0^3} \log \frac{E_{P_1}}{\mu}.$$

At high energies the total cross section for the production of pseudoscalar mesons with pseudoscalar coupling increases as  $\log \frac{E_{P_0}}{\mu}$ .

The value of  $g^2$  in the case of pseudoscalar coupling, which does not enter into the deuteron binding force is very uncertain. If we adopt  $g^2 = 0.3$ , the differential cross section becomes of the order of  $10^{-29} \text{ cm}^2$

$\left( \frac{g^6}{\chi^2} \frac{\mu^2}{M^2} \approx 10^{-29} \right)$ ; it is practically independent of the mass of the meson.

#### CONCLUDING REMARKS

The above result differs from that of the scalar theory with scalar coupling in which the total cross section decreases with energy as

$\frac{1}{E_{P_1}}$ , as obtained by Nordheim and Nordheim (1938) and Urban and Schwazi

(1946); this difference is due to the factor  $\left(1 - \frac{M}{E_{P_1}}\right) \approx \frac{1}{2} \frac{p'^2}{M^2}$ , whereas, in the

scalar coupling the analogous factor  $\left(1 + \frac{M}{E_{P_1}}\right)$  is about 2, as was mentioned

above. If the recoil of the nucleon initially at rest is neglected, the cross section vanishes with pseudoscalar coupling, with scalar coupling it does not. Our numerical value is of the same order as Foldy and Marshak (1949) computed from the analogy with photonic bremsstrahlung, this method replaces the process of virtual emission and absorption by an empirical potential between the two nucleons, and it is about 100 times smaller than that of Morette and Peng (1948) who based their calculation on a Moller-Rosenfeld mixture in non-relativistic approximation. The same cross section (pseudoscalar meson with pseudoscalar coupling) derived by Morette

(1949) from the invariant perturbation method varies as  $\frac{1}{E_{P_1}} \log \frac{ME_{P_1}}{2}$

(for  $E_{P_1} \gg M$ ); Takagi (1949) has computed the same problem from the invariant perturbation method. The reason for this discrepancy between the ordinary and the invariant perturbation methods is not quite obvious.

ACKNOWLEDGMENTS

This work was begun at the Dublin Institute for Advanced Studies during early 1950, the author wishes to express his sincere thanks to Prof. E. Schrödinger for his kind encouragement and to Prof. W. Heitler and Dr. W. Thirring for useful discussions. The recent emphasis on pseudoscalar theory has revived his interest to complete it.

REFERENCES

- Foldy and Marshak, 1949, *Phys. Rev.*, **75**, 1493.  
Heitler 1936, *Quantum Theory of Radiation*.  
Morette, 1949, *Phys. Rev.*, **76**, 1432  
Morette and Peng, 1948, *Proc. Roy. Irish Acad.*, **51A**, 217  
Nordheim and Nordheim, 1938, *Phys. Rev.*, **53**, 254.  
Takagi, 1949, *Proc. Theo. Physics*, IV, 557.  
Urban and Schwarzl, 1949, *Acta. Phys. Austr.*, **2**, 368.

## THE BAND SPECTRUM OF NICKEL FLUORIDE\*

By V. G. KRISHNAMURTY

DEPARTMENT OF PHYSICS, ANDHRA UNIVERSITY, WALTAIR

*(Received for publications, November 10, 1952)*

## Plate XIII

**ABSTRACT.** A characteristic band spectrum of nickel fluoride has been obtained using a heavy current discharge from a 2 K.W. D.C. generator. Regularities in wavenumber interval have led to the suggestion of a  ${}^2\Pi-{}^2\Sigma$  as the electronic transition giving rise to the band heads. The value of the ground state vibrational frequency obtained for this band system is  $740\text{ cm}^{-1}$  approximately.

Band spectra of the fluorides of transition group elements are among those that are least studied and understood. The only fluoride molecule for which a characteristic band spectrum has been obtained is  $\text{MnF}$ . Rochester and Olsson (1939) reported in  $\text{MnF}$  two systems in absorption—one in the region  $\lambda 3300$  to  $\lambda 3600$  consisting of five groups of violet degraded bands and the other in the region  $\lambda 2100$  to  $\lambda 2400\text{ \AA}$  which is of a simple sequence structure. They attributed the former system to the triatomic molecule  $\text{MnF}_2$  and the latter to the diatomic molecule  $\text{MnF}$  and suggested  ${}^1\Sigma-{}^1\Sigma$  as the probable electronic transition of the far ultraviolet system. The interpretation given above was completely revised in a very comprehensive work later by Bacher and Miescher (1948) who obtained both the systems in absorption and the near ultraviolet system also in emission in a heavy current discharge from a 1000 volts D.C. generator at 0.3 of an ampere using a specially designed discharge tube.  ${}^7\Pi-{}^7\Sigma$  was shown to be the electronic transition of the near ultraviolet system and a  ${}^7\Sigma-{}^7\Sigma$ , as the transition which gives rise to simpler sequence and vibrational structure of the far ultraviolet system. No other fluoride molecule seems to have been studied in detail.†

In continuation of the work on the chlorides and bromides of nickel and cobalt described in previous papers, the spectra of cobalt fluoride nickel fluoride have been investigated. The source of excitation is the same as that used previously—a heavy current discharge from a D. C. generator (2000 volts, 1 amp.). The experiments on cobalt fluoride have so far been un-

\* Communicated by Prof. K. R. Rao.

† Bands of the  $\text{MnF}$  molecule are photographed also in the region  $\lambda 4900$  to  $\lambda 5000$  by Bacher (1948) and P. T. Rao in this laboratory. The latter author analysed the system and assigned it to the transition  ${}^5\Pi-{}^7\Sigma$  (the results are in the course of publication).

successful. The main difficulty in obtaining fluoride bands arises from free fluorine (usually liberated during the exposure) which reacts with the walls of the discharge tube and emits silicon fluoride bands which are most easily excited. They often suppress the excitation of the bands of other fluorides (nickel or cobalt) or obliterate them due to overlapping when they occur in the same region. It was possible slightly to adjust the current flowing through the discharge tube such that the nickel fluoride bands are obtained somewhat more prominently than the silicon fluoride bands.

For nickel fluoride, the author succeeded in obtaining a characteristic band spectrum, a small portion of which is overlapped by silicon fluoride bands but a considerable portion being outside the region. This could be easily measured. The band spectrum is reproduced in Plate XIII (figure 2) which contains also SiF band spectrum in juxtaposition.

#### DESCRIPTION OF THE BANDS

The observed bands present a very characteristic appearance. They occur in well separated groups, the strongest one being the group at  $\nu$  22141.2  $\text{cm}^{-1}$  in which two band heads stand out prominently. In addition to this stronger group, two other weaker groups are observed on the lower frequency side at  $\nu$  21411.4 and 20686.5  $\text{cm}^{-1}$  [Plate XIII, figure 3]. Two other still weaker groups lying on the higher frequency side are also observable but they are masked by the strong silicon fluoride bands in this region and measurements could not be made. Each of the observed groups contains only a few band heads, about 4 or 5. 13 band heads have been measured altogether. No distinct degradation of the bands is noted. They are somewhat diffuse with a slight shading probably towards the red. A somewhat close structure leading to diffuseness of the band is noticed in the case of the strongest group at  $\nu$  22144.2  $\text{cm}^{-1}$ . If the structure and disposition of the individual bands are examined in each group, it will be seen that some three band heads occur close together while the remaining ones are situated at a larger interval from these. This grouping has suggested that two component levels (such as  $\pi_{1/2}$ ,  $\pi_{1\frac{1}{2}}$ ) may be involved.

#### ANALYSIS

The most intense group at  $\nu$  22144.2  $\text{cm}^{-1}$  is regarded as  $\Delta v = 0$  sequence and the other two groups on the longer wavelength side as  $\Delta v = -1$  and  $-2$  sequences respectively.  $\Delta v + 1$ ,  $+2$  sequences, as pointed out above, have been masked by silicon fluoride bands. The second sequence  $\Delta v = -1$ , served as the starting point of the analysis: Close scrutiny of this sequence shows that it consists of two separate groups, one of which has 3 heads and

the other, 2 heads, the intervals between the first members ( $\nu$  21411.4 and 21292.9) is  $118.5 \text{ cm}^{-1}$  which is of the same order as  $^3\Pi$  interval ( $103 \text{ cm}^{-1}$ )

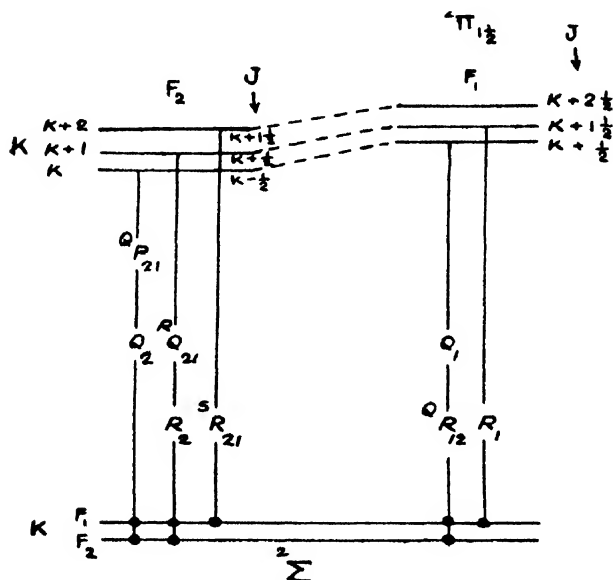


FIG. 1

Scheme of transition in  $^2\Pi(u) - ^2\Sigma$

observed in nickel chloride bands. This suggested the possibility of the transition  $^2\Pi - ^2\Sigma$ . The energy level diagram for this transition is drawn up and shown in figure 1. The diagram gives the expected band heads. Transition between  $^2\Pi_{1/2}$  and  $^2\Sigma$  gives rise to three resolvable heads.

(1)	(2)	(3)
$S_{R_{u1}}$	$R_2$	
	$R_{Q_{u1}}$	$Q_2$
		$Q_{P_{u1}}$

Similarly  $^2\Pi_{1/2}$  to  $^2\Sigma$  gives two resolvable heads.

(1)	(2)
$R_1$	$Q_{R_1}$
	$Q_1$

Thus five heads may be predicted for this transition.

Comparing these with the five component heads in the second group at  $\nu$  21411.4  $\text{cm}^{-1}$ , a close agreement between the predicted and observed heads is assumed.

With this identification and analysis of this group ( $\Delta\nu = -1$ ), the scheme is extended to the remaining two groups each of which consists respectively of four heads. It is also noticed that a wavenumber interval of about  $731 \text{ cm}^{-1}$  is found to be recurring between corresponding members of the  $\Delta\nu = 0$  and  $\Delta\nu = -1$  sequences shown below.



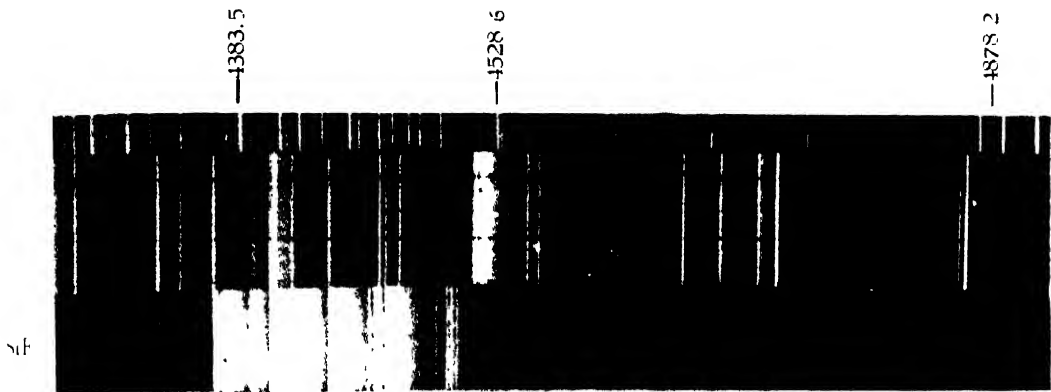


Fig. 2  
NiF and SiF bands

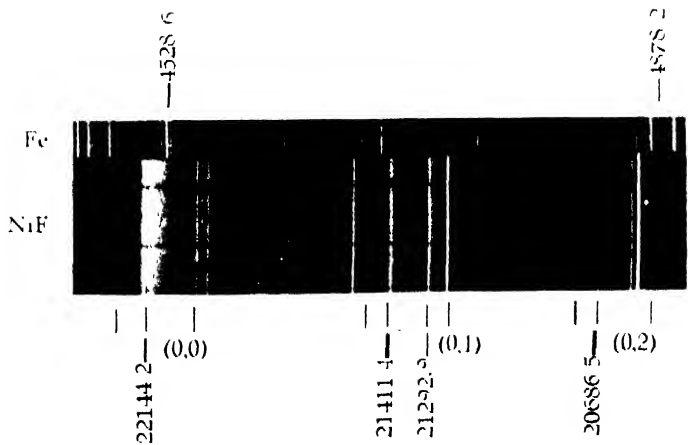


Fig. 3  
NiF bands.



22144.2	732.8
21411.4	
22124.1	730.5
21393.6	
22098.6	731.6
21367.0	

Again a slightly smaller interval recurs between the corresponding bands in  $\Delta v = -1$  and  $\Delta v = -2$  sequences.

21411.4	724.9
20686.5	
21367.0	727.4
20639.6	
21292.9	721.2
20571.7	
21270.7	718.9
20551.8	

These recurring intervals and the order of their value indicated that it may probably correspond to the ground state vibrational frequency  $\omega_e''$  ( $=740 \text{ cm}^{-1}$ ) since it agrees with the corresponding values in the other halides.

The complete analysis arrived at thus is shown in Table I which records also the wavenumbers of the band heads and their intensities.

Since sequences corresponding to  $\Delta v = +1$ ,  $+2$  are not measured it is not possible to determine the upper state vibrational frequency. The value of the vibrational frequency for the ground state is 740 wavenumber units approximately.

TABLE I  
NiF Bands

Wavenumber	Int.	$v', v''$	$\Delta J$		
			-1	0	+1
22144.2	7	0,0	$Q_{P_{21}}$	$RQ_{21}$	$SR_{21}$
124.1	9	0,0		$Q_2$	$R_2$
098.6	5	0,0			
040.7	6	0,0			$K_1$
21411.4	6	0,1	$Q_{P_{21}}$	$RQ_{21}$	$SR_{21}$
393.6	8	0,1		$Q_3$	$R_2$
367.0	5	0,1			
292.9	6	0,1			$R_1$
270.7	5	0,1	$Q_{P_{21}}$	$Q_1$	$QR_{11}$
20686.5	4	0,2		$Q_2$	$SR_{11}$
639.6	4	0,2			
571.7	5	0,2			$R_1$
551.8	3	0,2		$Q_1$	$QR_{11}$

## ACKNOWLEDGMENTS

The author wishes to express his grateful thanks to Prof. K. R. Rao for his kind guidance and interest in the work. He is grateful to the Government of India, Ministry of Scientific Research for the award of a Senior Research Scholarship.

## REFERENCES

- Bacher, J., 1948, *Helv. Phys. Acta.*, **21**, 379.  
Johnson and Jenkins., 1927, *Proc. Roy. Soc* , **116**, 327.  
Krishnamurty, V. G., 1951, *Curr. Sci.*, **20**, 323.  
    ,,                  1952,      ,,      **21**, 37.  
    ,,                  1952,      ,,      **21**, 98.  
    ,,                  1952, *Ind. J. Phys.* **26**, 207.  
Rao, P. T., *Proc Nat. Inst. Sci. India*. (In press).  
Rochester and Glisson 1939, *Z. f. Phys.*, **114**, 495

# OSCILLOGRAPHIC MEASUREMENTS OF VALVE NOISE IN AUDIO FREQUENCY CHANNELS

BY MISS. G. V. SUBHADRAMMA

WIRELESS LABORATORY, PHYSICS DEPARTMENT, BENARES HINDU UNIVERSITY

(Received for publication, October 23, 1952; received after revision, January 21, 1953)

**ABSTRACT.** An experimental study of over-all valve noise was made by an oscillographic method for different thermionic valves over a range of audio frequencies (375-1320 cycles/sec). The experimental results are summarised as follows:

(i) For a given anode voltage, the valve noise in any triode for any frequency channel was found to increase at first with the filament current attaining a maximum at some value of the filament current and then to decrease with further increase of filament current tending in some cases to a minimum value. In a particular tetrode, the noise voltage was found to increase with the increase of filament current tending to a saturation value.

(ii) For a given anode voltage, the *maximum* noise prevailed at the same value of filament current for all frequency channels but the magnitude of the maximum noise was found to increase with the increase of frequency channel tending in some cases to a saturation value.

(iii) For a given anode voltage, the magnitude of the *minimum* noise was found to vary with the frequency channel almost in the same manner as the maximum noise.

(iv) For a given filament current, the valve noise was found to decrease with the increase of anode voltage.

(v) The absolute values of the equivalent valve noise voltage was found to range from about 20 to about 200 microvolts in the several thermionic valves under the experimental conditions.

## I. INTRODUCTION

The noise in thermionic valves consists mainly of the following types: (i) shot noise, (ii) flicker noise, (iii) thermal noise, (iv) ionization noise, and (v) partition noise. In high vacuum triodes, however, the shot noise and the flicker noise constitute the major part of the valve noise. Much work, both theoretical and experimental, has been done since the discovery of shot effect by Schottky (1918). Besides the pioneer work of Schottky (1918, 1922), Hartmann (1921), Fry (1925), Johnson (1928), Llewellyn and others, (1930) the work of Kanazouski and Williams (1930), Thacker and Williams (1932), Moullin and Ellis (1934), Williams (1936), Bell (1938), Percival and Harwood (1938), Rack (1931) and others yielded useful information regarding valve noise. Later works by North (1940), Bell (1941) and others are also of importance.

From the experimental point of view the measurements of valve noise in audio frequency channels are liable to serious error due to slightest electrical disturbances and require extremely careful shielding arrange-

ments. It was, therefore, thought desirable to use a cathode ray oscillograph for delineating the noise patterns in different audio frequency channels after having amplified the noise voltage in the usual way. Reliable measurements of noise voltage by the oscillographic method was possible even though extraneous electrical disturbances were not altogether eliminated. Measurements of over-all valve noise were made by this method for a range of audio frequencies (375 to 1320 c/s) in the case of several thermionic valves viz. (i) Philips A 415 (ii) Mullard 1HF (iii) RCA 1H4G (iv) Mullard PM2 and (v) Philips A442.

With a fixed anode voltage for each of the thermionic valves, the over-all noise voltage was measured for different filament currents within the range of audio frequency channels (375-1320 c/s). From these measurements the variation of maximum noise in each valve with frequency channel was found. The variation of valve noise with varying plate voltages for maximum filament current was also studied in the same range of audio frequencies for one particular valve (Mullard PM2).

## 2. EXPERIMENTAL METHOD AND PROCEDURE

A suitable parallel combination of a coil and a condenser was placed in the anode circuit of the thermionic valve under investigation and the anode and filament of the valve were connected to input terminals of a high gain amplifier through a suitable blocking condenser. The coil-condenser combination was arranged to cover the desired range of resonance frequencies for the parallel circuits. It was also ensured that the equivalent impedance of the combination at its resonance frequency was very much higher than the impedance of the voltage amplifier which was used to amplify the valve noise. Under such condition, the noise frequencies in the valve ranging from 0 to  $\infty$  were confined, within a very narrow band, to the resonance frequency of the parallel circuit at the input end of the amplifier.

The amplified noise voltage for any frequency channel within the desired range was then applied to the Y-plates of an oscillograph, the linear time base having been connected to the X-plates. The pick-up from the 50 cycle converter lines invariably appeared on synchronization along with the superposed valve noise corresponding to the resonance frequency of the coil-condenser combination. The 50 cycle pick-up was, however, eliminated to a considerable extent by using a phase inverter unit constructed for the purpose and on further amplifying the noise voltage with the help of oscillograph amplifier, the average amplitude of the noise pattern was accurately measured on the fluorescent screen. Corresponding to the average amplitude in cms. of the noise pattern for each frequency channel, the equivalent noise voltage was obtained with the help of an audio oscillator and an attenuator. For equivalent noise measurements, calibration curves were drawn, one for each frequency channel, showing different A/F input voltages against corresponding amplitudes as measured in cms. on the oscillographic screen.

### 3. EXPERIMENTAL DETAILS

The experimental set up for the measurement of valve noise is illustrated in figure 1. The essential parts of the arrangement are as follows :

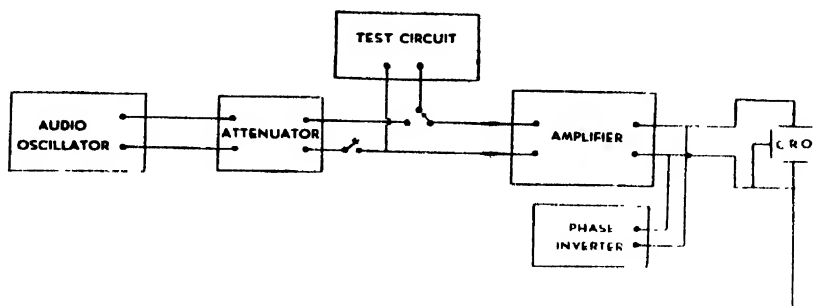


FIG. 1  
The experimental set-up

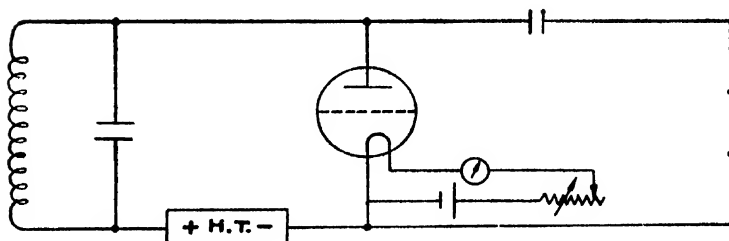


FIG. 2  
The test circuit

(i) *Test circuit.* The thermionic valve under investigation with suitable coil condenser parallel combination in its anode circuit was placed across the input impedance of a voltage amplifier through a blocking condenser. The coil in the combination was a 30-henry choke and the capacitance of the condenser ranged from  $0.0005 \mu\text{F}$  to  $0.006 \mu\text{F}$ , so that the resonance frequency of the combination could be varied from 375 to 1320 cycles/sec\* and the equivalent impedance of the combination at its resonance frequency was very much higher than the input impedance of the amplifier.

The circuit diagram of the test circuit with all the necessary connections is shown in figure 2. The coil condenser combination was kept in a double-walled metal enclosure. Other parts and connecting wires were all properly shielded.

(ii) *A/F voltage amplifier.* A Philips Modulation Amplifier (type 2845) with a maximum gain of 2300 was employed for amplifying the over-all noise

\* The resonance frequencies were calculated without considering the self-capacitance of the choke. The self-capacitance would cause a lowering of the frequency value to the extent of about 8% for the smallest value of the condenser used in these experiments. The observed noise patterns on the oscillographic screen showed also the same order of frequencies.

voltage across the thermionic valve under investigation. Suitable input and output channels were used. The high-tone filter in the amplifier unit was set for the straight line portion of the frequency characteristic and the low-tone filter was adjusted to cut off low frequencies as far as possible. The amplifier was worked with 220 volts of 50 cycles/sec.

(iii) *Cathode ray tube.* A Cossor's oscillograph was employed to delineate the noise patterns for different audio frequency channels. The noise pattern for any particular frequency channel was found superposed on the trace of the 50 cycle pick-up from the A/C power lines from the converter.

(iv) *Phase inverter unit.* The phase inverter unit, constructed for eliminating the 50 cycle pick-up, was essentially a unit of continuously varying phase and amplitude of the 50 cycle e. m. f. In this unit one arm of the circuit consisted of two similar capacitances and a potentiometer resistance in series, while the other arm had two similar inductances in series with another potentiometer resistance. Requisite conditions were satisfied regarding the magnitude of the elements. The output connections were taken from the variable points on the potentiometer resistances so that the phase of the output e.m.f. could be varied by changing the variable points on the two potentiometer resistances. The amplitude of the output e.m.f. was varied with a potentiometer across the supply voltage. The circuit for the phase inverter unit is shown in figure 3.

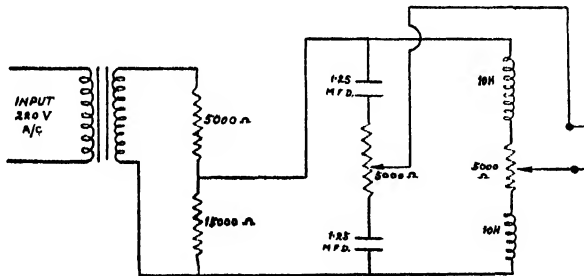


FIG. 3  
Phase inverter

The phase inverter output terminals were connected across the output of the A/F voltage amplifier. There was no shunting effect of the phase inverter, the output impedance of the phase inverter being very much higher than the output impedance of the amplifier.

#### 4. EXPERIMENTAL RESULTS

The variation of over-all valve noise with filament current and with frequency were studied in the case of all the valves under investigation with a fixed anode voltage. The grid of each valve was kept 'floating'. This evidently did not correspond to the usual operating conditions. In the case of the tetrode valve, the screen-grid voltage was about 70 volts.



The experimental results showing the variation of noise voltage with filament current are graphically shown in figures 4-6. It is to be noted

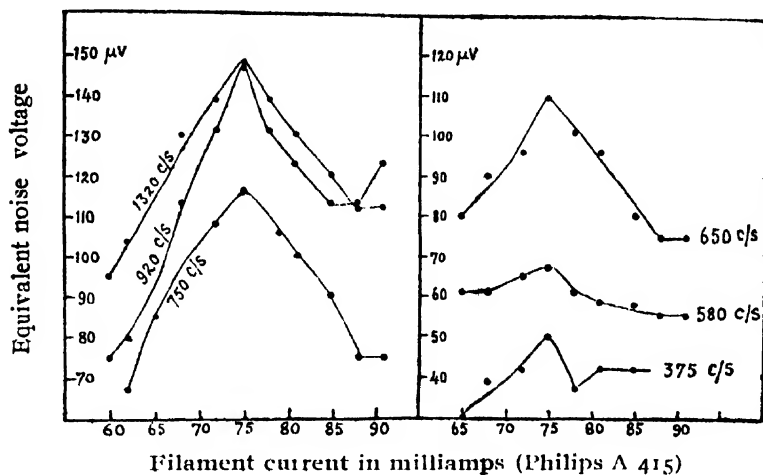


FIG. 4

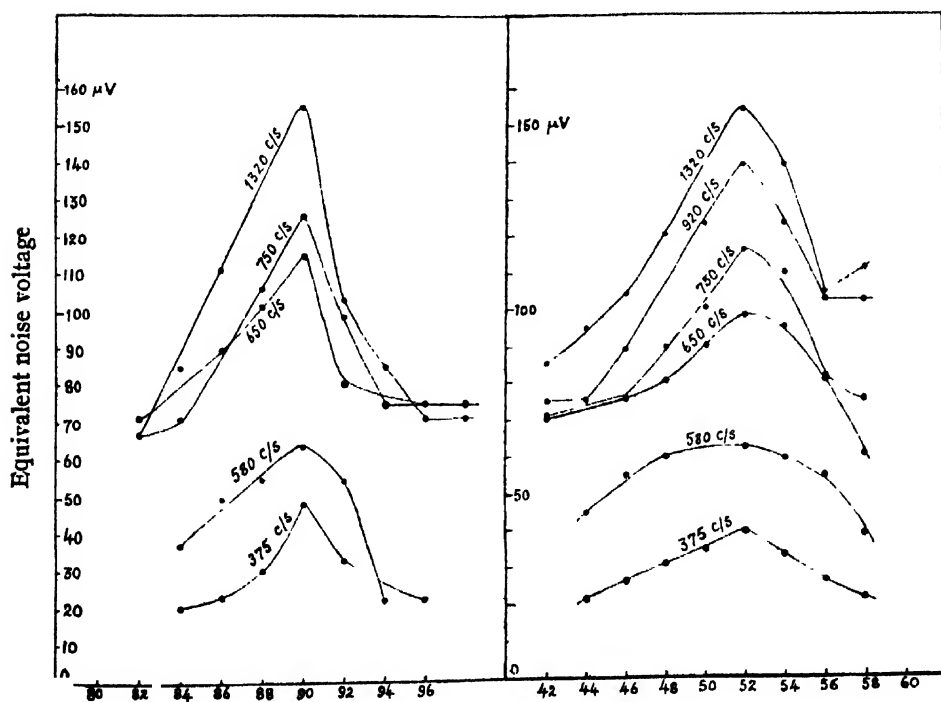


FIG. 5

Mullard 1HF

RCA 1H 4-G

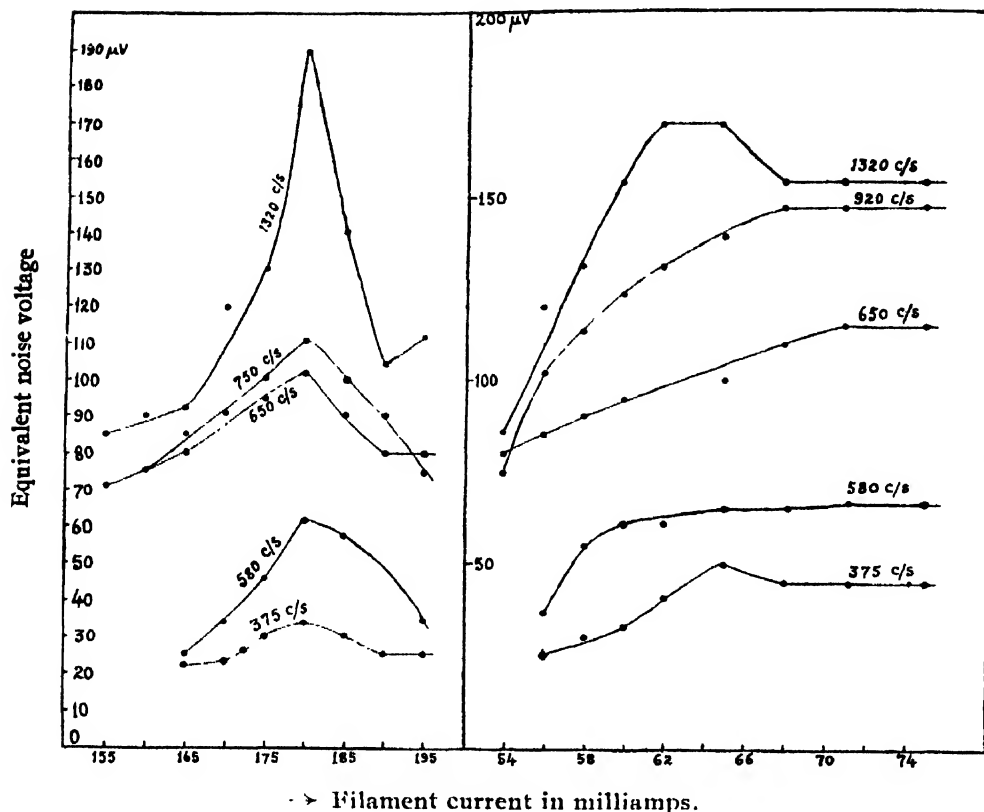


FIG. 6

Mullard PM 2

Philips A 442

that for all the frequency channels the equivalent noise voltage in all the triodes increased with the filament current and after attaining a maximum at a certain value of filament current decreased again to some minimum value. In the case of Philips A442 tetrode, the valve noise for the different frequency channels increased with filament current attaining a saturation value.

The maximum and the minimum values of the over-all valve noise in different triode valves, as determined for different frequency channels, are shown in figures 7 and 8. For all frequency channels the maximum noise was found to be at the same value of filament current but the maximum noise value in case of all the valves was found to increase with increase of frequency channel and in some cases it attained or tended to attain a saturation value. The minimum noise for all the valves showed a similar variation with frequency channel.

The variation of valve noise for a fixed filament current with varying anode voltages for three frequency channels was studied for only one valve (Mullard PM2). The valve noise was found to decrease with the increase of anode voltage. The experimental results are graphically shown in figure 9.

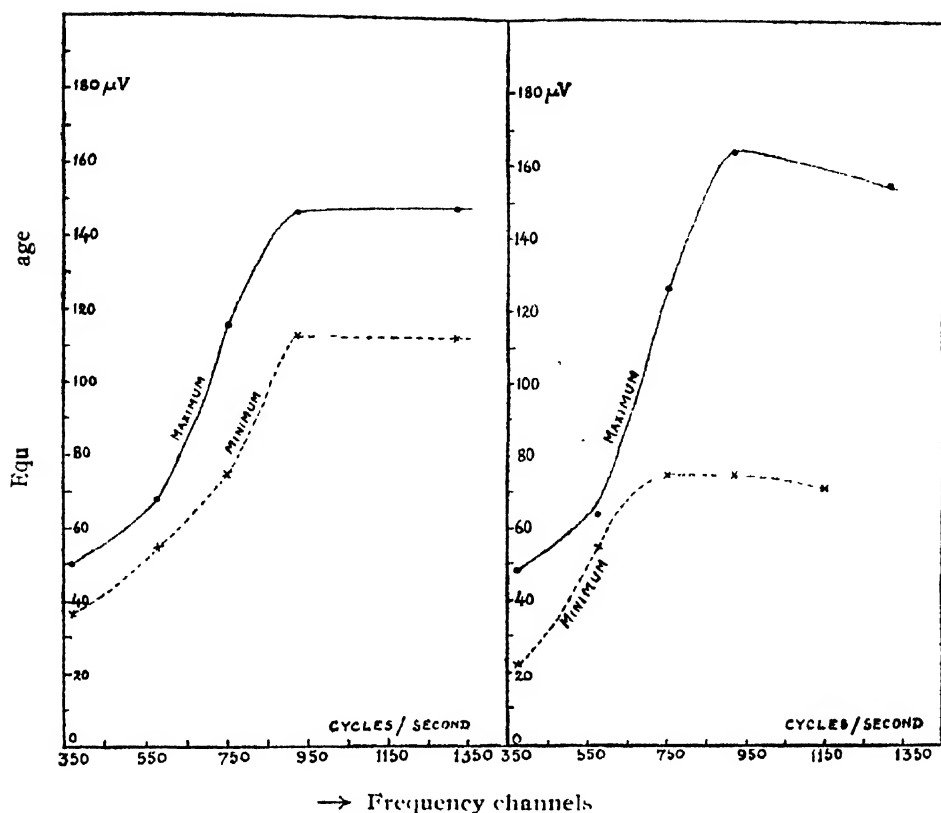


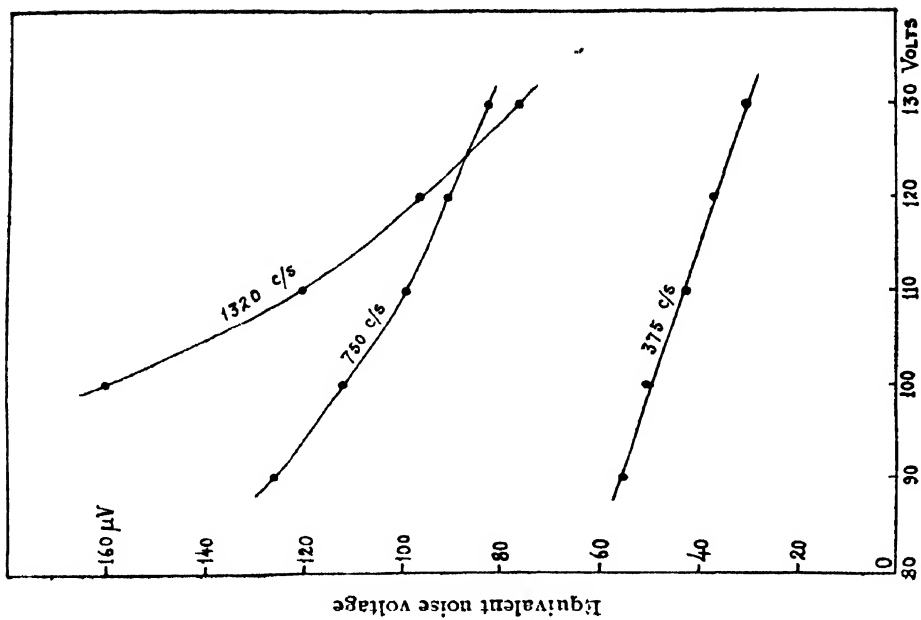
FIG. 7

Philips A 415

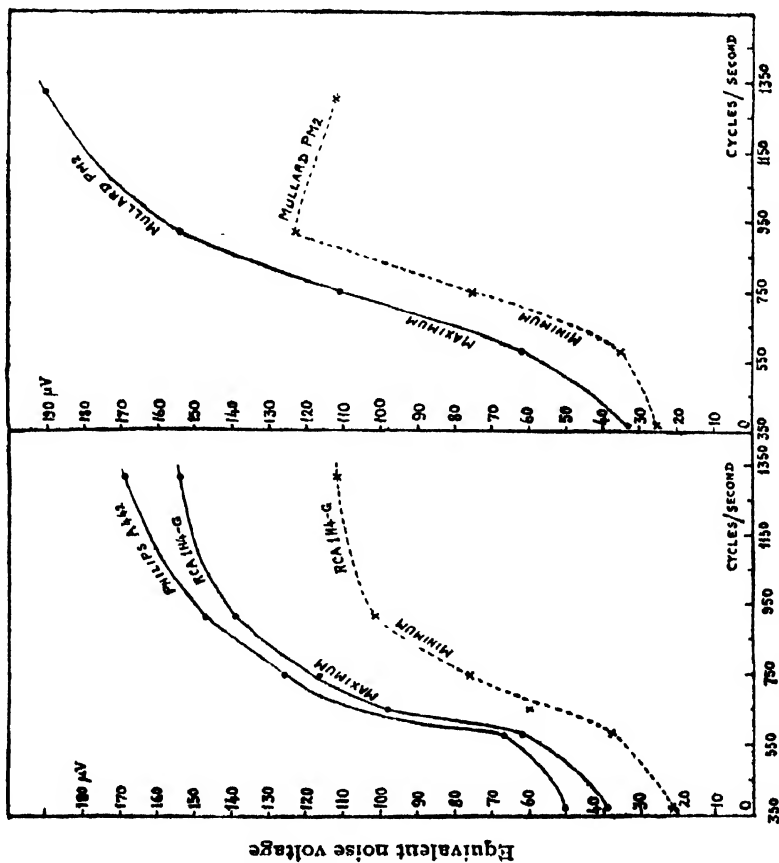
Mullard III F

## 5. CONCLUSIONS

The observed variation of valve noise with varying filament current for a fixed anode voltage showed the effect of space charge on the valve noise, as in the work of previous investigators. The observed increase in maximum and minimum valve noise with the increase of frequency channel in the experimental range (375-1320 cycles/sec.) is indeed significant. It is doubtful whether this signifies the validity of Hartmann-Schottky hypothesis. According to this hypothesis, a cooling is produced in the emitter after the emission of an electron and the emission of next electron become less probable for a short time compared to the frequency of the shot noise. It is accordingly expected that at very low frequencies which correspond to large time periods, the magnitude of the shot noise must be small. The observed decrease of valve noise with the increase of anode voltage for a given filament current in the case of one triode valve in three frequency channels within the experimental range is, however, contrary to expectation, as with higher anode voltage the space charge decreases and the shot noise is expected to increase with the increase of anode voltage. This requires further investigation. It was also found that the observed magnitude of the over-all valve



→ Anode voltage (Mullard PM 2)  
FIG. 9



→ Frequency channels  
FIG. 8

noise was appreciably higher than the value of the shot noise obtained according to Llewellyn's method of calculation. This is likely to be due to the preponderance of the flicker effect in the particular range of audio frequency channels.

## 6. ACKNOWLEDGMENTS

The author wishes to express her sincere thanks to Dr. S. R. Khastgir, D. Sc., F. N. I., for help and guidance during the progress of the work. Thanks are also due to Messrs, M. P. Varma, M. Sc. and B. A. P. Tantry, M. Sc. for their valuable technical assistance.

## REFERENCES

- Bell, A. D., 1938, *J. I. E. E.*, **82**, 522.  
 Bell, A. D., 1941, *Ibid.*, **89**, 207.  
 Fry, T. C., 1925, *J. Frank. Inst.*, **199**, 203.  
 Hartmann, C. A., 1921, *Ann. der. Physik*, **66**, 51.  
 Johnson, J. B., 1928, *Phys. Rev.*, **32**, 97.  
 Kanazowski, H. N., and Williams, N. H., 1930, *Phys. Rev.*, **36**, 13.  
 Llewellyn, F. B., 1930, *Proc. I. R. E.*, **18**, 24.  
 Moullin and Ellis, 1934, *J. I. E. E.*, **74**, 323.  
 North D. O., 1940, *R. C. A. Review*, **4**, 441.  
 „ „ „ „ *Ibid.*, **5**, 224.  
 Percival W. S., and Harwood, W. L., 1938 *Wireless Engineer and R. W.*  
 Rack, A. J., 1938, *Bell Sys. Tech. Jour.*, **17** (Oct).  
 Schottky, W., 1918, *Ann. der Physik*, **62**, 541.  
 „ „ „ „ *Ibid.*, **63**, 157.  
 Thacker, E. W., and Williams, N. H., 1932, *Phys. Rev.*, **39**, 174  
 Williams, F. C., 1936, *J. I. E. E.*, **78**, 326.  
 „ „ „ „ *Ibid.*, **89**, 219.

# INTENSITIES IN ${}^4\Sigma - {}^4\Sigma$ TRANSITION\*

By K. SURYANARAYANA RAO

DEPARTMENT OF PHYSICS, ANDHRA UNIVERSITY, WALTAIR

(Received for publication, October 23, 1952)

**ABSTRACT.** The intensity factors of the expected branches in a  ${}^4\Sigma - {}^4\Sigma$  transition are calculated and the expressions are reduced to a convenient form. Representative theoretical intensity curves are drawn for three of the branches, using the data on columbium oxide published by the author earlier.

## INTRODUCTION

The interpretation of the rotational structure of the bands of columbium oxide by the author led to the probability of assigning them to the electronic transition,  ${}^4\Sigma - {}^4\Sigma$ . As far as the author is aware, there is no band system till now investigated and ascribed to this transition. Hence the determi-

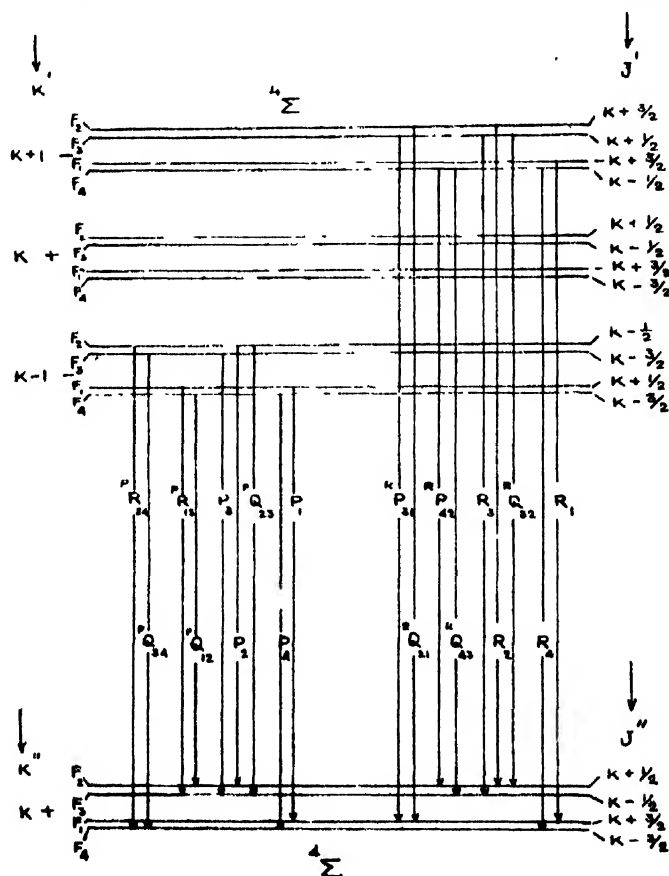


FIG. 1  
Expected transitions in  ${}^4\Sigma - {}^4\Sigma$

\* Communicated by Prof. K. R. Rao.

nation of all the characteristic features of a system belonging to this transition became necessary.

Budo derived expressions for the energy levels of a  $^1\Sigma$  state. These expressions enable the construction of the transition diagram for  $^1\Sigma - ^1\Sigma$  shown in figure 1. The other theoretical problem of the determination of the relative intensities of rotational lines in the expected branches, that is, the intensity factors has not been carried out so far. This calculation is shown in this paper.

For the calculation of the intensity factors of the branches in a transition in which both the states belong to Hund's case (b), a general method was first proposed by Mulliken who applied it to a  $^2\Sigma - ^2\Sigma$  transition. Later, he extended it to the cases  $\Delta\Lambda = 0$  and  $\pm 1$  and any values of  $\Lambda$  for doublet electronic states. This method, which has been extended in this paper to a  $^4\Sigma - ^4\Sigma$  transition, is briefly outlined below.

#### THEORY

The intensity formulae for any transition between two case(b) electronic states can be obtained in two steps: (1) First, neglecting the interaction between  $K$  and  $S$ , for a given value of  $\Delta\Lambda$  the relative intensities of the three cases  $\Delta K = 0, \pm 1$  are obtained in terms of  $K$  and  $\Lambda$ . These are identical with Honl and London's expressions given for Hund's case (a). It is to be noted that in case (b)  $\sigma$  and  $\sigma_K$  are the same (old notation). Substituting  $K$  and  $\Lambda$  in the appropriate Honl and London's equations, the intensity factors will be obtained. (2) Now introducing the interaction between  $K$  and  $S$  which will be analogous to the one between  $k$  and  $s$  in atomic spectra, the intensities are sub-divided. The relative intensities of transitions involving different values of  $\Delta J$  and of  $J'$  (or  $J''$ ) are given, for any fixed value of  $\Delta K$  and  $K'$  (or  $K''$ ) by precisely the same expressions as in line spectra, by merely replacing  $k$  for the line spectrum multiplet by  $K$ . In this case the equations of Sommerfeld and Honl can be utilised. Finally, combining the results of (1) and (2) explicit expressions are obtained for the relative intensities of the transitions. In a  $^1\Sigma - ^1\Sigma$  transition, according to the  $J, K$  and  $\pm \longleftrightarrow$  - selection rules eighteen branches will be obtained and these are shown in figure 1.

#### CALCULATIONS AND RESULTS

$\Sigma - \Sigma$  transitions of all multiplicities should be identical in structure and intensity relations provided the fine structure due to  $K$  and  $S$  interaction is ignored. The intensities of successive lines in each branch should be proportional to  $K$ . Considering the fine structure, two cases arise, namely,  $\Delta K = +1$  and  $\Delta K = -1$  which correspond to  $\Delta k = -1$  and  $\Delta k = -1$  in line spectra, expressions for which are given by Sommerfeld and Honl. The equations as slightly modified by Mulliken are :

For  $J \rightarrow J-1$ , if  $K \rightarrow K-1$ , or equally, for  $J-1 \rightarrow J$ , if  $K-1 \rightarrow K$

$$i_{\pm} = [(J+K)(J+K+1) - S(S+1)] [(J+K-1)(J+K) - S(S+1)] / JK$$

For  $J \rightarrow J$ , for either  $K \rightarrow K-1$  or  $K-1 \rightarrow K$

$$i^0 = (2J+1) [(J+K)(J+K+1) - S(S+1)] [S(S+1) - (J-K)(J-K+1)] / JK(J+1)$$

For  $J-1 \rightarrow J$ , if  $K \rightarrow K-1$ , or for  $J \rightarrow J-1$  if  $K-1 \rightarrow K$

$$i_{\pm} = [S(S+1) - (J-K)(J-K+1)] [S(S+1) - (J-K-1)(J-K)] / JK$$

in the present standard notation.

The relative intensities of the three forms associated with  $K$  transition are calculated according to the formulae given above, where  $S=3/2$  for a  $^4\Sigma$  state, and the sum of their intensities, as already mentioned, is proportional to  $K$ . To satisfy these conditions the relative intensities are first calculated by the help of the above formulae and are given below :

$$P_1 \quad \text{or} \quad R_1 \quad (J=K+3/2) \quad i_1 = (K+2)(2K-1)$$

$$P_2 \quad \text{or} \quad R_2 \quad (J=K+1/2) \quad i_2 = \frac{(K-1)(K+1)(2K-1)(2K+3)}{K(2K+1)}$$

$$P_3 \quad \text{or} \quad R_3 \quad (J=K-1/2) \quad i_3 = \frac{(K-1)(K+1)(2K+1)(2K-3)}{K(2K-1)}$$

$$P_4 \quad \text{or} \quad R_4 \quad (J=K-3/2) \quad i_4 = (K-2)(2K+1)$$

$${}^pQ_{12} \quad \text{or} \quad {}^nQ_{21} \quad (J=K+1/2) \quad i_5 = \frac{3(K+1)(2K-1)}{K(2K+1)}$$

$${}^pQ_{23} \quad \text{or} \quad {}^nQ_{32} \quad (J=K-1/2) \quad i_6 = \frac{16(K+1)(K-1)}{(2K+1)(2K-1)}$$

$${}^pQ_{34} \quad \text{or} \quad {}^nQ_{43} \quad (J=K-3/2) \quad i_7 = \frac{3(K-1)(2K+1)}{K(2K-1)}$$

$${}^nR_{13} \quad \text{or} \quad {}^nR_{31} \quad (J=K+1/2) \quad i_8 = K(2K+1)$$

$${}^pR_{24} \quad \text{or} \quad {}^nR_{42} \quad (J=K-1/2) \quad i_9 = \frac{3}{K(2K-1)}$$

In the above expressions a common factor 8 is omitted and also  $K$  represents always the larger of the two quantities  $K'$  and  $K''$ ; similarly with  $J$ .

Then we have

$$\Sigma i = 2(4K^2 - 1)$$

The relative intensities are then obtained by multiplying the above  $i$  values with  $2K/\Sigma i$ . The results thus obtained are presented below. These can be expressed in terms of  $J$  also by substituting for  $K$  in terms of  $J$ .

$$P_1 \quad \text{or} \quad R_1 ; i = \frac{K(K+2)}{(2K+1)}$$

$$P_2 \quad \text{or} \quad R_2 ; i = \frac{(2K+3)(K^2-1)}{2K+1)^2}$$



$$P_3 \text{ or } R_3; i = \frac{(2K-3)(K^2-1)}{(2K-1)^2}$$

$$P_4 \text{ or } R_4; i = \frac{K(K-2)}{(2K-1)}$$

$${}^PQ_{12} \text{ or } {}^RQ_{21}; i = \frac{3(K+1)}{2K+1}$$

$${}^PQ_{23} \text{ or } {}^RQ_{32}; i = \frac{16K(K^2-1)}{(2K-1)^2(2K+1)^2}$$

$${}^PQ_{31} \text{ or } {}^RQ_{13}; i = \frac{3(K-1)}{(2K-1)^2}$$

$${}^PR_{13} \text{ or } {}^RP_{31}; i = \frac{3}{(2K-1)(2K+1)^2}$$

$${}^PR_{21} \text{ or } {}^RP_{42}; i = \frac{3}{(2K+1)(2K-1)^2}$$

In the above expressions a common factor 2 is omitted. To obtain complete expressions for the intensities the above factors should be multiplied by the corresponding Boltzmann factors.

It is seen from the above relations that the main branches for which  $\Delta J = \Delta K$  are intense while the satellite  $Q$  branches are weak and the branches  ${}^PR_{13}$ ,  ${}^RP_{31}$ ,  ${}^PR_{21}$  and  ${}^RP_{42}$  exceedingly weak.

Representative theoretical curves are drawn for the  $P_1$ ,  ${}^PQ_{12}$  and  ${}^PR_{13}$  of (0,0) band of columbium oxide for which  $B' = 0.5325 \text{ cm}^{-1}$  and the

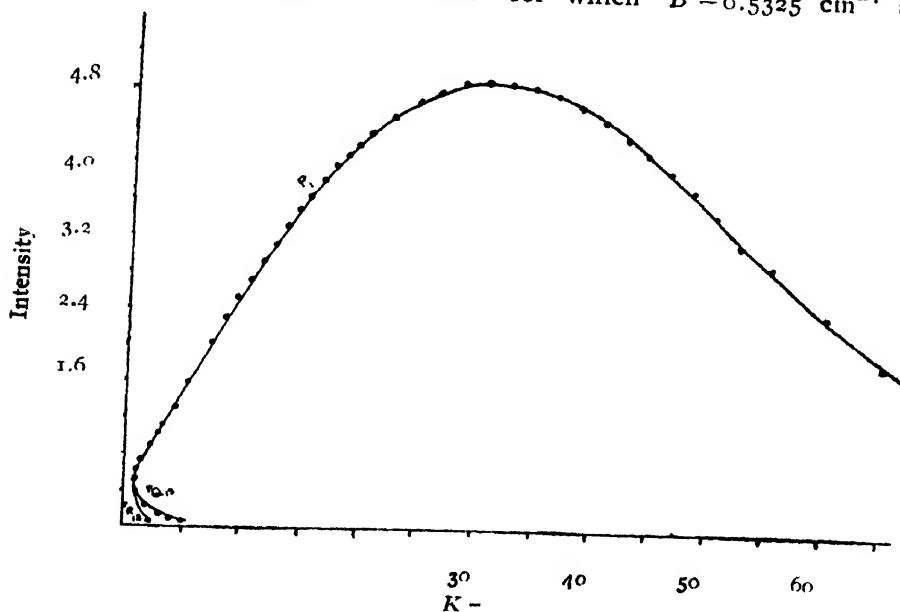


FIG. 2

effective temperature is taken as  $1500^{\circ}K$ . They are shown in figure 2. It may be remarked here that the theoretical intensity curves will be similar for the other corresponding main and satellite branches.

#### ACKNOWLEDGMENT

The author is deeply indebted to Prof.K.R.Rao for his valuable guidance during this investigation.

#### REFERENCES

- Budo, A , 1937, *Zeit.f.Phys.*, **105**, 73  
Honl, H and London, F., 1925, *ibid.*, **33**, 803  
Mulliken, R.S , 1927, *Phys. Rev.*, **30**, 138  
Sommerfeld, A. and Honl, H., 1925, *Sitzungsber. der Preuss. der Wiss., Phys. math. Klasse*, pp.141.

# ON THE DISTRIBUTION OF STRESS ROUND THE EDGE OF A HOLE IN A DEEP BEAM UNDER A UNIFORM BENDING MOMENT\*

BY B. KARUNES

DEPARTMENT OF APPLIED PHYSICS, UNIVERSITY COLLEGE OF SCIENCE AND TECHNOLOGY, CALCUTTA

(Received for publication, November 11, 1952)

**ABSTRACT.** A solution to the problem of stress concentration due to the presence of an unstressed hole of a fairly general shape in a deep plate beam under a uniform bending moment is obtained. The solution is verified for the cases of circular and elliptic holes which are already known, and is applied to obtain some new results.

## INTRODUCTION

The problems of stress distribution in an infinite plate containing an unstressed hole, under various types of load have been widely studied by finding the stress function  $\chi$  in suitable curvilinear coordinates, satisfying the biharmonic equation  $\nabla^4 \chi = 0$ . A method of solution to the problems of stress distribution in an infinite plate containing a hole of a fairly general shape has been developed by Green (1945). In the present paper Green's method has been applied to obtain the stress distribution round the edge of a hole in a deep plate beam under uniform bending moment.

This method can be applied when the hole is given by a curve  $\eta = 0$ , defined by the conformal transformation

$$Z = F(\zeta) \quad \dots (1)$$

where

$$Z = x + iy, \quad \zeta = \xi + i\eta$$

and

$$F'(\zeta) = a_0 e^{-i\zeta} + b_n e^{in\zeta}$$

it being assumed that  $\eta \rightarrow \infty$  when  $|Z| \rightarrow \infty$ . It is seen that the first term in  $F'(\zeta) \rightarrow \infty$  and the second term  $\rightarrow 0$  as  $\eta \rightarrow \infty$ .

It is known that the general solution of  $\nabla^4 \chi = 0$  is given by the real part of

$$F(Z) + \bar{Z}g(Z) \quad \dots (2)$$

where  $\bar{Z} = x - iy$  and where  $f'(Z)$  and  $g(Z)$  are regular functions of  $Z$ .

From (2) the stresses in curvilinear coordinates  $\xi, \eta$ , are found to be given by the real parts of (Green, 1945,)

\* Communicated by Prof. P. C. Mahanti

$$\begin{aligned}
 \widehat{\xi\xi} &= 2g'(Z) - \frac{F'(\zeta)}{F'(\zeta)} \left\{ f''(Z) + \bar{F}(\zeta)g''(Z) \right\} \\
 \widehat{\eta\eta} &= 2g'(Z) + \frac{F'(\zeta)}{F'(\zeta)} \left\{ f'(Z) + \bar{F}(\zeta)g''(Z) \right\} \\
 \widehat{\xi\eta} &= -i \frac{F'(\zeta)}{\bar{F}'(\zeta)} \left\{ f''(Z) + \bar{F}(\zeta)g''(Z) \right\}
 \end{aligned} \quad \dots \quad (3)$$

where dashes attached to  $g(Z)$  and  $f(Z)$  denote differentiation with respect to  $Z$  and dashes attached to  $F(\zeta)$  denote differentiation with respect to  $\zeta$

Introducing two functions of  $\zeta$ ,  $V(\zeta)$  and  $W(\zeta)$  which are finite at infinity and are of the form (Green, 1945,)

$$\begin{aligned}
 V(\zeta) &= -2g'(\zeta) - \frac{F'(\zeta)}{F'(\zeta)} \left\{ f''(Z) + F(\zeta)g''(Z) \right\} \\
 W(\zeta) &= \frac{F'(\zeta)}{\bar{F}'(\zeta)} \left\{ f''(Z) + F(\zeta)g''(Z) \right\}
 \end{aligned} \quad \dots \quad (4)$$

so that at  $\eta=0$ , the hole boundary, the real part of  $V(\zeta) = -\eta\eta_e$  and the imaginary part of  $W(\zeta) = \widehat{\xi\eta}_e$ , where  $\widehat{\xi\eta}_e$ ,  $\widehat{\eta\eta}_e$  denote stresses at the edge of the hole, we get the stresses in terms of  $V(\zeta)$  and  $W(\zeta)$  (Green, 1948) as the real parts of

$$\begin{aligned}
 \widehat{\xi\xi} &= -V(\zeta) - W(\zeta) - W'(\zeta) \frac{F'(\zeta)}{F'(\zeta)} - \frac{1}{2} \left\{ V'(\zeta) + W'(\zeta) \right\} \frac{F(\zeta) - \bar{F}(\zeta)}{\bar{F}'(\zeta)} \\
 \widehat{\eta\eta} &= -V(\zeta) - W(\zeta) + W(\zeta) \frac{\bar{F}'(\zeta)}{\bar{F}'(\zeta)} + \frac{1}{2} \left\{ V'(\zeta) + W'(\zeta) \right\} \frac{F(\zeta) - \bar{F}(\zeta)}{\bar{F}'(\zeta)} \\
 \widehat{\xi\eta} &= -iW(\zeta) \frac{\bar{F}'(\zeta)}{\bar{F}'(\zeta)} - \frac{1}{2}i \left\{ V'(\zeta) + W'(\zeta) \right\} \frac{\bar{F}(\zeta) - F(\zeta)}{F'(\zeta)}
 \end{aligned} \quad \dots \quad (5)$$

where dashes attached to  $V(\zeta)$  and  $W(\zeta)$  denote differentiation with respect to  $\zeta$ . From (5) we get the circumferential stress over the edge of the hole boundary given by the real part of

$$\widehat{\xi\xi}_e = -V(\zeta) - 2W(\zeta) \quad \dots \quad (6)$$

The solution of an individual problem depends on finding the suitable  $V(\zeta)$  and  $W(\zeta)$ .

#### THE SOLUTION

Let a bending moment  $M$  be applied to a plate beam of depth  $2b$  and thickness  $2c$ . When there is no hole in the plate we may take

$$\chi = R[f(Z) + \bar{Z}g(Z)] = Ay^3 \quad \dots (7)$$

where

$$A = \frac{M}{\pi z} \quad \dots (8)$$

so that

$$f(Z) = \frac{Ai}{4} Z^3, \quad g(Z) = -\frac{3Ai}{4} Z^2 \quad \dots (9)$$

Then we shall have the stresses in the plate given by the real parts of

$$\begin{aligned} \widehat{\xi\xi} &= -3Ai F(\zeta) - \frac{3Ai}{2} \cdot \frac{F'(\zeta)}{\bar{F}'(\zeta)} \left\{ F(\zeta) - \bar{F}(\zeta) \right\} \\ \eta\eta &= -3Ai F(\zeta) + \frac{3Ai}{2} \cdot \frac{F'(\zeta)}{\bar{F}'(\zeta)} \left\{ F(\zeta) - \bar{F}(\zeta) \right\} \quad \dots (10) \\ \widehat{\xi\eta} &= \frac{3A}{2} \cdot \frac{F'(\zeta)}{F'(\zeta)} \left\{ F(\zeta) - \bar{F}(\zeta) \right\} \end{aligned}$$

On the boundary  $\eta=0$ , these stresses have values given by the real parts of

$$\begin{aligned} \widehat{\xi\xi}_0 &= -3Ai F(\zeta) - \frac{3Ai}{2} \cdot \frac{F'(\zeta)}{F'(\zeta)} \left\{ F(\zeta) - \bar{F}(\zeta) \right\} \\ \widehat{\eta\eta}_0 &= -3Ai F(\zeta) + \frac{3Ai}{2} \cdot \frac{F'(\zeta)}{\bar{F}'(\zeta)} \left\{ F(\zeta) - \bar{F}(\zeta) \right\} \quad \dots (11) \\ \widehat{\xi\eta}_0 &= \frac{3A}{2} \cdot \frac{F'(\zeta)}{F'(\zeta)} \left\{ F(\zeta) - \bar{F}(\zeta) \right\} \end{aligned}$$

Superposing on the stress system (10) another which gives  $\widehat{\eta\eta}_r = -\widehat{\eta\eta}_0$  and  $\widehat{\xi\eta}_r = -\widehat{\xi\eta}_0$  on the boundary  $\eta=0$  and which tends to zero at infinity, we shall get the stress system in the plate beam containing the stress free hole  $\eta=0$  under the uniform bending moment  $M$ .

To obtain the required superposed stress system we first take

$$V_1(\zeta) = -3Ai F(\zeta) + \frac{3Ai}{2} \cdot \frac{F'(\zeta)}{\bar{F}'(\zeta)} \left\{ F(\zeta) - \bar{F}(\zeta) \right\} \quad (12)$$

Its real part  $= \widehat{\eta\eta}_0 = -\widehat{\eta\eta}_r$  on the boundary  $\eta=0$ .

To make  $V(\zeta)$  tend to zero when  $\eta \rightarrow \infty$ , we add the terms

$$3A(\bar{a}_0 e^{i\zeta} + a_0 e^{-i\zeta}) + \frac{3Ai}{2} \left\{ \frac{a_0 e^{i\zeta}}{F'(\zeta)} - \frac{a_0 e^{-i\zeta}}{\bar{F}'(\zeta)} \right\} \left\{ F(\zeta) - \bar{F}(\zeta) \right\} \quad \dots (13)$$

which sum up to give an imaginary quantity at  $\eta=0$ , so that on  $\eta=0$  the

real part of  $V(\zeta)$  is the same as that of  $V_1(\zeta)$  and is therefore equal to  $-\widehat{\eta\eta}_e$ . In choosing the terms in (13) care is taken not to include any term which produces no stress either at infinity or over the hole boundary.

If we take

$$W_1(\zeta) = -\frac{3Ai}{2} \frac{F'(\zeta)}{\bar{F}'(\zeta)} \left\{ F(\zeta) - \bar{F}(\zeta) \right\} \quad (14)$$

its imaginary part  $= \widehat{\xi\eta}_e = -\widehat{\xi\eta}_0$  over the hole boundary.

To make  $W(\zeta)$  tend to zero as  $\eta$  tends to infinity, we add the terms

$$\frac{3Ai}{2} \left\{ \frac{a_0 e^{-i\zeta}}{F'(\zeta)} + \frac{\bar{a}_0 e^{i\zeta}}{\bar{F}'(\zeta)} \right\} \left\{ F(\zeta) - \bar{F}(\zeta) \right\} \quad (15)$$

which sum up to give a real quantity on  $\eta=0$ , so that on  $\eta=0$  the imaginary part of  $W(\zeta)$  is equal to that of  $W_1(\zeta)$  and is therefore equal to  $\widehat{\xi\eta}_e$ .

We get from (12), (13), (14) and (15)

$$\begin{aligned} V(\zeta) &= 3A \left\{ \bar{a}_0 e^{i\zeta} - iF(\zeta) a_0 e^{-i\zeta} \right\} \\ &+ \frac{3Ai}{2} \left\{ \frac{F'(\zeta)}{\bar{F}'(\zeta)} - \frac{a_0 e^{-i\zeta}}{\bar{F}'(\zeta)} + \frac{\bar{a}_0 e^{i\zeta}}{F'(\zeta)} \right\} \left\{ F(\zeta) - \bar{F}(\zeta) \right\} \\ W(\rho) &= \frac{3Ai}{2} \left\{ -\frac{F'(\zeta)}{\bar{F}'(\zeta)} + \frac{a_0 e^{-i\zeta}}{F'(\zeta)} + \frac{\bar{a}_0 e^{i\zeta}}{\bar{F}'(\zeta)} \right\} \left\{ F(\zeta) - \bar{F}(\zeta) \right\} \end{aligned} \quad (16)$$

$V(\zeta)$  and  $W(\zeta)$  have finite values at infinity and their sum contains no poles.

The complete stress system is obtained from (5) and (16) together with the stresses (11) which are transmitted from infinity.

Calculating the stresses from (5) with the above values of  $V(\zeta)$  and  $W(\zeta)$  it is seen that the stresses tend to zero as  $\eta \rightarrow \infty$  only when  $n < \frac{3}{2}$ . Therefore (16) can be used for  $n=0$  or  $n=1$ . The circumferential stress over the edge of the hole, as calculated with the help of (6), is given by the real part of

$$\widehat{\xi\xi}_e = 6A \frac{\bar{a}_0 e^{i\zeta}}{F'(\zeta)} \left\{ \bar{F}(\zeta) - F(\zeta) \right\} \quad \dots \quad (17)$$

The terms in  $e^{(2-n)\zeta}$  in  $V(\zeta)$  and  $W(\zeta)$  produce infinite stresses at  $n > \frac{3}{2}$ , so for the cases where  $n \geq 2$  we subtract these terms  $V(\zeta)$  and  $W(\zeta)$  and add such new terms as to keep the stresses over the hole boundary unchanged. We get

$$\begin{aligned} V_n(\zeta) &= V(\zeta) - \frac{3A}{2} \frac{\bar{b}_n e^{-in\zeta}}{F'(\zeta)} + \frac{3A}{2} \frac{b_n e^{in\zeta}}{\bar{F}'(\zeta)} \\ W_n(\zeta) &= W(\zeta) - \frac{3A}{2} \frac{b_n e^{-in\zeta}}{F'(\zeta)} - \frac{3A}{2} \frac{\bar{b}_n e^{in\zeta}}{\bar{F}'(\zeta)} \end{aligned} \quad \dots \quad (18)$$

$V_n(\zeta)$  and  $W_n(\zeta)$  and the stresses produced by them tend to zero when  $\eta \rightarrow \infty$  for  $n > 0$ . But the new terms in them produce no stress either at infinity or over the hole boundary for  $n < \frac{3}{2}$ . So the use of these functions  $V_n(\zeta)$  and  $W_n(\zeta)$  will be valid only for  $n \geq 2$ . In this case the circumferential stress round the edge of the hole is the real part of

$$\widehat{\xi\xi}_r = 6Ai \frac{a_0 e^{\eta}}{F'(\zeta)} \left\{ F(\zeta) - F(\bar{\zeta}) - \frac{ib_n}{n} e^{-m\zeta} \right\} \quad (19)$$

#### APPLICATIONS

When  $n=1$  and  $b_n=0$ , we have a circular hole of radius  $ia_0$  when  $\eta=0$ . The circumferential stress round the edge of this hole, as calculated with the help of (17) is given by

$$\widehat{\xi\xi}_r = 12Aia_0 \sin \xi \cos 2\xi. \quad \dots (20)$$

which is in agreement with the results obtained by other authors.

When  $n=1$  and

$$a_0 = \frac{c}{2i} e^{\alpha+i\beta}, \quad b_n = -\frac{c}{2i} e^{-\alpha+i\beta}$$

we have an elliptic hole of semi-axes  $c \cosh \alpha$  and  $c \sinh \alpha$  with its major axis inclined at an angle  $\beta$  to the  $x$ -axis. The circumferential stress round the edge of this hole is obtained from (17) as

$$\widehat{\xi\xi}_r = 3Ac \frac{e^{\alpha} \sin(\xi-\beta) - e^{-\alpha} \sin(\xi+\beta)}{\cosh 2\alpha - \cos 2\xi} \left\{ e^{2\alpha} \cos 2(\xi-\beta) - \cos 2\beta \right\} \quad (21)$$

When  $\beta=0$ , it becomes

$$\widehat{\xi\xi}_r = 6Ac \frac{\sinh \alpha \sin \xi}{\cosh 2\alpha - \cos 2\xi} \left\{ e^{2\alpha} \cos 2\xi - 1 \right\} \quad (22)$$

and when  $\beta = \frac{\pi}{2}$ , it becomes

$$\widehat{\xi\xi}_r = 6Ac \frac{\cosh \alpha \cos \xi}{\cosh 2\alpha - \cos 2\xi} \left\{ e^{2\alpha} \cos 2\xi - 1 \right\} \quad (23)$$

These results also agree with those obtained by other authors.

When  $n=2$  and  $a_0 = -2b_n$ ,  $\eta=0$  represents approximately an equilateral triangular hole with rounded corners. The circumferential stress over the edge of this hole is calculated from (19) as

$$\widehat{\xi\xi}_r = \frac{3Ai a_0}{4 \cos 3\xi - 5} (2 \sin 4\xi - 8 \sin 3\xi + 4 \sin 2\xi - \sin \xi) \quad (24)$$

When  $n=3$  and  $a_0 = -3b_n$ ,  $\eta=0$  represents approximately a square hole with rounded corners. The circumferential stress of this hole is given by

$$\widehat{\xi\xi}_r = \frac{Aia_0}{3 \cos 4\xi - 5} (3 \sin 5\xi - 18 \sin 3\xi + 17 \sin \xi) \quad \dots (25)$$

## ACKNOWLEDGMENT

The author wishes to express his respectful thanks to Dr. S. Ghosh for suggesting the problem and for his constant guidance during the preparations of this paper.

## REFERENCE

Green, A. E., 1915, *Proc. Roy. Soc., A*, **104**, 231



# THE RAMAN SPECTRA OF 1, 1, 1- AND 1, 1, 2-TRICHLOROETHANE IN THE SOLID STATE AT $-180^{\circ}\text{C}^*$

By D. C. BISWAS

OPTICS DEPARTMENT, INDIAN ASSOCIATION FOR THE CULTIVATION OF SCIENCE,  
CALCUTTA-32

(Received for publication, May 20, 1953)

## Plate XIV

**ABSTRACT.** The Raman spectra of 1, 1, 1-trichloroethane and 1, 1, 2-trichloroethane in the solid state have been investigated and compared with those due to the two substances in the liquid state. It has been observed that in the case of 1, 1, 1-trichloroethane all the prominent Raman lines due to the liquid appear when the liquid is solidified, but in the case of the other molecule the two intense Raman lines  $638\text{ cm}^{-1}$  and  $786\text{ cm}^{-1}$  disappear with solidification of the liquid. A new Raman line  $13\text{ cm}^{-1}$  appears with solidification of 1, 1, 1-trichloroethane and a similar new line  $60\text{ cm}^{-1}$  has been also observed in the case of the other substance in the solid state. It has been also observed that some of the Raman lines due to the two liquids are totally depolarised. The significance of all these results has been discussed,

## INTRODUCTION

The Raman spectra of many substituted ethanes have been investigated for different states of the substances and it has been observed that the number of Raman lines due to the solid state of these compounds is less than that of the lines due to the liquid state and such results have been interpreted by assuming that in the liquid state there are two forms of the molecules while in the solid state one of the two forms of the molecules disappears (Mizushima and Morino, 1938).

It has also been reported recently (Sheppard and Szasz, 1949) that even in the case of aliphatic hydrocarbons in the solid state, the number of Raman lines observed is much less than those observed in the case of the liquid, and such disappearance of some of the Raman lines on solidification

\* Communicated by Prof S. C. Sirkar

has been interpreted on the assumption that in case of hydrocarbons also there are two forms of molecules in the liquid state and one of these two forms disappears with the solidification of the liquid.

The Raman spectra of 1, 1, 2-trichloroethane and 1, 1, 1-trichloroethane were not studied before in the solid state at low temperatures. The object of the present investigation is to find out whether the change in the relative positions of the chlorine atoms in the two molecules mentioned above influences the Raman spectra of these two substances in the solid state and also to find out whether any change in the structure of the molecules takes place with solidification at low temperatures. The polarisation of the Raman lines has also been studied in order to find out whether the molecules possess any symmetry.

#### EXPERIMENTAL

The liquids used were of C. P. quality and they were supplied by Eastman Kodak Co. They were repeatedly distilled in vacuum before exposure. A filter of 10 % solution of  $\text{NaNO}_2$  was used in the path of the incident light to cut off ultraviolet light, and this arrangement greatly reduced the intensity of fluorescence which was found to be produced by ultraviolet light.

In the case of 1, 1, 1-trichloroethane in the liquid state another filter of concentrated solution of  $\text{NaNO}_2$  was used to reduce appreciably the intensity of the  $4047 \text{ \AA}$  line, so that the assignment of the lines could be made correctly. The Raman spectra of the substances in the solid state were studied by solidifying the substances slowly in Pyrex containers which were gradually lowered in a transparent Dewar vessel containing liquid oxygen, and finally the lower portion of the container was completely immersed in liquid oxygen. A Fuess glass spectrograph was used to photograph the spectra and Ilford Zenith plates were used.

The polarisation of the Raman lines of the two liquids was studied in the usual manner by photographing the two components simultaneously with the help of a quartz double image prism. The polarisation of the Raman lines of carbon tetrachloride was also studied, using the same tube and the same arrangement, and from a comparison of these spectrograms the lines having degrees of polarisation of the order of  $6/7$  were found out.

#### RESULTS AND DISCUSSIONS

The spectrograms are reproduced in Plate XIV. The polarisation pictures are also reproduced to show that some of the lines are totally depolarised. The frequency shifts of the lines are given in Tables I and II.

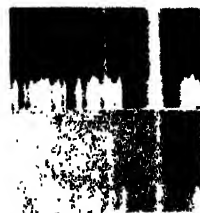
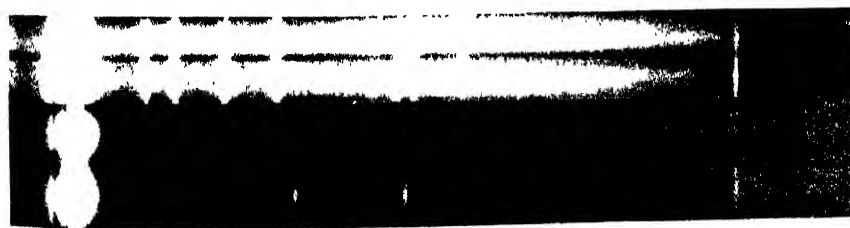
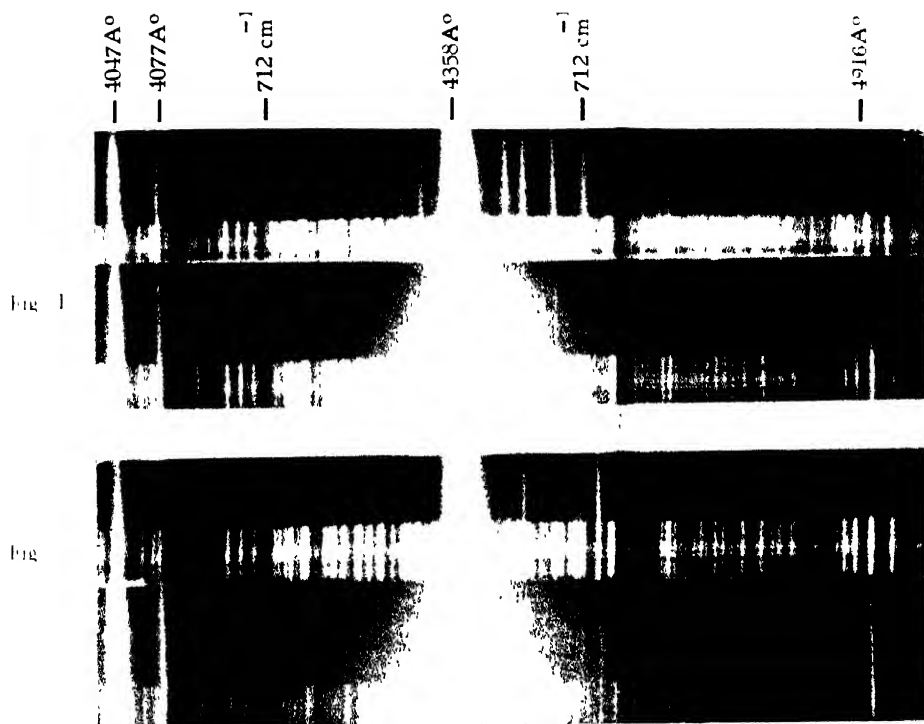


Fig. 3

Fig. 4

### Raman Spectra

Fig. 1 (a). 1, 1, 1-Trichloroethane at 28° C  
 (b) " " " at -180° C

Fig. 2 (a) 1, 2-Trichloroethane at 28° C  
 (b) " " " at -180° C

Fig. 3 Polarisation of Raman lines  
 (a) 1, 1, 1-Trichloroethane at 28° C.  
 (b) 1, 1, 2 " " at 28° C

Fig. 4 Raman spectra (magnified) of 1, 1, 2-trichloroethane  
 (a). at 28° C, (b). at -180° C.



TABLE I

1, 1, 1-Trichloroethane,  $\Delta\nu$  in  $\text{cm}^{-1}$ 

Liquid at 28°C

Solid at -180°C

Hull (1934)	Present author	Present author
* 241 (7)	241 (7), $\pm e, \pm k, i$ ; D	13 (2), k.
* 345 (10)	345 (8), $\pm e, \pm k$ ; P	243 (2), e, k
* 523 (9)	522 (10), $\pm e, \pm k$ ; P	347 (2), e, k
712 (7b)	712 (5b), e, k; D	522 (4), e, k
	973 (0), e; k; D	704 (2), e, k
{ 1071 (2)	1067 (2), e, k; P	
1086	1082 (1), e, k; P	1072 (1b), e
1175 (1)	1185 (0), k; ?	
1242 (1b)		
{ 1361 (1)		
1384		
{ 1424 (2)	1425 (2), e, k; D	
1451	1446 (2), e, k; D	1440 (0) ?
1592 (1b)		
2743 (1b)		
2943 (7)	2939 (6), e, k, i; P	2937 (3), e, k
3011 (6)	3007 (4), e, k; D	3007 (2), e, k

Observed also as anti-stokes lines

TABLE II

1, 1, 2-Trichloroethane  $\Delta\nu$  in  $\text{cm}^{-1}$ 

Liquid at 28°C

Solid at -180°C

Hull (1935)	Present author	Present author
	118 (2b) e, k; D	60 (2)
	190 (1b) e, k; D	166 (1) e
* 255 (4)	258 (4) $\pm e, k$ ; D	263 (1) e, k
* 283 (2)	287 (2) $\pm e, k$ ; P	
* 332 (10)	333 (10) $\pm e, k$ ; P	338 (3) e, k
* 395 (3)	391 (4) $\pm e, k$ ; P	385 (0) e
* 441 (1)		
525 (1)	525 (2) $\pm e, k$ ; P	525 (0) e
638 (3)	638 (4) $\pm e, k$ ; P	V
664 (5b)	668 (6) $\pm e, k$ ; P	670 (3) e, k
	697 (0) e, k; P	
	727 (0) e, k; P	
{ 772 (10)	775 (8) e, k; P	772 (6) e, k
{ 781	786 (5) e, k; P	V
931 (1)	934 (2) e, k; P	934 (0) e, ?
1056 (1b)	1041 (1) e, k; P	
1207 (2)		
1260 (2)	1260 (2) e, k; D	1260 (0) e
1304 (2)	1304 (3) e, k; P	1304 (0) e
1428 (2)	1430 (3) e, D	1427 (1) e
1475 (1b)		
2960 (8)	2961 (4) e, k, i; P	2961 (4) e, k
2996 (7)	3001 (2) e, k; P	3005 (3) e, k
3021 (5b)		

\* Observed also as anti-stokes lines

It can be seen from Table I that in the case of 1, 1, 1-trichloroethane in the liquid state the lines 1232, 1361 and 1384 and 1592  $\text{cm}^{-1}$  observed by Hull (1935) have not been observed in the present investigation. The spectrogram was a well exposed one, but no trace of these lines could be detected.

It is difficult to understand also how this molecule can yield a line 1592  $\text{cm}^{-1}$ , because there is no C=C bond. In the spectrogram obtained by using a concentrated solution of sodium nitrite to absorb the 4047 Å line in the incident light, it was verified that the line 2743  $\text{cm}^{-1}$  reported by Hull (1935) is actually a line 973  $\text{cm}^{-1}$  excited by 4358 Å. The line 2743  $\text{cm}^{-1}$  is not present in the spectrum. Similarly, the line supposed to be of frequency shift 1361  $\text{cm}^{-1}$  excited by 4358 Å was found to be the line 2939  $\text{cm}^{-1}$  excited by the line 4077 Å. Some of the lines due to the liquid are totally depolarised, and, therefore, the three-fold axis of rotation of the molecule is not disturbed in the liquid state.

In the solid state at  $-180^{\circ}\text{C}$  this compound yields a new line at 13  $\text{cm}^{-1}$ . This line is sharp but it is weak and cannot be due to the single molecule. It must be due to vibration of the whole molecule against other molecules in the lattice. Excepting the line 712  $\text{cm}^{-1}$  the other lines do not shift with solidification of the liquid. This shows that in this particular case the intermolecular field in the solid state does not change the strengths of the bonds appreciably.

In the case of 1, 1, 2-trichloroethane in the liquid state the lines observed by Hull (1935) were observed in the present investigation except the lines 441, 1207 and 1575  $\text{cm}^{-1}$ . This last line cannot be accounted for by assuming the known structure of the molecule. The lines 118 and 190  $\text{cm}^{-1}$  were not observed by Hull (1915). These lines are fairly intense and they can be clearly seen in the spectrograms reproduced in the Plate XIV. They may be due to torsional and deformation oscillation respectively. The lines 697 and 727  $\text{cm}^{-1}$  observed in the present investigation were not reported by Hull. The line 258  $\text{cm}^{-1}$  probably due to deformation oscillation of the C-C group is totally depolarised. Hence the molecule has some elements of symmetry.

Since this line persists in the solid state also the molecule in the solid state has an element of symmetry and this element may be a plane of reflection. It is, however, surprising that the line 3001  $\text{cm}^{-1}$  which might be due to antisymmetric C-H valence oscillation, is not totally depolarised, while the corresponding line due to 1, 1, 1-trichloroethane is totally depolarised. All the lines 638, 668, 697, 727, 775 and 786  $\text{cm}^{-1}$  are found to be polarised. These lines are due to C-Cl oscillations. Of these six lines the two lines 668 and 697  $\text{cm}^{-1}$  are extremely feeble. With the solidification of the liquid the lines 638 and 786  $\text{cm}^{-1}$  disappear and owing to the feebleness of the lines 668 and 697  $\text{cm}^{-1}$  it could not be ascertained whether they

also disappear with solidification. The line  $287\text{ cm}^{-1}$  also is seen to disappear with solidification. Such a disappearance of some of the lines was interpreted by previous workers in the case of disubstituted ethanes on the assumption that two types of molecules are present in the liquid and one of the two types transforms itself into the other type with solidification. In the case of ethylene dibromide, for instance, (Mizushima and Morino, 1938) some of the lines due to C-H valence and deformation oscillation also disappear with solidification along with a few lines due to C-Br oscillation. In the case of 1, 1, 2-trichloroethane, on the other hand, all the lines due to C-H valence and deformation oscillation persist when the liquid is solidified. This can happen only when the two types of molecules have the same frequencies for C-H oscillations, but in that case the frequencies of C-Cl vibration in the two types would not be so different from each other.

The appearance of the feeble line  $60\text{ cm}^{-1}$  in the case of the solid state may indicate formation of a dimer. It is significant that the line  $190\text{ cm}^{-1}$  probably, due to C-Cl deformation oscillation shifts to  $166\text{ cm}^{-1}$  with solidification of the liquid. However, the influence of intermolecular field in the liquid on the strength of the bonds can be determined only by studying the Raman spectrum of the substance in the vapour state. It has been observed by Mizushima, Morino, Watanabe, Simanouti and Yamaguchi (1949) that the intensity of those Raman lines of ethylene dichloride which disappear with solidification of the substance also diminishes when the substance is converted to vapour. This fact indicates a complicated influence of intermolecular field on the strength of the C-Cl bonds and the study of several such substances in the vapour state is necessary before definite conclusion can be drawn.

#### ACKNOWLEDGMENT

The author is indebted to Prof. S. C. Sirkar for his kind interest and guidance throughout the progress of the work.

#### REFERENCES

- Hull, G. F., 1935, *J. Chem. Phys.*, **3**, 534.  
 Mizushima, S. and Morino Y., 1938, *Proc. Ind. Acad. Sci.*, **8**, 315.  
 Mizushima, S., Morino Y., Watanabe, I., Simanoti, T. and Yamaguchi, S., 1949, *J. Chem. Phys.*, **17**, 591, 663.  
 Sheppard, N. and Szasz, G. I., 1949, *J. Chem. Phys.*, **17**, 86.





# SPECTROSCOPIC STUDY OF AMETHYST QUARTZ IN THE ULTRAVIOLET AND INFRARED REGIONS\*

BY M. K. VAINU BAPPU

PHYSICAL LABORATORY, NIZAM COLLEGE, HYDERABAD (DECCAN)

(Received for publication, October 10, 1952)

## Plate XV

**ABSTRACT.** In this paper a study is made of the absorption of light in the ultraviolet and infrared regions in amethyst quartz. In the ultraviolet the presence of the *V*-band is masked by the presence of iron impurity and it is difficult to assert its presence. That such a *V*-band exists was shown by Choong. In the near infrared three absorption bands are observed; the one on the long wavelength side can be identified with the *M*-band and the others as bands due to impurity. All these facts lead to the conclusion that the factors responsible for colour in the case of coloured alkali halides are also responsible for the coloration of amethyst quartz, with some slight difference.

## INTRODUCTION

In a previous paper (Vainu Bappu, 1952) a detailed study was made of the absorption of light in the visible region by amethyst quartz and it was shown that the observed absorption band, the *F*-band, was similar to the *F*-band observed by Pohl and his co-workers (1937, 38) in the alkali halides. Along with the study of the *F*-band in rocksalt, Pohl and his collaborators had subjected another band, observed in the ultra-violet, to intensive investigation. Molnar (quoted by Seitz, 1946) observed that when a crystal of colourless rocksalt was bombarded by X-rays, a band in the ultraviolet called the *V*-band was formed simultaneously with the *F*-band. The position of this band in the different alkali halides differed from each other but were all dependent on the lattice constant of the specimen under investigation. However, all these bands are always observed in conjunction with *F*-bands; as the band in the amethyst quartz has been ascribed to *F*-centres, it is quite logical to expect a *V*-band in the ultraviolet. Mollow (1935-37) observed an *M*-band in the long wave length side in the infrared. It appears that the *F*- and *M*-bands are associated with the trapped electrons loosened from the halogen or alkali metal ions, while the *V*-band is related to the holes in the closed shell structure. An attempt is made in this paper to see whether these bands are also present in the amethyst quartz.

## EXPERIMENTAL TECHNIQUE

(a) *Ultraviolet.* For absorption in ultraviolet the specimen was held in an aperture in a card board and interposed in the light beam. The

\* Part of a thesis approved for the M. Sc. degree of the Madras University.



# SPECTROSCOPIC STUDY OF AMETHYST QUARTZ IN THE ULTRAVIOLET AND INFRARED REGIONS\*

By M. K. VAINU BAPPU

PHYSICAL LABORATORY, NIZAM COLLEGE, HYDERABAD (DECCAN)

(Received for publication, October 10, 1952)

## Plate XV

**ABSTRACT.** In this paper a study is made of the absorption of light in the ultraviolet and infrared regions in amethyst quartz. In the ultraviolet the presence of the *V*-band is masked by the presence of iron impurity and it is difficult to assert its presence. That such a *V*-band exists was shown by Choong. In the near infrared three absorption bands are observed; the one on the long wavelength side can be identified with the *M*-band and the others as bands due to impurity. All these facts lead to the conclusion that the factors responsible for colour in the case of coloured alkali halides are also responsible for the coloration of amethyst quartz, with some slight difference.

## INTRODUCTION

In a previous paper (Vainu Bappu, 1952) a detailed study was made of the absorption of light in the visible region by amethyst quartz and it was shown that the observed absorption band, the *F*-band, was similar to the *F*-band observed by Pohl and his co-workers (1937, 38) in the alkali halides. Along with the study of the *F*-band in rocksalt, Pohl and his collaborators had subjected another band, observed in the ultra-violet, to intensive investigation. Molnar (quoted by Seitz, 1946) observed that when a crystal of colourless rocksalt was bombarded by X-rays, a band in the ultraviolet called the *V*-band was formed simultaneously with the *F*-band. The position of this band in the different alkali halides differed from each other but were all dependent on the lattice constant of the specimen under investigation. However, all these bands are always observed in conjunction with *F*-bands; as the band in the amethyst quartz has been ascribed to *F*-centres, it is quite logical to expect a *V*-band in the ultraviolet. Mollow (1935-37) observed an *M*-band in the long wave length side in the infrared. It appears that the *F*- and *M*-bands are associated with the trapped electrons loosened from the halogen or alkali metal ions, while the *V*-band is related to the holes in the closed shell structure. An attempt is made in this paper to see whether these bands are also present in the amethyst quartz.

## EXPERIMENTAL TECHNIQUE

(a) *Ultraviolet.* For absorption in ultraviolet the specimen was held in an aperture in a card board and interposed in the light beam. The

\* Part of a thesis approved for the M. Sc. degree of the Madras University.

transmitted light was condensed by means of quartz cylindrical lens on to the slit of the spectrograph. The photographs in Plate XV, figures 3 and 4 revealed a transmission limit of  $3800\text{\AA}$  for small exposures while for long exposures the limit was extended to  $3600\text{\AA}$ . To see if further exposure using a powerful light source would extend the transmission limit, a mercury arc was used and exposures of the order of 45 minutes could just reveal the bright line near  $3140\text{\AA}$ .

As complete opacity sets in by about  $3800\text{\AA}$  for reasonably moderate exposures, absorption spectra could be photographed easily using a gas filled tungsten lamp with a thin glass bulb. The glass for exposures of one minute absorbed wavelengths shorter than  $3100\text{\AA}$  transmitting freely in the region upto  $3200\text{\AA}$ . As such, a bulb of this type run on a higher voltage than usual was used as source for densitometric measurements, which were made in the usual way.

(b) *Infrared*. Studies in the infrared are usually carried out by thermopiles, but as the region of interest in this case was below  $10,000\text{\AA}$  a photocell sensitive to the red and near infra red regions was used. Though the photocell is quite at a disadvantage for spectral energy measurements, yet in the regions for which it is sensitive a great accuracy can be attained which is limited only by thermal emission and leakage between the electrodes. The measurement of currents greater than  $10^{-10}$  ampere was done by amplifying the photo-current by a D. C. amplifier. This was originally designed by Yu (1946) but in the present amplifying system (figure 1) certain changes were made.

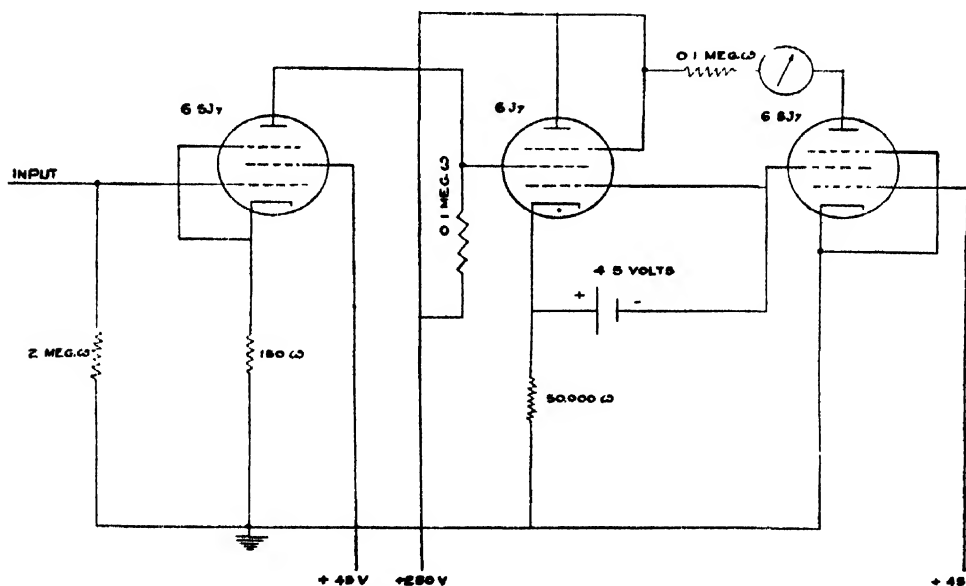


FIG. 1  
Circuit diagram of the amplifier

It was found that by introducing the galvanometer in the output of the second valve, a greater steadiness in output valve was obtained. To counteract the steady output current of the valve, an opposing current was passed through the galvanometer which could exactly balance it. But for currents lower than  $10^{-10}$  ampere, a Lindemann electrometer was used.

The source of light was a 150 candle power pointlight lamp, the radiation from which was condensed on to the slit of a spectrometer. A filter was used to cut off all radiations below  $5200\text{\AA}$ . As the dispersing element was a plane grating, the filter served the purpose of cutting off all radiations less than  $5200\text{\AA}$  in the second order spectrum thus enabling values to be obtained conveniently till  $10,000\text{\AA}$  in the first order. The specimen was held in a suitable holder and placed in between the filter and the collimator. The radiation from the grating is condensed on to a slit capable of admitting  $40\text{\AA}$  at a time in the red region, by means of long-focus achromatic lens. The photo cell was placed in a black housing with an aperture in front containing a narrow slit. The radiation ensuing from the first slit is condensed on to the second, by means of a quartz cylindrical lens. The photocell used had a caesium oxide surface sensitive to radiation between  $5000\text{\AA}$  and  $12000\text{\AA}$ . The current was measured by determining the time rate of increase of potential of a small high quality condenser.

$$\text{If } Q = CV$$

$$dQ/dt = i = C \frac{dV}{dt}$$

The capacity of the condenser was adjusted initially so that the time for charging the electrometer to a potential of one volt was between 10 and 35 seconds. The value finally adopted was 250 micro-micro farads. The absorption coefficients were determined by noting the times of charging the electrometer needle to potential of one volt, with and without the specimen before the slit of the instrument. As the times of charging are inversely proportional to the intensities of incident light the quantity  $\eta$  which is the transmitted fraction of the incident energy becomes equal to

$$\eta = \frac{I_2}{I_1} = \frac{t_1}{t_2}$$

were  $I_2$  is the transmitted energy,  $I_1$  the incident energy, and  $t_1$  and  $t_2$  being the times of charging the electrometer with and without the specimen, the mean of eight readings being finally adopted.

Figure 2 shows in detail, the arrangement of the infrared monochromator as well as the Lindemann electrometer.

The complete spectrometer was first calibrated for the mercury radiations  $5461\text{\AA}$  and  $5780\text{\AA}$  as well as  $D_1$  and  $D_2$  lines of sodium. As the voltage of the cell was quite low the photoelectric responses for different intensities were quite linear.

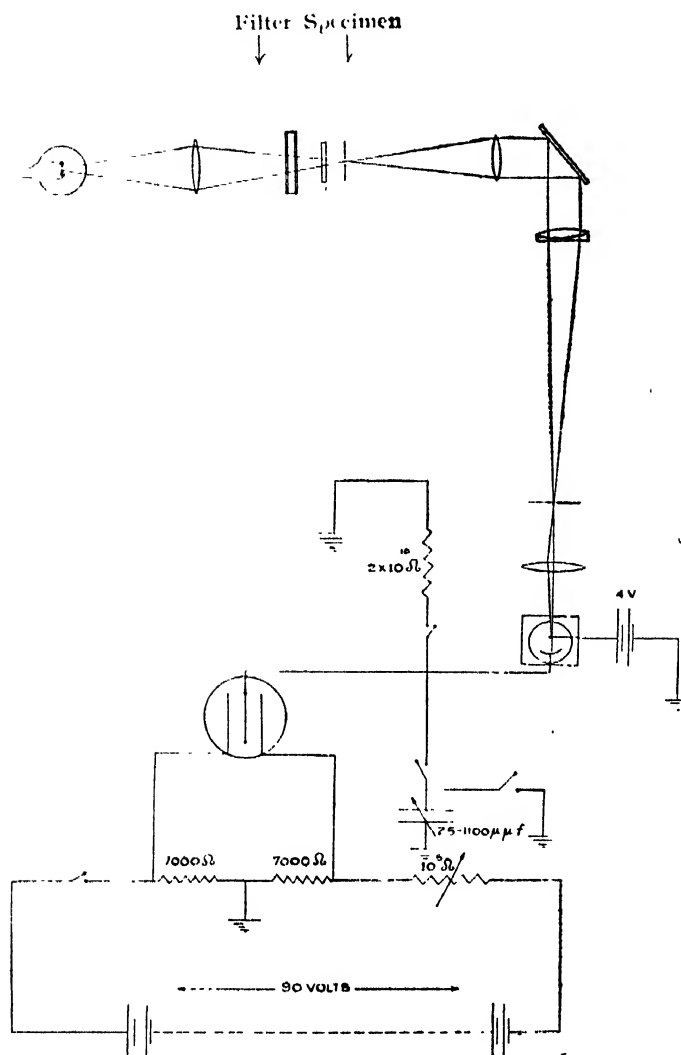


FIG. 2

Infrared monochromator together with the Lindemann electrometer and photocell

Much of the work was done in the winter months when the atmosphere was dry. As an additional precaution all work done with the electrometer was on sunny days with perfectly clear skies when reading could be reproduced properly.

For detecting the  $M$  band specimen,  $A_1$  was used while the decolorised specimen  $A_2$  was used to show which of the bands observed are due to impurities and which are not.

#### RESULTS AND DISCUSSION

Table I below gives the density values and corresponding absorption coefficients for different wavelengths. These can be seen diagrammatically represented in figure 6. An absorption band reaching opacity by  $3000\text{\AA}$

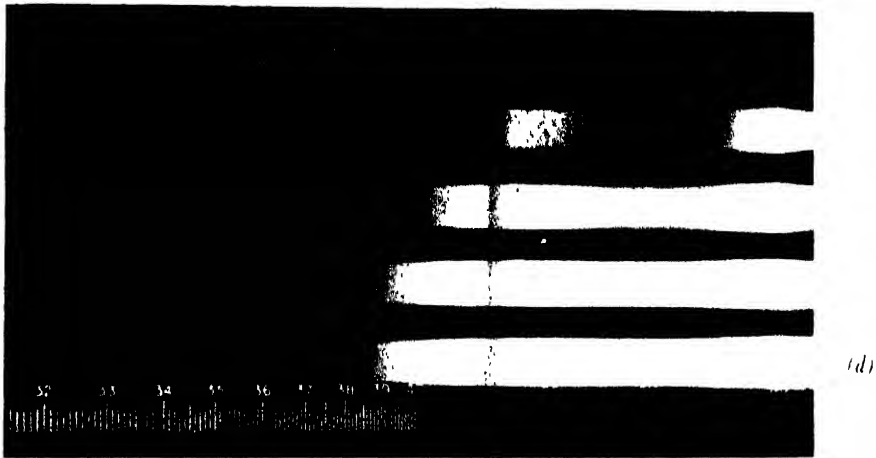


Fig. 3  
Transmission limits of amethyst quartz in the ultraviolet, - specimen  $A_1$ , for  
different exposure times  
(a) 1 minute, (b) 3 minutes, (c) 7 minutes, (d) 15 minutes

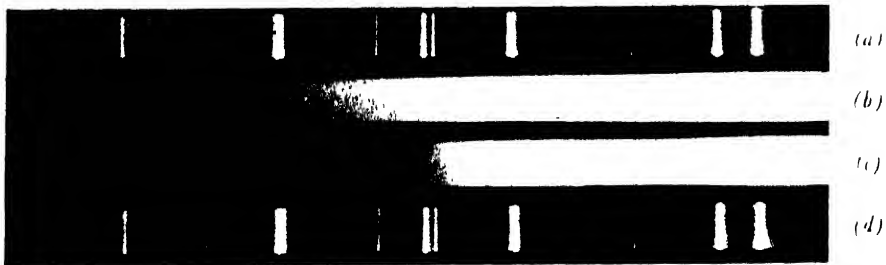


Fig. 4  
Absorption spectrum of amethyst quartz in the ultraviolet  
(a, d) Hg arc comparison spectrum  
(b) Decolorised specimen  $A_2$   
(c) Specimen  $A_1$





can be seen to be present. This band occupies just the same position and shape which a *V*-band in rocksalt does. To test whether this band is really a *V*-band, we have to resort to heat treatment.

TABLE I

Absorption coefficients for amethyst quartz in the ultraviolet

Wavelength in Angstrom units	Density	Absorption coefficient per cm
4046	0.077	10.93
3875	0.457	23.47
3620	0.591	30.10

The specimen used for the study of the removal of *F* centres by thermal treatment was used for absorption in the ultraviolet. No radical change in the transmission was noted after the heat treatment, even after removal of all the *F* centres. Consequently, we have to infer that the band in the ultraviolet in amethyst quartz is not a *V* band but it may be some band which masks entirely the effect of the *I*-centres, if any such exists.

In Plate XV, figure 4, we have the absorption in the visible and ultraviolet regions of both the specimens  $A_1$  and  $A_2$ . Specimen  $A_2$  has a greater transmission in the ultraviolet than the specimen  $A_1$ . But this was just the case before decoloration, and hence the increase in the transmission cannot be ascribed to thermal treatment. Plate XV-figure 3, shows the transmission limits in the ultraviolet for specimen  $A_1$  for different exposures. For very long exposures the limit does not exceed  $4630\text{\AA}$ .

Koch and others have noticed that small quantities of thallium halides may be dissolved in the alkali halides and that the resultant mixed crystals exhibit narrow absorption bands in the ultraviolet, visible and near infrared regions. As many previous investigators have detected iron in the form of  $\text{Fe}_2\text{O}_3$  in amethyst quartz, it is quite possible that the band in the ultraviolet is due to the presence of iron as impurity. Unaffected by thermal treatment, the band in the ultraviolet remains as it is, in spite of removal of *F*-centres [Plate XV, figure 4(b)]. Further, in the absorption spectra of specimens  $A_1$  and  $A_2$  we find different transmission limits, the limit in the case of  $A_2$  being about  $3300\text{\AA}$  for short exposures while that of  $A_1$  is in the neighbourhood of  $3800\text{\AA}$ . Thus we see that transmission limits do fluctuate from specimen to specimen. This can be explained as due to the difference in iron content of the two specimens. And this is all the more probable because specimen  $A_2$  was picked up from a different quarry.

The absorption curve for coloured amethyst quartz indicating the different bands in the infrared can be seen in figure 5. For coloured amethyst quartz we have three distinct bands with maxima at wavelengths

7850Å, 8350Å and 9200Å respectively. The bands at 7850Å and 8350Å are bell shaped and fairly narrow, whereas, that with maxima at 9200Å is very broad as can be seen clearly in curve(A) of figure 5. In the decolorised specimen we have two bands at 8350Å and 9200Å respectively, the positions and respective shapes being identical with the two bands in the coloured variety. The band at 7850Å is completely missing in decolorised specimen  $A_2$ , while the 8350Å band of  $A_2$  has a higher absorption than the corresponding one in  $A_1$ . But there is a decrease in the magnitude of the 9200Å band of  $A_2$  when compared with  $A_1$ .

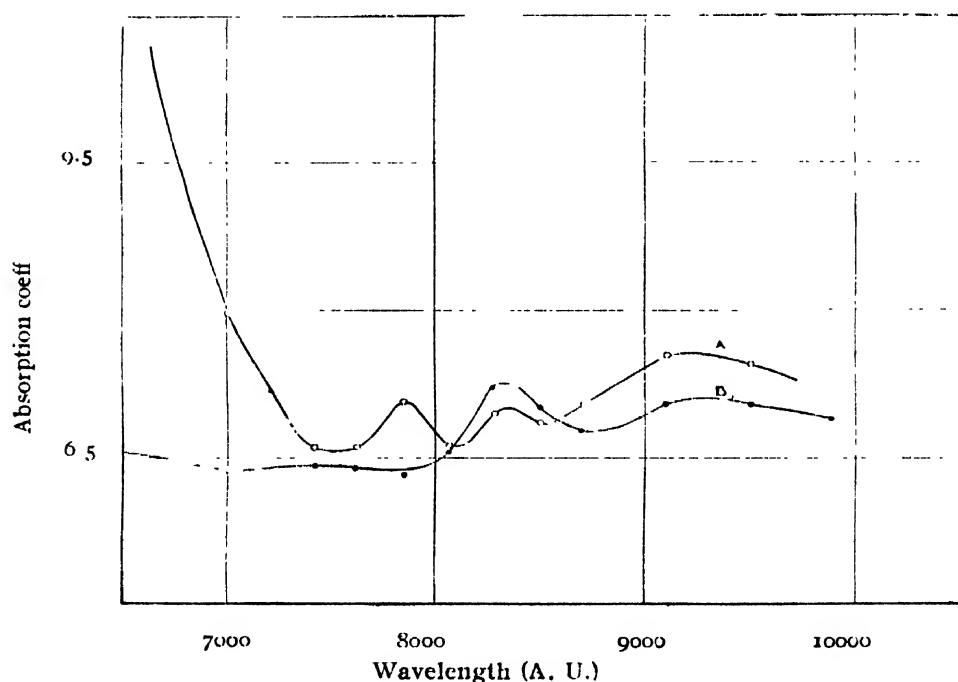


FIG. 5

The absorption curve of amethyst quartz in the near infrared.

A. Amethyst quartz specimen

B. Decolorised amethyst quartz

The 7850Å band is thus removed completely by thermal treatment, whereas, the other bands are not. Therefore, its origin is akin to that *F*-band. It can, therefore, be an *R*-band or an *M*-band. *R*-bands are usually found on the long wavelength foot while *M* bands are situated farther on, on the normal absorption curve. As the 7850Å band is slightly away from the long wavelength foot it may be considered to be an *M*-band.

Of the two other bands we find that thermal treatment has no effect on their structure. As such it cannot be due to any absorption centres of the type of *F*-and *M*-centres. And as we have an impurity band in the ultraviolet, it is quite probable that these may owe their origin to such impurities, in this case the impurity being iron.

## CONCLUSION

In figure 6 is given the complete absorption curve of amethyst quartz in the ultraviolet, visible and near infra-red regions, showing the *F*-bands, and *M*-bands and a band in the ultraviolet. The curve is almost similar to the one obtained by Molar in the case of potassium chloride irradiated by X-rays except for the band in the ultraviolet which may perhaps be due the iron impurity. Choong (1945) has, however, obtained a band in the ultraviolet in the case of fused quartz coloured violet by radium rays. The slight humps beyond the *F* and *M* bands may also be due to the impurity as these appear also in the infrared spectrum of the bleached crystal.

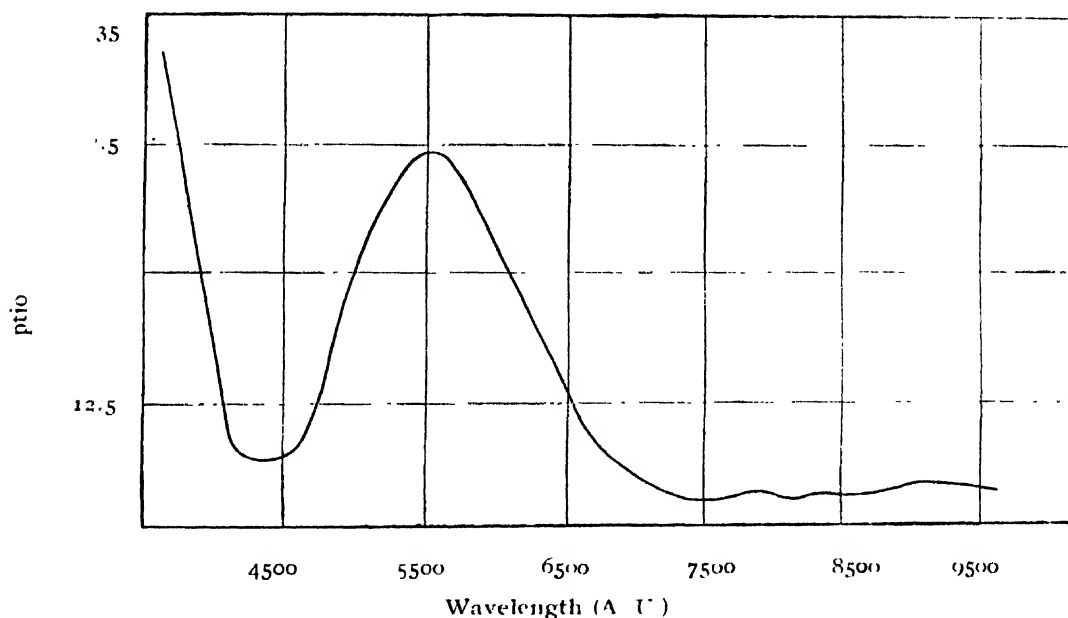


FIG. 6

Absorption curve of amethyst quartz in the ultraviolet, visible and near infrared regions

Seitz is of the view that a centre formed by combining an *F*-centre and a pair of vacancies may be responsible for the *M*-band. That the whole absorption phenomenon observed in the case of amethyst quartz is almost similar to those observed in coloured alkali halides, shows that the process responsible in both cases must be of same nature. These facts also establish that amethyst quartz behaves like a polar crystal, as far as absorption is concerned. This receives further support from the study of the photo-conductivity. Finally, it can be said with confidence that the colour of amethyst quartz is due to the colour centres formed by exposure to penetrating irradiation at some remote period in the evolution of the earth.

## ACKNOWLEDGMENT

In conclusion the author has great pleasure in expressing his deep gratitude to Dr. J. C. Kamesvara Rao, Professor of Physics, Nizam College, Hyderabad (Deccan), for his helpful guidance and keen interest in the investigation of this problem.

## REFERENCES

- Choong S. P., 1945, *Proc. Phys. Soc.*, **57**, 49.  
Koch, 1930, *Z. f. Phys.*, **57**, 638.  
Mollow, 1935, *Gottingen Nachrichten*, **1**, 190  
„ , 1937, *Ann. d. Physik.*, **29**, 394.  
Molnar, (Quoted by Seitz)  
Pohl, R. W., 1937, *Proc. Phys. Soc.* **49**, extra part 3.  
„ , 1938, *PhysZeit.*, **39**, 36  
Seitz, F., 1946, *Rev. Mod. Phys.*, **18**, 384.  
Vainu Bappu, 1951, *Ind. J. Phys.*, **26**, 1.  
Yu., 1946, *Electronics*.

# ON THE TEMPERATURE EFFECT IN GEIGER MULLER COUNTERS

By C. P. JOSHI

U. P. WIRELESS TELEGRAPHY SECTION, DILKUSHA, LUCKNOW

*Received for publication, April 9, 1957, received after revision, April 15, 1957*

**ABSTRACT** The effect of temperature on the plateau characteristics of self quenched and externally quenched counters was studied. Both types showed a deterioration of plateau from 20° to 60°C. inspite of the fact that they were quenched externally for 10 sec. The results have been explained on the hypothesis of the formation of long-lived metastable  $^{23}\text{P}_0$  states of mercury atoms. Traces of mercury vapour and free mercury are always present in counters due to the diffusion pumps, gauges etc. connected to filling manifolds. These metastable states return to normal in  $10^{-2}$  sec. and trigger a spurious discharge in doing so. The effect was more pronounced in argon-hydrogen counter than in argon-ether self-quenched counters.

## INTRODUCTION

The life of self-quenched Geiger counters is limited due to the disintegration of the polyatomic hydrocarbon molecules of the vapour of the quenching material. To run long term experiments on the time variation of cosmic rays a stable counter with a filling of permanent gases like argon and hydrogen is more reliable as there is no possibility of a progressive deterioration with time. But these counters show a change in their plateau characteristics with change of working temperature in much the same way as the self-quenched counters.

Other workers who have observed the temperature effect in self-quenched counters have attributed it to the adsorption of hydrocarbons on the cathode cylinder which increases its work function and diminishes its ability to produce photoelectrons (Korff, 1946; Prakash, 1949; Kimura, 1950 and Prakash and Kapur, 1950). On heating the counter this film is supposed to be evaporated thereby increasing the probability of the production of spurious counts and increasing the slope of the plateau. At low temperatures this hydrocarbon gets condensed and produces a short circuiting film inside the counter and thus the counter deteriorates. This hypothesis is quite convincing as far as the self-quenched counter is concerned but the possibility of other constituent gases playing an important role is not ruled out. The other gases are argon, with which the counter is filled, and traces of mercury vapour which is always present in counters due to the diffusion pumps, manometers and gauges connected to filling manifolds. The amount of mercury vapour present in the counter is a variable quantity and changes

with variations in temperature. This is due to some free mercury which appears in the counter as a result of back diffusion from the mercury diffusion pump which did not have a trap attached to it as has been mentioned earlier. The method by which the constituent responsible for the temperature effect can be singled out is by a process of elimination. This is, however, not possible in the case of the self-quenched counter in which the quenching vapour is essential for working and as such cannot be eliminated. This is the reason why the data on the temperature effect in argon-hydrogen counters become valuable as in this counter organic vapours, which are known to cause temperature dependence, are absent.

While designing the equipment for time variations of cosmic rays an externally quenched counter with a filling of argon and hydrogen was developed and the effect of the working temperature on the plateau characteristics of this counter was studied in some detail. For this purpose a comparative study was made of argon-hydrogen filled externally quenched counters and argon-ether filled self-quenched counters.

#### EXPERIMENTAL

The externally quenched counter was quenched by a special multi-vibrator circuit which is a modification of the Johnson circuit. To make the conditions identical the external quenching circuit was connected to the self-quenched counter also during these experiments. This circuit increased the dead time of the counter to  $10^{-3}$  sec by keeping the counter potential reduced by 300 volts for  $10^{-3}$  sec after a true discharge.

Both the counters were metal-in-glass type with a copper cathode and tungsten central wire. The argon-hydrogen counter was 12" long and had a diameter of 1.0". It was filled to a pressure of 20 cm. of Hg with 18 cm. of argon and 2 cm. of hydrogen. The self-quenched counter was 12" long and its diameter was 1.2". It was filled to a pressure of 9 cm. of Hg with 7 cm. of argon and 2 cm. of petroleum ether. The counters were evacuated to  $10^{-4}$  mm. Hg and the central wire was flashed. The argon used was spectroscopically pure. Evacuation was done with a mercury diffusion pump without a trap and a McLeod gauge and two mercury manometers were connected to the filling system.

The same quenching circuit was used throughout the tests and it was adjusted for maximum efficiency.

To study the effect of temperature on Geiger counters a thermostatic box was used. The temperature inside this box could be controlled to within  $1^{\circ}\text{C}$  between  $25^{\circ}\text{C}$  and  $80^{\circ}\text{C}$ . The counter was kept inside this box and it was given sufficient time at every temperature to settle down after the change. The characteristics have been obtained only after the counter had been sealed off from the filling manifold and after it had aged properly till there was no further improvement in the plateau with lapse of time.

The plateaus in both the counters were studied at three different temperatures and the characteristics in figures 1 and 2 are based on average values.

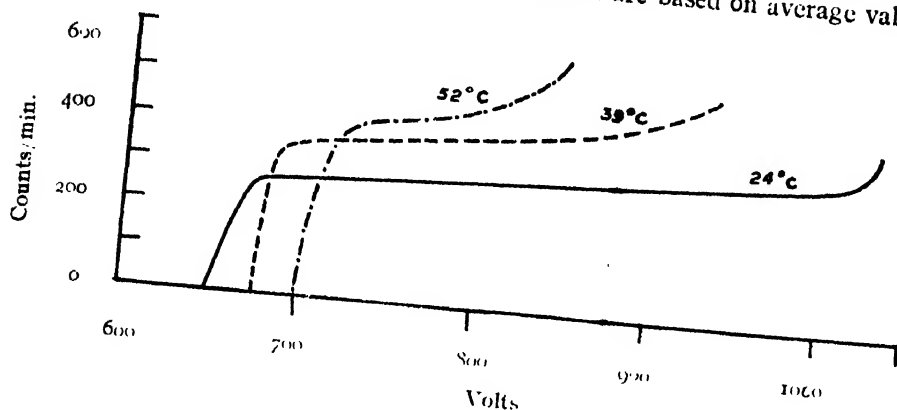


FIG. 1  
Self-quenched counter (argon-ether)

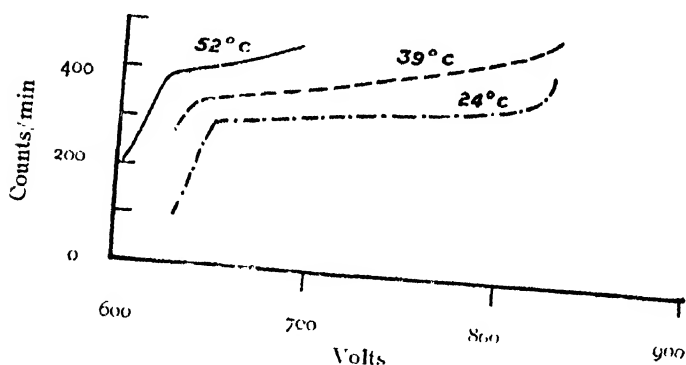


FIG. 2  
Externally quenched counter (A-H<sub>2</sub>)

## RESULTS

It will be apparent from the plateau characteristics given here that the effect of the increase of the working temperature is to raise the number of spurious counts which causes an increase in the slope of the plateau. This happens in both types of counters referred to above. In both the cases a substantially good and flat plateau at room temperature is completely ruined at about 52°C. The curve at 39°C clearly shows the trend of the process of deterioration.

The most significant fact emerging out of these observations is that the temperature effect is more marked in the argon-hydrogen counter than in the self-quenched counter and this is so inspite of the fact that a quenching circuit was reducing the counter voltage and keeping it low for  $10^{-8}$  sec.

## DISCUSSIONS

As mentioned earlier any one of the three gases present in a counter *i. e.* organic vapour, argon or mercury vapour, may be responsible for the temperature effect. In the argon-hydrogen counter the first is automatically eliminated.

Spurious counts in a Geiger counter are generated in many ways but one of the main processes responsible for them is the formation of metastable states of the counter gases with long life time. These metastable states return to normal and in doing so give rise to a spurious discharge. The addition of hydrogen results in the quenching of the metastable states of argon and since this is done within the dead time of the quenching circuit *i. e.*  $10^{-3}$  sec. we cannot except spurious counts arising out of this process.

Putnam (1948) has reported that self-quenched counters could be made substantially temperature independent by quenching them externally for  $10^{-3}$  sec. This suggests that the temperature effect in his case was due to second and third order phenomena which would not be initiated if the counter potential is kept low for  $10^{-4}$  sec or more after the initial avalanche.

The counters in the present experiment were quenched by a circuit which reduced the counter potential by about 300 volts and kept it down at that value for  $10^{-3}$  sec. Since both self-quenched and externally quenched counters connected to this circuit showed the temperature effect it is quite obvious that the phenomenon observed is quite different from that in the experiments of Putnam. One is naturally inclined to suspect some mechanism for the generation of spurious counts in which there is a time lag much more than  $10^{-3}$  sec. Korff (1946) has also observed "enormous" pulses at high pressures of mercury vapour.

The increase in the number of spurious counts in this experiment can be explained by the presence of mercury vapour in the counter. Normally in a sealed-in counter no variation of the quantity of mercury vapour can be anticipated with the increase of temperature. But in the present case traces of free mercury were also present in the counters after they were sealed as a result of back diffusion from the mercury diffusion pump. There is an increase in the amount of mercury vapour in the counter with the increase of temperature since at the higher temperature some free mercury will go into the gaseous state. The vapour pressure of mercury is  $10^{-3}$  mm at about  $20^{\circ}\text{C}$  but at  $80^{\circ}\text{C}$  it rises to 0.1 mm. This represents a change in the amount of mercury vapour by a factor of 100. The specific ionization of mercury vapour is almost twice as much as that of argon and, therefore, the change in the vapour pressure of mercury can be expected to be very effective. It was found that the starting potential was reduced on heating the counter and this can only be explained by the increase in the proportion of a gaseous constituent having a high specific ionization. This also



eliminates the possibility of the adsorption or absorption of hydrogen on the cathode and subsequent re-evaporation on heating being a significant process for the temperature effect. Had this been the case, the starting potential ought to have increased considerably since the specific ionization of hydrogen is only about a fifth of that of argon.

If mercury atoms present in the counter go into a metastable state of long duration (say greater than  $10^{-3}$  sec) and subsequently trigger an avalanche while returning to normal it would be possible to explain the temperature effect in argon-hydrogen counters which persists inspite of external quenching for  $10^{-3}$  sec. It is well known that mercury atoms in the  $2^3P_1$  metastable state pass into the long lived  $2^3P_0$  metastable state (17r) which has a life time of  $10^{-2}$  sec (Hughes and Dubridge, 1932 and also Dorgelo, 1925). If the initial discharge starts this mechanism any quenching circuit which reduces the counter potential for only  $10^{-3}$  sec would obviously be unable to deal with the spurious counts arising out of it. It is also known that the number of mercury atoms in the  $2^3P_0$  state increases considerably in the presence of argon (Hughes and Dubridge, 1932). In our counter containing argon and mercury vapour we can expect an increase in the number of long lived metastable atoms as we have the required conditions for this mechanism due to the presence of argon.

#### CONCLUDING REMARKS

From the above considerations it appears to be very likely that the argon-hydrogen counter containing traces of mercury vapour cannot be made temperature independent by quenching for  $10^{-3}$  sec. Putnam (1918) has reported complete temperature independence in self-quenched counters after external quenching was also used but in the experiments reported here although there was a marked improvement in self-quenched counters but still the temperature effect was evident to a large degree. This can only be due to the presence of mercury vapour.

These experiments on self-quenched and externally quenched counters suggest that mercury vapour can cause a large temperature effect. Although it has not been possible in these experiments to study the effect complete elimination of mercury from counters it will be attempted in future

#### ACKNOWLEDGMENTS

The author is thankful to Dr. Vikram A. Sarabhai, Professor of Cosmic Ray Physics in the Physical Research Laboratory, Ahmedabad and Dr. S. N. Ghoshal, Reader in the Department of Physics, Lucknow University, for their valuable help.

## REFERENCES

Dorgelo, H. B , 1925, *Zeit. f. Phys.*, **34**, 766.

Hughes and Dubridge, 1932, "Photoelectric Phenomena" McGraw-Hill, First Edition.

Kimura, M., 1950, *Phys. Rev.*, **80**, 761.

Korff, S. A , 1946, "Electron and Nuclear Counters"-Van Nostrand.

Prakash, O., 1949, *Phys. Rev.*, **76**, 568.

Prakash, O. and Kapur, P. L., 1950, *Proc. Phys. Soc.*, (Sec. A) **63**, 457.

Putnam, J. L., 1948, *Proc. Phys. Soc.*, **61**, 313.

# THE COMPLEX BAND SPECTRUM OF THE DIATOMIC MOLECULE CbO IN THE PHOTOGRAPHIC INFRARED \*

BY V. RAMAKRISHNA RAO AND D. PREMASWARUP

DEPARTMENT OF PHYSICS, ANDHRA UNIVERSITY, WALT AIR

(Received for publication, March 6, 1953)

## Plate XVI

**ABSTRACT.** Using Kodak 1-N plates a band system due to CbO molecule is obtained in the infrared for the first time. Bands in the region  $\lambda\lambda 7679-6033$  are reported with an analysis. Possible interpretations of the electronic transition are discussed. The following formula is obtained to represent the system

$$\begin{array}{l}
 15484.1 \\
 15431.3 \\
 15244.9 \\
 14880.6 \text{ J}
 \end{array}
 + 919.5(v' + 1/2) - 20.3(v' + 1/2)^2 - 996.0(v'' + 1/2) + 9.0(v'' + 1/2)^2.$$

## INTRODUCTION

The band spectrum of CbO molecule was first obtained by one of us (Rao, 1950) in various sources, primarily the D. C. arc of the conventional type. The bands were obtained in the region  $\lambda\lambda 4200-6450$  and divided into three systems: System A,  $\lambda\lambda 4200-5100$ , system B  $\lambda\lambda 5100-6100$  and system C,  $\lambda 6100$  to the limit of sensitivity of the panchromatic plates used at that time. A satisfactory analysis was then carried out for system A and tentative analyses were given for B and C. With regard to system C it was pointed out that only one group was obtained and there was considerable overlap between B and C. It was then suggested that possibly this group at  $\lambda 6100$  might be the  $\Delta v = +1$  sequence of a system extending further into the infrared. On an analogy with the TiO and ZrO (Lowater, 1929 and 1932) it was also pointed out that the analysis of this band system might provide a clue to the electronic states involved in all the band systems. In view of the above consideration an investigation of this band system C was taken up during his (Rao) stay in Chicago in 1950-51. Using Kodak 1-N type plates the complete band system was studied upto 8500 A.U, as predicated. A preliminary report of these bands in this region was made by V. R. Rao at the symposium on molecular structure and spectroscopy at Ohio State University, Columbus, Ohio, U. S. A, in June 1951. In the following pages a discussion of these bands is presented.

\* Communicated by Prof. K. R. Rao

## EXPERIMENTAL

The bands were easily obtained in the flame of a conventional D. C. arc at 110 volts, 3-4 amperes, run between metallic electrodes of columbium. Kodak 1-N plates were used to photograph the spectrum upto  $\lambda 8500$  A. U. For preliminary investigations a glass Littrow instrument at the University of Chicago was used. Pictures were also taken on the 10' grating at the Gas Institute, Illinois Institute of Technology, Chicago, and on the 21 foot concave grating in the first and second orders at the Yerkes Observatory, Williamsbay, Wisconsin, U. S. A. Thus we had pictures in dispersions 17, 5.2, 2.8 and 1.4 A. U. per mm. Measurements were made under all these dispersions on what appeared to be most probably the vibrational band heads.

## DESCRIPTION OF THE NEW SPECTRUM

The bands obtained in the region 6250-8500 A. U. are to be considered in conjunction with the group obtained in the earlier work (*loc. cit.*). The bands are all well degraded to long wavelengths. The band group between  $\lambda\lambda 6464$ -6830 is very intense and conspicuous. To the violet of this group and at about  $\lambda 6100$  lies the group discussed in the earlier work as part of system C. It is quite possible that some bands related to this system C may lie further into the violet thus extending into the region of what was previously designated as system B. On the red side of the first mentioned group of bands there is a group starting from 2920 A. U. with a systematic band structure. From  $\lambda 7200$  upto  $\lambda 7800$  the region is very difficult for recognising band heads, particularly on the 21' grating pictures. All indications are that system C might possibly terminate in this region. Rotational structure was open to different degrees on plates of both low and high dispersion. This feature is, however, rather unfortunate for a vibrational analysis, a definite location of a band head being not always easy. Spurious band heads (positions in which there may be some accidental grouping of rotational lines) are deceptive. Also if there is an atomic line in the vicinity of such a grouping, one gets the impression of a strong band. The latter difficulty is particularly troublesome with small dispersion spectrograms. It appears that an optimum dispersion of about 5 A.U. per mm. seems to be most desirable for bands of this type.

The wavelength, wavenumber together with intensity and assignment of these bands are given in Table I. Measurements were made only on what we considered to be the vibrational bands under all dispersions used. Plate XVI gives an impression of these bands and the more important assignments are marked on it.

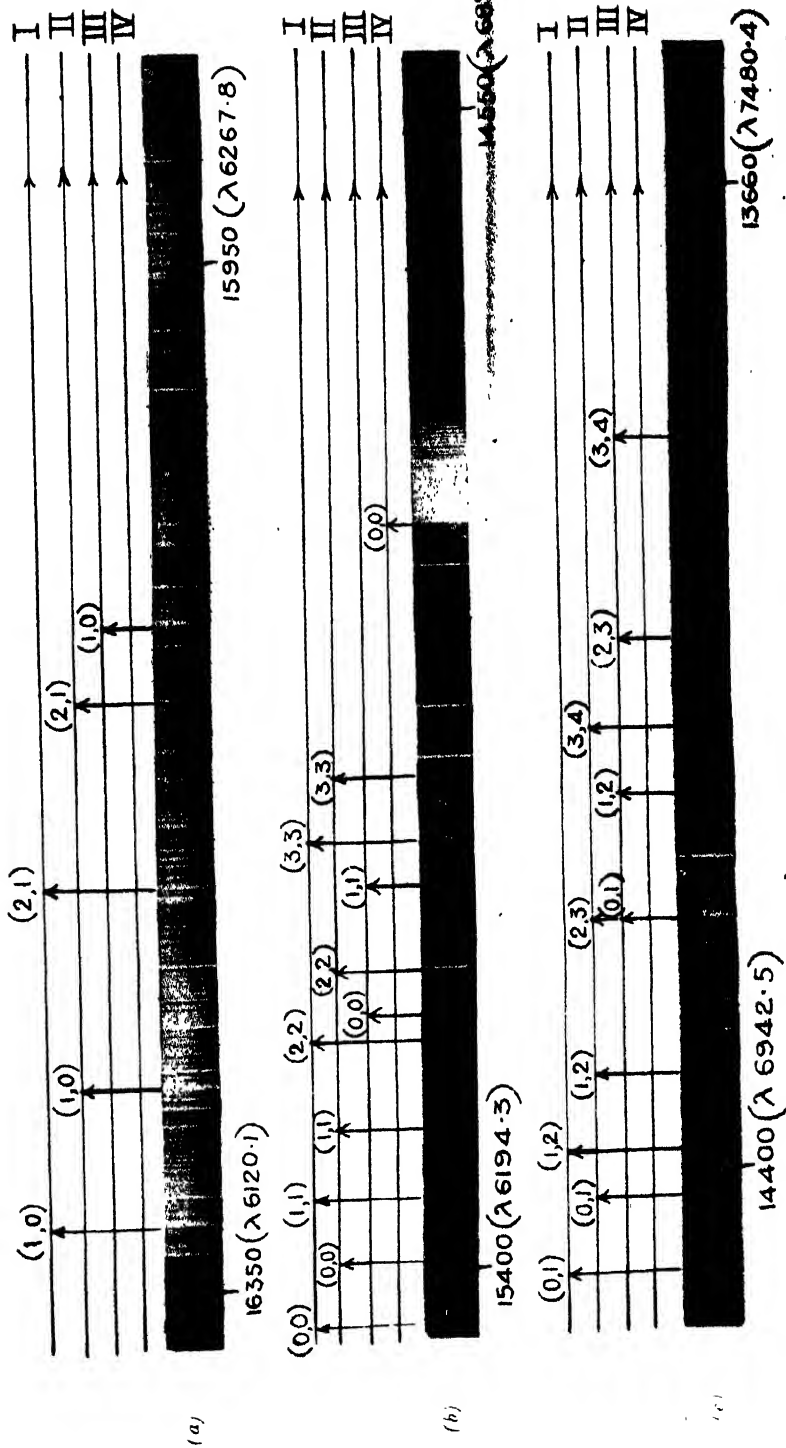




TABLE I  
Catalogue of CbO band heads

Wave length (A. U.)	Wave number observed	Int.	Assignment	Wave number Calculated (cm <sup>-1</sup> )	Deviation (cm <sup>-1</sup> )
7678.19	13020.3	3			
69.92	13034.4	3			
36.38	13091.6	2			
7584.93	13180.4	3			
7465.16	13391.9	2	II (1,3)	13388.4	3.5
32.6 *	13450		II (0,2)	13451.7	-1.7
7383.80	13539.3	3			
79.56	13547.2	3			
7263.98	13762.8	2			
07.72	13870.2	1			
7184.91	13911.2	3	III (3,4)	13913.8	0.4
63.35	13956.1	2			
35.90	1409.8	3			
20.42	14010.2	3	III (2,3)	14040.3	-0.1
7090.75	14099.0	3	II (3,1)	14100.2	-1.2
68.20	14141.0	2	III (1,2)	14144.2	-0.2
51.02	14178.4	2			
27.28	14226.3	4	II (2,3)	14226.7	-0.4
			III (0,1)	14225.5	0.8
19.61	14241.9	2			
6976.41	14330.1	3	II (1,2)	14330.6	-0.5
69.36	14344.6	4			
50.90	14382.7	4	I (1,2)	14383.4	-0.7
36.33	14412.9	2	II (0,1)	14411.9	-1.0
26.16	14431.0	2			
11.96	14463.7	1	I (0,1)	14464.7	-1.0
6873.29	14545.1	2			
6780.36	14744.4	3			
56.76	14795.9	4			
37.00	14839.1	5	III (3,3)	14838.3	0.9
			IV (0,0)	14839.4	-0.3
6694.15	14934.3	2			
75.66	14975.7	2			
54.52	15023.2	3	II (3,3)	15024.4	-1.2
32.94	15072.1	2	I (3,3)	15077.2	-5.1
18.68	15104.5	2	III (1,1)	15104.4	0.1
06.06	15133.4	3			
6594.03	15161.1	3			
90.82	15168.3	3	II (2,2)	15168.9	-0.6
75.61	15203.5	2	III (0,0)	15203.7	-0.2
66.1 *	15226		I (2,2)	15221.7	4.3
59.81	15240.1	2			
38.03	15290.9	2	II (1,1)	15290.8	0.1
20.44	15332.2	2			
15.18	15344.5	2	I (1,1)	15343.6	0.9
10.67	15355.2	3			
6499.41	15381.8	3			
95.64	15390.7	5			
94.84	15392.6	5	II (0,0)	15390.1	2.5
83.04	15420.6	3			
73.80	15442.7	3	I (0,0)	15442.9	-0.2
63.18	15468.0	1			
07.07	15603.5	1			
6387.86	15650.4	1			
85.80	15655.4	1			
72.92	15687.1	1			
70.93	15692.0	1			
59.9 *	15719		IV (1,0)	15718.3	0.7
29.21	15795.4	1			

\* These bands were measured on the Littrow spectrograms

TABLE I (contd.)

Wave length (A. U.)	Wave number observed (cm <sup>-1</sup> )	Int.	Assignment	Wave number calculated (cm <sup>-1</sup> )	Deviation (cm <sup>-1</sup> )
6309.18	15845.6	1			
6262.61	15963.4	2			
57.18	15977.2	1			
31.11	16044.1	2			
28.08	16051.9	2			
16.09	16082.8	2	III (1,0)	16082.6	0.2
6199.1 *	16127		II (2,1)	16129.1	-2.1
92.32	16144.4	2			
77.3 †	16184		I (2,1)	16181.9	2.1
76.07	16187.1	2			
54.73	16243.2	2			
45.06	16268.7	3	II (1,0)	16269.0	-0.3
28.57	16312.5	3			
24.01	16324.7	2	I (1,0)	16321.8	2.9
20.07	16335.2	4			
19.74	16336.1	4			
13.73	16352.1	1			
6096.64	16398.0	1			
87.98	16421.3	1			
77.88	16448.6	0			
66.09	16480.5	0			
47.34	16531.6	2			
34.23	16567.5	1			

\* These bands were measured on the Littrow spectrograms.

## ANALYSIS

The strong group of bands in the region  $\lambda 6400$  is evidently the  $\Delta v=0$  sequence. The intense and well defined nature of the bands, the marked degradation to the red and the general appearance of the system C gives at the first sight an impression of a very simple sequence structure of an open Franck-Condon parabola type. However, successive attempts at analysis proved this to be an erroneous impression, and the vibrational structure turned out to be more complex than it appeared. Various vibrational schemes were attempted with the strong bands of this group as members of a sequence without success. It was assumed that systems A and C might share a common state. The conspicuous red degradation of the bands indicates that  $\omega_e''$  must be considerably larger than  $\omega_e'$ . With this requirement it was seen that only the lower state could be common to the systems.

Several types of combinations with the strong bands in the region  $15393 \text{ cm}^{-1}$  as 0, 0 etc., were formed but the analysis did not progress. For example, one typical case was with 15468, 15442.7, 15420.6 and 15392.6 as the four components of the (0, 0) band. This means that multiplet separations are supposed to be much smaller than the vibrational separations in both states. Failure with this approach led us to a speculation of the possible order of magnitude of multiplet separation. It was found that the order of multiplet separation in TiO and VO (Keenan, 1952) are respectively 66, 75 and 73, 36, 87  $\text{cm}^{-1}$ . In ZrO the values are 292, 313  $\text{cm}^{-1}$ . We



find these values much larger than the corresponding values in TiO (the terms involved in both are triplets). It is reasonable, therefore, to expect multiplet separations to increase considerably when we go from VO to CbO. It is possible that system C of CbO and the infrared bands of VO discussed by Keenan may have similar electronic transition. Keenan pointed out the possibility of quartet term transition for the infrared system at the suggestion of the senior author (see foot-note, page 87, Keenan's paper). From his data it was, therefore, expected that the multiplet separations are of the order of  $300\text{ cm}^{-1}$ . It is also worthwhile noting that the values obtained by Keenan are not nearly equal; the second one is about half the value of the other two. An attempt on the above lines succeeded with comparative ease in building up the Deslander's Table (Table II) which includes practically all the intense bands in the spectrum. The important band heads are marked and shown in Plate XVI. The main features of this analysis are as follows: the lower state vibrational differences are nearly equal to those obtained in system A. The vibrational constants, as calculated from system C, are  $\omega_e'' = 996\text{ cm}^{-1}$  and  $x_e''\omega_e'' = 9.0\text{ cm}^{-1}$ . The corresponding values for system A are  $1000.9$  and  $6.5\text{ cm}^{-1}$  respectively. while taking note of the difference in values to the extent of  $6.7\text{ cm}^{-1}$  it should be pointed out that the values for A were obtained with glass Littrow

TABLE II

$v''$		0		1		2		3		4
$v'$										
0	I	15442.7	979 0	14463.7						
	II	15392.6	979 7	14412.9	963	13450				
	III	15203.5	977 2	14226.3						
	IV	14839.1								
		882.0		880.8						
		876.1		878.0		880				
		879.3		878.2						
		880								
1		16324.7	980 2	15344.5	961.8	14382.7				
		16268.7	977 8	15290.9	960.8	14330.1	938.2	13391.9		
		16082.8	978.3	15104.5	960.5	14144.0				
		15719								
				840		843				
				836		838.2		834.4		
2				16184	958	15226				
				16127	959	15168.3	942.0	14226.3		
								14040.2		
								796.9		
								798.9		
3								15072.1		
								15023.2	924.2	14099.0
								14839.1	924.9	13914.2

data. Work is in progress of obtain the values with higher dispersion spectra and compare for the two systems. The upper state has  $\omega'_e = 919.5$  and  $x'_e \omega'_e = 20.3 \text{ cm}^{-1}$ . The corresponding values for system *A* are 855.2 and  $3.9 \text{ cm}^{-1}$ .

The mean separations between I, II, III and IV are 52.8, 186.4 and  $364.3 \text{ cm}^{-1}$ . All the four bands are not identified in all  $v'$ ,  $v''$  positions. The  $\Delta v = 0$  and  $-1$  sequences could be followed upto four members. and  $\Delta v = 1$  sequence could be followed only upto two members. The following formula represents the bands.

$$\left. \begin{array}{l} 15484.1 \\ \nu = 15431.3 \\ 15244.9 \\ 14880.6 \end{array} \right\} + 919.5(v' + \frac{1}{2}) - 20.3(v' + \frac{1}{2})^2 - 996.0(v'' + \frac{1}{2}) + 9.0(v'' + \frac{1}{2})^2$$

Table I shows the calculated values and their deviation from the observed values.

The marking of the band heads shows a  $\Delta v = -1$  sequence superposing on the  $\Delta v = 0$  sequence of I. This possibly might account for the considerable difficulty experienced in the analysis.

#### DISCUSSION OF THE RESULTS

It was expected that a vibrational analysis of these bands may give a clue to the electronic transitions involved not only in this system *C* but also in system *A*. It must be admitted, however, that the hope was not fulfilled. The interpretation of what we designated as I, II, III and IV is far from clear. These four cannot possibly be treated as four different systems: for, then they cannot have both states common.

Considering the number of electrons for the molecule  $\text{CbO}$ , the electronic terms must be only of even multiplicity. In fact they can only be quartets and/or doublets. One possibility of explaining four branches is to consider the terms to be  $^4\Pi$  and  $^4\Sigma$ . In such a case the separations obtained are actually those of the 4 multiplet levels in the  $^4\Pi$  state as  $^4\Sigma$  may be treated as single for purposes of vibrational analysis. In  $\text{TiO}$  and  $\text{ZrO}$  the transitions for the corresponding systems are  $^3\Sigma - ^5\Pi$ . In vanadium oxide Keenan reported 8 bands in each position, four of which were multiplet heads and four others their rotational heads. We have not succeeded in obtaining 8 bands as in  $\text{VO}$ . For the above explanation to hold the rotational heads may have to be considered very weak. Even then the intervals observed are quite divergent. The multiplet separation (*A*) is generally about equal between any two levels. It may be added that it is not the case in  $\text{VO}$  as well. However, the evidence is not enough to assign this band system to the electronic transition  $^4\Sigma - ^4\Pi$ .

Another interpretation is the possibility of doublet terms. However, the lower state of system *A* has been suggested by one of us (V. R. Rao) to

be a quartet term. This was established by K. S. Rao by working out the rotational analysis of the (1, 0), (0, 0) and (0, 1) bands. If system C' is a doublet transition there cannot be a common state between A and C'. However, it is highly improbable that systems A and C' should not have at least one state in common. The intensity of the system does not easily permit a suggestion of an intercombination like doublet-quartet transition. Taking all these points into consideration we have to leave the question of electronic transition open.

## ACKNOWLEDGMENTS

Our thanks are due to Drs. R. S. Mulliken and John. R. Platt of the University of Chicago for the materials and facilities. The kind courtesy of the authorities of the Yerkes Observatory is gratefully acknowledged.

One of us (V. R. Rao) is grateful to the Andhra University for financial assistance during a part of his stay in U. S. A. We are thankful to Dr. K. R. Rao for his interest in the work.

## REFERENCES

- Keenan, P. C. and Schroeder, L. W., 1952, *Astrophysical Journal*, **115**, 82.
- Lowater, F., 1929, *Proc. Phys. Soc.*, **41**, 557.
- Lowater, F., 1932, *ibid*, **44**, 51.
- Rao, V. R., 1950, *Ind. J. Phys.*, **24**, 35.
- Survanarayana Rao, K., 1952, *Proc. Phys. Soc.*, (In Press).

# ON THE RAMAN SPECTRA OF 1, 2-DICHLOROETHANE AND 1, 1, 2-TRICHLOROETHANE IN THE VAPOUR STATE\*

BY MONOMOCHAN MAZUMDER

OPTICS DEPARTMENT, INDIAN ASSOCIATION FOR THE CULTIVATION OF SCIENCE, CALCUTTA-32

(Received for publication, July 7, 1953)

## Plate XVII

**ABSTRACT.** The ratio of intensities of the lines  $755$  and  $654\text{ cm}^{-1}$  in the Raman spectrum of 1, 2-dichloroethane vapour at  $135^{\circ}\text{C}$  has been measured quantitatively and compared with that reported for the vapour at  $170^{\circ}\text{C}$  by previous workers. It has been observed that a catastrophic change in the intensity ratio takes place with the change of state from liquid to vapour phase. The values of the intensity ratio, however, change only very slightly with the change of temperature of the vapour from  $135^{\circ}\text{C}$  to  $170^{\circ}\text{C}$ , so that the difference in energies of the two types of molecules to which the two lines are attributed remains the same in the case of the vapour as in the case of the liquid. It is pointed out that the catastrophic change in the intensity ratio cannot be explained on the assumption that two types of molecules co-exist in the liquid, the relative populations of the molecules depending on their partition functions and energy difference, and that some sort of stronger interaction between the molecules in the liquid state is to be postulated to explain the apparently anomalous results.

In the case of 1, 1, 2-trichloroethane the line  $775\text{ cm}^{-1}$  for the liquid at  $120^{\circ}\text{C}$  is totally absent in the spectrum due to the vapour at  $170^{\circ}\text{C}$ . It is pointed out that this change takes place with the change from liquid to the vapour state., Probable explanation for this phenomenon has been offered.

## INTRODUCTION

The Raman spectra of 1,2-dichloroethane in the liquid and solid phases have been investigated previously by Mizushima *et al* (1938) and Bishui (1948). It was observed that some of the prominent Raman lines disappear when the liquid is solidified. Mizushima *et al* (1938) pointed out that the Raman spectrum of the substance in the solid state can be explained on the assumption that the molecules are of the trans form in the solid state while the Raman lines due to the liquid phase are probably due to two types of molecules, one of the 'trans' configuration and the other of the 'gauche' configuration. They also studied the Raman spectrum of the substance in the vapour state at  $170^{\circ}\text{C}$  (Mizushima *et al*, 1949) and observed that the spectrum corresponds to that due to a mixture of trans and gauche molecules in the ratio 1 : 0.34, while in the liquid state the ratio was found

\* Communicated by Prof. S. C. Sirkar

to be 1 : 1.3. In the solid state the gauche molecules are found to be totally absent and all the molecules are of the trans type (Mizushima *et al*, 1938). It is thus evident that if the ratio of the two types of the molecules depended on temperature alone the proportion of molecules of the gauche type should have been larger in the case of the vapour at 170°C than that in the case of the liquid at room temperature. Actually, however, the proportion diminishes with increase of temperature. This behaviour is thus anomalous. The object of the present investigation was to find out whether at a temperature lower than 170°C the ratio of the intensities of the two lines 768 and 666  $\text{cm}^{-1}$ , assumed to be due to the trans and gauche molecules respectively in the vapour phase, is the same as or different from that observed in the case of the vapour at 170°C. It was also thought worthwhile to investigate whether any other substituted ethane behaves in the same way with the change from liquid to vapour phase as 1,2-dichloroethane. For this purpose the Raman spectrum of 1, 1, 2-trichloroethane in the vapour state at 170°C has been investigated and the results have been discussed in the present paper.

#### EXPERIMENTAL

A Pyrex tube about 6 cm in diameter and 38 cm long was used as the Wood's tube. Requisite quantity of the distilled liquid was introduced in the tube and it was sealed at the tail end after evacuation. The tube was placed in a horizontal cylindrical electric heater provided with two long windows parallel to its axis. The temperature of the vapour was raised to about 135°C and 170°C in the case of 1,2-dichloroethane and 1,1,2-trichloroethane respectively and the vapour filled the tube at pressure of about four atmospheres in both the cases. The temperatures were measured with a mercury thermometer inserted in the heater with tube inserted in it and two mercury arcs running in their positions. There was an excess of liquid in the tube, about 1 c.c. in volume, and this was contained in a blackened bulb at the tail end of the tube. The bulb was connected to the tube through a bent tube so that this liquid was not visible through the window of the Wood's tube. Two long mercury arcs of Pyrex glass made in the laboratory were placed near and parallel to the two windows of the heater and they were focussed on to the Wood's tube with two cylindrical mirrors made of polished aluminium sheets.

An Adam Hilger two-prism glass spectrograph was used to photograph the Raman spectra. The dispersion was about 21 Å per mm. in the 4046 Å region. An exposure of about 100 hours was necessary to record the Raman lines due to the vapour with moderate densities. Ilford Zenith plates taken from a fresh packet were used. Suitable stops were used to prevent extraneous light from entering into the spectrograph. In the case of 1, 2-dichloroethane vapour a strip of black paper was placed in the position of the 435 Å line to cut off this line, so that due to over exposure the line

might not produce blackening in its neighbourhood on the photographic plate.

In order to measure the relative intensities of the lines  $668$  and  $762\text{ cm}^{-1}$  of 1,2-dichloroethane intensity marks were taken on a plate taken from the same packet using light from a tungsten filament bulb reflected from a strip of white unglazed paper and by varying the width of the slit of the spectrograph. The plates containing the Raman spectrum and that containing the intensity marks were developed under identical conditions. Microphotometric records of the lines were taken with a Kipp and Zonen type self-recording microphotometer. The relative intensities of the two Raman lines were found out from the densities of the lines with the help of the blackening log-intensity curves for the two wavelengths corresponding to these two lines drawn with the help of the intensity marks. The background intensities were deducted from the total intensities at the centres of the lines in order to find out the relative intensities of the lines alone. In both cases Raman spectra of the liquids at room temperature and at temperatures slightly below the temperatures of the vapour were also photographed. As the line  $654\text{ cm}^{-1}$  is narrower than the line  $755\text{ cm}^{-1}$  in the case of the liquid as well as the vapour phase the intensities were multiplied by the relative widths of the lines to get the integrated intensities.

## RESULTS AND DISCUSSION

The Raman spectra of 1,2-dichloroethane in the vapour state at  $135^{\circ}\text{C}$  and in the liquid state at  $30^{\circ}\text{C}$  and  $130^{\circ}\text{C}$  are reproduced in the Plate XVII, figures 1(a), 1(b) and 1(c). The spectra for 1,1,2-trichloroethane in the vapour state at  $170^{\circ}\text{C}$  and in the liquid state at  $30^{\circ}\text{C}$  and  $120^{\circ}\text{C}$  respectively, are reproduced in figures 2(a), 2(b) and 2(c) in Plate XVII. The frequency-shifts are given in Tables I and II respectively. Microphotometric records of the lines due to 1,2-dichloroethane having frequency-shifts in the range  $500\text{--}1000\text{ cm}^{-1}$  are reproduced in figure 3.

It can be seen from Table I that when 1, 2-dichloroethane in liquid phase is heated to  $130^{\circ}\text{C}$  its Raman spectrum does not change appreciably. The Raman spectrum, however, undergoes considerable changes with the change from liquid to vapour phase. The lines  $755$ ,  $680$  and  $658\text{ cm}^{-1}$  due to the liquid at  $130^{\circ}\text{C}$  shift respectively to  $762$ ,  $702$  and  $668\text{ cm}^{-1}$  in the case of the vapour at  $135^{\circ}\text{C}$ . Also the lines  $2958$  and  $3005\text{ cm}^{-1}$  due to C-H valence oscillation, shift respectively to  $2972$  and  $3024\text{ cm}^{-1}$  with the change of state mentioned above. As regards the ratio of the intensity of the line  $755\text{ cm}^{-1}$  to that of the line  $654\text{ cm}^{-1}$  quantitative measurement by spectro-photometric method gave the results given in Table III, in which the data reported by Morino *et al* (1941) are also reported.

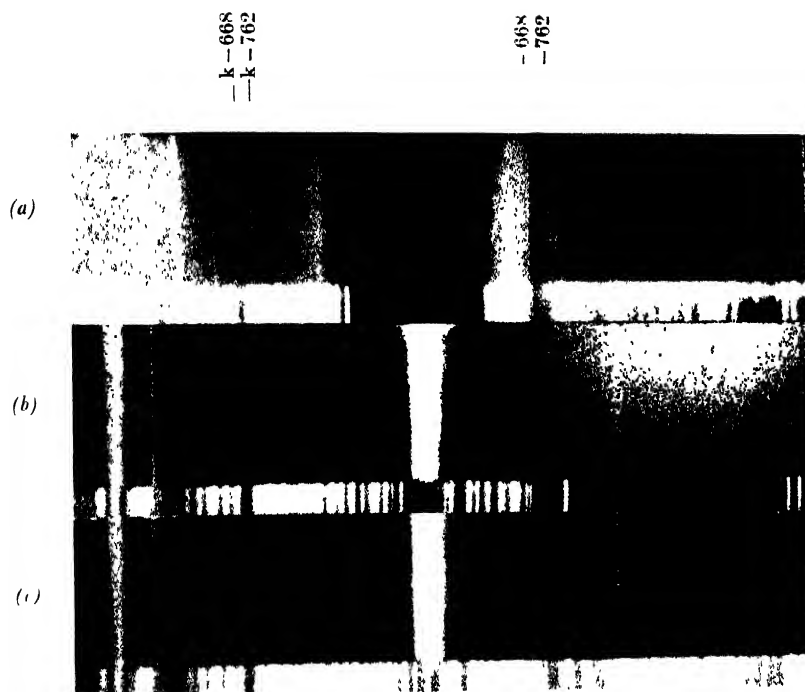


Fig. 1

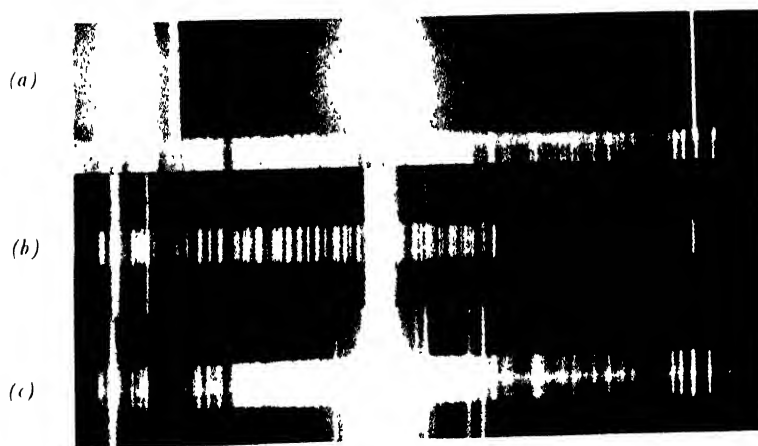


Fig. 2

Raman spectra

Fig. 1. 1, 2-Dichloroethane

(a) Vapour at 135°C

(b) Liquid at 130°C

(c) " " 30°C

Fig. 2. 1, 1, 2-Trichloroethane

(a) Vapour at 170°C

(b) Liquid at 120°C

(c) " " 30°C





TABLE I  
1, 2-Dichloroethane,  $\text{ClCH}_2\text{CH}_2\text{Cl}$ .  
 $\Delta\nu$  in  $\text{cm}^{-1}$

Liquid state		Vapour state.	
at 30°C°	at about 130°C°	at about 135°C°	at about 170°C°, Mizushima <i>et. al.</i> (1949)
128 (3b) e, k	128 (1) e, k		
265 (1) e	265 (1) e		
300 (6) e, k	300 (3) e, k	300 (3) e, k	301 (7)
409 (2) e, k	409 (11b)		
654 (8) e, k	658 (3) e, k	668 (1) e, k	666 (1)
675 (3) e, k	680 (6) e, k	702 (3) e, k	689 (6)
755 (10) e, k	755 (6) e, k	762 (4) e, k	768 (10)
833 (0) e, k	833 (0) e, k		950 (?)
946 (1) e, k	946 (1) e, k		
1051 (0) e, k	1051 (1) e, k		1040 (?)
1150 (0) k	1150 (0) k		
1250 (2) k	1250 (1) k		
1258 (3) e, k	1268 (2) e, k	1300 (1) e, k	1305 (3)
1430 (2) e, k	1430 (1) e, k		
1443 (2) e, k	1443 (1) e, k		
2880 (0) e, k	2880 (0) e, k	2880 (0) e, k	2887 (1) ?
2958 (8) k	2958 (2) k	2972 (3) e, k	2972 (8)
3005 (4b) e, k	3005 (2) e, k	3024 (1b) e, k	2978 (8)

TABLE II  
1, 1, 2-Trichloroethane,  $\text{CHCl}_2\text{CH}_2\text{Cl}$   
 $\Delta\nu$  in  $\text{cm}^{-1}$

Solid state at -180°C° Biswas (1953).	Liquid state.		Vapour state at about 170°C°.
	at 30°C°.	at about 120°C°.	
60 (1) e		118 (1) e, k	
125 (0) e	118 (2b) e, k		
156 (1) e			
263 (2) e, k	190 (1b) e	190 (0) e	
290 (0) e	258 (4) e, k	258 (3) e, k	
338 (3) e, k	287 (2) e, k	287 (1) e, k	
385 (0) e	333 (10) e, k	333 (6) e, k	333 (2) e, k
525 (1) e	390 (4) e, k	390 (2) e, k	
	525 (2) e, k	526 (1) e, k	
	638 (4) e, k	638 (2) e, k	
670 (3) e, k	668 (6) e, k	668 (3) e, k	668 (1b) e, k
	697 (0) e	697 (0) e	
	727 (0) e	727 (0) e	
772 (6) e, k	775 (8) e, k	775 (6) e, k	
	786 (5) e, k	786 (6) e, k	793 (4) e, k
934 (0) e ?	934 (2) e	934 (1) e	
	1041 (1) e, k	1041 (0) e, k	
1260 (0) e	1260 (2) e, k	1260 (1) e, k	
1304 (0) e	1304 (3) e, k	1304 (1) e, k	
1427 (1) e	1430 (3) e, k	1430 (1) e, k	
2961 (4) e, k	2961 (4) e, k	2962 (2) k	2976 (3) k
3005 (3) e, k	3001 (2) e, k	3002 (1) e, k	3001 (1) e, k

TABLE III

Intensity ratio  $I_{755}/I_{654}/(k\text{-excitation})$ 

Present author.			Morino <i>et al</i> (1941).		
Liquid at 30°C.	Liquid at 130°C.	Vapour at 135°C.	Liquid at 25°C.	Liquid at 150°C.	Vapour at 170°C.
1.8 : 1	2.0 : 1	4.5 : 1	1.9 : 1	2.1 : 1	5 : 1

It is thus evident that the line  $755\text{ cm}^{-1}$  not only shifts to  $762$  and  $768\text{ cm}^{-1}$  with vaporization and increase of temperature to  $130^\circ\text{C}$  and  $170^\circ\text{C}$  respectively, but also the ratio of the intensities of the two lines  $755\text{ cm}^{-1}$  and  $654\text{ cm}^{-1}$  increases with the change of state. Further, this ratio is found to be 4.5 : 1 in the case of the vapour at  $130^\circ\text{C}$ , while Morino *et al* (1941) found that in the case of the vapour at  $170^\circ\text{C}$  the ratio is 5 : 1. Hence the ratio changes only slightly with the rise of temperature of the vapour. There are some discrepancies between the results reported by Mizushima *et al* (1949) for the vapour at  $170^\circ\text{C}$  and those obtained in the present investigation. First, in place of the two lines  $2958$  and  $3005\text{ cm}^{-1}$  due to C-H valence oscillations of the 1, 2-dichloroethane in the liquid phase they observed two equally intense lines at  $2962$  and  $2978\text{ cm}^{-1}$  in the case of the vapour at  $170^\circ\text{C}$ . In the present investigation a strong line at  $2972\text{ cm}^{-1}$  and another faint line at  $3024\text{ cm}^{-1}$  have been observed in the case of the vapour at  $135^\circ\text{C}$ . Probably the line  $2972\text{ cm}^{-1}$  has been split up into components at  $170^\circ\text{C}$ , but at  $135^\circ\text{C}$  there is no indication of such a splitting or broadening of the line and the line  $3024\text{ cm}^{-1}$  is definitely present in the spectrum due to vapour at  $135^\circ\text{C}$ . Secondly, the faint line  $680\text{ cm}^{-1}$  due to the liquid at  $130^\circ\text{C}$  has been observed to shift to  $689\text{ cm}^{-1}$  by the authors mentioned above and they have found the intensity of the line to be of the order zero in the vapour state although that of the line  $666\text{ cm}^{-1}$  is 4. In the present investigation it is found that in the case of vapour at  $135^\circ\text{C}$  the line shifts to  $702\text{ cm}^{-1}$  and its intensity is about half that of the line  $668\text{ cm}^{-1}$ . This line can be clearly seen in the microphotometric records reproduced in figure 3.

The general conclusion drawn by Mizushima *et al* (1949) that the ratio of the intensity of the line  $755\text{ cm}^{-1}$  and that of the line  $654\text{ cm}^{-1}$  increases several times with vaporization of the liquid, is confirmed by the results of the present investigation. These results have been interpreted by the authors mentioned above on the assumption that the energy difference of the two types of molecules changes with the change from liquid to the vapour phase. Even if this assumption were correct, the shift and change in the relative intensity of the line  $676\text{ cm}^{-1}$  with vaporisation of the liquid could not be

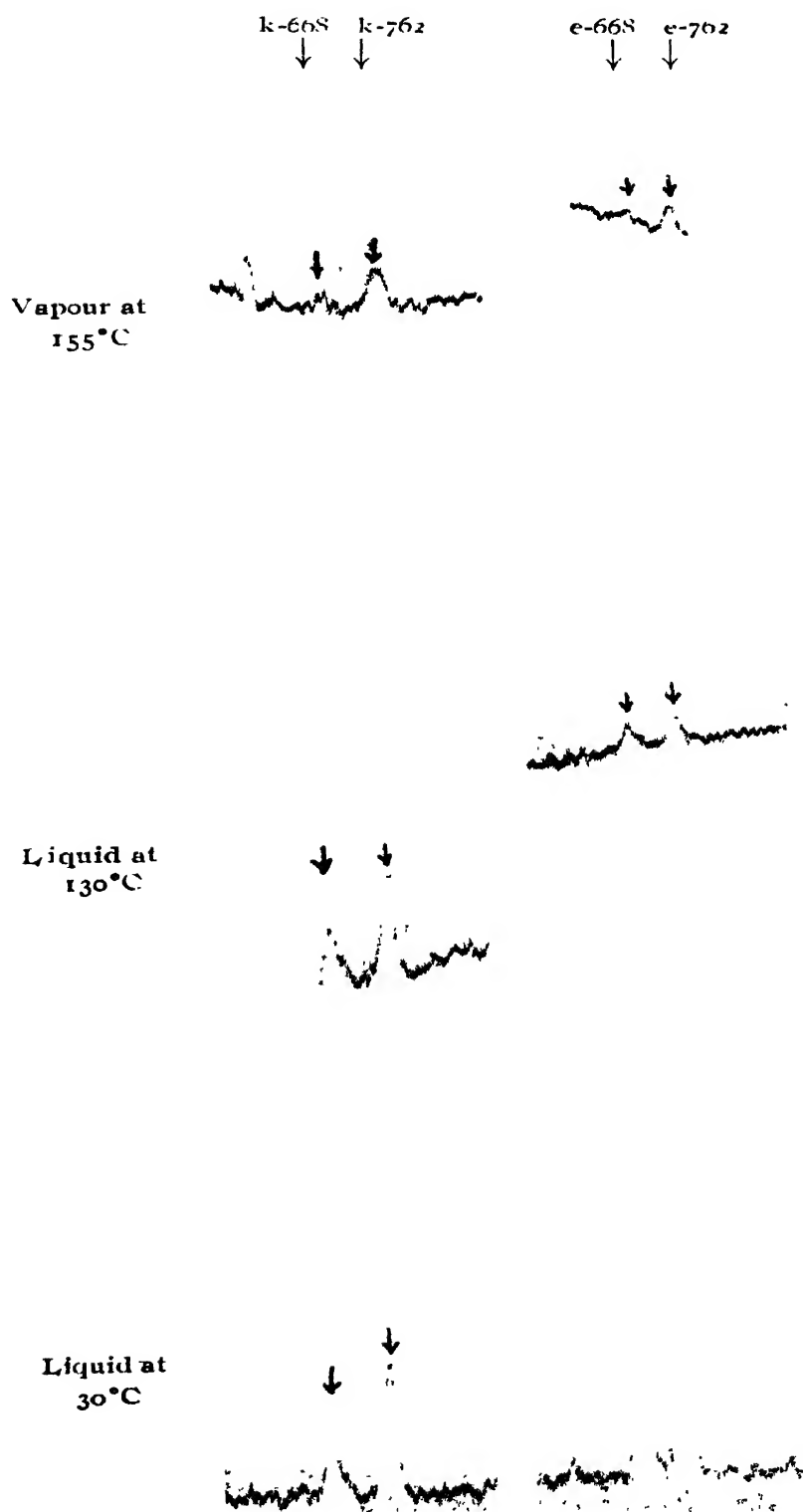


FIG. 3

explained on such a hypothesis. The results of the present investigation show that the ratio of the intensities of the lines  $762$  and  $668\text{ cm}^{-1}$  due to the vapour at  $135^\circ\text{C}$  is  $4.5:1$ , while the value of this ratio reported by Morino *et al* (1941) for the vapour at  $170^\circ\text{C}$  is  $5:1$ . This fact clearly shows that if the two lines  $655\text{ cm}^{-1}$  and  $751\text{ cm}^{-1}$  are attributed to the gauche and trans configurations of the molecules respectively the difference in potential energies of the two types in the vapour state is almost the same as that observed in the case of the liquid. This fact is contradictory to the conclusion arrived at by Mizushima *et al* (1949) that the change in the intensity ratio of the two lines mentioned above is due to a change in the difference of energies of the two types of molecules with vaporisation of the liquid. The ratio of the intensities of the two lines according to their hypothesis would depend on the ratio of partition functions and the difference of energies of the two configurations. The partition function cannot change with the change of state, because the frequencies of vibration do not change appreciably with vaporization. Since the difference in energies of the two forms also remains unaltered with the change from liquid to vapour state, as observed in the present investigation, the catastrophic change in the ratio of intensities of the two lines which takes place with the change from liquid to vapour phase can not be explained by the hypothesis put forward by Mizushima *et al* (1949). An alternative explanation is, therefore, to be found out for this catastrophic change.

The change in the relative intensities of the lines  $658$  and  $755\text{ cm}^{-1}$  with the change from liquid to vapour phase is, however, in the wrong direction, because it was observed by Mizushima *et al* (1938) that the line  $658\text{ cm}^{-1}$  disappears with lowering of temperature and solidification of the liquid. If the change were due to energy difference of two types of molecules the intensity of the  $658\text{ cm}^{-1}$  ought to have increased with increase of temperature of the liquid and the vapour. Actually, the reverse is true. The influence of the surrounding molecules in the liquid and solid states is thus mainly responsible for this anomalous behaviour of the molecule in these states of aggregation. Mizushima *et al* (1949) have stated that the presence of Onsüger field in the liquid is responsible for the change in the energy difference which is observed to take place with the changes from liquid to vapour phase. As pointed out earlier, no such change in the energy difference actually occurs with vaporisation and Onsüger field is not strong enough to produce the large change in the intensity ratio of the two lines mentioned above. Probably, some virtual bond is formed between neighbouring molecules in the liquid state so that the strength of one of the C-Cl bonds may be altered slightly. A satisfactory explanation of the observed changes in intensities of the two lines mentioned above cannot be given without collecting data for a few more molecules of the same type.

It would be interesting to find out whether 1,1,2-trichloroethane which is also a substituted ethane gives such anomalous results. Table II shows

that the intensity of the line  $786\text{ cm}^{-1}$  due to liquid at  $30^{\circ}\text{C}$  increases slightly when the temperature of the liquid is raised to  $120^{\circ}\text{C}$  and that of the line  $775\text{ cm}^{-1}$  diminishes a little. In the case of the vapour at  $170^{\circ}\text{C}$ , however, the latter line is totally absent and only a line at  $793\text{ cm}^{-1}$  is observed. The width of the line at  $793\text{ cm}^{-1}$  is much less than the total width of the doublet  $775$  and  $786\text{ cm}^{-1}$  observed in the case of the liquid phase at  $30^{\circ}\text{C}$ . It was further observed by Biswas (1953) that the line  $780\text{ cm}^{-1}$  is totally absent in the Raman spectrum of the crystals of 1,1,2-trichloroethane at  $-180^{\circ}\text{C}$ . Thus in this particular case the change in intensity of the line with change in state from solid to liquid phase and from liquid to vapour phase is in the same direction. These results can be interpreted by two alternative hypothesis. The lines  $775$  and  $780\text{ cm}^{-1}$  may be due to either two different configurations of the molecule or one may be due to strongly associated molecules in the state of aggregation and the other due to single molecules. In the latter case the vapour state of the substance contains single molecules. The influence of intermolecular field in the liquid state may be responsible for both the change in configuration or formation of virtual bonds between some of the neighbouring molecules and in the solid state all the molecules may be transformed into one of the two types or the associated type. The disappearance of the line  $775\text{ cm}^{-1}$  with vaporisation of the liquid is, however, not due to change of temperature of the molecule but it is due to change of state, because the line is as intense as the line  $786\text{ cm}^{-1}$  even in the case of the liquid at  $120^{\circ}\text{C}$ . Thus in this case also the intermolecular field is responsible for the appearance of this line. It is difficult to understand why the influence of intermolecular field is necessary for the coexistence of two different configurations of the molecule. On the other hand, the appearance of the line  $775\text{ cm}^{-1}$  only in the case of the liquid, may indicate that associated groups of molecules in the liquid are responsible for the origin of this line.

A comparison of the spectra of 1,2-dichloroethane and 1,1,2 trichloroethane in different states and at different temperatures thus shows that the behaviour of the former molecule is extremely anomalous and the hypothesis that two types of molecules coexist in the liquid and vapour phases cannot explain the observed facts satisfactorily.

Investigations with other similar compounds are in progress.

#### ACKNOWLEDGMENTS

The author is indebted to Prof. S. C. Sirkar, D.Sc., F.N.I., for his kind interest and helpful guidance throughout the progress of the work and to the Government of India for the award of a scholarship.

## REFERENCES

- Bishui, B. M., 1948, *Ind. J. Phys.*, **22**, 251.  
Biswas, D. C., 1953, *Ind. J. Phys.*, in Press  
Mizushima, S. and Morino, Y., 1938, *Proc. Ind. Acad. Sci. A*, **8**, 315.  
Mizushima, S., Morino, Y., Watanabe, I., Simanouti, T. and Yamagauchi, S., 1949,  
*Jour. Chem. Phys.*, **17**, 592.  
Morino, Y., Watanabe, I. and Mizushima, S., 1941, *Sci. Papers Inst. Phys. Chem.*  
*Research (Tokyo)*, **39**, 396.

# INTENSITY FORMULÆ FOR BANDS INVOLVING HIGH MULTIPLICITY TERMS. PART I. ${}^5\Sigma-{}^5\Sigma$ AND ${}^6\Sigma-{}^6\Sigma$ TRANSITIONS \*

BY D. PREMASWARUP

DEPARTMENT OF PHYSICS, ANDHRA UNIVERSITY, WALTAIR

(Received for publication, March 21, 1953)

**ABSTRACT.** The intensity expressions for the rotational lines in  ${}^5\Sigma-{}^5\Sigma$  and  ${}^6\Sigma-{}^6\Sigma$  transitions are derived. Representative theoretical curves are drawn for the branches showing the variation of the intensity with  $J$ .

## INTRODUCTION

The intensity distribution in the rotational lines of doublet and triplet bands was worked in detail by Mulliken (1927), Van Vleck (1928), Harls (1935) and others. For bands involving higher multiplicities this was investigated only in a few cases. Budo (1937) gave expressions for the intensity distribution in  ${}^4\Sigma-{}^4\Pi(a)$  and  ${}^4\Sigma-{}^4\Pi(b)$ , while Suryanarayana Rao (1952) calculated the expressions for the  ${}^4\Sigma-{}^4\Sigma$  bands. In the course of a study of the rotational structures of band systems of certain oxides such as CrO, MnO, TaO etc., the need was felt of a knowledge of the theoretical expressions for the intensities and the variation of the intensities with  $J$  in the different branches that are expected of a particular electronic transition. In these bands quintet and sextet terms which may be  $\Sigma$  or  $\Pi$ , may be anticipated. Hence theoretical calculations for the intensity distributions in bands involving these high multiplicities is undertaken at first as a preliminary step to the rotational analysis of these bands. This paper gives expressions derived for the intensities of the rotational lines of  ${}^5\Sigma-{}^5\Sigma$  and  ${}^6\Sigma-{}^6\Sigma$  bands. The other systems will be dealt with in subsequent papers.

## THEORY

Since in  $\Sigma-\Sigma$  transitions both the states always belong to Hund's case(b), the method first given by Mulliken for the doublet bands can be employed here. According to this method the calculation of the intensity factors,  $i$  (or more exactly the squares of the absolute values  $|q|^2$  of the dipole moment matrix elements) is done in two steps. Firstly, since the interaction between  $\Lambda$  and  $N$  giving the resultant  $K$  in case (b) is entirely analogous to that between  $\Omega$  and  $N$  giving the resultant  $J$  in case (a), if the

\* Communicated by Prof. K. R. Rao

fine structure resulting from the interaction between  $K$  and  $S$  is expurgated by averaging over the different  $J$  values consistent with a given  $K$ , the intensity factors for case (b) will be given by the same expressions as those for case (a) which are derived by Hönl and London (1925) if in the latter  $\Omega$  and  $J$  are respectively replaced by  $\Lambda$  and  $K$ . On the other hand, the interaction between  $K$  and  $S$  in case (b) is analogous to the interaction of  $k$  and  $s$  in the ordinary normal atomic multiplets; so that the proper relative intensities of the fine structure lines with different  $J$  but with same  $K$  are given by the same expressions as those give by Sommerfeld and Hönl (1925) for the atomic case when the  $k$  and  $j$  occurring in their expressions are replaced by  $K$  and  $J$  respectively. The superposition of these two expressions will then give the final intensity factors. The complete expressions for the intensities of the band lines assuming thermal equilibrium, in emission are then given by

$$I = g' \nu^A i e^{-E_1 / kT}$$

where  $g'$  is a constant in any one band and the other symbols have their usual significance.

#### CALCULATIONS AND RESULTS

The appropriate Sommerfeld-Hönl equations used here are given below after making the necessary substitutions cited earlier :

For  $\Delta J = \pm 1$  and  $\Delta K = \Delta J$

$$i = [(J+K)(J+K+1) - S(S+1)][(J+K-1)(J+K) - S(S+1)] / JK$$

For  $\Delta J = \pm 1$  and  $\Delta K = -\Delta J$

$$i = [S(S+1) - (J-K)(J-K+1)][S(S+1) - (J-K-1)(J-K)] / JK$$

For  $\Delta J = 0$  and  $\Delta K = \pm 1$

$$i = (2J+1)[(J+K)(J+K+1) - S(S+1)][S(S+1) - (J-K)(J-K+1)] / JK(J+1)$$

The intensities are first calculated according to these expressions. The final intensity factors  $i$ , are then obtained by a proper normalisation of these expressions to agree with the Hönl-London expression which for the particular case  $\Lambda=0$  and  $\Delta K = \pm 1$  (which is the only case we obtain in  $\Sigma - \Sigma$  transitions) is given by

$$i = \frac{2(K^2 - \Lambda^2)}{K} =$$

It is to be noted that in both the above sets of equations wherever  $K$  and  $J$  occur the greater of the two,  $K'$  and  $K''$ , and  $J'$  and  $J''$ , are to be used. The expressions thus obtained in  $K$  are converted into expressions in terms of  $J$ .

Figure 1 gives the transition scheme for the  ${}^5\Sigma - {}^5\Sigma$  bands while in Tables I and II are given the expressions for the intensity factors in terms of  $J$  for  ${}^5\Sigma - {}^5\Sigma$  and  ${}^6\Sigma - {}^6\Sigma$  bands respectively. In both the tables, it is the higher of the two,  $J'$  or  $J''$ , that is to be used for  $J$  in the expressions for the intensities.



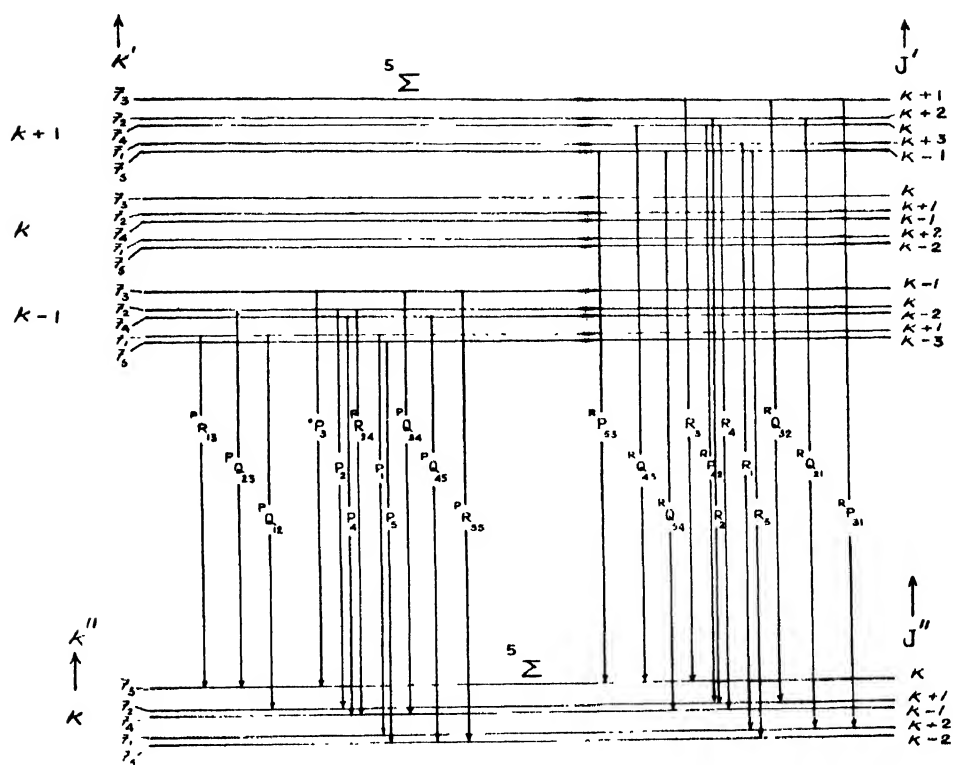


FIG. 1  
Expected branches in  $5\Sigma - 5\Sigma$  transition

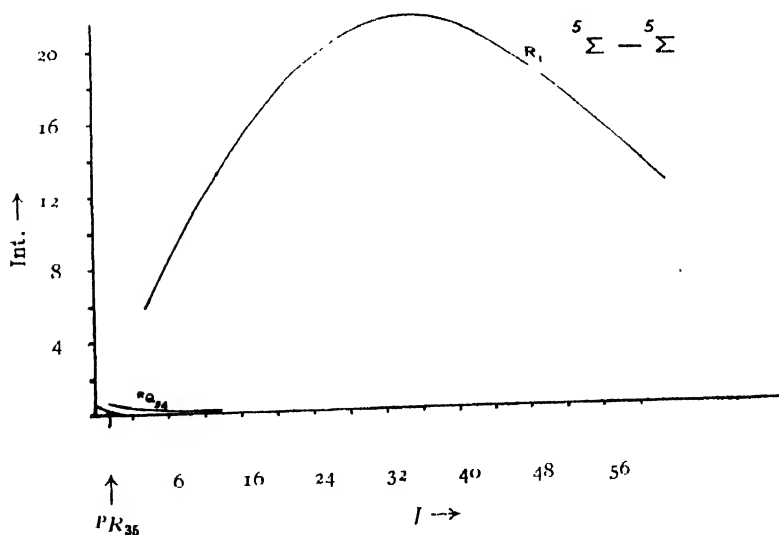


FIG. 2

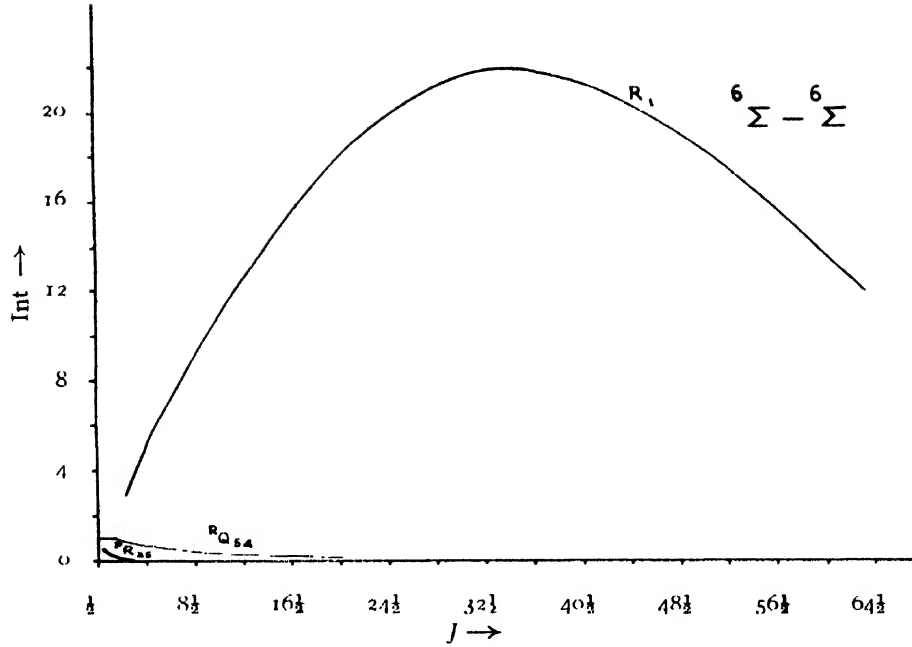


FIG. 3

TABLE I  
Intensity factors for  ${}^5\Sigma - {}^5\Sigma$  bands

Branches	Intensity factor
$P_1$ or $R_1$	$\frac{(2J+1)(J-2)}{(2J-3)}$
$P_2$ or $R_2$	$\frac{(J+1)(2J+1)(J-2)}{J(2J-1)}$
$P_3$ or $R_3$	$\frac{(2J+3)(J+1)(J-1)(J-3)}{(2J+1)J(2J-1)}$
$P_4$ or $R_4$	$\frac{(J+2)(2J-1)(J-1)}{(2J+1)J}$
$P_5$ or $R_5$	$\frac{(J+2)(2J-1)}{(2J+3)}$
$PQ_{12}$ or $RQ_{21}$	$\frac{2(2J+1)}{J(2J-1)}$
$PQ_{23}$ or $RQ_{32}$	$\frac{3(2J+3)(J-1)}{(J+1)J(2J-1)}$
$PQ_{34}$ or $RQ_{43}$	$\frac{3(J+2)(J-1)J}{(2J+3)(J+1)J}$
$PQ_{45}$ or $RQ_{54}$	$\frac{2(2J+1)}{(2J+3)(J+1)}$
$PR_{13}$ or $RP_{31}$	$\frac{6}{J(2J-1)(2J-3)}$
$PR_{24}$ or $RP_{42}$	$\frac{9}{(2J+1)J(2J-1)}$
$PR_{35}$ or $RP_{53}$	$\frac{6}{(2J+3)(2J+1)J}$

TABLE II  
Intensity factors for  ${}^{\infty}\Sigma - {}^{\infty}\Sigma$  bands

Branches	Intensity factor
$P_1$ or $R_1$	$\frac{(2J+1)(2J-5)}{(J-2)}$
$P_2$ or $R_2$	$\frac{(J+1)(2J+1)(2J-5)}{J(J-1)}$
$P_3$ or $R_3$	$\frac{(2J+3)(J+1)(2J-3)(J-1)}{J^2(J-1)}$
$P_4$ or $R_4$	$\frac{(J+2)(2J+3)(J-1)(2J-3)}{(J+1)J^2}$
$P_5$ or $R_5$	$\frac{(2J+5)(2J-1)(J-1)}{(J+1)J}$
$P_6$ or $R_6$	$\frac{(2J+5)(2J-1)}{(J+2)}$
${}^PQ_{12}$ or ${}^RQ_{21}$	$\frac{5(J+1)}{J(2J-1)}$
${}^PQ_{23}$ or ${}^RQ_{32}$	$\frac{2(2J+3)(2J+1)(2J-3)}{(J+1)J^2(J-1)}$
${}^PQ_{34}$ or ${}^RQ_{43}$	$\frac{9(J+2)(2J+1)(J-1)}{(J+1)^2J^2}$
${}^PQ_{45}$ or ${}^RQ_{54}$	$\frac{2(2J+5)(2J+1)(2J-1)}{(J+2)(J+1)^2J}$
${}^PQ_{56}$ or ${}^RQ_{65}$	$\frac{5(2J+1)}{(J+2)(J+1)}$
${}^PK_{13}$ or ${}^RP_{31}$	$J(J-1)(J-2)$
${}^PK_{24}$ or ${}^RP_{42}$	$\frac{18}{J^2(J-1)}$
${}^PK_{35}$ or ${}^RP_{53}$	$\frac{18}{(J+1)J^2}$
${}^PK_{46}$ or ${}^RP_{64}$	$\frac{10}{(J+2)(J+1)J}$

In figures 2 and 3 are shown the variation of the intensities of the band lines with  $J$  for the above two transitions, for some of the typical branches ( $R_1$ ,  ${}^RQ_{34}$  and  ${}^PK_{35}$ ). For the purpose of drawing these curves, thermal distribution corresponding to a temperature of 1500°C is assumed and  $B'$  is assigned the value 0.45. This value is calculated from the empirical relation between  $\omega_e'$  and  $r_e'$  using the  $\omega_e'$  values for  $\text{CrO}$  and  $\text{MnO}$ . The value thus calculated is at least as good as any other arbitrarily chosen value in the absence of one determined from the rotational structure data.

The expressions as well as the curves show that the intensity distribution for these bands is quite similar to that in other  $\Sigma - \Sigma$  bands of lower multiplicities. Thus, the intensity of the main branches ( $P$  and  $R$ ) starts from a low value at low  $J$  values, reaches a maximum at considerably high  $J$  values decreasing thereafter with increasing  $J$ ; the intensity of the satellite branches of the type  $^PQ$  and  $^RQ$  begins with a low value and falls off to still lower values as  $J$  increases, while the intensity of branches of the type  $^PR$  and  $^RP$  is still lower and falls off even more rapidly with increasing  $J$ .

#### ACKNOWLEDGMENT

The author wishes to acknowledge his deep indebtedness to Prof. K. R. Rao under whose invaluable guidance this work is carried out.

#### REFERENCES

- Budo, A., 1937, *Zeit. f. Phys.*, **108**, 73, 579.  
 Eairls, L. T., 1935, *Phys. Rev.*, **48**, 423.  
 Hönl, H., and London, F., 1925, *Zeit. f. Phys.*, **33**, 803.  
 Mulliken, R. S., 1927, *Phys. Rev.*, **30**, 138.  
 Nolan, P., and Jenkins, F. A., 1936, *ibid.*, **50**, 943.  
 Sommerfeld, A., and Hönl, H., 1925, *Sitzungsber. der Preuss. der Wiss., Phys. math. Klasse*, pp. 141.  
 Suryanarayana Rao, K., *Ind. J. Phys.*, (In Press)

# GLOBAL CHARACTERISTICS OF THE SEPARATION BETWEEN THE $F_1$ AND $F_2$ -LAYERS OF THE IONOSPHERE\*

By (Miss) MRINMAYEE GHOSH

, INSTITUTE OF RADIO PHYSICS AND ELECTRONICS, CALCUTTA UNIVERSITY

(Received for publication June 16, 1953)

**ABSTRACT.** Records of a number of ionospheric stations in north and south latitudes have been analysed to study the global characteristics of the seasonal and solar cycle variations of the separation between the  $F_1$  and  $F_2$  layers of the ionosphere. So far as the seasonal variation characteristics are concerned, they are found to be similar to those observed by Appleton for the height variation of the  $F_2$ -region. The variation of the separation with the sunspot activity shows the following unexpected features:

At high latitude stations the separation follows the trend of sunspot activity in local summer. In local winter, however, in such latitudes, there is no association between the two. At stations close to the geomagnetic equator, the separation is related to sunspot activity in an inverse manner in all the seasons. At stations of low intermediate latitudes, no appreciable correlation exists between variation of sunspot activity and the variation characteristics of the  $F_1$ - $F_2$  separation in any season. (The separations all refer to the mean noon values).

The seasonal and latitudinal variations can be explained (if the effect of tidal forces are taken into account) on the basis of the current hypothesis of the composite F-region formation, namely, that the  $F_1$  and  $F_2$  regions belong to a common bank of ionization and two maxima are produced in this common bank due to the peculiar physical characteristics of the atmosphere in this region. Regarding the variation characteristics of the separation with sunspot activity no simple explanation is possible with present state of our knowledge.

## 1. INTRODUCTION

It is well known that the separation between the two ionospheric layers  $F_1$  and  $F_2$  varies with the hour of the day, the season of the year, the latitude of the place of observation and with the phase of the solar cycle. A study of the separation phenomenon on a world-wide scale provides one with materials, on the one hand, for long term prediction of F-region characteristics and, on the other, for testing the correctness or otherwise of the hypotheses suggested regarding the production of these regions.

It is to be mentioned that since the height of the  $F_1$ -region (like that of the  $F_2$ -region) changes only to a small extent with the parameters listed above, study of the variation of the height of the  $F_2$ -region with reference to the ground will also give results similar to that of the study of the  $F_1$ - $F_2$  separation. However, in view of the recent hypothesis, that the two regions  $F_1$  and  $F_2$  belong to the same bank of ionization [Mohler, 1940;

\* Communicated by Prof. S. K. Mitra.

Bates and Massey, 1946; Mitra, 1952; Chatterjee, 1953] (*vide infra*), the latter form of study is more rational.

Results of study of the world-wide seasonal variation of the height of the bottom of the  $F_2$ -layer ( $h' F_2$ ) as has already been made by Appleton (1950), may be mentioned here. These are :

(1) In high latitude stations, northern or southern,  $h' F_2$  is maximum during the summer solstice (that is, in June in northern hemisphere and in December in southern hemisphere).

(2) In low latitude stations, there are two maxima, one in June and the other in December. The one in summer is more prominent, that is the June maximum is more prominent in the northern and the December maximum is more so in the southern hemisphere.

(3) On the geomagnetic equator both the June and December maxima are nearly equally prominent.

(4) The separation increases steadily from low southern latitudes to high northern latitudes in June. In December the state of affairs is reversed.

The maximum variation of  $h' F_2$ , as observed by Appleton, is of the order  $\pm 100$  km. This may be compared with the variation of  $\pm 25$  km of the  $F_1$  layer height and  $\pm 10$  km of the E layer height.

In the present paper, ionospheric data of stations in different latitudes as are available at this laboratory have been utilized for the study of the seasonal, latitudinal and solar cycle variations of the  $F_1$ - $F_2$  separation. For the seasonal variation the data for the year 1951 (low sunspot activity) have been used. The latitudinal variation is studied with the data for the years 1947, 1948 and 1949 (high sunspot activity). The solar cycle variation is examined with the data for the years 1945-52.

So far as the seasonal and latitudinal variations of the  $F_1$ - $F_2$  separation are concerned, the results agree generally with those obtained by Appleton for the  $F_2$ -layer height variation. The variation with solar activity, however, reveals certain new and unexpected characteristics. These, as also the general bearing of the results obtained on the current hypothesis regarding the production of the composite F-region, will be discussed in the following sections.

## 2. RESULTS OF ANALYSIS

*Seasonal variation of separation.* Figures.1(a) and 1(b) depict typical seasonal variation of separation (average monthly midday values) for two high latitude (northern and southern) and two low latitude (northern and southern) stations respectively, selected from amongst a large number of stations studied lying between latitudes  $60^\circ\text{N}$  and  $60^\circ\text{S}$ . It will be noticed that for the high latitude stations, there is only one peak of maximum separation, occurring during the summer solstice, i.e. in June in northern hemisphere and in December in southern hemisphere. For the low latitude stations lying between  $13^\circ\text{N}$  and  $21^\circ\text{S}$ , there are two peaks of maxima,

one in June-July and the other in December-January. It is also to be noted that while for Guam Island, in low northern latitude, the June-July maximum is more prominent, for Rarotonga in low southern latitude, the

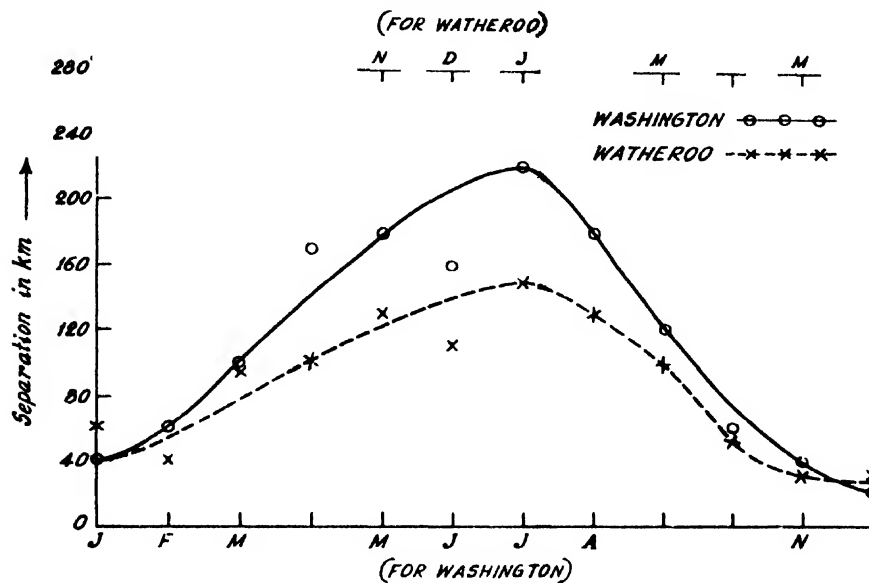


FIG. 1 (a)

Seasonal variation of  $F_1$ - $F_2$  separation for two high latitude stations Washington ( $38.7^\circ$  N,  $77.1^\circ$  W) and Watheroo ( $30^\circ$  S,  $115.9^\circ$  E)

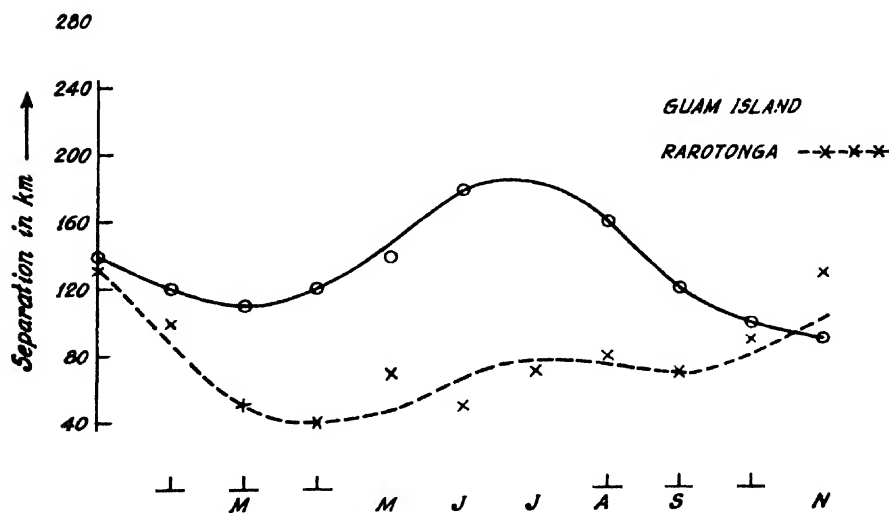


FIG. 1 (b)

Seasonal variation of  $F_1$ - $F_2$  separation for two low latitude stations, Guam Island ( $13.6^\circ$  N,  $144.9^\circ$  E) and Rarotonga ( $21.3^\circ$  S,  $159.8^\circ$  W)

December-January maximum is more prominent. (At Huancayo, near the geomagnetic equator, for which no curve is given the two maxima were found to be of nearly the same amplitude). All these features of the  $F_1$ - $F_2$  separation are in accord with the results obtained by Appleton regarding the variation of the  $F_2$ -layer height as mentioned above.

*Latitudinal variation of separation.* Figures 2 and 3 show the latitudinal distribution of separation (latitude  $70^{\circ}\text{N}$  to  $45^{\circ}\text{S}$ ) during the solstices (June

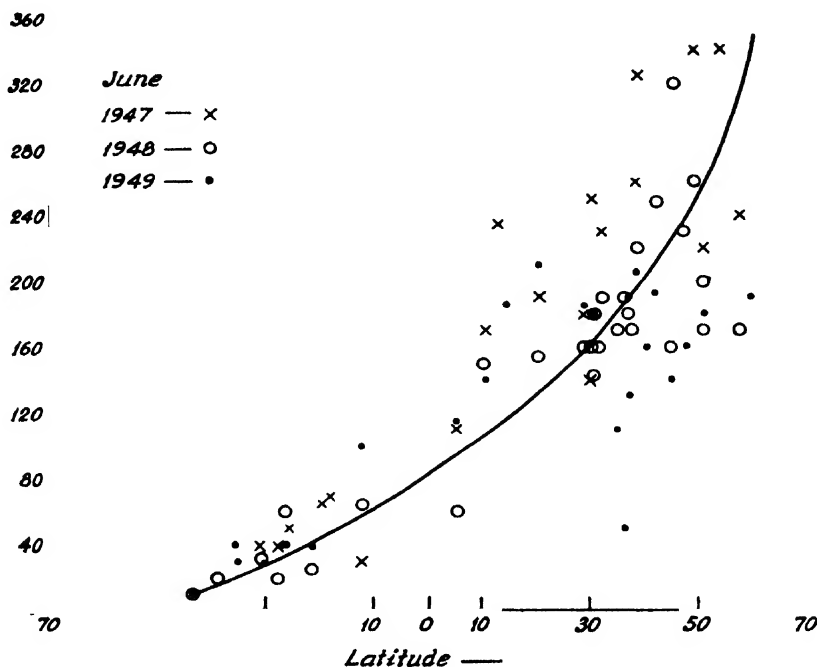


FIG. 2

Latitudinal variation of  $F_1$ - $F_2$  separation in June for the years 1947, 1948 and 1949.

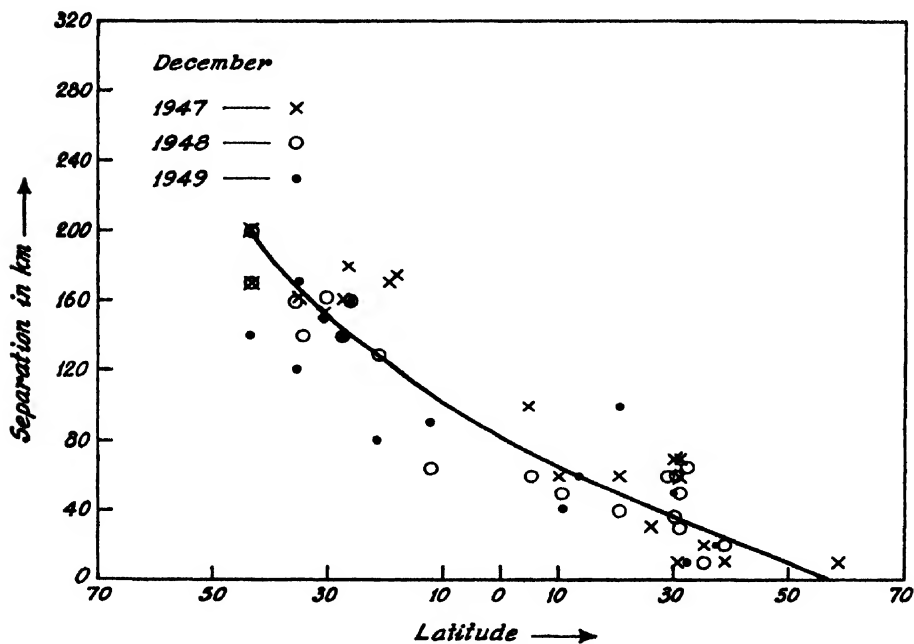


FIG. 3

Latitudinal variation of  $F_1$ - $F_2$  separation in December for the years 1947, 1948 and 1949.



and December). The values for three successive years, 1947-49, rather than those of the year of sunspot maximum (1947) alone, are all plotted. This is because due to the large scatter in the values, the plots for the three years together, years for which the mean sunspot number did not vary greatly, give a better picture of the mean latitudinal variation than the values of a single year. Figure 2 is for the June solstice, when the sun is overhead at  $23.5^\circ\text{N}$  at noon and figure 3 is for the December solstice when the sun is overhead at  $23.5^\circ\text{S}$  latitude at noon. It will be noticed that the general tendency of the separation is to increase from south to north in June and from north to south in December. This tendency is again the same as that observed by Appleton for the  $F_2$ -height variation.

*Solar cycle effect.* Figures 4(a) and 4(b) show how the separation changes with the sunspot activity in the summer solstice months for two high northern and two high southern latitude stations respectively. The stations are: Washington ( $39^\circ\text{N}$ ), Boston ( $42^\circ\text{N}$ ), Johannesburg ( $26.2^\circ\text{S}$ ) and Watheroo ( $30.3^\circ\text{S}$ ). Figure 5 shows the same variation in the winter solstice month. The curves show that while in the local summer month, at all the stations, the separation follows the trend of the increasing and decreasing sunspot activity, in the local winter months there is comparatively little variation of the separation.

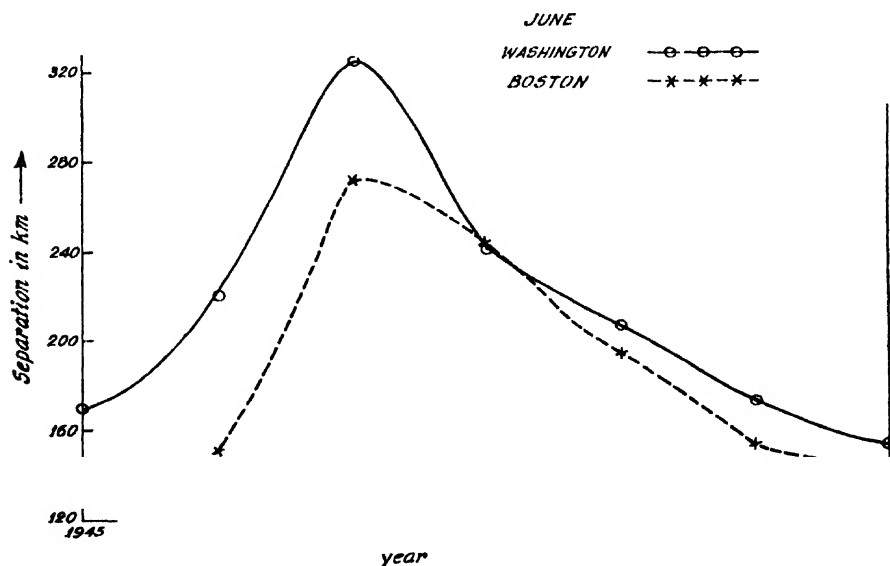


FIG. 4 (a)

Variation of  $P_1$ - $P_2$  separation with the variation of solar activity for two high north latitude stations in the month of June. Note that the variation follows the trend of solar activity, the year 1947 being one of maximum activity. Washington ( $38.7^\circ\text{N}$ ,  $77.1^\circ\text{W}$ ) and Boston ( $42.4^\circ\text{N}$ ,  $71.2^\circ\text{W}$ ).

Figure 6 shows the variation of the separation with sunspot activity for two low latitude stations, Trinidad ( $10.7^{\circ}\text{N}$ ) and Maui ( $20.8^{\circ}\text{N}$ ) for the month of December and June. It will be seen that unlike the curves in figures 4(a) and (b), the variations in all the curves are rather erratic, not following the sunspot trend in a regular manner.

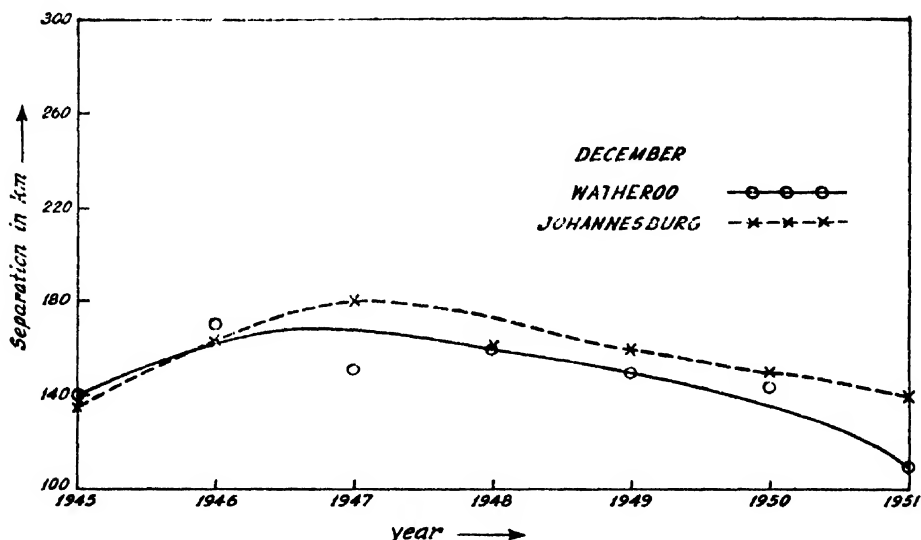


FIG. 4 (b)

Variation of  $F_1-F_2$  separation with sunspot activity for two high south latitude stations in the month of December. Note that the same remark applies as in the case of Fig. 4(a). Watheroo ( $30.3^{\circ}\text{S}$ ,  $115.9^{\circ}\text{E}$ ) and Johannesburg ( $26.2^{\circ}\text{S}$ ,  $28.1^{\circ}\text{E}$ ).

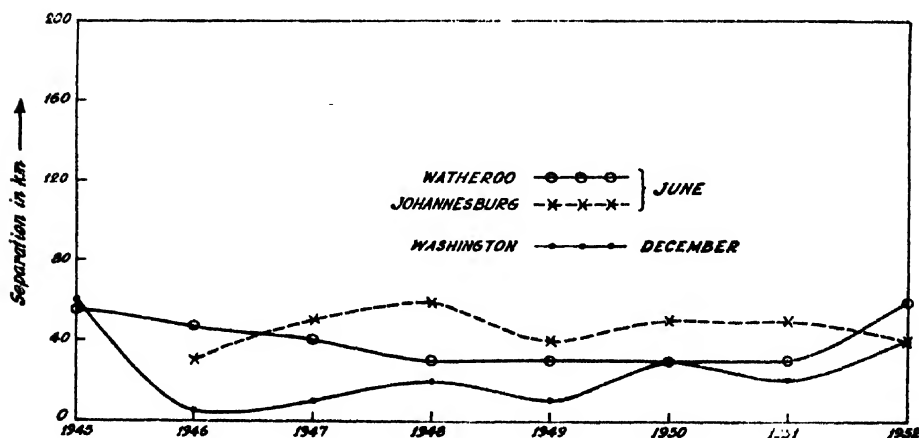


FIG. 5

Variation of  $F_1-F_2$  separation with solar activity for two high south latitude stations in June and one high north latitude station in December. Note that there is scarcely any association between the variation of solar activity and the variation of separation. Watheroo ( $30.3^{\circ}\text{S}$ ,  $115.9^{\circ}\text{E}$ ), Johannesburg ( $26.2^{\circ}\text{S}$ ,  $28.1^{\circ}\text{E}$ ), Washington ( $38.7^{\circ}\text{N}$ ,  $77.1^{\circ}\text{W}$ ).

Figure 7 shows the variation with sunspot activity for the station Huancayo, situated very near the geomagnetic equator, for the months of June and December. We notice here the curious fact that unlike the

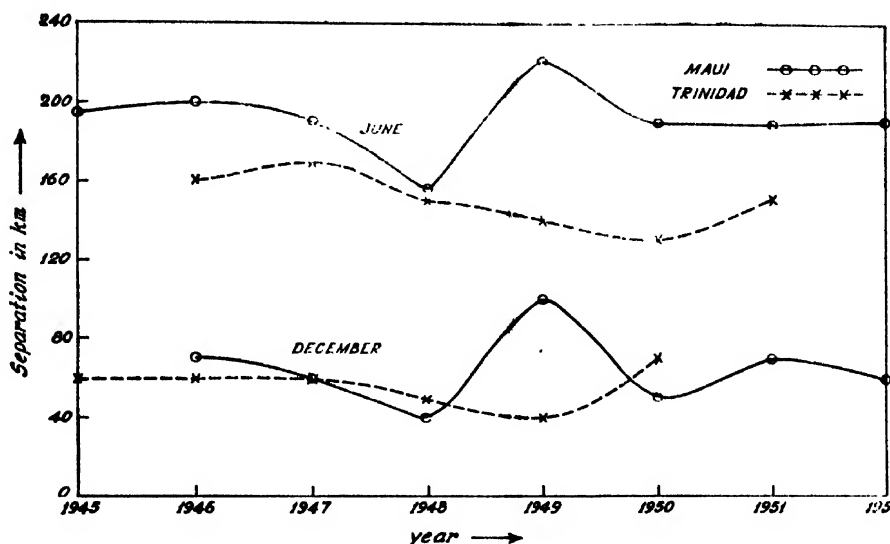


FIG. 6

Variation of  $F_1$ - $F_2$  separation with solar activity for two low latitude stations in the solstice months. Note that there is scarcely any association between sunspot activity and variation of separation either in June or in December Maui ( $20.8^\circ\text{N}$ ,  $156.5^\circ\text{W}$ ) and Trinidad ( $10.7^\circ\text{N}$ ,  $61.6^\circ\text{W}$ ).

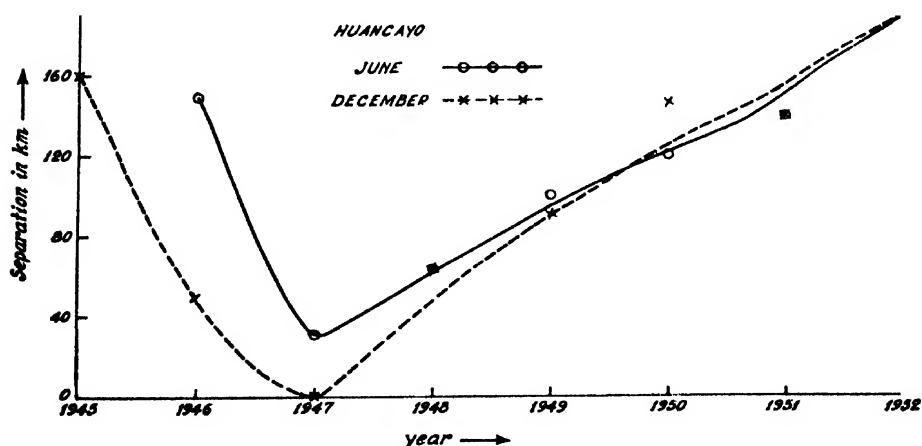


FIG. 7

Variation of  $F_1$ - $F_2$  separation with sunspot activity for Huancayo ( $12^\circ\text{S}$ ,  $75.3^\circ\text{W}$ , close to the geomagnetic equator. Note that the separation follows the trend of solar activity in an inverse manner in both June and December, the year 1947 being one of maximum activity.

variations in high latitude stations, the separation is related to sunspot activity in an inverse fashion, i. e. the separation increases as the sunspot activity decreases and vice versa. The same relation has been found to occur for the months of October and February, when the sun is nearly overhead at Huancayo.

### 3. DISCUSSION

Let us now consider how far the characteristic variations of the  $F_1$ - $F_2$  separation as described in the previous section are explainable on the current hypothesis of the formation of the two regions. As already mentioned, according to this hypothesis, the two maxima  $F_1$  and  $F_2$  belong to a common bank of ionization (produced by the ionization of atomic oxygen at its first ionization potential). In this common bank the lower maximum ( $F_1$ ) is produced by the normal Chapman process and the upper maximum ( $F_2$ ) is developed as a result of the peculiar physical characteristics of this region, namely, rapid rise of temperature and a rapid fall of the effective coefficient of recombination (which decreases with increasing temperature) with height. The former increases the concentration of the atmospheric constituents (including that ionized, viz., atomic oxygen) in the higher regions and the latter increases the ion concentration with height.

The increase in the  $F_1$ - $F_2$  separation in high latitude stations in local summer is evidently an effect of increased temperature in the high regions above the  $F_1$  maximum in this season. The  $F_2$  maximum is formed at a greater height and there is thus increased distance between  $F_1$  and  $F_2$ . The same explanation can be given of the increasing separation in June at noon, as one proceeds from southern to northern latitudes, and in December, as one proceeds from northern to southern latitudes (figures 2 and 3). In both the cases, due to the solar rays becoming less and less inclined to the vertical, there is greater and greater rise of temperature and the  $F_2$  maximum is produced higher and higher up increasing the separation. [The effect of increased temperature on the height of the formation of the  $F_2$ -layer has been fully discussed by Mitra (1952) and by Chatterjee (1953)]. There is, however, one point, in this connection, that needs consideration. The sun is overhead at latitude  $23.5^\circ$  north at noon during the summer solstice. Beyond this latitude the solar rays become more inclined to the vertical. It might, therefore, be thought that towards the pole from this latitude the temperature should also decrease in summer lowering the height of  $F_2$  maximum. Figure 2 and 3 show, however, that the increase in the separation persists well beyond this latitude. The explanation is that though in the higher latitudes the solar rays are incident more obliquely, the days are much longer. For example, at latitude  $40^\circ$ , at 200 km height in summer the sun shines for about 18 hours in 24 hours. Thus, the longer daylight period is able to maintain an average high temperature notwithstanding the larger zenith angle of the sun. The  $F_2$ -maximum is, therefore, formed

at a greater height even in these high latitudes and an increased separation between  $F_1$  and  $F_2$  is maintained.

Regarding the two seasonal maxima in figure 1(b), for the low latitude stations, one may be tempted to explain them also as due to the summer temperature rise (as in the case of the high latitude stations), because, of low latitude stations, the sun is overhead twice a year, and there are two summers, so to speak. However, it is noticed that the maxima occur in the same months, December and June, in all the latitudes studied, and not in the summer months which vary from latitude to latitude. In fact, in these latitudes the sun is nearly overhead all the year round and, as such, there cannot be any marked variation in temperature from month to month. The cause of these two maxima has, therefore, to be sought elsewhere. A possible explanation is that they are due to tidal effects, as are expected from Martyn's electrodynamical theory of tides, in the ionosphere. According to this theory, the motion of the ions due to tidal forces, has a strong vertical component. As a result of this vertical drift of ions, the diurnal and seasonal variations of both  $N_{\max}$  and  $h F_2$  become markedly different from those expected of a simple Chapman region (Mitra, 1950). It has been shown by a closer examination of the vertical drift effect, that at low latitude and equatorial stations the  $F_1$ - $F_2$  separation would attain maximum value both in December and in June (Chatterjee, 1953). The drift velocity also affects the separation in high latitude stations. But, as shown above, the major features of the variation of separation can be understood, at least, qualitatively, if the rise of temperature in the summer months is taken into account.

In regard to solar cycle variation we note that the curves in figures 4(a) - 7 indicate that for stations close to the geomagnetic equator, the  $F_1$ - $F_2$  separation follows the trend of sunspot activity in an inverse manner in all the months of the year. In high latitude stations, on the other hand, the  $F_1$ - $F_2$  separation follows the trend of sunspot activity in a direct manner, and that it does in summer months only, there being no association in the winter months. In low latitude stations, in no month of the year, there is any clear association between the variations of the sunspot activity and the separation. It is, however, to be noted that so far as the intensity of the ionization is concerned, it follows the trend of sunspot activity in all latitudes and in all months. It is, therefore, difficult to explain on any simple theory the anomalous behaviour of the variation of the  $F_1$ - $F_2$  separation in course of a sunspot cycle in different latitudes and in different months. One must wait for more observational results before attempting any explanation.

#### ACKNOWLEDGMENTS

The present work forms part of the programme of the Radio Research Committee of the Council of Scientific and Industrial Research, Government

of India and the author wishes to express her thanks to the Council for financial assistance during the work.

It is a pleasure to acknowledge debts to Professor S. K. Mitra for helpful guidance and interest throughout the progress of the work.

#### REFERENCES

- Appleton, E. V., 1950, *Jour. Atmos. Terr. Phys.*, **1**, 106.  
Bates, D. R. and Massey, H. S. W., 1946, *Proc. Roy. Soc. A*, **187**, 24.  
Chatterjee, R., 1953, "On the Ionization Distribution of the F-region". Communicated to the *Proc. Phys. Soc. (Lond.)*  
Martyn, D. F., 1947, *Proc. Roy. Soc. A*, **189**, 241.  
Mitra, A. P., 1950, *Ind. Jour. Phys.*, **24**, 387.  
Mitra, A. P., 1952, *Ind. Jour. Phys.*, **26**, 79.  
Mohler, R. L., 1940, *Bull. Std. Jour. Res.*, **25**, 50.

# ON THE LAW OF THE VARIATION OF E-REGION MAXIMUM WITH THE ZENITH DISTANCE OF THE SUN \*

By A. K. SAHA

INSTITUTE OF RADIO PHYSICS AND ELECTRONICS, UNIVERSITY COLLEGE OF SCIENCE, CALCUTTA

(Received for publication, July 17 1953)

**ABSTRACT.** The diurnal records of E-layer critical frequency ( $f^oE$ ) at Calcutta for the years 1949-52 are analysed to determine the value of  $n$  in Chapman's formula  $f^oE = f_0 (\cos \chi)^n$ .  $n$  is found to vary from 0.15 to 0.50 instead of remaining constant at the Chapman value of 0.25. The sub-solar frequency  $f_s$  also undergoes similar variations. There appears to be a seasonal component of  $n$  and  $f_s$ -variations which is most marked in the years 1950 and 1951. The mean trend of these variations follows that of the 12-month running average Zürich sunspot number. The results obtained are discussed in relation to those obtained by previous workers. The departures from the Chapman law may be attributed to changes in the height distribution of  $O_2$  in the transition region (where the atmospheric composition changes from one of  $O_2$  and  $N_2$  to one of  $O$  and  $N_2$ ) where the E-region is formed by the ionization of  $O_2$ . Detailed study of the variations of  $n$  and  $f_s$  will be helpful in the for accurate prediction of E-region transmission conditions.

## 1. INTRODUCTION

According to the well known Chapman process of formation of the ionospheric layers, the maximum ionization density for a layer, under equilibrium condition, varies as  $\sqrt{\cos \chi}$ , where  $\chi$  is the zenith distance of the sun. Records of observation show, however, that this law is obeyed only approximately for the case of the E and  $F_1$ -regions and very often not at all for the  $F_2$ -region. The subject of  $F_2$ -variation has received wide attention and many hypotheses have been put forward to explain its anomalous behaviours. The E and  $F_1$ -variations, however, appear to have received lesser attention. This is possibly because the departure of the variations from the  $\sqrt{\cos \chi}$ -law had been supposed to be only of minor importance. In recent years, however, the subject is being discussed by ionospheric workers and a number of investigations have been made, particularly to understand the morphology of the E and  $F_1$ -layer variations with zenith angle of the sun in different seasons and latitudes, and with the phase of the solar cycle. In the present paper the results of some studies that have been made for the latitude of Calcutta on the nature of the variation of E-layer maximum with  $\chi$  will be described. To understand better the significance of the results obtained a brief resumé will first be given of the investigations already made on the subject.

\* Communicated by Prof. S. K. Mitra

## 2. A RESUME OF CONTEMPORARY WORK ON THE SUBJECT

As mentioned in the introduction, according to Chapman's theory (Chapman, 1931) of ionized layer formation, the maximum ionization density of the layer, under equilibrium condition, varies as  $\sqrt{\cos \chi}$ , where  $\chi$  is the solar zenith angle. Since the penetration frequency ( $f$ ) of the incident wave (for a given angle of incidence) varies as the square root of the maximum ionization density, we write

$$f = f_s (\cos \chi)^n$$

where  $n=0.25$  and  $f_s$  is the sub-solar penetration frequency, that is, the penetration frequency when the sun is at the zenith.

The above law is found to hold generally for the E-layer except that the exponent  $n$  of  $\cos \chi$  is found to be different from 0.25. The value of  $n$  that gives the best fit with the observed results can be determined conveniently by plotting  $\log f$  against  $\log \cos \chi$ . One obtains a straight line and the slope of the line gives the value of  $n$ . The value of  $f_s$  is obtained by extrapolation of the straight line to  $\chi=0^\circ$ .

According to Tremmellen and Cox (1947) the average value of  $n$  at moderate latitudes may be taken as 0.31. They have also suggested a linear variation of  $f_s$ , with the sunspot number  $R$ , given approximately by the expression

$$f_s = 3.3(1 + 0.00228 R)$$

Harnischmacher (1951) has studied the month to month variations of the value of  $n$  for the stations Huancayo ( $12.0^\circ\text{S}$ ) Washington ( $38.7^\circ\text{N}$ ), Kochel ( $47.7^\circ\text{N}$ ) and Watheroo ( $30.3^\circ\text{S}$ ). He found the values to lie between 0.25 and 0.40, with a few exceptions. A seasonal variation of  $n$  was apparent at Washington with minima in winter and maxima in summer. At the other three stations no such regular variation could be observed, though, the value of  $n$  varied considerably from month to month. The value of the sub-solar penetration frequency  $f_s$  was found to be closely related to the sunspot number. It was different for the four different stations, being highest for Huancayo.

Values of  $n$  and  $f_s$  for the months of May, June and July for the years 1949 and 1950 have been derived by Scott (1952) for a large number of stations distributed throughout the globe. He found the average value of  $n$  to be about 0.33 at moderate latitudes, dropping sharply to between 0.10 and 0.20 near the north auroral zone and recovering again to 0.25 further north. Another sharp drop was found to appear at Calcutta (geomagnetic latitude  $12^\circ\text{N}$ ).

Scott has also studied the seasonal and solar cycle dependence of  $n$  and  $f_s$  at the Canadian stations, Ottawa ( $45.4^\circ\text{N}$ ), St. John's ( $47.6^\circ\text{N}$ ), Prince Rupert



(54.3°N) and Churchill (58.8°N)  $n$  and  $f_s$  were found to rise and fall together month by month. At Ottawa and Prince Rupert a seasonal variation was found with the minima occurring regularly in winter and the maxima either at the equinoxes or in summer. An approximately linear relationship was also found between  $f_s$  at these two stations and the 12-month running average sunspot number  $S$ , given by

$$f_s = 3.2 + 5.5 \times 10^{-3} S$$

### 3. ANALYSIS OF CALCUTTA DATA

The data for the period, June 1949 to December 1952, as recorded at the Ionosphere Laboratory, Calcutta (22.6°N) have been analysed for the determination of the monthly values of  $n$  and  $f_s$ . The method adopted for the determination was the same as explained in Sec. 2. The hourly mean values of  $f^oE$  for the months were plotted against the hourly mean values of  $\log \cos \chi$  on semi-log graph.  $n$  was obtained from the slope of the curve and  $f_s$  determined by extrapolation to  $\chi=0^\circ$ . Observations for zenith angles greater than  $84^\circ$  were omitted, as, for such large zenith angles, the  $\sqrt{\cos \chi}$ -law of Chapman ceases to hold. Two typical  $f^oE$ - $\log \cos \chi$  curves are shown in figure 1.

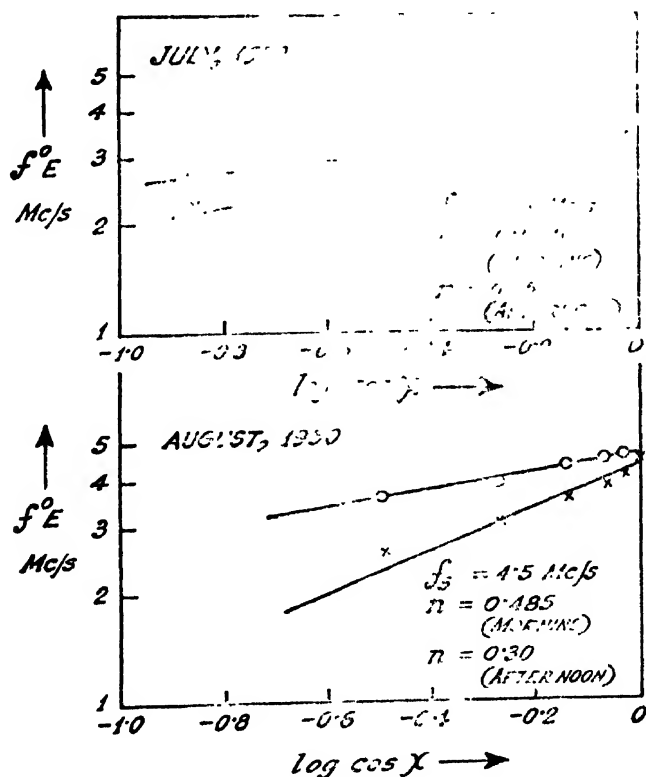


FIG. 1  
Typical  $f^oE$  vs  $\log \cos \chi$  curves showing the relation between  $f^oE$  and solar zenith angle  $\chi$ .

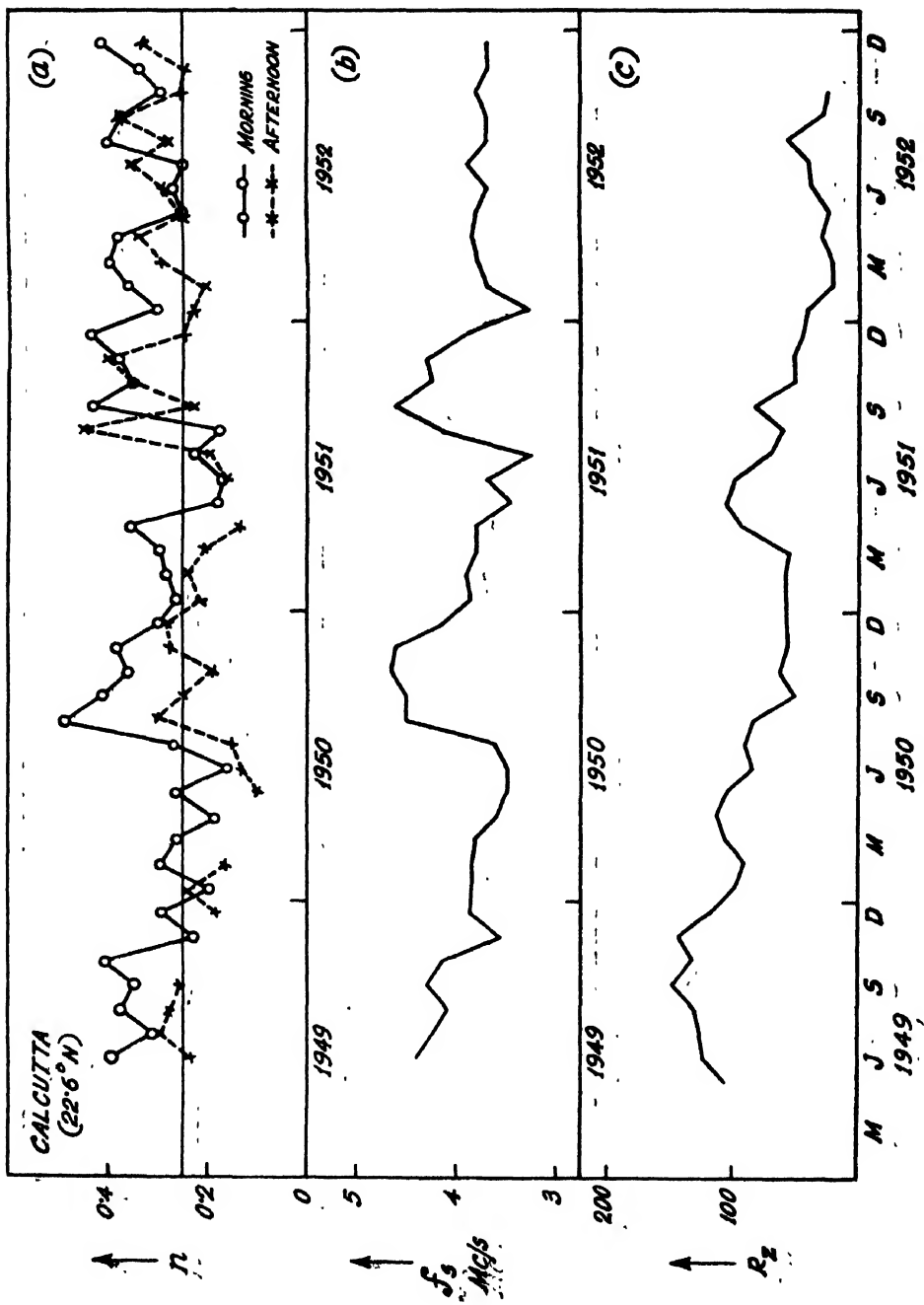


FIG. 2

The month to month variations of  $n$  and  $f_s$  at Calcutta from June 1949 to December 1952 [curves (a) and (b)]  
Curve (c) shows the monthly mean values of the Zürich sunspot number ( $R_z$ ).

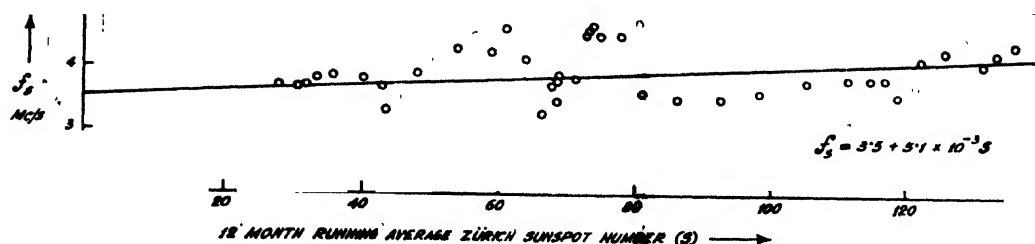


FIG. 3

The dependence of the sub-solar frequency  $f_s$  on the 12-month running average sunspot number  $S$ .

The month to month variations of  $n$  and  $f_s$  during the period under review are depicted in curves (a) and (b) in figure 2. Curve (c) shows the month to month variations of the Zürich sunspot number. It will be noted that the variations of  $n$  and  $f_s$  [curves (a) and (b)] are more or less parallel. There appears to be some sort of seasonal variation in both the  $n$  and  $f_s$ -curves, the variations being most marked for the years 1950 and 1951. A comparison of curves (b) and (c) shows, however, that what appears to be a seasonal variation of  $f_s$  may also be interpreted as a sort of rough inverse correlation between  $f_s$  and sunspot number variation. The  $f_s$ -variation has also a general tendency of following the trend of sunspot activity. In figure 3, the monthly mean values of  $f_s$  have been plotted against the 12-month running average sunspot number. The straight line giving the best fit is represented by

$$f_s = 3.5 + 5.1 \times 10^{-3} S$$

The values of  $f_s$  undergo large deviations about this mean trend.

## 5. DISCUSSION

The apparent seasonal variations of  $n$  and  $f_s$  at Calcutta and their parallelism, as seen in curves (a) and (b) of figure 2 are effects similar to those observed at Washington (Harnischmacher, 1951), Ottawa and Prince Rupert (Scott, 1952). However, it is to be noted that the phase of the Calcutta variations is different from that of Washington. At Washington the minima occur in winter and the maxima in summer, while at Calcutta the minima occur in summer and the maxima in autumn. Further, as already mentioned, regular seasonal variation has not been observed at all the stations studied, though, large month to month variations have been noted at Huancaayo, Kochel, Watheroo (Harnischmacher, 1951). This is also confirmed by the analysis of the Singapore records by the author as depicted in figure 4. It will be seen that though the general trend of the curve follows the sunspot activity (as at other stations) there is little or no seasonal variation.

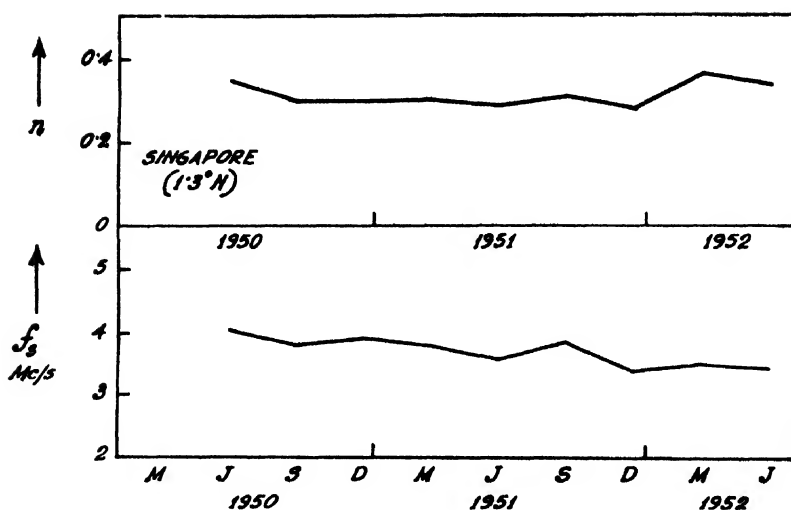


FIG. 4  
The variations of  $n$  and  $f_s$  at Singapore.

One interesting fact may be mentioned in this connection. As already mentioned, Scott in his study of the latitudinal variation of  $n$  (from analysis of the May, June, July records of 1949, 1950 of a number of stations), found that there is an unexpected drop in the value of  $n$  at Calcutta in the latitude variation curve. This he has explained as due to abnormal E-ionization which is very frequent at Calcutta in summer. The explanation is, however, not tenable, as the  $f^\circ E$  data, as recorded at Calcutta, are carefully made free from sporadic E-contamination. The result obtained by Scott is merely the effect of the apparent seasonal variation of  $n$  at Calcutta with the minima in summer.

Attempts have been made to explain the deviation of  $n$  from the Chapman value of 0.25 as due to variations in the scale height ( $H$ ) and recombination co-efficient ( $\alpha$ ) in the region of the E-layer.

According to Pfister (1950),  $H$  has a maximum around noon and the diurnal variation of  $H$  may be represented by some positive power of  $\cos \chi$ . However, a variation of  $H$  (*i.e.*, temperature) also causes a variation in the effective recombination co efficient  $\alpha$ , given by

$$\alpha = \alpha_0 \left( \frac{T}{T_0} \right)^r$$

where  $r \approx -1$  (Mitra and Jones, 1953). This would leave the maximum ionization in the Chapman formula

$$N_m^2 = \frac{Q}{\alpha H_0} \cos \chi$$

unaltered. Pfister has also shown that the combined influence of a linear scale height gradient ( $H$  increasing with height) and a recombination

co-efficient dependent only on the E-region maximum ionization would again leave  $N_m^*$  unaffected.

Nicolet (1950) has considered  $\alpha$  as a function of molecular concentration ( $\alpha$  decreasing with height). His analysis shows that the combined influence of such a gradient of  $\alpha$  and a linear gradient of scale height may lead to values of  $n$  above the normal 0.25 level. However, there are cases (*e.g.* Calcutta in summer) where  $n$  is less than 0.25. This, according to Nicolet's assumptions, is only possible if the scale height gradient becomes negative. This is improbable, since the temperature in the E-region is known to increase with height (*e.g.* rocket flight data).

Perhaps a solution of these difficulties may be found if the current theory of the E-layer formation is considered. According to this theory the E-ionization is due to ionization of molecular oxygen in the transition layer where the atmospheric composition changes rapidly from one of  $N_2$  and  $O_2$  to one of  $N_2$  and  $O$  due to dissociation of  $O_2$  by solar radiation ( $\lambda < 1760\text{\AA}$ ). The concentration of  $O_2$  in the transition layer decreases rapidly with height, the rate of dissociation being controlled principally by the physical processes controlling the dissociation equilibrium and not by the value of  $H$  as in the case of an isothermal atmosphere following Dalton's law. E-ionization with the solar zenith angle is, therefore, not expected to follow Chapman law of variation which is deduced on the assumption that the height variation of molecular concentration follows the simple exponential law of Dalton. The fact that it does so approximately is because investigations have shown that the decrease of  $O_2$  concentration with height in the transition layer follows approximately an exponential law, the constant factor in the exponent then taking the place of  $H$  in Chapman's formula. The observed departures from the Chapman variation are thus traceable to the departures of the height variation of  $O_2$  concentration from the exponential law. Further, as the value of the effective  $H$  must, of necessity, change with the solar zenith angle and with intensity of emission of the dissociating radiation from the sun, the values of  $n$  and  $f_1$  must also vary correspondingly. Also, it is likely that the dissociating solar radiation producing the transition layer ( $\lambda < 1760\text{\AA}$ ) and the ionizing radiation producing the E-layer [ $\lambda 900-1000\text{\AA}$  (Nicolet, 1945) or 325 eV photons (Hoyle and Bates, 1948)] vary independently of one another with the solar activity. This will tend to destroy any close parallelism between E-ionization variation and solar activity variation which may otherwise be expected. It is also not difficult to imagine that as a result of this, coupled with the variation of recombination co-efficient with height (due to variation of temperature), the ionization may vary in an inverse manner with solar activity as it appears from curves (b) and (c) in figure 2. However, detailed investigation of these problems is beyond the scope of the present paper and is left for future study.

In conclusion, attention, is drawn to the desirability of taking into account the great variability of the value of  $n$  in predicting transmission condition *via* E-layer. At present  $f^oE$  predictions are generally made with  $n=0.25$ , that is, on the assumption of  $\sqrt{\cos \chi}$ -law. Tremmellen and Cox (1947) have pointed out in this connection that a better value of  $n$  would be 0.31 instead of 0.25. But, in view of the abnormally high to abnormally low values (0.10 to 0.50) that  $n$  may take, assumption of a fixed value of  $n$  will lead to erroneous result. Further, the sub-solar frequency  $f_s$ , though found to follow the general trend of the solar cycle (similar to that assumed by Tremmellen and Cox and by Scott), is found to undergo large variations round the mean trend. All these factors have to be taken into account for more accurate prediction of the E-layer transmission conditions. And this will only be possible when characteristics of  $n$  and  $f_s$  variations are available over longer periods and from a larger number of stations distributed over the globe.

#### ACKNOWLEDGMENTS

The author is grateful to Professor S. K. Mitra for his kind advice and guidance during the progress of the work. The author's attention to the problem was drawn by Mr. A. P. Mitra (Visiting Professor at Pennsylvania State College) in a private communication.

The work forms part of the programme of the Radio Research Committee of the Council of Scientific and Industrial Research, Government of India, and the author wishes to express his thanks to the Council for financial assistance.

#### REFERENCES

- Chapman, S., 1931, *Proc. Phys. Soc.*, (London), **43**, 26.  
 Harnischmacher, E., 1951, *C. R. Acad. Sci.*, (Paris), **230**, 1301.  
 Hoyle, F. and Bates, D. R., 1948, *Terr. Mag. Atmos. Elec.*, **53**, 51.  
 Mitra, A. P. and Jones, R. E., 1953, Scientific Report No. 44, p. 55, Ionosphere Research Laboratory, Pennsylvania State College.  
 Nicolet, M., 1945, *Mén. Roy. Met. Inst.*, (Belgium), **19**, 124.  
 Nicolet, M., 1950, Proceedings of the Conference on Ionospheric Physics, Pennsylvania State College, p. VI-10.  
 Pfister, W., 1950, Proceedings of the Conference on Ionospheric Physics, Pennsylvania State College, p. TI-19.  
 Scott, J. C. W., 1952, *J. Geophys. Res.*, **57**, 362.  
 Tremmellen, K. W. and Cox, J. W., 1947, *J. Inst. Elec. Engineers*, **94**, Pt IIIA 200.

# STRESS DISTRIBUTION IN AN INFINITE PLATE WITH AN ELLIPTIC HOLE ACTED UPON BY A FORCE AND A COUPLE AT AN INTERNAL POINT \*

BY B. KARUNES

DEPARTMENT OF APPLIED PHYSICS, UNIVERSITY COLLEGE OF SCIENCE AND TECHNOLOGY, CALCUTTA

(Received for publication, March 2, 1953)

**ABSTRACT.** The Function theoretic method of Muschelisvili (1933) for solving two dimensional problems in elasticity is employed to obtain solutions of the problems of stress distribution in a large plate containing an elliptic hole under the action of an isolated force or a couple at any point inside the plate. From these solutions particular cases of the force and couple acting on the boundary of the hole are derived and the results are compared with those obtained by Rothman (1950), who used complex potentials as introduced by Stevenson (1945).

## INTRODUCTION

In a recent paper Rothman (1950) has obtained the solution of the problems of stress distribution in an infinite plate with elliptic and circular holes under the actions of isolated forces on the boundary of the hole. Following Stevenson (1945), he has introduced two functions  $\Omega(z)$  and  $\omega(z)$ , in terms of which the stresses can be expressed. In the present paper the solution is given of the problems of stress distribution in an infinite plate with an elliptic hole under the action of an isolated force or a couple at any point inside the plate. The method of Muschelisvili (1933) has been followed here. It may be mentioned that the complex stress functions introduced by Muschelisvili are connected with the complex potentials introduced by Stevenson. One of the functions of Stevenson is a constant multiple of one of the functions of Muschelisvili and the derivative of the second function of Stevenson is a constant multiple of the second function of Muschelisvili. Rothman's problems appear as particular cases of the problems solved here, if we make the point where the force is applied tend to the boundary of the hole. Another particular case is the problem of an infinite plate with a circular hole acted upon by a force at an internal point. This problem has been solved by Sen (1945) by a method which he has developed in the case of a force acting along a radius of the hole.

\* Communicated by Prof P. C. Mahanti

It has been shown by Muschelisvili (1933) that in state of generalised plane stress the stress combinations  $\widehat{xx} + \widehat{yy}$  and  $\widehat{yy} - \widehat{xx} + 2i\widehat{xy}$  of the average stresses are given by

$$\begin{aligned}\widehat{xx} + \widehat{yy} &= 4 \times \text{real part of } \phi_1'(z) \\ 2 &= [\phi_1'(z) + \bar{\phi}_1'(\bar{z})] \end{aligned} \quad \dots (1)$$

and

$$\widehat{yy} - \widehat{xx} + 2i\widehat{xy} = 2[z\phi_1''(z) + \psi_1'(z)] \quad \dots (2)$$

where  $\phi_1(z)$  and  $\psi_1(z)$  are two analytic functions of  $z (= x + iy)$  and a bar over a function represents the complex conjugate of the function.

The resultant traction across an arc  $AB$  (which the material on the right exerts on the left) is given by

$$X + iY = -i[\phi_1(z) + z\bar{\phi}_1'(\bar{z}) - \bar{\psi}_1(\bar{z})]_A^B \quad \dots (3)$$

and the moment of the traction across  $AB$  about the origin is given by

$$M_0 = \text{real part of } [-z\bar{z}\phi_1'(z) - z\psi_1(z) + \psi_2(z)]_A^B \quad \dots (4)$$

The displacements are obtained from the relation

$$2\mu(u + iv) = K\phi_1(z) - z\bar{\phi}_1'(\bar{z}) - \psi_1(\bar{z}) \quad \dots (5)$$

where

$$K = \frac{\lambda' + 3\mu}{\lambda' + \mu}.$$

To determine  $\phi_1(z)$  and  $\psi_1(z)$  when stresses are prescribed on the boundary, we have from (3)

$$\left. \begin{aligned} \phi_1(z) + z\bar{\phi}_1'(\bar{z}) + \bar{\psi}_1(\bar{z}) &= f_1 + if_2 \\ \bar{\phi}_1(\bar{z}) + z\phi_1'(z) + \psi_1(z) &= f_1 - if_2 \end{aligned} \right\} \quad \dots (6)$$

where

$$f_1 + if_2 = i \int_{n_s}^n (F_1 + iF_2) dS + \text{constant}.$$

$F_1(S) dS$  and  $F_2(S) dS$  being the  $x$  and  $y$  components of tractions across the arc  $dS$ .

For an isolated force  $X + iY$  at the origin supposed to be in the interior of the plate, the parts of  $\phi_1(z)$  and  $\psi_1(z)$  which give rise to the force are

$$\begin{aligned} \phi_1(z) &= -\frac{X + iY}{2\pi(K + 1)} \log z \\ \psi_1(z) &= \frac{K(X + iY)}{2\pi(K + 1)} \log z \end{aligned} \quad \dots (7)$$



For a couple of moment  $M$ , we have them as

$$\left. \begin{aligned} \phi_1(z) &= 0 \\ \psi_1(z) &= -\frac{iM}{2\pi Z} \end{aligned} \right] \quad \dots \quad (8)$$

When the force  $X + iY$  acts at the point  $z_0$ , the relevant parts of  $\phi_1(z)$  and  $\psi_1(z)$  are

$$\left. \begin{aligned} \phi_1(z) &= -\frac{X + iY}{2\pi(K + 1)} \log(z - z_0) \\ \psi_1(z) &= \frac{K(X - iY)}{2\pi(K + 1)} \log(z - z_0) + \frac{X + iY}{2\pi(K + 1)} \cdot \frac{\bar{z}_0}{z - z_0} \end{aligned} \right] \quad \dots \quad (9)$$

and when the couple acts at the point  $z_0$ , we have,

$$\left. \begin{aligned} \phi_1(z) &= 0 \\ \psi_1(z) &= \frac{iM}{2\pi} \cdot \frac{1}{z - z_0} \end{aligned} \right] \quad \dots \quad (10)$$

If  $z = \omega(\zeta)$  transforms the region outside the hole in the  $z$ -plane conformally on the region outside the unit circle  $\gamma$  in the  $\zeta$ -plane, we have on  $\gamma$

$$\left. \begin{aligned} \phi(\sigma) + \frac{\omega(\sigma)}{\omega'(\sigma)} \phi'(\sigma) + \psi(\sigma) &= f_1 + if_2 \\ \bar{\phi}(\bar{\sigma}) + \frac{\bar{\omega}(\bar{\sigma})}{\bar{\omega}'(\bar{\sigma})} \phi'(\sigma) + \psi(\sigma) &= f_1 - if_2 \end{aligned} \right] \quad (11)$$

where

$$\phi(\zeta) = \phi_1\{\omega(\zeta)\} \quad \text{and} \quad \psi(\zeta) = \psi_1\{\omega(\zeta)\}.$$

and  $\zeta = \sigma$  gives a point on  $\gamma$ , so that  $\sigma\bar{\sigma} = 1$ .

# INFINITE PLATE WITH AN ELLIPTIC HOLE ACTED UPON BY AN ISOLATED FORCE

Let the boundary of the hole be given by

$$\overline{R^2(1+m)^2} + \overline{R^2(1-m)^2} = 1 \quad \dots \quad (12)$$

The transformation

$$z = \omega(\zeta) = R\left(\zeta + \frac{m}{\zeta}\right), \quad 0 < m < 1, R > 0 \quad \dots \quad (13)$$

transforms the region outside the hole in the  $z$ -plane, to the region outside the circle  $\gamma$ ,  $|\xi| = 1$  in the  $\xi$ -plane and the point at infinity in the two planes correspond. Substituting from (13) in (11) and replacing  $\sigma$  by  $1/\sigma$ , we get on  $\gamma$

$$\begin{aligned}\phi(\sigma) + \frac{\sigma^2 + m}{\sigma(1 - m\sigma^2)} \phi' \left( \frac{1}{\sigma} \right) + \psi \left( \frac{1}{\sigma} \right) &= f_1 + if_2 \\ \bar{\phi} \left( \frac{1}{\sigma} \right) + \frac{\sigma(1 + m\sigma^2)}{\sigma^2 - m} \phi'(\sigma) + \psi(\sigma) &= f_1 - if_2\end{aligned}\quad \dots \quad (14)$$

If a force  $X + iY$  act at the point  $z_0$  of the plate, we may take

$$\begin{aligned}\phi_1(z) &= -\frac{X + iY}{2\pi(K + 1)} \log(z - z_0) + \phi_1^0(z) \\ \psi_1(z) &= \frac{K(X - iY)}{2\pi(K + 1)} \log(z - z_0) + \frac{X + iY}{2\pi(K + 1)} \frac{z_0}{z - z_0} + \psi_1^0(z),\end{aligned}\quad \dots \quad (15)$$

where  $\phi_1^0(z)$  and  $\psi_1^0(z)$  are analytic outside the elliptic hole (12),

Using the transformation (13) we write

$$\begin{aligned}\phi(\xi) &= -\frac{X + iY}{2\pi(K + 1)} \log \frac{(\xi - \xi_0)(\xi \xi_0 - m)}{\xi \xi_0} + \phi^0(\xi) \\ \psi(\xi) &= \frac{K(X - iY)}{2\pi(K + 1)} \log \frac{(\xi - \xi_0)(\xi \xi_0 - m)}{\xi \xi_0} \\ &\quad + \frac{X + iY}{2\pi(K + 1)} \frac{\xi \xi_0 (\xi_0^2 + m)}{\xi_0 (\xi - \xi_0)(\xi \xi_0 - m)} + \psi^0(\xi)\end{aligned}\quad \dots \quad (16)$$

where  $\phi^0(\xi)$  and  $\psi^0(\xi)$  are analytic outside the unit circle  $\gamma$  in the  $\xi$ -plane. Since the boundary of the hole is free from tractions, substituting in (14)  $f_1 = 0$ ,  $f_2 = 0$ , we get on the unit circle  $\gamma$

$$\begin{aligned}\phi^0(\sigma) + \frac{\sigma^2 + m}{\sigma(1 - m\sigma^2)} \phi'^0 \left( \frac{1}{\sigma} \right) + \psi^0 \left( \frac{1}{\sigma} \right) &= \frac{X + iY}{2\pi(K + 1)} \log \frac{(\sigma - \xi_0)(\sigma \xi_0 - m)}{\sigma \xi_0} \\ &\quad - \frac{K(X + iY)}{2\pi(K + 1)} \log \frac{(1 - \sigma \xi_0)(\xi_0 - m\sigma)}{\sigma \xi_0} + \frac{X - iY}{2\pi(K + 1)} \frac{\xi_0(\sigma - \xi_0)(\sigma \xi_0 - m)}{\xi_0(1 - \sigma \xi_0)(\xi_0 - m\sigma)} \\ \bar{\phi}^0 \left( \frac{1}{\sigma} \right) + \frac{\sigma(1 + m\sigma^2)}{\sigma^2 - m} \phi'^0(\sigma) + \psi^0(\sigma) &= \frac{X - iY}{2\pi(K + 1)} \log \frac{(1 - \sigma \xi_0)(\xi_0 - m\sigma)}{\sigma \xi_0} \\ &\quad - \frac{K(X - iY)}{2\pi(K + 1)} \log \frac{(\sigma - \xi_0)(\sigma \xi_0 - m)}{\sigma \xi_0} + \frac{X + iY}{2\pi(K + 1)} \frac{\xi_0(1 - \sigma \xi_0)(\xi_0 - m\sigma)}{\xi_0(\sigma - \xi_0)(\sigma \xi_0 - m)}.\end{aligned}\quad (17)$$

Multiplying these equations by  $\frac{1}{2\pi i} \frac{d\sigma}{\sigma - \zeta}$  and integrating along  $\gamma$  we get after a little reduction

$$\begin{aligned} \phi^0(\zeta) = & -\frac{X+iY}{2\pi(K+1)} \log \frac{\bar{\zeta}\bar{\zeta}_0}{\bar{\zeta}\bar{\zeta}_0 - m} + \frac{K(X+iY)}{2\pi(K+1)} \log \frac{\bar{\zeta}\bar{\zeta}_0}{\bar{\zeta}\bar{\zeta}_0 - 1} \\ & + \frac{X-iY}{2\pi(K+1)} \frac{(\bar{\zeta}_0 - m\bar{\zeta}_0)(1 - \bar{\zeta}_0\bar{\zeta}_0)}{\bar{\zeta}_0(\bar{\zeta}_0^2 - m)(1 - \bar{\zeta}_0\bar{\zeta}_0)} \\ \psi^0(\zeta) = & -\frac{X-iY}{2\pi(K+1)} \log \frac{\bar{\zeta}\bar{\zeta}_0}{\bar{\zeta}\bar{\zeta}_0 - 1} + \frac{K(X-iY)}{2\pi(K+1)} \log \frac{\bar{\zeta}\bar{\zeta}_0}{\bar{\zeta}\bar{\zeta}_0 - m} \\ & - \frac{X+iY}{2\pi(K+1)} \frac{m(1+m\bar{\zeta}^2)}{(\bar{\zeta}^2 - m)(\bar{\zeta}\bar{\zeta}_0 - m)} + \frac{X+iY}{2\pi(K+1)} \frac{(m\bar{\zeta}_0 - \bar{\zeta}_0)(\bar{\zeta}_0\bar{\zeta}_0 - m^2)}{\bar{\zeta}_0(\bar{\zeta}_0^2 - m)(\bar{\zeta}\bar{\zeta}_0 - m)} \\ & + \frac{K(X+iY)}{2\pi(K+1)} \frac{1+m\bar{\zeta}^2}{(\bar{\zeta}^2 - m)(\bar{\zeta}\bar{\zeta}_0 - 1)} - \frac{X-iY}{2\pi(K+1)} \frac{\bar{\zeta}\bar{\zeta}_0(\bar{\zeta}_0 - m\bar{\zeta}_0)(1+m\bar{\zeta}^2)(1 - \bar{\zeta}_0\bar{\zeta}_0)}{\bar{\zeta}_0(\bar{\zeta}_0^2 - m)(\bar{\zeta}_0^2 - m)(1 - \bar{\zeta}\bar{\zeta}_0)^2} \end{aligned}$$

... (18)

Hence we obtain from (16) and (18)

$$\begin{aligned} \phi(\zeta) = & -\frac{X+iY}{2\pi(K+1)} \log (\bar{\zeta} - \bar{\zeta}_0) + \frac{K(X+iY)}{2\pi(K+1)} \log \frac{\bar{\zeta}\bar{\zeta}_0}{\bar{\zeta}\bar{\zeta}_0 - 1} \\ & + \frac{X-iY}{2\pi(K+1)} \frac{(\bar{\zeta}_0 - m\bar{\zeta}_0)(1 - \bar{\zeta}_0\bar{\zeta}_0)}{\bar{\zeta}(\bar{\zeta}_0^2 - m)(1 - \bar{\zeta}\bar{\zeta}_0)} \\ \psi(\zeta) = & -\frac{X-iY}{2\pi(K+1)} \log \frac{\bar{\zeta}\bar{\zeta}_0}{\bar{\zeta}\bar{\zeta}_0 - 1} + \frac{K(X-iY)}{2\pi(K+1)} \log (\bar{\zeta} - \bar{\zeta}_0) \\ & - \frac{X+iY}{2\pi(K+1)} \frac{m(1+m\bar{\zeta}^2)}{(\bar{\zeta}^2 - m)(\bar{\zeta}\bar{\zeta}_0 - m)} + \frac{K(X+iY)}{2\pi(K+1)} \frac{1+m\bar{\zeta}^2}{(\bar{\zeta}^2 - m)(\bar{\zeta}\bar{\zeta}_0 - 1)} \\ & - \frac{X-iY}{2\pi(K+1)} \frac{\bar{\zeta}\bar{\zeta}_0(\bar{\zeta}_0 - m\bar{\zeta}_0)(1+m\bar{\zeta}^2)(1 - \bar{\zeta}_0\bar{\zeta}_0)}{\bar{\zeta}_0(\bar{\zeta}_0^2 - m)(\bar{\zeta}^2 - m)(1 - \bar{\zeta}\bar{\zeta}_0)^2} \\ & + \frac{X+iY}{2\pi(K+1)} \frac{(m\bar{\zeta}_0 - \bar{\zeta}_0)(\bar{\zeta}_0\bar{\zeta}_0 - m^2)}{\bar{\zeta}_0(\bar{\zeta}_0^2 - m)(\bar{\zeta}\bar{\zeta}_0 - m)} + \frac{X+iY}{2\pi(K+1)} \frac{\bar{\zeta}\bar{\zeta}_0(\bar{\zeta}_0^2 + m)}{\bar{\zeta}_0(\bar{\zeta} - \bar{\zeta}_0)(\bar{\zeta}\bar{\zeta}_0 - m)} \end{aligned}$$

... (19)

The equations (19), together with (1), (2) and (13) give the distribution of stress in an infinite plate with an elliptic hole, and acted upon by a force at any point inside the plate.

If the force  $X+iY$  acts at a point  $z_0$  on the boundary of the hole and if  $\zeta_0$  be the point on  $\gamma$  corresponding to  $z_0$ , we make  $\zeta_0 \rightarrow \sigma_0$  (in the  $\zeta$ -plane). The values of  $\phi(\zeta)$  and  $\psi(\zeta)$  in that case are easily deduced from (19) by making  $\zeta_0 \rightarrow \sigma_0$ , as

$$\left. \begin{aligned} \phi(\zeta) &= -\frac{X+iY}{2\pi} \log(\zeta - \sigma_0) + \frac{K(X+iY)}{2\pi(K+1)} \log \zeta \\ \psi(\zeta) &= \frac{X-iY}{2\pi} \log(\zeta - \sigma_0) - \frac{X-iY}{2\pi(K+1)} \log \zeta - \frac{m(X+iY)}{2\pi(K+1)} \\ &\quad + \frac{X+iY}{2\pi(K+1)} \frac{1+m\zeta^2}{\zeta^2-m} - \frac{X+iY}{2\pi} \frac{\sigma(1+m\zeta)}{(\zeta^2-m)(\sigma_0-\zeta)} \end{aligned} \right\} \dots \quad (20)$$

These results can be shown to be equivalent to those given by Rothman (1950) who has given a solution of the particular case by the method of Stevenson.

If we put  $m=0$ ,  $R=1$  in the transformation (13), we get the identical transformation

$$z = \omega(\zeta) = \zeta \quad \dots \quad (21)$$

Substituting the above in (19) we get the solution of the problem of an infinite plate containing circular hole of unit radius and acted upon by a force  $X+iY$  at a point  $z(z=z_0)$  within it as

$$\left. \begin{aligned} \phi(z) &= -\frac{X+iY}{2\pi(K+1)} \log(z - z_0) + \frac{K(X+iY)}{2\pi(K+1)} \log \frac{\bar{z}z_0}{z\bar{z}_0 - 1} \\ &\quad + \frac{X-iY}{2\pi(K+1)} \frac{1 - z_0\bar{z}_0}{z_0^2(1 - z\bar{z}_0)} \\ \psi(z) &= -\frac{X-iY}{2\pi(K+1)} \log \frac{\bar{z}z_0}{z\bar{z}_0 - 1} + \frac{K(X-iY)}{2\pi(K+1)} \log(z - z_0) \\ &\quad + \frac{K(X+iY)}{2\pi(K+1)} \frac{1}{z^2(\bar{z}z_0 - 1)} - \frac{X-iY}{2\pi(K+1)} \frac{1 - z_0\bar{z}_0}{z\bar{z}_0(1 - z\bar{z}_0)^2} \\ &\quad - \frac{X+iY}{2\pi(K+1)} \frac{1}{z\bar{z}_0} + \frac{X+iY}{2\pi(K+1)} \frac{\bar{z}_0}{z - z_0} \end{aligned} \right\} \dots \quad (22)$$

When the force acts along a radius of circular hole the stress distribution derived from (22) are found to agree with that given by Sen (1945).

If the force  $X + iY$  act on the boundary of the hole, we get  $\phi(z)$  and  $\psi(z)$  from (20)

$$\begin{aligned}\phi(z) &= -\frac{X+iY}{2\pi} \log(z-z_0) + \frac{K(X+iY)}{2\pi(K+1)} \log z \\ \psi(z) &= \frac{X-iY}{2\pi} \log(z-z_0) - \frac{X-iY}{2\pi(K+1)} \log z \\ &\quad + \frac{X+iY}{2\pi(K+1)} \cdot \frac{1}{z^2} + \frac{X+iY}{2\pi} \frac{z_0}{z^2(z-z_0)}\end{aligned} \quad \dots (23)$$

# INFINITE PLATE WITH AN ELLIPTIC HOLE ACTED UPON BY A COUPLE

If a couple  $M$  acts at the point  $z_0$ , we can write

$$\begin{aligned}\phi_1(z) &= \phi_1^{\circ}(z) \\ \psi_1(z) &= -\frac{iM}{2\pi(z-z_0)} + \psi_1^{\circ}(z)\end{aligned} \quad (24)$$

Using the transformation (13) we get

$$\begin{aligned}\phi(\xi) &= \phi^{\circ}(\xi) \\ \psi(\xi) &= -\frac{iM\xi}{2\pi R(\xi-\xi_0)\left(\xi-\frac{m}{\xi_0}\right)} + \psi^{\circ}(\xi)\end{aligned} \quad (25)$$

Substituting in (14) with  $f_1=f_2=0$  (as the boundary is free from traction) we have on the unit circle  $\gamma$

$$\begin{aligned}\phi^{\circ}(\sigma) + \frac{\sigma^2+m}{\sigma(1-m\sigma^2)} \phi^{\circ\prime}\left(\frac{1}{\sigma}\right) + \psi^{\circ}\left(\frac{1}{\sigma}\right) &= -\frac{iM\xi_0\sigma}{2\pi R(1-\sigma\xi_0)(\xi_0-m\sigma)} \\ \phi^{\circ}\left(\frac{1}{\sigma}\right) + \frac{\sigma(1+m\sigma^2)}{\sigma^2-m} \phi^{\circ\prime}(\sigma) + \psi^{\circ}(\sigma) &= -\frac{iM\xi_0\sigma}{2\pi R(\sigma-\xi_0)(\sigma\xi_0-m)}\end{aligned} \quad \dots (26)$$

Multiplying both sides of (26) by  $\frac{1}{2\pi i} \frac{d\sigma}{\sigma-\xi}$  and integrating along  $\gamma$ , we

get

$$\begin{aligned}\phi^{\circ}(\xi) &= \frac{iM\xi_0}{2\pi R(\xi_0^2-m)(1-\xi\xi_0)} \\ \psi^{\circ}(\xi) &= \frac{iM}{2\pi R} \left\{ \frac{m\xi_0}{(m-\xi_0^2)(m-\xi\xi_0)} - \frac{\xi\xi_0^2(1+m\xi^2)}{(\xi^2-m)(\xi_0^2-m)(1-\xi\xi_0)^2} \right\}\end{aligned} \quad \dots (27)$$

and therefore

$$\left. \begin{aligned} \phi(\zeta) &= \frac{iM\bar{\zeta}_0}{2\pi R(\bar{\zeta}_0^2 - m)(1 - \bar{\zeta}_0\zeta)} \\ \psi(\zeta) &= \frac{iM}{2\pi R} \left\{ \frac{\bar{\zeta}_0^2}{(\zeta - \bar{\zeta}_0)(\bar{\zeta}_0^2 - m)} - \frac{\bar{\zeta}_0^2(\zeta_0^2 + m\zeta^2)}{(\zeta^2 - m)(\bar{\zeta}_0^2 - m)(1 - \bar{\zeta}_0\zeta)^2} \right\} \end{aligned} \right] \quad \dots \quad (28)$$

If the couple  $M$  acts at a point  $z_0$  on the boundary of the hole and  $\sigma_0$  be the point on  $\gamma$  corresponding to  $z_0$ , we get, making  $\zeta_0 \rightarrow \sigma_0$  as before

$$\left. \begin{aligned} \phi(\zeta) &= -\frac{iM\sigma_0^2}{2\pi R(1 - m\sigma_0^2)(\sigma_0 - \zeta)} \\ \psi(\zeta) &= -\frac{iM\sigma_0^2}{2\pi R} \left\{ \frac{1}{(\sigma_0 - \zeta)(\sigma_0^2 - m)} + \frac{\zeta(1 + m\zeta^2)}{(\zeta^2 - m)(\sigma_0 - \zeta)^2(1 - m\sigma_0^2)} \right\} \end{aligned} \right] \quad \dots \quad (29)$$

Putting  $m=0$ , we get the case of a couple acting at a point of an infinite plate with a circular hole of radius  $R$ .

In the case of the couple acting at an internal point we have from (28)

$$\left. \begin{aligned} \phi(z) &= -\frac{iMR^2}{2\pi z_0(R^2 - zz_0)} \\ \psi(z) &= \frac{iM}{2\pi} \left\{ \frac{1}{z - z_0} - \frac{R^4}{z(R^2 - zz_0)^2} \right\} \end{aligned} \right] \quad \dots \quad (30)$$

and in the case of a couple acting at a point on the boundary, we have

$$\left. \begin{aligned} \phi(z) &= \frac{iMz_0^2}{2\pi(z_0 - z)} \\ \psi(z) &= -\frac{iM}{2\pi} \left\{ \frac{1}{z_0 - z} + \frac{R^2 z_0^2}{z(z_0 - z)^2} \right\} \end{aligned} \right] \quad \dots \quad (31)$$

#### ACKNOWLEDGMENTS

The author wishes to express his respectful thanks to Dr. S. Ghosh for his constant guidance during the preparation of this paper.

#### REFERENCES

- Muschelisvili, 1933, *Zelts. Angew. Math. u. Mech.*, Bd. 13, 264.  
 Rothman, 1950, *Quart. J. Mech. App Math.*, 3, 279.  
 Sen. B., 1945, *Bull. Cal. Math. Soc.*, 37, 37.  
 Stevenson, 1945, *Proc. Roy. Soc., ser. A*, 184, 125.

# ON THE RAMAN SPECTRA AND FLUORESCENCE OF ORTHO AND PARACHLOROTOLUENE IN THE SOLID STATE \*

BY S. B. SANYAL

OPTICS DEPT., INDIAN ASSOCIATION FOR THE CULTIVATION OF SCIENCE, CALCUTTA-32

(Received for publication, July 1, 1953)

## Plate XVIII

**ABSTRACT** The Raman spectra of ortho and parachlorotoluene in the solid state at  $-180^{\circ}\text{C}$  have been photographed and compared with those for the liquids at room temperature. Four new lines in the low-frequency region have been observed in each case, two of them having almost the same frequencies in the two cases. The intensities of these new lines are much smaller than those of the prominent lines due to the liquids. It is further observed that in the case of *o*-chlorotoluene some of the prominent Raman lines observed for the liquid state undergo large changes in intensity and position and the line  $2928\text{ cm}^{-1}$  splits up into three lines when the liquid is solidified and cooled to  $-180^{\circ}\text{C}$ . It is suggested that the line  $163\text{ cm}^{-1}$  of liquid *o*-chlorotoluene which shifts to  $185\text{ cm}^{-1}$  in the case of the solid might be due to a dimer. It is observed that these substances exhibit broad intense fluorescence bands in the visible region in the solid state, at  $-180^{\circ}\text{C}$ , and in the liquid state there is no fluorescence in the case of *p*-chlorotoluene, but *o*-chlorotoluene shows a continuous fluorescence in the whole visible region.

## INTRODUCTION

The Raman spectra of many substituted benzene compounds in the solid state at low temperatures were studied previously by Sirkar and Bishui (1946) and Ray (1950, 1951, 1952). It was observed by the latter author that in almost all the substituted benzene compounds several new lines appear in the low frequency region when the substances are solidified, and when they are further cooled down, some of the lines shift away from the Rayleigh line. The positions of the lines observed in the different substitution compounds, however, do not depend essentially on the moments of inertia of the molecules, and from this fact it was concluded by Ray (1951) that the lines are not produced by rotational oscillations of the molecules pivoted in the lattice as postulated by some previous workers (Kastler and Rousset, 1941). In order to find out whether in a di-substituted benzene compound the relative positions of the two substitution groups have an influence on the number and positions of the new lines in the low frequency region which may appear in the Raman spectra of these substances in the solid state, the Raman spectra of ortho- and parachlorotoluene in the solid state have been studied in the present investigation, and the results have been discussed in the light of the various theories put forward regarding the origin of the new lines in the low frequency region.

\* Communicated by Prof. S. C. Sirkar

## EXPERIMENTAL

Ortho and parachlorotoluene supplied by May and Baker of U. S. A. were distilled in vacuum, as usual. A preliminary investigation showed that the Raman spectrum of the second liquid does not exhibit any appreciable fluorescence although the first one shows a continuous fluorescence spectrum. The number of lines in each case, however, agreed with those published by previous workers. This proved the purity of the substances. The method used for studying the Raman spectra of these substances in the solid state at the temperature of liquid oxygen was the same as that used by previous workers in this laboratory (Bishui, 1948). Ilford Special Rapid plates were used to photograph the spectra for the solid state and a Fuess spectrograph with a dispersion of about  $10.8 \text{ \AA}$  per mm. in the  $4046 \text{ \AA}$  region was employed. The Raman spectra for the liquids at room temperature were also photographed with the same spectrograph in order to compare these with the Raman spectra for the solid state. The experimental tubes containing the solid was at  $-180^\circ\text{C}$ . No attempt was made to record very weak lines which might be present in the Raman spectra of the two substances in the liquid state.

## RESULTS AND DISCUSSION

(a) *Raman spectra.* The spectrograms for the two substances in the liquid state and in the solid state at  $-180^\circ\text{C}$  are reproduced in Plate XVIII. The frequency-shifts are given in Tables I and II. The frequencies of the Raman lines of the two substances reported by previous workers and given by Magat (1936) are also included in the tables for comparison.

A comparison of the data given in Tables I and II shows that both the substances yield four new Raman lines in the low frequency region in the solid state at  $-180^\circ\text{C}$  and two of these lines have the same frequencies in both the cases. The other two lines are at  $78$  and  $102 \text{ cm}^{-1}$  in the case of *o*-chlorotoluene and at  $85$  and  $129 \text{ cm}^{-1}$  in the case of *p*-chlorotoluene. These lines are, however, much feebler than similar lines observed in other disubstituted benzene compounds, such as *p*-dichlorobenzene or *p*-dibromobenzene. It was pointed out by Ray (1951) that all the monosubstituted benzenes studied by him yield in the solid state at  $-180^\circ\text{C}$  five new Raman lines in the low frequency region and that the positions of these lines cannot be correlated with the moments of inertia of the molecules about their three axes. The lines are also quite sharp and intense in all these cases. In the present case the two chlorotoluenes do not yield any such intense Raman lines and the lines are rather broad. Had these lines been due to rotational oscillations of the molecules pivoted in the lattice, as postulated by Kastler and Rousset (1941) they would be as intense as in the case of other similar



TABLE I  
Orthochlorotoluene  
 $\Delta \nu$  in  $\text{cm}^{-1}$

Liquid, Magat (1936)	Liquid at 25°C Present author	Solid at -180°C
163 (8)	163 (5) e, k	36 (o) e, k 50 (1) e, k 78 (o) e, k 102 (2) e, k 186 (5) e, k 243 (ob) e, k 363 (o) e 448 (1) e, k 550 (3) e, k 673 (5) e, k
247 (5)	247 (4) e, k	802 (3) e, k
361 (3)	361 (1) e	
447 (4)	443 (3) e, k	
552 (7)	550 (3) e, k	
675 (6)	673 (5) e, k	
745 (1)		
803 (4)	800 (4) e, k	
852 (oo)		
989 (1)		
1016 (o)		
1043 (8)	1040 (8) e, k	1034 (5) e, k
1132 (2)		
1156 (2)	1155 (2) e, k	1156 (1) e, k
1204 (5)	1205 (5) e, k	1210 (2) e, k
1279 (o)		
1378 (2)	1376 (4) e, k	1378 (1) e, k
1426 (o)		
1574 (3)	1572 (3) e, k	1572 (1) e, k
1592 (3)	1593 (3) e, k	1596 (1) e, k
2859 (o)		2905 (2) k
2926 (5)	2928 (5) e, k	2930 (2) k
3013 (o)		2956 (1b) k
3062 (7)	3062 (7) e, k	3066 (5) e, k

TABLE II  
Parachlorotoluene,  $\Delta \nu$  in  $\text{cm}^{-1}$

Liquid, Magat (1936)	Liquid at 25°C, Present author	Solide at -180°C
307 (8)	306 (3) e, k	38 (2) e, k 50 (1b) e, k 85 (1b) e, k 129 (2) e, k
376 (12)	374 (5) e, k	390 (1b) e, k
634 (5)	636 (3) e, k	372 (3) e, k 630 (1) e, k
692 (1)		
796 (12)	796 (8) e, k	792 (5) e, k
822 (2)	818 (1) e, k	
1090 (12)	1092 (10) e, k	1090 (5) e, k
1177 (1)		
1208 (7)	1210 (5) e, k	1210 (3) e, k
1303 (o)		
1379 (4)	1383 (2) e, k	
1454 (o)		
1596 (8)	1598 (8) e, k	1590 (2) e, k
2924 (8 I)	2930 (5) e, k	2920 (2) e, k
3031 (4)	3040 (3b)	
3064 (10 I)	3062 (10) e, k	3062 (5) e, k

molecules. Hence these lines may be due to intermolecular oscillations in groups of associated molecules as pointed out by Sirkar (1937) and also recently by Ray (1950, 1951).

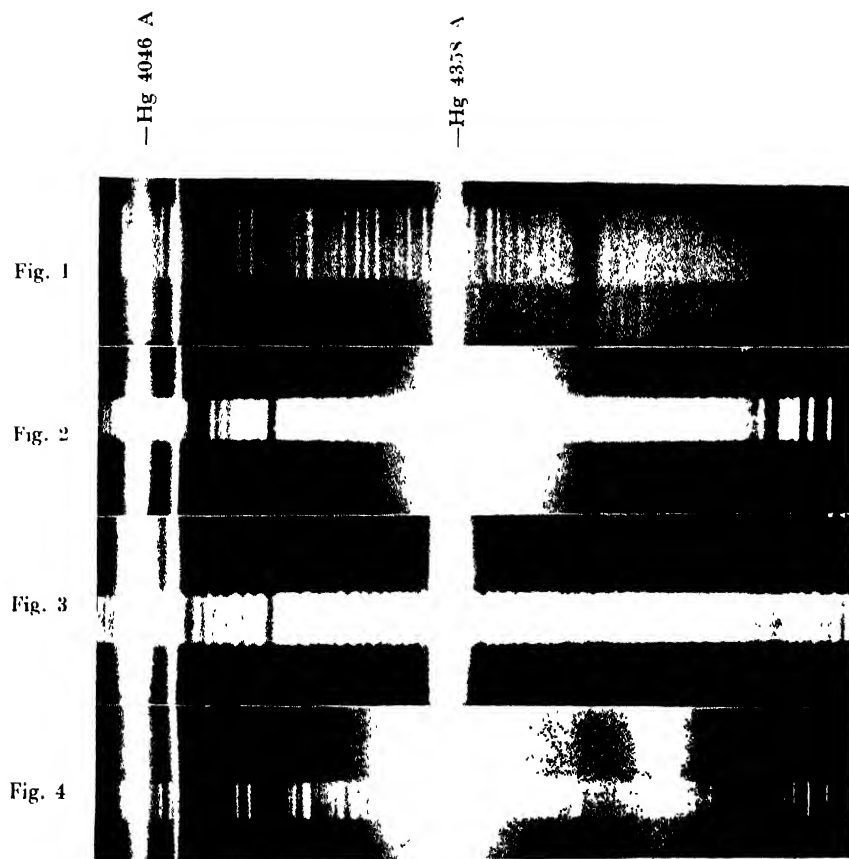
Some of the other Raman lines undergo changes in intensity and position with the solidification of these two substances. For instance, in the case of orthochlorotoluene the line  $163\text{ cm}^{-1}$  shifts to  $186\text{ cm}^{-1}$  the line  $246\text{ cm}^{-1}$  becomes much weaker and broader and the line  $2928\text{ cm}^{-1}$  splits up into three lines at  $2905$ ,  $2930$  and  $2956\text{ cm}^{-1}$  when the liquid is solidified and cooled down to  $-180^{\circ}\text{C}$ . In the case of parachlorotoluene the line  $306\text{ cm}^{-1}$  shifts to  $320\text{ cm}^{-1}$  and becomes broader while the lines  $1598$  and  $2930\text{ cm}^{-1}$  shift to  $1590$  and  $2920\text{ cm}^{-1}$  respectively with the solidification. Further, the lines  $1572$  and  $1503\text{ cm}^{-1}$  of *o*-chlorotoluene and the line  $1598\text{ cm}^{-1}$  of *p*-chlorotoluene become much weaker when the liquids are solidified. Since these lines are due to  $\text{C}=\text{C}$  oscillation, this diminution of intensity may indicate a diminution in the number of such double bonds in the molecule with the solidification. All these facts clearly indicate a strong influence of intermolecular field on the frequencies of oscillation of certain modes and this influence may be due to association of the molecules in the solid state which may be responsible also for the origin of the new lines in the low-frequency region.

(b) *Fluorescence spectra.* It can be seen from Plate XVII that the both the substances in the solid state at  $-180^{\circ}\text{C}$  exhibit fluorescence bands in the visible region. The positions of centres and width of the intense bands are are given in Table III.

TABLE III  
Fluorescence bands

<i>o</i> -Chlorotoluene			<i>p</i> -Chlorotoluene		
Position of band in Å. U.	Intensity	Width in Å. U.	Position of band in Å. U.	Intensity	Width in Å. U.
4400	5	100	4300	5	50
			4500	2	50
			4640	10	100
4760	2	50			

The spectrogram for *o*-chlorotoluene in the liquid state also shows a stronger continuous background extending from  $4100\text{ Å}$  upto about  $5100\text{ Å}$ . Even after distilling the liquid in vacuum repeatedly it was not possible to get rid of this fluorescence. The spectrogram for the substance in the solid state, however, shows weak continuous fluorescence over the region from about  $4250\text{ Å}$  upto about  $4400\text{ Å}$  and two bands, one strong and wide band at  $4400\text{ Å}$  and a feebler band at  $4760\text{ Å}$ . The frequency-difference is about  $1565\text{ cm}^{-1}$ . This frequency corresponds to the  $\text{C}=\text{C}$  valence oscillation.



## Raman spectra

- Fig. 1. *o*-Chlorotoluene, liquid at 26° C  
 Fig. 2. „ „ solid at -180° C  
 Fig. 3. *p*-Chlorotoluene, liquid at 26° C  
 Fig. 4. „ „ solid at -180° C



It is also an interesting fact that although *p*-chlorotoluene does not yield any Raman line with frequency-shift below  $306\text{ cm}^{-1}$ , *o*-chlorotoluene gives an intense line at  $163\text{ cm}^{-1}$ . This fact may indicate a fundamental difference between the nature of the molecules in the liquid state in two cases. Probably in the case of *o*-chlorotoluene the molecules exist as dimers which give rise to this line at  $163\text{ cm}^{-1}$  and also the continuous fluorescence mentioned above may be due to these dimers. In the case of *p*-chlorotoluene in the liquid state probably the molecules do not form such dimers and, therefore, the line  $163\text{ cm}^{-1}$  is absent in this case and no fluorescence is exhibited by this liquid. When the liquid is solidified, probably groups of strongly associated molecules are formed in this case also and they give rise to the fluorescence bands given in Table III as well as the new Raman lines given in Table II. The frequency-difference between the first and the second and the first and the third bands are approximately  $1530$  and  $1650\text{ cm}^{-1}$  respectively. It is significant that these frequencies correspond to those of the lines due to C-C and C=C oscillations of the molecule. Of course, the bands are very broad but this coincidence indicates that these valence oscillations are coupled to the electronic energy level of the ground state of the associated molecule during emission of the fluorescence radiation.

#### ACKNOWLEDGMENT

The author is indebted to Prof. S. C. Sirkar for his kind interest and guidance throughout the progress of the work.

#### REFERENCES

- Bishui, B. M., 1948, *Ind. J. Phys.*, **22**, 167.  
Kastler, A. and Rousset, A., 1941, *Comptes Rendus*, **212**, 645.  
Magat, M., 1936, *Annual Table of Constants*, Parts, p. 26-77.  
Ray, A. K., 1950, *Ind. J. Phys.*, **24**, 111.  
Ray, A. K., 1951, *Ind. J. Phys.*, **25**, 131.  
Sirkar, S. C., 1937, *Ind. J. Phys.*, **11**, 343.  
Sirkar, S. C. and Bishui, B. M., 1946, *Ind. J. Phys.*, **20**, 111.

# OSCILLATION OF VISCOUS LIQUIDS IN TUBES AND THE CRITERION OF STREAM LINE MOTION

BY S. VENKATARAMAN

PHYSICAL LABORATORY, NIZAM COLLEGE, HYDERABAD-(DN)

(Received for publication, February 2, 1953)

**ABSTRACT.** In this paper the problem of oscillation of liquids in cylindrical tubes is investigated. It is found that the logarithmic decrement  $\frac{1}{2} \nu k^2 T$ , where  $k = 1.2197 \pi/a$ , enables us to determine the viscosity of the liquid.

It is also found that for stream line flow the radius of the tube must be such that the number  $a^2/\nu T$  (where  $T$  is the periodic time), must lie between 5 and 37

By this method the viscosities of fairly viscous liquids, viz. the higher alcohols, was determined and the values thus obtained agree well with the standard values given in International Critical Tables.

## INTRODUCTION

In a paper published by the author (Venkataraman, 1933) a photographic method was described for the determination of the viscosity of mobile liquids.

Investigations on the oscillatory motion of a fluid along a circular tube was carried by Christopherson, *et al* (1938). The authors tried to find the viscosity of a liquid. They found that it was not possible to determine the coefficient of viscosity by finding the logarithmic decrement of the free oscillation. After an elaborate mathematical analysis they found an expression which was ultimately used to measure viscosity, but probably they overlooked the work of the author (Venkataraman, 1933), where the problem of damping of free oscillations of a cylindrical liquid column was already solved. They found in their investigation that turbulent flow can be avoided by using small bore or small displacement and suggested that the question of setting in of turbulence could be settled only by experiment.

The problem of steady flow in tubes was investigated by Reynolds, who stated that when the velocity of flow was greater than a certain maximum,  $w_0$ , turbulence sets in. For stream line flow the Reynolds' number  $\frac{w_0 a}{\nu}$  should be a constant. The turbulent motion of oscillating liquids was not so far investigated. It is proposed to study this experimentally in this paper.

The method may be briefly described. The liquid under investigation is allowed to oscillate either in a U-tube or in two vertical tubes projecting

out of a bottle filled with the same liquid. The oscillations of the portion of the liquid meniscus near the axis of the tube are photographed by means of Raman's vibrograph camera. The logarithmic decrements of the damped oscillations of the liquids are determined from the photographs. The kinematic viscosity and hence the coefficient of viscosity of the liquid is determined from the relation :

$$\text{Logarithmic decrement } \delta = \frac{1}{2} \nu k^2 T,$$

where  $k = \frac{1.2197\pi}{a}$ ,  $a$  is the radius of the tube and  $T$  is the period of oscillation. The above relation can be rewritten as

$$\nu = 0.136 \delta \frac{a^2}{T} \text{ or } \eta = 0.136 \frac{\delta a^2 \rho}{T}, \text{ as } \nu = \frac{\eta}{\rho} \quad \dots (1)$$

As at that time the interest was only to develop a new method of measuring the absolute coefficient of viscosity, it was found sufficient to obtain an expression for logarithmic decrement, which was easily deduced from Stokes' dissipation function and no attempt was made to study the limits for which oscillation of liquids in tubes is stream line.

It was pointed out in that paper, that for satisfactory results, the oscillations should be neither too large nor too small. Amplitudes between 1.2 and 0.8 cm gave the best results for the mobile liquids investigated, it was found that the radii of the tubes should lie between certain limits. In this paper an attempt is made to carry the problem a step further and also to find out the effect of the viscosity of the liquid and radius of the tube on the stream line motion of the liquid.

#### THEORY

Starting from Navier Poisson equations the modulus of decay of the motion of liquid in a circular cylinder was already solved in the general case (Lamb).

The particular solution in the present case can be written as

$$\psi = \left\{ \frac{J_0(kr)}{J_0(ka)} - 1 \right\} e^{-\nu h t} \quad \dots (2)$$

where  $\psi$  is the stream function and  $a$  is the radius of the tube.

To satisfy the condition that the tangential velocity may vanish when  $r=a$ , we have :

$$J'_0(ka) = 0, \text{ i. e. } J_1(ka) = 0 \quad \dots (3)$$

the first root is given by  $ka = \frac{1.2197}{\pi}$

The above relations completely determine the motion of the liquid in the tube. In the case of very viscous liquids, the motion will no longer be periodic; the motion gradually subsides and by measuring the time taken for a certain displacement we can measure the viscosity of very viscous liquids like glycerine.

## CONDITIONS FOR STREAMLINE FLOW

In order that the logarithmic decrement may be constant, it is necessary that the motion should be stream line. We shall, therefore, investigate the conditions for which the motion is streamline.

Let equation (1), be written in the form

$$a^2/vT = \frac{1}{0.1368 \delta}. \quad (4)$$

It will be noticed that the expression on the left hand side of (4) is dimensionless, and may be regarded as a quantity playing the same role in oscillatory motion, as Reynolds' number in steady flow.

If we plot  $a^2/vT$  against  $1/\delta$ , the curve should obviously be a straight line. Its actual form is as shown in figure 1. The photographs obtained with all the tubes used in this as well as the previous investigation on the subject, were used in plotting the curve.

It is clear that the graph is a straight line for values of  $\frac{a^2}{vT}$  lying

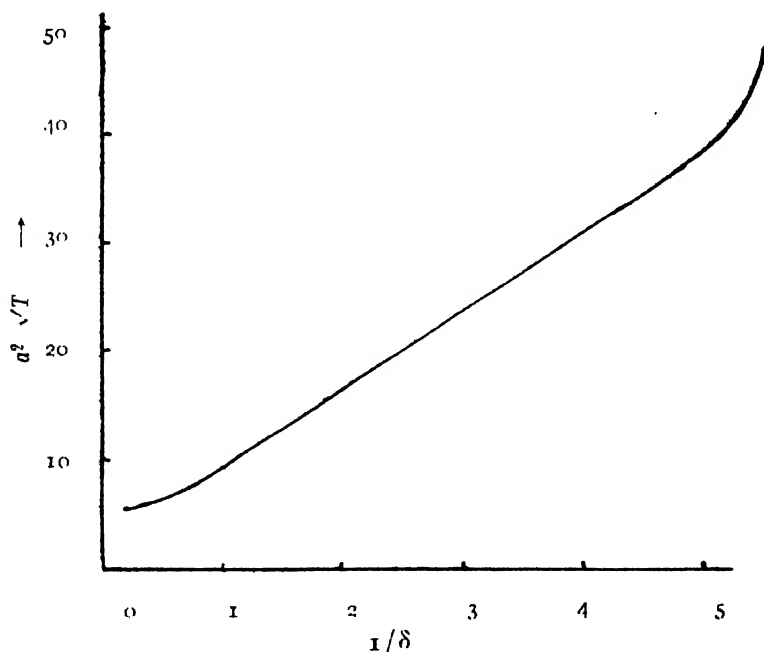


FIG. 1

approximately between 5 and 37 or for  $1/\delta$  values between 0.5 and 5.1. That is to say, for satisfactory results by this method, the values of  $\delta$  should lie approximately between 2 and 0.2. Values of  $\delta > 2$ , tend to give a higher value for  $\eta$  and values of  $\delta > 0.2$  give a lower value. For the success of this method the following conditions must be observed. Large oscillations, where drainage of the liquid along the walls of the tube appear to have a vitiating influence on the results, should be avoided. So also very small oscillations, where the motion is so slow that only the layers of the liquid



about the axis appear to move, should be avoided. Influence of surface tension is negligible for moderate amplitudes but appear to have some influence for very small amplitudes.

#### RESULTS FOR MODERATELY VISCOUS LIQUIDS

As a further confirmation of the correctness of the method, it has now been used for the determination of viscosities of comparatively viscous liquids, the higher alcohols and aniline, using tubes of 0.77 to 1.12 cm diameter, and the results are recorded in Table I.

TABLE I  
Length of the oscillating column, 51-54 cm  
Period (experimental), 1.14 secs

Liquid	Density at 30°C	Tube 1 $a=0.385$ cm		Tube 2 $a=0.48$ cm		Tube 3 $a=0.50$ cm		$\eta$ (From I. C. T.)
		$\delta$	$\eta$	$\delta$	$\eta$	$\delta$	$\eta$	
Normal propyl alcohol	0.7958	1.60	0.0178	1.02	0.0177	0.755	0.0177	0.01732 (at 30°. 83°C)
Isopropyl alcohol	0.7774	1.63	0.0177	1.04	0.0176	0.763	0.0176	0.017275 (,, 30°. 55°C)
Normal butyl alcohol	0.8029	2.01	0.0224	1.26	0.0221	0.929	0.022	0.02172 (,, 31°. 73°C)
Isobutyl alcohol	0.7944			1.65	0.0386	1.21	0.0285	0.03658 (,, 21°. 77°C)
Aniline	1.013			1.47	0.0324	1.07	0.0322	0.02977 (,, 31°. 76°C)

#### CONCLUSION

As seen from columns (8) and (9) the values of viscosities of fairly viscous liquids determined by this method agree remarkably well with the values given in the International Critical Tables. For getting accurate results the motion should not be turbulent. To ensure this tubes of proper radii should be selected and the amplitude of oscillation should neither be too large nor too small. The reason for this was pointed out above.

The determination of the viscosity of mercury by this method is of some interest for many reasons. Preliminary observations confirm the results obtained. Hence it is proposed to study the oscillation of this liquid in detail and it is also proposed to apply this method to the determination of the viscosities of other liquid metals and very viscous liquids like glycerine, where the liquids do not oscillate at all.

## ACKNOWLEDGMENT

The author welcomes this opportunity to express his gratitude to Dr. J. C. Kamesvara Rao, Professor of Physics, Nizam College, at whose suggestion and under whose guidance this investigation was carried out, for kind interest throughout the progress of the work.

## REFERENCES

- Christopherson, D. C., A Gemant, H. A. Hogg and R. W. Southwell., 1938, *Proc Roy Soc.*, **168 A**, 351.  
Lamb, Hydrodynamics. 4th edn. p. 365.  
Merrington, Viscometry p. 84.  
Venkataraman. S., 1933, *Ind. Jour. Phys*, **8**, 25.

# THE ULTRAVIOLET ABSORPTION SPECTRA OF PHENETOLE AND *n*-BUTYLBENZOATE IN DIFFERENT STATES \*

BY A. R. DEB

OPTICS DEPARTMENT, INDIAN ASSOCIATION FOR THE CULTIVATION OF SCIENCE, CALCUTTA 32

(Received for publication, August 12, 1953)

**ABSTRACT.** The absorption spectra of phenetole in the liquid and solid states and those of *n*-butylbenzoate in the vapour, liquid and solid phases have been photographed in the region between 2820 and 2500 Å U., using thin films of the substances in the case of the liquid and solid phases

In the absorption spectrum of phenetole in the liquid state at 30°C, three broad bands are observed with the  $\nu_0$ -band at  $35771\text{ cm}^{-1}$  and other bands corresponding to a progression of vibrational frequency  $901\text{ cm}^{-1}$ . In the solid state at  $-180^\circ\text{C}$  the broad bands observed for the liquid state become much sharper and each is accompanied by three faint bands. The bands correspond to the vibrational frequencies 500, 773, 922, 945 and  $1272\text{ cm}^{-1}$  and their combinations. The  $\nu_0$ -band in the solid state at  $-180^\circ\text{C}$  is shifted towards longer wavelengths by  $38\text{ cm}^{-1}$  from its position in the liquid state and by  $629\text{ cm}^{-1}$  from its position in the vapour state

The absorption spectrum of *n*-butylbenzoate in the vapour state yields 9 bands with the  $\nu_0$ -band at  $36099\text{ cm}^{-1}$  and progression of vibrational frequencies 360 and  $944\text{ cm}^{-1}$  and their combinations. In the liquid state at  $32^\circ\text{C}$  the substance yields only three bands corresponding to vibrational frequency  $952\text{ cm}^{-1}$  and the whole spectrum is shifted by about  $573\text{ cm}^{-1}$  towards longer wavelengths. When the liquid is solidified and cooled to  $-180^\circ\text{C}$  the bands shift by about  $100\text{ cm}^{-1}$  towards longer wavelengths and become a little sharper.

These results have been discussed in detail.

## INTRODUCTION

The investigations of the absorption spectra of some aromatic organic compounds in different states and at different temperatures carried out recently in this laboratory (Deb, 1951, 1952, 1953; Sirkar and Swamy 1952; Swamy 1952, 1953) yielded results which furnish much information regarding the influence of the intermolecular field on the electronic energy levels of the molecules in the liquid and solid states. The investigations referred to above were mainly confined to substituted benzene compounds and a few double-ring compounds. Yet the changes taking place in the absorption spectra with change of state were found to be of widely different characters for different molecules with, of course, some characteristics common to all the substances. For example, the  $\nu_0$ -band and the spectrum as a whole are

\* Communicated by Prof. S. C. Sirkar

shifted towards longer wavelengths in all the cases with the change from vapour to liquid state. The number of bands also become much smaller with liquefaction of the vapour, but the subsequent changes taking place in the spectrum on solidification of the substances are found to be different for different molecules. In some cases the electronic energy level is split up into several components with solidification and lowering of temperature of the substances (Sirkar and Swamy 1952, Swamy 1952). In the case of other molecules such as diphenylmethane, dibenzyl (Deb 1953), *p*-dichlorobenzene (Swamy, 1952), etc., the bands due to the liquid phase become sharper in the spectrum due to the solid state at low temperature, and as a result of this sharpening some weak bands due to  $\sigma \rightarrow \pi$  transitions, which are absent in the case of the liquid phase, are distinctly resolved in the spectra due to the solid phase. The sharpening of the bands were attributed to cessation of angular oscillations of the molecules in the crystal at low temperatures.

There is still a third group of compounds, the absorption spectra of which do not undergo the changes mentioned above with the change of state from liquid to solid phase. Methyl and ethyl benzoates were found to belong to this group (Deb, 1951b, 1953).

Further, the shift of the  $\nu_0$ -band with solidification in the case of all compounds studied so far was found to be different from each other in magnitude and direction, for different compounds. The vibrational frequencies for the excited state were also found to be changed in the case of some compounds with solidification and lowering of temperature of the substances.

The investigations were continued in order to get information regarding other compounds and the present paper reports the results obtained in the case of phenetole ( $C_6H_5OC_2H_5$ ) and *n*-butylbenzoate ( $C_6H_5COOC_4H_9$ ). The data obtained in the case of phenetole have been compared with those in the vapour state reported by Sreeramamurty (1951) and in the other case the spectra for all the three states have been investigated.

#### EXPERIMENTAL

The experimental technique used in these investigations has been described previously (Deb, 1951a). The ultraviolet continuum was obtained from a hydrogen discharge tube run at about 3 K. V. The thickness of the absorbing film in the solid and liquid states, required for the production of bands in the absorption spectrum was about a few microns in the case of phenetole and less than 0.1 mm in the other case. For investigations at low temperatures a Dewar vessel made of fused silica was used as before.

The substances studied were of chemically pure quality. Phenetole was supplied by B. D. H. and *n*-butylbenzoate by Fisher Scientific Co. of U. S. A. They were redistilled in evacuated double bulbs before use.

The length of the of the absorption tube used in the investigation of the spectrum of *n*-butylbenzoate in the vapour state was 90 cm, the ends being closed by quartz windows, sealed with sodium silicate cement. A Cenco

Hyvac pump was used to evacuate the tube. The temperature of the tube as well as the bulb containing the liquid, connected to the tube was maintained much above room temperature by playing the flame of a burner over the tube and bulb intermittently.

All the photographs were taken on Ilford H. P. 3 films using a Hilger E 1 quartz spectrograph which has a dispersion of about 3 Å.U. per mm in the region, 2600 Å. Iron arc comparison was recorded in each photograph and microphotometric records of the spectra were taken using a Kipp and Zonen self-recording microphotometer. In each record a known iron line at one end of the spectrum was taken as the reference line. The wavelengths of the bands were calculated from these records from the known ratio used (1.6 : 1) and the distance of peaks from the reference line mentioned above.

# RESULTS AND DISCUSSION

The microphotometric records of the spectra have been reproduced in figures 1 and 2 and the wave numbers of the bands and their assignments are given in Tables I and II. For comparison, the wave numbers and assignments of several prominent bands of phenetole in the vapour state, reported by Sreeramamurty (1951) have been included in columns 1 and 2 of Table I. Column 3 of the same table gives the excited state frequencies of phenetole vapour reported by Robertson, *et al* (1950).

TABLE I

Ultraviolet absorption bands of phenetole  $\left( \langle \text{C}_6\text{H}_5 \rangle - \text{O} - \text{C}_2\text{H}_5 \right)$

Vapour (Sreeramamurty, 1951 (Prominent bands only))		Vapour (Robertson <i>et al</i> , 1950)	Liquid at 30°C (Present author)		Solid at -180°C (Present author)	
$\nu$ (cm <sup>-1</sup> ) and Int.	Assign- ment	Excited st frequencies (cm <sup>-1</sup> )	$\nu$ (cm <sup>-1</sup> ) and Int.	Assign- ment	$\nu$ (cm <sup>-1</sup> ) and Int	Assignment
36362 (vvs)	$\nu_0$	155 (w)	35771 (vs)	$\nu_0$	35733 (vvs)	$\nu_0$
36916 (ms)	$\nu_0 + 554$	340 (w)			36293 (ms)	$\nu_0 + 560$
37106 (vs)	$\nu_0 + 744$	760 (vs)			36506 (s)	$\nu_0 + 773$
37130 (ms)	$\nu_0 + 744 + 27$	940 (vs)	36672 (vvs)	$\nu_0 + 901$	36635 (w)	$\nu_0 + 902$
		1255 (m)			36678 (vvs)	$\nu_0 + 945$
37269 (vs)	$\nu_0 + 907$				37005 (w)	$\nu_0 + 1272$
37314 (ms)	$\nu_0 + 952$	The $\nu_0$ band at 36352 cm <sup>-1</sup>	37572 (w)	$\nu_0 + 2 \times 901$	37239 (ms)	$\nu_0 + 945 + 560$
37625 (vs)	$\nu_0 + 1272$				37449 (w)	$\nu_0 + 945 + 773$
					57625 (ms)	$\nu_0 + 2 \times 945$
					37953 (w)	$\nu_0 + 945 + 1272$
					38182 (vw)	$\nu_0 + 2 \times 945 + 560$
					38561 (vvw)	$\nu_0 + 3 \times 945$
					38898 (vvw)	$\nu_0 + 2 \times 945 + 1272$

Microphotometric record of the ultraviolet absorption spectra of phenetole

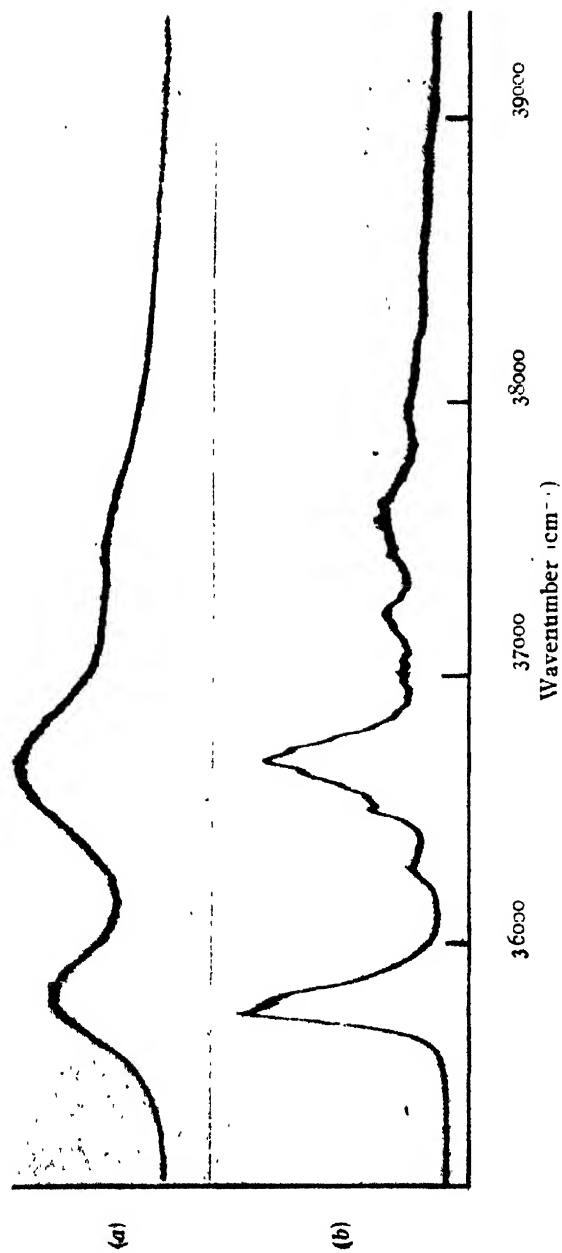


FIG. 1

(a) Liquid at 30°C

(b) Solid at -180°C

Microphotometric records of the ultraviolet absorption spectra of *n*-butylbenzoate

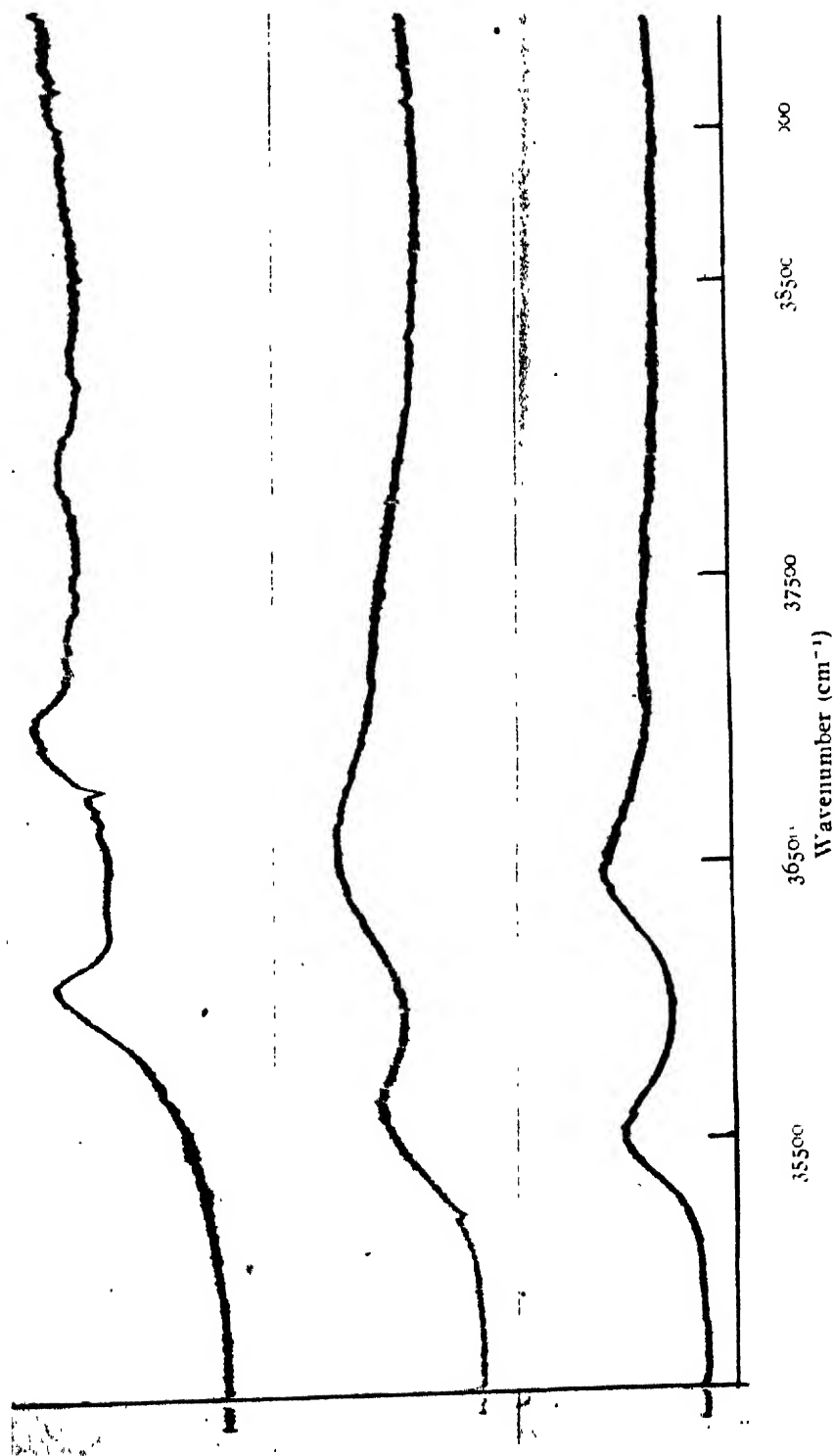
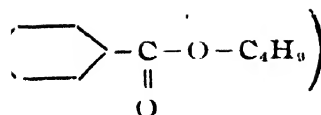


FIG. 2

TABLE II

Ultraviolet absorption bands of *n*-butylbenzoate

Vapour		Liquid at 32°C		Solid at -185°C	
$\nu$ (cm <sup>-1</sup> ) and Int.	Assignment	$\nu$ (cm <sup>-1</sup> ) and Int.	Assignment	$\nu$ (cm <sup>-1</sup> ) and Int.	Assignment
35703 (vww)	$\nu_0 - 396$				
36099 (vs)	$\nu_0$	35627 (vs)	$\nu_0$	35526 (vs)	$\nu_0$
36459 (w)	$\nu_0 + 360$				
37043 (vvs)	$\nu_0 + 944$	36579 (vvs)	$\nu_0 + 952$	36478 (vs)	$\nu_0 + 952$
37400 (w)	$\nu_0 + 944 + 360$				
37986 (s)	$\nu_0 + 2 \times 944$	37526 (w)	$\nu_0 + 2 \times 952$	37428 (w)	$\nu_0 + 2 \times 952$
38348 (vw)	$\nu_0 + 2 \times 944 + 360$				
38920 (vw)	$\nu_0 + 3 \times 944$				
39290 (vww)	$\nu_0 + 3 \times 944 + 360$				

*Phenetole:*

It is seen from Table I as well as from figure 1 that the fine structure of the bands of phenetole vapour reported by Sreeramamurty (1951) is completely absent in the spectrum of the substance in the liquid state. Only three broad bands are present in the liquid state. The first one on the longer wavelength side, which is at 35771 cm<sup>-1</sup> is taken as the  $\nu_0$ -band. The  $\nu_0$ -band in the vapour state (Sreeramamurty, 1951) is at 36362 cm<sup>-1</sup>. Thus there is a shift of the  $\nu_0$ -band by about 391 cm<sup>-1</sup> towards longer wavelengths with the liquefaction. The only vibrational frequency in the excited state observed in the case of the liquid state is 901 cm<sup>-1</sup> measured from these broad bands. In the case of the solid phase at -180°C, the broad bands of the liquid phase become much sharper, so that several other feeble bands which are merged in the broad bands in the spectrum of the liquid state are clearly resolved out. The vibrational frequency 901 cm<sup>-1</sup> deduced from the centres of the broad bands in the case of the liquid state is found to be resolved into two bands at 902 and 945 cm<sup>-1</sup> in the case of the solid state. The other new bands are found to have frequency-differences 560, 773 and 1272 cm<sup>-1</sup> from the  $\nu_0$ -band and their combinations with the frequency 945 cm<sup>-1</sup> or its harmonics. These bands, therefore, are due o- $\nu$  transitions and not due to the splitting of electronic energy levels. Some of the excited state frequencies observed in the case of the vapour (Sreeramamurty, 1951) are 554, 744, 907, 952 and 1252 cm<sup>-1</sup>. Robertson, *et al* (1950) reported the excited state frequencies 760, 940 and 1255 cm<sup>-1</sup> besides a few more, in the case of the vapour state. But there is one significant difference between the spectrum due to the vapour and that due to the solid. It is quite evident that the bands representing the frequencies 560, 773 and 1272 cm<sup>-1</sup> in the case of the solid state are much weaker than the corres-



ponding bands observed in the case of the vapour. Thus the transitions are restricted by neighbouring molecules in the solid state. The sharpening of the bands observed in this case is evidently due to cessation of some motions of the molecules in the lattice, which, as has been pointed out earlier (Swamy, 1952 ; Deb, 1953) might be the angular oscillations of the molecules. The influence of the intermolecular field on the electronic energy level is clearly indicated by the shift of the  $\nu_0$ -band with liquefaction. The cessation of angular motions of the molecules is probably caused by the formation of virtual bonds between neighbouring molecules. The shift of the  $\nu_0$ -band is towards longer wavelengths both with liquefaction of the vapour and solidification of the liquid phase in this case, and this may indicate a gradual strengthening of the virtual bands with lowering of temperature.

The absorption spectrum of anisole, the lower homologue of phenetole is exactly similar to that of phenetole in the liquid state. In the solid state, however, they are not exactly similar. In the case of anisole only one more vibrational frequency, in addition to that of the liquid state was observed in the solid state at low temperature (Deb, 1951a) ; whereas in the present case three more vibrational frequencies and several combination frequencies are also observed.

#### *n*-Butylbenzoate :

In the vapour state *n*-butylbenzoate yields 9 bands. The strong and sharp band on the long wavelength side of the spectrum at  $36099\text{ cm}^{-1}$  has been assigned as the  $\nu_0$ -band of the system. The other bands are then found to correspond to vibrational frequencies 360 and  $944\text{ cm}^{-1}$  and their harmonics and combinations. One very feeble band on the long wavelength side of the  $\nu_0$ -band is observed at a distance of  $390\text{ cm}^{-1}$  from the  $\nu_0$  band. This band is totally absent in the spectra due to the liquid and solid states. Evidently, this represents a ground state vibrational frequency which probably fall to the value  $360\text{ cm}^{-1}$  in the excited state.

In the liquid state at  $32^\circ\text{C}$ , the substance yields only three broad bands, the distance between the centres of the successive bands being  $952\text{ cm}^{-1}$ . The  $\nu_0$ -band shifts towards longer wavelengths by  $472\text{ cm}^{-1}$  from its position in the vapour state, when the vapour is liquefied. When the substance is solidified and cooled to  $-180^\circ\text{C}$ , the bands again shift towards longer wavelengths, the shift of the  $\nu_0$ -band being  $100\text{ cm}^{-1}$ . No further changes are observed in this case, except a slight sharpening of the bands with lowering of temperature to  $-180^\circ\text{C}$ . The vibrational frequency  $944\text{ cm}^{-1}$  in the vapour state remains practically the same in the liquid and solid states in this case.

These results are similar to those observed in the case of ethylbenzoate (Deb, 1953) and methylbenzoate (Deb, 1951b). The influence of the intermolecular field thus lowers the excited state energy levels of these molecules,

this lowering for the change from vapour to liquid phase being much larger than that for the change from liquid to solid phase. The absence of any appreciable sharpening of bands at  $-180^{\circ}\text{C}$  points out that the angular motions of the molecules, which are supposed to be the cause of the broadening of bands in the liquid state, persist in this case even at  $-180^{\circ}\text{C}$ . The linking of the molecules with the neighbouring ones at low temperatures is thus less favoured in this case than in the case of phenetole. From an observation of similar results in the case of ethylbenzoate it was suggested that the shape of the molecule might be the determining factor in allowing the formation of virtual bonds in such a way that angular motions of the molecules are very much restricted. Evidently, in all these benzoic acid esters the presence of the flexible groups  $\text{C}(\text{O})\text{-C}_2\text{H}_5$  etc. is responsible for the fluctuation of intermolecular field even in the solid state at  $-180^{\circ}\text{C}$ . The  $\nu_{\text{C}}\text{-band}$  is a little sharper in these cases than the other bands. This shows that the vibrational transitions of the molecules broaden the electronic energy level in the excited state.

#### ACKNOWLEDGMENT

The author wishes to express his indebtedness of Prof. S. C. Sirkar, D. Sc., F. N. I., for his kind interest and guidance throughout the progress of the work.

#### REFERENCES

- Deb, A. R. 1951a, *Ind. J. Phys.*, **25**, 233.  
" " 1951b, *Ibid.*, **25**, 433.  
" " 1952, *Ibid.* **26**, 201.  
" " 1953, *Ibid.* **27**, 183.  
Robertson, W. W. Scriff, A. J. and Matsen, R. A., 1950, *J. Am. Chem. Soc.*, **72**, 1539  
Sirkar S. C., and Swamy, H. N., 1952, *J. Chem. Phys.*, **20**, 1177.  
Sreeramamurty K., 1951, *Ind. J. Phys.*, **25**, 123.  
Swamy, H. N., 1952, *Ind. J. Phys.*, **26**, 233, 445.  
" " 1953, *Ibid.* **27**, 55, 119.

# RADIATION PROPERTIES OF THE OPEN END OF A RECTANGULAR WAVEGUIDE WHEN THE END PLANE IS INCLINED TO THE GUIDE AXIS\*

By G. S. SANYAL

INSTITUTE OF RADIO PHYSICS AND ELECTRONICS, CALCUTTA UNIVERSITY

(Received for publication, August 14, 1953)

**ABSTRACT.** The far-zone field intensity pattern due to radiation from the obliquely cut open end of a rectangular waveguide is studied experimentally and theoretically in the microwave frequency range. The waveguide used had internal dimensions of 0.9" x 0.4" and the exciting wavelength was in the range 3.2 to 3.5 cms. The experimentally obtained radiation patterns show that in the  $H$ -plane of the waveguide, the beam width of the major lobe decreases with the increase of the angle of inclination of the end plane to the guide axis and a compromise between the beam width and the intensities of the minor lobes is affected when the inclination is  $50^\circ$ . Making certain simplifying assumptions the normalised radiation patterns are calculated by applying the diffraction theory. The possible sources of discrepancy between the calculated and experimental patterns are discussed. To check the matching property of the open end to free space, V.S.W.R. (voltage standing wave ratio) measurements have also been carried out for various inclinations of the end plane. It has been found that the V.S.W.R. in the wavelength range tested is not high and the matching properties improve when the inclination is large, e.g.,  $70^\circ$ .

## 1. INTRODUCTION

Of the many types of apertures employed as radiating elements in the microwave frequency range, one of the simplest is the open end of a rectangular waveguide. Such open ends, with the end plane perpendicular to the waveguide axis, are often utilised to serve as the primary feed of microwave antenna systems. The radiation properties of such apertures have been investigated by Chu (1940).

Radiation properties of open ends, with the end plane inclined to the axis of the waveguide appears, however, not to have been studied, though, such obliquely cut apertures are likely to be of use as feeds. The present paper describes the results of such study, both experimental and theoretical, made in the microwave range with a rectangular waveguide with the open end perpendicular to the  $H$ -plane, but inclined to the guide axis at various angles. It has been found that as the inclination of the end plane to the guide axis increases, the direction of maximum radiation deviates away from the normal to the plane towards the waveguide axis. At the same

\* Communicated by Prof. S. K. Mitra.

time, the width of the major lobe in the H-plane decreases. When the inclination is very large, minor adjacent lobes of appreciable intensity appear. When the inclination is about  $50^\circ$ , a compromise is effected between the beam width of the major lobe and intensities of the minor lobes. It has been found that the radiation pattern in the E-plane is practically unaffected by the change of inclination of the cut. This, of course, is as expected, because, the shorter sides of the rectangular end plane are unaffected by changes in the inclination.

Attempt has also been made to calculate, on the basis of the diffraction theory, the normalised radiation pattern of the opening. Fair agreement has been obtained between the calculated and experimental patterns. The possible sources of discrepancy between the two are discussed.

To check the matching property of the open end to free space, V.S.W.R. (voltage standing wave ratio) measurements have also been carried out for various inclinations of the endplane. It has been found that the V.S.W.R. in the wavelength range tested (3.2 to 3.5 cms) is not high and the matching properties improve when the inclination is large.

## 2. EXPERIMENTAL OBSERVATIONS

As mentioned in the Introduction, measurements were carried out, (i) on the radiation properties of the obliquely cut open end of the rectangular waveguide and (ii) on the V.S.W.R. in the waveguide for various inclinations of the end plane. The waveguide used had internal dimensions  $0.9'' \times 0.4''$ . The exciting wavelength was in the range 3.2 to 3.5 cms.

(i) *Measurement of the radiation pattern.* The waveguide with its H-plane horizontal was suitably mounted about 5 ft. above the floor level. To obtain radiation from the open end (which will hereinafter be referred to as "antenna"), the waveguide was fed from a C.W. klystron oscillator. The output of the oscillator was controlled by an attenuator and was delivered to the 'antenna' through a flexible R.F. co-axial cable with waveguide adapter at its ends. A reaction type cavity wavemeter was incorporated to note the frequency.

To measure the field intensity, a moderately directive pyramidal horn, with aperture dimensions  $3\frac{1}{2}'' \times 3\frac{1}{8}''$  and  $3\frac{1}{4}''$  long was used as a pick-up antenna. The horn was suitably mounted on a movable base at the same height above the floor level as the antenna (1 ft.). The axis of the horn was horizontal and, when taking measurements, always pointed towards the centre of the antenna. The horn terminated in a crystal detector and a D.C. microammeter read the crystal current. The microammeter readings were periodically calibrated by a precision variable waveguide attenuator.

The far-zone radiation pattern was measured in the horizontal plane, 5 ft. above the floor level, by moving about the receiving horn. For each case, two measurements of the H-plane radiation pattern were made by turning the waveguide from one of its broadsides to another. Almost

identical radiation patterns were obtained indicating that the effect of stray reflections from neighbouring objects was negligible. E-plane radiation patterns were measured in the same manner. The patterns obtained for various inclinations of the end plane are shown in figures 1(a) to 1(i).

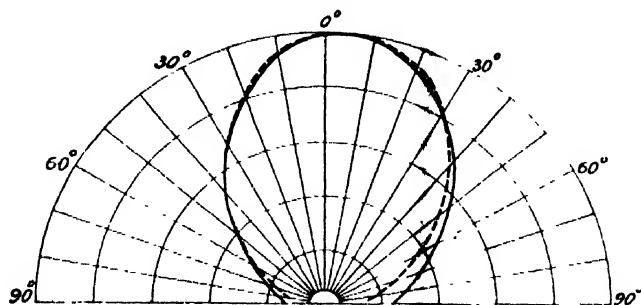


FIG. 1(a)

H-plane radiation pattern Broken line curve—experimental Continuous line curve—theoretical Guide dimensions (internal):  $0.9'' \times 0.1''$  with  $0.1''$  all;  $\lambda = 3.35$  cms;  $\alpha = 0^\circ$

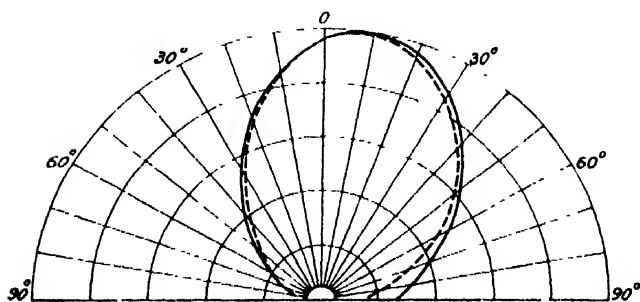


FIG. 1(b)

Same as Fig. 1(a) with  $\alpha = 20^\circ$

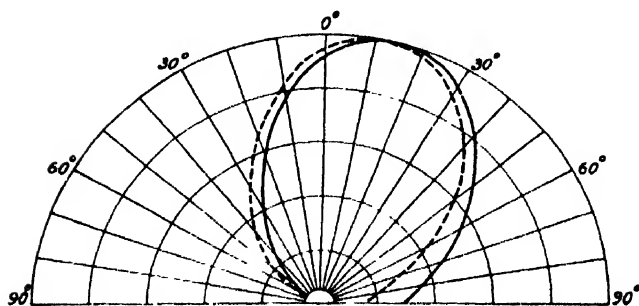


FIG. 1(c)

Same as Fig. 1(a) with  $\alpha = 30^\circ$ .

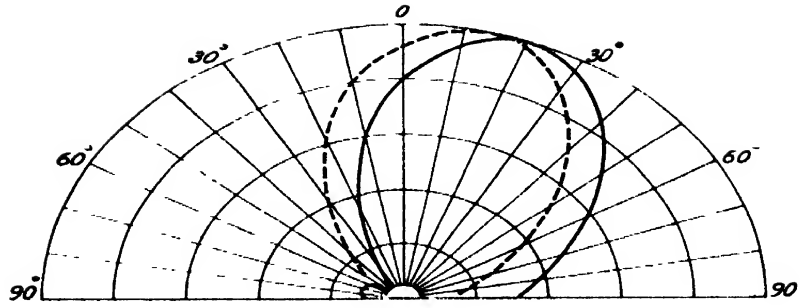


FIG. 1(d)  
Same as Fig. 1(a) with  $\alpha = 40^\circ$ .

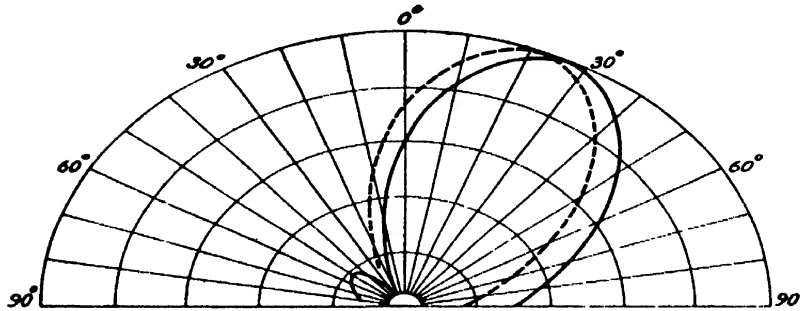


FIG. 1(e)  
Same as Fig. 1(a) with  $\alpha = 50^\circ$ .

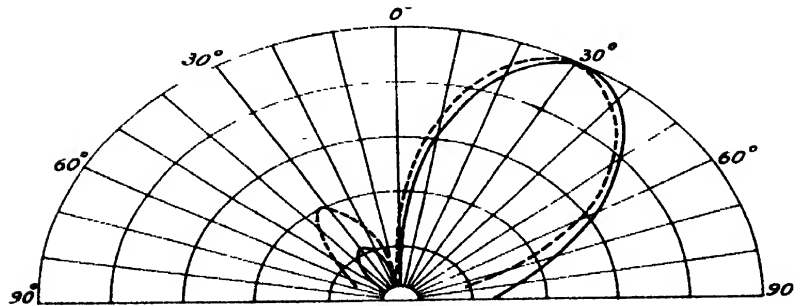


FIG. 1(f)  
Same as Fig. 1(a) with  $\alpha = 60^\circ$ .

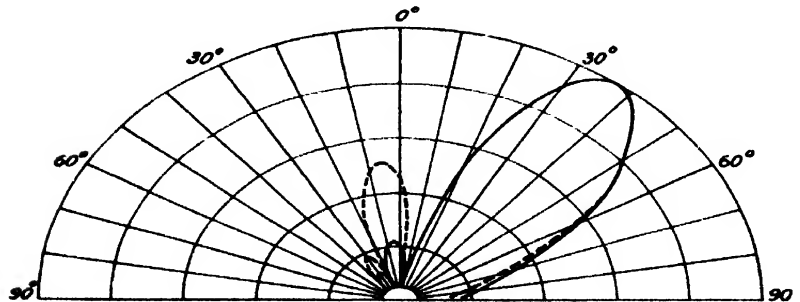


FIG. 1(g)  
Same as Fig. 1(a) with  $\alpha = 70^\circ$ .

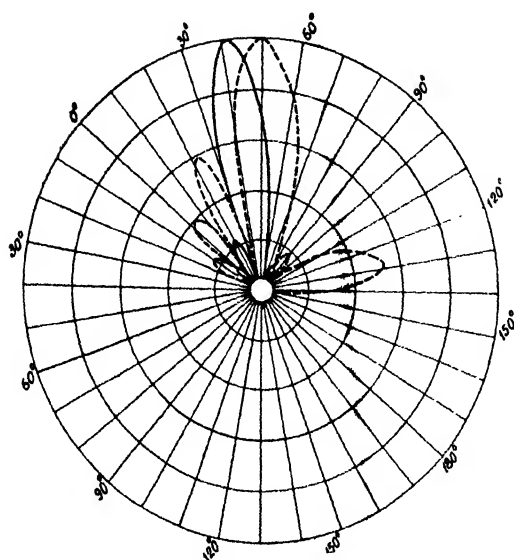


FIG. 1(h)  
Same as Fig. 1(a) with  $\alpha = 90^\circ$ .

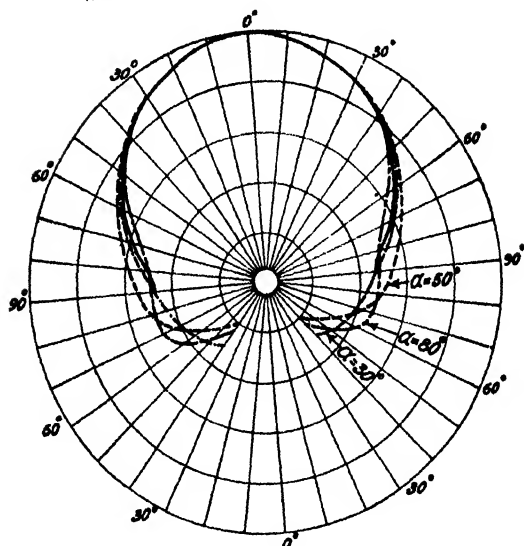


FIG. 1(i)  
E-plane radiation patterns. Broken line curves—experimental. Solid line curve—  
theoretical. Guide dimensions (internal):  $0.9'' \times 0.4''$  with  $0.1''$  wall,  $\lambda = 3.35$   
cms.

(ii) *V. S. W. R. Measurements.* The V. S. W. R. produced in the waveguide, due to the mismatching of the open end to free space, was measured by a precision waveguide slotted section together with a probe

detector unit. A fixed 15 db attenuator and a precision variable attenuator were interposed between the R. F. source (C. W. klystron oscillator) and the standing wave line. To measure the V. S. W. R. the probe detector carriage was placed at a voltage minimum. The probe was then shifted to its adjacent maximum and the extra attenuation required to bring the level of detected current to its previous minimum was a measure of the V. S. W. R. The klystron output and frequency was monitored through a directional coupler by a reaction type wavemeter and a crystal detector. A schematic diagram of the set up is shown in figure 2. V. S. W. R. obtained is shown in figure 3.

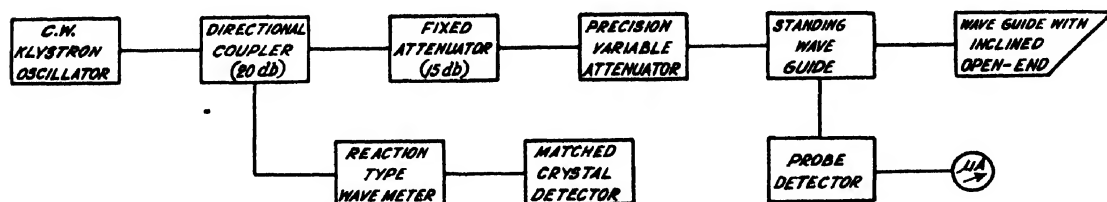


FIG. 2

Block diagram of the experimental arrangement for the measurement of the V. S. W. R. in the guide.

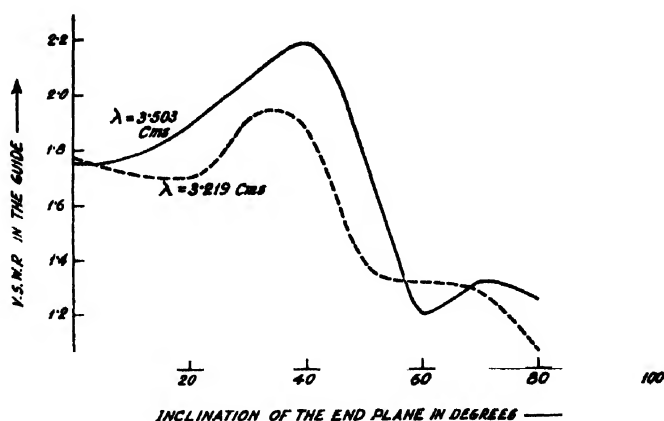


FIG. 3

V. S. W. R. in the guide versus inclination of the end plane of the waveguide.

### 3. THEORETICAL ANALYSIS

In order to calculate the intensity of the radiated field at any point in the far-zone, it is first necessary to know the distribution of the field—the amplitude and the phase—over the aperture plane which acts as the radiating antenna. For this we shall make the following simplifying assumptions.



(i) *Phase Distribution.* The dominant mode ( $TE_{01}$ ) of the field advancing along the axis of the waveguide produces a field distribution, uniformly polarised in the aperture plane  $XOY$  (figure 4) with the electric field vector along the  $Y$ -direction. We assume that the phase distribution in the aperture plane is the same as that, which would have existed if the waveguide had not been cut and continued along the right (figure 5)

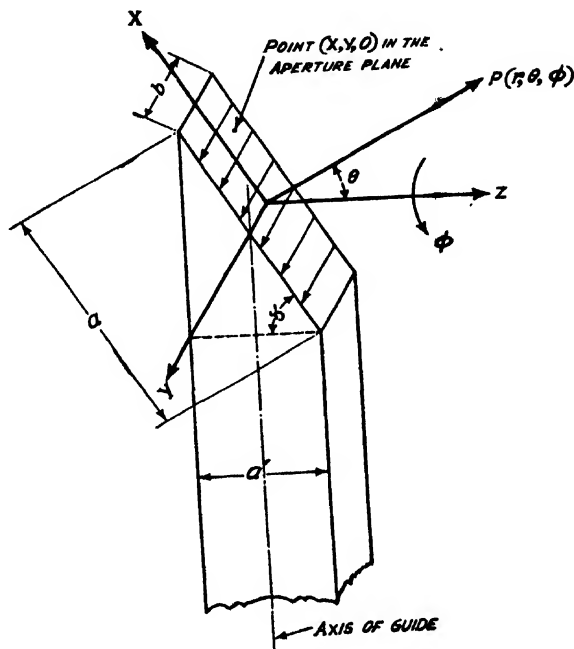


FIG. 4

View of the inclined end plane of the waveguide showing the co-ordinate systems.

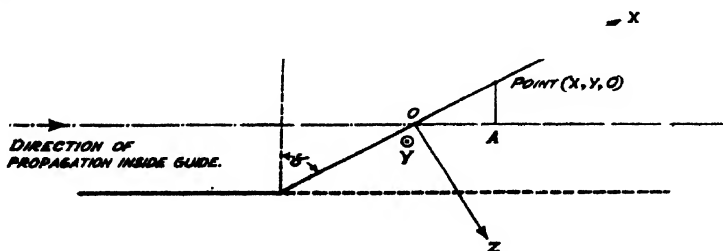


FIG. 5

Diagram illustrating the phase shift at a point  $(x, y, 0)$  relative to the origin in the end-plane. Distance  $OA$  corresponds to the phase lag associated with the point.

Hence, remembering that the cut leaves the narrow dimension unaltered, the phase distribution over the aperture with reference to the centre point of the plane is given by

$$\left. \begin{aligned} \psi_1(x) &= (2\pi/\lambda_g)x \sin \alpha \\ \psi_2(y) &= 0 \end{aligned} \right\} \dots (1)$$

where  $\lambda_g$  is the wavelength inside the waveguide given by

$$\lambda_g = \lambda / \sqrt{1 - (\lambda/2a')^2} \quad \dots (2)$$

$a'$  being the broad dimension of the waveguide.

(ii) *Amplitude distribution.* With the dominant  $TE_{01}$  mode if, as before, the waveguide is imagined to be continued beyond the cut end, one has to assume that the amplitude distribution (normalised to have a maximum value of unity) in the  $X$ -direction is sinusoidal, being given by  $a(x) = \cos(\pi x/a)$ . Since the guide is limited at the aperture plane, higher order mode fields of the type  $TE_{on}$  are locally generated in the region of the same. Though, it is not possible to assess the individual contributions due to such high order modes, it may reasonably be assumed that field ( $TE_{on}$ ) due to these higher order modes, together with the dominant mode, will tend to make the amplitude distribution over the aperture plane more or less uniform. The amplitude distribution may thus be assumed to be approximately uniform *i.e.*, we write

$$a_1(x) = 1, \quad -a/2 < x < a/2 \quad \dots (3)$$

Since the narrow dimension of the guide is left unaltered by the oblique cut and since modes of the type  $TE_{on}$  only are assumed to be present, the amplitude distribution in the  $Y$ -direction is also constant and we write\*

$$a_2(y) = 1, \quad -b/2 < y < b/2 \quad \dots (4)$$

(iii) There will be currents flowing over the exterior surface of the guide. There will also be reflected component of the dominant mode field in the aperture. The effects of these are, however, small and are neglected.

With the above assumptions, the field distribution function  $f(x, y)$  for the aperture may be written simply, from Eqs. (3) and (4), as

$$f(x, y) = \exp[-j(2\pi/\lambda_g)x \sin \alpha] \quad \dots (5)$$

The far-zone field intensity pattern in the direction  $\theta, \phi$  due to the radiating aperture having a field distribution as given by Eq. (5), may, therefore, be written according to the usual diffraction formula (Silver, 1949) as follows :

$$g(\theta, \phi) = \int_{-a/2}^{a/2} \int_{-b/2}^{b/2} f(x, y) (\cos \theta + S_z) \exp[j\beta \sin \theta (x \cos \phi + y \sin \phi)] dx dy \quad \dots (6)$$

where  $\beta = 2\pi/\lambda$  is the freespace phase constant,

$\lambda$  is the freespace wavelength,

and  $S_z$  is the  $z$ -component of a unit vector along a ray through the aperture.

Since the phase distribution in the aperture plane has been assumed to be that due to the  $TE_{01}$  mode alone in the guide,  $S_z$  is given by

\* The effects of the modes of the type  $TE_{mn}$  ( $m > 0$ ) on the amplitude distribution are neglected. The variations that are possibly introduced by the presence of the higher modes of propagation are also neglected in writing out the expression for the phase distribution.)

$$S_z = [1 - (1/\beta^2)(\partial\psi_1/\partial x)^2 - (1/\beta^2)(\partial\psi_2/\partial y)^2]^{1/2} \\ = [1 - (\lambda/\lambda_g)^2 \sin^2 \alpha]^{1/2} \quad \dots (7)$$

Substitution for  $f(x, y)$  from Eq. (5) in Eq. (6) yields

$$g(\theta, \phi) = (\cos \theta + S_z) \int_{-a/2}^{a/2} \exp[j\{\beta \sin \theta \cos \phi - (2\pi/\lambda_g) \sin \alpha\} x] dx \\ \times \int_{-b/2}^{b/2} \exp[j(\beta \sin \theta \sin \phi) y] dy \\ = ab(\cos \theta + S_z) \left\{ \frac{\sin \{(\pi a/\lambda) \sin \theta \cos \phi - (\pi a/\lambda_g) \sin \alpha\}}{(\pi a/\lambda) \sin \theta \cos \phi - (\pi a/\lambda_g) \sin \alpha} \right. \\ \left. \times \left[ \frac{\sin \{(\pi b/\lambda) \sin \theta \sin \phi\}}{(\pi b/\lambda) \sin \theta \sin \phi} \right] \right\} \quad \dots (8)$$

The principal plane patterns are therefore :

In the XZ or H-plane ( $\phi=0$ ),

$$g(\theta) = (\cos \theta + S_z) \frac{\sin [(\pi a/\lambda) \sin \theta - (\pi a/\lambda_g) \sin \alpha]}{(\pi a/\lambda) \sin \theta - (\pi a/\lambda_g) \sin \alpha} \quad \dots (9)$$

In the YZ or E-plane ( $\phi=\pi/2$ ),

$$g(\theta) = (\cos \theta + S_z) \frac{\sin [(\pi b/\lambda) \sin \theta]}{(\pi b/\lambda) \sin \theta} \quad \dots (10)$$

The field patterns in the H-plane given by Eq. (9) were computed for values of  $\alpha$  at 10° degree intervals and normalised by setting  $(g_\theta)_{\max}$  to be unity. The computed patterns are shown, along with those obtained experimentally, in figures 1(a) to 1(h).

It will be seen from Eq.(10) that the pattern in the E-plane has a maximum along  $\theta=0$  and is symmetrical. The variation in  $S_z$  due to different values of  $\alpha$ , will modify the patterns only to a minor extent. In computing patterns in this plane, therefore,  $S_z$  is put equal to unity for all values of  $\alpha$ . This computed pattern together with those experimentally obtained are shown in figure 1(i).

#### 4. DISCUSSION

It will be seen from the H-plane radiation patterns that so far as the major lobes are concerned, the agreement between experimental and theoretical results is quite satisfactory. This is notwithstanding the several simplifying assumptions that have been made in carrying out the computation. The zeroes and maxima of the adjacent side lobes—then they occur—are nearly at the predicted angles. The beam width of the major lobe, as measured between the two half-power points on either side of the maximum,

gradually becomes narrower and the side lobes are of negligible intensity up to the case with  $\alpha = 60^\circ$  degrees.

Since the E-plane radiation pattern is symmetrical and is almost independent of  $\alpha$ , the assumption of constant amplitude distribution in the Y-direction of the aperture, [*e.g.*,  $a_2(y) = 1$ ] is justified. The patterns would have been considerably distorted if the higher order modes of type  $TE_{m,n}$  ( $m > 0$ ) were present.

Let us now discuss the radiation patterns in the H-plane a little more closely. Figures 1(a) to 1(h) show that for angles ( $\alpha$ ) less than  $70^\circ$  degrees, the patterns are deviated towards the normal to the aperture more than is predicted by theory. This deviation of the pattern from the predicted angle is maximum for an angle ( $\alpha$ ) of about  $40^\circ$  degrees and becomes least for an angle of about  $70^\circ$  degrees. Thereafter, the deviation is in the other sense, that is, away from the normal. The shift of the pattern towards the normal from the predicted angle may be due to the presence of unequal wall currents flowing on the exterior narrow surfaces of the guide. This effect is augmented by the fact that the energy density in the aperture plane is not uniform, as assumed, due to the continuous spilling over of energy from inside the guide to the open space across the aperture. This will produce a gradual decrease of aperture illumination in the X-direction. Also, since the phase velocity in the guide in the region of the aperture is higher than the free space velocity, the incident wavefront will tilt towards the normal; thus, the effective angle of incidence of the wave on the aperture plane (*i. e.*,  $\alpha$ ) is less than the actual angle of cut. However, as the inclination of the end plane increases, the guide wavelength  $\lambda_g$  in the region of the aperture approaches the free space wavelength  $\lambda$ , and a greater phase shift per unit length in the X-direction is produced. This greater phase shift will deviate the direction of maximum intensity away from normal. An opposing effect thus comes into play making the agreement with the theoretical results better as  $\alpha$  increases (*cf.*  $\alpha = 70^\circ$  degrees). For still larger angles (*e.g.*  $\alpha = 80^\circ$  degrees), the aperture dimension, which is proportional to  $\sec \alpha$ , increases very rapidly and the counterbalancing effect becomes predominant. This accounts for the deviation of the measured radiation pattern in the direction away from the normal.

It will be seen from figure. 3 that the reflection, corresponding to the dominant mode, set up in the guide, increases as the angle  $\alpha$  increases, reaching a maximum in the neighbourhood of  $\alpha = 40^\circ$  degrees. Thereafter, it decreases continuously. This shows that the effect of the higher order modes on the impedance transformation from guide to free space becomes more pronounced with increasing values of  $\alpha$ . For large values of  $\alpha$  ( $\alpha > 50^\circ$ ), however, the transition region from the waveguide to free space becomes more gradual and hence the guide is more effectively matched to free space.

ACKNOWLEDGMENT

The author wishes to take this opportunity of recording his grateful thanks to Professor S. K. Mitra for his interest in the work and for many helpful discussions.

REFERENCES

Chu, L. J , 1940 *Jour. App. Phys* , 11, 603.

Silver, S., 1949, *Microwave Antenna Theory and Design* (Mc Graw-Hill), p p. 160-174.



# ON THE RELAXATION TIME OF POLAR MOLECULES IN THE LIQUID STATE

By S. C. SIRKAR

OPTICS DEPARTMENT, INDIAN ASSOCIATION FOR THE CULTIVATION OF SCIENCE, CALCUTTA 32

(Received for publication September, 11, 1953)

**ABSTRACT.** It is pointed out that the values of  $\lambda_m$ , deduced by previous workers from Cole and Cole equation do not agree with the values actually observed by some recent workers in the case of a few polar liquids. Debye's theory is extended to the case of a liquid containing a mixture of monomeric and dimeric molecules and an expression for the complex dielectric constant has been deduced. It is found that the expression is too complicated to yield a simple condition for maximum absorption.

The various causes for the discrepancy between the actual molecular volume and the volume of the rotor calculated from Debye's theory observed in certain cases have been discussed.

## INTRODUCTION

It is well known that the value of the permanent electric moment,  $\mu$  of the molecule in the liquid state calculated from the Debye equation from the observed values of  $\epsilon_0$  and  $\epsilon_\infty$ , the dielectric constant of the liquid for fields of zero and infinite frequencies respectively, do not generally agree with the values observed in the case of the respective vapours. Attempts have been made by Onsager (1936) and Kirkwood (1939) to modify the Debye equation, taking into account the influence of intermolecular field so that the values of  $\mu$  calculated from the modified equations may agree with those observed for the vapour. In the region of very high frequencies certain polar liquids exhibit absorption and the dielectric constant  $\epsilon^*$  is complex due to the presence of a relaxation time  $\tau$  which should be given by the Debye equation

$$\epsilon^* = \epsilon_\infty + \frac{\epsilon_0 - \epsilon_\infty}{1 + iB\omega\tau}, \quad \dots (1)$$

where

$$B = \frac{\epsilon_0 + 2}{\epsilon_\infty + 2}$$

Actually, however, it is observed that in the case of many liquids equation (1) cannot explain the complex dielectric constant for different frequencies if a suitable fixed value of  $\tau$  is assumed in equation (1). To overcome this difficulty existence of a distribution in the relaxation time in such cases has been assumed. In order to take into account the distribution

of relaxation time Cole and Cole (1941) suggested the following empirical expression for the complex dielectric constant

$$\epsilon^* = \epsilon_\infty + \frac{\epsilon_0 - \epsilon_\infty}{1 + (i\omega\tau_0)^{1-\alpha}} \quad \dots \quad (2)$$

where  $\tau_0$  is the most probable relaxation time corresponding to a frequency at which the absorption is maximum and  $\alpha$  is the empirical constant with values between 0 and 1.

Hennelly, Heston and Smyth (1948) observed that in the case of certain alkyl bromides such as octyl bromide etc., there is a distribution of relaxation time,  $\alpha$  being greater than zero. Franklin *et al* (1950) have discussed the values of  $\alpha$  for certain alkyl halides dissolved in different solvents and have shown that  $\alpha$  has a value different from zero in the case of solutions in certain solvents, but in some other cases  $\alpha$  is zero.

Branin and Smyth (1952) have pointed out that in the arc plot with  $(\epsilon' - \epsilon_\infty)/(\epsilon_0 - \epsilon_\infty)$  as abscissa and  $\epsilon''/(\epsilon_0 - \epsilon_\infty)$  as the ordinate, where  $\epsilon'$  and  $\epsilon''$  are defined by the equation  $\epsilon^* = \epsilon' - i\epsilon''$ , the following expressions can be assumed to take account of the distribution of relaxation time

$$\begin{aligned} \frac{\epsilon' - \epsilon_\infty}{\epsilon_0 - \epsilon_\infty} &= \int_0^\infty \frac{G(\tau) d\tau}{1 + \omega^2 \tau^2} \\ \frac{\epsilon''}{\epsilon_0 - \epsilon_\infty} &= \int_0^\infty \frac{\omega \tau G(\tau) d\tau}{1 + \omega^2 \tau^2} \end{aligned} \quad (3)$$

where  $G(\tau)$  is a function of  $\tau$ . Two forms of the function, the Cole and Cole function (1941) and the Wagner-Yager (1936) function have been discussed and compared with experimental results by these authors.

It is the object of the present paper to point out that results of investigations on the absorption of U. H. F. and microwaves reported by Sen (1950, 1951), Kastha (1952) and Ghosh (1953a, 1953b) indicate the presence of several discrete values of  $\tau$  in the case of some of the liquids studied by them and that in calculating the complex dielectric constant in such cases these discrete values of  $\tau$  should be taken into account instead of a distribution given by the  $G$ -function. It has also been pointed out by Ghosh (1953) that new absorption maxima due to dimers appear in some cases only when the liquids are cooled down to low temperatures. In such cases, therefore, a single value of  $\tau$  should explain the observed dielectric constant for different frequencies at higher temperatures. This is corroborated by the results reported by Hennelly, Heston and Smyth (1948) who observed that the value of  $\alpha$  in Cole and Cole equation is small in the case of certain liquids and it diminishes almost to zero with rise of temperature of the liquids. Some of these liquids are *i*-propyl bromide, *i*-butyl bromide, chlorobenzene, bromobenzene, ethylene chloride etc. These facts clearly indicate that the agents which are responsible for the



deviation from Debye equation at lower temperatures tend to disappear at higher temperatures. These agents are evidently dimers which are present in the liquid in considerable proportions at lower temperatures and gradually break up into monomers at higher temperatures, as observed in the case of many liquids by Sen (1950, 1951), Kastha (1952) and Ghosh (1953a).

#### DIFFICULTIES WITH DISTRIBUTION OF RELAXATION TIME THEORY

The Cole and Cole empirical relation would explain the observed facts satisfactorily if a distribution of relaxation time dependent only on temperature and consequently on the viscosity of the liquid were present in the liquid. As pointed out above, actually, more than one discrete relaxation time, instead of a continuous distribution, are observed in many cases at any particular temperature. Hence although the empirical equation can explain the dielectric constant of the liquid for different frequencies with a suitably adjusted value of  $\alpha$  for each temperature, the value of  $\lambda_m$ , the wave length showing maximum absorption at each temperature, deduced from the Cole and Cole equation may not agree with the actual value observed by the method of direct determination of absorption coefficient of the liquid for different frequencies. It can be seen from a comparison of the two sets of values given in Table I that such a discrepancy actually occurs in some cases.

TABLE I

Liquid	Temperature	$\lambda_m$ deduced from Cole and Cole equation (Hennelly <i>et al.</i> , 1948)	$\lambda_m$ actually observed by direct method (Ghosh, 1953a)
Chlorobenzene	25°C	1.94 cm	36.5 cm
Bromobenzene	1°C	4.53 cm	34.5 cm

The absorption peak at 36.5 cm observed by Ghosh (1953a) is assumed by him to be due to dimers and that due to monomers should, of course, be at a smaller wave length, but the consistent value of  $\lambda_m$  due to the monomer deduced from that for the dimer is about 28 cm, and it cannot be so small as 1.94 cm deduced from Cole and Cole equation. In the case of bromobenzene at 0°C the peak observed at 34.5 cm (Ghosh, 1953a) has been assumed to be due to a monomer. So the value 4.53 cm deduced by Hennelly *et al.* (1948) from Cole and Cole equation is much too low. It has further been observed by Ghosh (1953c) that bromobenzene does not show any absorption maximum for the wave length 3.18 cm in the temperature range 0°–80°C, and therefore, the  $\lambda_m$  deduced by Hennelly *et al.* (1948) from Cole and Cole equation is not actually observed. Similar discrepancies have also been observed in the case of ethylene chloride and ethylene bromide by Ghosh (1953b).

# APPLICABILITY OF DEBYE'S THEORY IN PRESENCE OF BOTH MONOMERS AND DIMERS IN THE LIQUID

It has to be pointed out that the values of the radius of the rotor have been calculated so far by previous authors from Debye's theory on the assumption that there is only one type of rotor in the liquid. As actually both monomers and dimers are present in the liquid, it is not possible to obtain the accurate value of  $\tau$  from the relation

$$\omega\tau = \frac{\omega + 2}{\epsilon_0 + 2} \sqrt{\frac{\epsilon_0}{\epsilon_\infty}} \quad \dots (4)$$

unless the relative concentration of the monomers and dimers and their contributions to  $\epsilon_0$  and  $\epsilon_\infty$  are known and equation (4) is suitably modified to take into account these contributions. If  $f_1$  and  $f_2$  be the mole fractions of the single and double molecules respectively the equation for the complex dielectric constant  $\epsilon$  given by Debye (1929) can be modified in the case of a mixture assuming Mosotti's hypothesis to hold. The modified equation for the mixture becomes

$$\frac{\epsilon - 1}{\epsilon + 2} \cdot \frac{Mf_1 + M'f_2}{\rho} = P_1(\omega)f_1 + P_2(\omega)f_2 \quad \dots (5)$$

where

$$P_1(\omega) = \frac{4\pi N}{3} \left[ \alpha_0 + \frac{\mu^2}{3kT} \cdot \frac{1}{1 + i\omega\tau} \right],$$

$$P_2(\omega) = \frac{4\pi N}{3} \left[ \alpha'_0 + \frac{\mu'^2}{3kT} \cdot \frac{1}{1 + i\omega\tau'} \right],$$

$\alpha_0$ ,  $\mu$ ,  $M$  and  $\tau$  are respectively the polarisability, permanent electric moment, molecular weight and relaxation time of the single molecule and  $\alpha'_0$ ,  $\mu'$ ,  $M'$  and  $\tau'$  are the corresponding quantities for the dimer. Let the quantities  $\epsilon_0$ ,  $\epsilon_\infty$ ,  $\epsilon'_0$  and  $\epsilon'_\infty$  for the monomeric and dimeric molecules respectively be defined as follows according to Debye (1929) :—

$$\begin{aligned} \frac{\epsilon_0 - 1}{\epsilon_0 + 2} \cdot \frac{M}{\rho} &= \frac{4\pi N}{3} \left( \alpha_0 + \frac{\mu^2}{3kT} \right) \\ \frac{\epsilon'_0 - 1}{\epsilon'_0 + 2} \cdot \frac{M'}{\rho'} &= \frac{4\pi N}{3} \left( \alpha'_0 + \frac{\mu'^2}{3kT} \right) \\ \frac{\epsilon_\infty - 1}{\epsilon_\infty + 2} \cdot \frac{M}{\rho} &= 4\pi N \alpha_0 \\ \frac{\epsilon'_\infty - 1}{\epsilon'_\infty + 2} \cdot \frac{M'}{\rho'} &= \pi N \alpha'_0 \end{aligned} \quad (6)$$

Here  $\epsilon_0$  and  $\epsilon_\infty$  are the dielectric constants of the liquid containing only monomeric molecules, for frequencies zero and infinity respectively and  $\epsilon'_0$  and  $\epsilon'_\infty$  are the corresponding quantities for the liquid containing only

dimeric molecules and  $\rho$  and  $\rho'$  are the corresponding densities of the liquids.

Then from (5) and (6) we get,

$$f_1 P_1(\omega) + f_2 P_2(\omega) = \frac{\epsilon_\infty - 1}{\epsilon_\infty + 2} \cdot \frac{f_1 M}{\rho} + \frac{\epsilon_\infty' - 1}{\epsilon_\infty' + 2} \cdot \frac{f_2 M'}{\rho'} + \frac{M f_1}{\rho} \left( \frac{\epsilon_0 - 1}{\epsilon_0 + 2} - \frac{\epsilon_\infty - 1}{\epsilon_\infty + 2} \right) \frac{1}{1 + i\omega\tau} + \frac{M' f_2}{\rho'} \left( \frac{\epsilon_0' - 1}{\epsilon_0' + 2} - \frac{\epsilon_\infty' - 1}{\epsilon_\infty' + 2} \right) \frac{1}{1 + i\omega\tau'} \quad \dots \quad (7)$$

If it is now assumed that  $\epsilon_\infty = \epsilon_\infty' = n^2$ , where  $n$  is the refractive index of the actual liquid containing both monomeric and dimeric molecules and that  $\rho = \rho'$ , we get,

$$f_1 P_1(\omega) + f_2 P_2(\omega) = \frac{1}{\rho} \cdot \frac{n^2 - 1}{n^2 + 2} (M f_1 + M' f_2) + \frac{M f_1}{\rho} \cdot \left( \frac{\epsilon_0 - 1}{\epsilon_0 + 2} - \frac{n^2 - 1}{n^2 + 2} \right) \frac{1}{1 + i\omega\tau} + \frac{M' f_2}{\rho} \cdot \left( \frac{\epsilon_0' - 1}{\epsilon_0' + 2} - \frac{n^2 - 1}{n^2 + 2} \right) \frac{1}{1 + i\omega\tau'} \quad \dots \quad (8)$$

From (5) we get,

$$\epsilon = \frac{1 + \frac{2\rho}{M f_1 + M' f_2} \{P_1(\omega) f_1 + P_2(\omega) f_2\}}{1 - \frac{\rho}{M f_1 + M' f_2} \{P_1(\omega) f_1 + P_2(\omega) f_2\}} \quad \dots \quad (9)$$

From (8) and (9) we get,

$$\begin{aligned} \epsilon = & \frac{1 + \frac{2(n^2 - 1)}{n^2 + 2} + \frac{2M f_1}{M f_1 + M' f_2} \cdot \frac{1}{(1 + i\omega\tau)} \left( \frac{\epsilon_0 - 1}{\epsilon_0 + 2} - \frac{n^2 - 1}{n^2 + 2} \right) + \frac{2M' f_2}{M f_1 + M' f_2} \cdot \frac{1}{(1 + i\omega\tau')} \left( \frac{\epsilon_0' - 1}{\epsilon_0' + 2} - \frac{n^2 - 1}{n^2 + 2} \right)}{1 - \frac{n^2 - 1}{n^2 + 2} - \frac{M f_1}{M f_1 + M' f_2} \cdot \frac{1}{(1 + i\omega\tau)} \left( \frac{\epsilon_0 - 1}{\epsilon_0 + 2} - \frac{n^2 - 1}{n^2 + 2} \right) - \frac{M' f_2}{M f_1 + M' f_2} \cdot \frac{1}{(1 + i\omega\tau')} \left( \frac{\epsilon_0' - 1}{\epsilon_0' + 2} - \frac{n^2 - 1}{n^2 + 2} \right)} \\ & \frac{\frac{\epsilon_0}{\epsilon_0 + 2} + \frac{M' f_2}{M f_1} \cdot \frac{(1 + \omega^2 \tau \tau')}{(1 + \omega^2 \tau'^2)} \left\{ \frac{\epsilon_0'}{\epsilon_0' + 2} - \frac{\omega^2 \tau' (\tau - \tau') n^2}{n^2 + 2} \right\}}{+ i\omega \left[ \frac{n^2}{n^2 + 2} \cdot \tau + \frac{M' f_2}{M f_1 (1 + \omega^2 \tau'^2)} \left\{ \frac{(1 + \omega^2 \tau \tau') \tau' n^2}{n^2 + 2} + \frac{\epsilon_0' (\tau - \tau')}{\epsilon_0' + 2} \right\} \right]} \\ = & \frac{1}{\epsilon_0 + 2} + \frac{M' f_2 (1 + \omega^2 \tau \tau')}{M f_1 (1 + \omega^2 \tau'^2)} \left\{ \frac{1}{\epsilon_0' + 2} - \frac{\omega^2 \tau' (\tau - \tau')}{n^2 + 2} \right\} + i\omega \left[ \frac{\tau}{n^2 + 2} + \frac{M' f_2}{M f_1 (1 + \omega^2 \tau'^2)} \left\{ \frac{\tau' (1 + \omega^2 \tau \tau')}{n^2 + 2} + \frac{\tau - \tau'}{\epsilon_0' + 2} \right\} \right] \quad \dots \quad (10) \end{aligned}$$

When  $M=M'$ ,  $f_1=f_2$  and  $\tau=\tau$ , equation (10) reduces to the following form :

$$\epsilon = \frac{\epsilon_0}{\epsilon_0 + 2} + \frac{\epsilon_\infty}{\epsilon_\infty + 2} \frac{i\omega\tau}{1 + i\omega\tau} \quad \dots \quad (11)$$

Equation (11) is the well known Debye equation for the dielectric constant of the liquid having only one type of molecules. The condition for maximum absorption deduced by Debye (1929) from (11) is given by the relation

$$\omega\tau = \frac{\epsilon_\infty + 2}{\epsilon_0 + 2} \sqrt{\frac{\epsilon_0}{\epsilon_\infty}} \quad \dots \quad (12)$$

As equation (10) is more complicated than equation (11), the simple condition for the maximum absorption given in (12) cannot be deduced from (10). Hence it is clear that the value of  $\tau$  deduced from (12) in the case of a mixture of monomeric and dimeric molecules cannot be accurate. In certain cases, however, it is found that equation (12) gives some values of  $\tau$  which lead to values of volume of the rotors agreeing with those of the dimers calculated from the density. Chlorobenzene, *o*-xylene and *m*-xylene are such substances. As reported by Ghosh (1953a), the absorption peaks due to the dimers in these cases are exhibited in the range 500–900 Mc/sec at different temperatures and those due to the single molecules may be observed at still higher frequencies.

It is unlikely that all the molecules in any of these liquids are dimers. The validity of equation (12) in these cases probably indicates that the absorption coefficient in the neighbourhood of the frequency of maximum absorption is determined predominantly by that frequency of maximum absorption, the influence of the other frequency of maximum absorption due to single molecules being negligible. Also, the values of  $\epsilon_0$  for the two types of molecules should not differ widely from each other if we want to get any reliable value of  $\tau$  from equation (12). This condition may be satisfied in the case of all the three molecules mentioned above, because the dielectric constant being low in all these cases, the contribution of the permanent electric moment to the dielectric constant is not very great and it may not change very much with the formation of dimers.

#### VISCOUS FORCES ACTING ON THE MOLECULES IN POLAR LIQUIDS

It has been pointed out by many previous authors that the volume of the rotor calculated from the relation  $\tau = 4\pi\eta a^3/kT$ , where  $\eta$  is the viscosity of the liquid, does not agree in many cases with the volume of the molecule calculated from the density of the liquid. For instance, Whiffen and

Thompson (1946) observed that in the case of solution of chloroform in heptane the volume calculated from Debye's equation is too small. The results obtained recently by Ghosh (1953*b*) in the case of pure chloroform, ethylene chloride and glycerine in the liquid state also lead to the same conclusion. Whiffen and Thompson suggested that the discrepancy is due to the fact that internal viscosity acting on the polar molecule is different from the macroscopic viscosity. It has to be pointed out, however, that the macroscopic viscosity leads to correct value of the volume of the molecule in in many pure liquids such as chlorobenzene, bromobenzene etc., (Ghosh, 1953*a*). The discrepancy is actually enormous in the case of liquids having high macroscopic viscosity, such as glycerine. This may be due to the fact that in such liquids there is strong association among neighbouring molecules. Each group of associated molecules being large in volume, the macroscopic viscosity is large, as the rate of flow is determined predominantly by the flow of the large groups. There may be, however, many single molecules in the liquid not strongly associated with their neighbours and these may orient freely along external electric field. The viscous forces acting on these molecules during the orientation are much smaller owing to want of association with neighbouring molecules. As the volume of the rotor is inversely proportional to  $\eta$  according to Debye's equation, the volume calculated with the smaller value of  $\eta$  will be much larger than that calculated taking the macroscopic viscosity in place of  $\eta$ .

In the case of other liquids having smaller coefficient of viscosity the discrepancy between the calculated value of the volume of the rotor and the actual volume of the molecule, deduced from density, may be due to two causes. As pointed out earlier, if the liquid contains both monomeric and dimeric molecules, the value of  $\tau$  calculated from Debye's equation is not correct and so the volume of the rotor deduced from the value of  $\tau$  cannot be correct. In the case of solution, presence of dimers is ruled out and the discrepancy is obviously due to the difference between the actual viscous force acting on the molecule during orientation and the macroscopic viscosity. The viscosity of heptane, for instance, is determined by the viscous forces acting on the long heptane molecule when it moves in the liquid. The chloroform molecule being almost spherical and much smaller, the viscous forces acting on it during its orientation when it is dissolved in heptane are much smaller than the macroscopic viscosity of pure heptane. If this smaller viscous force be taken into account in calculating the volume of the rotor, the volume will come out much larger than that deduced by Whiffen and Thompson (1946) assuming  $\eta$  to be equal to the macroscopic viscosity of heptane. It is difficult, however, to measure the actual viscous forces acting on the chloroform molecule when it is dissolved in heptane. In the case of such a solution of simple molecules in liquids of low viscosity if the value of  $\tau$  and the volume of the molecule calculated from its density are taken in calculating the value of  $\eta$  from Debye's equation probably the

'internal' viscous forces acting on the dissolved molecule can be roughly estimated.

## REFERENCES

- Branin, F. H. and Smyth, C. P., 1952, *J. Chem. Phys.*, **20**, 1121.  
Cole, K. S., and Cole, R. H., 1941, *J. Chem. Phys.*, **9**, 341.  
Debye, P., 1929, Polar Molecules, Chemical Catalog Co., P. 92.  
Franklin, A. D., Heston, W. M., Hennelly, E. J. and Smyth, C. P., 1950, *J. Amer. Chem. Soc.*, **72**, 3447.  
Hennelly, E. J., Heston, W. M. and Smyth, C. P., 1948, *J. Amer. Chem. Soc.*, **70**, 4102.  
Ghosh, D. K., 1953a, *Ind. J. Phys.*, **27**, 285.  
,, 1953b, *Ind. J. Phys.*, **27**, this issue.  
,, 1953c, unpublished results.  
Kastha, G. S., 1952, *Ind. J. Phys.*, **26**, 103.  
Kirkwood, J. G., 1939, *J. Chem. Phys.*, **7**, 911.  
Onsager, L., 1936, *J. Amer. Chem. Soc.*, **58**, 1486.  
Sen, S. N., 1950, *Ind. J. Phys.*, **24**, 163.  
,, 1951, *Ind. J. Phys.*, **25**, 25, 187, 237.  
Whiffen, D. H. and Thompsyn, H. W., 1946 *Trans. Farad. Soc.*, **42A**, 122.  
Yager, W. A., 1936, *Physics*, **7**, 434.

# ON THE USE OF THE SCINTILLATION COUNTER AS A GAMMA RAY SPECTROMETER, USING STILBENE CRYSTAL

BY SOBHANA DHAR AND SUNIL KUMAR SEN

INSTITUTE OF NUCLEAR PHYSICS, CALCUTTA UNIVERSITY.

(Received for publication September 7, 1953).

**ABSTRACT.** A preliminary investigation on the use of the scintillation counter as a gamma ray spectrometer has been reported here, using the organic crystal stilbene and the 1P28 photomultiplier tube. Pulse height distribution curves have been obtained for the  $\text{Co}^{60}$  source with a thin lead radiator and a thin aluminium foil respectively.  $\text{Co}^{60}$  emits two gamma rays of energies 1.17 and 1.33 Mev.; an attempt has been made to explain the formation of the peaks in the distribution curves in the light of the different processes through which gamma rays lose energy in the crystal material; the positions of the peaks agree well with the positions expected from theoretical considerations. The results have been discussed with mentions of the reports of different workers in this line. The electronic circuits and the experimental arrangements designed for the present purpose have been described in detail.

## INTRODUCTION

The scintillation counter has proved to be an extremely useful and efficient tool for the detection of nuclear radiations. The investigations on the proportional behaviour of the scintillation counter (that is, the proportionality between the energy of the incident radiation and the light output from the phosphor) have opened up another important field of application of this type of counter. Different workers have successfully utilised the proportional behaviour of the scintillation counters in measuring the energies of beta and gamma radiations. Such a device is designated as a 'scintillation spectrometer.'

The principle of a scintillation spectrometer will be best followed by recapitulating the different ways through which gamma rays lose energy in the crystal material. When gamma rays impinge on the crystal, they may interact with the crystal by three processes, namely (i) photo-electric effect (ii) Compton effect and (iii) pair production. The relative importance of the different processes will ultimately depend on the nature of the constituent elements of the crystal and the energies of the incident radiations.

The photo-electric effect is more pronounced for heavy elements and at energies below about 1 MeV.

The probability of Compton scattering decreases with energy and increases with electron density; this effect is predominant in all materials below about 5 MeV.

The third process, namely pair-production, cannot occur with a quantum energy less than 1.02 MeV and its cross section increases with energy, giving large contribution to energy loss for energies of gamma rays, greater than 10 MeV, and with elements of high atomic number for energies above 5 MeV.

In organic crystals like anthracene, stilbene, naphthalene etc., the constituent elements are light and hence for them Compton effect is most predominant. For a monochromatic beam of gamma ray of energy  $E_\gamma$ , the maximum energy  $E_c$  of Compton electrons released is given by

$$E_c = E_\gamma \frac{1}{1 + E_0/2E_\gamma} \quad \text{where } E_0 = \text{self energy of electron} = 0.511 \text{ MeV.}$$

The number of recoil electrons reaches a maximum at greatest energy and then there is a sharp fall. Hence by measuring the energy of the peak points in the pulse height distribution curve, gamma ray energies can be easily calculated.

In inorganic crystals, such as NaI(Tl) or KI(Tl) containing elements of higher atomic number, the photo-electric and pair-production processes have appreciable cross section. These processes result in more well-defined peaks in the pulse height distribution curves.

#### PREVIOUS WORKS AND RESULTS:

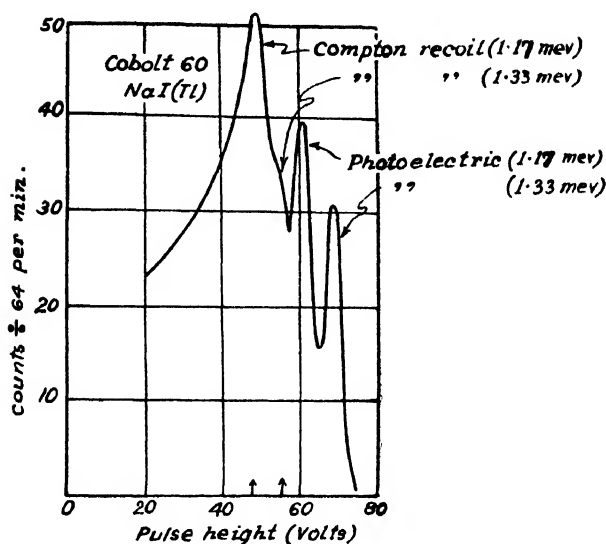
Earlier contributions in the development of the scintillation spectrometer were made by workers like Jordan and Bell (1949), Hofstadter and McIntyre (1950), Pringle, et al (1950), Johansson (1950) and Bell and Cassidy (1950).

Jordan and Bell (1949) reported the use of a scintillation gamma ray spectrometer using anthracene crystal and 1P21 tube. The accuracy of their results was checked with a similar set of data from a lens spectrometer and the agreement was remarkably well.

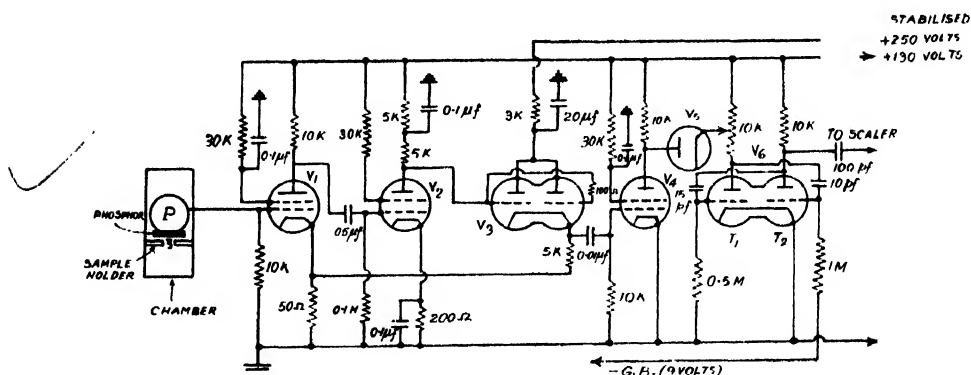
Hofstadter and McIntyre (1950) have made extensive experiments on gamma ray scintillation spectrometers with a number of sources emitting one or more gamma rays of different energies and using NaI(Tl) as the scintillator. Figure 1 shows the pulse height distribution curve obtained by them using  $\text{Co}^{60}$  source and 0.5 inch cube of NaI(Tl) crystal. They have also calculated the theoretical pulse distribution curves for different gamma ray energies and have found experimental evidence for the reality of the curves. More accurate and unique measurements of energy have also been reported by them (1950) using the combination of two crystals in coincidence. The resolution obtained by these workers is claimed to be about  $\frac{1}{10}$  to  $\frac{1}{30}$  of that in a good  $\beta$ -ray spectrograph.

Johansson (1950) has also used NaI(Tl) phosphor in combination with 1P21 tubes for the measurement of beta and gamma energies. Maienschein and Bair (1951) reported a three-crystal scintillation coincidence spectrometer with NaI(Tl) crystal which proves to be very useful in unique measurements of gamma energies above 1.5 MeV. We have made, in our laboratory a





preliminary investigation on the use of the scintillation counter as a gamma ray spectrometer. The experiments have been performed using the organic crystal stilbene in conjunction with a  $^{10}\text{P}28$  photomultiplier tube. Inorganic crystals in transparent form and of appreciable size were not available to us.



painted black inside. The sample under investigation is mounted on a holder and is fixed within the chamber so as to give a constant spacing and geometry of the source relative to the phosphor. The phosphor used is a transparent stilbene crystal of dimensions  $2'' \times 3'' \times \frac{3}{4}''$ , covered with a very thin aluminium foil which serves the purpose of a light reflector. The spectral

response of 1P28 tube has been found to be well matched to the fluorescence emission characteristics of the stilbene crystal used. 1P28 tubes exhibit maximum response in the neighbourhood of 4000 Å.

Pulses from the anode of the photomultiplier are amplified by a three-staged degenerative feedback amplifier (figure 2). The amplifier has a gain 80 and a band-width of 5 Mc/s. The negative pulses from the amplifier are inverted by  $V_1$  (6AK5), and are allowed finally to trigger the discriminator. The discriminator, circuit, made of  $V_6$  (6J6), is a plate-coupled multivibrator triggered only by positive pulses. The coupling between the inverter  $V_4$  and the multivibrator is made by a diode  $V_5$  (6H6). The plate voltage of  $V_5$  is the same as that of the anode voltage of  $V_4$ , while its cathode voltage may be continuously varied. The cathode of 6H6 is always positive with respect to its anode making 6H6 normally non-conducting. Only the positive pulses above a pre-determined amplitude at the anode of  $V_4$  make it conducting and can trigger the multivibrator  $V_6$ . By changing cathode voltage of  $V_5$ , pulses of different minimum amplitudes are sorted out to trigger the multivibrator. For every value of the cathode voltage of 6H6, the difference between the anode and the cathode voltage of 6H6 has been calibrated by a valve voltmeter. The grid bias of 6J6 is supplied from 9-volt dry batteries. The discriminator bias can be converted into the corresponding minimum pulse height from the relation,

$$x = V_{ca} + (V_g - V_k)$$

where  $V_{ca}$  = the voltage difference between the cathode and the anode of 6H6.

$V_g$  = grid voltage of 6J6.

$V_k$  = the voltage of the grid of 6J6 at which the multivibrator just starts to oscillate.

The negative pulses from the discriminator operate the standard laboratory scaler of 128 and are finally recorded in a mechanical register.

Highly stabilised power supplies were used for the electronic recording circuits and the counter. The A.C. mains supply was also stabilised by a magnetic stabiliser. The stabilised H.V. circuit for the scintillation counters is a new one developed by us and is represented in figure 3. The stabilisation has been measured and the variations have been found to be less than 0.1 volt in 1200 volts.

The experiments performed with a  $\text{Co}^{60}$  source, which emits two gamma rays of energies 1.17 MeV and 1.33 MeV consisted of observing the number of pulses recorded per minute for each setting of the 6H6 cathode voltage.

Integral bias curves were taken under two conditions, namely (a) with a thin aluminium foil interposed between the source and the phosphor and (b)



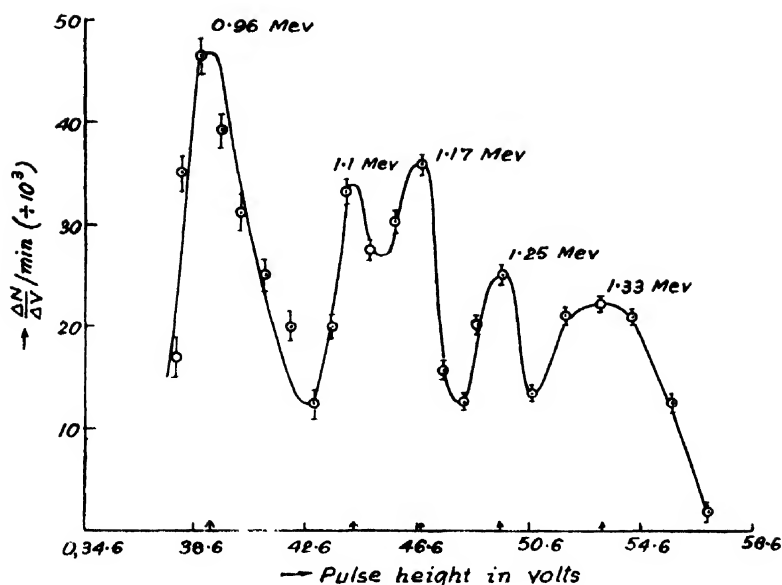


FIG. 4(b)

distribution curves, and it can be shown that 40 volts in the voltage scale corresponds to one Mev energy.

#### RESULTS AND DISCUSSION

Altogether five peaks appear in figure 4 (b). Actually however we should expect to get six peaks in this distribution curve and they occur in the following way.

The crystal chosen by us is an organic one and so  $\text{Co}^{60}$  gamma rays lose energy in the crystal primarily through Compton process. The maximum energies of Compton electrons for 1.17 MeV and 1.33 MeV gamma rays are calculated to be 0.96 MeV and 1.11 MeV respectively. The Pb-sheet was interposed between the source and the phosphor as a radiator to obtain the photo-electrons in lead. The energies of photo-electrons from lead due to  $\text{Co}^{60}$  gamma rays will be the energies of gamma rays less the binding energy of electrons in the K-shells. Two cases may arise then; when the accompanying X-rays enter the crystal simultaneously with the photo-electrons, we shall get the peaks at the full energies of the gamma rays, that is, at 1.17 MeV and 1.33 MeV. On the other hand, during photo-electric process, some of the accompanying K X-radiation of lead may escape from the other surface of lead and these do not enter the crystal. Since K-shell binding energy of lead is about 84 KeV, the energy of photo-electrons produced will be about  $(1.17 - .08) = 1.09$  MeV and  $(1.33 - .08) = 1.25$  MeV respectively, and they will give rise to the formation of the so-called 'escape peaks'.

Summing up the above considerations, we would expect to obtain six peaks, namely, those at 0.96 MeV, 1.09 MeV, 1.1 MeV, 1.17 MeV, 1.25 MeV and 1.33 MeV. The limit of resolution of the present system will not

allow the two peaks at 1.09 MeV and 1.1 MeV to be shown separated; so they coincide and we get ultimately five peaks as shown in figure 4(b).

The appearance of the 'escape peaks' in scintillation counters has been reported by West, *et al* (1951). More recently, Graham, *et al* (1952) also obtained the 'escape peaks' in their pulse height distribution curves taken with scintillation counters.

West *et al* (1951) and also Graham, *et al* (1952) performed their experiments with the inorganic NaI (Tl) crystal and naturally therefore, the 'escape peaks' are attributed to be due to the escape of the K -X-rays of iodine from the surface of the crystal itself. The escape peaks are reported to be situated at energies 28 KeV (Graham, *et al*, 1952) and 33 KeV lower than the incident photon energies (West, *et al*, 1950), where 28 KeV (or 33 KeV) is taken to be the K-shell binding energy of iodine.

In figure 4(a), the distribution curve is obtained by placing a thin Al-foil in front of the crystal and the source being covered with a bakelite sheet so as just to cut off the .3 MeV  $\beta$ -ray from  $\text{Co}^{60}$ . Four peaks are found to be formed; the first and the third one appear at pulse heights exactly corresponding to 0.96 MeV and 1.1 MeV respectively and they are identified to be due to Compton recoil electrons produced by the two  $\text{Co}^{60}$  gamma rays in the Al-foil and in the crystal material. The other two peaks are attributed to be due to the internally converted electrons from the two gamma rays of  $\text{Co}^{60}$ . Their energies should be very nearly equal to the energies of the gamma rays (since  $K_{\alpha}$  X-ray energy for  $\text{Ni}^{60}$  is  $\sim 8.3$  KeV). Actually, in figure 4(a), the peaks due to internally converted electrons seem to be slightly shifted towards the lower energy region and the peaks correspond to energy values 1.03 MeV and 1.2 MeV respectively. The reason of these shifts may be sought in the fact that while passing through the thickness of the bakelite sheet and the Al-foil (total thickness of which comes out of the order of 70 mgm/cm<sup>2</sup>) the internal conversion electrons lose a part of their energies which results in the displacements of the maxima in the curve towards the lower energy region. From range-energy data compiled by Evans (1947) the thickness of material required to bring about this change in the maximum energy values (namely from 1.17 MeV to 1.03 MeV and from 1.33 MeV to 1.2 MeV) are of the order of 75 mgm/cm<sup>2</sup> and 70 mgm/cm<sup>2</sup> respectively. These figures agree reasonably well with the actual thickness interposed between the source and the crystal.

The detection efficiency for the conversion electrons is 100% with the present arrangement. Hence, though the internal conversion co-efficients are fairly low, it can be shown that quite an appreciable number of conversion electrons are detectable with a source of the order of microcurie strength.

For an inorganic crystal made of heavier elements, the photo-electric effect is a predominant factor and the peaks due to internally converted electrons and those due to the photo-electrons are situated very close together

- Bell, P. and Cassidy, J., 1950, *Phys. Rev.*, **79**, 173.  
 Evans, R. D., 1947, Science and Engineering of Nuclear Power, Vol. I, p. 52.  
 Graham R. L. et al, 1952, *Canadian Jour. Phys.*, **30** 459.  
 Hofstadter, R. and McIntyre, J. A., 1950, *Phys. Rev.*, **78**, 617 and 619.  
   1950, *Phys. Rev.*, **79**, 389.  
   1950, *Phys. Rev.*, **80**, 631.  
   1950, *Nucleonics*, **7**, No. 3, 32.  
 Hopkins, J. I., 1950, *Phys. Rev.*, **77**, 406.  
 Johansson, S. A. E., 1950, *Nature*, **166**, 396.  
 Jordan, W. H. and Bell, P. R , 1949, *Nucleonics* **5**, No. 4, 30.  
 Mainenschlein, F. C. and Bair, J. K., 1951, *Phys. Rev.* ,**82**, 317.  
 Pringle, R. W., et al, 1950, *Rev. Sci. Inst.* **21**, 216.  
 West, H. I., et al, 1951, *Phys. Rev.*, **81**, 141.

# LIMIT OF INTERFERENCE IN OPTICAL INSTRUMENTS

By AMAR NATH NIGAM, YATENDRA PAL VARSHNI  
AND MAHENDRA SINGH SODHA

DEPARTMENT OF PHYSICS, UNIVERSITY OF ALLAHABAD, ALLAHABAD.

(Received for publication, November 3, 1952)

**ABSTRACT.** A rigorous theory has been given for the limit of interference in Lummer Gehrcke plate, transmission and reflection echelons and the grating on the lines of Saha's treatment for Fabry-Perot interferometer.

## INTRODUCTION

The theory of the limit of interference in optical instruments has been worked out by Lippich (1870), Schönrock (1906) and Rayleigh (1915). They have shown that when the pressure is small, the critical distance  $D$  (or the limit of interference) is connected by the following formula with the wavelength  $\lambda$  of light, the temperature  $T$  of the tube and mass  $M$  of the emission centres.

$$\frac{D}{\lambda} = A \sqrt{\frac{M}{T}} \quad \dots (1)$$

However, their value of  $A$  was deduced from approximate and not altogether satisfactory theoretical considerations. Saha (1917) gave a rigorous solution for the case of Fabry-Perot interferometer taking into account the infinite number of interfering beams and the effect of reflection. Gilchrist (1926) has discussed the case of Lummer Gehrcke plate but has neglected the term  $4a^4 \sin^2 (N\delta/2)$ , thereby getting the same result as Saha. In the present communication a rigorous theory has been developed for the cases of Lummer Gehrcke plate, transmission and reflection echelons and the grating.

## DEDUCTION OF THE FORMULÆ

The general expression for intensity in case of the above mentioned instruments is given by

$$I = I_0 \frac{(1 - a^N)^2 + 4a^N \sin^2 (N\delta/2)}{(1 - a)^2 + 4a \sin^2 (\delta/2)} \quad \dots (2)$$

where

$$\delta = \frac{2\pi}{\lambda} \Delta$$

$\Delta$  is the path difference between two consecutive interfering beams.

$N$  is the number of interfering beams.

and  $a$  is equal to

(i)  $Re^{-k't \sec r}$  in case of Lummer Gehrcke Plate (Sodha, 1952).

$R$  = reflection coefficient

$k'$  = intensity absorption coefficient.

$t$  = thickness of plate

$r$  = angle of refraction.

(ii)  $e^{-k't/2}$  in case of Transmission echelon (Sodha, 1953)

$k'$  = intensity absorption coefficient

$t$  = height of the step of the echelon

(iii) 1 in case of reflection echelon

(iv) 1 in case of grating.

The number of particles having their velocity between  $v$  and  $v + dv$  is  $Ae^{-\beta v^2} dv$ , and the frequency of radiation emitted by these particles is  $\nu(1 + v/c)$  where  $\nu$  is the frequency of light emitted by the particles at rest. In the expression for retardation in phase, we must, therefore, replace  $\lambda$  by  $\lambda/(1 + \frac{v}{c})$  and write  $\frac{2\pi\Delta}{\lambda}(1 + \frac{v}{c})$  in place of  $\frac{2\pi\Delta}{\lambda}$ .

The intensity of light emitted by molecules having their velocity between  $v$  and  $v + dv$  is

$$dI = B \cdot \frac{(1 - a^N)^2 + 4a^N \sin^2 \left\{ \frac{N\delta}{2} (1 + v/c) \right\}}{(1 - a)^2 + 4a \sin^2 \left\{ (\delta/2)(1 + v/c) \right\}} \cdot e^{-\beta v^2} dv \quad \dots (3)$$

The total intensity

$$I = B \int_{-\infty}^{+\infty} \frac{(1 - a^N)^2 + 4a^N \sin^2 \left\{ \frac{N\delta}{2} (1 + v/c) \right\}}{(1 - a)^2 + 4a \sin^2 \left\{ (\delta/2)(1 + v/c) \right\}} \cdot e^{-\beta v^2} dv \quad (4)$$

We have by trigonometric expansion

$$\frac{1 - a^2}{(1 - 2a \cos \delta + a^2)} = 1 + 2a \cos \delta + 2a^2 \cos 2\delta + \dots \quad \dots (5)$$

Further, we have

$$\int_{-\infty}^{+\infty} e^{-\beta v^2} dv \sin \frac{n\delta v}{c} = 0 \quad \dots (6)$$

$$\int_{-\infty}^{+\infty} e^{-\beta v^2} dv \cos \frac{n\delta v}{c} = \sqrt{\frac{\pi}{\beta}} e^{-\frac{1}{\beta} \left( \frac{n\delta}{c} \right)^2} \quad \dots (7)$$

The integral (4) can be broken up into two integrals.

$$\text{First integral} = B(1 - a^N)^2 \int_{-\infty}^{+\infty} \frac{e^{-\beta v^2} dv}{(1 - a)^2 + 4a \sin^2 \left\{ \frac{\delta}{2} (1 + v/c) \right\}}$$



$$\begin{aligned}
 &= B(1-a^N)^2 \int_{-\infty}^{+\infty} \frac{e^{-\beta v^2} dv}{1-2a \cos \delta \left(1 + \frac{v}{c}\right) + a^2} \\
 &= \frac{B(1-a^{N+2})}{1-a^2} \sqrt{\frac{\pi}{\beta}} \left[ 1 + 2 \sum_{n=1}^{\infty} a^n e^{-(1/\beta)(n\delta/c)^2} \cos n\delta \right] \quad (8)
 \end{aligned}$$

by using (5), (6) and (7).

$$\begin{aligned}
 \text{Second integral} &= 4Ba^N \int \frac{\sin^2 \frac{N\delta}{2} \left(1 + \frac{v}{c}\right) e^{-\beta v^2} dv}{1-2a \cos \delta \left(1 + \frac{v}{c}\right) + a^2} \\
 &= \frac{4Ba^N}{1-a^2} \int \left\{ 1 + 2 \sum_{n=1}^{\infty} a^n \cos n\delta \left(1 + \frac{v}{c}\right) \right\} \sin^2 \frac{N\delta}{2} \left(1 + \frac{v}{c}\right) e^{-\beta v^2} dv \\
 &= \frac{4Ba^N}{1-a^2} \left[ \int \sin^2 \frac{N\delta}{2} \left(1 + \frac{v}{c}\right) e^{-\beta v^2} dv \right. \\
 &\quad \left. + 2 \int \sum_{n=1}^{\infty} a^n \cos n\delta \left(1 + \frac{v}{c}\right) \sin^2 \frac{N\delta}{2} \left(1 + \frac{v}{c}\right) e^{-\beta v^2} dv \right] \\
 &= \frac{4Ba^N}{1-a^2} \left[ \frac{1}{2} \int \left\{ 1 - \cos N\delta \left(1 + \frac{v}{c}\right) \right\} e^{-\beta v^2} dv \right. \\
 &\quad \left. + \sum_{n=1}^{\infty} a^n \int \cos n\delta \left(1 + \frac{v}{c}\right) \left\{ 1 - \cos N\delta \left(1 + \frac{v}{c}\right) \right\} e^{-\beta v^2} dv \right] \\
 &= \frac{4Ba^N}{1-a^2} \left[ \frac{1}{2} \int e^{-\beta v^2} dv - \frac{1}{2} \int \cos N\delta \cos \frac{N\delta v}{c} e^{-\beta v^2} dv \right. \\
 &\quad + \frac{1}{2} \int \sin N\delta \sin \frac{N\delta v}{c} e^{-\beta v^2} dv + \sum_{n=1}^{\infty} a^n \int \cos n\delta \left(1 + \frac{v}{c}\right) e^{-\beta v^2} dv \\
 &\quad \left. - \sum_{n=1}^{\infty} a^n \int \cos n\delta \left(1 + \frac{v}{c}\right) \cos N\delta \left(1 + \frac{v}{c}\right) e^{-\beta v^2} dv \right] \\
 &= \frac{4Ba^N}{1-a^2} \left[ \frac{1}{2} \sqrt{\frac{\pi}{\beta}} - \frac{1}{2} \cos N\delta \cdot \sqrt{\frac{\pi}{\beta}} e^{-(1/\beta)(N\delta/c)^2} + \sum_{n=1}^{\infty} a^n \cos n\delta \sqrt{\frac{\pi}{\beta}} e^{-(1/\beta)(n\delta/c)^2} \right. \\
 &\quad - \frac{1}{2} \sum_{n=1}^{\infty} a^n \int \cos (N+n)\delta \left(1 + \frac{v}{c}\right) e^{-\beta v^2} dv \\
 &\quad \left. - \frac{1}{2} \sum_{n=1}^{\infty} a^n \int \cos (N-n)\delta \left(1 + \frac{v}{c}\right) e^{-\beta v^2} dv \right]
 \end{aligned}$$

$$\begin{aligned}
&= \frac{4Ba^N}{1-a^2} \left[ \frac{1}{2} \sqrt{\frac{\pi}{\beta}} - \frac{1}{2} \sqrt{\frac{\pi}{\beta}} \cos N\delta e^{-(1/\beta)(N\delta/c)^2} + \sqrt{\frac{\pi}{\beta}} \sum a^n \cos n\delta e^{-(1/\beta)(n\delta/c)^2} \right. \\
&\quad \left. - \frac{1}{2} \sum a^n \cos (N+n)\delta \sqrt{\frac{\pi}{\beta}} e^{-(1/\beta)\{(N+n)\delta/c\}^2} \right. \\
&\quad \left. - \frac{1}{2} \sum a^n \cos (N-n)\delta \sqrt{\frac{\pi}{\beta}} e^{-(1/\beta)\{(N-n)\delta/c\}^2} \right] \dots (9)
\end{aligned}$$

Hence the total expression for intensity is

$$\begin{aligned}
I = B \cdot \frac{(1-a^N)^2}{1-a^2} \sqrt{\frac{\pi}{\beta}} &\left[ 1 + 2 \sum a^n e^{-(1/\beta)(n\delta/c)^2} \cos n\delta \right] \\
&+ \frac{2Ba^N}{1-a^2} \sqrt{\frac{\pi}{\beta}} \left[ 1 - \cos N\delta e^{-(1/\beta)(N\delta/c)^2} + 2 \sum a^n \cos n\delta e^{-(1/\beta)(n\delta/c)^2} \right. \\
&\left. - \sum a^n \cos (N+n)\delta e^{-(1/\beta)\{(N+n)\delta/c\}^2} - \sum a^n \cos (N-n)\delta e^{-(1/\beta)\{(N-n)\delta/c\}^2} \right] \dots (10)
\end{aligned}$$

$I$  will be maximum, when  $\frac{\delta}{2} = m\pi$  or  $\delta = 2m\pi$

$I$  will be minimum, when  $\frac{\delta}{2} = (2m+1) \frac{\pi}{2}$  or  $\delta = (2m+1)\pi$

Putting  $D = \frac{B(1-a^N)^2}{1-a^2} \sqrt{\frac{\pi}{\beta}}$  and  $E = \frac{2Ba^N}{1-a^2} \sqrt{\frac{\pi}{\beta}}$  and neglecting higher

terms in  $ae^{-(1/\beta)(\delta/c)^2}$  and  $e^{-(1/\beta)(\delta/c)^2}$  because  $-(1/\beta)(\delta/c)^2 \sim 10^8$  and  $a \leq 1$ , we have

$$\begin{aligned}
I_{\max} = D[1 + 2ae^{-(1/\beta)(\delta/c)^2}] + E[1 + 2ae^{-(1/\beta)(\delta/c)^2} - a^{N-1}e^{-(1/\beta)(\delta/c)^2} \\
- a^N - a^{N+1}e^{-(1/\beta)(\delta/c)^2}]
\end{aligned}$$

$$\begin{aligned}
I_{\min} = D[1 - 2ae^{-(1/\beta)(\delta/c)^2}] + E[1 - 2ae^{-(1/\beta)(\delta/c)^2} + a^{N-1}e^{-(1/\beta)(\delta/c)^2} \\
- a^N + a^{N+1}e^{-(1/\beta)(\delta/c)^2}]
\end{aligned}$$

Hence the visibility

$$\begin{aligned}
V &= \frac{I_{\max} - I_{\min}}{I_{\max} + I_{\min}} \\
&= \frac{D \cdot 4ae^{-(1/\beta)(\delta/c)^2} + E[4ae^{-(1/\beta)(\delta/c)^2} - 2a^{N-1}e^{-(1/\beta)(\delta/c)^2} - 2a^{N+1}e^{-(1/\beta)(\delta/c)^2}]}{2D + 2E - 2E \cdot a^N} \\
&= 2ae^{-(1/\beta)(\delta/c)^2} \left[ \frac{1 - a^{2N-2}}{1 - a^{2N}} \right] \dots (11)
\end{aligned}$$

Now

$$\beta = \frac{m}{2kT}$$

$m$  = weight of radiant atoms in gms.

$k$  = Boltzmann constant

$T$  = temperature in absolute scale.

Then we have

$$-\frac{1}{\beta} \left( \frac{2\pi\Delta}{\lambda c} \right) = \log_e \frac{V}{2a} \left\{ \frac{1-a^{2N}}{1-a^{2N-2}} \right\}$$

$$\text{or} \quad \frac{\Delta}{\lambda} = \frac{c}{2\pi} \sqrt{\frac{m}{2kT}} \log_e \frac{2a}{V} \left( \frac{1-a^{2N-2}}{1-a^{2N}} \right) \quad \dots (12)$$

(i) Lummer Gehrcke plate: Putting  $a = Re^{-k't \sec r}$  in expression (12), we get :

$$\frac{\Delta}{\lambda} = \frac{c}{2\pi} \sqrt{\frac{m}{2kT}} \log_e \frac{2Re^{-k't \sec r}}{V} \left[ \frac{1-R^{2N-2}e^{-(2N-2)k't \sec r}}{1-R^{2N}e^{-2Nk't \sec r}} \right] \quad (13)$$

(ii) Transmission echelon:  $a = e^{-k't/2}$

$$\frac{\Delta}{\lambda} = \frac{c}{2\pi} \sqrt{\frac{m}{2kT}} \log_e \frac{2e^{-k't/2}}{V} \left[ \frac{1-e^{-(N-1)k't}}{1-e^{-Nk't}} \right] \quad (14)$$

(iii) Reflection echelon :

$$\frac{\Delta}{\lambda} = \frac{c}{2\pi} \sqrt{\frac{m}{2kT}} \log_e \frac{2(N-1)}{N} \quad (15)$$

(iv) For grating also expression (15) holds.

#### ACKNOWLEDGMENTS

The authors express their grateful thanks to Dr. G. B. Deodhar, Dr. K. Majumdar and Dr. D. Sharma for their interest in the work.

#### REFERENCES

- Gilchrist, I., 1926, *Phys. Rev.*, **27**, 596.  
 Lippich, 1870, *Pogg. Ann. t.*, CXXXIX, 465.  
 Rayleigh, 1915, *Phil. Mag*, **99**, 274.  
 Saha, M. N., 1917, *Phys. Rev.*, **10**, 6, 782,  
 Schönrock, 1906, *Ann der Physik.*, **20**, 905.  
 Sodha, M. S., 1952, *I. Sci. Ind. Research.*, **11B**, 9, 395.  
 Sodha, M. S., 1953, *Sci. & Cult*, **18**, 489

# ON THE GENERATION OF HIGH INTENSITY ULTRASONIC ENERGY AND MEASUREMENT OF THE OUTPUT POWER DENSITY OF A QUARTZ CRYSTAL \*

By T. C. BHADRA

BOSE INSTITUTE, CALCUTTA-9

*(Received for publication April 6, 1953)*

## Plate XIX

**ABSTRACT.** An account of the measurement of the output power of a piezo-electric quartz crystal is given. The determination of the power output by a calorimetric substitution method is described. An output of  $42.2 \text{ watts/cm}^2$  for the quartz crystal, has been attained at a frequency of 1000 kc/s.

## INTRODUCTION

The increasingly wide range of applications of ultrasonics in various fields necessitates an accurate knowledge of the density of output ultrasonic energy. Accordingly, the attention of many workers, in this line, has been drawn on the necessity of measuring the maximum power density attainable from a quartz ultrasonic generator, operating at resonance. Unfortunately, there exists an incompatibility in the results of the various workers in this subject. Richard (1939) reported that at an output of the order of  $3 \text{ watts/cm}^2$ , the crystal was shattered. For a pretty long time,  $10 \text{ watts/cm}^2$  was considered to be the maximum power attainable from a quartz crystal. Recently, however, Wood and Loomis (1927) reported a ceiling value of about  $35 \text{ watts/cm}^2$  while Epstein, Anderson and Harden's (1947) value is as high as  $43 \text{ watts/cm}^2$ . Richard used a crystal 5 cm in diameter and an electrical input of about 200 watts. In the present experiment, a crystal having 6.25 sq. cm. in area and 0.287 cm. in thickness did not break even with an electrical input of the order of 500 watts. It appears from the present experiment that more electrical power can be given to the crystal without the attending risk of mechanical break-down, provided that the dielectric strength of the medium surrounding the crystal does not yield under the electrical pressure. In fact, the maximum power that can be radiated by the crystal transducer without shattering the crystal, depends more upon the system of mounting, oscillation frequency and the physical properties of the medium surrounding the crystal.

\* Communicated by Dr. D. M. Bose

By suitable design of the crystal holder and other factors as described below, power level of 42.2 watts/cm<sup>2</sup> has been obtained.

# THEORETICAL CONSIDERATION FOR MAXIMUM POWER DENSITY

Many workers attributed the crystal break-down to the intensity vibration i. e. mechanical failure of the crystal. But computation from elastic constants of quartz and the surrounding medium shows that for X-cut quartz crystal operating in insulating oil, the upper limit of power density is of the order of 10<sup>4</sup> watts/cm<sup>2</sup> before the mechanical breakdown of the quartz crystal sets in. The expression for the power density in an unidirectional plane wave, as given by Morse (1936), is

$$T_{max} = \frac{1}{2} \rho_0 v_0 [\pi v_1 (E_{max}/2E)]^2 \quad \dots (1)$$

where  $A$  = amplitude of the wave,

$d$  = thickness of the quartz crystal,

$v_1$  = velocity of sound in quartz,

$\rho_0$  = density of the medium,

$v_0$  = velocity of sound in the medium,

$E$  = Young's modulus,

$E_{max}$  = Break-down tensile strength along the direction of the applied stress.

Substituting the values of the constants obtained from the International Critical Table,  $T_{max}$  comes out to be of the order of 10<sup>4</sup> watts/cm<sup>2</sup>. Therefore, it is obvious that the cause of the break-down of the quartz crystal is to be sought in the electrical rather than in the elastic properties of the system. The dielectric strength of quartz is much higher than that of the surrounding medium. When the break-down occurs in the oil, intense localised heat in the resulting arc deposits carbonaceous substances and establishes a short-circuiting path between the electrodes. This factor produces uneven strains in the crystal and causes its ultimate break-down. Moreover, for X-cut crystal with air backing, and functioning at resonance, the power density expression as given by Cady, may be written in the following way :

$$T_{max} = 2e_{11}^2 [1/\rho_0 v_0 (V/300d)_0] \text{ erg/sec-cm}^2 \quad \dots (2)$$

where  $V$  = peak voltage applied across the crystal thickness  $d$ .

$e_{11}$  = Piezoelectric stress coefficient of the quartz =  $5.2 \times 10^4$  C. G. S. units,

$\rho_0$  = density of the medium,

$v_0$  = velocity of sound in the medium.

This formula indicates that  $T_{max}$  for any given medium is independent of frequency, on the assumption that the dielectric strength of the medium is independent of the frequency of the applied electrical power and of the thickness of the sample. Actually, the dielectric strength of the oil is not a true constant. It is dependent both on frequency and on thickness. So

the variation of  $(V/d)_{\max}$  with thickness and frequency may be expressed approximately according to the following relation :

$$(V/d)_{\max} = (V/d)_0 e^{-\alpha d} \quad \dots (3)$$

where  $(V/d)_0$  and  $\alpha$  are constants depending on the nature of the medium dimensions, and test electrodes. Combining (2) and (3) and expressing  $d$  in terms of frequency  $\nu$  by the relation  $\nu = v_1/2d$ , where  $v_1$  is the velocity of sound in quartz, the expression for power density may be written in the following way :

$$T_{\max} = 2e^2_{11} [1/\rho_0 v_0 (V/300d)_0 e^{-\alpha v_1/\nu}] \text{ erg/sec-cm}^2 \quad \dots (4)$$

It has been experimentally shown by Epstein, Anderson, and Harden (1947) that  $T_{\max}$  tends to the maximum value of about 814 watts as  $\nu$  tends to infinity. Substituting the values of  $\rho_0$  and  $v_0$  of transformer oil used in the present experiment, and taking the maximum value of  $V/d$  as experimentally determined,  $T_{\max}$  comes out to be of the order of 508 watts/cm<sup>2</sup> for  $\nu = \infty$  \*.

#### EXPERIMENTAL DESCRIPTION

##### 1. Ultrasonic Generator :

A single high power valve (Osram MT9) was used to generate the radio-frequency voltage. The circuit used was of the conventional Hartely type. The  $Q$  value of the coil, used in the tank circuit, was kept high. D. C. high voltage was obtained from a half-wave rectifier unit, equipped with suitable filter system. The schematic detail of the circuit, shown in the diagram, is self explanatory (figure 1).

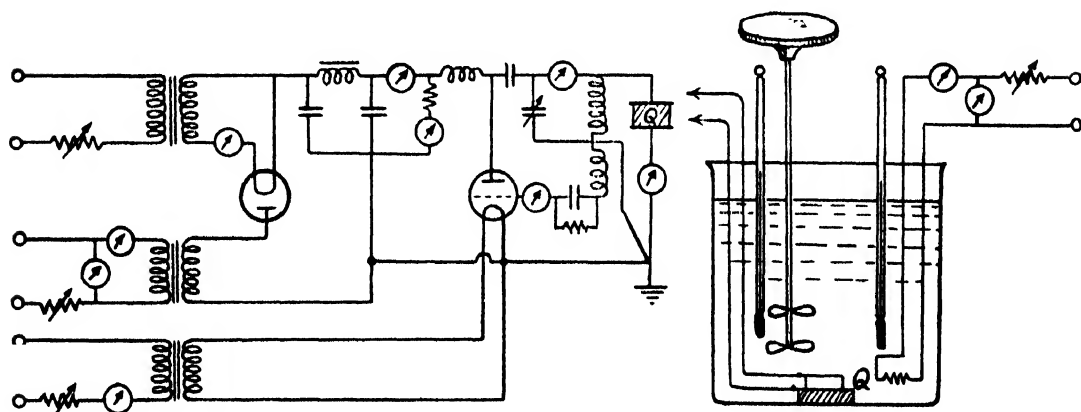


FIG. 1

The crystal transducer was connected directly across the tank circuit. It was mounted at the centre of the bottom of a thick-walled cylindrical glass vessel containing about 8 liters of transformer oil. At resonant frequency, the amplitude of vibration of the crystal was maximum which was

\* The value of  $V/d$  for the particular transformer oil used in the present investigation was found experimentally to be 10.5 kv/cm, the value of  $\rho_0$  and  $v_0$  being .90 g/cm<sup>3</sup> and  $1.41 \times 10^5$  cm/sec respectively.



Fig. 2  
Photograph of the experimental set-up

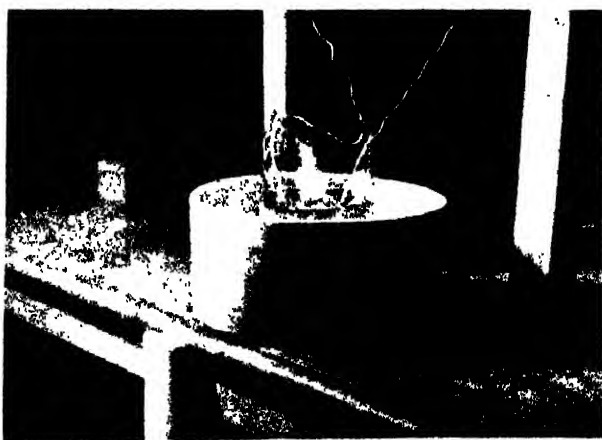


Fig. 3  
Photograph of the fountain formed in the  
oil medium at resonance frequency





simultaneously indicated by the height of the fountain formed in the oil medium (cf. figure 3), and the corresponding maximum reading of the r. f. meter inserted in the circuit.

A photograph of the actual set-up is shown in figure 2, Plate XIX.

## 2. Crystal transducer :

An X-cut quartz crystal having 6.25 sq. cm. surface area and 0.287 cm thickness was used as the crystal transducer. The faces of the crystal were chemically silvered. The silvered surface consisted of an area of about 4.50 sq cm at the central portion of the face of the crystal forming its effective area. In the present experiment two types of crystal holders were used, viz. an airbacking type and a lead block backing type (figure 4).

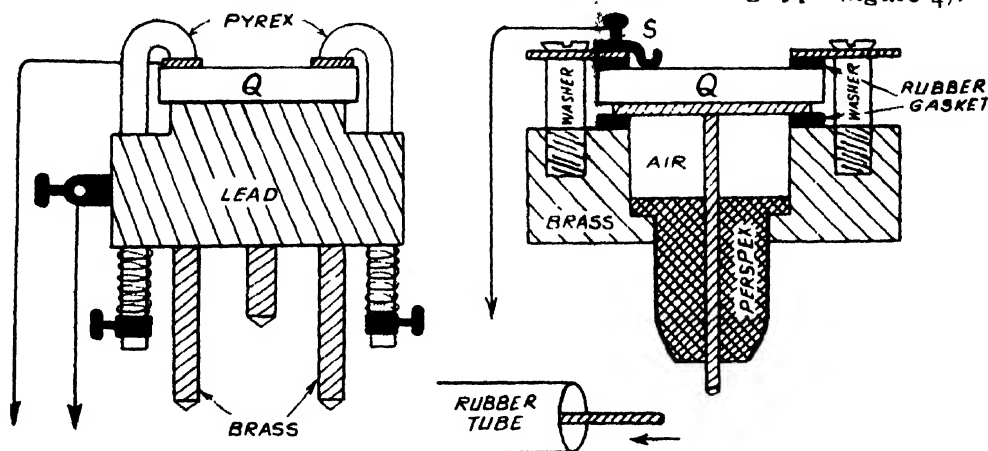


FIG. 4

In both the cases, one face of the crystal was in direct contact with the liquid in which the crystal transducer was placed. The electrodes used for the application of high voltage to the faces of the crystal were polished with fine emery powder, so as to maintain good electrical contact. The areas of the electrodes were made smaller than that of the crystal, in order to increase the length of the insulated path between the two electrodes. Edges of the crystal were rounded off. The thickness of the lead block was about some multiple of quarter wavelength.

## 3. Power measurement :

A mechanical stirrer fitted with a series of propeller blades and operating at 400 r. p. m., churned the oil bath which was simultaneously heated by an immersion heater with 500 watts rating. Two thermometers recorded the actual temperature of the oil bath and the rate of rise of its temperature. For the latter purpose, a Beckmann thermometer to read temperature within 1/100th of a degree, was used. The immersion heater was used to calibrate the oil bath, but it was left inside the vessel permanently for maintaining

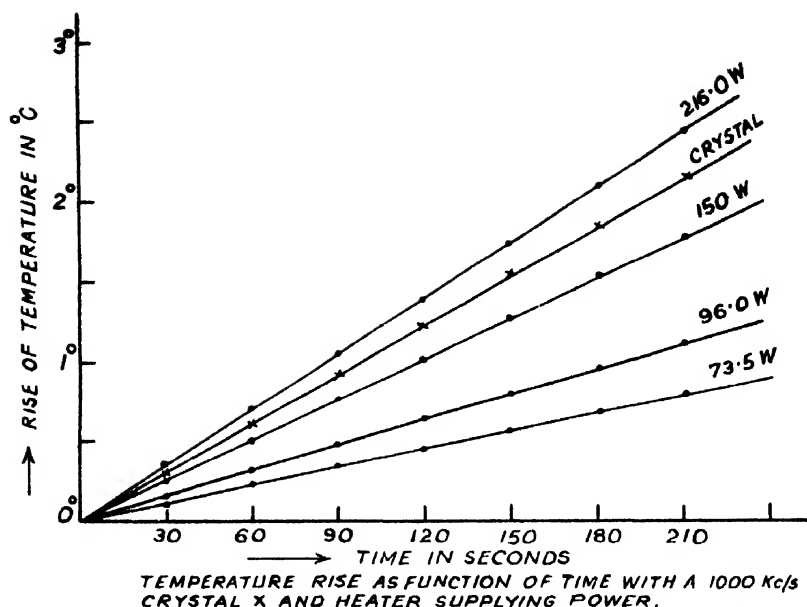


FIG. 5

the heat capacity of the system unchanged during the period of measurements. The input power given to the heater was measured by means of substandard voltmeter and ammeter, with a range of accuracy of  $\pm \frac{1}{2}\%$ . While the stirrer was operating and the crystal oscillating, the rise of temperature was measured by means of the Beckmann thermometer at intervals of 30 seconds.

## RESULTS

A mean graph was drawn with the rise of temperature against the time interval. The plot was linear and passed through the origin. The slope of the plot was taken to be the measure of the rate of rise of temperature i.e.,  $\Delta T/\Delta t$ , where  $\Delta T$  represents the difference of temperature during the interval of time  $\Delta t$ . Similar graphs were drawn (figure 5) when the crystal was not oscillating, but the stirrer was operating, for different input power applied to the immersion heater. In each case  $\Delta T/\Delta t$  was found out from the mean graph. Finally, another mean graph (figure 6) was plotted with  $\Delta T/\Delta t$  against the input power to the heater. This plot was also linear and passed through the origin. From this graph the corresponding value of the power for  $\Delta T/\Delta t$  of the crystal was found out. This power was taken as the average output power of the piezo-electric quartz crystal. By linear interpolation, the total output power comes out to be 190.0 watts, with a probable error of  $\pm 5$  watts. Effective area being 4.50 sq. cm. the power output per sq. cm. is 42.2 watts.

Table I gives the results of measurements for a heater and also for a 1000 kc/s quartz crystal, driven by 500 watts r. f. energy. \*

Figures. 5 and 6 depict the corresponding graphs.

TABLE I  
Room temperature was kept constant within  $\pm 3^{\circ}\text{C}$

No.	Source	$\Delta T/\Delta t$ deg./sec	Power (W)	Output ultrasonic power (watt/cm <sup>2</sup> )
1	Heater	0.683	216.0	
2	do	0.50	150.0	
3	do	0.313	99.0	
4	do	0.22	73.5	
5	Crystal	0.60	190.0 (from graph)	42.2

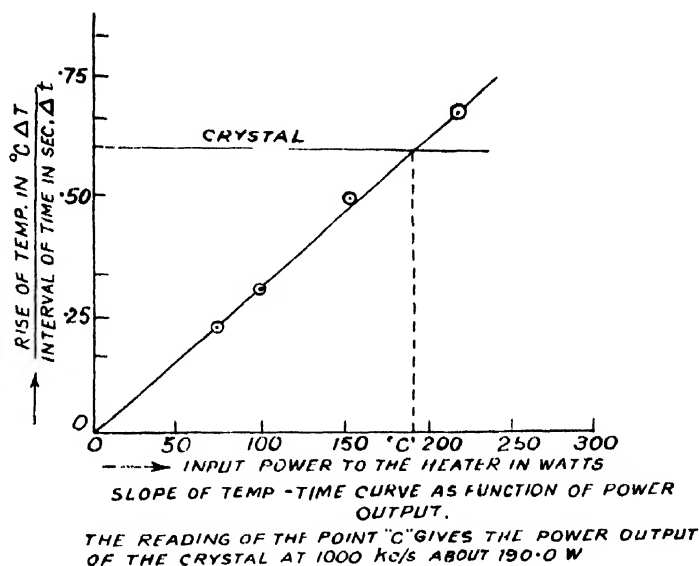


FIG 6

## DISCUSSIONS

The maximum ultrasonic power density  $T_{\text{max}}$  obtained in the present experiment is considerably lower than the theoretical value computed from the electrical and mechanical properties of quartz. The value of  $T_{\text{max}}$  agrees well with that experimentally obtained by Epstein, Anderson and Harden (1947) but it is higher than that obtained by other previous workers. It has been possible to obtain the value of 42.2 watts/cm<sup>2</sup> in the present experi-

\* The input D. C. power  $P$  to the oscillating valve was calculated from the product of  $V \times I$ , where  $V$  = D. C. plate potential = 10 kv, measured by an electrostatic voltmeter  
 $I$  = D. C. plate current of the valve = 72 mA

$$P = V \times I = 10 \text{ kv} \times 72 \text{ mA} = 720 \text{ watts}$$

Taking the efficiency of the class 'C' oscillator valve to be 70%, the r. f. power was calculated to be 504 watts

ment, chiefly by the improvement made in the design of the crystal holder. But the transformer oil used did not conform with the specification of an ideal dielectric medium. In fact, the percentage of moisture content in the oil was rather high making it impossible to inject sufficiently high voltage between the two electrodes of the crystal. Thus, it is apparent that in the generation of high intensity ultrasonic energy, transformer oil used as an insulating medium plays an important role. If the dielectric strength of the medium is improved, one can inject higher voltage to the crystal, resulting in higher output of ultrasonic energy.

The efficiency of conversion of the present system is about 38%, the remaining 62% being lost in the matching network and elsewhere. In the present experiment it is assumed that the ultrasonic energy generated in the thick-walled glass vessel is entirely confined to the vessel and practically there is no transmission of ultrasonic energy outside the vessel. The energy thus measured is assumed to be total energy. However, this is not strictly correct, because ultrasonic energy forms only a part of the total energy. In the present experiment, the rate of rise of the temperature of the oil bath due to the absorption of ultrasonic energy generated by using air backing type or lead block backing type crystal holder was found practically the same, so the results are not shown separately. The efficiency of the lead block type crystal holder was increased by adjusting the thickness of the block by trial and error to some multiple of quarter wavelength. Further work is being carried out to resolve the existing discrepancy in the value of the power density obtained experimentally and that calculated from theoretical considerations.

#### SOME INCIDENTAL OBSERVATIONS IN CONNECTION WITH POWER MEASUREMENTS

1. The crystal was replaced by a glass plate of the same dimension as that of the crystal. On the application of the r. f. voltage between the electrodes, the glass plate shattered immediately even when there was no break-down of the insulating oil. However, a quartz plate, cut in an arbitrary manner, did not break but acted as a dielectric medium between electrodes. The r. f. current through this quartz plate was less than that flowing through the X-cut crystal, while operating at resonance; the current through the X-cut plate at resonant condition being 0.40A, while the maximum current through the other plate was 0.15A. No appreciable rise of temperature was noticed in the latter case. It may, therefore, be concluded that the contribution of the r. f. current in raising the temperature of the bath, during the measurements, is negligible.

2. At resonant frequency, the crystal vibrated at its maximum amplitude. The height of the fountain formed at this condition was about 8 cm but some of the oil droplets attained a height of about 25 cm. A photograph of the fountain is shown in figure 3. It was also noticed that

when  $L/C$  ratio of the tank circuit was high, the cross section of the fountain was smaller but the ultrasonic beam was more directive. With low value of  $L/C$  ratio, practically no formation of fountain was observed. But when the  $L/C$  ratio was kept at some intermediate value, the cross section of the fountain increased accompanied by a great agitation in the oil bath.

3. A long narrow glass tube with flat bottom and containing a steel ball about 1 mm in diameter in water medium, was held vertically on the fountain head. The ball was elevated to a height of about 30 cms. against gravity. It was, however, found that the height through which the ball was pushed through was not the same when the tube was held near the face of the crystal, the place of maximum ultrasonic intensity

4. The temperature of the scattered droplets of the oil fountain was found subjectively to be much higher than that of the oil bath.

The phenomena described in (3) and (4) are evidently manifestations of the conversion of the radiant ultrasonic energy traversing the liquid medium at the liquid-air boundary surface into kinetic energy of motion. A further discussion of these and the allied phenomena will form the subject matter of a subsequent communication.

#### ACKNOWLEDGMENT

The author is indebted to Dr. D. M. Bose, Director, Bose Institute, Calcutta, for his keen interest, guidance and invaluable discussions. His thanks are also due to Prof. A. K. Dutta of Utkal University for pointing out the importance of the present set of measurements and to Dr. S. D. Chatterji of Science College, Calcutta University, for his valuable advice.

#### REFERENCES

- Ludwig Bergmann, *Der Ultraschall* (Third edition)  
 Cady, W. G., 1945, *Piezoelectricity* (McGraw-Hill Book Company)  
 Richard, W. T., 1939, *Rev. Mod. Phys.*, **11**, 36.  
 Wood, R. W. and Loomis, A. L., 1927, *Phys. Rev.*, **29**, 373, (1127), *Phil. Mag.* **4**, 417.  
 Epstein, L. F., Anderson, W. M. A and Harden, L. R., 1947, *J. Acous. Soc. America*, **19**, 248.  
 Morse, P. M., 1936, *Vibration and Sound* (McGraw-Hill Book comp., New York, p, 18)9.

# CALCULATION OF THE EXCITED LEVELS OF INDENE

BY S. RAMAMURTY

DEPARTMENT OF MATHEMATICAL PHYSICS, ANDHRA UNIVERSITY, WALTAIR

(Received for publication, July, 7, 1953)

**ABSTRACT** The energy of the excited levels of indene is calculated by the method of anti-symmetrised Molecular Orbitals. The observed band system at 2.52A is assigned to a  $^1J_1 - ^3J_1$  transition. The results of the M.O. and the A.O. methods of treatment are compared.

## INTRODUCTION

It may be generally stated that the concept of unique electron configuration is valid for molecules also. This electron configuration is assigned for a given molecule by two methods usually called the Atomic Orbital (A.O.) and the Molecular Orbital (M.O.) methods. In the first method, a molecule is treated as compounded of several atoms and ions. The electron configuration is made up of the electron configurations of the different atoms. The wavefunctions of the molecule are written down as products of atomic orbitals (A.O.'s)—one electron wavefunctions in atoms. Energy values are then obtained by a variation method, as the roots of a secular equation. In the second method, the molecule is treated, as far as possible, as a unit. The wavefunction of the molecule is written down as (anti-symmetrised) product of a set of molecular orbitals (M.O.'s). These are solutions of Schrodinger's equation for an electron in the field due to the nuclei and all other electrons. In practice, this equation cannot be solved. The M.O.'s are written as linear combinations of a complete set of functions. This set might well be the A.O.'s of any one of the atoms of the molecule. But the difficulty, in this case is that the M.O.'s thus constructed converge too slowly. The use of orbitals of all the atoms of the molecule leads to better convergence. M.O.'s thus constructed as linear combinations of the A.O.'s of the concerned atoms, are called the L.C.A.O. forms of the M.O.'s. Having thus assigned the electron configuration, the calculation of energy levels was carried out on the basis of the theorem that the value of energy in a state  $\phi$  is  $\int \phi^* H \phi d\tau$ ,  $H$  being the Hamiltonian.

The A.O. method has been employed by Viswanath (1953) recently to calculate the energy levels of indene. Excited levels are predicted with energy values 3.84, 8.25, 105.67 eV above the ground level. All the levels conform to singlet symmetrical states  $^1A$ . In benzene and other molecules, the M.O. method is sometimes stated to give a better approximation than the A.O. method (Longuet-Higgins, 1948). The purpose

of this paper is to apply the second, antisymmetrised molecular orbital method to the indene molecule. The treatment of the problem is similar to that followed by Goeppert-Mayer and Sklar (1938) for benzene. The results are presented, in detail, in the following sections. A brief preliminary report has been published in "Current Science" (Ramanurthy, 1953).

#### ANALYTICAL PART

The structure of indene is shown in figure 1. The molecule belongs to the symmetry group  $C_{2v}$ . In indene (as in benzene) only the  $2p\pi$

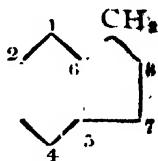


FIG. 1

electrons are spectroscopically active and hence only the molecular states of these electrons need be considered. These have a node in the plane of the molecule. There are eight  $2p\pi$  electrons in indene, as was assumed by Viswanath in the A.O. calculations previously. The same assumption is made here also. The numbering of the electrons is shown above.

Representing the electrons by Greek letters  $\mu, \nu$  (ranging from 1 to 8) and the  $2p\pi$  eigenfunction on the  $k$ th atom by  $K(\nu)$  (ranging from I to VIII) and taking these to be positive on the same side of the indene plane, the molecular orbitals employed in this work are

$$\phi_l = \frac{1}{\sqrt{8\sigma_l}} \sum_{k=1}^8 e^{\frac{2\pi i l k}{8}} K(\nu)$$

with  $l=0, \pm 1, \pm 2, \pm 3, 4$ .  $\sigma_l$ 's are normalising factors. Evidently  $\phi_l = \phi_{-l}^*$ .  $\phi_l, \phi_{-l}$  have the same energy ( $\epsilon_l$ , say). Also neglecting overlap integrals and integrals over products of non-neighbouring A.O.'s, the energy of the  $\phi'_l$ 's rises with  $|l|$ .

The energy of the molecule is lowest if the eight electrons are distributed in  $\phi_0, \phi_1, \phi_{-1}, \phi_2$  two in each. The eigenfunction for the whole molecule is therefore

$$\psi_0 = \phi_0(1)\phi_0(2)\phi_1(3)\phi_1(4)\phi_{-1}(5)\phi_{-1}(6)\phi_2(7)\phi_2(8).$$

The excited levels arise by a  $\phi_2$  electron jumping into  $\phi_3, \phi_{-3}$  or  $\phi_4$ . They are

$$\phi_0(1)\phi_0(2)\phi_1(3)\phi_1(4)\phi_{-1}(5)\phi_{-1}(6)\phi_2(7)\phi_3(8)$$

$$\phi_0(1)\phi_0(2)\phi_1(3)\phi_1(4)\phi_{-1}(5)\phi_{-1}(6)\phi_2(7)\phi_{-3}(8)$$

$$\phi_0(1)\phi_0(2)\phi_1(3)\phi_1(4)\phi_{-1}(5)\phi_{-1}(6)\phi_2(7)\phi_4(8).$$

All states belong to the symmetry type  $A_1$ .

These must be multiplied by the appropriate spin factors. If two electrons are in the same M.O., they must have opposite spins. Thus for the ground state, the spin factor is

$$\alpha(1)\beta(2)\alpha(3)\beta(4)\alpha(5)\beta(6)\alpha(7)\beta(8).$$

For the excited levels the  $\phi_2$ ,  $\phi_3$  or the  $\phi_2$ ,  $\phi_{-3}$  or the  $\phi_2$ ,  $\phi_4$  electrons may have their spins opposed or parallel. In the first case, the spin factor must be anti-symmetric and is

$$\frac{1}{\sqrt{2}} \alpha(1)\beta'(2)\alpha(3)\beta(4)\alpha(5)\beta(6)[\alpha(7)\beta(8) - \alpha(8)\beta(7)].$$

In the second case, the spin factor must be symmetric; there are three of them and these are

$$\alpha(1)\beta(2)\alpha(3)\beta(4)\alpha(5)\beta(6)\alpha(7)\alpha(8)$$

$$\alpha(1)\beta'(2)\alpha(3)\beta(4)\alpha(5)\beta(6)\beta(7)\beta(8)$$

$$\frac{1}{\sqrt{2}} \alpha(1)\beta(2)\alpha(3)\beta(4)\alpha(5)\beta'(6)[\alpha(7)\alpha(8) + \beta(7)\beta(8)].$$

In the first case, the states are said to be singlets. In the second case, they are said to be triplets. As we neglect in our calculation the spin-orbit interaction, the triplet will not be separated.

The totally anti-symmetrised wavefunction is then obtained by multiplying the orbital with the spin factor and applying the anti-symmetrising operator. Thus the anti-symmetrised wavefunction of the ground state is

$$\Psi_0 = \frac{1}{\sqrt{8!}} \sum (-1)^P P \phi_0(1)\phi_0(2)\phi_1(3)\phi_1(4)\phi_{-1}(5)\phi_{-1}(6)\phi_2(7)\phi_2(8) \\ \alpha(1)\beta(2)\alpha(3)\beta(4)\alpha(5)\beta(6)\alpha(7)\beta(8).$$

The energy of the state is then equal to the sum of the energies of the separate M.O.'s and the energy due to the interaction of the electrons. The latter has the potential

$$H^{(1)} = \sum_{\nu=1}^8 \frac{e^2}{r\nu\mu} \\ \mu < \nu$$

The energy of the ground state is thus

$$2\epsilon_0 + 4\epsilon_1 + 2\epsilon_2 + \int \Psi_0^* H^{(1)} \Psi_0 d\tau.$$

The integral expressing the average value of  $H^{(1)}$  can be expanded in terms of two types of integrals, viz.,

$$J_{\mu\nu} = \iint \frac{e^2}{r\nu\mu} |\phi_i(\nu)|^2 |\phi_i'(\mu)|^2 d\tau_\nu d\tau_\mu$$

$$\delta_{\mu\nu} = \iint \frac{e^2}{r\nu\mu} \phi_i(\nu)\phi_i'(\mu)[\phi_i(\mu)\phi_i'(\nu)]^* d\tau_\nu d\tau_\mu$$



The energies including the electronic interaction for the ground state and the excited singlet and triplet levels are

$$E_g = 2\epsilon_0 + 4\epsilon_1 + 2\epsilon_2 + \gamma_{0,0} + 8\gamma_{0,1} + 4\gamma_{0,2} + 6\gamma_{1,1} + 8\gamma_{1,2} + \gamma_{2,2} \\ - 4\delta_{0,1} - 2\delta_{0,2} - 2\delta_{1,-1} - 2\delta_{1,2} - 2\delta_{-1,2}$$

$$(\phi_2 \rightarrow \phi_4) E_s = 2\epsilon_0 + 4\epsilon_1 + \epsilon_2 + \epsilon_3 + \gamma_{0,0} + 8\gamma_{0,1} + 2\gamma_{0,2} + 2\gamma_{0,3} + 6\gamma_{1,1} \\ + 4\gamma_{1,2} + 4\gamma_{1,3} + \gamma_{2,3} - 4\delta_{0,1} - \delta_{0,2} - \delta_{0,3} - 2\delta_{1,-1} - \delta_{1,2} \\ - \delta_{-1,2} - \delta_{1,3} - \delta_{-1,3} + \delta_{2,3}$$

$$(\phi_2 \rightarrow \phi_{-3}) E_s = 2\epsilon_0 + 4\epsilon_1 + \epsilon_2 + \epsilon_3 + \gamma_{0,0} + 8\gamma_{0,1} + 2\gamma_{0,2} + 2\gamma_{0,-3} + 6\gamma_{1,1} \\ + 4\gamma_{1,2} + 4\gamma_{1,-3} + \gamma_{2,-3} - 4\delta_{0,1} - \delta_{0,2} - \delta_{0,-3} - 2\delta_{1,-1} \\ - \delta_{1,2} - \delta_{-1,2} - \delta_{1,-3} - \delta_{-1,-3} + \delta_{2,-3}$$

$$(\phi_2 \rightarrow \phi_1) E_s = 2\epsilon_0 + 4\epsilon_1 + \epsilon_2 + \epsilon_3 + \gamma_{0,0} + 8\gamma_{0,1} + 2\gamma_{0,2} + 2\gamma_{0,1} + 6\gamma_{1,1} \\ + 4\gamma_{1,2} + 4\gamma_{1,1} + \gamma_{2,1} - 4\delta_{0,1} - \delta_{0,2} - \delta_{0,4} - 2\delta_{1,-1} \\ - \delta_{1,2} - \delta_{-1,2} - \delta_{1,1} - \delta_{-1,1} + \delta_{2,1}$$

$$(\phi_2 \rightarrow \phi_4) E_t = 2\epsilon_0 + 4\epsilon_1 + \epsilon_2 + \epsilon_3 + \gamma_{0,0} + 8\gamma_{0,1} + 2\gamma_{0,2} + 2\gamma_{0,3} + 6\gamma_{1,1} \\ + 4\gamma_{1,2} + 4\gamma_{1,3} + \gamma_{2,3} - 4\delta_{0,1} - \delta_{0,2} - \delta_{0,3} - 2\delta_{1,-1} \\ - \delta_{1,2} - \delta_{-1,2} - \delta_{1,3} - \delta_{-1,3} - \delta_{2,3}$$

$$(\phi_2 \rightarrow \phi_{-3}) E_t = 2\epsilon_0 + 4\epsilon_1 + \epsilon_2 + \epsilon_3 + \gamma_{0,0} + 8\gamma_{1,0} + 2\gamma_{0,2} + 2\gamma_{0,-3} + 6\delta_{1,1} \\ + 4\gamma_{1,2} + 4\gamma_{1,-3} + \gamma_{2,3} - 4\delta_{0,1} - \delta_{0,2} - \delta_{0,3} - 2\delta_{1,-1} \\ - \delta_{1,2} - \delta_{-1,2} - \delta_{1,-3} - \delta_{-1,-3} - \delta_{2,-3}$$

$$(\phi_2 \rightarrow \phi_1) E_t = 2\epsilon_0 + 4\epsilon_1 + \epsilon_2 + \epsilon_3 + \gamma_{0,0} + 8\gamma_{0,1} + 2\gamma_{0,2} + 2\gamma_{0,1} + 6\gamma_{1,1} \\ + 4\gamma_{1,2} + 4\gamma_{1,1} + \gamma_{2,1} - 4\delta_{0,1} - \delta_{0,2} - \delta_{0,4} - 2\delta_{1,-1} \\ - \delta_{1,2} - \delta_{-1,2} - \delta_{1,1} - \delta_{-1,1} - \delta_{2,1}$$

$g$  indicates ground state ;  $s$ , singlet and  $t$ , triplet state

#### NUMERICAL CALCULATIONS

The integral  $\gamma$ 's and  $\delta$ 's over  $M$ ,  $O$ .'s are expressed in terms of integrals over  $A$ ,  $O$ .'s by using the Huckel type orbitals written above.

First of all, the normalising factors  $\sigma_l$ 's are determined by the following equation :

$$\sigma_l = \frac{1}{k} \int \sum e^{-\frac{2\pi i l k}{8}} K(v) \sum e^{-\frac{2\pi i l k}{8}} K(v) d\tau, \\ = \frac{1}{k} \left[ 8 + \left( 12 \cos \frac{\pi l}{4} + 2 \cos \frac{5\pi l}{4} \right) S_1 + \left( 12 \cos \frac{\pi l}{2} + 4 \cos \pi l \right) S_2 \right. \\ \left. + \left( 8 \cos \frac{3\pi l}{4} + 2 \cos \frac{\pi l}{4} \right) S_3 \right]$$

Where  $S_1 = \int I(v) II(v) d\tau_v$ ,  $S_2 = \int I(v) III(v) d\tau_v$ ,  $S_3 = \int I(v) IV(v) d\tau_v$  and overlap integrals over electrons 1, 2, 3, 4 on the one hand and 7, 8 on the other are neglected.

Next, the expansions of integrals  $\gamma_{ll'}$ ,  $\delta_{ll'}$ , will contain the following types of integrals :

$$A_K = \iint \frac{e^2}{rv\mu} I^2(v)(K+1)^2(\mu) d\tau_v d\tau_\mu$$

$$B = \iint \frac{e^2}{rv\mu} I^2(v) I(\mu) II(\mu) d\tau_v d\tau_\mu$$

$$C = \iint \frac{e^2}{rv\mu} I(v) II(v) I(\mu) II(\mu) d\tau_v d\tau_\mu$$

Interaction between electrons which are partially on atoms which are not closest neighbours as also between electrons 1, 2, 3, 4 on the one hand and 7, 8 on the other are neglected.

Lastly, we have

$$\begin{aligned} e_l &= \int \frac{1}{\sqrt{8\sigma_l}} \sum e^{-\frac{2\pi i l h}{8}} K(v)(T+H_0) \frac{1}{\sqrt{8\sigma_l}} \sum e^{-\frac{2\pi i l h}{8}} K(\gamma) d\tau_v \\ &= \frac{1}{8\sigma_l} \int I(v)(T+H_0) \left\{ 8I(v) + \left( 2 \cos \frac{5\pi l}{4} + 12 \cos \frac{\pi l}{4} \right) II(v) \right. \\ &\quad \left. + \left( 4 \cos \pi l + 12 \cos \frac{\pi l}{2} \right) III(v) + \left( 2 \cos \frac{\pi l}{4} + 8 \cos \frac{3\pi l}{4} \right) IV(v) \right\} d\tau_v \end{aligned}$$

where  $T$  is the kinetic energy and  $H_0$  the potential energy. Neglecting the effect of hydrogen atoms completely

$$H_0 = \sum H_K$$

where  $H_K$  is the potential of the attraction of the  $k$ th carbon nucleus and of the repulsion of the other five electrons on the  $k$ th nucleus. Obviously,  $H_K$  is the difference between the potential of a neutral carbon atom  $\bar{H}_K$  and the potential of a  $2p\pi$  electron,

$$H_K = \bar{H}_K - \int \frac{e^2}{rv\mu} K^2(\mu) d\tau_\mu$$

Also as  $K(v)$  is a  $2p\pi$  eigenfunction,

$$(T+H_0)K(v) = W_{2p}K(v)$$

where  $W_{2p}$  is the energy of a  $2p$  level in carbon atom in a valence state. Bearing this in mind and substituting for  $H_0$  as above, two new kinds of integrals arise in the expression of  $e_l$  namely,

$$Q = - \int \bar{H}_1(v) II^2(v) d\tau_v,$$

$$\text{and } R = - \int \bar{H}_1(v) I(v) II(v) d\tau_v.$$

All interaction between non-neighbours is neglected. Then

$$e_l = \frac{1}{\sqrt{8\sigma}} \left( 8\sigma_l W_{2p} - 8(2Q + 2A_1 + 2A_2 + A_3) - \left( 2 \cos \frac{5\pi l}{4} + 12 \cos \frac{\pi l}{4} \right) (R+B) \right)$$

Assuming the C=C distance in indene to be  $1.39\text{\AA}$  i.e. equal to that in benzene, the values of the integrals  $S_1, S_2, S_3, A_0, A_1, A_2, A_3, B, C, Q, R$  can be taken over from the benzene calculations of Goeppert-Mayer and Sklar (1938). The energy levels of indene, relative to the ground level, are obtained to be 0, 0.36, 3.89, 8.39, 10.615, 10.628, 11.82.

The energy levels are shown in figure 2. It is clear from it that the observed band system at  $2952\text{\AA}$  arises from a jump  $\phi_2 \rightarrow \phi_3$  ( ${}^1A_1 - {}^3A_1$ ) i.e., from a singlet to triplet transition. Such transitions are highly probable in complex molecules (Kasha, 1950).

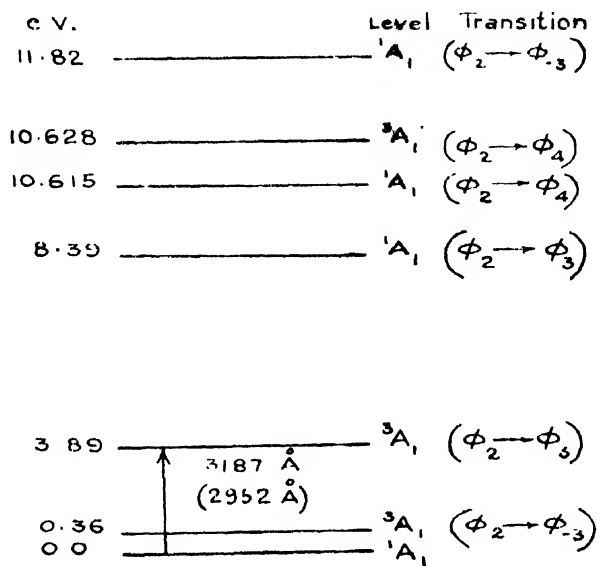


FIG. 2

Comparing the results of A.O. and M.O. calculations, they give nearly the same values for lower excited levels. The lower excited level at 0.36 eV, however, does not appear in the A.O. treatment. The M.O. method gives even in respect of lower excited levels a better approximation to the experimental values, for indene by  $40\text{\AA}$ . Also the M.O. method enables us to calculate the energy levels state by state, taking the group-theoretical aspect also into account in the calculation itself. Further, the M.O. method is clear as to the multiplicity and symmetry character of the state.

#### SUMMARY

The energy levels of indene have been calculated by the method of anti-symmetrised molecular orbitals. In applying this method the following assumptions have been made

1. The molecule has eight  $2p\pi$  electrons.
2. Huckel type M.O. forms are used

$$\varphi_k = \sqrt{8\sigma_k} \quad k=1'$$

3. Interaction between electrons partially on non-neighbouring atoms as also between electrons 1, 2, 3, 4 on the one hand and 7, 8 on the other have been neglected. Effect of hydrogen atoms and spin-orbit interaction is also neglected.

4. The C=C distance in indene is taken as  $1.39\text{\AA}$ .

Reckoning from the ground state the energy levels are obtained to be 0, 0.36, 3.89, 8.39, 10.615, 10.628, 11.82 eV. The observed band system at  $2952\text{\AA}$  should arise, according to this treatment, from the ground state to a triplet excited level.

#### ACKNOWLEDGMENT

The author would like to express his indebtedness to Prof. K. R. Rao for his kind guidance and interest in the work.

#### REFERENCES

- Goeppert-Mayer, M. and Sklar, A. L., 1938, *J. Chem. Phys.*, **6**, 645.  
Kasha, M., *Disc. Farad. Soc.*, No. 9, 14.  
Longuet-Higgins, H. C., 1948, *Proc. Phy. Soc. Lond.*, **60**, 270.  
Ramamurty, S., 1953, *Curr. Sci.*, **22**, 168.  
Viswanath, G., 1953, *Ind. J. Phys.*, **27**, 251.

# ON THE ABSORPTION MAXIMA EXHIBITED BY SOME ORGANIC LIQUIDS IN THE MICROWAVE REGION. I \*

By DILIP KUMAR GHOSH

OPTICS DEPARTMENT, INDIAN ASSOCIATION FOR THE CULTIVATION OF SCIENCE, CALCUTTA 32

(Received for publication, September 11, 1953)

**ABSTRACT** The absorption of 3.18 cm. microwaves in chloroform, ethylene chloride, ethylene bromide and glycerine at different temperatures has been studied by the direct method avoiding formation of standing waves. A maximum in the absorption-temperature curve has been exhibited by each of the four liquids. The temperatures for maximum absorption are  $-45^{\circ}\text{C}$ ,  $-10^{\circ}\text{C}$ ,  $21^{\circ}\text{C}$  and  $100^{\circ}\text{C}$  for chloroform, ethylene chloride, ethylene bromide and glycerine respectively. It is pointed out that the values of  $\lambda_m$ , the wave length corresponding to the maximum absorption calculated by previous workers from the Cole and Cole empirical relation on the assumption of the existence of a distribution of relaxation time do not agree with the values observed by the direct method in the present investigation. It is further pointed out that actually different discrete values of the relaxation time, more than one in number, are present in most of the liquids, instead of a continuous distribution of relaxation time assumed in Cole and Cole empirical relation.

The radius of the rotor calculated from Debye's equation comes out to be too low in all the four cases and the reasons for this discrepancy have been discussed.

## INTRODUCTION

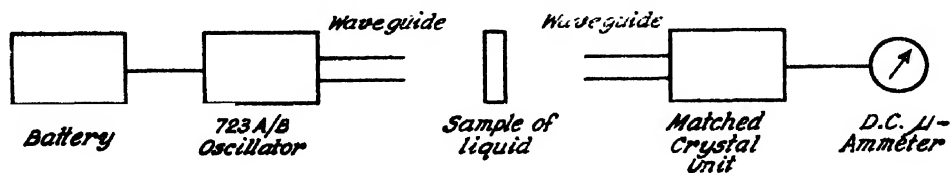
The dielectric constant of many organic liquids in solution for two different frequencies in the microwave region has been investigated by Whiffen and Thompson (1946a) and from the experimental value of  $\tan \delta$ , the loss tangent, the value of the relaxation time has been determined in each case with the help of the Debye equation. Whiffen and Thompson (1946b) also found out the value of  $\tan \delta$  for 1.27 cm. waves in the case of pure *o*-xylene and *p*-cymene at different temperatures and also in the case of solutions of a few organic compounds in heptane at temperatures ranging from those below the freezing points of the liquids upto about their boiling points. Heston, Hennelly and Smyth (1948), on the other hand, measured the dielectric constant of a large number of organic halogen compounds for 1.27 cm. microwaves at four different temperatures and determined the value of loss tangent in each case. Hennelly, Heston and Smyth (1948) determined the values of  $\tau_0$ , the most probable relaxation time, using the Cole and Cole equation (1941) deduced empirically on the assumption of the existence of a distribution of relaxation time. It was, however, observed recently (Ghosh, 1953) that some of the liquids studied by the authors mentioned above exhibit

\* Communicated by Prof. S. C. Sirkar

absorption maxima in the range 500-920 Mc/sec at suitable temperatures, and at other temperatures the absorption was found to be negligible in this region. Also, the radius of the rotor calculated from Debye's theory indicated that the rotor in some of the cases is a dimer. These facts indicated that instead of a continuous distribution of relaxation time over wide limits only two or three discrete values are to be taken into account in these cases. This has been pointed out recently by Sirkar (1953). As the absorption due to single molecules was expected to be observed in the microwave region in the case of some liquids having simple molecules, it was thought worthwhile to determine by the optical method the temperatures at which maximum absorption of 3.18 cm. microwaves are exhibited by these liquids and to find out the value of  $\tau$  and the radius of the rotor from Debye's theory. In such a method it is not necessary to use any empirical relation like the Cole and Cole equation, as has been done by the previous workers mentioned above. The preliminary results observed in the case of chloroform, ethylene chloride, ethylene bromide and glycerine are reported in this paper.

#### EXPERIMENTAL

A klystron oscillator of type 723 A-B was used as the source of microwaves, the power being derived from dry batteries. The frequency of oscillations used was 9415 Mc/sec and it was measured with a calibrated reaction type cavity wavemeter. The absorption of the radio waves coming out through a wave guide cut open at a distance of about 14 cm. from the tuning plunger and of cross section 2.3 cm  $\times$  1 cm was studied by optical method. For the detection of the transmitted waves another wave guide and a matched crystal detector were used as shown in figure 1.



BLOCK DIAGRAM OF THE EXPERIMENTAL ARRANGEMENT.

FIG. 1

It was first observed that even when a thin glass plate was placed between the two wave guides after the positions of the plungers had been adjusted for maximum current in the detecting microammeter, reflection of waves at the glass plate occurred for certain distances of the plate from the open end of the transmitting wave guide, but for certain other distances full transmission of the waves through the glass plate was observed. It was also observed that the distance between successive positions of the glass plate for which the transmission was maximum was about  $\lambda/2$ , where  $\lambda$  is the wave length of the microwaves in air. It was thus evident

that when the distance between the glass plate and tuning plunger was a multiple of  $\lambda/2$ , stationary waves were formed and there was very little transmission through the plate in this case and for other distances equal to  $n\lambda/2 + \lambda/4$  there was no reflection at the surfaces of the glass plate. When a glass cell with a distance of 1 cm between inner surfaces was placed between the two transmitting and receiving wave guides the transmission through the glass walls of the cell was not cent per cent for any position of the cell. When, however, the cell was filled with benzene, full transmission was observed for certain distance of the cell from the end of the transmitting wave guide. This arrangement was, therefore, used for observing the maximum absorption in the liquids studied in the present investigation. Incidentally, it might be pointed out that the assumption made by Whiffen and Thompson (1946) that the reflection at the mica walls of the cell used by them is identical both for the empty cell and for the cell filled with the liquid is probably not correct.

The liquids studied are chloroform, ethylene chloride, ethylene bromide and glycerine of chemically pure quality. They were purchased from U. S. A. and they were all distilled in vacuum after proper dehydration. In order to study the absorption at different temperatures the cell filled with the liquid was placed in baths at different temperatures and when the liquid attained the temperature of the bath the cell was taken out and its outer surfaces were cleaned. The cell was then placed between the wave guides and its distance from the open end of the transmitting wave guide was adjusted till maximum deflection in the detecting circuit was observed. The temperature of the liquid was measured just before starting this adjustment. The ratio of the current in the detecting circuit observed with the cell filled with the liquid placed in its position and that observed with the cell removed was noted for different temperatures of the liquid. The reflection at the glass-liquid interface was thus neglected in this method. Preliminary results obtained with chloroform and ethylene bromide at high temperatures clearly showed that reflection at glass-liquid interfaces was negligible, because there was full transmission through the liquids at certain temperatures.

#### RESULTS AND DISCUSSIONS

The values of apparent absorption coefficient,  $\mu$ , were calculated from the

relation,

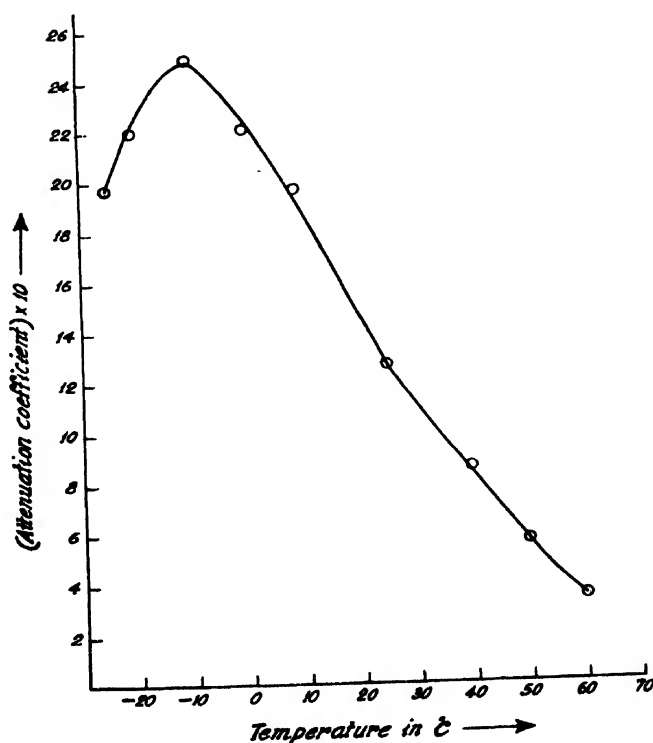
$$\mu = \frac{2.34}{x} \log_{10} \left( \frac{I_0}{I} \right)$$

where  $x$  is the thickness of the liquid,  $I$  is the observed maximum current in the microammeter in the detecting crystal circuit with the liquid absorber in its position and  $I_0$  the current with the cell removed. The values of  $\mu$  have been plotted against the temperature of the liquid in figures 2, 3 and 4. It can be seen from the figures that as the temperature of the liquid increases from a certain low value, the value of  $\mu$  gradually increases and after attaining a maximum at a particular temperature, it diminishes again. In the case

of chloroform at 35°C and ethylene bromide at 70°C the transmission is cent per cent. Since dielectric constant changes from 6.12 to 4.4 in the case of chloroform with change of temperature of the liquid from -45°C to 35°C and in the case of ethylene bromide the dielectric constant is almost constant throughout the range from 21°C to 70°C, it is quite evident that the change in dielectric constant of the liquid cannot be responsible for the change in the absorption coefficient which takes place with the change of temperature of the liquid. This is further corroborated by the results obtained with glycerine. It is observed that when the temperature of pure glycerine free from water is raised from 17°C up to 200°C the value of  $\mu$  gradually increases and after attaining a very large value in the range 80°C to 120°C, it diminishes again, although the value of dielectric constant gradually diminishes with the rise of temperature of the liquid. The results shown in figures 2, 3, 4 and 5 show that the value of  $\lambda_m$ , the wave length for maximum absorption exhibited by the liquids at the particular temperature is 3.18 cm. This wave length is thus determined directly in the present investigation. The values of  $\tau$  at the respective temperatures of maximum absorption which have been calculated from Debye's theory from the relation,

$$\omega\tau = \frac{\epsilon_0 + 2}{\epsilon_1 + 2} \sqrt{\frac{\epsilon_1}{\epsilon_0}},$$

where  $\omega$  is the angular frequency at the maximum absorption,  $\epsilon_0$  and  $\epsilon_1$  are



Ethylene chloride

FIG. 2



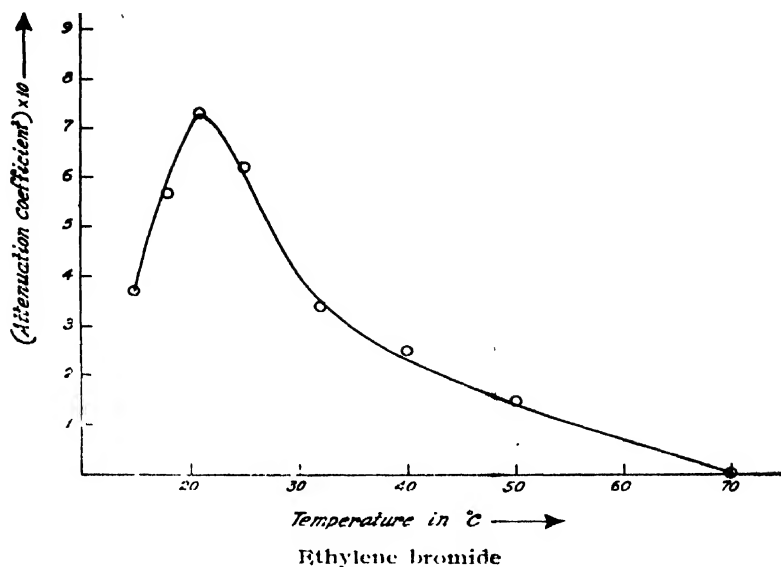


FIG. 3

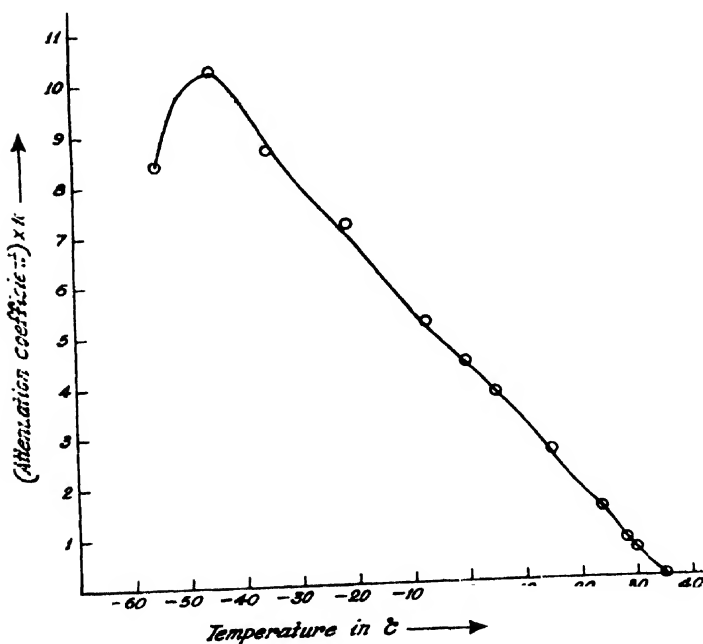


FIG. 4

dielectric constants for infinite frequency and zero frequency respectively, are given in Table I.

The value of  $\eta$  are obtained by extrapolation from the results reported in Handbook of Chemistry and Physics published by Chemical Rubber Publishing Co. The values of  $\eta$  for glycerine at temperatures above 30°C are taken from the results reported by Vand (1947). The value of  $\epsilon_1$  has

been obtained from the table of dielectric constant of pure liquids published by National Bureau of Standards, United States, Department of Commerce. The value of  $\epsilon_0$  has been assumed to be equal to the square of  $n$ , the refractive index at 20°C for sodium D-line, because the values of  $n$  at lower temperatures were not available. The values of radius of the rotors calculated from Debye's theory are also given in Table I.

TABLE I  
 $\omega/2\pi = 9415$  Mc/sec

Liquid	T°K for max. absorption	$\epsilon_1$	$\epsilon_0$	$\tau \times 10^{11}$	$\eta \times 100$	$a \times 10^8$ cm
Chloroform	228	6.12	2.094	1.455	1.12	1.478
Ethylene chloride	263	12.7	2.084	1.16	1.2	1.405
Ethylene bromide	294	4.8	2.364	1.545	1.7	1.420

*Ethylene chloride and Ethylene bromide :*

The values of  $\lambda_m$ , the wave length for maximum absorption exhibited by the liquids at the particular temperature as deduced by Hennelly, Heston and Smyth (1948) for ethylene chloride and ethylene bromide applying the empirical relation suggested by Cole and Cole (1941) on the assumption of the presence of distribution of relaxation time  $\tau$  are compared with the value obtained by the optical method in the present investigation in Table II.

TABLE II

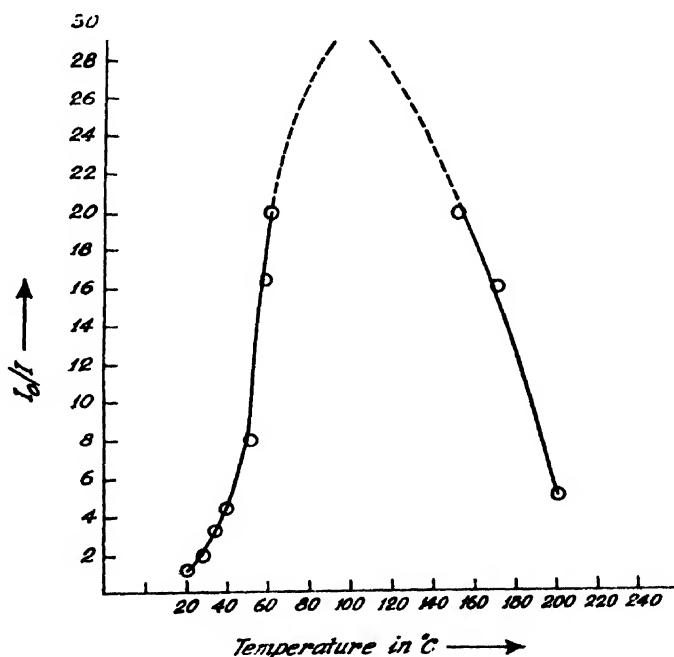
Liquid	Present author		Hennelly <i>et al</i> (1948)	
	Temperature	$\lambda_m$ in cm	Temperature	$\lambda_m$ in cm
Ethylene chloride	-10°C	3.18	1°C	1.83
Ethylene bromide	21°C	3.18	25°C	2.18

The value of  $\lambda_m$  deduced from Cole and Cole equation in the case of ethylene chloride at 1°C is 1.83 cm and this will lead to a value 2.16 cm at -10°C if the change in viscosity with temperature is taken into consideration. The value observed directly in the present investigation, however, is 3.18 cms. Similarly, in the case of ethylene bromide at 25°C the value of  $\lambda_m$  deduced by the previous authors is 2.18 cms and the value observed by

the direct method in the present investigation is 3.18 cms at 21°C. Thus it is evident that the empirical relation mentioned above leads to wrong value of  $\lambda_m$ . Therefore, the fundamental assumption that there is a continuous distribution of  $\tau$  in these liquids is not quite correct as pointed out by Sirkar (1953).

*Chloroform :*

In the case of chloroform solution in heptane at -45°C Whiffen and Thompson (1946) found the value of  $\tau$  to be equal to  $7.4 \times 10^{-12}$  sec. The viscosity of heptane at this temperature, as extrapolated from the values at higher temperatures, is 0.7 centipoise and the viscosity of chloroform at this temperature is 1.12. Hence the value of  $\tau$  in pure chloroform at -45°C deduced from the values of the solution in heptane at the same temperature is  $1.18 \times 10^{-11}$  sec. This does not differ much from the value  $1.45 \times 10^{-11}$  sec obtained in the present investigation.



Glycerine

FIG. 5

*Glycerine :*

It can be seen from figure 5 that the value of  $I_0/I$  increases with temperature till it reaches enormously high values beyond 80°C and it begins to diminish again beyond about 100°C. Thus the value of  $\lambda_m$  for glycerine at about 100°C is 3.18 cm. Previous authors (Mizushima, 1928, Sirkar and Sen, 1949) observed that glycerine at about 31°C shows absorption peak at about 60 cms. Since the viscosity of glycerine at 31°C is very high, being 620 centipoise the value of the radius of the rotor calculated from these data from

Debye equation comes out to be of the order of  $0.4 \times 10^{-8}$  cms. The value is obviously too small to correspond to even a small part of the molecule. The radius of the rotor calculated similarly with the help of  $\eta$  for  $100^\circ\text{C}$  observed in the present investigation is about  $0.6 \times 10^{-8}$  cms. This value also is too low. The high value of viscosity is evidently responsible for these discrepancies because as the viscosity decreases to one tenth of its value with the change from  $31^\circ\text{C}$  to  $100^\circ\text{C}$  the discrepancy also is reduced to some extent. The cause for this discrepancy has been discussed by Sirkar (1953) in another paper.

It is thus quite evident from the facts mentioned above that although the method adopted in the present investigation is the simplest of all the methods used so far the measurement of maximum absorption, the results obtained regarding the value of  $\lambda_m$  at particular temperature of the liquid are quite accurate and they show that such results deduced from Cole and Cole empirical relations are not quite correct in some cases. These results further show the hypothesis of the presence of continuous distribution of  $\tau$  in the range from 0 to  $\infty$  in the case of all the liquids is not quite correct, because in the case of three of the four liquids studied in the present investigation, discrete absorption peaks have been observed. These maxima in the present case seem to be due to single molecules. Peaks at lower frequencies may be observed at low temperatures and those peaks will be due to dimers, because such peaks due to dimers have been observed in other cases (Ghosh, 1953).

The value of  $a$ , the radius of the rotor calculated from the Debye's equation  $\tau = \frac{4\pi\eta a^3}{kT}$  is almost the same for all the three liquids—chloroform

ethylene chloride and ethylene bromide, and it is less than the C-Cl distance. Even in the case of chloroform the value is too small to lead to the correct volume of the molecule deduced from the density of the liquid. This discrepancy may be due to the presence of dimers in the liquid which has not been taken into account in the calculation, as pointed by Sirkar (1953).

The fact that the value of  $a$  is almost the same in ethylene chloride or ethylene bromide as in chloroform may indicate that only the C-Cl or C-Br group orientates along the impressed field due to the freedom of rotation about the C-C bond. This can happen only when the other half of the molecule is held rigidly in the liquid, which means that the molecules may be associated with the neighbouring molecules so that the freedom of motions of the portion of the molecules directly linked to each other is very much restricted. At higher temperatures the associated molecules are expected to break up into single molecules and the whole molecule is expected to orientate along the impressed field. Further investigations with other liquids are in progress.

ACKNOWLEDGMENT

The author's thanks are due to Prof. S. C. Sirkar, D. Sc., F. N. I. for kindly suggesting the problem and for his guidance throughout the progress of the work.

REFERENCES

- Cole, K. S. and Cole, R. H., 1941, *J. Chem. Phys.*, **9**, 341  
Ghosh, D. K., 1953, *Ind. J. Phys.*, **27**, 285  
Hennelly, F. J., Heston, W. M. and Smyth, C. P., 1948, *J. Am. Chem. Soc.*, **70**, 4102  
Heston, W. M., Hennelly, F. J. and Smyth, C. P., 1948, *J. Am. Chem. Soc.*, **70**, 4093  
Mizushima, S., 1928, *Sci. Pap. Inst. Phys. and Chem. Research (Tokyo)*, **9**, 209  
Sirkar, S. C., 1953, *Ind. J. Phys.*, **27**, (in press)  
Sirkar, S. C. and Sen, S. N., 1949, *Nature*, **164**, 1048  
Vand, V., 1947, *Research (London)* **1**, 44.  
Whiffen, D. H. and Thompson, H. W., 1946a, *Trans. Farad. Soc.*, **42 A**, 114.  
Whiffen, D. H. and Thompson, H. W., 1946b, *Trans. Farad. Soc.*, **42 A**, 122.

# LATENT HEAT OF SUBLIMATION OF FIFTEEN SALTS FROM SPECTROSCOPIC AND THERMOCHEMICAL DATA

BY MAHENDRA SINGH SODHA \* AND YATENDRA PAL VARSHNI

DEPARTMENT OF PHYSICS, ALLAHABAD UNIVERSITY, ALLAHABAD

(Received for publication November 11, 1952, received after revision September 5, 1953)

**ABSTRACT.** The latent heat of sublimation of fifteen salts, which have not been experimentally determined, are calculated from spectroscopic and thermochemical data.

The latent heat of sublimation  $L(MX)$  of a salt  $MX$  can be obtained from spectroscopic and thermochemical data by means of the following equations :

$$(MX)_{\text{gas}} = M_{\text{gas}} + X_{\text{gas}} - D_o(MX)$$

$$(MX)_{\text{solid}} + L(MX) = (MX)_{\text{gas}}$$

$$M_{\text{gas}} = M_{\text{solid}} + L(M)$$

$$X_{\text{gas}} = \frac{1}{2}(X_2)_{\text{gas}} + \frac{1}{2}D_o(X_2)$$

$$\frac{1}{2}(X_2)_{\text{gas}} = \frac{1}{2}(X_2)_{\text{solid}} + L(X)$$

$$M_{\text{solid}} + \frac{1}{2}(X_2)_{\text{solid}} = (MX)_{\text{solid}} + F$$

$$\text{or } L(MX) = F + L(M) + L(X) + \frac{1}{2}D_o(X_2) - D_o(MX)$$

where  $F$  is the heat of formation of  $MX$  ;  $L(M)$  and  $L(X)$  are the latent heats of  $M$  and  $X$  respectively,  $D_o(M)$  and  $D_o(X_2)$  are the heats of dissociation of  $MX$  and  $X_2$  respectively.

The calculations for the latent heats of the salts are shown in Table I.

## REMARKS

(1) The values of heats of formation are those given by Bichowsky and Rossini (1936).

(2) The values of  $L(M)$  are given by Landolt-Börnstein (1936).

(3) The values of  $L(X)$  are those used by Mathur (1937).

(4) The values of  $D_o(X_2)$  and  $D_o(MX)$  are those given by Herzberg (1950) except those which are marked with asterisks and are given by Gaydon (1947).

(5) Whenever a range is given only the mean value has been used.

(6) Calculated  $L(\text{PbO})$  agrees closely with the value 61.6 Kcal./mole given by Landolt-Börnstein, which shows the correctness of  $D_o(\text{PbO})$ .

\* Now at Defence Science Laboratory, New Delhi.

TABLE I  
Calculation of latent heats of fifteen salts

S. No.	MX	F in Kcal/mol	L(M) in Kcal/mole	L(X) in Kcal/mole	$D_0(X_2)$ in e. v.	$\frac{1}{2}D_0(X_2)$ in Kcal/mole	$F + L(M) + L(X) + \frac{1}{2}D_0(X_2)$ in Kcal/mole	$D_0(MX)$ in e. v.	$D_0(MX)$ in Kcal/mole	L(MX) in Kcal/mole
1	PbO	52.5	47.2	gas	5.080	58.1	157.8	4.3	99.2	58.6
2	PbSe	20.0	47.2	17.4	2.8*	32.3	116.9	4.7	108.4	8.5
3	PbTe	6.0	47.2	13.2	2.3*	26.5	92.9	3.5	80.7	12.2
4	SnO	67.7	68.0	gas	5.08	58.1	193.8	3.2	73.8	120.1
5	SnS	22.7	68.0	14.7	4.4	50.7	156.1	7.0	90.3	86.8
6	FeO	34.3	96.6	gas	5.08	58.1	219.0	4.8	110.8	108.2
7	CuO	38.5	81.7	gas	5.08	58.1	178.3	4.5	103.7	74.6
8	MgO	146.1	34.4	gas	5.08	58.1	238.6	3.7	85.3	153.3
9	MnO	66.5	69.0	gas	5.08	58.1	223.0	4.4	101.5	122.1
10	CsH	12.0	18.7	gas	4.476	51.6	82.3	1.9	13.8	38.5
11	KH	10.0	21.9	gas	4.476	51.6	83.5	1.6	11.5	42.0
12	LiH	21.6	36.0	gas	4.476	51.6	109.2	2.5	57.6	51.6
13	NaH	14.0	26.2	gas	4.476	51.6	91.8	2.2	50.7	41.1
14	RbH	12.0	20.6	gas	4.476	51.6	84.2	1.9	43.8	40.4
15	AgCl	8.3	90.7	gas	2.475	28.5	127.5	3.5	80.7	46.8
16	MgS	82.2	34.4	14.7	4.4	50.7	182.0	2.9	66.9	115.1

## ACKNOWLEDGMENTS

The authors express grateful thanks to Dr. K. Majumdar and Dr. D. Sharma for their interest in the work.

## REFERENCES

- Bichowsky and Rossini, 1936, *Thermochemistry of Chemical Substances*, Reynhold Publishing Corporation, New York .
- Gaydon : 1947 *Dissociation Energies and Spectra of Diatomic Molecules* (Chapman and Hall, London) p. 204.
- Herzberg, 1939, *Molecular Spectra and Molecular Structure Part I Diatomic Molecules* (D Van Nostrand Co., London) 5. 501-581.
- Landolt-Bornstein, 1936, *Physikalish Chemische Tabellen*
- Mathur, L. S., 1937, *Proc. Roy. Soc.*, **908**, 162, 63
- Mathur, L. S., 1937, *Ind. J. Phys.*, **11**, 177.



# THE FOCUSSED AND MAGNETIC ANALYSIS OF A BEAM FROM A RADIO-FREQUENCY ION SOURCE

By A. N. BANERJEE

BOSE INSTITUTE, CALCUTTA-9

(Received for publication, September 11, 1953)

**ABSTRACT.** The operation of a radio-frequency type of positive ion source is described, in which the excitation was produced by a 22 Mc sec., 200 watt r.f. oscillator. Using an extraction voltage of 22 KV, a total positive ion current of 175 microamperes was delivered at the target. The extraction voltage beam current characteristics show that this current can be increased further to attain a saturation value with increasing extraction voltage. By suitably adjusting the ratio of the extraction voltage to the focussing voltage a 6 to 10 mm diameter beam could be realized in the region of accelerator space. A magnetic analysis of the beam revealed that its atomic ion content was more than 60%.

## INTRODUCTION

The success of Cockroft and Walton in 1932 in producing artificial disintegration of light elements by means of accelerated protons stimulated intensive efforts in different countries for developing efficient positive ion sources and diverse methods for accelerating them. The various types of ion sources that came into being comprise, *inter alia*, the following types: (a) The high voltage discharge, (b) The low voltage arc discharge and (c) The capillary arc discharge. The large energy spread of the ions generated in a high voltage discharge source was eliminated in the subsequently evolved low voltage arc source. However, the presence of metallic surfaces, within the discharge tube acting as bases for recombination of the atomic ions into the molecular forms rendered the apparatus, rather less efficient for atomic ion production. In the U.S.A. several capillary arc type of sources were designed and although many of the desirable characteristics were combined in these instruments, the requirements of occasional replacement of the filament remained a discouraging feature. The introduction by Thonemann (1946) of the radio-frequency discharge technique for the production of ion source was soon taken up by a large number of workers in different countries (Thonemann, *et al*, 1948; Bayly, *et al*, 1948; Hall, 1948; Moak, *et al*, 1951) and the working of several efficient ion sources have since been reported. Different workers have chosen frequencies ranging from 15 Mc/sec to 450 Mc/sec; the method of excitation for the lower frequencies being by means of a resonated coil wound round the discharge tube. For higher frequencies, the excitation

is by two external electrodes placed near the ends of the discharge tube, with an axial magnetic field, presumably to reduce the power requirements of the radio-frequency oscillator. Brascfield (1930) measured the conductivity of hydrogen at low pressure in a discharge tube and found that it was maximum at a frequency of 15 Mc/sec and a pressure between 10 and 20 microns. Herzberg (1927) obtained a very low intensity of the molecular spectrum of hydrogen in a discharge tube held inside the h.f. coil. Moreover, good impedance matching can be attained after a few trials with the dimension of the exciting coil. All these considerations led to the use of the lower frequencies in this laboratory. A 22 Mc/sec, 200 watt oscillator was used for the excitation of discharge. Using an extraction voltage of 2.2 KV, the source, a hydrogen discharge tube is capable of delivering 175 microamperes of positive ion current of which more than 60% are atom ions.

The condition of focus of the beam largely determines the extent to which it can be used in a high voltage accelerator. Even in the absence of a workable theory this problem received a satisfactory experimental solution in the provision of a focussing lens, which was a cylindrical electrode placed close to the extraction canal and charged to an appropriate potential sufficient to converge an initially divergent beam. This method quite efficiently passed on a moderately focussed beam into the accelerator space. Further, by dividing the total accelerating voltage over a number of electrodes the condition of focus could be considerably improved. However, there is very little available information regarding the shape of the beam emerging from the canal before being subjected to the action of the focussing lens, and the extent to which the various factors are responsible for determining such a shape. An occasion arose in the course of the present investigation to determine the beam cross section at a suitable distance from the canal. The method used for this purpose was based on the formation of a well-defined area on a clean brass surface when the beam is allowed to strike against it for a few minutes. In this way a study of the effect of various electrode shapes, mutual space-charge effect of the ions and the geometry of the extraction canal assembly could be made. For the beam current and the extraction voltage used the geometry of the extraction canal was found to be predominantly responsible for determining the shape of the beam while the mutual space-charge repulsion and the shape of the probe electrode had little effect in this respect.

#### EXPERIMENTAL ARRANGEMENT: OPERATION OF THE ION SOURCE

Hydrogen was obtained by the electrolysis of water from a glass U-tube with platinum electrodes. The gas was collected by the displacement of mercury through an 80 cm narrow glass tube and after drying passed into an one litre pyrex flask. Only 3 cc of liquid was necessary for electrolysis.

The reservoir was connected to the discharge tube by means of a needle valve. Recently, however, arrangements have been made for the regulation of the flow of gas by diffusion through a heated palladium tubing.

The discharge tube (figure 1) consisted of a 4 cm outer diameter pyrex tube, 15 cm in length. A tungsten wire anode was fused at one end of the tube and it was hidden from the main part of the discharge tube by means

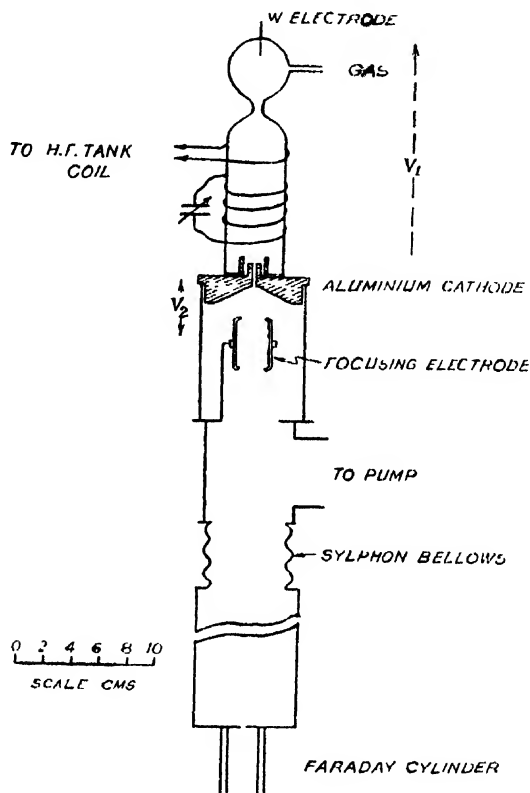


FIG. 1

of a constriction in the glass tube. The cathode was a flat tip of aluminium with a canal 1.5 mm in diameter and half an inch in length. The outer diameter of the tip was 6 mm and it was covered by a pyrex tube which extended 3/16 inch beyond the tip into the discharge tube. A 200 watt, 22 megacycles/sec radio-frequency source consisting of one type 6V6 driver oscillator, an 807 buffer amplifier and a pair of 805 in push pull power amplifier stage, supplied the energy necessary for the discharge. The radio-frequency energy was transferred to a resonant circuit whose coil was placed axially with the discharge tube by link coupling. The diameter of the coil was 2.5 inches and it consisted of four turns of silver coated  $\frac{1}{8}$ " diameter copper wire. The variable condenser had seven plates with a separation of 3 mm between the plates and was placed inside a glass jar containing transformer oil. The rotor of the condenser was attached to a long insulated handle to operate it from a distance.

The same power source (figure 2) was used for the probe and focussing voltages. A single phase 50 cycles transformer with a half-wave rectifier tube type 8013A and a pair of 1 mfd condensers provided 15 kilovolts which

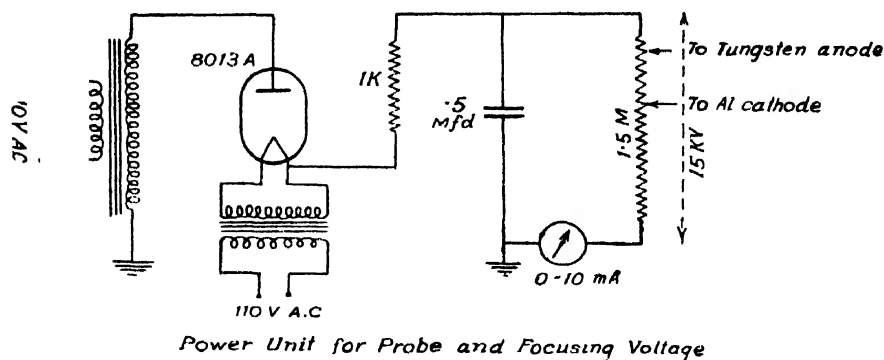


FIG. 2

was fed to a chain of resistances with a total value of 1.5 megohms. With a number of tappings on the resistance chain the desired voltage ratios and different total voltages could be used.

The pressure within the discharge tube was maintained at about 10 microns and with the oscillator operated at the maximum power output level, the colour of the discharge was bright red and the Balmer lines of the hydrogen spectrum were brightly displayed when observed by a direct vision spectroscope. From the general appearance of the discharge it was observed that there was a deeper tinge in the middle of tube along the axis and it gradually faded at the walls.

*Focussing of the ion beam:* A great deal of information is available from the work of Tuve *et al.* (1935) who used a variety of lens system consisting of different sizes and shapes of and gaps between electrodes kept at various potentials and found some practical methods for delivering a moderately focussed beam into an accelerator space. No satisfactory theory exists to account for the behaviour of ion beams, under the action of a lens and the straightforward application of the results of investigations of Pierce (1940) for electron beam focussing to the case of ion beams is not possible. An understanding of the phenomenon would naturally require a complete mapping out of the beam cross section along its entire path. The recording of the photographic impression of the beam rendered luminous by traces of gas in high vacuum, as developed by Buechner, Lamar and Van de Graaff (1941) was an effort in this direction. In this laboratory it was found that by exposing a polished brass surface against the beam at a suitable distance from the canal a well defined spot could be formed and this spot gave directly the cross section of the beam at that particular distance. This method could be used to determine (1) the natural broadening of the beam on account of its own space charge, (2) the effect of different shapes of the

probe electrode, and (3) the effect of the geometry of the extraction canal assembly.

In Table I it is shown that when the space-charge effects are nearly completely eliminated for moderate probe voltages; widely varying electrode shapes do not seem to exert a marked influence upon the shape of the emergent beam and that the geometry of the extraction canal plays a very important role in determining the beam shape before it is delivered to the focussing lens. The geometrical cone had its apex at the centre of the canal and was formed by joining it with the boundary of the canal at the exit end. The above considerations would suggest the desirability of having the correct design of the canal assembly for the usable beam-current and the functions of the focussing lens and the accelerating electrodes could then be carried out with maximum efficiency.

TABLE I  
Beam current = 100  $\mu$ a, extraction voltage = 2500V

Electrode shape	Canal diameter	Distance from centre of canal	Geometrical cone	Spot diameter	Beam cone
1. Flat	1.5 mm	4.35 cm	14°	1.2 cm	16°
2. 90° cone	2 mm	4.6 cm	18°	1.5 cm	18°
3. 135° cone	2 mm	4.35 cm	18°	1.1 cm	15°

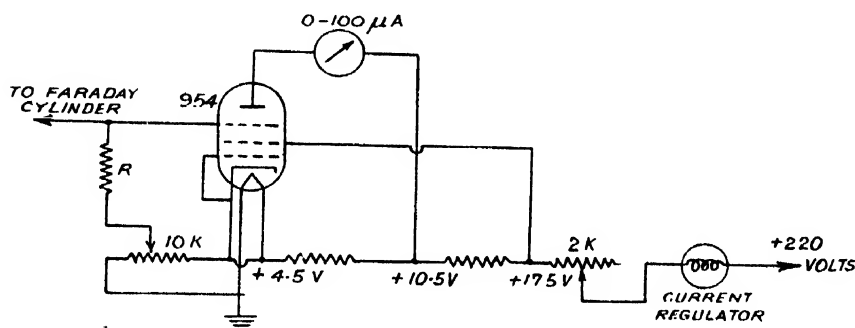
The ions after emergence from the canal were subjected to a larger electrostatic field and made to focuss on to the slit of a Faraday cylinder at a distance of 62 cms from the canal. A maximum of 2.2 KV was used for probe extraction and the focussing voltage was so adjusted as to maintain a ratio in excess of five with the former. A cylindrical electrode with edges rounded off was used with a gap of one inch from the canal. The focussing effect of charged particles in electrostatic field arrangements is analogous to the optical behaviour of a pencil of rays relating the change in velocity at the boundary of a medium to the refraction of the rays. Equations of electron optical image-forming systems do not hold good for high intensity ion beams. The parameters are connected empirically. In Table II is shown the effectiveness of large voltage ratios on the conditions of focus of the beam at distances where further focussing can be effected by means of accelerating electrodes.

TABLE II

Extraction voltage $V_1$ in volts	Beam current $\mu$ a	Focussing voltage $V_2$ in volts	$V_2/V_1$	Distance from canal	Diameter of spot
700	50	6600	9.4	42 cms	6 mm
2173	175	14500	6.7	60 cms	10 mm

## MAGNETIC ANALYSIS OF THE ION BEAM

The ions drawn out of the canal and focussed by means of the electrostatic focussing lens to form a narrow beam were subjected to a uniform magnetic field by means of a pair of Helmholtz coils, 14.5 inches in diameter. The beam was received on the slit ( $1\frac{1}{4}'' \times \frac{1}{4}''$ ) of a brass plate attached to the end of a 30 cm glass tube. The beam was received on a Faraday cylinder opposite the slit and the current measured by type 954 tube in an electrometer tube circuit (figure 3) where the control grid was connected to the cathode and the suppressor grid assumed the functions of the control grid. For the grid resistor,  $R$ , the value of  $1M$  was used for the measurements and a microammeter of  $100 \mu A$  full scale was placed on the plate circuit. All the measurements were confined to the linear portion of



Electrometer tube circuit for mass analyser

FIG. 3

the grid voltage plate current characteristic curve. Considerable precautions were taken for shielding the electrometer circuit from external pick-up due to its operation in the proximity of the powerful r.f. source. The measurements were taken by removing the slit from the path of the beam to a desired distance by tightening or loosening the screws connected to the sylphon bellows, and then bringing each component of the slit by adjusting the magnet current.

In a magnetic field of strength  $H$  (gauss) the radius of curvature of the path followed by the ions of mass  $m$  (in atomic mass units) having an energy of  $V$  (electron volts) is given by the relation (Nier, 1940)

$$m/c = 4.82 \times 10^{-5} r^2 H^2 / V$$

where  $e$  is the electronic charge and  $r$  the radius of curvature in cm.

The method of mass analysis as adopted by Dempster, Nier and others consists in keeping  $r$  and  $H$  fixed in the arrangement and gradually varying  $V$  for the different  $m/e$  ratios. By using the pair of Helmholtz coils for providing the magnetic field it was found possible to vary  $H$  by changing the current  $i$  passing through the coils keeping  $r$  and  $v$  constant. Such a procedure was adopted to obviate a variation of  $V$ , upon which the condition

of focus of the beam depended considerably. Table III shows the approximate linearity of  $H$  with  $V$ .

TABLE III

Total voltage volts	Magnetic current for peak mass $1$ ion current in $\mu$ amperes	$H^2/V$
4030	3.8	.0036
5270	4.3	.0035
6665	5.0	.0038

The magnetic analysis of the ion beam was carried out for two constructions of the discharge tube extraction canal assembly. In the first instance (case I) the canal tip was bevel shaped and sharp. Only 36% of atomic ions resulted. In the second case (case II) the tip was machined flat and its outer surface was covered with pyrex tube extending  $3/16$  inch above the tip and the atomic ions increased to 61%. The slit of the Faraday cylinder was removed to different distances in the two cases. Results of analysis are given in Table IV. Figure 4 is drawn from the peak values of the beam

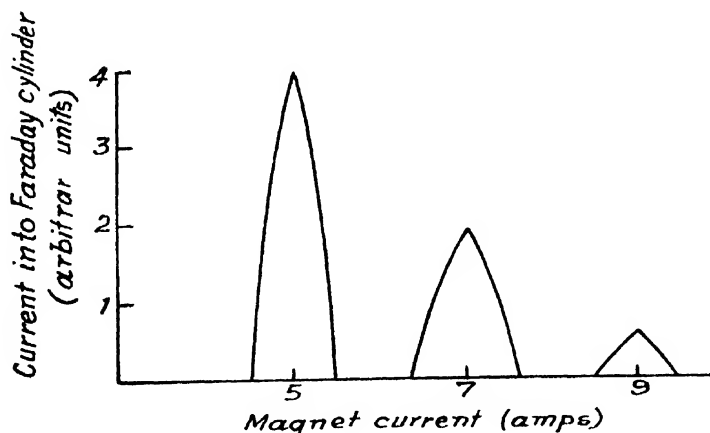


FIG. 4

current components and the half value width of the magnet current beam current curve.

TABLE IV (a)

Case I, extraction voltage = 430 volts, shap of cathode, sharp and tip uncovered.

Coil current (amps)	Significant ions	Meter deflection (scale division)	Percentage
2.2	$H_1$	23	36.5
3.4	$H_2$	30	47.6
4.1	$H_3$	10	15.9

TABLE IV (b)

Case II, Extraction voltage = 430 volts, shape of cathode, flat tip covered with pyrex tubing.

Coil current (amps)	Significant ions	Meter deflection (scale division)	Percentage
5	$H_1$	40	61.5
7	$H_2$	19	29.2
9	$H_2$	6	9.2

It will be apparent from the above observations that by covering the protruded portion of the canal with a pyrex tube the proton percentage was markedly increased. The total current obtainable in Case II also increased considerably. While only 60 microamperes of total current was obtained in Case I for an extraction voltage of 1860 volts, in Case II the current was 175 microamperes for 2200 volts.

THE TOTAL BEAM CURRENT

In order to determine the characteristics of the ion source the total ion current was measured as a function of the extraction voltage, In this case the beam was received on a brass plate which was held at a positive potential of 100 volts to arrest the liberation of secondary electrons from the plate and the current was measured with a microammeter. The extraction voltage-beam current characteristics are shown in Table V and figure 5.

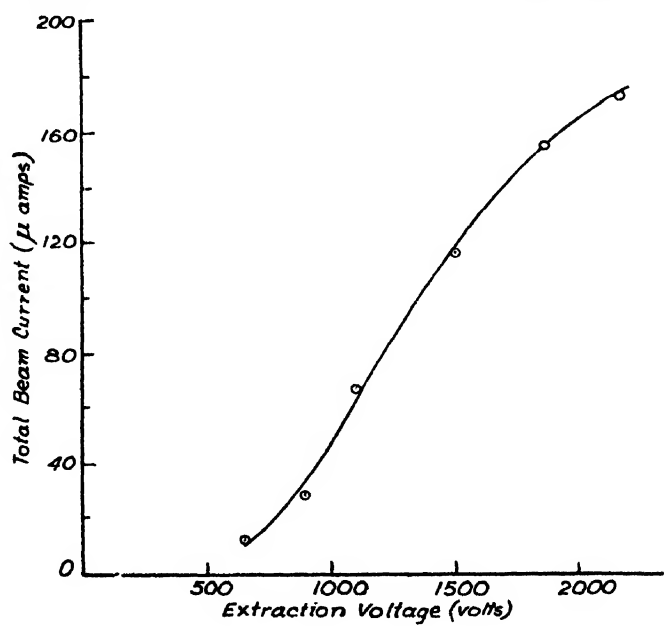


FIG. 5



TABLE V

Extraction voltage in volts	Beam current in $\mu$ amps
650	13
900	28
1100	68
1500	117
1850	156
2175	175

The rising part of figure 5 presumably represents a space charge limited current as it relates to the particular conditions of the discharge. With further increase in the extraction voltage this increasing current is supposed to attain a saturation value in an analogous way to the thermionic emission from hot cathode. So the possibility of a substantial increase in the total ion current with further increase of extraction voltage is indicated. The space charge equation for singly charged ions with molecular wt.  $M$  is given by (Langmuir *et al*, 1931).

$$I = 5.462 \times 10^{-8} M^{-1/2} V^{3/2} X^{-2} \text{ amps cm}^{-2}$$

where  $V$  is in volts and  $X$  the distance between anode and cathode.

The partial neutralization of space charge in bipolar current discharges consisting of a flow of positive ions in one direction and electrons in the opposite direction manifests itself as a more rapid increase of current than the above equation suggests. From the results of the above measurements an equation of the following form has been worked out.

$$I = K V^{2.1} X^{-2} \text{ amps cm}^{-2}$$

where  $K$  is a constant.

#### CONCLUSION

The large majority of ion sources developed in recent years recorded the atomic ion percentage in the beam at between 50 and 60. A few, however, were reported to have an yield between 80% and 90%. This improvement was caused, firstly, by reducing the metallic parts within the discharge tube to its possible limit and secondly by designing the extraction assembly in such a way that only the ions from the cone of the discharge tube were drawn out. The incorporation of this latter means of improvement in the design of the present ion source would be necessary before any further increase in its atomic ion content, from its present value of 61.5%, could be contemplated. It is proposed, at present, to utilize this ion source for neutron production from D-D Reaction in a 150 KV accelerator.

## ACKNOWLEDGMENTS

In conclusion the author takes great pleasure in recording his sincere thanks to Dr. D. M Bose, Director, Bose Research Institute, Calcutta, for constant encouragement and helpful suggestions and for the provision of all laboratory facilities. Thanks are also due to Atomic Energy Commission, Government of India, for financial assistance in support of this work.

## REFERENCES

- Bayly, A. J. Ward, A. G. 1948, *Can. J. Research A*, **26** 69.  
 Brasefield, C. J., 1930, *Phys. Rev*, **35**, 1073.  
 Buchner, W. W., Lamar, E. S. and Van de Graaff, R. S. 1941, *J. Appl. Phys.*, **12**, 141.  
 Hall, R. N., 1948, *Rev. Sci. Instr.*, **19**, 905.  
 Herzberg, G., 1927, *Ann. Phys. Lpz.*, (4), **84**, 565.  
 Langmuir, I. and Compton, K. T. 1931, *Rev. Mod. Phys.*, **3**, 191.  
 Moak, C. D. Reese, H. Wood, W. M. 1951, *Nucleonics* **9**, 18.  
 Nier, A., 1940, *Rev. Sci. Instr.*, **11**, 212.  
 Pierce, J. B., 1940, *J. Appl. Phys.*, **11**, 548.  
 Thonemann, P. C. 1946, *Nature*, **168**, 61.  
 Thonemann, P. C., Moffatt, J., Roaf, D. and Sanders, J. H., 1948, *Proc. Phys. Soc.*, (Lond) **61**, 433.  
 Tuve, M. A., Dahl, O. and Hafstad, L. R., 1935, *Phys. Rev*, **48** 241.

# THE EFFECT OF FLUID MOTION ON HEAT TRANSMISSION. PART II. DETERMINATION OF THE FORCED CONVECTION CONSTANT

By D. G. KAPADNIS\*

PHYSICS DEPARTMENT, FACULTY OF SCIENCE, MAHARAJA SAYAJIRAO UNIVERSITY OF BARODA  
BARODA

(Received for publication, March 16, 1953)

**ABSTRACT.** In this paper a detailed experimental study of the forced convection constant has been made. It is shown that the value of this constant is  $7.56 \times 10^{-6}$ , the heat being measured in calories, and that it depends on the physical properties of the fluid. This value is in fair agreement with the theoretical value obtained from Nusselt's equation. The slight deviation from the theoretical value has been accounted for by considering the variation with temperature of the quantities involved in Nusselt's equation.

## INTRODUCTION

Despite the evident practical importance of the problem of forced convection, the transport of heat from a hot solid by a stream of relatively cool fluid or vice versa, it cannot be said that our knowledge of it is as yet, especially from a theoretical standpoint, at all complete. The most general problem, where the shape of the solid is not simple, and the thermal expansion, compressibility and viscosity of the fluid, and the temperature variations of these and of the specific heat are taken into account, presents very considerable difficulties. Straight mathematical solutions of the differential equations representing this type of heat transmission have been worked out in a few cases and only under certain simplifications of the considered problems. However, the principle of similitude has been and is being widely employed to obtain an insight into the complex mechanisms of the processes of heat convection.

The results arrived at mathematically by some workers in both the regions, laminar as well as turbulent, of forced convection suggest that the experimental data of this problem of the effect of fluid motion on heat transmission may be examined in the light of a very simple formula

$$H = bV^n + c \quad \dots (1)$$

where  $H$  is the rate of heat dissipation per unit area of the surface of the hot cylinder immersed in a moving fluid,  $V$  is the fluid velocity, the index

\* Now at National Physical Laboratory of India, New Delhi 12

$n$  is a constant and  $b$  and  $c$  are functions of the characteristic dimension of the cylinder immersed, and of the excess of temperature of the cylinder over that of the surrounding fluid. The term  $bV^n$  represents the heat dissipation due to forced convection, while  $c$  includes the energy losses due to radiation and natural convection.

In this paper a detailed experimental study of the forced convection constant has been made in the light of the above formula.

### EXPERIMENTAL

This paper is in continuation with the previous one by the present author (Kapadnis, 1953). The same experimental technique (Kapadnis and Gogate, 1952) was, therefore, used to record a few more observations, sample series of which are given in Tables I and II. In all, five cylindrical vessels were used to collect the necessary experimental data, the velocity of the air stream issuing from the electric fan, made uniform by introducing a wire-mesh between the fan and the cylindrical vessel, ranging from about 80 cm per sec. to 1100 cm per sec., and an excess of temperature of the cylinder surface over that of the surrounding air stream from 30°C to 68°C. If in this case the rate of heat dissipation per unit area is plotted against the  $n$ th power of air velocity for each temperature excess, one should obtain a family of straight lines from which the values of the functions  $b$  and  $c$  in expression (1) can be calculated. Figures 1 and 2 show this conclusion to

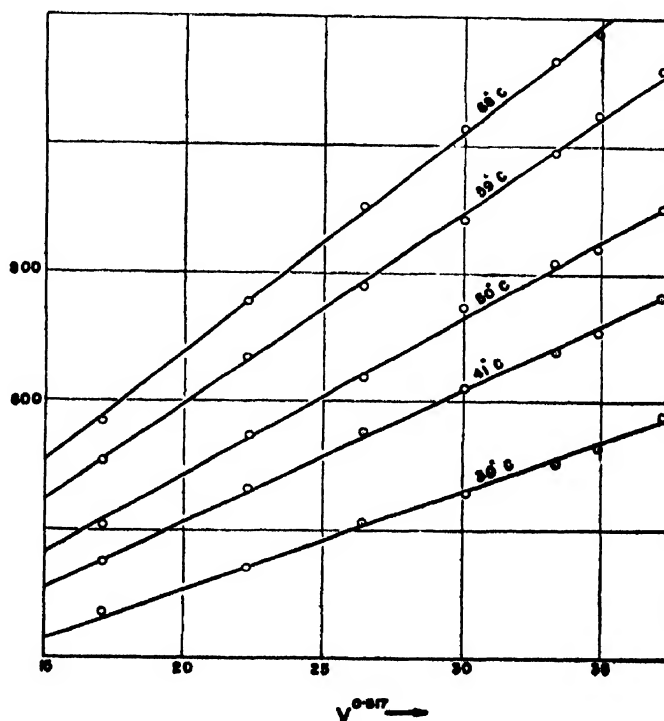


FIG. 1

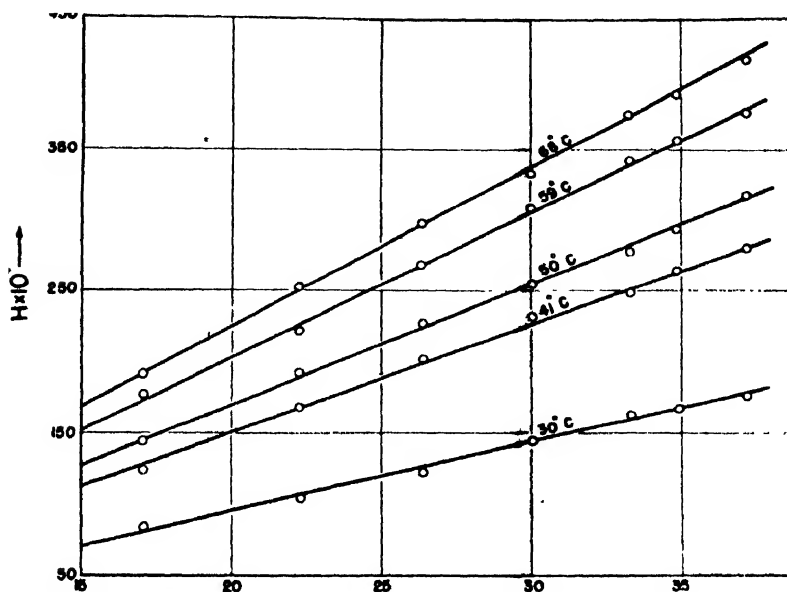


FIG. 2

be justified within the limits of experimental error. The accuracy of the observations was tested by plotting for each vessel this family of straight lines corresponding to the various temperatures and in this way a check was obtained in the determination of the constant function  $b$ . The values of  $b$  obtained in this manner are recorded with the excess of temperature and the diameter of the cylinder in Table III.

As the Nusselt's equation, used by the present author in his previous work of which this investigation is a continuation, does not take account of the heat losses due to natural convection and radiation; all the values of the rate of heat dissipation are corrected for these losses in the same manner the present author followed in his previous work. The question of the second function,  $c$ , representing the heat losses due to radiation and natural convection, therefore, does not arise here. The study of this constant function,  $c$ , will be made separately.

#### DETAILED ANALYSIS

As mentioned above the term  $b$  in expression (1) is a function of the temperature excess and the cylinder diameter. For a constant value of the cylindrical vessel, therefore, expression (1) represents a surface in space, which gives in  $H-V''$  plane a family of straight lines for different temperatures. The slope of each line gives the value of the forced convection constant function  $b$  for the corresponding value of the excess of temperature of surface of the hot cylinder over that of the surrounding stream of air. Values of  $b$  corresponding to different values of  $\Delta\theta$ , the temperature excess, in the case of cylinders of various diameters are recorded

TABLE I

Effect of air velocity on heat transmission for different temperature excesses

Diameter of the cylinder  $D=2.5$  cm

Air velocity $V$ in cm/sec.	$V^{0.517}$	Rate of heat dissipation per unit area in cals /sec /sq.cm $\times 10^4$ for an excess of temperature of				
		30°C	41°C	50°C	59°C	68°C
242	17.06	273	352	406	507	569
405	22.28	343	465	546	667	754
563	26.42	410	552	637	778	903
721	30.06	458	619	744	883	1,023
882	33.34	504	677	815	987	1,103
967	34.91	528	705	838	1,046	1,172
1,095	37.24	577	761	902	1,118	1,258

TABLE II

Effect of air velocity on heat transmission for various values of excess temperature

Diameter of the cylinder  $D=21.8$  cm

Air velocity $V$ in cm./sec.	$V^{0.517}$	Rate of heat dissipation per unit area in cals./sec./sq. cm. $\times 10^4$ for an excess of temperature of				
		30°C	41°C	50°C	59°C	68°C
242	17.06	85	125	145	177	192
405	22.28	105	168	192	223	252
563	26.42	123	202	227	268	298
721	30.06	145	233	255	308	333
882	33.34	163	248	278	342	376
967	34.91	168	265	294	356	389
1,095	37.24	178	282	318	377	414

in Table III. Figures 1 and 2 give typical plot of the convective rate of heat transmission per unit area against the  $n$ th power of air velocity for two cylinders, the smallest and the biggest among those tried in these investigations. A remarkable feature of the forced convection constant function revealed by the record and the graphs as well is that its values show a systematic increase with the temperature excess, but a striking decrease with increasing values of cylinder diameter. This suggests that the constant function  $b$  be examined in the light of the expression  $b = \beta \Delta \theta$ , where  $\beta$  is the function of the cylinder diameter only.

TABLE III

Variation of the forced convection constant function with the excess of temperature in the case of cylinders of different sizes

Diameter of the cylinder $D$ in cm.	Values of the forced convection constant function $(b) \times 10^{-3}$ for an excess of temperature of				
	30°C	41°C	50°C	59°C	68°C
2.4	1.53	2.05	2.43	2.95	8.38
5.2	1.01	1.45	1.66	2.00	2.28
10.7	0.78	0.99	1.10	1.38	1.64
15.0	0.62	0.87	0.98	1.22	1.45
21.8	0.48	0.76	0.85	1.02	1.12

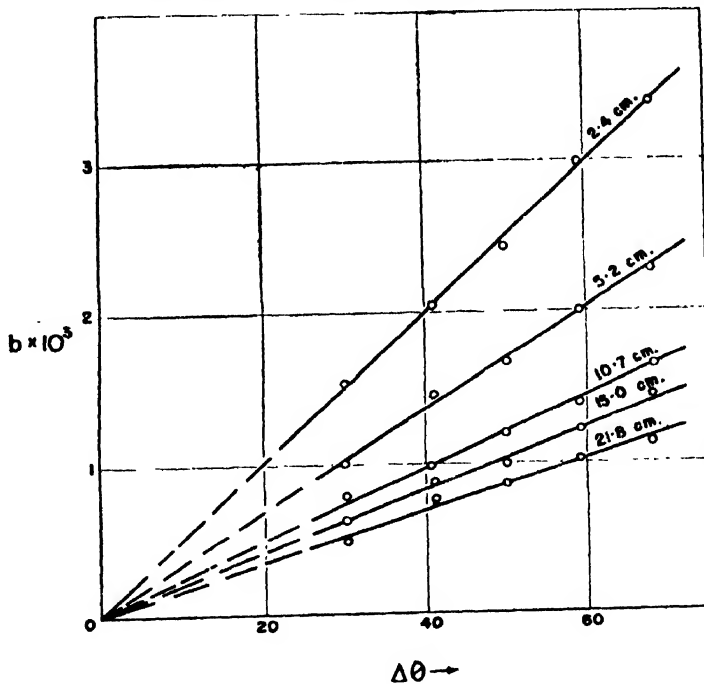


FIG. 3

The values of the constant function  $b$  are, therefore, plotted against the excess of temperature of the surface of the cylinder over that of the surrounding stream of air, for different cylinder diameters (figure 3) in order to get the various values of  $\beta$ .

It is seen from the values of  $\beta$  obtained in this way that  $\beta$  is very nearly independent of the temperature. The slight increase in its values with increasing temperature may be represented by a small temperature coefficient such that  $\beta = \beta_0 (1 + \alpha \Delta\theta)$ ; and which may be interpreted as due to the combined variation of the dimensions of the vessel and the density, viscosity and heat conductivity of air with temperature. It has been found

in these experiments that this variation of  $\beta$  with the temperature excess is negligibly small, very slightly greater than that due to the experimental errors.

The present author (Kapadnis, 1953) obtained by using the method of dimensional analysis the following partial theoretical expression, co-ordinating experimental data, in the case of heat dissipation by forced convection :

$$\left( \frac{1}{A\Delta\theta} \frac{dQ}{dT} \frac{D}{K} \right) = 0.56 \left( \frac{VD}{\xi} \right)^{0.517}$$

$$\text{i. e. } H = \frac{1}{A} \frac{dQ}{dT} = \frac{0.56K}{\xi^{0.517}} \frac{\Delta\theta V^{0.517}}{D^{0.483}} \quad \dots (2)$$

where  $\frac{dQ}{dT}$  is the rate of heat transmission ;

$A$ , the area of the cylinder exposed ;

$D$ , the characteristic dimension of the cylindrical vessel (vessel diameter) ;

$\Delta\theta$ , the excess of the surface temperature of the cylinder over that of the surrounding air-stream ;

$V$ , the velocity of the air stream ;

$K$ , the heat conductivity of air ;

and  $\xi$ , is the ratio of the viscosity of air to its density.

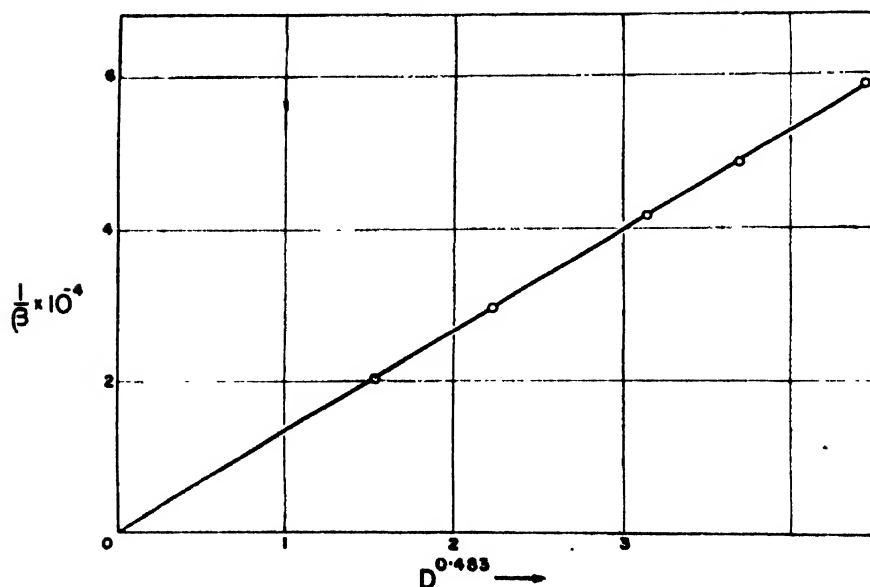


FIG. 4

It is evident from the present author's experimental results in the previous paper and also from expression (2) that  $\beta$  varies inversely as the 0.483rd power of the diameter of the cylinder. Figure 4 gives a plot of the reciprocal of  $\beta$  against the 0.483rd power of the cylinder diameter,



which is a straight line showing clearly that the product of  $\beta$  and  $D^{0.488}$  is constant. The constancy of this product is shown very satisfactorily in the last column of Table IV. The mean value of this product as the result of all the observations is given by

$$\beta D^{0.488} = 7.56 \times 10^{-5} \quad \dots (3)$$

the units of heat being in calories.

The theoretical expression (2) requires that  $\beta$  be given by

$$\beta = \frac{0.56K}{\xi^{0.517} D^{0.488}} \quad \dots (4)$$

TABLE IV

Variation of  $\beta$  with the size of the cylinder

$D$	$\beta$	$D^{0.488}$	$\frac{1}{\beta}$	$\beta D^{0.488}$
	$\times 10^{-5}$		$\times 10^{-4}$	$\times 10^{-5}$
2.4	5.00	1.53	2.00	7.65
5.2	3.37	2.22	2.97	7.48
10.7	2.40	3.14	4.17	7.54
15.0	2.06	3.70	4.85	7.62
21.8	1.70	4.43	5.88	7.53

Taking from International Critical Tables the value of the heat conductivity of air,  $K = 5.755 \times 10^{-5}$  cal./cm. sec. ( $^{\circ}\text{C}$ ,  $\text{cm}^{-1}$ ); that of the viscosity of air,  $\mu = 185.6 \times 10^{-6}$  poise; and that of the density of air,  $\rho = 0.001165$  gms./ $\text{cm}^3$ , (all at  $30^{\circ}\text{C}$ ), for the numerical calculation of the theoretical constant factor  $0.56K/\xi^{0.517}$  in expression (2), we get

$$\frac{0.56K}{\xi^{0.517}} = 8.33 \times 10^{-5} \quad (5)$$

which is in agreement with the factor (3) arrived at purely from the experimental data. However, the agreement between these experimental and theoretical factors is not very close.

In these investigations the temperature of the air-stream was measured at a considerable distance from the surface of the cylinder, because it is well-known from theory and experience that at the very surface of the cylinder the temperature of the air-stream is not different from the surface temperature. The values of heat conductivity, density and viscosity of air were taken at the temperature of the stream of air. Considerable variation of these quantities with temperature takes place. But, in the present investigations the temperature excess never exceeded  $68^{\circ}\text{C}$ . The error due to the neglect of the variation in the above quantities with temperature was,

therefore, thought to be small in comparison with the experimental error. So expression (2) used here was not modified to take account of the abovementioned variations with temperature.

The root cause of the slight disagreement between the theoretical and experimental factors (5) and (3) respectively lies most probably in the theoretical expression (2) which has been derived by assuming that the density, heat conductivity and viscosity of the surrounding air-stream remain constant when the excess of temperature of the hot cylinder over that of the surrounding stream of air has got a small value.

#### ACKNOWLEDGMENTS

The author tenders his grateful thanks to Dr. K. S. Krishnan, Director, National Physical Laboratory, New Delhi, for his valuable suggestions; and to Dr. D. V. Gogate, Head of the Physics Department of M. S. University of Baroda, for his guidance and keen interest in this work.

The experimental observations were taken in the Physics Laboratory of the Faculty of Science of the Maharaja Sayajirao University of Baroda. The rest was carried out while the author was receiving a research scholarship from the M. S. University of Baroda, for which grateful acknowledgment is made.

#### REFERENCES

Kapadnis, D. G., 1953, *Ind. J. Phys.*, **27**, 77.

Kapadnis, D. G., and Gogate, D. V., 1952, *Ind. J. Phys.*, **26**, 171.

# DYNAMICS OF PLASTIC DEFORMATIONS IN A BAR EXHIBITING STRAIN-RATE EFFECT AND SUBJECTED TO ALTERNATING STRESSES

By S. K. GHOSH

DEPARTMENT OF PHYSICS, CHANDERNAGORE COLLEGE, WEST BENGAL

(Received for publication February 28, 1953)

**ABSTRACT.** Dynamics of the vibration of a bar exhibiting strain-rate effect when subjected to an alternating mechanical stress has been worked out, following the operational method. Expression for the amplitude of vibration at the free end in terms of resonance frequency and fractional detuning at 3 db point has been derived. An accurate formula is also derived for the resonance frequency. An expression giving the displacement at any point along the bar has also been derived. The work of previous authors have also been critically discussed.

## INTRODUCTION

The theory of the extensional vibrations of a bar excited by impact of a 'rigid' load has been worked out by a number of workers. (Boussinesq, 1885 ; Ghosh, 1936 ; Ghosh and Dhar, 1930). Ghosh and Ghosh (1950) extended the case, applying the powerful operational method, for an elastic load struck at the free end of a bar, the other end being fixed. In a subsequent paper (Ghosh and Ghosh, 1952) dealing with the transmission of stress under the conditions of rapidly applied loading, the author has calculated the time of collision during impact for each epoch and has derived many important conclusions therefrom. But in formulating the earlier theories the effect of internal friction in solids was neglected. Thereupon the author has built up the complete dynamics of the elastic strain-waves due to axial impulse and has extended the theory to cover plastic behaviour exhibited by most metals. In formulating all these theories the author has always used the powerful operational method, which is also employed here for solving the present problem. In the present theory the effect of viscosity, which arises out of internal friction, in metals on the transmission of strain-waves through a solid bar subjected to an alternating mechanical stress has been considered. The characteristic of viscosity is that in a moving fluid, the stresses differ from a state of pressure uniform in all directions about a point, by quantities depending on the 'rates of strain'.

It is usually assumed that these quantities are linear functions of the rates of strain. At least in the high polymers, a complete model of the solid

must comprise an indefinitely large number of elements all obeying this linear model, but with differing values of appropriate elastic and viscous moduli. From our present standpoint this is sufficiently justified by the fact that the strain-velocities are regarded as infinitely small.

### THEORY

For mathematical convenience, it is common in problems on vibrations to consider the relation between the stress,  $p$ , and the strain,  $e$ , in a solid to be of the form :

$$p = Ec + \eta \frac{de}{dt}$$

where  $E$  and  $\eta$  are the associated elastic and viscous moduli.

The equation of longitudinal motion in a thin bar or tube (Cady, 1922) exhibiting strain-rate effect, is then :

$$\rho \frac{d^2 \omega}{ds^2} = E \frac{d^2 \omega}{ds^2} + \eta \frac{d^3 \omega}{dt \cdot ds^2} \quad (1)$$

where  $s$  = longitudinal co-ordinate,  
 $\omega$  = longitudinal displacement,  
 $\rho$  = density of the bar,  
 $E$  = Young's modulus of the bar,  
 and  $\eta$  = associated viscosity coefficient of the bar.

Equation (1) is equivalent to :

$$\frac{d^2 \omega}{ds^2} = \frac{D_1^2 \omega}{C^2} \quad (1.1)$$

where

$$D_1 = D[1 + \eta_1 D]^{-1/2}$$

$$C^2 = E/\rho$$

$$\eta_1 = \eta/E \text{ and } D = \text{the operator } \frac{d}{dt}.$$

The general solution of equation (1.1) is

$$\omega = A \cosh \frac{D_1 s}{C} + B \sinh \frac{D_1 s}{C} \quad (1.2)$$

If a periodic force of any period be applied at one end of the bar, any portion of it will vibrate with the same periodicity as the force, so that in the steady state,

$$\omega_s = \psi(s) \cdot \frac{D}{D - in} \quad (1.21)$$

expressed in operational form in which  $n$  represents the frequency of vibration.

At the free end of the bar, there being no external force, we have,

$$\text{at } s=0, \quad \frac{d\omega_s}{ds} = 0 \quad (1.3)$$

Also, the displacement at the free end ( $s=0$ ) may be expressed as

$$u_0 = \psi(s)_{s=0} \cdot \frac{D}{D - in} \quad \dots \quad (1.4)$$

With the help of equations (1.3) and (1.4), equation (1.2) becomes :

$$\omega_s = \psi(s)_{s=0} \cosh \frac{D_1 s}{c} \cdot \frac{D}{D - in} \quad \dots \quad (2)$$

The operational solution of equation (2) yields :

$$\omega_s = \psi(s)_{s=0} \left[ \cosh^2 \frac{\beta s}{c} - \sin^2 \frac{n s}{c} (4 - 3\alpha) \right]^{1/2} e^{i(nl + \dots)} \quad \dots \quad (2.1)$$

where  $\alpha = 1 + \frac{1}{8} \eta_1^2 n^2$ ,  $\beta = \frac{1}{2} \eta_1 n^2$  ... (2.11)

and  $\tan \epsilon = \tanh \frac{\beta s}{c} \cdot \tan \frac{n s}{c} (4 - 3\alpha)$  ... (2.12)

If the bar of length  $l$  be excited at one end ( $s=l$ ) by a periodic stress  $F \cdot e^{i(nl + \dots)}$  of peak value  $F$ , the equation of motion at  $s=l$  is

$$E \left( \frac{d\omega}{ds} \right)_{s=l} + \eta D \left( \frac{d\omega}{ds} \right)_{s=l} = F \cdot e^{i(nl + \dots)} \quad \dots \quad (3)$$

Substituting values of  $\left( \frac{d\omega}{ds} \right)_{s=l}$  from equation (2), equation (3) becomes,

$$F \cdot e^{i(nl + \dots)} = \frac{E}{c} \psi(s)_{s=0} D [1 + \eta_1 D]^{1/2} \sinh \frac{D_1 l}{c} \cdot e^{i n l}$$

$$\frac{E}{c} \psi(s)_{s=0} [x^2 n^2 + \beta^2]^{1/2} \left\{ \cosh^2 \frac{\beta l}{c} - \cosh^2 \frac{n l}{c} (4 - 3\alpha) \right\}^{1/2} e^{i(nl + \dots)} \quad \dots \quad (3.1)$$

where  $\epsilon_1 = \epsilon + \phi + \pi$ , and  $\tan \phi = \frac{\tanh \frac{\beta l}{c} \cot \frac{n l}{c} (4 - 3\alpha) - \frac{\beta}{\eta n}}{\frac{\beta}{\alpha n} \tanh \frac{\beta l}{c} \cot \frac{n l}{c} (4 - 3\alpha) + 1}$

at  $s=l$ .

The amplitude of vibration at the free end  $s=0$  is, therefore, given by

$$\psi(s)_{s=0} = \frac{F}{c} [x^2 n^2 + \beta^2]^{1/2} \left[ \cosh^2 \frac{\beta l}{c} - \cosh^2 \frac{n l}{c} (4 - 3\alpha) \right]^{1/2} \quad \dots \quad (4)$$

Equation (4) is in agreement with the result given by Lethersich and Pelzer (1950) upto terms containing  $\eta_1^2 n^2$ .

Also from equation (2.1) we get the displacement at any point along the bar in terms of the amplitude of vibration at the free end and is given by

$$|\omega_s| = \psi(s)_{s=0} \left[ \cosh^2 \frac{\beta s}{c} - \sin^2 \frac{n s}{c} (4 - 3\alpha) \right]^{1/2} \quad \dots \quad (5)$$

Differentiating the expression under the radical sign in equation (4) with respect to  $n$  and equating to zero, the maxima of the amplitude are found to occur when,

$$n = \frac{S\pi c}{l} \left( 1 + \frac{3}{8} \eta_1^2 n^2 \right)^{-1} \quad \dots (6)$$

where  $S = 1, 2, 3 \dots$  etc.

Similarly, an inspection of equation (5) shows that minimum values of displacement (nodes) occur at distances given by

$$\frac{nS}{c} \left( 1 - \frac{3}{8} \eta_1^2 n^2 \right) = S' \frac{\pi}{2} \quad \dots (7)$$

where  $S' = 1, 3, 5 \dots$  etc.

### DISCUSSIONS

Experiments (Lethersich, *et al*, 1950) made on a number of plastics indicate that at a frequency of  $2 \times 10^3$  c/s,  $\eta_1^2 n^2$  lies between 0.00016 and 0.003. Thus if  $\eta_1^2 n^2 < 0.00016$ , the minimum value for most plastics,  $(1 - 3\alpha)$  of equations (4) and (5) approaches unity.

Under this condition equation (6) shows that resonances occur at or near multiples of frequency when  $n = n_r$ ,

$$\text{where } n_r = \frac{S\pi c}{l}, S = 1, 2, 3 \dots \text{etc.}$$

Therefore expanding the cosh and cosine terms in equation (4) and using the approximate relations :

$$\cosh \theta = 1 + \frac{\theta^2}{2} + \frac{\theta^4}{24},$$

$$\cos \theta = 1 - \frac{\theta^2}{2} + \frac{\theta^4}{24},$$

a simplified expression for the amplitude near the resonance peaks is given by

$$\psi(s)_{s=0} = \frac{2F}{S\pi(\rho E)^{1/2}} \cdot \left[ \frac{n^6 \eta_1^2}{2n_r^2} + \frac{4n^2(n - n_r)^2}{n_r^2} \cdot \left( 1 - \frac{\eta_1^2 n^2}{8} \right) - \frac{4S^2 \pi^2 n^2 (n - n_r)^4}{3n_r^4} \left( 1 - \frac{\eta_1^2 n^2}{2} \right) \right]^{1/2} \quad \dots (4.1)$$

Equation (4.1) gives the resonance amplitude at the free end, in terms of the harmonic number  $S$  and the fractional detuning. The resonant amplitude can, however, be found more accurately by using the relation (6) i.e., replacing  $n$  in equation (4.1) by

$$\frac{S\pi c}{l} \left( 1 + \frac{3}{8} \eta_1^2 n^2 \right)^{-1}.$$

Relation (6), therefore, gives an accurate value for the resonance frequency and indicates that some sources of error creep in due to successive approximation in deriving a similar relation by Lethersich and Pelzer.

Relation (6) thus amends Lethersich and Pelzer's similar relation and improves the accuracy of Wegel and Walther's (1935) expression giving the band-width at the 3 db. point.

Equation (7) gives minimum values of displacement at distances given by

$$\frac{2n_s}{c} = S'\pi, S' = 1, 3, 5 \dots \text{etc.}$$

when  $\eta_1^2 n^2 < 0.00016$ . This is also in agreement with Lethersich and Pelzer's relation giving the position of nodes.

With the above approximation, the displacement at the centre of the bar vibrating in its simplest mode at resonance is

$$\omega_{1/2} = \psi(s)_{s=0} \sinh \frac{\eta_1 n^2 l}{4c} \dots (5.1)$$

which is the only minimum value at the fundamental. The displacement at the centre of the bar for the same mode, when the amplitude of vibration at the free end has dropped by a factor of  $\sqrt{2}$  (i.e., 3 db.) on either side of the peak is obtained by putting  $(n_r \pm \Delta)$  for  $n$  in equation (5),  $\Delta$  being the band-width at the 3 db. point. This gives

$$\omega = \psi(s)_{s=0} \left[ \cosh^2 \frac{\eta_1 n_r^2 l}{4c} \left( 1 + \frac{\Delta}{n_r} \right)^2 - \cosh^2 \frac{\Delta l}{2c} \right]^{1/2} \dots (5.2)$$

Neglecting  $\frac{\Delta}{n_r}$  compared to unity and using Wegel and Walther's relation,

$$\Delta = \frac{\eta_1 n_r^2}{2} \text{ at 3 db. point, we get,}$$

$$\omega_s \simeq \sqrt{2} \omega_{s=\frac{l}{2}} \dots (5.3)$$

Equation (5.3) is also in agreement with Lethersich and Pelzer's similar expression.

#### ACKNOWLEDGMENT

The author wishes to thank Dr. M. Ghosh, Professor of Physics, City College, Calcutta, for his kind suggestions and helpful discussions.

#### REFERENCES

- Boussinesq, 1885, Application des potential.  
Cady, W. G., 1922, *Phys. Rev.*, **10**, 1.

Ghosh, M., 1936, *Bull. Cal. Math. Soc.*, **27**, 1.

Ghosh, M. and Dhar, S. C., 1930, *Bull. Cal. Math. Soc.*, **27**, 171.

Ghosh, M. and Ghosh, S. K., 1950, *Ind. J. Phys.*, **25**, 75.

Ghosh, M. and Ghosh, S. K., 1952, *Ind. J. Phys.*, **26**, 9.

Leathersich, W., 1950, Rheological Study of the Creep of Dielectrics over short Times and its Relation to Dynamic properties, R. R. A. Report Ref : L/T 212.

Leathersich, W. and Pelzer, H. Britt, 1950, *J. Appl. Phys.*, **1**, 18

Wegel, R. L., and Walther, H., 1935, *Physics*, **6**, 141.

Love, The Mathematical Theory of Elasticity, 4th Ed., P. 431.



# ON THE STUDY OF BI-PARTITION AND TRI-PARTITION OF URANIUM NUCLEUS\*

BY S. P. DUTTA

BOSE RESEARCH INSTITUTE, CALCUTTA 6

(Received for publication, September 12, 1953)

**ABSTRACT.** In the present paper binary and ternary fissions of uranium under the action of slow neutron have been studied by photographic emulsion technique and it is intended to establish the fact that in the case of tri-partition the third fragment may not necessarily be a light particle, of the nature of an  $\alpha$ -particle, but can have a mass greater than 4. Accordingly, it was necessary to desensitize the experimental nuclear plates by increasing the concentration of  $\text{UO}_2(\text{NO}_3)_2 \cdot 6\text{H}_2\text{O}$  in alcohol. A concentration of 12 to 16% was found most favourable due to various factors. More than 20,000 cases of bi-partition and one interesting case of tri-partition were observed. The calculated mass values were 166, 43 and 30; but from the nature of ionisation, the mass value of the third fragment is expected to lie between 15 to 20 instead of 30. The calculated kinetic energy of this tri-partition is  $2 \times 10^9$  electron-volts instead of  $1.5 \times 10^8$  electron-volts and hence it is assumed that the fission has been initiated by a high energy fast neutron (of cosmic ray origin) the direction and value of which only can help to determine the correct mass values. In such highly desensitized plate the total range distribution of the two fission fragments has been shown by a histogram and most of them lie between 20 and  $21\mu$ . The corresponding value in a non-desensitized plate is  $24\mu$  approximately.

## INTRODUCTION

The phenomenon of excited nucleus, namely that of uranium or thorium breaking up into two fragments during the fission process have been observed by various methods e.g., ionisation chamber, Wilson chamber etc. and the projectile used to have brought out this fission process was generally the neutron. Though in the past Ilford Half-tone and other similar types of photographic plates were used to study the fission phenomenon along with the other studies on nuclear reaction and cosmic rays, they served only a limited useful purpose. Recently, the production of a new specially concentrated emulsion (manufactured mainly by two photographic firms, namely, Ilford Ltd and Kodak Ltd) for the investigation of nuclear processes has brought a wide development in the field of nuclear research (Powell, Occhialini, Livesey and Chilton, 1946). Using the new photographic emulsions the observation of tracks due to fission fragments has been studied by a number of workers. In addition to bi-partition of uranium nucleus which is commonly observed, tri-partition of uranium has also been reported by some workers, namely, Green and Levesey (1947), and others. The aim of the present investigation is

(a) to search for the tri-partition of uranium nucleus under the action of neutron by photographic emulsion technique and if observed,

\* Communicated by Dr. D. M. Bose.

(b) to establish the fact that the third fragment emitted in addition to the other two fragments which are equivalent to those in binary fission may not necessarily be a light particle of the nature of an  $\alpha$ -particle, but can have a mass value greater than 4 mass units.

#### EXPERIMENTAL TECHNIQUE AND RESULT

The study of fission fragments by the photographic emulsion requires some special treatment of the nuclear research emulsion due to the difficulties arising out of the technique employed. Firstly, uranium itself emits  $\alpha$ -particles which create a considerable amount of background tracks along with those due to fission fragments. The number of these  $\alpha$ -particles depends upon the quantity of uranium present in the emulsion. Secondly, in the present investigation the fission of the uranium nucleus is brought about under the action of neutrons, there is every chance of having recoil proton tracks in the emulsion. Thirdly, the neutron-source was a radium-beryllium one and so the back-ground fogging due to  $\gamma$ -rays has to be eliminated. Moreover, the aim of the present work is to search for a tri-partition of uranium nucleus which when observed, should also indicate, whether the particle has a mass equal to or greater than 4; thus the problem requires that a large number of uranium-fission fragments should be produced in the plate, and carefully scrutinized under the microscope for observation of such rare events.

To eliminate the effect of the back-ground due to less energetic radiation i.e.,  $\alpha$ -particles, recoil proton tracks etc., desensitizers like  $\text{CrO}_3$ ,  $\text{K}_3\text{Fe}(\text{CN})_6$  etc. were tried but with no satisfactory result, as the quantity of uranium with which a plate can be loaded cannot be increased beyond an appreciable value. If uranium in the form of its salt is used in large quantity then further desensitizing action of uranium salt (actually solution of uranyl nitrate in ethyl alcohol was used) made the fission tracks much weaker; it could be hardly visible, but the total number of fission events was increased. The desensitizing action of uranium-salt which increases with the increase of uranylion, is found to be most suitable for the present purpose of studying the rare event in connection with the fission of uranium nucleus, as was also suggested by Green and Livesey (1946). The choice of the particular concentration of uranyl nitrate  $[\text{UO}_2(\text{NO}_3)_2, 6\text{H}_2\text{O}]$  in ethyl alcohol was found by performing a number of preliminary experiments, by increasing successively the concentration of uranyl nitrate a little. The plates, being bathed in the requisite concentration of solution for half an hour, were dried, kept for a few days and then developed as usual. When the tracks due to  $\alpha$ -particles were completely suppressed, but tracks due to fission fragments were easily distinguishable, the corresponding value of the particular concentration was chosen and it

was found to be between 12 to 16 gms of uranyl nitrate crystals dissolved in 100 c.c. of ethyl alcohol. The use of alcohol was found to be suitable for impregnation, as it helps in quick drying out of the plates especially in moist weather.

Some Ilford nuclear plates of different types, namely, C<sub>2</sub>, R<sub>1</sub>, D<sub>1</sub> etc. were impregnated with the above concentration of solution of uranyl nitrate, and were dried quickly in a specially constructed wooden chamber (kept in a dark room). The construction of the chamber is very simple and is shown in the figure 1.

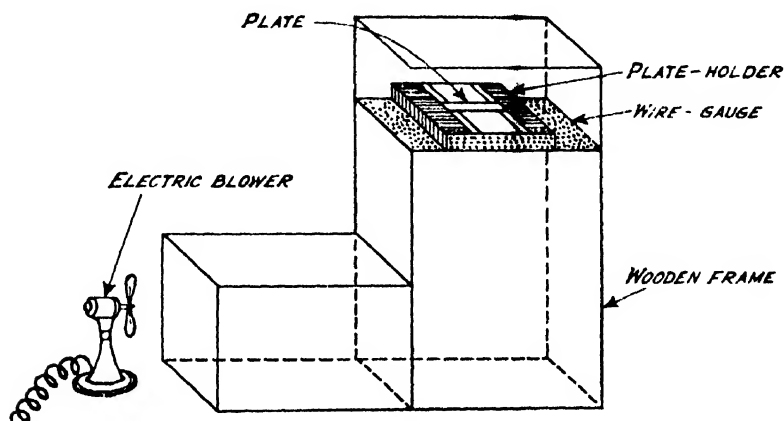


FIG. 1

Drying chamber

It consists of a tall upright rectangular wooden frame-work open at the top and closed at the bottom; there is a small similar frame-work attached to a side near the end. Through the mouth of the side frame-work air is blown from an electric blower. Slightly below the mouth of the upright frame-work but inside it there is a metallic wire-gauge over which there is a plate holder in which the impregnated plates are put with the emulsion surface facing downwards. The whole chamber both inside and outside is painted black so that any transient illumination due to sparking in the electric blower may not affect the emulsion due to reflection from the sides. The dried plates are placed within a brass box which in turn was kept within another thin brass box. The plates were then placed before a neutron source (radium-beryllium) surrounded by paraffin bricks. The effect of the  $\gamma$ -rays was almost cut off by interposing some lead bricks, of total thickness 12 cms, between the plates and the source. The plates were kept as such in an atmosphere of slow neutrons; some few fast neutrons, however, coming directly from the source without being slowed down were included. After four or five weeks the plates were developed as follows:

The development was done with great care taking all necessary precautions. Firstly, the plate was washed with running cold water for 50 minutes

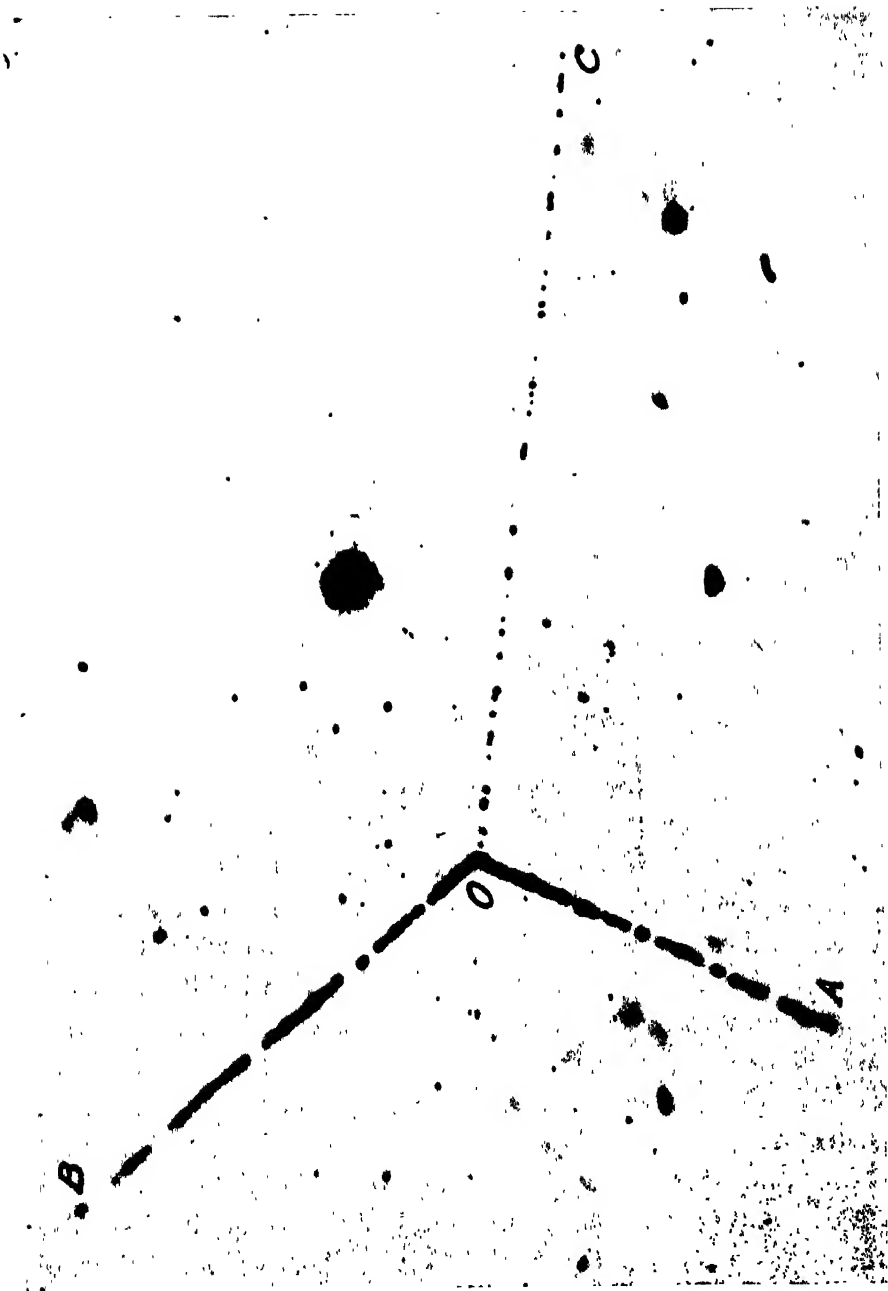


FIG. 2  
Photograph of the tri-partition of uranium nucleus, magnification,  
2000 nearly.

(for  $50\mu$  plate) to make it free from uranium-salt and then developed with Ilford 1D-19 developer diluted with water in the ratio 1 : 3 for 20 minutes at about  $18^{\circ}\text{C}$ ; the results, however, were not satisfactory as considerable back-ground effects were present. Also some tracks were found to be present in the developed plates. These tracks are attributed to the  $\alpha$ -particles ejected during the time of washing out the uranium-salt. The result was improved by developing the plates in the same way as above without washing the uranium-salt but by simply pre-soaking the emulsion with water for ten to fifteen minutes for  $50\mu$  plate. In addition, by using the same developer but diluted in the ratio 1 : 6 and developing for 12 to 15 minutes at  $20^{\circ}\text{C}$  (for  $50\mu$  plate), the results were further improved. Though in the latter case the developing condition was not ideal still the number of such tracks due to  $\alpha$ -particles was greatly reduced and if found, it was mainly near the surface of the emulsion.

After proper development, the plates were carefully scanned under a research binocular microscope (Leitz Ortholux) using  $1/12$  oil immersion fluorite objective (95 X and N. A = 1.32). The overall magnification used during scanning was nearly 1000. Out of the total number of fission events taking place in the plate, only 61.3 per cent of them had tracks due to fission fragments which ended in the emulsion. The total number of fissions observed was more than 20,000. In addition to binary fission of uranium nucleus, only one interesting case of ternary fission was observed in an Ilford E1 plate and its photomicrograph is shown in figure 2. All the three fission fragments which ended in the emulsion, are hereby in the same plane and could be reproduced in a single photomicrograph. The ends of the tracks OA and OB are slightly out of focus. According to the procedure of the experiments described above, the third fragment in addition to the two fission fragments must have a mass greater than that of an  $\alpha$ -particle. Moreover, in the cases of tripartition of uranium nucleus reported by several investigators, namely Green and Livesey (1947) the two heavy fission particle tracks are almost in a straight line, to which the 3rd particle makes different angles; but in the present case the angle between the two heavy fission particles was much less than  $180^{\circ}$ , to balance the relatively high value of the momentum of the 3rd particle. Such relatively high value of momentum requires for its interpretation, a relatively high value for the mass of the third particle. Tsiang, Wei, *et al.* (1947) have also reported to have observed one particular case of tri-partition, in which the calculated masses of the fragments were about 127, 77, and 32 respectively. In the present case the tracks due to the two heavy fission fragments have a grain-density gradually decreasing towards the end which is a feature characteristic of a binary fission event as generally observed, due to the loss of multiple charges of the fission fragments. The silver grains forming the first few microns of these tracks are densely packed into a continuous solid line, while those at the end are distinctly separated from one another. The

nature of the fission fragment tracks gives an idea about the degree of desensitising action of the uranyl ion, on track latent images. Such high degree of desensitising reduces the total range of the two binary fission fragment tracks because the latent images near the last portion of the real range of the tracks are not developable. The total range distribution in the case of a binary fission has been discussed later.

The ranges and angular distribution of the three fragments (figure 2) are given below with reference to a separate simplified diagram (figure 3).

The ranges are as follows :

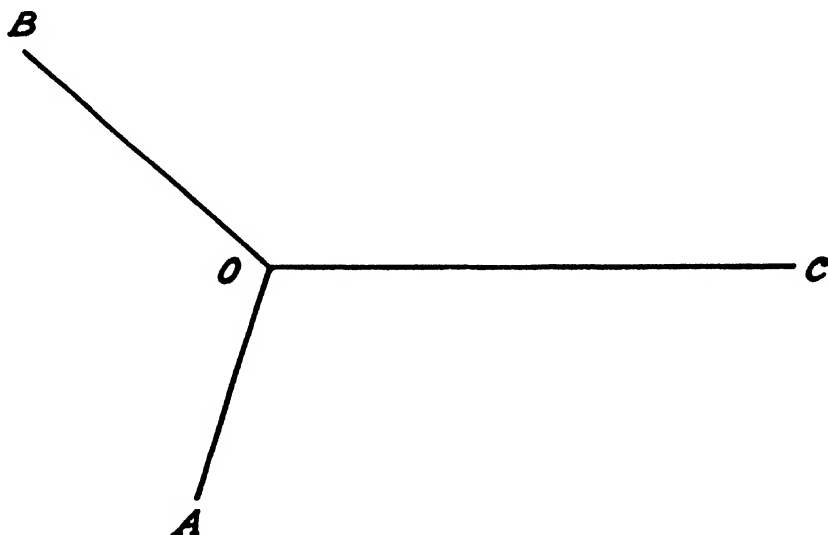


FIG. 3

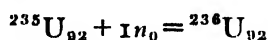
$$OA = 27\mu, \quad OB = 35\mu \quad \text{and} \quad OC = 54\mu,$$

while in the case of bi-partition the total track length of the two fragments together is between 20 and 21  $\mu$ .

The angular distribution is as follows :

$$\angle AOB = 118^\circ, \quad \angle BOC = 136^\circ \quad \text{and} \quad \angle COA = 106^\circ$$

The mass values of the three fragments as well as the kinetic energy of this tri-partition of uranium nucleus have been calculated out by applying a method similar to that adopted by Tsing, Wei, Chastel and Vigueron (1947). It is assumed that firstly a compound nucleus is formed by the absorption of a neutron according to the following equation :



Then the compound nucleus  $^{236}\text{U}_{92}$  thus formed explodes with three ionisable fragments. It is further assumed that no neutron is emitted during the process. Let the masses and velocities of the three fragments

$OA$ ,  $OB$  and  $OC$  be represented by  $M_1$ ,  $M_2$ ,  $M_3$  and  $V_1$ ,  $V_2$ ,  $V_3$  respectively. From the conservation of mass we have

$$M_1 + M_2 + M_3 = 236 \quad \dots (1)$$

Further from the conservation of momentum and the resolution of the momenta in two mutually perpendicular directions  $OX$  and  $OY$  (figure 4) we get

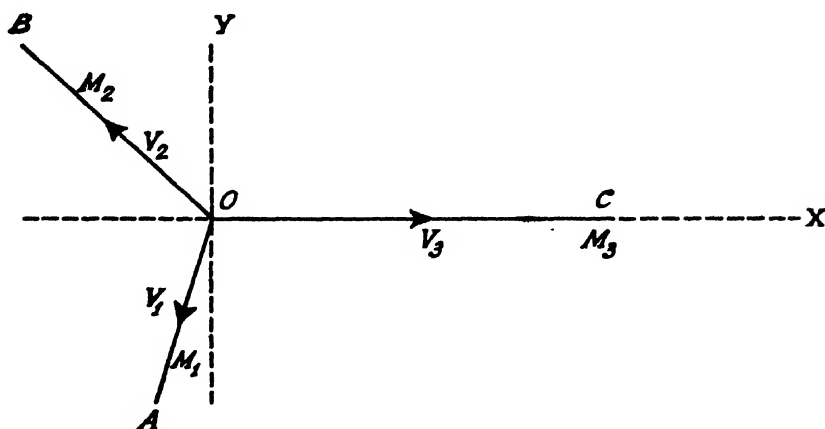


FIG. 4

$$M_1 V_1 \cos \widehat{AOC} + M_2 V_2 \cos \widehat{BOC} + M_3 V_3 = 0 \quad (2)$$

$$M_1 V_1 \sin \widehat{AOC} - M_2 V_2 \sin \widehat{BOC} = 0 \quad (3)$$

(It is to be noted that the calculations are being done in the centre of mass system of the incident particle).

If the relation between velocity and mass be known for a definite value of the range of fragment then by the use of the above three equations it is easy to calculate masses of the three fragments by trial and error method. To deduce the relation between velocity and mass for a particular value of the range the following procedure was adopted :

First of all the ranges (in emulsion) of the three fragments were converted to their air equivalent from known values of stopping power. Their air equivalent ranges have been used in subsequent calculation. According to Bohr, the ratio between the range  $R_F$  of a fission fragment and the range  $R_\alpha$  of an  $\alpha$ -particle with the same initial velocity  $V_i$  is given by

$$\frac{R_F}{R} = 5 \left\{ \frac{M}{Z^{2/3}} \cdot \frac{V_o}{V_i} \right\} \quad (4)$$

where  $Z$  and  $M$  are the charge and mass respectively of the fission fragment and  $V_o$  is given by  $\frac{2\pi e^2}{h}$ . Therefore, in equation (4) by substitut-

ing a known value of  $V_i$  corresponding to  $R_a$ , we get on calculation the value of  $\frac{M}{Z^{2/3}}$ . As  $Z$  is known corresponding to a particle of mass  $M$ , a curve can be drawn with different values of  $\frac{M}{Z^{2/3}}$  and  $M$  as co-ordinates. From this curve the value of  $M$  can be found out from known value of  $\frac{M}{Z^{2/3}}$  determined from the known value of  $V_i$  by the use of equation (4). Thus, by giving different values of  $V_i$  we get different values of  $M$  corresponding to one particular value of the range of the fission fragment. Putting these values of the range, we get the corresponding different velocity-mass curves as shown in figure 5.

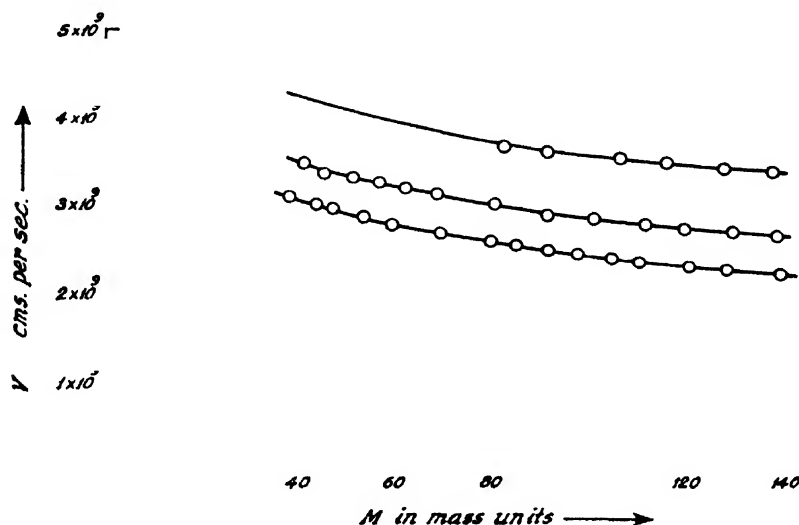


FIG. 5  
Velocity-mass curves

By choosing different sets of values of velocity and mass, using equation (1), (2) and (3) and by trial and error we get the three mass values corresponding to the three fragments as 166, 43 and 30 mass units.

From the nature of ionization along the track  $OC$  and also from minimum ionization tracks, the mass value most probably will lie between 15 and 20 instead of the calculated value 30. Similarly, the calculated mass value 43 seems to be a bit lower as its grain density along the track suggests a higher value than 43. However, taking the mass values as 166, 43 and 30 the kinetic energy of tri-partition comes out to be  $2 \times 10^9$  electron-volts which is large compared to the energy of fission of value  $1.5 \times 10^8$  electron-volts approximately induced by a neutron. Due to such large kinetic energy released in the present case of tri-partition, the phenomenon can only be explained by the assumption that the fission has been initiated by a high energy fast neutron of cosmic ray origin. The chance of its being initiated by a high energy proton or  $\alpha$ -particle cannot be totally excluded.



Though the present study on tri-partition of uranium nucleus is mainly concentrated on the work with desensitised plates, the experiments were first begun with non-desensitised plates. Nearly 1 gm of uranyl nitrate was dissolved in 100 c. c. of water and some C<sub>2</sub> plates were bathed in that solution for half an hour. Then they were dried, put in thin brass box and kept as such in an atmosphere of slow neutron. After 2 or 3 weeks they were developed for 10 minutes with Ilford ID-19 developer diluted in the ratio 1 : 3. The plates were scanned as usual and only some binary fission tracks were observed with a back-ground of  $\alpha$ -particles ejected from uranium and recoil proton tracks. The total range of the two fragments was measured for different binary fissions in these plates by means of a calibrated reticule and has an average value of 23.95 or 24 $\mu$  approximately. Thus the concentration of uranyl nitrate solution was gradually increased and following the same procedure it was observed that the total range value for bi-partition of uranium nucleus was becoming less and less. Finally, at a concentration in which the tri-partition was observed it has already been mentioned that the total range of the binary fission fragment tracks was reduced due to the desensitising action of the uranium on the formation of latent images due to fission fragments. This range distribution of the two fragments (in E1 plate) has been shown by a histogram in figure 6.

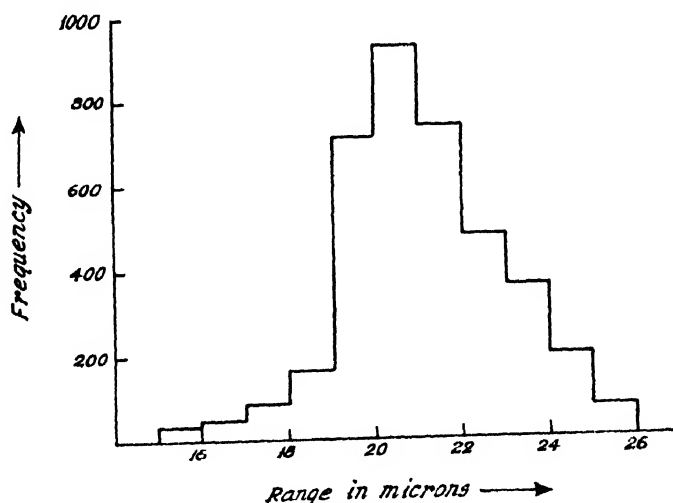


FIG. 6

Total range frequency histogram of two binary fission fragments in E1 plate.

Most of the fission fragments have a total range lying between 20 to 21 $\mu$ . Sometimes tracks of very small range appeared near the upper surface of the emulsion and this was discarded by considering it to be due to  $\alpha$ -particle. Such a chance for the formation of their latent images is due to the fact that while rinsing the plate after bathing in the requisite highly concentrated

solution of uranyl nitrate the upper surface of the emulsion may have every chance of reduction in concentration of uranyl nitrate and thereby reducing the intensity of the disensitising action by a little. The readings for the histogram in figure 6 are taken in Ilford Fx plates in which the tri-partition was observed. Further experiments are in progress and more rare events like tri-partition etc. are expected to be observed.

#### ACKNOWLEDGMENTS

The work was carried out under the general supervision of Dr. D. M. Bose, M. A., Ph. D., F. N. I., Director, Bose Research Institute, Calcutta, to whom the author is indebted for his interest and support. The author wishes to thank Mr. H. P. De, M. Sc., P. R. S., for valuable discussions during the progress of the work. Thanks are also due to Messrs. Ilford Selo (India) Ltd. for their help in supplying the nuclear research emulsion plates.

#### REFERENCES

- Bohr, N. 1941, *Phys. Rev.*, **59**, 270.  
 Green L. L. and Livesey, D. L. 1949, *Nature*, **158**, p. 272.  
 Powell, C. F. Occhialini, G. P. S. Livesey D. L. and Chilton 1946, *Jour. Sci. Inst.*, **23** 102-106.  
 Tsien San-Tsiang, Chastel, R. Ho Zah-Wei and Vigneron, R. 1946, *Compts. Rendus*. **223**, 986  
 „ „ 1947, *Nature*, **159**, p. 773.  
 Tilterton, E. W. and Brinkely, T. A. 1950, *Phil. Mag.*, **41**, 316, p. 500.  
 Tsien San-Tsiang, Chastel, R. Ho Zah-Wei and Vigneron, R. 1947, *Jour. de. Phys. et. Radium.*, **8**, 165  
 „ „ 1947, *Jour. de. Phys. et. Radium*, **8**, 200.

# PROTON-PROTON SCATTERING AT HIGH ENERGIES

By PRABUDDHA BANERJEA \*

DEPARTMENT OF THEORETICAL PHYSICS, INDIAN ASSOCIATION FOR THE CULTIVATION OF SCIENCE, CALCUTTA 32

(Received for publication, October 8, 1953)

**ABSTRACT.** In this paper the differential cross sections for proton-proton scattering have been calculated in the Born's approximation using potentials consisting of the tensor operator multiplied respectively by  $\frac{e^{-\lambda r}}{\lambda^2}$  and  $\frac{e^{-\lambda r}}{\lambda^{2/3}}$ . Results for the second potential have been shown to give marked angular isotropy which agree qualitatively better with the experimental results of proton-proton scattering at 345 MeV energy than the existing calculations made with potentials derivable from field theories.

## INTRODUCTION

Chamberlain *et al* (1951) have recently determined proton-proton scattering cross sections at high energies. Their results for 345 MeV show that the differential cross section between  $90^\circ$  and  $15^\circ$  is very much independent of the angles having the value  $3.8 \times 10^{-27}$  cm<sup>2</sup>/steradian (centre of mass system). Such spherically symmetric scattering could qualitatively be explained by saying that the scattering is due to an interaction in the S state. But this is not a possible explanation of the observed results because the cross sections, as calculated on the basis of an interaction in the S state, are too low in comparison with the experimentally determined values.

So far, it has not been possible to explain even qualitatively the observed isotropic scattering in the above-mentioned case with the help of potentials as obtained from field theoretical considerations. Some workers have, however, tried to approach the problem in a phenomenological manner. Case and Pais (1951) have attempted to explain the observed angular isotropy by introducing a spin-orbit coupling in the nuclear interaction. Christian and Noyes (1950) have used a combination of central and tensor potentials. The central potential is a square well of range  $2.6 \times 10^{-13}$  cms.

and the tensor potential is of the form  $V_t \frac{e^{-r/R}}{(r/R)^2}$  with  $R = 1.6 \times 10^{-13}$  cms. ;

$V_t = \pm 18$  MeV. Their curve, however, rises steadily and rapidly below  $40^\circ$ . They also have plotted a curve for which the tensor term is of the Yukawa type and also another curve for no tensor potential. Their curves clearly show that the tensor term not only flattens the curve, but also raises the

\* Now at Ravenshaw College, Cuttack

value of the scattering cross sections at large angles. Furthermore, the singular tensor curve ( $\frac{1}{r^2}$ -singularity) is flatter than the Yukawa tensor curve. In the present paper, the central term has been omitted altogether, thus allowing scattering to take place in the triplet states only. Furthermore, a potential with  $\frac{1}{r^3}$ -singularity has been tried to investigate the effect of radial dependence on the cross section. As will be seen, the term with  $\frac{1}{r^2}$ -singularity shows considerable variation of the differential cross section with angle; and hence it is not likely that the Yukawa tensor potential will give isotropic scattering. Hence it has not been tried. Jastrow (1951) has attempted to explain the high energy proton-proton scattering taking an interaction consisting of a hard core of finite radius in the singlet state in addition to an exponential radial dependence outside the core; and a triplet potential consisting of tensor and exchange terms in addition to an exponential radial dependence. So far, his calculations seem to fit the experimental data best. The existence of a hard core of finite radius is, however, questionable on the point of view of relativity.

In this paper, proton-proton scattering cross sections have been calculated in the centre of mass system taking the potentials

$$V_1 = \frac{f^2}{4\pi} \cdot S_{12} \cdot \frac{e^{-\lambda r}}{\lambda r^2} \quad \dots (1)$$

$$V_2 = \frac{f^2}{4\pi} \cdot S_{12} \cdot \frac{e^{-\lambda r}}{\lambda^2 r^3} \quad \dots (2)$$

where  $f^2$  is the coupling constant,  $S_{12}$ , the tensor operator  $= 3(\sigma_1 \cdot \frac{\vec{r}}{r})(\sigma_2 \cdot \frac{\vec{r}}{r}) - (\sigma_1 \cdot \sigma_2)$ ;  $\sigma_1$  and  $\sigma_2$  denote the spin vectors of the two protons taking part in the collision;  $\vec{r}$  denotes the vector joining the two protons; and  $\lambda = 1.3 \times 10^{-13} \text{ cm}^{-1}$ .

#### METHOD OF CALCULATION

Born approximation has been used for the present calculations, the method being given by Ashkin and Wu (1948). As the above paper gives a fairly exhaustive treatment of the subject, some of the details of the method have been left out here.

According to Born approximation the scattering matrix of proton-proton scattering (without exchange), for a potential of the form  $V = S_{12}J(r)$  is given by

$$S'_{m, 'm, ''}(\theta, \phi) = C(\theta) \zeta_{m, 'm, ''}(\theta, \phi), \quad \dots (3)$$

$$\text{where } C(\theta) = (M/\hbar^2) \int_0^r J_1(r) \left[ \frac{\sin Kr}{Kr} - 3 \frac{\cos Kr}{(Kr)^3} - \frac{\sin Kr}{(Kr)^5} \right] dr, \quad \dots (4)$$

$$\text{where } K = 2k \sin \theta/2 \text{ and } k^2 = \frac{4\pi^2 ME}{h^2} \quad \dots (5)$$

$M$  is the mass of the proton;  $E$  is the energy of the incident proton in the centre of mass system and  $\zeta_{m, 'm, ''}$  is defined by the equation

$$\zeta(\theta, \phi) \chi_{m, 'm, ''} = \sum_{m, 'm, ''=-1}^{+1} \zeta_{m, 'm, ''}(\theta, \phi) \chi_{m, 'm, ''}, \quad \dots (5')$$

where  $\chi_{m, '}$  and  $\chi_{m, ''}$  are the spin eigenfunctions

$$\text{and } \zeta(\theta, \phi) = \sigma_1 \cdot \sigma_2 - 3 \sigma_1 \cdot n_0 - n_0 \cdot \sigma_2, \quad n_0 = n$$

$\bar{\sigma}_1, \bar{n}_0 = \bar{n}$  and  $\sigma_2, n_0 = \bar{n}$  being the components of  $\sigma_1$  and  $\sigma_2$  in the direction of momentum transfer. The values of the matrix elements  $\zeta_{m, 'm, ''}(\theta, \phi)$  have been tabulated by Ashkin and Wu as also by Burhop and Yadav (1949).  $\theta$  and  $\phi$  are the polar and azimuthal angles of the scattered direction with respect to the direction of incidence. For proton-proton scattering, due to exchange, the scattering matrix will be modified to

$$S_{m, 'm, ''}(\theta, \phi) = S'_{m, 'm, ''}(\theta, \phi) - S'_{m, 'm, ''}(\pi - \theta, \pi + \phi) \quad \dots (6)$$

the negative sign appearing because here scattering takes place in the triplet state only.

The triplet scattering cross section is then given by

$$\sigma_t = \frac{1}{3} \sum_{m, 'm, ''} |S_{m, 'm, ''}|^2 \quad \dots (7)$$

The total cross section is therefore

$$\sigma = \frac{3}{4} \cdot \sigma_t = \frac{1}{4} \sum_{m, 'm, ''} |S_{m, 'm, ''}|^2 \quad \dots (8)$$

This reduces to

$$\sigma = 6 \left( \frac{M}{\hbar^2} \right)^2 \left\{ C(\theta)^2 + C(\pi - \theta)^2 + C(\theta)C(\pi - \theta) \right\} \quad \dots (9)$$

For the first potential (eq. 1), we have

$$C_1(\theta) = \frac{f^2}{4\pi} \left( \frac{M}{\hbar^2} \right)^2 \cdot \frac{1}{\lambda} \left[ \frac{3\lambda}{2K^2} - \left( \frac{3\lambda^2}{2K^3} + \frac{1}{2K} \right) \tan^{-1} \frac{K}{\lambda} \right] \quad \dots (10)$$

Similarly for the second potential

$$C_2(\theta) = \frac{f^2}{4\pi} \left( \frac{M}{\hbar^2} \right)^2 \cdot \frac{1}{\lambda^2} \left[ \frac{\lambda^2}{2K^2} + \left( \frac{\lambda}{2K} + \frac{\lambda^3}{2K^3} \right) \tan^{-1} \frac{K}{\lambda} \right] \quad (11)$$

Accordingly, the differential cross sections are

$$\sigma_1 = 6 \cdot \frac{1}{\lambda^2} \left( \frac{M}{\hbar^2} \cdot \frac{f^2}{4\pi} \right)^2 \left\{ \left[ \frac{3\lambda}{2K^2} - \left( \frac{3\lambda^2}{2K^3} + \frac{1}{2K} \right) \tan^{-1} \frac{K}{\lambda} \right]^2 \right.$$

$$+ \left[ \frac{3\lambda}{2K'^2} - \left( \frac{3\lambda^2}{2K'^3} + \frac{1}{2K'} \right) \tan^{-1} \frac{K'}{\lambda} \right]^2 + \left[ \frac{3\lambda}{2K^2} - \left( \frac{3\lambda^2}{2K^3} + \frac{1}{2K} \right) \tan^{-1} \frac{K}{\lambda} \right]^2 \\ \times \left[ \frac{3\lambda}{2K'^2} - \left( \frac{3\lambda^2}{2K'^3} + \frac{1}{2K'} \right) \tan^{-1} \frac{K'}{\lambda} \right] \left[ \frac{3\lambda}{2K^2} - \left( \frac{3\lambda^2}{2K^3} + \frac{1}{2K} \right) \tan^{-1} \frac{K}{\lambda} \right] \} \quad \dots \quad (12)$$

$$\sigma_2 = 6 \cdot \frac{1}{\lambda^4} \left( \frac{M}{\hbar^2} \cdot \frac{f^2}{4\pi} \right)^2 \left\{ \left[ -\frac{\lambda^2}{2K^2} + \left( \frac{\lambda}{2K} + \frac{\lambda^3}{2K^3} \right) \tan^{-1} \frac{K}{\lambda} \right]^2 \right. \\ + \left[ -\frac{\lambda^2}{2K'^2} + \left( \frac{\lambda}{2K'} + \frac{\lambda^3}{2K'^3} \right) \tan^{-1} \frac{K'}{\lambda} \right]^2 + \left[ -\frac{\lambda^2}{2K^2} + \left( \frac{\lambda}{2K} + \frac{\lambda^3}{2K^3} \right) \tan^{-1} \frac{K}{\lambda} \right] \\ \times \left[ -\frac{\lambda^2}{2K'^2} + \left( \frac{\lambda}{2K'} + \frac{\lambda^3}{2K'^3} \right) \tan^{-1} \frac{K'}{\lambda} \right] \left. \right\} \quad \dots \quad (13)$$

where  $K' = 2k \cos \theta/2$ .

## RESULTS

A preliminary analysis of the calculations reveal that  $\sigma_2$  shows much less variation with angle than  $\sigma_1$ . The magnitude of  $f^2$  is adjusted so as to give the best agreement between the theoretical and experimental results and its value is taken to be  $2.642 \times 10^{-17}$  ergs. cm. For proton energies of 345 Mev, the numerical values of the differential cross sections  $\sigma_1$  and  $\sigma_2$  are given below.

Angle in degrees	$\sigma_1$	$\sigma_2$
	in $10^{-27}$ cm <sup>2</sup> /steradian	in $10^{-27}$ cm <sup>2</sup> /steradian
20	0.365	4.061
25	0.1351	3.936
30	0.04601	3.774
35	0.05402	3.688
40	0.05810	3.524
45	0.06241	3.399
50	0.06691	3.298
55	0.07117	3.268
60	0.07154	3.096
65	0.07564	3.053
70	0.0777	3.002
80	0.08091	2.949
90	0.08307	2.934

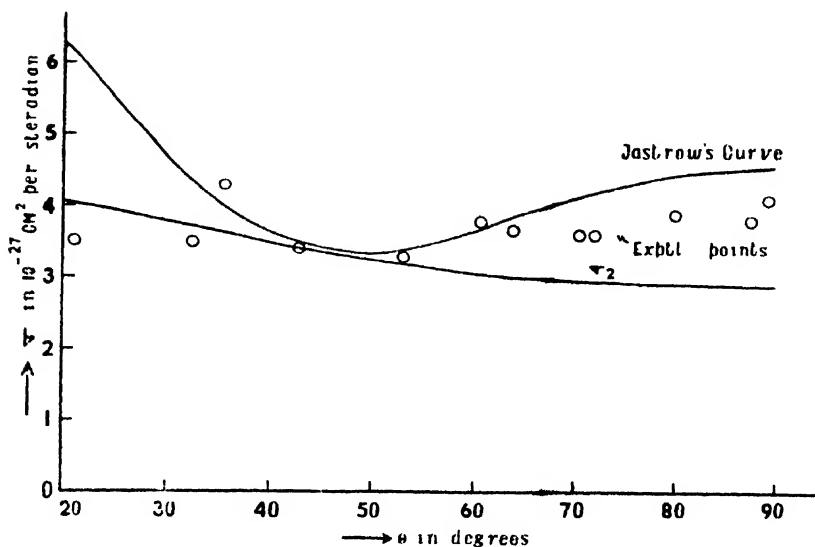


FIG. 1

In the accompanying graph  $\sigma_2$  as well as Jastrow's curve for 345 MeV proton-proton scattering have been drawn. The circles given there denote the experimental values of Chamberlain *et al.* It may be seen that  $\sigma_2$  fits more closely with the experimental points than Jastrow's curve. At present however, it does not appear appropriate to say that the potential  $V_2$  chosen in this paper does give the exact law of interaction between protons at high energies of collision: the reason being that the experimental data are not sufficiently reliable and the calculations of the author have been performed in the non-relativistic approximation. All that can be said is that of the chosen potentials,  $V_2$  can account for the angular isotropy of the differential cross sections to a great extent. Furthermore, it remains to be seen what justification the chosen potentials have in the light of a field theory.

## ACKNOWLEDGMENTS

The author is thankful to Dr. M. N. Saha, F. R. S. for taking keen interest in the work and also for permission to use the library of the Indian Association for the Cultivation of Science, and to Dr. D. Basu, Head of the Department of Theoretical Physics of the same institution, for suggesting the problem as a research topic and for his kind guidance throughout the progress of the work.

## REFERENCES

- Ashkin and Wu, 1948, *Phys. Rev.*, **73**, 973  
 Burhop and Yadav, 1949, *Proc. Roy. Soc.*, **197**, 505.  
 Case and Pais, 1950, *Phys. Rev.*, **80**, 203.  
 Chamberlain *et al.*, 1951, *Phys. Rev.*, **83**, 923.  
 Christian and Noyes, 1950, *Phys. Rev.*, **79**, 85

## MOTION OF A SINGLE CLOUD IN THE IONOSPHERE

By S. N. MITRA

ALL INDIA RADIO, NEW DELHI

*(Received for publication, September 29, 1953)*

## Plate XX

**ABSTRACT.** The fading on pulsed transmission is known to be due to interference between waves scattered from local irregularities in the ionosphere, the irregularities having both random and steady motion. The nature of the fading pattern indicates that a large number of irregularities is involved in the process. But, under favourable conditions, it is possible to detect a single cloud in the ionosphere, the fading of the received signal being caused by its bodily motion with the existing wind velocity.

In a previous communication the author (Mitra, 1949) has described how the wind in the ionosphere could be investigated by a study of fading on pulsed transmissions as recorded simultaneously on a system of spaced receivers. The fading is supposed to be due to interference between a large number of wavelets diffractively scattered from local irregularities in the ionosphere. A wind in the ionosphere causes these irregularities to be bodily moved and the fading patterns as recorded in a system of spaced receivers are similar in nature but show a time-shift with respect to one another. The velocity of the wind could be obtained from the time-shift. A random motion of the irregularities amongst themselves causes the fading patterns to be dissimilar and when the random motion predominates, the time-shift caused by the wind is difficult to be determined due to the dissimilarity between fading patterns. Experiments have indicated that when the distance between any two receivers is of the order of a wavelength, the presence of a wind could usually be detected from the fading patterns except when the fading becomes too rapid under disturbed ionospheric conditions. The investigation of fading by pulsed transmission has shown that under favourable conditions, it is possible to deduce from the fading pattern, the motion of a single cloud in the ionosphere.

The nature of fading pattern caused by the interference of scattered wavelets is usually random without any noticeable periodicity. But in the absence of irregularities in the ionosphere, the down-coming wave will not 'fade' and the received amplitude will not vary with time. Let us assume such an idealised condition when the echo amplitude remains steady. We then enquire what happens if a single cloud comes within the receiving zone and moves past with the existing wind velocity. There will be interference between the wave reflected from the 'smooth' ionosphere and the wave scattered from the cloud. The resultant amplitude at any instant



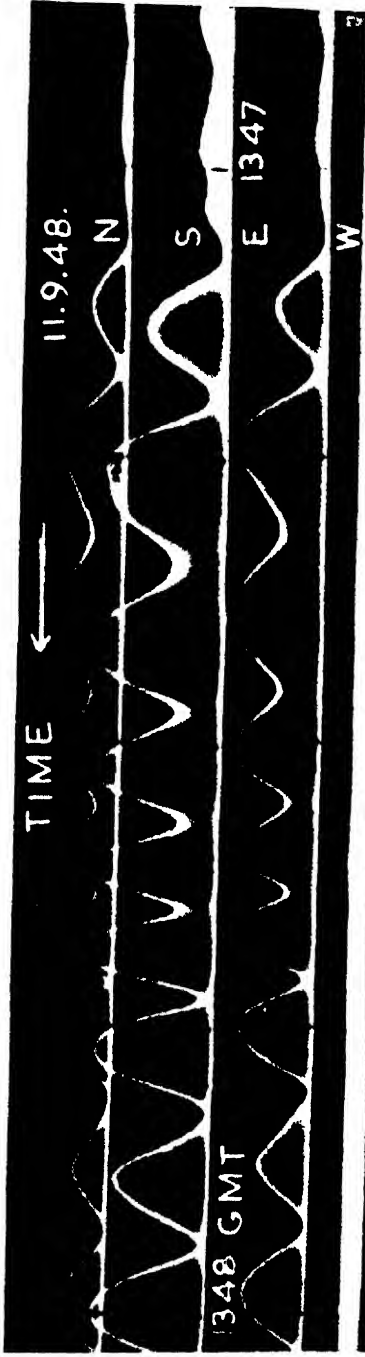
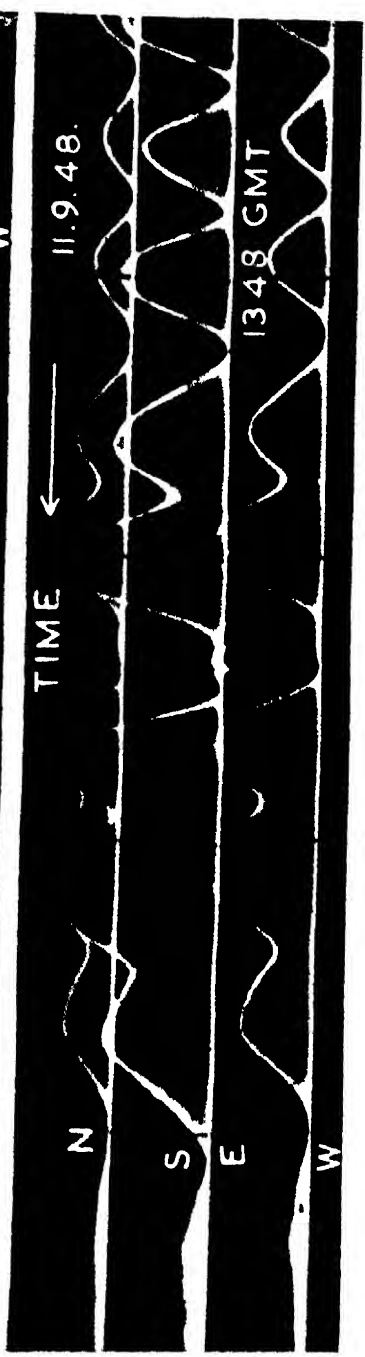


Fig.



Fig

Fading records indicating the motion of a single cloud in the ionosphere. Frequency = 4 Mc/sec. Reflection from the F-layer. Figure 2 is the continuation of Figure 1



will depend upon the phase difference between the scattered wave and the wave reflected from the ionosphere.

The problem may be studied in another way. A single scattering cloud behaves as a radiating antenna and will have a characteristic polar diagram. The polar diagram, however, will depend upon the dimension of the cloud in relation to the wavelength. The situation is simplified if the back-ground reflection is due to the radiation emitted by such an antenna in that case the polar diagram becomes the same as that of a horizontal antenna radiating some distance above the ground and the ground is regarded as a perfect reflector. In our case, the ionosphere is the 'ground' and the radiating cloud becomes the 'horizontal wire antenna'. In such a case, the polar diagram will consist of several minor lobes placed symmetrically round a major lobe in the centre. Now, if this pattern is being moved bodily, the intensity of the radiation at the receiver will go through a series of maxima and minima roughly equally spaced and the variation of intensity with time will be periodic. When the radiating cloud goes out of the "contributing zone" for the receiver, the intensity at the receiver will again become steady. Thus, if a periodic fading pattern is observed preceded and followed by steady signal, the pattern may be interpreted as due to a cloud moving past in the ionosphere. It should, however, be ensured by using polarised receiving aerial that the periodic fading pattern is not due to an interference between the two magneto-ionic components (Mitra, 1950).

Such types of rather ideal fading patterns have been observed in the author's (Mitra, 1949) spaced receiver experiment on only a few occasions. It has been observed that for some time the echo amplitude was remaining more or less steady and no shift was being shown between the fading patterns at the spaced receivers. Then the periodic fading started which lasted for a short time and then the amplitude became steady again. Figures 1 and 2 (Plate XX) show a typical example. (Figure 2 is the continuation of the fading pattern shown in figure 1). It will be noted from these figures, that the echo amplitude was small but steady before the periodic fading started. The periodic fading lasted for a little more than one and a half minute and after that the fading became steady. The three patterns at the three receivers are very much similar in nature and the steady shift between the fading patterns could be easily noticed from the record. The velocity of the wind can also be calculated from the shift which comes to about 80 m/sec., its direction being towards SSE.

An ideal condition of a horizontal radiating antenna representing a scattering cloud cannot be realised in practice. Complications will arise due to the back-ground reflection and the true polar diagram for such a system. Nevertheless, some useful informations, although approximate, can be obtained from such a periodic pattern.

It is known that the number of lobes in such a system of horizontally radiating antenna is equal to the total number of half-wavelengths contained

within the length of the antenna. In the present example, the total number of maxima (each maximum corresponds to a lobe) is 14. Thus, the horizontal length of the cloud is about one kilometre (wavelength used was 75 metres). Moreover, the total time of the periodic fading gives an idea of the diameter of the "contributing zone," by which is meant the horizontal distance the cloud will have to go before the radiation from the cloud ceases producing any effect on the received intensity of the down-coming wave. Knowing the speed with which the cloud is moving (wind speed), the horizontal distance comes out to be about 10 km. The height of reflection was about 250 km; the diameter of the first Fresnel zone for a 75-metre wave is of the order of 9 km. Thus, the assumption that when a scattering centre is outside the first few Fresnel zones, it has negligible contribution to the intensity fluctuation of a down-coming wave (Pawsey, 1935) is approximately satisfied.

In the course of his investigations on fading using pulsed transmissions and a system of spaced receivers (Mitra, 1949), the author has found that such types of periodic fading of the down-coming wave, implying the motion of a single cloud in the ionosphere, are rarely observed. Most of the fading patterns do not show such effects and are mainly caused by interference of waves scattered from a number of irregularities. The presence of a single irregularity in the form of an ion cloud within the "contributing zone" is rather a rare occurrence. But when such phenomenon is observed, it gives information regarding the size of the cloud and the area of the "contributing zone" which otherwise would be difficult to determine. The origin of an ion cloud is not yet definitely established but the ionized trail left by the passage and evaporation of a meteor may constitute such an irregularity in the ionosphere.

#### ACKNOWLEDGMENTS

The work described in this note was carried out by the author in connection with his investigation on wind and turbulence in the ionosphere at the Cavendish Laboratory, University of Cambridge during the tenure of a State Scholarship of the Government of India. The author is grateful to Mr. A. C. Ramchandani, Chief Engineer, All India Radio for kind permission to publish this note.

#### REFERENCES

- Mitra, S. N., 1949, *Proc. Inst. Elec. Engrs.*, **63**, 441.
- Mitra, S. N., 1950, *Ind. J. Phys.*, **24**, 197.
- Pawsey, J. L., 1935, *Proc. Camb. Phil. Soc.*, **31**, 125

# ON THE FAITHFUL REPRODUCTION OF THE FLAT TOP OF A PULSE IN A HIGH FIDELITY PULSE AMPLIFIER (PART II)\*

BY BIMALKRISHNA BHATTACHARYYA  
INSTITUTE OF NUCLEAR PHYSICS, CALCUTTA UNIVERSITY,  
92, UPPER CIRCULAR ROAD, CALCUTTA

(Received for publication, August 29, 1953)

Plates XXIA-B

**ABSTRACT.** An experimental verification of the theory on the transient response of a pulse amplifier so far as the reproduction of the flat top of a pulse is concerned, is presented. This paper indicates the error in assuming the plate current of a pentode to be an exact replica of the input pulse. The sag in plate current is considerable if the  $RC$  time constants are not properly chosen.

## INTRODUCTION

In a previous communication (Bhattacharyya, 1953) we have studied theoretically the influence of the interactions of the cathode, screen, plate and grid circuits on the reproduction of the flat top of a pulse in a pulse amplifier. Expressions for the overall response of the amplifier circuit were developed after following a careful examination of the interactions of the various circuits in two different ways.

In the first method of analysis we derived the formulae of the reduction factors in the overall gain of the amplifier due to voltages produced in the screen and cathode circuits. These reduction factors were employed to determine the actual current flowing in the plate.

In the second method the total current in the plate was taken to be the combination of currents resulting from three voltage sources, (i) the input voltage  $e_g$  at the grid, (ii) the voltage  $e_{s,g}$  developed across the screen impedance and (iii) the voltage  $e_K$  developed across the cathode circuit.

When the actual current that is flowing in the plate is known, the output voltage can be easily determined by a nodal analysis of the plate circuit.

This paper presents an experimental verification of the theory given in the previous publication (Bhattacharyya, 1953) for developing the response functions of the amplifier. It has been demonstrated clearly that the sag in the plate current due to two  $RC$  circuits in the cathode and screen is considerable if the time constants are not properly chosen. The

\* Communicated by Sri B. M. Banerjee

sag in the output voltage is still greater due to the  $C_g R_{H_g}$  circuit in the grid. This can be reduced to a great extent if decoupling circuits are used in the plate.

### THEORETICAL DISCUSSION

In this section we shall deal with the theoretical response functions which were derived in the previous publication and a few modified forms of these functions. The basic amplifier stage is shown in figure 1.

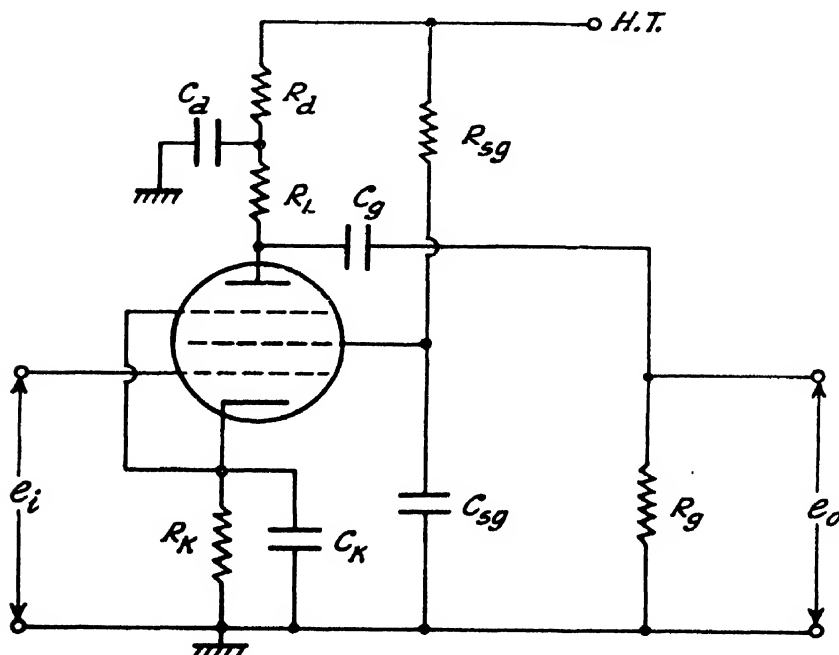


FIG. 1

A resistance-capacitance coupled amplifier

*Plate current response :*

In the first method of analysis the plate current is given by,

$$i_p i_{gm} = \frac{a^2 x}{b' c d} + \frac{(a - b')}{(-b')} \frac{(a x - a_0 b' + b'^2)}{(c - b') (d - b')} e^{-b' t} + \frac{(a - c)}{(-c)} \frac{(a x - a_0 c + c^2)}{(b' - c) (d - c)} e^{-c t} \\ + \frac{(a - d)}{(-d)} \frac{(a x - a_0 d + d^2)}{(b' - d) (c - d)} e^{-d t} \quad \dots (1)$$

where,

$$\left. \begin{aligned} a &= 1 / C_{sg} R_{sg} \\ b' &= (r_{sg} + R_{sg}) / r_{sg} C_{sg} R_{sg} \\ x &= 1 / R_K C_K \\ a_0 &= a + x, \\ c + d &= b' + x + g_m i' C_K \end{aligned} \right\} \quad \dots (2)$$

and

$$cd = b' x + a g_m / C_K$$

Now the first term  $a^2\gamma/b'cd$  in equation (1) can be written as

$$\frac{a^2\gamma}{b'cd} = \frac{a^2}{b'(b' + a g_m R_K)} \quad \dots (3)$$

So with the variation of the value of the cathode capacitor this factor will not change.

If the second method is followed, the plate current is given by

$$i_p = g_m e_g + g_{m2} e_{s,g} + g_k e_K \quad \dots (4)$$

where

$g_m$  = transconductance of the plate with respect to grid  $= \partial i_p / \partial e_g$

$g_{m2}$  = transconductance of the plate with respect to screen grid  $= \partial i_p / \partial e_{s,g}$

$g_k$  = transconductance of the plate with respect to cathode  $= -\partial i_p / \partial e_K$

$e_g$  = input voltage at the grid.

$e_{s,g}$  = voltage developed across the screen circuit and

$e_K$  = voltage developed across the cathode impedance.

Now for all practical purposes we can assume that

$$g_k = -g_m \quad \dots (5)$$

Equation (4) can now be written as

$$\begin{aligned} \frac{i_p}{g_m} = & \left[ 1 - \frac{\mu_s(K+1)}{C_K r_{s,g}} \cdot \frac{a}{\omega_0^2} - \frac{\mu_s g_{m2}}{g_m} \cdot \frac{1}{C_{s,g} r_{s,g}} \cdot \frac{\gamma}{\omega_0^2} \right] \\ & - \frac{e^{-m t}}{n-m} \left[ \frac{\mu_s(K+1)}{C_K r_{s,g}} (1-a/n) + \frac{\mu_s g_{m2}}{g_m} \cdot \frac{1}{C_{s,g} r_{s,g}} (1-\gamma/n) \right] \\ & + \frac{e^{-n t}}{n-m} \left[ \frac{\mu_s g_{m2}}{g_m} \cdot \frac{1}{C_{s,g} r_{s,g}} (1-\gamma/n) + \frac{\mu_s(K+1)}{C_K r_{s,g}} (1-a/n) \right] \quad \dots (6) \end{aligned}$$

where  $(-m)$  and  $(-n)$  are the roots of the equation :

$$p^2 + 2bp + \omega_0^2 = 0$$

$2b$  and  $\omega_0^2$  are given by

$$2b = \frac{r_{s,g}(R_{s,g}C_{s,g} + R_K C_K) + R_{s,g}R_K C_K + \{1 + \mu_s(K+1)\}R_K R_{s,g}C_{s,g}}{R_{s,g}C_{s,g}R_K C_K r_{s,g}}$$

and

$$\omega_0^2 = \frac{r_{s,g} + R_{s,g} + R_K \{1 + \mu_s(K+1)\}}{R_{s,g}C_{s,g}R_K C_K r_{s,g}}$$

We shall now consider a special case when  $C_K$  is removed altogether. In the first method of analysis the factor  $B$  which arises due to the presence of  $R_K C_K$  circuit in the cathode, may be neglected and the response is given by the function

$$i_p/g_m = \frac{a}{b'} - \frac{(a-b')}{b'} e^{-b't} \quad \dots (7)$$

In the second method if the contribution of  $e_K$  towards the increase of sag in plate current is assumed to be negligible due to the absence of  $C_K$ , the plate current response can be written as

$$\frac{i_p}{g_m} = 1 - \frac{1}{a_1 b C_{s,g}} (1 - e^{-a_1 t}) \quad \dots (8)$$

Since the magnitudes of the screen resistance  $R_{s,u}$  and the screen by-pass condenser  $C_{s,u}$  are generally very high, the time constant  $R_{s,u}C_{s,u}$  is almost always very large. But in the case of the cathode circuit, a very large value of  $C_K$  which is practically not obtainable, would have to be chosen in order to make  $R_K C_K$  time constant large, since the value of  $R_K$  is usually very small. Due to this reason, the variation of plate current response with the change in  $C_K$  has been studied both theoretically and experimentally. Plots of plate current for different values of  $C_K$  have been given in figures 2, 3 and 4. The experimental plots have also been included in these figures for the sake of comparison. In every figure the responses for two separate values of  $C_K$  are drawn in order to show clearly any alteration in response with change in the value of  $C_K$ .

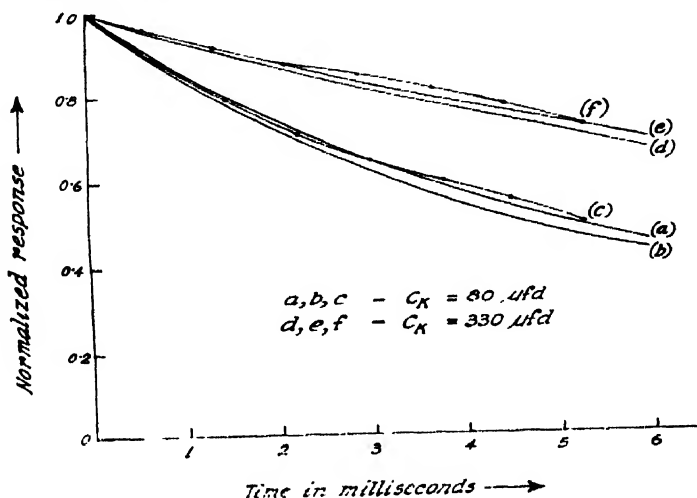


FIG. 2

Plot of plate current with time

(a), (d)—for the first method (b), (e)—for the second method (c), (f)—experimental plots

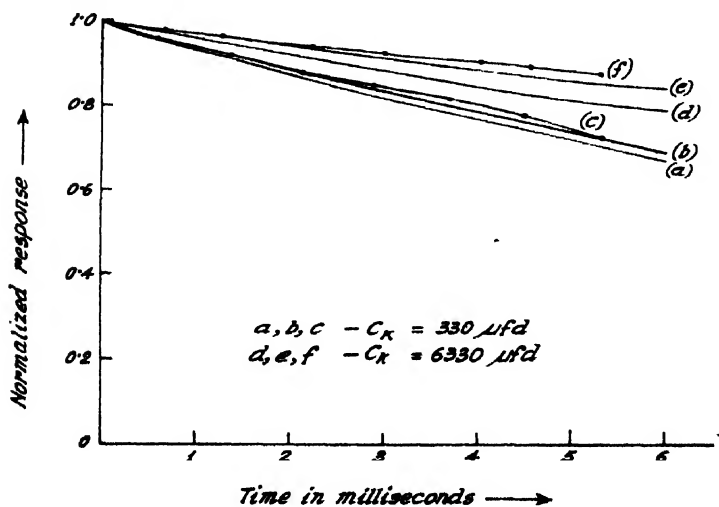


FIG. 3

Plot of plate current with time

(a), (d)—for the first method (b), (e)—for the second method (c), (f)—experimental plots



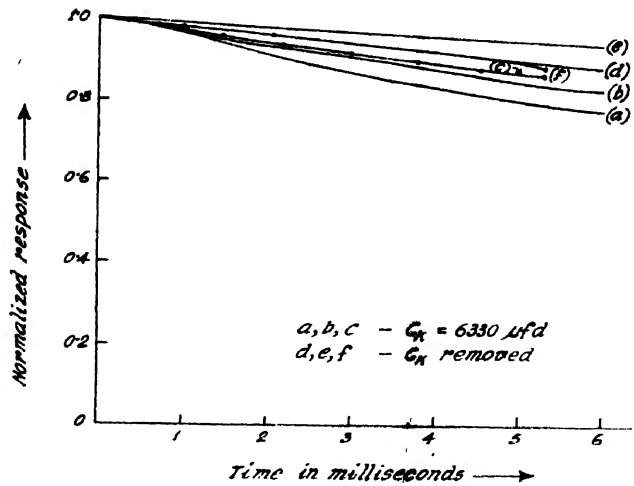


FIG. 4

Plot of plate current with time  
(a), (d)—for the first method (b), (c)—for the second method (e), (f)—experimental plots.

The values of the circuit elements are chosen to be  $R_{s0} = 60K\Omega$ ,  $C_{s0} = 2\mu fd$  and  $R_K = 180\Omega$ . The tube constants have been determined experimentally and are given below :

$$g_m = -g_K = 9000 \mu \text{ mhos}, g_{m2} = 206 \mu \text{ mhos} \\ r_{s0} = 25K \Omega, \mu_{s0} = 62.5$$

It is evident from the plots that the response improves definitely as we increase the value of  $C_K$ . The best possible response can be obtained at the cost of gain, if  $Z_K$  is purely resistive.

*Output voltage wave-form without compensation.*

In the first method of analysis, the output voltage response is given by the expression :

$$f(t) = \frac{(a-\beta)(a^2-a_0\beta+\beta^2)}{(b'-\beta)(c-\beta)(d-\beta)} e^{-\beta t} + \frac{(a-b')(a^2-a_0b'+b'^2)}{(\beta-b')(c-b')(\alpha'-b')} e^{-b't} \\ + \frac{(a-c)(a^2-a_0c+c^2)}{(\beta-c)(b'-c)(d-c)} e^{-ct} + \frac{(a-d)(a^2-a_0d+d^2)}{(\beta-d)(b'-d)(c-d)} e^{-dt} \quad \dots (9)$$

where  $\beta = 1/R_0C_0$

If the second method of analysis is applied, the normalized response can be written as

$$f(t) = Ae^{-\beta t} + Be^{-mt} + Ce^{-nt} \quad \dots (10)$$

where

$$A = 1 + \left[ \frac{\mu_s g_{m2}}{g_m} \cdot \frac{(\beta - \alpha)}{C_{s0} r_{s0}} + \frac{\mu_s (K+1)}{C_K r_{s0}} (\beta - a) \right] \frac{1}{(m-\beta)(n-\beta)}, \\ B = \left[ \frac{\mu_s g_{m2}}{g_m} \cdot \frac{(m-\alpha)}{C_{s0} r_{s0}} + \frac{\mu_s (K+1)}{C_K r_{s0}} (m-a) \right] \frac{1}{(m-\beta)(m-n)}$$

and

$$C = \frac{\mu_s g_{m2}}{g_m} \cdot \frac{(n-\alpha)}{C_{su} \tau_{su}} + \frac{\mu_s (K+1)}{C_K \tau_{su}} \cdot (n-a) \quad (\beta-n)(m-n)$$

The output voltage wave-forms have been plotted in figures 5 and 6 for different cases. The values of the circuit elements are chosen to be :

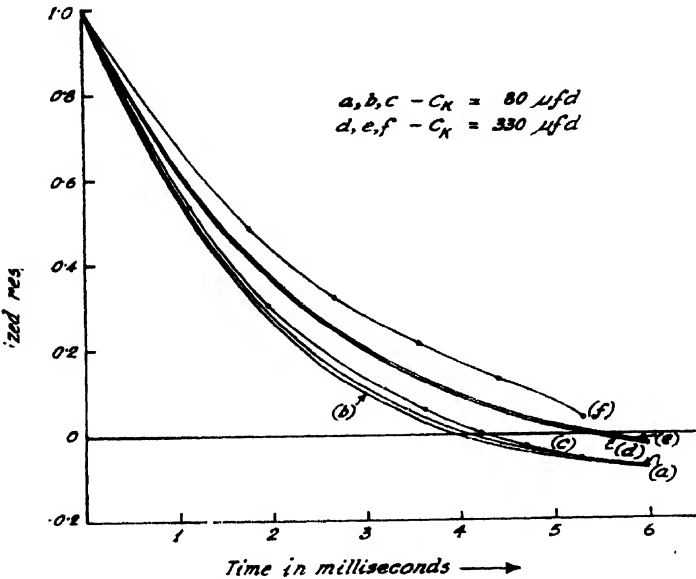


FIG. 5

Relative output response curve (without compensation)

(a), (d)—for the first method (b), (e)—for the second method (c), (f)—experimental plots.

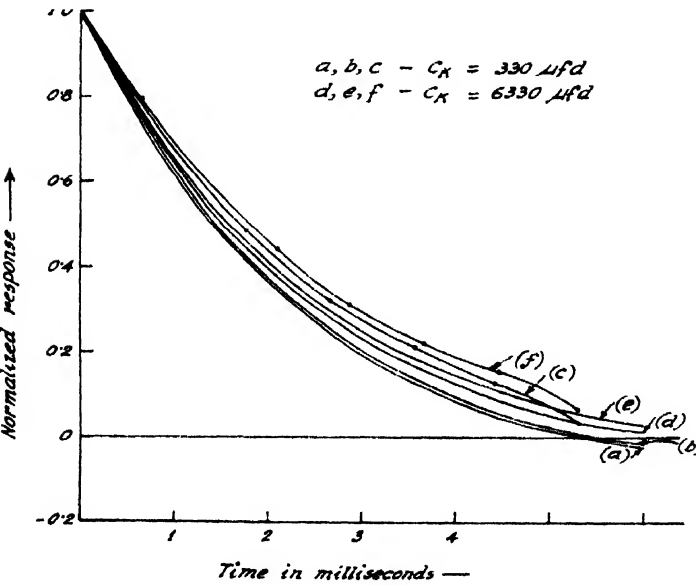


FIG. 6

Relative output response curve (without compensation)

(a), (d)—for the first method (b), (e)—for the second method (c), (f)—experimental plots

$$R_K = 180 \Omega, \quad R_{\nu} = 60K \Omega, \quad C_{\nu} = 2\mu fd, \\ R_L = 10K \Omega, \quad C_{\mu} = 0.01\mu fd \text{ and } R_{\nu} = 250K \Omega.$$

Output voltage wave-form with compensation :

When decoupling networks are used, the response is given by the following expression in the first method of analysis :

$$f(t) = A_1 e^{-\alpha' t} + A_2 e^{-\beta' t} + A_3 e^{-b' t} + A_4 e^{-c' t} + A_5 e^{-d' t} \quad \dots (11)$$

where

$$\alpha' = \frac{1}{R_{\nu} C_{\nu}}, \quad \beta' = \frac{1}{R_L C_{\mu}}, \quad \gamma' = \frac{1}{R_L C_{\nu}}, \\ A_1 = \frac{(\gamma' + \beta' - \alpha')(a - \alpha')(\alpha'^2 - a_0 \alpha' + a^2)}{(\beta' - \alpha')(b' - \alpha')(c - \alpha')(d - \alpha')}, \\ A_2 = \frac{\gamma'(a - \beta')(\beta'^2 - a_0 \beta' + a^2)}{(\alpha' - \beta')(b - \beta')(c - \beta')(d - \beta')}, \\ A_3 = \frac{(\gamma' + \beta' - b')(a - b')(\beta'^2 - a_0 b' + a^2)}{(\alpha' - b')(\beta' - b')(c - b')(d - b')}, \\ A_4 = \frac{(\gamma' + \beta' - c)(a - c)(c^2 - a_0 c + a^2)}{(\alpha' - c)(\beta' - c)(b - c)(d - c)}, \\ \text{and} \\ A_5 = \frac{(\gamma' + \beta' - d)(a - d)(d^2 - a_0 d + a^2)}{(\alpha' - d)(\beta' - d)(b - d)(c - d)}.$$

With the help of the second method of analysis, we can show that the step-function response  $f(t)$  is the Laplace transform of

$$F(p) = \frac{(p + \gamma' + \beta')}{(p + \alpha')(p + \beta')} - \frac{\mu_s g_{m2}}{g_m C_{\nu} \tau_{s \nu}} \cdot \frac{(p + \alpha)(p + \gamma' + \beta')}{(p + m)(p + n)(p + \alpha')(p + \beta')}, \\ - \frac{\mu_s (K + 1)}{C_K \tau_{s \nu}} \cdot \frac{(p + a)(p + \gamma' + \beta')}{(p + m)(p + n)(p + \alpha')(p + \beta')} \quad \dots (12)$$

so  $f(t)$  is given by the equation

$$f(t) = P e^{-\alpha' t} + Q e^{-\beta' t} + R e^{-m t} + S e^{-n t} \quad \dots (13)$$

where

$$P = \frac{(\gamma' + \beta' - \alpha')}{(\beta' - \alpha')} - \frac{(\gamma' + \beta' - \alpha')}{(m - \alpha')(n - \alpha')(\beta' - \alpha')}, \\ \left[ \frac{\mu_s g_{m2}}{g_m} \cdot \frac{(\alpha - \alpha')}{C_{\nu} \tau_{s \nu}} + \frac{\mu_s (K + 1)}{C_K \tau_{s \nu}} (a - \alpha') \right] \\ Q = \frac{\gamma'}{(\alpha' - \beta')} - \frac{\gamma'}{(m - \beta')(n - \beta')(\alpha' - \beta')}, \\ \left[ \frac{\mu_s g_{m2}}{g_m} \cdot \frac{(\alpha - \beta')}{C_{\nu} \tau_{s \nu}} + \frac{\mu_s (K + 1)}{C_K \tau_{s \nu}} (a - \beta') \right],$$

$$R = - \frac{(\gamma' + \beta' - m)}{(\alpha' - m)(\beta' - m)(n - m)}$$

$$\left[ \frac{\mu_s g_{m2}}{g_m} \cdot \frac{(\alpha - m)}{C_{s,q} r_{s,q}} + \frac{\mu_s (K + 1)}{C_K r_{s,q}} (a - m) \right]$$

and

$$S = - \frac{(\gamma' + \beta' - n)}{(\alpha' - n)(\beta' - n)(m - n)}$$

$$\frac{\mu_s g_{m2}}{g_m} \frac{(\alpha - n)}{C_{s,q} r_{s,q}} + \frac{\mu_s (K + 1)}{C_K r_{s,q}} (a - n)$$

The nature of the decoupled output voltage is now shown in figures 7 and 8 for the case  $\alpha' = \gamma'$ . The slope of the response curve at  $t=0$  is practically zero when the capacitance across  $Z_K$  is removed altogether, because in this case the sag in plate current is not very appreciable. It is known (Bhattacharyya, 1953) that if a step-function current pulse is assumed to be present in the plate of the amplifier,  $\alpha' = \gamma'$  is the condition which is to be satisfied to obtain zero slope at  $t=0$  in the reproduced output pulse.

The values of the circuit elements chosen are

$$R_l = 2K \Omega, \quad R_d = 15K \Omega, \quad C_d = 1 \mu fd, \quad C_u = 0.01 \mu fd,$$

$$R_u = 200K \Omega, \quad R_K = 180 \Omega, \quad R_{s,q} = 60K \Omega \quad \text{and} \quad C_{s,q} = 2 \mu fd.$$

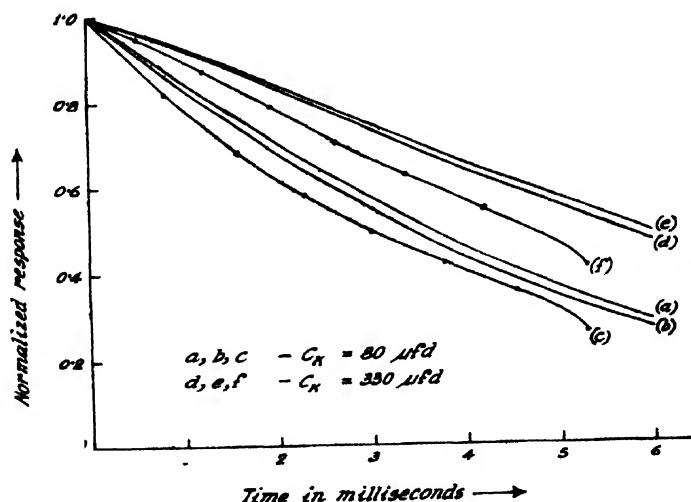


FIG. 7

Relative output response curve  
(with decoupling network)

(a), (d)—for the first method

(b), (e)—for the second method

(c), (f)—experimental plots.

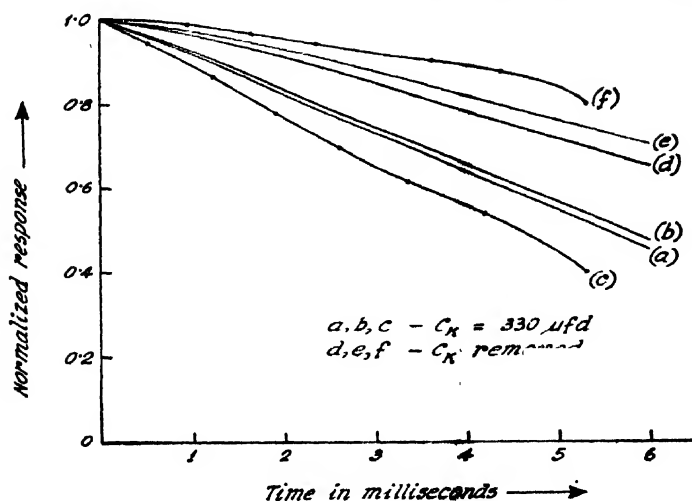


FIG. 8  
Relative output response curve  
(with decoupling network)  
(a), (d)—for the first method  
(b), (e)—for the second method  
(c), (f)—experimental plots.

The effect of increasing the value of the coupling condenser  $C_c$  is shown in figures 9 and 10. The values of the circuit elements are :

$$R_l = R_a = 5K \Omega, \quad C_a = 1 \mu\text{fd} \quad \text{and} \quad R_o = 300K \Omega.$$

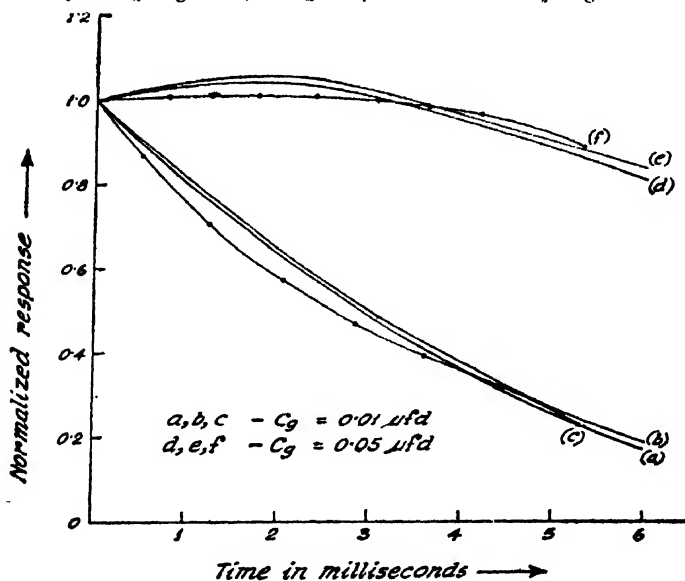


FIG. 9  
Relative output response curve  
(with decoupling network)  
(a), (d)—for the first method  
(b), (e)—for the second method  
(c), (f)—experimental plots.

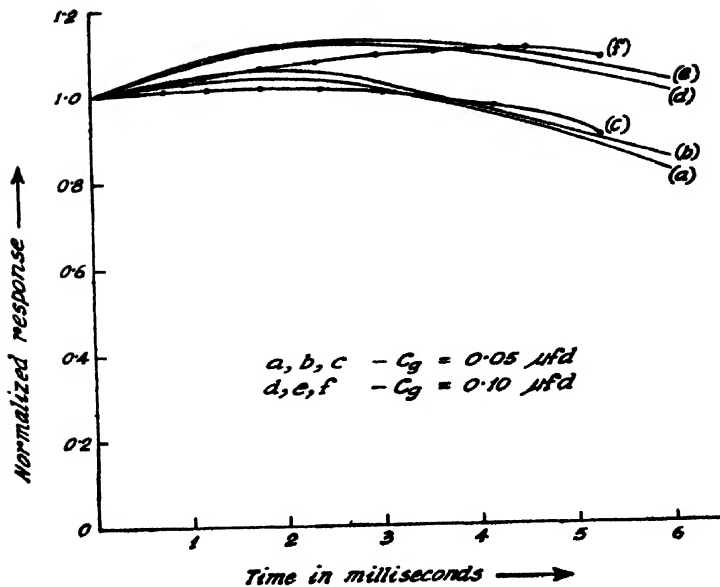


FIG. 10

Relative output response curve  
(with decoupling network)

(a), (d) — for the first method

(b), (e) — for the second method

(c), (f) — experimental plots.

#### EXPERIMENTAL PROCEDURE

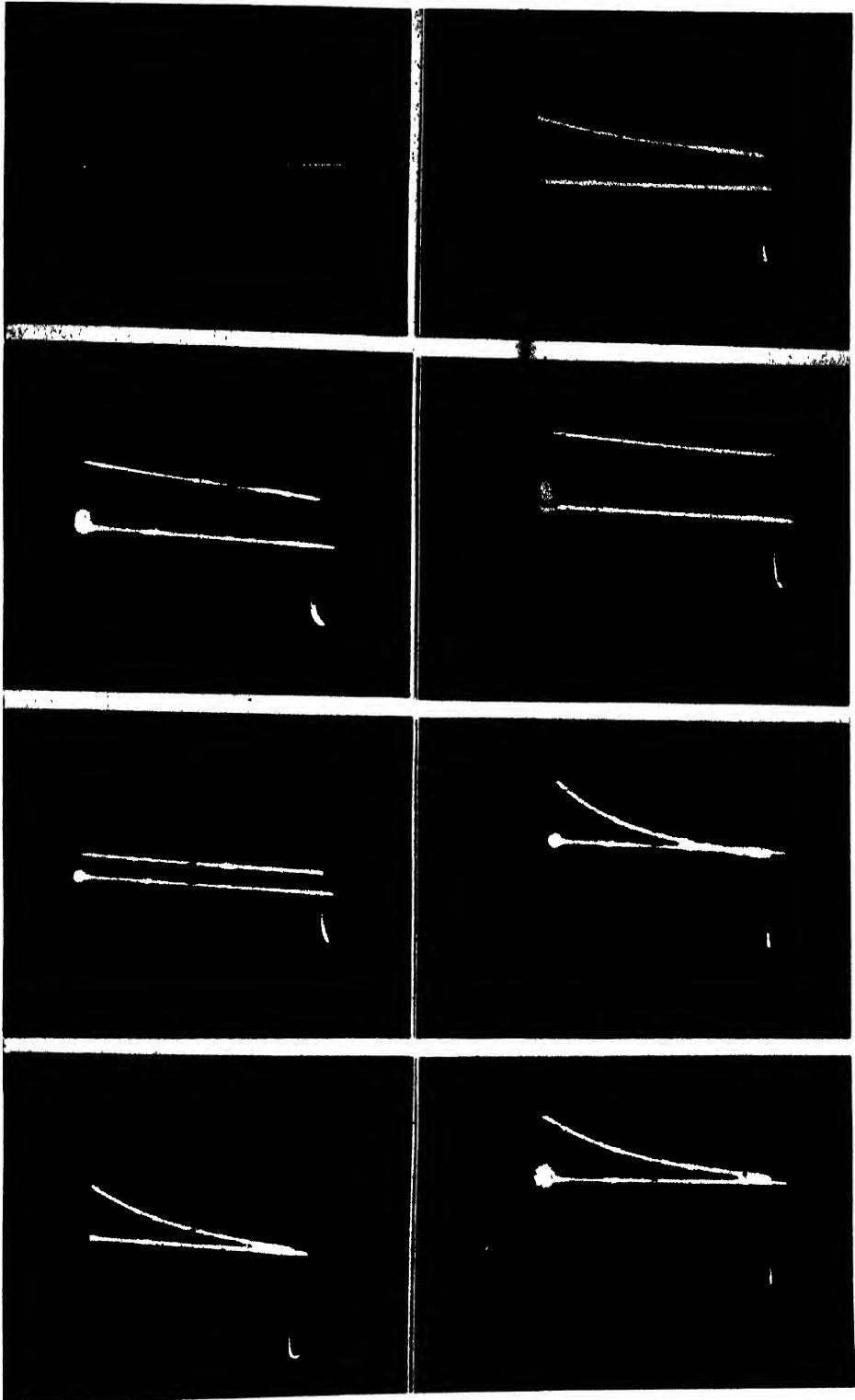
In order to study the response characteristics of a RC-coupled amplifier to a flat top pulse, it was necessary to generate a rectangular pulse with its top perfectly flat. Model 50 pulse generator described by Ilmore and Sands, (1949) is suitable for this purpose. A similar pulse generator was constructed. The pulse generator furnishes flat topped pulses of duration 5.33 milliseconds.

The amplifier stage (figure 1) utilises a tube type 6AC7.

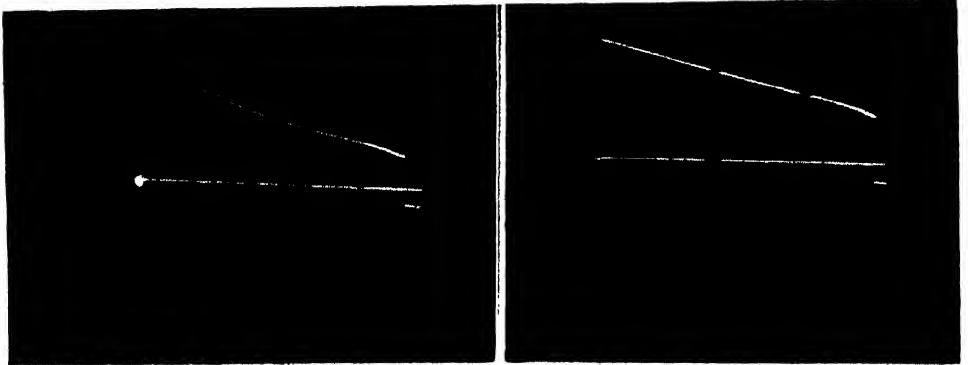
The negative pulses from the univibrator of the pulse generator were used to drive the sweep and the voltage wave-forms were applied to the  $Y_2$ -plate of a Cossor double-beam oscilloscope (Model No. 1035). The  $Y_1$ -beam was utilised to show the base-line of the reproduced pulses. Oscillograms were taken with the help of a plate camera.

When there is only a load resistance  $R_L$  in the plate, the shape of the plate point voltage is an exact replica of the plate current wave-form and so in figures (ii), (iii), (iv) and (v) we have taken the oscillograms of the plate-point voltages for the various conditions mentioned in Table I.

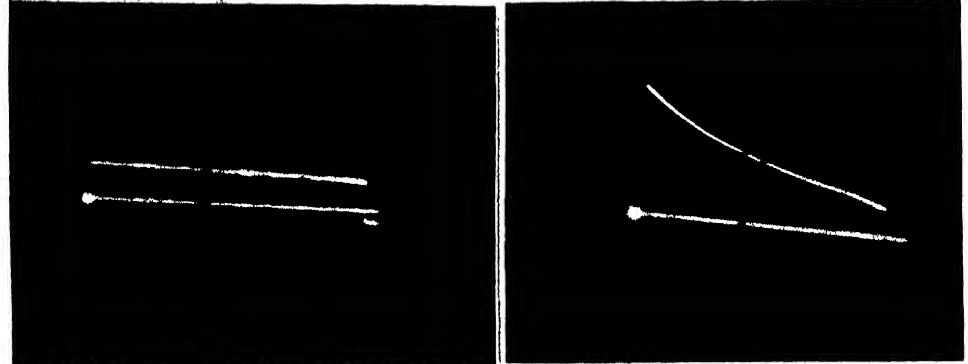
The following cases mentioned in Table I were shown in the oscillograms (see Plates XXIA, B) :



ix



xi



ciii

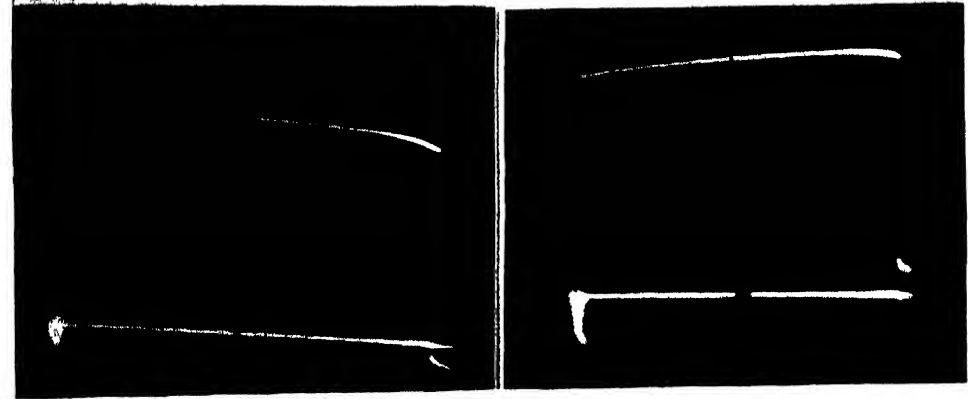




TABLE I

No. of Figs:	Values of the circuit constants:		Nature of the pulse
	Constant parameters	Variable parameters	
(i)			Input pulse.
(ii)	$R_{\theta} = 60\text{K } \Omega$ , $C_{\theta} = 2\mu\text{fd}$ , $R_K = 180\text{ } \Omega$ .	$C_K = 80\mu\text{fd}$	Plate current.
(iii)	"	$C_K = 330\mu\text{fd}$	"
(iv)	"	$C_K = 6330\mu\text{fd}$	"
(v)	"	$C_K$ removed	"
(vi)	$R_{\theta} = 60\text{K } \Omega$ , $C_{\theta} = 2\mu\text{fd}$ , $R_K = 180\text{ } \Omega$ , $C_g = 0.01\mu\text{fd}$ , $R_g = 250\text{K}$ , $R_i = 10\text{K}$ .	$C_K = 80\mu\text{fd}$	Output voltage without compensation.
(vii)	"	$C_K = 330\mu\text{fd}$	"
(viii)	"	$C_K = 6330\mu\text{fd}$	"
(ix)	$R_i = 2\text{K} \Omega$ , $R_d = 15\text{K} \Omega$ $C_d = 1\mu\text{fd}$ , $C_g = 0.01\mu\text{fd}$ , $R_g = 300\text{K} \Omega$ Other parameters same as before.	$C_K = 80\mu\text{fd}$	Output voltage with compensation.
(x)	"	$C_K = 330\mu\text{fd}$	"
(xi)	"	$C_K$ removed	"
(xii)	$R_i = 5\text{K} \Omega$ , $R_d = 5\text{K} \Omega$ , $R_g = 300\text{K} \Omega$ $C_d = 1\mu\text{fd}$ , $C_K = 300\mu\text{fd}$ , other parameters same as before.	$C_g = 0.01\mu\text{fd}$	"
(xiii)	"	$C_g = 0.05\mu\text{fd}$	"
(xiv)	"	$C_g = 0.1\mu\text{fd}$	"

## DISCUSSION

The flat-top pulses were generated with a very low repetition rate so that it may be safely said that there is negligible influence of the previous pulse on the response of the amplifier to the in-coming pulse.

(a) *Plate current response*: The sag in plate current is mainly due to the  $R_K C_K$  combination in the cathode if the  $R_{\theta} C_{\theta}$  time constant is sufficiently high. This is shown in the four cases both experimentally and theoretically. That the theoretically plotted curves and the experimentally obtained responses tally with each other, may be seen from figures 2-4 where the experimental points have been accurately measured in the oscillograms by a travelling microscope.

All figures indicate the error which is often done by assuming that the plate current of a pentode is always constant and is an exact replica of the

input pulse. The sag in plate current is above 50% if the cathode by-pass condenser is not suitably chosen, [cf. figure (ii) of the oscillograms].

(b) *Output voltage wave-forms without compensation*: The sag in plate current actually causes the output voltage wave-form to become slightly negative in the end. If the  $C_g R_g$  time constant is not sufficiently high, the mere increase of the value of the cathode capacitor cannot improve the shape of the wave-form very much.

It is found from a comparison of the calculated and experimental values (figures 5 and 6) that the theory and experiment are in very good agreement with each other in this case also.

(c) *Output voltage wave-forms with compensation*. The sag present in the output voltage wave-form may be compensated by a decoupling network in the plate. There is a considerable improvement in the response of the amplifier which can further be modified for the better by inserting suitable by-pass capacitor in the cathode or removing it altogether [figures (ix)-(xi)]. This has been predicted by a study of the plots of the response functions derived theoretically. A comparison between the calculated and the experimental values may be made with the help of figures 7 and 8.

The discrepancy which is found in the theoretical plots and experimental oscillograms is due to several reasons. First of all, the values of the mutual conductance  $g_m$  of the tube, the screen resistance  $r_{s,0}$  and the screen amplification factor  $\mu_{s,0}$  which are so-called tube constants are variable due to non-linear nature of tube characteristics. The values taken for the calculation represent only a rational and logical choice obtaining in the operating region of the tube.

In figures 9 and 10 and oscillograms (xii-xiv) it is found that the output voltage wave-form shows an exponential rise with time as the value of the coupling condenser is increased. This is due to the fact that the output voltage of the network (figure 11) increases exponentially with a time constant  $R_d C_d$  if the input is a step-function current pulse.

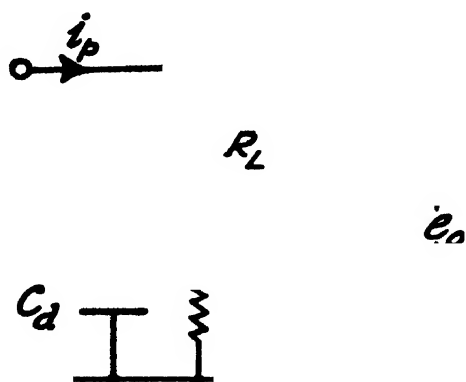


FIG. 11  
Decoupling filter network

## CONCLUSION

It is evident from a comparison of the theoretical curves and experimental oscillograms that the complicated interactions of the various resistance-capacitance networks in the plate, screen-grid, cathode and control grid, must be carefully taken into account in order to have a clear idea about the response characteristics of the amplifier. The nature of the response functions as obtained theoretically closely tallies with the oscillograms.

It may be concluded from the experiment that the time constant of the  $R_K C_K$  circuit in the cathode has a very great influence on the reproduced pulse shapes of the amplifier. The choice in taking  $C_K$  as the variable element in the experiment was due to the fact that the cathode resistance is generally small and a condenser of very high value is not always available. The time constant of the  $R_{s,g} C_{s,g}$  circuit in the screen can be easily increased by a suitable choice of the values of the components. So it was not considered essential to vary this time constant and study its effect on the output wave-forms.

This experimental verification of the analysis (Bhattacharyya, 1953) presented sometime ago is concerned mainly about the matter of flat top compensation in terms of the transient response. It was customary to assess the transient behaviour of an amplifier from a measurement of the gain and phase functions over the entire frequency range. That this method is not quite suitable is well-known and has been so stated by various workers (Elmore and Sands, 1949). The methods adopted here are not only more logical and direct but also far less laborious and troublesome.

## ACKNOWLEDGMENTS

The author is deeply indebted to Prof. M. N. Saha, D.Sc., F.R.S. and Prof. B. D. Nag, Ph.D. for their kind interest in the work. He also desires to express his sincere thanks to Sri B. M. Banerjee for his help and advice throughout the progress of the work. He is also grateful to Sri A. P. Patro and Sri B. Basu for their help in taking photographs presented here.

## REFERENCES

- Bhattacharyya, B. K., 1953, *Ind. J. Phys.*, **27**, 39.  
Elmore, C. W., and Sands, M., 1949, *Electronics (Experimental Techniques)*, First Edition, McGraw-Hill Book Co. Inc., p. 128-136, 320-322.  
Gardner, M. F., and Barnes, J. L., 1947, *Transients in Linear Systems*, Vol. I, Wiley, New York.  
Valley, G. E. and Wallman, H., 1948, *Vacuum Tube Amplifiers*, McGraw-Hill Book Co., New York.

# INTENSITY FORMULAE FOR BANDS INVOLVING HIGH MULTIPLICITY TERMS. PART II. ${}^5\Pi - {}^5\Sigma$ , ${}^5\Pi - {}^5\Pi$ , AND ${}^4\Pi - {}^4\Pi$ TRANSITIONS

By D. PREMASWARUP

DEPARTMENT OF PHYSICS, ANDHRA UNIVERSITY, WALTAIR

(Received for publication June 10, 1953)

**ABSTRACT.** In continuation of the author's previous work on  ${}^5\Sigma - {}^5\Sigma$ ,  ${}^6\Sigma - {}^6\Sigma$  transitions, intensity formulae have been derived for the rotational lines of bands due to the transitions  ${}^5\Pi(a) - {}^5\Sigma$ ,  ${}^5\Pi(b) - {}^5\Sigma$ ;  ${}^5\Pi(a) - {}^5\Pi(a)$ ,  ${}^5\Pi(a) - {}^5\Pi(b)$ , and  ${}^5\Pi(b) - {}^5\Pi(b)$ ; and  ${}^4\Pi(a) - {}^4\Pi(a)$ ,  ${}^4\Pi(a) - {}^4\Pi(b)$ , and  ${}^4\Pi(b) - {}^4\Pi(b)$ .

## INTRODUCTION

In this paper which is a continuation of an earlier one by the author (1953), expressions are derived for the intensities of the rotational lines in  ${}^5\Pi - {}^5\Sigma$  and  ${}^5\Pi - {}^5\Pi$  bands. Incidentally as the calculation of the intensity distribution in the rotational structure of  ${}^4\Pi - {}^4\Pi$  bands has not been previously attempted, expressions are derived for the intensities of the rotational lines in these bands also.

## THEORY

We can approach the general intermediate case of coupling, starting either from case (a) or case (b) (Hill and Van Vleck, 1928). If we start from case (a) the procedure will be simplified to a great extent, as will be evident from the following calculations. The general procedure will be similar even if case (b) is taken as the starting point. If  $q_a$  is the amplitude matrix for the case (a) - (a) transition and  $q$ , that of the general case, we have from quantum mechanics the relation

$$q = S' q_a \tilde{S}''^*$$

where  $S'$  is the transformation matrix of the initial state from case (a) to the general case and  $\tilde{S}''^*$  is the matrix obtained by transposing the columns of the complex conjugate of  $S''$ , the transformation matrix for the final state. The elements  $S_{ik}$  of  $S$  are obtained by solving the set of simultaneous equations

$$W_{ii} S_{ii} - \sum_k (k, i') S_{ik} = 0$$

where  $i, i'$  and  $k$  assume all values of  $K$  consistent with a given set of values for  $\Lambda, J$ , and  $S$ , i.e.,  $i, i', k = |J - S|, \dots, (J + S - 1), (J + S)$  and

$W_{ii}$  are the energies and  $H(k, i')$  the elements of the energy matrix for the particular state under consideration, the energy matrix being obtained by starting from case (a) coupling and introducing the effect of molecular rotation on spin as a perturbation. Expressions for these elements have already been derived by Van Vleck (1929).

#### CALCULATIONS AND RESULTS

As expressions for the intensities of the individual band lines will be extremely complicated in the general case, expressions are here derived only for the limiting cases. As such, we recognize three types of transitions, namely, transitions in which both states belong to case (a), those in which both states belong to case (b) and those in which one of the states belongs to case (a) while the other belongs to case (b). When both states belong to case (a) the intensity factors  $i$ , (which are identical with the squares of the absolute values of the amplitude matrix elements, i.e.,  $|q_{nm}|^2$ ) are calculated directly from the Hönl-London expressions given below by substituting the proper values for  $\Omega$  and  $S$  occurring therein.

$$\begin{aligned} \text{For } \Delta\Omega=0 \text{ with } \Delta J=0, & \quad i=2(2J+1)\Omega^2/J(J+1). \\ \text{For } \Delta\Omega=0 \text{ with } \Delta J=\pm 1, & \quad i=2(J^2-\Omega^2)/J. \\ \text{For } \Delta\Omega=\pm 1 \text{ with } \Delta J=0, & \quad i=(2J+1)(J+\Omega)(J-\Omega+1)/J(J+1). \\ \text{For } \Delta\Omega=\pm 1 \text{ with } \Delta J=\Delta\Omega, & \quad i=(J+\Omega)(J+\Omega-1)/J. \\ \text{For } \Delta\Omega=\pm 1 \text{ with } \Delta J=-\Delta\Omega, & \quad i=(J-\Omega)(J-\Omega+1)/J. \end{aligned}$$

For transitions in which both states belong to case (b), the method adopted to calculate the intensity factors is the same as that used for bands with  $\Sigma-\Sigma$  transitions. This method has already been described in detail in Part I of this series. The Sommerfeld-Hönl expressions for case  $\Delta K=0$  which are not given in the previous paper and which are required for these calculations are given below. In these expressions as well as in the above Hönl-London expressions it is to be noted that the higher of the two  $K'$  or  $K''$ ,  $J'$  or  $J''$ , and  $\Omega'$  or  $\Omega''$  are to be used respectively for  $K$ ,  $J$  and  $\Omega$  occurring therein.

$$\text{For } \Delta K=0 \text{ with } \Delta J=0, \quad i=(2K+1)(2J+1)[J(J+1)+K(K+1) \\ -S(S+1)]/JK(J+1)(K+1)$$

$$\text{For } \Delta K=0 \text{ with } \Delta J=\pm 1, \quad i=(2K+1)[(J+K)(J+K+1)-S(S+1)]^{1/2} \\ [S(S+1)-(J-K-1)(J-K)]^{1/2}/JK(K+1)$$

For transitions from a case (a) to a case (b) state the method outlined above is applied. It is to be remembered that for any case (a) state the transformation matrix is the unit matrix, so that the expression for  $q_{ik}$  is given by

$$q_{ik}(J', J'') = \sum_m q_{aim}(J', J'') S_{kkm}(J'')$$

Herein we see the convenience in starting from case (a), for, since the  $q_a$

## D. Premaswarup

matrix is diagonal the summation over  $m$ , in the expression for  $q_k$  is removed, which would not have been the case if we had started from case (b). Thus the above equation is simplified to

$$q_{ik}(J', J'') = q_{ai}(J', J'') S_{ki}(J'')$$

so that the intensity factors are given by

$$i = |q_{ik}(J', J'')|^2 = [q_{ai}(J', J'')]^2 [S_{ki}(J'')]^2$$

The  $[q_{ai}(J', J'')]^2$  are the intensity factors for the case (a) - (a) transition and hence have been derived already. For the purpose of determining the transformation matrices  $S$ , the case (b) energy values, given by the general equation

$$W = BK(K+1) - B\Lambda^2$$

are used, the different energies being obtained by putting  $K = |J-S|$ ,  $|J-S+1|$ , ...  $(J+S)$ . The elements of the energy matrix are determined from the following equations (Hill and Van Vleck, 1928).

$$H(\Sigma, \Sigma) = A\Lambda\Sigma + B[J(J+1) - (\Lambda + \Sigma)^2] + B[S(S+1) - \Sigma^2]$$

$$H(\Sigma, \Sigma \pm 1) = B[J(J+1) - (\Lambda + \Sigma)(\Lambda + \Sigma \pm 1)]^{1/2} [S(S+1) - \Sigma^2]^{1/2}$$

The transformation matrices are then obtained for the three states  $^5\Sigma$ ,  $^5\Pi(b)$  and  $^4\Pi(b)$ , by substituting for the energies and the matrix elements the expressions obtained as above in the set of simultaneous equations and solving for  $S_{ik}$ . The matrix for the  $^4\Pi(b)$  state is given below as an illustration.

$$S[^4\Pi(b)] =$$

$$\begin{pmatrix} \left(\frac{2J-3}{16J}\right)^{1/2} & \left(\frac{3(2J-3)}{16J}\right)^{1/2} & \left(\frac{3(2J+3)(2J-3)}{16J(2J-1)}\right)^{1/2} & \left(\frac{(2J+5)(2J+3)}{16J(2J-1)}\right)^{1/2} \\ \left(\frac{3(2J+1)}{16(J+1)}\right)^{1/2} \left(\frac{(2J+5)^2}{16(J+1)(2J+1)}\right)^{1/2} & \left(\frac{(2J+3)(2J-7)^2}{16(J+1)(2J+1)(2J-1)}\right)^{1/2} & \left(\frac{3(2J+5)(2J+3)(2J-3)}{16(J+1)(2J+1)(2J-1)}\right)^1 \\ \left(\frac{3(2J+1)}{16J}\right)^{1/2} \left(\frac{(2J-3)^2}{16(2J+1)J}\right)^{1/2} & \left(\frac{(2J+9)^2(2J-1)}{16(2J+3)(2J+1)J}\right)^{1/2} & \left(\frac{3(2J+5)(2J-1)(2J-3)}{16(2J+3)(2J+1)J}\right)^1 \\ \left(\frac{(2J+5)}{16(J+1)}\right)^{1/2} \left(\frac{3(2J+5)}{16(J+1)}\right)^{1/2} & \left(\frac{3(2J+5)(2J-1)}{16(2J+3)(J+1)}\right)^{1/2} & \left(\frac{(2J-1)(2J-3)}{16(2J+3)(J+1)}\right)^{1/2} \end{pmatrix}$$

The final intensity factors in the limiting cases for the  $^5\Pi - ^5\Sigma$ ,  $^5\Pi - ^5\Pi$  and  $^4\Pi - ^4\Pi$  transitions are given in Tables I, II and III respectively. To get the actual expressions for the intensities of the individual band lines these intensity factors have to be multiplied by the respective Boltzmann factors. The following conclusions can, however, be drawn from consideration

TABLE I

 Intensity factors for  ${}^b\Pi - {}^5\Sigma$  bands

Branches		Intensity factors	
${}^b\Pi \rightarrow {}^5\Sigma$	${}^5\Sigma \rightarrow {}^b\Pi$	${}^5\Pi(a)$	${}^5\Pi(b)$
$P_1(J)$	$R_1(J-1)$	$\frac{(J+2)^2(J+1)^2}{4(2J+1)J(2J-1)}$	$\frac{(2J+1)(J-3)}{(2J-3)}$
$Q_1(J)$	$Q_1(J)$	$\frac{(J+2)^2(J-1)}{4J(2J-1)}$	$\frac{(J+1)(2J+1)(J-2)}{J(J-1)}$
$R_1(J)$	$P_1(J+1)$	$\frac{(J+2)J(J-1)}{4(2J+1)(2J-1)}$	$\frac{(2J+3)J}{(2J-1)}$
$QP_{21}(J)$	$QR_{12}(J-1)$	$\frac{(J+1)^2(J-1)}{(2J+1)(2J-1)}$	$\frac{2(2J+1)}{J(J-1)}$
$RQ_{21}(J)$	$PQ_{12}(J)$	$\frac{(J+1)(J-1)}{(2J-1)}$	$\frac{2(2J+1)}{(2J-1)(J-1)}$
$PQ_{12}(J)$	$RQ_{21}(J)$	$\frac{(J+3)^2(J+2)(2J+1)(J-1)}{2(J+1)J(5J+3)(J^2+2J+3)}$	$\frac{2(2J+1)(J-2)}{J(2J-1)(J-1)}$
$QR_{12}(J)$	$QP_{21}(J+1)$	$\frac{(J+3)^2(J+2)J(J-1)}{2(J+1)(5J+3)(J^2+2J+3)}$	$\frac{2(2J+3)}{(J+1)J}$
$P_2(J)$	$R_2(J-1)$	$\frac{(J+3)^2(J+1)(J-1)}{2(5J+3)(J^2+2J+3)}$	$\frac{(J+1)(2J+1)(J-2)^2}{J(2J-1)(J-1)}$
$Q_2(J)$	$Q_2(J)$	$\frac{(J+3)^2(2J+1)(J-1)}{2(5J+3)(J^2+2J+3)}$	$\frac{(2J+1)(J^2-3)^2}{(J+1)J^2(J-1)}$
$R_2(J)$	$P_2(J+1)$	$\frac{(J+3)^2J(J-1)}{2(5J+3)(J^2+2J+3)}$	$\frac{(J+2)(2J+3)(J-1)}{(2J+1)J}$
$QP_{32}(J)$	$QR_{23}(J-1)$	$\frac{3(J+1)J(J-1)^2}{(5J+3)(J^2+2J+3)}$	$\frac{3(J+1)(2J-3)}{J^2(J-1)}$
$RQ_{32}(J)$	$PQ_{23}(J)$	$\frac{3(J+1)(2J+1)J(J-1)}{(5J+3)(J^2+2J+3)}$	$\frac{3(2J+3)(J-1)}{J^2(2J-1)}$
$PQ_{23}(J)$	$RQ_{32}(J)$	$\frac{3(2J+1)}{2(2J+3)(2J-1)}$	$\frac{3(2J+3)(J-1)^2}{(J+1)J^2(2J-1)}$
$QR_{23}(J)$	$QP_{32}(J+1)$	$\frac{3J}{2(2J+3)(2J-1)}$	$\frac{3(J+2)(2J-1)}{(J+1)^2J}$
$P_3(J)$	$R_3(J-1)$	$\frac{(J+1)J(J-1)}{(2J+3)(2J-1)}$	$\frac{(2J+3)(J+1)(J-1)^2(2J-3)}{(2J+1)J^2(2J-1)}$
$Q_3(J)$	$Q_3(J)$	$\frac{(J+1)(2J+1)J}{(2J+3)(2J-1)}$	$\frac{(2J+1)(J^2+J-3)^2}{(J+1)^2J^2}$
$R_3(J)$	$P_3(J+1)$	$\frac{(J+2)(J+1)J}{(2J+3)(2J-1)}$	$\frac{(2J+5)(J+2)^2J(2J-1)}{(2J+3)(J+1)^2(2J+1)}$
$QP_{43}(J)$	$QR_{34}(J-1)$	$\frac{3(J-1)(J-2)}{2(2J+3)J(2J-1)}$	$\frac{3(2J+3)J(J-1)}{(J+1)J^2}$
$RQ_{43}(J)$	$PQ_{34}(J)$	$\frac{3(J+2)(2J+1)(J-1)}{2(2J+3)(J+1)J(2J-1)}$	$\frac{3(J+2)^2(2J-1)}{(2J+3)(J+1)^2J}$

TABLE I (contd.)

Branches		Intensity factors	
${}^5\Pi \rightarrow {}^5\Sigma$	${}^5\Sigma \rightarrow {}^5\Pi$	${}^5\Pi(a)$	${}^5\Pi(b)$
${}^PQ_{34}(J)$	${}^RQ_{43}(J)$	$\frac{3(J+2)(2J+1)(J+1)J}{(5J+2)(J^2+2)}$	$\frac{3(J+2)(2J-1)}{(2J+3)(J+1)^2}$
${}^Q R_{34}(J)$	${}^QP_{43}(J+1)$	$\frac{3(J+2)^2(J+1)J}{(5J+2)(J^2+2)}$	$\frac{3(2J+5)J}{(J+2)(J+1)^2}$
${}^P_4(J)$	${}^R_4(J-1)$	$\frac{(J+2)(J-1)(J-2)^3}{2(5J+2)J(J^2+2)}$	$\frac{(J+2)(2J-1)(J-1)}{(J+1)(2J+1)}$
${}^Q_4(J)$	${}^Q_4(J)$	$\frac{(J+2)^2(2J+1)(J-1)(J-2)^2}{2(J+1)J(5J+2)(J^2+2)}$	$\frac{(2J+1)(J^2+2J-2)^2}{(J+2)(J+1)^2J}$
${}^R_4(J)$	${}^P_4(J+1)$	$\frac{(J+3)(J+2)^2(J-2)^2}{2(J+1)(5J+2)(J^2+2)}$	$\frac{(J+3)^2(2J+1)^2J}{(J+2)(2J+3)(J+1)}$
${}^QP_{54}(J)$	${}^QR_{45}(J-1)$	$\frac{(J-1)(J-2)^3(J-3)}{2(5J+2)J(J^2+2)}$	$\frac{2(2J-1)}{(J+1)J}$
${}^RQ_{54}(J)$	${}^PQ_{45}(J)$	$\frac{(J+3)(2J+1)(J-2)^3(J-1)}{2(J+1)J(5J+2)(J^2+2)}$	$\frac{2(J+3)(2J+1)}{(J+2)(2J+3)(J+1)}$
${}^PQ_{45}(J)$	${}^RQ_{54}(J)$	$\frac{(J+2)^2(J-1)}{(2J+3)(J+1)}$	$\frac{2(2J+1)}{(J+2)(2J+3)}$
${}^QR_{45}(J)$	${}^QP_{54}(J+1)$	$\frac{(J+3)(J+2)^2J}{(2J+3)(J+1)(2J+1)}$	$\frac{2(2J+1)}{(J+2)(J+1)}$
${}^P_5(J)$	${}^R_5(J-1)$	$\frac{(J-1)(J-2)(J-3)}{4(2J+3)(2J+1)}$	$\frac{(J+1)(2J-1)}{(2J+3)}$
${}^Q_5(J)$	${}^Q_5(J)$	$\frac{(J+3)(J-1)(J-2)}{4(2J+3)(J+1)}$	$\frac{(J+3)(2J+1)J}{(J+2)(J+1)}$
${}^R_5(J)$	${}^P_5(J+1)$	$\frac{(J+4)(J+3)(J-1)}{4(2J+3)(2J+1)}$	$\frac{(J+4)(2J+1)}{(2J+5)}$

of the tables. In  ${}^5\Pi-{}^5\Sigma$  transition if the  $\Pi$  state belongs to case (a) coupling the intensities of almost all the branches (main as well as satellites) are of the same order with the  $Q$  branches, twice as intense as the  $P$  and  $R$  branches, while if the  $\Pi$  state belongs to case (b) only the main branches are present with the intensities of the  $Q$  branches twice that of the  $P$  or  $R$  branches. In both the cases the intensities of all the branches first increase with  $J$  to a maximum and thereafter decrease with increasing  $J$ . In  ${}^5\Pi-{}^5\Pi$ , in all the three cases the intensities of the  $P$  and  $R$  branches increase with  $J$  attaining a maximum after which they decrease with increasing  $J$ , while the intensities of the  $Q$  branches are initially low and decrease with increasing  $J$  even at low values. When at least one of the  $\Pi$  states belongs to case (a) the branches  ${}^RQ_{21}$ ,  $Q_3$ ,  ${}^PQ_{23}$ ,  ${}^OQ_{24}$  and  ${}^NQ_{25}$  are completely absent. The intensities in the  ${}^4\Pi-{}^4\Pi$  bands show the same type of behaviour except that here no branches are completely absent,



For the Sake of brevity, in Table I, the intensity factors are given only for branches with  $\Delta J=0, \pm 1$ , and  $\Delta K=0, \pm 1$ , while in Tables II and III these are given only for branches with  $\Delta J=\Delta K=0, \pm 1$ . The expressions for the remaining branches are omitted as their inclusion will make the tables inconveniently long.

TABLE II

Intensity factors for  ${}^3\Pi \leftarrow {}^3\Pi$  bands

Branch	${}^3\Pi(a) \rightarrow {}^3\Pi(a)$	${}^3\Pi(a) \rightarrow {}^5\Pi_1(b)$	${}^3\Pi(b) \rightarrow {}^5\Pi(b)$
$P_1(J)$	$\frac{(J+1)(J-1)}{J}$	$\frac{(J+1)^2(J-1)(J-2)}{4(2J+1)(2J-1)}$	$\frac{(2J+1)(J-1)(J-3)}{(2J-3)(J-2)}$
$Q_1(J)$	$\frac{(2J+1)}{(J+1)J}$	$\frac{(J-2)}{4J(2J-1)}$	$\frac{(J+1)(2J+1)}{J(J-1)^2}$
$R_1(J)$	$\frac{(J+2)J}{(J+1)}$	$\frac{(J+2)J(J-2)}{4(2J+1)(2J-1)}$	$\frac{(2J+3)J(J-2)}{(2J-1)(J-1)}$
$P_2(J)$		$\frac{(J+1)J}{2(2J+1)}$	$\frac{(J+1)(2J+1)(J-2)^2}{(2J-1)(J-1)^2}$
$Q_2(J)$			$\frac{(2J+1)(J^2-3)^2}{(J+1)J^3(J-1)^2}$
$R_2(J)$	$(J+1)$	$\frac{(J+1)^2}{2(2J+1)}$	$\frac{(J+2)(2J+3)(J-1)^2}{(2J+1)J^2}$
$P_3(J)$	$\frac{(J+1)(J-1)}{J}$	$\frac{(J-1)(J^2+J-3)^2}{(2J+3)J^2(2J-1)}$	$\frac{(2J+3)(J+1)^2(J-1)^2(2J-3)}{(2J+1)J^3(2J-1)}$
$Q_3(J)$	$\frac{(2J+1)}{(J+1)J}$	$\frac{(2J+1)(J^2+J-3)^2}{(2J+3)(J+1)^2J^2(2J-1)}$	$\frac{(2J+1)(J^2+J-3)^2}{(J+1)^3J^3}$
$R_3(J)$	$\frac{(J+2)J}{(J+1)}$	$\frac{(J+2)(J^2+J-3)^2}{(2J+3)(J+1)^2(2J-1)}$	$\frac{(2J+5)(J+2)^2J^2(2J-1)}{(2J+3)(J+1)^3(2J+1)}$
$P_4(J)$	$\frac{(J+2)(J-2)}{J}$	$\frac{(J+4)^2(J-1)(J-2)}{2(J+1)(2J+1)J}$	$\frac{(J+2)^2(2J-1)(J-1)}{(J+1)^2(2J+1)}$
$Q_4(J)$	$\frac{4(2J+1)}{(J+1)J}$	$\frac{2(J+4)^2(J-1)}{(J+2)(J+1)^2J}$	$\frac{(2J+1)(J^2+2J-2)^2}{(J+2)^2(J+1)^3J}$
$R_4(J)$	$\frac{(J+3)(J-1)}{(J+1)}$	$\frac{(J+4)^2(J+3)(J-1)^2}{2(J+2)(J+1)^2(2J+1)}$	$\frac{(J+3)^2(2J+1)J}{(J+2)^2(2J+3)}$
$P_5(J)$	$\frac{(J+3)(J-3)}{J}$	$\frac{(J+3)(J-1)(J-2)(J-3)}{4(J+2)(2J+3)(2J+1)}$	$\frac{(J+3)(J+1)(2J-1)}{(J+2)(2J+3)}$
$Q_5(J)$	$\frac{9(2J+1)}{(J+1)J}$	$\frac{9(J-1)(J-2)}{4(J+2)(2J+3)(J+1)}$	$\frac{(2J+1)J}{(J+2)^2(J+1)}$
$R_5(J)$	$\frac{(J+4)(J-2)}{(J+1)}$	$\frac{(J+4)J(J-1)(J-2)^2}{4(J+2)(2J+3)(J+1)(2J+1)}$	$\frac{(J+4)(J+2)(2J+1)}{(J+3)(2J+5)}$

TABLE III

Intensity factors for  ${}^4\Pi - {}^4\Pi$  bands

Branch	${}^4\Pi(a) \rightarrow {}^4\Pi(b)$	${}^4\Pi(a) \rightarrow {}^4\Pi(b)$	${}^4\Pi(a) \rightarrow {}^4\Pi(b)$
$P_1(J)$	$\frac{(2J+1)(2J-1)}{J}$	$\frac{(2J+1)(2J-1)(2J-3)}{16J^2}$	$\frac{(2J+1)(2J-1)(2J-5)}{(J-1)(2J-3)}$
$Q_1(J)$	$\frac{(2J+1)}{(J+1)J}$	$\frac{(2J+1)(2J-3)}{16(J+1)J^2}$	$\frac{16(J+1)(2J+1)}{J(2J-1)^2}$
$R_1(J)$	$\frac{(2J+3)(2J+1)}{(J+1)}$	$\frac{(2J+3)(2J+1)(2J-3)}{16(J+1)J^2}$	$\frac{(2J+3)(2J+1)(2J-3)}{J(2J-1)^2}$
$P_2(J)$	$\frac{(2J+1)(2J-1)}{J}$	$\frac{(2J+5)^2(2J-1)}{16(J+1)J}$	$\frac{(J+1)(2J+1)^2(2J-3)^2}{J^2(2J-1)^2}$
$Q_2(J)$	$\frac{(2J+1)}{(J+1)J}$	$\frac{(2J+5)^2}{16(J+1)J^2}$	$\frac{16(2J^2+1)(J-4)^2}{(J+1)(2J+1)J(2J-1)^2}$
$R_2(J)$	$\frac{(2J+3)(2J+1)}{(J+1)}$	$\frac{(2J+5)^2(2J+3)}{16(J+1)^2}$	$\frac{(J+2)(2J+3)^2(2J-1)^2}{(J+1)^2(2J+1)^2}$
$P_3(J)$	$\frac{(2J+3)(2J-3)}{J}$	$\frac{(2J+9)^2(2J-1)(2J-3)}{16(2J+1)J^2}$	$\frac{(2J+3)^2(2J-1)^2(J-1)}{(2J+1)^2J^2}$
$Q_3(J)$	$\frac{9(2J+1)}{(J+1)J}$	$\frac{9(2J+9)^2(2J-1)}{16(2J+3)(J+1)J^2}$	$\frac{16(2J^2+3J-3)^2}{(2J+3)^2(J+1)(2J+1)J}$
$R_3(J)$	$\frac{(2J+5)(2J-1)}{(J+1)}$	$\frac{(2J+9)^2(2J+5)(2J-1)^2}{16(2J+3)(J+1)(2J+1)J}$	$\frac{(2J+5)^2(2J+1)^2J}{(2J+3)^2(J+1)^2}$
$P_4(J)$	$\frac{(2J+5)(2J-5)}{J}$	$\frac{(2J+5)(2J-1)(2J-3)(2J-5)}{16(2J+3)(J+1)J}$	$\frac{(2J+5)(2J+1)(2J-1)}{(2J+3)(J+1)}$
$Q_4(J)$	$\frac{25(2J+1)}{(J+1)J}$	$\frac{25(2J+1)(2J-1)(2J-3)}{16(2J+3)(J+1)^2J}$	$\frac{16(2J+1)J}{(2J+3)^2(J+1)}$
$R_4(J)$	$\frac{(2J+7)(2J-3)}{(J+1)}$	$\frac{(2J+7)(2J-1)(2J-3)^2}{16(2J+3)(J+1)^2}$	$\frac{(2J+7)(2J+3)(2J+1)}{(2J+5)(J+2)}$

## ACKNOWLEDGMENTS

The author wishes to acknowledge his deep indebtedness to Prof. K. R. Rao for his invaluable guidance while carrying out this work.

## REFERENCES

- Hill, E. L. and Van Vleck, J. H. 1928, *Phys. Rev.*, **32**, 250.  
Hönl, H. and London, F. 1925, *Zett. f. Phys.*, **33**, 803.  
Premaswarup, D. 1953, *Ind. J. Phys.*, **27**, 415.  
Somerfeld, A. and Hönl, H. 1929, *Sitzungsber. der Preuss. der. Qiss., Phys-math. Klasse*, pp. 141.  
Van Vleck, J. H. 1929, *Phys. Rev.*, **33**, 467.

# TERM VALUES IN THE SPECTRUM OF CHROMIUM II\*

By V. SURYANARAYANA AND V. RAMAKRISHNA RAO

DEPARTMENT OF PHYSICS, ANDHRA UNIVERSITY, WALTAIR

(Received for publication October 28, 1953)

**ABSTRACT.** Term values for the configurations  $3d^5$ ,  $3d^4.4s$ ,  $3d^3.4s^2$  in CrII are calculated and compared with the experimental data due to Kiess. The values of the unidentified terms are predicted from these theoretical calculations.

## INTRODUCTION

An extensive experimental analysis of the spectrum of CrII was recently published by Kiess (1951). The even terms arising out of the configurations  $3d^5$ ,  $3d^4.4s$  and  $3d^3.4s^2$  were worked in fairly good detail and their values were given. A theoretical calculation of these term values appeared desirable for (a) checking the analysis and (a) predicting the terms yet to be established. The results of these calculations are presented and discussed in the following pages.

The theory of the calculations was first given by Slater (1929) and developed later by Van Vleck (1934). The working details were given by Rao (1948) in his paper on "Term values in Complex Spectra (Columbium I and II)". Tables I, II and III embody the results. The observed values of the terms are the statistical means of the multiplet levels of each term. The formulae used in the calculations are given in the last column. For the evaluation of the parameters  $F_0$ ,  $F_2$ ,  $F_4$  and  $G_2$  the method of normal equations was employed (Rao, 1948). Low lying terms are used for this purpose (marked in the table with asterisks) as their assignment is generally more certain.

In Table I the term values of the lowest configuration  $3d^5$  of CrII are given. In the calculated values, the  $a^6S$  term is reduced to zero and correspondingly all the other terms shifted to that scale. The percentage of discrepancy, between observed and calculated values is given in column 4. There is in general good agreement. Considerable disagreement is found between the values for  $a^4P$ . Of all the quartet terms, this should be the highest according to Hund's rule (lowest 'L' value). However, the  $b^4D$  and  $b^4F$  terms are larger than  $a^4P$ . This involves a certain amount of perturbation in the term scheme which may possibly be due to slight deviation from rigorous R-S coupling assumed in theoretical considerations. Terms  $a^3D_+$  and  $a^3P_+$  are not identified in experimental work as these are considerably high. The lines arising out of these levels and an excited state generally lie in the far infrared and so was not obtained. These values could,

\* Communicated by Prof K. R. Rao.

in general, be only predicted from theory and fitted into the term scheme. Their values are given in column (3). Table II gives the results of calculation for the configuration  $3d^4.4s$  of CrII which is the next higher configuration to the above one namely  $3d^5$ . In this, calculations are made in two ways. The values obtained by straight calculations with formulae (column 1) are given in column 5. In column 4 the data are obtained from calculations through ion data. The configuration  $3d^4$  of CrIII is the ionic configuration of  $3d^4.4s$  of CrII. Van Vleck (1934) gave the necessary theory for such a calculation and the working details may be found in Rao's paper (1948). This calculation helps us to verify CrII spectra as against Cr III spectrum. A good agreement between the two data indicates the consistency of assignments of both the spectra of the configurations dealt with. However, the calculation is limited by the number of terms known in  $3d^4$  configuration in CrIII. The first column gives the base terms of  $3d^4$  of CrIII on which those of CrII are built up by the addition of a  $4s$  electron. Columns 6 and 7 give the percentage of discrepancy between the observed values on one hand and the calculated values from ion data (column 6) and from formulae (column 7) given in the last column. It is seen that where calculation could be made for ion data, the discrepancy is very small, confirming the assignments of terms in the configurations of both CrII and CrIII. In the calculated data from the formulae, it would be found that the percentage of discrepancy is more than in case of the  $3d^5$  configuration, though in itself it is not much. However, this may be attributed to the fourth parameter  $G_2$  entering the formulae, The deviation from R-S coupling may be considerable in the case of  $3d^4.4s$  electrons.

Table III gives term values for the  $3d^3.4s^2$  configuration of CrII. In this configuration the unit  $3d^3$  is shielded by the complete subshell  $4s^2$  and so the deviation from the R-S coupling may be considered to be much less than in the earlier configurations. The configuration gives rise to the same terms as  $3d^3$  and values are given in column (3). The percentage of discrepancy is small. The terms,  $^2F$ ,  $^2H$ ,  $^2D_+$  and  $^2D_-$  are predicted in the spectrum. In view of the general good agreement it may be reasonably expected that these predicted values can lie within 4 percent of the values given. The formulae given in the last column of this table are obtained by neglecting the  $G$ 's in the formulae for the  $d^3s$  configuration by Bowman (1941).

TABLE I

Term values of chromium II

Configuration  $3d^5$ 

Term symbol	Observed value	Calculated value (author)	Percentage of discrepancy	Formula (Laporte 1942)
$a^6S^*$	0.0	0.0	0.0	$10F_0 - 35F_2 - 315F_4$
$a^4G^*$	20516.0	20498.5	-0.1	$11F_0 - 25F_2 - 190F_4$
$b^4F$	32848.2	31666.7	-0.7	$10F_0 - 13F_2 - 180F_4$
$b^4D^*$	25039.9	25721.2	+2.7	$11F_0 - 18F_2 - 225F_4$
$a^4P^*$	21823.7	23475.2	+7.6	$10F_0 - 28F_2 - 105F_4$
$a^3I^*$	30147.2	29067.1	-3.5	$10F_0 - 24F_2 - 50F_4$
$b^3H$	35664.0	35774.3	+0.3	$10F_0 - 22F_2 - 30F_4$
$a^2G$	36197.9	37274.2	+3.1	$10F_0 - 13F_2 - 115F_4$
$d^2G$	52311.2	34426.8	+4.0	$10F_0 + 3F_2 - 155F_4$
$a^2F$	32459.2	33536.0	-3.3	$10F_0 - 25F_2 - 15F_4$
$c^2F$	39821.1	40258.6	+1.1	$10F_0 - 9F_2 - 165F_4$
$d^2D$	47361.4	49204.5	+3.9	$10F_0 - 4F_2 - 120F_4$
$a^2D_-$	31420.1	33018.5	+5.1	$10F_0 - 3F_2 - 90F_4$
$a^2D_+$		72096.9		$+ (513F_2^2 - 4500F_2F_4 + 2700F_4^2)^{1/2}$
$a^2P$		67110.5		$10F_0 + 20F_2 - 210F_4$
$a^2S$	44307.0	44735.2	+1.4	$10F_0 - 3F_2 - 195F_4$

$$10F_0 = 62378.0 \text{ cm}^{-1},$$

$$F_2 = 1118.6 \text{ cm}^{-1},$$

$$F_4 = 74.5 \text{ cm}^{-1}.$$

**Note:**—In this and the following tables the suffixes + and - indicate higher and lower of two similar terms and the corresponding formulae must be taken with the respective sign.

The terms Marked with asterisks are those taken for the calculation of the constants.

TABLE II  
Configuration  $3d^4 4s$ .

Base term	Term symbol	Observed value	Calculated value (from data)	Calculated value (by formula)	Percentage discrepancy		Formula (Rao, 1948)
					(Ion data)	(Formula)	
$^5D$	$a^5D^*$	12295.0	12296.0	11476.7	0.0	-6.7	$6F_0 - 21F_2 - 189F_4 - 3G_2$
	$a^5D^*$	19848.9	19850.8	20059.2	0.0	+4.1	$6F_0 - 21F_2 - 189F_4 + 2G_2$
$^3H$	$a^3H^*$	30286.3	30286.3	29752.0	+1.9	-1.8	$6F_0 - 17F_2 - 69F_4 - 2G_2$
	$a^3H^*$	34731.2	35382.5	35261.5	+1.9	+1.5	$6F_0 - 17F_2 - 69F_4 + G_2$
$^3G$	$b^3G^*$	33592.2	34305.4	33920.5	+2.1	+1.0	$6F_0 - 12F_2 - 94F_4 + G_2$
	$b^3G$	39763.0	38830.5	39430.0	-2.3	-8.3	$6F_0 - 12F_2 - 94F_4 - 2G_2$
$^3F_+$	$4^3F_+$			57121.2			$6F_0 - 5F_2 - 76.5F_4 - 2G_2$
$a^3F_-$	$a^3F_-$	31166.3	31951.3	32219.6	+2.6	+3.4	$\pm \frac{1}{2}(612F_2 + 2002F_4 - 4860F_2F_4)^{1/2}$
$^3F_+$	$^3F_+$			52630.7			$6F_0 - 5F_2 - 76.5F_4 + G_2$
$a^3F_-$	$a^3F_-$	31166.3	31951.3	32219.6		+6.0	$\pm \frac{1}{2}(612F_2 + 2002F_4 - 4860F_2F_4)^{1/2}$
$a^3D$	$b^3D$	38309.1		39755.4	+2.5	+3.8	$6F_0 - 5F_2 - 129F_4 - 2G_2$
	$b^3D$	42031.3		45265.9		+5.4	$6F_0 - 5F_2 - 129F_4 + G_2$
$^3P_+$	$4^3P_+$			57553.6			$6F_0 - 5F_2 - 76.5F_4 - 2G_2$
$a^3P_-$	$b^3P_-$	30577.5	31054.3	31777.2	+1.5	+3.9	$\pm \frac{1}{2}(912F_2 + 3802F_4 - 9960F_2F_4)^{1/2}$

TABLE II (contd.)

Base term	Term symbol	Observed value	Calculated value (ion data)	Calculated value (by formula)	Percentage discrepancy		Formula (Rao, 1948)
					(Ion data)	(Formula)	
$3P_+$	$2P_+$			63073.1			$\{6F_0 - 3F_2 - 76.5F_4 + G_2$
$3P_-$	$2P_-$	35181.9	35587.5	37286.7	+1.2	+6.0	$\pm 1/2(912F_2^2 + 38025F_4^2 - 9960F_2F_4)^{1/2}$
$3I$	$2I$	40214.1		39807.9		-1.0	$6F_0 - 15F_2 - 9F_4 - G_2$
$1G_+$	$2G_+$			66757.3			$\{6F_0 - 5F_2 - 6.5F_4 - G_2$
$3G_-$	$2G_-$	38539.5		39360.5		+2.1	$\pm 1/2(708F_2^2 + 30825F_4^2 - 6420F_2F_4)^{1/2}$
$3F$	$2F$	50675.8		49241.5		-2.8	$6F_0 - 84F_4 - G_2$
$1D_+$	$2D_+$			82348.6			$\{6F_0 - 9F_2 - 76.5F_4 - G_2$
$1D_-$	$2D_-$	45707.7		47002.6		+2.8	$\pm 1/2(1206F_2^2 + 30825F_4^2 - 10440F_2F_4)^{1/2}$
$1S_+$	$2S_+$			104918.0			$\{6F_0 + 10F_2 + 6F_4 - G_2$
$3S_-$	$2S_-$	40415.3		42591.2		+5.4	$\pm 1/2(3088F_2^2 + 133200F_4^2 - 20640F_2F_4)^{1/2}$
$6F_0 = 62012.3 \text{ cm}^{-1}$			$F_2 = 1301.7 \text{ cm}^{-1}$	$F_4 = 93.6 \text{ cm}^{-1}$	$G_2 = 1856.5 \text{ cm}^{-1}$		

TABLE III

Term values in chromium II.

Configuration  $3d^3.4s^2$ 

Term	Observed value	Calculated value	Percentage of discrepancy	Formula
$^4P$	55045.7	55658.9	+1.1	$F_0 - 147F_4$
$^2P$	59112.8	57292.7	-3.2	$F_0 - 6F_2 - 12F_4$
$^4F$	53574.4	52970.9	-1.1	$F_0 - 15F_2 - 72F_4$
$^2F$		59980.7		$F_0 + 9F_2 - 87F_4$
$^2G$	54576.2	56396.7	+3.3	$F_0 - 11F_2 + 13F_4$
$^2H$		57292.7		$F_0 - 6F_2 - 12F_4$
$^3D_+$		62709.6		$F_0 + 5F_2 + 3F_4$
$^3D_-$		59430.2		$\left\{ \begin{array}{l} \pm \frac{1}{2}(193F_2^2 - 1650F_2F_4 \\ - 8325F_4^2)^{1/2} \end{array} \right.$

$$F_0 = 59451.5 \text{ cm}^{-1}$$

$$F_2 = 308.2 \text{ cm}^{-1}$$

$$F_4 = 25.8 \text{ cm}^{-1}$$

## ACKNOWLEDGMENT

The authors wish to take this opportunity to express their thanks to Prof. K. R. Rao, for his kind interest in the work.

## REFERENCES

- Bowman, D. S., 1941, *Phys. Rev.*, **59**, 386.  
 Kiess, C. C., 1951, *Jour. Res. Nat. Bur. Stand.*, **47**, 423.  
 Rao, V. R., 1948, *Ind. Jour. Phys.*, **22**, 429.  
 Serber, 1934, *Phys. Rev.*, **45**, 461.  
 Slater, J. C. 1929, *Phys. Rev.*, **34**, 1293.  
 Van Vleck, J. H., 1934, *Phys. Rev.*, **45**, 405.



## ON THE PHOTOCONDUCTIVITY OF AMETHYST QUARTZ\*

By M. K. VAINU BAPPU

PHYSICAL LABORATORY, NIZAM COLLEGE, HYDERABAD, DECCAN

*(Received for publication, August, 2, 1953).*

**ABSTRACT.** This paper describes an investigation of the photoconducting nature of amethyst quartz. Measurements of photocurrent were made for varying voltages, intensities, radiations and temperatures. A spectral sensitivity curve of photoconductivity duplicates the optical absorption in the visual region identified as the F-band. The photocurrent is found to be proportional to light intensity and voltage; in the latter case secondary currents deviate the relationship from strict linearity. Under constant irradiation of light in the maximum of the F-band, the crystal is shown to be "excited". Lastly, measurements of photocurrent at different temperatures under radiation sources that yield both the electron primary current and the positive primary current, show that the curves obtained are identical with those obtained by Pohl and collaborators in the case of coloured rocksalt. The similarity of the behaviour of amethyst quartz and coloured rocksalt is so very striking that it seems very reasonable to ascribe the colouring of amethyst quartz to F-centres caused by high frequency radiations.

## INTRODUCTION

Systematic studies of the photoconductivity of crystals have shown that we can classify them into two categories. Idiochromatic crystals are those whose photoelectric properties are determined by the material itself and not by any naturally present or artificially introduced impurities. Allochromatic crystals on the other hand are inactive photoelectrically in the pure state, but active when foreign atoms or particles are dispersed through their volume. The naturally and artificially coloured alkali halides, studied extensively by Gudden, Pohl and collaborators in Germany fall into this latter class.

The differences between allochromatic and idiochromatic crystals become readily apparent when one studies their absorption spectra and their photoconducting nature. In idiochromatic crystals the photoelectric current is directly proportional to the incident light quanta and increases as we go to the ultraviolet, until a high rate of recombination is reached in the crystal. In allochromatic crystals, where F-centres are responsible for the colour as well as the enhanced electrical conductivity under the influence of light, the spectral response curve of photoconductivity follows closely the F-band. The "excited" spectral response also duplicates closely the trend indicated by the F-band.

In an earlier investigation the author (Bappu, 1952) has shown from a study of the absorption spectrum in the visible region that amethyst quartz may be considered as essentially an allochromatic crystal. The absorption in the

\* Part of the thesis accepted for the M. Sc. research degree of the Madras University.

ultraviolet and near infrared regions (Bappu, 1953) also confirms this hypothesis and reveals the slight deviations present from the identical behaviour of an alkali halide crystal exposed to high frequency radiation. In what follows, we shall report on a study of the photoconductivity of amethyst quartz and show conclusively that its colour is acquired in a fashion similar to that of an allochromatic crystal.

#### EXPERIMENTAL

The conductivity was measured by the well known Curie method with the aid of a Lindemann electrometer. The electrodes used were crocodile clips and the springs in them had sufficient tension to ensure a good contact between the specimen and electrodes. An earthed copper guard ring prevented any possible surface leakage. The current was measured by noting the charging rate of a precision high quality condenser. The value of the condenser used for measuring very low currents was  $94 \mu\text{f}$  while for appreciable currents, of the order of  $10^{-12}$  amperes, a value of  $110 \mu\text{f}$  was employed. The high tension source for values less than 180 volts was a set of dry batteries, the output of which for all purposes may be taken as constant over the period. For voltages greater than 180 volts, a rectifier capable of giving potentials up to 500 volts was used.

The source of light employed for exciting the F-centres was a 250 watt tungsten filament lamp run on A. C. voltage; the light from this lamp was focused on to the entire area of the specimen between the electrodes. Three spectral regions with effective wavelengths of  $5500 \text{ \AA}$ ,  $4600 \text{ \AA}$  and  $5900 \text{ \AA}$  and having bandwidths of about  $500 \text{ \AA}$  were isolated by means of filters. Light from a 150 C. P. pointolite lamp, after passing through a red filter, acted as the source of long wavelength radiation. In the study of the variation of photocurrent with light intensity, the relative intensities were deduced by applying the inverse square law.

For maintaining the specimen at a temperature higher than that of the surroundings, a heater provided with two mica windows as entrances for the exciting light and red light was used. Measurements were made only when steady temperatures were attained and maintained for at least half an hour, as indicated by a thermometer placed virtually in contact with the specimen.

#### RESULTS

(a) *Dependence of photocurrent on light intensity and applied voltage.* One of the most significant features of the primary photoelectric current that has been observed in every photoconducting crystal, is the strict proportionality between the current and the intensity of the exciting light. Secondary currents do bring in their own complications to upset this rigorous proportionality, as will be seen in the intensity curve of molybdenite, obtained by Coblenz and collaborators and reproduced by

Nix (1932). In the case of the variation of primary current with voltage, we get curves showing saturation for fairly high values of electric field. Saturation could be attained fairly easily in idiochromatic crystals, while in allochromatic crystals they can be found only with great difficulty.

To determine the variation with intensity in the case of amethyst quartz, a current obtained fifteen seconds after illumination had started, was utilized. The variation was studied with two different radiations, green and yellow. The current obtained was strictly proportional to the intensity of the light. As can be seen in figure 1, both the curves are parallel to each other showing that the difference in value of photocurrent was caused by a difference in absorption.

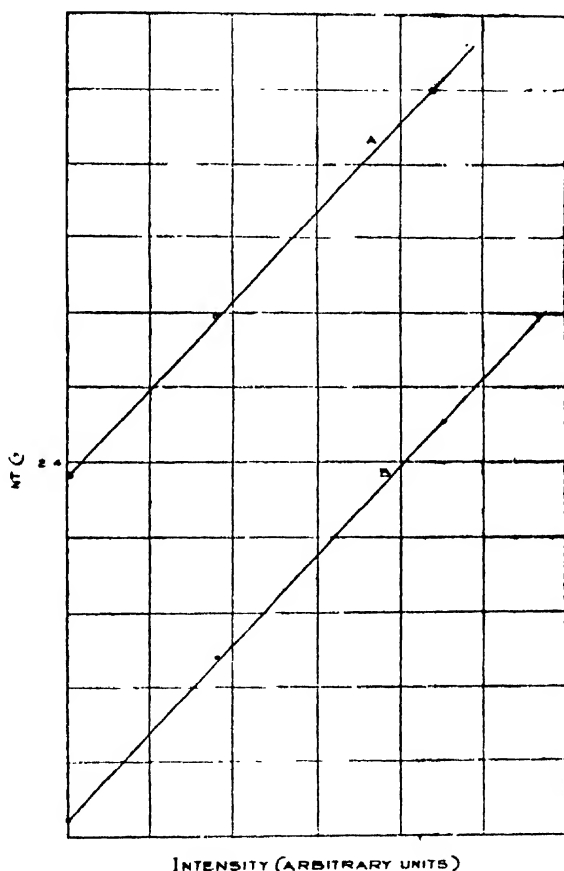


FIG. 1

Variation of photoelectric current with light intensity

A. Green light.

B. Yellow light

To test the dependence on voltage, readings were taken one minute after the beginning of illumination in the blue and green regions of the spectrum.

These measurements were taken in a way that facilitated the indication of the presence of secondary currents. No tendency for saturation occurred

as can be seen in figure 2. On the contrary the current increased considerably with higher voltages, thus indicating the major share taken up by secondary currents.

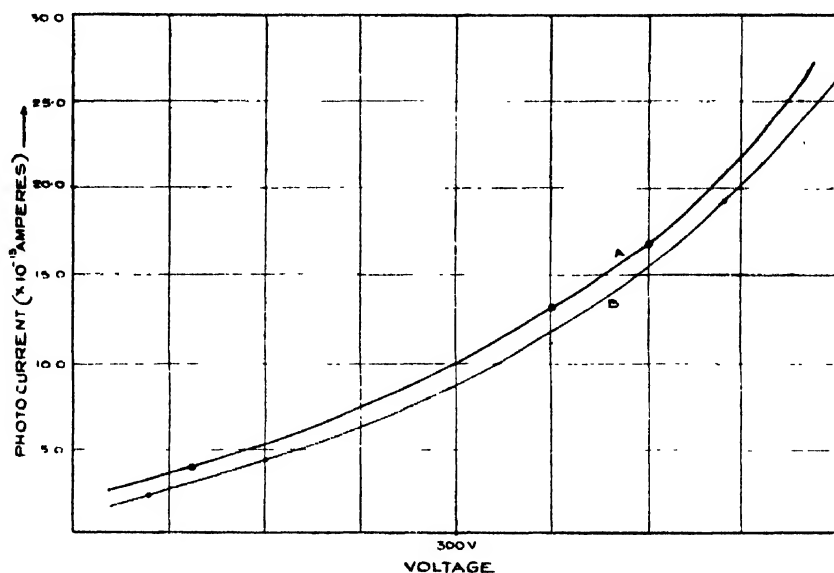


FIG. 2

Variation of photocurrent with applied voltage

A. Green light      B. Blue light

(b) *Photoelectric responses for different wavelengths*: For investigating spectral sensitivity it is essential that the spectral regions isolated from a light source by filters or by a monochromator should have the same spectral energy. In the following experiments accurate spectral energy measurements could not be made and so the different spectral regions could not be equalised with respect to their energy contents. However, by combining the energy distribution of the tungsten lamp with the transmission data of the filters, the assumption that for all practical purposes the relative transmitted energies of the three filters are equal, seems valid. The measurements of the initial jumps of the primary current are used to obtain an idea of the degree of excitation, produced by the different radiations, of the F-centres.

Figure 3 demonstrates the photoelectric responses of a specimen of amethyst quartz to green, blue and yellow light and also to white light. The measurements being green, blue and yellow exciting radiations constitute a continuous run, the crystal being irradiated with red light at the end of each dark period that follows one of excitation. Let us consider first the effect of green light alone. Instantly on illumination we have a sudden rise of  $1.2 \times 10^{-13}$  amperes in the value of the current. This is the primary current. If at this stage the primary current had continued steadily, the current curve would have been parallel to the time axis. But

instead we find a slow but regular increase in the value of current showing that with time the resistivity of the crystal has decreased. This current is the secondary current because it has developed here with the aid of the primary current and with a time lag. Intense lighting, together with imperfections are responsible for the formation of secondary currents. Hence in crystals with twinnings, some glasses, and tablets of compressed powders the primary photoelectric current is largely suppressed and only a high secondary current is observed. In view of this fact it is not surprising, if in amethyst quartz, the lattices of which are distorted by the presence of metallic impurity, a secondary current manifests itself.

The decrease in value of current at the fifth minute after illumination is due to the formation of a space charge which tends to nullify the regular inflowing current. The mechanism of the secondary current can be considered as follows: When the crystal is irradiated with light in the F-band, photoelectrons are released, and under the influence of the electric field they move towards the anode. A large or small number of photoelectrons is released depending on the absorbed energy and we get correspondingly a large or small primary current. The continued passage of the primary current appears to break down the resistance of the crystal, so that electrons can enter the crystal from the cathode and pass to the anode. When the primary current flows, a few of the photoelectrons are trapped at impurity centres or at surfaces of discontinuity, forming channels as a result of which the effective resistance of the crystal decreases. This current constitutes the secondary current. Due to the flow of the photoelectrons, a positive charge builds up in the crystal and tends to annul the incoming electron flow. This accounts for the decrease in current after the fifth minute. A few of the incoming electrons neutralise the positive charges behind, while further positive charges are formed continuously due to the drift of the photoelectrons under the influence of light. The saturation value is obtained when a number of electrons coming in from the cathode neutralises the positive charges, the current being observed due to the motion of the photoelectrons. At the eighth minute when the light has been turned off there are no more photoelectrons released and a sudden fall in the current is noticed, showing that the photoelectrons do not contribute anymore to the current. After this sudden drop the current decays with a time lag until the normal value of the dark current is reached, because the conducting channels lose the electrons of which they are made.

In the case of the photoelectric response with blue light we find an initial jump of  $0.95 \times 10^{-13}$  amperes constituting the primary current. The development of the secondary current can be noticed, but there is again a space charge formed which decreases the current. The absence of a sudden fall immediately on turning off the light, indicates, that the incoming flow of electrons just neutralises the positive charges released.

With yellow light we have a rise of  $0.85 \times 10^{-13}$  amperes constituting

the primary current. The secondary current formed, keeps increasing without any space charge being formed, showing, that the positive charges are being nullified by the electron flow from the cathode. The conducting channels decay rather rapidly to restore normal conditions once again.

Comparing the initial jumps in values of the current, under the influence of green, blue and yellow radiations we find that the green radiations have a greater effect in producing photoelectrons than the blue and yellow regions of the spectrum. This indicates that the photoelectric spectral distribution curve has a maximum in the green region, with blue and yellow having lower values, thus forming a bell shaped curve similar in shape to that of optical absorption. This behaviour is just as expected, for amethyst quartz has been proved optically to be essentially an allochromatic crystal.

The above measurements were repeated after 24 hours, so that the crystal may revert to its original condition. The full radiation of the lamp was turned on, as the source of white light. A different electrode spacing gave a slightly higher field, which in turn accounts for a slight increase in value of the dark current. The variation in current under the influence of white light, as seen in figure 3, shows that the difference between the final value of the current and the dark current is more than twice that in the case of green light. As white light consists of radiations both on the short wavelength and on the long wavelength side of the F-band, we can assume that a large number of photoelectrons is created and conduction channels are formed, while the locations of the positive charges formed are made mobile by the long wavelength radiations of the red and infrared regions. As secondary currents depend on primary currents for their formation, which in turn depend on the exciting wavelength, we have indirectly a relation between the magnitudes of the secondary currents and the respective wavelengths responsible for their creation. This can be found in the case of molybdenite where the secondary currents due to  $\lambda 9900$  are about eight fold greater than those due to  $\lambda 24100$ . In amethyst quartz, we have the secondary current assuming large proportions because of the sum total of the roles is played by all the different wavelengths. The rapid decay in darkness shows that under the influence of long wavelength light most of the locations of positive charges had slipped to the cathode. It is because of the simultaneous flow of the positive primary current along with the ordinary flow that the final value of the current in the case of white light is more than double that in the case of green light. The definite time lag present in the decay after illumination with white light illustrates that conduction channels play an appreciable part.

(c). *Excitation in amethyst quartz*: Rontgen and Joffe (1921) found that the spectral sensitivity of coloured rocksalt by X-rays was influenced by the order in which measurements are made. Later investigations on rocksalt have shown that the crystal when excited yields a spectral sensitivity

curve which has a maximum of lower value than in the unexcited condition. In amethyst quartz, excitation and effect of current flow were observed together and are shown diagrammatically in figure 4. The crystal was irradiated and kept in darkness, measurements being taken in the meanwhile. Two more runs of this type were made without giving any time for the crystal to come back to normal condition.

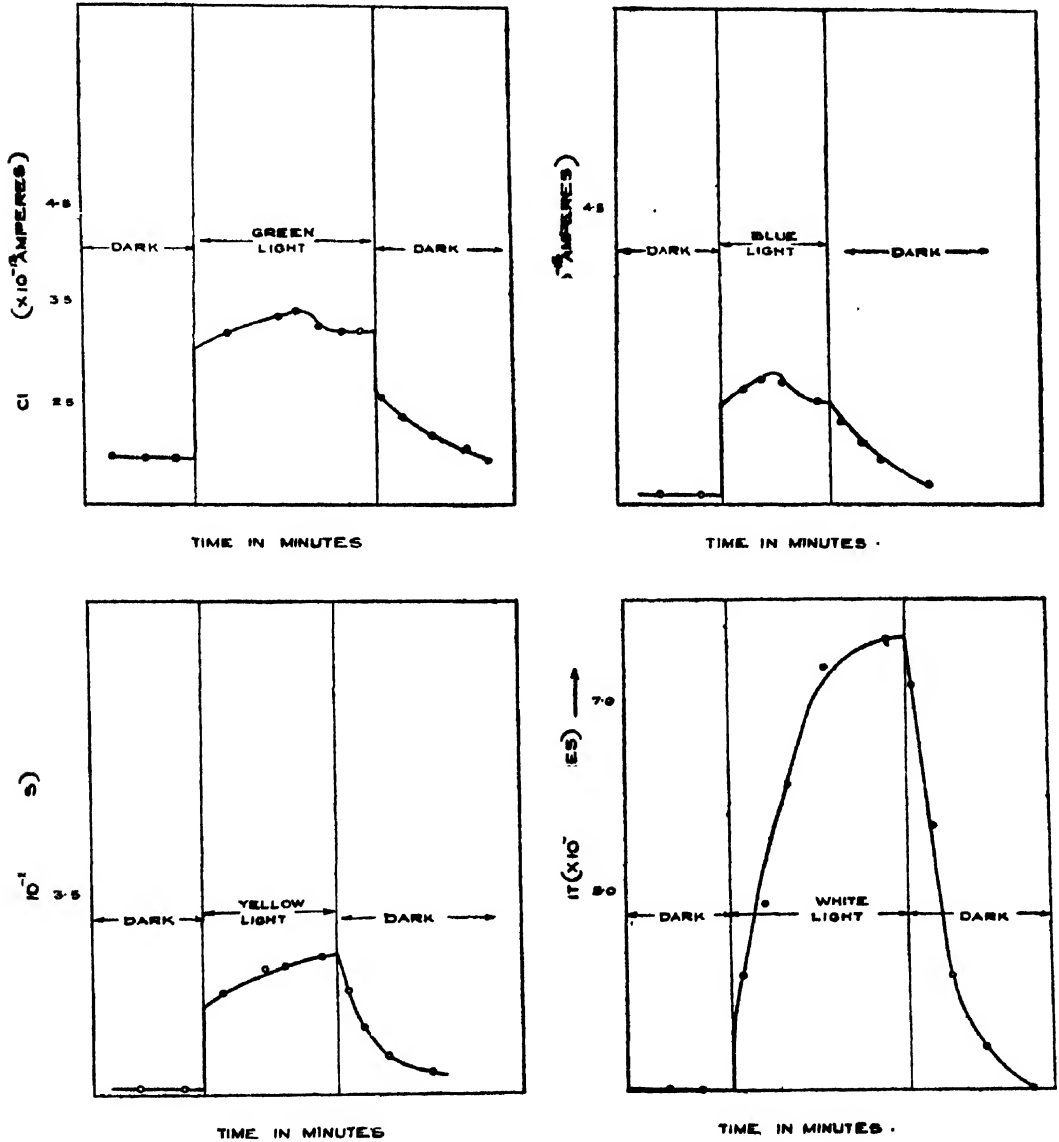


FIG. 3

Photoelectric response vs time of illumination

A comparison of diagrams (a), (b) and (c) will show the changes that have taken place. The transition from digram (a) to (c) indicates a decrease

in dark current of  $0.25 \times 10^{-13}$  amperes. This decrease can be ascribed to polarisation which is so often found in insulators of the type of quartz.

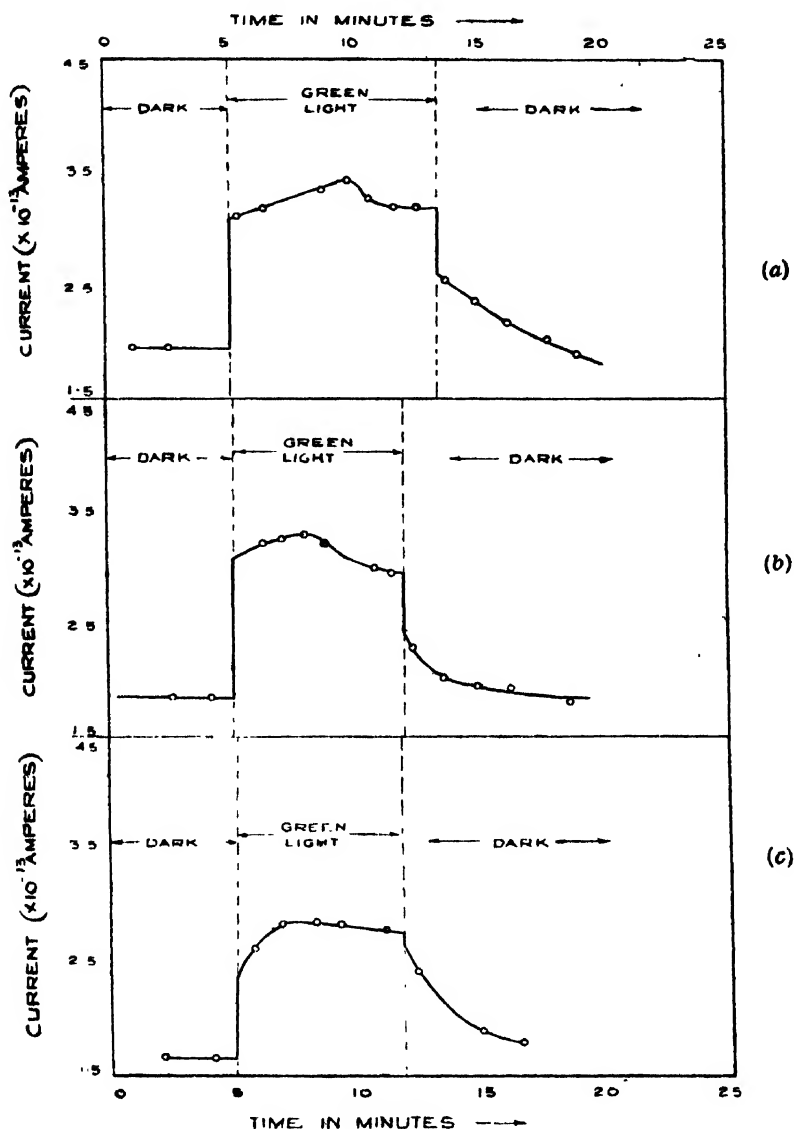


FIG. 4

Excitation in amethyst quartz

On illumination we find in case (a) a primary current of  $1.2 \times 10^{-13}$  amperes as against one of  $0.65 \times 10^{-13}$  amperes in case (c). Also on the termination of illumination the fall in the first run is  $0.53 \times 10^{-13}$  amperes and  $0.2 \times 10^{-13}$  amperes in the third case. The difference between the fall in current in the first and second runs is not as striking as in the case of the first and third. Such a behaviour is due to the different periods of illumination in the two cases and hence if in the second run the crystal was bathed for a greater duration with green radiation, the magnitude of the



fall in current when the light intensity is turned off would have been much less than observed. The decrease in values of the primary currents from (a) to (c) is a clear and definite illustration of 'excitation' in amethyst quartz.

(d). *Photoelectric currents at different temperatures*: Gudden and Pohl have studied exhaustively the photocurrents obtained at different temperatures in the case of yellow sodium chloride. Figure 16 of Pohl's survey article (1937) gives a diagrammatic representation of the data obtained at four different temperatures. In figure 5 the results obtained in the case of amethyst quartz for the temperatures  $33^{\circ}\text{C}$ ,  $90^{\circ}\text{C}$  and  $128^{\circ}\text{C}$  can be seen. The procedure followed was exactly that adopted in the case of sodium chloride. After a dark interval the crystal was exposed to green light (corresponding to the F-band), followed by an interval of darkness. Lastly, the crystal was flooded with red light. A voltage of 90 volts was applied, the distance between the electrodes being 0.7 cms.

At room temperature a primary photocurrent of  $0.1 \times 10^{-13}$  amperes was obtained. Such a value does not seem high when compared with previous measures, but in view of the fact that the experiment was carried out with a smaller value of the electric field and a lower light intensity, this jump is not too low. The current increased with time upto the fifth minute after illumination, and reached a saturation value of  $2.6 \times 10^{-13}$  amperes. At the end of the eighth minute after illumination the light was turned off. A drop in value of  $0.4 \times 10^{-13}$  amperes occurred, followed by a decay to  $1.9 \times 10^{-13}$  amperes in current value, was noticed. This decays quickly at first and slowly afterwards with time, reaching the dark current value obtained before the experiment was performed.

At  $90^{\circ}\text{C}$  the dark current was  $8.75 \times 10^{-13}$  amperes. Instantly on illumination, a primary current of  $6.25 \times 10^{-13}$  amperes was noted. A steady increase in current value could be seen, but it was not much when compared with the increase at  $33^{\circ}\text{C}$ . A drop in value of  $1.0 \times 10^{-13}$  amperes occurred when the illumination terminated. After four minutes of darkness an instantaneous rise in value of  $1.5 \times 10^{-13}$  amperes was noted with the red source on, followed by a current decay back to the initial value.

The dark current at  $128^{\circ}\text{C}$  was  $14.5 \times 10^{-13}$  amperes. An observation made half a minute after the beginning of illumination revealed an increase of  $17.0 \times 10^{-13}$  amperes. But even when the green light was on there existed a steady decay in the behaviour of the current. The decay continued still further in darkness. On turning the source of red radiation on, an increase of  $3.5 \times 10^{-13}$  amperes was noted.

At  $33^{\circ}\text{C}$  the fall in value of current immediately on turning off the green light source is nearly four times the initial jump. A possible explanation of this can be given as follows. A few of the electrons are trapped. Due to the electron flow by virtue of the primary current these are released temporarily and some of them get trapped once more in vacancies or with

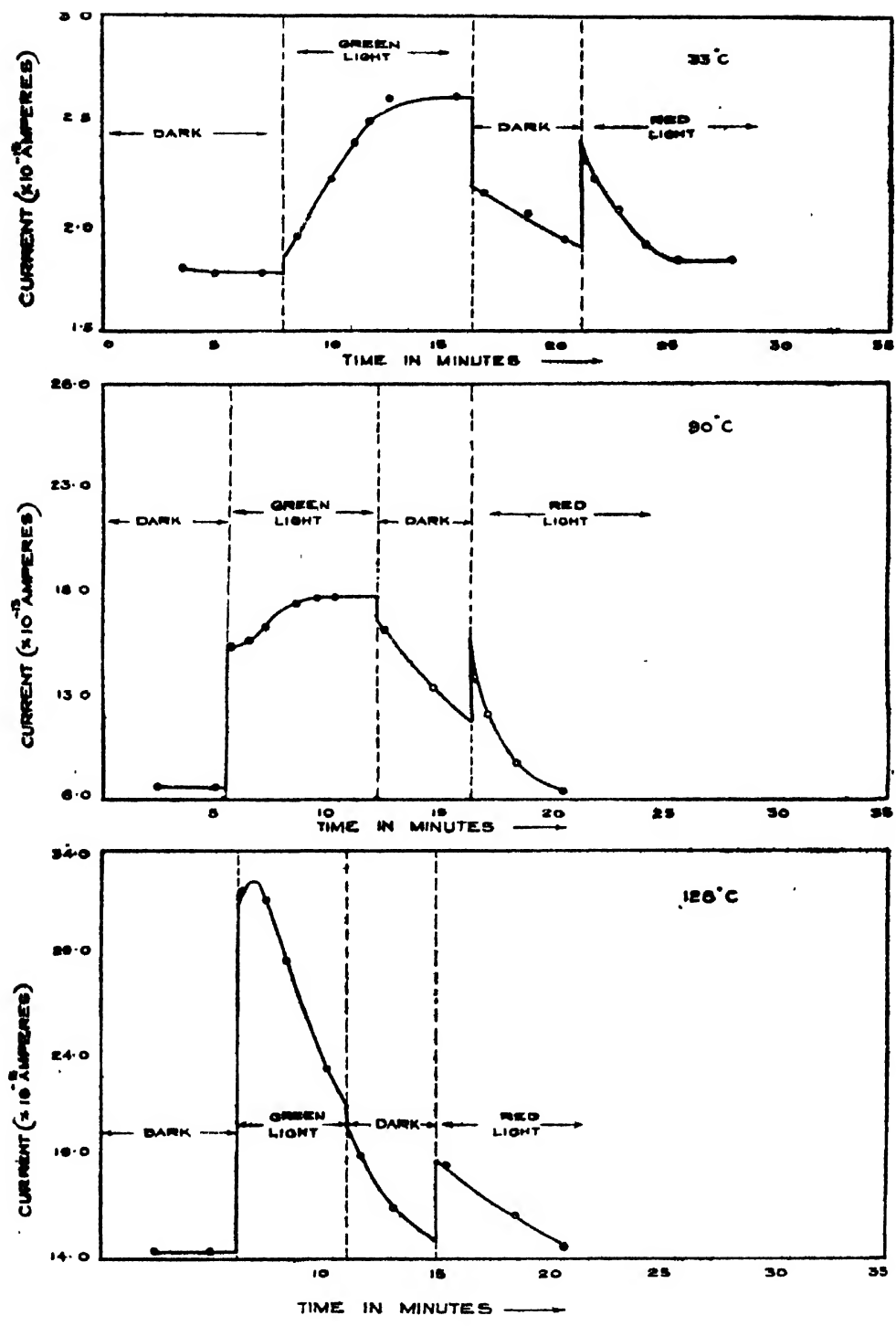


FIG. 5  
Variation of photocurrent with temperature

interstitial ions. The green light releases them and they again move a certain distance. Consequently, the number of electrons moving under the influence of light now is greater than initially and hence when the light is turned off a greater fall in value of current is observed. During the dark period the conduction channels formed, decay. The location of a few positive charges slip back to the cathode, thus causing a slight flow of the positive primary current in darkness also. On illumination with red light the positive charges are neutralised completely, as shown by the increased value of the current.

At  $90^{\circ}\text{C}$  a very high jump in value of current, immediately on illumination, is noticed. This is because, simultaneously with the electron primary current, a little of the positive primary current flows as a result of the thermal energy being able to move the electrons further. As most of the positive primary current flows during illumination with green light as well as when the crystal is in darkness, we have a rise in value of current under the influence of red light equal to only two thirds the value of the initial jump on illumination.

The behaviour at  $128^{\circ}\text{C}$  is just a magnification of that at  $90^{\circ}\text{C}$ . But now as a result of the high value of current flowing by virtue of the negative and positive primary currents, the current decreases due to an increasing polarisation which effects the drift of the electrons. A low dark current is observed and the flow of the positive primary current under the influence of red light is very little.

A comparison of the three curves indicating behaviour under the influence of red light will show that with time, at room temperature the current decay is quick initially and slow later. At  $90^{\circ}\text{C}$  it decays fairly quickly while at  $128^{\circ}\text{C}$  it varies linearly with time. This difference is due to the increased mobility of the locations of positive charges at high temperatures.

Thus the phenomena of spectral sensitivity, excitation and variation of photocurrent with temperature, exhibited by yellow sodium chloride, are duplicated essentially by amethyst quartz. Along with the optical studies, this investigation indicates rather definitely that amethyst quartz possesses its colour as a result of the presence of F-centres, formed possibly by high frequency radiation.

#### ACKNOWLEDGMENT

It is a pleasure to acknowledge indebtedness to Dr. J. C. Kamesvara Rav, Professor of Physics, Nizam College, Hyderabad, Dn., for his constant encouragement and keen interest during the course of this investigation.

## REFERENCES

- Bappu, M. K. V., 1952, *Ind. J. Phys.*, **26**, 1.  
" " 1953, " " " **27**, 385.  
Nix, F. C., 1932, *Rev. Mod. Phys.*, **4**, 753.  
Pohl, R. W., 1937, *Proc. Phys. Soc.*, **49**, extra part  
Rontgen and Joffe, 1921, *Ann. d. Phys.*, **46**, 1.

# ON THE ULTRAVIOLET ABSORPTION SPECTRA OF TOLUIDINES IN THE LIQUID AND SOLID STATES \*

By (Miss) USHA RANI GUHA BISWAS

OPTICS DEPT. INDIAN ASSOCIATION FOR THE CULTIVATION OF SCIENCE,  
CALCUTTA 32

(Received for publication, November 18, 1953)

**ABSTRACT.** The ultraviolet absorption spectra of *ortho*, *meta*, and *para* toluidine have been studied in the liquid and solid phases of the substances and the spectra have been compared with those of the substances in the vapour state. The results for the *para* compound in the vapour state agree with those reported by Tintea (1933). It has been observed that when the substances are liquefied the narrow bands are replaced by an extended broad band. This broad band persists even when the liquids are solidified and cooled down to  $-180^{\circ}\text{C}$ .

The region of this extended absorption shifts towards longer wavelengths in each case with liquefaction of the vapour and it does not shift appreciably with the solidification of the liquids and lowering of temperature of the solid to  $-180^{\circ}\text{C}$ .

These results are compared with those for chlorotoluenes and dichlorobenzenes reported by Swamy (1952) and it is pointed out that the behaviour of the bands with solidification of toluidines is opposite to that observed in the case of chlorotoluenes and dichlorobenzenes

## INTRODUCTION

The absorption spectra of some disubstituted benzene compounds in the solid state at low temperatures were studied recently in this laboratory by Swamy (1952*a*, 1952*b*, 1952*c*, 1953) and it was observed that the changes which take place with solidification and lowering of temperature of the *para* compounds to  $-180^{\circ}\text{C}$  are different from those observed in the case of *ortho* or *meta* compounds. In the case of *ortho* and *meta* chlorotoluene and *ortho* dichlorobenzene in the solid state each of the bands was found to be accompanied by satellites which were produced by the splitting of the energy level. No such splitting was observed in the other disubstituted compounds studied by him. It is not possible, however, to draw the general conclusion from these results that the presence of chlorine atom is responsible for the splitting unless results are obtained in the case of a large number of such disubstituted benzene compounds. It was thought worthwhile to investigate this problem more thoroughly, and in the present investigation the absorption spectra of *ortho*, *meta* and *para* toluidine in the solid and liquid states have been photographed and the results have been compared with those for other disubstituted compounds studied by Swamy (1952, 1953).

## EXPERIMENTAL

The substances were supplied by B. D. H. They were distilled in vacuum repeatedly, rejecting each time the residual coloured portion till the

\* Communicated by Prof. S. C. Sirkar

collected portions were perfectly colourless. The absorption spectra of the vapours of ortho, meta and para toluidine were studied by introducing the vapour in the absorption tube at room temperature which was about  $30^{\circ}\text{C}$ . As *p*-toluidine is solid at  $30^{\circ}\text{C}$  the bulb containing the substance attached to the side tube of the long absorption cell was heated a little to melt the solid. The width of the slit of the Hilger L1 spectrograph used in these investigations was about .2 mm. The length of the absorption tube was 25 cm.

The technique used for photographing the absorption spectra of the substances in the liquid state and in the solid state at low temperatures was the same as that used by Deb (1951).

The thickness of the absorbing film was very small, being of the order of a few microns. Microphotometric records of the spectrograms were obtained with the help of a Kipp and Zonen type self-recording microphotometer.

#### RESULTS AND DISCUSSION

Tracings of the microphotometric records are reproduced in figures 1, 2 and 3. The position of the bands observed in the case of the three states of the substances are given in Tables I, II and III. The absorption spectra of these substances in the vapour state were studied by previous workers, but as the literature was not available the data could not be included in the tables.

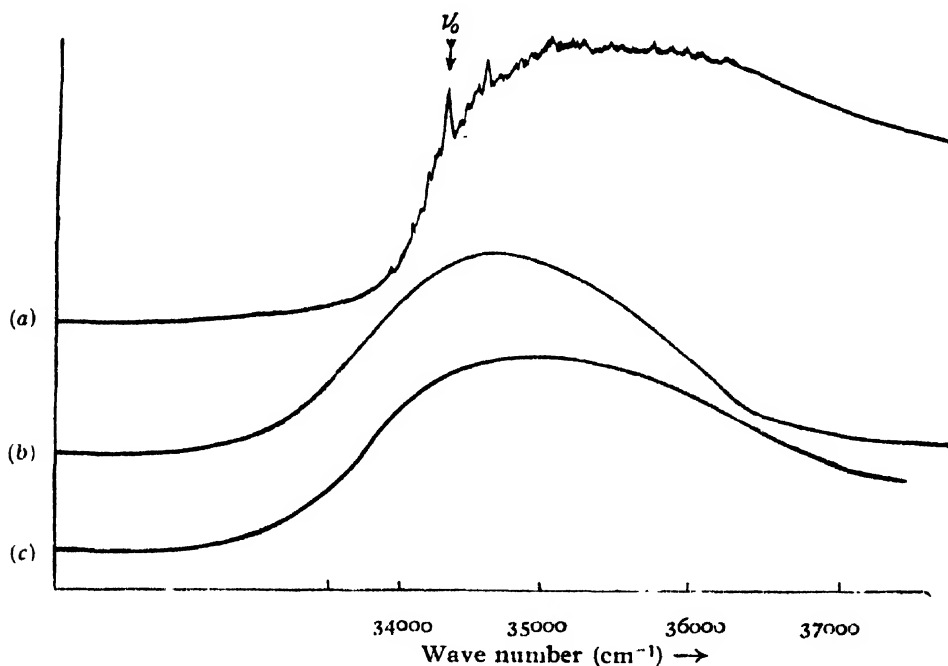


FIG. 1

Microphotometric records of the ultraviolet absorption spectra of *o*-toluidine

(a) Vapour at  $30^{\circ}\text{C}$ , (b) Liquid at  $30^{\circ}\text{C}$ ; (c) Solid at  $-180^{\circ}\text{C}$

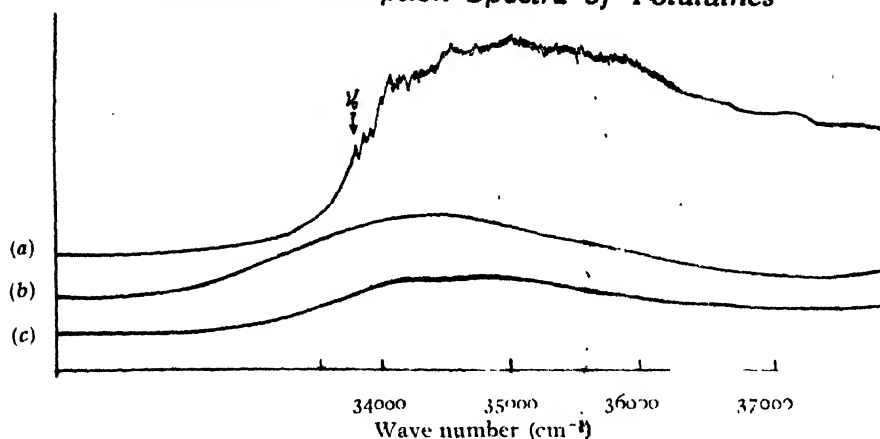


FIG. 2

 Microphotometric records of the ultraviolet absorption spectra of *m*-toluidine

(a) Vapour at 30°C; (b) Liquid at 30°C; (c) Solid at -180°C

TABLE I

 Absorption bands of *o*-toluidine:  $\nu$  in  $\text{cm}^{-1}$ 

Vapour (prominent bands)	Assignment	Liquid at 30°C	Solid at -180°C
33888 (w)	$\nu_0 - 433$		
34171 (w)	$\nu_0 - 150$		
34213 (m)	$\nu_0 - 180$		
34245 (m)	$\nu_0 - 76$		
34321 (v.s)	$\nu_0$		
34412 (m)	$\nu_0 + 91$		
34470 (m)	$\nu_0 + 220 - 76$	One broad band from	One broad flat band from
34541 (m)	$\nu_0 + 220$		
34602 (v.s)	$\nu_0 + 281$		
34695 (m)	$\nu_0 + 281 + 91$		
34780 (m)	$\nu_0 + 468$		
34821 (m)	$\nu_0 + 281 + 220$	32803 $\text{cm}^{-1}$	32803 $\text{cm}^{-1}$
34921 (m)	$\nu_0 + 281 + 220 + 91$	to	to
35053 (m)	$\nu_0 + 732$	36670 $\text{cm}^{-1}$	36671 $\text{cm}^{-1}$
35274 (m)	$\nu_0 + 732 + 220$		
35481 (m)	$\nu_0 + 1160$	max. at	
35756 (m)	$\nu_0 + 1160 + 281$		
35851 (m)	$\nu_0 + 1160 + 281 + 91$	34684 $\text{cm}^{-1}$	
35947 (m)	$\nu_0 + 1160 + 468$		

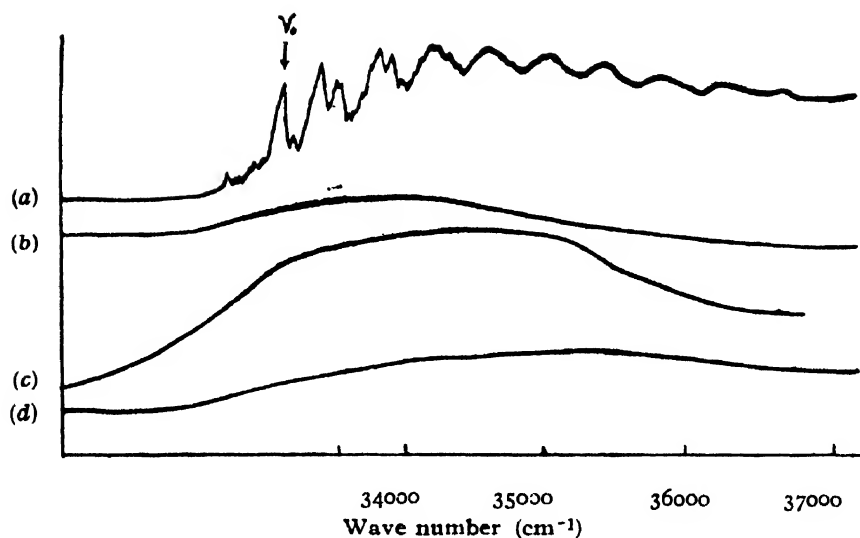


FIG. 3

Microphotometric records of the ultraviolet absorption spectra of *p*-toluidine

- (a) Vapour at 30°C; (b) Liquid at 60°C;  
(c) Solid at 30°C; (d) Solid at -180°C

TABLE II

Absorption bands of *m*-toluidine :  $\nu$  in  $\text{cm}^{-1}$

Vapour (prominent bands)	Assignment	Liquid at 30°C	Solid at -180°C
33813 (m)	$\nu_0$		
33882 (m)	$\nu_0 + 69$		
33931 (m)	$\nu_0 + 118$		
34018 (m)	$\nu_0 + 205$		
34087 (s)	$\nu_0 + 274$		
34157 (m)	$\nu_0 + 274 + 69$	Broad band from 32606 $\text{cm}^{-1}$ to 36198 $\text{cm}^{-1}$	Broad band from
34203 (m)	$\nu_0 + 274 + 118$		32803 $\text{cm}^{-1}$
34295 (m)	$\nu_0 + 274 + 205$		to
34496 (m)	$\nu_0 + 274 + 2 \times 205$		36350 $\text{cm}^{-1}$
34556 (s)	$\nu_0 + 743$		and
34772 (m)	$\nu_0 + 2 \times 274 + 2 \times 205$		Broad band peaks
34991 (s)	$\nu_0 + 1178$		at 34084 $\text{cm}^{-1}$
35057 (m)	$\nu_0 + 1178 + 69$		and
35190 (m)	$\nu_0 + 1178 + 205$		34834 $\text{cm}^{-1}$



TABLE III

 Absorption bands of *p*-toluidine :  $\nu$  in  $\text{cm}^{-1}$ 

Vapour (prominent bands)	Assignment	Liquid at $60^\circ\text{C}$	Solid at $30^\circ\text{C}$	Solid at $-180^\circ\text{C}$
32650 (w)	$\nu_0 - 437$			
32860 (w)	$\nu_0 - 227$			
32914 (w)	$\nu_0 - 173$			
33029 (s)	$\nu_0 - 58$			
33087 (v.s)	$\nu_0$			
33157 (w)	$\nu_0 + 298 - 227$			
33327 (s)	$\nu_0 + 298 - 58$			
33385 (v.s)	$\nu_0 + 298$			
33461 (s)	$\nu_0 + 427 - 58$	One broad band from	One broad band from	One broad band from
33514 (s)	$\nu_0 + 427$			
33683 (m)	$\nu_0 + 2 \times 298$	32606 $\text{cm}^{-1}$	32606 $\text{cm}^{-1}$	32606 $\text{cm}^{-1}$
33748 (m)	$\nu_0 + 427 + 298 - 58$	to	to	to
33808 (s)	$\nu_0 + 427 + 298$	35688 $\text{cm}^{-1}$	36198 $\text{cm}^{-1}$	36670 $\text{cm}^{-1}$
33895 (s)	$\nu_0 + 808$			
33940 (m)	$\nu_0 + 2 \times 427$			
34011 (m)	$\nu_0 + 982 - 58$			
34069 (m)	$\nu_0 + 982$			
34176 (s)	$\nu_0 + 1143 - 58$			
34230 (s)	$\nu_0 + 1143$			
34318 (m)	$\nu_0 + 808 + 427$			
34654 (s)	$\nu + 1143 + 427$			
34958 (w)	$\nu_0 + 1143 + 427 + 298$			
35084 (s)	$\nu_3 + 1143 + 2 \times 427$			
35510 (s.b)	$\nu_0 + 1143 + 3 \times 427$			
35939 (s.b)	$\nu_0 + 1143 + 4 \times 427$			
36366 (s.b)	$\nu_0 + 1143 + 5 \times 427$			
36792 (s.b)	$\nu_0 + 1143 + 6 \times 427$			

The ultraviolet and absorption spectra of ortho, meta and para toluidine in the vapour state were studied previously by Pizlo (1934) and also by Horio (1934). As mentioned earlier, these data were not available. The data

for para-toluidine reported more recently by Tintea (1949) show that the bands can be classified into two series given by the following equations:

$$\text{Series I. } \nu = 33090 + (p' - p_0)817 + (q' - q_0)431 + (r' - r_0)297 - 20p_0(q_0) - 10r_0$$

$$\text{Series II } \nu = 33030 + (p' - p_0)817 + (q' - q_0)431 + (r' - r_0)297 - 20p_0(q_0) - 10r_0$$

The data given in Table III show that the band at  $33029 \text{ cm}^{-1}$  is a weak one while that at  $33087 \text{ cm}^{-1}$  is a strong one. So the latter band has been taken as the  $\nu_0$  band. The progressions of vibration frequencies, 288, 427 and  $808 \text{ cm}^{-1}$  agree fairly well with those observed by Tintea. There seems to be a second system displaced from the first towards longer wavelengths by  $58 \text{ cm}^{-1}$  with  $\nu_0$  at  $33029 \text{ cm}^{-1}$ . When the vapour is liquefied the bands are washed off and a very broad band extending over the whole region from  $32606 \text{ cm}^{-1}$  to  $85688 \text{ cm}^{-1}$  is observed. Either solidification or cooling down of the solid mass to  $-180^\circ\text{C}$  does not produce any appreciable influence on the position of this broad band. As the  $\nu_0$  band in the case of the vapour is at  $33087 \text{ cm}^{-1}$  there seems to be a little shift of the band system towards longer wavelengths with liquefaction of the vapour. Evidently, the broadening of the bands in the case of the liquid state is due to some influence of intermolecular field due to surrounding molecules on the position of the energy level. The distance between any molecule and its neighbours may vary in the liquid due to either irregularity of arrangement of the molecules or motions of the molecules inside the liquid. The fact that even in the case of the solid state in which the arrangement of the molecules is regular the bands are broad shows that some sort of oscillatory motion of the molecules is responsible for the larger width of the bands and that such motions do not cease even at  $-180^\circ\text{C}$ . This behaviour of this particular molecule is quite different from that of para substituted benzene compounds containing chlorine as the substituent atoms (Swamy, 1952). The  $\text{NH}_2$  group thus makes the solid behave as the liquid as far as oscillatory motion is concerned, and it does not favour formation of strong virtual bonds among neighbouring molecules, as observed in the case of disubstituted benzene compounds with chlorine as a substituent.

Ortho toluidine behaves in a manner quite different from that of *p*-toluidine as far as changes in the band system with liquefaction of the vapours are concerned. It can be seen from Table I that although this molecule in the vapour state yields sharp bands which can be assigned to progressions of certain vibration frequencies, the liquid state yields a single broad band in a region shifted towards longer wavelengths by about  $1300 \text{ cm}^{-1}$ . This shift is much larger than that observed in the case of *p*-toluidine. This broad band does not shift appreciably when the liquid is solidified and cooled to  $-180^\circ\text{C}$ . This fact supports the view that the bands shift towards longer wavelengths with liquefaction of the vapour, because there cannot be  $\nu \rightarrow 0$  transitions of large frequencies at  $-180^\circ\text{C}$ . The spectrum due

to the vapour, when analysed, yields progressions of frequencies 91, 220, 281, 468, 732 and 1160  $\text{cm}^{-1}$ .

In the case of the meta compound the spectrum due to the vapour seems to yield two series separated by 69  $\text{cm}^{-1}$ . The progressions of frequencies 118, 205, 274, 743 and 1178  $\text{cm}^{-1}$  have been observed. The spectrum seems to shift by about 1200  $\text{cm}^{-1}$  towards longer wavelengths with liquefaction of the vapour and the bands become broader and merge into one another. When the liquid is solidified and cooled to  $-186^{\circ}\text{C}$  the broad band splits up into two narrower but still broad bands with peaks at 3408.4 and 3483.4  $\text{cm}^{-1}$  giving a frequency difference of 750  $\text{cm}^{-1}$  which may correspond to the frequency 743  $\text{cm}^{-1}$  observed in the case of the liquid.

It is thus evident that in all these three molecules the bands broaden out owing to the fluctuating intermolecular field in the liquid state and the width persists even in the case of the solid at  $-180^{\circ}\text{C}$ . This fact shows that it is the nature of the presence of  $\text{NH}_2$  group and not its position with respect to the  $\text{CH}_3$  group in the molecule that is responsible for the persistence of the angular oscillations of the molecules even at  $-180^{\circ}\text{C}$ .

Investigations with other molecules are in progress.

#### ACKNOWLEDGMENTS

The author's thanks are due to Prof. S. C. Sirkar for kindly suggesting the problem and for his guidance throughout the progress of the work and to the Govt. of India for the award of a scholarship.

#### REFERENCES

- Deb, A. R., 1951, *Ind. J. Phys.*, **28**, 233.  
 Horio, M., 1934, *Bull Intern. J. Soc. Chem. Ind. Japan*, **37**, 283.  
 Pizlo, M. J., 1934, *Acad. Polonaise Classe Sci. Math. Nat.*, **22**, 41.  
 Swamy, H. N., 1952a, *Ind. J. Phys.*, **26**, 119.  
 Swamy, H. N., 1952b, *Ind. J. Phys.*, **26**, 233.  
 Swamy, H. N., 1952c, *Ind. J. Phys.*, **26**, 445.  
 Swamy, H. N., 1953, *Ind. J. Phys.*, **27**, 55.  
 Tintea, H., 1942, *Bull. Soc. Roumaine Phys*, **43**, 9.

# CALCULATION OF PARTIAL MOLAR VOLUME AT INFINITE DILUTION FROM REFRACTIVE INDEX MEASUREMENTS

By ANIL K. SIRCAR AND SANTI R. PALIT

INDIAN ASSOCIATION FOR THE CULTIVATION OF SCIENCE, CALCUTTA 32

(Received for publication, November, 12, 1953)

**ABSTRACT.** A method for the determination of partial specific volume  $(\bar{v}_2)_0$  or the partial molar volume  $(V_2)_0$  at infinite dilution from refraction measurements only without any solution density measurements at all, has been proposed.

The equation,  $(\bar{V}_2)_0 = \frac{1}{r_1} \left\{ v_1 R_2 - 6M_2 \gamma_0 n \left( \frac{v_1}{n_1^2 + 2} \right)^2 \right\}$  has been deduced and calculated values of  $(\bar{V}_2)_0$  obtained from this equation with a few recent data of  $n_D$  and  $d$  are found to be in quite good agreement with observed ones.

The partial molar volume of a solute at infinite dilution is an important physicochemical quantity and is generally measured by accurate density measurements of a series of solutions of graded dilution. We propose to demonstrate that it is possible to make a fairly correct estimate of the partial specific volume,  $(\bar{v}_2)_0$  or the partial molar volume,  $(\bar{V}_2)_0$  at infinite dilution of a solute by refractive index measurements only without making density measurements at all.

## THEORY

By definition of specific refraction constant, we have

$$r = \frac{n^2 - 1}{n^2 + 2} \cdot \frac{1}{d} = \frac{n^2 - 1}{n^2 + 2} \cdot v \quad \dots (1)$$

where  $n$  is the refractive index and  $d$  is the density and  $v$  is the specific volume of the solution. We shall use the subscript 1 for solvent, 2 for the solute, none for a solution and zero for infinite dilution. We shall use small letters for specific terms and capital letters for molar terms.

Differentiating equation (1) with respect to  $\omega_2$ , the weight fraction of the solute, we obtain,

$$\frac{\partial r}{\partial \omega_2} = \frac{r_1}{v_1} \cdot \frac{\partial v}{\partial \omega_2} + 3 \frac{v_1}{(n_1^2 + 2)^3} \frac{\partial n^2}{\partial \omega_2} \quad \dots (2)$$

Now proceeding to infinite dilution, we obtain,

$$\left(\frac{\partial r}{\partial \omega_2}\right)_0 = \frac{r_1}{v_1} \left(\frac{\partial v}{\partial \omega_2}\right)_0 + \frac{3v_1 \left(\frac{\partial n^2}{\partial \omega_2}\right)_0}{(n_1^2 + 2)^2} \quad \dots (3)$$

Now, specific refraction is an extensive property like specific volume and so admits of treatment by the partial concept. This has already been hinted at by Guggenheim (1950). We may, therefore, regard partial specific refraction of a solute at infinite dilution as a characteristic property of the solute-solvent system independent of any concentration effect, and this quantity according to the fundamental equation of partial quantities must satisfy the following equation :

$$\infty r_2 = (\bar{r}_2)_0 = r_1 + \left(\frac{\partial r}{\partial \omega_2}\right)_0 \quad \dots (4)$$

Inserting the value of  $\left(\frac{\partial r}{\partial \omega_2}\right)_0$  from equation (3) we obtain

$$\infty r_2 = r_1 \left\{ 1 + \frac{1}{v_1} \left(\frac{\partial v}{\partial \omega_2}\right)_0 \right\} + \frac{3v_1 \left(\frac{\partial n^2}{\partial \omega_2}\right)_0}{(n_1^2 + 2)^2} \quad (5)$$

Now,  $v$  being an extensive property, the following equation for partial quantity will also be applicable in this case.

$$(\bar{v}_2)_0 = v_1 + \left(\frac{\partial v}{\partial \omega_2}\right)_0 \quad \dots (6)$$

Combining equations (5) and (6) we obtain

$$\infty r_2 = \frac{r_1(\bar{v}_2)_0}{v_1} + \frac{6v_1 n}{(n_1^2 + 2)^2} \cdot \left(\frac{\partial n}{\partial \omega_2}\right)_0 \quad \dots (7)$$

Writing  $\gamma_0$  for  $\left(\frac{\partial n}{\partial \omega_2}\right)_0$  and multiplying the above equation throughout by the molecular weight of the solute, we have

$$(\bar{R}_2)_0 = \infty r_2 \times M_2 = \frac{M_2 r_1 (\bar{v}_2)_0}{v_1} + \frac{6M_2 v_1 \gamma_0 n}{(n_1^2 + 2)^2} \quad \dots (8)$$

This is our basic equation. We now take it as a postulate that the value of partial molar refraction of a solute at infinite dilution remains constant from solvent to solvent, and in most cases is equal to that of the pure solute, i.e.  $(\bar{R}_2)_0 = R_2$ , particularly when the solute is an organic liquid. The above assumption of constancy of refraction is only approximate and is justified on experimental grounds wherever data (Weissberger, 1949) are available. On theoretical grounds we shall also expect such a behaviour because it is

hardly likely that weak solvation forces of the Van der Waals type would affect the electronic polarisation. Hence equations (7) and (8) are recast in the following form for convenience in calculation,

$$(\bar{v}_2)_0 = \frac{1}{r_1} \left\{ v_1 r_2 - 6\gamma_0 n \left( \frac{v_1}{n_1^2 + 2} \right)^2 \right\} \quad \dots (9)$$

$$(\bar{V}_2)_0 = \frac{1}{r_1} \left\{ v_1 R_2 - 6M_2\gamma_0 n \left( \frac{v_1}{n_1^2 + 2} \right)^2 \right\} \quad \dots (10)$$

It would be observed that equation (10) contains constants for pure solute and solvent only and none for the solution except  $\gamma_0$  to determine which refractive index measurements of dilute solution are necessary. Hence, if  $R_2$  is known from bond refraction table or is calculated from  $n$  and  $d$  of the pure liquid with the help of equation (1), or is calculated from equation (8) in one solvent, we can immediately calculate with the help of equation (10) the value of  $(\bar{v}_2)_0$  or  $(\bar{V}_2)_0$  in any solvent by refraction measurements in solution. Thus, if the above assumptions are correct, we have arrived at a method of calculating partial molar volume of a solute at infinite dilution from refractive index measurements of its solutions; at least, when its refraction is known in one solvent, we can calculate its partial molar volume in different other solvents from only refractive index measurements of its dilute solutions.

#### CALCULATIONS

In order to illustrate the degree of accuracy attainable with equation (10) we have made calculations with a few recent data (Few and Smith, 1949a, 1949b; Barclay *et al*, 1950) where both refractive index and density of dilute solutions are available so that we can not only make a check of how far the calculated values of  $(\bar{v}_2)_0$  agree with the experimentally observed ones but also can test how far our basic postulate of constency of refraction is experimentally justified in these cases. This has been done in Tables I and

II. In applying equations (9) and (10) we calculated  $\left( \frac{\partial v}{\partial \omega_2} \right)_0$  and  $\left( \frac{\partial n}{\partial \omega_2} \right)_0$

by the statistical least square slope of  $v$  versus  $\omega_2$ , and  $n$  versus  $\omega_2$  respectively assuming the points to be linear. It should be pointed out that the refractive index data on which calculations have been made are not of a high order of accuracy as has been evidenced from the high scatter of the points about the least square line. It seems that for our purpose it would be more convenient to have differential refractive index values as are easily obtainable to an extremely high degree of accuracy with a Raleigh interferometer and such data would provide a real test of equations (9) and (10),

TABLE I  
Refractivity in different solvents

Solute	$R_2$ in C. C		
	Pure liquid	In benzene	In dioxane
Aniline	30.55	30.71	30.29
Methylaniline	35.62	35.68	36.12 34.71
Dimethylaniline	40.85	41.28	41.19
<i>n</i> -Butylamine	24.01	24.45	24.40
Triethylamine	33.96	33.70	

It would be observed that the molar refraction has almost the same value in the two solvents, benzene and dioxane and this value is practically equal to that of the pure liquid.

TABLE II  
Partial molar volume (c. c. 20°C) at infinite dilution

Solute	In benzene		In dioxane	
	Calc *	Observed **	Calc *	Observed **
Aniline	90.94	91.55	88.16	86.93
Methylaniline	107.32	107.32	106.27	107.50
Dimethylaniline	124.68	126.14	126.09	127.44
<i>n</i> -Butylamine	99.03	100.51	99.17	100.15
Triethylamine	139.30	138.74		

\* Calculated according to eqn (10) using  $R_2$  value for the pure liquid.

\*\* Calculated from solution density data by standard formula.

It would be observed from Table II that there is a fair degree of agreement between the calculated and the observed values. Whether the slight discrepancy between the calculated and observed values is due to weakness of the theory or to the inaccurate character of the experimental data on refractive index as already commented upon has to remain an open question until more precise data from work, which has been already undertaken in this laboratory using interferometer, are available.

It is suggested that the proposed method would be helpful in estimating the partial specific volume of proteins and similar compounds (Cohn and Edsall, 1943).

## ACKNOWLEDGMENT

One of the authors (A. K. S.) wishes to express his thanks to the Council of Scientific & Industrial Research, Government of India, for granting him a Research Assistantship.

## REFERENCES

- Barclay, G., Lefevre, R. and Smythe, B , 1950, *Trans Farad. Soc* , **46**, 815.
- Cohn, E. J. and Edsall, J. T., 1943, Proteins. Amino-acids and Peptides as ions and dipolar ions, Second Printing, Reinhold Publishing Corporation, U. S. A. page 157.
- Few, A. V., and Smith, J. W., 1949a, *J. C. S.*, Part I, 753.
- Few, A. V., and Smith, J. W., 1949b, *Ibid*, Part IV, 2664.
- Guggenheim, E. A., 1950, "Thermodynamics", second edition, North Holland Publishing Co., Amsterdam, p. 172.
- Weissberger, A., 1949, Physical Methods of Organic Chemistry, Part II, P. 1160-1170, 1151. (Inter Science Publishers, Inc. New York)



# A STUDY OF D. C. RESISTIVITY OF CALCUTTA SOIL

By S. P. BHATTACHARYYA AND P. C. MAHANTI

DEPARTMENT OF APPLIED PHYSICS, CALCUTTA UNIVERSITY

(Received for publication, November 18, 1953)

**ABSTRACT.** The paper reports the results of study of d.c. resistivity of soil in and around the city of Calcutta and of its variation with time, temperature and humidity. The effect of endosmosis has also been ascertained.

## INTRODUCTION

It is well known that for the protection and safety of electrical machines and equipment as well as of human and animal lives, all electrical power systems are earthed. Even to the earliest part of the present century, the resistivity of the earth was commonly believed to be so low as to make the potential at any point on the earth's surface practically zero. But recent researches have shown it otherwise. One may, therefore, apprehend that whenever a fault in a power system occurs, it may lead to dangerous consequences if the resistance of the path to the fault current through the earth is not sufficiently low. This resistance is considered to consist of three separate parts, viz., (1) the resistance of the connecting link to the earth connection and of the material of the earth connection itself, (2) the contact resistance between the metal of the earth connection and the surrounding earth and (3) the resistance of the earth surrounding the earth connection. Of these the first is easily calculated from a knowledge of the dimensions and material of the link and the earth electrode but for evaluating the other two factors, a knowledge of resistivity of earth at the locality in question is essential. It may be noted that the resistivity of soil at any locality depends not only on its chemical composition and physical structure but also on its moisture content and temperature as well as on the nature of current, direct or alternating, passing through it and also on the frequency of current when alternating. Furthermore, endosmosis and polarisation may set in and influence the value of its resistivity when direct current flows through the soil.

Almost in all progressive countries elaborate investigations have been carried out for the determination of resistivities, both d.c. and a.c., and contact resistance between the earth and earth electrodes. The a.c. resistivity has been measured not only at power frequencies but also at audio and radio frequencies. Important contributions in this direction have been made by several scientists in U.K. Higgs (1930) made investigations on

d.c. and a.c. resistivities of soil at power frequency and observed changes in their values due to polarisation and endosmosis. Ratcliff and White (1930), Strutt (1930) and Collard (1932) measured the conductivity of soil not only at power frequency but also at telephonic and radio frequencies. Smith-Rose (1934), however, made a comprehensive study of the electrical properties of soil with alternating current at various frequencies. He found the electrical conductivity of the soil to increase rapidly with moisture-content but slowly with frequency. Measurements of conductivity of soil at medium frequencies were also made by Dellinger (1933) in America and by Cheery (1930) in Australia. In India, the resistivity of soil has so far been measured at radio frequencies only, notably by Joshi (1938), Rahaman and Mulhi (1944) and by Khastgir, Roy and Banerjee (1946). Joshi studied also the effect of temperature on the electrical constants of soil. He found the temperature co-efficient of its electrical conductivity to be positive having a value of 2.0 percent per degree centigrade at 20°C and to increase with frequency. But no attempt has yet been made to ascertain the value of resistivity, d.c. or a.c., of Indian soil which may throw further light on the system of earthing to be satisfactorily adopted in our country by the power engineers. It is, therefore, proposed to carry out a systematic investigation of resistivity of soil of different parts of India. In the present paper are reported the results of measurement of d. c. resistivity of soil in and around the city of Calcutta.

Samples of soil used in this investigation have been taken from Sinthee in the north, from Beliaghata in the east, from Tollygunge in the south and from Dockyard in the west of the city of Calcutta. Samples have also been taken from the compound of the University College of Science and Technology at 92, Upper Circular Road to represent the nature of soil of the central part of the city. As Calcutta is situated on the bank of the Ganges, a sample from the river silt has also been included in the investigation.

#### *Experimental cylinder :*

The experimental cylinder, as shown in figure 1, is a porcelain tube of length 25.4 cm., of thickness 1.6 cm. and of internal diameter 10 cm. The cylinder is fitted with adjustable brass electrodes. It may be mentioned

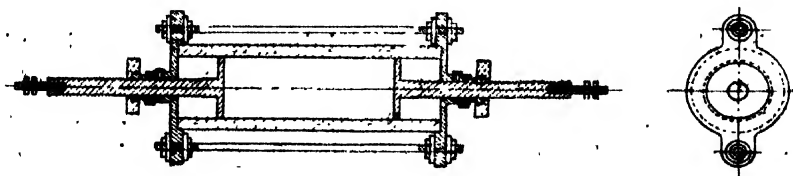


FIG. 1

here that attempts were first made to use a glass cylinder, but it proved futile as even the best quality of glass locally available was found unsuitable to stand the effects of unequal heating during the experiment.

*Preparation of the sample for test :*

Each sample of soil is first dried as completely as possible in an electrically heated oven, the temperature of which never exceeds  $105^{\circ}\text{C}$ . It is found that if dried sample is stored in a dry place for several days it does not absorb more than one percent of moisture. It is then powdered and packed tightly into the experimental cylinder. To prepare a sample with a desired value of moisture content a given quantity of the dried sample was taken and a calculated amount of water was intimately mixed with it.

*Experimental arrangement.*

The experimental arrangement for measuring the resistance is shown in figure 2. The well known ammeter-voltmeter method was used. All the voltmeters and ammeters used in the measurement were calibrated with the help of a potentiometer in conjunction with a Weston standard cadmium cell and standard resistances. The d.c. voltage was taken directly from 220 volt d. c. supply mains and with the help of a potential divider, the voltage across the experimental cylinder was maintained at a nominal value of 120 volts (true value = 124 V) throughout the experiment.

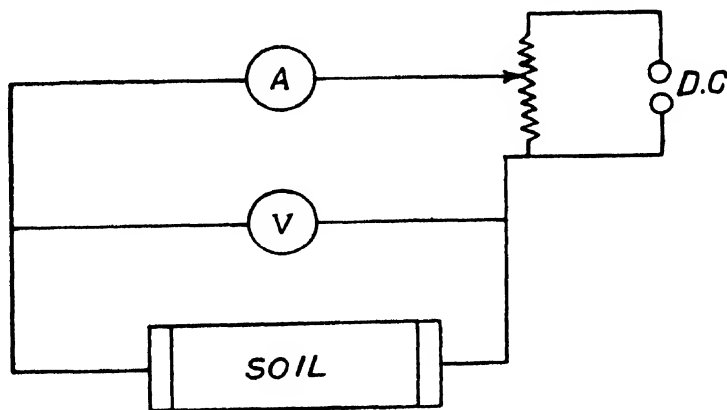


FIG. 2

*Determination of the percentage of moisture content :*

The moisture content of the soil was found out from the difference in weight of the moist soil and dried soil. A quantity of soil under test was taken in a weighing bottle and weighed. It was then dried in a muffle furnace maintained at a temperature between  $100^{\circ}-105^{\circ}\text{C}$ . and weighed again until its weight was found constant. The difference in weight gave the amount of moisture content in the sample and the percentage of moisture could then be easily calculated.

## EXPERIMENTAL RESULTS

*D. C. Resistivity :*

The data of d.c. resistivity of different samples of soil are given in Table I. To obtain these data, measurements were made at a room temperature of 30°C, each sample having a moisture content of 15 per cent.

TABLE I

Soil taken from	D. C. Resistivities in ohm-cm.
North (Sinthee)	1450
East (Beliaghata)	3250
South (Tollygunge)	1400
West (Dockyard)	1415
Central (Science College)	2850
Silt (Ganges)	1365

It is seen from the table that the value of d. c. resistivity of each of the samples of soil taken from the northern, southern and western parts of Calcutta which are nearer to the Ganges is nearly equal to that of the sample taken from the Ganges silt, while it differs considerably in the case of the sample taken from the central and eastern parts of the city, which are away from the river. The sample of soil taken from Beliaghata, which is farthest from the river on the eastern part of the city has the highest value of resistivity.

TABLE II

Sample of soil taken from the central part of the city. Percentage of moisture content = 16.2

Time in minutes	Ammeter reading (m amp.)	Temp. °C	d. c. resistivity in ohm-cm	Time in minutes	Ammeter reading (m amp.)	Temp. °C	d. c. resistivity in ohm-cm.
0	96.5	31.1	2469	180	56.2	41.7	4238
10	106.0	36.2	2248	360	26.8	34.5	8174
30	117.0	42.5	2079	540	20.8	33.4	11450
45	118.5	46.0	2012	720	16.8	32.7	14220
60	118.5	48.0	2012	1500	9.2	31.5	25890
90	110.5	49.5	2152	1620	9.2	31.5	25890
120	86.0	47.4	2771				

TABLE III

Sample of soil taken from the southern part of the city. Percentage of moisture content = 15.4

Time in minutes	Ammeter reading (m amp.)	Temp. °C.	d. c. resistivity in ohm-cm.	Time in minutes	Ammeter reading (m amp.)	Temp. °C.	d. c. resistivity in ohm-cm.
0	145.2	31.1	1811	255	54.7	44.7	4808
10	151.7	38.1	1737	315	36.9	38.7	7125
20	156.7	42.8	1678	375	29.2	36.0	9007
25	158.2	44.5	1663	435	19.3	34.5	13630
30	158.2	45.7	1663	495	18.3	33.8	14370
60	154.2	51.4	1705	1380	12.0	32.9	21920
135	126.8	55.1	2074	1500	12.0	32.5	21920
195	100.5	51.9	2617	1620	12.0	32.5	21920

TABLE IV

Sample of soil taken from the Ganges silt. Percentage of moisture content = 12.1

Time in minutes	Ammeter reading (m amp.)	Temp. °C.	d. c. resistivity in ohm-cm.	Time in minutes	Ammeter reading (m amp.)	Temp. °C.	d. c. resistivity in ohm-cm.
0	125.0	30.0	1905	120	68.6	42.6	3473
10	137.5	34.2	1733	180	52.7	37.6	4522
20	147.2	39.7	1617	240	41.8	35.0	5699
30	154.2	43.1	1545	390	31.2	32.7	7645
55	165.0	48.8	1443	510	26.5	32.4	8989
60	165.0	49.6	1443	1290	15.4	31.7	12280
70	148.7	50.9	1603	1470	15.4	31.7	12280
90	91.0	47.8	2619	1620	15.4	31.7	12280

*Time-current characteristics :*

A steady d.c. voltage was applied across a sample of soil and the readings of ammeter at suitable intervals noted until the current was found to attain a constant value. Along with each ammeter reading the temperature of the test sample was also recorded with the help of a sensitive

thermometer introduced into it through a hole along the axis of the cylinder. Such observations were made on the samples of soil taken from the central and southern parts of the city as well as from the Ganges silt. These data are given in Tables II, III and IV which also include the corresponding values of d.c. resistivity of the sample. The results are also shown graphically in figures 3, 4 and 5.

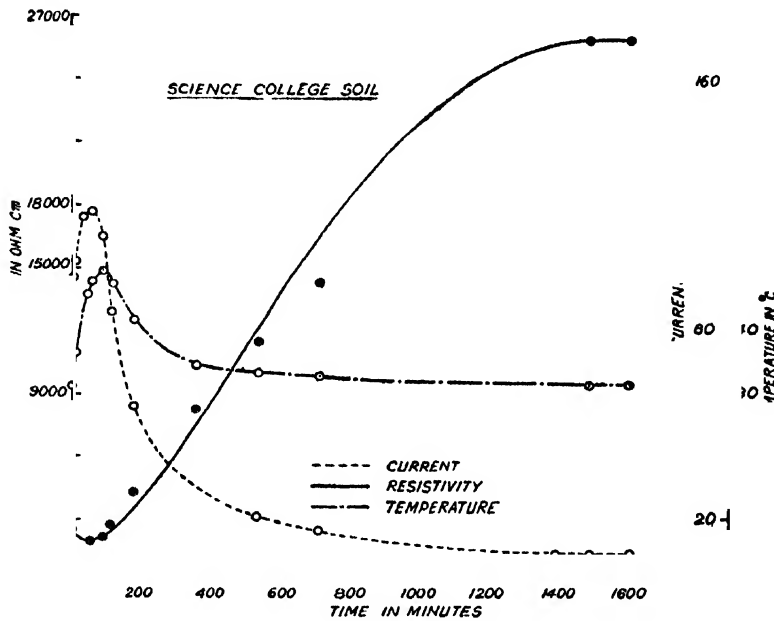


FIG. 3

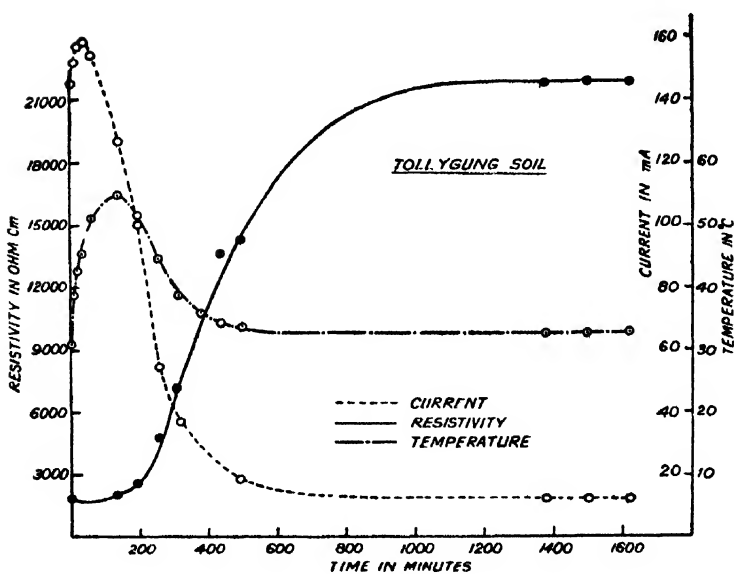


FIG. 4

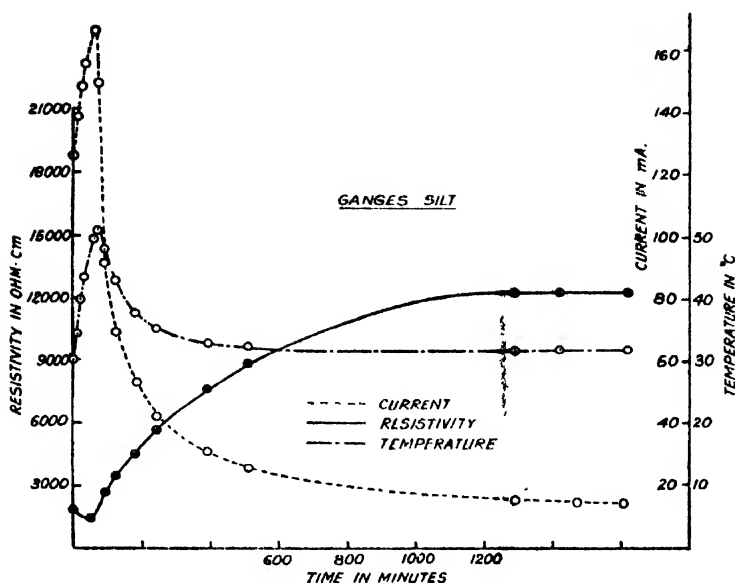


FIG. 5

It may be noted that as one would expect the time-temperature curves are similar in nature to the time-current characteristic curves. It will be seen further that for each sample of soil, the current at first increases, reaches a maximum and then decreases to a minimum value. Such a behaviour may be explained by assuming the soil to consist of many electrolytic salts in its composition.

The current passing through the sample increases its temperature. This increase of temperature decreases the resistance of the soil thereby increasing the magnitude of the current flowing through it. This increase of current further increases the temperature. Thus the current increases with time. This state of affair would have continued for a long time had there been no polarisation and endosmosis effects in the soil. The last two effects tend, however, to decrease the current. Thus the value of the resultant current depends on the relative magnitude of these effects. One may, therefore, be led to infer that at first the heating effect but finally the effect of endosmosis becomes predominant.

#### *Effect of endosmosis :*

It is well known that the process of preferential movement of moisture contained in a body from one part to another is called endosmosis. It is, therefore, of interest to study how endosmosis affects the resistivity and hence the current distribution and the voltage drop in the body of the soil when subjected to a constant d.c. voltage.

A sample of soil taken from the Ganges slit, having a moisture content of 18 per. cent. was taken in the experimental cylinder. The soil was divided approximately into three equal parts by two perforated zinc

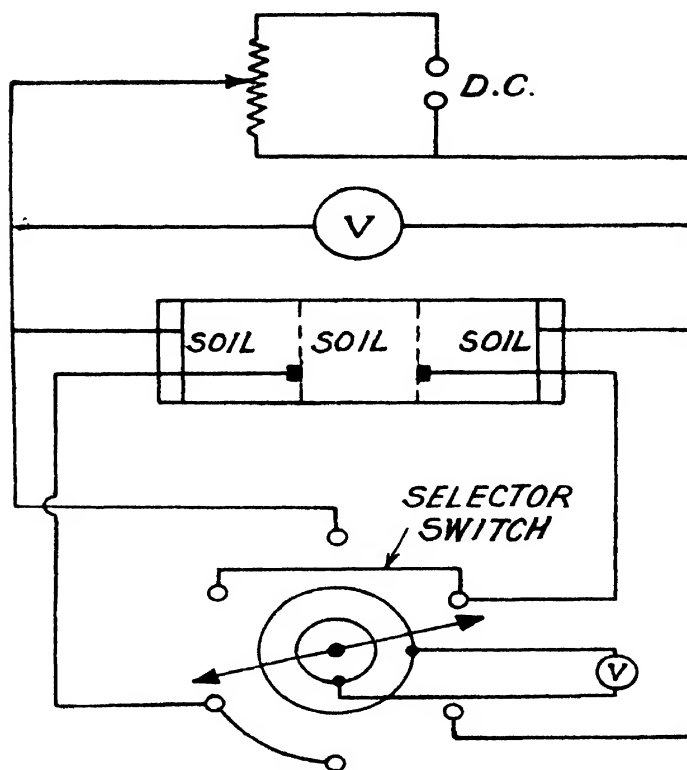


FIG. 6

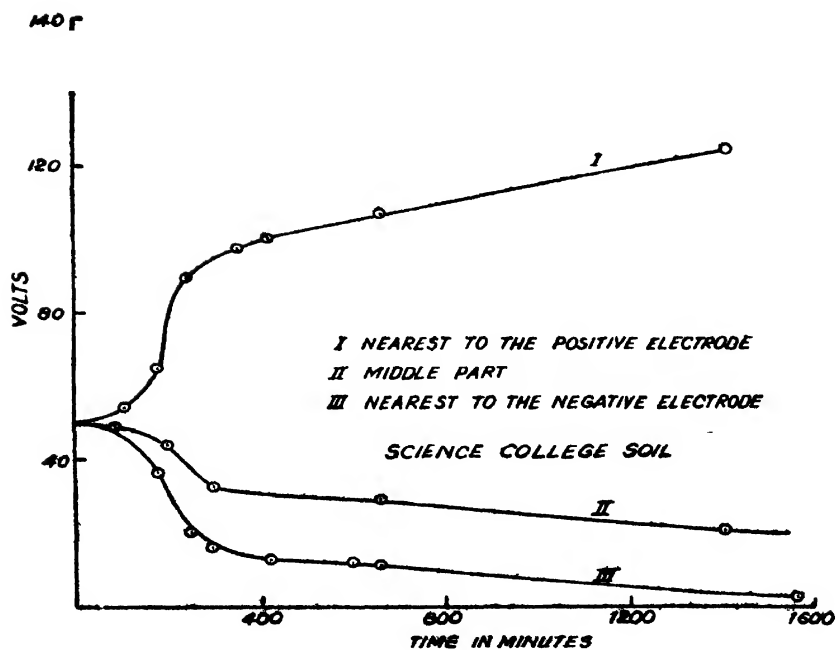


FIG. 7



electrodes. A constant d. c. voltage was applied across the outer electrodes and the current allowed to flow continuously. The voltage drop across each section was noted. For this purpose it was necessary to introduce one low range voltmeter (0-75V) and a selector switch into the previous arrangement. The experimental arrangement is given in figure 6. At the end of the experiment the percentage of moisture content of each section was found out in the usual way.

The percentage of moisture content of the section adjacent to the negative electrode was the highest and that to the positive electrode the lowest, being 22 and 9.5 respectively. The middle section showed a moisture content of 17.5%. Curves showing the variations of voltage drop across each section with time are given in figure 7.

From the curves it is seen that the potential drop across the soil section adjacent to the positive electrode increases while that in each of the other two sections decreases with time. It will be further seen that the section adjacent to the negative electrode has the lowest voltage drop. Such a variation of voltage drop across the different sections with time may be attributed to the fact that since a constant voltage is applied across the body of the soil, it is the movement of moisture from one section to the other with time in the direction of the current flow that produces this variation. Similar observations have previously been made by Higgs (1930). The nature of the curves also reveals the direction of the movement of moisture amongst different sections of the soil when carrying current.

#### *Effect of moisture :*

Samples of soil from a particular locality and having different values of moisture content were taken in the experimental cylinder and their d.c. resistivity calculated from the readings of the voltmeter and the ammeter. The data of d. c. resistivity and conductivity of a soil with different values of moisture content are given in Tables V, VI and VII and shown graphically in figure 8.

It will be seen from the graphs that with the increasing value of moisture content of a soil, its d.c. resistivity decreases or its conductivity increases. This may be explained by assuming the dry soil to contain many air packets, so that with increasing moisture content, more and more air packets are reduced thereby diminishing the resistivity of the soil. On the other hand, if the soil contains electrolytic salts, one would expect its resistivity to increase with increasing moisture content. The observed decrease of resistivity with moisture content may, therefore, be attributed to the superposition of these two effects.

It will be further seen that the rate of decrease of resistivity (or increase of conductivity) at first increases and then decreases with increasing value of moisture content. This shows that the conductivity of a soil approaches a saturation value after a certain value of its moisture content. This pheno-

TABLE V

Sample of soil taken from the central part of the city. Temp. = 30°C

Percent. moist. content	D. C.	
	Resistivity in ohm-cm.	Conductivity mho-cm $\times 10^{-6}$
4.7	28540	35.0
6.5	10010	99.9
8.9	5442	183.8
13.4	3070	325.8
16.2	2580	387.6
20.7	1481	675.0

TABLE VI

[Sample of soil taken from the southern part of the city. Temp. = 30°C.]

Percent. moist. content	D. C.	
	Resistivity in ohm-cm.	Conductivity mho-cm $\times 10^{-6}$
1.6	139700	7.2
5.3	7725	129.4
9.0	3485	286.9
13.0	1811	552.1
15.7	1334	749.8
21.0	1287	776.9

TABLE VII

Sample of soil taken from the Ganges silt. Temp. = 30°C

Percent. moist. content	D. C.	
	Resistivity in ohm-cm.	Conductivity mho-cm $\times 10^{-6}$
3.7	28990	34.5
7.7	4919	203.2
12.1	1905	524.7
16.8	1153	883.9
19.5	914	1094.0

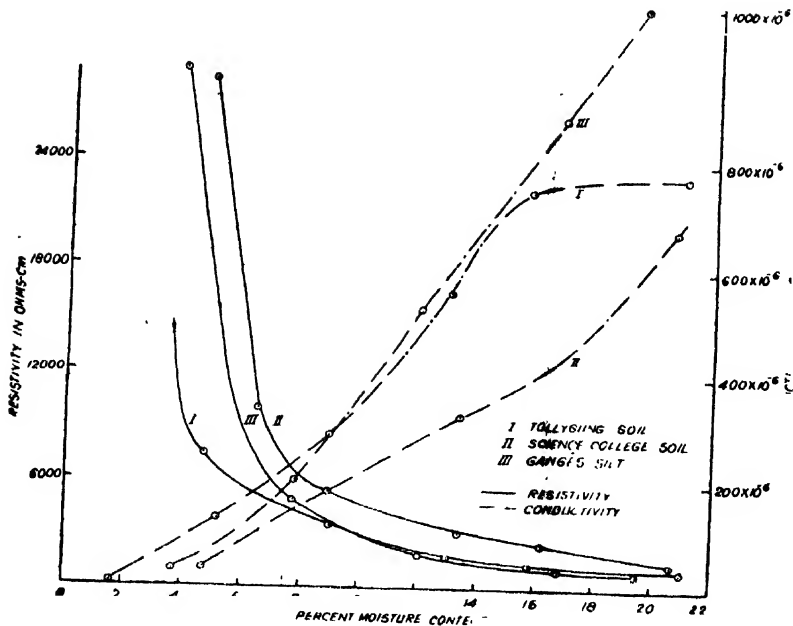


FIG. 8

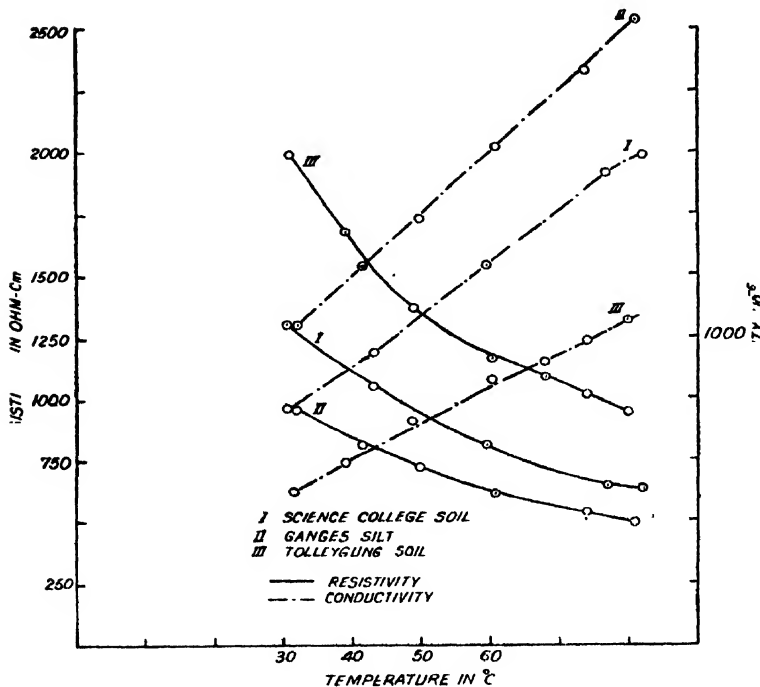


FIG. 9

menon was observed for the samples of soil taken from the Ganges silt and the southern part of the city but not from the central part for even a moisture content of 20 per. cent., the maximum limit used in the present work. This shows that the saturation point is not the same for all kinds of soil but it is dependent on the composition of the soil.

*Effect of temperature :*

The experimental cylinder was wound with insulated nichrome wire and covered with an asbestos sheet to minimise heat losses. By regulating the heating current the temperature of the test soil in the cylinder was kept at desired values and could be maintained constant for at least half an hour. From the readings of the ammeter and voltmeter, the d.c. resistivity was determined at each temperature. Tables VIII, IX and X give the data of d.c. resistivities and conductivities for three different soils.

TABLE VIII

Sample of soil taken from the central part of the city.

Moisture content = 20.7%

Temperature in °C.	Resistivity in ohm-cm.	Conductivity mho-cm $\times 10^{-6}$
30.4	1305	766.5
43.0	1049	953.0
59.5	811	1233.0
76.7	653	1531.0
82.1	631	1585.0

TABLE IX

Sample of soil taken from the southern part of the city.

Moisture content = 12.8%

Temperature in °C	Resistivity in ohm-cm.	Conductivity mho-cm $\times 10^{-6}$
31.4	1988	502.9
39.0	1677	596.4
48.2	1368	731.1
60.2	1165	858.2
68.0	1085	921.7
74.0	1015	985.4
80.0	939	1055.0

TABLE X

Ganges silt. Moisture content = 16.9%

Temperature in °C.	Resistivity in ohm-cm.	Conductivity mho-cm $\times 10^{-8}$
31.8	959	1042
41.5	811	1233
49.8	721	1387
60.7	619	1615
73.7	536	1865
81.0	493	2029

Figure 9 shows the variation of d.c. resistivity with temperature. It will be seen that for each sample of soil the resistivity decreases with increase of temperature. This leads one to infer that the conduction in moist soil is predominately electrolytic in nature as it is well known that the resistivity of an electrolyte decreases with increase of temperature. Conductivity-temperature curves are drawn to find out the value of temperature co-efficient of conductivity. From these curves it is seen that the increase of conductivity with temperature follows a linear law and that within the observed range of temperature, the co-efficient of conductivity varies from 2 to 2.4 per-cent per degree centigrade.

#### REFERENCES

- Cheery, 1930, *Proc. Phys. Soc. Lond.*, **42**, 192  
 Collard, 1932, *Jour. I. E. E.*, **71**, 674.  
 Dellinger and others, 1933, *Proc. I. R. E.*, **21**, 1419.  
 Higgs, 1930, *Jour. I. E. E.*, **68**, 736.  
 Joshi, 1938, *Ind. J. Phys.*, **12**, 1.  
 Khastgir, Roy and Banerjee, 1946, *Ind. Jour. Phy.*, **20**, 119  
 Rahaman and Muhi, 1944, *Ind. Jour. Phy.*, **18**, 31.  
 Ratcliff and White, 1930, *Phil. Mag.*, **10**, 667.  
 Smith-Rose, 1934, *Jour. I. E. E.*, **73**, 221.  
 Strutt, 1930, *Elek. Nach-Tech.*, **7**, 387.

# ON A CONSISTENCY TEST OF THE THEORIES OF STRONG ELECTROLYTES IN SOLUTION \*

By M. SENGUPTA

DEPARTMENT OF PHYSICAL CHEMISTRY, UNIVERSITY COLLEGE OF SCIENCE, CALCUTTA 9

(Received for publication, December 30, 1952)

**ABSTRACT.** In the original Debye Hückel theory the Poisson equation has been evaluated on the assumption that

$$e^{-\frac{e\psi}{kT}} = 1 - \frac{e\psi}{kT}, \text{ i.e. } \frac{e\psi}{kT} \ll 1$$

In this paper it has been shown that the value of  $\frac{e\psi}{kT}$  with which the actual thermodynamic calculations have been made in the theory, is generally  $> 1$ . Thus at least in this respect the original calculations of Debye and Hückel are inconsistent. Incidentally, a similar test applied to the theory of Bagchi shows that this theory is generally consistent in this respect.

In the theory of strong electrolytes due to Debye and Hückel, (1923) the interionic field is assumed to satisfy the Poisson equation :

$$\Delta^2 \psi = -\frac{4\pi}{D} \rho$$

where  $\rho$  is calculated by applying Boltzmann's distribution formula. In the general case, when the solution contains ions of different species 1, 2, ..., i, j, ..., s. the above reduces to :

$$\Delta^2 \lambda_i = -\frac{4\pi e^2}{DkT} \sum_{j=1}^i n_j Z_j e^{-Z_j \lambda_i} \quad \dots (1)$$

where,

$\psi_i$  = electrostatic potential round any central ion of the  $i$ th type

$$\lambda_i = \frac{e\psi_i}{kT}$$

$n_i$  and  $Z_i$  are the number density and valence, respectively of the  $i$ th sort of ions in solution,  $\epsilon$ ,  $D$ ,  $k$ , and  $T$  have their usual significance.

To facilitate the integration of the above partial differential equation (1),  $\sum_{j=1}^i n_j z_j e^{-Z_j \lambda_i}$  has been replaced by  $-\sum_{j=1}^i (n_j z_j^2) \cdot \lambda_i$  on the assumption that

$$Z_j \lambda_i \ll 1 \quad \dots (2)$$

The expression then obtained for  $\lambda_i$  as a function of the distance  $r$  from the central ion of charge  $Z_i$  is :

\* Communicated by Prof. S. N. Bose.

$$\lambda_i = \frac{Z_i e^2 e^{K a_i}}{D k T (1 + K a_i)} \cdot \frac{e^{-K r}}{r} \quad (3)$$

where,

$$K^2 = \frac{4\pi e^4}{D k T} \sum_{j=1}^{\infty} n_j Z_j^2 \text{ and}$$

$a_i$  = the average value of the distance upto which the surrounding ions can approach the central ion.

The additional free energy of the ions due to the interionic field which only is of real significance in the theory, is calculated from consideration of an ideal process of charging-discharging of the ions, or by other thermodynamic methods. However, it is significant that all these methods utilise only the value of the potential at the surfaces of the ions (really, the surfaces of the "Deckungssphären" of ions).

Now if contrary to the condition (2), it is found that  $Z_j \lambda_i \geq 1$ , then the higher powers of  $Z_j \lambda_i$  in the exponential series become significantly large compared to  $Z_j \lambda_i$ , and cannot be neglected. Since, moreover, only the value of  $\lambda_i$  at  $r = a_i$  is important, it is obvious that the consistency of the theory demands that  $Z_j (\lambda_i) r = a_i < 1$ .

This simple requirement of the theory has been tested here (Table I) by calculating  $Z_j (\lambda_i) a_i$  from equation (3) for different ions, at different concentrations (molar) and at 25°C. The values of  $a$  used in these calculations are those which have been found to give the closest fit between theoretical and observed values of activity coefficients, (Harned and Owen, 1950), and of osmotic coefficients, (Falkenhagen, 1934). Since  $a_+$  is assumed to be equal to  $a_-$ ,  $\lambda_+ = \lambda_-$  in the case of the uni-univalent electrolytes. In the case of unsymmetrical electrolytes, where  $Z \neq Z_-$ , the tabulated values of  $Z_j \lambda_i$  correspond to the lower value of  $Z_j$  for obvious reasons.

TABLE I

	$a(\text{\AA})$	.001m	.01m	.1m
NaCl	(a) 4.02	1.704	1.568	1.252
	(b) 4.4	1.586	1.417	1.112
KCl	(a) 3.76	1.827	1.689	1.364
	(b) 4.10	1.669	1.533	1.22
HCl	(b) 5.6	1.204	1.08	.805 *
$\text{K}_2\text{SO}_4$ $\text{K}^+ \quad \text{SO}_4^{--}$	(a) 2.69	2.528	2.30	1.787
		5.056	4.600	3.574
$\text{La}(\text{NO}_3)_3$ $\text{La}^{+++} \quad \text{NO}_3^-$	(a) 4.97	3.822	3.076	1.901
		1.274	1.025	.634 *

Table I shows that except in two cases (marked with asterisk), the condition for the validity of the above approximation is not satisfied, and that it is especially so in the case of polyvalent ions or ions of small radius. This latter fact has already been mentioned by Müller (1927). Further  $\lambda_a$  is seen to increase with dilution, which is also evident from equation (3). Thus the approximation becomes less justified in dilute solutions.

Gronwall (1928) has pointed out some other inconsistencies of the Debye Hückel theory, but has failed to notice the above simple one.

Recently Bagchi (1950) has obtained a better fit between the calculated and the experimental values of activity coefficients by replacing Boltzmann's distribution in the Debye Hückel theory, by a new distribution function which has subsequently been supported theoretically. (Dutta and Bagchi, 1950; Dutta, 1947). The Poisson equation in this case reduces to (for a single electrolyte in solution, giving two sorts of ions) :

$$\nabla^2 \lambda_+ = \frac{4\pi e^-}{DkT} Z_+ Z_- [Z_+ e^{Z_+ \lambda_+} + Z_- Z_- e^{-Z_- \lambda_+} + Z_+] n_+ + n_- \dots \quad (4)$$

where,  $\psi_+$  = potential round the central positive ion,

$\lambda_+ = \frac{e\psi_+}{kT}$ , and  $n_+$ ,  $n_-$ ,  $Z_+$ ,  $Z_-$ ,  $D$ ,  $k$  and  $T$  have the same significance as in Debye's theory.

Bagchi has solved the above equation (4) by approximating in the following way :

(i) for  $\lambda_+ \approx 0$ , equation (4) reduces to :

$$\nabla^2 \lambda_+ = K^2 \lambda_+ \quad (5a)$$

where,

$$K^2 = \frac{4\pi e^2}{DkT} \cdot \frac{Z_+ Z_- (Z_+^2 + Z_-^2)}{(Z_+ + Z_-)^2} (n_+ + n_-)$$

with the solution :

$$\lambda_{+(1)} = B \frac{e^{-\xi}}{\xi} \dots \quad (5)$$

where  $\xi = Kr$

and (ii) for  $\lambda_+ \approx \infty$ , the equation (4) reduces to :

$$\nabla^2 \lambda_+ = K^2 m_+ \quad (6a)$$

where,

$$m_+ = \frac{(Z_+ + Z_-)^2}{Z_+ (Z_+ + Z_-^2)}$$

with the solution :

$$\lambda_{+(2)} = m_+ \left[ \frac{\xi^2}{6} + C + \frac{H}{\xi} \right] \quad (6)$$



The constants  $B$ ,  $C$  and  $H$  have been determined by fitting the two solutions (5) and (6) together on the surface  $\lambda_+ = m_+$  so that (5) should hold for  $\lambda_+ < m_+$  and (6) for  $\lambda_+ > m_+$ .

The electrical free energy has been calculated after Debye; thus, here also, only the surface potential of the central ion is significant. Since however, Bagchi has used only the second solution in calculating the free energy, it is evident that we should have  $(\lambda_{i(2)})r = a_i > m_i$ ;  $i = +, -$ .

This has been tested in Table II, by calculating  $(\lambda_{i(2)})a_i$  by means of equation (6) for different ions, at different concentrations (molar) and at 25°C. The values of  $a_i$  used in the calculations are the same as those used by Bagchi for calculating the activity coefficients. The univalent ions are supposed to be derived from uni-univalent electrolytes. The values of  $m_i$  are also included for comparison.

TABLE II

	$a_i$ (Å)	$m_i$	.01 $m$	1 $m$	4 $m$
K <sup>+</sup>	1.33	2	5.204	4.146	3.367
	2.76	"	2.428	1.587 *	1.244 *
Rb <sup>+</sup>	1.48	"	4.66	3.62	2.88
Cs <sup>+</sup>	1.67	"	4.113	3.097	2.411
Cl <sup>-</sup>	1.81	"	3.78	2.787	2.141
Br <sup>-</sup>	1.96	"	3.481	2.505	1.906 *
I <sup>-</sup>	2.19	"	3.10	2.16	1.626 *
Na <sup>+</sup>	3.2	"	2.071	1.303 *	1.03 *
Na <sup>+</sup> , H <sup>+</sup> , Cl <sup>-</sup>	5	"	1.28 *	.83 *	.828 *
Ba <sup>++</sup>	1.31	.9	10.405	8.019	6.4
BaCl <sub>2</sub>					
Cl <sup>-</sup>	1.81	1.8	3.665	2.239	1.56 *
La <sup>+++</sup>	1.06	.533	19.33	15.71	13.03
LaCl <sub>3</sub>					
Cl <sup>-</sup>	1.81	1.6	3.54	1.83	1.22 *

From Table II it is clear that the assumption  $(\lambda_{i(2)})a_i > m_i$  is justified in most cases, and that most of the cases where it does not hold (marked with an asterisk) are those where Bagchi has taken large artificial values for the ionic radii to get a closer fit between the calculated and the experimental values of activity coefficients.

Thus it is clear that at least with respect to the consistency of method, as put forward in this note, the calculations of Bagchi are more satisfactory than those of Debye and Hückel.

## ACKNOWLEDGMENTS

The author's thanks are due to Prof. S. N. Bose for his kind interest in this work, and especially to Dr. M. Dutta for his suggesting the problem and helpful guidance.

## REFERENCES

- Bagchi, S. N. 1950, *J. Ind. Chem. Soc.*, **27**, 204.  
Debye, P., and Hückel, E. 1923, *Phys. Zt.*, **24**, 185.  
Dutta, M. and Bagchi, S. N., 1950, *Ind. J. Phys.*, **24**, 61,  
Dutta, M. 1947, *Proc. Nat. Inst. Sci. Ind.*, **13**, 247.  
    ,, 1948,           ,,           **24**, 163.  
    ,, 1951,           ,,           **17** 27, 445.  
Falkenhagen, H. 1934, *Electrolytes*, "English Translation. Oxford University Press 256.  
Gronwall, T. H., LaMer, V. K., and Sandved, 1928, *Phys. Zt.*, **29**, 358.  
Harned, H. S., and Owen, B. B. 1959, "Physical Chemistry of Electrolytic solutions,"  
    Reinhold Publishing Corporation, p. 380.  
Müller, H., 1927, *Phys. Zt.*, **28**, 324.